Handbook of Size Exclusion Chromatography and Related Techniques

Second Edition, Revised and Expanded

edited by
Chi-san Wu
International Specialty Products
Wayne, New Jersey, U.S.A.

MARCEL DEKKER, INC. NEW YORK • BASEL

© 2004 by Marcel Dekker, Inc.

First edition: *Handbook of Size Exclusion Chromatography* (1995).

Although great care has been taken to provide accurate and current information, neither the author(s) nor the publisher, nor anyone else associated with this publication, shall be liable for any loss, damage, or liability directly or indirectly caused or alleged to be caused by this book. The material contained herein is not intended to provide specific advice or recommendations for any specific situation.

Trademark notice: Product or corporate names may be trademarks or registered trademarks and are used only for identification and explanation without intent to infringe.

Library of Congress Cataloging-in-Publication Data
A catalog record for this book is available from the Library of Congress.

ISBN: 0-8247-4710-0

This book is printed on acid-free paper.

Headquarters
Marcel Dekker, Inc., 270 Madison Avenue, New York, NY 10016, U.S.A.
tel: 212-696-9000; fax: 212-685-4540

Distribution and Customer Service
Marcel Dekker, Inc., Cimarron Road, Monticello, New York 12701, U.S.A.
tel: 800-228-1160; fax: 845-796-1772

Eastern Hemisphere Distribution
Marcel Dekker AG, Hutgasse 4, Postfach 812, CH-4001 Basel, Switzerland
tel: 41-61-260-6300; fax: 41-61-260-6333

World Wide Web
http://www.dekker.com

The publisher offers discounts on this book when ordered in bulk quantities. For more information, write to Special Sales/Professional Marketing at the headquarters address above.

Copyright © 2004 by Marcel Dekker, Inc. All Rights Reserved.

Neither this book nor any part may be reproduced or transmitted in any form or by any means, electronic or mechanical, including photocopying, microfilming, and recording, or by any information storage and retrieval system, without permission in writing from the publisher.

Current printing (last digit):

10 9 8 7 6 5 4 3 2 1

PRINTED IN THE UNITED STATES OF AMERICA

© 2004 by Marcel Dekker, Inc.

CHROMATOGRAPHIC SCIENCE SERIES

A Series of Textbooks and Reference Books

Editor: JACK CAZES

1. Dynamics of Chromatography: Principles and Theory, *J. Calvin Giddings*
2. Gas Chromatographic Analysis of Drugs and Pesticides, *Benjamin J. Gudzinowicz*
3. Principles of Adsorption Chromatography: The Separation of Nonionic Organic Compounds, *Lloyd R. Snyder*
4. Multicomponent Chromatography: Theory of Interference, *Friedrich Helferich and Gerhard Klein*
5. Quantitative Analysis by Gas Chromatography, *Josef Novák*
6. High-Speed Liquid Chromatography, *Peter M. Rajcsanyi and Elisabeth Rajcsanyi*
7. Fundamentals of Integrated GC-MS (in three parts), *Benjamin J. Gudzinowicz, Michael J. Gudzinowicz, and Horace F. Martin*
8. Liquid Chromatography of Polymers and Related Materials, *Jack Cazes*
9. GLC and HPLC Determination of Therapeutic Agents (in three parts), *Part 1 edited by Kiyoshi Tsuji and Walter Morozowich, Parts 2 and 3 edited by Kiyoshi Tsuji*
10. Biological/Biomedical Applications of Liquid Chromatography, *edited by Gerald L. Hawk*
11. Chromatography in Petroleum Analysis, *edited by Klaus H. Altgelt and T. H. Gouw*
12. Biological/Biomedical Applications of Liquid Chromatography II, *edited by Gerald L. Hawk*
13. Liquid Chromatography of Polymers and Related Materials II, *edited by Jack Cazes and Xavier Delamare*
14. Introduction to Analytical Gas Chromatography: History, Principles, and Practice, *John A. Perry*
15. Applications of Glass Capillary Gas Chromatography, *edited by Walter G. Jennings*
16. Steroid Analysis by HPLC: Recent Applications, *edited by Marie P. Kautsky*
17. Thin-Layer Chromatography: Techniques and Applications, *Bernard Fried and Joseph Sherma*
18. Biological/Biomedical Applications of Liquid Chromatography III, *edited by Gerald L. Hawk*
19. Liquid Chromatography of Polymers and Related Materials III, *edited by Jack Cazes*
20. Biological/Biomedical Applications of Liquid Chromatography, *edited by Gerald L. Hawk*
21. Chromatographic Separation and Extraction with Foamed Plastics and Rubbers, *G. J. Moody and J. D. R. Thomas*
22. Analytical Pyrolysis: A Comprehensive Guide, *William J. Irwin*
23. Liquid Chromatography Detectors, *edited by Thomas M. Vickrey*
24. High-Performance Liquid Chromatography in Forensic Chemistry, *edited by Ira S. Lurie and John D. Wittwer, Jr.*
25. Steric Exclusion Liquid Chromatography of Polymers, *edited by Josef Janca*
26. HPLC Analysis of Biological Compounds: A Laboratory Guide, *William S. Hancock and James T. Sparrow*

© 2004 by Marcel Dekker, Inc.

27. Affinity Chromatography: Template Chromatography of Nucleic Acids and Proteins, *Herbert Schott*
28. HPLC in Nucleic Acid Research: Methods and Applications, *edited by Phyllis R. Brown*
29. Pyrolysis and GC in Polymer Analysis, *edited by S. A. Liebman and E. J. Levy*
30. Modern Chromatographic Analysis of the Vitamins, *edited by André P. De Leenheer, Willy E. Lambert, and Marcel G. M. De Ruyter*
31. Ion-Pair Chromatography, *edited by Milton T. W. Hearn*
32. Therapeutic Drug Monitoring and Toxicology by Liquid Chromatography, *edited by Steven H. Y. Wong*
33. Affinity Chromatography: Practical and Theoretical Aspects, *Peter Mohr and Klaus Pommerening*
34. Reaction Detection in Liquid Chromatography, *edited by Ira S. Krull*
35. Thin-Layer Chromatography: Techniques and Applications. Second Edition, Revised and Expanded, *Bernard Fried and Joseph Sherma*
36. Quantitative Thin-Layer Chromatography and Its Industrial Applications, *edited by Laszlo R. Treiber*
37. Ion Chromatography, *edited by James G. Tarter*
38. Chromatographic Theory and Basic Principles, *edited by Jan Åke Jönsson*
39. Field-Flow Fractionation: Analysis of Macromolecules and Particles, *Josef Janca*
40. Chromatographic Chiral Separations, *edited by Morris Zief and Laura J. Crane*
41. Quantitative Analysis by Gas Chromatography: Second Edition, Revised and Expanded, *Josef Novák*
42. Flow Perturbation Gas Chromatography, *N. A. Katsanos*
43. Ion-Exchange Chromatography of Proteins, *Shuichi Yamamoto, Kazuhiro Nakanishi, and Ryuichi Matsuno*
44. Countercurrent Chromatography: Theory and Practice, *edited by N. Bhushan Mandava and Yoichiro Ito*
45. Microbore Column Chromatography: A Unified Approach to Chromatography, *edited by Frank J. Yang*
46. Preparative-Scale Chromatography, *edited by Eli Grushka*
47. Packings and Stationary Phases in Chromatographic Techniques, *edited by Klaus K. Unger*
48. Detection-Oriented Derivatization Techniques in Liquid Chromatography, *edited by Henk Lingeman and Willy J. M. Underberg*
49. Chromatographic Analysis of Pharmaceuticals, *edited by John A. Adamovics*
50. Multidimensional Chromatography: Techniques and Applications, *edited by Hernan Cortes*
51. HPLC of Biological Macromolecules: Methods and Applications, *edited by Karen M. Gooding and Fred E. Regnier*
52. Modern Thin-Layer Chromatography, *edited by Nelu Grinberg*
53. Chromatographic Analysis of Alkaloids, *Milan Popl, Jan Fähnrich, and Vlastimil Tatar*
54. HPLC in Clinical Chemistry, *I. N. Papadoyannis*
55. Handbook of Thin-Layer Chromatography, *edited by Joseph Sherma and Bernard Fried*
56. Gas–Liquid–Solid Chromatography, *V. G. Berezkin*
57. Complexation Chromatography, *edited by D. Cagniant*
58. Liquid Chromatography–Mass Spectrometry, *W. M. A. Niessen and Jan van der Greef*
59. Trace Analysis with Microcolumn Liquid Chromatography, *Milos Krejcl*

© 2004 by Marcel Dekker, Inc.

60. Modern Chromatographic Analysis of Vitamins: Second Edition, *edited by André P. De Leenheer, Willy E. Lambert, and Hans J. Nelis*
61. Preparative and Production Scale Chromatography, *edited by G. Ganetsos and P. E. Barker*
62. Diode Array Detection in HPLC, *edited by Ludwig Huber and Stephan A. George*
63. Handbook of Affinity Chromatography, *edited by Toni Kline*
64. Capillary Electrophoresis Technology, *edited by Norberto A. Guzman*
65. Lipid Chromatographic Analysis, *edited by Takayuki Shibamoto*
66. Thin-Layer Chromatography: Techniques and Applications, Third Edition, Revised and Expanded, *Bernard Fried and Joseph Sherma*
67. Liquid Chromatography for the Analyst, *Raymond P. W. Scott*
68. Centrifugal Partition Chromatography, *edited by Alain P. Foucault*
69. Handbook of Size Exclusion Chromatography, *edited by Chi-san Wu*
70. Techniques and Practice of Chromatography, *Raymond P. W. Scott*
71. Handbook of Thin-Layer Chromatography: Second Edition, Revised and Expanded, *edited by Joseph Sherma and Bernard Fried*
72. Liquid Chromatography of Oligomers, *Constantin V. Uglea*
73. Chromatographic Detectors: Design, Function, and Operation, *Raymond P. W. Scott*
74. Chromatographic Analysis of Pharmaceuticals: Second Edition, Revised and Expanded, *edited by John A. Adamovics*
75. Supercritical Fluid Chromatography with Packed Columns: Techniques and Applications, *edited by Klaus Anton and Claire Berger*
76. Introduction to Analytical Gas Chromatography: Second Edition, Revised and Expanded, *Raymond P. W. Scott*
77. Chromatographic Analysis of Environmental and Food Toxicants, *edited by Takayuki Shibamoto*
78. Handbook of HPLC, *edited by Elena Katz, Roy Eksteen, Peter Schoenmakers, and Neil Miller*
79. Liquid Chromatography–Mass Spectrometry: Second Edition, Revised and Expanded, *W. M. A. Niessen*
80. Capillary Electrophoresis of Proteins, *Tim Wehr, Roberto Rodríguez-Díaz, and Mingde Zhu*
81. Thin-Layer Chromatography: Fourth Edition, Revised and Expanded, *Bernard Fried and Joseph Sherma*
82. Countercurrent Chromatography, *edited by Jean-Michel Menet and Didier Thiébaut*
83. Micellar Liquid Chromatography, *Alain Berthod and Celia García-Alvarez-Coque*
84. Modern Chromatographic Analysis of Vitamins: Third Edition, Revised and Expanded, *edited by André P. De Leenheer, Willy E. Lambert, and Jan F. Van Bocxlaer*
85. Quantitative Chromatographic Analysis, *Thomas E. Beesley, Benjamin Buglio, and Raymond P. W. Scott*
86. Current Practice of Gas Chromatography–Mass Spectrometry, *edited by W. M. A. Niessen*
87. HPLC of Biological Macromolecules: Second Edition, Revised and Expanded, *edited by Karen M. Gooding and Fred E. Regnier*
88. Scale-Up and Optimization in Preparative Chromatography: Principles and Biopharmaceutical Applications, *edited by Anurag S. Rathore and Ajoy Velayudhan*
89. Handbook of Thin-Layer Chromatography: Third Edition, Revised and Expanded, *edited by Joseph Sherma and Bernard Fried*

© 2004 by Marcel Dekker, Inc.

90. Chiral Separations by Liquid Chromatography and Related Technologies, *Hassan Y. Aboul-Enein and Imran Ali*
91. Handbook of Size Exclusion Chromatography and Related Techniques: Second Edition, Revised and Expanded, *edited by Chi-san Wu*

ADDITIONAL VOLUMES IN PREPARATION

© 2004 by Marcel Dekker, Inc.

Preface to the Second Edition

Gel permeation chromatography (GPC), or size exclusion chromatography (SEC), has evolved steadily since its development in the 1960s. New columns, detectors, and methodologies have been introduced at a timely pace to push the limits of technology. In the most recent Waters International GPC 2003 and ISPAC-16 Symposium (Baltimore, Maryland, June 7–12, 2003), more than 80 very interesting papers were presented by scientists from all over the world. This demonstrates that the interest in determining the molecular weight and molecular weight distribution of polymers accurately, precisely, and efficiently has remained high throughout the years.

The first edition of the *Handbook of Size Exclusion Chromatography* was published in 1995 to fill the need for a book dedicated to the practical applications of SEC. To better serve the practitioners in SEC, the publisher took the initiative to commission this second edition, to incorporate the important developments in SEC in the years since 1995. Most chapters in this new edition have been updated and six new chapters have been added. Therefore, the title has been expanded to *Handbook of Size Exclusion Chromatography and Related Techniques* to reflect these significant additions.

The credit for this book undoubtedly goes to all the contributors. By spending weeks of their own time to prepare their respective chapters, they have demonstrated one of the finest attributes of professional scientists—commitment

© 2004 by Marcel Dekker, Inc.

to sharing their valuable experiences. It is a humbling experience to work with these scholars and experts.

I thank Mr. Russell Dekker for taking the initiative to develop this second edition and Ms. Karen Kwak for doing an outstanding job as the production editor. Finally and once again, I would like to thank Dr. Edward G. Malawer, Director of the Analytical Department and Quality Assurance of International Specialty Products, Wayne, New Jersey, for his generous support in allowing me to take on the task of preparing this volume.

Chi-san Wu

© 2004 by Marcel Dekker, Inc.

Preface to the First Edition

Molecular weight and molecular weight distribution are well known to affect the properties of polymeric materials. Even though for decades viscosity has been an integral part of product specifications used to characterize molecular weight of polymeric materials in industry, the need to define the molecular weight distribution of a product has attracted little attention. However, in recent years producers and users of polymeric materials have become ever more interested in value-added polymers with not only specific molecular weights but also optimal molecular weight distribution to offer performance advantages to products.

In fact, molecular weight distribution has become an important marketing feature for polymeric products in the 1990s. It is very common these days to see new grades of polymeric materials introduced to the marketplace that are specially designed to have either narrow or bimodal molecular weight in composition distribution throughout the entire molecular weight distribution. Therefore, the need to improve the analytical capability in R&D to characterize molecular weight distribution by size exclusion chromatography or gel permeation chromatography has become increasingly urgent in recent years.

Determination of molecular weight distribution of a polymer is very often not a simple task. This is one of the reasons it is still not commonly used as a final product specification. Many books have been published on size exclusion chromatography. However, there has still been a need for a book that stresses practical applications of size exclusion chromatography to the important

© 2004 by Marcel Dekker, Inc.

polymeric materials in industry. Hopefully the valuable experiences of the authors in this book will be helpful to the practitioners of size exclusion chromatography in their efforts to obtain molecular weight distribution of the polymers thay have to work with and to improve the quality and efficiency of their current operations.

To achieve this goal, authors from universities and industries with years of experience in either specific areas of size exclusion chromatography or its application to important polymers have been assembled to share their wisdom with the readers. It is a great honor to receive this degree of support from these scholars and experts; their effort to prepare the respective chapters on top of busy schedules is much appreciated, and they have done great service to the industry.

It is a formidable task to put together a book on size exclusion chromatography with such wide coverage and so many contributing authors. Without the help, guidance, and patience from the following persons, the publication of this book would not have been possible: Lisa Honski and Walter Brownfield of Marcel Dekker, Inc.; Jack Cazes, editor of the *Journal of Liquid Chromatography*; and Edward Malawer, director of the Analytical Department of International Speciality Products.

Chi-san Wu

© 2004 by Marcel Dekker, Inc.

Contents

Preface to the Second Edition
Preface to the First Edition
Contributors

1. **Introduction to Size Exclusion Chromatography**
   Edward G. Malawer and Laurence Senak

2. **Semirigid Polymer Gels for Size Exclusion Chromatography**
   Elizabeth Meehan

3. **Modified Silica-Based Packing Materials for Size Exclusion Chromatography**
   Roy Eksteen and Kelli J. Pardue

4. **Molecular Weight Sensitive Detectors for Size Exclusion Chromatography**
   Christian Jackson and Howard G. Barth

5. **Characterization of Copolymers by Size Exclusion Chromatography**
   Gregorio R. Meira and Jorge R. Vega

© 2004 by Marcel Dekker, Inc.

6. **Size Exclusion Chromatography of Polyamides, Polyesters, and Fluoropolymers**
Christian Dauwe

7. **Size Exclusion Chromatography of Natural and Synthetic Rubber**
Terutake Homma and Michiko Tazaki

8. **Size Exclusion Chromatography of Asphalts**
Richard R. Davison, Charles J. Glover, Barry L. Burr, and Jerry A. Bullin

9. **Size Exclusion Chromatography of Acrylamide Homopolymer and Copolymers**
Fu-mei C. Lin

10. **Size Exclusion Chromatography of Polyvinyl Alcohol and Polyvinyl Acetate**
Dennis J. Nagy

11. **Size Exclusion Chromatography of Vinyl Pyrrolidone Homopolymer and Copolymers**
Chi-san Wu, James F. Curry, Edward G. Malawer, and Laurence Senak

12. **Size Exclusion Chromatography of Cellulose and Cellulose Derivatives**
Elisabeth Sjöholm

13. **Molar Mass and Size Distribution of Lignins**
Bo Hortling, Eila Turunen, and Päivi Kokkonen

14. **Contribution of Size Exclusion Chromatography to Starch Glucan Characterization**
Anton Huber and Werner Praznik

15. **Size Exclusion Chromatography of Proteins**
John O. Baker, William S. Adney, Michelle Chen, and Michael E. Himmel

16. **Size Exclusion Chromatography of Nucleic Acids**
Yoshio Kato and Shigeru Nakatani

© 2004 by Marcel Dekker, Inc.

17. **Size Exclusion Chromatography of Low Molecular Weight Materials**
Shyhchang S. Huang

18. **Two-Dimensional Liquid Chromatography of Synthetic Macromolecules**
Dušan Berek

19. **Methods and Columns for High-Speed Size Exclusion Chromatography Separations**
Peter Kilz

20. **Automatic Continuous Mixing Techniques for On-line Monitoring of Polymer Reactions and for the Determination of Equilibrium Properties**
Wayne F. Reed

21. **Light Scattering and the Solution Properties of Macromolecules**
Philip J. Wyatt

22. **High Osmotic Pressure Chromatography**
Iwao Teraoka and Dean Lee

23. **Size Exclusion/Hydrodynamic Chromatography**
Shyhchang S. Huang

© 2004 by Marcel Dekker, Inc.

Contributors

William S. Adney, M.S. Biotechnology Division for Fuels and Chemicals, National Bioenergy Center, National Renewable Energy Laboratory, Golden, Colorado, U.S.A.

John O. Baker, Ph.D. Biotechnology Division for Fuels and Chemicals, National Bioenergy Center, National Renewable Energy Laboratory, Golden, Colorado, U.S.A.

Howard G. Barth, Ph.D. Central Research and Development, E. I. du Pont de Nemours and Company, Wilmington, Delaware, U.S.A.

Dušan Berek, Doc. Ing., Dr.Sc. Laboratory of Liquid Chromatography, Polymer Institute of the Slovak Academy of Sciences, Bratislava, Slovakia

Jerry A. Bullin, Ph.D. Department of Chemical Engineering, Texas A&M University, College Station, Texas, U.S.A.

Barry L. Burr Department of Chemical Engineering, Texas A&M University, College Station, Texas, U.S.A.

Michelle Chen Wyatt Technology Corporation, Santa Barbara, California, U.S.A.

© 2004 by Marcel Dekker, Inc.

James F. Curry Analytical Department, Research and Development, International Specialty Products, Wayne, New Jersey, U.S.A.

Christian Dauwe* PSS Polymer Standards Service, Mainz, Germany

Richard R. Davison, Ph.D. Department of Chemical Engineering, Texas A&M University, College Station, Texas, U.S.A.

Roy Eksteen, Ph.D.† Liquid Separations, Supelco, Inc., Bellefonte, Pennsylvania, U.S.A.

Charles J. Glover, Ph.D. Department of Chemical Engineering, Texas A&M University, College Station, Texas, U.S.A.

Michael E. Himmel, Ph.D. Biotechnology Division for Fuels and Chemicals, National Bioenergy Center, National Renewable Energy Laboratory, Golden, Colorado, U.S.A.

Terutake Homma Department of Chemical Technology, Kanagawa Institute of Technology, Atsugi, Japan

Bo Hortling, Ph.D. KCL, Espoo, Finland

Shyhchang S. Huang, Ph.D. Measurement Science, Noveon, Inc., Brecksville, Ohio, U.S.A.

Anton Huber Institut für Chemie (IFC), Kolloide and Polymere, Karl-Franzens-Universität Graz, Graz, Austria

Christian Jackson Central Research and Development, E. I. du Pont de Nemours and Company, Wilmington, Delaware, U.S.A.

Yoshio Kato Nanyo Research Laboratory, TOSOH Corporation, Yamaguchi, Japan

Peter Kilz, Ph.D. PSS Polymer Standards Service GmbH, Mainz, Germany

Päivi Kokkonen KCL, Espoo, Finland

**Current affiliation*: YMC-Europe GmbH, Schermbeck, Germany
†*Current affiliation*: Sales and Marketing, TOSOH Bioscience LLC, Montgomeryville, Pennsylvania, U.S.A.

© 2004 by Marcel Dekker, Inc.

Dean Lee Othmer Department of Chemical and Biological Sciences and Engineering, Herman F. Mark Polymer Research Institute, Polytechnic University, Brooklyn, New York, U.S.A.

Fu-mei C. Lin, Ph.D. Department of Chemistry, University of Pittsburgh, Pittsburgh, Pennsylvania, U.S.A.

Edward G. Malawer, Ph.D. Analytical Department and Quality Assurance, International Specialty Products, Wayne, New Jersey, U.S.A.

Elizabeth Meehan, Ph.D. Chromatography Solutions, Polymer Laboratories Ltd, Church Stretton, Shropshire, United Kingdom

Gregorio R. Meira INTEC (Universidad Nacional del Litoral and CONICET), Santa Fe, Argentina

Dennis J. Nagy, Ph.D. Analytical Technology Center, Air Products and Chemicals, Inc., Allentown, Pennsylvania, U.S.A.

Shigeru Nakatani TOSOH Bioscience LLC, Montgomeryville, Pennsylvania, U.S.A.

Kelli J. Pardue Liquid Separations, Supelco, Inc., Bellefonte, Pennsylvania, U.S.A.

Werner Praznik Institut für Chemie, Universität für Bodenkultur, Vienna, Austria

Wayne F. Reed, Ph.D. Physics Department, Tulane University, New Orleans, Louisiana, U.S.A.

Laurence Senak, Ph.D. Analytical Department, Research and Development, International Specialty Products, Wayne, New Jersey, U.S.A.

Elisabeth Sjöholm, Ph.D. Chemical Analysis, Swedish Pulp and Paper Research Institute (STFI), Stockholm, Sweden

Michiko Tazaki Department of Chemical Process Engineering, Kanagawa Institute of Technology, Atsugi, Japan

© 2004 by Marcel Dekker, Inc.

Iwao Teraoka, Ph.D. Othmer Department of Chemical and Biological Sciences and Engineering, Herman F. Mark Polymer Research Institute, Polytechnic University, Brooklyn, New York, U.S.A.

Eila Turunen KCL, Espoo, Finland

Jorge R. Vega INTEC (Universidad Nacional del Litoral and CONICET), Santa Fe, Argentina

Chi-san Wu, Ph.D. Analytical Department, Research and Development, International Specialty Products, Wayne, New Jersey

Philip J. Wyatt, Ph.D. Wyatt Technology Corporation, Santa Barbara, California, U.S.A.

© 2004 by Marcel Dekker, Inc.

1
Introduction to Size Exclusion Chromatography

Edward G. Malawer and Laurence Senak
International Specialty Products
Wayne, New Jersey, U.S.A.

Size exclusion chromatography (SEC), the technique that is the subject of this monograph, is the generic name given to the liquid chromatographic separation of macromolecules by molecular size. It has been taken to be generally synonymous with such other names as gel permeation chromatography (GPC), gel filtration chromatography (GFC), gel chromatography, steric exclusion chromatography, and exclusion chromatography. The "gel" term generally connotes the use of a nonrigid or semirigid organic gel stationary phase whereas SEC can pertain to either an organic gel or a rigid inorganic support. Despite this, the term GPC is commonly used interchangeably with SEC. In this chapter we shall focus on high-performance (or high-pressure) SEC, which requires the use of rigid or semirigid supports to effect rapid separations, lasting typically 20 minutes to one hour. (More recently, a series of high-throughput SEC columns have been introduced by several vendors. While these columns are not capable of the same degree of quantitative discrimination as the analytical SEC column, they offer a nominal five minute analysis time for comparative purposes.)

The primary purpose and use of the SEC technique is to provide molecular weight distribution (MWD) information about a particular polymeric material.

© 2004 by Marcel Dekker, Inc.

The graphical data display typically depicts a linear detector response on the ordinate vs. either chromatographic elution volume or, if processed, the logarithm of molecular weight on the abscissa. One may ask, if SEC relates explicitly to molecular *size*, how can it directly provide molecular *weight* information? This arises from the relationship between linear dimension and molecular weight in a freely jointed polymeric chain (random coil): either the root mean square end-to-end distance or the radius of gyration is proportional to the square root of the molecular weight (1). It follows that the log of either distance is proportional to (one-half) the log of the molecular weight.

1 THE SEC EXPERIMENT AND RELATED THERMODYNAMICS

A stylized separation of an ideal mixture of two sizes of macromolecules is presented in Fig. 1. In the first frame, the sample is shown immediately after injection on the head of the column. A liquid mobile phase is passed through the column at a fixed flow rate, setting up a pressure gradient across its length. In the next frame the sample polymer molecules pass into the column as a result of this pressure gradient. The particles of the stationary phase (packing material) are porous with controlled pore size. The smaller macromolecules are able to penetrate into these pores as they pass through the column, but the larger ones are too large to be accommodated and remain in the interstitial space as shown in the third frame. The smaller molecules are only temporarily retained and will flow

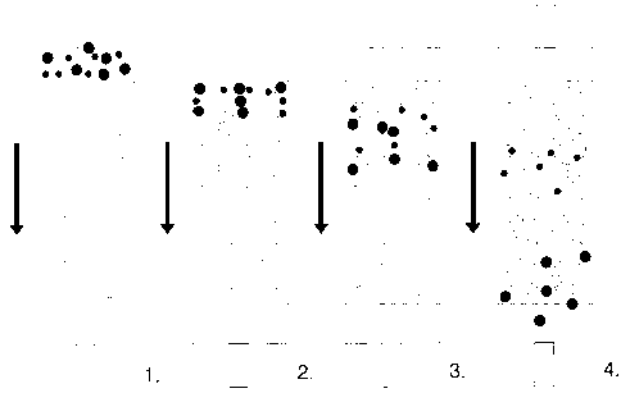

Figure 1 SEC separation of two macromolecular sizes: (1) sample mixture before entering the column packing; (2) sample mixture upon the head of the column; (3) size separation begins; and (4) complete resolution.

© 2004 by Marcel Dekker, Inc.

down the column until they encounter other particles' pores to enter. The larger molecules flow more rapidly down the length of the column because they cannot reside inside the pores for any period of time. Finally the two molecular sizes are separated into two distinct chromatographic bands as shown in the fourth frame. A mass detector situated at the end of the column responds to their elution by generating a signal (peak) for each band as it passed through, whose size would be proportional to the concentration. A real SEC sample chromatogram would typically show a continuum of molecular weight components contained unresolved within a single peak.

If a series of different molecular weight polymers was injected onto such a column they would elute in reverse size order. It is instructive to consider the calibration curve that would result from a series of molecular weights such as those depicted in Fig. 2. Here the molecular weight is plotted on the ordinate and the retention volume (V_r) on the abscissa. The left-hand edge of the chart represents the point of injection. The retention volume labelled V_o is the void volume or total exclusion volume. This is the total interstitial volume in the chromatographic system and is the point in the chromatogram before which no

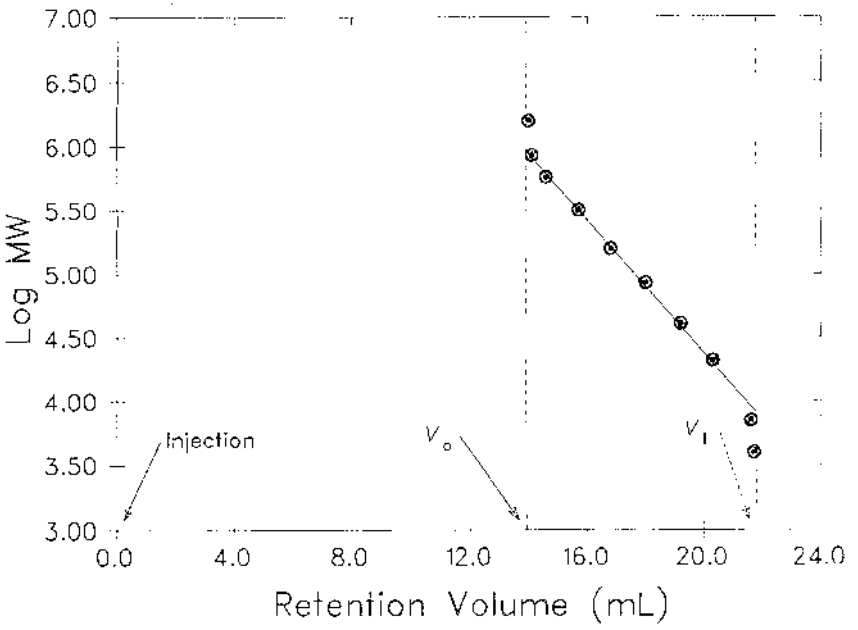

Figure 2 Typical SEC calibration curve: logarithm of molecular weight vs. retention volume.

© 2004 by Marcel Dekker, Inc.

polymer molecule can elute. The total permeation volume (V_t) represents the sum of the interstitial volume and the total pore volume. It is the point at which the smallest molecules in the sample mixture would elute. All SEC separation takes place between V_o and V_t. This retention volume domain is called the selective permeation range. In this figure the largest and smallest molecular weight species are too large and small, respectively, to be discriminated by this column and thus appear at the two extremes of the selective permeation range.

The capacity factor, k', is an index used in chromatography to define the elution position of a particular chromatographic component with respect to the solvent front, which in the case of SEC occurs at V_t. Because all macromolecular separation in SEC occurs before V_t, k' is negative. In all other forms of liquid chromatography k' is positive. One consequence of this difference is that separation in SEC occurs over one column set volume (in the selective permeation range) whereas in other forms of high-performance liquid chromatography (HPLC) separation may occur over many column volumes. Thus components in a mixture analyzed by other HPLC forms are commonly baseline-resolved while SEC separations of macromolecules tend to be broad envelopes. It should be noted that it is not necessary to separate polymer molecules by the number of repeat units in order to determine the molecular weight distribution. (It is possible to resolve very low molecular weight components if a sufficient number of small pore size columns are utilized.) To understand how these differences come about one must consider the thermodynamics of chromatographic processes.

For any form of (gas or liquid) chromatography one can define the distribution of solute between the stationary and mobile phases by an equilibrium (2). At equilibrium the chemical potentials of each solute component in the two phases must be equal. The driving force for solute migration from one phase to the other is the instantaneous concentration gradient between the two phases. Despite the movement of the mobile phase in the system, the equilibrium exists because the solute diffusion into and out of the stationary phase is fast compared to the flow rate. Under dilute solution conditions the equilibrium constant (the ratio of solute concentrations in the stationary and the mobile phases) can be related to the standard Gibbs free energy difference between the phases at constant temperature and pressure:

$$\Delta G^\circ = -RT \ln K \tag{1}$$

and

$$\Delta G^\circ = \Delta H^\circ - T\,\Delta S^\circ \tag{2}$$

where ΔH° and ΔS° are the standard enthalpy and entropy differences between the phases, respectively. R is the gas constant and T is the absolute temperature.

© 2004 by Marcel Dekker, Inc.

In other modes of liquid chromatography (LC) the basis of separation involves such phenomena as partitioning, adsorption, or ion exchange, all of which are energetic in nature since they involve intermolecular forces between the solute and stationary phase. In such cases the free energy can be approximated by the enthalpy term alone since the entropy term is negligible and the equilibrium constant is given by

$$K_{\mathrm{LC}} \simeq \exp(-\Delta H^{\circ}/RT) \tag{3}$$

The typical exothermic interaction between the solute and stationary phase leads to a negative enthalpy difference and hence a positive value for the exponent in Eq. (3). This, in turn, leads to an equilibrium constant greater than one and causes solute peaks to elute later than the solvent front.

In SEC the solute distribution between the two phases is controlled by entropy alone; that is, the enthalpy term is here taken to be negligible. In SEC the equilibrium constant becomes

$$K_{\mathrm{SEC}} \simeq \exp(\Delta S^{\circ}/R) \tag{4}$$

The entropy, S, is a measure of the degree of disorder and can be expressed as (3)

$$S = k \ln \Omega \tag{5}$$

where k is the Boltzmann constant and Ω is the number of equally probable micromolecular states. The relative ability of a small and a larger macromolecule to access an individual pore greater in size than the larger molecule is depicted in Fig. 3. Here the number of ways in which the individual molecules can occupy space within the pore is given by the number of grid positions (representing

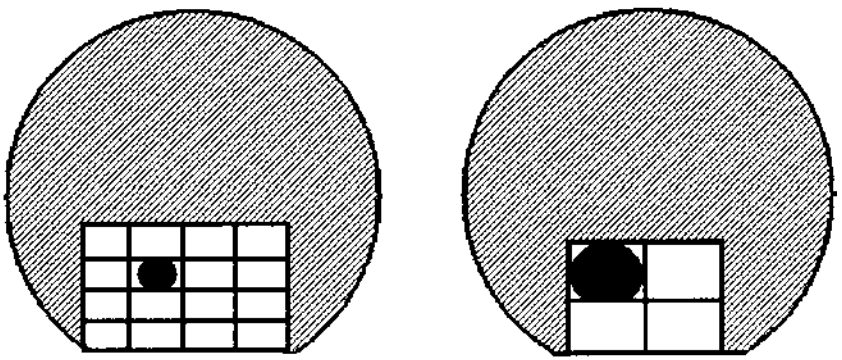

Figure 3 Entropy of macromolecular retention in a pore: the smaller molecule on the left has four times as many possibilities for retention as the molecule on the right.

© 2004 by Marcel Dekker, Inc.

individual states) allowed to them. The smaller molecule is retained longer within the pore than the larger one because its number of equally probable states is greater (and hence it possesses a larger entropy). Yet because the number of equally probable states is much smaller inside the pore than in the interstitial space for an individual molecule, solute permeation in SEC results in a *decrease* in entropy. This results in a negative exponent in Eq. (4). K_{SEC} is less than one and solutes elute before the solvent front. SEC is also inherently temperature independent, in contrast to the other liquid chromatographic separation phenomena, as can be seen by comparing Eqs (3) and (4). (Temperature does in fact have an indirect effect on SEC separations through its influence on the viscosity of polymeric solutions. The viscosity determines the mass transfer rate of polymer molecules into and out of the pores of the packing material and hence the elution of the sample.)

2 EXPERIMENTAL CONDITIONS FOR SEC

2.1 System Overview

A typical SEC system is essentially a specialized isocratic high-performance liquid chromatograph. An idealized schematic is presented in Fig. 4. First a solvent reservoir, typically 1–4 L in size, is filled with the SEC mobile phase. It is commonly sparged with helium or treated ultrasonically in order to degas it and prevent air

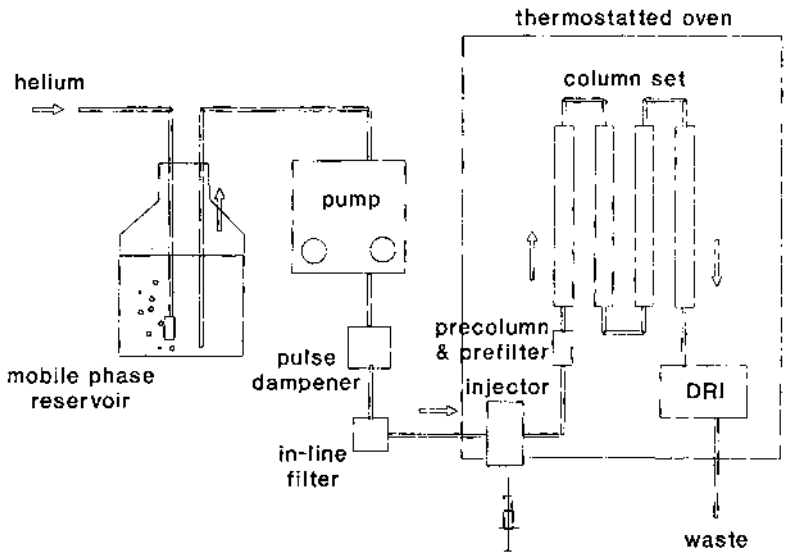

Figure 4 Schematic representation of a generic size exclusion chromatograph.

© 2004 by Marcel Dekker, Inc.

bubbles from entering the detector downstream. A high-pressure pump capable of operating at pressures up to 6000 psi forces the mobile phase through line filters and pulse dampeners to the sample injector where an aliquot of dilute polymer solution (prepared using the same mobile phase batch as contained in the reservoir) is introduced.

The sample, which initially exists as a narrow band in the system, is then carried through the precolumn and the analytical column set where molecular size discrimination occurs. The discriminated sample elutes from the column set and passes through a universal detector, which generates an electrical (mV) signal proportional to the instantaneous sample concentration. The sample and mobile phase then exit the detector and are carried to a waste container while the electrical signal is transmitted to an integrator, recorder, or computer for display and/or further processing.

2.2 Universal (Concentration) Detectors

The most common type of universal detector by far is the differential refractive index (DRI) detector. (Here, the word "universal" denotes the ability to respond to all chemical functionalities.) It senses differences in refractive index between a moving (sample-containing) stream and a static reference of mobile phase using a split optical cell. It responds well (at a moderate concentration level) to most polymeric samples provided that they are different in refractive index from the mobile phase in which they are dissolved. Despite the temperature independence of the SEC separation phenomenon, the DRI is highly temperature sensitive as a result of the strong temperature dependence of refractive index. Thus one normally maintains the DRI in a constant temperature oven along with the columns and injector (as in Fig. 4). The temperature chosen is at least $5-10^{\circ}C$ above ambient.

It is generally assumed that the DRI's response is equally proportional to polymer concentration in all molecular weight regimes. Unfortunately this assumption breaks down at low molecular weights (less than several thousand atomic mass units (amu)) where the polymer end-groups represent a non-negligible portion of the molecules' mass and do change the refractive index. The DRI is also very sensitive to backpressure fluctuations due to variations in flow rate caused by the pump. This effect (especially of reciprocating piston pumps) is compensated for by the use of pulse dampeners as shown in Fig. 4.

Other common types of concentration detectors are the ultraviolet (UV) and infrared (IR) detectors. Neither are truly universal detectors, but they are able to respond to a variety of individual chemical functional groups (chromophores) provided that these functional groups are not contained in the mobile phase. The IR detector is slightly more sensitive than the DRI detector while the UV detector is several orders of magnitude more sensitive. The last is most commonly employed for polymers containing aromatic rings or regular backbone

© 2004 by Marcel Dekker, Inc.

unsaturation while the IR detector has been used largely to characterize polyolefins. Other less commonly utilized concentration detectors include the fluorescence, dielectric constant, flame ionization, and evaporative light scattering detectors.

2.3 Mobile Phase and Temperature

The mobile phase should be chosen carefully to fit certain criteria: it must completely dissolve the polymer sample in a continuous solution phase (non-θ condition), it must be low enough in viscosity in order for the SEC system to operate in a normal pressure range, and it must effectively prevent the polymer molecules from interacting energetically with the stationary phase (for example, through adsorption). Failure to achieve even one of these criteria would result in the inability of the system to properly characterize the sample. Temperature is a useful parameter to adjust when one or more of these conditions have not been met but where one is constrained to use a particular mobile phase. Certain polymers (for example, polyesters and polyolefins) may achieve dissolution only at elevated temperatures. The viscosity of inherently viscous mobile phases may also be lowered by raising the temperature.

The analysis of polymers containing one or more formal, like charges in every repeat unit (i.e., polyelectrolytes) incurs one additional requirement of the mobile phase. When solubilized in water, the repulsion of like charges along the polyelectrolyte chain causes it to take on an extended conformation (4). In order for normal SEC to be performed on a polyelectrolyte in an aqueous medium, its conformation must be made to reflect that of a random coil (Gaussian chain). This counteracting of the "polyelectrolyte effect" is generally accomplished by sufficiently raising the ionic strength with the use of simple salts and sometimes with concomitant pH adjustment. The former provides counterions to screen the like polymeric charges from one another and permits the extended chain to relax. The latter is used to neutralize all residual acidic or basic groups. (When fully charged these groups are no longer available to participate in hydrogen bonding interactions with the stationary phase.)

For example, it has been demonstrated that normal SEC behavior can be obtained for poly(methyl vinyl ether-co-maleic acid) with the use of a mobile phase consisting of a pH 9 buffer system (prepared from tris(hydroxymethyl)-aminomethane and nitric acid) modified with 0.2 M $LiNO_3$ (5). Halide salts should be completely avoided as they tend to corrode the stainless steel inner surfaces of the SEC system, which in turn causes injector fouling and column contamination.

2.4 Stationary Phases

When selecting an optimum stationary phase there are additional criteria to be met: the packing material should not interact chemically with the solute (i.e., the

© 2004 by Marcel Dekker, Inc.

sample), it must be completely wetted by the mobile phase but should not suffer adverse swelling effects, it must be stable at the required operating temperature, and it must have sufficient pore volume and an adequate range of pore sizes to resolve the sample's molecular weight distribution. For high-performance SEC, either semirigid polymeric gels or modified, rigid silica particles are typically used.

Columns are available from a number of vendors packed with monodisperse or mixed-bed pore size particles. The latter are useful for building a column set that will discriminate (usually on a log-linear basis) at least four molecular weight decades (i.e., several hundred to several million amu). For rigid particles it is also possible to design a column set consisting of individual columns of different, single pore sizes yielding a calibration curve log-linear in molecular weight if the pore size and total pore volume of each column type are known (6). Typical available pore sizes range from 60 to 4000 Å. High-performance packing materials generally have particle sizes in the range of 5 to 10 μm with efficiencies of several thousand theoretical plates per 15-cm column.

For organic mobile phases, the most common column packings are crosslinked (with divinylbenzene) polystyrene gels or trimethylsilane-derivatized silica. For aqueous mobile phases the most common are crosslinked hydroxylated polymethacrylate or poly(propylene oxide) gels (7) or glyceryl (diol) derivatized silica (8). In general, rigid packings have several advantages over semirigid gel packings: they are tolerant of a greater variety of mobile phases, they equilibrate rapidly on changing solvents, they are stable at the elevated temperatures required to characterize certain polymers, and their pore sizes are more easily defined, which facilitates column set design. Silica-based rigid packings are prone to adsorptive effects, however, and must be carefully derivatized to react away or screen labile silanol groups. An overview of typical column packing/mobile phase combinations has been recently published by Yau *et al.* (9). The reader is referred to comprehensive discussions of SEC stationary phases covered in Chapter 2 (semirigid polymeric gels) and Chapter 3 (modified, rigid silica) of this monograph.

2.5 Sample Size and Mobile Phase Flow Rate

Sample size is defined by both the volume of the aliquot injected as well as by the concentration of the sample solution. Use of excessively large sample volumes can lead to significant band broadening, resulting in loss of resolution and errors in molecular weight measurement. As a rule of thumb, sample volumes should be limited to one-third or less of the baseline volume of a monomer or solvent peak measured with a small sample (10). The optimum injection volume will be a function of the size and number of the columns employed but will generally range between 25 and 200 μL.

© 2004 by Marcel Dekker, Inc.

Sample concentration should be minimized consistent with the sensitivity of the concentration detector employed. The use of high sample concentrations can result in peak shifts to lower retention volumes and band broadening due to "viscous fingering" or spurious shoulders appearing on the tail of the peak. These phenomena are likely related to a combination of causes including chain entanglements and an inability to maintain the equilibrium between solute concentrations inside the pores and in the interstitial space. These effects are particularly problematic for high molecular weight polymers (of the order of one million amu). Optimum sample concentrations may range from 0.1% for high molecular weight samples to greater than 1.0% for low molecular weight samples.

Another unwanted viscosity effect, the shear degradation of high molecular weight polymers at high flow rates, which results in erroneous (larger) retention volumes and (lower) molecular weights, is avoided by minimizing the flow rate. In addition, the use of high flow rates can result in considerable loss of column efficiency because, under such conditions, mass transfer or diffusion in and out of the pores is not fast enough vis-à-vis the solute migration rate along the length of the column. Thus, flow rates in the general vicinity of 1 mL/min are most commonly employed for sets of SEC columns and represent a good compromise between analysis time and resolution. For single column separations, a flow rate of 0.5 ml/min is commonly used. The reader is referred to Chapter 5 (aqueous SEC) and Chapter 6 (nonaqueous SEC) of this monograph for comprehensive discussions of sample size and flow rate optimizations.

3 CALIBRATION METHODOLOGY AND DATA ANALYSIS IN SEC

In modern high-performance SEC there are only four commonly employed calibration methods. Three of these can be utilized in conjunction with a single (i.e., concentration) detector SEC system: direct (narrow) standard calibration, polydisperse or broad standard calibration, and universal calibration. The fourth type of SEC calibration requires the use of a second, molecular weight sensitive detector connected in series with the concentration detector (and in front of it in the case of the DRI). The purpose of calibration in SEC is to define the relationship between molecular weight (or typically its logarithm) and retention volume in the selective permeation range of the column set used and to calculate the molecular weight averages of the sample under investigation.

3.1 Direct Standard Calibration

In the direct standard calibration method, narrowly distributed standards of the same polymer under analysis are used. The retention volume at the peak maximum of each standard is equated with its stated molecular weight. While this is the

© 2004 by Marcel Dekker, Inc.

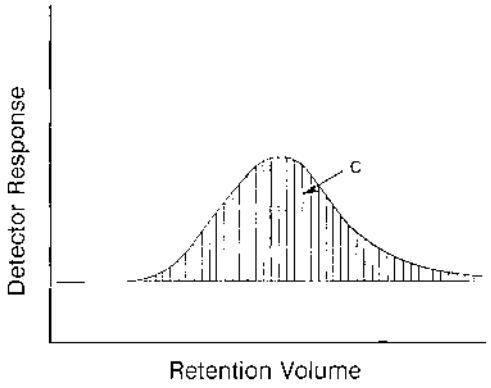

Figure 5 Time-sliced peak output from a concentration detector (DRI).

simplest method it is generally restricted in its utility owing to the lack of availability of many different polymer standard types. It also requires a sufficient number of standards of different molecular weights so as to completely cover the entire dynamic range of the column set or, at least, the range of molecular weights spanned by the samples' molecular weight distributions. Narrow standards currently available include polystyrene, poly(methyl methacrylate), poly (ethylene), (used for nonaqueous GPC), and poly(ethylene oxide) or poly(ethylene glycol), poly(acrylic acid), and polysaccharides (used in aqueous GPC) are common commercially available standards. It is instructive to study the mechanism of narrow standard calibration since all of the other methods are based upon it. A thorough review of this subject has been provided by Cazes (11).

In this approach, the raw chromatogram obtained as output from the concentration detector is divided into a number of time slices of equal width as depicted in Fig. 5. For a polydisperse sample the number of time slices must be greater than 25 for the computed molecular weight averages to be unaffected by the number of time slices used. (Most commonly available SEC data programs utilize a minimum of several hundred time slices routinely for each analysis.) An average molecular weight is assigned to each time slice based upon the calibration curve and it is further assumed for computational purposes that each time slice is monodisperse in molecular weight. A table is constructed with one row assigned to each time slice. The following columns are created for this table: retention volume, area (A_i), cumulative area, cumulative area percent, molecular weight (M_i), A_i divided by M_i, and A_i times M_i. The area column and the last two factors are also summed for the entire table.

Once this data table has been completed it is possible to compute the molecular weight averages or moments of the distribution. The most common

© 2004 by Marcel Dekker, Inc.

averages defined in terms of the molecular weight at each time slice and either the number of molecules, n_i, or the area of each time slice are as follows:
Number average:

$$\bar{M}_{\mathrm{N}} = \frac{\sum_i n_i M_i}{\sum_i n_i} = \frac{\sum_i \Lambda_i}{\sum_i A_i / M_i} \tag{6}$$

Viscosity average:

$$\bar{M}_{\mathrm{V}} = \left[\frac{\sum_i n_i M_i^{1+a}}{\sum_i n_i M_i}\right]^{1/a} = \left[\frac{\sum_i A_i M_i^{a}}{\sum_i A_i}\right]^{1/a} \tag{7}$$

where, a is the Mark–Houwink exponent.
Weight average:

$$\bar{M}_{\mathrm{W}} = \frac{\sum_i n_i M_i^2}{\sum_i n_i M_i} = \frac{\sum_i A_i M_i}{\sum_i A_i} \tag{8}$$

"Z" average:

$$\bar{M}_{\mathrm{Z}} = \frac{\sum_i n_i M_i^3}{\sum_i n_i M_i^2} = \frac{\sum_i A_i M_i^2}{\sum_i A_i M_i} \tag{9}$$

The dispersity or polydispersity, D, is given by the ratio of the weight to the number average molecular weight and is a measure of the breadth of the molecular weight distribution. The SEC number, viscosity, weight, and "Z" averages correspond to those obtained classically by osmometry, capillary viscometry (intrinsic viscosity), light-scattering photometry, and sedimentation equilibrium methods, respectively. The viscosity average molecular weight approaches the weight average as the Mark–Houwink exponent, a (described in Sec. 3.4 of this chapter), approaches one. (See the subsequent discussion concerning universal calibration.) The "Z" and weight average molecular weights are most influenced by the high molecular weight portion of the distribution whereas the number average is influenced almost exclusively by the low molecular weight portion. Narrow standards employed in this calibration method are ideally monodisperse but practically must have dispersities less than 1.1.

3.2 Band Broadening Measurement and Correction

It is important to review the molecular weight distribution generated for symmetric and unsymmetric band broadening that will result in non-negligible errors in computed molecular weight averages. An American Society for Testing and Materials (ASTM) method describes a procedure to calculate the magnitude of these effects and to correct the molecular weight averages (12). It is necessary to know both $\bar{M}_{\mathrm{W}}$ and $\bar{M}_{\mathrm{N}}$ for each standard of the entire series of narrow standards

© 2004 by Marcel Dekker, Inc.

used. The symmetric band broadening factor, Λ, is calculated for each standard according to

$$\Lambda = \frac{1}{2}\left[\frac{\bar{M}_{\mathrm{N}}(t)}{\bar{M}_{\mathrm{N}}(u)} + \frac{\bar{M}_{\mathrm{W}}(u)}{\bar{M}_{\mathrm{W}}(t)}\right] \tag{10}$$

The skewing or unsymmetric factor, sk, is calculated according to

$$sk = \frac{\Phi - 1}{\Phi + 1} \tag{11}$$

where

$$\Phi = \frac{\bar{M}_{\mathrm{N}}(t)\,\bar{M}_{\mathrm{W}}(t)}{\bar{M}_{\mathrm{N}}(u)\,\bar{M}_{\mathrm{W}}(u)} \tag{12}$$

and t and u refer to the true and uncorrected moments. Under ideal conditions, $\Lambda = 1$ and $sk = 0$ and no corrections are necessary. Practically this is never the case but if these values are 1.05 and 0.05 or less, respectively, then the resulting corrections are small and can be ignored. If, on the other hand, they are larger than these values, the sample's distribution moments may be corrected according to

$$\bar{M}_{\mathrm{N}}(t) = \bar{M}_{\mathrm{N}}(u)(1 + sk)(\Lambda) \tag{13}$$

and

$$\bar{M}_{\mathrm{W}}(t) = \frac{\bar{M}_{\mathrm{W}}(u)}{(1 - sk)\Lambda} \tag{14}$$

A description of the correction for band broadening of the entire molecular weight distribution is beyond the scope of this introduction to SEC but the interested reader is referred to the technique described by Tung (13,14). A better approach is to employ sufficiently good experimental practices so as to obviate the need for band spreading corrections altogether. This has been demonstrated when sufficiently long column lengths and low flow rates are used (15).

3.3 Polydisperse or Broad Standard Calibration

In the polydisperse standard method one employs a broadly distributed polymer standard of the same chemical type as the sample. The sample and the standard are frequently the same material. The main requirements of this technique are that the MWD of the standard must span most if not all of the sample's dynamic range and that two moments of the standard's distribution, $\bar{M}_{\mathrm{N}}$ and either $\bar{M}_{\mathrm{W}}$ or $\bar{M}_{\mathrm{V}}$, must be accurately known as a result of ancillary measurements. This method is particularly useful when narrow MWD standards and molecular weight sensitive detectors are unavailable and universal calibration is impractical due to lack of

© 2004 by Marcel Dekker, Inc.

information regarding appropriate Mark–Houwink coefficients and/or the inability to perform intrinsic viscosity measurements.

Balke, Hamielec et al. described a computer method to determine a calibration curve expressed by

$$V_e = C_1 - C_2 \log_{10} M \tag{15}$$

where V_e is the elution (or retention) volume and M is the molecular weight (16). Their original method involved a cumbersome, simultaneous search for the constants C_1 and C_2, which was prone to false convergence. Revised methods featured a sequential, single-parameter search (17,18). These methods rely on the fact that the dispersity, D, is a function of the slope, C_2, alone. Arbitrary values are first assigned to the two constants. The resulting calibration equation is iteratively applied to the time slice data while the slope value is optimized to minimize the difference between the true and computed dispersities. Once the slope has been determined it is fixed and the intercept, C_1, is optimized to minimize the difference between the true and computed moments (either individually or their sum).

3.4 Universal Calibration

Benoit and co-workers demonstrated that it is possible to use a set of narrow polymer standards of one chemical type to provide absolute molecular weight calibration to a sample of a different chemical type (19,20). In order to understand how this is possible, one must first consider the relationship between molecular weight, intrinsic viscosity and hydrodynamic volume, the volume of a random, freely jointed polymer chain in solution. This relationship has been described by both the Einstein–Simha viscosity law for spherical particles in suspension

$$[\eta] = C\left(\frac{V_h}{M}\right) \tag{16}$$

and the Flory–Fox equation for linear polymers in solution

$$[\eta] = \Phi\left(\frac{\langle s^2\rangle^{3/2}}{M}\right) \tag{17}$$

where $[\eta]$ is the intrinsic viscosity, V_h, is the hydrodynamic volume, $\langle s^2\rangle^{1/2}$ is the root-mean-square radius of gyration of the polymer chain, and C and Φ are constants (21). If either equation is multiplied by M, the molecular weight, the resulting product, $[\eta]M$, is seen as proportional to hydrodynamic volume. (Note that the cube of the root-mean-square radius of gyration is also proportional to volume.) Benoit and co-workers plotted this product versus elution volume for a number of chemically different polymers investigated under identical SEC

© 2004 by Marcel Dekker, Inc.

conditions and found that all points lay on the same calibration curve (19,20). This calibration behavior was said to be "universal" for all the polymer types studied.

In actual practice one would establish the following relationship

$$[\eta]_1 M_1 = [\eta]_2 M_2 \tag{18}$$

where the subscripts 1 and 2 refer to the standard and sample polymers, respectively. Even if the intrinsic viscosities are known or can be measured for each standard, it is unlikely that the value of intrinsic viscosity would be known for each time slice in the molecular weight distribution of the sample polymer. Thus, Eq. (18) must be further modified to make it more useful. This can be accomplished with the use of the Mark–Houwink equation

$$[\eta] = KM^a \tag{19}$$

where the coefficient, K, and exponent, a, are known as the Mark–Houwink constants. These constants are a function of both the polymer and its solvent environment (including temperature). If the constants are available from the literature or can be determined for the sample polymer using narrow fractions in the SEC mobile phase, then one can substitute the Mark–Houwink term for $[\eta]$ into Eq. (18) to yield

$$\log_{10} M_2 = \frac{1}{1+a_2} \log_{10} \frac{K_1}{K_2} + \frac{1+a_1}{1+a_2} \log_{10} M_1 \tag{20}$$

which is an expression for the sample molecular weight in terms of the standard molecular weight and both sets of Mark–Houwink constants.

3.5 Molecular Weight Sensitive Detectors

It is possible to add a second molecular weight sensitive detector to an SEC system in order to provide a direct means of absolute molecular weight calibration without the need to resort to external standards. These detectors represent refinements in classical techniques such as light-scattering photometry, capillary viscometry (for intrinsic viscosity), and membrane osmometry for on-line molecular weight determination. Yau has published a review of this subject with comparisons of the properties and benefits of the principal detectors currently in use (22). The present discussion will be restricted to light-scattering and viscometry detectors. The reader is referred to Chapter 4 of this monograph for a comprehensive discussion of molecular weight sensitive detectors.

3.5.1 Low Angle Laser Light Scattering Detection

The low angle laser light scattering detector (LALLS or LALS) was originally developed by Kaye (23,24) and was formerly marketed by Chromatix and LDC

© 2004 by Marcel Dekker, Inc.

Analytical. Two models, the KMX-6 and the CMX-100, are no longer commercially available. Although the former was said to be capable of a small scattering angle variation, both units were essentially fixed, low angle photometers. Overviews of the basic operating principles were provided by McConnell (25) and Jordan (26). A low angle laser light scattering detector is still offered, however, by Viscotek in the Triple Detector Array (see below).

The working equation for the determination of the weight average molecular weight by light scattering (using unpolarized light), due to Debye, is

$$\frac{Kc}{\Delta R_\theta} = \frac{1}{\bar{M}_W P(\theta)} + 2A_2 C \tag{21}$$

where the constant, K, is given by

$$K = \frac{2\pi^2 n^2}{N_o \lambda^4} \left(\frac{dn}{dc}\right)^2 \tag{22}$$

and N_o is Avogadro's number, n is the refractive index of the solution at the incident wavelength λ, and A_2 is the second virial coefficient, a measure of the compatibility between the polymer solute and the solvent. The term dn/dc is known as the specific refractive index increment and reflects the change in solution refractive index with change in solute concentration. The term ΔR_θ is called the excess Rayleigh ratio and represents the solution ratio of scattered to incident radiation minus that of the solvent alone. The particle scattering function, $P(\theta)$, which is the angular dependence of the excess Rayleigh ratio, is defined by

$$\frac{1}{P(\theta)} = 1 + \frac{16\pi^2}{3\lambda^2} \langle s^2 \rangle \sin^2(\theta/2) \tag{23}$$

where $\langle s^2 \rangle$ is the mean-square radius of gyration of the polymer chain. The Debye equation [Eq. (21)] is actually a virial equation which includes higher power concentration terms; these higher terms can be neglected if the concentrations employed are small.

In the classical light scattering experiment one solves the Debye equation over a wide range of angles and concentrations for unfractionated polymer samples. The data are plotted in a rectilinear grid known as a Zimm plot in which the ordinate and abscissa are $Kc/\Delta R_\theta$ and $[\sin^2(\theta/2) + kc]$, respectively, where k is an arbitrary constant used to adjust the spacing of the data points (27). The Zimm plot yields parallel lines of either equal concentration or angle. The slope of the $\theta = 0$ line yields $\langle s^2 \rangle$ while that of the $c = 0$ line yields A_2. The intercept of either of these lines is $\bar{M}_W$. One of the major problems associated with classical light scattering experiments relates to the effect of dust: if the entire solution contained in the large cell volume typically used is not kept scrupulously free of dust, large scattering errors can result.

© 2004 by Marcel Dekker, Inc.

The LALLS device developed by Kaye provides three significant changes that make it amenable as an SEC molecular weight detector: an intense, monochromatic light source (a HeNe laser, $\lambda = 632.8$ nm) is used, the cell volume is reduced to 10 μL and the scattering volume to 0.1 μL (26), and the single scattering angle employed is in the range of $2-7^{\circ}$. The net result is that the device is extremely sensitive; it can readily distinguish scattering due to an individual dust particle flowing through the cell from that due to the sample, and the angular dependence is removed from the Debye equation. The latter follows from the fact that the value of $\sin^2(\theta/2)$ for a small angle is essentially zero. Under this condition the Debye equation becomes

$$\frac{Kc}{\Delta R_\theta} = \frac{1}{\bar{M}_{\mathrm{W}}} + 2A_2C \tag{24}$$

or

$$\bar{M}_{\mathrm{W}} = \frac{1}{Kc/\Delta R_\theta - 2A_2C} \tag{25}$$

and $\bar{M}_{\mathrm{W}}$ can be obtained at a single finite concentration provided that A_2 is known from the literature or is determined from the slope of Eq. (24) using a series of concentrations. However, the removal of the angular variability from the LALLS detector means that it cannot be used to determine molecular size, that is, $\langle s^2 \rangle$.

The SEC/LALLS experiment is then conducted as follows. The LALLS and concentration detectors are connected in series after the SEC column set and interfaced with the computing system. Time slice data from both detectors is acquired, as shown in Fig. 6, so as to have corresponding time slices in each distribution. In order to accomplish this the time delay between the detectors must be accurately known. The instantaneous concentration in either detector, c_i, may be computed using

$$c_i = \frac{mA_i}{V \sum_i A_i} \tag{26}$$

where m is the sample mass injected, V is the effluent volume passing through the cell in the time of a single time slice, and A_i is the area of a concentration detector time slice. If one assumes that each time slice is sufficiently narrow so as to be monodisperse, then the instantaneous molecular weight is determined using Eq. (25). This data collectively constitute the absolute molecular weight distribution calibration.

It is generally acknowledged that LALLS used either as a stand-alone light-scattering photometer or as an SEC detector provides accurate values for $\bar{M}_{\mathrm{W}}$. Yet in 1987 a number of independent workers reported that the ability of SEC/LALLS to accurately determine $\bar{M}_{\mathrm{N}}$ was dependent on the polydispersity of the sample: the

© 2004 by Marcel Dekker, Inc.

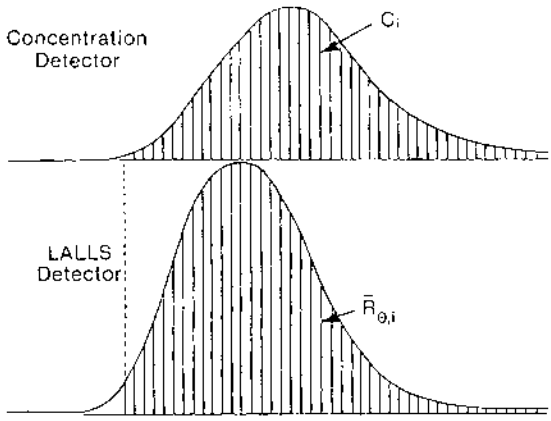

Figure 6 Overlay of time-sliced peak output from a dual (DRI/LALLS) detector system.

greater the polydispersity, the poorer the estimate of $\bar{M}_N$ (28–30). In performing SEC/LALLS on high molecular weight poly(vinyl pyrrolidone), Senak *et al.* (28) demonstrated that this phenomenon is caused by the lack of sensitivity of the LALLS detector toward the low molecular weight portion of a broad distribution ($D = 6.0$). As shown in Fig. 7, the DRI detector is still responding (the shaded area) in a region where the LALLS detector is not. As discussed by Hamielec *et al.*,

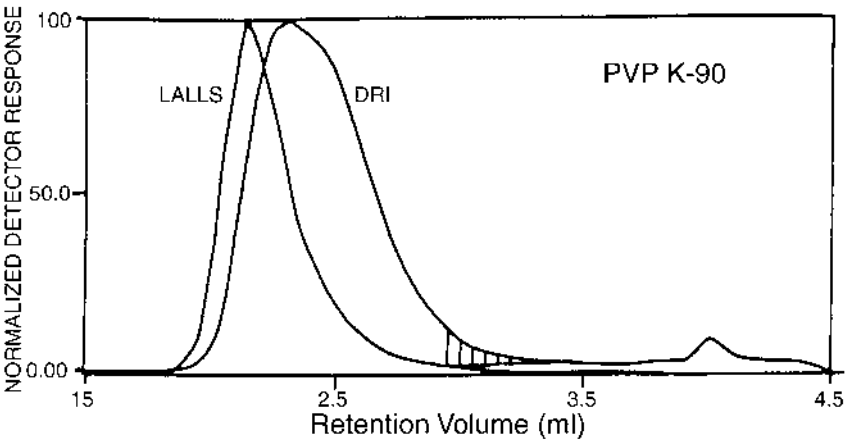

Figure 7 Relative sensitivity of a LALLS vs. a DRI detector for a broadly dispersed sample of poly(vinyl pyrrolidone).

© 2004 by Marcel Dekker, Inc.

an electronic switching device and a technique for optimizing the signal-to-noise ratio of the LALLS detector throughout the LALLS chromatogram is needed to improve its utility (31).

The LALLS detector coupled to an SEC has also been reported to be useful in measuring the relative amount of branching of a branched relative to a linear polymer of the same chemical type (32–34). The parameter of interest is g_M, defined by Zimm and Stockmayer (35) as

$$g_M = \left(\frac{\langle s^2\rangle_b}{\langle s^2\rangle_l}\right)_M = \left(\frac{[\eta]_b}{[\eta]_l}\right)M \tag{27}$$

or the ratio of the mean-square radii of gyration of a branched to a linear polymer at a constant molecular weight and, through the Flory–Fox equation [Eq. (17)], the ratio of their intrinsic viscosities (35). The measured quantity in the SEC/LALLS experiment, however, is g_V, the branching index at constant elution volume: the ratio of molecular weights of branched to linear polymers. It has been shown that the Mark–Houwink equation [Eq. (19)] can be used to convert g_V to g_M to give

$$g_M = g_V^{a+1} = \left(\frac{M_l}{M_b}\right)_V^{a+1} \tag{28}$$

where a is the Mark–Houwink exponent of the linear polymer (32,33). In principle, the variation in the branching index can be determined as a function of molecular weight provided that the exponent, a, is known. Complications may arise if there is significant band broadening in the SEC system and/or if the samples are highly polydisperse as previously discussed. It must be emphasized that the ability of the SEC/LALLS to produce branching information is strictly due to the discrimination of molecular size by the SEC column set since LALLS has no molecular size capability itself.

3.5.2 Multi-Angle Laser Light Scattering Detection

The multi-angle laser light scattering detectors (MALLS or MALS) developed and produced by Wyatt Technology Corp. (Santa Barbara, California), (the models DAWN B and DAWN F, and currently the EOS), unlike LALLS, have the ability to measure scattered light at either 15 (23–128°) or 18 (5–175°) different angles depending upon the model selected (36,37). In addition, these data can be obtained simultaneously using an array of detectors. The mathematics employed is essentially based upon Eqs (21) to (23). One of the capabilities of this instrument is the determination of polymer radius of gyration distribution when used as an on-line SEC detector. Used off line this instrument is capable of producing Zimm plots supplying weight-average molecular weight, radius of gyration, and second virial coefficient information. The ability of MALLS to make this measurement

© 2004 by Marcel Dekker, Inc.

accurately for very large and very small polymer molecules has been disputed (38,39). Other MALLS instruments are available from Polymer Laboratories (Shropshire, U.K.) which offers a dual angle (15° and 90°), which is also available with a dynamic (quasielastic) light scattering detector as an option, and from Brookhaven Instruments (Holtsville, New York, U.S.A.) who offers an array of seven detectors in their MALLS unit. For a complete discussion of MALLS the reader is referred to Chapter 21.

3.5.3 Right-Angle Laser Light Scattering Detection and Triple Detection

At the 1991 International GPC Symposium (San Francisco, California) M. Haney of Viscotek Corp. introduced a new laser light scattering detector (RALLS), which operates at a fixed angle of 90° (40). Because the particle scattering function, $P(\theta)$, cannot be neglected at this angle (for large molecules), this device must be used in conjunction with another molecular weight sensitive detector (that is, a viscosity detector) and a concentration detector in order to yield absolute molecular weight information. An iterative calculation is performed on each chromatogram time slice using a simplified form of the Debye equation [Eq. (21)], the Flory–Fox equation [Eq. (17)] and the particle scattering function equation [Eq. (23)]. The convergence condition used is no further change in either molecular weight, radius of gyration, or $P(\theta)$. Viscotek claims an inherently better signal-to-noise ratio (due to lower noise) for the RALLS detector vs. either LALLS or MALLS operating at close to 0°. The use of a three detector array such as RALS, viscosity, and RI (as a concentration detector) is referred to as "Triple Detection." The current configuration of the Triple Detection instrument includes RALS, LALS and viscosity as molecular weight sensitive detectors. Also offered in this design are RI and UV as universal or concentration dependent detectors.

3.5.4 Viscometric Detection

An alternative type of molecular weight sensitive detector is the on-line viscometer. All of the current instrument designs depend upon the relationship between pressure drop across a capillary through which the polymer sample solution must flow and the viscosity of that solution. This relationship is based upon Poiseuille's law for laminar flow of incompressible fluids through capillaries:

$$\eta = \frac{\pi \Delta P r^4 t}{8 V l} \tag{29}$$

where η is the absolute viscosity, ΔP is the observed pressure drop, t is the efflux time, and r, l, and V are the radius, length, and volume of the capillary, respectively. In a capillary viscometer operating at ambient pressure, one can define the relative viscosity, η_r, as the ratio of the absolute viscosities of solution to solvent, which is equal to the ratio of their efflux times at low concentrations.

© 2004 by Marcel Dekker, Inc.

Yet when such a capillary is used as an SEC detector, the flow time is constant and the relative viscosity becomes

$$\eta_r = \frac{\eta}{\eta_o} = \frac{\Delta P}{\Delta P_o} \tag{30}$$

the ratio of the solution to solvent pressure drops. Since the intrinsic viscosity, $[\eta]$, is defined as

$$[\eta] = \lim_{c \to 0} \left(\frac{\ln \eta_r}{c} \right) \tag{31}$$

one can combine Eqs (30) and (31) to give

$$[\eta] = \frac{\ln (\Delta P / \Delta P_o)}{c} \tag{32}$$

provided that c is very small. (It is generally less than 0.01 g/dL under SEC conditions.)

Thus an on-line viscosity detector is capable of providing intrinsic viscosity distribution information directly using time slicing analogous to laser light-scattering detection. In order to act as a molecular weight detector, however, one must either obtain the Mark–Houwink constants in order to use the Mark–Houwink equation or possess a set of molecular weight standards that obeys the universal calibration behavior. If both intrinsic viscosity and absolute molecular weight information are available for each time slice, the Flory–Fox equation may be employed to generate a similar distribution for the mean-square radius of gyration (22).

A single capillary detector developed by Ouano (41) and further advanced by Lesec and colleagues (42–44) and Kuo *et al.* (45) has been internally incorporated into the Millipore/Waters model 150 CV SEC system. Chamberlin and Tuinstra developed a single-capillary detector that was directly incorporated within a conventional DRI detector (46,47). Haney developed a four-capillary detector with a Wheatstone bridge arrangement, which was commercialized by Viscotek Corp. (48,49) and further evaluated by other workers (50,51). A dual, consecutive capillary detector developed by Yau (22) (and also commercialized by Viscotek Corp.) was said to be superior to the other designs because it was better able to compensate for flow rate fluctuations: its series arrangement would cause the two capillaries to be simultaneously and equally affected, thus exactly offsetting any disturbance.

© 2004 by Marcel Dekker, Inc.

4 GENERAL REFERENCES

The interested reader is referred to several additional general references for supplemental information on the principles of SEC separations and selected applications. The first four (52–55) are compilations of papers presented by leading authorities at various International GPC Symposia sponsored by Waters Associates (Milford, Massachusetts). The next two volumes (56,57) are introductory books published by two other HPLC/SEC vendors. Finally, an early monograph edited by J. J. Kirkland (58) contains an excellent introductory chapter on GPC (SEC). Although all of these books are relatively old, they nevertheless contain valuable information that is still applicable and useful today.

5 ACKNOWLEDGEMENTS

The author is grateful to C. S. Wu for his encouragement and for useful discussions, to J. F. Tancredi for his support, to M. Krass and J. Bager for help in creating several figures, and to International Specialty Products for permission to publish this review.

6 REFERENCES

1. FW Billmeyer. Textbook of Polymer Science. 2nd ed. New York: Wiley-Interscience, 1971, p 28.
2. WW Yau, JJ Kirkland, DD Bly. Modern Size Exclusion Chromatography. New York: Wiley-Interscience, 1979, p 27 ff.
3. GS Rushbrooke. Introduction to Statistical Mechanics. Oxford, UK: Oxford University, 1949, p 11.
4. B Vollmert. Polymer Chemistry. Heidelberg, Germany: Springer-Verlag, 1973, p 537 ff.
5. CS Wu, L Senak, EG Malawer. J Liq Chromatogr 12(15):2901–2918, 1989.
6. EG Malawer, JK DeVasto, SP Frankoski, AJ Montana. J Liq Chromatogr 7(3):441–461, 1984.
7. T Hashimoto, H Sasaki, M Aiura, Y Kato. J Polym Sci, Polym Phys Ed 16:1789, 1978.
8. LR Snyder, JJ Kirkland. Introduction to Modern Liquid Chromatography. 2nd ed. New York: Wiley-Interscience, 1979, p 489.
9. WW Yau, JJ Kirkland, DD Bly. Size Exclusion Chromatography. In: PR Brown, RA Hartwick, eds. Chemical Analysis: High Performance Liquid Chromatography. New York: Wiley-Interscience, 1989, pp 293–295.
10. WW Yau, JJ Kirkland, DD Bly. Modern Size Exclusion Chromatography. New York: Wiley-Interscience, 1979, p 240.
11. J Cazes. J Chem Ed 43(7)A576, 1966 and A3(8)A625, 1966.

© 2004 by Marcel Dekker, Inc.

12. ASTM Method D 3593-77. Standard Test Method for Molecular Weight Averages and Molecular Weight Distribution of Certain Polymers by Liquid Exclusion Chromatography (Gel Permeation Chromatography—GPC) Using Universal Calibration.
13. LH Tung. J Appl Polym Sci 13:775, 1969.
14. LH Tung, JR Runyan. J Appl Polym Sci 13:2397, 1969.
15. MR Ambler, LJ Fetters, Y Kesten. J Appl Polym Sci 21:2439–2451, 1977.
16. ST Balke, AE Hamielec, BP LeClair, SL Pearce. Ind Eng Chem, Prod Res Dev 8:54, 1969.
17. MJ Pollock, JF MacGregor, AE Hamielec. J Liq Chromatogr 2:895, 1979.
18. EG Malawer, AJ Montana. J Polym Sci, Polym Phys Ed 18:2303–2305, 1980.
19. H Benoit, Z Grubisic, P Rempp, D Decker, JG Zilliox. J Chim Phys 63:1507, 1966.
20. Z Grubisic, H Benoit, P Rempp. J Polym Sci, Polym Lett B5:753–759, 1967.
21. C Tanford. Physical Chemistry of Macromolecules. J Wiley & Sons, 1961, p. 333 ff, p. 390 ff.
22. WW Yau. Chemtracts: Makromol Chem 1(1):1–36, 1990.
23. W Kaye. Anal Chem 45(2):221A, 1973.
24. W Kaye, AJ Havlik. Appl Opt 12:541, 1973.
25. ML McConnell. Am Lab 10(5):63, 1978.
26. RC Jordan. J Liq Chromatogr 3(3):439–463, 1980.
27. NC Billingham. Molar Mass Measurements in Polymer Science. J Wiley/Halsted, 1977, p 128 ff.
28. L Senak, CS Wu, EG Malawer. J Liq Chromatogr 10(6):1127–1150, 1987.
29. P Froment, A Revillon. J Liq Chromatogr 10(7):1383–1397, 1987.
30. O Prochazka, P Kratochvil. J Appl Polym Sci 34:2325–2336, 1987.
31. AE Hamielec, AC Ouano, LL Nebenzahl. J Liq Chromatogr 1(4):527–554, 1978.
32. RC Jordan, ML McConnell. Characterization of Branched Polymers by Size Exclusion Chromatography with Light Scattering Detection. In: T Provder, ed. Size Exclusion Chromatography (GPC). ACS Symposium Series, No. 138, ACS, 1980 pp 107–129.
33. LP Yu, JE Rollings. J Appl Polym Sci 33:1909–1921, 1987.
34. HH Stuting, IS Krull, R Mhatre, SC Krzysko, HG Barth. LC-GC 7(5):402–417, 1989.
35. BH Zimm, WH Stockmayer. J Chem Phys 17:1301, 1949.
36. PJ Wyatt, C Jackson, GK Wyatt. Am Lab 20(5):86, 1988.
37. PJ Wyatt, C Jackson, GK Wyatt. Am Lab 20(6):108, 1988.
38. WW Yau, SW Rementer. J Liq Chromatogr 13:627, 1990.
39. PJ Wyatt. J Liq Chromatogr 14(12):2351–2372, 1991.
40. MA Haney, C Jackson, WW Yau. Proceedings of the 1991 International GPC Symposium, 1991, pp 49–63.
41. AC Ouano. J Polym Sci: Symp. No. 43. 43:299–310, 1973.
42. L Letot, J Lesec, C Quivoron. J Liq Chromatogr 3(3):427–438, 1980.
43. J Lesec, D Lecacheux, G Marot. J Liq Chromatogr 11(12):2571–2591, 1988.
44. J Lesec, G Volet. J Liq Chromatogr 13(5):831–849, 1990.
45. CY Kuo, T Provder, ME Koehler. J Liq Chromatogr 13(16):3177–3199, 1990.

© 2004 by Marcel Dekker, Inc.

46. TA Chamberlin, HE Tuinstra. US Patent 4,775,943, October 4, 1988.
47. TA Chamberlin, HE Tuinstra. J Appl Polym Sci 35:1667–1682, 1988.
48. MA Haney. J Appl Polym Sci 30:3037–3049, 1985.
49. MA Haney. Am Lab 17(4):116–126, 1985.
50. PJ Wang, BS Glasbrenner. J Liq Chromatogr 11(16):3321–3333, 1988.
51. DJ Nagy, DA Terwilliger. J Liq Chromatogr 12(8):1431–1449, 1989.
52. J Cazes, ed. Liquid Chromatography of Polymers and Related Materials (Chromatographic Science Series, volume 8). New York: Marcel Dekker, 1977.
53. J Cazes, X Delamare, eds. Liquid Chromatography of Polymers and Related Materials II (Chromatographic Science Series, volume 13). New York: Marcel Dekker, 1980.
54. J Cazes, ed. Liquid Chromatography of Polymers and Related Materials III (Chromatographic Science Series, volume 19). New York: Marcel Dekker, 1981.
55. J Janca, ed. Steric Exclusion Liquid Chromatography of Polymers (Chromatographic Science Series, volume 25). New York: Marcel Dekker, 1984.
56. RW Yost, LS Ettre, RD Conlon. Practical Liquid Chromatography, an Introduction. Perkin-Elmer, 1980.
57. N Hadden, F Baumann, F MacDonald, M Munk, R Stevenson, D Gere, F Zamaroni, R Majors. Basic Liquid Chromatography. Palo Alto, CA: Varian Aerograph, 1971.
58. KJ Bombaugh. The Practice of Gel Permeation Chromatography. In: JJ Kirkland, ed. Modern Practice of Liquid Chromatography. New York: J Wiley & Sons, 1971, pp 237–285.

© 2004 by Marcel Dekker, Inc.

2
Semirigid Polymer Gels for Size Exclusion Chromatography

Elizabeth Meehan
Polymer Laboratories Ltd
Church Stretton, Shropshire, United Kingdom

1 INTRODUCTION

The earliest developments in polymeric packings for size exclusion chromatography (SEC) involved the application of lightly crosslinked, microporous soft gels, used with aqueous-based eluents, for the analysis of water soluble polymers (1). Although work continued to optimize such systems, greater attention was directed to developing stationary phases that would be compatible with organic solvents for the analysis of synthetic polymers. In 1964, Moore (2) introduced a range of rigid macroporous crosslinked polystyrene resins that proved to be successful in the analysis of a wide range of synthetic organic soluble polymers. Since that time polystyrene/divinylbenzene (PS/DVB) packing materials have continued to dominate in the field of organic SEC, although more recent years have seen the introduction of some more polar polymeric stationary phases for specific application areas. For aqueous SEC separations, the original soft gel packing materials have also given way to a new generation of highly crosslinked macroporous polymeric materials, although no single chemistry has proven to be universally applicable. Today, a wide variety of high-performance porous packing

© 2004 by Marcel Dekker, Inc.

materials are commercially available for SEC, including both silica- and polymer-based media. This chapter discusses in detail the technology and application of polymer-based packings for SEC using both organic- and aqueous-based eluents.

2 COLUMN PACKING AND PERFORMANCE

Columns of semirigid polymer gels are generally packed using a balanced density slurry packing technique at pressures in the range 2000–4000 psi (3). Column internal diameters of 7–8 mm i.d. have been employed traditionally, although in recent years narrow bore (4–6 mm i.d.) columns have become more commonplace for environmental and safety reasons because they require reduced solvent consumption. Column lengths are typically 200–600 mm and the overall dimensions of SEC columns available today represent a good compromise between resolution and analysis time using flow rates and operating pressures in accordance with common high-performance liquid chromatography equipment.

Column performance is usually assessed by performing a plate count measurement using a relatively low viscosity eluent and a totally permeating test probe, such as toluene in tetrahydrofuran for organic-based packings or glycerol in water for aqueous SEC columns (4,5). Several methods for measuring plate count (N) from the elution profile of the test probe are well documented and Fig. 1 illustrates the commonly used half height method for plate count calculation as well as the symmetry factor. This type of column test is useful because it provides reference performance data for future comparison during the lifetime of the column. It is important to remember, however, that such data should always be

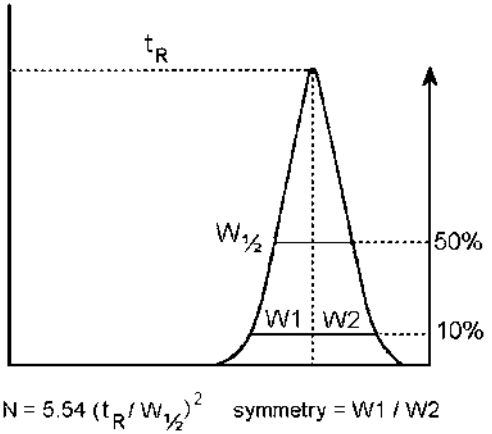

Figure 1 Calculation of plate count, N, and symmetry factor.

© 2004 by Marcel Dekker, Inc.

generated using the same chromatographic conditions of flow rate, eluent, temperature, apparatus, and test solute.

3 ORGANIC SEC

By far the most widely used organic SEC packings are based on porous PS/DVB particles. This is primarily because they are easily produced in a wide range of pore size and particle size and they exhibit minimal absorptive characteristics for a diverse selection of polymers and solvents. However, in recent years alternative packing materials, based on more polar polymeric beads, have been developed to address some applications where the polymer under investigation exhibits hydrophobic interaction with the PS/DVB stationary phase, particularly when analyzed using a more polar organic solvent. Table 1 briefly outlines the range of organic SEC columns commercially available, while more comprehensive information is documented elsewhere (6).

3.1 Manufacture

Polystyrene/divinylbenzene materials are prepared by suspension polymerization using a two-phase organic/aqueous system (7). The crosslinking polymerization is performed in the presence of inert diluents which are miscible with the starting monomers but must not dissolve in the aqueous phase. Submicron particles (microbeads) form as the styrene/divinylbenzene polymerizes and precipitates out of solution and these microbeads fuse together to form macroporous particles. Initially a network of microporosity may be present in the microbeads and polymerization conditions must be controlled to minimize this type of porosity as it results in a less effective packing for the reasons outlined in Table 2. After forming the crosslinked PS/DVB porous particles any residual reactants, diluents, and surfactants must be removed by thorough washing.

3.2 Particle Size

A range of particle sizes can be produced from the reaction described above. For packing materials to be as homogeneous as possible with uniform flow channels, particles of equal size are most suitable. Narrow particle size distributions and regular, spherical particles are therefore desirable (8). If the particle size distribution is too broad then the permeability of the column will decrease. Refinement of particle size distribution by some form of particle classification is used to produce narrow distributions for optimum performance.

Information regarding the particle shape and size can be readily obtained by microscopic methods. However particle sizing equipment is vital for the accurate determination of particle size distribution. For SEC packings, particle diameters in

© 2004 by Marcel Dekker, Inc.

Table 1 Commercial Column Packing Materials for Organic SEC

Type	Chemistry	Pore size range	Particle size range (μm)	Comments	Supplier*
PLgel	PS/DVB	50 Å–10E6 Å + MIXED	3–20	All organic solvents up to 210°C operation	1
OligoPore	PS/DVB	100 Å	6	Oligomeric separations	1
PL HFIPgel	PS/DVB	multipore	9	HFIP applications	1
Shodex KF	PS/DVB	801–807 + MIXED	6–18	THF applications	2
Shodex K	PS/DVB	801–807 + MIXED	6–18	Chloroform applications	2
Shodex KD	PS/DVB	801–807 + MIXED	6–18	DMF applications	2
Shodex HT, UT	PS/DVB	803–807 + MIXED	13–30	High temperature applications	2
Shodex HFIP	PS/DVB	803–807 + MIXED	7–18	HFIP applications	2
Shodex LF	PS/DVB	multipore	6	All organic solvents	2
TSK-GEL H6	PS/DVB	G1000–G7000 + MIXED	13	All organic solvents	3
TSK-GEL H8	PS/DVB	G1000–G4000	10	All organic solvents	3
TSK-GEL HXL	PS/DVB	G1000–G7000 + MIXED	5–13	All organic solvents	3
TSK-GEL HHR	PS/DVB	G1000–G7000 + MIXED	5	All organic solvents	3
TSK-GEL SuperH	PS/DVB	1000–7000 + MIXED	3–5	All organic solvents	3
TSK-GEL Alpha gel	Polar Polymer	α2500–α6000 + MIXED		Polar organic solvents and water	3
TSK Multipore	PS/DVB	multipore	6	All organic solvents	3
Styragel HR	PS/DVB	HR0.5–HR6 + MIXED	5	All organic solvents	4
Styragel HT	PS/DVB	HT2–HT6 + MIXED	10	All organic solvents, high temperature	4
Styragel HMW	PS/DVB	HMW2, HMW7 + MIXED	20	All organic solvents	4
PSS SDV	PS/DVB	100 Å–10E7 Å + MIXED	3–20	All organic solvents	5
PSS PFG	Polar fluoro gel	100 Å–4000 Å + MIXED	7	Fluorinated solvents	5

*1: Polymer Laboratories (www.polymerlabs.com)
2: Shodex (www.sdk.co.jp/shodex)
3: Tosoh (www.tosohbiosep.com)
4: Waters Corporation (www.waters.com)
5: Polymer Standards Service (www.polymer.de)

© 2004 by Marcel Dekker, Inc.

Table 2 Comparison of Macroporous and Microporous Polymeric Packings

Property	Macroporous	Microporous
Structure	Rigid polymer	Soft gel
Crosslink density	High, $>20\%$	Low, 2–12%
Volumetric swell in solvents	Low	High
Pore size	Independent of eluent	Determined by eluent and crosslink density
Mechanical strength	Good, <6000 psi	Poor, <2000 psi
Operating conditions	High pressure, high flow rate	Low pressure, low flow rate
Examples	PS/DVB, hydroxylated PMMA	4–8% PS/DVB, agarose, polyacrylamide

the range 3–20 μm are commercially available. Smaller particles offer improved resolution but result in higher operating pressures and can prove more difficult to pack. The Van Deemter equation (9) predicts that H, the theoretical plate height, is proportional o the square of the particle diameter. Originally, packing materials were manufactured as 37–70 μm particles and typical column sets consisted of four 4 ft columns resulting in analysis times of 3–4 hours (10). Over the last ten years the gradual reduction in particle size of analytical packings has resulted in much higher efficiency columns and a corresponding reduction in analysis time to typically 10–30 minutes (11). However, for the analysis of very high molecular weight polymers, larger particle size columns are still preferred to avoid any incidence of on-column shear degradation.

3.3 Porosity

The pore size of PS/DVB particles when swollen in solvent is difficult to measure and for convenience is usually assessed by testing the packing material with molecular probes (12,13). These are most commonly polymer calibrants of known molecular weight and very narrow polydispersity. This produces an SEC calibration for the packing where log (molecular weight) vs. elution time or volume is plotted. From this plot the exclusion and total permeation limits can be determined as well as the region of shallowest slope, which essentially define the operating range and pore volume of the packing. For PS/DVB packings pore sizes are commonly expressed in angstrom units (Å). This is not, however, the actual pore size but is related to the extended molecular chain length of a polystyrene molecule that is just excluded from the pores. Various manufacturers' Å sizes are based on different molecular models for polystyrene and are therefore not

© 2004 by Marcel Dekker, Inc.

necessarily comparable. For this reason comparisons of packing materials are best made based on the exclusion limit and pore volume calculated from the SEC calibration curves supplied by the manufacturer. A typical range of calibration curves are shown in Fig. 2 for PLgel individual pore size gels.

Individual pore size packings for SEC have a finite separation capacity, which is concentrated in a limited molecular weight range. Although the resolution of such columns is high, the relatively narrow range of molecular weight limits their use to SEC analyses of narrow molecular weight distribution polymers or samples. In practise, SEC columns of different pore size are connected in series to provide a wider molecular weight separation range (14). Most SEC users prefer convenient systems that provide a wide molecular weight separation range to analyse polymers of different molecular weight and distribution without having to change and recalibrate columns. In combining individual pore size columns for this purpose it is important to consider the pore size distributions of each column type. The dimensions of all the columns will remain constant but pore volume may vary from one gel to another. This has the effect of giving variable degrees of resolution over specific regions of molecular weight. Columns with widely overlapping molecular weight resolving ranges were often used in series, for example, 10^6, 10^5, 10^4, 10^3, 500 Å. However with the development of smaller particles yielding higher column efficiencies, this number of columns, and therefore analysis times, has become excessive (15).

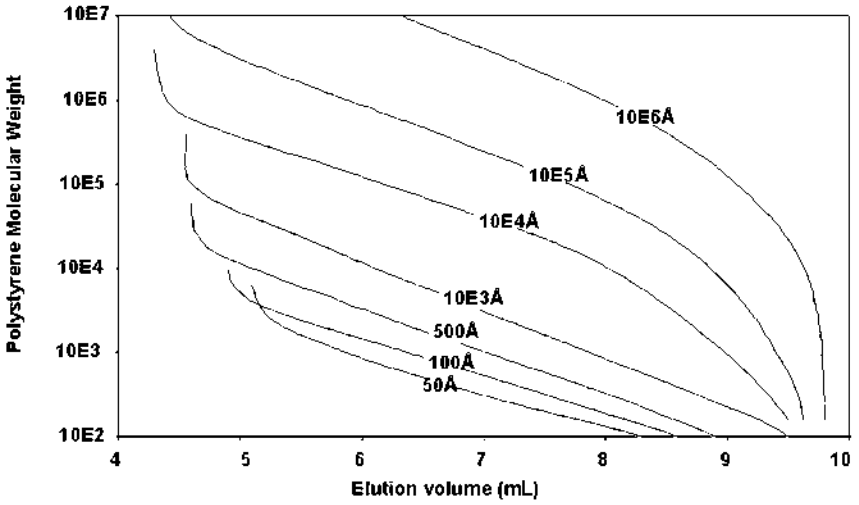

Figure 2 SEC calibration curves for PLgel individual pore size gels, column dimensions 300 × 7.5 mm, eluant tetrahydrofuran, flow rate 1 mL/min, calibrants narrow polydispersity polystyrene, detector ultraviolet (UV) 254 nm.

© 2004 by Marcel Dekker, Inc.

Yau *et al.* (16) described a quantitative theory of producing individual columns in which the pore size distribution, and hence molecular weight resolving range, was broadened by blending two or more gels together. It was shown that the use of a single packing material greatly simplified the column inventory and allowed the use of reduced numbers of columns while maintaining the high chromatographic resolution and accurate molecular weight measurements associated with high-performance SEC. The application of this theory to mixed gel packings based on PS/DVB gels has been shown to yield similar improvements (17).

Mixed gel, extended range, or linear SEC packings can be produced by blending together selected pore size gels and packing them as a homogeneous mixture to produce a column that exhibits a linear calibration. The highest pore size gel in the blend will determine the final exclusion limit of the packing and the blended packing material may consist of up to five or more individual pore size gels. The linear calibration plot, as shown in Fig. 3 for a range of PLgel MIXED gels, results in equal resolution per decade of molecular weight over the full operating range of each packing.

In recent years, several manufacturers have released SEC column products that are based on so called "multipore" technology. These packing materials are produced by suspension polymerization, but the manufacturing conditions are

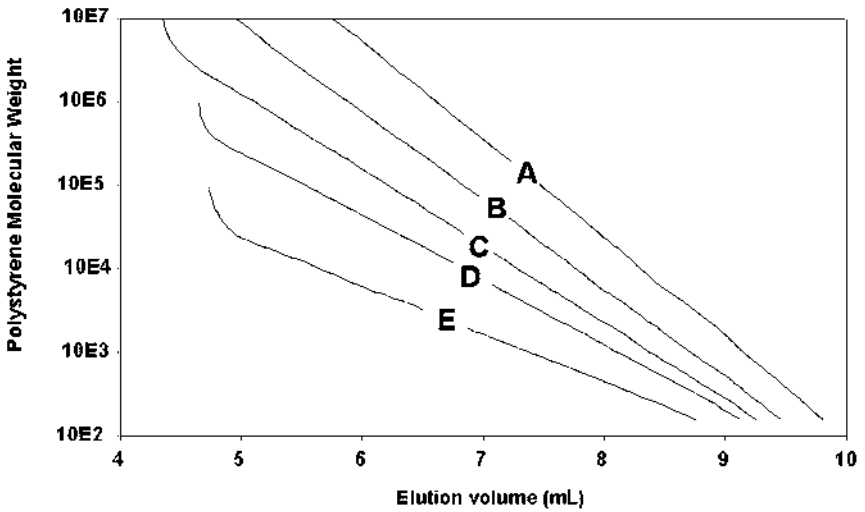

Figure 3 SEC calibration curves for PLgel MIXED gels, column dimensions 300 × 7.5 mm, eluant tetrahydrofuran, flow rate 1 mL/min, calibrants narrow polydispersity polystyrene, detector UV 254 nm.

© 2004 by Marcel Dekker, Inc.

adjusted such that the pore size distribution obtained is wider than conventional single pore size packings. The resultant SEC column calibration exhibits extended resolving range, comparable to that of mixed gel technology, although overall linearity of the calibration curve is somewhat compromised.

3.4 Mechanical and Chemical Stability

All packing materials are subject to the development of back pressure under flow conditions. The mechanical stability of the gel will determine its maximum allowable flow rate in operation. The pressure/flow characteristics, as illustrated in Fig. 4, reveal both the permeability of the packing, from the initial linear portion of the graph, and the point at which the gel will compress and deform. The

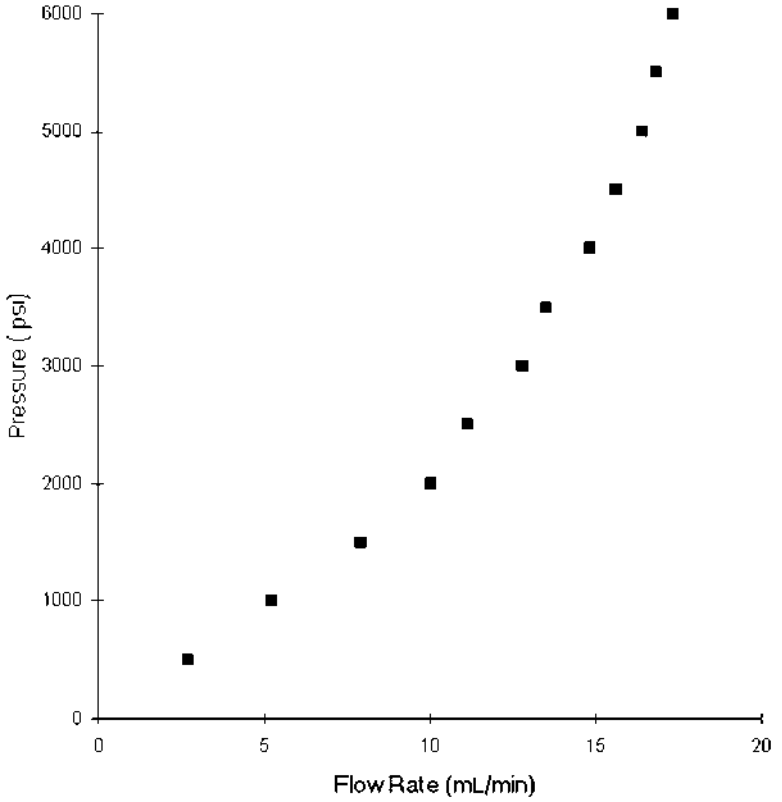

Figure 4 Flow rate vs. column pressure measured for a PLgel 5 μm, 100 Å, 300 × 7.5 mm column, eluant acetone.

© 2004 by Marcel Dekker, Inc.

maximum operating pressure of the packing should fall well below the compression point to avoid permanent damage and effective repacking of the column.

The chemical stability of the gel is usually most relevant to solvent compatibility. Solvents of varying solubility parameter will cause a polymeric gel to swell to differing degrees. The extent of swell in different solvents will depend on the degree of crosslinking and for this reason highly crosslinked gels perform best across the widest range of solvent polarity (18). Generally, modern SEC packings can be used with a wide range of organic solvents although, as manufacturing processes may vary, the solvent compatibility of a packing material will depend on the chemistry and packing techniques employed. Therefore it is always recommended that the manufacturers' guidelines for solvent compatibility should be consulted. When transferring columns from one solvent to another it is important to check the miscibility of the two solvents and the solubility of any additives/stabilizers present. Column blockage could occur if either of these two considerations are overlooked.

Some solvents may exhibit high viscosity at room temperature and elevated temperature (50–120°C) can be used to reduce the viscosity, thus improving mass transfer, reducing operating pressure, and prolonging column lifetime. High-temperature SEC (130–210°C) is also required for the analysis of polymers that only dissolve at higher temperatures and readily crystallize out of solution on cooling, classically polyolefins (19). In such cases there may be a general reduction in the lifetime of the packing brought about by two mechanisms:

1. Thermal or oxidative degradation of the gel, which alters the swell characteristics and changes the pore size distribution, eventually breaking down the particle. Although ultimately some degradation can be expected under such aggressive conditions, this can be reduced substantially by the addition of antioxidants to the mobile phase.
2. The production of "solvent tracks" through the gel bed brought about by heating/cooling cycles. This phenomenon occurs when damage to the column packing results in regions of different packed bed density giving rise to varying flow paths through the column. The effects can easily be observed as broad peaks or split peaks in the chromatogram. The lifetime of the gel is significantly improved by minimizing thermal shock to the columns, which means maintaining low flow rate through the column while changing the temperature at rates of around 1°C/min or less depending on the manufacturer.

3.5 Column Selection/Applications

The first criterion for column selection is the molecular weight of the sample to be analyzed. For some applications where resolution is required over a relatively

© 2004 by Marcel Dekker, Inc.

narrow molecular weight range, individual pore size packings are suitable. This is particularly the case for small molecule separations as shown in Fig. 5. For polymer analyses, where resolution is required covering several decades of molecular weight, mixed gel or linear columns are widely applicable. Figure 6 illustrates the application of mixed gels columns to the analysis of polyethylene, which typically has a high polydispersity.

Resolution in SEC is dependent on:

1. the slope of the calibration plot $d\log M/dv$, and
2. efficiency.

These two parameters should be manipulated in order to optimize resolution (20). Calibration slope can be decreased by the addition of more columns in series and the effect on resolution is illustrated in Fig. 7. Efficiency is dependent on particle size and smaller particle size, higher efficiency columns are generally preferred. The effect of particle size on the separation of polystyrene oligomers is shown in Fig. 8. Column sets should comprise packing materials of the same particle size as the full potential efficiency of the system will never be achieved if large and small particle size columns are combined.

In a chromatographic bed the largest tangential shear stresses in the moving eluent stream would be expected to be in the most open areas subject to the highest flows, that is, in the spaces between the particles. It has been estimated (21) that

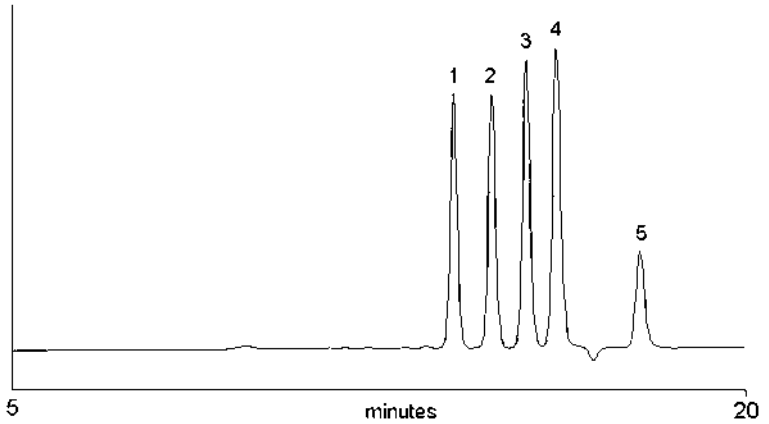

Figure 5 Separation of dialkylphthalates, two columns PLgel 3 μm, 100 Å, 300 × 7.5 mm, eluant tetrahydrofuran, flow rate 1 mL/min, detector refractive index (RI); (1) dioctyl phthalate, (2) dibutyl phthalate, (3) diethyl phthalate, (4) dimethyl phthalate, (5) toluene.

© 2004 by Marcel Dekker, Inc.

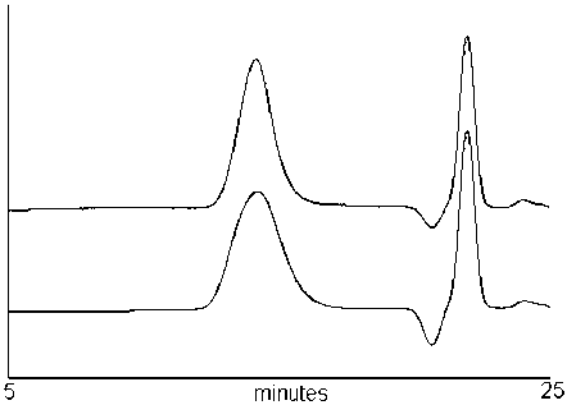

Figure 6 Analysis of two commercial polyethylene samples, three columns PLgel 10 μm MIXED-B, 300 × 7.5 mm, eluant trichlorobenzene, flow rate 1 mL/min, temperature 160°C, detector refractive index (RI).

these "capillaries" may have effective diameters 0.4 times the particle diameter. Therefore it can be predicted that higher shear rates associated with small particle size packings would prove to be more likely to incur polymer shear degradation in SEC (22). This phenomenon is most relevant to the analysis of high molecular weight polymers that exhibit high intrinsic viscosity in solution since shear stress $\tau = \eta\gamma$, where η is the viscosity of the polymer solution and γ is the shear rate. In order to minimize the effects of shear degradation in SEC it is therefore necessary to use larger particle size packings to reduce γ and lower sample concentrations to

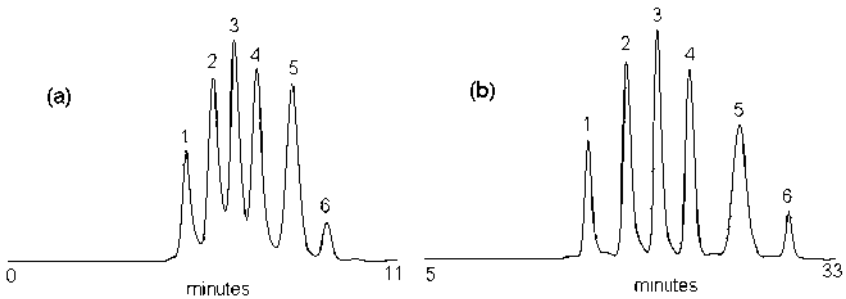

Figure 7 Effect of column length on separation using PLgel 10 μm MIXED-B columns, eluant tetrahydrofuran (THF), flow rate 1 mL/min, detector RI, (a) one 300 × 7.5 mm, (b) three 300 × 7.5 mm, PL EasiCal polystyrene standards; (1) $M_p = 3{,}040{,}000$; (2) $M_p = 330{,}000$; (3) $M_p = 66{,}000$; (4) $M_p = 9200$; (5) $M_p = 580$; (6) toluene.

© 2004 by Marcel Dekker, Inc.

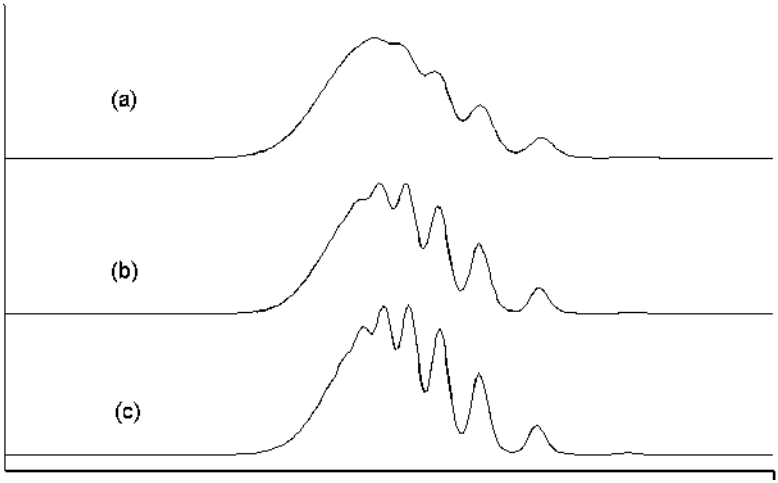

Figure 8 Effect of particle size on polystyrene oligomer separation using PLgel 100 Å column, 300 × 7.5 mm; (a) 10 μm, (b) 5 μm, (c) 3 μm; eluant tetrahydrofuran, flow rate 1 mL/min, detector UV 254 nm.

reduce η. In addition the porous frits at the inlet and outlet of SEC columns present a further potential source of shear as they are comprised of narrow channels that can also be considered as capillaries. The frit porosity should be selected in accordance with the particle size of the packing so as to contain the packing material while not inducing polymer shear degradation.

Molecular shear phenomena are evidenced by peak splitting or lower than expected calculated molecular weight values (23). Experimental data (24) have shown that using 5 μm particle size, packings errors of 15–30% in molecular weight can be observed for narrow distribution polystyrene standards greater than 4,000,000 g/mol. In these applications larger particle size (10–20 μm) columns are most suitable and compensation for their lower efficiency is made by the addition of more columns in series.

4 AQUEOUS SEC

4.1 Introduction

The first polymeric packings were developed primarily for the analysis of natural polymers and they were based on lightly crosslinked polymer networks that produced soft gel packings (8). These soft gels, based on dextran or agarose, develop porosity between the polymer chains or between clusters of polymer

© 2004 by Marcel Dekker, Inc.

chains in their swollen state. They were found to be much less susceptible to secondary interaction effects than silica-based packings so that separations dominated by size exclusion were readily achieved. However, the disadvantage was that the highly swollen, microporous networks had poor mechanical strength and were therefore not really suitable for high-performance SEC performed with relatively short, low capacity columns at high eluent flow rates.

Packings for high performance aqueous SEC have therefore been developed (25,26) which are rigid, which have functionalities similar to those of the soft gels, and which can tolerate a wide range of pH. Table 3 summarizes the range of commercial high-performance aqueous SEC packings available, while more comprehensive information is documented elsewhere (6).

Many of the comments referred to in Secs. 3.2–3.5 apply equally to aqueous SEC. The remainder of this section will discuss other important parameters specific to semirigid polymeric packings for aqueous SEC.

4.2 Porosity

Pore size distribution is expressed in the form of an SEC calibration plot, log M vs. elution volume, but whereas for organic SEC polystyrene standards are used almost exclusively, for aqueous SEC packings resolving ranges are commonly quoted in terms of polyethylene oxide/glycol (PEO/PEG), polysaccharides, or

Table 3 Commercial Column Packing Materials for Aqueous SEC

Type	Chemistry	Pore size range	Particle size range (μm)	Supplier*
PL aquagel–OH	Macroporous with OH functionality	AOH30–AOH60 + MIXED	8–15	1
Shodex OHpak	Hydroxylated PMMA	SB802HQ–SB806HQ + MIXED	8–13	2
TSK-GEL PW	Hydroxylated PMMA	G1000–G6000 + MIXED	6–25	3
Ultrahydrogel	Hydroxylated PMMA	120 Å–2000 Å		4
PSS HEMA	Acrylic	40 Å–1000 Å + MIXED	10	5
PSS Suprema	OH-acrylic	30 Å–30,000 Å + MIXED	5–20	5

*1: Polymer Laboratories (www.polymerlabs.com)
2: Shodex (www.sdk.co.jp/shodex)
3: Tosoh (www.tosohbiosep.com)
4: Waters Corporation (www.waters.com)
5: Polymer Standards Service (www.polymer.de)

© 2004 by Marcel Dekker, Inc.

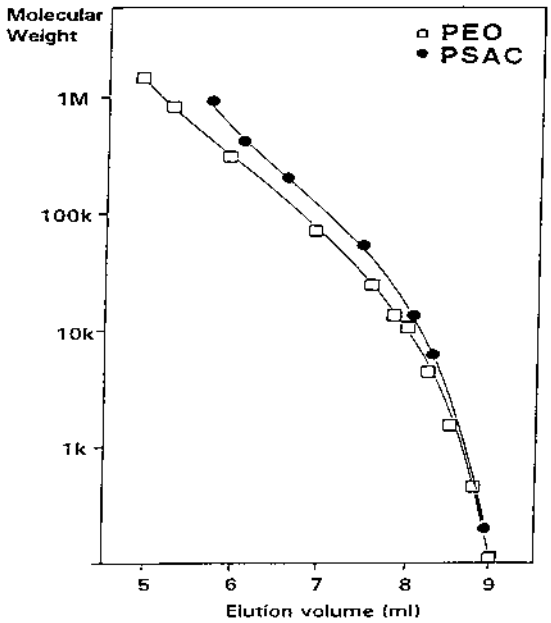

Figure 9 SEC calibration using polyethylene oxide (PEO) and polysaccharide (PSAC) standards, column PL aquagel–OH 50, 300 × 7.5 mm, eluant water, flow rate 1 mL/min, detector RI.

globular proteins. A comparison of PEO/PEG and Pullulan polysaccharide calibrations is shown in Fig. 9. These molecular probes vary considerably in hydrodynamic volume and can therefore be expected to yield quite different calibration curves (25). It is therefore important to base column selection on a calibration that is relevant to the application.

4.3 Surface Chemistry

Ideally a packing material for aqueous SEC should be highly hydrophilic and should not possess any charge. These requirements arise from the nature of the polymers to be analyzed. Both natural and synthetic water-soluble polymers can be either nonionic (neutral) or ionic (polyelectrolyte) and in turn either hydrophilic or relatively hydrophobic. A polymeric packing material that is not highly hydrophilic may result in hydrophobic sample to column interactions. In addition, charged sites on the surface of the packing material can give rise to ionic interactions with polyelectrolyte polymers (27).

© 2004 by Marcel Dekker, Inc.

In practise, most high-performance aqueous SEC packings exhibit some degree of hydrophobicity and ionic charge due to the chemistries involved in their manufacture. Because a variety of chemistries are available commercially (Table 3) the ionic and hydrophobic characteristics of packing materials may differ. Often the chemistry applied is necessary to obtain a compromise between the chemical and physical properties of the final packing material. Both ionic and hydrophobic character are undesirable because they result in nonsize exclusion phenomena and although manufacturers of packing materials aim to minimize such interactions, eluent modification to suppress them is routine. This normally involves the use of salt/buffer solutions (ionic interaction) and/or the addition of organic modifiers (hyrophobic interaction) to the eluent. An advantage of using such eluent systems is that the presence of salts effectively reduces polyelectrolyte viscosity, which can otherwise be excessive due to intramolecular electrostatic attractions within the polymer chains giving rise to viscous fingering effects in SEC (28).

Depending on the chemistry adopted by the column manufacturer, eluent selection may be limited with respect to pH and type/level of organic solvent that can be tolerated. For example, the choice and level of crosslinking agent in polyvinyl alcohol based packings influences both the pH stability and organic solvent compatibility. In all cases the manufacturers' literature should specify eluent compatibility.

4.4 Eluent Selection

The selection of the eluent in aqueous SEC is critical as it is often the only means of controlling secondary interactions between the sample and the column. Specific interactions can be exploited if the separation of discrete components in a sample is to be achieved, for example, purification of biological compounds. However, if SEC is to be used to derive a polymer molecular weight distribution then nonsize exclusion behavior is undesirable (29). Although it is sometimes difficult to eliminate interactions completely, they can often be suppressed by selection of an appropriate eluent. The selection of eluent will be dependent on the type of sample and on the surface chemistry of the packing material. Although it cannot be assumed that an eluent used for a separation on one manufacturer's columns will be suitable for a separation using a different type of column, certain general rules apply as outlined in Table 4.

Adsorption effects can be identified by phenomena such as a sharp leading edge followed by tailing of the peak, small peak area, retardation of elution, and poor reproducibility. Ion exclusion effects can be seen by early elution close to or even slightly prior to the void volume. When optimizing eluent composition, the reproducibility of chromatograms resulting from systematic changes in composition can be used as an indicator to determine the best set of conditions.

© 2004 by Marcel Dekker, Inc.

Table 4 Typical Eluent Systems for Synthetic Water Soluble Polymers

Type of polymer	Typical sample	Suitable eluent
Nonionic, hydrophilic	Polyethylene oxide, polyethylene glycol	Pure water
Nonionic, hydrophobic	Polyvinylpyrrolidone	0.1–0.2 M salt/buffer with 20–50% organic solvent
Anionic, hydrophilic	Sodium polyacrylate, sodium hyaluronate, carboxymethyl cellulose	0.1–0.3 M salt/buffer, pH 7–9
Anionic, hydrophobic	Sodium polystyrene sulfonate	0.1–0.3 M salt/buffer, pH 7–9 with 20–50% organic solvent
Cationic, hydrophilic	Chitosan, poly-2-vinyl pyridine	0.3–0.8 M salt/buffer, pH 2–7
Cationic, hydrophobic	Polyethyleneimine	0.3–0.8 M salt/buffer, pH 2–7 with 20–50% organic solvent

For nonionic polymers, pure water can often be used as eluent although a low ionic strength is a good safety measure and adds a degree of reproducibility to the system. Polyethylene oxide and polyethylene glycol are characteristic of this sample category.

For ionic samples it is recommended that salt/buffer systems are used as eluents. The salts most commonly used are sodium sulfate, sodium nitrate, and sodium acetate, because these cause little corrosion to stainless steel column hardware even at low pH. Ionic strength is varied according to sample type but generally does not exceed 1.0 M as increasing salt concentration will promote hydrophobic interaction. Often a buffer is used to allow pH to be controlled.

Anionic polymers may be eluted using 0.1–0.3 M salt/buffer at pH 7–9. Figure 10 shows the analysis of polyacrylic acid (sodium salt), which is a typical example. Polystyrene sulfonate (sodium salt) is also an anionic polymer, but often does not elute under such conditions as it is relatively hydrophobic. Although the salt/buffer system is sufficient to suppress the ionic interaction, adsorption due to hydrophobic interaction occurs and this has to be overcome by introducing some organic modifier to the mobile phase as shown in Fig. 11. In the case of PL aquagel–OH, methanol is recommended as an organic modifier although with other packings different solvents may be used (e.g., acetonitrile with TSK PW columns). The manufacturers' recommendations on the use of organic solvents with aqueous packings should always be followed carefully as the wrong choice of solvent may irreversibly damage the column.

Cationic polymers may be eluted using rather higher salt concentrations, 0.3–1.0 M, and pH in the range 2–7. A typical analysis of poly-2-vinyl pyridine is shown in Fig. 12. As with the anionic samples, if there is a high degree of

© 2004 by Marcel Dekker, Inc.

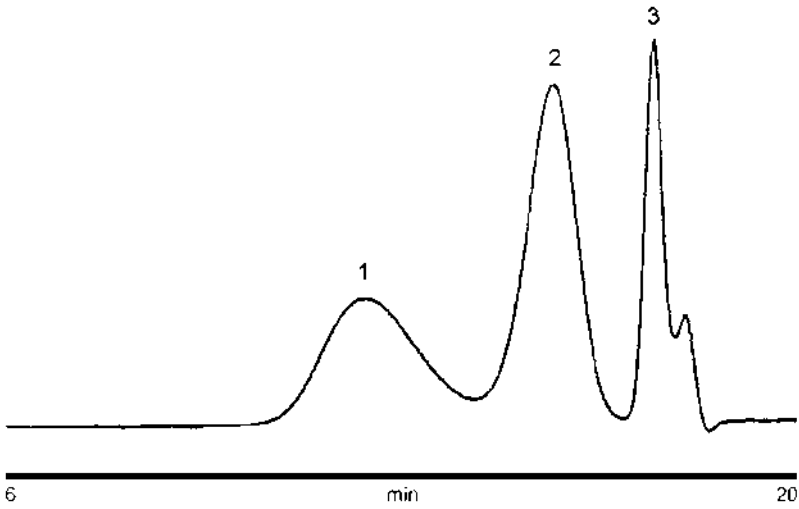

Figure 10 Analysis of polyacrylic acid standards: two columns PL aquagel–OH 50, 300 × 7.5 mm, eluant 0.25 M $NaNO_3$ and 0.01 M NaH_2PO_4, pH 7, flow rate 1 mL/min, detector RI: (1) $M_p = 272{,}900$; (2) $M_p = 16{,}000$; (3) salt peak.

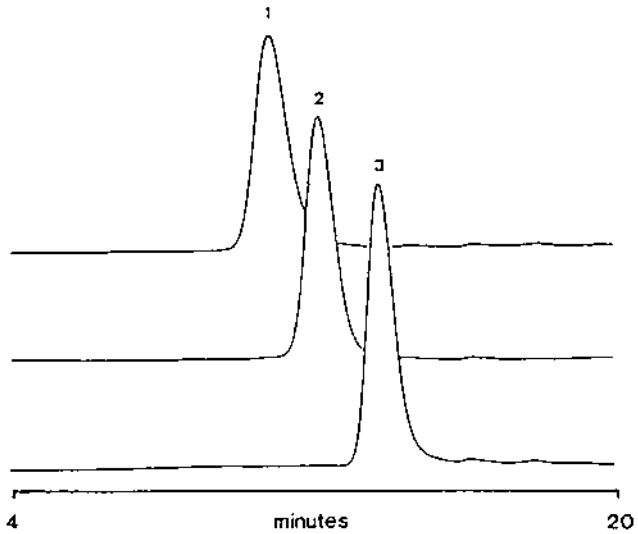

Figure 11 Analysis of polystyrene sulfonate (sodium salt) standards: two columns PL aquagel–OH 40, 300 × 7.5 mm, eluant 80% vol/vol 0.3 M $NaNO_3$ and 0.01 M NaH_2PO_4, pH 9, +20% vol/vol methanol, flow rate 1 mL/min, detector RI: (1) $M_p = 100{,}000$; (2) $M_p = 35{,}000$; (3) $M_p = 4600$.

© 2004 by Marcel Dekker, Inc.

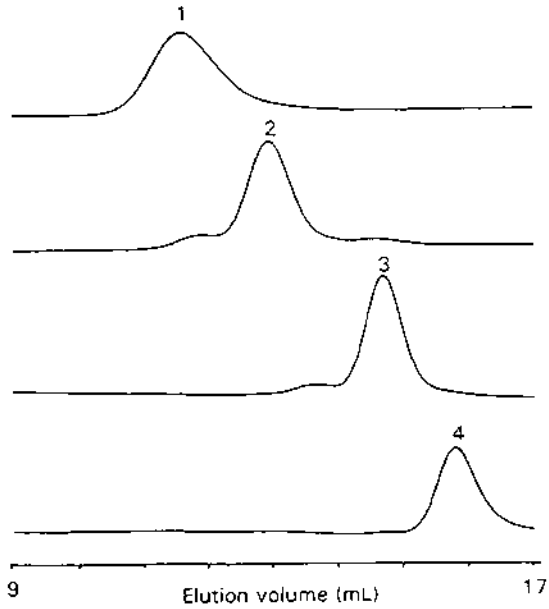

Figure 12 Analysis of poly-2-vinyl pyridine standards: two columns PL aquagel–OH 50, 300 × 7.5 mm, eluant 0.25 M $NaNO_3$ and 0.01 M NaH_2PO_4, pH 3, flow rate 1 mL/min, detector RI: (1) $M_p = 600{,}000$; (2) $M_p = 200{,}000$; (3) $M_p = 50{,}000$; (4) $M_p = 20{,}000$.

hydrophobicity in the sample then it may be necessary to add some organic modifier to the mobile phase.

Even if the ionic sample solutions are prepared from the eluent, when the mobile phase consists of a salt solution there will often be a peak near total permeation due to the salt. This is believed to be due to ion inclusion (30) where the porous packing acts like a semipermeable membrane and an equilibrium is established such that the ion of the same charge as the excluded sample is forced into the pores, giving rise to a permeated peak. This can be problematic as it may interfere with sample components and in this case column selection may have to be adjusted to give more resolution for very small molecules.

5 CONCLUSION

A wide variety of commercial semirigid polymer gels exists for both organic and aqueous SEC. Following the introduction of smaller particle size packings, high-

© 2004 by Marcel Dekker, Inc.

performance columns are available that can provide rapid analysis of compounds covering an extensive range of chemical composition and molecular weight. Mixed gel or linear columns are becoming increasingly popular for the analysis of polymers as they permit accurate molecular weight determinations using a reduced number of columns. The chemical and thermal stability of organic SEC columns may become more important in the characterization of new polymers where more exotic solvents and higher temperatures are required. Environmental considerations may increase the usage of high-performance aqueous SEC columns in the future as more water-based polymer systems are developed.

6 REFERENCES

1. J Porath, P Flodin. Nature 183:1657, 1959.
2. JC Moore. J Polym Sci, Part A 2:835, 1964.
3. B Ravindranath. Principles and Practice of Chromatography. Ellis Horwood Ltd, UK, 1989, p 317.
4. PA Bristow. Liquid Chromatography in Practise. UK: Hept, 1976, p 16.
5. AB Littlewood. Gas Chromatography. New York: Academic Press, 1970.
6. C Wu. Column Handbook for Size Exclusion Chromatography. New York: Academic Press, 1999.
7. J Seidl, J Malinsky, K Dusek, W Heitz. Adv Polym Sci 5:113, 1967.
8. G Glockner. Polymer Characterisation by Liquid Chromatography. J Chromatogr Libr 34:170, 1987.
9. WW Yau, JJ Kirkland, DD Bly. Modern Size-Exclusion Liquid Chromatography. New York: John Wiley & Sons, 1979, p 63.
10. JM Evans. RAPRA Members J, August 1973.
11. E Meehan, JA McConville, FP Warner. Polym Int 26:23–38, 1991.
12. FV Warren, BA Bidlingmeyer. Anal Chem 56:6, 1984.
13. AA Gorbunov, LYa Solovyova, VA Pasechnik. J Chromatogr 448:307–332, 1988.
14. WW Yau, JJ Kirkland, DD Bly. Modern Size-Exclusion Liquid Chromatography. New York: John Wiley & Sons, 1979, p 267.
15. FP Warner, Z Dryzek, LL Lloyd. New criteria influencing the selection of high performance GPC columns for polymer analysis. Presented at Antec, Boston, 1986.
16. WW Yau, CR Ginnard, JJ Kirkland. J Chromatogr 149:465–487, 1978.
17. E Meehan, JA McConville, S Oakley, FP Warner. Performance criteria for mixed gel GPC columns. Presented at the International GPC Symposium, San Fransisco, 1991.
18. WG Lloyd, T Alfrey. J Polym Sci 62:301–316, 1962.
19. MR Haddon, JN Hay. In: BJ Hunt, SR Holding, eds. Size Exclusion Chromatography. Glasgow and London: Blackie & Son, 1989, p 57.
20. WW Yau, JJ Kirkland, DD Bly, HJ Stoklosa. J Chromatogr 125:219, 1976.
21. JC Giddings. Adv Chromatogr 20:217, 1982.
22. HG Barth, FJ Carlin. J Liq Chromatogr 7(9):1717–1738, 1984.
23. JG Rooney, G ver Strate. In: J Cazes, ed. Liquid Chromatography of Polymer and Related Materials III. New York: Marcel Dekker, 1981, p 207.

© 2004 by Marcel Dekker, Inc.

24. E Meehan, S O'Donohue. The role of column and media design in the SEC characterisation of high molecular weight polymers. Presented at ISPAC 5, Inuyama, Japan, 1992.
25. E Meehan, LL Lloyd, JA McConville, FP Warner, NP Gabbott, JV Dawkins. J Appl Polym Sci, Appl Polym Symp 48:3–17, 1991.
26. Y Kato, T Matsuda, T Hashimoto. J Chromatogr 332:39–46, 1985.
27. HG Barth. J Chromatogr Sci 18:409–429, 1980.
28. C Abad, L Braco, V Soria, R Garcia, A Campos. Br Polym J 19:489–508, 1987.
29. DJ Nagy, DA Terwilliger, BD Lawrey, WF Tiedge. Characterisation of cationic polymers by aqueous SEC/differential viscometry. Presented at the International GPC Symposium, Newton, 1989.
30. PL Dubin, IJ Levy. J Chromatogr 235:377–387, 1982.

© 2004 by Marcel Dekker, Inc.

3
Modified Silica-Based Packing Materials for Size Exclusion Chromatography

Roy Eksteen* and Kelli J. Pardue
Supelco, Inc.
Bellefonte, Pennsylvania, U.S.A.

1 INTRODUCTION

Size exclusion chromatography (SEC), gel filtration chromatography (GFC) and gel permeation chromatography (GPC) are chromatographic techniques based on discrimination by differences in the size of the analytes. GFC uses an aqueous mobile phase and GPC an organic mobile phase. The general term SEC covers both uses. GFC was first applied in 1959 at the University of Uppsala by Porath and Flodin (1), who showed that proteins were separated as a function of their molecular weight on porous dextran beads because of their (partial) exclusion by the pores. Similarly, GPC was first employed in 1964 by Moore at Dow Chemical Company, who demonstrated the separation of organic soluble polymers on a column packed with a cross-linked polystyrene gel using an organic solvent as the mobile phase (2). Following their discoveries, GFC and GPC developed quickly

**Current affiliation*: TOSOH Bioscience, LLC, Montgomeryville, Pennsylvania, U.S.A.

© 2004 by Marcel Dekker, Inc.

into accepted laboratory techniques through the availability of commercial supplies of agarose- and polystyrene-based packing materials.

During the initial stages of development, the particle size of SEC packings did not decrease as rapidly as that of silica-based packings employed in high-performance liquid chromatography (HPLC) techniques. According to theory, the performance of HPLC columns improves in direct proportion to a decrease in particle size (3). This prediction was proven correct during the latter part of the 1960s. It was not until the late 1970s, however, that this concept led to the use of small silica-based particles for size exclusion chromatography supports. The 5-μm silica gel particles were first shown to be an efficient substitute for traditional resin-based particles in GPC (4). Later, the potential of silica and porous glass for use in GFC was demonstrated, following their chemical bonding with hydrophilic ligands to prevent adsorption of proteins and nucleic acids (5).

Since their introduction in 1978, high-performance silica-based SEC packings have made a great impact in the analysis and purification of biopolymers. Columns filled with 10-μm spherical particles and nominal pore sizes of 125, 250, and 500 Å (10 Å = 1 nm) became the state of the art for protein separations during the 1980s (6). Further improvements in speed and resolution were obtained by reducing the size of the particles from 10 to 5 μm (7). Columns filled with these high-performance particles are now manufactured and distributed by several companies. Although this chapter discusses several aspects of the use of silica-based packings for biopolymer analysis, consult Chapters 15 and 16 for details on the application of SEC for the separation of proteins and nucleic acids, respectively.

For the analysis of organic-soluble and water-soluble synthetic polymers, silica-based packing materials have not become as widely used as was originally envisioned (8). Major improvements in the properties of polymer-based supports have contributed to their increased use in GPC. Columns packed with polystyrene divinylbenzene particles are now as efficient as those filled with silica particles of the same size. Because polymer-based packings can be synthesized with very small (<60 Å) and very large (>4000 Å) pores, they provide better selectivity than silica columns for the separation of monomers, as well as for very high molecular weight (5–20 million dalton) polymers.

The use of (modified) silica gels for size exclusion chromatography has been the topic of many recent reviews and books. The 1979 book from Yau *et al.*, enriched by the authors' contribution to the development of high-performance silica-based SEC packings, is still an often-used reference for new and experienced workers alike (8). The application of silica-based packing materials for biopolymer separations is discussed in detail in Refs 9–14. References 15–17 focus mainly on gels (organic nonrigid packing materials), which are exclusively discussed in Refs 18 and 19. Refer to the comprehensive review from Barth and Boyes (20) for recent references for the analysis of organic- and water-soluble industrial

© 2004 by Marcel Dekker, Inc.

polymers. References describing the use of controlled pore glass in chromatography have been compiled in a commercial bibliography (21).

This chapter first discusses the characteristics of silica as it pertains to size exclusion chromatography. Next, several methods for molecular weight calibration in SEC are examined and the effects of secondary retention discussed. The chapter concludes with an overview of practical aspects associated with the application of size exclusion chromatography.

2 PROPERTIES OF SILICA

Silicon dioxide (SiO_2), silica gel, or silica is the most abundant compound in the Earth's crust. Many industries depend on it being readily and abundantly available in relatively pure form. Traditionally, silica has been an important natural resource for the glass industry. More recently, ultrapure silica particles have become the raw material for manufacturing computer chips. Other common applications of silica include its widespread use as a drying agent, food ingredient, and its incorporation in floor waxes to impart nonskid properties (22). The properties of porous silica and its use as a support in column liquid chromatography (LC) were described in a book by Unger (23). The chemistry of silica is the topic of a comprehensive book by Iler (24). Silica as a backbone of LC column packings was recently reviewed by Berthod (25). Henry discussed the design requirements of silica-based matrices for biopolymer chromatography, including their use in SEC (26).

2.1 Structure, Synthesis, and Purity

Silica gel has an amorphous structure, is highly porous, and exhibits a very large surface area, most of which is located in the pores. It consists of a three-dimensional network of SiO_2 repeating units with siloxane and silanol terminal units on the surface. Silica gel can be synthesized into particles ranging in diameter from millimeters to micrometers; the particle size of silica sols (colloids consisting of discrete silica particles—nonporous, spherical, and amorphous) is in the nanometer range. Refer to Refs 22–24 for thorough treatments of the synthesis of silica gel particles for use in chromatography.

The purity of silica has been a topic of debate among those studying interactive modes of liquid chromatography. The effect of metal ion impurities on the retention of basic solutes and chelating compounds was first addressed by Verzele *et al.* (27). Depending on the manufacturing process, chromatographic silica gel contains impurities in concentrations ranging from low to high parts per million. Although to the knowledge of the authors this issue has not yet been discussed in the context of silica-based size exclusion chromatography, it is expected that the use of high-purity silica gels can lead to further improvements in obtaining true SEC retention behavior, as well as improved recovery of

© 2004 by Marcel Dekker, Inc.

Table 1 Trace Metal Impurities in Commercial Silica Gels (ppm)

Element Periodic table group	Na Ia	K Ia	Mg IIa	CA IIa	BA IIa	Ti IVb	Zr IVb	Cr VIb	Fe VIII	Cu Ib	Al IIIa	Sb Va	Analysis method[b]	Reference
Capcell SG120	NO[a]	NO	NO	NO		7	3		1		6		ICP-AES	28
Hypersil	3360								260		300		AAS	30
Hypersil Lot 180	4176		61	48					192		344		ICP-AES	[c]
Hypersil Lot 180	3945		60	43					230		340		ICP-AES	[c]
Hypersil Lot 195	3818		58	48					187		345		ICP-AES	[c]
Kromasil	10								40		20		AAS	30
LiChrospher 60 RP Select B	190	<10				26	10		<5		7		ICP	31
LiChrospher Si-100	172		10	<5					48		150		ICP-AES	[c]
LiChrospher Si-100	130								420		300		AAS	30
LiChrospher Si-200	2900			NO	81	235	NO	NO	445	NO	1100	625	ICP-AES	29
Matrex	500								110		350		AAS	30
Nova Pak C18	380	18				47	160		57		25		ICP	31
Nucleosil 100-5	56			130	6	57	NO	NO	76	9	NO	NO	ICP-AES	29
Nucleosil 100-10	50								50		<10		AAS	30
Nucleosil 100-10	6	3	78	123	1	61	10	1	12		100	<1	Neutron activation	27
Nucleosil 100-30	250								110		30		AAS	30
Nucleosil C18	240	12				52	<5		9		10		ICP	31
Nyacol 2040	4404		3	2					69		107		ICP-AES	[c]
Partisil	15								75		60		AAS	30
Partisil ODS-1	23	7	79	216	2	246	4	2	8			<1	Neutron activation	27
Sephasil 120				NO	NO	30	20	10	40	1	30	NO	X-ray fluorescence	32
Spherisorb	5600								420		300		AAS	30
Spherisorb S5W	4220		22	40					303		128		ICP-AES	[c]
Supelcosil LC-18-DB	1050	65				48	58		94		120		ICP	31
Supelcosil LC-Si	2012		64	15					128		128		ICP-AES	[c]
Suplex pKb-100	1050	38				47	54		100		120		ICP	31

© 2004 by Marcel Dekker, Inc.

TSKgel ODS-80Ts	290	<10				<5	<5		8		<5		ICP	31
Vydac TP	4		63	444					<1		<1		ICP-AES	[c]
Vydac TPB-2030	30								45		10		AAS	30
YMC 120A-S5	4		9	<2					4		6		ICP-AES	[c]
Zorbax BP-SIL	20								80		60		AAS	30
Zorbax BP-SIL	37		4	<5					24		20		ICP-AES	[c]
Zorbax PSM-60	105			NO	NO	41	<25	115	68	245	NO		ICP-AES	29
Zorbax PSM-60, EDTA	NO			NO	NO	NO	NO	NO	NO	NO	NO	NO	ICP-AES	29
Zorbax Rx-C18	48	<10				<5	<5		13		<5		ICP	31

[a]Not observed.
[b]AAS = atomic absorption spectrometry; AES = atomic emission spectroscopy; ICP = inductively coupled plasma.
[c]R. Eksteen, unpublished results, 1986.

© 2004 by Marcel Dekker, Inc.

mass and biological activity, for metal binding proteins. Table 1 shows that the concentrations of sodium, calcium, iron, and aluminum vary greatly in commercial silicas. Note that the metal ion levels when measured by spectroscopic techniques represent bulk properties, not the levels present at the accessible silica surface. Deactivation procedures, such as the treatment of silica with strong acids or bases (28) or chelating agents (29), effectively remove metal ion impurities from the silica surface. The effect of surface treatments on the concentration of metal ion impurities is shown for Supelcosil LC-18-DB in comparison with that of untreated Supelcosil LC-Si. Metal ions present in Zorbax PSM-60 were removed by EDTA treatment (29). The reproducibility for the measurement of metal ions in silica by ICP-AES is excellent as demonstrated by the data from duplicate blind measurements for Lot 180 of 5 μm 120 Å Hypersil silica. The reproducibility of the manufacturing process is given for two lots of Hypersil (Lot 180 and Lot 195). Of course, the level of metal ions in a silica depends on that of the raw materials. For example, Table 1 also contains data for Nyacol 2040, a commercial silica sol of 20 nm nominal particle size, used in the manufacturing of HPLC-grade silicas.

2.2 Chromatographic Characteristics

The attributes of an SEC column packing material are listed in Table 2. As indicated, the support must be optimized with respect to specific resolution, efficiency, column pressure, and mechanical, chemical, and thermal stability. Recovery of mass and activity is particularly important in the analysis and purification of biopolymers. It also plays a role in the analysis of nonbiochemical synthetic polymers on silica-based SEC columns. In addition to recovery losses by adsorption, the recovery for both groups of polymers can also be reduced by polymer degradation as a result of, for instance, mechanical shear.

As explained elsewhere in this book, resolution in SEC can be expressed in terms of the peak standard deviation and the slope of the calibration curve. As in other HPLC modes, the efficiency of SEC columns can be improved by decreasing particle size. The relationship between column efficiency (or plate number N) and velocity can be expressed in dimensionless (reduced) parameters. The reduced plate height h is equal to the ratio of the height of a theoretical plate and the particle size as shown in Eq. (1). The reduced velocity v is equal to the product of the linear velocity $\langle v \rangle$ and particle size d_p divided by the solute diffusion coefficient D_m, as shown in Eq. (2).

$$h = \frac{H}{d_p} \tag{1}$$

$$v = \frac{\langle v \rangle \, d_p}{D_m} \tag{2}$$

© 2004 by Marcel Dekker, Inc.

Table 2 Characteristics of SEC Packing Materials

Attribute	Variable	Relationship	Typical range
Specific resolution	Particle size	$1/\sigma$	$R_{sp} = 1–5$[a]
	Pore size/pore volume	$1/D_2$	Porosity 55–80%[b]
Efficiency, HETP	Particle size	$\backsim dp^2$	5–20 μm
	Linear velocity	$\backsim\langle v\rangle$	0.4–1.0 mm/min
Column pressure	Particle size	Constant/dp_2	5–10 MPa
	Particle shape	Form factor Θ	$\equiv 1$ for spherical, $\simeq 2$ for irregular
Mechanical stability	Support type	Inorganic supports are in general more rigid; for all supports, the larger the pore size (and pore volume), the weaker the particle; at constant pore size and pore volume, particle strength decreases with size.	
Chemical stability	Support/bonded phase	Silica slowly dissolved above pH 7; enhanced stability possible from surface treatment or bonding reaction(s); most polymer-based matrices are stable up to pH 10 or higher, allowing high-pH column regeneration in biopurification and wider access to buffers, detergents, and chaotropic salts.	
Thermal stability	Support/bonded phase	Silica columns have few temperature limitations; when using polymer columns at $\geq 140^\circ$C, do not cool to ambient between high-temperature analyses to avoid resettling of the packet bed; most modern SEC packings can be sterilized.	
Recovery	Mass	Water-soluble biopolymers, synthetic polymers, and polyelectrolytes may adsorb on polymer- and silica-based columns depending on mobile-phase conditions.	
	Activity	Maintenance of biological activity (and mass recovery) for proteins depends on mobile-phase conditions, column type, and contact time.	

[a]According to $R_{sp} = 0.58/\sigma D_2$, specific resolution is inversely proportional to the product of the peak standard deviation σ and the slope of the calibration curve D_2. See page 103 of Ref. 8 for details.

[b]Pore size of commercial materials varies from very small to very large, depending on the application. For each pore size, the requirement for a large pore volume is balanced against the need for a pressure-stable particle. In a study of commercial silica-based SEC packings, the percentage of pore volume per particle varied from 55 to 80% (Ref. 33).

© 2004 by Marcel Dekker, Inc.

Experimental efficiency vs. velocity data can be fitted to any of a number of $h-v$ equations, of which the Knox equation (34) is the most widely used.

$$h = \frac{B}{v} + Av^{0.33} + Cv \tag{3}$$

The A, B, and C terms of Eq. (3) symbolize contributions to sample dispersion from the interparticle flow structure A, axial diffusion B, and finite rate of equilibration of the solute between mobile and stationary phases C. The values of the coefficients A, B, and C are obtained from curve fitting of experimental data to Eq. (3) for a sufficiently wide velocity range. For very good columns, $A = 0.5$, $B = 2$, and $C \simeq 0.05$ (35). Independent of particle size and solute molecular weight, h reaches an optimal value of 2–3 for a "well-packed" column, when v is in the range 3–5. For a given solute, the linear velocity at this optimum increases with decreasing particle size. For example, for a solute with a molecular weight of 200 ($D_m \simeq 1 \times 10^{-5}$ cm^2/s), a column filled with 5-μm particles provides the best efficiency when operated at a linear velocity of 0.6–1.0 mm/s.

The definition of linear velocity is based on the retention time for the first eluting component. In interactive modes of chromatography, linear velocity is calculated by dividing the length of the column by the retention time of an unretained (small) molecule that can freely access the total available pore structure. In SEC, linear velocity is based on the retention time of a totally excluded solute. Because the interparticle volume is about as large as the pore volume, the linear velocity in SEC $\langle v \rangle_{SEC}$ is roughly twice that in interactive modes when operating the column at the same flow rate. In other words, as in the preceding example, an SEC column filled with 5-μm particles provides the best efficiency for a 200 dalton molecular weight solute when $\langle v \rangle_{SEC}$ is 1.2–2.0 mm/s. Similarly, for a protein with a molecular weight of 100,000 dalton and a diffusion coefficient of 3×10^{-7} cm^2/s, the column efficiency is optimal when $\langle v \rangle_{SEC}$ is in the range 0.036–0.060 mm/s. In the remainder of this chapter $\langle v \rangle$ represents $\langle v \rangle_{SEC}$.

The analysis time in SEC is given by the retention time for an unretained small molecular weight solute. Thus, the optimal analysis time for analysing *small* molecular weight solutes on a well-packed 30 cm (5 μm) column is 5–8 minutes. For proteins, the optimal analysis time is 3–5 h, which necessitates the use of very low flow rates. These approximations are in agreement with the calculations of Guiochon and Martin (36), who predicted an optimum analysis time of 1.6 h at a reduced velocity of 10. Sjodahl first put this principle into practice for SEC of proteins by operating a 30 cm × 7.5 mm inner diameter (ID), 10 μm, TSKgel G3000SW column at a flow rate of 50 μL/min, as shown in Fig. 1 (37). Although excellent resolution is obtained during the 12-h analysis time, most users prefer to work at linear velocities of 0.4–1.0 mm/s to keep the analysis time below 30 minutes.

© 2004 by Marcel Dekker, Inc.

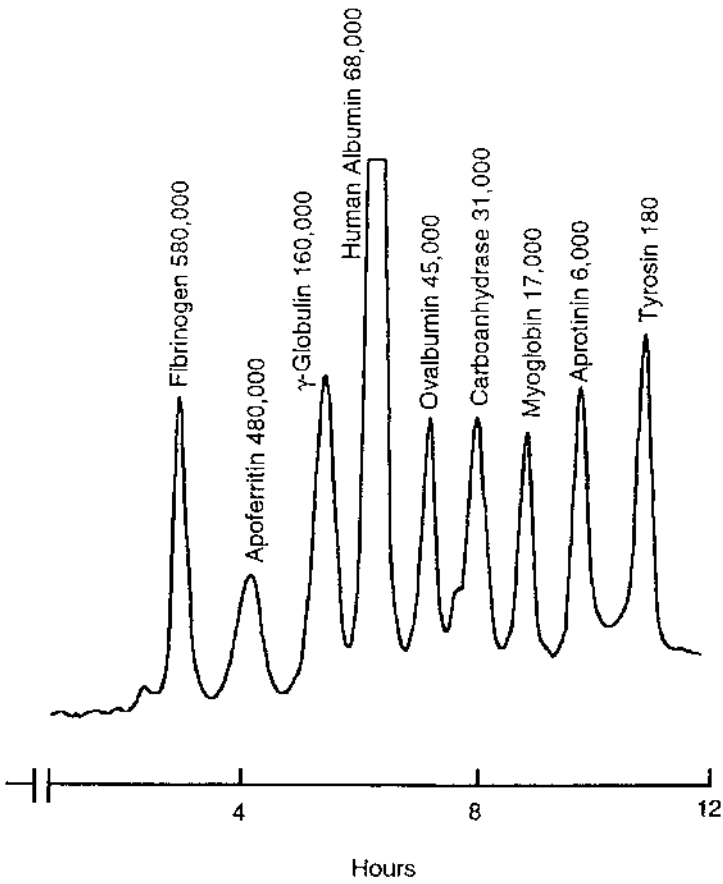

Figure 1 Analysis of proteins at very low flow rate. Column, TSKgel G3000SW, 10 μm, 60 cm × 7.5 mm; mobile phase, 0.1 M sodium dibasic phosphate, pH 6.8, +0.1 M sodium chloride; flow rate, 50 μL/min; detection, 280 nm, UV; temperature, 22°C; injection, 75 μL; sample, 5–10 μg each protein.

In terms of efficiency, an optimal packing material should exhibit high performance as well as the appropriate specific resolution, and the column backpressure should be low. The properties of silica gel that are important for its application as a SEC packing material are listed in Table 3. Also listed are the typical values and the range of values for each of the properties discussed here. Table 4 provides general data for controlled pore glasses, which have been used extensively for biopolymer analyses but are not available in particle sizes typically used for HPLC separations. Porous glass is produced from a ternary system of

© 2004 by Marcel Dekker, Inc.

Table 3 Properties of SEC Silica Gels

Property	Common values	Range
Particle size, μm	10	5–10
Particle shape	Spherical	Spherical, irregular
Pore size, Å	125, 250, 500	60–4000
Specific pore volume, mL/mL[a,b]	0.40	0.30–0.50
Pore volume, mL/g[c]	1.2	0.9–1.8
Interparticle porosity, %[a]	40	35–45
Particle porosity, %[a]	60	55–80
Surface modification	Diol	Diol-polyether

[a]Data from Ref. 33.
[b]Specific pore volume expressed as mL pore volume per mL column volume.
[c]Pore volumes (mL/g) of several commercial SEC silica gels.

Pore size (Å)	SW TSK-GEL	SW_{XL} TSK-GEL	Beckman	Bio-Rad
125	1.25	1.00	0.95	0.9
250	1.55	1.30	1.35	1.2
500	1.85	1.50	1.55	1.2

Source: Courtesy of Dr. Paul Shieh (Beckman) and Wai-Kin Lam (Bio-Rad).

silica (50–75%), sodium oxide (1–10%), and boric acid (to 100%), and such substances as alumina or lime are added to obtain better hydrolytic stability or larger pore sizes (38).

Silica and its bonded phases are characterized by a variety of techniques, including chemical, physical, spectroscopic, and chromatographic methods. A discussion of these techniques can be found in Refs. 39 and 40.

Table 4 Properties of Controlled Porosity Glasses for SEC

Property	BIORAN[a]	CPG[b]
Pore size, Å	300–4000	75–3000
Specific pore volume, mL/g	0.5–1.2	0.4–0.8
Specific surface area, m^2/g	10–300	7–340
Particle size, μm	30–250	37–177
Surface modification	Diol	Diol

[a]BIORAN: Schott Glaswerke BioTech, Mainz, Germany.
[b]CPG: for address see Ref. 21.
Source: Adapted from Ref. 38.

© 2004 by Marcel Dekker, Inc.

2.3 Particle Morphology

As mentioned, reducing particle size was crucial in making liquid chromatography a high-performance technique. Early in the development of HPLC, small silica particles were obtained by grinding and sieving larger silica gels used in the purification of natural products by open-column liquid chromatography. Once the potential of "high-pressure" LC had been demonstrated (41,42), columns packed with 10-μm irregularly shaped silica became readily available. Although such particles are still widely used in routine analyses, most analyses and column development work in academia and industry is performed with spherical 5-μm particles. In recent years, 5-μm particles have become widely available for gel filtration of proteins. The use of even smaller particle sizes in SEC has been advocated by Guiochon and Martin (36) and Engelhardt and Ahr (43), who investigated the optimum particle size for analysing proteins.

One of the main advantages of a column packed with spherical particles is that the pressure drop is lower by as much as a factor of 2 compared with a column packed with irregular particles of the same average size. Also, although the hardness of silica depends mainly on the size of the pores together with the pore volume per particle, there is some evidence for the widely held belief that irregular particles are more prone to breakage during the column-packing process (44). It is also considered more difficult to prepare a well-packed column with irregular particles (45). Particle shape does not influence the kinetic and thermodynamic properties that describe the chromatographic process.

The relationship between particle size and column efficiency is now well understood, although the exact form of the equations, including the Knox equation [see Eq. (3)], is still debated (46). The 3–5 μm particle size of modern HPLC columns allows fast analysis of small molecular weight compounds at near optimal column efficiency. As discussed, larger molecular weight compounds, because of their smaller diffusion coefficients, require much lower flow rates to elute with maximum column efficiency. Because of the usual variation in polymer molecular weight, it is not possible to operate the column at the optimal speed for all components in the sample.

2.4 Column Dimensions

A common internal diameter for an SEC column is 7.5 or 7.8 mm vs. 4.6 mm for non-SEC columns. The length of an SEC column has traditionally been 30 cm, but 60-cm columns have also been available for 10-μmm packings. Initial packing studies showing higher efficiencies for larger bore columns contributed to the choice of 7–8 mm as the internal diameter for most high-performance SEC columns (47,48). Advantages of such larger ID columns are (1) a reduction of the importance of extra column contributions to the volume of the sample band, (2) increased sample capacity for preparative purposes, and (3) the ability to

© 2004 by Marcel Dekker, Inc.

operate at a flow rate that can easily be maintained with the available HPLC instrumentation. Recent studies have demonstrated that capillary SEC columns can be packed with equivalent or higher efficiency than SEC columns of standard dimensions. An example is shown in Fig. 2, in which the efficiency of 28- and 50-μm ID columns were evaluated using bovine serum albumin (BSA), chicken ovalbumin, and bovine α-chymotrypsinogen as test solutes at linear velocities (based on a totally excluded solute) varying from 0.01 to 0.9 mm/s (49). The microcolumns were packed with 4.5-μm, 150 Å, Zorbax GF-250XL particles that were treated with a zirconium salt and derivatized with a diol functionality. The diffusion coefficients ($\times 10^{-7}$ cm^2/s) for these proteins, ranging in molecular weight from 69,000 to 43,000 and 26,000, were experimentally determined to be 5.65, 6.68, and 8.23, respectively. Note that the optimum reduced plate height was as low as 2 for BSA and as high as 4 for α-chymotrypsinogen. In all cases, the reduced velocity at h_{min} was approximately 5. As measured by the half-height method, the efficiency of a 30 cm × 50 μm ID column compared favorably with that of a standard 25 cm × 9.4 mm ID column filled with the same packing material, and the performance of the capillary column was much better when calculated by statistical moments or based on the Dorsey–Foley equation (50).

Because of the larger ID when operating a standard diameter SEC column at a flow rate of 1 mL/min, the linear velocity is 2.5 times lower than when the same flow rate is used on a 4.6-mm ID column. Thus, an SEC column is operated closer to the velocity at which the column performs at optimal efficiency. As discussed, however, at least a 10-fold drop in flow rate is required for the column to perform near its optimum for most proteins. This effect is illustrated in Fig. 3, in which a protein test mixture is separated at various flow rates on a 25 cm × 4.1 mm ID column packed with 10-μm, 250 Å, amide-bonded silica (51). Clearly, resolution improves with decreasing flow rate: the optimum efficiency had not yet been reached at a flow rate of 65 μL/min or a linear velocity at 0.13 mm/s.

According to Eq. (2), reduced velocity is inversely proportional to the solute diffusion coefficient. Under the same conditions, solutes of varying molecular weight show optimal column performance at different flow rates. This is illustrated in Fig. 4. The relationship between the logarithm of molecular weight (MW) and the otimal flow rate is plotted for 50 peptides and glycine (MW 50–10,000) analyzed under denaturing mobile-phase conditions (52). As shown, the optimal flow rate is inversely and linearly related to log MW. Over the narrow molecular weight range, the optimum flow rate decreases roughly 2-fold for a 10-fold increase in molecular weight.

2.5 Porosity

Except for nonporous particles, all packing materials contain a variation of pore sizes around a mean value. This pore size distribution determines the range of

© 2004 by Marcel Dekker, Inc.

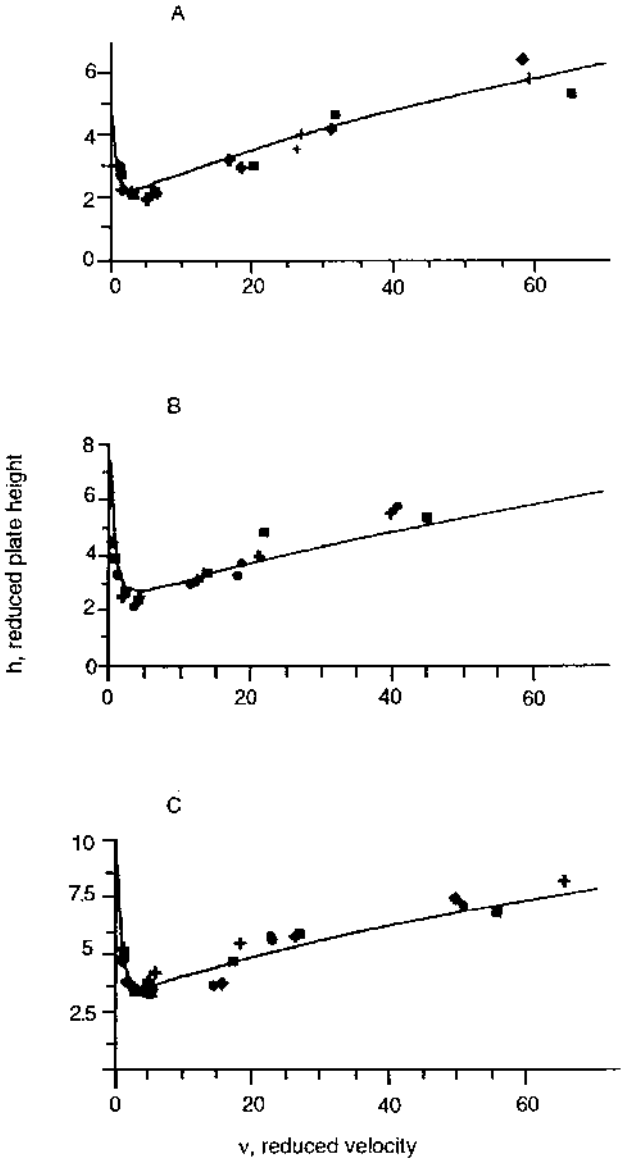

Figure 2 Column efficiency for 28 and 50 μm ID SEC columns. Column, Zorbax GF-250, 4.5 μm, 30 cm × 28 μm (pluses) or 50 μm (squares, diamonds, and circles); mobile phase, 0.25 M sodium sulfate and 0.1 M sodium phosphate, pH 7.0; linear velocity, 0.001–0.09 cm/s; detection, fluorescence, excitation 254 nm, emission 340 nm; sample (A) bovine serum albumin, (B) ovalbumin, (C) α-chymotrypsinogen A.

© 2004 by Marcel Dekker, Inc.

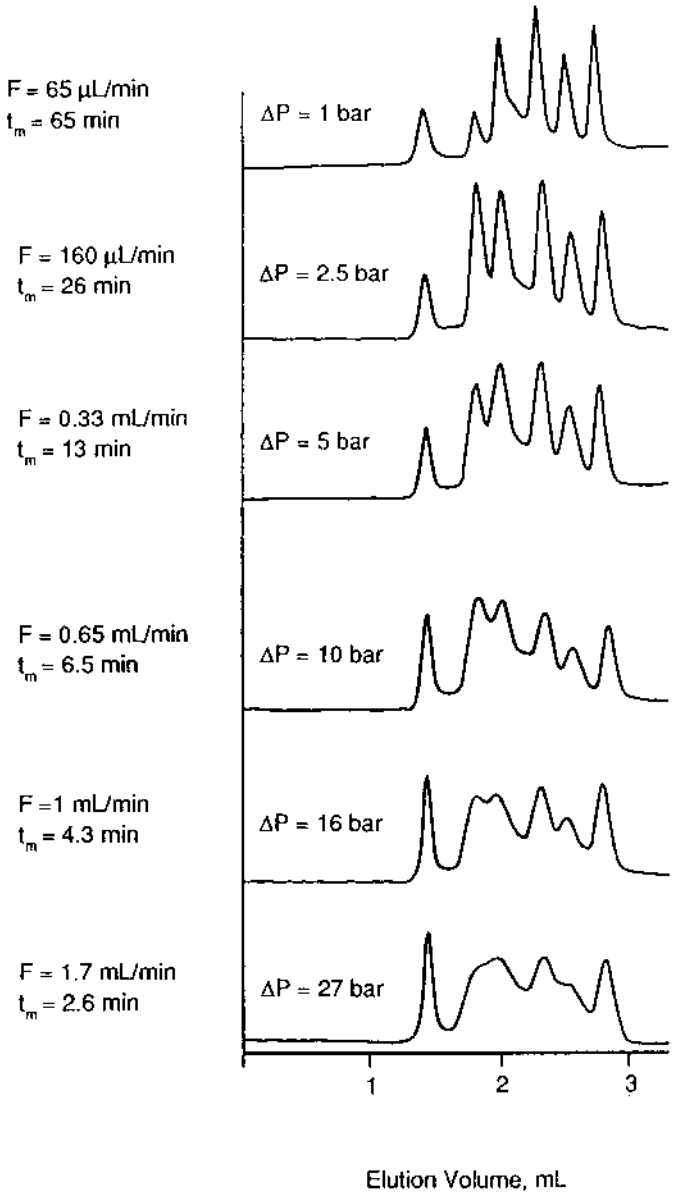

Figure 3 Efficiency of amide-bonded SEC columns as a function of flow rate. Column, amide-bonded Grace 250 A silica, 10 µm, 25 cm × 4.1 mm; mobile phase, 0.1 M Tris, pH 7, +0.4 M sodium chloride; detection, 280 nm, UV; elution order, thyroglobulin, alcohol dehydrogenase, conalbumin, myoglobin, cytochrome c, and dinitrophenylglutamic acid.

© 2004 by Marcel Dekker, Inc.

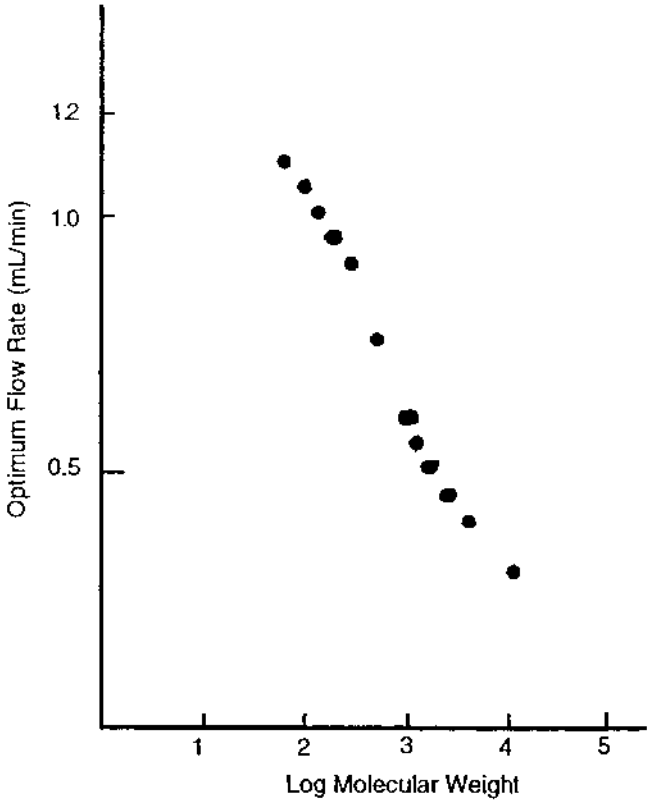

Figure 4 Optimum flow rate as a function of peptide molecular weight. Column, TSKgel G3000SW, 60 cm × 7.5 mm; mobile phase, 0.15 M phosphate, pH 7.4, +1 M sodium chloride, 20% methyl Cellosolve, and 1% SDS; detection, fluorescence, *o*-phthalaldehyde method (J Benson, P Hare. Proc Natl Acad Sci USA 72:619, 1979); temperature, 22°C; injection, 0.2 nmol peptide.

molecular weights that can be separated, and the available pore volume throughout the pore size distribution determines the quality of the separation. In general, the larger the volume of the pores per unit column volume, the better the resolution.

As shown in Eq. (4), the pore volume V_p is equal to the empty column volume V_C minus the sum of the interparticle or interstitial volume V_i and the volume of the solid particle matrix V_S.

$$V_p = V_C - (V_i + V_S) \tag{4}$$

The pore volume per unit column volume can be maximized by decreasing the interparticle volume and/or by decreasing the volume of the solid matrix. For

© 2004 by Marcel Dekker, Inc.

mechanically stable packing materials, such as silica, the interparticle volume occupies about 40% of the empty column volume. Irregular particles can give rise to larger interparticle volumes than spherical particles because of particle bridging (53), although V_i values as low as 35% of the column volume have been found, presumably caused by smaller particles fitting tightly between larger particles (54). Note that because silica is a rigid support, the interparticle volume cannot be reduced by deforming the particles, an approach successfully demonstrated by Hjerten and Liao for reducing the interparticle volume of soft gel agarose-composite particles (55).

The comparison of SEC columns that differ in length and diameter is simplified by converting the relevant volumes to porosities, dimensionless parameters defined in Eqs (5) to (8):

Interparticle or interstitial porosity

$$\epsilon_i = \frac{V_i}{V_C} \tag{5}$$

Intraparticle or internal porosity

$$\epsilon_P = \frac{V_P}{V_C} \tag{6}$$

Fraction filled by solid packing

$$\epsilon_S = \frac{V_S}{V_C} \tag{7}$$

Mobile-phase porosity

$$\epsilon_T = \epsilon_i + \epsilon_P \tag{8}$$

The mobile-phase porosity ϵ_T represents the fraction of the column occupied by the mobile phase between the particles and in the pores; it is readily calculated from Eq. (9):

$$\epsilon_T = \frac{4Ft_0}{\pi d_C^2 L} \tag{9}$$

where F is the flow rate, t_0 the elution time of an (unretained) small molecular weight molecule, and d_C and L are the column internal diameter and length. Also commonly used is the particle porosity ϵ_{SP}:

$$\epsilon_{SP} = \frac{V_P}{V_P + V_S} \tag{10}$$

Equation (10) can also be expressed as the ratio $V_{SP}/(V_{SP} + V_{SS})$, in which V_{SP} is

© 2004 by Marcel Dekker, Inc.

the specific pore volume (mL/g adsorbent) and V_{SS} is the volume of pure solid per gram. Equation (11) presents the relationship between particle porosity and internal porosity:

$$\epsilon_P = \epsilon_{SP}(1 - \epsilon_i) \tag{11}$$

The range for the interparticle porosity ϵ_i listed in Table 3 is largely based on data from Ref. 33. It was found that GFC columns packed with spherical particles have interparticle porosities ranging from 0.35 to 0.39, but columns packed with irregular particles showed V_i values as high as 0.47. These values are in reasonable agreement with earlier findings from Giddings (53), who reported ϵ_i values in the range 0.37–0.43. Experiments by the authors with spherical 5-μm, 100 Å pore size silicas have repeatedly found a value of 0.40 for the interparticle porosity and 0.75–0.80 for the mobile-phase porosity. Values as low as 0.34 for ϵ_i were measured when these silicas were more fragile and had mobile-phase porosities ϵ_T of 0.80–0.84. Examples of these two types of silicas are shown later. Engelhardt reported 0.42 for the interstitial porosity of solid glass beads and 0.80–0.88 for the mobile-phase porosity of totally porous supports (56).

For particles with very large pores, pore volume is sometimes sacrificed for mechanical stability. For example, when particles varying in pore size from 10 to 385 nm, but with nearly identical porosities, were subjected to pressure tests, those with the largest pore sizes collapsed at lower pressure drops (see Ref. 23, p. 174). Thus, the mechanical stability of larger pore size particles can only be maintained by reducing the pore volume. Alternatively, larger pore size particles must be slurry packed at lower pressures, thereby decreasing the stability and lifetime of the packed bed.

Chemical modification of the silica surface results in a loss of pore volume. Thus, the bonded phase layer must be optimized to reduce effectively interactions with silanol groups while minimizing the thickness of the bonded layer to avoid reducing the pore volume and preventing slow transport kinetics in the stationary phase. For example, the thickness of the stationary phase layer was estimated as 0.56 nm for a C3-alkyl functional group and 2.45 nm for C18-alkyl, assuming that the ligands stand upright on the surface (57). This assumption is thought to be correct under conditions that fully solvate the stationary phase layer, which is the case in GFC as well as GPC, in which the stationary and mobile phases have similar polar or nonpolar characteristics, respectively. Under such conditions, however, the bonded phase layer can be partially penetrated by the solutes and, thus, the loss of pore volume is smaller than expected based on the volume of the bonded-phase layer. Henry recently showed the shift in the pore diameter distribution for a polyethyleneimine phase with a layer thickness of 0.85 nm (26).

The average pore size of modern analytical HPLC packings is 100 Å, range 60–120 Å. Figure 5 shows the internal surface area vs. pore diameter for four

© 2004 by Marcel Dekker, Inc.

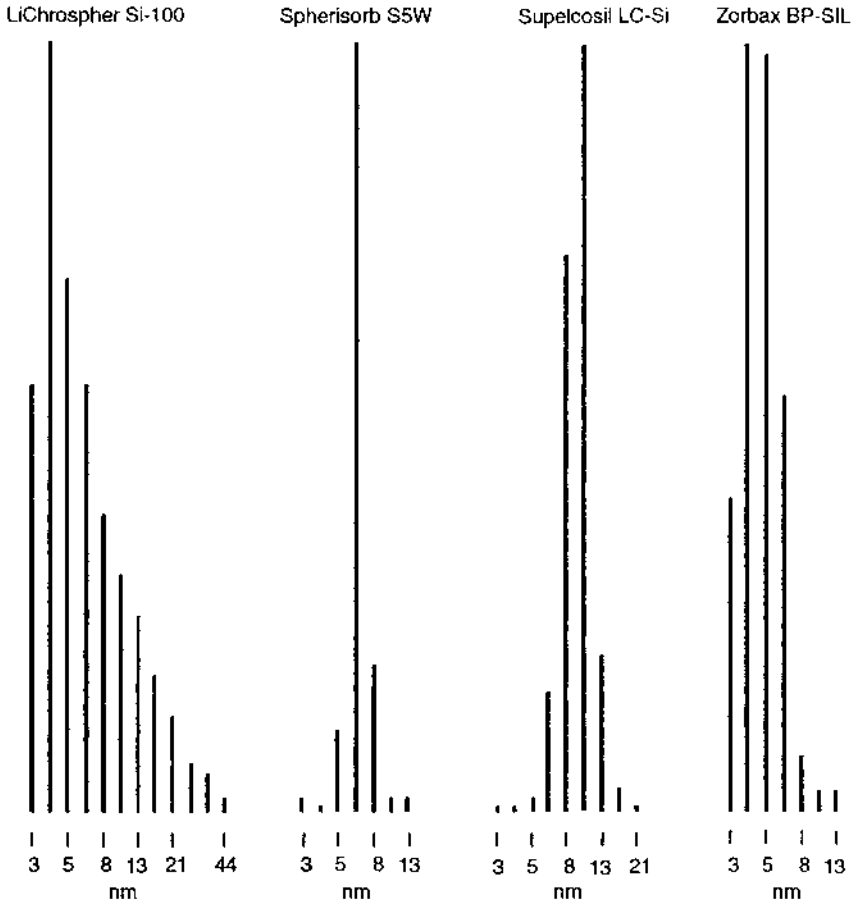

Figure 5 Pore size distributions of HPLC silicas. Internal surface area vs. pore diameter for four commercial 5-μm silicas were determined by mercury intrusion using Micromeritics Autopore II 9200 at pressures up to 60,000 psi (400 MPa). Packing materials, LiChrospher Si-100 (Lot 602F659316), Spherisorb S5W (Lot F5259), Supelcosil LC-Si (Lot 180-86), and Zorbax BP-Sil (Lot 20357-58).

commercial 5-μm silicas with pore sizes ranging from 60 to 120 Å as determined by mercury porosimetry (R. Eksteen, unpublished results, 1986). This technique can measure pore diameters down to 30 Å, which is the upper limit of the size range for micropores. Note that the data in Fig. 5 are biased toward the smallest pore sizes, which by virtue of their number can contribute significantly to the total surface area while representing a relatively smaller fraction of the total pore

© 2004 by Marcel Dekker, Inc.

volume. It is clear, however, that Spherisorb and Superlcosil have narrower pore size distributions than Zorbax and, particularly, LiChrospher.

The application of the silicas shown in Fig. 5 in SEC is demonstrated in Fig. 6, in which six narrow molecular weight polystyrene standards ranging from 4,480,000 to 890 dalton are separated on 15 cm × 4.6 mm ID columns packed with 5-μm LiChrosorb Si-100, Spherisorb S5W, Supelcosil LC-Si, and Zorbax BP-SIL, respectively (R. Eksteen, unpublished results, 1986). Toluene is included in the mix to mark the total inclusion volume. The calibration curves for the four silicas, as well as for Nucleosil 120-5 and YMC-GEL SIL 120A S5, are shown in Fig. 7. To simplify the comparison of the different packing materials, normalized retention volume $(V_E/V_i) - 1$, is plotted on the x-axis instead of elution volume. The normalized retention volume, which is zero for a totally excluded solute, is a direct measure of the retention of a compound beyond the interstitial volume.

It is evident from the chromatograms in Fig. 6 that of all the columns, LiChrospher provides the best separation for polystyrenes above 17,500 dalton molecular weight, followed by Supelcosil. LiChrospher is also the best choice for separations below 17,500 dalton molecular weight, followed closely by Zorbax. This last result is expected based on the large number of small pores that were measured for LiChrospher and Zorbax in Fig. 5. In support of the data shown in Fig. 5, the calibration curve for LiChrospher Si-100 in Fig. 7a also confirms the presence of pores much larger than 100 Å. In terms of the available pore volume, both the LiChrospher and the YMC silicas are considerably more porous than the other silicas shown in Fig. 7. Although this property is particularly attractive for their use in SEC, silicas with large pore volumes are more fragile, as shown later in this section. It is interesting to note that the interparticle porosity for both high pore volume silicas was only 34% of the empty column volume, but that of the other siicas was 40%. A low interparticle porosity can result when a silica has a broad particle size distribution such that the smallest particles can occupy the interparticle space between the larger particles. It is also possible that some particle fracturing took place during column packing. The backpressure for the LiChrospher column was about 25% higher than that for the more robust Spherisorb, Supelcosil, Nucleosil, and Zorbax columns, and the backpressure for the YMC column was twice as high. In comparison with the stronger silicas, the efficiency for the 15-cm LiChrosorb and YMC columns was about 7000 vs. 10,000 theoretical plates and the peak asymmetry factor was 0.6 vs. 0.9, respectively. Despite these lower values for the column performance parameters, it is clear from Fig. 6 that good overall peak shape and resolution were obtained for the polystyrene test mixture on the more fragile LiChrospher silica. Note also that all silicas shown in Figs 5 to 7 were primarily developed for analysing small molecular weight compounds. Although, as shown in Fig. 7, even small solutes are partially excluded from entering all pores, silicas with pores in the range

© 2004 by Marcel Dekker, Inc.

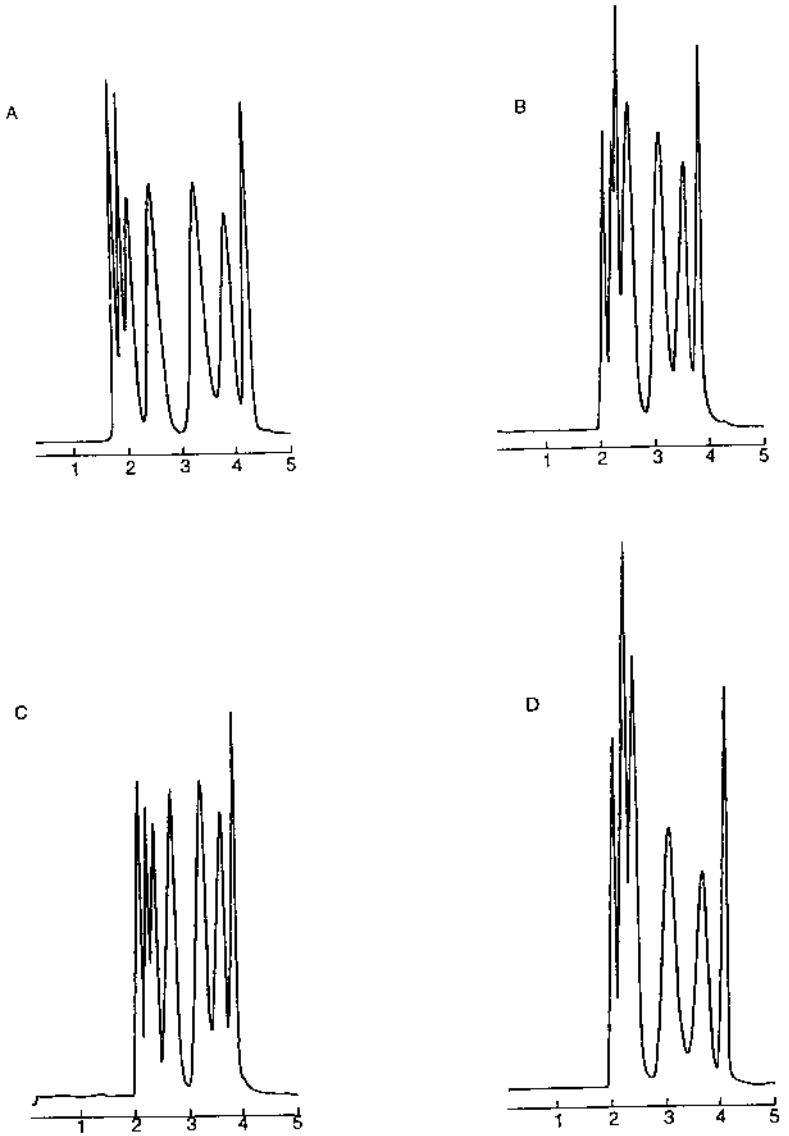

Figure 6 Separation of polystyrenes on small pore size silica columns. Columns LiChrospher Si-100 (A), Spherisorb SSWL (B), Supelcosil LC-Si (C), and Zorbax BP-Sil (D). Lot numbers as in Fig. 5, 15 cm × 4.6 mm; mobile phase, methylene chloride; flow rate, 0.5 mL/min; detection, 254 nm, UV; temperature, 35°C; sample, polystyrenes, MW 4,480,000, 450,000, 50,000, 17,500, 4000, and 890 dalton, and toluene (Ref. 91), time scale in minutes.

© 2004 by Marcel Dekker, Inc.

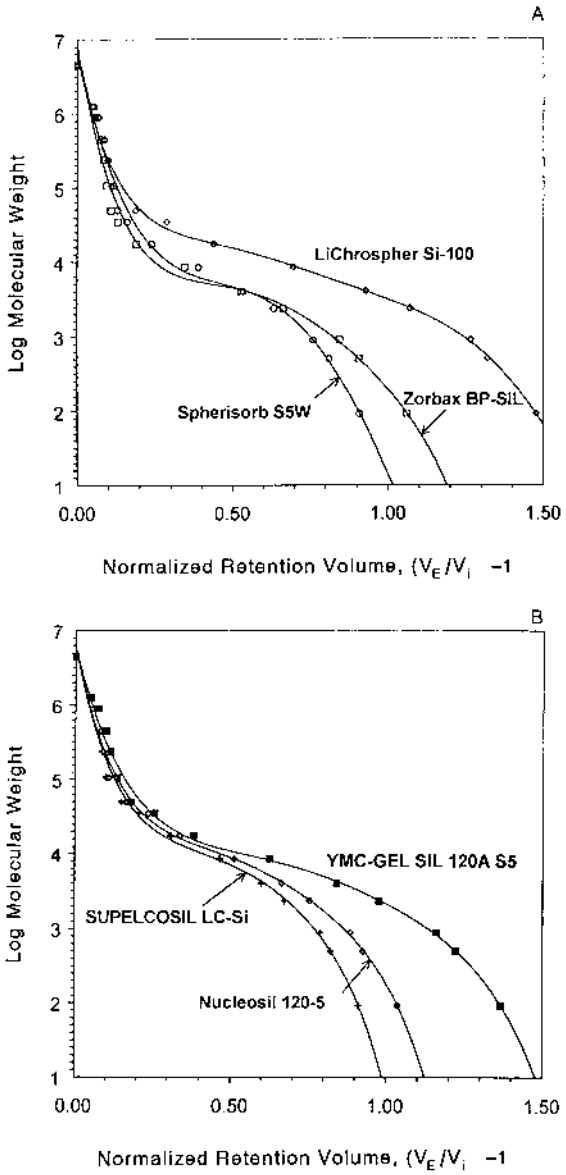

Figure 7 Polystyrene calibration curves for small pore size silicas. Columns, 5 μm, (A) LiChrospher Si-100, Spherisorb S5W, Zorbax BP-Sil, (B) YMC-GEL SIL 120A S5 (Lot 600327), Supelcosil LC-Si, and Nucleosil 120-5 (Lot 4101), 15 cm × 4.6 mm; sample, polystyrenes as in Fig. 6 plus MW 1,260,000, 240,000, 107,000, 35,000, 8500, 2350, and 500 dalton; other conditions as in Figs. 5 and 6.

© 2004 by Marcel Dekker, Inc.

60–120 Å are large enough to be fully accessible for the molecular weight range (below 2000 dalton) of most organic compounds analyzed by HPLC.

Unlike silica, polymer-based particles are readily available in smaller pore sizes. Small pore size silicas, such as Merck 40 or Davisil 20, are not commercially available in the 5–10 μm particle size range suitable for high-performance SEC. Syloid 63, a food additive produced by WR Grace, is an irregular 9 μm particle size silica with 22 Å pores and 0.4 mL/g pore volume. Its broad particle size distribution does not make it readily suitable for high-performance SEC of small molecules.

Table 5 lists two lines of commercially available silica-based gel permeation columns. The selection was limited to the Zorbax and LiChrospher silicas because these materials were specifically developed for gel permeation chromatography. Zorbax silica has a 6 μm particle size for optimum efficiency. The pore sizes were chosen such that a linear calibration curve is obtained when coupling columns of different pore sizes. In addition to plain silicas, Zorbax silicas are also available derivatized with trimethylchlorosilane, providing a surface that is less adsorptive for certain organic soluble polymers. Several important water-soluble industrial polymers, such as polyacrylamide, polyacrylic acid, and polyvinyl alcohol, do not require deactivation of the silica surface to obtain ideal size exclusion behavior. LiChrospher silicas are 10 μm in size; they vary in pore size from 100 to 4000 Å to allow the separation of very large polymers.

Table 6 summarizes the most well-known silicas used in gel filtration chromatography. Note that all the siicas are derivatized. The diol functionality, or some variation thereof, is the most widely used. Because most proteins have molecular weights well below 1 million dalton, they can be separated on silica-based SEC columns with pore sizes of 500 Å or less. Table 7 shows the fractionation ranges for globular proteins in common buffers and under denaturing conditions on TSK-GEL SW columns varying in pore size from 125 to 500 Å (58). Table 7 also shows the fractionation ranges for double-stranded DNA fragments (59). Note that globular proteins are more compact in solution than double-stranded DNA fragments. Using acrylic-based TSK-GEL PW_{XL} columns, DNA fragments of up to 10 times this size can be separated (60).

2.6 Surface Area

Independent of other qualities, surface area is a crucial parameter in the development of an adsorbent because it determines its capacity for purifying or drying chemicals or for catalyzing a reaction. In contrast to the techniques used in interactive chromatography or catalysis, an ideal size exclusion support is not chemically or physically attractive to any sample component. Size exclusion requires the presence of pores, and thus surface area is still a critical factor in the design of SEC packing materials. A discussion of hydrodynamic size exclusion

© 2004 by Marcel Dekker, Inc.

Table 5 Selected Silica-Based Columns for Gel Permeation Chromatography

Column description	Supplier/ manufacturer	Stationary phase	Dimensions (cm × mm)	Particle size (μm)	Pore size (Å)	Exclusion limit (polystyrenes)
Zorbax	Mac-Mod	C_1, also silica	25 × 6.2	6	60	1×10^4
PSM-60					300	3×10^5
PSM-300					1000	1×10^6
PSM-1000						
LiChrospher	Merck	Silica	25 × 4	10	100	PEG[a]: 1×10^4
Si 100				10	300	7×10^4
Si 300				10	500	4×10^5
Si 500				10	1000	1×10^6
Si 1000				10	4000	1×10^7

[a]Polyethylene glycol.

© 2004 by Marcel Dekker, Inc.

Table 6 Selected Silica-Based Columns for Gel Filtration Chromatography

Column description	Supplier/ manufacturer	Stationary phase	Dimensions (cm × mm)	Particle size (μm)	Pore size (Å)	Exclusion limit (proteins)
UltraSpherogel	Beckman	Polyether				
SEC 2000			30 × 7.5	5	140	2.5×10^5
SEC 3000				5	230	7×10^5
SEC 4000				5	350	2×10^6
Bio-Sil	Bio-Rad	—				
SEC 125			30 × 7.8	5	125	6×10^4
SEC 250				5	250	3×10^5
SEC 400				5	400	1×10^7
Zorbax	Mac-Mod	Diol on				
GF-250, 250XL		Zr-clad	25 × 9.4	6, 4	150	4×10^5
GF-450, 450XL		silica		6, 4	300	9×10^5
LiChrospher	Merck	Diol				
Si 100 DIOL			25 × 4	10	100	PEG, 1×10^4
Si 300 DIOL				10	300	7×10^4
Si 500 DIOL				10	500	4×10^5
Si 1000 DIOL				10	1000	1×10^5
Si 4000 DIOL				10	4000	1×10^7
Protein-Pak	Waters	Diol				
Protein-Pak 60			30 × 7.8	—	60	2×10^4
Protein-Pak 125				—	125	8×10^4
Biosep-SEC	Phenomenex	—				
S2000			30 × 7.5	5	145	3×10^4
S3000				5	290	7×10^5
S4000				5	500	2×10^6

© 2004 by Marcel Dekker, Inc.

SynChropak	SynChrom	Diol				K_D 0.2–0.8
GPC Peptide			25 × 4.6,	5	50	3.5×10^4
GPC100			30 × 7.8	5	100	1.6×10^5
GPC300				5	300	1×10^6
GPC500				7	500	1×10^6
GPC1000				7	1000	1×10^7
GPC4000				10	4000	—
TSKgel	Tosoh/	Glycol ether				
2000SW and SW_{XL}	TosoHaas,		SW: 30, 60 × 7.5	10, 5	130	1×10^5
3000SW and SW_{XL}	Supelco,		SW_{XL}: 30 × 7.8	10, 5	240	5×10^5
4000SW and SW_{XL}	others			13, 8	450	7×10^6

© 2004 by Marcel Dekker, Inc.

Table 7 Separation Ranges for Polymers on TSK-GEL SW Columns

Sample and mobile phase	TSK-GEL G2000SW	TSK-GEL G3000W	TSK-GEL G4000SW
Polyethylene glycol, water	500–15,000	1,000–35,000	2,000–250,000
Dextran, water	1,000–30,000	2,000–70,000	4,000–500,000
Globular proteins[a]			
Common buffers[b]	5,000–100,000	10,000–500,000	20,000–7,000,000
6 M guanidine–HCl[c]	1,000–25,000	2,000–70,000	3,000–400,000
0.1% SDS[d]	15,000–25,000	10,000–100,000	15,000–30,000
Common buffers[e]	$<30{,}000$	30,000–500,000	$>500{,}000$
6 M guanidine–HCl[e]	$<10{,}000$	10,000–70,000	$>70{,}000$
0.1% SDS[e]	—	$<60{,}000$	$>60{,}000$
RNA[f]	70,000	150,000	1,500,000
DNA[g]	50,000	100,000	300,000

[a]Data from Ref. 58.
[b]Examples: 0.05 M sodium phosphate buffer (pH 7.0) containing 0.3 M NaCl, or 0.05 M Tris–HCl containing 0.2 M NaCl, or 0.2 M disodium (or dipotassium) hydrogen phosphate and 0.2 M sodium (or potassium) dihydrogen phosphate.
[c]Guanidine hydrochloride (6 M) in 0.1 M sodium phosphate, pH 6.0.
[d]Aqueous sodium dodecyl sulfate (0.1%) in 0.1 M sodium phosphate, pH 7.0.
[e]Optimum separation range.
[f]Exclusion limit in 0.1 M phosphate buffer (pH 7.0) containing 0.1 M NaCl and 1 mM EDTA (Ref. 59).
[g]Exclusion limit for double-stranded DNA in mobile phase listed in Note d (Ref. 59).

chromatography, in which polymer particles are separated by size on the external surface of the (porous or nonporous) particles, falls outside the scope of this chapter (61).

The surface area of a 60 Å silica is approximately 500 m^2/g; that of a 500 Å silica is about 50 m^2/g. The packing density of silica, although dependent on the type, is approximately 0.5 g/mL. Thus, a 25 cm × 4.6 mm column contains about 2 g silica, which, depending on the pore size, has a surface area of from 100 to 1000 m^2. Equation (12) shows that surface area is inversely proportional to pore diameter (see Ref. 23, p. 37):

$$D_P = 4 \times 10^3 \frac{V_{SP}}{S_{BET}} \tag{12}$$

where D_P is the mean pore diameter (nm), V_{SP} is the specific pore volume (mL/g), and S_{BET} is the surface area (m^2/g). In theory, pore volume does not change when preparing silicas of different pore diameter by the same procedure. As discussed, the relationship between pore size and surface area is at best approximate because a balance must be struck between particle strength and pore volume. Given the

© 2004 by Marcel Dekker, Inc.

same pore volume, large-pore particles are more brittle than those with small pores. Operation under HPLC conditions requires that the particles withstand the high pressures required for packing. Although small-particle SEC packings are usually operated at low linear velocity, silica-based columns must be packed at relatively high pressures to ensure physical stability of the column. Figure 8 shows the results of a simple test to determine the pressure at which particles fracture (62). The experiment was performed with a constant pressure pump. After filling the column for 5 minutes at 3000 psi, the pressure was increased in 1000 psi increments to 12,000 psi, at which point the hysteresis was determined by lowering the pressure to 4000 psi. Note that the relationship between flow rate and pressure for 100 Å Supelcosil LC-Si silica is linear over the entire pressure range, but that the pressure–flow rate curve for LiChrospher Si-100 starts to deviate from linearity at 6000 psi. Flow rates at higher pressures are lower than expected, and

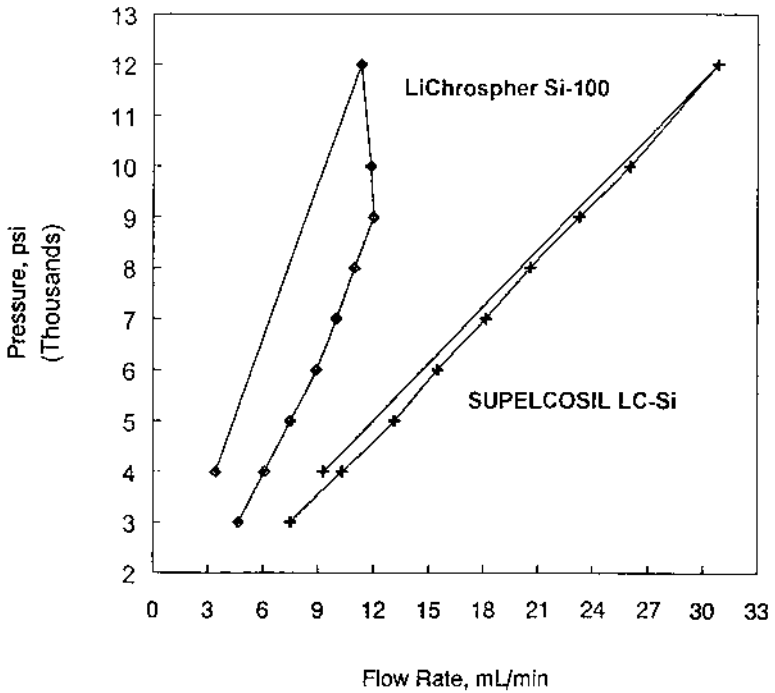

Figure 8 Stability of HPLC silicas during column packing. Packing materials, 2.25 g of 5 μm Supelcosil LC-Si and 1.35 g of 5 μm LiChrospher Si-100; columns, 15 cm × 4.6 mm; extension, 10 cm × 4.6 mm; slurry reservoir, 35 mL; Haskel pneumatic amplifier Model DSTV-122C; slurry and driving solvent, methanol; see text for details.

© 2004 by Marcel Dekker, Inc.

the decline in permeability is permanent. Similar results (not shown) were found for YMC-GEL 120A silica, which started to deviate from linearity at 5000 psi. It was shown earlier that the pore volumes of LiChrospher Si-100 and YMC-GEL SIL 120A S5 were considerably higher than that for Supelcosil LC-Si. A standard procedure to strengthen silica is to sinter the particles at high temperature (23,63). As a result, the distribution of the pores shifts toward larger sizes, and if performed in the presence of a high-melting salt, pore volume can be maintained.

2.7 Silanol Groups

The strong affinity of silica toward polar solutes, which makes it an excellent choice as an adsorbent in adsorption chromatography, is responsible for it being a less than ideal column packing material for size exclusion chromatography. The amorphous nature of silica is reflected in the random distribution of various chemical structures on the surface, as shown in Fig. 9 (23). Free silanols are isolated from other hydroxyl groups by an O—O bond distance larger than 0.30 nm, that is, the average bond distance between two hydrogen-bonded silanol groups. Vicinal and geminal silanols are not commonly discriminated and are referred to as *bound silanols*. Because silica is hydroscopic at room temperature, it contains physically adsorbed water. Heating under vacuum at 473 K for several hours drives off most of this water. At higher temperatures, however, condensation of bound silanols results in the formation of *siloxane bonds.* The total concentration of silanol groups (free and bound) on silica is about 8 $\mu mol/m^2$. Of these groups, the free silanol groups constitute the premier adsorption and reaction sites. The bound silanol groups play a secondary role in the adsorption process.

It is well known in HPLC that silica-based packings have two important shortcomings: the silica matrix is not stable at alkaline pH, and most silane-bonded phases can be cleaved at a pH below 2. After chemical modification, approximately 4 $\mu mol/m^2$ of silanol groups remains unbonded. These residual silanol groups are negatively charged above pH $\simeq$ 3 and, when accessible, may interact with positive charges on a polymer surface. Because of the use of organic solvents in GPC, chemical stability of the silica is not a concern. The limited stability at high pH, however, is a potential problem in GFC. In general, proteins are most stable at pH 7–8, which is the upper limit of the accepted pH range for silica-based packing materials. By removing metal impurities in the starting material, several manufacturers have been able to produce highly purified silicas, although it is not yet clear whether ultrapure silica particles have the same chemical stability as standard silica particles. Taking the opposite approach, silica particles when covered with 1 $\mu mol/m^2$ of zirconium oxide before performing the diol bonding reaction, allowed extended operation at pH 8 or greater without degrading the column performance (64). An alternative approach involves the preparation of polymerized bonded phases. The bonded layer makes the $\equiv$Si—O—Si bond less

© 2004 by Marcel Dekker, Inc.

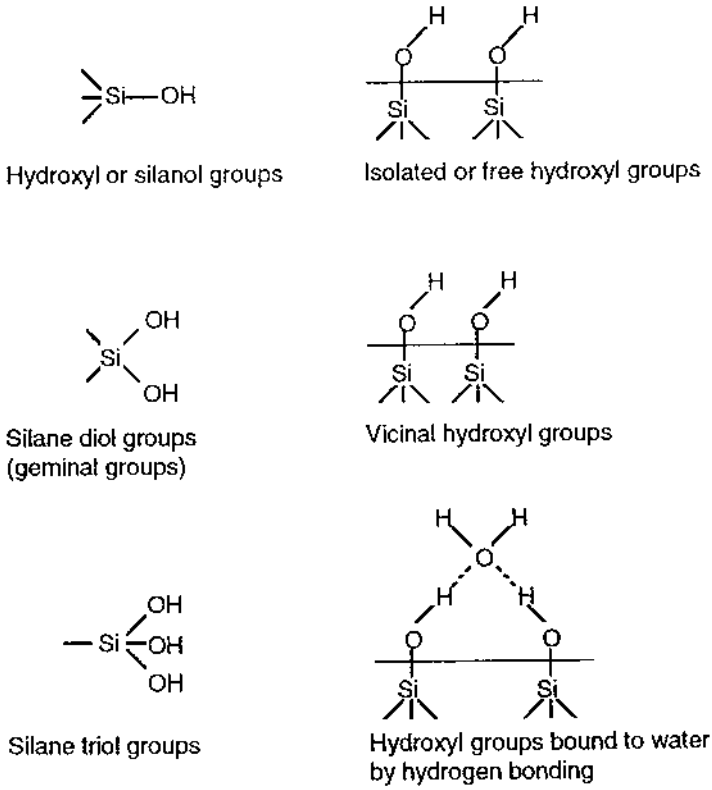

Figure 9 Silanol groups on silica surface.

accessible to nucleophilic attack, and it requires cleavage of multiple bonds to cause loss of bonded phase. The performance of polymer bonded or encapsulated phases have been reported for a C18-silicone polymer bonded to high-purity silica (28), but this approach has not been extended to the development of silica-based SEC packing materials.

2.8 Deactivation

The use of mobile-phase additives to deactivate silanol groups is the most practical way to make them inaccessible to solute molecules. This approach is based on the well-known observation from adsorption chromatography that the activity of silica gel is strongly dependent on the presence and amount of water in a (largely) nonaqueous mobile phase. Thus, in adsorption chromatography, the retention of

© 2004 by Marcel Dekker, Inc.

sample components can be varied by adjusting the amount of water in the mobile phase. (Because sometimes a variation of as little as 10 ppm water can make the difference between a good separation and no separation at all, alcohol is frequently used to modify retention, which requires a larger volume and is thus easier to control.)

Early successful attempts at reducing the activity of silanol groups on porous glass supports included the use of mobile-phase modifiers (65) and coating the surface with 20,000 dalton polyethylene oxide (66). A more permanent way to deactivate silanol groups is to convert them through chemical reaction. Regnier and Noel (5) first demonstrated that by reacting controlled porosity glass beads with glycidoxypropyltrimethoxysilane, followed by opening the epoxide ring under acid conditions, resulted in a hydrophilic surface suitable for analysis of proteins, nucleic acids, and polysaccharides by a size exclusion mechanism. Other examples of modifications are discussed here.

2.9 Chemical Modification

As mentioned in the introduction, the explosive growth of HPLC would not have taken place without the recognition that instead of coating the stationary phase to the silica surface, a permanent bonded phase would do away with some important limitations of physically held phases (67–69). Among these limitations were slow equilibration, decreasing retention as a function of time, and the inability to inject samples dissolved in solvents that were miscible with the stationary phase. Early investigations in bonded phase synthesis (68,69) employed esterification of surface silanols to form a $\equiv$Si—O—C bond, which, however, was found to hydrolyse in aqueous solutions (70). It was replaced by the silylation reaction, leading to the formation of the more stable $\equiv$Si—O—Si—C bond (71). Initial bonded phase columns did not have the required physical stability and reproducibility of retention and selectivity. Development of improved packing and bonding procedures (72–74) corrected these weakenesses, resulting in the design of reliable, automated HPLC-based analysers (75).

It is interesting to note that the first prepared HPLC bonded phase, named C18 after the octadecylsilane bonding reagent, soon became the most popular column type. According to a 1991 survey, this continues to be the case today with almost half of all HPLC analyses being performed on this column type (76). Chemical modification of the silica surface with long-chain alkyl groups creates a nonpolar, hydrophobic surface that interacts with sample molecules through weak dispersion (van der Waals) forces. Retention is in direct proportion to the hydrophobic surface area of the molecule, and elution is accomplished with a mobile phase consisting of a mixture of water and an organic solvent, such as methanol or acetonitrile. The use of an aqueous mobile phase has greatly simplified the injection of samples studied in the life and food sciences and related

© 2004 by Marcel Dekker, Inc.

industries (particularly the pharmaceutical industry), as well as in the chemical industry. Because the polarities of the mobile and stationary phases were the opposite of those in adsorption chromatography, this mode of liquid chromatography is generally referred to as reversed phase LC.

Several polar bonded phases were developed based on the same bonding chemistry used to prepare C18, C8, and other alkyl bonded phases. Cyanopropyldimethylchlorosilane, 1,2-epoxy-3-propoxypropyltriethoxysilane, and aminopropyltriethoxysilane were reacted to obtain cyano, diol, and amino polar bonded phases, respectively. The cyano phase is a weaker adsorbing surface than plain silica, but it shares the benefit of bonded phases in that equilibrium is reached within minutes and retention is not strongly affected by traces of water in the mobile phase. Because of the presence of the propyl anchor group, the cyano phase has also been used as a weak alkyl bonded phase with aqueous/organic mobile phases. Under such conditions, the cyano group imparts special polar selectivity, such as seen in the analyses of tricyclic antidepressants and PTH (phenylthiohydantoin) amino acids. The amino phase has mainly been applied to the analysis of carbohydrates using water/acetonitrile mobile phases. The separation mode resembles adsorption (normal phase) chromatography in that an increase in the percentage of water decreases retention. Although the diol phase has been applied as a substitute for silica in the analysis of steroids, for example, its main use has been as a support in gel filtration chromatography, as discussed later in more detail. Columns packed with cyano, amino, or diol bonded phase silica are more popular in adsorption chromatography than plain silica columns (76).

Figure 10 shows the type of chemistry for the preparation of the diol bonded phase, the usefulness of which was first demonstrated for SEC by Regnier and Noel (5). The 1,2-epoxy-3-propoxypropyltriethoxysilane reagent is bonded to the silica following a reaction in toluene at 120°C for 12 h. After a washing step, the epoxide ring is opened by heating the bonded silica in strong acid for 1 h. In aqueous mobile phases, unreacted ethoxy groups are converted into silanol groups that can contribute to extra retention and adsorption effects. The bonding chemistry shown in Fig. 10 for preparing GFC phases is similar to the standard procedures for preparing deactivated phases for GPC. In this case, trimethylchlorosilane is bonded with silica in the presence of toluene as a solvent. Usually the reaction is repeated to maximize the coverage of trimethylsilyl groups. This "end-capping" step is also used as a second reaction in the preparation of reserved-phase packing materials but is not common for most polar bonded phases.

The diol functional group has been commercialized by several manufacturers (see Table 6), but other functional groups are worth mentioning. Engelhardt and co-workers have investigated the properties of, in particular, the amide bonded phase, which is prepared by reacting *N*-(3-triethoxysilylpropyl) acetamide with silica under similar conditions as used for the diol phase (51,77).

© 2004 by Marcel Dekker, Inc.

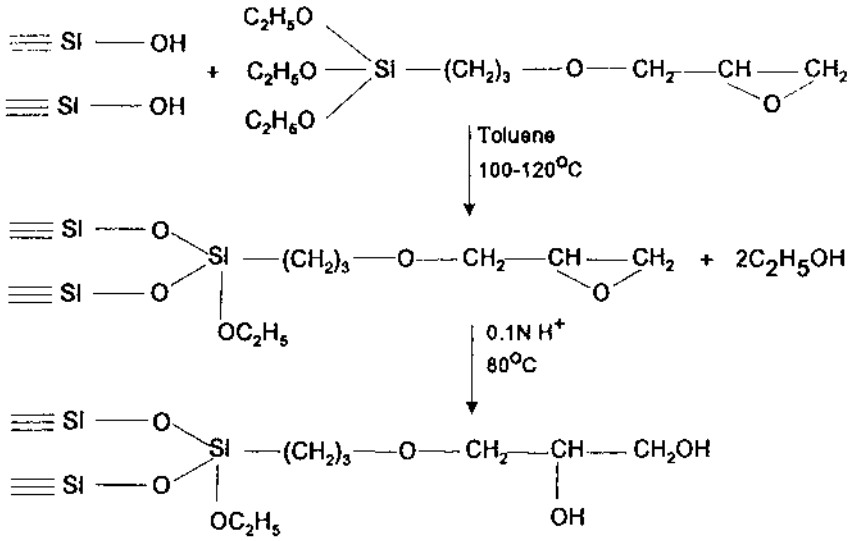

Figure 10 Diol bonding reactions.

In a related paper, the same authors demonstrated the fractionation of milligram quantities of polypeptides and proteins up to 50,000 dalton molecular weight, with excellent recovery of biological activity on amide columns prepared from LiChrosorb Si-100 silica (78). Miller *et al.* (79) synthesized an ether bonded phase of the general formula $\equiv Si-O-Si(CH_2)_3-O-(CH_2-CH_2-O)_n-R$, where $n = 1$, 2, or 3 and R = methyl, ethyl, or *n*-butyl. Resulting phases allowed the separation of proteins under hydrophobic interaction or SEC conditions. Functional groups were bonded to the silica as trialkoxysilane reagents. The reaction was performed in the presence of water to control the formation of a bonded phase network that is more stable in aqueous solutions than those produced from di- or monofunctional silanes (80). When operated in the SEC mode, an ether bonded phase column showed stable elution volumes for basic proteins in high ionic strength (0.5 M ammonium acetate, pH 6.0) mobile phase after flushing the column for 40,000 column volumes. At low ionic strength (0.05 M ammonium acetate, pH 6.0), the retention of lysozyme increased 2-fold during the same experiment. Recently, Poppe and colleagues discussed the inertness and stability of a maltose stationary phase (81). Effective shielding of the silica surface was obtained by reacting maltose to aminopropyl bonded silica. Stability against hydrolysis greatly improved by using acid-washed silica, by adding a small amount of water to the silica before bonding with aminopropylsilane, and by polymerizing the glucose units in the maltose groups

© 2004 by Marcel Dekker, Inc.

at 100°C under vacuum. The hydrophilic nature of the "polymaltose" phase allowed the exclusion of all but the most basic proteins. The chemistry of the popular TSK-GEL SW columns has not been described in the open literature. The SW stationary phase has been referred to as a "glycol ether-type bonded phase" similar in nature to the diol phase (82), containing the structure $-CH_2C(OH)HCH_2O-$ (14).

3 CALIBRATION

As mentioned in the introduction, in high-performance gel filtration chromatography, silica- rather than resin-based packing materials are more widely used for biopolymer separations. This is true for peptides, proteins, and possibly also for nucleic acids, although size exclusion is not a common technique for determining the molecular weight or for isolating this class of compounds. Polymer-based packings are the material of choice for most other water-soluble polymers, including oligo- and polysaccharides and the many examples of natural and synthetic polymers discussed in other chapters.

GPC is routinely used for determining the average molecular weight of an organic soluble polymer and the distribution of the molecular weights around this mean. Although desirable, it is often not possible to obtain a reliable value for the molecular weight of a protein by GFC. Despite elaborate bonding procedures, all available silica-based (and polymer-based) packings show some deviation from ideal size exclusion behavior for proteins. Unreacted and accessible silanol groups are responsible for secondary retention mechanisms, resulting in inaccurate MW estimates. This section discusses calibration curves for proteins and other biopolymers. A review of the various parameters responsible for nonideal elution behavior follows.

Under ideal SEC conditions, all solutes elute at a retention volume V_E that is larger than the interparticle volume V_i but smaller than the mobile-phase volume V_T (which is the sum of V_i and the pore volume V_P). The distribution coefficient K_D for elution by ideal SEC is given by Eq. (13), in which K_D varies from zero for a fully excluded solute to 1 for a small molecular weight solute capable of penetrating all the pores:

$$V_E = V_i + K_D V_P \tag{13}$$

The selectivity curve of a packing material is obtained by plotting the elution volume, or some function of V_E, vs. an expression of the solute size. It is known that the size for a random coil of a linear polymer is correlated with its molecular weight. Thus, for polystyrene standards of known molecular weight, a unique pore diameter can be assigned at which the polymer is excluded from the pores of a packing material. With dextrans, the relative volume of the random coil is smaller

© 2004 by Marcel Dekker, Inc.

because of the higher relative molecular mass per unit chain length. As a result, dextrans possess larger elution volumes than polystyrenes of identical molecular weights. Proteins, more dense than random coils, elute as even "smaller" molecules, and their calibration curves are displaced from polystyrene and dextrans of the same molecular weight. Figure 11 (83) shows this effect for calibration curves of polyethylene glycols, dextrans, and proteins on TSK-GEL SW columns containing spherical 10-μm particles with pore sizes of 130 Å (G2000SW), 240 Å (G3000SW), and 450 Å (G4000SW). The data in Fig. 11 emphasize that calibration should occur with standards possessing the same shape and hydrodynamic volume characteristics as the solute.

Several references have outlined the various methodologies for obtaining correct calibration curves (8,17,18,45,84,85). The simplest is the *peak position calibration* method. It can be used for macromolecules that have a unique molecular weight (such as proteins) or a narrow distribution of molecular weights. The logarithm of the molecular weight for a series of known molecular weight standards ($M_W/M_N \leq 1.1$, where M_W and M_N are the weight- and number-average molecular weights) is plotted vs. their elution volumes. In the

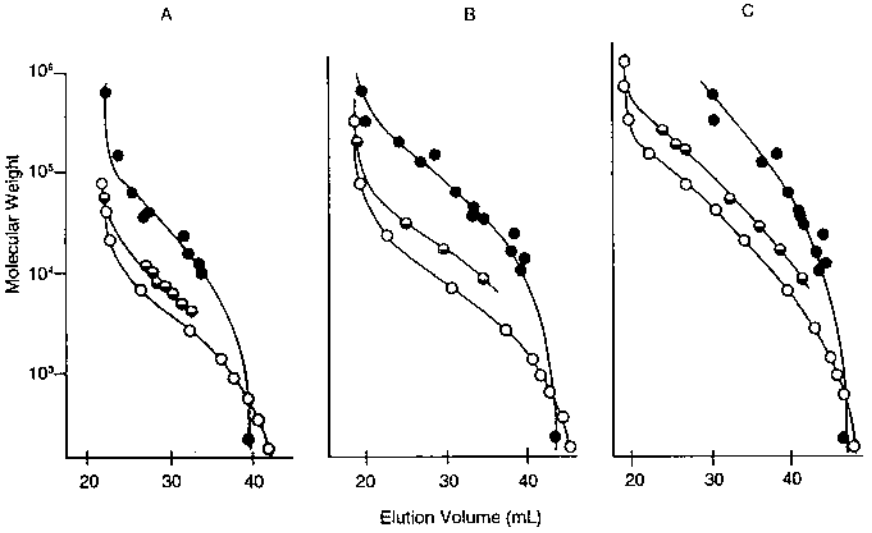

Figure 11 Calibration curves for proteins (closed circles), polyethylene glycols (open circles), and dextrans (half-closed circles). Columns, TSKgel SW, 10 μm, 60 cm × 7.5 mm, two in series. (A) G2000SW, (B) G3000SW, (C) G4000SW. Mobile phase, proteins: 0.1 M phosphate, pH 7, +0.3 M sodium chloride; dextrans and polyethylene glycols: distilled water; flow rate, 1.0 mL/min; detection, 220 nm, UV.

© 2004 by Marcel Dekker, Inc.

absence of secondary (i.e., non-SEC) retention mechanisms, the resulting calibration curve is the well-known S-shaped curve containing a linear portion. Thus, a column is selected for which the solutes of interest elute on the linear portion of the curve. This method requires narrow distribution standards and samples that have the same molecular conformation as the standards. Without appropriate standards, the calculated molecular weight for an unknown can be in error by a factor of 2 or 3 and up to an order of magnitude under the most unfavorable conditions (45).

The effect of pore diameter upon K_D values for globular proteins was investigated by Gooding and Hagestam Freiser (11). For the same protein, the K_D value was approximately 0.2 units lower on a 100 Å material vs. a 300 Å material. The slope of the linear portion of the calibration curve indicates the homogeneity of the pore structure. The smaller the slope, the more pores there are of the same size and the higher the potential for resolution of two solutes with similar molecular weight (10, 19,33). The steeper the slope, the larger the variety of pores of different size and the broader the range of molecular weights that can be separated.

When no narrow molecular weight distribution standards are available, then the *single broad standard calibration* or integral molecular weight distribution method provides the most accurate molecular weight measurements. Reference 8 outlines this method, which requires knowledge of the complete molecular weight distribution [i.e., weight- (M_W) and number-averaged (M_N) molecular weights] for a single broad molecular weight polymer. Unlike narrow standard methods, calibrations obtained by broad standard methods are affected by instrumental peak broadening. Without corrections, this calibration error can cause errors in the molecular weight analysis of polymer samples. The GPC calibration curve is obtained by matching those molecular weight and elution volume values that correspond to the same value of sample weight fraction on the molecular weight distribution and GPC elution curves (8).

Approximate molecular weights can be obtained when the single broad standard method or universal calibration method is not feasible (8,45). The accuracy of this method depends upon the unknown polymer having the same structure and molecular weight distribution as the standard.

The *universal calibration method* can be utilized for the molecular weight determination of known polymers. This method is valid when polymer retention is determined only by its hydrodynamic volume. In this case, a plot of the logarithm of the intrinsic viscosity times molecular weight, $\log[\eta]MW$ vs. the elution volume of the polymer provides a calibration curve that applies to all polymers. The resulting universal calibration curve is approximately the same for all polymers (random coil, rigid rod, or spherical). First, a peak position calibration is performed for the molecular weight range of interest using narrow molecular weight standards, such as polystyrene, providing a value for M_2. After obtaining

© 2004 by Marcel Dekker, Inc.

values for k_1, k_2, and α, the unknown molecular weight M_1 can be calculated from Eq. (14):

$$M_1 = \left(\frac{k_2}{k_1}\{M_2^{\alpha_2}\}\right)^{1/\alpha_1} \tag{14}$$

where M_2 is the molecular weight determined by the peak position calibration curve method, k_1 is the coefficient of the analyzed polymer, k_2 is the coefficient of the molecular weight standard, and α_1 and α_2 are the second coefficients of the polymer and the molecular weight standard, respectively. Equations (15) and (16) show how k and α are calculated:

$$k = 6.19 \times 10^9 K^{1/3} \tag{15}$$

$$\alpha = \tfrac{1}{3}(1 + a) \tag{16}$$

where K and a are Mark–Houwink constants that account for the molecular weight dependence of the intrinsic viscosity. The universal calibration method is broadly applicable given the availability of Mark–Houwink constants. Reference 86 summarizes Mark–Houwink constants for a number of common polymers. Sources of error for the universal calibration method are discussed in Refs 8, 85, and 87. As can be expected, serious errors occur if mechanisms other than size exclusion are at work. Cassassa (88) stated that $[\eta]$MW is not a true universal elution parameter, although both theory and experience indicate good results for species of similar type. Based on theoretical considerations, Cassassa predicted a common $[\eta]$MW dependence, however, between random coil polymers and rodlike structures over a narrow range of molecular weight. Indeed, a good fit to universal calibration for dextrans and some native proteins was found over a narrow (1×10^6 to 1.2×10^7) molecular weight range (89).

It was mentioned earlier in this section that the hydrodynamic volume and shape of the standards, in addition to their molecular weight, plays a role in calibration. A claim can be made that the elution behavior of a protein is better related to its Stokes radius R_S than to its molecular weight (90). However, this relationship is not widely employed. The plot of R_S vs. the inverse error function erf^- of $(1 - K_D)$ can be linear if the pore distribution is Gaussian with respect to the Stokes radii of the macromolecules. Work with detergent-soluble membrane proteins emphasizes the need to calibrate with similar standards and the effectiveness of R_S plots (90). Different standards are required for water-soluble globular and detergent-soluble membrane proteins. Often the membrane proteins may be excluded or retarded. A smooth, although nonlinear, relationship was obtained for the plot of R_S vs. $\text{erf}^-(1 - K_D)$, and a scatter of points was observed for log MW vs. K_D. Detergent-bound proteins behave differently, and their Stokes radii may be off by 10–30% when calibration curves are based on the elution volumes of water-soluble proteins. Figure 12 (90) shows the selectivity curve for

© 2004 by Marcel Dekker, Inc.

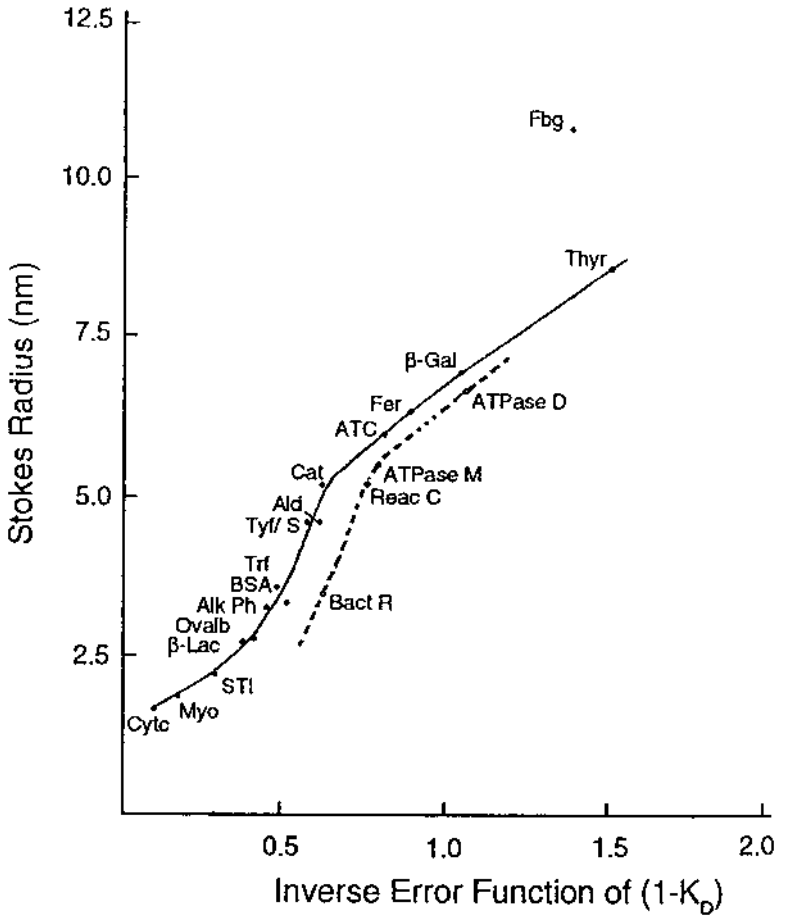

Figure 12 Calibration curves for water-soluble proteins (closed circles) and detergent-soluble membrane proteins (open circles). Column, TSKgel G3000SW, 10 μm, 30 cm × 7.5 mm; mobile phase, 200 mM sodium acetate, 10 mM imidazole, 30 mM HEPES, and 0.1 mM calcium chloride, pH 7.0, and 0.5 mg/mL of $C_{12}E_8$; detection, 280 nm, UV; injection, 20–250 μL containing 1 μg to 2 mg. Abbreviations: Fbg, fibrinogen; Thyr, thryoglobulin; β-galactosidase; Fer, ferritin; ATC, aspartate transcarbamylase; Cat, catalase; Ald, aldolase; Tyr/S, tyrosyl-tRNA synthetase; Trf, transferring; BSA, bovine serum albumin; Alk Ph, alkaline phosphatase; Ovaib, ovalbumin; β-Lac, β-lactoglobulin; TI, soybean trypsin inhibitor; Myo, myoglobin; Cytc, cytochrome c; ATPase D, Ca^{2+}-ATPase dimer M, Ca^{2+}-ATPase monomer; Reac C, reaction center; Bact R, bacteriorhodopsin.

© 2004 by Marcel Dekker, Inc.

water-soluble and detergent-soluble membrane proteins. All the points for the water-soluble proteins lie on a sigmoid curve (except fibrinogen, which has different behavior as a result of its asymmetrical shape). The membrane proteins clearly fall outside the calibration curve for water-soluble proteins, so that the Stokes radii estimated from this curve are high by 10–30%.

Himmel and Squire (84) found significant improvement in the determination of protein molecular weight using denaturing conditions. Their study reconciles the size parameters of proteins and random coils by determining $F_{(v)}$ in Eq. (17):

$$F_{(v)} = \left(\frac{V_E^{1/3} - V_i^{1/3}}{V_T^{1/3} - V_i^{1/3}} \right) \tag{17}$$

Much less error for the molecular weight determination is found when plotting $F_{(v)}$ vs. $MW^{1/3}$ than K_D vs. log MW, R_S vs. $MW^{1/3}$, or $K_D^{1/3}$ vs. $MW^{1/3}$. Tarvers and Church (91), working with TSKgel G3000SW columns, utilized both native and denatured proteins to compare plots of $F_{(v)}$ vs. $MW^{1/3}$, R_S vs. $\text{erf}^-(1 - F_{(v)})$, and R_S vs. $\text{erf}^-(1 - K_D)$ and confirmed plots of $F_{(v)}$ vs. $MW^{1/3}$ provided a better estimate of protein molecular weight. The method of Himmel and Squire (for example, $F_{(v)}$ vs. $MW^{1/3}$) has been used to produce linear curves with native proteins (92–94), denatured proteins (95), and, independently, globular proteins (96).

Denaturing gel filtration with 0.1% sodium dodecyl sulfate (SDS) or 6 M guanidine hydrochloride results in better resolution, increased accuracy, and an extended linear range. This provides a simple, rapid, and sensitive means of separating protein mixtures and determining protein molecular weights that deviate only 5–7% from reported values measured by gel filtration, sedimentation equilibrium, or SDS–polyacrylamide gel electrophoresis (97). On TSKgel G3000SW (Fig. 13), the linear part of the calibration curve for proteins denatured in guanidine hydrochloride extends from molecular weight 9000 to 43,000. Using the same column, the calibration curve for SDS-denatured proteins is linear from 9000 to 93,000, and nondenaturing conditions provide a linear curve from 30,000 to 93,000 with no resolution below 30,000. Similar work by Kato (58) provided the optimum separation ranges presented in Table 7. Good agreement on protein behavior was seen between the various studies for G3000SW columns.

4 SECONDARY RETENTION

Schmidt *et al.* (98) showed how retention volumes of globular proteins varied on silica-based diol bonded phase columns depending on the pH and ionic strength of the mobile phase and their effective charge. Because most proteins elute within the interstitial pore volume, size exclusion is the dominant effect; other possible mechanisms are secondary order effects (99). Pfankoch *et al.* (33) investigated

© 2004 by Marcel Dekker, Inc.

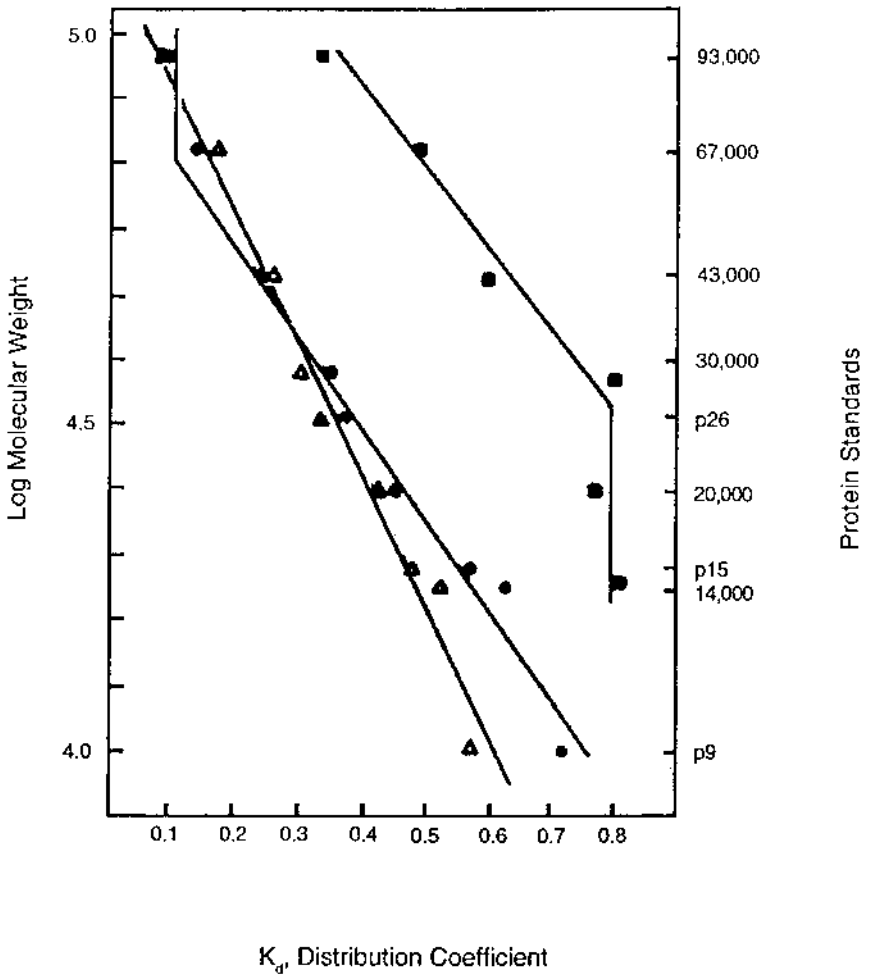

Figure 13 Protein calibration curves for denaturing and nondenaturing conditions. Column, TSKgel G300SW, 10 μm, 30 cm × 7.5 mm; mobile phase (circles), 20 mM sodium phosphate, pH 6.5, +6 M guanidine hydrochloride; (triangles) 50 mM sodium phosphate, pH 6.5, +0.1% SDS; (squares) 50 mM sodium phosphate, pH 6.5; flow rate, 0.2–0.4 mL/min; detection, 280 nm, UV; temperature, 25°C, sample, 1 mg/mL of each protein. Sample preparation: (circles) 20 mM sodium phosphate, pH 6.5, +8 M guanidine hydrochloride and 1% 2-mercaptoethanol, heated at 100°C for 2 minutes; (triangles) 10 mM sodium phosphate, pH 7.2, +1% SDS, heated at 100°C for 2 minutes; (squares) 50 mM sodium phosphate, pH 6.5.

© 2004 by Marcel Dekker, Inc.

the importance of secondary retention mechanisms for several commercial GFC columns. As discussed, after derivatization with a hydrophilic bonded phase, silica-based packings exhibit residual and accessible silanol groups that dissociate within the usable pH range as a function of the pretreatment of the base silica. It was found that the pH of a solution of TSKgel G3000SW packing material in 0.5 M NaCl was slightly below 5 and that the number of dissociated silanol groups reached 0.013 meq/mL packing material at pH 8 (100). As a consequence, a basic solute, such as arginine, or a protein, such as lysozyme, is retained longer than expected because of interaction with the negatively charged silanol groups; acid proteins or small acids, such as citric acid, are repelled from the surface and elute earlier than expected based on their size. This is illustrated in Table 8, in which the distribution coefficients for citric acid and arginine are listed for various commercial columns as a function of the ionic strength of a pH 7.05 phosphate buffer (33). Normal SEC behavior for citric acid and arginine, that is, elution from

Table 8 K_D Values for Citrate, Arginine, and Phenylethanol as a Function of Ionic Strength for Commercial Silica-Based Gel Filtration Columns[a]

Solute and ionic strength	TSKgel G3000SW	LiChrosorb Diol	SynChropak GPC 100	TSKgel G2000SW	Waters I-125
Citrate					
$\mu = 0.026$	0.66	0.54	0.46	0.43	0.39
0.12	0.89	0.81	0.76	0.75	0.72
0.24	0.92	0.95	0.89	0.84	0.79
2.40	0.94	0.99	0.91	0.88	0.88
Arginine					
$\mu = 0.026$	1.30	1.53	1.35	1.57	1.70
0.12	1.05	1.15	1.06	1.06	1.23
0.24	1.02	1.05	1.01	1.02	1.16
0.60	1.00	0.99	—	0.99	1.08
2.40	0.98	1.07	0.98	0.98	1.00
Phenylethanol					
$\mu = 0.026$	1.47	2.49	1.44	1.95	1.83
0.12	1.50	2.56	1.49	2.02	1.88
0.24	1.53	2.64	1.53	2.10	1.88
0.60	1.61	2.93	1.63	2.30	2.03
1.20	1.81	3.52	1.81	2.71	2.29
2.40	2.35	5.31	2.35	4.01	3.03

[a]The distribution coefficient K_D (or K_{SEC}) is defined by $V_E = V_i + K_D V_P$, in which V_E is the solute retention volume, V_i the interparticle or interstitial volume, and V_P the pore volume. Mobile phase: pH 7.05 phosphate buffer of indicated ionic strength.
Source: Ref. 33.

© 2004 by Marcel Dekker, Inc.

the column in the void volume, can be expected on most commercial columns when operated at a mobile phase ionic strength of 0.24 or above. That the behavior of small molecular weight compounds does not always extrapolate to that for proteins is shown in Fig. 14, in which the distribution coefficient K_D for lysozyme is plotted as a function of ionic strength for the same set of commercial columns

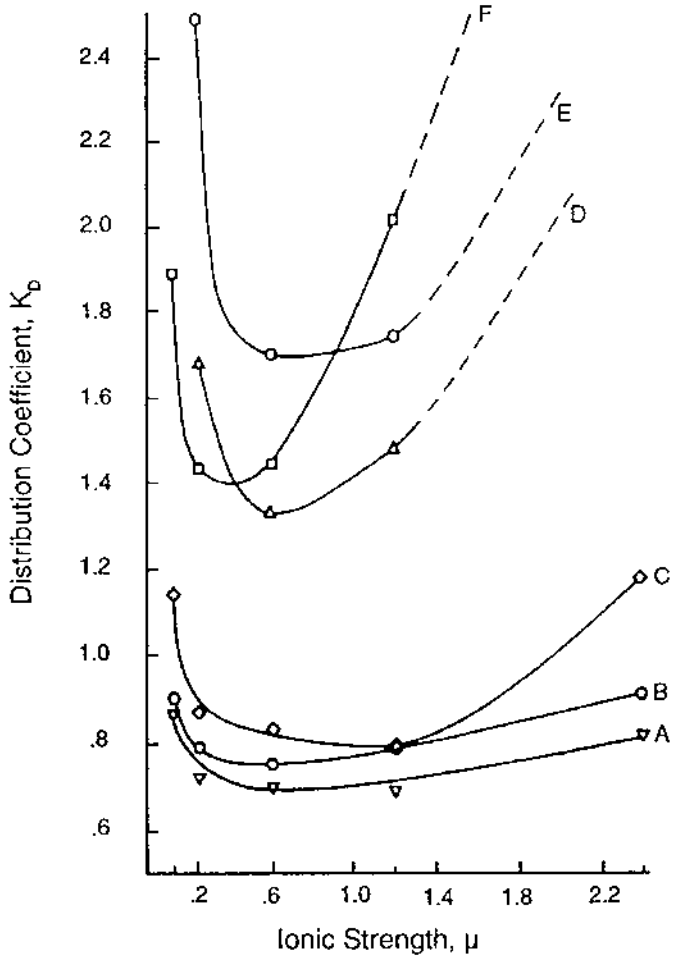

Figure 14 K_D of lysozyme for commercial hydrophilic bonded silicas. Columns, 10 μm: (A) TSKgel G2000SW, 30 cm × 7.5 mm; (B) TSKgel G3000SW, 30 cm × 7.5 mm; (C) LiChrosorb Diol, 24 cm × 4.1 mm; (D) Shodex OH Pak B-804, 50 cm × 8 mm; (E) Waters I-125, 30 cm × 7.8 mm; (F) SynChropak GPC 100, 25 cm × 4.6 mm; mobile phase, phosphate, pH 3.0; detection, 254 nm, UV.

© 2004 by Marcel Dekker, Inc.

discussed in Table 8 (33). Based on the data in Table 8, it was expected that the TSKgel G3000SW and SynChropak GPC 100 columns would show similar behavior, but larger K_D values were expected for the remaining columns. Instead, lysozyme shows similar retention on the TSKgel and the LiChrosorb columns and much longer retention on SynChropak and Waters columns.

The importance of hydrophobic interactions as another secondary retention mechanism is also illustrated in Table 8, in which the distribution coefficient for phenylethanol is listed as a function of ionic strength for the same set of commercial GFC columns (33). Indicative of hydrophobic interaction, K_D values increase with increasing ionic strength for this uncharged solute. Thus, a balance must be stuck between the need to increase ionic strength to reduce ionic interactions and to decrease ionic strength to limit hydrophobic interaction. In practise, hydrophobic interaction is not a strong component of protein retention in size exclusion chromatography because the hydrophobic side chains of the amino acids are predominantly located in the interior of the protein. The addition of 5–20% of a nondenaturing solvent, such as ethylene glycol, to a high ionic strength mobile phase was shown to eliminate the hydrophobic interaction of globular proteins on a diol bonded phase column (98). In contrast to proteins, hydrophobic interaction can be significant in SEC of peptides, some of which may require high concentrations of organic solvents to obtain retention dominated by size exclusion (101,102). Mant *et al.* (103) demonstrated the effectiveness of 0.1% trifluoroacetic acid or addition of organic solvents to overcome hydrophobic interactions. Additionally, the advantageous use of nonideal SEC behavior is detailed.

Kato and co-workers recommend the use of 0.05 M sodium phosphate buffer (pH 7.0) containing 0.3 M NaCl to obtain true size exclusion behavior for most proteins on 5-μm TSK-GEL SW_{XL} columns (7). Not surprisingly, Mori and Kato (104) recommend a very similar mobile phase, 0.1 M phosphate and 0.1 M NaCl at pH 7.0, for size exclusion on diol bonded porpous glass columns. Okazaki and Hara (105) recommend 0.15 M NaCl with lipoproteins, but various aqueous buffers with salts are satisfactory as long as the pH is less than 8.5. Salt contcentration, buffering, and pH all may alter the lipoprotein separation and improve resolution. Increasing the buffering substance or salt concentration leads to peak broadening, indicating a salting-out effect.

5 PRACTICAL CONSIDERATIONS

5.1 Extracolumn Effects

Since the advent of high-performance liquid chromatography, it has been emphasized that the analyst be aware of the influence of the HPLC system components on column efficiency. In a chromatographic system, the observed column efficiency is caused not only by dispersion processes in the column.

© 2004 by Marcel Dekker, Inc.

The peak volume is also broadened by dispersion outside of the column, including broadening of the sample band by the injector, injection volume, the detector cell, detector time constant, and connecting tubing. Once an HPLC system has been assembled, the extracolumn effects are constant factors that may or may not take away from the quality of the separation obtained in the column, depending on the column dimensions and the relative importance of each of the individual extracolumn effects.

The volume in which a band elutes from an HPLC column V_{PV} is defined as four peak standard deviations σ. The relationship between peak volume, retention volume V_E and efficiency of the peak N is given by the equation

$$V_{PV} = \frac{4V_E}{N^{1/2}} \tag{18}$$

in which V_E (earlier described as $V_i + K_D V_P$) can be expressed as a function of the column volume as shown in Eq. (19):

$$V_E = \tfrac{1}{4}\pi(d_c)^2 L(1 + K_D)\epsilon_i \tag{19}$$

Substitution of Eq. (19) into Eq. (18) gives the following expression for the peak volume:

$$V_{PV} = \pi(d_c)^2 L(1 + K_D)\epsilon_i N^{-1/2} \tag{20}$$

It is clear from Eq. (20) that peak volumes are directly proportional to the volume of the column and that samples elute with smaller peak volumes from the same column when filled with a more efficient, that is, smaller size, packing material. The more efficient the column, the narrower are the sample bands and the more important is the effect of extracolumn band broadening. Wider columns provide for more peak volume, and this reduces the importance of extracolumn band broadening.

In ideal SEC, K_D ranges from zero for a fully excluded solute to 1 for a fully included solute. Unlike that in interactive liquid chromatography, in which efficiency is roughly independent of the retention factor, the highest efficiency in SEC is obtained for the smallest molecular weight compound that elutes last from the column, that is, in the total mobile-phase volume. Larger compounds that are partially excluded from the pores have broader peaks as a result of slower and restricted diffusion into the pores. The relative importance of extracolumn band broadening diminishes with increasing peak volume. Thus, in SEC, the contribution of the system to extracolumn band broadening is best studied for a small molecular weight solute that elutes in the total inclusion volume.

Sternberg (106) first showed that the variance of the chromatographic output function can be written as the sum of the variances of the distributions of the

© 2004 by Marcel Dekker, Inc.

individual dispersion processes inside and outside the column, as shown in Eq. (21):

$$\begin{aligned}\sigma^2_{\text{obs}} &= \sigma^2_{\text{col}} + \sigma^2_{\text{inj}} + \sigma^2_{\text{det}} + \sigma^2_{\text{ct}} \\ &= \sigma^2_{\text{col}} + \sum \sigma^2_{\text{ec}}\end{aligned} \tag{21}$$

where σ^2_{obs} is the observed variance or output variance and σ^2_{col} is the variance due to column band broadening. The other variances represent the contributions from injector, capillary tubing, and detector, respectively, and $\sum \sigma^2_{\text{ec}}$ is the sum of extracolumn variances. If needed, Eq. (21) can be extended with other variances, such as those caused by the electronics of the recording system. The validity of Eq. (21) is limited to random dispersion processes that give rise to a Gaussian distribution. This condition is generally assumed in chromatographic applications. The equations describing the individual contributions from extracolumn band broadening are discussed in detail elsewhere (106–110).

Although ideally the observed variance is equal to the column variance, most HPLC systems detract from the column efficiency. Equation (22) can be used to calculate the importance of extracolumn effects:

$$\begin{aligned}\sigma^2_{\text{obs}} &= \sigma^2_{\text{col}} + \sigma^2_{\text{ec}} \\ &= \sigma^2_{\text{col}} + \theta^2 \sigma^2_{\text{col}}\end{aligned} \tag{22}$$

where θ^2 is the fractional increase of the column variance caused by extracolumn effects. A 10% loss of column efficiency (or a 5% increase in bandwidth) as a result of extracolumn effects, $\theta^2 = 0.1$, is considered acceptable in practise.

Injection effects as a result of mass and volume overloading or the injection technique can detract from column efficiency. As with other extracolumn effects, injection effects become more critical with smaller bore columns, which require smaller injection volumes and low flow rates; refer to Ref. 109 for a discussion of extracolumn effects in microcolumn systems.

Equation (23) relates the maximum injection volume to the column dimensions, particle size d_p, mobile-phase porosity ϵ_T, θ, and reduced plate height (110). The constant K_{inj} depends on the injection technique; $K^2_{\text{inj}} = 12$ for plug flow injection and varies from 2 to 9 for most commercial injectors (74). Equation (23) is valid for a small molecular marker that elutes in the total mobile-phase volume:

$$(V_{\text{inj}})_{\max} = \tfrac{1}{4}\pi K_{\text{inj}} \epsilon_T \theta (d_c)^2 (L h d_p)^{1/2} \tag{23}$$

For a reasonably efficient ($h \simeq 8$) 30 cm × 7.5 mm, 10-μm, SEC column, Eq. (23) predicts a maximum injection volume of 165 μL for $K_{\text{inj}} = 3$, $\theta^2 = 0.1$, and $\epsilon_T = 0.8$. Figure 15 shows experimental data for the effect of injection volume on column efficiency for bovine serum albumin on a 30 cm × 7.5 mm, 10-μm,

© 2004 by Marcel Dekker, Inc.

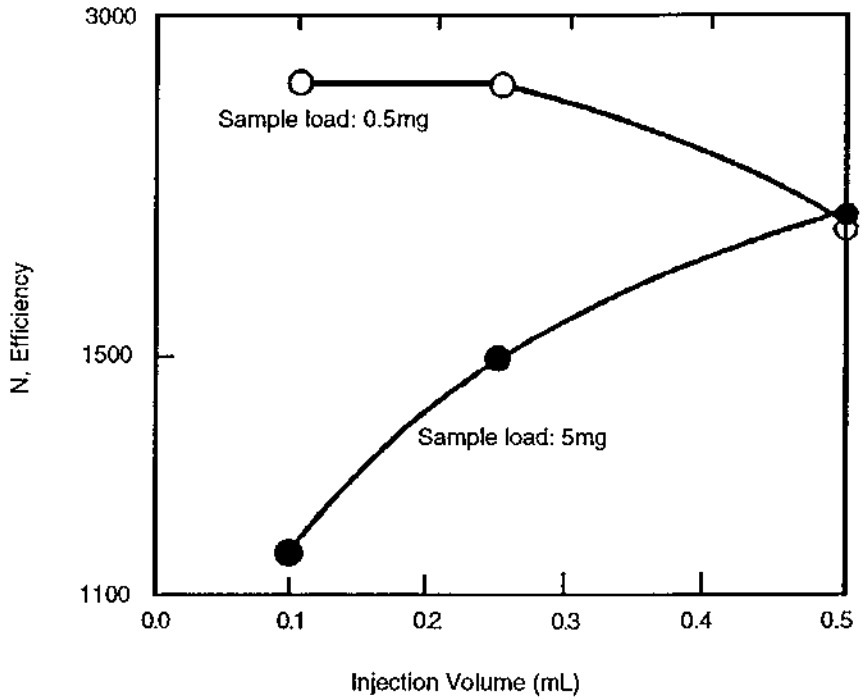

Figure 15 Effect of sample volume on column efficiency. Column, TSKgel G3000SW, 10 μm, 60 cm × 7.5 mm; mobile phase, 0.1 M phosphate and 0.2 M sodium chloride, pH 7.0; flow rate, 1.0 mL/min; detection, 280 nm, UV. (Adapted from Ref. 83.)

TSKgel G3000SW column (83). For a 0.5-mg sample load, column efficiency does not decline until the injection volume increases above 250 μL, or 2% of the empty column volume, in reasonable agreement with the predicted value. Note that mass overloading can be detrimental at much lower injection volumes. As demonstrated, dilution of the sample actually improves efficiency beyond the injection volume at which volume overload becomes apparent.

The construction of the detector cell and detector electronics can seriously detract from the efficiency of the column. Although generally some capillary tubing is contained in the detector, we assume that this can be neglected in comparison with the amount of capillary tubing used to connect the column to the injector and detector. This assumption is not valid when the column effluent is directed through a large-volume heat exchanger before entering the detector cell, as in most refractive index detectors. To minimize the band broadening of early peaks, the volume of the cell should be less than one-tenth the volume of the peak of interest (8,45).

© 2004 by Marcel Dekker, Inc.

The detector time constant can distort column efficiency when the peak width (in time units) becomes of the same order of magnitude as the response time. High-efficiency columns produce very sharp peaks, and detectors with response times greater than 0.5 s can contribute significantly to band broadening. Electronic filtering can increase response time and cause measurable broadening of sharp peaks. Refer to Ref. 108 for an exhaustive discussion of extracolumn effects in detector systems.

Capillary tubing should be kept as narrow and short as possible, while remaining practical. The length of tubing for a maximum band width increase of 5% can be calculated from Eq. (24), taken from Ref. 45:

$$L = \frac{40 V_E^2 D_m}{\pi F N d_{ct}^4} \tag{24}$$

in which D_m is the solute diffusion coefficient in cm^2/s, F is the flow rate in mL/s, d_{ct} is the ID of the capillary in cm, N is the plate number, and the retention volume (V_E) was earlier given by Eq. (19). Equation (24) can also be used to calculate the dimensions of a detector cell for the ideal situation in which no mixing occurs in the cell, that is, the plug flow model. Bending, coiling, or deforming the tubing permits longer lengths with the same degree of band broadening as shorter lengths of straight tubing (111).

5.2 Sample

As discussed, there is a limit to how much can be injected into an HPLC column in terms of sample mass and volume at which the resolution deteriorates beyond acceptable levels. SEC has the lowest loading capacity (g sample/g packing material) for high-performance HPLC techniques because the separation is performed under isocratic mobile-phase conditions and because the separation takes place within the interstitial pore volume, that is, in the absence of a stationary phase. In general, samples are injected as a large volume of a dilute solution. As the increasing concentration overloads the inlet, asymmetrical and broad peaks are seen and resolution decreases. Gooding *et al.* (112) derived Eq. (25) to calculate the theoretical protein load in milligrams for a 25 cm long column:

$$C \simeq \frac{r^2}{4.4} \tag{25}$$

where C is the loading capacity and r is the column radius in mm. Thus, for a column ID of 7.5 mm, the protein loading capacity is $\backsim$3.2 mg/injection. Kirkland and Antle (113) determined that 0.1 mg of a 4800 dalton polystyrene polymer could be injected per gram packing material in GPC on 47 Å silanized silica. Roumeliotis and Unger (99) found that 0.1 mg protein can be loaded per gram LiChrosorb Diol material. They demonstrated that load is proportional to

© 2004 by Marcel Dekker, Inc.

the cross-sectional area of the column regardless of particle size. They determined 1 and 8 mg, respectively, for 60 cm × 7.5 mm (10 g packing) and 60 cm × 21.5 mm (80 g packing) TSKgel G3000SW columns. Freiser and Gooding (114) reported loads of 2–4 mg without band broadening on a 300 × 7.8 mm SynChropak GPC 100 column. For best resolution, it is recommended that samples be 0.01–0.5% (wt/vol). However, very dilute samples (< 10 μg) sometimes lead to skewed peaks and/or poor recovery (58). For preparative protein purification, loads are usually 10–20 mg/mL (15). The concentration dependence of polymers is a special case and is discussed next.

For macromolecules, the sample size may be limited by viscosity. As a rule of thumb, the sample injected should have a viscosity no greater than twice the viscosity of the mobile phase. For proteins, this equals 70 mg/mL in a dilute aqueous mobile phase (9). Thus, viscosity of the sample is seldom an issue with proteins, although it can be a problem when glycerol or sucrose is used as stabilizing agent or ethylene glycol is present to prevent protein adsorption. Increasing viscosity causes restricted diffusion and irregular flow patterns, which lead to broad and tailing peaks (115). With high molecular weight synthetic polymers, a sample concentration ≤ 0.1% is often required to eliminate undesirable effects on both molecular coil dimensions and sample viscosity (8). As the sample load increases, the polymer elutes at higher elution volumes (116). The concentration dependence can be attributed to contraction of polymer coils with increasing concentration. It may also be accounted for by the combined effects of coil contraction and sample viscosity in the interstitial pore volume. The viscosity effect can be operative to different extents, depending upon the column system. Viscosity can drastically affect retention volume and peak width (for molecules that elute within the interstitial pore volume), accounting for 80% of the total concentration effect. With other systems, coil contraction can account for 50–80% of the total concentration effect (116).

For small volumes, peak height increases with increasing sample volume, but retention time and resolution are not affected. At some critical volume, a noticeable decrease in retention time occurs (see Fig. 15), as well as loss of resolution and efficiency. Theoretically, the maximum injection volume for protein SEC is equal to the separation volume between two proteins of interest, but in practice, microturbulence, nonequilibrium between stationary phase and mobile phase, and long diffusion lead to additional band broadening (115). As a general rule, the maximum injection volume is 1–2% of the total column volume (for example, 265–530 μL for a 60 cm × 7.5 mm column), which agrees with the data shown in Fig. 15. Injection volumes less than 1% of the column volume do not necessarily improve resolution. The manufacturer of TSK-GEL SW columns recommends injection volumes up to 0.5% of the analytical column volume (58).

© 2004 by Marcel Dekker, Inc.

5.3 Mobile Phase

A mobile phase is primarily chosen for its effectiveness in solubilizing and stabilizing the sample. Because of the short contact time related to the isocratic conditions, proteins remain stable if the appropriate mobile phase and column are used. As discussed earlier, nonideal SEC behavior may be observed on silica-based columns. Mobile phase considerations therefore play an important role in SEC. Elimination of protein adsorption is crucial, but the effect of the eluant on protein structure must also be considered. Additionally, polyelectrolytes expand and condense with changes in macro-ion concentration within the buffer (117).

Aqueous buffers around pH 6–8 are a good environment for many proteins and are suitable for silica-based SEC columns. The most common nondenaturing aqueous buffers are phosphate ($pK_a = 7.2$) and tris(hydroxymethyl)amino-methane ($pK_a = 8.1$) (19,115). Phosphate buffer is most utilized because of the pH 2–7 limitation for silica-based materials. An ionic strength of 0.1–0.5 M is typically sufficient to prevent adsorption to the weakly anionic silica surface while avoiding hydrophobic effects. Hagel (19) suggested the use of Good's buffers (118) if the buffer capacity of phosphate is too low or its properties are incompatible with the sample; phosphate is known to inhibit certain enzymes (119). It has also been noted that borate may interact with glycopeptides (120). The type of buffer anion has a significant influence on adsorption of proteins to silica. Polyvalent anions, such as sulfate and phosphate, are more effective in preventing adsorption than monovalent anions (chlorine, perchlorate, and acetate). However, sulfates may salt-out proteins and promote hydrophobic interactions with the matrix. In those cases, chaotropic ions, such as perchlorate, can be used to increase the ionic strength of the buffer (19), if sodium chloride is undesirable because of its corrosive properties in the presence of stainless steel components.

Nonionic interactions can be eliminated by reversing the conditions used to prevent ionic interactions (that is, increase pH and/or decrease ionic strength) or by adding a small amount of ethylene glycol, glycerol, organic modifier, or detergent. These additives do not affect the physical properties of silica-based matrices. This stability is an advantage over less rigid SEC supports. Kelner and co-workers (121) examined enzyme recovery from TSKgel G3000SW columns. The addition of glycerol reduces hydrophobic interactions and lessens denaturation. A more pronounced effect was seen for the recovery of α-amylase, and a striking increase in activity was found for adenosine deaminase. Increasing sodium chloride concentration led to a marked decrease in enzyme recovery as a result of hydrophobic interactions. Protein denaturation was more pronounced on the polymer-based TSKgel G3000PW column. The addition of glycerol did not overcome the observed lower mass or activity recoveries. Sykes and Flatman (122) report the use of organic modifier to decrease hydrophobic interactions of human calcitonin gene-related peptide to a TSKgel G2000SW$_{XL}$ column.

© 2004 by Marcel Dekker, Inc.

Acetonitrile–trifluoroacetic acid eluants are attractive for reducing hydrophobic interactions and because of the volatile nature and ultraviolet (UV) transparency of this mobile phase. Protein resolution is dependent upon the acetonitrile concentration and requires the low pH trifluoroacetic acid provides. However, a severe limitation is the low solubility of proteins larger than 15,000 dalton in the 30–45% acetonitrile needed for optimum resolution. This low solubility leads to severe protein aggregation and limits the use of this mobile phase to peptides and low molecular weight proteins.

Detergents may be utilized to stop protein hydrophobic interactions with silica matrices. Some detergents are mild and allow nondenaturing conditions (for example, sodium deoxycholate, Triton, and Nonidet P40). Deoxycholate is the most versatile detergent, with little absorbance at 280 nm. Triton and Nonidet P40 both exhibit strong absorbance in the UV range. The detergent binds to the hydrophobic portion of the protein without forming large micelle structures (this is controlled with the critical micelle concentration, CMC, of each detergent). Triton and Nonidet form large micelles that decrease resolution. Typically, deoxycholate can be used at 0.1%, pH 7.6–8.0, without forming large micelles (115). Detergents, such as SDS, may cause multisubunit proteins to divide into individual subunits, may change the protein quaternary structure from globular to elongated, or, through adsorption, may increase the size of the protein. SDS is always used at its CMC, and the amount of SDS bound is sensitive to the buffer concentration within the range 0.1–0.4 M (123).

The use of denaturing mobile phases is particularly helpful in the analysis of the composition of oligomeric structures (that is, cell organelles, viruses, and multimeric enzymes), because they disrupt most noncovalent protein–protein interactions. Most common denaturing conditions utilize 0.1% SDS or 6 M guanidine hydrochloride. As mentioned earlier, denaturing conditions may be advantagcous for molecular weight determination and lead to in increase in resolution. The use of SDS provides much better resolution than phosphate–guanidine hydrochloride systems because of the extended and uniform conformations of proteins. Takagi *et al.* (123) and Konishi (124) report the effect of salt concentration (phosphate) on complexes of SDS and polypeptides. Takagi found good resolution within the phosphate concentration range 0.05–0.15 M, although, in general, retention is a strong function of buffer concentration in SDS systems. This effect can only partially be explained by the change in the effective size of the complexes as a result of their polyelectrolyte-like nature. Ion exclusion appears to be at play for the lower concentrations. The complexes were totally excluded at lower buffer concentrations, repelled by the negative charges on residual and accessible silanol groups. Konishi found a linear relationship between log MW and K_D for polypeptides ranging from 1000 to about 80,000 dalton when eluted in a 0.20 M phosphate buffer in the presence of 0.1% SDS (124). At lower phosphate concentrations, the calibration curves were steep, but linear, up to 15,000 dalton and

© 2004 by Marcel Dekker, Inc.

less steep and still linear at higher molecular weights. Furthermore, although the slope of the curves at high molecular weight were independent of salt concentration, below 15,000 dalton the slope became steeper with decreasing phosphate concentration. No marked effect of SDS concentration was detected for polypeptides 10,000 dalton or higher. For polypeptides with molecular weight less than 10,000 dalton, the plot in 1% SDS lost linearity and became steeper.

If SEC is being performed for preparative purification or desalting, such volatile buffers as ammonium bicarbonate or acetate may be preferred because they are readily removed by freeze drying. Organic modifiers, such as acetonitrile, are volatile but may lead to protein aggregation. Triethylamine formate, pH 3.0, is also a volatile denaturing agent. Reference 119 lists more volatile buffer systems.

As shown in Fig. 3, mobile phase flow rate has a strong influence on resolution. For larger molecules (polynucleotides and proteins), the mass transfer term is much larger and the flow rate must be correspondingly decreased. Typical flow rates are 0.5–1.0 mL/min for 7.5-mm ID columns, and although better resolution can be obtained at much lower flow rates (see Fig. 1), these rates represent the best compromise between separation efficiency and time.

5.4 Temperature

Although most SEC applications are run at room temperature, increased temperature may be utilized to improve the resolution of difficult separations or to decrease the viscosity. As long as the macromolecule is well dissolved, the influence of temperature on the slope and position of a molecular weight calibration curve is relatively minor (8). Some high molecular weight polyolefins and polyamides require temperatures of 100–135°C because the samples are not soluble at lower temperatures (45). With low molecular weight molecules, increasing the temperature may decrease adsorption. The extent and rate of formation of aggregates was investigated by Watson and Kenney using SEC at elevated temperatures (125). They found that the formation of aggregated species was the main reason for loss of monomer for interleukin-2 analog and γ-interferon.

6 REFERENCES

1. J Porath, P Flodin. Nature 183:1657, 1959.
2. J Moore. J Polym Sci, Part A 2:835, 1964.
3. J Giddings. Anal Chem 35:2215, 1963.
4. J Kirkland. J Chromatogr 125:231, 1976.
5. F Regnier, R Noel. J Chromatogr Sci 14:316, 1976.
6. K Fukano, K Komiya, H Sasaki, T Hashimoto. J Chromatogr 166:47, 1978.
7. Y Kato, Y Yamasaki, H Moriyama, K Tokunaga, T Hashimoto. J Chromatogr 404:33, 1987.

© 2004 by Marcel Dekker, Inc.

8. W Yau, J Kirkland, D Bly, eds. Modern Size-Exclusion Liquid Chromatography. New York: John Wiley & Sons, 1979.
9. K Unger. In: W Jakoby, ed. Methods in Enzymology, Vol. 104, Part C: Enzyme Purification and Related Techniques. New York: Academic Press, 1984, Ch. 7.
10. K Gooding, F Regnier. In: K Gooding, F Regnier, eds. HPLC of Biological Macromolecules. New York: Marcel Dekker, 1990, Ch. 3.
11. K Gooding, H Hagestam Freiser. In: C Mant, R Hodges, eds. High Performance Liquid Chromatography of Peptides and Proteins: Separation, Analysis, and Conformation. Boca Raton, FL: CRC Press, 1991, pp 135–144.
12. G Welling, S Welling-Wester. In: R Oliver, ed. HPLC of Macromolecules. A Practical Approach. Oxford: IRL Press, 1989, Ch. 3.
13. A Preneta. In: E Harris, S Angal, eds. Protein Purification Methods. A Practical Approach. Oxford: IRL Press, 1989, Ch. 6.
14. J Dawkins. In: K Unger, ed. Packings and Stationary Phases in Chromatographic Techniques. New York: Marcel Dekker, 1990, Ch. 7.
15. R Scopes. Protein Purification. Principles and Practice. 2nd ed. New York: Springer, 1987, Ch. 6, pp 186–220.
16. E Stellwagen. In: M Deutscher, ed. Methods in Enzymology, Vol. 182: Guide to Protein Purification. New York: Academic Press, 1990, Ch. 25.
17. K Makino, H Hatano. In: P Dubin, ed. Aqueous Size-Exclusion Chromatography. Amsterdam: Elsevier, 1988, Ch. 9.
18. T Klemmer, L Boross, eds. Gel Chromatography. Theory, Methodology, Applications. Chichester: John Wiley & Sons, 1979.
19. L Hagel. In: J-C Janson, L Ryden, eds. Protein Purification. Principles, High Resolution Methods, and Applications. New York: VCH Publishers, 1989, Ch. 3.
20. H Barth, B Boyes. Anal Chem 64:428R, 1992.
21. Bibliography on Controlled-Pore Glass Chromatography and Related Subjects, 32 Pier Lane West, Fairfield, NJ: CPG, Inc., 07006, 1986.
22. G Alexander. Silica and Me. Washington, DC: ACS, 1973.
23. K Unger. Porous Silica. Amsterdam: Elsevier, 1979.
24. R Iler. The Chemistry of Silica. New York: Wiley, 1979.
25. A Berthod. J Chromatogr 549:1, 1991.
26. M Henry. J Chromatogr 544:413, 1991.
27. M Verzele, M de Potter, J Ghysels. J HRC & CC 2:151, 1979.
28. Y Ohtsu, Y Shiojima, T Okumura, J-I Koyama, K Nakamura, O Nakata, K Kimata, N Tanaka. J Chromatogr 481:147, 1989.
29. J Kohler, D Chase, R Farlee, A Vega, J Kirkland. J Chromatogr 352:275, 1986.
30. M Nystron, W Hermann, D Sanchez, P Moller. Kromasil, a New High Performance Silica for Liquid Chromatography. S-44501, Surte, Sweden: EKA Nobel.
31. K Komiya, H Moriyama, Y Kato. Poster, Pittsburgh Conference, New Orleans, LA, 1993.
32. T Nyhammer. Pharmacia Biotech AB, Uppsala, Sweden, personal communication, 1992.
33. E Pfankoch, K Lu, F Regnier, H Barth. J Chromatogr Sci 18:430, 1980.
34. J Knox, M Saleem. J Chromatogr Sci 7:614, 1969.

© 2004 by Marcel Dekker, Inc.

35. P Bristow, J Knox. Chromatographia 10:279, 1977.
36. G Guiochon, M Martin. J Chromatogr 326:3, 1985.
37. J Sjodahl, A Winter. Protides. In: H Peeters, ed. Biol Fluids, Proc Colloq, Vol. 30, 1982, p 693.
38. R Schnabel, P Langer. J Chromatogr 544:137, 1991.
39. L Sander, S Wise. Crit Rev Anal Chem 18:299, 1987.
40. K Unger. Packings and Stationary Phases in Chromatographic Techniques. New York: Marcel Dekker, 1990.
41. J Huber, J Hulsman. Anal Chim Acta 38:305, 1967.
42. L Snyder. Anal Chem 39:698; 39:705, 1967.
43. H Engelhardt, G Ahr. J Chromatogr 282:385, 1983.
44. T Wilson, D Simmons. Poster 116, HPLC '92, Baltimore, MD, 1992.
45. L Snyder, J Kirkland. Introduction to Modern Liquid Chromatography. 2nd ed. New York: Wiley, 1979.
46. R Scott. Liquid Chromatography Column Theory. New York: Wiley, 1992.
47. J Kirkland. J Chromatogr 125:231, 1976.
48. D Herman, L Field, S Abbott. J Chromatogr Sci 19:470, 1981.
49. R Kennedy, J Jorgenson. J Microcol Sep 2:120, 1990.
50. B Bidlingmeyer, J Warren. Anal Chem 56:1583A, 1984.
51. H Engelhardt, U Schon. Chromatographia 22:388, 1986.
52. Y Shioya, H Yoshida, T Nakajima. J Chromatogr 250:341, 1982.
53. J Giddings. Dynamics of Chromatography. New York: Marcel Dekker, 1965.
54. C Dewaele, M Verzele. J Chromatogr 260:13, 1983.
55. S Hjerten, J Liao. J Chromatogr 457:165, 1988.
56. H Engelhardt. Practice of High Performance Liquid Chromatography. New York: Springer, 1986.
57. G Berendsen. Thesis, Delft University, Delft, The Netherlands, 1980, Ch. 5.
58. Y Kato. LC-GC 1:540, 1983.
59. Y Kato, H Parvez, S Parvez. In: H. Parvez and S Parvez, eds. Progress in HPLC, Vol. 1. Utrecht, The Netherlands: VNU Science Press, 1985.
60. Y Kato, Y Yamasaki, T Hashimoto. J Chromatogr 320:440, 1985.
61. G Stegeman, JC Kraak, H Poppe. J Chromatogr 550:721, 1991.
62. G Huntzinger, R Eksteen. Poster 508, HPLC '86, San Francisco, CA, 1986.
63. J van de Venne, J Rindt, G Coenen, C Cramers. Chromatographia 13:11, 1980.
64. RW Stout, JJ DeStefano. J Chromatogr 326:63, 1985.
65. T Mizutani, A Mizutani. J Chromatogr 111:214, 1975.
66. H Crone, R Dawson, E Smith. J Chromatogr 103:71, 1976.
67. G Howard, A Martin. Biochem J 56:32, 1950.
68. I Halasz, I Sebastian. Angew Chem Int Ed 8:453, 1969.
69. J Kirkland, J DeStefano. J Chromatogr Sci 8:309, 1970.
70. A Pryde. J Chromatogr Sci 12:486, 1974.
71. R Majors, M Hopper. J Chromatogr Sci 12:767, 1974.
72. J Kirkland. J Chromatogr Sci 9:206, 1971.
73. R Majors. Anal Chem 44:1722, 1972.
74. R Eksteen. Thesis, Northeastern University, Boston, MA, 1984, Ch. 1 and 2.

© 2004 by Marcel Dekker, Inc.

75. J Dolan, R Gant, N Tanaka, R Giese, B Karger. J Chromatogr 16:616, 1978.
76. R Majors. LC-GC 9:686, 1991.
77. H Engelhardt, D Mathes. J Chromatogr 142:311, 1977.
78. H Engelhardt, G Ahr, M Hearn. J Liq Chromatogr 4:1361, 1981.
79. N MilIer, B, Feibush, B Karger. J Chromatogr 316:536, 1985.
80. T Waddell, D Leyden, M DeBello. J Am Chem Soc 103:5305, 1981.
81. R Huisden, T Ooms, J Kraak, H Poppe. Chromatographia 31:263, 1991.
82. T Alfredson, C Wehr, L Tallman, F Klink. J Liq Chromatogr 5:489, 1982.
83. H Watanabe, M Umino, T Sasagawa. Sci Rep Toyo Soda 28:1, 1984.
84. M Himmel, P Squire. Int J Peptide Protein Res 17:365, 1981.
85. M Himmel, P Squire. In: P Dubin, ed. Aqueous Size-Exclusion Chromatography. Amsterdam: Elsevier, 1988, Ch. 1.
86. J Brandrup, E Immergut, eds. Polymer Handbook. 3rd ed. New York: Wiley Interscience, 1989.
87. J Janca. In: J Giddings, E Grushika, J Cazes, P Brown, eds. Advances in Chromatography. Vol. 19. New York: Marcel Dekker, 1981, Ch. 2.
88. E Cassassa. Macromolecules 9:182, 1976.
89. R Frigon, J Leypoldt, S Uyeji, L Henderson. Anal Chem 55:1349, 1983.
90. M LeMaire, L Aggerbeck, C Monteilhet, J Andersen, J Moller. Anal Biochem 154:525, 1986.
91. R Tarvers, F Church. Int J Peptide Protein Res 26:539, 1985.
92. P Squire. J Chromatogr 210:433, 1981.
93. T Burcham, D Osuga, H Chino, R Feeney. Anal Biochem 139:197, 1989.
94. M Dennis, C Lazure, N Seidah, M Chretien. J Chromatogr 266:163, 1983.
95. C Lazure, M Dennis, J Rochemont, M Seidah, M Chretien. Anal Biochem 125:406, 1982.
96. J Bindels, H Hoenders. J Chromatogr 261:381, 1983.
97. R Montelaro, M West, C Issel. Anal Biochem 114:398, 1981.
98. D Schmidt, R Giese, D Conron, B Karger. Anal Chem 52:177, 1980.
99. P Roumeliotis, K Unger. J Chromatogr 218:535, 1981.
100. Y Kato, T Hashimoto. JHRC & CC 6:45, 1983.
101. S Lau, A Taneja, R Hodges. J Chromatogr 317:192, 1984.
102. A Taneja, S Lau, R Hodges. J Chromatogr 317:1, 1984.
103. C Mant, J Parker, R Hodges. J Chromatogr 397:99, 1987.
104. S Mori, M Kato. J Liq Chromatogr 10:3113, 1987.
105. M Okazaki, I Hara. In: P Dubin, ed. Aqueous Size-Exclusion Chromatography. Amsterdam: Elsevier, 1988, Ch. 11.
106. J Sternberg. Adv Chromatogr 2:205, 1966.
107. B Karger, M Martin, G Guiochon. Anal Chem 46:1640, 1974.
108. R Scott. Liquid Chromatography Detectors. 2nd ed. Amsterdam: Elsevier, 1986.
109. D Ishii, ed. Introduction to Microscale High Performance Liquid Chromatography. Weinheim, Germany: VCH, 1988.
110. G Guichon, H Colin. In: P Kucera, ed. Macrocolumn High Performance Liquid Chromatography. New York: Elsevier, 1984.
111. E Katz, R Scott. J Chromatogr 268:169, 1983.

© 2004 by Marcel Dekker, Inc.

112. K Gooding, K Lu, G Vanecek, F Regnier. 4th International Symposium on Column Liquid Chromatography, Boston, MA, 1979.
113. J Kirkland, P Antle. J Chrom Sci 15:137, 1977.
114. H Freiser, K Gooding. J Chromatogr 544:125, 1991.
115. R Montelaro. In: P Dubin, ed. Aqueous Size-Exclusion Chromatography. Amsterdam: Elsevier, 1988, Ch. 10.
116. O Chiantore, M Guaita. J Liq Chromatogr 7:1867, 1984.
117. B Stenlund. In: Advances in Chromatography. Vol. 14. New York: Marcel Dekker, 1976, Ch. 2.
118. N Good, G Winget, W Winter, T Connoly, S Izawa, R Singh. Biochemistry 5:467, 1966.
119. D Perrin, B Dempsey. Buffers for pH and Metal Ion Control. London: Chapman & Hall, 1976.
120. R Rothman, L Warren. Biochim Biophys Acta 955:143, 1988.
121. D Kelner, J Mayhew, J Hobbs. American Biotechnology Laboratory, 40, February, 1989.
122. A Sykes, S Flatman. Poster, Tenth International Symposium on the HPLC of Proteins, Peptides, and Polynucleotides, Wiesbaden, Germany, 1990.
123. T Takagi, K Takeda, T Okuno. J Chromatogr 208:201, 1981.
124. K Konishi. In: H Parvez, S Parvez, eds. Progress in HPLC. Vol. 1. Utrecht, The Netherlands: VNU Science Press, 1985.
125. E Watson, W Kenney. J Chromatogr 436:289, 1988.

© 2004 by Marcel Dekker, Inc.

4
Molecular Weight Sensitive Detectors for Size Exclusion Chromatography

Christian Jackson and Howard G. Barth
E. I. du Pont de Nemours and Company
Wilmington, Delaware, U.S.A.

1 INTRODUCTION

Size exclusion chromatography (SEC) provides a rapid, high-resolution method for determining molecular weight distributions (MWD) of macromolecules. In the conventional mode, the molecular weight is determined by calibrating the column to determine the relation between elution volume and molecular weight. The size exclusion separation mechanism is based on the effective hydrodynamic volume of the molecule, not the molecular weight, and as a result the system must be calibrated using standards of known molecular weight and homogeneous chemical composition. The chemical composition must be the same as the standards to he analyzed, and the calibrated molecular weight range must be greater than the range of molecular weights to be analyzed. The calibration curve is thus specific to a given polymer–solvent system.

For many commercial polymers the columns cannot be calibrated because well-characterized standards are unavailable. The situation is further complicated

© 2004 by Marcel Dekker, Inc.

for branched polymers or copolymers, for which there is no single calibration curve relating elution volume to molecular weight (1).

An additional potential source of error is the sensitivity of the calibration curve to alterations in the experimental conditions. Anything that alters the elution time of a given molecular weight species, such as changes or fluctuations in flow rate, column degradation, or enthalpic interactions with the column packing, can lead to serious errors in the measurement of molecular weight.

Because of these limitations, it is clearly desirable to measure the molecular weight, or some property related to molecular weight, directly as the sample elutes from the columns. This is generally done by connecting either a light-scattering detector or a viscometer to the SEC system. The eluting polymer flows through the detector cell as it leaves the column and before it reaches the concentration detector. In a light-scattering detector, the excess light scattered by the eluting polymer is proportional to molecular weight. For an on-line viscometer, the specific viscosity can be used to calculate the molecular weight either in conjunction with the Mark–Houwink coefficients of the polymer solution or by using the method of universal calibration.

This chapter reviews the principles and methodology of molecular weight determination by light scattering and viscometry in conjunction with SEC. The emphasis is on those aspects of molecular weight measurement relevant to SEC analysis; more detailed general treatments of light scattering, viscometry, and polymer solutions are available elsewhere (2–10). Applications of both methods are discussed with particular emphasis on molecular weight determination of polymers that are heterogeneous in composition or architecture; it is in these areas that molecular weight sensitive detectors offer the greatest advantage over conventional SEC.

2 PRINCIPLES

2.1 Viscometry

At a constant flow rate, the pressure drop across a capillary tube P is proportional to the viscosity of the liquid flowing through the tube. For a polymer solution, the ratio of this pressure to the pressure for the pure solvent P_0 is equal to the relative viscosity η_r of the solution,

$$\frac{P}{P_0} = \frac{\eta}{\eta_0} = \eta_r \tag{1}$$

where η is the solution viscosity and η_0 is the solvent viscosity. The specific viscosity is defined as

$$\eta_{sp} = \frac{\eta - \eta_0}{\eta_0} = \eta_r - 1 \tag{2}$$

© 2004 by Marcel Dekker, Inc.

which is a measure of the increase in viscosity caused by the addition of the polymer to the solvent. The reduced viscosity η_r/c, where c is the polymer concentration, is a measure of the specific capacity of the polymer to increase the solution relative viscosity. In the limit of infinite dilution this quantity is known as the intrinsic viscosity:

$$[\eta] = \left(\frac{\eta_{sp}}{c}\right)_{c\to 0} \tag{3}$$

The reduced viscosity has a concentration dependence in dilute solutions described by the Huggins equation,

$$\frac{\eta_{sp}}{c} = [\eta] + k'[\eta]^2 c \tag{4}$$

where k' is the Huggins constant. In SEC the concentration of the solute is usually low, so that the assumption of infinite dilution is generally valid and the conditions for Eq. (3) hold. Thus, the intrinsic viscosity of an eluting polymer can be determined from measurements of the specific viscosity and concentration of the eluting polymer solution at each elution volume.

The intrinsic viscosity of a polymer solution is related to its molecular weight by the empirical relation known as the Mark–Houwink equation:

$$[\eta] = KM^a \tag{5}$$

where K and a are the Mark–Houwink coefficients, which depend on the polymer, solvent, and temperature.

Measurement of the specific viscosity requires that both the solution and the solvent viscosity be measured at the same flow rate. This can be achieved by measuring the solvent viscosity baseline before and after the polymer peak elutes or by measuring the solution viscosity as the peak elutes using a reference capillary. An example of such a flow-referenced viscometer is shown in Fig. 1 (6). This is a fluid analog of the electrical circuit known as a Wheatstone bridge. With only solution flowing through the viscometer, the flow resistances R1, R2, R3, and R4 are balanced and the differential pressure transducer signal is zero. When a polymer solution enters the viscometer, it fills capillaries R1, R2, and R3, but the reservoir prevents it from reaching the fourth capillary, R4, which still contains flowing solvent. A pressure transducer measures the resultant difference in pressure between the two sides of the bridge. The specific viscosity η_{sp} is calculated from the ratio of this differential pressure to the pressure drop across the bridge. Other types of viscometers include single-capillary (7) and referenced dual-capillary (8) designs. A listing of commercial instrumentation is given in the appendix.

Figure 2 shows the viscometer and refractometer tracings as a function of elution volume for a mixture of equal amounts of three nearly monodisperse

© 2004 by Marcel Dekker, Inc.

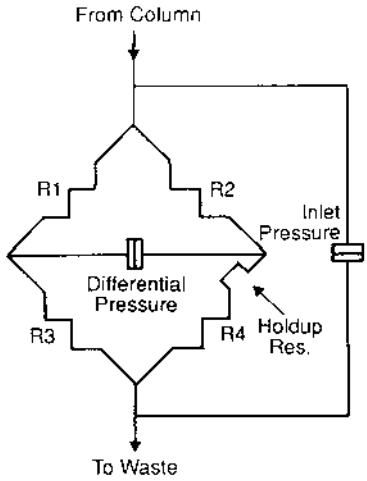

Figure 1 "Bridge design" flow-referenced capillary viscometer. See text for details. (Adapted from Ref. 6, with permission from John Wiley and Sons, Inc.)

polystyrene standards. Note that the refractometer is proportional to concentration c; the signal from the viscometer is proportional to $[\eta]c$. By dividing the viscometer output by the refractometer signal, we can then determine $[\eta]$ at each elution volume increment.

2.2 Light Scattering

The intensity of the light scattered by a polymer solution, above that scattered by the pure solvent, is related to the molecular weight of the polymer by (9)

$$\frac{K^*c}{R(\theta)} = \frac{1}{M_w P(\theta)} + 2A_2c \tag{6}$$

where c = polymer concentration, M_w = weight-average molecular weight of the polymer, A_2 = second virial coefficient of the polymer–solvent system, $R(\theta)$ = measured excess scattering intensity of the solution over that of the pure solvent, the Rayleigh ratio, $P(\theta)$ = particle scattering function as a function of angle relative to the incident beam, and K^* is an optical constant for the scattering system, given by

$$K^* = \frac{4\pi^2 n_0^2 (dn/dc)^2}{\lambda_0^4 N_A} \tag{7}$$

© 2004 by Marcel Dekker, Inc.

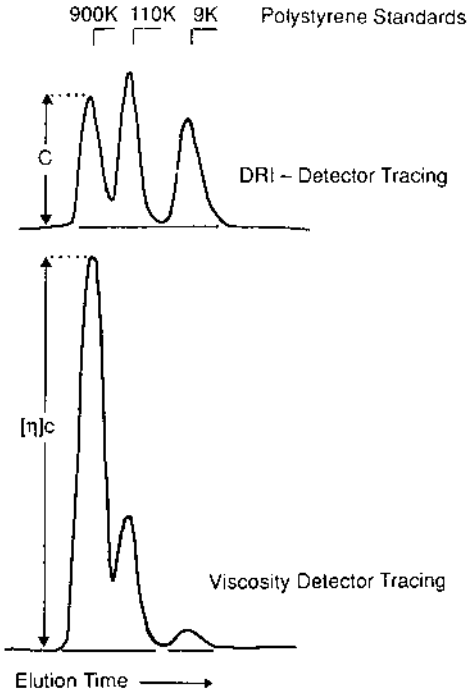

Figure 2 SEC chromatogram of a mixture of three polystyrene standards showing the outputs of both a differential refractometer (top) and a viscometer (bottom).

where n_0 = refractive index of the solvent, dn/dc = specific refractive index increment of the solution, λ_0 = wavelength of the incident light in a vacuum, N_A = Avogadro's number.

The particle-scattering function describes the angular variation of the scattered light intensity and depends upon the polymer size and shape. At low scattering angles it can be approximated by

$$\frac{1}{P(\theta)} = 1 + \left(\frac{4\pi}{\lambda}\right)^2 \sin^2\left(\frac{\theta}{2}\right) \frac{\langle Rg^2\rangle_z}{3} \tag{8}$$

where λ is the wavelength of the incident light in the solution and $\langle Rg^2\rangle_z$ is the mean-square radius of gyration of the molecules in solution.

Figure 3 shows a simplified schematic of a light-scattering photometer. In a typical instrument, a laser light source, vertically polarized, irradiates a sample solution. The intensity of the scattered light is measured at a given angle with respect to the forward direction. Instrumentation is available (see appendix) that

© 2004 by Marcel Dekker, Inc.

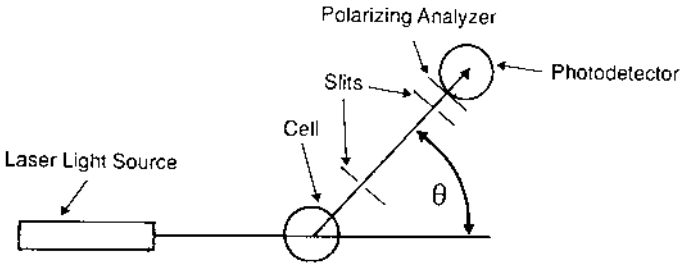

Figure 3 A light-scattering photometer. Polymer solution in cell is irradiated with an incident beam, and scattered light intensity is measured at angle θ.

utilizes a single angle measurement at $< 10^\circ$ (10) or 90° (11), two angles (12), or multiangles (13,14).

The weight-average molecular weight, the radius of gyration, and the second virial coefficient can be determined by measuring the scattered intensity as a function of angle for a series of different dilute concentrations. These parameters are determined from a Zimm plot of $K^*c/R(\theta)$ against $\sin^2(\theta/2) + kc$ for these data (Fig. 4), where k is an arbitrary constant used to spread out the data. A value of $k = 1/c_{\max}$, where $c_{\max}$ is the maximum concentration used, has been found to work well (2). The data are extrapolated to zero angle and zero concentration, and

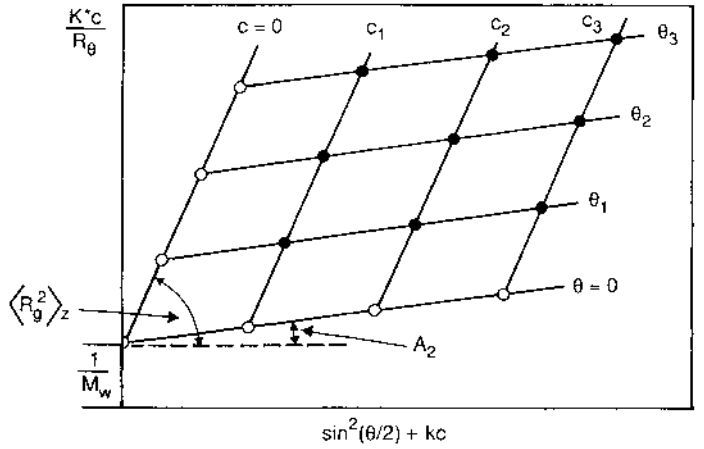

Figure 4 Zimm plot, which is a double-extrapolation procedure used in light-scattering measurements for determining the second virial coefficient A_2, mean square radius of gyration $\langle R_g^2 \rangle$ and weight-average molecular weight M_w.

© 2004 by Marcel Dekker, Inc.

the double extrapolation to zero angle and zero concentration intercepts the $K^*c/R(\theta)$ axis at a value equal to the inverse of the molecular weight,

$$\left(\frac{K^*c}{R(\theta=0)}\right)_{c\to 0} = \frac{1}{M_w} \tag{9}$$

The initial slope at zero angle is proportional to the second virial coefficient, and the initial slope of the graph at zero concentration, divided by the intercept, is proportional to the mean-square radius of gyration.

When combined with SEC, the light-scattering intensity can only be measured at a single concentration for each molecular weight fraction eluting from the column. Thus, to determine molecular weight, the second virial coefficient must be known beforehand or must be assumed to be zero. In most cases, setting the second virial coefficient to zero is a valid approximation because the eluting polymer concentration is usually low. In general, the resultant error is less than experimental error. Making this approximation and measuring the scattered light intensity at a number of angles, we can determine the molecular weight and mean-square radius of gyration for each elution slice by extrapolation to zero angle. The data points thus obtained approximate to the zero concentration points in Fig. 4. In practice, the radius of gyration can only be determined for molecules greater than about 20 nm in diameter; below this size it is extremely difficult to measure variation in scattered intensity with angle.

If a single low-angle scattering intensity is measured, typically $< 10^\circ$, then for most polymer molecules scattering intensity in this region this can be considered a valid approximation to the zero-angle intensity and no extrapolation is required. The molecular weight is then proportional to the scattered intensity divided by the concentration.

3 METHODOLOGY

3.1 Viscometry

3.1.1 Universal Calibration

Benoit and co-workers (15) showed that SEC separates polymer molecules by hydrodynamic volume. The hydrodynamic volume can be expressed as the product of intrinsic viscosity and molecular weight:

$$h\nu = [\eta]M \tag{10}$$

It is therefore possible to generate a universal calibration curve of polymer hydrodynamic volume against elution volume that is valid for different types of polymers as well as copolymers and branched polymers (Fig. 5). This is achieved by using narrow molecular weight distribution standards with known molecular

© 2004 by Marcel Dekker, Inc.

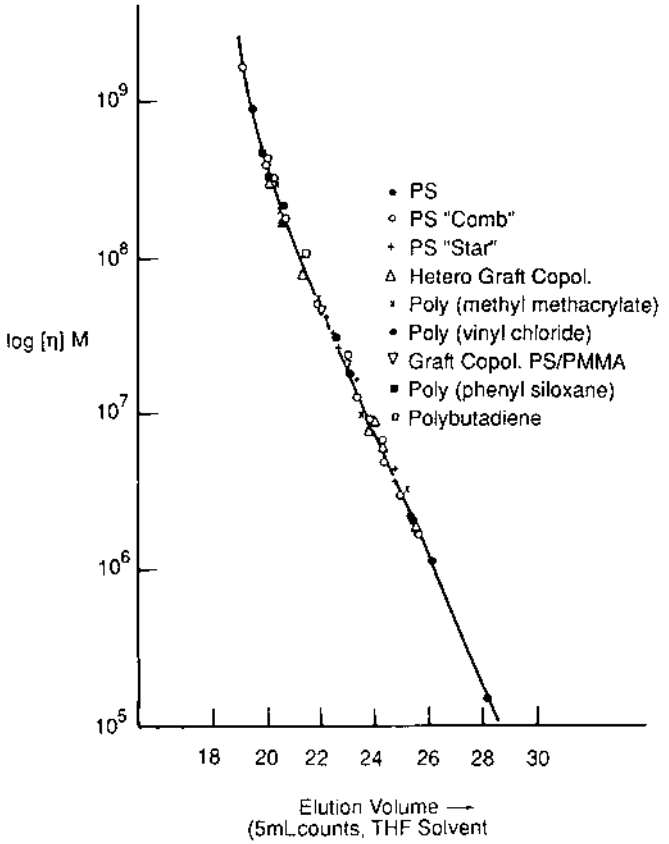

Figure 5 SEC universal calibration curve demonstrates that molecular hydrodynamic volume $[\eta]M$ governs the separation mechanism. (From Ref. 15, with permission from John Wiley and Sons, Inc.)

weights and known intrinsic viscosities, either measured or calculated from the Mark–Houwink coefficients. The calibration curve is then constructed from a plot of $\log[\eta]M$ against the measured elution volume. The molecular weight of each fraction of an unknown eluting polymer can then be calculated from the universal calibration curve and either the measured polymer intrinsic viscosity or the Mark–Houwink coefficients:

$$M = \frac{hv}{[\eta]} = \left(\frac{hv}{K}\right)^{1/(a+1)} \tag{11}$$

© 2004 by Marcel Dekker, Inc.

If the intrinsic viscosity of the eluting unknown polymer is measured at each elution volume using an on-line viscometer, universal calibration can be used to calculate the molecular weight at each volume, and thus the molecular weight distribution, without knowledge of the Mark–Houwink coefficients.

For branched polymers or copolymers, the molecules eluting at a given volume may be polydisperse in molecular weight. Molecules with the same hydrodynamic volume but different structure or composition have different molecular weights. In this case the molecular weight in a given elution volume increment measured by universal calibration is the number-average molecular weight M_n (16).

Universal calibration is valid only when there are no enthalpic interactions between the polymer sample and the column packing and the separation is entirely a result of the size exclusion mechanism. Furthermore, chromatographic concentration effects must be absent. Another consideration is that the molecular weight of the standards used to construct the universal calibration curve must be known accurately.

3.1.2 SEC-Viscometry Without a Concentration Detector

SEC-viscometry combined with universal calibration can provide measurements of molecular weight distribution even when it is not possible to use a concentration method (17), for example at temperatures at which a concentration detector can no longer operate or in solvents in which there is no measurable difference between solution and solvent refractive index, such as polyolefins in decalin.

The method requires that the Mark–Houwink exponent a for the polymer–solvent system and the sample amount injected be known. The concentration at each elution slice is then calculated from the viscometer output η_{sp}, the universal calibration curve, and the Mark–Houwink exponent. From the Mark–Houwink equation and the definition of hydrodynamic volume in universal calibration, it can be shown that the concentration at each elution volume increment is given by (M. Haney, personal communication)

$$c_i = \frac{(\ln \eta_r)_i}{[K^{1/a}(h\nu)_i]^{a/(a+1)}} \tag{12}$$

where

$$K = \frac{\sum (\ln \eta_r)_i}{\sum c_i} \left[\frac{\sum (\ln \eta_r)_i / h\nu_i}{\sum c_i} \right]^{1/a} \tag{13}$$

and

$$\sum c_i = m\Delta V \tag{14}$$

© 2004 by Marcel Dekker, Inc.

where $h\nu$ is the hydrodynamic volume at each slice from the calibration curve, m is the total sample amount injected, and ΔV is the retention volume increment between data points.

A special case of this approach is the method of calculating the number-average molecular weight from the viscometer output, the universal calibration curve, and the sample amount injected (18):

$$M_n = \frac{\sum c_i}{\sum (\ln \eta_r)_i / h\nu_i} \tag{15}$$

In this case the Mark–Houwink exponent is not required, and thus this method can be used when the Mark–Houwink exponent is unknown or when it may vary with elution volume, as for copolymers and polymer blends.

3.1.3 Intrinsic Viscosity Distribution

Another approach to the SEC-viscometry data is that of Kirkland *et al.* (19). The intrinsic viscosity is a fundamental property of the polymer sample in solution, and thus polymers may be characterized in terms of their intrinsic viscosity distribution (IVD) without attempting to convert this into a molecular weight distribution. Moments of the IVD may be calculated similar to those for the MWD (20). The advantage is that the intrinsic viscosity distribution is directly measured and is not subject to the errors introduced when universal calibration is used to calculate molecular weight.

If the Mark–Houwink coefficients for the polymer–solvent system are known, then the IVD measured by SEC-viscometry can be converted into the molecular weight distribution using the Mark–Houwink relation. This should give greater precision in the measurement of molecular weight distribution than SEC-viscometry with universal calibration, because the IVD measurement is much less sensitive to experimental conditions than a calibration curve.

3.1.4 Radius of Gyration Measurement

If universal calibration is used with SEC-viscometry, it is also possible to calculate the radius of gyration for linear polymers at each elution volume using the Flory–Fox equation (21),

$$R_g = \frac{1}{\sqrt{6}} \left(\frac{M[\eta]}{\Phi} \right)^{1/3} \tag{16}$$

where

$$\Phi = 2.55 \times 10^{21} (1 - 2.63\epsilon + 2.86\epsilon^2) \tag{17}$$

© 2004 by Marcel Dekker, Inc.

and

$$\epsilon = \frac{2a - 1}{3} \tag{18}$$

The ϵ parameter [Eq. (18)] is used to take into account deviations from θ conditions (22). This approach has been evaluated with good success using polystyrene samples (20,23). If a viscosity detector is used in series with a right-angle light-scattering detector, Eq. (16) can be used in an iterative procedure to correct for angular asymmetry (see Sec. 3.2.6).

3.2 Light Scattering

3.2.1 Determination of the Specific Refractive Index Increment and Solvent Refractive Index

The accuracy of the light-scattering measurement depends on prior determinations of the solvent refractive index and of the specific refractive index increment dn/dc of the sample in the solvent [Eq. (7)]. The solvent refractive index can be measured with a conventional refractometer or values found in the literature. The dn/dc value can be measured using either a differential refractometer or, less frequently, an interferometer. Measurements should be made at the same temperature as the light-scattering measurement and ideally at the same wavelength. Because of the dependence of the optical constant on the square of dn/dc, extreme care must be taken with the measurement because any error is doubled in the calculated molecular weight. Detailed discussions of the measurement principles and methods can be found in Refs. 2 and 24.

A comprehensive tabulation of experimental values for dn/dc has been published (25). Many of these values are at different wavelengths, and the value at the desired wavelength can be obtained by extrapolation of a plot of dn/dc against the inverse of the wavelength squared using the relationship

$$\frac{dn}{dc} = k' + \frac{k''}{\lambda^2} \tag{19}$$

where k' and k'' are the intercept and slope, respectively.

Values of dn/dc have a nearly linear dependence on solvent refractive index, so that if values are not available in the solvent to be used it can also be determined by extrapolation from other solvent systems. If the polymer refractive index n_p and the partial specific volume of the polymer in the solvent ν_p are known, then dn/dc can be estimated by the Gladstone–Dale rule (2),

$$\frac{dn}{dc} = \bar{\nu}_p(n_p - n_0) \tag{20}$$

© 2004 by Marcel Dekker, Inc.

It should be noted that dn/dc also varies with molecular weight. Typically, the dn/dc value increases with increasing molecular weight and reaches an asymptotic limit for molecular weights greater than approximately 20,000g/mol. For polymers with fractions in this low-molecular-weight regime, this effect should be taken into consideration because it generally leads to an error in the measurement of the low-molecular-weight region of the distribution; that is, the number-averge molecular weight is most affected. For example, if dn/dc decreases with molecular weight, then the molecular weight at each elution volume is overestimated, especially M_n. If the entire polymer MWD is below 20,000, then dn/dc values should be determined separately for the required molecular weight range.

One other consideration is the effect of ionic groups on synthetic polyelectrolytes and biopolymers. To measure a reliable value for dn/dc, the polymer solution, containing electrolyte, must be dialysed against the solvent system until a constant chemical potential is obtained. Details on the determination of dn/dc of polyelectrolytes can be found in Refs. 2, 24, and 26.

3.2.2 Instrument Calibration

Determination of the Rayleigh ratio from the scattered light intensity requires that the light-scattering detector be calibrated to account for detector sensitivity, cell geometry, and so on. Utiyama (27) discusses calibration procedures and standards for light-scattering measurements. Because procedures vary depending upon instrument and cell design, discussion of instrument calibration is not presented here and the reader is advised to consult manufacturers' instruction manuals.

3.2.3 Measurement of Molecular Weight Distribution

When dn/dc and n_0 have been determined, and the instrument calibrated, the molecular weight can be calculated from the light-scattering intensity and the concentration at each elution volume [Eq. (9)]. These values can then be used to determine the molecular weight distribution. If there is any polydispersity at a given elution volume caused by heterogeneity of composition or structure, the calculated value is a weight-average molecular weight.

3.2.4 Measurement of Sample M_w

It can be shown that the weight-average molecular weight can be determined from the ratio of the area of the light-scattering intensity measured at low angle, $< 10^\circ$, and the concentration chromatograms, corrected for their respective calibration constants (28):

$$M_w = \frac{\sum M_i c_i}{\sum c_i} = \frac{\sum R_{\theta i}/K^*}{\sum c_i} \tag{21}$$

© 2004 by Marcel Dekker, Inc.

Thus, an accurate M_w value can be obtained from the light-scattering signal alone if the injected mass is known. Alternatively, the area measurement can be used instead of a point-by-point summation of calculated molecular weights to avoid the effect of baseline noise at the peak edges. This method has been shown to give greater precision than the summation of individual values at each elution volume (29,30). This approach can also be used for samples that contain a high-molecular-weight fraction that is detected only by the light-scattering detector, not by the concentration detector.

The inverse problem occurs at the low-molecular-weight end of many distributions, at which the light-scattering signal is too small to determine a reliable molecular weight estimate but there is still a signal from the refractometer. In this case, extrapolation of the column calibration curve from measured data can improve the accuracy of M_n, as shown in Fig. 6.

3.2.5 SEC-Light Scattering with Universal Calibration

Light scattering can also be used in conjunction with universal calibration to obtain an estimate of the intrinsic viscosity of the sample (see Sec. 5). Because of the greater complexity of the measurement and the lower light-scattering

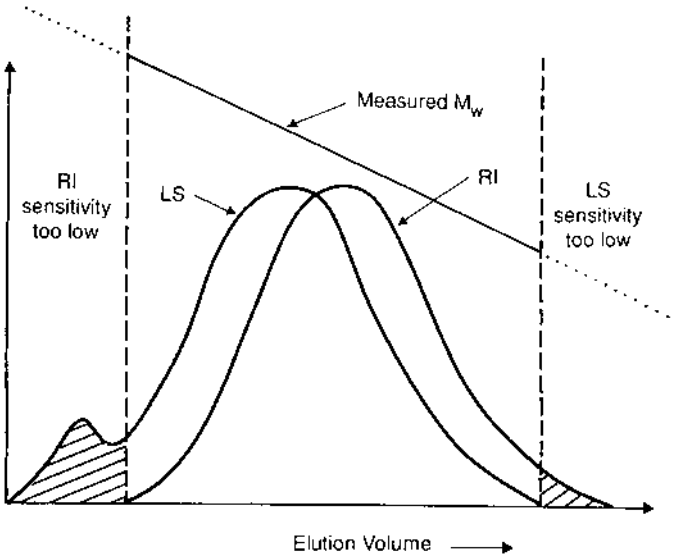

Figure 6 SEC tracings from light-scattering and differential refractive index detectors showing the low sensitivity of each detector at the ends of a hypothetical distribution.

© 2004 by Marcel Dekker, Inc.

sensitivity for many samples compared with viscometry, this approach is rarely used.

3.2.6 Right-Angle Laser Light Scattering

Haney *et al.* (11) used a right-angle light-scattering (LS) detector combined with SEC-viscometry to measure directly both the intrinsic viscosity and molecular weight of each elution slice. For molecules with molecular weights less than about 100,000 g/mol, there is no measurable scattering asymmetry and the right-angle intensity provides a good measurement of the molecular weight. For higher molecular weights, the Flory–Fox equation [Eq. (16)] is used in an iterative procedure to correct for any asymmetry in the scattering and thus determine a good approximation to the correct molecular weight. Thus, with this approach, both molecular weight and the radius of gyration [Eq. (16)] can be determined. The method gave accurate molecular weights for polystyrene in THF up to 3×10^6 g/mol.

3.3 Concentration Measurement

One of the advantages of conventional SEC is that the absolute concentration of the sample at each elution slice is not required to calculate the MWD. With both SEC-LS and SEC-viscometry it becomes necessary to determine an absolute concentration measurement if the MWD is to be determined.

There are two approaches to determining the concentration: one is to use the injected sample mass, and the other is to calibrate the concentration detector. In the following discussion it is assumed that a refractometer is being used to determine concentration, but the same applies to ultraviolet (UV) detectors, except that the UV absorbance of a sample replaces the dn/dc value.

In the first method, the area under the concentration detector chromatogram is taken to be proportional to the total sample mass injected m:

$$k = \frac{m}{\Delta V \sum h_{\mathrm{i}}} \tag{22}$$

and thus the concentration at each elution slice c_{i} may be calculated from the detector output at each slice h_{i} by $c_{\mathrm{i}} = kh_{\mathrm{i}}$.

The advantages of this method are that it is straightforward and is not affected by different dn/dc values for different samples. The disadvantage is that the injected amount of sample must be known accurately. This implies that the injection volume is known accurately.

In the second method, the concentration detector is calibrated with a series of solutions of different concentrations and known refractive indices. This provides a

© 2004 by Marcel Dekker, Inc.

calibration constant for the detector k' that converts the signal into a change in refractive index, such that for each chromatogram slice,

$$c_i = \frac{k'}{dn/dc} h_i \tag{23}$$

This avoids the problems with the peak mass not corresponding to the injected mass and thus increases the measurement precision, but it means that dn/dc for the sample must be known. Because dn/dc must be known for the light-scattering calculation, this clearly does not require any additional work for SEC-light scattering. Furthermore, once the concentration detector is calibrated, dn/dc for unknown polymers can be determined using Eq. (23) if the injected mass is known. With this approach it is best to use a monochromatic light source for the refractometer having the same wavelength as the light source used for the light-scattering experiment.

3.4 Interdetector Delay Volume

When a molecular weight sensitive detector is added as a second detector to an SEC system, it is essential that the dead volume in the connecting tubing between the measurement points of the two detector cells be known precisely. If this is not done, the calculated values contain significant errors. In particular, the measured polydispersity and Mark–Houwink coefficients are extremely sensitive to errors that may be incurred in the interdetector dead volume.

A number of approaches can be used to determine the interdetector volume. The obvious procedure is to calculate the geometric offset volume from the connection volume between detectors. As discussed by Bruessau (31) and Lecacheux and Lesec (32), however, these calculated values are not correct because they do not take into account peak shape changes that can occur. The most commonly used approach for determining interdetector volume for either viscometers or light-scattering detectors is to measure peak maxima differences of a narrow molecular weight distribution polymer standard or a monodisperse solute, such as a protein. In a viscometer, a solute, such as methanol, can be employed for aqueous SEC. Measurement of peak onset difference, as well as the peak maxima difference of an excluded polymer peak, has been reported (33).

A different procedure was used by Lecacheux and Lesec (32) for determining interdetector volume for both a viscometer and a light-scattering detector. In this approach, an excluded monodisperse polymer standard is injected. When the correct interdetector volume is selected, the calculated intrinsic viscosity, or molecular weight, is equal to the expected value and remains constant as a function of elution volume.

To determine the interdetector delay volume for a viscometer, a broad molecular weight distribution standard can be injected and a Mark–Houwink plot,

© 2004 by Marcel Dekker, Inc.

that is, $\log[\eta]$ vs. $\log M$, generated using universal calibration. The interdetector volume is adjusted until the expected Mark–Houwink exponent is obtained (34).

Another approach to determining the interdetector volume of a viscometer is first to establish an $[\eta]$ vs. elution volume calibration curve using a series of narrow polymer standards of known intrinsic viscosities. A broad molecular weight standard is then injected and the interdetector volume is adjusted to obtain superimposition of the intrinsic viscosity calibration curve (35).

With a light-scattering detector, a $\log M$ vs. elution volume calibration curve is constructed from a series of narrow molecular weight distribution polymer standards. A broad molecular weight distribution standard is then injected, and an iterative procedure finds the interdetector volume that superimposes the broad MWD standard calibration curve onto the one established by the narrow standards (36).

Finally, a spectrophotometric method has been proposed in which a low-angle laser light-scattering (LALLS) detector is used as an absorption photometer (33). Interdetector volume is then determined by injecting a solute that absorbs radiation from the LALLS detector. Mourey and Miller (33) used copper cyclohexanebutyrate as the solute and determined interdetector volume using the peak onsets of the LALLS detector and refractometer.

3.5 Band Broadening

SEC does not provide infinite resolution of species with different hydrodynamic volumes; as a result each slice has some residual polydispersity. This is primarily the result of the finite time required for a given polymer to diffuse into and out of the stationary phase. The effect can be compounded by extra dead volume in the detectors or connecting tubing. In conventional SEC, band broadening leads to an overestimate of sample polydispersity. This is because the eluting peak is broadened so that it appears to cover a wide molecular weight range.

If a light-scattering detector is used as a detector, then the true molecular weight at each elution volume can be directly measured. If there is any band broadening, each elution volume is polydisperse in molecular weight, and the measured quantity is a weight average. The slope of the measured M_w against elution volume is flatter than the calibration curve for the molecular weight because of band broadening, and the sample appears less polydisperse. Although the weight-average molecular weight for the sample can still be measured correctly, the number-average molecular weight is overestimated because of the lack of resolution. As a result, polydispersity is underestimated. The error introduced to molecular weight parameters as a function of band broadening is given in Fig. 7. These results are based on computer simulation studies (37).

© 2004 by Marcel Dekker, Inc.

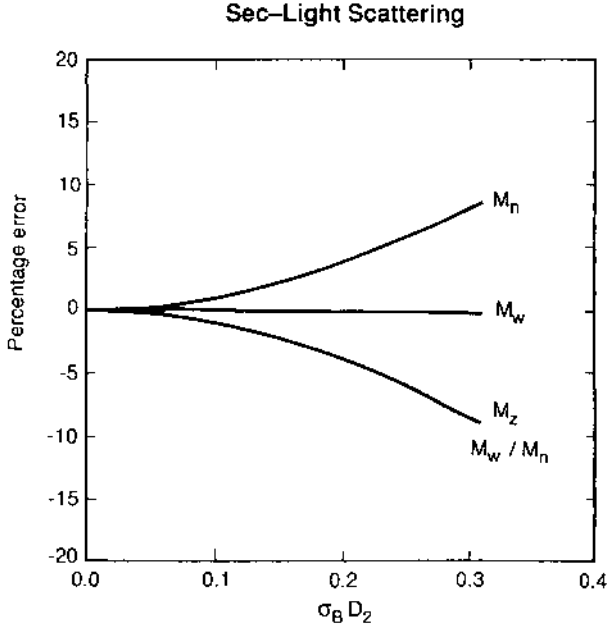

Figure 7 Effect of band broadening for a polymer with polydispersity 2 on the measured moments of the molecular weight distribution by light scattering, where D_2 is the slope of log molecular weight and elution volume and σ_B is the peak variance caused by band broadening. (From Ref. 37.)

The measured polydispersity can be corrected for band broadening using the method of He *et al.* (38). For columns with a linear calibration curve in log MW with slope D_2, the true polydispersity is given by

$$\left(\frac{\bar{M}_w}{\bar{M}_n}\right)_{TRUE} = e^{D_2 D_2'(1-D_2'/D_2)\sigma_T^2}\left(\frac{\bar{M}_w}{\bar{M}_n}\right)_{SEC\text{-}LALLS} \tag{24}$$

where D_2' is the experimental calibration curve measured by the light-scattering detector and σ_T^2 is the variance of the experimental concentration chromatogram. A more general form of the correction, which does not assume a Gaussian peak shape, has been developed by Lederer *et al.* (39) and Billiani and co-workers (40–42). The same correction also applies to the intrinsic viscosity distribution, the width of which is also underestimated.

In SEC-viscometry with universal calibration, as in conventional SEC, the effect of band broadening is an apparent increase in polydispersity as the peak broadens (Fig. 8). Although the true intrinsic viscosity is measured at each slice,

© 2004 by Marcel Dekker, Inc.

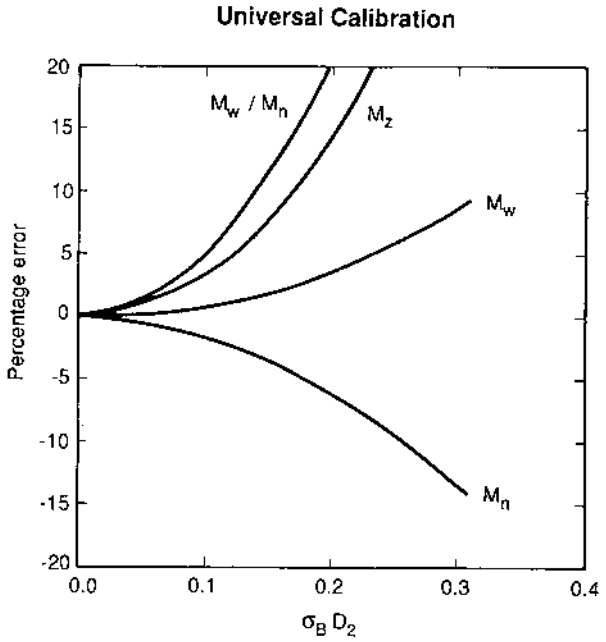

Figure 8 Effect of band broadening for a polymer with polydispersity 2 on the measured moments of the molecular weight distribution by viscometry and universal calibration, where D_2 is the slope of log molecular weight and elution volume and σ_B is the peak variance caused by band broadening. (From Ref. 37.)

the effect of band broadening means that the molecular weight profile no longer has a one-to-one correspondence to the intrinsic viscosity elution profile, from which the universal calibration curve is determined. The corrected intrinsic viscosity, without band broadening, can be calculated using the method of Hamielec (43):

$$[\eta](V) = \frac{F(V)}{F(V - E_2\sigma^2)} e^{1/2(E_2\sigma)^2} [\eta](V)_{\text{exp}} \tag{25}$$

where $[\eta](V)$ is the corrected intrinsic viscosity at each elution volume V and $[\eta](V)_{\text{exp}}$ is the experimentally determined intrinsic viscosity at each elution volume, F is the concentration chromatogram, σ is the Gaussian band-broadening parameter, and E_2 is the slope of the intrinsic viscosity calibration curve

$$[\eta](V) = E_1 e^{-E_2 V} \tag{26}$$

From this, the true molecular weight calibration curve can be determined and can then be used to calculate the correct MWD.

© 2004 by Marcel Dekker, Inc.

In general, band-broadening corrections are still required if a molecular weight sensitive detector is added to SEC, especially if the molecular weight distribution or the Mark–Houwink coefficients are being determined. As mentioned, some average values of the distribution M_w by SEC-LS and $[\eta]$ by SEC-viscometry are unaffected. In SEC-LS and SEC-viscometry used with Mark–Houwink coefficients, the errors in the determination of the MWD are less than in conventional SEC. In SEC-viscometry with universal calibration, these errors are greater, as shown in Fig. 8. A detailed discussion on the effect of band broadening with viscometers and light-scattering detectors can be found in Ref. 38.

One related problem is that of interdetector band broadening. Detectors with larger cell volumes, if placed after other detectors in the SEC system, exhibit a broader peak than other detectors. In SEC-LS, for example, the light-scattering peak is generally narrower than the concentration-sensitive detector peak because of the smaller cell volume. This can lead to a mismatch of the two detector signals, even with correct compensation for the interdetector volume. In the SEC-LS example, this mismatch leads to an overestimate of the molecular weight in the center of the peak and an underestimate at the leading and tailing edges. If molecular weight is plotted as a function of elution volume for a narrow MWD sample, it appears as an *n*-shaped curve rather than a nearly flat line. The weight-average molecular weight in this example is unaffected, but the number and *Z* averages are distorted (37).

This effect can be corrected by injecting a narrow MWD sample and measuring the variance of the peaks in each detector. Because the peak shape is nearly Gaussian, it should, ideally, be the same for all detectors. If it is not, the additional variance can be calculated for one of the detectors. In subsequent data analysis, the narrower peak can be digitally broadened using Gaussian band spreading to correct for this mismatch.

4 APPLICATIONS

4.1 Viscometry

4.1.1 Molecular Weight Distribution

SEC-viscometry and universal calibration has been widely used to determine the MWD of synthetic polymers, and selected applications are listed in Table 1. On-line viscometers have been successfully used at high temperatures: Pang and Rudin (48) measured the MWD of polyolefins dissolved in 1,2,4-trichlorobenzene at 145°C, and Stacy (17) measured the MWD of polyphenyl sulfide in 1-chloronaphthalene at 220°C.

SEC-viscomettry has also been applied to natural polymers with more complex molecular weight distributions. Timpa (59) used universal calibration and on-line viscometry to measure the MWD of cotton fibers to evaluate different fiber

© 2004 by Marcel Dekker, Inc.

Table 1 Measurement of Molecular Weight Distribution by SEC-Viscometry: Selected Applications

Macromolecule	References
Homopolymers	
Polystyrene	34,44–46
Polymethyl methacrylate	34,45–47
Polyolefins	48
Polyvinyl chloride	34,45
Polyvinyl acetate	45
Polyvinyl alcohol	49
Polyallylamine	50
Polyethylene oxide	51
Polyamides	52,53
Polyphenylene sulfide	54
Copolymers	
Ethylene-vinyl acetate	55
Natural polymers and derivatives	
Lignin	56–58
Cotton	59
Starch	60
Pectin	61,62
Biopolymers	
Proteins	63,64

strains by determining the relationship between molecular composition and fiber strength and length.

4.1.2 Copolymer Molecular Weight Distribution

The difficulty with copolymer analysis is in the measurement of the concentration of each elution volume. On-line viscometers measure the correct specific viscosity for copolymers. If universal calibration holds, the problem with which we are faced is converting the specific viscosity into an intrinsic viscosity. Only if there is no compositional drift with elution volume does the output from a refractometer or UV detector correspond directly to concentration. If there are compositional changes, then the signal reflects these changes through changes in the detector response factor. If the composition changes with molecular weight, then a second detector can be used that is sensitive to only one component of the copolymer (65). This method was used recently by Grubisic-Gallot *et al.* (66) to characterize polystyrene-b-methyl methacrylate block copolymers. A UV detector set at 262 nm, at which wavelength polymethyl methacrylate does not absorb, was used

© 2004 by Marcel Dekker, Inc.

to measure the polystyrene content, and the refractometer was used to measure the total change in refractive index. The UV signal was then used to correct for changes in polymer refractive index and allow the concentration of both components at each elution volume to be calculated. Figure 9 shows the weight fraction of styrene for two samples as a function of elution volume.

Another approach is to use a method proposed by Goldwasser (18). This is applicable to copolymers and polymer blends and allows the number-average molecular weight to be calculated if the sample injected mass is known without a concentration detector. Figure 10 shows chromatograms from blends of equal concentrations of polystyrene and polymethyl methacrylate (20). The measured M_n is in good agreement with the value calculated from the known molecular weight of the two components. Note that the refractometer response is twice as sensitive to the polystyrene because of the larger dn/dc.

4.1.3 Branching

One of the most important applications of molecular weight sensitive detectors is in the characterization of branched polymers. A branched molecule in solution has

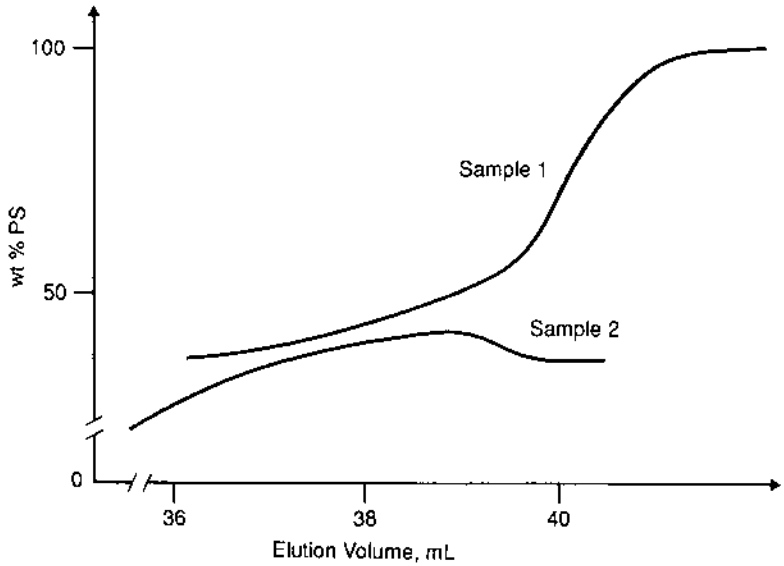

Figure 9 Weight fraction of polystyrene vs. elution volume for two samples of polystyrene-b-methyl methacrylate. Sample 1 contains residual polystyrene homopolymer in the low-molecular-weight region of the distribution. (From Ref. 66, with permission from Springer-Verlag Publishers.)

© 2004 by Marcel Dekker, Inc.

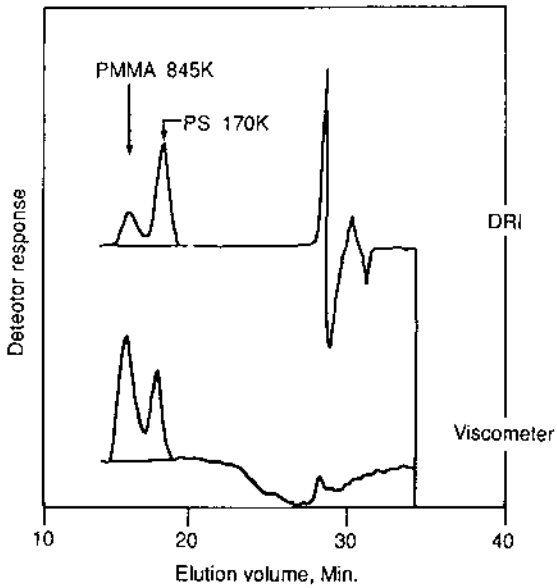

Figure 10 Differential refractometer (DRI) and viscometer outputs for a 1 : 1 mixture of 845,000 g/mol of polymethyl methacrylate and 170,000 g/mol of polystyrene. With this method (for example, see Ref. 15), the determined M_n was 265,000 g/mol, compared with an expected value of 283,000 g/mol. (From Ref. 20, with permission from John Wiley and Sons, Inc.)

a smaller size than a linear molecule of the same molecular weight. This smaller size also means a correspondingly smaller intrinsic viscosity. By comparing the measured intrinsic viscosity of the branched molecule at each elution volume increment to the intrinsic viscosity of the linear molecule with the same molecular weight, a branching factor g', defined as

$$g' = \left(\frac{[\eta]_b}{[\eta]_l}\right)_M \tag{27}$$

can be determined, where the subscripts b and l correspond to the branched and linear polymers, respectively. For a linear polymer g' is unity. For a branched polymer it decreases as the number of branch points per molecule increases.

Zimm and Stockmayer (67) determined the extent of the relative decrease in the radius of gyration under θ conditions for a given number and type (tri- or

© 2004 by Marcel Dekker, Inc.

tetrafunctional) of branch points. This is defined in terms of another branching factor,

$$g = \left(\frac{Rg_b^2}{Rg_l^2}\right)_M \tag{28}$$

where Rg^2 is the mean-square radius of gyration. For different branching architectures, g can be related to the number of branches per molecule (4).

This branching factor g is related to the intrinsic viscosity branching factor g' by

$$g' = g^{\epsilon} \tag{29}$$

where ϵ is a structure factor not specified by the theory. Typical values for ϵ range from 0.5 to 1.5. Experimentally determined values for a variety of polymer–solvent systems have been tabulated (68). Because of the uncertainty in ϵ and because SEC measurements are always made in good solvents, whereas g is defined for θ conditions, there is too much uncertainty to use g' to obtain the number of branch points per molecule. In many cases, only the branching ratio g' is reported, where it serves as a useful measure of the relative degree of branching and is a useful parameter for comparing variations among polymer samples.

Kuo *et al.* (34) used this method to study randomly branched and star polystyrene, as well as branched polyvinyl acetate. Figure 11 shows the Mark–Houwink plots for the linear and branched polystyrenes and a plot of the branching index g' for the branched polystyrene as a function of molecular weight. As expected, g' for randomly branched polystyrene decreases with increasing molecular weight. Siochi *et al.* (69,70) used this method to study model graft polymethyl methacrylates and found that in this case, g' increased with increasing molecular weight. They speculated that this was possibly caused by a difference between macromer and the backbone monomer polymerization kinetics.

Note that the intrinsic viscosity-molecular weight data for the corresponding linear polymer are required to calculate g'. Ideally this should be determined from a linear sample analyzed by SEC-viscometry. Alternatively, literature values for the Mark–Houwink parameters for the linear polymer may be used. If neither of these data are available, the least branched sample or a secondary linear standard can be used as the control. Table 2 lists selected references on the use of SEC-viscometry for branching studies.

4.1.4 Mark–Houwink Coefficients

An important application of SEC-viscometry in conjunction with universal calibration is to determine the Mark–Houwink coefficients for a given polymer

© 2004 by Marcel Dekker, Inc.

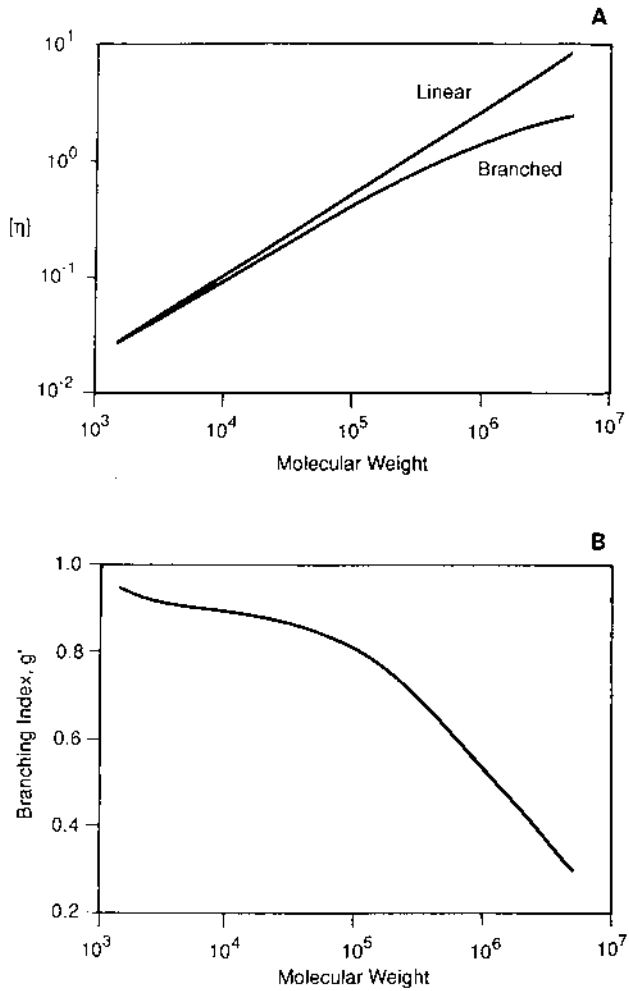

Figure 11 (A) Mark–Houwink plot of $\log[\eta]$ vs. $\log M$ for a linear and a branched polystyrene. (B) Plot of branching index g' as a function of molecular weight for the randomly branched polystyrene. (From Ref. 34, with permission from the American Chemical Society.)

system. The coefficients can provide information about solvent quality and molecular conformation. In addition, once the coefficients for a polymer–solvent system are known, that polymer can then be characterized using conventional universal calibration without an on-line viscometer. All references listed in Table 1 report the Mark–Houwink coefficients for the systems studied.

© 2004 by Marcel Dekker, Inc.

Table 2 Measurement of Branching by SEC-Viscometry: Selected Applications

Macromolecule	References
Polystyrene	34
Polyvinyl acetate	34,45,71
Polyethylene	72–75
Acrylic polymers	69,70,76
Polybutadiene	77,78

4.1.5 Biopolymer Characterization

In our laboratory, SEC-viscometry has been used to estimate the aspect ratio of proteins (79). This ratio, which describes the shape of proteins, is calculated from the Scheraga–Mandelkern β function (80). To determine this function, the intrinsic viscosity of the protein must be known accurately. Through the use of SEC-viscometry, proteins can be separated from interfering conformers and associated species, and intrinsic viscosities can be determined accurately.

4.2 Light Scattering

4.2.1 Molecular Weight Distribution

SEC-LS is used to measure molecular weight distribution directly as a polymer elutes from the SEC without universal calibration. For each polymer–solvent system, the specific refractive index increment dn/dc is required, and for most instruments the solvent refractive index is also needed. Table 3 lists selected papers describing SEC-LS measurements of synthetic polymers, copolymers, polysaccharides, cellulosics, and related polymers.

SEC-LS has been used at temperatures of 145°C, for example, for polyolefln analysis. It has also been used with aqueous mobile phases. In the latter case particulate contamination of the mobile phase is a serious problem, and the solvent requires careful filtration before use.

Aggregation has been studied by SEC-LS (see later) as well as the polyelectrolyte effect. Schorn *et al.* (93) used SEC-LS to illustrate how electrolyte was required to suppress the polyelectrolyte effect for nylon 6 in hexafluoroisopropanol. Without the electrolyte, bimodal peaks were observed by conventional SEC.

4.2.2 Copolymer Molecular Weight Distribution

The analysis of copolymers by SEC-LS is complicated by the compositional heterogeneity of the sample in two ways: first is in the determination of the

© 2004 by Marcel Dekker, Inc.

Table 3 Measurement of Molecular Weight Distribution by SEC-LS: Selected Applications

Macromolecule	References
Homopolymers	
Polystyrene	81–85
Polyolefins	42,86–91
Polyamides	92–96
Acrylic polymers	97–102
Polyphosphazines	103
Polyvinyl butyral	104
Polyqinolines	105
Urea-formaldehyde resins	40
Polyesters	106–108
Polyvinyl alcohol	109
Polycarbonate	93,110
Phenolic resins	111
Polyethers	108
Polyethylene oxide	97
Polyethylene terephthate	107
Polybutadiene/polyisoprene	112–115
Copolymers	
Polyacrylates	116,117
Stryene-based	118–123
Polyesters	108
Others	124
Polysaccharides	
Carrageenans	125
Dextran	97,126,127
Guar gum	128
Heparin	129
Pectin	130,131
Starch	132–135
Xanthan	136, 137
Others	138–142
Cellulosics	
Cellulose	143–151
Nitrocellulose	152,153
Humic acids	154
Lignin	154,155

© 2004 by Marcel Dekker, Inc.

concentration at each elution volume fraction, and second is the effect of the copolymer dn/dc on the light-scattering signal. If the composition is heterogeneous, an apparent weight-average molecular weight M_w^* is measured, which depends on the solvent refractive index n_0. To determine the true molecular weight, the light-scattering intensity must be measured in at least three solvents with different refractive indices (2,156). This can be understood from Eq. (7), which shows that the scattered intensity depends on $(dn/dc)^2$, for two components this is the sum of the respective dn/dc values squared. The measured dn/dc, however, is merely a straight summation. In an extreme case, the solvent refractive index may lie between the refractive indices of the two components and the dn/dc could be zero. However, such a copolymer would still scatter light and M_w^* would be infinite. If the composition distribution is homogeneous, as in a random copolymer, or if the refractive indices of the two components are equal, then M_w^* is equal to M_w. When these conditions are obtained, SEC-LS can be applied successfully to copolymers.

Grubisic-Gallot *et al.* (66) studied block copolymers of ethyl methacrylate and deuterated methyl methacrylate by SEC-LALLS. The dn/dc values in tetrahydrofuran were nearly equal, 0.084 and 0.079 mL/g, respectively. They found good agreement between the measured molecular weight and the theoretical value obtained using the molecular weights of the blocks. Malihi *et al.* (123) used static measurements of a styrene–butylacrylate emulsion copolymer in a series of solvents with different refractive indices to obtain the correct M_w and also to find the best solvent for SEC-LS. The best solvent is that in which M_w^* is closest to M_w as determined from the multiple solvent measurements, that is, when the component dn/dc values are relatively closest. They found good agreement between SEC-LS results and static measurements.

Dumelow (121) used SEC-LALLS with dual concentration detectors to study the variation in compositional heterogeneity with molecular weight in polystyrene–polydimethylsiloxane block copolymers. The results showed that some of the copolymers were in fact blends. The largest errors in the analysis were found to arise if it were assumed that there was no molecular weight distribution at each elution slice. By avoiding this assumption the results were improved.

The relationship between the radius of gyration and the light-scattering asymmetry is also dependent on copolymer composition and is not the same as for homopolymers. Unless dn/dc is equal for both components, the spatial distribution of the component that scatters the most dominates the angular distribution of scattered light and thus the measured radius of gyration (156).

4.2.3 Branching

Light scattering has been widely used to study branching. The molecular weight of the branched polymer M_b is measured for each elusion slice, and the

© 2004 by Marcel Dekker, Inc.

size information is derived from universal calibration. Equation (27) can be rewritten as

$$g' = \left(\frac{M^*}{M_b}\right)^{a+1} \tag{30}$$

where M^* is the molecular weight of the linear molecule with the same hydrodynamic volume as the branched molecule calculated from universal calibration and a is the Mark–Houwink exponent for the linear molecule. Figure 12 illustrates the effect of branching on the molecular weight calibration curve.

The value of M_b in Eq. (30) is a number-average molecular weight, and because light scattering measures the weight-average molecular weight, values of g' do not agree with those measured by viscometry if there is significant polydispersity at each elution slice. This occurs when species with different degrees of branching have the same hydrodynamic volume.

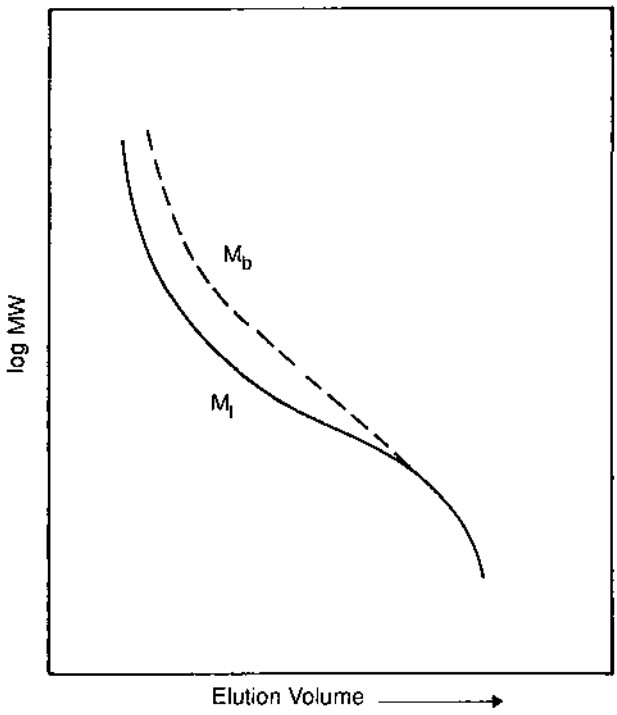

Figure 12 Typical SEC calibration curves for linear and branched polymers.

© 2004 by Marcel Dekker, Inc.

Selected applications are listed in Table 4. One of the most widely studied branched polymers is polyethylene. Rudin and co-workers (165,166) used SEC-LALLS to study branching in polyethylene in conjunction with intrinsic viscosity measurements. They found no appreciable difference between the two methods, indicating that there was little molecular weight polydispersity in each elution volume. They also compared SEC-LALLS results with static LALLS results and found that the latter were significantly larger, possibly because of the poor refractometer signal at the high-molecular-weight end of the distribution. This is because of the molecular weight sensitivity of LS, which makes it especially sensitive to small amounts of highly branched material, or "microgel," which are either filtered out by the SEC columns or give too low a signal in the refractometer.

4.2.4 Biopolymers

Studies relating to the use of SEC-LS for several classes of polysaccharides and cellulosics are listed in Table 3. In addition, Dean and Rollings (184) studied polysaccharide depolymerase activity in fermentation with SEC-LS. Agarose and agarose-type polysaccharides, within a molecular weight range 80,000–140,000 g/mol, were also analyzed by SEC-LS (142).

Table 5 lists selected applications of SEC-LS for biopolymers, mainly proteins. An earlier review of SEC-LS of biopolymers can be found in Ref. 209. It is of interest that there has been only one reported study on the use of SEC-LS for the analysis of nucleic acids (207).

For protein characterization, SEC-LS has been used as an analytical procedure for determining the molecular weights of unknown samples and also

Table 4 Characterization of Branched Polymers by SEC-LS: Selected Applications

Macromolecule	References
Polyolefins	157–168
Polyvinyl chloride	166
Polyvinyl alcohol	169–172
Polychloroprene	171
Polystyrene	170,173,174
Polyoctenamer	175
Polybutadiene/polyisoprene	118,176–178
Polysaccharides	179,180
Dextran	127
Polymethyl methacrylate	181
Polyesters	182

© 2004 by Marcel Dekker, Inc.

Table 5 Molecular Weight Distribution by SEC-LS: Biopolymers: Selected Applications

Macromolecule	References
Proteins	97,184–198
Membrane proteins	198–204
Enzymes	205,206
Nucleic acids	207

for studying protein association. In using an on-line light-scattering detector for SEC of proteins, it seems logical to use assigned dn/dc values for individual proteins, determined off line using purified samples. In many cases, however, purified standard proteins are not available, there is limited sample availability, or the identity of proteins in a sample is not known. Because of the uncertainty in dn/dc values, many investigators have used both a differential refractometer and a UV spectrophotometer, in series with a light-scattering detector, to determine dn/dc values of eluting species. For example, Maezawa and Takagi (198) used this approach to determine the molecular weights of glycoproteins. A light-scattering-UV-DRI (differential refractive index) detection system has also been used for determining molecular weights of ATPases (192,206) and membrane proteins (208). Recently, Krull and co-workers (185,209) investigated the advantages of using the LS-UV-DRI approach for protein characterization and found that on-line dn/dc measurements were in good agreement with off-line measurements. Furthermore, these investigators demonstrated the use of gradient elution high-performance liquid chromatography (HPLC) with an on-line light-scattering detector and applied this technique to examine aggregation of bovine alkaline phosphate (186,210), ribonuclease A (186), lysozyme (186), and pituitary and recombinant human growth hormones (184).

Dollinger *et al.* (211) used an HPLC fluorimeter as a 90° light-scattering detector for proteins analyzed by reversed-phase HPLC. The excitation and emission wavelengths were both set to 467 nm. Because of the small size of the proteins, there was no measurable scattering asymmetry for molecular weights below 1×10^6 g/mol, and the scattered intensity at 90° was found to be proportional to molecular weight. The light-scattering method was further simplified, in this case, by assuming that the second virial coefficient was negligible under HPLC conditions and that dn/dc values for all proteins under similar chromatographic conditions were equal. Figure 13 shows the LS and UV responses for lysozyme analyzed by reversed-phase HPLC. The double peaks have the same molecular weight and correspond to different conformers rather than aggregates.

© 2004 by Marcel Dekker, Inc.

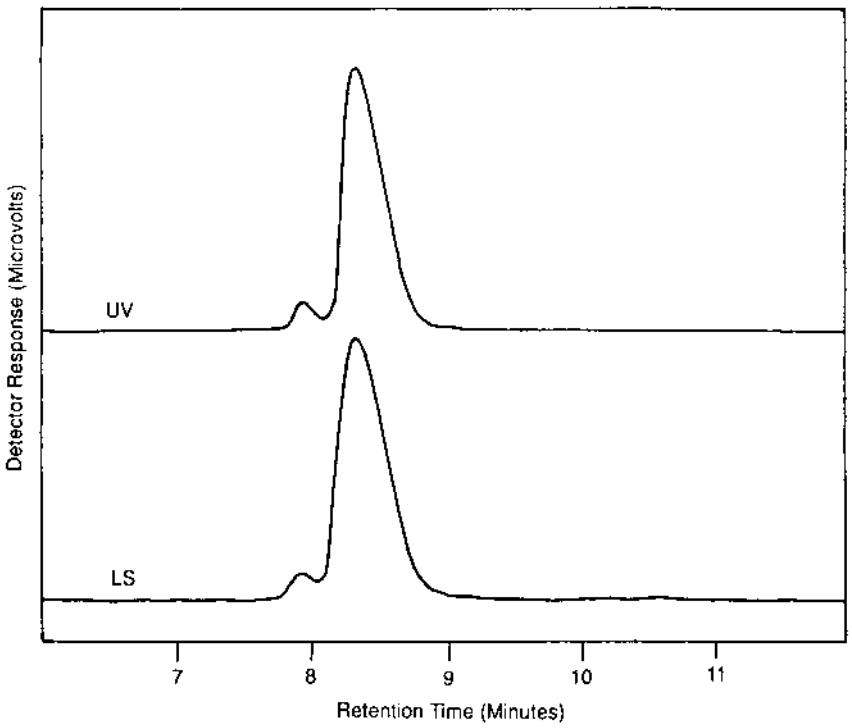

Figure 13 Gradient reversed-phase HPLC of lysozyme showing two conformers in both the UV and light-scattering tracings. Light scattering was measured using an HPLC fluorimeter at 90°. (From Ref. 211, with permission from Elsevier Science Publishers.)

5 SPECIAL APPLICATIONS

Cotts (105) showed that SEC-LALLS could be combined with universal calibration to determine the intrinsic viscosity at each elution volume increment. As in SEC-viscometry with universal calibration, the accuracy of the calculated values depends upon the chromatograms being corrected for axial dispersion. In addition, the Mark–Houwink coefficients can be determined from a plot of molecular weight and intrinsic viscosity at each elution volume for the whole molecular weight distribution. However, it was noted that the values obtained were also sensitive to axial dispersion. Another source of error arises from the polydispersity in individual elution volume increments, because universal calibration requires that the number-average molecular weight be used to calculate intrinsic viscosity.

© 2004 by Marcel Dekker, Inc.

By measuring the scattered intensity at more than one angle, both the radius of gyration and the molecular weight can be determined for each elution volume. Jackson *et al.* (212) used multi-angle LS to determine the radius of gyration of monodisperse and polydisperse polystyrenes. For the nearly monodisperse standards, measurements for radii greater than 10 nm were possible. For the polydisperse sample the lower limit was 18 nm. A similar LS detector was used to determine the relationship between radius of gyration and molecular weight for linear polyethylene (87), cross-linked polystyrene (213), and polyamic acid (214). Figure 14 shows a plot of R_g vs. M_w for a polyamic acid.

The combination of a light-scattering detector and an on-line viscometer with SEC provides a method of directly measuring MWD and intrinsic viscosity distribution, as well as MWD, from universal calibration in a single experiment. Such a combined instrument has been used by Lesec and Volet (215,216) to characterize a range of linear and branched synthetic polymers. Tinland and co-workers (217) used an SEC-viscometry-LS instrument to characterize xanthan and dextran. Grubisic-Gallot *et al.* (66) added a second concentration detector to an SEC-viscometry-LS instrument to characterize block copolymers. Pang and Rudin (48) showed how each detector (light-scattering, viscometer, and DRI) provided

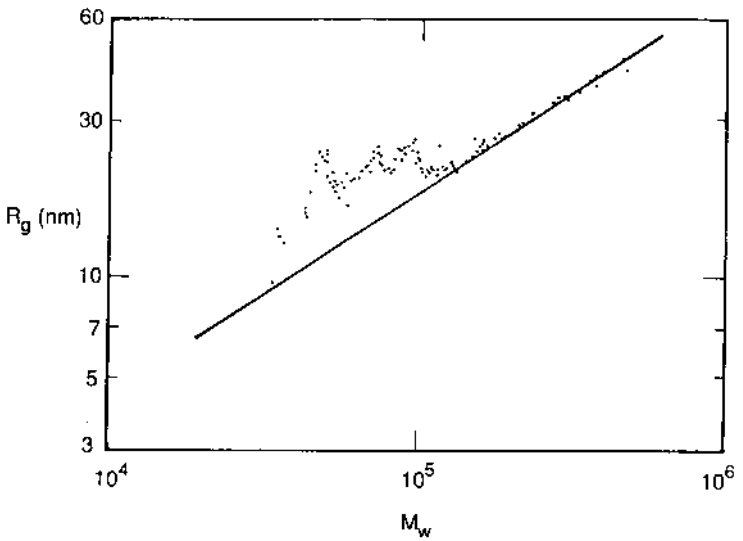

Figure 14 Radius gyration R_g vs. weight-average molecular weight of a diethyl ester of a polyamic acid as determined using SEC with an on-line multi-angle laser light-scattering detector. The line through the data is the linear regression fit for molecular weight greater than 10^5 g/mol. (Adapted from Ref. 213, with permission from John Wiley and Sons, Inc.)

© 2004 by Marcel Dekker, Inc.

useful information in the analysis of linear polyolefins at high temperature. They also demonstrated, for the polymer studied, that no single detector was able to give a complete picture of the MWD because of different sensitivity ranges. Jackson and co-workers (218) showed that the Mark–Houwink exponent of polystyrene in toluene could be measured with a relative standard deviation of less than 1% with a single injection of a broad MWD standard.

As discussed earlier, a combination of a right-angle laser light-scattering detector and a viscometer has proved to be a useful system for determining not only molecular weight and intrinsic viscosity data but also radius of gyration of linear polymers (11). Light-scattering measurements made at 90° simplify the design of light-scattering instrumentation and, in principle, give a less noisy signal by reducing spikes from particle contamination and stray light. In fact, a commercially available HPLC fluorescence detector can be employed for these measurements (212).

6 SUMMARY

The use of molecular weight sensitive detectors has increased dramatically the information content that can be obtained from an SEC analysis. With these detection systems, accurate measurements of fundamental molecular parameters, both average and distributed values, can be determined readily. Furthermore, the use of light-scattering detectors, and viscosity detectors for IVD, eliminates the need for column calibration, which greatly increases the precision and reliability of these measurements. However, as, in any other analytical instrumental procedure, good chromatographic practise must be exercised: signal-to-noise ratio of detector outputs must be maximized, defined polymer solutions injected, and instrument calibration parameters and proper interdetector volumes established.

In addition to applications in the area of synthetic polymers, we foresee exciting uses of molecular weight sensitive detectors for biopolymer characterization and with interactive modes of separation, such as reversed-phase gradient elution or ion-exchange chromatography. Finally, the combination of on-line spectroscopic detectors, including UV-diode array, Fourier transform infrared, mass spectrometry and possibly nuclear magnetic resonance with molecular weight sensitive detectors represent a significant breakthrough for the characterization of complex polymeric materials.

7 ACKNOWLEDGEMENTS

The authors gratefully acknowledge the valuable input and discussions with our colleague Wallace W. Yau. We also thank the Corporate Center for Analytical Sciences of the DuPont Company for giving us opportunity to prepare this chapter.

© 2004 by Marcel Dekker, Inc.

8 APPENDIX: INSTRUMENT COMPANIES

8.1 Light-Scattering Detectors for SEC

Brookhaven Instruments Corp., 750 Blue Point Rd, Holtsville, NY 11742: CCD-based seven-angle light-scattering detector.

Precision Detectors, Inc., 34 Williams Way, Bellingham, MA 02019: dynamic light-scattering and dual-angle light-scattering detectors.

Viscotek Corp., 15600 West Hardy Rd, Houston, TX 77060: right-angle and dual-angle light-scattering detectors.

Wyatt Technology Corp., 30 South La Patera Lane, Santa Barbara, CA 93117: dynamic light scattering, multiangle and triple-angle light-scattering detectors.

8.2 Viscometers for SEC

Viscotek Corp., 15600 West Hardy Rd, Houston, TX 77060: four capillary bridge design.

Waters Corp., 34 Maple St., Milford, MA 01757: flow-referenced capillary design.

9 REFERENCES

1. WW Yau, JJ Kirkland, DD Bly. Modern Size Exclusion Liquid Chromatography. New York: John Wiley and Sons, 1979.
2. P Kratochvil. Classical Light Scattering from Polymer Solutions. New York: Elsevier, 1987.
3. M Bohdanecky, J Kovar. Viscosity of Polymer Solutions. New York: Elsevier, 1982.
4. H Yamakawa. Modern Theory of Polymer Solutions. New York: Harper and Row, 1971.
5. H Fujita. Polymer Solutions. New York: Elsevier, 1990.
6. MA Haney. J Appl Polym Sci 30:3023, 1985; 30:3037, 1985.
7. JL Ekmanis, RA Skinner. J Appl Polym Sci, Appl Polym Symp 48:57, 1991.
8. WW Yau, SD Abbott, GA Smith, MY Keating. ACS Symp Ser 352:80, 1987.
9. BH Zimm. J Chem Phys 16:1093, 1948.
10. ML McConnell. Am Lab 10(5):63, 1978.
11. MA Haney, C Jackson, WW Yau. Proc Int Gel Permation Chromatography Symp 1991, San Francisco, 1993, p 49.
12. Precision Detectors, Application Notes, Amherst, MA.
13. PJ Wyatt, DL Hicks, C Jackson, GK Wyatt. Lab 20(6):108, 1988.
14. PJ Wyatt, C Jackson, GK Wyatt. Am Lab 20(5):86, 1988.
15. Z Grubisic, P Rempp, H Benoit. J Polym Sci, Part B, Polym Lett 5:753, 1967.
16. AE Hamielec, AC Ouano. J Liq Chromatogr 1:111, 1978.
17. CJ Stacy. J Appl Polym Sci 32:3959, 1986.

© 2004 by Marcel Dekker, Inc.

18. JM Goldwasser. Proc Int Gel Permation Chromatography Symposium 1989, Newton, MA, 1990, p 150.
19. JJ Kirkland, SW Rementer, WW Yau. J Appl Polym Sci 48:39, 1991.
20. WW Yau. Chemtracts-Macromol Chem 1:1, 1990.
21. PJ Flory, TG Fox, Jr. J Am Chem Soc 73:1904, 1951.
22. OB Ptitsyn, YE Eizner. Sov Phys Tech Phys 4:1020, 1960.
23. HG Barth, WW Yau. Proc Int Gel Permation Chromatography Symp 1989, Newton, MA, 1990, p 26.
24. MB Huglin, ed. Light Scattering from Polymer Solutions. New York: Academic Press, 1972, Ch 6.
25. MB Huglin. In: J Brandrup, EH Immergut, eds. Polymer Handbook, 3rd ed. New York: John Wiley and Sons, 1989.
26. H Eisenberg. Biological Macromolecules and Polyelectrolytes in Solution. Oxford: Clarendon Press, 1987.
27. H Utiyama. In: MB Huglin, ed. Light Scattering from Polymer Solutions. New York: Academic Press, 1989, Ch 4.
28. M Martin. Chromatographia 15:426, 1982.
29. O Prochazka, P Kratochvil. J Appl Polym Sci 3:919, 1986.
30. O Prochazka, P Kratochvil. J Appl Polym Sci 34:2325, 1987.
31. R Bruessau. In: J Cazes, ed. Liquid Chromatography of Polymers and Related Material—II. New York: Marcel Dekker, 1983, p 73.
32. D Lecacheux, J Lesec. J Liq Chromatogr 5:2227, 1982.
33. TH Mourey, SM Miller. J Liq Chromatogr 13:693, 1990.
34. C-Y Kuo, T Provder, ME Koehler, AF Kah. ACS Symp Ser 352:130, 1987.
35. ST Balke, P Cheung, L Jeng, R Lew. J Appl Polym Sci, Appl Polym Symp 48:259, 1991.
36. TH Mourey, SM Miller, ST Balke. J Liq Chromatogr 13:435, 1990.
37. C Jackson, WW Yau. J Chromatogr 645:209, 1993.
38. Z He, X Zhang, R Cheng. J Liq Chromatogr 5:1209, 1982.
39. K Lederer, G Imrich-Scwarz, M Dunky. J Appl Polym Sci 32:4751, 1986.
40. J Billiani, DK Lederer, M Dunky. Angew Makromol Chem 180:199, 1990.
41. J Billiani, I Amtmann, T Mayr, K Lederer. J Liq Chromatogr 13:2973, 1990.
42. J Billiani, DK Lederer. J Liq Chromatogr 13:3013, 1990.
43. AE Hamielec. In: J Janca, ed. Steric Exclusion Liquid Chromatography of Polymers. Chromatographic Science Series, Vol. 25. New York: Dekker, 1984, Ch 3.
44. MA Haney, JE Armonas, L Rosen. ACS Symp Ser 352:119, 1987.
45. MG Styring, JE Armonas, AE Hamielec. ACS Symp Ser 352:104, 1987.
46. FB Malihi, CY Kuo, ME Kochler, T Provder, AF Kah. Org Coat Appl Polym Sci Proc 48:760, 1983.
47. FB Malihi, CY Kuo, ME Koehler, T Provder, AF Kah. ACS Symp Ser 245:281, 1984.
48. S Pang, A Rudin. Polymer 33:1949, 1992.
49. DJ Nagy. Int GPC Symp '87, 1987, p 250.
50. DJ Nagy, DA Terwilliger. J Liq Chromatogr 12:1431, 1989.
51. DJ Nagy. J Liq Chromatogr 13:677, 1990.
52. G Marot, J Lesec. Int GPC Symp '87, 1987, p 113.

© 2004 by Marcel Dekker, Inc.

53. G Marot, J Lesec. J Liq Chromatogr 11:3305, 1988.
54. T Housaki, K Sato. Polym J (Tokyo) 20:1163, 1988.
55. D Lecacheux, J Lesec, C Quivoron, R Prechner, R Panaras. J Appl Polym Sci 29:1569, 1984.
56. ME Himmel, K Tatsumoto, KK Oh, DK Johnson, HL Chum. ACS Symp Ser 397:82, 1989.
57. ME Himmel, K Tatsumoto, K Grohmann, DK Johnson, HL Chum. J Liq Chromatogr 498:93, 1990.
58. EJ Siochi, MA Haney, W Mahn, TC Ward. ACS Symp Ser 397:100, 1989.
59. JD Timpa. J Agric Food Chem 39:270, 1991.
60. BP Wasserman, JD Timpa. Starch/Staerke 43:389, 1991.
61. ML Fishman, DT Gillespie, SM Sondey, RA Bardord. J Agric Food Chem 37:584, 1989.
62. ML Fishman, DT Gillespie, SM Sondey. Carbohydr Res 215:91, 1991.
63. PK Dutta. J Chromatogr Sci 28:119, 1990.
64. PK Dutta, K Hammons, B Willeby, MA Haney. J Chromatogr 536:113, 1991.
65. HE Adams. In: KH Altgelt, L Segal, eds. Gel Permeation Chromatography. New York: Dekker, 1971, p 391.
66. Z Grubisic-Gallot, JP Lingelser, Y Gallot. Polym Bull (Berlin) 23:389, 1990.
67. BH Zimm, WH Stockmayer. J Chem Phys 17:1301, 1949.
68. J Roovers. In: Encyclopedia of Polymer Science and Technology, Vol. 2, 2nd ed. New York: J. Wiley and Sons, 1989, p 478.
69. EJ Siochi, JM DeSimone, AM Hellstern, JE McGrath, TC Ward. Polym Prep (Am Chem Soc Div Polym Chem) 30(1):141, 1989.
70. EJ Siochi, JM DeSimone, AM Hellstern, JE McGrath, TC Ward. Macromolecules 23:4696, 1990.
71. C Kuo, T Provder, ME Koehler. Polym Mater Sci Eng 65:142, 1991.
72. FM Mirabella, Jr, L Wild. Polym Mater Sci Eng 59:7, 1988.
73. DG Moldovan. Int GPC Symp '87, 1987, p 129.
74. D Lecacheaux, J Lesec, C Quivoron. J Appl Polym Sci 27:4867, 1982.
75. D Lecacheux, J Lesec, C Quivoron. Polym Prepr (Am Chem Soc, Div Polym Chem) 23(2):126, 1982.
76. PJ Wang, RJ Rivard. J Liq Chromatogr 10:3059, 1987.
77. C Jin, S Sun, S Sui. Yingyong Huaxe 3:50, 1986.
78. C Jin, S Sun, R Hou, R Cheng. Gaofenzi Xuebao 2:113, 1987.
79. BE Boyes, HG Barth, WW Yau. 200th ACS National Mtg., Washington, D.C., August 1990, Dn. Agr. Food Chem., Abstract 147.
80. KE van Holde. Physical Biochemistry. 2nd ed. Englewood Cliffs, NJ: Prentice-Hall, 1985.
81. W Zhang, M Wang, J Sun, X Zhang, Z He. Yingyong Huaxue 7(3):57, 1990.
82. F Schosseler, H Benoit, Z Grubisic-Gallot, C Strazielle, L Leibler. Macromolecules 22:400, 1989.
83. WG Rand, AK Mukherji. J Appl Polym Sci. Polym Lett Ed 20:501, 1982.
84. A Lapp, C Strazielle. Makromol Chem 184(9):1877, 1984.

© 2004 by Marcel Dekker, Inc.

85. Y Tsukahara, K Tsutsumi, Y Yamashita, S Shimada. Macromolecules 23:5201, 1990.
86. JG Rooney, G Ver Strate. In: J Cazes, ed. Liquid Chromatography of Polymers and Related Materials III. New York: Marcel Dekker, 1981, p 207.
87. T Housaki, K Satoh. Makromol Chem Rapid Commun 9:257, 1988.
88. AW Degroot. J Appl Polym Sci, Appl Polym Symp 43:85, 1989.
89. V Grinshpun, KF O'Driscoll, A Rudin. Org Coat Appl Polym Sci Proc 48:745, 1983.
90. V Grinshpun, KF O'Driscoll, A Rudin. J Appl Polym Sci 29:1071, 1984.
91. V Grinshpun, A Rudin. J Appl Polym Sci 30:2413, 1985.
92. G Pastuska, J Just, H August. Angew Makromol Chem 107:173, 1982.
93. H Schorn, R Kosfeld, M Hess. J Chromatogr 353:273, 1986.
94. DJ Goedhart, JB Hussem, BPM Smeets. Chromatogr Sci 13 (Liq Chromatogr Polym Relat Mater 2):203, 1980.
95. PJ Wang, BS Glassbrenner. J Liq Chromatogr 11:3321, 1988.
96. A Huber. Biochem Soc Trans 19:505, 1991.
97. M Fukutomi, M Fukuda, T Hashimoto. Toyo Soda Kogyo KK Japan 24:33, 1980.
98. CJ Kim, AE Hamielec, A Bendek. J Liq Chromatogr 5:1277, 1982.
99. WM Kulicke, N Boese. Colloid Polym Sci 262:197, 1984.
100. G Muller, C Yonnet. Makromol Chem, Rapid Commun 5:197, 1984.
101. T Kato, T Tokuya, T Nozaki, A Takahashi. Polymer 25:218, 1984.
102. R Jenkins, RS Porter. J Polym Sci, Polyn Lett Ed 18:743, 1980.
103. R De Jaeger, D Lecacheaux, P Potin. J Appl Polym Sci 39:1793, 1990.
104. EE Remsen. J Appl Polym Sci 42:503, 1991.
105. PM Cotts. J Polym Sci, Part B, Polym Phys 24:1493, 1986.
106. A Kinugawa, Y Kise. Kobunshi Ronbushu 45:531, 1988.
107. S Berkowitz. J Appl Polym Sci 29:4353, 1984.
108. DB Cotts. Org Coat Appl Polym Sci Proc 48:750, 1983.
109. DJ Nagy. Polym Sci, Part C, Polym Lett 24:87, 1986.
110. C Bailly, D Daust, R Legras, JP Mercier, C Straziell, A Lapp. Polymer 27:1410, 1986.
111. JD Wellons, L Gollob. Wood Sci 13:68, 1980.
112. S Bo, R Cheng. J Liq Chromatogr 5:1404, 1982.
113. T Honma, M Tazaki. Nippon Gomu Kyokaishi 60:636, 1987.
114. SA Gusev, IB Tsvetkovski, V Valuev. Kauch Rezina 3:32, 1984.
115. X Wang, X Zhang, Z He. Yingyong Huaaxue 2:77, 1985.
116. CS Wu, L Senak. J Liq Chromatogr 13:851, 1990.
117. FC Lin, GD Getman. Int GPC Symp '87, 225, 1987.
118. RC Jordan, SF Silver, RD Sehon, RJ Rivard. Org Coat Appl Polym Sci Proc 48:755, 1983.
119. RJ Cramer. Report 1987, NWC-TP-6774, SBI-AD-E900674; Order No. AD-A182149, Avail. NTIS.
120. T Dumelow, SR Holding, LJ Maisey, JV Dawkins. Polymer 27:1170, 1986.
121. TJ Dumelow. Macromol Sci Chem A26:125, 1989.
122. R Murakoe. Petrotech (Tokyo) 10:175, 1987.
123. FB Malihi, CY Kuo, T Provder. J Appl Polym Sci 29:925, 1984.
124. V Grinshpun, A Rudin. Polym Mater Sci Eng 54:174, 1986.

© 2004 by Marcel Dekker, Inc.

125. D Slootmaekers, JAPP Van Dijk, FA Varkevisser, CJ Bloys Van Treslong.
126. CJ Kim, AE Hamielec, A Bendek. J Liq Chromatogr 5:425, 1982.
127. JAPP Van Dijk, FA Varkevisser, JAM Smit. J Polym Sci, Part B, Polym Phys 25:149, 1987.
128. BR Vijayendran, T Bone. Carbohydr Polym 4:299, 1984.
129. D Lecacheaux, Y Mustiere, A Denis. Spectra 2000 122:57, 1987.
130. MG Kontominas, JL Kokoni. Lebensm-Wiss Technol 23:174, 1990.
131. WE Hennink, JWA Van den Berg, J Feijen. Thromb Res 45:463, 1987.
132. A Heyraud, M Rinaudo. ACS Symp Ser 458 (Biotechnol Amylodextrin Oligosaccharides):171, 1991.
133. K Lederer, C Huber, M Dunky, JK Fink, HP Ferber, E Nitsch. Arzneim-Forsch 35:610, 1985.
134. S Hizurkuri, T Takagi. Carbohydr Res 134:1, 1984.
135. T Takagi. Kagaku Zokan (Kyoto) 102:253, 1984.
136. JA Hunt, TS Young, DW Grenn, GP Willhite. SPE Reservoir Eng 3:835, 1988.
137. F Lambert, M Milas, M Rinaudo. Polym Bull (Berlin) 7:185, 1982.
138. A Corona, JE Rollings. Sep Sci Technol 23:855, 1988.
139. D Lecacheaux, R Panaras, G Brigand, G Martin. Carbohydr Polym 5:423, 1985.
140. D Lecacheaux, Y Mustiere, R Panaras, G Brigand. Carbohydr Polym 6:447, 1986.
141. M Miya, R Iwamoto, S Yoshikawa, S Mima. Kobunshi Ronbushu 43:83, 1986.
142. C Rochas, M Lahaye. Carbohydr Polym 10:129, 1989.
143. JM Lauriol, P Froment, F Pla, A. Robert. Holzforschung 41:109, 1987.
144. JM Lauriol, J Comtat, P Froment, F Pla, A Robert. Holzforschung 41:165, 1987.
145. JM Lauriol, J Comtat, P Froment, F Pla, A Robert. Holzforschung 41:215, 1987.
146. JJ Cael, KJ Cietek, FJ Kolpak. J Appl Polym Sci, Appl Polym Symp 37:509, 1983.
147. T Kato, T Tokuya, A Takahasi. Kobunshi Ronbunshu 39:293, 1981.
148. WD Eigner, J Biliani, A Huber. Papier 41:680, 1987.
149. A Wirsen. Makromol Chem 189:833, 1988.
150. PJ Wood, J Weisz, W Mahn. Cereal Chem 68:530, 1991.
151. JT Cheng, MJ Langsam. Macromol Sci Chem A21:403, 1984.
152. A Wirsen, E Helleday. Report 1986, FOA-C-20602-D-1; Order No. PB86-88067/GAR, (Sweden). Avail. NTIS from Gov. Rep. Announce. Index (USA) 1986, 86(16), Abstract No. 635,623.
153. AF Cunningham, C Heathcote, DE Hillma, JI Paul. Chromatogr Sci 13 (Liq Chromatogr Polym Relat Mater 2):175, 1980.
154. DS Argyropoulos, HIJ Bolker. Wood Chem Technol 7:1, 1987.
155. ES Olson, JW Diehl. J Chromatogr 349:337, 1985.
156. H Benoit. In: MB Huglin, ed. Light Scattering from Polymer Solutions. New York: Academic Press, 1972.
157. FJ Kolpak, DJ Cietek, W Fookes, JJ Cael. J Appl Polym Sci, Appl Polym Symp 37:491, 1983.
158. DE Axelson, WC Knapp. J Appl Polym Sci 25:119, 1980.
159. BD Dickie, RJ Koopmans. J Polym Sci, Part C, Polym Lett 28:193, 1990.
160. W Zhang, M Wang, J Sun, Z He. Yingyong Huaxue 7(3):48, 1990.
161. TB MacRury, ML McConnell. J Appl Polym Sci 24:651.

© 2004 by Marcel Dekker, Inc.

162. LI Kulin, NL Meijerink, P Starck. Pure Appl Chem 60:1403, 1988.
163. DC Bugada, A Rudin. Eur Polym J 23:847, 1987.
164. V Grinshpun, A Rudin, KE Russel, MV Scammell. J Polym Sci, Part B, Polym Phys 24:1171, 1986.
165. V Grinshpun, A Rudin. Makromol Chem Rapid Commun 6:219, 1985.
166. A Rudin, V Grinshpun, KF O'Driscoll. J Liq Chromatogr 7:1809, 1984.
167. S Shiga, Y Sato. Nippon Gomu Kyokaishi 57:811, 1984.
168. S Shiga. Nippon Gomu Kyokaishi 59:162, 1986.
169. AE Hamielec, AC Ouano, LI Nebenzahl. J Chromatogr 1:527, 1978.
170. ZL Gallot. Chromatogr Sci 13 (Liq Chromatogr Polym Relat Mater 2):113, 1980.
171. RC Jordan, ML McConnell. AGS Symp Ser 138 (Size Exclusion Chromatogr):107, 1980.
172. SH Agarwal, RF Jenkins, RS Porter. J Appl Polym Sci 27:113, 1982.
173. A Hasegawa, T Nakamura, S Teramachi. Kogakuin Daigaku Kenkyu Hokoku 60:25, 1986.
174. Z He, M Yuan, X Zhang, X Wang, X Jin, J Huang, C Li, L Wang. Eur Polym 2:597, 1986.
175. T Usami, Y Gotoh, S Takayama. Eur Polym J 21:885, 1985.
176. X Zhang, X Wang, Z He. Shiyou Huagong 15:349, 1986.
177. EP Piskareva, GG Kartasheva. Kauch Rezina 1:27, 1988.
178. RC Jordan, SF Silver, RD Sehon, RJ Rivard. ACS Symp Ser 2245:295, 1984.
179. LP Yu, JE Rollings. J Appl Polym Sci 33:1909, 1987.
180. LP Yu, JE Rollings. J Appl Polym Sci 35:1085, 1988.
181. P Lang, W Burchard. Makromol Chem, Rapid Commun 8:451, 1987.
182. BL Neff, JR Overton. Polym Prepr (Am Chem Soc, Div Polym Chem) 23(2):130, 1982.
183. SW Dean, JE Rolling. Biotechnol Tech 3:161–185, 1989.
184. HH Stuting, IS Krull. J Chromatogr 539:91, 1991.
185. HH Stuting, IS Krull. Anal Chem 62:2107, 1990.
186. R Mhatre, IS Krull, HH Stuting. J Chromatogr 502:21, 1990.
187. W Flapper, PJM Van den Oetelaar, CPM Breed, J Steenbergen, HJ Hoenders. Clin Chem (Winston-Salem, NC) 32:363, 1986.
188. T Takagi. In: H Peeters, ed. Proc. 30th Colog Proteides Biol Fluids, Brussels, 1982. Oxford: Pergamon Press, 1982; pp 701–704.
189. T Takagi. Tanpakushitsu Kakusan Koso 27:1526, 1982.
190. T Takagi, SJ Hizukuri. Biochem (Tokyo) 95:1459, 1984.
191. T Takagi. Prog HPLC, 1 (Gel Permeation Ion-Exch Chromatogr Proteins Pept):27, 1985.
192. T Takagi, S Maezawa, YJ Hayashi. Biochem (Tokyo) 101:805, 1987.
193. A Kato, T Takagi. J Agric Food Chem 35:633, 1987.
194. JG Bindels, BM De Man, HJ Hoenders. J Chromatogr 252:255, 1982.
195. JG Bindels, HJ Hoenders. Chromatographia 15:475, 1982.
196. JG Bindels, BM De Man, H Bloemendal, HJ Hoenders. Lens Res 1:89, 1983.
197. K Kameyama, T Nakae, T Takagi. Biochim Biophys Acta 706:19, 1982.
198. S Maezawa, T Takagi. J Chromatogr 280:124, 1983.
199. JG Bindels, HJ Hoenders. J Chromatogr 261:381, 1983.

© 2004 by Marcel Dekker, Inc.

200. JG Bindels, GJJ Bessems, BM De Man, HJ Hoenders. Comp Biochem Physiol B 76B:47, 1983.
201. Y Hayashi, H Matsui, T Takagi. Methods Enzymol 172 (Biomembranes, Pt S):514, 1989.
202. Y Hayashi, K Mimura, H Matsui, T Takagi. Biochim Biophys Acta 983:217, 1989.
203. S Maezawa, Y Hayashi, T Nakae, J Ishii, K Kameyama, T Takagi. Biochim Biophys Acta 747:291, 1983.
204. T Fujitani, G Maeki, T Nakao. Kenkyu Nenpo-Tokyo-toritsu Eisei Kenkyu-sho 34:406, 1983.
205. T Nakao, T Ohno-Fujitani, MJ Nakao. Biochem (Tokyo) 94:689, 1983.
206. Y Hayashi, T Takagi, S Maezawa, H Matsui. Biochim Biophys Acta 748:153, 1983.
207. T Nicolai, L Van Dijk, JAAP Van Dijk, JAM Smit. J Chromatogr 389:286, 1987.
208. JN Ishii, T Takagi, K Kameyanna, T Nakae. J Exp Clin Med 7(suppl.):157, 1982.
209. HH Stuting, IS Krull, R Mhatre, SC Krzysko, HG Barth. LC-GC, 7:402, 1989.
210. IS Krull, HH Stuting, SC Krzysko. J Chromatogr 442:29, 1988.
211. G Dollinger, B Cunico, M Kunitani, D Johnson, R Jones. J Chromatogr 592:215, 1992.
212. C Jackson, LM Nilsson, PJ Wyatt. J Appl Polym Sci, Appl Polym Symp 45 (Polym Anal Charact 2):191, 1990.
213. SH Kim, PM Cotts, W Volksen. J Polym Sci, Part B, Polym Phys 30:177, 1992.
214. C Johann, P Kilz. J Appl Polym Sci, Polym Symp 48 (Polym Anal Charact 3):111, 1991.
215. J Lesec, G Volet. J Appl Polym Sci, Appl Polym Symp 45 (Polym Anal Charact 2):177, 1990.
216. J Lesec, G Volet. J Liq Chromatogr 13:831, 1990.
217. B Tinland, J Mazet, M Rinaudo. Makromol Chem, Rapid Commun 9:69, 1988.
218. C Jackson, HG Barth, WW Yau. Proc Int Gel Permation Chromatography Symposium 1991, San Francisco, 1993, p 751.

© 2004 by Marcel Dekker, Inc.

5
Characterization of Copolymers by Size Exclusion Chromatography

Gregorio R. Meira and Jorge R. Vega
INTEC (Universidad Nacional del Litoral and CONICET)
Santa Fe, Argentina

1 INTRODUCTION

Copolymers are characterized by a chemical composition distribution (CCD) that is represented by the mass fraction of molecules of a given copolymer composition vs. the copolymer composition. This characteristic considerably complicates the determination of the molecular weight distribution (MWD) of a copolymer by size exclusion chromatography (SEC) (1–7). However, there are two situations where copolymers can be almost treated as homopolymers from the point of view of the MWD estimation: (1) when the CCD is very narrow, or (2) (more generally) when the average composition does not change with hydrodynamic volume. Copolymers with narrow CCDs are in general desirable from the point of view of their end properties, and a control of the chemical composition along the copolymerization may be necessary for producing narrow CCDs. More normally, however, the average composition changes along the polymerization, and also

© 2004 by Marcel Dekker, Inc.

possibly with hydrodynamic volume (8). In this work, we shall limit our discussion to copolymers containing only two repeating units types.

From the point of view of the SEC analysis, block copolymers are simpler than statistical copolymers. This is because important properties such as the specific refractive index increment or the hydrodynamic volume may be estimated by simply averaging the corresponding homopolymer properties (6). Also, linear copolymers are simpler than branched copolymers from the point of view of their MWD determination. A long-branched copolymer of a given molar mass and composition exhibits a smaller hydrodynamic volume than its linear homolog, and the volume reduction is more pronounced with an increasing branching functionality (9,10).

The molecular macrostructure of a linear copolymer is totally determined by the bivariate distribution of molar masses and chemical composition (2–6). The univariate distributions of molar masses and chemical composition are obtained by appropriate integration of such bivariate distribution. A branched copolymer molecule is characterized by the number of branches and their functionality (9–12). In this work, we shall restrict our discussion to long-branched copolymers of functionality 3. The branching distribution (BD) is represented by the mass of molecules containing 1, 2,... branches/molecule vs. the number of branches (11,12). The complete molecular macrostructure of a trifunctionally branched copolymer is represented by a set of bivariate distributions of molecular weights and chemical composition, with one bivariate distribution for each branched topology. Presently, it is impossible to measure such detailed molecular macrostructure.

SEC is the main analytical technique for measuring the MWD of a polymer. For copolymers, several problems complicate this determination (13–15). Consider first the instantaneous mass. With homopolymers, the instantaneous mass is proportional to the differential refractometer (DR) signal, except perhaps for molar masses lower than 10,000 g/mol, where the specific refractive index increment shows a dependence on the molar mass (15,16). With copolymers, the specific refractive index increment depends on the instantaneous composition, and this last variable may change with hydrodynamic volume. Thus, the copolymer mass cannot be determined from the DR signal alone (6,15). Errors in the instantaneous mass affect not only the MWD ordinates. More importantly, it affects derived variables that are obtained from a signals ratio where the instantaneous mass is in the denominator. This is the case for the molar mass (when determined through an in-line detector) and for the chemical composition (when determined through a detector that responds to a single repeating unit type). The difficulties with the DR spurred the development of other more "universal" mass detectors such as the evaporative-light scattering detector or the on-line densimeter. Evaporative detectors present some fundamental difficulties for quantifying the instantaneous mass, but enable their interface with Fourier Transform Infrared (FTIR) detectors. This allows the determination of the

© 2004 by Marcel Dekker, Inc.

composition of the different deposited dried fractions. However, the poor film morphology produced by the evaporative interface can seriously affect the FTIR spectral accuracy, and a film posttreatment may be required (17–19). On-line densimeters are, in general, less sensitive than DRs (20).

The instantaneous molar mass is also difficult to estimate. In the more normal situation, in-line molar mass sensors are not available, and a molecular weight calibration is employed. Since copolymer standards are, in general, unavailable, the universal calibration is generally employed (21,22). The universal calibration assumes that at any elution volume V, the hydrodynamic volume is proportional to $\{M(V) \times [\eta](V)\}$, where M is the molar mass and $[\eta]$ is the intrinsic viscosity. Unfortunately, this concept yields only approximate molar masses. This is because $\{M(V) \times [\eta](V)\}$ represents the hydrodynamic volume of flexible molecules under Θ-conditions, while good solvents are used in SEC. Furthermore, to transform $[\eta]$ into molar mass, the Mark–Houwink parameters of the analyzed copolymer are required. Unfortunately, these parameters are generally unknown because they depend on many variables (not only on the solvent and the temperature, but also on the chemical composition, the molar mass, the polymer microstructure, and the level of branching) (23,24). For block copolymers, it has been suggested to estimate the Mark–Houwink parameters by interpolation (with the chemical composition) between the Mark–Houwink parameters of the corresponding homopolymers. This procedure includes a correction term for statistical copolymers with many sequence alternations (25).

Consider the direct molar mass measurement through an intrinsic viscometer (IV) or a light-scattering (LS) detector. Their signals are proportional to the instantaneous molar mass (15,16,26–28), and for this reason the measurements are insensitive to low molar masses (e.g., lower than 30,000 g/mol). LS sensors have the advantage of not requiring any molecular weight calibration. However, the specific refractive index increment of the instantaneously analyzed fraction must be *a priori* known, and this information is in general unavailable. However, even if it were, only an apparent (rather than a true) molar mass would be determined by LS (15,28). For the IV signal, either the universal calibration or the Mark–Houwink parameters of the analyzed copolymer are required. Both approaches only produce approximate molar masses, however. In spite of all their limitations, IVs are generally preferred to LS sensors for analysing copolymers, except for the rather special case where the specific refractive index increments of both repeating unit types are identical (14). Through triple detection SEC (i.e., DR + IV + LS sensor) it is in principle possible to characterize a chromatographically complex polymer without resorting to any molecular weight calibration (28,29). However, its applicability to copolymers with a varying composition along the elution volume has not yet been fully demonstrated. Also, $\overline{M}_n$ may be directly obtained from the IV signal and the universal calibration, without requiring an instantaneous mass measurement (30).

© 2004 by Marcel Dekker, Inc.

An insurmountable limitation of SEC is that molecules are fractionated according to hydrodynamic volume rather than by molar mass. This determines that (even under perfect resolution) the instantaneous MWD is not monodisperse, except perhaps for the rather special case where both repeating unit types exhibit identical specific densities and are noninteracting. The variety of molar masses in the detector cell when a "chromatographically complex" polymer is analyzed introduces some bias in the MWD (31). The bias is further magnified under imperfect resolution. Imperfect resolution results from a combination of: (a) nonexclusion (secondary or enthalpic) fractionation (32,33), and (b) instrumental broadening in the columns, fittings, and detectors (33–37). Nonexclusion effects may shift and distort the chromatograms, yielding both positive and negative molecular weight deviations. Instrumental broadening is important when the MWD is narrow or multimodal. If the instrumental broadening is not corrected for, then the polydispersity $\overline{M}_w/\overline{M}_n$ is typically: (a) overestimated when the molecular weights are calculated from a calibration obtained with narrow standards, (b) underestimated when obtained from LS sensors, and (c) under- or overestimated when obtained from IVs (37,38).

In liquid adsorption chromatography (LAC), copolymer molecules are fractionated according to their enthalpic interactions with the column substrate. When the repetitive unit types exhibit a difference in their adsorption–desorption behavior and such behavior is independent of the molar mass, then LAC can be used to determine the CCD (39).

In many practical situations, copolymers are mixed with their corresponding homopolymers, and it may be impossible to quantitatively isolate the copolymer prior to its SEC analysis. This involves a serious complication, because SEC detectors cannot distinguish a copolymer from a homopolymer mixture with the same hydrodynamic volume and an equivalent global composition. Even in the presence of polymer mixtures, the bivariate distribution of the molecular weights and chemical composition may still be estimated if the repeating unit types exhibit a difference in their adsorption–desorption behavior. First, preparative LAC is used to isolate the copolymer from the homopolymers and to fractionate the copolymer by composition. Then, SEC is used to determine the MWD of thin slices of the LAC eluogram (40,41). With less success, previous developments have been proposed that first fractionate by hydrodynamic volume and then analyze the eluted slices by chemical composition (42).

In some special cases, SEC alone is capable of determining both the MWD and the CCD (43–45). To this effect, the following (rather hard) conditions must be verified: (1) the instantaneous distributions of the molecular weights and of the chemical composition are both narrow, and (2) the instantaneous average composition varies monotonically with the molecular weights. Eventually, the second condition could be relaxed if the first condition were strictly verified. Similarly, both the MWD and the DB of a branched copolymer may be determined

© 2004 by Marcel Dekker, Inc.

by SEC alone (11,12,46). In this case, the following is required: (1) the instantaneous distributions of the molecular weights and of the number of branches per molecule are both narrow, (2) the average number of branches per molecule increases monotonically with the molar mass, and (3) the CCD is narrow, or (at least) the average composition does not change with the molar mass (11,12). The first condition is again the most important. All three conditions are approximately verified in a copolymerization where both reactivity ratios are close to 1, and where long branches are produced by reaction with the accumulated polymer.

In the remaining sections, three styrene–butadiene (SB) copolymers are analyzed by SEC alone. In Example 1, the aim is to determine the MWD of a statistical SBR obtained in an emulsion process. In Example 2, the aim is to determine the MWD and CCD of a linear diblock SB rubber obtained in a sequential anionic polymerization. In Example 3, the aim is to determine the MWD and BD of a graft SB copolymer contained in high-impact polystyrene. Examples 2 and 3 have been previously presented with greater detail (11,12,45), but in this work they will be reconsidered in a more general fashion. In all three examples, the measurements were carried out with a Waters ALC244 size exclusion chromatograph fitted with a DR, a UV sensor at 256 nm, and a full set of 6 μ-Styragel® columns. In all three cases, the carrier solvent was tetrahydrofurane (THF) at 1 mL/min and 25°C. In example 3, an in-line IV (Viscotek Corp., Houston, Texas) was added to the dual-detection system. The detector signals were sampled as follows: every 0.118 mL in Example 1, every 0.150 mL in Example 2, and every 0.027 mL in Example 3.

2 EXAMPLE 1: MOLECULAR WEIGHT DISTRIBUTION

Let us first discuss the more general problem of analysing an SB copolymer by SEC with standard dual-detection and a set of narrow PS and PB standards of known molecular weights. A UV sensor at 256 nm was used. This detector "sees" only the phenyl groups of the S repeating units, but not the B repeating units. The following equations can be written for the baseline-corrected UV and DR chromatograms [$s_{UV}(V)$ and $s_{DR}(V)$, respectively] (1,6,43–45):

$$s_{UV}(V) = k_{UV} p_S(V) w(V) \tag{1}$$

$$s_{DR}(V) = k_{DR}\{\nu_{PS} p_S(V) + \nu_{PB}[1 - p_S(V)]\} w(V) \tag{2}$$

where $w(V)$ is the instantaneous mass, $p_S(V)$ is the instantaneous mass fraction of S; k_{UV}, k_{DR} are the UV and DR sensor gains; and ν_{PS}, ν_{PB} are the specific refractive index increments of PS and PB, respectively. From Eq. (2), $w(V)$ is proportional

© 2004 by Marcel Dekker, Inc.

to $s_{DR}(V)$ when either $\nu_{PS} = \nu_{PB} = \text{constant}$, or when (more generally) $p_S(V) = \text{constant}$. Solving for the unknowns in Eqs (1) and (2), one obtains:

$$w(V) = \left(\frac{1}{k_{DR}\nu_{PB}}\right)s_{DR}(V) + \left(\frac{\nu_{PB} - \nu_{PS}}{k_{UV}\nu_{PB}}\right)s_{UV}(V) \tag{3}$$

$$p_S(V) = \frac{1}{\left(\frac{\nu_{PB} - \nu_{PS}}{\nu_{PB}}\right) + \left(\frac{k_{UV}}{k_{DR}\nu_{PB}}\right)\frac{s_{DR}(V)}{s_{UV}(V)}} \tag{4}$$

The signal-to-noise ratio of a chromatogram is high at its maximum but low near to the baseline. Also, large systematic errors can occur at the chromatogram tails. In Eqs (3) and (4), the values in parentheses are constants. Thus, the following can be noted: (a) $w(V)$ results from a linear combination of the chromatograms, and therefore it is relatively "well behaved" from the point of view of the propagation of errors, and (b) $p_S(V)$ is obtained from a signals ratio, and therefore acceptable estimations are only feasible in the midchromatogram region.

From the PS and PB standards, the individual calibrations $\log M_{PS}(V)$ and $\log M_{PB}(V)$ are obtained. Then, the copolymer molar mass $M(V)$ can be calculated by interpolation with the copolymer composition, as follows (43):

$$\log M(V) = p_S(V)\log M_{PS}(V) + [1 - p_S(V)]\log M_{PB}(V) \tag{5}$$

Alternatively, the following expression has been derived on the basis of the universal calibration, and for cases where the homopolymer calibrations are linear and parallel to each other (47):

$$M(V) = \frac{M_{PS}(V)}{1 + (r-1)[1 - p_S(V)]} \tag{6}$$

where $r = M_{PS}(V)/M_{PB}(V) = \text{constant}$. Equation (6) has been later extended for cases where the homopolymer calibrations exhibit different slopes (48).

Equations (1–6) are strictly applicable to linear block SB copolymers as in Example 2. However, the same equations are here applied to the SBR copolymer of Example 1. In Examples 1 and 2, a common set of calibrations were used. The detectors were calibrated as follows (45): (a) different masses of PS and PB homopolymers were injected, (b) the total chromatogram areas were represented vs. the injected masses, (c) three straight lines were adjusted, and (d) the slopes yielded $k_{UV} = 25800$; $k_{DR} \times \nu_{PS} = 272{,}300$ and $k_{DR} \times \nu_{PB} = 223{,}500$. The homopolymer calibrations are represented in Figs 1c and 2c. Their analytical expressions are: $\log M_{PS} = -0.1821\ V + 12.8219$, and $\log M_{PB} = -0.1821\ V + 12.5202$.

© 2004 by Marcel Dekker, Inc.

Figure 1 illustrates the SEC analysis of a commercial SBR (grade 1502), obtained from a continuous emulsion process. The copolymer is mainly linear, and it exhibits a statistical distribution of (short) S and B sequences. The nominal mass fraction of S was 24.5%; and the B microstructure was: 54% 1,4-cis; 38%

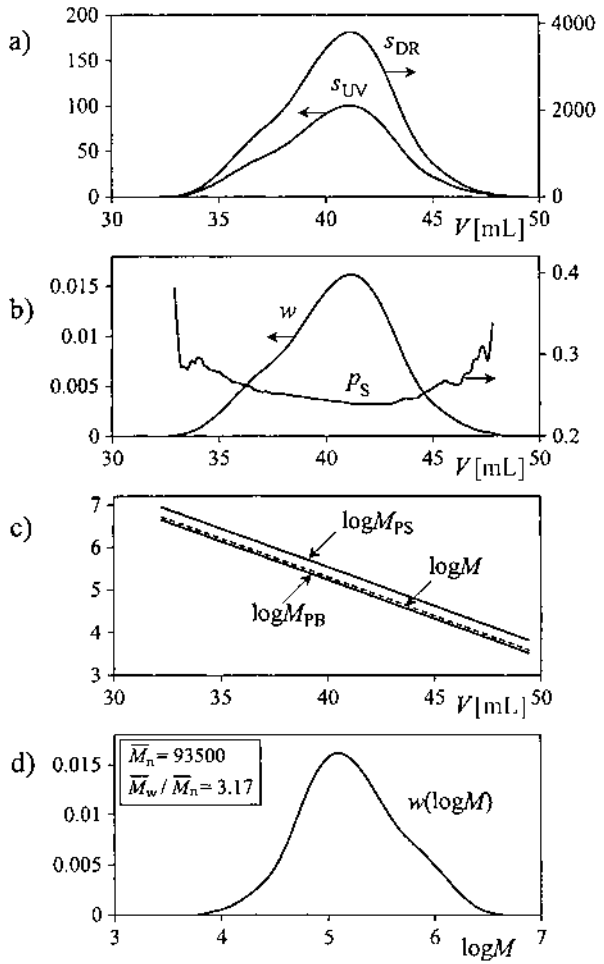

Figure 1 Example 1: MWD of an emulsion SBR as determined by SEC with standard dual detection: (a) UV chromatogram $s_{UV}(V)$ and DR chromatogram $s_{DR}(V)$; (b) instantaneous mass $w(V)$ and instantaneous mass fraction of S $p_S(V)$; (c) homopolymer calibrations $\log M_{PS}(V)$ and $\log M_{PB}(V)$, and copolymer molecular weights $\log M(V)$; (d) MWD $w(\log M)$.

© 2004 by Marcel Dekker, Inc.

1,4-trans; and 8% 1,2-vynil. The global CCD is narrow because (a) both reactivity ratios are close to 1, and (b) the average chain length is much larger than the average S or B sequence. Two potential complications are (a) the polymer exhibits some degree of branching, and (b) the high molecular weight fraction may be totally excluded from the column pores and/or subject to degradation. These difficulties are expected to be unimportant, however, and will be neglected in the present analysis. Consequently, both $\overline{M}_w$ and the polydispersity $\overline{M}_w/\overline{M}_n$ are expected to give slightly underestimated results.

Figure 1a shows the baseline-corrected chromatograms $s_{DR}(V)$ and $s_{UV}(V)$. The UV signal was shifted with respect to the DR signal, to account for the time lag between detectors. The chromatograms are seen to be almost proportional to each other. The instantaneous mass $w(V)$ and the instantaneous mass fraction of S $p_S(V)$ were obtained through Eqs (3) and (4) (Fig. 1b). The following is observed: (a) $w(V)$ is proportional to both chromatograms, and (b) $p_S(V)$ is essentially constant in the midchromatogram region (and close to the global nominal composition of 24.5%), while deviations are observed at the chromatogram tails.

The molecular weights were calculated from Eq. (5) with $p_S(V) \cong 0.245$, resulting in $\log M = -0.1821\ V + 12.5941$ (Fig. 1c). From this expression and $w(V)$, the MWD of Fig. 1d was obtained. This distribution is relatively broad and unimodal, with $\overline{M}_w/\overline{M}_n = 3.17$. This indicates that a correction for instrumental broadening is not required. Also, since $\log M(V)$ is linear, the ordinates of $w(\log M)$ are proportional to the ordinates of $w(V)$.

3 EXAMPLE 2: CHEMICAL COMPOSITION DISTRIBUTION

Figure 2 represents the SEC analysis of a narrow-distributed linear SB diblock copolymer (45). The calibrations of Example 1 are here readopted. The sample was produced in a sequential anionic polymerization. First, the butadiene solution was slowly loaded into the initiator solution. Then, the styrene solution was slowly added until almost complete conversion. The nominal weight fraction of S in the copolymer was 20%. The impurities contained in the stock comonomer solutions produced a continuous deactivation of living ends along the polymerization, and for this reason the copolymer S content increases with the molar mass.

The $s_{UV}(V)$ and $s_{DR}(V)$ chromatograms are represented in Fig. 2a. The instantaneous mass and mass fraction of S [$w(V)$ and $p_S(V)$, respectively] were directly calculated from the chromatograms and Eqs (3) and (4) (Fig. 2b). In the midchromatogram region, $p_S(V)$ increases monotonically with the molar mass, while oscillations are observed at the chromatogram tails as a result of the propagation of errors. In summary, the copolymer exhibits a broad CCD and a continuous variation of the chemical composition with the molecular weight.

© 2004 by Marcel Dekker, Inc.

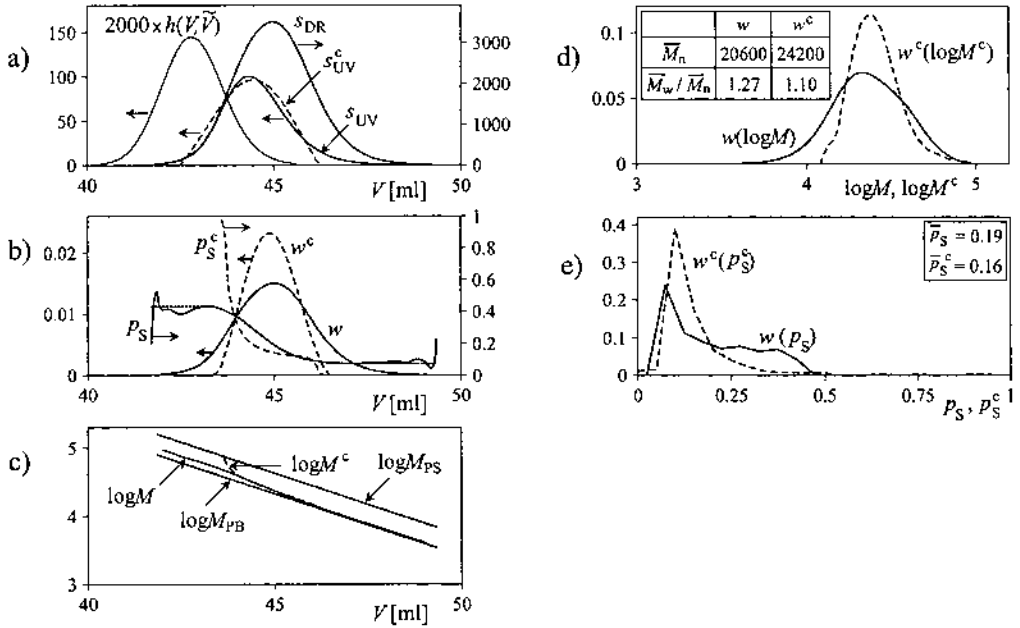

Figure 2 Example 2: MWD and CCD of an anionic diblock SB copolymer as determined by SEC with standard dual detection: (a) UV chromatogram $s_{UV}(V)$ and DR chromatogram $s_{DR}(V)$, instrumental broadening function $h(V, \tilde{V})$, and corrected UV chromatogram $s^c_{UV}(V)$; (b) instantaneous mass $w(V)$ and instantaneous mass fraction of S $p_S(V)$, as determined from the chromatograms, and the same functions but corrected for instrumental broadening [$w^c(V)$ and $p^c_S(V)$, respectively]; (c) homopolymer calibrations $\log M_{PS}(V)$ and $\log M_{PB}(V)$, and copolymer molecular weights with and without correction for instrumental broadening [$\log M^c(V)$ and $\log M(V)$, respectively]; (d) MWDs with and without correction for instrumental broadening [$w^c(\log M)$ and $w(\ldots \log M)$, respectively]; (e) CCDs with and without correction for instrumental broadening [$w^c(p^c_S)$ and $w(p_S)$, respectively].

© 2004 by Marcel Dekker, Inc.

The goal is to find the MWD and CCD. The main assumption is that the instantaneous CCD is narrow.

Let us first neglect the instrumental broadening. The copolymer molecular weights were directly calculated from Eq. (6) with $r = 2.003$, yielding $\log M(V)$ of Fig. 2c. [Although not shown, very similar results were obtained by application of Eq. (5).] From $w(V)$ and $\log M(V)$, the uncorrected MWD $w(\log M)$ of Fig. 2d was calculated. Because $\log M(V)$ is nonlinear, an ordinates correction was necessary to transform $w(V)$ into $w(\log M)$. Finally, the uncorrected CCD is represented by $w(p_S)$ in Fig. 2e, and was obtained from $w(V)$ and $p_S(V)$. In this last transformation, the oscillations of $p_S(V)$ at the chromatogram tails were "flattened" as indicated by the horizontal dashed lines in Fig. 2b. This results in "accumulation peaks" at the low and high composition limits of $w(p_S)$ (Fig. 2e).

In spite of the living ends deactivation, the chromatograms are quite narrow and a correction for instrumental broadening is required. In Fig. 2a the chromatograms are compared with the (uniform) instrumental broadening function $h(V, \tilde{V})$, which in turn was obtained through a recycle technique (49). $\tilde{V}$ represents the average retention volume of a hypothetical monodisperse sample. In Fig. 2a only the broadening function for $\tilde{V} = 42.75\,\text{mL}$ is represented. At any other $\tilde{V}$, the function is identical but shifted with respect to $h(V, 42.75\,\text{mL})$.

For narrow MWDs, the instrumental broadening can be considered uniform as in Fig. 2a. More generally, however, this function is nonuniform in the sense that its shape changes with $\tilde{V}$ (37,50–52). [A nonuniform broadening $h(V, \tilde{V})$ is in theory obtained by injecting a series of strictly monodisperse standards of different mean retention volumes $\tilde{V}$.] To correct for the instrumental broadening, the normal procedure is to correct the raw chromatograms prior to calculating the derived variables. The broadening process is modeled by assuming that each measurement is obtained by filtering a true (or corrected) chromatogram through a noncausal (and in general volume-varying) linear filter. The broadening filter is common to all chromatograms. In standard dual-detection, the following equations can be written [35–37,50]:

$$s_{DR}(V) = \int h(V, \tilde{V}) s^c_{DR}(\tilde{V})\, d\tilde{V} \tag{7a}$$

$$s_{UV}(V) = \int h(V, \tilde{V}) s^c_{UV}(\tilde{V})\, d\tilde{V} \tag{7b}$$

where $s^c_{DR}(V)$ and $s^c_{UV}(V)$ are the corrected chromatograms. The corrected chromatograms can be retrieved from the measurements by numerical inversion. However, this operation is particularly ill-conditioned, and therefore a robust inversion algorithm is required (50–52).

© 2004 by Marcel Dekker, Inc.

Consider an alternative procedure to Eqs (7). In Eq. (3), replace first $w(V)$, $s_{UV}(V)$, and $s_{DR}(V)$ with $w^c(V)$, $s^c_{DR}(V)$, and $s^c_{UV}(V)$, respectively. If the resulting equation is combined with Eq. (7), then the following can be derived:

$$w(V) = \int h(V, \tilde{V}) w^c(\tilde{V})\, d\tilde{V} \tag{8}$$

Equation (8) suggests an alternative procedure for calculating $w^c(V)$: (a) use Eq. (3) to obtain the (broadened) mass "chromatogram" $w(V)$, and (b) correct $w(V)$ for instrumental broadening through Eq. (8). Compared with the normal procedure of inverting Eq. (7), this method requires of a single inversion, and it is therefore preferable from the point of view of the propagation of errors.

Equation (8) cannot be extended to $p_S(V)$, however. This is because [unlike Eq. (3)], Eq. (4) is nonlinear. We here propose to calculate $p^c_S(V)$ as follows [see Eq. (1)]:

$$p^c_S(V) = \frac{s^c_{UV}(V)}{k_{UV} w^c(V)} \tag{9}$$

where $s^c_{UV}(V)$ is the corrected UV chromatogram [obtained by inversion of Eq. (7b)]; and $w^c(V)$ is the corrected mass "chromatogram" [obtained by inversion of Eq. (8)].

Figure 2b presents the corrected mass "chromatogram" $w^c(V)$, when calculated by inverting $w(V)$ through Eq. (8) with a singular value decomposition algorithm (53). The corrected UV chromatogram $s^c_{UV}(V)$ of Fig. 2a was calculated from $s_{UV}(V)$ using the same inversion algorithm (53). In the midchromatogram region, the slope of $p^c_S(V)$ increases steadily with the molar mass. Also, large errors in $p^c_S(V)$ are apparent at the chromatogram tails, where compositions larger than 1 and lower than 0 were obtained. The corrected molecular weights $\log M^c(V)$ of Fig. 2c were calculated by interpolation with $p^c_S(V)$. From $w^c(V)$ and $\log M^c(V)$, the corrected MWD of Fig. 2d was found. As expected, this distribution is narrower than the uncorrected MWD. The change in breadth is quantified by the (rather large) variation in the polydispersity (from 1.27 without correction to 1.10 with correction, Fig. 2d).

The CCDs (with and without correction for instrumental broadening) are presented in Fig. 2e. The corrected CCD [$w^c(p^c_S)$] was obtained from $w^c(V)$ and $p^c_S(V)$. Unlike the MWD, the corrected CCD is broader than the uncorrected CCD. By assuming accurate measurements of the instantaneous mass and composition, the global average composition is unaffected by the instrumental broadening. For this reason, it seems preferable to calculate the global composition directly from $w(V)$ and $p_S(V)$, rather than from $w^c(V)$ and $p^c_S(V)$. The corrected and uncorrected global compositions ($\bar{p}^c_S$ and $\bar{p}_S$, respectively) are compared in Fig. 2e.

© 2004 by Marcel Dekker, Inc.

As expected, $\bar{p}_S$ is closer to the nominal value of 20%. The deviation in $\bar{p}_S^c$ is a consequence of the propagation of errors during the inversion operations.

4 EXAMPLE 3: BRANCHING DISTRIBUTION

Consider the analysis of a PB-*graft*-PS copolymer contained in high-impact polystyrene (i.e., a mixture of free PS, graft copolymer, and unreacted PB) (11,12,54). The high-impact polystyrene was produced in a solution polymerization of styrene in the presence of PB and a chemical initiator, and the sample corresponds to a monomer conversion of 18%. Prior to the SEC analysis, the graft copolymer was isolated from the homopolymers through a solvent extraction technique (54). The copolymer branching points are mainly trifunctional, and are produced by a free radical attack to the double bonds of the B repeating units. Tetrafunctional branching points (or crosslinks) are neglected in the present analysis. The instantaneous CCD is broad, but the average composition does not change with the molar mass. For this reason, SEC alone is incapable of determining the CCD. On the positive side, if one also assumes that in dilute solution the PS branches are noninteracting with the PB backbones, then the graft copolymer can be considered as a branched homopolymer from the chromatographic point of view. The rate of branching is proportional to the molar mass of the reacted PB chain. For this reason, the larger copolymer molecules are also the more highly branched, and a SEC fractionation by hydrodynamic volume also implies a fractionation by the number of branches.

The instantaneous molar mass $M(V)$ and the instantaneous number-average number of grafted branches per molecule $b_n(V)$ were obtained from intrinsic viscosity measurements $[\eta](V)$ combined with the universal calibration. The universal calibration was determined from narrow PS standards of known molar masses and intrinsic viscosities. At any given elution volume, $\{M \times [\eta]\}$ is a constant. For a branched polymer, $[\eta](V)$ is lower than its linear homolog, while the opposite is verified for $M(V)$. To obtain $b_n(V)$, the following procedure (originally developed for branched homopolymers) was employed:

1. Calculate the instantaneous intrinsic viscosity from:

$$[\eta](V) = k_{IV} \frac{s_{IV}(V)}{s_{DR}(V)} \tag{10}$$

   where $s_{IV}(V)$ is the IV chromatogram, $s_{DR}(V)$ is the mass chromatogram, and k_{IV} is a calibration constant.
2. Calculate $[\eta](M)$ from $[\eta](V)$ and the universal calibration $\log\{M(V) \times [\eta](V)\} = A - B\,V$.

© 2004 by Marcel Dekker, Inc.

3. Calculate the g' branching parameter from the ratio (at any given molar mass) between the intrinsic viscosity of the branched polymer and the intrinsic viscosity of the linear homolog, yielding:

$$g'(M) = \frac{[\eta](M)}{KM^{\alpha}} \leq 1 \tag{11}$$

where K and α are the Mark–Houwink parameters of the linear homolog.

4. Calculate the g branching parameter (which is based on the radii of gyration), which is related to g' through the following empirical expression:

$$[g(M)]^{\varepsilon} = g'(M) \tag{12}$$

where ε depends on the polymer, the solvent, and the temperature, and is generally unknown for copolymers.

5. Calculate $b_n(M)$ by inverting the following nonlinear equation, which was theoretically derived for trifunctional branching points (9,12):

$$g(M) = \left[\left(1 + \frac{b_n(M)}{7}\right)^{1/2} + \frac{4b_n(M)}{9\pi}\right]^{-1/2} \leq 1 \tag{13}$$

An SEC analysis may be improved when measurements are compared with predictions produced by representative polymerization models. For the investigated graft copolymer, the ε exponent of Eq. (12) was adjusted from comparing SEC measurements of $g'(M)$ with theoretical predictions of $g(M)$ provided by a polymerization model (11,12,54). For THF at 25°C, the exponent resulted in $\varepsilon \cong 2$ (12). For the same solvent and temperature, the Mark–Houwink parameters of a linear SB diblock copolymer with a similar global composition and equivalent molecular weight range were taken from the literature, yielding $K = 3.2 \times 10^{-4}$ dL/g and $\alpha = 0.693$ (23).

The IV and DR chromatograms are presented in Fig. 3a. From the ratio $s_{DR}(V)/s_{UV}(V)$ and Eq. (4), an almost constant $p_S(V)$ was observed. For this reason, the DR signal was made proportional to the instantaneous mass. The intrinsic viscosity $[\eta](V)$ was calculated from Eq. (10), but is not presented here. The universal calibration resulted in $\log\{M(V) \times [\eta](V)\} = 18.09 - 0.3041\ V$ (12). The experimental MWD of Fig. 3c was determined from $[\eta](V)$ and the universal calibration. The experimental BD was estimated from Eqs (10)–(13) (Fig. 3d). This function is represented by a continuous curve in Fig. 3d, but with the data points concentrated at integer values of the number of branches.

Finally, compare the SEC results with theoretical predictions by a polymerization model (Figs. 3b, c, and d). For the total copolymer, the following

© 2004 by Marcel Dekker, Inc.

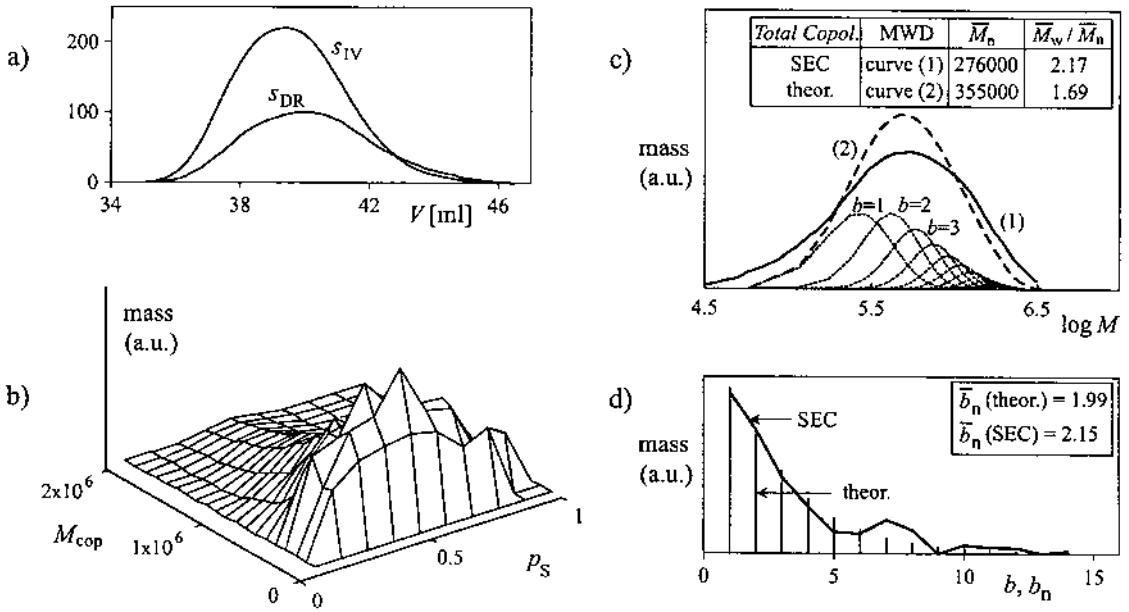

Figure 3 Example 3: MWD and BD of a PB-*graft*-PS copolymer as determined by SEC with standard dual detection plus an IV; (a) DR chromatogram $s_{DR}(V)$ and IV chromatogram $s_{IV}(V)$; (b) theoretical bivariate distribution of the molecular weights and the chemical composition; (c) theoretical and measured MWDs (the theoretical MWD for the total copolymer results from adding the MWDs of the different branched topologies represented by $b = 1, 2, \ldots$); (d) theoretical and measured BDs.

© 2004 by Marcel Dekker, Inc.

was predicted by the mathematical model: (a) the bivariate distribution of molecular weights and chemical composition of Fig. 3b, (b) the MWD of Fig. 3c, and (c) the BD of Fig. 3d. The bivariate distribution indicates that the average composition is almost independent of the molar mass, and that the derived univariate CCD is expected to be quite broad. The experimental MWD is broader than the theoretical MWD (Fig. 3c). The experimental BD is quite similar to the theoretical BD (Fig. 3d).

The mathematical model also predicted the MWDs of the different branched topologies that integrate the total graft copolymer (Fig. 3c). Each branched topology b (= 1, 2, 3, . . .) is characterized by the number of trifunctional grafting points per molecule. The MWD of the total copolymer is obtained by adding the individual MWDs (Fig. 3c). The areas under the individual MWDs of Fig. 3c are represented by vertical bars in the theoretical BD of Fig. 3d. An important observation is that the MWDs of the individual topologies are relatively little overlapped at the low molar masses, but moderately overlapped at the high molar masses. For this reason, a good fractionation according to the number of branches is expected to be produced at the low molar masses, while a relatively poorer fractionation is expected to occur at the high molar masses.

5 REFERENCES

1. S Mori, T Suzuki. Problems in determining compositional heterogeneity of copolymers by size-exclusion chromatography and UV-RI detection system. J Liq Chromatogr 4:1685–1696, 1982.
2. LH García-Rubio, JF MacGregor, AE Hamielec. Size exclusion chromatography of copolymers. In: C Craver, ed. Polymer Characterization. Spectroscopic, Chromatographic, and Physical Instrumental Methods. Adv Chem Ser 203. Washington, DC: American Chemical Society, 1983, pp 311–344.
3. GR Meira, LH García-Rubio. Corrections for instrumental and secondary broadening in the chromatographic analysis of linear copolymers. J Liq Chromatogr 12:997–1021, 1989.
4. GR Meira. Data reduction in size exclusion chromatography of polymers. In: HG Barth, JW Mays, ed. Modern Methods of Polymer Characterization. New York: John Wiley & Sons, Inc., 1991, pp 67–101.
5. ST Balke, TH Mourey, TC Schunk. Size exclusion chromatography: practical methods for quantitative results. Polym React Eng 7:429–452, 1999.
6. P Kilz. Copolymer analysis by LC methods, including two-dimensional chromatography. In: J Cazes, ed. Encyclopedia of Chromatography. New York: Marcel Dekker, Inc., 2001, pp 195–200.
7. S Mori. Copolymer composition by GPC-SEC. In: J Cazes, ed. Encyclopedia of Chromatography. New York: Marcel Dekker, Inc., 2001, pp 200–202.
8. C Hagiopol. Copolymerization. Toward a Systematic Approach. New York: Kluwer Academic/Plenum Publishers, 1999, pp 1–18.

© 2004 by Marcel Dekker, Inc.

9. BH Zimm, WH Stockmayer. The dimension of chain molecules containing branches and rings. J Chem Phys 17:1301–1314, 1949.
10. JM Liu, CS Chang, RCC Tsiang. Method of determining the degree of branching from the gel permeation chromatogram for star-shaped SBS thermoplastic block copolymers. J Appl Polym Sci, Polym Chem 35:3393–3401, 1997.
11. DA Estenoz, JR Vega, HM Oliva, GR Meira. Analysis of a styrene–butadiene graft copolymer by size exclusion chromatography. I. Computer simulation study for estimating the biases induced by branching under ideal fractionation and detection. Int J Polym Anal Charact 6:315–337, 2001.
12. JR Vega, DA Estenoz, HM Oliva, GR Meira. Analysis of a styrene–butadiene graft copolymer by size exclusion chromatography. II. Determination of the branching exponent with the help of a polymerization model. Int J Polym Anal Charact 6:339–348, 2001.
13. A Rudin. Determination of molecular weight distributions of copolymers by size exclusion chromatography. In: C Wu, ed. Handbook of SEC. New York: Marcel Dekker, 1995, pp 147–159.
14. S Mori. Copolymer molecular weights by GPC-SEC. In: J Cazes, ed. Encyclopedia of Chromatography. New York: Marcel Dekker, Inc., 2001, pp 202–203.
15. C Jackson, HG Barth. Molecular weight sensitive detectors for size exclusion chromatography. In: C Wu, ed. Handbook of SEC. New York: Marcel Dekker, 1995, pp 103–145.
16. PJ Wyatt. Light scattering and the absolute characterization of macromolecules. Anal Chim Acta 272:1–40, 1993.
17. PC Cheung, ST Balke, TC Schunk, TH Mourey. Assessment and development of evaporative interfaces for SEC-FTIR. J Appl Polym Sci, Symp Ed 52:105–124, 1993.
18. TC Schunk, ST Balke, PC Cheung. Quantitative polymer composition characterization with a liquid chromatography–Fourier transform infrared spectrometry-solvent-evaporation-interface. J Chromatogr A 661:227–238, 1994.
19. PC Cheung, ST Balke, TC Schunk. Size-exclusion chromatography–Fourier transform IR spectrometry using a solvent-evaporative interface. Adv Chem Ser 247:265–279, 1995.
20. WL Elsdon, JM Goldwasser, A Rudin. Densimeter detector in gel permeation chromatography of copolymers. J Polym Sci, Polym Chem Ed 20:3271–3283, 1982.
21. Z Grubisic, P Rempp, H Benoit. A universal calibration for GPC. J Polym Sci B 5:753–759, 1967.
22. AE Hamielec, AC Ouano. Generalized universal molecular weight calibration parameter in GPC. J Liq Chromatogr 1:111–120, 1978.
23. G Kraus, CJ Stacy. Molecular weight and long-chain branching distributions of some polybutadienes and styrene–butadiene rubbers. Determination by GPC and Dilute Solution Viscometry. J Polym Sci A-2 10:657–672, 1972.
24. J Brandrup, EH Immergut. Polymer Handbook. 3rd ed. New York: J Wiley, 1989, pp VII/1–VII/60.
25. JM Goldwasser, A Rudin. Analysis of block and statistical copolymers by gel permeation chromatography: estimation of Mark–Houwink constants. J Liq Chromatogr 6:2433–2463, 1983.

© 2004 by Marcel Dekker, Inc.

26. M Haney. The differential viscometer. I. A new approach to the measurement of specific viscosities of polymer solutions. J Appl Polym Sci 30:3023–3036, 1985.
27. M Haney. The differential viscometer. II. On-line viscosity detector for size-exclusion chromatography. J Appl Polym Sci 30:3037–3049, 1985.
28. Y Brun. Data reduction in multidetector size exclusion chromatography. J Liq Chromatogr & Relat Technol 21:1979–2015, 1998.
29. SV Greene. SEC with on-line triple detection: light scattering, viscometry, and refractive index. In: J Cazes, ed. Encyclopedia of Chromatography. New York: Marcel Dekker, Inc., 2001, pp 200–202.
30. ST Balke, TH Mourey, CA Harrison. Number-average molecular weight by size exclusion chromatography. J Appl Polym Sci 51:2087–2102, 1994.
31. W Radke, PFW Simon, AHE Müller. Estimation of number-average molecular weights of copolymers by gel permeation chromatography-light scattering. Macromol 29:4926–4930, 1996.
32. D Berek, K Marcinka. Gel chromatography. In: Z Deyl, ed. Separation Methods. Amsterdam: Elsevier, 1984.
33. PJ Wyatt. Mean square radius of molecules and secondary instrumental broadening. J Chromatogr 648:27–32, 1993.
34. KP Hupe, RJ Jonker, G Rozing. Determination of band spreading effects in high-performance liquid chromatographic instruments. J Chromatogr 285:253–265, 1984.
35. LH Tung. Method of calculating MWD from gel permeation chromatograms. III. Application of the method. J Appl Polym Sci 10:1271–1283, 1966.
36. M Netopilik. Correction for axial dispersion in gel permeation chromatography with a detector of molecular masses. Polymer Bull 7:575–582, 1982.
37. AE Hamielec. Correction for axial dispersion. In: J Janca, ed. Steric Exclusion Liquid Chromatography of Polymers. Chromatogr Sci Ser 25. New York: Marcel Dekker, 1984, pp 117–160.
38. C Jackson, WW Yau. Computer simulation study of size exclusion chromatography with simultaneous viscometry and light scattering measurements. J Chromatogr 645:209–217, 1993.
39. D Berek. Coupled liquid chromatographic techniques for the separation of complex polymers. Prog Polym Sci 25:873–908, 2000.
40. H Pasch, B Trathnigg. HPLC of Polymers. Berlin: Springer-Verlag, 1997.
41. P Kilz, H Pasch. Coupled liquid chromatographic techniques in molecular characterization. In: RA Meyer, ed. Encyclopedia of Analytical Chemistry. New York: Wiley, 2000.
42. ST Balke. Orthogonal chromatography and related advances in liquid chromatography. In: T Provder, ed. Detection and Data Analysis in Size Exclusion Chromatography. Am Chem Soc Symp Ser 352. New York: Am Chem Soc, 1987, pp 59–77.
43. JR Runyon, DE Barnes, JF Rudd, LH Tung. Multiple detectors for molecular weight and composition analysis of copolymers by gel permeation chromatography. J Appl Polym Sci 13:2359–2369, 1969.
44. HE Adams. Composition of butadiene–styrene copolymers by gel permeation chromatography. Separ Sci 6:259–273, 1971.

© 2004 by Marcel Dekker, Inc.

45. RO Bielsa, GR Meira. Linear copolymer analysis with dual-detection size exclusion chromatography: correction for instrumental broadening. J Appl Polym Sci 46:835–845, 1992.
46. L Mrkvicková. Characterization of chemical heterogeneity of graft copolymer by conventional SEC. J Liq Chrom & Relat Technol 22:205–214, 1999.
47. FSC Chang. Molecular weight analysis of block copolymer by gel permeation chromatography. J Chromatogr 55:67–71, 1971.
48. W Keqiang, H Honghong. A method for determining molecular weight of copolymer by GPC. J Liq Chromat & Relat Technol 23:523–529, 2000.
49. D Alba, GR Meira. Calibration for instrumental spreading in size exclusion chromatography by a novel recycle technique. J Liq Chromat 9:1141–1161, 1986.
50. JR Vega, GR Meira. SEC of simple polymers with molar mass detection in presence of instrumental broadening. Computer simulation study on the calculation of unbiased molecular weight distributions. J Liq Chrom & Relat Technol 24:901–919, 2001.
51. LM Gugliotta, JR Vega, GR Meira. Instrumental broadening correction in size exclusion chromatography. Comparison of several deconvolution techniques. J Liq Chromatogr 13:1671–1708, 1990.
52. GR Meira, JR Vega. Axial dispersion correction methods in GPC/SEC. In: J Cazes, ed. Encyclopedia of Chromatography. New York: Marcel Dekker, Inc., 2001, pp 71–76.
53. JM Mendel. Lessons in Estimation Theory for Signal Processing, Communications, and Control. New Jersey: Prentice Hall PTR, 1995, pp 44–57.
54. DA Estenoz, IM González, HM Oliva, GR Meira. Polymerization of styrene in presence of polybutadiene. Determination of molecular structure. J Appl Polym Sci 74:1950–1961, 1999.

© 2004 by Marcel Dekker, Inc.

6
Size Exclusion Chromatography of Polyamides, Polyesters, and Fluoropolymers

Christian Dauwe*
PSS Polymer Standards Service
Mainz, Germany

1 INTRODUCTION

Gel permeation chromatography (GPC, also known as SEC or size exclusion chromatography) has become a well accepted analytical method since its introduction in the late 1950s by works of Porath and Flodin (1) and Moore (2). Polymer Standards Service (PSS) share this long-standing tradition as universal and stable sorbent manufacturer for all types of polymer applications.

The analytical departments of PSS have collected much practical experience regarding GPC analysis of polyamides and polyesters, and also to some extent in the field of fluoropolymer analysis.

The group of polymers including polyamides, polyesters, and fluoropolymers is often called performance polymers due to their unique mechanical and

**Current affiliation*: YMC-Europe GmbH, Schermbeck, Germany.

© 2004 by Marcel Dekker, Inc.

solubility properties. They are used for many technical applications. A common property of these polymers is their poor or nonsolubility in many solvents (THF, toluene, trichloromethane, water, and so on). This makes GPC using these frequently used eluents unsuccessful. Good GPC analysis of these polymers can, however, be carried out using very special eluents and columns. Laboratory personnel performing these analyzes should be very experienced in order to ensure that valuable GPC results are obtained. When no practical experience is available, it is necessary to request expert advice. Customers in research and quality control are therefore invited to ask PSS, a long-standing developer and manufacturer of GPC systems, for expert advice and customer support.

An overview of theoretical aspects, methods known in the literature, and PSS experience in the field of polyester, polyamide, and fluoropolymer analysis is provided in the following sections.

2 THEORETICAL ASPECTS

Polyesters such as polyethyleneterephthalate (PET), polybutyleneterephthalate (PBT), or the biodegradable polylactides often show a high crystallinity. This high crystallinity decreases the solubility in many solvents and so it becomes difficult to dissolve these substances completely. For this reason the solvents have to be strong enough to destroy this crystallinity. Hexafluoroisopropanol (HFIP) and trifluoroethanol (TFE) are the most frequently and successfully used solvents.

Polyamides such as polyamide 6 or silk contain ionic functional groups (amides) that tend to associate via hydrogen bonding. These intermolecular associations decrease the solubility and increase the observed molecular size and respective molecular weight. These associations must be destroyed prior to analysis. In order to destroy these associations and in order to perform satisfactory GPC analysis, the highly polar solvent hexafluoroisopropanol (HFIP), containing 0.05% sodium trifluoroacetate, is the most used solvent.

Some fluoropolymers can be investigated using GPC. These polymers typically contain fluorocarbon groups and "normal" organic groups such as ether or ester functions or aliphatic groups. This makes some of them soluble in perfluoroalkyl-methylethers (HFE 7100) or in HFIP. Unfortunately GPC analyzes performed in HFE 7100 cannot be calibrated with commercially available polymeric standards. This disadvantage is related to the insolubility of these standards in HFE 7100.

3 GPC METHODS IN THE LITERATURE

3.1 Polyesters

Most of the published analytical work in the field of polyester GPC was carried out on investigation of PET. PET was analyzed by GPC using meta-cresol at

© 2004 by Marcel Dekker, Inc.

100–135°C (3,4). Later investigations have shown that meta-cresol can cause degradation of PET through acid-catalysed hydrolysis (5). For this reason a mixture of nitrobenzene-tetrachloroethane was developed as a solvent for PET analysis at room temperature (5). The following eluent systems have also been developed successfully: ortho-chlorphenol/chlorform (25/75, v/v) for GPC at room temperature (6), ortho-chlorphenol (8), 1,1,2,2-tetrachloroethane/phenol (9) and methylene chloride/dichloroacetic acid (10).

Later 1,1,1,3,3,3-hexafluoroisopropanol (HFIP) was developed to carry out successful GPC analysis of PET at room temperature (11). This method has the disadvantage of being very expensive. As a consequence, mixtures of HFIP with less expensive solvents were developed. Mixtures of methylene chloride/HFIP (12) and chloroform/HFIP (e.g., 98/2, v/v) allow GPC analysis at room temperature (13–15).

3.2 Polyamides

Polyamides such as nylon have been investigated in HFIP containing 0.05 M potassium or sodium trifluoroacetate (16,17). This highly polar eluent is needed in order to interact with the very polar amide groups in polyamides. Sodium trifluoroacetate destroys the intermolecular hydrogen bonding between the amide groups, thus single polymers appear as single molecules and not as polymeric associations.

3.3 Fluoropolymers

GPC methods for fluoropolymers are known. In particular, perfluoroether or polymers containing fluorinated side chains have been the subject of literature-described investigations. They were performed in special partly fluorinated eluents or in DMAc (18). For a successful GPC analysis of this very special polymer group a detailed investigation on structure and solubility is recommended.

4 GPC METHODS USED AT POLYMER STANDARDS SERVICE

Polyester and polyamide GPC analyzes are typically performed using HFIP containing 0.05 M potassium or sodium trifluoroacetate. The standard column combinations for these analyzes are the highly resistant PerFluoroGel (PFG) columns: PSS-PFG 100 Å, 7 μm, 8 × 300 mm + PFG 1000 Å, 7 μm 8 × 300 mm. Alternatively a combination of 2×PFG linXL, 7 μm, 8 × 300 mm is used. This system covers the full range of molecular weights of polycondensates and allows the analysis of oligomers up to 1 or 2 Mio D. The calibration of this system with PMMA standards allows the determination of the relative molecular weight of the analytes. The viscosity or light-scattering coupling allows the

© 2004 by Marcel Dekker, Inc.

determination of the absolute molecular weights (if also necessary). For the calculation and presentation of the results PSS WinGPC 6.20 (Polymer Standards Service, Mainz, Germany) was used.

Successful fluoropolymer GPC analysis strongly depend on details of their structure and solubility. Over recent years we have investigated some fluoropolymers by GPC methods, but have not seen structures originating from a large group of customers. Thus a method covering a large field of interests cannot be given.

Pure and very expensive fluorinated eluents are used because of the high reproducibility of the results obtained in the following described applications. The high price of the eluent can be reduced when a company specialized in high purity recycling ($>99.8\%$) of expensive eluents is used as a supplier to the analytical laboratory. Contact details for such a source can be given by the author on request.

4.1 Polyesters

Most of the interest in investigating polyesters relates to polyethyleneterephthalates (PET), polybutyleneterephthalates (PBT), and the biodegradable polylactides. Figures 1 to 5 show typical results that are obtained on polyester analysis using PSS methods.

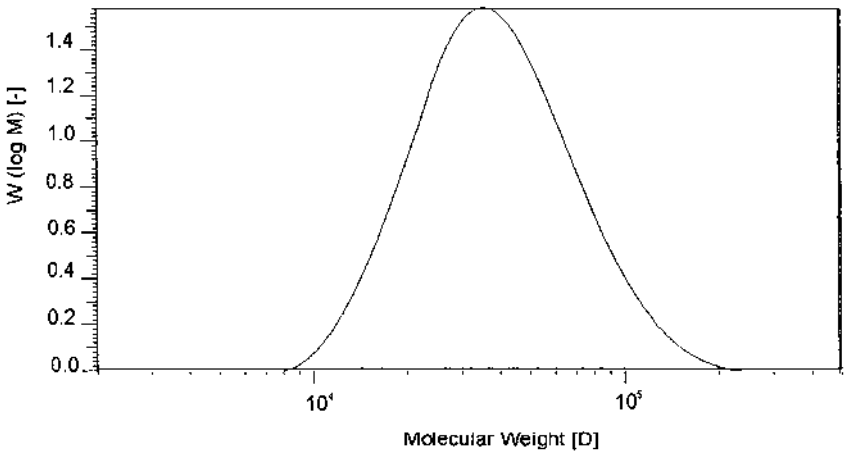

Figure 1 Result of a PET analysis. Eluent: HFIP + 0.05 M potassium-trifluoroacetate. Flow rate: 1 mL/min. Columns: PSS PFG 100 Å, 7 μm, 8 × 300 mm + PFG 1000 Å, 7 μm, 8 × 300 mm. Temperature: 25°C. Detection: RI. Standards: 12 PSS PMMA calibration standards.

© 2004 by Marcel Dekker, Inc.

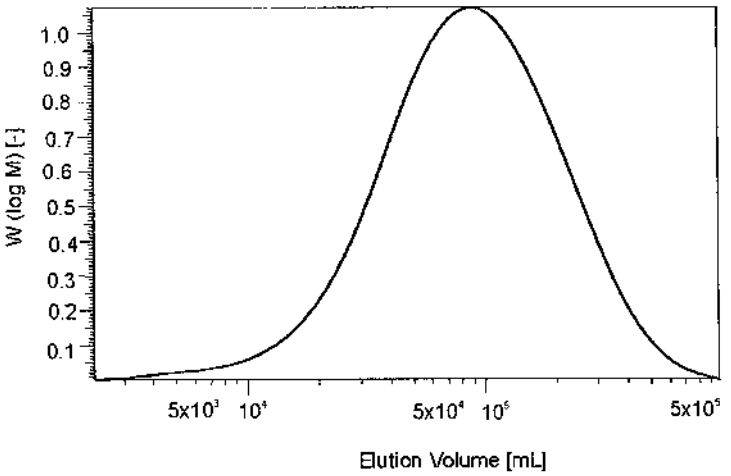

Figure 2 Result of a different PET analysis: For analytical conditions, see Fig. 1.

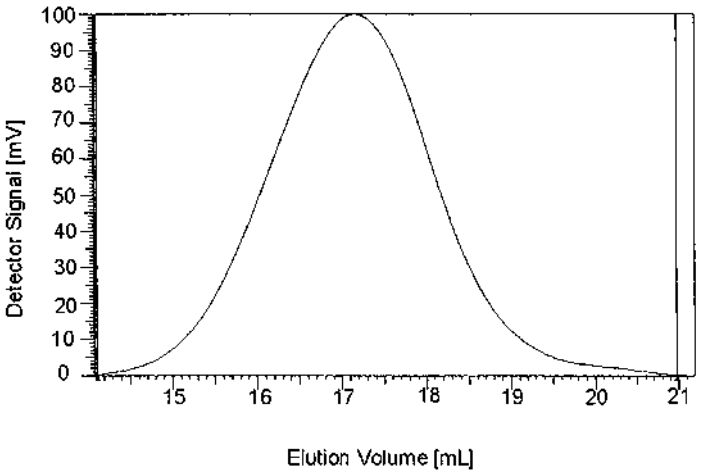

Figure 3 Elution profile of PBT. Eluent: HFIP + 0.05 M potassium-trifluoroacetate. Flow rate: 1 mL/min. Columns: 2 × PSS PFG LinXl, 7 μm, 8 × 300 mm. Temperature: 25°C. Detection: RI. Standards: 12 PSS PMMA calibration standards.

© 2004 by Marcel Dekker, Inc.

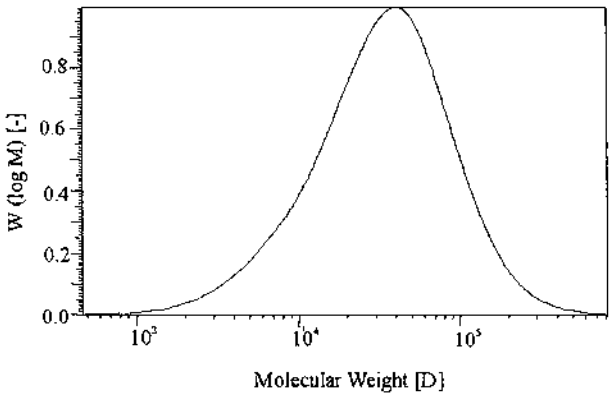

Figure 4 Result of the PBT analysis: molecular weight distribution relative to PMMA calibration.

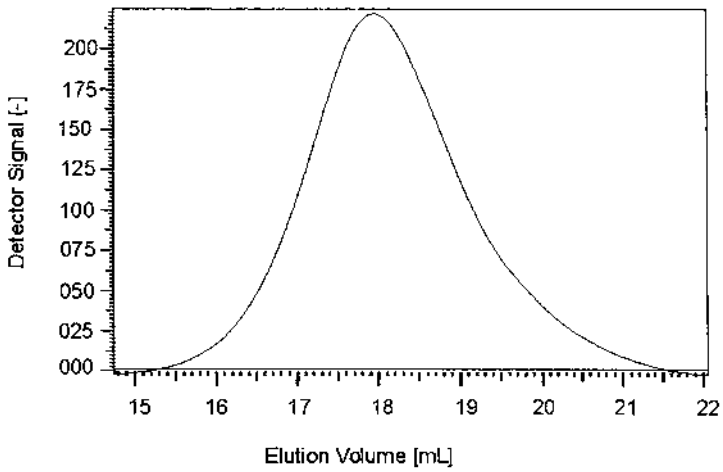

Figure 5 Elution profile of a biodegradable poly(lactic acid). Eluent: 2,2,2-trifluoroethanol + 0.1 M sodium-trifluoroacetate. Flow rate: 1 mL/min. Columns: PSS PFG 100 Å, 7 μm, 8 × 300 mm + PFG 1000 Å, 7 μm, 8 × 300 mm. Temperature: 25°C. Detection RI. Standards: 12 PSS PMMA calibration standards.

4.2 Polyamides

Most of the interest in investing polyamides is related to the aliphatic polyamides polyamide 6 or 6,6. Figures 6 to 8 show typical results that are obtained on polyamide analysis in fluorinated eluents using PSS methods.

© 2004 by Marcel Dekker, Inc.

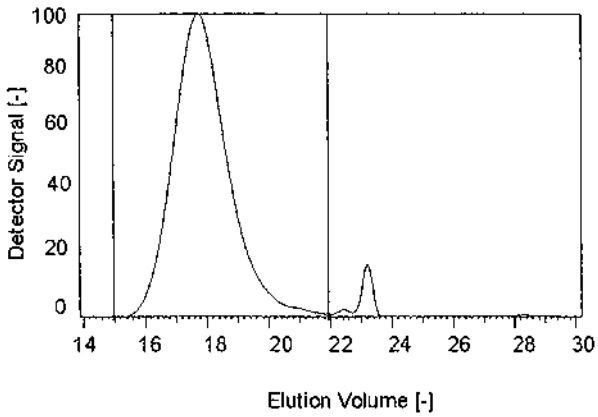

Figure 6 Elution profile of PA6. Eluent: HFIP + 0.05 M potassium-trifluoroacetate. Flow rate: 1 mL/min. Columns: 2 × PSS PFG LinXl, 7 μm, 8 × 300 mm. Temperature: 25°C. Detection: RI. Standards: 12 PSS PMMA calibration standards.

Biopolymers such as silk and the very versatile group, proteins, can also be regarded as polyamides. For protein GPC analysis we have observed that PSS-NOVEMA columns driven in aqueous solvents became the most successful (19). Owing to the complex structure of proteins, complex GPC methods are often used. The large theoretical background that is needed for protein analysis makes it necessary to describe it in a separate article (19).

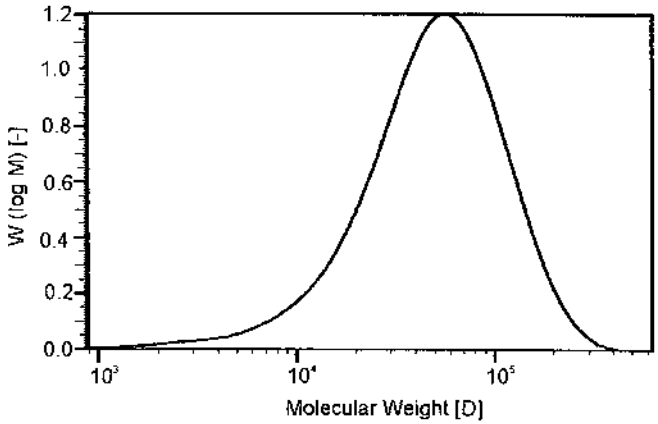

Figure 7 Result of the PA6 analysis: molecular weight distribution relative to PMMA calibration.

© 2004 by Marcel Dekker, Inc.

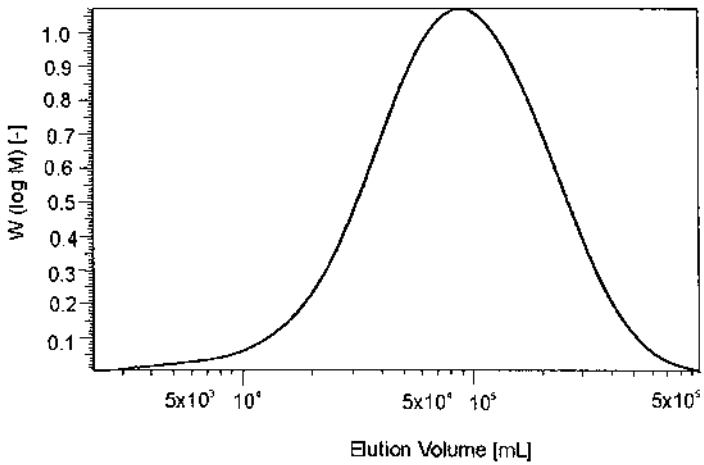

Figure 8 Result of natural spider silk analysis. Eluent: HFIP + 0.1 M sodium-trifluoroacetate. Flow rate: 1 mL/min. Columns: PSS PFG 100 Å, 7 μm, 8 × 300 mm + PFG 1000 Å, 7 μm, 8 × 300 mm. Temperature: 25°C. Detection RI. Standards: 12 PSS PMMA calibration standards.

5 CONCLUSION

The previous section described the most frequently used PSS methods for analysing polyesters and polyamides. We know from our long experience that the methods presented are the most reliable and reproducible. In routine analysis in the laboratories of PSS and of our customers it normally takes many years before the presented systems lose any efficiency.

Molecular weight calibrations can be carried out very easily with the readily available PMMA standards; of course, polyester or polyamide standards also can be used.

Owing to the unusually poor solubility of these polymers it is very important for customers to be in contact with a column supplier which knows how to overcome the difficulties that result and which is able to assist its customers. This assistance will become more and more important for customers because of the many modifications that will be made to high-performance plastics in the future.

6 ACKNOWLEDGEMENTS

The author thanks the editor for his support and all the colleagues at PSS who contributed their work to this chapter. The author also thanks his wife Susanne and his son Jan-Luca for the care they took of him while writing.

© 2004 by Marcel Dekker, Inc.

7 REFERENCES

1. J Porath, P Flodin. Nature 183:1657, 1959.
2. JC Moore. J Polym Sci A2:835, 1964.
3. G Shaw. 7th Int GPC Seminar Proc, Waters Assoc, Monte Carlo, 1964, p 309.
4. JR Overton, J Rash, LD Moore. 6th Int GPC Seminar Proc, Waters Assoc, Miami Beach, FL, 1968, p 422.
5. EE Paschke, BA Bidlingmeyer, JG Bergmann. J Polym Sci, Polym Chem Ed 15:983, 1977.
6. Sang Ming-Min, Jin Nan-Ni, Jlang Er-Fang. J Liq Chromatogr 5:1665, 1982.
7. SA Jaban, Dc Balduff. J Liq Chromatogr 5:1825, 1982.
8. L Martin, M Marvine, ST Balke. J Liq Chromatogr 15:1817, 1992.
9. CV Uglea, S Azleovici, A Mihescu. E Polym J 21:577, 1985.
10. TH Mourey, TG Bryan, J Greaner. J Chromatogr A 657:377, 1993.
11. EE Orott. In: J Cazers, ed. Liquid Chromatography of Polymers and Related Materials (Chromatographic Sci Ser Vol 8). New York: Dekker, 1976, 41.
12. JR Overton, HL Browning. In: T Provder, ed. Size Exclusion Chromatography (ACS Symp Ser Vol 245). Washington D.C.: Am Chem Soc 1984, 219.
13. K Weisskopf. J Polym Sci, A Polym Chem 26:1919, 1988.
14. N Chikazumi, Y Mukoyama, H Sugiatani. J Chromatogr 479:85, 1989.
15. B Gemmel. Chem Fibers Internat (CFI) 45:104, 1995.
16. H Suzuki, S Mori. In: Chi-San Wu, ed. Column Handbook for Size Exclusion Chromatography. New York: Academic Press, 1999, p 190.
17. P Kilz. In: Chi-San Wu, ed. Column Handbook for Size Exclusion Chromatography. New York: Academic Press, 1999, p 300.
18. H Jordi. In: Chi-San Wu, ed. Column Handbook for Size Exclusion Chromatography. New York: Academic Press, 1999, p 367.
19. C Dauwe, G Reinhold. CLB—Chemie in Labor und Biotechnik 52:176, 2001.

© 2004 by Marcel Dekker, Inc.

7
Size Exclusion Chromatography of Natural and Synthetic Rubber

Terutake Homma and Michiko Tazaki
Kanagawa Institute of Technology
Atsugi, Japan

1 INTRODUCTION

In the early years of the rubber industry, natural rubber was the only material used for final products, and there was no need to know precisely the molecular characteristics such as average molecular weights and molecular weight distribution. However, since the introduction of various kinds of synthetic rubbers to the rubber industry, efforts have been devoted to understanding the correlations between their molecular weight characteristics and physical properties and processability. Apart from this technological aspect, considering the reaction of the chemical modification of current rubbers or the synthesis of new rubbers, elucidation of the molecular characteristics is the first necessary step for development. Until the introduction of gel permeation chromatography (GPC) to the method of polymer characterization in 1964 by Moore (1), a tedious molecular weight fractionation method or ultracentrifugal analysis was employed for these measurements. However, since then, GPC has been recognized as an invaluable

© 2004 by Marcel Dekker, Inc.

method for the study of the molecular characterization of rubbers. At present, the term "size exclusion chromatography" (SEC) is more frequently used than GPC, and this is becoming much more refined in both hardware and software, as described elsewhere.

It is always necessary to dissolve the rubber sample in SEC solvents before SEC analysis. Natural rubbers as well as many synthetic rubbers are mainly composed of diene and vinyl units and are in an amorphous solid state. Therefore, in general, no problems are encountered when performing SEC measurements. Much data for SEC for rubbers have been obtained. These data are listed in the Appendix to this chapter to provide SEC experimental conditions, and some consideration is given here to the SEC analysis of rubbers.

2 CLASSIFICATION OF RUBBERS

In addition to natural rubber, many synthetic rubbers are now commercially available. Although there are several ways to classify these rubbers, the American Society for Testing and Materials (ASTM) Standard D1418-85 gives the classification and designation of rubbers based on their chemical composition. Therefore, in this chapter, the classification and naming of rubbers are based on this standard. For convenience, the nomenclature is reproduced in Table 1, extracted from the standard.

Table 1 Abbreviation of Rubbers According to ASTM D1418-85

ABR	acrylate-butadiene
BR	butadiene
CIIR	chloro-isobutene-isoprene
CR	chloroprene
IIR	isobutene-isoprene
IR	isoprene, synthetic
NBR	nitrile-butadiene
NCR	nitrile-chloroprene
NIR	nitrile-isoprene
NR	natural rubber
SBR	styrene-butadiene
SCR	styrene-chloroprene
SIR	styrene-isoprene rubbers
Z	polyorganophosphazene
Q	polysiloxane rubber
FKM	fluoro rubber of polymethyrene type having substituent fluoro and perfluoroalkoxy groups on the polymer chain

© 2004 by Marcel Dekker, Inc.

As pointed out earlier, rubber must first be dissolved in SEC solvent when SEC analysis is attempted. Almost all final rubber products, however, are produced by vulcanization, in which raw rubbers tend to become completely insoluble. Therefore, SEC of rubbers is limited to raw rubbers only. This criterion, however, is not obeyed for SEC of low-molecular-weight compounds in vulcanized rubbers. Vulcanized rubbers contain many additives, such as curatives, antioxidants, and modifiers. These additives can be easily analyzed by SEC if their forms are soluble in SEC solvents, as demonstrated by Zimbo *et al.* (34) for the SEC analysis of the extender oil bloom on EPDM (terpolymer of ethylene, propylene, and a diene) vulcanizates.

3 GENERAL REMARKS

To manifest the particular property of rubber, high elasticity, rubbers have high molecular weights with a broad molecular weight distribution compared with other polymeric materials. This is seen typically in the molecular weight distribution curve for natural rubber (NR), shown in Fig. 1. Synthetic commercial rubbers were initially produced after natural rubber, and their molecular weight distributions were also almost the same as that of natural rubber. Therefore, the SEC characteristics of the various rubbers are considered together.

The convenience of SEC for the determination of molecular weight data for a wide variety of synthetic rubbers was appreciated early after the introduction of

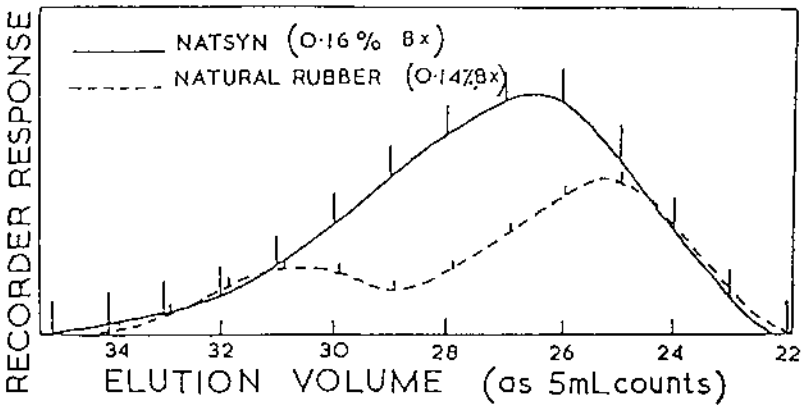

Figure 1 Chromatograms of Natsyn 400 and natural rubber. Instrument: Waters Model 200. Column: 10^6, 10^5, 5×10^4, 10^3 Å porosities. Mobile phase: THF (0.05% wt/vol antioxidant). Flow rate: 0.91, 0.95 mL/min. Temperature: 35°C. (From Ref. 8.)

© 2004 by Marcel Dekker, Inc.

SEC. One of the reasons is that they are generally easily soluble in SEC solvents and need no specific SEC experimental condition, such as high temperature.

In some cases, however, it is difficult to perform SEC analysis, especially when attempting SEC of new rubbers. An example is polyorganophosphazene rubber (30,31). For SEC, the choice of SEC conditions should be made first. The SEC/low-angle laser light-scattering (LALLS) or SEC/LALLS/viscosity detector coupling systems give effective results. By these techniques, the dilute solution properties of the rubber polymer, which are closely related to their behavior in SEC, are understood simultaneously. Cooperative data from SEC and dilute solution properties give information on molecular branching, molecular weight distribution, and compositional heterogeneity so that more precise molecular characterization can be obtained.

3.1 Solvents of Rubber for SEC

SEC is a separation technique based on differences in molecular sizes in solution. The most essential condition in the SEC of rubbers is that they be dissolved completely in SEC solvents. Solvents used for the SEC of rubbers are summarized in Table 2. The most common solvent is tetrahydrofuran (THF).

So-called organic solvent-resistant rubbers and heat-resistant rubbers exist. Also, there are rubbers that contain microcrystalline parts or molecular associations even in their solution state. NBR, CR, Z, Q, FKM, and EPDM (see Appendix) are examples. An example of SEC analysis of these rubbers is seen in phosphazene rubbers (30,31). In the SEC of such rubbers, difficulties arise in finding suitable SEC solvents. In principle, such methods as increasing the temperature to enhance the solubility are needed for these rubbers. In EPDM or EPM (copolymers of ethylene and propylene), for instance, normal room temperature SEC was once used, but today use of a high-temperature SEC is most commonly used because they may contain some crystalline parts depending on the block of C_2 or C_3 segments. Choice of other solvents depends on the required sensitivity of the detectors.

Care should be taken when handling rubber solutions because rubbers have considerable amounts of unsaturated double bonds and are prone to oxidation by the peroxide in THF or even by the oxygen in air. The addition of suitable antioxidants is very common to reduce the incidence of such oxidative degradation. Also, the solution should not be exposed to light or high storage temperature. Common antioxidants used in SEC for rubbers are shown in Table 3.

3.2 Presence of Gel

Both natural and synthetic rubbers normally have a gel component, which is a part that remains undissolved in a solvent (61,62). The gel component is probably produced by chain branching during the polymerization process or by slight

© 2004 by Marcel Dekker, Inc.

Table 2 Various Solvents and Operating Temperatures in the Literature for SEC Analysis of Rubbers[a]

Polymer	Solvent	Temperature (°C)	References
EPDM	TCB	135	70
	THF		39
EVA (high VA)	THF	Ambient	70
EVA (low VA)	ODCB	140	70
NR	Toluene	80	70
	THF	24	5
	THF	27	6
	THF	35	7,9
	THF	40	3
	THF		10
Polyacrylonitrile	DMF	80	70
Polybut-1-ene	TCB	140	70
BR	Toluene	80	70
	THF	40	29
	THF		22,24,28
Q	Toluene	80	70
	THF	Ambient	70
Polyurethane	THF	Ambient	70
	DMF	80	70
SBR	Toluene	80	70
	THF	40	21
	THF		20
IR	THF	Ambient	58
	Toluene	80	70
Z	THF	30	30
	Acetone + cyclohexane		31

[a]EVA, polyethylene + vinyl acetate; TCB, 1,2,4-trichlorobenzene; ODCB, 1,2-dichlorobenzene.

crosslinking when handling rubbers. The most common example is seen in unmilled natural rubbers. When such a component is present, SEC analysis affords only the molecular weight data on the soluble fraction, excepting the gel fraction. In this case, to understand the viscoelastic properties of the rubbers connected with the SEC data is not appropriate because the gel contributes to these properties. Studies of the influence of the gel fraction on the mechanical properties of natural rubber are listed in a relevant article (61). The suggestion is that, in natural rubber, the gel tends to be soluble in SEC solvents when suitably masticated.

A common practice in SEC is to filter the sample solution through an approximately 0.5 μm filter used for the injection. This means that the gel

© 2004 by Marcel Dekker, Inc.

Table 3 Antioxidants Used for SEC Analysis of Rubbers

Antioxidant	Concentration (%)	References
4,4-Thiobis-3-methyl-6-*tert*-butylphenol (Santonox)	0.1 wt/vol	40,61
2,4-Di-*tert*-butylphenyl phosfite (D-13 168)	0.1 wt/vol	61
2,6-Di-*tert*-butyl-4-methylphenol (Ionol)	0.03	30
	1 for polymer	44
	0.05 wt/wt	43

or aggregates that cannot pass through the filter are removed from the SEC columns.

3.3 SEC Calibration

As is well known, an SEC system should be calibrated by plotting the elution volume V_e of the peak maxima of a series of calibrants with narrow molecular weight distribution against the log molecular weight M before SEC analysis is made. Commonly, standard polystyrenes are used for the calibrants. The calibration curve log M vs. V_e for the polystyrene calibrants is valid only for SEC analysis of linear polystyrene samples. For rubbers, rubber standards of the same type of rubber in question should be used. The difference in the calibration curves between polystyrene and polyisoprene standards is depicted in Fig. 2 (6). However, only a limited number of commercial rubber standards are available, as shown in Table 4.

An alternative approach to calibrating an SEC system has been to use a single broad molecular weight distribution calibrant. However, this method is not common.

A method to overcome this is Benoit's universal calibration plot (63) of $\log[\eta]M$ against V_e, where $[\eta]$ is intrinsic viscosity. However, this method needs the constants from the Mark–Houwink $[\eta]M$ relationships for the rubber samples to be analyzed in the SEC solvents before the SEC analyses. However, a literature survey showed that few constants for rubbers are available, as shown in Table 5. Another method is to use the Q factor (64), which is defined as the ratio of the extended chain length between polystyrene and rubber samples. This method is valid only for vinyl polymers and is empirically crude (6).

A much more satisfactory calibration method is to use LALLS coupling with the usual refractive index (RI) detector in the SEC system so that the molecular weight corresponding to each elution volume can be obtained directly (30,38). The molecular weight distributions of the polyorganophosphazenes have

© 2004 by Marcel Dekker, Inc.

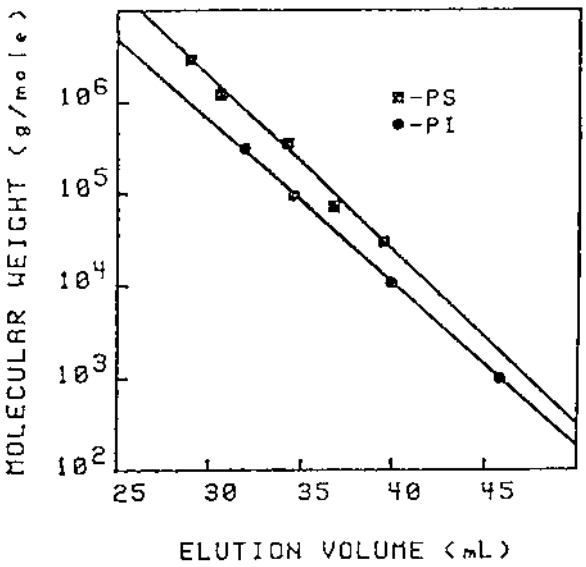

Figure 2 Typical GPC calibrations with PS ($Q = 60.4\,g/\text{Å}$) and PI molecular weight standards. Instrument: Waters Model 244. Column: 10^6, 10^5, 10^4, 10^3, 500 Å porosities. Mobile phase: THF. Flow rate: 1 mL/min. Temperature: 27°C. Detector: RI. (From Ref. 6.)

been obtained by this method; they cannot be obtained with other methods because of their complex behavior in SEC solvent.

It is not always necessary to calculate the correct molecular weight distribution to obtain information from SEC chromatograms. Simple inspection of chromatograms often reveals important information, as shown in Fig. 3. The comparison is valid only for data obtained under the same SEC conditions, however, because an SEC chromatogram is a function of molecular weight

Table 4 Molecular Weight Standards for SEC Analysis of Rubbers

Polybutadiene
Polyisoprene
Polyisobutylene
Polystyrene-isoprene diblock
Polystyrene-butadiene diblock
Polystyrene-butadiene star block

Source: Ref. 71.

© 2004 by Marcel Dekker, Inc.

Table 5 Mark–Houwink Viscometric Constant for Rubbers Used for SEC

Polymer	Solvent	Temperature (°C)	$K \times 10^{-4}$	α	Reference
Natural rubber	THF	25	1.09	0.79	72
Polybutadiene	THF	25	2.36	0.75	72
Polyisoprene	THF	25	1.77	0.735	72
SBR (28% styrene)	THF	25	4.51	0.693	72
Polybutadiene	ODCB	135	2.7	0.746	72
Polydimethylsiloxane	ODCB	135	3.83	0.57	72
	$CHCl_3$	30	0.54	0.77	72
Polyaryloxyphosphazene	THF	30	0.0119	0.649	30

distribution as well as the SEC system, including columns and instrumentation. Although the fingerprinting method is qualitative, it is the most frequently used method for the design of syntheses of new rubber polymers. SEC chromatograms indicate polymerization recipes and polymerization conditions (47,50,52).

3.4 SEC of Molecular Branching

Both natural rubber (*Hevea*) and synthetic rubbers have molecular chain branching. The presence of branched molecules affects the SEC behavior to a great extent, because a branched molecule has a smaller hydrodynamic volume than a linear chain molecule of the same molecular weight and is eluted later. Therefore, when branched molecules are present, an erroneous molecular weight distribution curve results by analyzing the SEC curve as if there are only linear molecules. Subramaniam (8) has shown an example in the SEC analysis of NR.

Many modern SEC systems include LALLS. As described earlier, this gives information about both the molecular weight distribution and the extent of chain branching in the same SEC analysis time. It is convenient for simultaneous determination of chain branching and molecular weight distribution. Even when LALLS is not used, a combination of SEC and viscometric measurements can estimate chain branching using the universal hydrodynamic calibration method (63). Fuller and Fulton (3) studied the relation between molecular branching and the mechanical behavior of NR.

3.5 SEC of Copolymer Rubbers and Blends

As can be seen in Table 1, several rubbers have a copolymer structure. The physical properties of the copolymers are affected not only by the molecular weight distribution but also by the compositional distribution. Therefore, it is desirable to know the compositional distribution in addition to the molecular

© 2004 by Marcel Dekker, Inc.

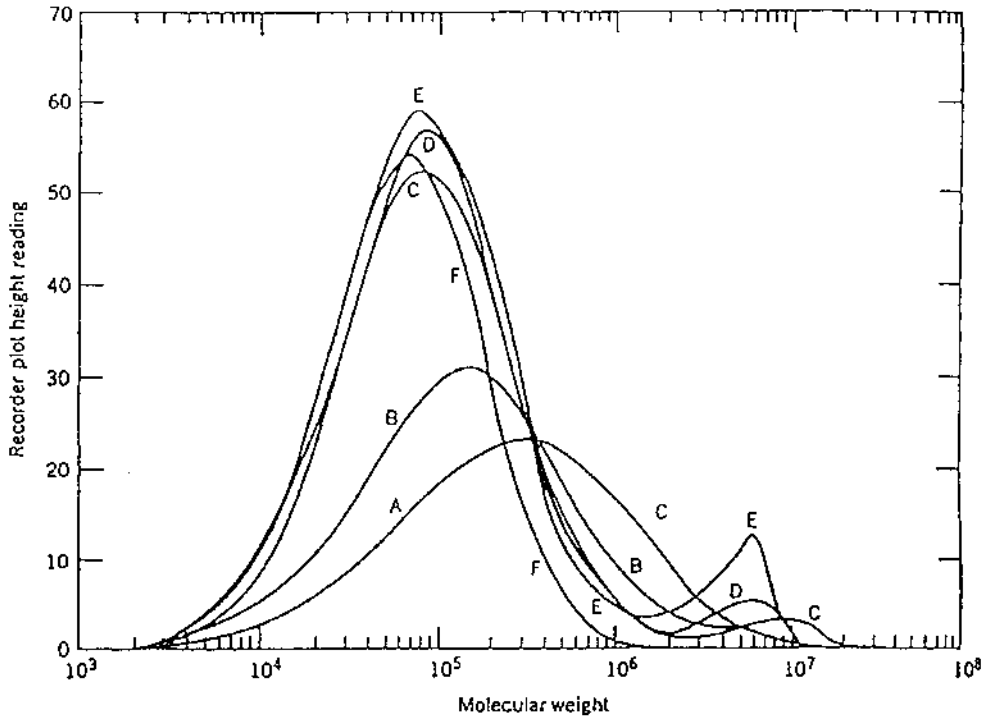

Figure 3 Gel permeation chromatograms showing the effect of NR mastication. (A) 8 minutes milling time; (B) 21 minutes; (C) 38 minutes; (D) 43 minutes; (E) 56 minutes; and (F) 76 minutes. (From Ref. 66.)

© 2004 by Marcel Dekker, Inc.

weight distribution. This type of analysis is often performed by SEC systems having more than two detectors.

When one of the constituents *A* or *B* of a copolymer has ultraviolet (UV) absorption and the other does not, a UV-RI dual-detector system can be used for the detection of the chemical heterogeneity of the copolymer. As with molecular weight distribution, 1:1 eluant–eluant composition against the retention volume V_e is calculated from the two chromatograms, and a compositional variation is plotted as a function of molecular weight. However, the response factors of the two components in the two detectors must be calibrated first. This method has been applied to the determination of chemical heterogeneity for styrene–butadiene copolymers (14,59). SBR is one of the most widely used synthetic rubbers. In the earliest stage of introduction of SEC for SBR, the molecular weights and molecular weight distribution were only included in the analysis by RI detection. However, by using a UV absorption detector, additional comonomer styrene UV maxima can be obtained separately. If a UV photodiode array detector is used, various low-molecular-weight additives that have different UV maxima can be detected at one time (14).

Other detection methods, such a turbidometric titration (19) and Fourier transform infrared spectrometry (35), have been used for compositional detection in copolymer rubbers.

Recently, rubbers have been modified by blending or by chemical reaction to suit specific needs for the product. In these cases, the compositional analysis is very important. The same SEC analysis is used as an effective companion method.

For the SEC of rubber blends, it is crucial that SEC equipped with two or three properly selected detectors, instead of the conventional single RI detector, be used (65).

3.6 Preparative SEC for Rubbers

From the beginning, preparative SEC was applied to the preparation of narrow molecular weight samples of a specified rubber polymer. Nevertheless, the literature survey shows that only a few studies have been reported. The reason, as Chaturcedi and Patel (43) describe, is that the preparative SEC method is tedious and time consuming compared with the conventional preferred precipitation method.

Fractionation of *trans*-1,4-polyisoprene by preparative SEC was reported by Chaturcedi and others (43). However, they obtained only three fractions that could be measured by further viscometry.

4 TYPICAL APPLICATIONS OF SEC RUBBERS

4.1 SEC for NR and IR

Although the molecular weight distribution of NR has been studied extensively, different results have been reported. The reason appears to be that there is a

© 2004 by Marcel Dekker, Inc.

variation between different samples of NR depending on both the origin of trees and processing methods. Also, samples of NR have an additional complication as a result of the oxidation and gelation that take place in the bulk state or even in solution.

In 1972, Subramaniam (8) reported a comprehensive study on the molecular weight distribution of selected samples of NR by SEC. Solutions of NR were prepared on fresh latex obtained from six clones of *Hevea brasiliensis*. Figure 1 shows the SEC chromatogram of the purified natural rubber sample. It can be seen in this curve that NR has a very broad molecular weight distribution with a distinctive bimodal curve. Comparing this to that obtained on a sample of synthetic polyisoprene (IR), Natsyn 400, the bimodality can be seen more clearly. Using the universal calibration method (63), he showed that the integral molecular weight distribution curves for six clones of NR ranges from 10^4 to 10^7. However, the average molecular weights derived from SEC curves are too low compared with values obtained conventionally. He pointed out that this error was a result of not considering chain branching. In other words, by this method chain branching was not completely detected. Further study is needed to use SEC/LALLS or other relevant methods.

Subramaniam also described difficulty with the practice of SEC for NR. This difficulty was the partial blockage of the columns experienced with some rubber samples. This is caused by the gel "plug" in the NR solution. When plugged, the plugged gel parts are usually removed by opening the column. Another remedy to this problem was to clean the plugged gel by injecting a 3% (vol/vol) solution of xylyl mercaptan, which had no effect on the efficiency of the columns in fractionating polymers.

The degradation of NR during milling has been studied by SEC. A representative graph shows that the molecular weight distribution is narrowed as the rubber is milled for an increasingly longer time under fixed milling conditions (Fig. 3) (66). The peak of the distribution curve shifts to lower and lower molecular weights with increased milling time. The molecular weight distribution curve becomes much narrower than the original curve.

A comparison of the milling down rate of different diene rubbers was measured easily by SEC. From the SEC analysis results for different diene rubbers under fixed milling conditions, the milling down rate is in the order NR $>$ IR $>$ SBR $\simeq$ BR (67).

4.2 SEC of Polyorganophosphazene Rubber Z

A typical example of the application of SEC for difficult samples is seen in the molecular weight analysis of polyorganophosphazene rubber. The molecular characterization of Z by SEC has been studied extensively in recent years. Nevertheless, no satisfactory results were obtained until the work

© 2004 by Marcel Dekker, Inc.

by the De Jaeger and Mourey groups (30,31). A reason for this is that Z rubbers show a molecular association in solution caused by their chemical nature.

It was reported that the SEC of Z (polydiphenoxy, polyaryloxy, and polyfluoroalkoxy) in pure THF shows an unusually shaped chromatogram, suggesting adsorption or other nonsize exclusion phenomena (30). The reason is attributed to the behavior of polyelectrolytes arising from the polydichlorophosphazene residue that is the precursor of Z. Also it is responsible for the formation of aggregates in SEC eluants. The addition of salts, for example LiBr (0.1 M), is enough to remove such aggregates. This was also confirmed by dilute solution viscosity data using an SEC/LALLS system. Figure 4 shows typical SEC chromatograms of polytrifluoroethoxyphosphazene and polydiphenoxyphosphazene obtained by an SEC/LALLS system in THF.

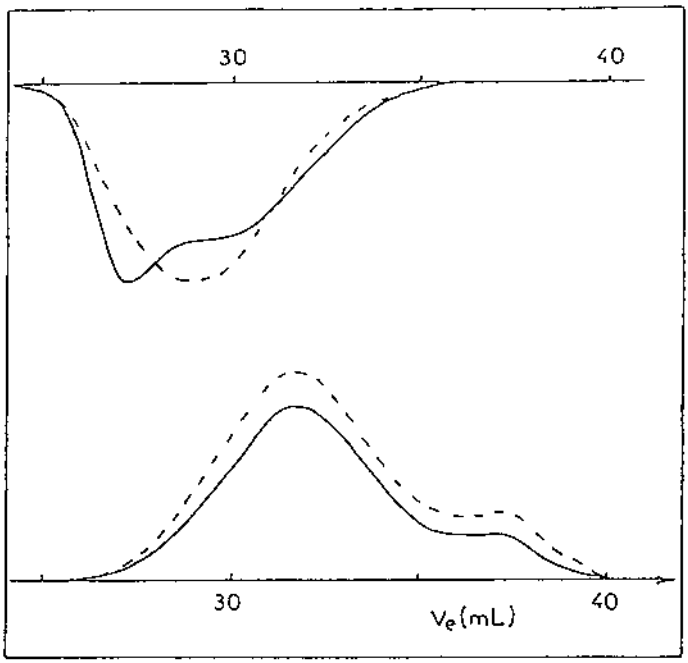

Figure 4 Comparison of two polydiphenoxyphosphazene samples of very similar RI chromatogram (lower trace). The LALLS detector seems to reveal some aggregates. Instrument: Waters Model 150 ALC/GPC. Column: Shodex 80M. Mobile phase: THF (0.03% antioxidant, 2,6-di-*tert*-butyl-4-methylphenol). Flow rate: 1 mL/min. Temperature: 30°C. Detector: RI, LALLS. (From Ref. 30.)

© 2004 by Marcel Dekker, Inc.

Another example, shown in Fig. 5 (31), uses a viscosity detector system. The intrinsic viscosity decreases nearly linearly with retention volume across the main peak of the distribution, but it then drops distinctly near the low-molecular-weight region of the chromatogram.

Their conclusions on the SEC analysis of Z are that SEC/LALLS coupling is an effective characterization technique and the eluant should be free or chosen so that association is eliminated. Despite its mineral backbone, polyorganophosphazene also confirms the universality of the universal calibration concept, and examination of dilute solution viscosity behavior is a simple method of screening a potential solution for SEC analysis.

When using SEC to study rubber samples having the same unusual characteristics, properly selected dual or triple detectors yield much more comprehensive information on molecular characteristics. Otherwise, the use of a single detector in SEC for such samples may lead to erroneous conclusions. Commercially available detectors are LALLS, UV, infrared, and evaporative detector (ED) photometers with conventional RI detectors.

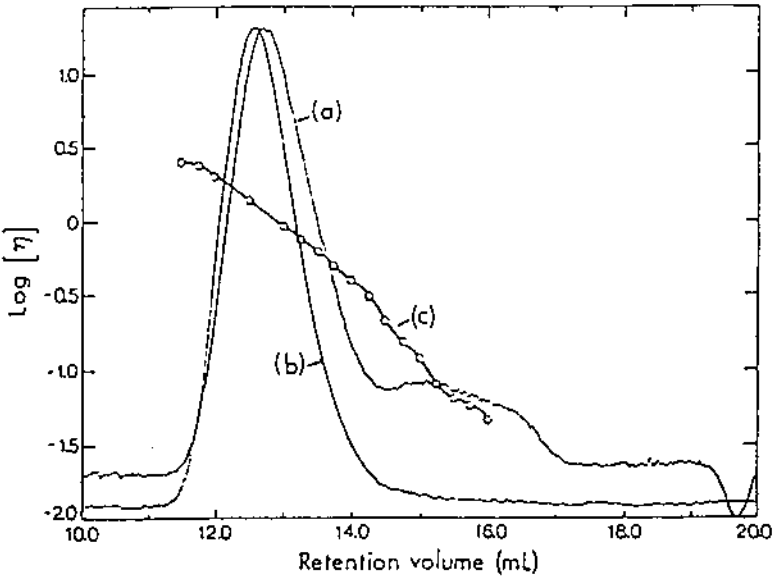

Figure 5 Chromatograms of polybistrifluoroethoxyphosphazene using different detectors: (a) differential refractometer, (b) differential viscometer, and (c) intrinsic viscosity. Column: PLgel mixed bed. Mobile phase: acetone, cyclohexanone. Temperature: 30°C, 40°C. (From Ref. 31.)

© 2004 by Marcel Dekker, Inc.

5 SPECIAL APPLICATIONS OF SEC FOR RUBBERS

SEC is used for the characterization of the molecular weight parameters of rubbers; however, there is an inverse SEC consideration in which the determination of the porous structure of the column packings (if the packings are vulcanized rubber) might be elucidated by examining the retention data for polymers having known molecular weights. This technique is called inverse SEC. This seems to be a natural extension of inverse gas chromatography (68).

In 1984, Haidar and others (39) reported their inverse SEC results for the elucidation of structural differences in networks prepared by chemical and photochemical reactions of EPDM. They used conventional GPC for their inverse SEC, except for the columns, in which fine powders of crosslinked EPDM were packed. Polystyrenes of various molecular weights were used as the probe.

Their elution data for standard polystyrenes from EPDM packed columns showed clearly the differences presented between two vulcanizing methods: one was photo-crosslinked and the other was peroxide-cured EPDM. From this study they concluded that the M_c, the molecular weight between crosslinking junctions, was different for the two samples.

In 1985, Capillon and others (69) gave the criticism that the inverse SEC gives erroneous results when used in gels that swell too much, such as vulcanized rubbers.

Subsequently, very little work has been done using inverse SEC for the characterization of the network structure of rubbers.

6 CONCLUSION

Rubbers based on dienes can easily be analyzed for their molecular characterization by SEC; however, special rubbers, such as polyorganophosphazenes, show some difficulty because of their imperfect dissolution in SEC solvents. Fluoro-rubbers are hard to dissolve in solvents. The application of SEC to such rubbers is not covered in the literature cited in Table 5.

Recent application trends of SEC to rubbers are multidetector systems to obtain much more information on the molecular characteristics in a single SEC run. A properly arranged SEC system gives almost a complete molecular characterization of rubbers if the rubbers are dissolved in SEC solvents.

For the appendix we could not find a role for SEC in the quality control of rubber production processes despite its technological importance. Furthermore, we expect that much work on the correlation between SEC analysis and mechanical properties of rubbers is in development.

© 2004 by Marcel Dekker, Inc.

APPENDIX: SEC CONDITIONS FOR RUBBERS

Polymer	Columns	Mobile phase	Comments	Reference
NR (masticated)				2
NR (not crosslinked)	Two 60 cm mixed bed columns (Polymer Laboratories)	THF 0.5 mL/min 40°C	UV (215 nm) Polystyrene standard	3
NR	10^6, 10^5, 10^3, 100, 50 Å PLgel	0.8 mL/min 70°C	UV, RI Polyisoprene standard Polystyrene (PS) standard	4
Guayule Parthenium		THF 1 mL/min 24°C	Polyisoprene standard	5
Guayule	10^6, 10^5, 10^4, 10^3, 500 Å μStyragel	THF 1 mL/min 27°C	RI Polystyrene standard Polyisoprene standard	6
Guayule	10^7, 10^6, 5×10^5, 1×10^5 to 3×10^5, 5×10^3 to 1×10^4 Å Styragel	THF 1 mL/min 35°C	Water Ana-Prep chromatograph RI Universal calibration	7
NR, IR	10^5, 5×10^4, 1.5×10^4, 10^3 Å 10^6, 10^5, 5×10^4, 10^3 Å	$C_6H_5CH_3$ THF 0.91 mL/min 0.95 mL/min 35°C	Polystyrene standard Toluene a good solvent for NR and quite stable, but refractive index in crement between it and NR small	8
NR, IR, SBR, BR masticated	10^7, 10^6, 10^5, 10^4 Å	THF 1 mL/min		9
NR, IR, SBR, BR	7×10^7, 10^6, 10^4 Å	35°C		
NR latex (modified with peracetic acid epoxidation)		THF	Solubility decreases with increasing level of epoxidation because of higher gel content	10

© 2004 by Marcel Dekker, Inc.

Appendix (*Continued*)

Polymer	Columns	Mobile phase	Comments	Reference
Copolymer of NR and nylon 6	Two Shodex AD-80M/S	1,1,2,2-Tetra-chloroethane ($CH_2Cl_2CH_2Cl_2$) 1.0 mL/min Ambient temperature	RI + UV (260 nm) (37% nylon 6 mechanically blend)	11
NR (lightly masticated) IR (lightly masticated) BR (lightly masticated)	10^6, 10^5, 10^4, 10^3, 5×10^2 Å	THF 1 mL/min	UV Graft copolymers	12
SBR VSBR (vinyl styrene butadiene rubber)			Molecular weight distribution (MWD) bimodal, each peak with a narrow MWD	13
SBR	Ultrastyragel linear column	THF 1.0 mL/min	RI Photodiode array detector	14
SIR Styrene–ethylene–butadiene copolymer Styrene–butyl-methacrylate copolymer	Ultrastyragel 500 Å (Waters)	38°C		
SBR (ozonolysis)	Styrene–divinylbenzene gel (21.2 mm inner diameter, ID, 60 cm, three)	Chloroform 2 mL/min	UV (254 nm)	15
SBR lattices	Bimodal-S kit (DuPont)	THF BHT (butylated hydroxy-toluene)	UV, RI Vistex solution	16
SBR (ozonolysis) BR (ozonolysis)	Styrene–divinylbenzene gel (7.5 mm ID, 500 mm)	Chloroform	UV	17

© 2004 by Marcel Dekker, Inc.

Appendix (*Continued*)

Polymer	Columns	Mobile phase	Comments	Reference
PS-BR-THF ternary system PS-BR-tetralin ternary system BR	Styragel, 5×10^6, $1.5-1.7 \times 10^5$, $1.5-5 \times 10^4$, $2-5 \times 10^3$ Å	THF 1 mL/min Tetralin	Ternary-phase studies (blend) Phase diagram determination RI + UV 254 nm	18
Anionic polymerized Dimethyl-formamide SBR	Styragel (Waters) 10^7, 10^6, 10^5, 10^4 Å (0.1% Ionol)	THF (0.3% $NaNO_3$) 0.5 mL/min 26°C	Compositional distribution Universal calibration	19
SBR		THF	(Waters Associates, Inc.)	20
SBR BR	Glaskugel	THF 40°C	RI, UV	21
BR (OH terminated)	Analytical GPC μStyragel 10^4, 10^3, 500, 100 Å Preparative GPC Styragel 10^4, 10^3 Å	THF 2 mL/min THF 10 mL/min	RI, UV Universal calibration	22
1,4-BR-b-1, 2-BR	PLgel columns (2) 10^5, 10^3 Å	Chloroform 1 mL/min	RI Polystyrene standard	23
BR Waste rubber	μBondagel E linear columns	THF	Mixture of 1,4-BR, 1,4-*trans*, and 1,2-vinyl polybutadiene	24
Phosphorus-terminated BR	Divinyl-benzene crosslinked polystyrene bead (10 μm) 10^5-10^2 Å		RI Universal PS calibration	25
BR *cis*-1,4-polybutadiene (branched)	Waters 200 GPC		Determination of long-chain branching	26
ω-Functional group terminated BR (liquid polymer)			Polymers polymerized with different kinds of initiator were measured (different organometallic initiators)	27
BR	Silicagel Lichrospher	THF 0.5 mL/min	Polystyrene standard	28

© 2004 by Marcel Dekker, Inc.

Appendix (*Continued*)

Polymer	Columns	Mobile phase	Comments	Reference
cis-BR (Taktene 1220)		THF 3 mL/min (two columns) 1 mL/min (four columns) 40°C	Polystyrene standard	29
PZ (polyorgano-phosphazene) FZ (polyfluorophos-phazene)	Two Shodex 80 M (stabilized with 0.03% 2,6-di-*tert*-butyl-4-methylphenol)	THF + LiBr 0.1 mol/L, + ethylene-glycol, or + diethylene glycol 1 mL/min 30°C	LALLS-RI in series Aggregates form because of the presence of P—Cl, P—O bonds or P—OH, P—O, and N—H bonds	30
FZ Polydichlorophos-phazene Z	Polystyrene–divinylbenzene	Acetone + cyclohexanone, 30°C, 40°C, Ammonium nitrate	Dilute solution properties in acetone, THF, cyclohexane in the presence of TBAN (tetrabutylammonium butyrate) examined to choose optimum eluant conditions for SEC; acetone in SEC caused concentration-induced chain compression; poorer solvent, cyclohexane, reduced this effect	31
Modified phosphazenes	μBondagel	THF with 0.01 *N* tetra-*n*-butylammonium bromide (added to break up polymer association)	Anomalies in GPC data attributed to separation by chemical heterogeneity as well as molecular size	32
PZ	Five 4 ft/in. Styragel columns of porosity rating 5×10^6, two of $1.5–7 \times 10^5$, 10^5, $1.5–5 \times 10^4$ Å	THF 1 mL/min	Polystyrene standard	33

© 2004 by Marcel Dekker, Inc.

Appendix (*Continued*)

Polymer	Columns	Mobile phase	Comments	Reference
Extender oil bloom on the surface of EPDM vulcanizates	100 Å UltraStyragel (300, 7.8 mm ID)	THF 1.0 mL/min 30°C	Dissolution part in hexane RI	34
EPM (copolymers of ethylene and propylene)	Shodex columns 802, 803, 804, 805	TCB 0.5 mL/min 135°C	Composition drift collecting solvent-free polymer film from a high-temperature GPC	35
EP (C_3 = mol% 51–36) M_w/M_n 3.2–12.9	Styragel 10^7, 10^6, 10^5, 10^4, 10^3 Å 10^7, 10^6, 10^4, 10^3 Å	ODCB 1 mL/min 135°C	Double peaks	36
EPM-g-SAN (styrene–acrylonitrile copolymer)	Styragel (5×10^3, 10^7 Å)	THF 1 mL/min	UV RI	37
EPM	μStyragel (500, 10^6 Å)			
EPM	Styragel 10^6, 10^5, 10^4, 10^3 Å	1,2,4-Trichloro-benzene	GPC-LALLS RI	38
EPDM	Waters	140°C		
EPDM	Packed with polymer pieces of crosslinked elastomer (EPDM)	THF 0.4 mL/min	Inverse GPC	39
EPDM	11 × 300 mm PLGel column (2×10^6, 1×10^3 Å)	Trichlorobenzene 1 mL/min 135°C	LALLS (ED, DRI (differential refractive index))	40
IR	DuPont Z or latex PSM	THF	M_w of complex polymer can be determined by SEC on-line viscometry detector	41
IR	μStyragel	THF 25°C	Polyisoprene standard No indication of aggregates found Association behavior in end-functionalized polymer	42
Trans-1,4-IR	10^6, 10^5, 10^4, 10^3 Å	Toluene 2 mL/min 30°C		43

© 2004 by Marcel Dekker, Inc.

Appendix (*Continued*)

Polymer	Columns	Mobile phase	Comments	Reference
Hydroxytelechelic polybutadiene	For analytical GPC Styragel 1000, 500, 100, 50 Å	THF	30 g Arco-R45M fractionated into five fractions; fractions recovered from solutions by vacuum and characterized by nuclear magnetic resonance, VPO, and GPC RI (Waters R401) Polystyrene standard Polybutadiene standard	44
U (thermoplastic)	PI-Gel 10 μm	THF (250 ppm BHT) 1.0 mL/min 40°C	RI	45
U	Not given	Not given	GPC curves of fragments obtained by decomposition of U in *n*-$BuNH_2$/ dimethyl-sulfoxide solution shown	46
Polyisobutyrene (PIB) Isoprene Living polymerization Telechelic living PIB Cyclopolyisoprene cy-PIP/PIB multiblock (tr-1,4-PIP)-b-PIB-b-(tr-1,4-PIP) (PIB is a thermoplastic elastomer)			Polymerization Polyisobutadiene standard Polystyrene standard RI For MW determination	47
NBR (low conversion) Acrylonitrile in polymer 20, 26, 34, 37, 50 wt%	Crosslinked 2-chloro-acrylonitrils gel Shodex H-2005	Chloroform/*n*-hexane (gradient) 0.5 mL/min Chloroform 3.5 mL/min	Evaporative mass detector (Model 750/ 14ACS Co.) Mixture of three commercial NBR of different AN contents separated	48

© 2004 by Marcel Dekker, Inc.

Appendix (*Continued*)

Polymer	Columns	Mobile phase	Comments	Reference
Antioxidant in CR (chloroprene) (methylene-4426-s, KY-405, phenothiazine)	MCH-5N-CAP	MeOH-$CHCl_2$-H_2O		49
Triflate ($-OSO_2CF_3$) terminated PIB	μStyragel 10^5, 10^4, 10^3, 500, 100 Å	THF 1 mL/min	Synthesize triblock and star-block copolymers consisting of central PIB and external PTHF (polytetra-hydrofuran); polystyrene standard UV, RI	50
Polyether-amide block copolymer Thermoplastic elastomer	μStyragel 10^5, 10^4, 10^3, 500 Å	Benzyl alcohol (0.5% di-*t*-butyl-paracresol)	RI IR	51
Polyisobutyrene Living polymerization	UltraStyragel 10^5, 10^4, 10^3, 500, 100 Å	THF 1 mL/min 1 mL/min	Living polymerization of IB polymerization conditions followed by SEC	52
S-B-S, S-I-S triblock copolymers Their ozonolysis products	Polystyrene gel Preparative column 3×10^3 Å Analytical column 7×10^5, 2×10^5, 1×10^5, 5×10^4 Å	Chloroform 2 mL/min (preparation) 1 mL/min (analytical)	Polystyrene standard Commercial S-B copolymer KX-65, Solprene-411, Clearen 530-L Commercial S-I block copolymer Kraton-1107, TR-1112 Chemical composition distribution determined by high-performance liquid chromatography using acrylonitrile gel of hexane–chloroform mixture	53
Polystyrene–polydimethyl–siloxane block copolymer PS-PDMS (polysimethyl-siloxane) blend	Four 30 cm 10 μm packings (Polymer Laboratories 10^6, 10^5, 10^4, 10^3 Å)	$C_2H_2Cl_4$ (tetrachloro-ethylene) quoted pore size concentration 5×10^{-3} g/cm^3 or less	RI, LALLS (dual detector) Compositional heterogeneity correlation with MWD	54

© 2004 by Marcel Dekker, Inc.

Appendix (*Continued*)

Polymer	Columns	Mobile phase	Comments	Reference
Toluene diisocyanate Diphenyl-methane diisocyanate in poly-urethane polymers	500, 100, 100 Å Styragel	CH_2Cl_2 1 mL/min 30 cm × 78 mm ID	Urethane	55
Polyepichloro-hydrin	TSKgel (two G2000H8, G3000H8, G40000H8)	THF 40°C	RI UV (254 nm)	56
Polyurethane-based copolymer with polyether and polyamide	TSK G3000HXL, G4000HXL	THF	Polystyrene standard	57
Polyorgano-siloxane–polyarylester block copolymers (perfectly alternating) functional siloxane oligomers	50, 10^6, 10^5, 10^4 Å μStyragel	THF 1.0 mL/min	RI, UV Step growth reactions of the two oligomers confirmed from SEC chromato-grams	58
SB (styrene–butadiene copolymer)	10^6, 10^5, 10^4, 10^3, 800 Å	THF	UV, RI Polystyrene standard Polybutadiene standard	59
Polyalkenylenes	Not given	Not given	Bimodal molecular weight distribution curve of polyoctenylene shown	60

REFERENCES

1. JC Moore. J Polym Sci A2:835, 1964.
2. H Bartels, ML Hallensleben, G Pampus, G Scholz. Angew Macromol Chem 180:73, 1990.
3. KNG Fuller, WS Fulton. Polymer 31:609, 1990.
4. H Bartels, ML Hallensleben, G Pampus, G Scholz. Angew Makromol Chem 180:73, 1990.

© 2004 by Marcel Dekker, Inc.

5. J West, E Rodriguez. Rubber Chem Technol 60:888, 1987.
6. CL Swanson, ME Carr, HC Nielsen. J Polym Mater 3:211, 1986.
7. T Hager, A MacArthur, D McIntyre, R Seeger. Rubber Chem Technol 52:693, 1979.
8. A Subramaniam. Rubber Chem Technol 45:346, 1972.
9. T Homma, N Tagata, H Hibino. Nippon Gomu Kyokaishi 41:242, 1968.
10. IR Gelling. Rubber Chem Technol 58:86, 1985.
11. T Ogawa, M Sakai. J Liq Chromatogr 8(6):1025, 1985.
12. DS Campbell, AJ Tinker. Polymer 25:1146, 1984.
13. RR Rahalkar. Polymer 31:1028, 1990.
14. JK Del Rios. Am Lab 20:78,80, 1988.
15. Y Tanaka, H Sato, J Adachi. Rubber Chem Technol 59:16, 1986.
16. DL Bender, JJ Beres, RB Timmer. Int GPC Symp '87, 1, 1987.
17. Y Tanaka, H Satou, Y Nakafutami. Polymer 22:1721, 1981.
18. DR Lloyd, V Narasimhan, CM Burns. J Liq Chromatogr 3(8):1111, 1980.
19. M Hoffmann, H Urban. Makromol Chem 178:2683, 1977.
20. Y Minoura, Y Hatanaka. Nippon Gomu Kyokaishi 43:838, 1970.
21. HJ Cantow, J Probst, C Stojanov. Kautschuk Gummi 21:609, 1968.
22. KN Ninan, VP Balagangadharan, KB Catherine. Polymer 32:628, 1991.
23. S Poshyachinda, HGM Edwards, AF Johnson. Polymer 32:334, 1991.
24. G Adam, A Sebenik, U Osredkar, Z Veksli, F Ranogajec. Rubber Chem Technol 63:660, 1990.
25. WE Lindsell, K Radha, I Soutar, MJ Stewart. Polymer 31:1374, 1990.
26. J Chunshan, G Qipeng. J Appl Polym Sci 41:2383, 1990.
27. RA Livigni, IG Hargis, HJ Fabris, JA Wilson. J Appl Polym Sci, Appl Polym Symp 44:11, 1989.
28. L MrKvickova, I Kucharikova, S Pokorny, J Cermak. Plaste Kautsch 34:17, 1987.
29. G Kraus, CJ Stacy. J Polym Sci A-2, 10:657, 1972.
30. R De Jaeger, D Lecacheux, P Potin. J Appl Polym Sci 39:1793, 1990.
31. TH Mourey, SM Miller, WT Ferrar, TR Molaire. Macromol 22:4286, 1989.
32. WT Ferrar, AS Marshall, EC Flood, KE Goppert, DY Myers. Polm Prepr (Am Chem Soc, Div Polym Chem) 28(1):444, 1987.
33. GL Hagnauer, BR LaLiberte. J Polym Sci, Polym Phys Ed 14:367, 1976.
34. M Zimbo, LM Skewes, AN Theodore. J Appl Polym Sci 41:835, 1990.
35. AH Dekmezian, T Morioka. Anal Chem 61:458, 1989.
36. KQ Wang, SY Zhang, J Xu, Y Li. J Liq Chromatogr 5:1899, 1982.
37. A De Chirico, S Arrighetti, M Bruzzone. Polymer 22:529, 1981.
38. BJR Scholtens, TL Welzen. Macromol Chem Phys 182:269, 1981.
39. B Haider, A Vidal, H Balard, JB Donnet. J Appl Polym Sci 29:4309, 1984.
40. V Grinshpun, A Rudin. J Appl Polym Sci 32:4303, 1986.
41. WW Yau, SW Rementer. J Liq Chromatogr 13(4):627, 1990.
42. NS Davidson, LJ Fetters, WG Funk, WW Graessley, N Hadjichristidis. Macromol 21:112, 1988.
43. PN Chaturcedi, CK Patel. J Polym Sci Polym Phys 23:1255, 1985.
44. I Descheres, O Paisse, JN Colonna-Ceccaldi, QT Pham. Macromol Chem 188:583, 1987.
45. DJ Keller, EG Kolycheck. J Liq Chromatogr 13(10):2035, 1990.
46. K Murakami, H Oikawa, T Nagai. Nichon Reoroji Gakkaishi 17:77, 1989.

© 2004 by Marcel Dekker, Inc.

47. G Kaszas, JE Puskas, JP Kennedy. J Appl Polym Sci 39:119, 1990.
48. N Asada, H Hosozawa, A Toyoda, H Sato. Rubber Chem Technol 63(2):181, 1990.
49. Y Wang, Y Peng. Sepu (China) 7(6):391, 1989.
50. A Gadkari, JP Kennedy. J Appl Polym Sci, Appl Polym Symp 44:19, 1989.
51. G Marot, J Lesec. J Liq Chromatogr 11:3305, 1988.
52. G Kaszas, J Puskas, JP Kennedy. Makromol Chem, Macromol Symp 13/14:473, 1988.
53. Y Tanaka, H Sato, J Adachi. Rubber Chem Technol 60:25, 1987.
54. T Dumelow, SR Holding, LJ Maisey, JV Dawkins. Polymer 27:1170, 1986.
55. K Taymaz. J Liq Chromatogr 9(15):3347, 1986.
56. S Kohjiya, S Ohta, S Yamashita. Polym Bull 5:463, 1981.
57. H Kazama, M Hoshi, H Nakajima, D Horak, Y Tezuka, K Imai. Polymer 31:2207, 1990.
58. PJA Brandt, CLS Elsbernd, N Patel, G York, JE McGrath. Polymer 31:180, 1990.
59. JR Runyon, DE Barnes, JF Rudd, LH Tung. J Appl Polym Sci 13:2359, 1969.
60. A Draxler. In: AK Bhowmick, HL Stephens, eds. Handbook of Elastomers. New York: Marcel Dekker, 1988, p. 665.
61. KNG Fuller. In: AD Roberts, ed. Rheology of Raw Rubber in Natural Rubber Science and Technology. Oxford, New York, 1988, Ch. 5.
62. DC Blackley. Synthetic Rubbers, Their Chemistry and Technology. Oxford: Elsevier Applied Science, 1983.
63. Z Grubisic, P Rempp, H Benoit. J Polym Sci, Part B 5:753, 1967.
64. FW Billmeyer, Jr. J Paint Technol 41:209, 1969.
65. S Mori. In: BJ Hunt, SR Holding, eds. Size Exclusion Chromatography. Glasgow and London: Blackie, 1989, p. 100.
66. JF Johnson. In: JI Kroschwitz, ed. Encyclopedia of Polymer and Engineering. Vol. 3. New York: Wiley, 1985, p. 520.
67. T Homma *et al.* Nippon Gomu Kyokaishi 41:242, 1968.
68. DR Lloyd, TC Ward, HP Schreiber, eds. Inverse Gas Chromatography, ACS Symposium Series 391, Washington, D.C., 1989.
69. J Capillon, R Audebert, C Quivoron. Polymer 26:575, 1985.
70. BJ Hunt, SR Holding, eds. Size Exclusion Chromatography. Glasgow and London: Blackie, 1989, p. 277.
71. BJ Hunt, SR Holding, eds. Size Exclusion Chromatography. Glasgow: Blackie, 1989, p. 275.
72. BJ Hunt, SR Holding, eds. Size Exclusion Chromatography. Glasgow: Blackie, 1989, p. 279.

© 2004 by Marcel Dekker, Inc.

8
Size Exclusion Chromatography of Asphalts

Richard R. Davison, Charles J. Glover, Barry L. Burr, and Jerry A. Bullin
Texas A&M University
College Station, Texas, U.S.A.

1 INTRODUCTION

Early researchers in the application of size exclusion chromatography (SEC) to asphalt (1–7) noted that size exclusion chromatography (SEC) [also called gel permeation chromatography (GPC)] was very sensitive to differences in asphalts and to changes in composition. This was exploited by Adams and Holmgreen (8) to show differences between various asphalts and between asphalts from the same supplier at different locations. Glover *et al.* (9,10) used SEC to show how asphalts from a number of suppliers changed with the seasons. It has also been used to compare fractions produced by preparative SEC and other methods (9,11–24).

SEC can be quite sensitive to contamination by material of low molecular weight or narrow molecular weight distribution. This was used by Burr *et al.* (25) to prove incomplete solvent removal by standard American Society for Testing and Materials (ASTM) extraction and recovery procedures.

Bynum and Traxler (4) were the first to use SEC to study road aging. SEC is very sensitive to the changes that occur when an asphalt hardens. Minshull (5) and

© 2004 by Marcel Dekker, Inc.

Haley (26) showed that the large molecular size material increased greatly following air blowing. A series of studies on Texas test sections (8,9,27,28) showed a progressive growth in large molecular size (LMS) material. This material is usually defined as that comprising about the first third of the chromatogram elution time. Similar results are reported for oven aging (12,29–32) and for aging during the hot-mix operation (30,33,34). Asphalts also change when in contact with solvents, and this is detected by an increase in the LMS region (35).

A procedure has been developed (36) using preparative chromatography with toluene as the carrier and a florescence detector (36–40). The normal florescence of aromatics under UV radiation is apparently quenched by association. The nonradiating fraction I is largely LMS material. The remaining fraction II is also sometimes further fractionated. Jennings *et al.* (18) ran SECs on fraction I, II, and whole asphalts. Values of LMS calculated from fraction I and II were usually less than the whole asphalt measured values. McCaffrey (41) has described an "ultra-rapid" procedure using one column and a high flow rate of a 95:5 chloroform:methanol carrier solvent. Three distinct peaks are obtained, which are correlated with both physical and chemical properties.

Many tests have been proposed for simulating hot mix and road aging, and SEC may be used to compare laboratory and field aging (33,42). The effectiveness of recycling agents in restoring aged asphalt for reuse has also been studied by comparing the SEC chromatograms of the old, new, and restored asphalts (14,42–45).

Since Bynum and Traxler (4) there have been a number of attempts to relate road performance to SEC results. Plummer and Zimmerman (46) studied test sections in Michigan and Indiana and found that a greater LMS percentage seemed to correlate with cracking. Jennings and co-workers (14,42,47–51) conducted a major study relating cracking of roads to higher percentage LMS, primarily in Montana but also in other regions of the United States. Both Jennings and Pribanic (50) and Hattingh (29) showed that low-percentage LMS can result in rutting.

There have been many attempts to correlate asphalt properties to the shape of the SEC chromatograph, including both aged and unaged material. Beazley *et al.* (52) used SEC and nuclear magnetic resonance to estimate asphalt yield and viscosity from crude oil. Woods *et al.* (53) used SEC fractions to study the differences in maltenes from tar sand bitumens. The most common procedure has been to divide the chromatograph into segments, ranging in number from 3 to 12, and correlating properties to the relative size of these segments (10,54–65). When the chromatograph is divided into many segments, a reduced set is often chosen on the basis of statistical significance. Some of these studies include modified material (32,65,66). The properties of compacted mixes were correlated by Price and Burati (66) to the SEC chromatograph of the base asphalt.

The measurement of molecular weight by SEC, as with other methods, is greatly complicated by the tendency of the more polar asphalt constituents to

© 2004 by Marcel Dekker, Inc.

associate. Girdler (67) and Speight *et al.* (68) report large ranges of molecular weights measured by various methods. SEC molecular weight curves must be calibrated by some external standard, such as against vapor pressure osmometry (VPO) measurements of preparative SEC fractions of the asphalt (1,12,69–76). The results are thus limited by the accuracy of the standard, and these methods are very dependent on the solvent and concentration. Markedly different retention times for molecules of different structure but the same molecular weight are a major complicating factor (9,12,68,69,71–73), and data of Bergman and Duffy (77) with model compounds indicate that this is very solvent dependent. A number of researchers have used intrinsic viscosity data in an attempt to eliminate the effect of structurally dependent elution volumes (12,69,71,73,78), but it has been demonstrated (79) that the assumption of a constant relation between molecular volumes and elution volumes does not apply to the differing structural types in asphalt. Domin *et al.* (80) compared SEC measured MWs using N-methyl pyrrolidinone to VPO and mass spectrophotometric values.

Because of the tendency of asphalts to associate and also to be adsorbed on the column (7,10,42,69,81–83), the choice of solvent is very important. Jennings *et al.* (42) reported that the relative percentage of LMS between asphalts could be reversed by using chloroform instead of tetrahydrofuran (THF). Altgelt and Gouw (81) report that 5% methanol in chloroform or benzene is an excellent solvent. Bishara and McReynolds (84) added 5% pyridine to THF to reduce adsorption of polar materials. Brulé (12) compared several solvents: the greater the polarity, the smaller the LMS region. Although increasing polarity tends to decrease the percentage LMS, this is not automatic and depends on the specific interactions. Jennings *et al.* (85) showed 5% methanol (MeOH) in THF increasing the percentage of LMS. Done and Reid (82) and Donaldson *et al.* (86) compared THF and toluene. Higher concentrations, higher flow rates, as well as a poorer solvent can cause an increase in the LMS region (12,41,83,87,88). A lengthy residence time of asphalt in a solvent also causes a growth in the LMS region (12,35,89).

There is an increasing use of polymers in asphalt and these are easily detected by SEC. One of the most common uses is to detect the changes in polymer molecular size as it is mixed with asphalt at high temperature (66,90,91). SEC is also used to detect the changes in polymer molecular size as oxidation occurs (92–96).

2 ASPHALT CHEMISTRY

Asphalt is probably the most complex material routinely studied by SEC. Asphalt is the residual left when practically everything that can be recovered from crude oil by high-vacuum, high-temperature distillation has been vaporized. Alternatively, the residuum may be propane extracted to remove even more material and the

© 2004 by Marcel Dekker, Inc.

resulting very hard asphalt may be cut back with lighter fractions. Regardless of how it is produced, the result is a sticky, near solid containing a vast array of high-molecular-weight compounds varying from paraffins to highly condensed aromatics. Included within these compounds, especially in the more condensed material, are the so-called heteroatoms, O, N, S, and metals, especially Ni and V.

To simplify asphalt analysis, a common practice is to fractionate the material to divide it into groupings of simpler constitution. A large number of methods have been proposed, but most are based on either selective solvent extraction or chromatographic separation or, frequently, a combination of solvent precipitation and chromatographic separation.

One of the most used procedures, an ASTM standard, D4124, was developed by Corbett (97) and separates asphalt into four fractions. Asphaltenes are precipitated by heptane, and the remaining solution is divided into saturates, naphthene aromatics, and polar aromatics by a series of successively more polar solvents on an alumina column. Similar procedures produce fractions variously known as asphaltenes, resins, and oils or saturates, aromatics, resins, and asphaltenes, for example. Although similar, the methods are not identical and produce fractions that overlap those of other methods.

Corbett (97,98) used a densometric procedure coupled with molecular weight determination by VPO at 37°C to determine the structure of his fractions, as shown in Table 1. Asphaltenes could not be characterized completely because of the difficulties in molecular weight determination as a result of asphaltene molecular association.

Table 2 (99) shows additional structural data estimated for the fractions. These results are all dependent on the composition of the source crude oil, particularly heteroatom content and metals. Both Ni and V are found primarily in the heptane-precipitated asphaltenes and are evenly distributed without regard to molecular size. They seem to be interchangeable in structure in that in fractions of a given asphalt the ratio of V to Ni is constant over wide ranges of composition. These metals often exist in porphyrin structures and have been implicated in higher rates of asphalt oxidation.

Heteroatoms are important because of an inordinate contribution to properties. Large increases in asphalt hardening occur with the uptake of only 1 wt% oxygen. Petersen (100,101) has carried out extensive work on heteroatom analysis. A typical analysis is shown in Table 3 (101). When asphalt oxidizes, the principle increase is in ketones and sulfoxides. Carboxylic acids and anhydrides tend to concentrate at the aggregate surface in asphalt concrete and may produce sensitivity to water damage.

Studies have shown that increases in asphalt viscosity with oxidation can be correlated with increases in carbonyl formation (28) which has been shown to be proportional to oxygen uptake (102). Almost certainly this hardening results from hydrogen bonding between heteroatom groups in asphaltene molecules and also

© 2004 by Marcel Dekker, Inc.

Table 1 Fractions Obtained Using Corbett Analysis

Group	Wt% range	Average MW	Fraction aromatic	Rings/mole		Description
				Naphthene	Aromatic	
Saturates	5–15	650	0	3	0	Pure paraffins + pure naphthenes + mixed paraffin–naphthenes
Naphthene aromatics	30–45	725	0.25	3.5	2.6	Mixed paraffin–naphthene–aromatics + sulfur-containing compounds
Polar aromatics	30–45	1150	0.42	3.6	7.4	Mixed paraffin–naphthene–aromatics in multi-ring structures + sulfur, oxygen, nitrogen-containing compounds
Asphaltenes	5–20	3500	0.5	—	—	Mixed paraffin–naphthene–aromatics in polycyclic structures + sulfur, oxygen, nitrogen-containing compounds

Source: Ref. 97.

© 2004 by Marcel Dekker, Inc.

Table 2 Elemental Characterization of Corbett Fractions

Element	Average number of atoms per molecule in			
	Saturates	Naphthene aromatics	Polar aromatics	Asphaltenes
Carbon				
Paraffin chain	31	21	24	85
Naphthene ring	14	17	18	29
Aromatic ring	0	13	25	115
Hydrogen	85	94	105	350
Sulfur	0	0.5	1	4
Nitrogen	0	0	1	3
Oxygen	0	0	1	2.5
Average molecular weight	625	730	970	3400

Source: Ref. 99.

between polar aromatics, which then may become asphaltenes (23,103–106). This association strongly impacts attempts to measure molecular size by SEC or colligative properties.

There is considerable evidence that, contrary to the data in Tables 1 and 2 and much published data, the single asphaltene molecule is actually no larger than those of other fractions. Figure 1 shows an SEC chromatogram of a badly oxidized

Table 3 Distribution of Functional Groups in Fractions from Corbett Separation[a]

	Concentration in fraction (M)				
	Whole asphalt	Saturates	Naphthene aromatics	Polar aromatics	Asphaltenes
Ketones	0	0	0	0.11	Trace
Carboxylic acids	0.027	0	0	0	0.034
Anhydrides	0	0	0	Trace	Trace
2-Quinolone types	0.021	0	0	0.023	0.046
Sulfoxides	0.019	0	Trace	0.12	0.09
Pyrrolics	0.17	0	0	0.21	0.23
Phenolics	0.035	0	0	0.055	0.075

[a]Yield of fractions based on whole asphalt were saturates, 9.9%; naphthene aromatics, 25.3%; polar aromatics, 38.1%; asphaltenes, 21.6% loss (which should be added to polar aromatics), 5.1%.
Source: Ref. 101.

© 2004 by Marcel Dekker, Inc.

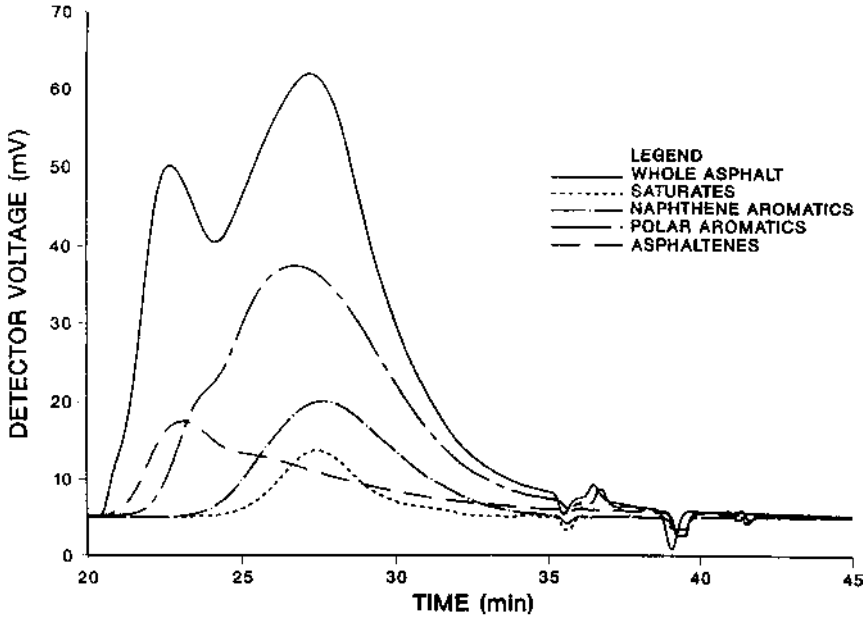

Figure 1 SEC analyses of an aged asphalt and its Corbett fractions (500/50 Å, 60 cm PLgel, THF at 1 mL/min, 100 μL, RI detector). The whole asphalt is analysed using a 7 wt% solution; the Corbett fractions are adjusted according to their weight fraction.

asphalt from a road core along with chromatograms of its Corbett fractions. It is seen that the saturates appear slightly larger than the naphthene aromatics. There is a shift to larger size with the polar aromatic fractions and a greater shift with asphaltenes, but it is these latter fractions that tend to associate, thereby giving a false impression of molecular size.

Boduszynski *et al.* (107,108), using field ionization mass spectroscopy (FIMS), obtained average molecular weights from 873 to 1231 for the Corbett fractions, with asphaltenes actually the smallest molecules. The VPO value for asphaltenes was over 4000. The values obtained for polar aromatics was 1020 by FIMS and over 1400 by VPO. Results for naphthene aromatics and saturates were quite close by the two methods. It should be realized that the designation of asphaltenes is arbitrary, depending on the precipitating solvent (109,110). Propane precipitates most of the polar aromatics, and pentane asphaltenes can be nearly twice the heptane asphaltenes.

Many of the properties of asphalt are determined by the variety of chemical types and their divergent properties. The asphaltenes and saturates are immiscible. Mixtures of asphaltenes and naphthene aromatics are highly non-Newtonian at

© 2004 by Marcel Dekker, Inc.

100°F, but polar aromatics and asphaltene mixtures are Newtonian (99). It has long been proposed (111,112) that asphalt exists as asphaltene micelles or clusters solubilized by polar aromatics.

Yen and associates (113–116), based on x-ray analysis, proposed that asphaltenes and resins (polar aromatics) existed as flat, condensed aromatic disks to which alkyl and naphthenic side chains were attached, forming a unit sheet. Through π bonding between aromatic sheets, and no doubt hydrogen bonding between heteroatom groups, the unit sheets arrange themselves in stacks, forming a particle or cluster. Unless two sheets are connected by a side chain, the unit sheet weight is approximately the molecular weight. In asphalt, polar aromatic sheets can combine in a stack with asphaltene sheets and, being less condensed, help to solubilize the asphaltenes in the remaining, less miscible fractions. When an asphalt is dissolved in a solvent, the polar aromatics may be extracted from the stack, causing the depleted asphaltene particles to clump, increasing apparent molecular weight and perhaps causing precipitation. Although Yen's work involves a number of structural assumptions, his unit sheet weights are similar to those obtained by FIMS and, like FIMS, yield higher molecular weights for resins than for asphaltenes.

Others (70,71,117–120), using nuclear magnetic resonance and elemental analysis with certain structural assumptions, have obtained very similar results for unit sheet weights. Several researchers have applied this procedure to asphalt fractions produced by preparative SEC. The unit sheet weights are always less than SEC- or VPO-determined molecular weights. Kiet *et al.* (71) found nearly constant sheet weights for his large molecular size fractions, which exhibited an over four-fold change in VPO molecular weights that he attributed to an increasing number of sheets per stack in the heavier fractions. Haley (26) hardened preparative SEC fractions by air blowing: VPO molecular weights showed a considerable increase. The unit sheet weights increased for the heavier fractions, reflecting an increase in aromaticity and some crosslinking, but considerably less than the VPO molecular weights. There are a number of studies indicating that these asphaltene conglomerates exist in disclike structures. This is discussed in some detail by Baltus (121) and Lin *et al.* (122). Ravey *et al.* (123) separated asphaltenes into a number of fractions by SEC and used small angle neutron scattering to obtain particle dimensions. In dilute THF the dimensions were roughly 13 nm diameter and 0.5 nm thickness. The diameter increased in polar solvents. Lin *et al.* (122) developed a suspension viscosity model for asphaltenes in asphalt which predicted a disc-shaped particle with an aspect ratio that varied from about 18 to 24. Acevedo (124) predicted a disc shape for octylated asphaltenes based on viscosity measurements and SEC data.

Domke *et al.* (125,126) showed that oxidation kinetics of asphalt was affected by oxygen diffusion into the asphaltene particle and its associated material. The results were also affected by the nature of the solvating material.

© 2004 by Marcel Dekker, Inc.

Apparently more polar compounds are shielded by less polar and less reactive material (127). It is clear that the tendency of both asphaltenes and polar aromatics to associate, which is affected by other asphalt constituents and the polarity of carrier solvents, has a number of implications for SEC analysis.

3 APPLICATIONS OF SEC TO ASPHALTS

3.1 Asphalt Fingerprinting, Compositional Analysis, and Aging

Asphalt from each source crude oil has its own characteristic chromatogram that usually changes only slightly with grade. For this reason SEC is a very effective tool for detecting changes in asphalt as a result of processing changes, crude source, or contamination. Glover *et al.* (9) ran monthly SEC chromatograms on 11 asphalts for a period of a year. Each asphalt exhibited its characteristic shape, but some of these showed considerable seasonal change, probably reflecting processing changes. It must be emphasized that characterizations of this kind require that all SEC parameters be held constant. This is a major disadvantage, making comparisons difficult between laboratories and even over time. An asphalt standard should be run periodically to confirm constant operating parameters. Garrick (61,63) divided asphalts into groups depending on the shape of the SEC profile. This was based on width, location, and height of the peak maximum, and so on, and showed that properties such as temperature susceptibility and viscosity ratio before and after thin film oven test (TFOT) oxidation tended to fall into these groups.

Low-molecular-weight contaminants, or any material having a narrow molecular weight range, produce a peak on the chromatogram and are easily detected, often at very low concentrations. Before asphalts from roads or hot-mix plants can be studied chemically, they must be separated from the aggregate. There are standard ASTM procedures for extracting the asphalt and then removing the extracting solvent. Burr *et al.* (25) showed that the standard procedures often left sufficient solvent in the asphalts to affect properties significantly. The literature is replete with work that has been marred in this manner. By using SEC, the solvent can be detected at low concentrations, and Burr *et al.* developed methods to assure complete solvent removal. It is prudent to use SEC routinely to assure complete solvent removal from recovered asphalt.

SEC analysis can be used very effectively in combination with Corbett separation, solvent or supercritical solvent fractionation, and other fractionation procedures for the purpose of understanding asphalt composition and aging. Figure 2 shows chromatograms for an asphalt cut into a 60% top fraction and a 40% bottom fraction by supercritical pentane (15). The top 60% was fractionated into four fractions by supercritical pentane (Fig. 3), and the bottom

© 2004 by Marcel Dekker, Inc.

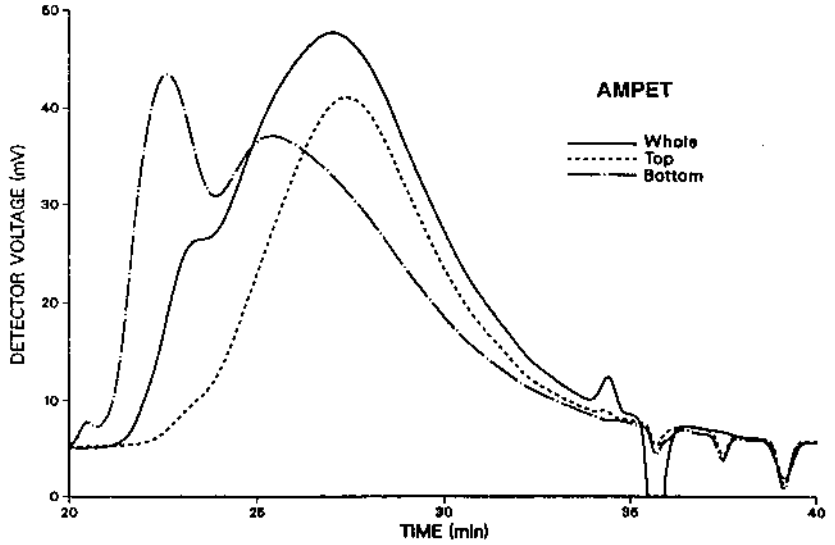

Figure 2 SEC analyses of an asphalt and its light (top, 60%) and heavy (bottom, 40%) supercritically separated fractions (500/50 Å, 60 cm PLgel, THF at 1 mL/min, 100 μL of 5 wt% solution, RI detector).

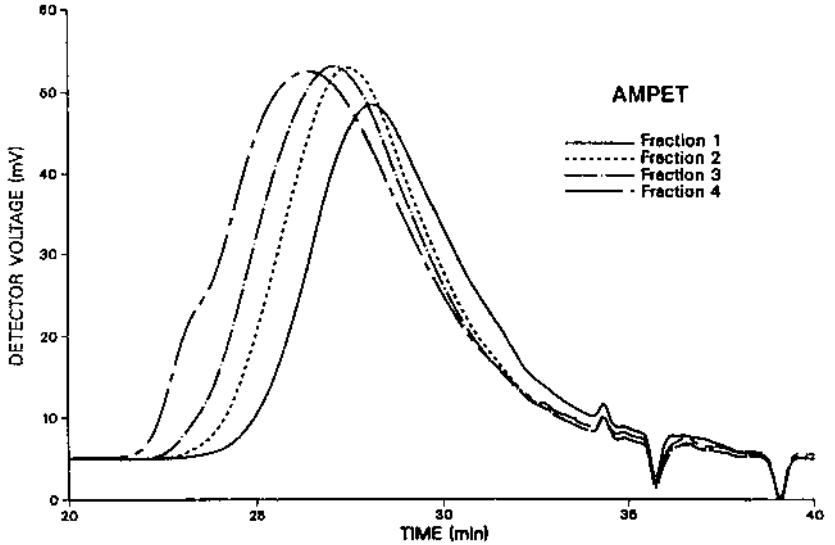

Figure 3 SEC analyses of an asphalt's supercritical fractions 1–4 (500/50 Å, 60 cm PLgel, THF at 1 mL/min, 100 μL of 5 wt% solution, RI detector).

© 2004 by Marcel Dekker, Inc.

40% was fractionated into four fractions by pentane and pentane–cyclohexane mixtures under ambient conditions. The slight hump in fraction 4 probably results from the small amount of asphaltenes in this fraction. Figure 4 shows saturates and Fig. 5 polar aromatics from the supercritically separated top fractions. The saturate curves are typical, being symmetrical and having relatively little variation in molecular size from one fraction to the next. The polar aromatics, in contrast, grow progressively higher in molecular size in heavier fractions and show signs of considerable association in the higher molecular size fractions by the growing hump in the LMS region. Asphaltenes (Fig. 6) from fraction 4, separated from the top material, are markedly lower in size than the material from the fractions of the bottom 40%.

As asphalts age, the characteristic change to the SEC chromatogram is growth in the LMS region, which sometimes changes shape in the process. Figure 7 shows tank asphalts and cores for a single asphalt used in test sections at three Texas locations. The difference in the cores is primarily the percentage of air voids in the finished concrete. In 1987, the air voids at Lufkin were 1.8% and the 60°C viscosity was 5400 P (1 P = 1 dPa · s). At Dumas it was 8.5% and 55,000 P, and at Dickens it was 11% and 376,000 P. These differences are clearly shown in the chromatograms.

This percentage LMS growth is directly related to oxidation but may be highly asphalt dependent. Figure 8 shows the change in percentage LMS with

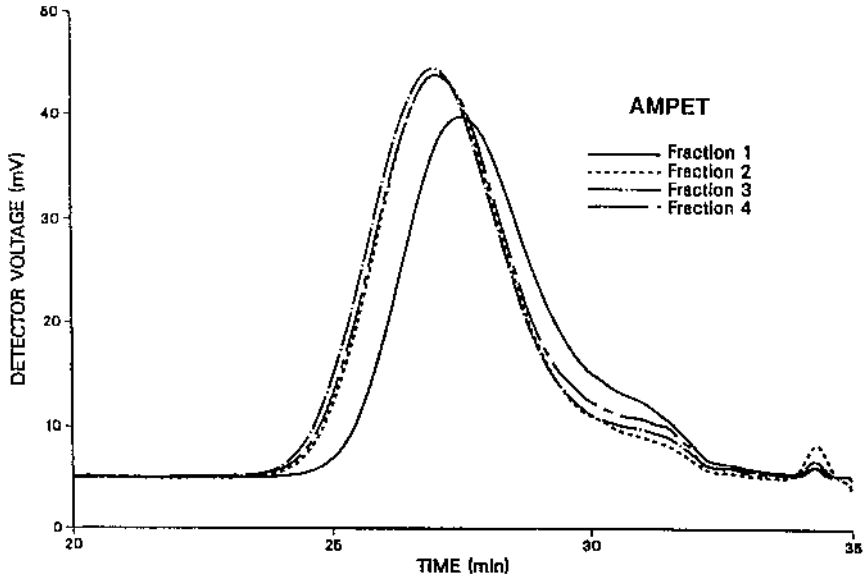

Figure 4 SEC analyses of the saturates from an asphalt's supercritical fractions 1–4 (500/50 Å, 60 cm PLgel, THF at 1 mL/min, 100 μL of 5 wt% solution, RI detector).

© 2004 by Marcel Dekker, Inc.

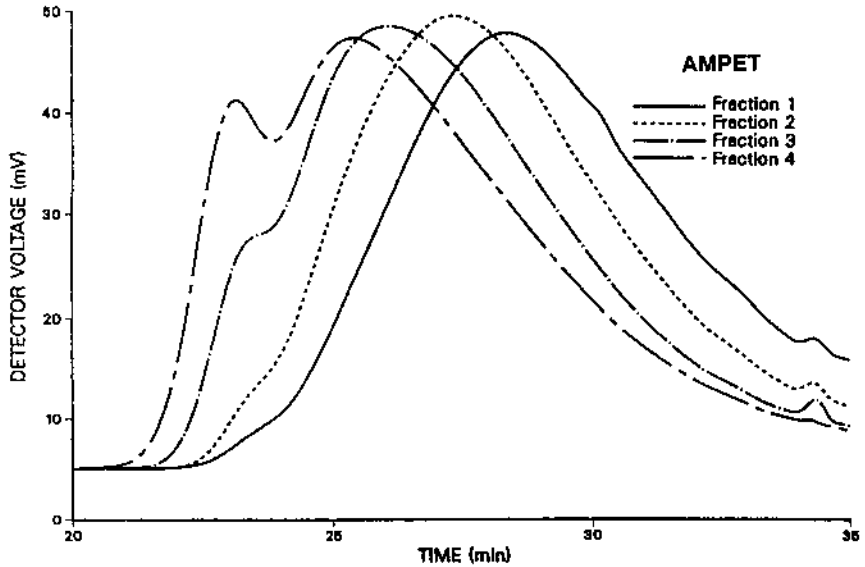

Figure 5 SEC analyses of the polar aromatics from an asphalt's supercritical fractions 1–4 (500/50 Å, 60 cm PLgel, THF at 1 mL/min, 100 μL of 5 wt% solution, RI detector).

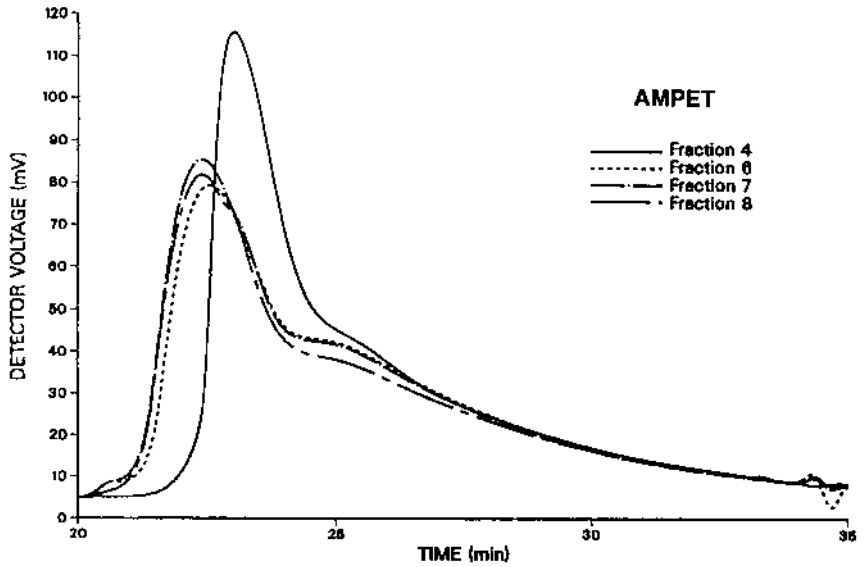

Figure 6 SEC analyses of the asphaltenes from an asphalt's fractions 4 and 6–8 (500/50 Å, 60 cm PLgel, THF at 1 mL/min, 100 μL of 5 wt% solution, RI detector).

© 2004 by Marcel Dekker, Inc.

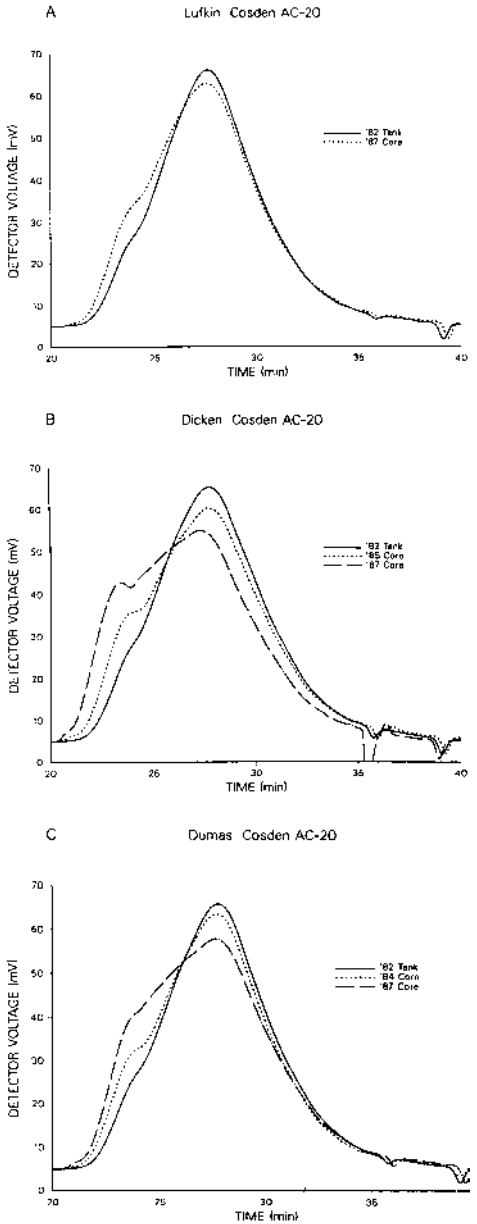

Figure 7 SEC analyses of an unaged asphalt and its aged binder recovered from highway test pavements at three locations A, B, C (500/50 Å, 60 cm PLgel, THF at 1 mL/min, 100 μL of 7 wt% solution, RI detector).

© 2004 by Marcel Dekker, Inc.

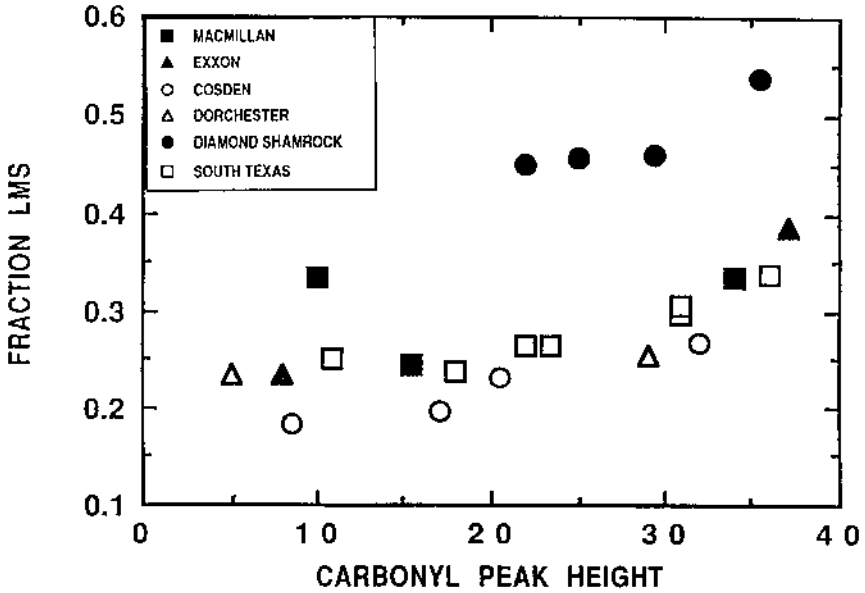

Figure 8 SEC LMS fraction vs. Fourier transform infrared spectroscopy carbonyl peak height for asphalts recovered from aged pavement cores (500/50 Å, 60 cm PLgel, THF at 1 mL/min, 100 μL of 7 wt% solution, RI detector).

growth in the carbonyl peak, an excellent measure of oxidation effects. The open circles in this figure include the data in Fig. 7 and show a steady growth in the LMS region with carbonyl increase, but it is seen that with some asphalts, the growth in percentage LMS is small until higher levels of oxidation are reached.

Several tests, including SEC, were used to compare two standard oven-aging tests (the thin-film oven test, TFOT, ASTM D1754, and the rolling thin-film oven test, RTFOT, ASTM D2872) and to determine their accuracy in simulating the changes that occur in the hot-mix plant (33). The tests were also performed at extended times, and these data are designated ETFOT and ERTFOT. Asphalts and hot-mix were taken from nine plants using six different suppliers and with two grades from one supplier. The asphalts were aged in the oven tests and compared using six parameters. Figure 9 shows the agreement in the percentage of LMS, and similar agreement was obtained for the other parameters, confirming that the oven tests are interchangeable. The oven tests were then compared to asphalts from the extracted hot mixes. Figure 10 shows the disagreement between the oven tests and the recovered hot-mix asphalts, disagreements also confirmed by the other parameters. The tests were designed to reproduce the 60°C viscosity and do this reasonably well,

© 2004 by Marcel Dekker, Inc.

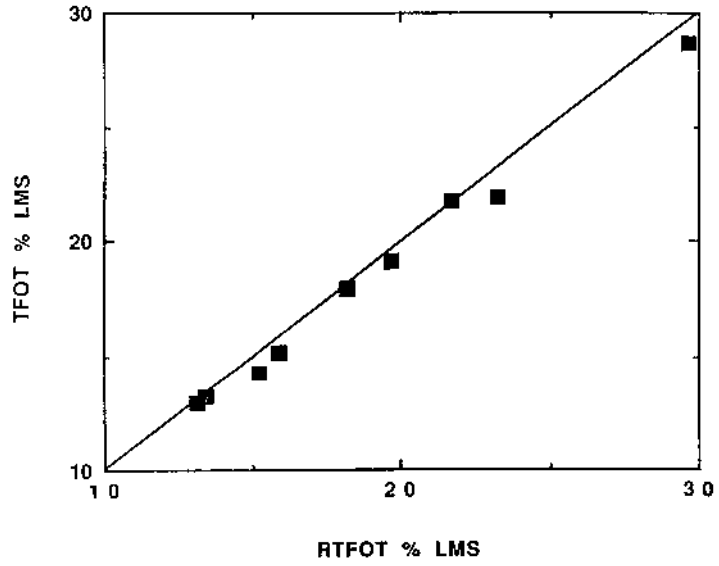

Figure 9 Comparison of percentage LMS for TFOT- and RTFOT-aged asphalts (500/50 Å, 60 cm PLgel, THF at 1 mL/min, 100 μL of 7 wt% solution, RI detector).

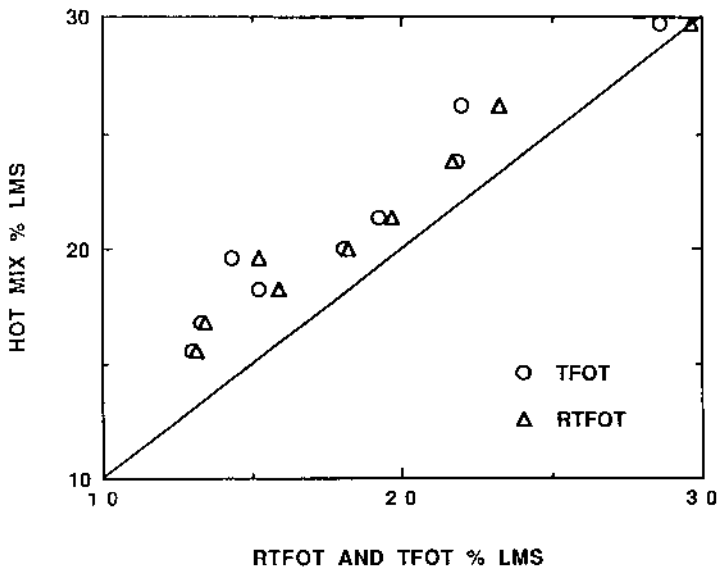

Figure 10 Comparison of percentage LMS for hot-mix and oven-aged asphalts (500/50 Å, 60 cm PLgel, THF at 1 mL/min, 100 μL of 7 wt% solution, RI detector).

© 2004 by Marcel Dekker, Inc.

but obviously not by the same mechanisms. Asphalts oxidized to the same viscosity at 100 and 103°C also show differences in the chromatographs (128).

Asphalts also tend to age on contact with solvents, and this is manifested by both viscosity and LMS increases (35). Simply dissolving an asphalt in a good solvent and recovering it immediately produces about a 10% viscosity increase; 2 days contact at room temperature causes a 50% or greater increase in viscosity. If samples are made and run immediately or within hours at room temperature, the effect on the SEC chromatogram is negligible, but days or even hours at a higher temperature can produce significant growth in the LMS region.

The Corbett analysis of an asphalt is also altered by aging. In Fig. 11 chromatograms are shown of Corbett fractions of a tank asphalt and a 1984 core from one of the Texas test sections. As expected, there is no change in the saturates. There is a decrease in quantity but not in elution time for naphthene aromatics. The polar aromatics change little in quantity as material is gained from the naphthene aromatic fraction and lost to the asphaltenes, which increase in quantity. Despite this considerable shifting of material, the elution time is little changed. The large tailing effect with asphaltenes is probably caused by column adsorption.

The change in molecular size of Corbett fractions with oxidation was studied extensively by Liu *et al.* (22,129) using SEC. They found that while naphthene aromatics oxidize to polar aromatics, they subsequently converted to asphaltenes only after extensive oxidation. Newly produced polar aromatics and asphaltenes produced by oxidation of naphthene and polar aromatics respectively tend to be smaller than the original material. Large-sized polar aromatics and naphthene aromatics are converted to asphaltenes and polar aromatics more rapidly than smaller sized material.

Huang and Bertholf (20) oxidized previously separated Corbett fractions using UV irradiation. SEC analysis before and after oxidation showed an increase in molecular size of all fractions. The saturate fractions showed a striking increase, which is significant as saturates do not normally react with oxygen.

3.2 Use of SEC to Predict Pavement Performance

Plummer and Zimmerman (46) studied roads in Michigan and Indiana and found that an increase in the LMS region correlated with increased cracking. Hattingh (29) found that in the hot South African climate, roads with a low asphaltene content and a small LMS region were subject to bleeding. By far the most extensive effort of this kind is that of Jennings and co-workers (42,47–51), conducted primarily in Montana but extended nationwide. The principal road problem addressed was that of cracking.

A total of 39 roads in Montana constructed with asphalt from four refineries were cored, extracted, and analysed by SEC (42,48). The condition of the roads

© 2004 by Marcel Dekker, Inc.

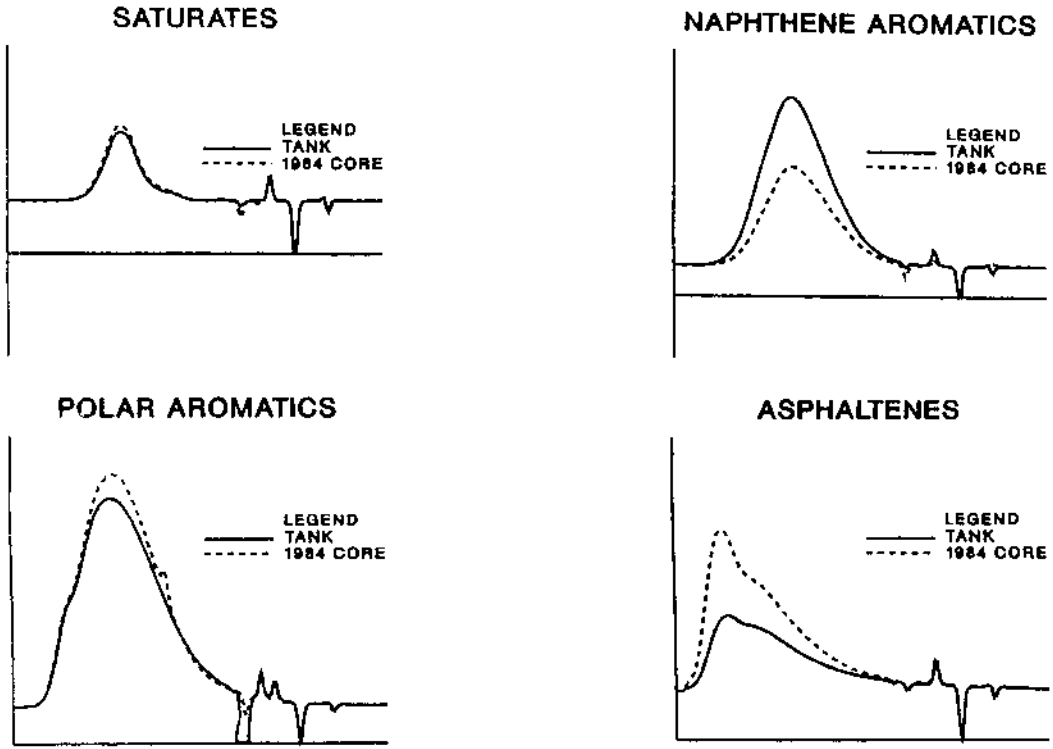

Figure 11 Comparison of SEC chromatograms of Corbett fractions for an unaged and aged (recovered pavement binder) asphalt (500/50 Å, 60 cm PLgel, THF at 1 mL/min, 100 μL, RI detector). The solution concentrations are adjusted according to each Corbett fraction's weight fraction in the asphalt.

© 2004 by Marcel Dekker, Inc.

was noted and categorized as excellent, good, poor, or bad, based on both the age of the pavement and the extent of cracking. A 19-year-old road in excellent condition was chosen as a standard. It had a low LMS region, and a high degree of correlation was found between the condition of the other roads and the similarity of their SEC chromatograms to that of this standard, particularly in the LMS region. This is clearly seen in Figs 12 and 13, in which the standard is labeled Gallatin Gateway-South. A correlation with the percentage of asphaltenes was also found, which is not surprising because the percentage of asphaltenes and percentage LMS region are strongly correlated, although not all asphalts fit. Based on these results, a range of the LMS region from 8 to 10% and an asphaltene content from 12.5 to 16.5% was recommended for Montana roads.

Jennings and Pribanic (51) expanded this study to include samples from 15 other states. The nation was divided into zones of similar climate, and the condition of roads within each zone was compared on the basis of the molecular size distribution. In general, in each zone there was a percentage of LMS above which all roads were poor or bad, and most of the good and excellent roads were those of lower percentage LMS. However, there was a very large difference between the percentage of LMS that could be tolerated in warm zones and that in very cold zones. Furthermore, there was evidence from the warm zones that too low a percentage of LMS correlated with rutting.

There were many exceptions, particularly poor and bad roads with low percentage LMS, but of course there are many factors unrelated to asphalt quality that can cause road failure. Jennings presented evidence that some asphalts failed because of poor viscosity temperature susceptibility even though they had a satisfactory percentage of LMS.

There have been objections to this approach (16), partly because of the arbitrariness of the procedure in which the percentage of LMS is very much an artifact of the SEC operating parameters. It is also thought that it is the mechanical properties that cause failure, and these do not correlate well with chemical properties, such as SEC; thus if ex post facto measurements are to be used, they may as well be the physical properties of the old asphalt. There are several studies that indicate that there is a limiting ductility below which all roads fail (130,131). It has been suggested (132) that penetration at 4°C, a good predictor of the limiting stiffness temperature, be used to predict the tendency to crack.

There are other problems in that some asphalts with a very high percentage of LMS do not fit at all; the black circles in Fig. 8 are for a good-performing asphalt of very high percentage LMS. The use of old road data is also a problem, whether for percentage LMS or physical properties. Figure 7 shows that the same asphalt can have greatly different percentages of LMS at the same age depending on nonasphalt factors. High-percentage LMS is an indication of aging without regard to what caused it. In the Texas study, the asphalts at Lufkin all had lower percentage LMS because they were not aging. The same asphalts had much higher

© 2004 by Marcel Dekker, Inc.

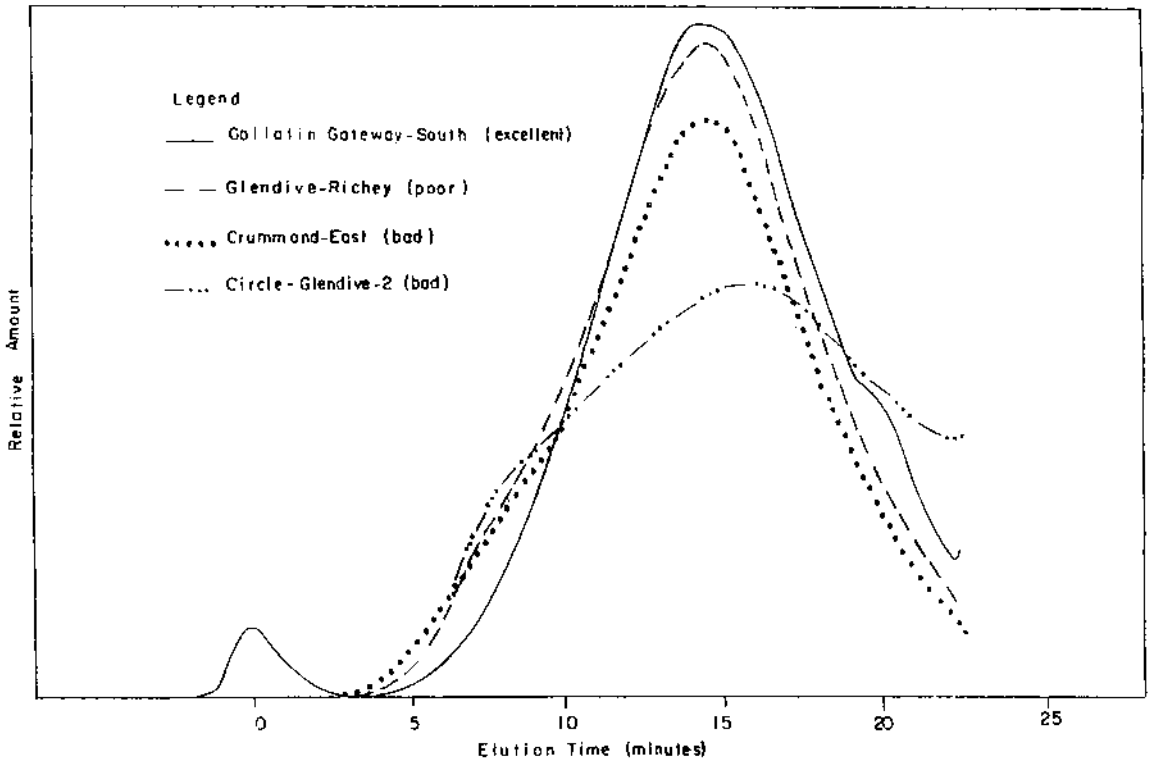

Figure 12 Comparisons of SEC chromatograms using a refractive index detector of asphalt from Montana roads for the chosen standard and three poorly or badly performing pavements. The small peak at zero time is a polystyrene standard. (From Ref. 49, p. 23.)

© 2004 by Marcel Dekker, Inc.

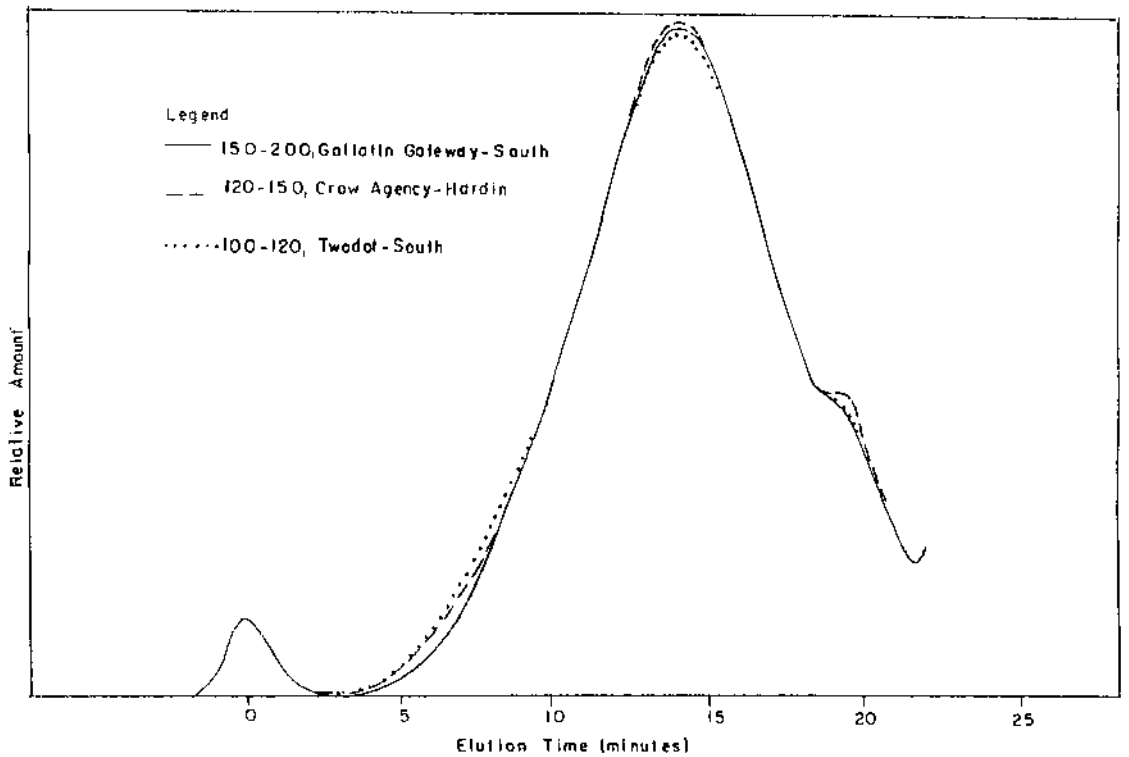

Figure 13 Comparisons of SEC chromatograms using a refractive index detector of asphalts from Montana roads for the chosen standard and two excellently or well performing pavements. The number range for each sample is the binder penetration grade, and the small peak at zero time is a polystyrene standard. (From Ref. 49, p. 29.)

© 2004 by Marcel Dekker, Inc.

percentage LMS at the other locations. Even so, Jennings' results are too impressive to be ignored.

As noted, Jennings also found some connections between rutting and a low LMS region. This is confirmed by the data in Fig. 14. Here six asphalts have been rated by users according to "tenderness" (slow setting that can result in rutting). A high score indicates tenderness. Clearly there is a correlation between the tenderness rating and the size of the LMS region.

Jennings has also done some work with asphalt recycling. In this process old road material in bad condition is stripped from the roadway, mixed with a softening agent, and relaid. Sufficient new material is generally added to restore viscosity and ductility to levels approximating those of new asphalt. This does not usually reduce the percentage of LMS to that of new asphalt. One roadway done with a commercial recycling agent having 0% LMS showed a high percentage of LMS even though the resulting mixture was quite soft. As recycling agents contain little or no asphaltenes, it has been suggested that the reduction in the LMS region could be used as a rapid method to check recycling agent content (45).

3.3 Correlating Physical Properties with SEC Results

Attempts to correlate asphalt physical properties with chemical properties have not been particularly successful. This no doubt is primarily the result of the lack of uniqueness in the chemical properties that are used. For instance, a Corbett fraction from one asphalt may have very different physical properties from those of the same fractions from another asphalt. Also, two asphalts with similar physical properties can have radically different SEC chromatograms.

Bishara *et al.* (58,59) report good correlation of viscosity temperature susceptibility and LMS to medium molecular size ratio.

The viscosity temperature susceptibility from 60 to 135°C of the Texas test section tank asphalts were correlated with percentage LMS and percentage small molecular size using both THF and toluene as carriers. The penetration index would not correlate, and later attempts to extend this to aged asphalts were not successful. Inclusion of other parameters can improve results. For instance, the viscosities of all the asphalts represented in Fig. 8, except the anomalous Diamond Shamrock (black circles), were correlated by log viscosity at $60^{\circ}\mathrm{C} = A + B(\%\mathrm{LMS})^{-0.6} + C(\mathrm{IR})^{0.9}$, $r^2 = 0.968$, in which IR is the area of the carbonyl peak (27). Infrared carbonyl area and Heithaus parameters (a measure of asphalt compatibility) were more successful in correlating other properties than percentage LMS. The carbonyl peak was one of the best parameters, and because it is strongly cross-correlated with percentage LMS, the efficiency of the latter is affected.

Because of the crudeness of representing the shape of the SEC chromatograph by three sections, Garrick and co-workers (55–57,61) divided

© 2004 by Marcel Dekker, Inc.

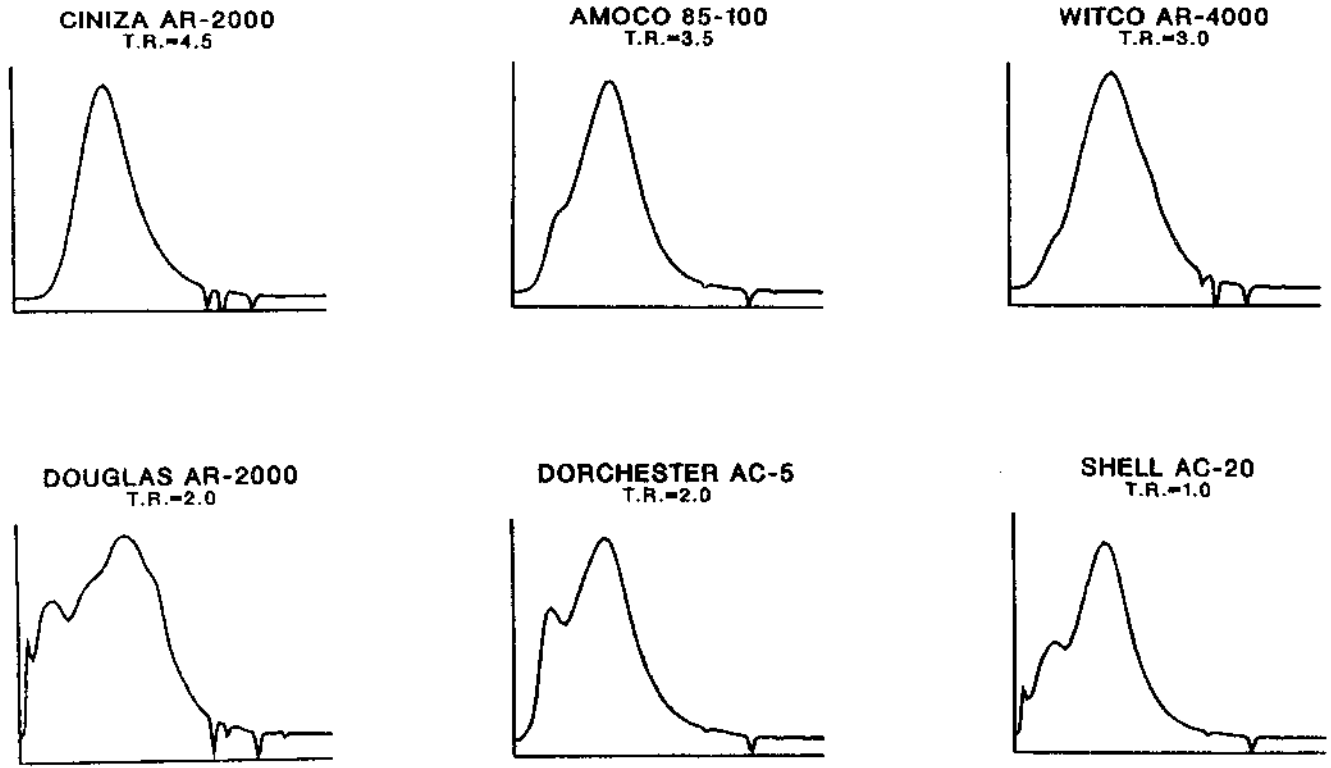

Figure 14 Comparison of SEC chromatograms to tenderness rating for six asphalts (500/50 Å, 60 cm PLgel, THF at 1 mL/min, 100 μL of 7 wt% solution, RI detector).

© 2004 by Marcel Dekker, Inc.

the total area into up to 12 sections. Correlations were then attempted using some or all of the sections as parameters. A good correlation with temperature susceptibility was obtained using three of twelve sections chosen statistically.

Kim *et al.* (133) used slices of SEC chromatographs to predict the properties of dry and water-soaked compacted asphalt, aggregate mixes, and road cores. Chromatographs of neat and solvent-extracted material were divided into ten slices and correlated to tensile strength and the resilient modulus of the mixes. Using all ten slices some very good correlations were obtained and fair correlations were obtained using three slices in the LMS region for the dry mixes. Viscosity and penetration of 27 asphalts before and after aging were correlated with ten slices and reduced sets chosen statistically (62).

Similar studies (32,65) have been reported that include modified asphalts. Correlations were attempted with a variety of properties including Superpave performance specifications (134). Up to 12 slices were included in the correlations, which improved steadily with the number of slices. Correlation was much better with equal time slices than with equal area slices, but only a few were good. The inclusion of modified asphalts, which have a large effect on the LMS region, doubtless affected the results.

3.4 Determination of Asphalt Molecular Weight Distribution

Because SEC responds directly to apparent molecular size, it appears to be a simple method for obtaining the molecular weight distribution of asphalt. However, it turns out not to be a straightforward determination for a number of reasons. The first, already discussed, is that some asphaltic fractions associate in solution. These same fractions also may tend to be adsorbed in the column. A final factor is the chemical complexity of asphalt. It is well known that the order of elution of polar and nonpolar compounds can be considerably altered by changing solvents, so it is difficult to choose calibrating compounds for such a complex mixture.

The common calibration procedure for asphalt depends on preparative SEC fractionation. Fractions thus obtained are then subjected to analytical SEC analysis to obtain mean elution values, and the fraction molecular weights are determined by an independent method, such as VPO. In general, a single plot of molecular weight vs. elution volume holds rather well for most asphalts (12), but upon aging asphalts by air blowing, a series of such curves is produced for different degrees of hardening (26).

Molecular weight–elution volume curves are actually very sensitive to composition. Champagne *et al.* (73) plotted molecular weight vs. retention time for a series of pure compounds along with polystyrenes, obtaining separate and distinct curves for the polystyrenes, long-chain asphaltenes, and nonfused polyaromatics. For fused polyaromatics scatter was obtained.

© 2004 by Marcel Dekker, Inc.

The SEC elution times are dependent on molecular hydrodynamic volume rather than molecular weight, M, as is the intrinsic viscosity, $[\eta]$. Thus the idea of a universal calibration curve is proposed (78) in which $\log[\eta]M$ is plotted vs. the elution volume. Brulé (12) shows a single curve for a number of asphalts, although it still deviates from the universal curve established for polystyrene or other polymers (71). In fact, there is considerable deviation from the universal curve for aromatic and highly condensed compounds (79,135). Lafleur and Nakagawa (136), using N-methyl pyrrolidone as the carrier solvent, investigated molecular weight vs. retention times for a variety of molecules in the 100 to 300 MW range. For polar molecules the retention was largely independent of size effects. Most impressive were results for 19 naphthalene derivatives for which retention volumes varied from 19 to 30 mL for the same MW.

There are a variety of limitations for any SEC asphalt calibration procedure. First, it is no better than the method used to establish the fraction molecular weights. This in turn is affected by the solvent, the concentration, and the temperature, with no certainty that complete dissociation has been attained. The SEC chromatogram is also affected by all these conditions plus others imposed by the column and detector.

Both Girdler (67) and Speight *et al.* (68) published data showing an enormous range of asphalt molecular weights determined by various methods. Table 4 shows a summary of some of these data in which the entries are average molecular weights for 14 asphaltenes measured by VPO. Molecular weights so determined usually decrease with decreasing concentration; elution times for large, associating material tend to increase with greater dilution. However, Moschopedis *et al.* (137) show that even if the molecular weight does not decrease with dilution in one solvent, it may still show a much lower molecular weight in another.

Noting that VPO molecular weights become relatively constant in hot nitrobenzene, Moschopedis assumed that these molecular weights corresponded to the individual asphaltene particles. Based on this assumption, Nali and Manclossi (75)

Table 4 VPO Molecular Weight Variations with Solvent Properties

Solvent	Temperature (°C)	Molecular weight
C_6H_6	37	5047
CH_2Br_2	37	4015
C_2H_5N	37	2766
$C_6H_5NO_2$	100	1900
$C_6H_5NO_2$	115	1857
$C_6H_5NO_2$	130	1798

Source: Ref. 137.

© 2004 by Marcel Dekker, Inc.

attempted to develop an SEC method that would agree with hot nitrobenzene VPO values for asphaltenes. The SEC samples were run at 25 and 40°C in THF at high dilution and several calibrations were used; the best was a mixture of vanadyl-porphyrine and polycarbonates of bisphenol A. Though several low values of molecular weight were obtained, none agreed well with the VPO values. Attempts to solve the calibrations problems have been made using octylated asphaltenes (138,139) but the molecular sizes reported for asphaltenes are still quite high. Thus, regardless of how measured, molecular weights for associating species are dependent on the parameters used in the procedure. The same is equally true for the shape of the SEC chromatograms.

Generally, the parameter set in the molecular weight determination that yields the lowest value is preferred, bearing in mind that any method based on colligative properties is very sensitive to low-molecular-weight contaminants, such as solvents. Similarly, the SEC parameters giving the largest elution volume should be preferred, except that column adsorption will increase the elution volume. Fortunately, solvents that minimize association also tend to minimize adsorption. Thus, using a very good solvent for the associating species at a low concentration may give molecular weight values approaching complete dissociation. The lowest values in Table 4, for instance, are still about twice the values obtained by Boduszynski *et al.* (107) using FIMS. Actually both VPO and SEC can be fairly reliable for the less polar components of asphalt (24,107).

The chief utility of SEC in molecular size distribution measurements is not to obtain absolute values but to measure the degree of association in asphalts of different properties and composition, particularly to note the changes that occur during aging. It is likely that the effect of solvent power on the change in apparent molecular size carries information about the internal stability of the asphalt.

4 SOLVENT AND CONCENTRATION EFFECTS

Choice of the solvent system is of great importance, particularly with a complex material like asphalt. The solvent system includes not only the solvent but also the concentration, temperature, sample size, and even the flow rate because of effects apart from the effect on column performance. All these factors interact to determine the solution characteristics on which the column must act. The key factors are the tendency of polar materials in asphalt to associate and to be adsorbed on the column. To a lesser, but still important extent, the results are also affected by interactions with the solvent that affect the apparent hydrodynamic volume. For instance, associating substances, such as asphaltenes, show much higher molecular size in a poor solvent, but a smaller size polar substance, such as a C_{12}—C_{18} normal alcohol, shows a considerably larger elution time (smaller size) in, say, toluene than in THF, even though the latter is a better solvent for alcohols.

© 2004 by Marcel Dekker, Inc.

Association is such an important characteristic of asphalts, believed by many to be an indicator of asphalt performance, that attempts have been made to use poorer solvents to emphasize this feature. Unfortunately, poorer solvents lead to column fouling and bad tailing of the adsorbed material. Figure 15 is an extracted core asphalt and its Corbett fractions run in toluene and is similar to the material in Fig. 1. In both instances the asphaltenes tail badly, but in toluene this is the predominant effect, largely displacing the larger material to much lower apparent size. Similar results have also been reported for Corbett fractions in THF (140).

All the evidence discussed previously indicates that if SEC is to be employed in molecular weight determinations the best solvent system for the associating material should be used. These include data at low concentrations and extrapolation to infinite dilution. Elevated temperatures probably help, but the choice of solvent is especially important.

There are two particularly useful schemes for choosing solvents. The oldest is the solubility parameter method of Hildebrand and Scott (141) with the modifications of Hansen and colleagues (142–144). Hildebrand's solubility

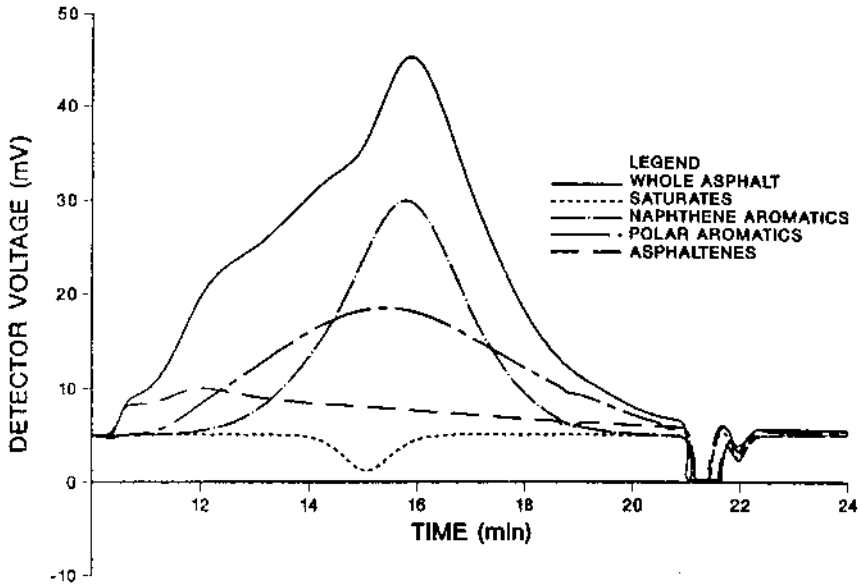

Figure 15 SEC analyses of the same samples as in Fig. 1 with a toluene carrier solvent (500 Å, 60 cm PLgel, toluene, 1 mL/min, 100 μL, RI detector). The whole asphalt is analysed using a 7 wt% solution; the Corbett fractions are adjusted according to their weight fraction.

© 2004 by Marcel Dekker, Inc.

parameter is based on the internal pressure, defined as the square root of the molar internal energy of vaporization divided by the molar volume. Strictly speaking, the formulation applies only to solutions having an ideal entropy of mixing, but in fact it is also remarkably good for a wide range of nonpolar and weakly polar mixtures. In the modification of Hansen it is assumed that the effective solubility parameter can be divided into three factors resulting from dispersion forces, polarity, and hydrogen bonding. The dispersion forces were estimated from the hydrocarbon homomorph. The polar factor was calculated from theoretical considerations based on measurements of dielectric constant, dipole moment, and refractive index. It is then assumed that the measured parameter is the sum of the dispersive, polar, and hydrogen bonding components, and the latter is calculated from the difference. The parameter has found many applications and was applied to asphalt by Hagen *et al.* (145). In this treatment the polar and hydrogen bonding components were combined and solubility correlated on a two-dimensional scale. They found that asphalt solubility could be represented as contours on this two-dimensional plot. The maximum solubility occurred in a region occupied by such solvents as THF, chloroform, and toluene. That these solvents are far from equal shows the imperfections in the system, but they also found that as the asphalts aged, the maximum solubility moved in the direction of an increasing hydrogen bonding parameter.

The significance is that the material exhibiting maximum association is also the most oxidized material, and the solvent should be chosen for this material, not the whole asphalt. Thus with increasing oxidation, a solvent of increasing hydrogen bonding should be chosen. This is seen in the data of Cipione *et al.* (146), in which the highly oxidized material, which is most tightly bound to the aggregate in aged asphalt concrete, is much better extracted if ethanol is added to the solvent.

A second useful treatment is that of Snyder (147), in which solvents are evaluated on the basis of a polarity index calculated from the solvent interaction with three test solutes: dioxane, ethanol, and nitromethane. Figure 16 (12) shows an SEC chromatogram of an asphalt for the four solvents indicated. The results show significant decrease in association at 800 Å as one goes from tetraline to benzonitrile. Although tetraline has the lowest dielectric constant and benzonitrile the highest, the order is reversed for THF (E = 7.25) and chloroform (E = 4.806). On the basis of Snyder's polarity parameter P', however, the order is THF ($P' = 4.2$), chloroform ($P' = 4.4$), and benzonitrile ($P' = 4.6$), which agrees with the 800 Å order.

As with any system, the effect of sample size depends on the response characteristics of the detector, but with asphalt this is complicated by the greater association in more concentrated solutions and the dissociation kinetics following injection. There is usually a decrease in the percentage of LMS as lower concentrations are injected.

© 2004 by Marcel Dekker, Inc.

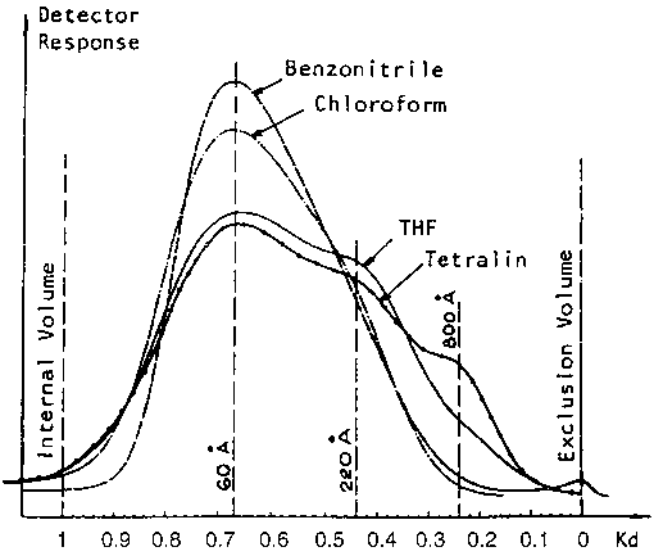

Figure 16 Comparisons of asphalt SEC chromatograms using four different carrier solvents. (From Ref. 12, p. 225.)

Flow rate has much the same effect. Brulé (12) injected the same sample size at different flow rates and found that the percentage of LMS increased with flow rate. Despite the great dilution in the carrier solvent, the dissociation rate is sufficiently slow that the results largely reflect the state in the injected solution. Thus the faster the flow, the less dissociation had occurred. McCaffrey used this effect to obtain three peaks using a flow rate of 3.5 mL/min and 95:5 chloroform:methanol (90).

Brulé also ran asphalt samples at extended intervals following preparation: 4 h and 7, 14, and 21 days. In these samples the LMS region increased with aging. This involves the phenomenon of solvent hardening that occurs, particularly in dilute solutions, in all solvents and increases rapidly with increasing temperature. Burr *et al.* (35,89) gave results for a variety of solvents and asphalts, but of particular significance is the infrared spectra for five asphalts after two days at room temperature in 15% ethanol in trichloroethylene. The viscosity of the recovered asphalts increased from 50 to 90%, and all but one of the asphalts showed significant changes in infrared spectra. The changes were different for each asphalt, however, and were not correlated with the viscosity changes. Because the exposure to solvent changes the SEC chromatograms with time, samples should generally be run the same day they are prepared.

© 2004 by Marcel Dekker, Inc.

5 MODIFIED ASPHALTS

The addition of modifiers to asphalts, polymers, or ground tire rubber has increased because of generally improved properties and the necessity of meeting more stringent specifications. The new performance grade (PG) specifications (134) require that the asphalt meet certain rheological requirements at a specified temperature. For instance, a PG 64-22 must meet the upper temperature requirement at 64°C and the lower temperature requirement at −22°C. Polymers are most often used to improve the upper grade while allowing a softer base asphalt to be used to meet the lower grade, although the benefit is asphalt dependent. At the same time there is evidence that modifiers can slow the hardening of asphalt as it oxidizes.

The polymers are higher molecular weight than asphalt and show a very distinct peak on the chromatograph. The polymers degrade on oxidation, reducing the peak and shifting material to longer times and this is clearly visible with SEC (90,93–95,148). Figure 17 is an SEC chromatograph of an asphalt containing 3% SBR polymer before and after one year of thin-film (1 mm) aging at 60°C. This chromatograph also shows the extreme sensitivity of the viscosity detector to the

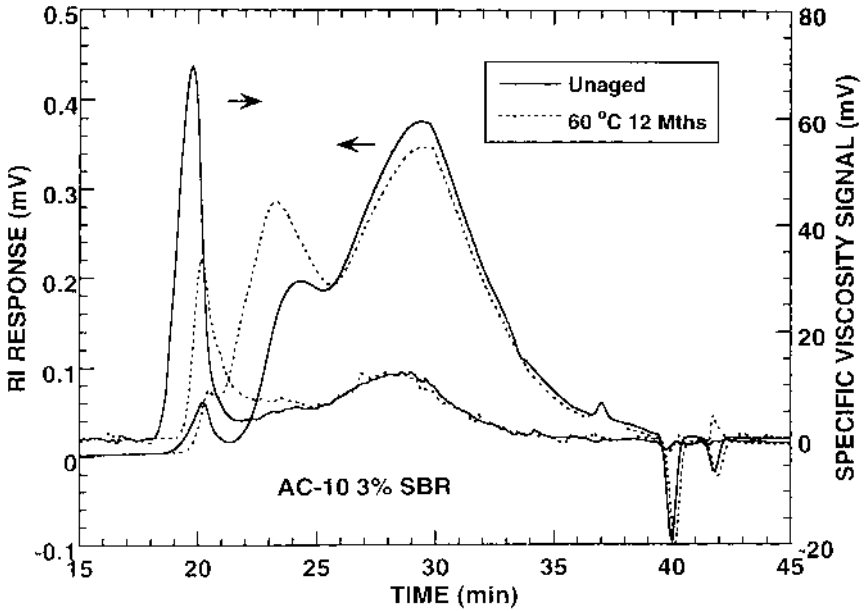

Figure 17 Effect of aging on apparent molecular size for an SBR-modified asphalt as determined by refractive index (RI) and intrinsic viscosity (IV) detectors 1000/500 Å (30 cm ultrastyragel)/50 Å (60 cm PLgel). THF at 1 mL/min, 100 μL of 2 wt% solution.

© 2004 by Marcel Dekker, Inc.

high-molecular-weight material as well as the reduction and shifting of the peak as the polymer degrades. The small response of the asphalt to the specific viscosity detector results from scaling to keep the polymer peak on scale. The RI response is typical of asphalts and much more nearly represents the actual amount of polymer present, but it is much less sensitive to the changes that occur. It also shows the usual growth with oxidation in the LMS peak near 24 minutes.

When ground tire rubber is blended with asphalt at high temperature, some of the rubber degrades sufficiently to go into solution and this is clearly visible with SEC (66,91). Billiter *et al.* (92,149,150) used SEC with a viscosity detector to study the effect of mixing variables on rubber disassociation in asphalt and the effect on properties. Figure 18 shows the effect of high shear mixing of rubber into asphalt. Initially a peak appears at about 200,000 MW by polystyrene standards, but with curing the peak grows and then degrades. The size of the peak compared to the peak in Fig. 17 shows that a relatively small fraction of the rubber actually dissolves, but the degradation of this peak is a fair measure of the reduction in size of the remaining products.

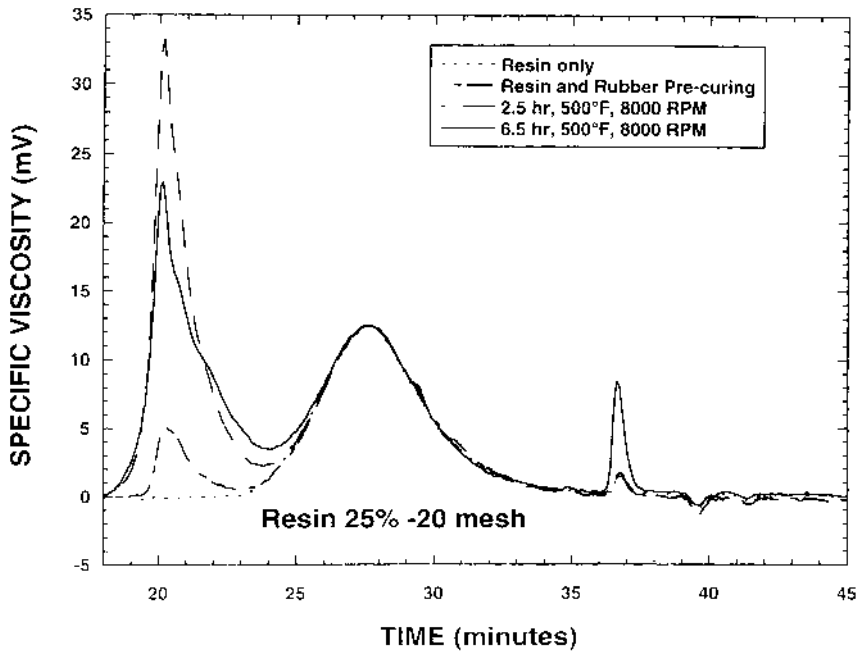

Figure 18 SEC analyses of a crumb-rubber modified resin at different stages of curing and its base asphalt (1000/500 Å, 30 cm ultrastyragel, 50 Å, 60 cm PLgel, THF at 1 mL/min, 100 μL, 2 wt% solution, IV detector).

© 2004 by Marcel Dekker, Inc.

Oxidation of the rubber and asphalt can be used to speed up the dissolution process (96). Starting with a less viscous base, asphalt material which is hardened as the rubber disintegrates yields a material with excellent PG characteristics with the 21-minute peak shown in Fig. 18 almost completely degraded.

6 DETECTORS AND "MASS DETECTION"

Researchers have used a wide variety of detectors to analyze asphalts in SEC studies. Generally, the aim is to characterize rapidly the molecular or, more correctly, the apparent size distributions. This implies the need to determine the concentration of asphalt in the eluant, which in turn requires a detector having uniform sensitivity to mass at all retention times and for all types of asphalts, regardless of differences in the materials' functionalities and degrees of molecular association. Such an ideal detector would be a true mass detector. Because of asphalt's complicated structure and composition, all detectors used to analyze asphalts by SEC fall short of being true mass detectors (68,151,152). Consequently, no single detector has gained universal appeal.

By far, the most popular on-line detectors for asphalt SEC are the differential refractive index (RI) and the ultraviolet absorption (UV) detectors. The RI detector measures differences in refractive index between the pure carrier solvent and the SEC eluant. These differences are related to the amount of solute in the eluant. The UV detector measures the eluant's absorbance of UV light at a selected wavelength. Here also, the response is related to sample concentration for a given solute.

Asphalt contains many different compounds that vary not only in molecular, or particle, size but also in UV absorptivity or refractive index. Figure 19 shows the relation between detector response per unit mass and apparent molecular size for some asphalts (12). Neither detector is uniform, as a mass detector would be. The UV detector is much less uniform than the RI detector. This is mainly because paraffinic hydrocarbons, known as saturates, which comprise roughly 10–20% of a typical asphalt, are very weak absorbers of UV light, and the aromatic components in the asphalt are strong UV absorbers. Consequently, a UV detector's response to a saturate is much less than to an aromatic compound (151,153). The effect of molecular association (which occurs in the large molecular size region) on detector sensitivity is probably significant but is not well understood (68,85,87).

The RI and UV detectors are popular because they are commonly used in other high-performance liquid chromatography applications, relatively inexpensive, reliable, and easy to operate. The UV detector is preferred by some because it has much lower detection limits, whereas others prefer the RI detector because it has more uniform response across the entire range of asphalt constituents.

© 2004 by Marcel Dekker, Inc.

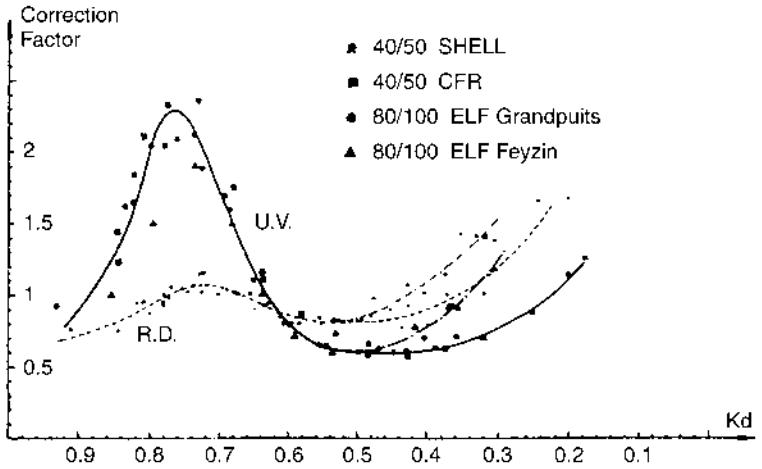

Figure 19 Comparison of the response of UV and RI detectors to materials of different apparent molecular size. (From Ref. 12, p. 239.)

The multiple-wavelength UV detector simultaneously scans several wavelengths in the UV and visible spectra. Spectra from this detector provide information about which size of molecules, or particles, contain certain UV-sensitive functionalities. Vanadyl porphyrins, for instance, have specific UV absorbances at 410 nm and are suspected of affecting asphalt aging processes. The multiple-wavelength UV detector shows (Fig. 20) that the vanadyl porphyrins are present at all molecular sizes but are concentrated in the small molecular size region (17,154,155).

Recently, several evaporative on-line detectors have been developed and are reported to be true mass detectors. However, when applied to asphalts and heavy petroleum fractions, these detectors' responses show signs of being solute dependent.

Two types of evaporative flame ionization detectors (FID) are the moving wire (156,157) and the rotating disc detectors (158–160). These convey the eluant along a wire or quartz disc into an evaporation chamber, where the volatile carrier solvent is removed. The nonvolatile sample is then passed through an FID. Any unburned sample is removed in an ashing chamber before the wire or disc returns to its eluant-collecting position.

The FIDs rely only on the amount of combustible material present, rather than light absorption or refraction characteristics of the solvent. This should make them respond more uniformly to mass over the particle size spectrum than RI or UV detectors. However, the literature indicates that nonuniformities are still a problem. Saturates and aromatics gave different response factors, possibly as a

© 2004 by Marcel Dekker, Inc.

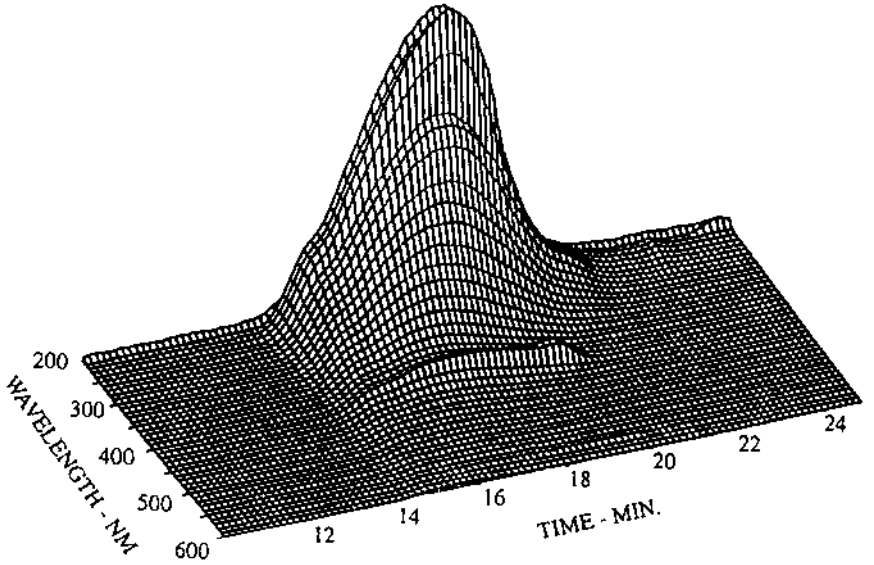

Figure 20 SEC chromatogram for an asphalt using a multiple-wavelength UV detector. (From Ref. 154, p. 172.)

result of different carbon–hydrogen ratios in the materials. The differences in response were comparable to those in RI or UV detectors. These detectors are generally more expensive and more difficult to operate than RI or UV detectors, however.

Another evaporative on-line detector is the evaporative light-scattering detector (ELSD) (152,160–164). In the ELSD, the eluant is nebulized with an inert gas to form an aerosol. The solvent in the dispersed eluant droplets is evaporated and removed in a heated chamber. The resulting solute particles fall through a light-scattering detector. The scattered light is related to the amount of mass in the particles, which in turn corresponds to the amount of solute in the eluant.

The light scattering is supposed to be minimally dependent upon the structure and functionality of the solutes. The sparse literature pertaining to asphalt and heavy petroleum fractions indicates that the detector's response varies with different solutes, however. Pentane solubles gave markedly lower response than asphaltenes and benzene insolubles. The response to pentane solubles also varied with evaporator temperature, which is usually a sign of solute loss by evaporation. This seems unlikely with a material as nonvolatile as asphalt. Like the evaporative FIDs, the ELSD is more expensive and more difficult to operate than the RI or UV detectors.

© 2004 by Marcel Dekker, Inc.

"Universal" detectors, which combine continuous RI and intrinsic viscosity (IV) detection, propose to remove some of the error caused by chemical functionality differences within a sample. SEC columns separate on the basis of hydrodynamic volume, or the volume a molecule or association of molecules occupies in solution. Hydrodynamic volume is converted to molecular weight using calibrations of standard molecular weight molecules, such as polystyrene. However, molecules having the same molecular weights can have considerably different hydrodynamic volumes because of differences in molecular structure. Linear molecules, such as paraffins, have higher hydrodynamic volumes than branched molecules, like polar aromatics, of the same weight. Therefore, in SEC with conventional concentration detection, these molecules elute at different times and appear to have different molecular weights. Intrinsic viscosity detection gathers information on molecular structure (degree of branching or compactness), which is used to convert hydrodynamic volumes to molecular weights.

The only universal detector sensitive enough to detect asphalt (because of its relatively low molecular weight) is the differential viscometer (165,166). It utilizes a Wheatstone bridge flow resistance scheme that measures intrinsic viscosity differences between the column eluant and the carrier solvent. Other viscosity detectors measure absolute intrinsic viscosity of the eluant and are not as precise. In Fig. 21, several supercritically refined asphalt fractions having a variety of molecular weights (M_w) are seen to have similar RI and IV molecular weights in the low-molecular-weight regions (19). In high-molecular-weight regions, where fractions have higher asphaltene contents, viscosity detection results in higher molecular weights than RI detection. This is because asphaltenes are much more compact than polystyrene, have lower hydrodynamic volumes relative to molecular weight, and therefore elute at the same time as a smaller polystyrene molecule. Maltenes and polystyrene seem to have similar compactness. The detector still cannot account for errors caused by tailing or molecular associations in solution. At present, there are no instances of universal detection providing improved characterization in terms of chemical composition or performance properties.

Other on-line detectors receive rare mention in the literature and are used for specialty applications. Nickel and vanadium detectors have been used to detect the distribution of metal porphyrins in asphalts (167). Fluorescence detectors have been used to detect cut-points between associated and nonassociated constituents (36).

While searching for a mass detector, it must be remembered that other chromatographic problems still prevent the determination of asphalt molecular size distributions. Large, polar molecules tend to interact with the column packing and cause adsorption–desorption tailing in the chromatograms. Therefore, material that appears to have low molecular size may actually be of very large molecular size. Also, asphalt forms associations of molecules that may individually be of

© 2004 by Marcel Dekker, Inc.

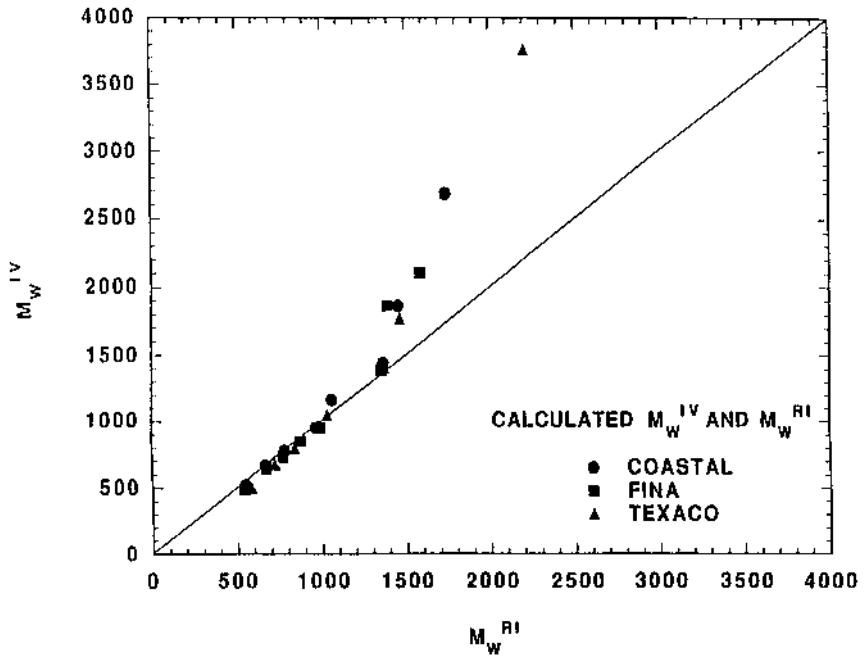

Figure 21 Comparisons of apparent molecular size as determined by intrinsic viscosity (IV) and refractive index (RI) detectors.

average size but collectively appear to be very large molecules. A mass detector may determine how much material is in the form of large particles but does not reveal the true size of the particles' component molecules. If different asphalts form molecular associations to different degrees, then it is pointless to draw conclusions on asphalt molecular size distributions purely from SEC.

7 SUMMARY

Size exclusion chromatography has been used extensively for the study of asphalts. Conditions that have been reported in the literature are summarized in Table 5. SEC of asphalts is especially useful for observing differences between asphalts, changes that occur to an asphalt upon oxidative aging, and for detecting low molecular size contaminants. Correlations of SEC chromatograms with physical properties, although aggressively sought, have been elusive, undoubtedly because of the role of other factors besides size, such as the chemical nature of the molecules and the compatibility of the many components in the asphalt blend.

© 2004 by Marcel Dekker, Inc.

Table 5 Reported Conditions for SEC Determinations of Asphalt and Related Materials[a]

Polymer	Column type/ pore sizes (Å)	Mobile-phase solvent/flow rate (mL/min)	Comments		References
			Detector	Injection volume (μL)/ concentration (mass %)	
Asphalt[b]	PS/—[c]	Bz + 10% MeOH/1.5	Prep	10 mL/10	1,2
	PS/10^4 + 2 at 400 + 100	THF/1	RI	—/0.5	3
	PS/10^4 + 10^3 + 500 + 50	THF/—	RI	—/1.08	4
	PS/—	Bz/—	Prep	—	5
	PS/—	Bz + 5% MeOH/—	Prep	—	7
	PS/—	THF/—	RI	—	8
	PS/500 + 50	THF/1	RI	100/7	9,10,25,27,28, 30,33,35,86
	PS/500 + 50	Tol/1	RI	100/7	9,10,86
	PS/—	Bz + 10% MeOH/250	Prep	300 g/0.2 g/mL	11[d]
	PS/10^3 + 10^4 + 10^5 + 10^6 or PS/10^3 + 10^4	THF, $CHCl_3$, Bznt, Tet/several	RI; UV (254) UV (350)	Several	12
	PS/10^4 + 10^3	THF/3.5	RI; UV (350)	15/2	13
	—	THF/—	—	50 to 2 × 10^3/ 0.2–0.5	14
	PS/500 + 50	THF/1	RI	100/5	15
	PS/—	Bz + 10% MeOH/2	Prep	5 mL/20	26,70,120
	—	THF/—	Prep	—	29
	PS/10^3 + 500 + 100	—	UV (—)	—	34
	PS/10^5 + 10^3 + 4 at 500	Several	UV (254)	Several	42

© 2004 by Marcel Dekker, Inc.

S/—	THF/2	RI	0.5 mL/1	44
PS/10^3 + 3 at 500 + 10^5 + 100	THF/3	RI	1 mL/2	45
PS/10^3 + 2 at 500	THF/0.9	RI; UV (340)	100/0.5 g/mL	50
PS/10^3 + 3 at 500 + 10^5 + 100	THF/2	RI; UV (254)	1 mL/2	54
PS/10^3 + 3 at 500 + 10^5 + 10^6	THF/2	RI	0.5 mL/1	55
PS/10^3 + 2 at 500	THF/1	UV (290)	50/0.5	56
PS/3 at 500 + 10^3 + 100	THF/2	UV (340)	—/2	60
PS/50% 100–50% 250 + 2 at 10^3 + 10^4	$CHCI_3$ + 5% MeOH/2	UV (370)	0.45 mL/0.02 g/mL	69
PS/60 + 100 + 10^3 + 5 × 10^3 + 10^5	THF/1	RI	—/0.25	71
PS/10^4 + 3 × 10^3 + 800 + 250 + 100	THF/1	RI	2 mL/0.5 mg/mL	72
PS/10^4 + 10^3 + 500 + 100	THF/1.5	RI, UV (—)	—	73
—	Several	—	—	77
PS/—	Bz + 5% MeOH/10	Prep	—	81
PS/60	THF or Tol/1.15	RI	10–30/30	82[d]
PS/10^3 + 10^4	THF/3.5	UV (350)	10/10	87
PS/10^3 + 10^4	—	—	—	88
PS/8500 + 10^3 + 500 + 70	THF/1	—	—/0.5	108
PS/400 + 100	Bz/1	Prep	1.7 g	135
PS/500	THF + 5% Pyr	RI; UV/(354)	100–200/6–8 mg	153
PS/4000 + 40 + 4	THF/1	MW UV visible	50/0.5	154

© 2004 by Marcel Dekker, Inc.

Table 5 (*Continued*)

Polymer	Column type/ pore sizes (Å)	Mobile-phase solvent/flow rate (mL/min)	Comments		References
			Detector	Injection volume (μL)/ concentration (mass %)	
	Several	Several	RI; UV (313 + 365); MW-FID	Several	157[d]
	PS/1000 + 500 + 100	THF/1.2	RD-FID; ELSD; RI	—	160
	PS/10^4 + 0–1000 Mixed bed + 150	Xyl + 20% Pyr + 0.5% Crs/1	ICP	100/0.1 g/mL	167[c,d]
	PS/10^4 + 10^3 + 500 + 100	THF/—	RI	0.25 mL/2	148
	PD v B[f]/500	NMP[g]/0.6	UV (270–600)	—/1 mg/mL	136
	PS/10^3 + 500 + 500	THF/1	UV (290)	50/0.5	61
	Jordi GPC Gel/10^3	THF/0.9	MW UV	—/0.5	17
	PS/1000 + 500 + 100	THF/1	RI	500/10 mg/mL	90
	PS/1000	CH_3Cl–5% MeOH/3.5	UV (340)	10/0.5 g/L	41
	PS/500	THF/1	MW UV;ELSD;VI	—	164
	PS/1000 + 500 + 500	THF/1	RI;UV (254)	100/0.25	62
	Bio-beads SX1	Tol/3.5	Florescence	150 mL/0.11 g/mL	37
	PS/1000 + 500 + 500	THF/1	UV (290)	50/0.5	63
	PS/10^4 + 10^3 + 500 +500 + 100 + 100	THF/1	RI	Various/0.05–0.5	75
	PS/1000 + 500 + 50	THF/1	RI;VI	100/—	19

© 2004 by Marcel Dekker, Inc.

	PS/10^4 + 10^3 + 500 + 100	THF/1	RI;UV (230,340)	—	64
	PS/10^4 + 10^3 + 500 + 100	THF/—	RI	—	32
	PS/10^4 + 10^3 + 500	THF/1	RI	20/5%	93
	PS/10^4 + 10^3 + 500 + 100	THF/1	RI	100/5	65
	PS/10^4 + 10^3 + 500 or PS/1000 + 500 + 100	THF/1	RI	50/6 g/L	24
	PS/10^4 + 10^3 + 500	THF/1	RI	20/5	94, 93
	PS/1000 + 500 + 50	THF/—	VI	—/0.2 g/10 mL	96
Asphalt 25,35°C	PS/10^5 + 2 at 10^4 + 10^3	THF/—	—	—/0.25	114
Asphalt 25,40°C	PS/1000 + 500 + 500	THF/1	RI	100/0.25	133
Asphalt 30°C	PS/3 × 10^3 + 500 + 250 + 60	THF/—	Prep	—	6
	PS/10^4	Tol/2	MW UV	50/various	83
	PS/500 + 500 + 100	THF/1	UV (340)	20/1	128
	PS/Mixed (100–40,000)	THF/0.7	RI	20/5 mg/mL	140
	PS/Mixed-E	THF/0.7	RI	20/5 mg/mL	20
	PS/1000 + 500 + 500	THF/1 Decalin/0.7	UV (340)	20/0.5	23
Asphalt 40°C	Bio-beads SX1/170	Tol/3.6	Florescence	150 mL/0.11 g/mL	74
	Bio-beads SX1	Tol/3.6	Florescence	—	39
	PS/1000 + 500 + 50	THF/1	RI	100/0.7	129
	PS/500 + 500 + 100	Tol/1	RI;Florescence	220/24 mg/220 μL	91
	PS/1000+ 100 + 50	THF/1	RI;VI	—/0.2–0.25 g/mL	149
Asphalt 45°C	PS/10^3 + 500 + 500	THF/1	RI	200/0.5	66

© 2004 by Marcel Dekker, Inc.

Table 5 (*Continued*)

Polymer	Column type/ pore sizes (Å)	Mobile-phase solvent/flow rate (mL/min)	Comments		References
			Detector	Injection volume (μL)/ concentration (mass %)	
Asphalt 80°C	Mixed-D PS-DVB	NMP/0.5	MW UV	20/—	80
Asphalt 90°C	S/60	THF/1	UV (220)	25/0.05	59

[a]Analyses are at 25°C or room temperature unless otherwise noted. PS = polystyrene, S = silica, THF = tetrahydrofuran, Tol = toluene, MeOH = methanol, Bz = benzene, $CHCl_3$ = chloroform, Bznt = benzonitrite, Tet = tetraline, Pyr = pyridine, Xyl = xylene, Crs = cresol, RI = refractive index, UV(λ) = UV detector at λ nm, Prep = preparative SEC, detector not used, ELSD = evaporative light-scattering detector, RD-FID = rotating disk FID, MW-FID = moving wire FID, ICP = inductively coupled plasma, MW UV = multiwavelength UV visible, VI = viscosity detector.
[b]May include aged asphalt material, air-blown residue, asphalt fractions, or crude oils.
[c]Data not reported.
[d]Crude oil or its fractions.
[e]Nickel and vanadium determinations.
[f]Poly(divinylbenzene) Jordi-gel.
[g]N-methylpyrrolidinone.

© 2004 by Marcel Dekker, Inc.

Nevertheless, SEC of asphalts is established as an important analytical technique, especially when used in concert with other methods.

REFERENCES

1. KH Altgelt. J Appl Polym Sci 9:3389–3393, 1965.
2. KH Altgelt. Makromol Chem 88:75–89, 1965.
3. WB Richman. Proc AAPT 36:106–113, 1967.
4. D Bynum, Jr, RN Traxler. Proc AAPT 39:683–702, 1970.
5. JA Minshull. Australian Road Res Board 428:1468–1476, 1968.
6. JJ Breen, JE Stephens. AAPT 38:706–712, 1969.
7. CA Stout, SW Nicksic. Separation Sci 5(6):843–854, 1970.
8. CK Adams, RJ Holmgreen. FHWA/TX-86/287-4F, 1986.
9. CJ Glover, JA Bullin, JW Button, RR Davison, GR Donaldson, MW Hlavinka, CV Philip. FHWA/TX-87/419-1F, 1987.
10. CJ Glover, RR Davison, JA Bullin, JW Button, GR Donaldson. Trans Res Rec 1171:71–81, 1988.
11. KH Altgelt, E Hirsch. Separation Sci 5(6):855–862, 1970.
12. B Brulé. In: J Cazes, X Delamare, eds. Liquid Chromatography of Polymers and Related Materials II. New York: Marcel Dekker, 1980, pp 215–248.
13. C Such, B Brulé, C Baluja-Santos. J Liq Chromatogr 2:437–453, 1979.
14. PW Jennings. Proc AAPT 54:635–651, 1985.
15. JR Stegeman, AL Kyle, BL Burr, HB Jemison, RR Davison, CJ Glover, JA Bullin. Fuel Sci Tech 10:767–794, 1992.
16. JL Goodrich, JE Goodrich, WJ Kari. Trans Res Rec 1096:146–167, 1986.
17. PW Jennings, JAS Pribanic, TM Mendes, JA Smith. Fuel Sci Technol Int 10(4–6):809–823, 1992.
18. PW Jennings, JAS Pribanic, JA Smith, TM Mendes. Am Chem Soc Preprint 37(3):1313–1319, 1992.
19. HB Jemison, RR Davison, CJ Glover, JA Bullin. Fuel Sci Technol Int 13(5):605–638, 1995.
20. J Huang, D Bertholf. Petrol Sci Technol 15(1&2):37–49, 1997.
21. MM Liu, JM Chaffin, RR Davison, CJ Glover, JA Bullin. Ind Eng Chem Res 36:2177–2183, 1997.
22. M Liu, JJ Chaffin, RR Davison, CJ Glover, JA Bullin. Trans Res Rec 1638:40–46, 1998.
23. PR Herrington, Y Wu. Pet Sci Technol 17(3&4):291–318, 1999.
24. S Peramanu, BB Pruden, P Rahimi. Am Chem Soc Preprint 38:3121–3130, 1999.
25. BL Burr, RR Davison, CJ Glover, JA Bullin. Trans Res Rec 1269:1–8, 1990.
26. GA Haley. Anal Chem 47(14):2432–2437, 1975.
27. RR Davison, JA Bullin, CJ Glover, BL Burr, Jr, HB Jemison, ALG Kyle, CA Cipione. FHWA/TX-90/458-1F, 1990.
28. KL Martin, RR Davison, CJ Glover, JA Bullin. Trans Res Rec 1269:9–19, 1990.
29. MM Hattingh. Proc AAPT 53:197–215, 1984.

© 2004 by Marcel Dekker, Inc.

30. CJ Glover, RR Davison, SM Ghoreishi, HB Jemison, JA Bullin. Trans Res Rec 1228:177–182, 1989.
31. AS Noureldin. In: JC Hardin, ed. Physical Properties of Asphalt Cement Binders. ASTM STP 1241. Philadelphia: American Society for Testing and Materials, 1995, pp 137–174.
32. M Asi, HI Al-Abdul Wahhab, IA Al-Dubabi, MF Ali. J Mater Eng Perform 6(4):503–510, 1997.
33. HB Jemison, RR Davison, CJ Glover, JA Bullin. Trans Res Rec 1323:77–84, 1991.
34. BH Chollar, JA Zenewitz, JG Boone, KT Tran, DT Anderson. Trans Res Rec 1228:145–155, 1989.
35. BL Burr, RR Davison, HB Jemison, CJ Glover, JA Bullin. Trans Res Rec 1323:70–76, 1991.
36. JC Petersen, RE Robertson, JF Branthaver, PM Harnsberger, JJ Duvall, SS Kim, DA Anderson, DW Christensen, HU Bahia, R Dongré, CE Antle, MG Sharma, JW Button, CJ Glover. Binder Characterization and Evaluation, Volume 4: Test Methods. SHRP-A-370. Strategic Highway Research Program. Washington, D.C.: National Research Council, 1994, pp 79–83.
37. JF Branthaver, JJ Duvall, JC Petersen. In: J Youtcheff, T Mill, co-chairmen. Symposia of Chemistry and Characterization of Asphalts. Washington, D.C.: American Chemical Society, 35(3):407–414, 1990.
38. RE Robertson, JF Branthaver, H Plancher, JJ Duvall, EK Ensley, PM Harnsberger, JC Peterson. Proc AAPT 60:413–436, 1991.
39. JF Branthaver. Fuel Sci Technol Int 11(1):123–139, 1993.
40. YW Jeon, CW Curtis, BA Coker. Pet Sci Technol 15(9&10):873–905, 1997.
41. G McCaffrey. Fuel Sci Technol Int 10(4–6):519–530, 1992.
42. PW Jennings, JA Pribanic, KR Dawson. FHWA-MT 82/001, 1982.
43. DE Newcomb, BJ Nusser, BM Kiggundu, DM Zallen. Trans Res Rec 968:66–77, 1984.
44. AS Noureldin, LE Wood. Trans Res Rec 1228:191–197, 1989.
45. JE Shoenberger, RS Rollings, RT Graham. In: JC Hardin, ed. Physical Properties of Asphalt Cement Binders, ASTM STP 1241. Philadelphia: American Society for Testing and Materials, 1995, pp 199–213.
46. MA Plummer, CC Zimmerman. Proc AAPT 53:138–159, 1984.
47. PW Jennings. FHWA-MT 7927, 1977.
48. PW Jennings, JA Pribanic, W Campbell, KR Dawson, RB Taylor. FHWA-MT-7930, 1980.
49. PW Jennings, JAS Pribanic. Big Timber Test Section Report. Bozeman Montana: Montana State University, 1984.
50. PW Jennings, JAS Pribanic. FHWA/MT-85/001, 1985.
51. PW Jennings, JAS Pribanic. Fuel Sci Technol 7(9):1269–1287, 1989.
52. PM Beazly, LE Hawsey, MA Plummer. Trans Res Rec 1115:46–50, 1987.
53. JR Woods, LS Koflyar, DS Montgomery, BD Sparks, JA Ripmeester. Fuel Sci Technol 8(2):149–171, 1990.
54. EL Dukatz, Jr, DA Anderson, JL Rosenberger. Proc AAPT 53:160–185, 1984.
55. NW Garrick, LE Wood. Trans Res Rec 1096:35–41, 1986.

© 2004 by Marcel Dekker, Inc.

56. NW Garrick, RR Biskur. Trans Res Rec 1269:26–39, 1990.
57. NW Garrick, LE Wood. Proc AAPT 57:26–40, 1988.
58. SW Bishara, RL McReynolds, ER Lewis. Trans Res Rec 1323:1–9, 1991.
59. SW Bishara, RL McReynolds. Trans Res Rec 1342:35–49, 1992.
60. BH Chollar, JG Boone, WE Cuff, EF Bailey. Public Roads 49(1):7–12, 1985.
61. NW Garrick, RR Biskur. Proc AAPT 59:33–53, 1990.
62. KW Kim, JL Burati, Jr. J Mater Civil Eng 5(1):41–52, 1993.
63. NW Garrick. J Mater Civil Eng 6(3):376–389, 1994.
64. HI Abdul Wahhab, MF Ali, IM Asi, IA Dubabe. Am Chem Soc Preprint 41(4):1296–1301, 1996.
65. HI Al-Abdul Wahhab, IM Asi, FM Ali, IA Al-Dubabi. J Mater Civil Eng 11(1):6–14, 1999.
66. RP Price, JL Burati, Jr. Proc AAPT 59:1–32, 1990.
67. RB Girdler. Proc AAPT 34:45–79, 1965.
68. JG Speight, DL Wernick, KA Gould, RE Overfield, BML Rao, DW Savage. Rev Inst Fr Petrole 40(1):51–61, 1985.
69. LR Snyder. Anal Chem 41(10):1223–1227, 1969.
70. GA Haley. Anal Chem 43(3):371–375, 1971.
71. HH Kiet, LP Blanchard, SL Malhotra. Separation Sci 12(6):607–634, 1977.
72. H Reerink, J Lijzenga. Anal Chem 47(13):2160–2167, 1975.
73. PJ Champagne, E Manolakis, M Ternan. Fuel 64:423–425, 1985.
74. JF Branthaver, JJ Duvall, JC Petersen, H Plancher, RE Robertson. Fuel Sci Technol Int 10(4–6):1003–1032, 1992.
75. M Nali, A Manclossi. Fuel Sci Technol Int 13(10):1251–1264, 1995.
76. JF Branthaver, RE Robertson, JJ Duvall. Trans Res Rec 1535:10–14, 1996.
77. JG Bergman, LJ Duffy. Anal Chem 43(1):131–133, 1971.
78. Z Grubisic, P Rempp, H Benoit. J Polym Sci, Part B 5:753–759, 1967.
79. HH Oelert, DR Latham, WE Haines. Separation Sci 5(5):657–668, 1970.
80. M Domin, A Herod, R Kandiyoti, JW Larsen, M-J Lazaro, S Li, P Rahimi. Energy & Fuels 13:552–557, 1999.
81. KH Altgelt, TH Gouw. Adv Chromatogr 13:71–175, 1975.
82. JN Done, WK Reid. Separation Sci 5(6):825–842, 1970.
83. SI Andersen. J Liq Chromatogr 17(19):4065–4079, 1994.
84. SW Bishara, RL McReynolds. In: J Youtcheff, T Mill, co-chairmen. Symposia of Chemistry and Characterization of Asphalts. Washington, D.C.: American Chemical Society, 35(3):396–406, 1990.
85. PW Jennings, MA Desando, MF Raub, JO Hoberg, R Moats, FF Stewart. In: J Youtcheff, T Mill, co-chairmen. Symposia of Chemistry and Characterization of Asphalts. Washington, D.C.: American Chemical Society, 35(3): 440–444, 1990.
86. GR Donaldson, MW Hlavinka, JA Bullin, CJ Glover, RR Davison. J Liq Chromatogr 11(3):749–765, 1988.
87. B Brulé, G Ramond, C Such. Trans Res Rec 1096:22–34, 1986.
88. I Ishai, B Brulé, JC Vaniscote, G Ramond. Proc AAPT 57:65–93, 1988.
89. BL Burr, RR Davison, CJ Glover, JA Bullin. Trans Res Rec 1436:47–53, 1994.

© 2004 by Marcel Dekker, Inc.

90. S Linde, U Johansson. In: KR Wardlaw, S Shuler, eds. Polymer Modified Asphalt Binders, ASTM STP 1108. Philadelphia: American Society for Testing and Materials, 1992.
91. JJ Duvall. Am Chem Soc Preprint 41(4):1267–1275, 1996.
92. TC Billiter, RR Davison, CJ Glover, JA Bullin. Trans Res Rec 1586:50–56, 1997.
93. X Lu, U Isacsson. Fuel 77(9&10):961–972, 1998.
94. X Lu, U Isacsson. Trans Res Rec 1661:83–92, 1999.
95. JF Chipps, RR Davison, CJ Glover. Energy & Fuels 15:637–647, 2001.
96. SE Leicht, P Juristyarini, RR Davison, CJ Glover. Pet Sci Technol 19(3&4):317–334, 2001.
97. LW Corbett. Anal Chem 41:576–579, 1969.
98. LW Corbett. Anal Chem 36(10):1967–1972, 1964.
99. LW Corbett. Proc AAPT 39:481–491, 1970.
100. JC Petersen. Trans Res Rec 999:13–30, 1984.
101. JC Petersen. Trans Res Rec 1096:1–11, 1986.
102. M Liu, MA Ferry, RR Davison, CJ Glover, JA Bullin. Ind Eng Chem Res 37:4669–4674, 1998.
103. RV Barbour, JC Petersen. Anal Chem 46(2):273–277, 1974.
104. JC Petersen. Fuel 46:295–305, 1967.
105. SE Moschopedis, JG Speight. Fuel 55:187–192, 1976.
106. JF McKay, PJ Amend, TE Cogswell, PM Harnsberger, RB Erickson, DR Latham. In: PC Uden, S Siggia, eds. Analytical Chemistry of Liquid Fuel Sources. Advances in Chemistry Series 170. Washington, D.C.: American Chemical Society, 1978, pp 128–142.
107. MM Boduszynski, JF McKay, DR Latham. Proc AAPT 49:123–143, 1980.
108. MM Boduszynski. In JW Bunger, NC Li, eds. Chemistry of Asphaltenes. Advancement in Chemistry Series 195. Washington, D.C.: American Chemical Society, 1981, pp 119–135.
109. DL Mitchell, JG Speight. Fuel 52:149–152, 1973.
110. JG Speight, RB Long, TD Trowbridge. Fuel 63:616–620, 1984.
111. FJ Nellensteyn. J Inst Petrol Technol 14:134–138, 1928.
112. JPh Pfeiffer, RNJ Saal. Phys Chem 44:139–149, 1940.
113. TF Yen, JG Erdman, SS Pollack. Anal Chem 33(11):1587–1594, 1961.
114. JP Dickie, TF Yen. Anal Chem 39(14):1847–1852, 1967.
115. TF Yen, JP Dickie. J Inst Petrol Technol 54(530):50–53, 1968.
116. TF Yen. In: J Youtcheff, T Mill, co-chairmen. Symposia of Chemistry and Characterization of Asphalts. Washington, D.C.: American Chemical Society, 35(3):314–319, 1990.
117. SW Ferris, EP Black, JB Clelland. Ind Eng Chem Prod Res Dev 6(2):127–132, 1967.
118. FE Dickson, BE Davis, RA Wirkkala. Anal Chem 41(10):1335–1337, 1969.
119. FE Dickson, RA Wirkkala, BE Davis. In: KH Altgelt, L Segal, eds. Gel Permeation Chromatography. New York: Marcel Dekker, 1971, pp 579–591.
120. GA Haley. Anal Chem 44(3):580–585, 1972.
121. RE Baltus. In: OC Mullins, EY Sheu, eds. Structures and Dynamics of Asphaltenes. New York: Plenum Press, 1998, pp 303–335.

© 2004 by Marcel Dekker, Inc.

122. M-S Lin, JM Chaffin, RR Davison, CJ Glover, JA Bullin. In: OC Mullins, EY Sheu, eds. Structures and Dynamics of Asphaltenes. New York: Plenum Press, 1998, pp 267–302.
123. JC Ravey, G Ducouret, D Espinat. Fuel 67:1560–1567, 1988.
124. S Acevedo, G Escobar, MA Ranaudo, LB Gutiérrez. Fuel 73(11):1807–1809, 1994.
125. CH Domke, RR Davison, CJ Glover. Trans Res Rec 1961:114–121, 1999.
126. CH Domke, RR Davison, CJ Glover. Ind Eng Chem Res 39:592–598, 2000.
127. MM Liu, MS Lin, JM Chaffin, RR Davison, CJ Glover, JA Bullin. Pet Sci Technol 16(7&8):827–850, 1998.
128. PR Herrington, GFA Ball. Fuel 75(9):1129–1131, 1996.
129. M-S Liu, RR Davison, CJ Glover, JA Bullin. Trans Res Rec 1507:86–95, 1995.
130. WJ Halstead. Proc AAPT 32:247–270, 1963.
131. PS Kandhal, WC Koehler. Trans Res Rec 999:41–50, 1984.
132. JL Goodrich, LH Dimpfl. Proc AAPT 55:57–91, 1986.
133. KW Kim, JL Burati, Jr, SN Amirkhanian. J Mater Civil Eng 5(4):447–459, 1993.
134. Asphalt Institute, Performance Graded Asphalt Binder Specification and Testing, Superpave Series No. 1 (SP-1), 1994.
135. HJ Coleman, JE Dooley, DE Hirsch, CJ Thompson. Anal Chem 45:1724–1737, 1973.
136. AL Lafleur, Y Nakagawa. Fuel 28:742–752, 1989.
137. SE Moschopedis, JF Fryer, JG Speight. Fuel 55:227–232, 1976.
138. S Acevedo, G Escobar, LB Gutiérrez, JD Aquino. Fuel 71:1077–1079, 1992.
139. S Acevedo, G Escobar, MA Ranaudo, A Rizzo. Fuel 77(8):853–858, 1998.
140. J Huang, D Bertholf. Fuel Sci Technol Int 14(8):1037–1047, 1996.
141. J Hildebrand, R Scott. Solubility of Non-Electrolytes. 3rd ed. New York: Reinhold, 1949.
142. CM Hansen, K Skaarup. J Paint Technol 39(511):511–514, 1967.
143. CM Hansen. Ind Eng Chem Prod Res Dev 8(1):2–11, 1969.
144. CM Hansen, A Beerbower. In: RE Kirk, DF Othmer, eds. Encyclopedia of Chemical Technology. 2nd ed., Supplement Volume. New York: John Wiley and Sons, 1971, pp 889–910.
145. AP Hagen, R Jones, RM Hofener, BB Randolph, MP Johnson. Proc AAPT 53:119–137, 1984.
146. CA Cipione, RR Davison, BL Burr, CJ Glover, JA Bullin. Trans Res Rec 1323:47–52, 1991.
147. LR Snyder. J Chromatogr 92:223–230, 1974.
148. JL Goodrich. Proc AAPT 57:117–175, 1988.
149. TC Billiter, RR Davison, CJ Glover, JA Bullin. Pet Sci Technol 15(3&4):205–236, 1997.
150. TC Billiter, JS Chun, RR Davison, CJ Glover, JA Bullin. Pet Sci Technol 15(5&6):445–469, 1997.
151. HV Drushel. J Chromatogr Sci 21:375–384, 1983.
152. KD Bartle, N Taylor, MJ Mulligan, DG Mills, C Gibson. Fuel 62:1181–1185, 1983.
153. SW Bishara, RL McReynolds. Trans Res Rec 1269:40–47, 1990.
154. JAS Pribanic, M Emmelin, GN King. Trans Res Rec 1228:168–176, 1989.

© 2004 by Marcel Dekker, Inc.

155. PW Jennings, JAS Pribanic, TM Mendes, JA Smith. In: J Youtcheff, T Mill, co-chairmen. Symposia of Chemistry and Characterization of Asphalts. Washington, D.C.: American Chemical Society, 35(3):383–388, 1990.
156. HV Drushel. In: PC Uden, S Siggia, eds. Analytical Chemistry of Liquid Fuel Sources. Advances in Chemistry Series 170. Washington, D.C.: American Chemical Society, 1978, pp 295–306.
157. EW Albaugh, PC Talarico. J Chromatogr 74:233–253, 1972.
158. JB Dixon. Chimia 38(3):82–86, 1984.
159. CD Pearson, SG Gharfeh. Anal Chem 58:307–311, 1986.
160. S Coulombe. J Chromatogr Sci 26:1–6, 1988.
161. TH Mourey, LE Oppenheimer. Anal Chem 56:2427–2434, 1984.
162. M Righezza, G Guiochon. J Liq Chromatogr 11(9/10):1967–2004, 1988.
163. KD Bartle, M Burke, DG Mills, S Pape, S Lu. In: J Youtcheff, T Mill, co-chairmen. Symposia of Chemistry and Characterization of Asphalts. Washington, D.C.: American Chemical Society, 35(3):415–420, 1990.
164. KD Bartle, M Burke, DG Mills, S Pape, S-L Lu. Fuel Sci Technol Int 10(4–6):1071–1082, 1992.
165. M Haney. American Laboratory, March and April, 1985.
166. M Haney. U.S. Patent No. 4,463,598. Official Gazette 54, August 7, 1984.
167. CD Pearson, JB Green. Fuel 68:465–474, 1989.

© 2004 by Marcel Dekker, Inc.

9
Size Exclusion Chromatography of Acrylamide Homopolymer and Copolymers

Fu-mei C. Lin
University of Pittsburgh
Pittsburgh, Pennsylvania, U.S.A.

1 INTRODUCTION

Acrylamide monomer is a white crystal, available commercially as a 50 wt% aqueous solution. Acrylamide monomer can be polymerized to a very-high-molecular-weight (10^6–10^7 g/mole) homopolymer, copolymer, or terpolymer. Polyacrylamide (PAM) is a nonionic polymer. The anionic polyacrylamide species can be obtained from the hydrolysis of the amide (—$CONH_2$) functional group of the homopolymer, or from the copolymerization of acrylamide with an anionic monomer, such as acrylic acid (AA) or 2-acrylamino 2-methyl propane sulfonic acid (AMPS). Acrylamide can be copolymerized with a cationic monomer, such as dimethyl diallylammonium chloride (DMDAAC) or acryloyloxyethyl trimethyl ammonium chloride (ALETAC), to form the cationic acrylamide polymer.

© 2004 by Marcel Dekker, Inc.

Acrylamide can simultaneously react with anionic and cationic monomers to form a polyampholyte. The acrylamide homopolymer, copolymers, and terpolymers are synthesized (1–20) by free radicals via solution or emulsion or other polymerization methods. Adamsky and Beckman (21) reported the inverse emulsion polymerization of acrylamide in supercritical carbon dioxide. The product classes of acrylamide polymers include liquid, dry, and emulsion.

The nonionic, anionic, and cationic acrylamide polymers have been used for many industrial applications (1–3,13,22,23). The polymer selection for a particular application depends upon the desired chemical structure, chemical composition, molecular weight (MW), and molecular weight distribution (MWD). Some applications of acrylamide polymers are shown in Table 1. Size exclusion chromatography (SEC) is an excellent technique to determine MW and MWD. Yau *et al.* (24) have discussed the SEC technique. Barth (25) has reported a practical approach to steric exclusion chromatography of water-soluble polymers. However, SEC is not easily carried out for the subject polymers because of the high molecular weight (10^6–10^7 g/mole) and the polyelectrolyte characteristics of the charged polymers. In order to obtain meaningful SEC data, the columns, mobile phase, concentration of polymer solution, sample preparation method, flow rate, and shear degradation of the polymer should be considered in an SEC experiment.

Several authors (26–29) have discussed concentration effects in SEC. Barth and Carlin (30) have proposed mechanisms and possible sources of polymer shear degradation in SEC. Giddings (31) determined the shear degradation of PAM. Omorodion *et al.* (32) studied the effects of pH, ionic strength, and nonionic surfactants on polymer dimensions and elution volume for aqueous SEC of PAM with controlled-porc glass (CPG) columns. Onda *et al.* (33,34) analyzed PAM by SEC using CPG columns in formamide and aqueous media. They also studied the effects of salt addition on the retention volume. Klein and Westerkamp (35) separated PAM, acrylamide/sodium acrylate copolymers, dextrans, and poly(sodium styrene sulfonates) by using CPG columns. They investigated the thermal degradation of PAM at 50 and 75°C. Letot *et al.* (36) used polyvinylpyrrolidone-coated silica columns and pure water to chromatograph PAM and other water-soluble polymers. El-Awady and co-workers (37) investigated the MW and MWD of PAM in side chains and in homopolymer by SEC during grafting of cellulose acetate with acrylamide monomer. McCormick and Park (38) studied the effects of Fe(II), H_2O_2, acrylamide, and dextran concentration on the hydrodynamic volumes of dextran-grafted acrylamide copolymers by SEC. Muller and Yonnet (39) studied a high MW hydrolyzed polyacrylamide (HYPAM) and a 74/26 mole% AM/AA high MW copolymer by SEC, static low-angle laser light scattering (LALLS) and photon correlation light scattering. Huang (40) evaluated the chemical structural heterogeneity of cationic acrylamide copolymers by high-performance liquid

© 2004 by Marcel Dekker, Inc.

Table 1 Applications of Acrylamide Polymers

Application	Polymer	Change (%)	Molecular weight
Liquid/solid separation			
Process water clarification	Anionic PAM	High	High
Filtration aid	PAM	None	High
	Anionic PAM	High	High
Primary waste water clarification	PAM	None	High
	Anionic PAM	High	High
	Cationic PAM	Medium	High
Secondary waste water clarification	Cationic PAM	High	High
Sludge thickening and sludge dewatering for biological waste	Cationic PAM	High	High
Sludge thickening and sludge dewatering for mineral	PAM	None	High
	Anionic PAM	High	High
Retention/drainage aid	Cationic PAM	Medium to high	High
	Anionic PAM	Low to medium	High
Dry strength aids for paper	Anionic PAM + polyamine	Low	Medium
		High	Low
Wet strength aids for paper	Gloxated cationic PAM (lightly Crosslinked PAM)	Low	Medium
Hair and skin conditioners in personal care applications	Cationic PAM	Medium to high	High
	Amphoteric	Low (net charge)	High
Oil field applications			
Mobility control	Anionic PAM	Low–high	High
Recovery of petroleum	PAM gel or powder	None	High
	PAM + 5% HYPAM	Low	High
Lubricant–coolant	Ethylene/maleic Anhydride + PAM	None	Medium
Reducing friction losses	PAM	None	Medium to high
	Anionic PAM		
	Cationic PAM		

PAM, polyacrylamide; HYPAM, hydrolyzed polyacrylamide.
Source: Refs. 1–3, 13, 22, and 23.

© 2004 by Marcel Dekker, Inc.

chromatography. Abdel-Alim and Hamielec (41) used a broad MWD PAM standard A to create a linear calibration curve that covers the molecular weight range from 10^3 to 10^7 g/mole. This calibration was used to characterize two other broad-MWD standards B and C.

The Micropak TSK Gel PW, TSK Gel PWXL and Shodex OHpak Q-800, B-800, and KB-800 series are more recently available columns developed for analyzing the acrylamide polymers and other water-soluble polymers in aqueous SEC. The TSK columns have been evaluated by Barth (25), Alfredson *et al.* (42), Sasaki *et al.* (43), and Lin and Getman (44). Dhowa Denko (45) reported the SEC analysis of PAM by Shodex OHpak columns. The narrow MWD polyacrylamide standards ($M_w = 1.2 \times 10^4$ to 9.0×10^6 g/mole) produced by the American Polymer Standards Corporation are listed in Table 2. However, some acrylamide copolymers and terpolymers are heterogeneous (40) in terms of chemical structure and MW, and the standards having chemical structures similar to the samples are not commercially available. The absolute MW and MWD of these polymers are difficult to determine using conventional SEC with a single refractive index (RI) detector and using narrow MWD standards for calibration. The on-line dual or multidetectors were used in an SEC system to solve the above problems.

Kim and co-workers (46) developed a methodology for using RI/LALLS dual detectors to establish the MW calibration curve and peak broadening parameter for a wide range of MW for PAM. Lin and Getman (44) determined the absolute MW and MWD of PAM, HYPAM, acrylamide/acrylic acid

Table 2 Polyacrylamide Standards (Reported by American Polymer Standards Corporation)

	Nonionic, 100% water-soluble powder			
Catalog #	$\overline{M}_w$ (g/mole)	M_p (g/mole)	$\overline{M}_n$ (g/mole)	IV[a] (dL/g)
PAAM9000K	9,000,000	6,500,000	4,250,000	14.600
PAAM6000K	5,500,000	3,695,000	2,460,000	10.385
PAAM1000K	1,140,000	725,000	465,300	3.800
PAAM500K	524,000	331,000	209,600	2.250
PAAM350K	367,000	193,400	141,000	1.650
PAAM80K	79,000	50,500	44,400	0.645
PAAM60K	58,400	46,100	36,500	0.545
PAAM20K	21,900	17,300	13,700	0.255
PAAM10K	11,530	7,950	7,600	0.160

[a]IV = Intrinsic viscosity in dL/g in 0.05 M sodium sulphate at 30°C.
$[\nu] = kM^a$, $a = 0.66$, $k = 0.000373$.

© 2004 by Marcel Dekker, Inc.

(AM/AA), and acrylamide/dimethyldiallylammonium chloride (AM/DMDAAC) copolymers by Micropak TSK Gel PW and PWXL columns with an RI/LALLS dual detecting system. Also, the authors determined the molecular weight reduction and mass loss of degraded AM/AA copolymer in a boiler by SEC with RI detector. Lesec and Volet (47) applied RI/LALLS/on-line viscometer triple detectors to determine the absolute MW and MWD of PAM.

A Calgon in-house computer simulation program developed by Min and Cha (48) has been applied to construct a conventional calibration curve. This program is written in Fortran. It needs two standards for a linear fit and four standards for a third-order fit. The required parameters are the $\overline{M}_w$ and $\overline{M}_n$ (number-average molecular weight) of each standard. The different weighted factor (0 to 1) can be entered into the program to specify the degree of importance of the given $\overline{M}_w$ or $\overline{M}_n$ value.

Rand and Mukherji (49) reported a MW calibration technique with the assistance of a computer program to handle the routine analysis of a specific polymer with a special set of columns, identical mobile phase, and identical SEC experiment. This method deals with modifying the previous calibration curve by shifting the retention times of the upper and/or lower limits to obtain a new calibration curve for the current experiment.

A list of the SEC conditions used in the above references will be compiled in the Appendix of this chapter.

The methodology and applications of SEC for characterizing acrylamide polymers will be discussed in this chapter from a practical point of view.

2 EXPERIMENTAL

2.1 Column and Mobile Phase

The selections of columns and mobile phase depend on the chemistry and molecular weight of the polymer to be analyzed. Important factors (31,32) such as chemistry, pore size, particle size, ionic group, and adsorptive properties of the stationary phase, the resolving power, molecular weight separation range, solvent compatibility, lifetime, sample loading capacity, and temperature stability should be considered before selecting a column. When a high-molecular-weight ($>10^6$ g/mole) polymer is analyzed, the shear degradation of the polymer in the columns is an important factor, which influences the accuracy of the MW and MWD determinations. Giddings (31) reported the reduction in intrinsic viscosity of polyacrylamide solution ($\overline{M}_w = 6.25 \times 10^6$ g/mole) after passing through a CPG-10 column (3000 Å pore size and 39–75 μm particle size) at a flow velocity as low as 0.025 cm/s.

© 2004 by Marcel Dekker, Inc.

When an anionic or cationic acrylamide polymer is analyzed, the ionic group of the stationary phase should be considered before selecting a column. Sasaki and colleagues (43) reported that the TSK Gel PWXL columns have small amounts of weakly anionic groups. Lin and Getman (44) observed the adsorption of a high MW acrylamide/DMDAAC cationic polymer in the TSK Gel PWXL columns. Therefore, the TSK Gel PW columns are recommended for analyzing cationic and amphotoric acrylamide polymers.

Simple salts such as sodium chloride or sodium sulfate are added to the mobile phase to minimize the polyelectrolyte effect of the charged acrylamide polymers. The optimal ionic strength of the mobile phase can be determined by measuring the intrinsic viscosity $[\eta]$ of the polymer solutions with increasing concentration of simple salt until the intrinsic viscosity becomes constant. If a linear calibration curve is desired, the different pore sizes of columns should be investigated for a particular range of MW. If a very slow flow rate such as $0.1-0.3$ mL/min is required for a very-high-molecular-weight sample in a narrow MW range, a single column may be used to reduce the analysis time. Research should be conducted to provide adequate information for selecting columns and mobile phase. The columns and mobile phases that have been used to analyse polyacrylamide and its copolymers and terpolymers are summarized in a list of SEC conditions, which are compiled in the Appendix at the end of this chapter.

2.2 Sample Preparation

Sample preparation is a very important step for SEC analysis. The MW of a polymer can be changed unintentionally during sample preparation. Use the mobile phase to prepare samples. If the low MW tail of the chromatogram overlaps with the salt peak, replace the mobile phase with an appropriate amount of water to obtain a negative polarity salt peak. The quantity of water to be used depends on the concentration to be prepared and the percentage of active polymer in the sample. It can be determined from a series of SEC experiments with varying amounts of water added to the sample until a negative polarity salt peak is obtained. The optimum concentration of SEC sample depends on the MW of the polymer. Lundy and Hester (50) suggested that the polymer solution injected into the columns should not be greater than one-half the reciprocal of its intrinsic viscosity. If an unusual pressure trace caused by a high viscosity of a solution is observed during the injection, reduce the concentration and remove the precolumn filter, if such a filter is present.

Filter size selection depends on the MW and solution concentration. Use an appropriate size of filter to prepare polymer solutions, so the large molecules will not be excluded by the filter. If there is no information about the MW of the

© 2004 by Marcel Dekker, Inc.

polymer, a large size filter of 5, 8, or 10 μm is recommended. Examples are shown below.

Weight-average molecular weight $\overline{M}_w$ (g/mole)	Concentration (g/100 mL)	Filter size (μm)
10^2–10^4	0.1–0.15	0.22
10^5	0.1	0.45
10^6	0.05–0.08	1.2–3.0
$>10^6$	0.03–0.05	5.0–10.0

The mixing method can change the actual MW and MWD. In this work, different methods were used to prepare three types of samples.

2.2.1 For Solution Samples

The magnetic stirring method at low speed is recommended.

2.2.2 For Solid Samples

It is very difficult to dissolve high MW solid PAM or its copolymers in a high-ionic-strength mobile phase directly. A special process is recommended as follows. Pour about 60 mL filtered water into a bottle and stir the water with a magnetic stir bar at high speed. Sprinkle the correct amount of solid sample into the bottle. When the solid sample disperses homogeneously in the water, cap the bottle tightly and place the bottle containing the sample in a shaker with low speed at 50°C overnight. Remove the sample from the shaker when the solid sample is dissolved completely. Add the correct amount of salt to the above sample solution and adjust the total volume to 100 mL by adding filtered water. Mix the solution very well and filter the solution with an appropriate size of filter. Degas the polymer solution in a flask, then transfer the polymer solution to a 4 mL vial.

2.2.3 For Emulsion Samples

Dilute the emulsion sample with xylene or hexane, then precipitate the dilute solution into isopropyl alcohol (IPA) or acetone. Filter the mixture to obtain the solid sample. Dry the precipitated sample in a vacuum oven at 40°C overnight to remove the residual IPA or acetone. A solution of the precipitated sample for SEC analysis can be prepared by the same method used for preparing solid samples.

© 2004 by Marcel Dekker, Inc.

3 RESULTS AND DISCUSSION

3.1 Chromatographic System

PAM, HYPAM, and AM/AA copolymers can be analyzed by TSK Gel PWXL (44), TSK Gel PW (25,44), Shodex OHpak (25,45), CPG (31–34,38,41,46), Sephacryl S1000 (39), polyvinylpyrrolidone-coated silica columns (36) with an appropriate mobile phase. For cationic acrylamide copolymers, the Gel TSK PW columns (44) have a better separation capability than the Gel PWXL columns. This is probably due to the higher number of residual anionic sites found in PWXL columns (44). When a cationic polyacrylamide is analyzed, conditioning the columns is very important. This process can be achieved by injecting the lower MW solution (or first sample) that has the same chemical structure as the samples into the columns before data are collected for analysis. The MW range that can be separated by TSK PW or TSK PWXL columns is 10^3–10^7 g/mole.

The high-ionic-strength mobile phase creates some difficulty in maintaining a constant flow rate during the SEC experiment. About 0.025 to 0.05 min fluctuations in retention time at 1 mL/min flow rate have been observed in 50 min run times. The consistency of flow rate during the SEC analysis can be evaluated by comparing the elution times of salt peaks among chromatograms of samples. Data generated from inconsistent flow rates will give incorrect MW information. Lundy and Hester (51) designed a syringe pump to obtain 0.15 mL/min consistent flow rate for characterizing large water-soluble macromolecules.

Figure 1 shows the chromatograms of PAM and HYPAM from TSK PWXL columns and AM/DMDAAC copolymer from TSK PW columns. The MW of five PAM samples will be discussed later. The narrower line width of the chromatogram of the highest MW sample (PAM 1, $\overline{M}_w = 6 \times 10^6$ g/mole) is probably due to the insufficient separation capability of the columns (TSK Guard column + G6000V + G5000 + G4000 PWXL). Figure 2 shows the chromatogram of a very broad-MWD PAM standard, which was obtained by mixing these five PAM samples. The MW information, which is summarized in Table 3, was determined from five PAM samples using peak MW calibration techniques. Using this single broad-MWD standard rather than several PAM standards can save SEC analysis time for routine samples. The 50/50 wt% monomer charge ratio of AM/DMDAAC contains a narrow high MW portion and low MW tail [negative skewness defined by Chen and Hu (52)]. The high and low MW portions have been separated by precipitating the copolymer solution in isopropyl alcohol (IPA). Both precipitated solid (high MW portion) and supernatant (low MW portion) were dried in a vacuum oven at 40°C. The dried samples were redissolved in H_2O and analysed by proton NMR spectroscopy. Based on the copolymer composition determined from proton NMR analysis, the high MW portion is acrylamide-rich AM/DMDAAC copolymer, and the polymer in the low MW fraction is DMDAAC-rich AM/DMDAAC copolymer. The copolymer composition of

© 2004 by Marcel Dekker, Inc.

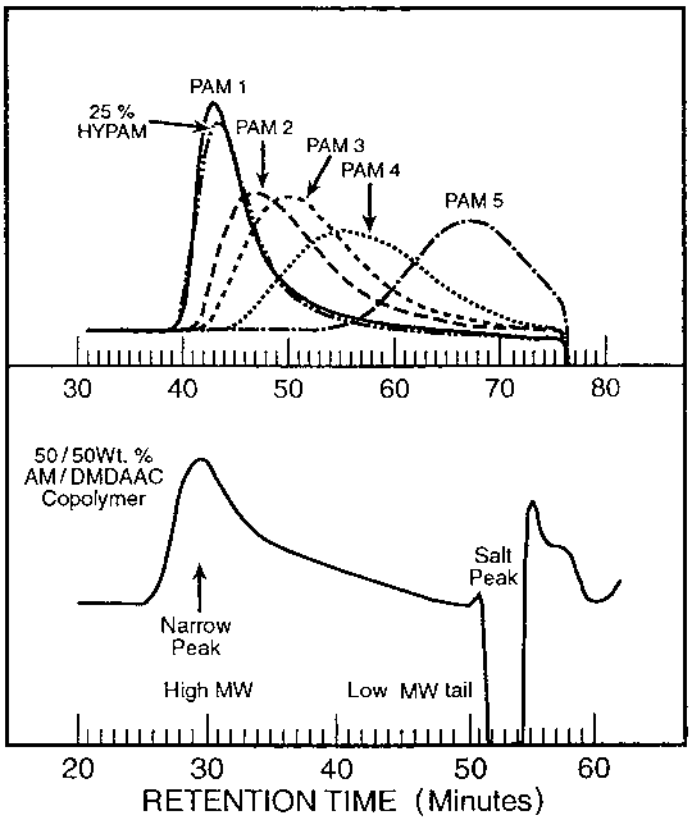

Figure 1 Size exclusion chromatograms of PAM, HYPAM, and AM/DMDAAC copolymer (raw data).

AM/DMDAAC copolymer is a function of MW. This phenomenon is caused by the different copolymer reactivity ratios of acrylamide and DMDAAC ($r_{AM} = 2.36$, $r_{DMDAAC} = 0.046$) monomers. Again, the narrow line shape of the high MW portion may be due to the poor separation capability of the columns at the upper MW end (about 5×10^6 g/mole). Langhorst and co-workers (53) stated that the combination of hydrodynamic chromatography (HDC) and LALLS detection can be applied to determine MW and MWD of partially hydrolysed PAM up to $\overline{M}_w = 9 \times 10^6$ g/mole.

Figure 3 shows two chromatograms of low MW 90/10 wt% AM/DMDAAC copolymer samples with solvent peaks of different polarity. The low MW tail of the chromatogram overlaps with the salt peak. Therefore, the final processing time is difficult to determine and the $\overline{M}_w$, $\overline{M}_n$, and $\overline{M}_w/\overline{M}_n$ values

© 2004 by Marcel Dekker, Inc.

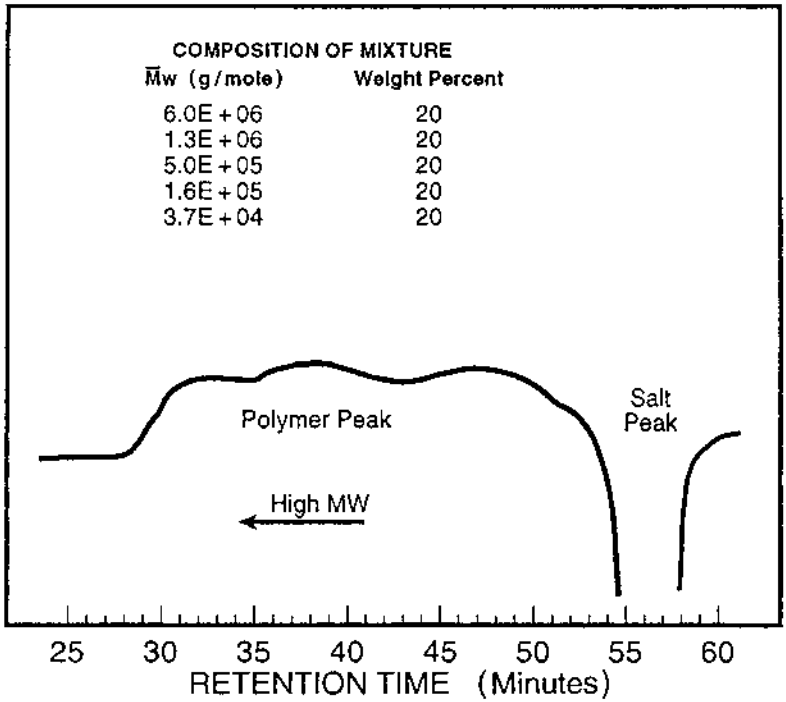

Figure 2 A broad-MWD PAM standard obtained from five individual PAM samples.

depend on the choice of the final process time. With the positive salt peak, a significant amount of area was eliminated in the MW and MWD determination. This results in a narrower polydispersity. With the negative salt peak, a small area of the salt peak was included in the MW and MWD determination. This results in a broader polydispersity.

The RI, UV, LLAS, and viscometer detectors have been successfully used in this work. The FTIR detector has been applied to study protein by Remsen and Freeman (54). It is difficult to obtain a strong signal from the conductivity detector (Waters Model 430) because of the high-ionic-strength mobile phase.

3.2 Characterization of Molecular Weight Standards

3.2.1 Static LALLS Experiment

This experiment determines the absolute $\overline{M}_w$ of a polymer in solution. It requires the specific refractive index increment $[(dn/dc)_{T,\lambda,\mu}]$ (55–57) of the polymer

© 2004 by Marcel Dekker, Inc.

Table 3 MW and MWD of a Broad-MWD PAM Standard Shown in Fig. 2

PAM Standards: PAM 1, PAM 2, PAM 3, PAM 4, PAM 5, and PAM 6 ($\overline{M}_w = 3.7 \times 10^4$ to 6.0×10^6 g/mole)
$\overline{M}_w = 1.1 \times 10^6$ g/mole
$\overline{M}_n = 5.2 \times 10^4$ g/mole
$\overline{M}_w/\overline{M}_n = 24$

Cumulative wt%	Slice MW (g/mole)
0.045	34,409,572
0.432	16,696,033
1.622	8,682,435
6.391	2,829,109
12.761	1,140,318
21.184	544,627
38.745	224,933
56.957	106,853
68.643	65,451
74.720	50,499
86.133	28,440
94.563	14,351
97.324	9,653
99.183	6,216
100.000	3,812

Columns: Guard column + TSK G6000 PW + G5000 PW + G3000 PW.
Mobile phase: 0.15 M Na_2SO_4 + 1% acetic acid, pH = 3.1, temperature: 35°C.

solution in order to calculate $\overline{M}_w$. The dn/dc measurement should be carried out under the same temperature (T) and same wavelength (λ) as the LALLS experiment and at a constant chemical potential (μ). The conditions for a constant chemical potential can be achieved by dialyzing the polymer solution against the filtered mobile phase until the dn/dc of the polymer solution becomes constant. In addition, the final concentration of the polymer solution should be determined after dialysis. It was found that when a 0.1 g/100 mL-high MW PAM solution was dialyzed against 2000 mL of mobile phase with a 1000 MW cut-off dialysis membrane, it took about three to four days to obtain a constant dn/dc and resulted in a 3 to 5 wt% mass loss. The concentration of polymer solution was decreased from 0.1 g/100 mL to 0.097 g/100 mL to 0.095 g/100 mL. Other parameters that may affect the dn/dc value are the molecular weight of the polymer and the temperature of the experiment. Research should be conducted to define the correct conditions for the dn/dc measurement. Also, it

© 2004 by Marcel Dekker, Inc.

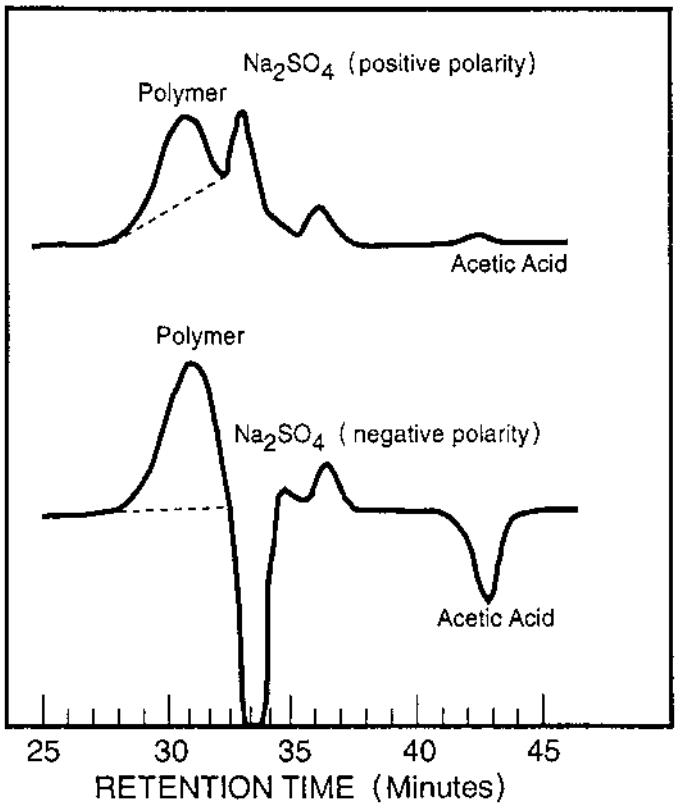

Figure 3 Size exclusion chromatograms of low MW 90/10 wt% AM/DMDAAC copolymer with positive or negative salt peak.

should be noted that the measured dn/dc of an acrylamide copolymer is an average of its components.

3.2.2 SEC Analysis with RI/LALLS Dual Detectors

This type of analysis provides the absolute MW and MWD without standards (44,46,47). The $\overline{M}_w$, $\overline{M}_n$ polydispersity, and molecular weight vs. cumulative % area of polymer can be obtained. $(dn/dc)_{T,\lambda,\mu}$ of the polymer solution should be used for MW determination. Samples characterized by this technique can be used as SEC MW standards.

The LALLS detector is insensitive to low MW and low concentration species. Therefore, the $\overline{M}_n$ determined by this method may be erroneously high.

© 2004 by Marcel Dekker, Inc.

Another commercially available MW detector is a Multi Angle Laser Light Scattering (MALLS) photometer. It should be noted that a good chromatographic system is required for obtaining a meaningful MW and MWD, even if a MW detector (LALLS or MALLS) is used. In other words, the MW detector cannot solve chromatographic problems.

3.2.3 Intrinsic Viscosity Determination

The intrinsic viscosity and Mark–Houwink constants of standards can be determined from a static capillary viscometer or an on-line viscometer detector in an SEC system. If the intrinsic viscosity is to be used for constructing a universal calibration curve, it is important to use identical conditions in performing the SEC analysis and the intrinsic viscosity measurement. A Mark–Houwink plot for five PAM standards and one PAA standard is shown in Fig. 4. The intrinsic viscosity of PAM may decrease with time and becomes constant after about one week. It is recommended that the PAM solution be analyzed while still fresh.

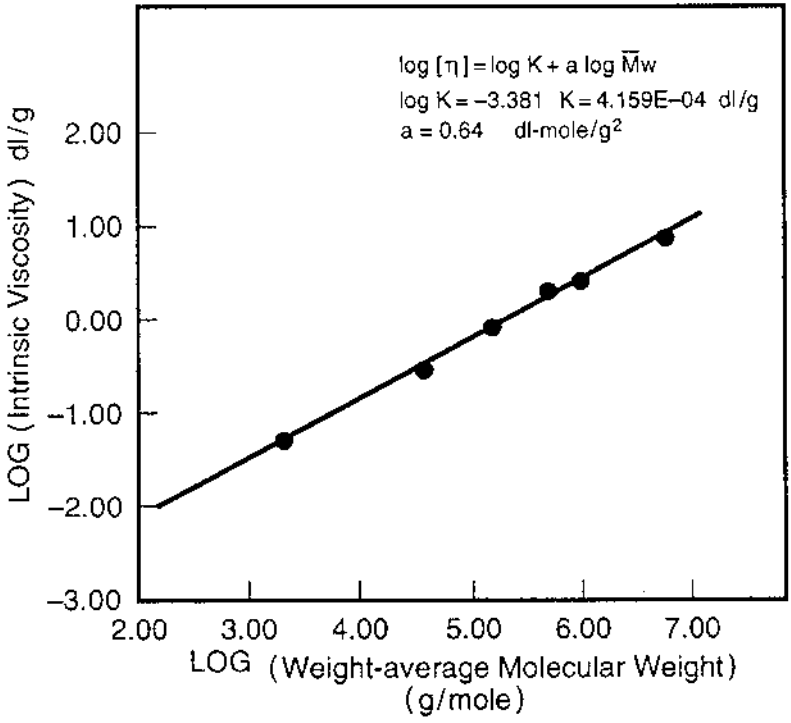

Figure 4 Mark–Houwink plot of five polyacrylamides and one polyacrylic acid.

© 2004 by Marcel Dekker, Inc.

3.3 Factors Influencing the MW Determination

3.3.1 MW and Chemical Structure of Standards

Table 4 shows the average molecular weights and polydispersities of four 80/20 w/w AM/DMDAAC high MW copolymers. It appears that the use of poly (DMDAAC) as a standard results in the reporting of a higher molecular weight and polydisperity of the copolymer. It is also important to note that the chain microstructure (stereostrucrure, end groups, or monomer sequence distribution) of a polymer may affect the molecular size when in solution. Every effort should be made to use a polymer with a similar chain microstructure for standardization when determining MW. Otherwise, erroneous values may be obtained because even though a polymer may have the same chemistry, it may have a different chain microstructure and behave differently in solution. When comparing relative MW, the same MW standards must be used for all determinations.

3.3.2 MW and Calibration Technique

Table 5 shows the given $\overline{M}_w$ (determined by LALLS) and intrinsic viscosities determined from an on-line viscometer (Viscotek Model 110) and the measured $\overline{M}_w$ determined by different calibration techniques for six samples. The deviations $\{[(\text{measured } \overline{M}_w - \text{given } \overline{M}_w)/(\text{given } \overline{M}_w)] \times 100\}$ between the measured $\overline{M}_w$ and those given $\overline{M}_w$ for PAM are -10 to $+15\%$ by universal calibration and -8 to $+4\%$ by peak position calibration. The universal calibration technique gives relatively higher deviations, probably due to the fact that the intrinsic viscosity was determined from a single point (58) or the universal calibration curves included two different types of polymers (five PAM and one low MW polyacrylic acid) as shown in Fig. 5, or the polydispersity of PAM is not narrow (59). Bose and co-workers (60) found that the universal calibrations of polystyrene sulfonate and dextrans do not coincide. For a 25% hydrolyzed PAM, its absolute $\overline{M}_w$

Table 4 Molecular Weight of 80/20 w/w Acrylamide/DMDAAC Copolymers

	Relative to poly(DMDAAC) standards			Relative to polyacrylamide standards		
Sample	$\overline{M}_w$	$\overline{M}_n$	$\overline{M}_w/\overline{M}_n$	$\overline{M}_w$	$\overline{M}_n$	$\overline{M}_w/\overline{M}_n$
Copolymer 1	6.13×10^6	1.57×10^6	3.90	3.06×10^6	8.45×10^5	3.62
Copolymer 2	7.59×10^4	1.18×10^4	6.43	7.16×10^4	3.48×10^4	2.06
Copolymer 3	2.66×10^5	3.13×10^4	8.50	1.58×10^5	6.76×10^4	2.34
Copolymer 4	1.85×10^6	8.38×10^4	22.1	8.47×10^5	1.48×10^5	5.72

© 2004 by Marcel Dekker, Inc.

Table 5 Weight-Average Molecular Weight ($\overline{M}_w$) and Intrinsic Viscosity of PAM ad 25% Hydrolyzed PAM

Sample	$[\eta]$ dL/g	Given $\overline{M}_w$ (g/mole) by LALLS	Measured $\overline{M}_w$ (g/mole) (relative to PAM standards)	
			Universal calibration	Peak position calibration
HYPAM	16.483	—	1.8×10^6	5.0×10^6
PAM 1	8.095	6.0×10^6	5.4×10^6	5.9×10^6
PAM 2	2.975	1.3×10^6	1.5×10^6	1.2×10^6
PAM 3	2.210	5.0×10^5	5.4×10^5	5.2×10^5
PAM 4	0.896	1.6×10^5	1.8×10^5	1.6×10^5
PAM 5	0.312	3.7×10^4	3.4×10^4	3.7×10^4

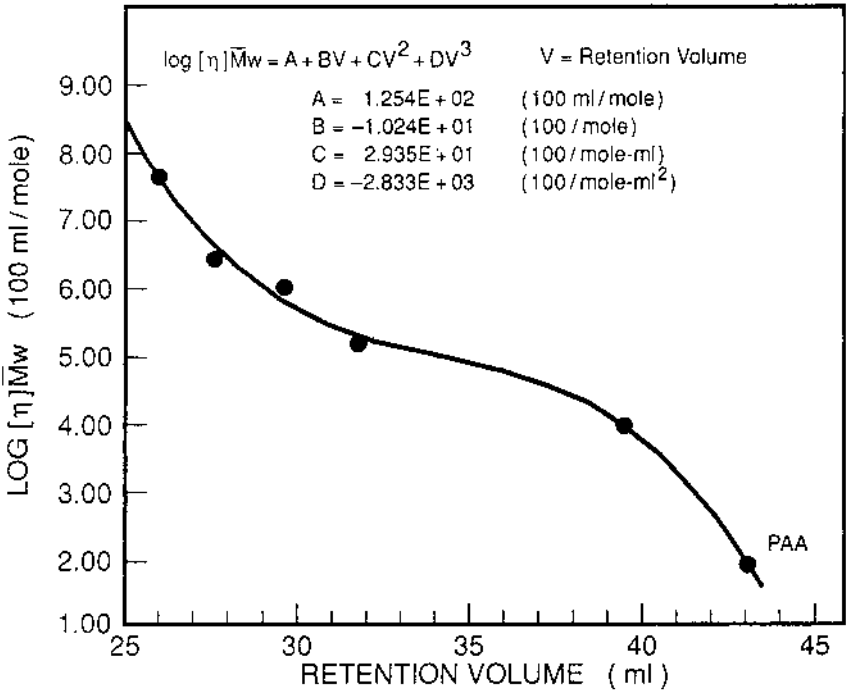

Figure 5 Universal calibration curve of five PAM and one PAA samples.

© 2004 by Marcel Dekker, Inc.

Table 6 Weight-Average Molecular Weight ($\overline{M}_w$) and Polydispersity ($\overline{M}_w/\overline{M}_n$) of Polyacrylamides

Sample	Given $\overline{M}_w$ by LALLS (g/mole)	Measured $\overline{M}_w$ and $\overline{M}_w/\overline{M}_n$ (relative to PAM standards)			
		Determined from column set 1		Determined from column set 2	
		$\overline{M}_w$ (g/mole)	$\overline{M}_w/\overline{M}_n$	$\overline{M}_w$ (g/mole)	$\overline{M}_w/\overline{M}_n$
PAM 1	6.0×10^6	5.85×10^6	3.83	5.78×10^6	3.87
PAM 2	1.3×10^6	1.18×10^6	3.99	1.16×10^6	3.95
PAM 3	5.0×10^5	5.15×10^5	2.92	5.23×10^5	3.38
PAM 4	1.6×10^5	1.64×10^5	1.93	2.02×10^5	2.44
PAM 5	3.7×10^4	3.70×10^4	2.03	3.66×10^4	1.93

Column Set 1: TSK G6000/5000/4000/3000/PWXL,
0.3 M NaCl + 0.1 M KH_2PO_4, pH = 7.0;
Column Set 2: TSK G6000/5000/4000 PW,
0.15 M Na_2SO_4 + 1% (v/v) acetic acid, pH ∽ 3.1.

(1.8×10^6 g/mole) determined from universal calibration is about one-third of its relative $\overline{M}_w$ (5.0×10^5 g/mole) determined from PAM standards.

3.3.3 MW and Column Pore Size Distribution

Table 6 shows the $\overline{M}_w$ determined from two column pore size distributions and two mobile phases. The $\overline{M}_w$ values determined from two systems for four PAM samples 1, 2, 3, and 5 agree very well. Also, their $\overline{M}_w$ values agree with the given values. However, for sample 4, the $\overline{M}_w$ (l.6 $\times 10^5$ g/mole) determined from four columns (TSK G6000/5000/4000/3000 PWXL) and the neutral pH mobile phase agrees with the given $\overline{M}_w$ while the $\overline{M}_w$ (2.0×10^5 g/mole) determined from three columns (TSK G6000/5000/3000 PW) and the acidic pH (3.1) mobile phase is about 25% higher than the given $\overline{M}_w$ (1.6×10^5 g/mole). It seems that the pore size of a TSK G4000PWXL column gives a better separation for the MW range of 1.0×10^4 to 2.0×10^5 g/mole.

4 APPLICATIONS OF SEC

SEC is mainly used for determining MW and MWD simultaneously. Other applications of SEC technique for various studies in industry have been reported in Refs 25, 37, 38, and 40. Additional projects, which have been carried out by the author, will be discussed in this section.

© 2004 by Marcel Dekker, Inc.

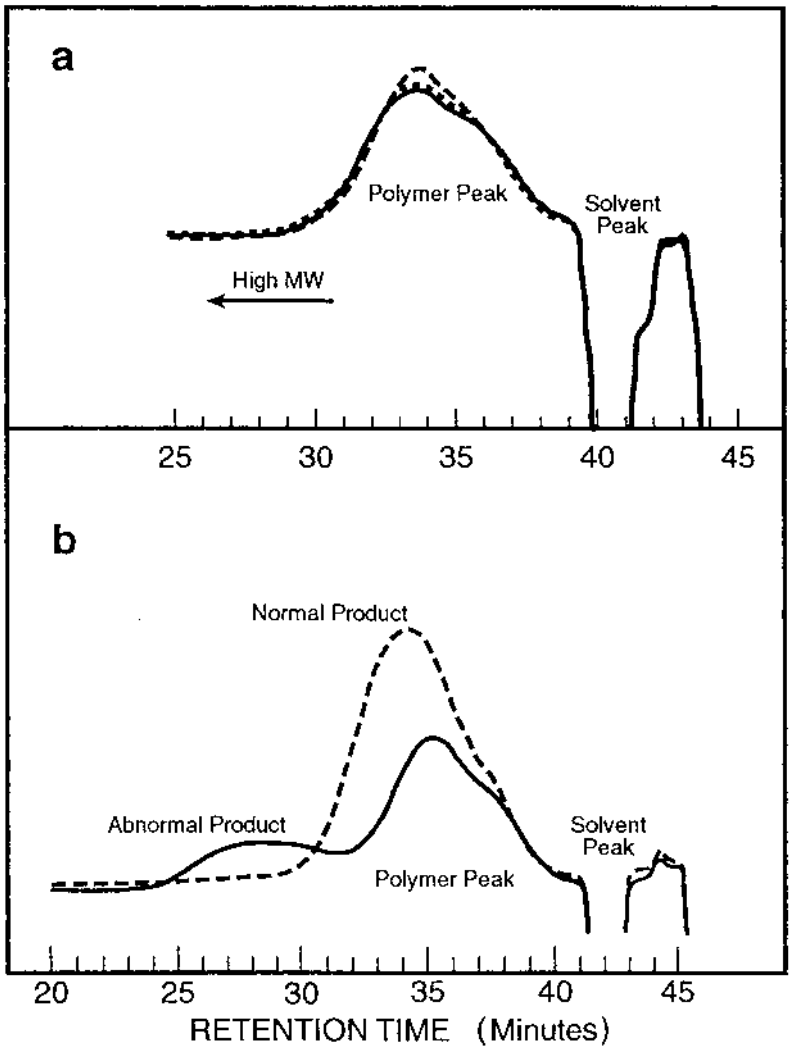

Figure 6 (a) Size exclusion chromatograms of three lots of 65/35 wt% AM/AA copolymers which have a consistent MW and MWD; (b) Comparison between the size exclusion chromatograms of a normal and an abnormal product of 65/35 wt% AM/AA copolymers.

© 2004 by Marcel Dekker, Inc.

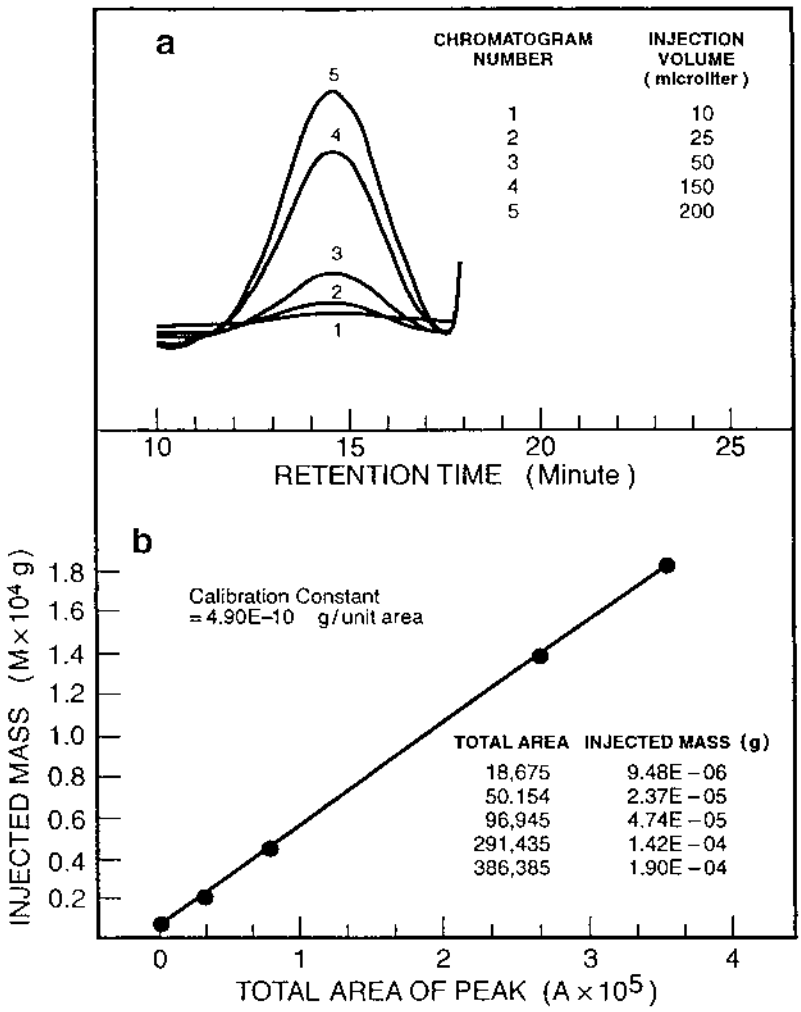

Figure 7 Size exclusion chromatograms and concentration calibration curve of low MW AM/AA copolymer ($\bar{M}_w = 8000$ g/mole).

4.1 For Anionic Acrylamide Polymers

4.1.1 Monitoring the MW and MWD of Products for Manufacturing

Figure 6a shows three lots of 65/35 wt% AM/AA having a consistent MW and MWD. Figure 6b shows that an abnormal lot of product contains high MW species

© 2004 by Marcel Dekker, Inc.

compared to a normal product. By comparing the raw chromatograms of any lots of product to a control, the abnormal lot of product can be easily identified.

4.1.2 Determining Percent Active Polymer in Solution Product

Figure 7a shows the chromatograms obtained using an RI single detector for five low MW AM/AA solutions. The injected mass of the five solutions varies from 9.48×10^{-6} to 1.90×10^{-4} g. A calibration curve that relates the injected mass and total area of the polymer peak for the five solutions is shown in Fig. 7b. Utilizing the calibration constant (4.90×10^{-10} g/unit area) obtained from Fig. 7b, the active polymer in the copolymer sample has been determined to be 30.2%. This is about 0.6% higher than the expected value (29.6%).

4.1.3 Determining the Molecular Weight Reduction and Mass Loss of Degraded Polymer

Figure 8 shows SEC chromatograms of 75/25 wt% AM/AA copolymer treated at various conditions (44). The 4000 ppm solution treated in an autoclave at 350°C and 2400 psi pressure has about 82% $\overline{M}_w$ reduction and about 71% mass loss. This mass loss can be determined from the reduction of area for the degraded polymer in

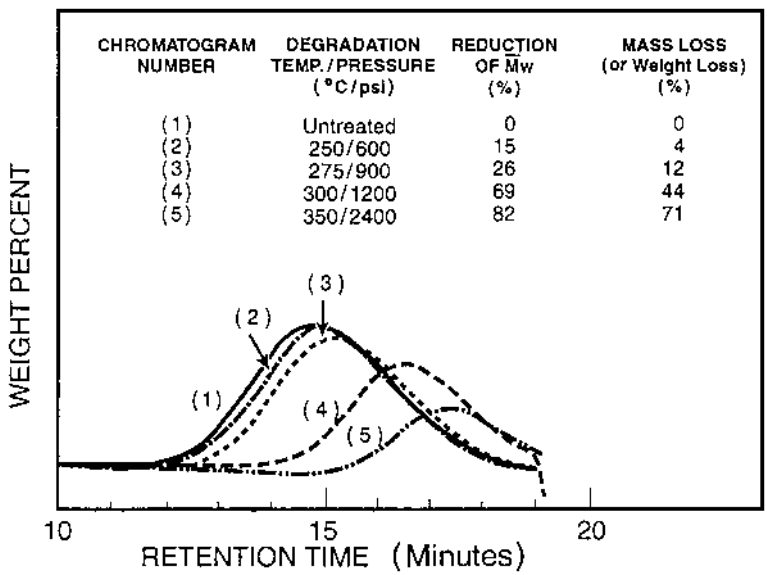

Figure 8 Size exclusion chromatograms of A 75/25 wt% AM/AA copolymer treated at various conditions (4000 ppm solution). (Courtesy of Millipore Corporation, Billerica, Massachusetts, U.S.A.)

© 2004 by Marcel Dekker, Inc.

each sample. Both proton and carbon-13 NMR analyses indicated that the lost mass was converted to the low MW degradation products. It appears that the hydrolysis of AM and chain scissoring of the polymer chains occurred during the heating process in an autoclave. The molecular weight of the degradation product is lower than the separation limit (MW is about 600 g/mole) of the columns at the low molecular end.

4.2 For Cationic Acrylamide Polymers

4.2.1 Providing a Guideline for Process Development in the Polymer Synthesis Area

Studying Structure/Performance Relationship. Figure 9 shows the chromatogram of two precipitated samples of AM/AA/DMDAAC emulsion terpolymers. The high MW and narrow peak width in chromatogram (1) is due to crosslinked species in the sample. The same phenomenon is not observed in chromatogram (2). This structure difference leads to different behaviors in a paper industrial application. The partially crosslinked terpolymer performs well and the noncrosslinked terpolymer performs poorly. Based on this information, a crosslinking agent may be added during the polymerization process to modify the structure until the desired structure is obtained.

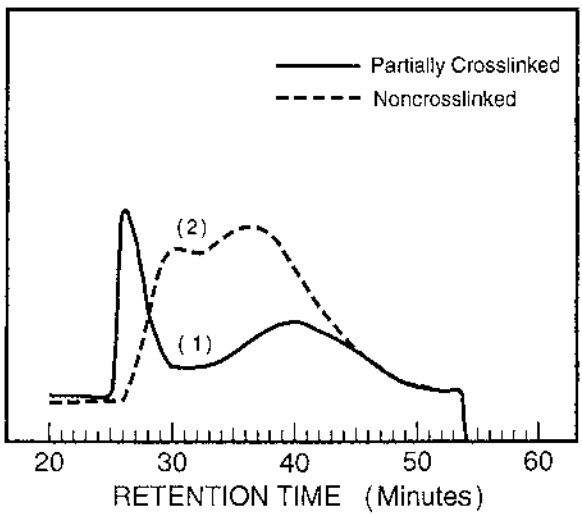

Figure 9 Size exclusion chromatograms of two precipitated AM/AA/DMDAAC emulsion terpolymers: (1) partially crosslinked terpolymer; (2) noncrosslinked terpolymer.

© 2004 by Marcel Dekker, Inc.

Studying the Kinetics of a Chemical Reaction. Four 90/10 wt% AM/DMDAAC copolymers were synthesized with different initiator levels. The correlation between log $\overline{M}_w$ and initiator level for four copolymers is a third-order equation as shown in Fig. 10. For a desired MW range, the required initiator level can be predicted from Fig. 10.

4.2.2 Studying the Distribution of Dansyldiallylamine Incorporation Along an AM/DMDAAC Copolymer

Figure 11 shows the RI and UV scans of dansyldiallylamine tagged AM/DMDAAC (50/50 w/w monomer charge ratio) copolymers. No UV signal can be observed for the copolymer synthesized at pH 6.5, so dansyldiallylamine did not incorporate into this copolymer chain. However, the chromatograms of UV and RI scans for a copolymer synthesized at pH 3.0 are similar. This indicates that

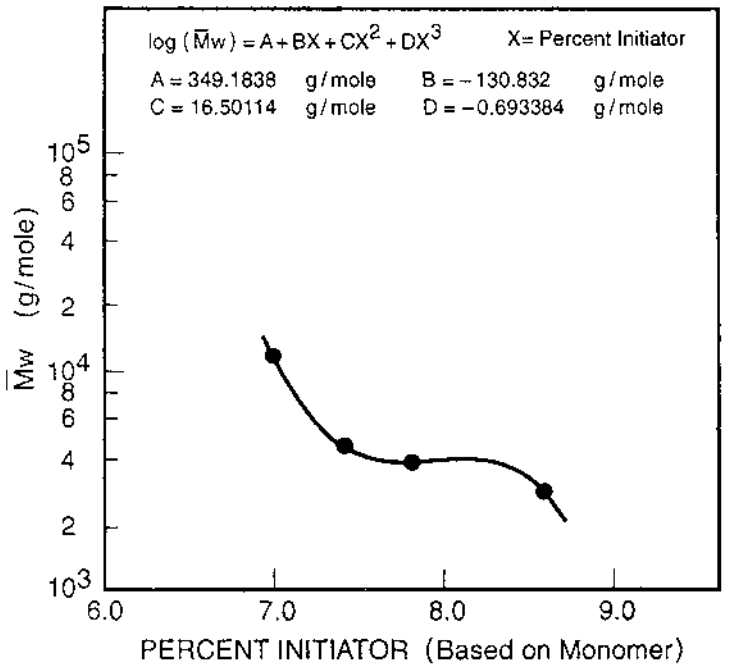

Figure 10 Plot of log $\overline{M}_w$ (relative to PolyDMDAAC standards) vs. % initiator for 90/10 wt% AM/DMDAAC copolymers.

© 2004 by Marcel Dekker, Inc.

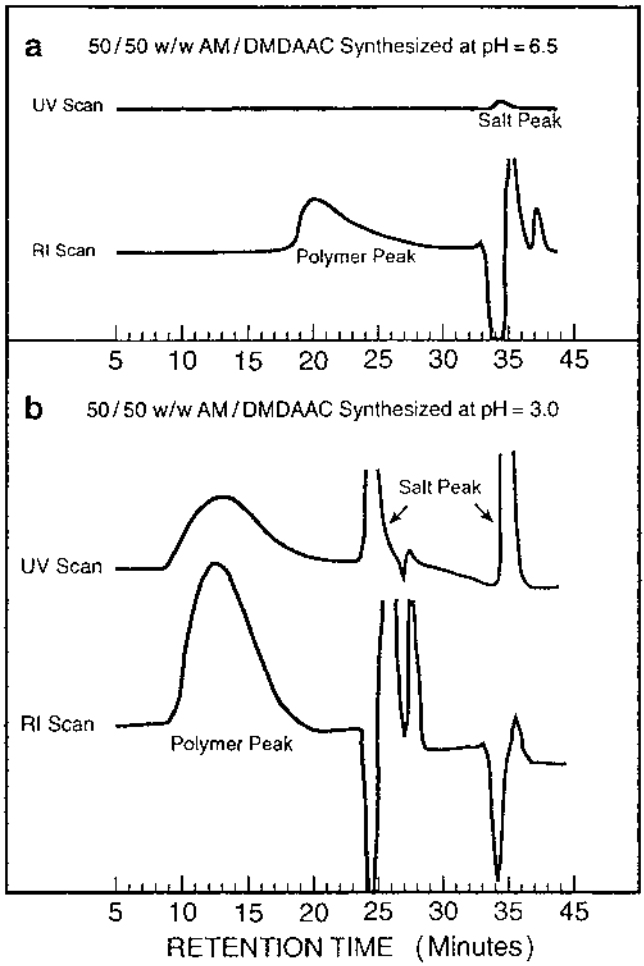

Figure 11 Size exclusion chromatograms (raw data) of dansyldiallylamine tagged 50/50 wt% AM/DMDAAC copolymers.

the dansyldiallylamine has been incorporated evenly throughout the entire copolymer chain.

4.2.3 Studying Formulation of Polymer Blends

In Figure 12, chromatogram (a) is a blend of 90/10 w/w AM/AA copolymer and epichlorohydrin polyamine. The composition determined by NMR spectroscopy for this polymer blend is 65/35 wt% copolymer/polyamine. Based on

© 2004 by Marcel Dekker, Inc.

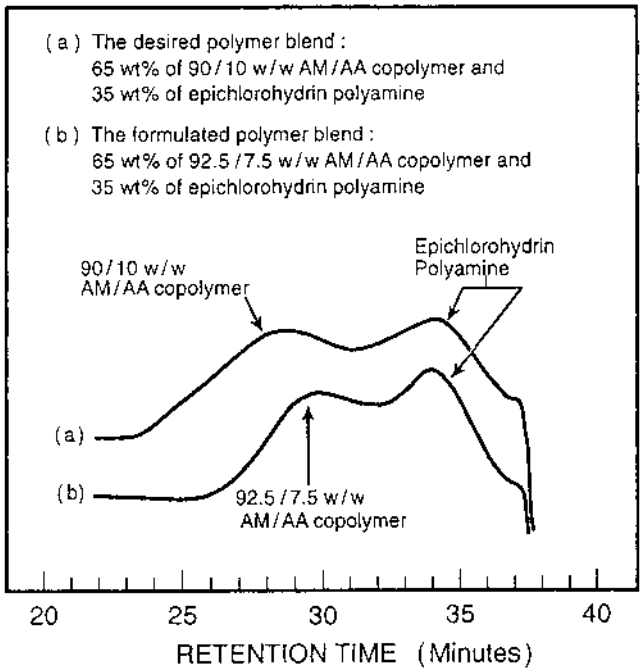

Figure 12 Size exclusion chromatograms of polymer blends.

this information, the higher MW peak is AM/AA copolymer and the lower MW peak is polyamine. Chromatogram (b) is a formulated blend of 92.5/7.5 wt% AM/AA copolymer and polyamine. In a comparison of the two chromatograms, the molecular size of the copolymer in the formulated blend is found not to be as large as the molecular size of the copolymer in the desired blend. In industrial applications, these two polymer blends may behave differently. The area ratio of two overlapping chromatographic peaks can be more easily determined by using a deconvolution technique reported by Vaidya and Hester (61).

5 CONCLUSIONS

SEC is a very powerful tool for characterizing polymers and studying the relationship of their various properties and performances in industrial applications. Additionally, the SEC technique demonstrates the capability for guiding process development in polymer synthesis and studying the kinetics of a chemical

© 2004 by Marcel Dekker, Inc.

reaction. The combination of SEC and NMR techniques is especially useful for studying the formulation of polymer blends and the degradation of polymers. However, the high-molecular-weight ($\overline{M}_w > 5 \times 10^6$ g/mole) acrylamide polymers are difficult to separate efficiently by the commercially available columns at the present time. The chromatographic systems, sample preparation, characterization of MW standards, and calibration technique affect SEC MW and MWD determination. Therefore, values obtained for SEC MW and MWD should be interpreted carefully.

References 62–85 have been added since the publication of the first edition of this book.

6 ACKNOWLEDGEMENT

The author expresses her appreciation to Calgon Corporation for its permission to publish this article and for its support on all research work.

APPENDIX: SEC EXPERIMENTAL CONDITIONS

Polymer	Column	Mobile phase	Comments	Chapter/ reference
Polyacrylamide	Controlled-porosity glass (CPG-10) Mean pore diameter: 3000, 3000, 2000, 1000, and 729 Å Column size = 4 ft × 3/8 in. ID	Aqueous solution Contains Na_2SO_4 (ionic strength = 0.25), 0.025 g/L polyethylene oxide, 1.5 g/24 L Tergitol, 2.5% CH_3OH, pH = 7.0	RI detector	32
Polyacrylamide	Controlled-porosity glass Mean pore diameter: 3125, 486, 255, and 75 Å Column size = 4 ft × 3/8 in. ID	Formamide with 10^{-1} M to 5×10^{-3} M KCl	RI detector	33

© 2004 by Marcel Dekker, Inc.

Appendix (*Continued*)

Polymer	Column	Mobile phase	Comments	Chapter/ reference
Polyacrylamide	Controlled-porosity glass Mean pore diameter: 3125, 2000, 973, 493, 240, and 123 Å Column size = 4 ft × 3/8 in ID	Aqueous solution with 0.005 M KCl	RI detector	34
Polyacrylamide Acrylamide/ sodium acrylate copolymer Dextrans, polystyrene sulfonated	Controlled-porosity glass Mean pore diameter: 16.4–300 nm Column size: 620 mm long 7 mm ID	Aqueous solution with 0.1 M Na_2SO_4, which contained 10 ppm biocide Kathon WT	RI detector Cubic B-spline calibration technique	35
Polyacrylamide Polyethylene oxide Polyvinyl alcohol Hydroxyethyl cellulose	Polyvinyl-pyrrolidone (PVP)-coated silica Mean pore diameter: 100, 500, 1000, and 4000 Å Column size: 30 cm length 48 mm ID	Water	RI detector Universal calibration	36
Hydrolysed polyacryl-amide, 26/74 mole % Acrylate/ acrylamide copolymer	Wet-packed Sephacryl S 1000 superfine (Pharmacia Fine Chemicals) Column size: 2.6 cm diameter 70 cm or 100 cm bed height	Aqueous solution with 1 M NaCl	Collected fractions and analysed by LALLS. Determined diffusion coefficients by photon correlation light scattering	39
Cellulose acetate-grafted acrylamide copolymer	CPG-10 Mean pore diameter: 2023, 1223, 723, 129 Å Column size: 90 cm × 9 mm ID	Water	RI and UV detectors	37

© 2004 by Marcel Dekker, Inc.

Appendix (*Continued*)

Polymer	Column	Mobile phase	Comments	Chapter/ reference
Dextran-grafted acrylamide copolymer	Porous glass Mean pore diameter: 3000, 1400, 700, 350, 240, 170 Å Column size: 60 × 0.762 cm ID	Aqueous solution with 0.05 M potassium biphthalate	RI detector	38
Polyacrylamide CPG-10 2000 Å	Bio glass 2500 Å, 125/240/370 Å Porasil DN 400/800 Å Porasil CX 200/400 Å	Water	RI detector	41
Polyacrylamide	Dry-packed controlled porosity glass Mean pore diameter: 700, 1000, and 3000 Å Particle size: 200/400 mesh Column size: 3.8 in. ID 4–6.5 ft long	Aqueous solution with 0.2 M Na_2SO_4 + 1 g/25 L Tergital NPX (Union Carbide Corp.)	DRI/LALLS dual detectors	47
Polyacrylamide hydrolysed polyacryl-amide Acrylamide/ acrylic acid copolymers	TSK columns: Guard + G6000 PWXL + G5000 PWXL + G4000 PWXL + G3000 PWXL	Aqueous solution with 0.3 M NaCl + 0.1 M KH_2PO_4 adjusted pH = 7.0 by 50/50 w/w NaOH	RI/LALLS dual detectors	44
Polyacrylamide Acrylamide/ dimethyl diallyl-ammonium chloride copolymers	TSK columns: Guard + G6000 PW + G5000 PW + G3000 PW	Aqueous solution with 0.3 M Na_2SO_4 + 1% acetic acid pH = 3.1	RI/LALLS dual detectors	44
Polyacrylamide	Shodex OH-Pak or Ultrahydrogel	Pure water or 0.5 M $LiNO_3$ aqueous solution	LALLS/ Viscometer/ RI triple detectors	46

© 2004 by Marcel Dekker, Inc.

Appendix (*Continued*)

Polymer	Column	Mobile phase	Comments	Chapter/ reference
Methacryloxy-ethyl trimethyl-ammonium chloride/AM copolymer, diallyl dimethyl ammonium chloride copolymer	TSK PWH guard column + TSK PWXL mixed-bed column	0.24 M aqueous sodium formate pH 3.7	RI	40

REFERENCES

1. Acrylamide polymers. In: Encyclopedia of Science and Technology. 1st ed., Vol. 1. New York. Interscience Publishers, 1964, pp. 177–197, and references therein by WM Thomas, American Cyanamid Company.
2. Acrylamide polymers. In: Encyclopedia of Science and Engineering, 2nd ed., Vol. 1. New York: John Wiley & Sons, 1985, pp 169–211, and references therein by WM Thomas, American Cyanamid Company.
3. DN Schulz. Kinetic and Practical Aspects of Water Soluble Polymer Synthesis. Water Soluble Short Course sponsored by The University of Southern Mississippi, Dept of Polymer Science, February 24–25, 1992.
4. RAM Thomson. Methods of polymerization for preparation of water soluble polymer. In: CA Finch, ed. Chemistry and Technology for Water Soluble Polymer. New York: Plenum, 1983, pp 31–70.
5. NM Bikales. Water soluble polymers. In: NM Bikales, ed. Polymer Science and Technology. Vol. 2. New York: Plenum, 1973, pp 213–225.
6. N Yoshida, Y Ogana, R Handa. U.S. Patent 4,306,045. Assigned to Nitto Chemical Company, Dec. 15, 1981.
7. K Plochoka. J Makromol Sci Rev Macromol Chem C20(1):67, 1981.
8. KY Park, ER Santee, HJ Harwood. ACS Polym Prepr 27(2):81, 1986.
9. U.S. Patent 4,022,731, May 10, 1977. Assigned to American Cyanamide Company.
10. U.S. Patents 3,624,019, Rc28,474, July 8, 1974. Assigned to Nalco Chemical Co.
11. DN Schulz, JJ Mauer, J Bock. U.S. Patents 4,463,151 and 4,463,152. Assigned to Exxon, July 31, 1984.
12. WM Kulicke, R Kniewske, J Klein. Prog Polym Sci 8:373, 1982.
13. RH Yocum, EB Nyquist, eds. Functional Monomers, Vol. 1. New York: Marcel Dekker, Inc., 1973, pp 23–52.

© 2004 by Marcel Dekker, Inc.

14. R Schulz, G Renner, H Henglien, W Kern. Makromol Chem 12:20, 1954.
15. WB Crummett, RA Hummell. J Amer Waterworks Ass 55:209, 1963.
16. T Chung-li Shen. Controlled Polymerization of Acrylamide to Produce Copolymers with Unique Solution and Viscosity Properties. PhD Dissertation, University of Southern Mississippi, University of Microfilms International, 1977.
17. Muyen Michael Wu. Polymerization of Acrylamide in Water-In-Oil Microemulsion. PhD Dissertation, University of Akron, University Microfilms International, 1983.
18. RAM Thomson. A kinetic study of the adiabatic polymerization of acrylamide. J Chem Educ 63(4):362–364, 1986.
19. T Ishige, AE Hamielec. J Appl Poly Sci 17:1479–1506, 1973.
20. W-C. Hsu, C-Y Chen, J-F Kuo, EM Wu. Polymer 35(4):849–856, 1994.
21. FA Adamsky, EJ Beckman. Inverse emulsion poymerization of acrylamide in supercritical carbon dioxide. Macromolecules 27(1):312–314, 1994.
22. YL Meltzer. Water-Soluble Resins and Polymers Technology and Applications. New Jersey: Moyes Data Corp., 1976, pp 14–44.
23. JA Caskey. The Effect of Polyacrylamide Molecular Structure on Flocculation Activity of Domestic Sewage. Final report to National Science Foundation Thermodynamic and Mass Transfer Division of Engineering for Research Grant, July 15, 1977.
24. W Yau, J Kikland, D Bly. Modern Size Exclusion Chromatography. New York: John Wile & Sons, 1979.
25. HG Barth. J Chrom Science 18:409–429, 1980.
26. O Chiantore, M Guaita. J Liq Chrom 9:1867–1885, 1984.
27. M Song, G Hu. J Liq Chrom 8(14):2543–2556, 1985.
28. M Song, G Hu. J Liq Chrom 11(2):363–381, 1988.
29. S Pokorny, J Zábranský, M Bleha. J Liq Chrom 7(9):1887–1901, 1984.
30. HG Barth, FJ Carlin, Jr. J Liq Chrom 7(9):17, 1984.
31. JC Giddings. Adv Chromatogr 20:217–258, 1982.
32. SNE Omorodion, AE Hamielec, JL Brash. ACS Symp Ser 138, Size Exclusion Chromatography (GPC) 267–284, 1980.
33. N Onda, K Furusawa, N Yamaguchi, S Komuro. J Appl Poly Sci 23:3631–3638, 1979.
34. N Onda, K Furusawa, N Yamaguchi, M Tokiwa, Y Hirai. J Appl Poly Sci 25:2363–2372, 1980.
35. J Klein, A Westerkamp. J Poly Sci, Poly Chem Edn 19:707–718, 1981.
36. L Letot, J Lesec, C Duivoron. J Liq Chrom 4(8):1311–1322, 1981.
37. NI El-Awady, NA Ghanem, WB Pedersen, K Singer. Eur Polym J 15:1017–1024, 1979.
38. C McCormick, L Park. J Appl Poly Sci 26:1705–1717, 1981.
39. G Muller, C Yonnet. Makromol Chem, Rapid Commun 5:197–201, 1984.
40. Shyhchang S Huang. J Chrom 536:203–209, 1991.
41. AH Abdel-Alim, A Hamielec. J Appl Poly Sci 18:297–300, 1974.
42. TV Alfredson, CT Wehr, L Tallman, F Klink. J Liq Chrom 5(3): 489–524, 1982.
43. H Sasaki, T Matsuda, O Ishikawa, T Takamatsu, K Tanaka, Y Kato, T Hashimoto Scientific Report of Toyo Soda Manufacturing Company, Ltd 29(1):37–54, 1985.
44. FC Lin, GD Getman. Internal GPC Symposium'87, Millipore Corp., pp 225–245, 1984.
45. KK Dhowa Denko. Shodex application data on Shodex aqueous GPC columns.

© 2004 by Marcel Dekker, Inc.

46. CJ Kim, A Hamielec, A Bendek. J Liq Chromatog 5(7):1277–1294, 1982.
47. J Lesec, G Volet. Internal GPC Symposium'89, Millipore Corp., pp 386–405, 1989.
48. K Min, C Cha. Technical Report, Calgon Corporation, 1981.
49. W Rand, A Mukerji. J Liq Chromatog 5(5):841–851, 1982.
50. CE Lundy, RD Hester. J Liq Chrom 7(10):1911–1934, 1984.
51. CE Lundy, RD Hester. J Poly Sci, Part A, Polym Chem 24:1829–1839, 1986.
52. SA Chen, HC Hu. J Poly Sci, Polym Chem 21:3373–3380, 1983.
53. MA Langhorst, FW Stanley, Jr, SS Cutie, JH Sugarman, LR Wilson, DA Hoagland, RK Prud'homme. Anal Chem 58(11):2242–2247, 1986.
54. EE Remsen, JJ Freeman. Appl Spectroscopy, 45(5):868–873, 1991.
55. ThG Scholte. Techniques and Methods of Polymer Evaluation, Vol. 4. New York: Marcel Dekker Inc., 1975, pp 542–547.
56. MB Huglin. Determination of molecular weight by light scattering. In: Top Curr Chem 77 (Inorg Phys Chem). New York: Springer-Verlag, 1979, pp 155–208.
57. J Stejskal, J Horska. Makromol Chem 183:2527–2535, 1982.
58. KK Chee. J Appl Poly Sci 34:891–899, 1987.
59. D Lecacheux, J Lesec, C Quivoron. J Liq Chrom 5(2):217–228, 1982.
60. A Bose, J Rollings, J Caruthers, M Okos, G Tsao. J Appl Poly Sci. 27:795–810, 1982.
61. RA Vaidya, RD Hester. J Chrom 287:231–244, 1984.
62. K Furusawa, N Onda, N Yamaguchi. Chem Lett 3:313–314, 1978.
63. CL McCormick, RD Hester, HH Neidlinger, GC Wildman. Surf. Phenom. Enhanced Oil Recovery [Proc. Symp.], 1981, pp 741–742.
64. R Brian, JV Dawkins. Eur Polym J 20(2):129–133, 1984.
65. G Muller, C Yonnet. Makromol Chem, Rapid Commun 5(4):197–201, 1984.
66. W Ling, P Shi, Z Xu, W Chen. Zhongnan Kuangye Xuebao 1:103–108, 1985.
67. CG Overberger, W Ferng, Minn Shong Chi. J Polym Sci, Part A, Polym Chem 24(12):3365–3379, 1986.
68. R Nielson. International GPC Symposium'87, Millipore Corp., 1987, p 455.
69. KJ McCarthy, CW Burkhardt, DP Parazak. J Appl Polym Sci 33(5):1699–1714, 1987.
70. J Lesec, G Volet. J Appl Polym Sci, Appl Polym Sci 45 (Polym Anal Charact 2):177–189, 1990.
71. W-M Kulicke, A Jacobs. Makromol Chem, Macromol, Symp 61:59–74, 1992.
72. Shigeki Ono, Kobunshi Ronbunshu, 49(5), 467–9 (1992).
73. SC De Vos, M Moeller. Makromol Chem, Macromol Symp 75:223–229, 1993.
74. Meiling Ye, Dong Han, Lianghe Shi, Lin Li, Yi Liu. Sepu 13(1):15–20, 1995.
75. Tianru Fang, Jiahang Wang, Zheng Fang, Peiyan Liu. Chinese J Poly Sci 13(3):244–251, 1995.
76. Qicong Ying, Guangwei Wu, B Chu, R Farinato, L Jackson. Macromolecules 29(13):4646–4654, 1996.
77. EF Lucas, CX Silva, GS Pereira. Polym Bull (Berlin) 39(1):73–78, 1997.
78. Fu-mei C Lin. 38th Experimental Nuclear Magnetic Resonance Conference (ENC), Poster 148, p 113, 1997.
79. T Osaki. Fukuoka Kogyo Daigaku Erekutoronikusu Kenkyusho Shoho 16:55–58, 1999.
80. R Hecker, PD Fawell, A Jefferson, JB Farrow. J Chrom A 837:139–151, 1999.
81. Zhidong Guuo, Hongguang Huang. Fenxi Huaxue 28(10):1314, 2000.

© 2004 by Marcel Dekker, Inc.

82. M Bednarek, T Biedron, P Kubisa. Centrum Badan Molekularnych Makromoleularnych PAN, Lodz, Pol. Polimery (Warsaw) 45(10):664–673, 2000.
83. KA Klimchuk, S Lowen. J Poly Sci, Part A, Poly Chem 38(17):3128–3145, 2000.
84. KA Klimchuk, MB Hocking, S Lowen. J Poly Sci, Part A, Poly Chem 38(17):3146–3160, 2000.
85. MB Hocking, KA Klimchuk, S Lowen. J Polym Sci Part A Polym Chem 39(12):1960–1977, 2001.

© 2004 by Marcel Dekker, Inc.

10
Size Exclusion Chromatography of Polyvinyl Alcohol and Polyvinyl Acetate

Dennis J. Nagy
Air Products and Chemicals, Inc.
Allentown, Pennsylvania, U.S.A.

1 INTRODUCTION

Polyvinyl alcohol (PVA) and polyvinyl acetate (PVAc) share a common link, since PVAc is the precursor used in the synthesis of PVA. Over 2 billion pounds of vinyl acetate monomer are produced annually in the United States alone and most of this is used for synthesizing PVAc homopolymer and copolymers. These polymers are used in paints, adhesives, coatings, nonwoven fabrics, and some food products (1). PVA is the world's largest volume synthetic, water-soluble polymer. It is commercially produced via a continuous process from the hydrolysis of PVAc, usually in methanol, and is available in a wide range of molecular weights. The degree or extent of hydrolysis can be carefully controlled, yielding partially acetylated PVA copolymers. The two most common types are fully hydrolyzed PVA (98 mole%) and partially hydrolyzed PVA (88 mole%). Intermediate hydrolysis grades of PVA are also available. PVA is used in a wide range of applications because of its excellent physical properties, to include adhesives,

© 2004 by Marcel Dekker, Inc.

fibers, textile and paper sizing, emulsion polymerization, and the production of polyvinyl butyral. It is also used in joint cements for building construction and water-soluble packaging for herbicides, pesticides, and fertilizers (2).

PVA and PVAc are sold to various markets based on molecular weight. Physical properties and end uses are both strongly governed by molecular weight and molecular weight distribution. For example, the molecular weight of PVA has a direct influence on solution viscosity, tensile strength, block resistance, water and solvent resistance, adhesive strength, and dispersing power. Size exclusion chromatography (SEC) has proven to be a very reliable method over the years for characterizing the molecular weight distribution of both PVA and PVAc. Aqueous SEC coupled to on-line, differential viscometry (DV) and/or multi-angle laser light scattering (MALLS) has been successfully used for PVA for several years (1–4). Characterization of the molecular weight distribution, intrinsic viscosity, roots-mean-square radius, and solution conformation are possible using these techniques. PVAc is usually characterized using tetrahydrofuran (THF), although other solvents such as trichlorobenzene (TCB) can be used.

The characterization of PVA and other types of water-soluble polymers by SEC has closely followed the advances in column and detection technology since the 1960s. Aqueous SEC can often be more challenging than the analysis of polymers such as PVAc under organic-based, solvent conditions. Several mechanisms that compete with the size exclusion process, can easily complicate the characterization process in aqueous SEC. These include such phenomena as ion exchange, ion inclusion, adsorption, and viscous "fingering." Ideally, one wants only the size exclusion as the operable mechanism when characterizing PVA for molecular weight distribution. The composition of the mobile phase must be carefully chosen to prevent enthalpic interactions between polymer and packing. Because partially hydrolyzed PVA is, in essence, a copolymer of vinyl alcohol and vinyl acetate, hydrophobic forces as well as hydrogen bonding can lead to adsorption. The presence of the hydrophobic acetate functionality along the polymer chain can contribute to secondary effects such as interaction between the polymer and column packing material. Thus, mobile phase composition and column chemistry play an important role in the utilization of an effective SEC process for polymer separation (4,5).

In addition to competing, nonsize exclusion effects, the detection system used in aqueous SEC can also present additional challenges. On-line, differential viscometry detection requires the use of polymer standards and the obeyance of universal calibration for the determination of molecular weights. Multi-angle laser light scattering (MALLS) requires a particulate-free mobile phase to eliminate excessive background scatter. Prior knowledge of the specific refractive index increment of the polymer under the conditions of analysis is also required for these types of light scattering measurements.

© 2004 by Marcel Dekker, Inc.

A relatively new technique utilizing a triple detection system (TDS) has been combined with SEC to provide even more information about polymer structure. TDS utilizes a concentration detector, a viscometry detector, and a right-angle laser light scattering detector. Adding TDS to SEC provides one with a three-dimensional approach to molecular characterization. The first dimension is the size exclusion, chromatographic process which separates PVA according to molecular size. A differential refractometer index (DRI) detector is commonly used to measure polymer concentration as a function of elution time. The second is light-scattering detection, which determines absolute molecular weight data. The third dimension comes from the viscometer, which measures intrinsic viscosity. Using TDS, all of these together provide a detailed picture of molecular structure. The use of a triple detection system (TDS), sometimes referred to as SEC^3, provides the capability to simultaneously capture absolute molecular weight, intrinsic viscosity, radius of gyration, and conformational information. In addition, Mark–Houwink constants can also be determined using TDS.

The original work described in the *Handbook of Size Exclusion Chromatography* for PVA and PVAc was carried out prior to 1995. This chapter will highlight and review some of the recent advances in SEC characterization of PVA and PVAc. The emphasis will be on the use of SEC interfaced to TDS for both polymers.

2 RECENT ADVANCES FOR CHARACTERIZATION OF PVA

Since 1995, aqueous SEC coupled to multi-angle laser light scattering (MALLS), differential viscometry detection, and TDS have been major areas of investigation. In addition, characterization of PVA using thermal field-flow fractionation (TFFF) and reverse phase, gradient liquid chromatography for hydrolysis distribution have been reported (6,7). A brief review of the theory behind TDS follows.

2.1 SEC Triple Detection

The use of TDS with aqueous SEC provides the capability to simultaneously capture absolute molecular weight, intrinsic viscosity, and conformational information about PVA. In addition, Mark–Houwink constants can also be determined using TDS. TDS utilizes three modes for simultaneous detection. The differential refractometer provides a signal, Y_i, which is proportional to concentration of polymer as it elutes from the SEC column:

$$Y_i = K_{ri}\left(\frac{dn}{dc}\right)c_i$$

© 2004 by Marcel Dekker, Inc.

where for species i, K_{ri} = refractometer constant, dn/dc = specific refractive index increment, and c_i = concentration. The viscometer provides a signal proportional to the specific viscosity of the sample:

$$\eta_{sp} = \frac{4\Delta P}{(I_p - 2\Delta P)}$$

where η_{sp} is the specific viscosity, ΔP is the differential pressure across the middle of the capillary bridge of the viscometer, and I_p is the inlet pressure. Thus, at every elution increment,

$$\Delta P_i = \frac{1}{2}\left[\frac{\eta_{spi}}{(2 + \eta_{spi})}\right] I_p$$

At the very dilute concentrations used in SEC, the intrinsic viscosity at each increment, $[\eta]_i = \eta_{spi}/c_i$. Thus, the set of data points c_i and $[\eta]_i$ are collected across the entire SEC chromatogram. These dilute concentrations also enable simplification of the basic Rayleigh light scattering equation to:

$$\frac{kc_i}{R(\Theta)_i} = \frac{1}{M_i P(\Theta)}$$

where k is a constant dependent upon wavelength, refractive index, dn/dc, and $R(\Theta)$ is the excess Rayleigh scattering factor (2). The $P(\Theta)$ term approaches unity for molecules having sizes less than $1/20$ of the wavelength of the incident light. In TDS, the hydrodynamic radius of the molecule, R_h is given by:

$$R_h = \left\{\frac{3}{4}\pi\left(\frac{[\eta]M}{0.025}\right)\right\}^{1/3}$$

The radius of gyration, R_g, can be determined from the Flory–Fox and Ptitsyn–Eizner equations (8,9):

$$R_g = \left(\frac{1}{6}\right)^{1/2}\left(\frac{[\eta]M}{\Phi}\right)^{1/3}$$

where,

$$\Phi = 2.55 \times 10^{21}(1 - 2.63\varepsilon + 2.86\varepsilon^2) \text{ and } \varepsilon = (2a - 1)/3$$

© 2004 by Marcel Dekker, Inc.

where a is the exponent of the Mark–Houwink equation,

$$[\eta] = KM^a$$

2.2 Experimental TDS Work for PVA

Figure 1 is a schematic of an experimental setup used by this author for aqueous SEC with a TDS interface. This system also employs a three-angle MALLS detector for the simultaneous capture of data from both TDS and MALLS detection. Table 1 summarizes the specific conditions used. The MALLS photometer (Mini-Dawn from Wyatt Technology, Santa Barbara, California, U.S.A.) is configured in series between the SEC instrument and a DRI detector (Waters Corporation Model 410, Milford, Massachusetts, U.S.A.). The TDS detector (Viscotek Model T60A, Houston, Texas, U.S.A.) is configured in a parallel arrangement with the DRI detector so that the flow is split evenly between the two detectors. The aqueous mobile phase of 0.05 M sodium nitrate was prefiltered through a 0.45 μ membrane (Gelman) to remove any particulates. Data acquisition and processing were carried out using ASTRA version 4.72 software for MALLS and Viscotek TriSEC Version 3.0 software for TDS.

The offset volume between the RI and TDS detector was determined using a poly(ethylene glycol) standard of 22,800 molecular weight. The offset volume

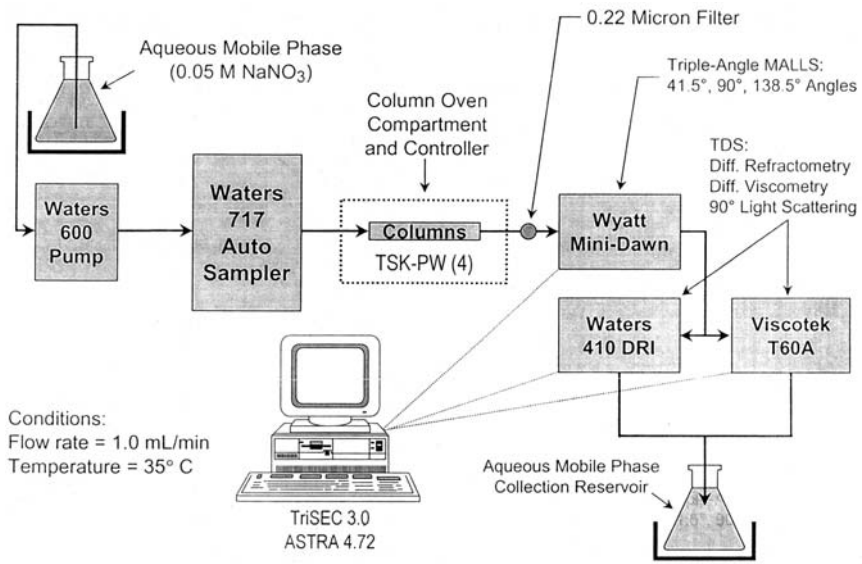

Figure 1 TDS/MALLS experimental setup. (Reprinted from American Laboratory, Vol. 35, 1, Copyright 2003 by International Scientific Communications, Inc.)

© 2004 by Marcel Dekker, Inc.

Table 1 Experimental Summary for TDS/MALLS System

Columns	Toyo Soda, TSK-PW 2000, 3000, 4000, 5000 Å
Refractometer	Waters Model 410
Triple detector	Viscotek Model T60A
MALLS detector	Wyatt Technology Mini-Dawn
Auto sampler	Waters Model 717
Mobile phase	Aqueous solution of 0.05 M sodium nitrate
Flow rate	1.00 mL/min
Temperature	35°C
Injection volume	0.250 mL
Sample concentration	0.20–0.50% by weight

between the DRI and MALLS detectors was determined using a 23,000 molecular weight poly(saccharide) standard from Polymer Laboratories. Airvol® PVA used in this study was supplied by Air Products and Chemicals, Inc., (Allentown, Pennsylvania, U.S.A.). These PVA grades consisted of various molecular weight types in the range from 88 to 99% degree of hydrolysis. The PVA types used are listed in Table 2. Molecular weights are expressed as 4% solution viscosities in water at 20°C. Solutions of PVA were prepared in the aqueous mobile phase by heating to 90°C for 30 minutes.

An overlay of TDS chromatograms for a medium molecular weight, fully hydrolyzed PVA is shown in Fig. 2. The DRI, viscometry, and 90° light-scattering chromatograms all exhibit excellent signal response. These chromatograms represent a fairly typical type of chromatography one obtains for all different molecular weight grades of PVA, including partially hydrolyzed types (10). Figure 3 is an overlay of the MALLS chromatograms from the Mini-Dawn and DRI detectors for the same PVA shown in Fig. 2. All of these chromatograms also exhibit excellent signal response, similar to the TDS chromatograms. Note that the

Table 2 Summary of PVA Types[a]

Partially hydrolyzed (88%)	Fully hydrolyzed (98%)
Super-low (2 cP)	Super-low (3 cP)
Low (5 cP)	Low (7 cP)
Medium–low (13 cP)	Medium (25 cP)
Medium (23 cP)	High (50 cP)
High (40 cP)	

[a]Expressed as 4% solution viscosity in water at 20°C.

© 2004 by Marcel Dekker, Inc.

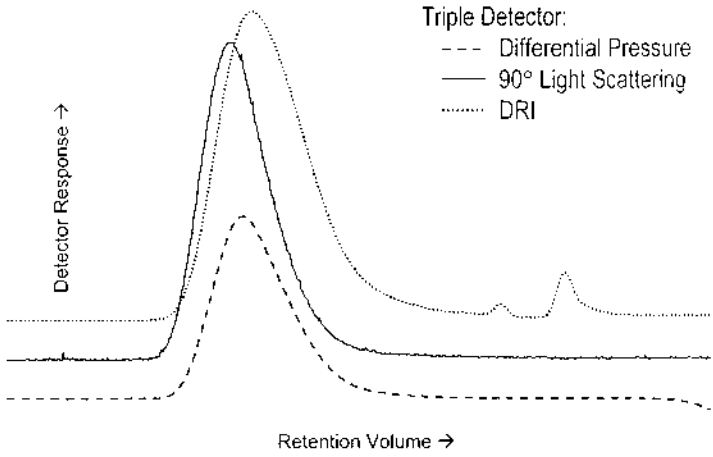

Figure 2 TDS chromatograms for fully hydrolyzed, medium molecular weight PVA. (Reprinted from American Laboratory, Vol. 35, 1, Copyright 2003 by International Scientific Communications, Inc.)

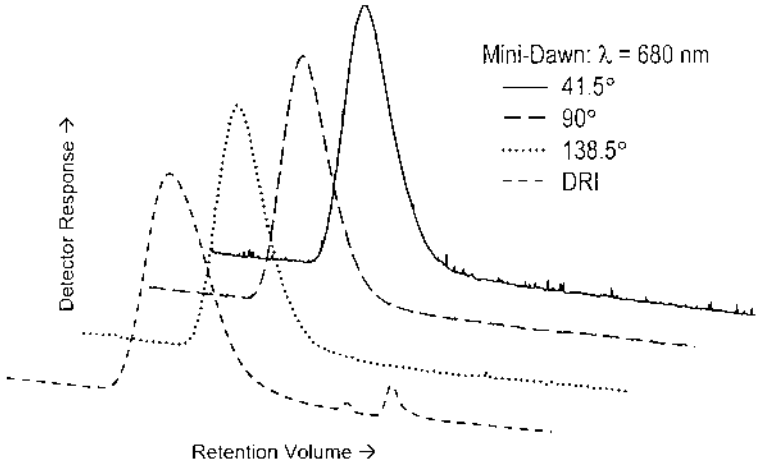

Figure 3 MALLS chromatograms for fully hydrolyzed, medium molecular weight PVA.

lowest angle chromatogram (41.5°) shows slightly more noise than the higher angle chromatograms.

TDS 90° light scattering and viscometry raw chromatograms for a low molecular weight, fully hydrolyzed PVA are shown in Fig. 4. Overlaid with these chromatograms are the molecular weight vs. retention volume and intrinsic

© 2004 by Marcel Dekker, Inc.

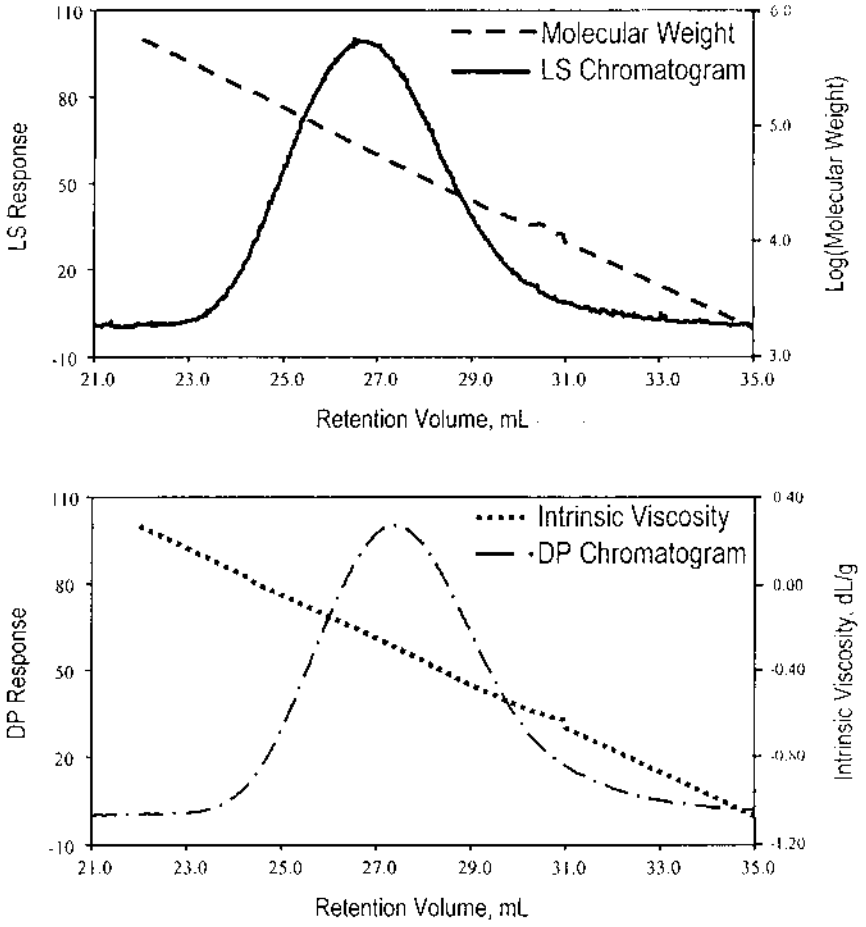

Figure 4 TDS chromatograms for low molecular weight, fully hydrolyzed PVA.

viscosity vs. retention volume curves. As expected, a linear response for both molecular weight and intrinsic viscosity is demonstrated.

A comparison of molecular weight distributions obtained from TDS and MALLS is shown in Figs 5 and 6. Figure 5 overlays the molecular weight distributions for all five partially hydrolyzed grades used in this study. Figure 6 overlays the molecular weight distributions for the four fully hydrolyzed grades. The molecular weight distribution calculations used a specific refractive index (dn/dc) value of 0.143 for partially hydrolyzed PVA and a value of 0.150 for fully hydrolyzed PVA (2). The molecular weight distribution plots determined from TDS compare reasonably well with those from MALLS and the Mini-Dawn.

© 2004 by Marcel Dekker, Inc.

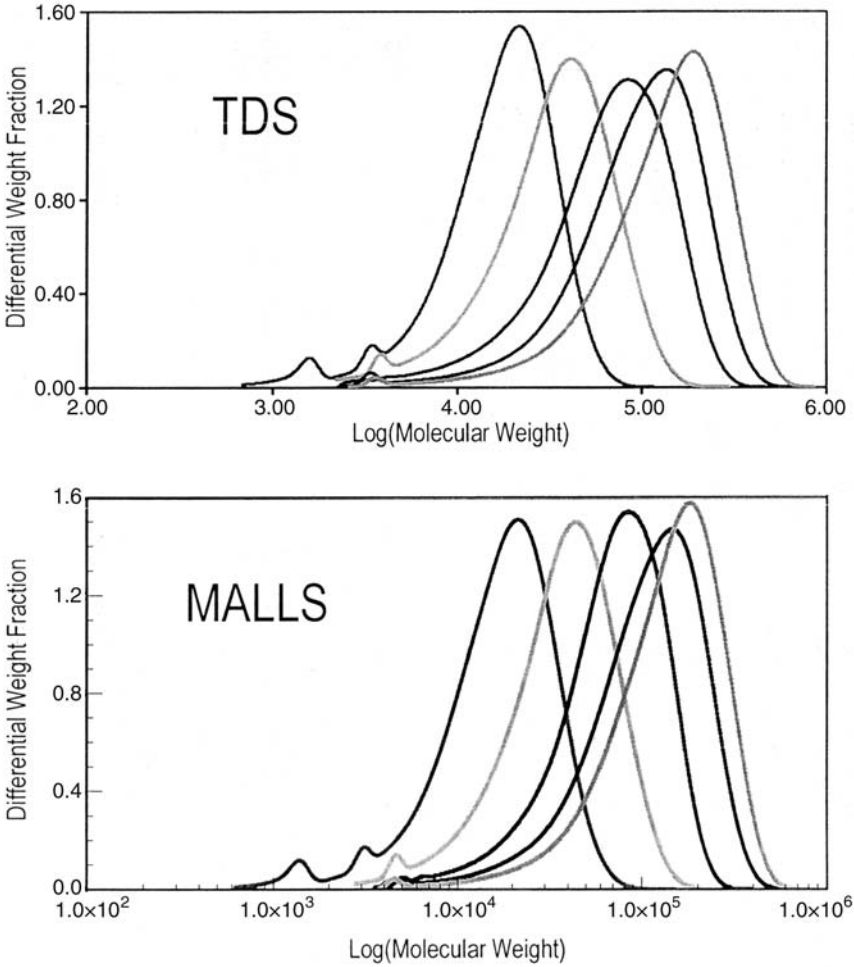

Figure 5 Comparison of molecular weight distributions for partially hydrolyzed PVA, molecular weight order, left to right: super-low, low, medium–low, medium, high.

Molecular weight data from TDS and MALLS data for partially and fully hydrolyzed PVA are summarized in more detail in Table 3 (10). The M_w, M_n, and M_w/M_n data from TDS and MALLS are included, as well as the intrinsic viscosity, and Mark–Houwink K and a values. Overall, the molecular weight and polydispersity values exhibit very good agreement between TDS and MALLS for both partially hydrolyzed and fully hydrolyzed PVA. The average ΔM_w between TDS and MALLS for the partially hydrolyzed grades is 3.6% and the average ΔM_n

© 2004 by Marcel Dekker, Inc.

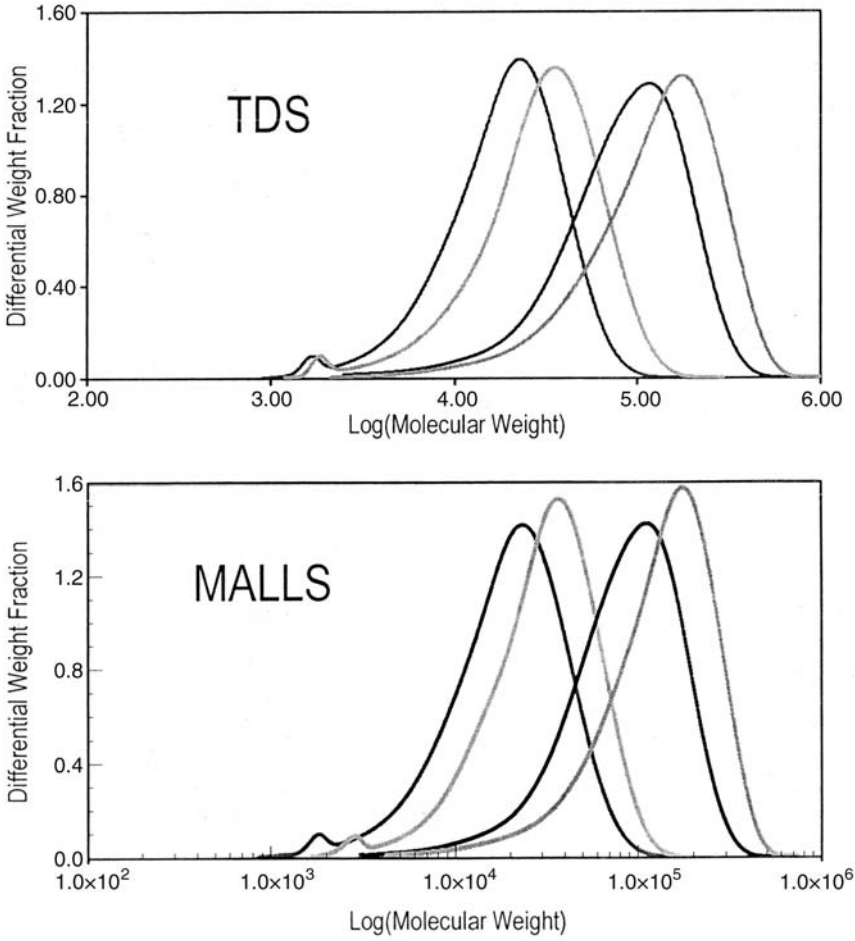

Figure 6 Comparison of molecular weight distributions for fully hydrolyzed PVA, molecular weight order, left to right: super-low, low, medium, high.

between TDS and MALLS is 6.7%. For the fully hydrolyzed grades the average ΔM_w between TDS and MALLS is 4.7% and the average ΔM_n between TDS and MALLS is 4.8%. As expected, the intrinsic viscosity values track closely to the molecular weight.

A comparison of molecular weight data between MALLS and TDS for intermediate hydrolyzed grades of PVA are also summarized in Table 3 (10). These grades of PVA fall in the 92 to 96% hydrolyzed range and are high, medium, and medium–low molecular weight types. A high molecular weight, super-hydrolyzed

© 2004 by Marcel Dekker, Inc.

Table 3 Summary of TDS Molecular Weight Data for PVA[a]

Molecular weight (Hydrolysis %)	M_w	M_n	M_w/M_n	$[\eta]$, dL/g	a	$\log(K)$
Super–low (88%)	20,900	11,900	1.8	0.287	0.645	−3.306
	20,100	**10,700**	1.9			
Low (88%)	43,000	23,900	1.8	0.426	0.631	−3.265
	43,600	**26,200**	1.7			
Medium–low (88%)	85,500	44,800	1.9	0.658	0.602	−3.124
	80,300	**48,400**	1.7			
Medium (88%)	128,000	67,900	1.9	0.833	0.623	−3.238
	127,000	**69,100**	1.8			
High (88%)	173,000	88,900	1.9	1.010	0.624	−3.241
	162,000	**88,700**	1.8			
Super-low (98%)	23,400	13,200	1.8	0.343	0.618	−3.137
	23,900	**13,200**	1.8			
Low (98%)	37,400	19,400	1.9	0.443	0.602	−3.077
	35,800	**21,200**	1.7			
Medium (98%)	110,000	55,900	2.0	0.847	0.605	−3.099
	101,000	**57,300**	1.8			
High (98%)	161,000	76,400	2.1	1.069	0.618	−3.162
	155,000	**86,900**	1.8			
Medium–low (92%)	93,100	44,400	2.0	0.711	0.610	−3.154
	91,900	**49,200**	1.9			
High (92%)	176,000	81,300	2.1	1.062	0.627	−3.240
	169,000	**89,200**	1.9			
Medium (96%)	114,000	53,200	2.1	0.882	0.619	−3.161
	105,000	**56,100**	1.9			
High (99+%)	156,000	79,300	2.0	1.046	0.616	−3.153
	153,000	**83,100**	1.8			

[a]MALLS data expressed in bold.
Source: Reprinted from American Laboratory, Vol. 35, 1, Copyright 2003 by International Scientific Communications, Inc.

PVA grade is also included. As observed for both partially and fully hydrolyzed grades, the agreement between the two techniques is very good. The average ΔM_w between TDS and MALLS is 4.0% and the average ΔM_n between TDS and MALLS is 7.7%.

The Mark–Houwink K and a values are determined directly from the log–log plot of intrinsic viscosity vs. molecular weight. An overlay of these

© 2004 by Marcel Dekker, Inc.

Mark–Houwink plots for the five partially hydrolyzed molecular weight grades of PVA and the four molecular weight grades of fully hydrolyzed PVA are shown in Fig. 7 (10). The curves for the fully hydrolyzed PVAs are super-imposed with little or no variation. The curves for the partially hydrolyzed PVAs show slighter more scatter. This may be due to the presence of some slight secondary effects of

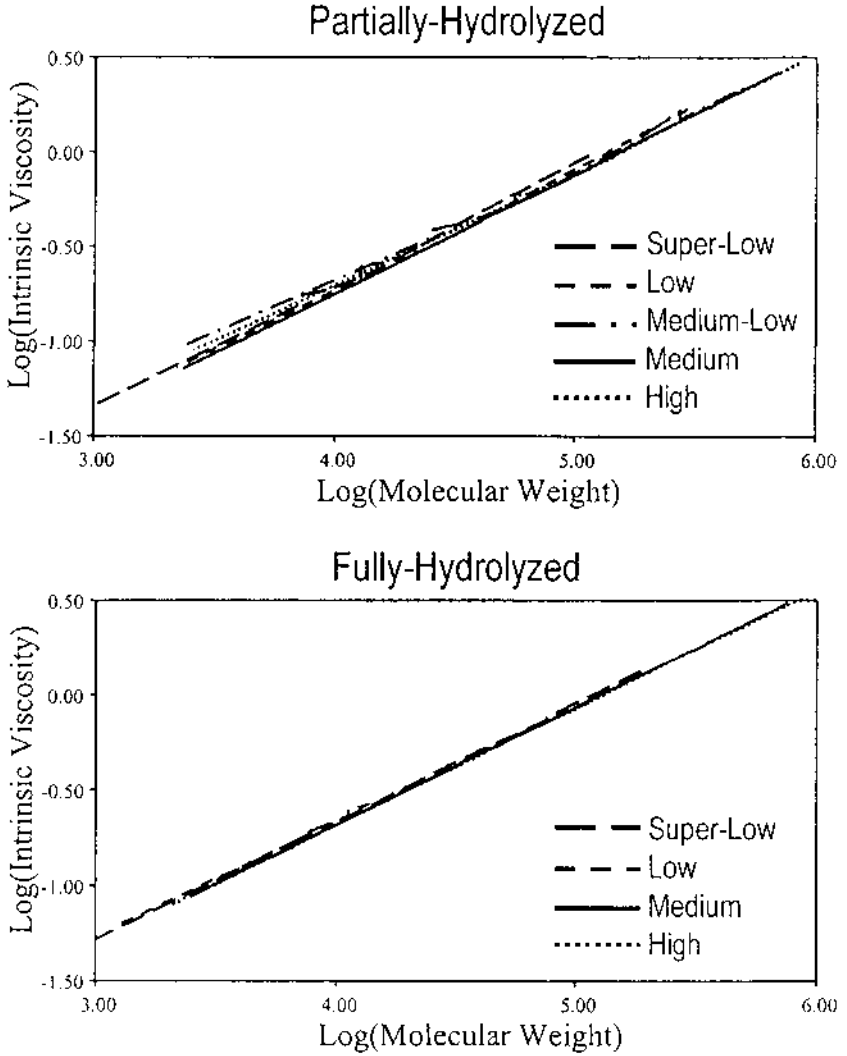

Figure 7 Mark–Houwink plots. (Reprinted from American Laboratory, Vol. 35, 1, Copyright 2003 by International Scientific Communications, Inc.)

© 2004 by Marcel Dekker, Inc.

the partially hydrolyzed PVA with the column packing (1). The Mark–Houwink K and a values calculated from TDS measurements (Table 3) fall within a relatively narrow range (0.602–0.631). Only the super-low, partially hydrolyzed grade exhibits an a value outside that range (0.645). The log(K) values fall in the range −3.124 to −3.265, except for the super-low, partially hydrolyzed PVA grade, which shows log(K) = −3.306. The log(K) and a values appear to be independent of molecular weight and degree of hydrolysis.

Table 4 shows a summary of the average log(K) and a value for partially hydrolyzed and fully hydrolyzed PVA from this study and four other published works (11–14). The values obtained from TDS compare quite favorably to these published values, except for Ref. (11). That work utilized on-line viscometry and universal calibration with aqueous SEC to determine K and a for fully hydrolyzed PVA. The value for a from universal calibration is somewhat lower than that obtained from TDS, 0.560 vs. 0.611. The TDS results may challenge how well universal calibration behavior was in force in the previous study (11).

TDS provides an effective means to measure radius of gyration (R_{gz}) and conformation of PVA. Overlays of the conformation plots (log–log plot of RMS radius vs. molecular weight) for the five partially hydrolyzed molecular weight grades of PVA and the four molecular weight grades of fully hydrolyzed PVA are shown in Fig. 8. As was observed for the Mark–Houwink plots in Fig. 7, the curves for the fully hydrolysed PVAs fall right on top of each other with virtually no variation. The curves for the partially hydrolyzed PVAs show slighter more scatter.

Table 5 summarizes a comparison of R_{gz} values obtained from TDS and MALLS. The MALLS data show both R_{gz} values from the Mini–Dawn triple-angle detection and the Wyatt Technology Dawn-F multi-angle detection. The Dawn-F data are from Ref. 2. Over the full range of molecular weights used for both partially and fully hydrolyzed PVA, the R_{gz} values range from 6.5 to 20.4 nm.

Table 4 Summary of Mark–Houwink Constants for PVA

PVA type	a	log(K)
Partially hydrolyzed		
This study	0.625	−3.325
Fully hydrolyzed		
This study	0.611	−3.119
Ref. 11	0.560	−2.875
Ref. 12	0.61	−3.161
Ref. 13	0.62	−3.052
Ref. 14	0.64	−3.125

© 2004 by Marcel Dekker, Inc.

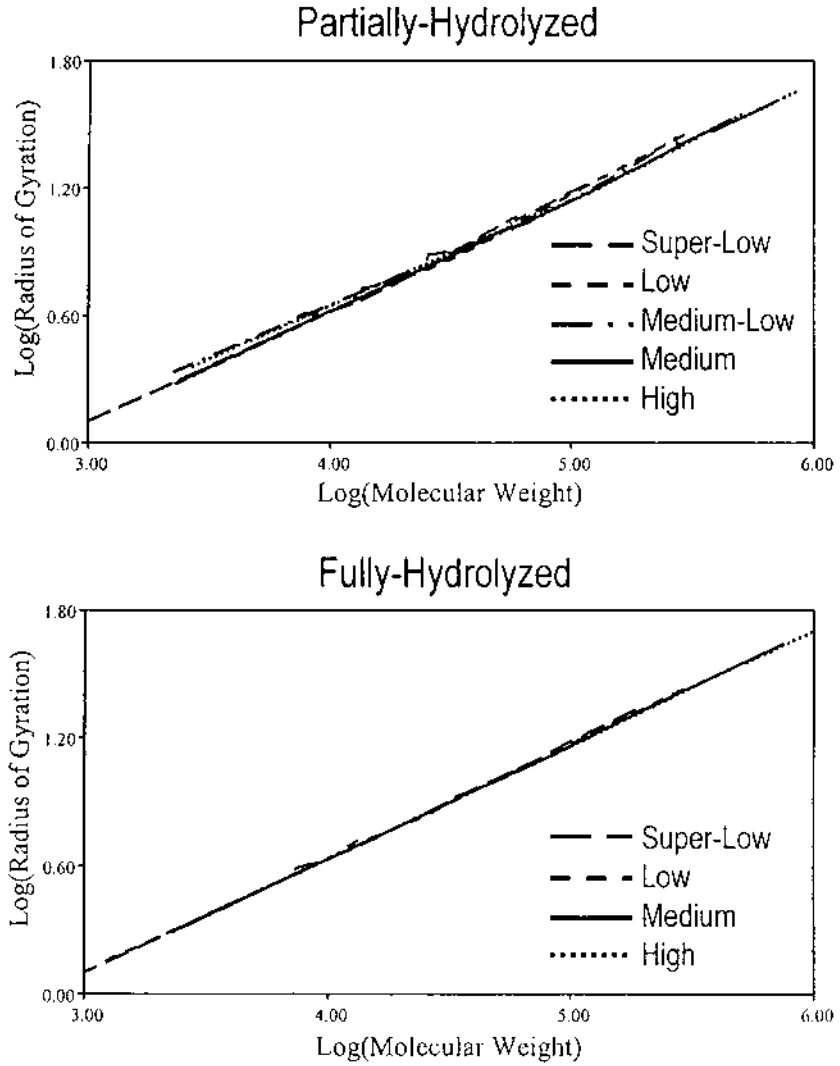

Figure 8 Conformation plots.

There does not appear to be any significant change with R_{gz} based on the degree of hydrolysis. For example, medium molecular weight grades of 88, 96 and 98% degree of hydrolysis exhibit R_{gz} values of 16.9, 16.7, and 16.3 nm, respectively. High molecular weight grades of 88, 92, 98, and 99% degree of hydrolysis exhibit R_{gz} values of 19.9, 20.4, 20.0, and 19.5 nm, respectively. The same is true for the

© 2004 by Marcel Dekker, Inc.

Table 5 Summary of Conformation and R_g Data for PVA

PVA type/Mol. wt.	TDS[a] α	TDS[a] R_{gz} (nm)	Mini-Dawn R_{gz} (nm)	Dawn-F (Ref. 2) R_{gz} (nm)
88%				
Super-low	0.550	6.5		
Low	0.541	9.5		11.7
Medium–low	0.546	13.8	15.4	
Medium	0.554	16.9	25.8	17.1
High	0.554	19.9	21.6	21.6
98%				
Super-low	0.536	7.1		6.8
Low	0.532	9.1		7.7
Medium	0.540	16.3	17.7	16.1
High	0.553	20.0	26.4	19.4
92% Medium–low	0.549	14.5	17.7	
92% High	0.555	20.4	29.0	
96% Medium	0.553	16.7	12.4	
99% High	0.554	19.5	33.8	

[a]TDS data from Ref. 10.

super-low, low, and medium–low molecular weight grades of PVA. The R_{gz} values obtained from TDS compare more favorably to those obtained using the Dawn-F. The agreement is not as good using the Mini-Dawn. This may well be a consequence of using only three detection angles with the Mini-Dawn vs. 12 to 15 angles with the Dawn-F.

Also included in Table 5, are the conformational α values obtained from TDS. The α value is virtually constant over the entire range of PVA molecular weights and degrees of hydrolysis (0.536 to 0.555). These α values confirm that under these conditions, PVA exhibits characteristics very close to that of a random-coil polymer in a good solvent. Previous work using only Dawn-F MALLS detection measured $\alpha = 0.48$ for partially hydrolyzed PVA and $\alpha = 050$ for fully hydrolyzed PVA (2). Values from TDS appear to be slightly larger than those from the Dawn-F MALLS measurements.

Figure 9 shows the molecular weight distribution, Mark–Houwink plot, and conformation plot for a broad distribution PVA with a 92% degree of hydrolysis. This PVA is produced via a batch process of PVAc followed by subsequent hydrolysis, as opposed to the more traditional continuous polymerization of PVAc. This results in a broader molecular weight distribution with a polydispersity index of 3.4. Molecular weight values from TDS and MALLS compare favorably (Fig. 10). The calculated Mark–Houwink values for this particular PVA are

© 2004 by Marcel Dekker, Inc.

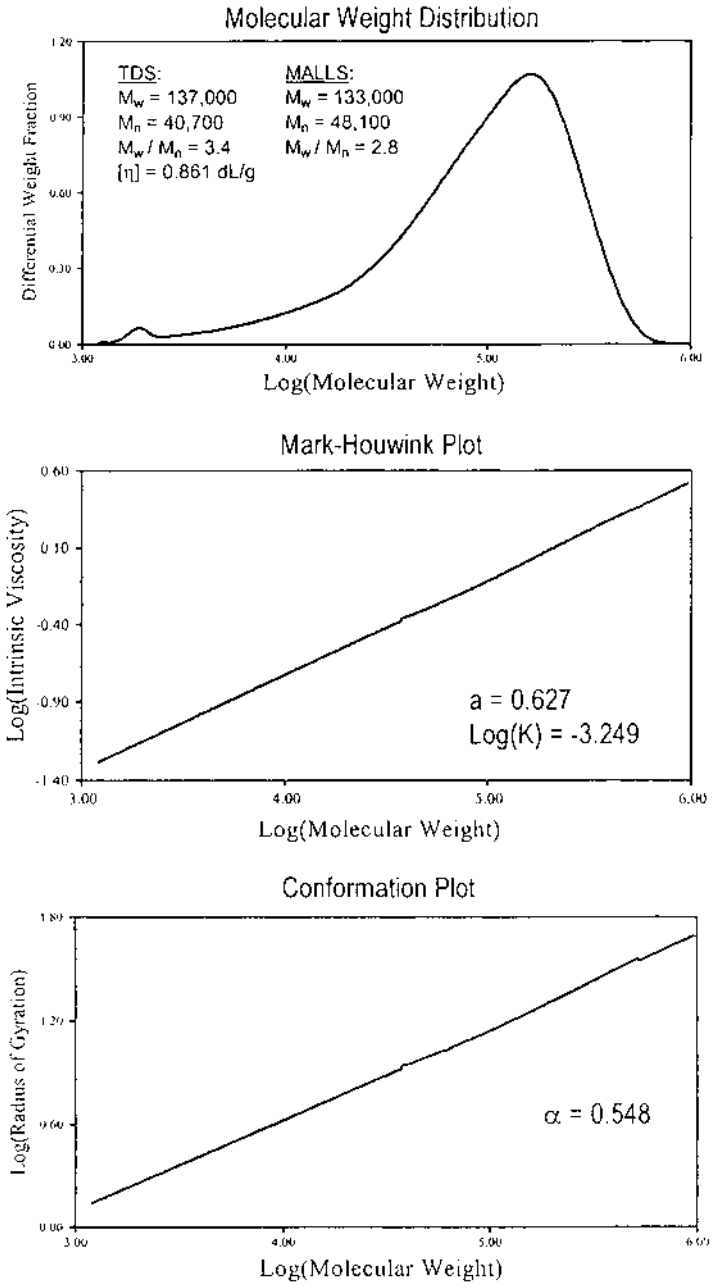

Figure 9 Broad distribution PVA, 92% hydrolyzed, from TDS.

© 2004 by Marcel Dekker, Inc.

$a = 0.627$ and $\log(K) = -3.249$. These are consistent with the values for partially and fully hydrolysed PVA summarized in Table 3.

TDS can be a valuable tool for examining the presence of gel material within a PVA sample. Figure 10 shows TDS chromatograms and the corresponding molecular weight distribution for PVA obtained from the aqueous fraction of a PVAc emulsion (10). Partially hydrolyzed PVA is often used as a protective colloid in the emulsion polymerization of poly(vinyl acetate) homopolymer and

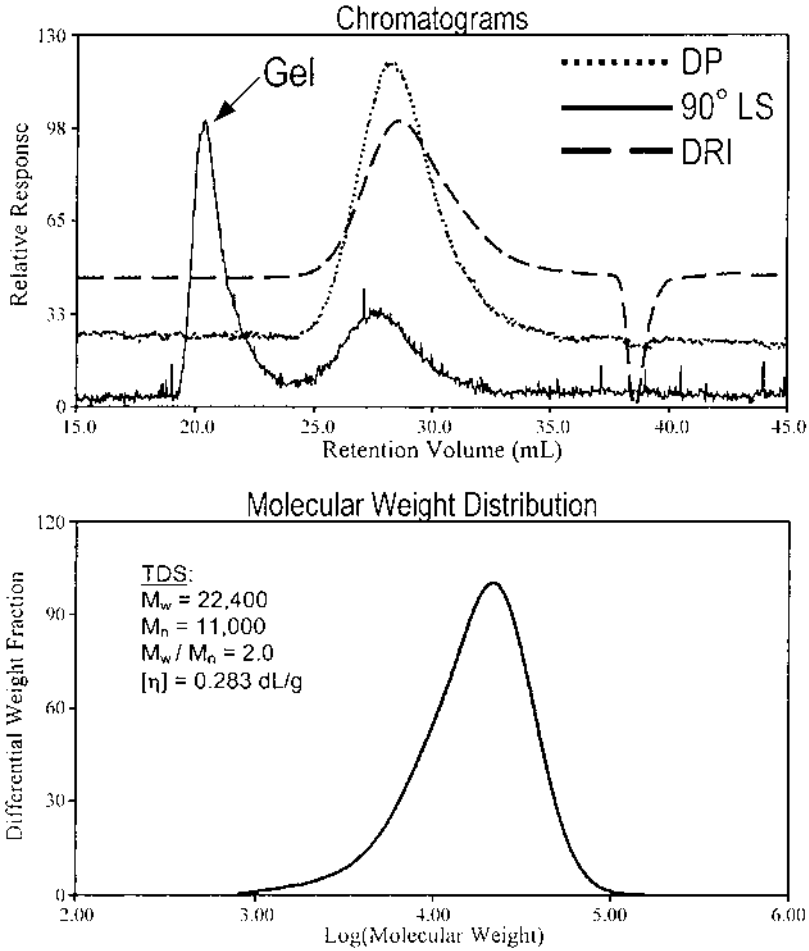

Figure 10 PVA-containing gel. (Reprinted from American Laboratory, Vol. 35, 1, Copyright 2003 by International Scientific Communications, Inc.)

© 2004 by Marcel Dekker, Inc.

copolymer emulsions. The aqueous fraction was collected by ultracentrifugation of the emulsion. The 90° light scattering signal clearly reveals the presence of gel, which is absent in the viscometry and DRI responses. The presence of this small amount of gel does not add any significant molecular weight to the distribution. The calculated molecular weight is typical of that for a low viscosity type PVA.

2.3 Other SEC Characterization of PVA

Wang and colleagues studied the effect of γ-ray irradiation on PVA using aqueous SEC-viscometry and dynamic and static light scattering (15). Because PVA can be crosslinked by γ-ray irradiation, chain branching and polydispersity were studied. Their SEC system consisted of a Shimamura Model YRD-89 differential refractometer and a Viscotek Model H502-02 differential viscometer detector. The analyses were performed at 40°C using a 0.05 M LiCl aqueous solution as the eluant. Two Shodex Asahipak columns were used for the separations. Increases in $[\eta]$, M_w, R_g, and R_h and a decrease in A_2 (the second virial coefficient) were observed after γ-ray irradiation. However, both the values of $[\eta]$ and A_2 for the irradiated PVA fell below the data of unirradiated PVA solutions. This structural change of PVA as a result of γ-ray irradiation was also observed by the decrease in the Mark–Houwink a value from 0.54 to 0.26 by SEC-viscometry. For γ-ray irradiated aqueous PVA solutions, the a values are lower than those for the corresponding linear PVA. This indicates branched polymer chains and that a decreases with increasing irradiation dose (15). Overall, this work is an excellent example of the usefulness of SEC-viscometry for probing changes in polymer microstructure.

The work by Dunn for the SEC characterization of residual levels of PVA from a drug delivery system involved the use and examination of evaporative light scattering detectors (ELSD) from three manufacturers (16). PVA is used in the manufacture of poly(DL-lactide-co-glycolide) microparticles for the delivery of drugs in an injectable implant form. The levels of PVA can affect the release or injectability of the microparticles and must be controlled. Previous work had shown that the use of visible detection of iodine–borate complexes of PVA were insensitive and prone to interferences from other formulation components and the sample solvents required. Refractive index detection also lacked the sensitivity to detect low levels of PVA. Evaporative light scattering detection was found to be more sensitive and less prone to interferences from the sample matrix. The PVA analyzed was extracted using a hot, aqueous solution of 0.1%(vol) of trifluoroacetic acid. An Alltech Model 500 and Polymer Laboratories Model PL-ELS 100 exhibited excellent low limits of detection. Typically, evaporative light-scattering detectors exhibit nonlinear response vs. concentration. However, Dunn showed that a log–log plot of PVA peak area vs. concentration was linear.

© 2004 by Marcel Dekker, Inc.

The limits of detection of the PVA ranged from 0.8 to 4 μg on column depending on the detector used (16).

2.4 Compositional Characterization of PVA

Dawkins and colleagues used reversed phase high-performance liquid chromatography (HPLC) to characterize the compositional distribution of partially hydrolyzed PVA (7). This study was a continuation and expansion of the originally published work on compositional characterization of PVA by Meehan *et al.* in 1994 (17). This type of separation was accomplished to establish quantitatively a compositional distribution, independent of molecular weight. Since partially hydrolysed PVA is actually a copolymer of vinyl alcohol and vinyl acetate, this

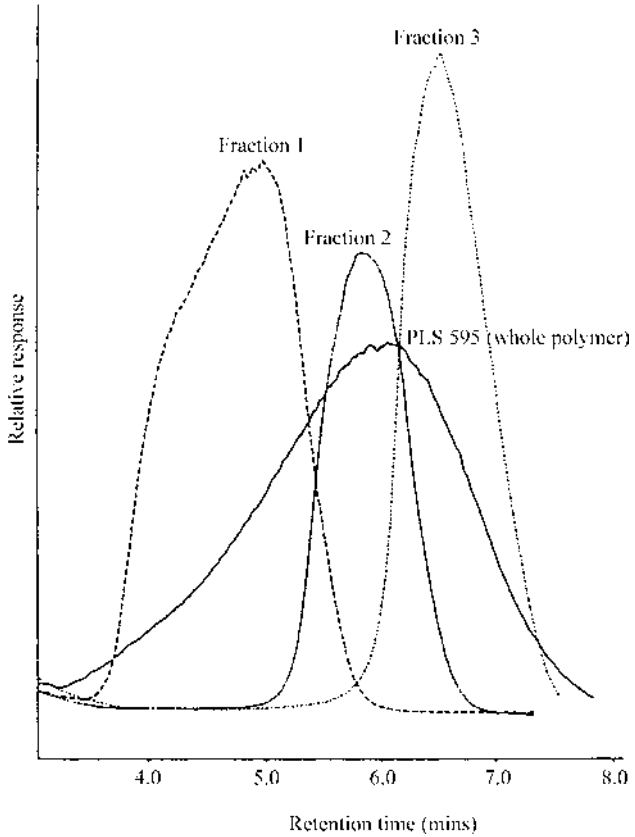

Figure 11 HPLC chromatogram of PVA hydrolysis fractions. (From Ref. 7.)

© 2004 by Marcel Dekker, Inc.

procedure was used to determine a hydrolysis distribution, similar in manner to the measurement of a molecular weight distribution.

The fractionation of PVA by composition rather than molecular weight was carried out using a gradient liquid chromatography system comprising two Model 64 pumps and a Model 50 programmer (Knauer, Germany), a Model 7125 injection valve (Rheodyne, USA), and a Model 950 evaporative mass detector (Polymer Laboratories, UK). The HPLC column was a polystyrene–divinylbenzene-based type with a particle size of 8 μ and a pore size of 4000 Å, 50 × 7.5 mm. A linear gradient of water:THF (98:2%, v/v) to water:THF (30:70%, v/v) over a 9-min period was employed.

These conditions yielded a separation where the first components to elute are the high hydrolysis PVA fractions followed by lower hydrolysis PVA components. An average degree of hydrolysis of 70% or greater produces satisfactory results using this methodology. Figure 11 is an overlay of three chromatograms from the reversed phase HPLC of PVA fractions with degrees of hydrolysis (determined by ^{1}H-NMR spectroscopy) of 88.0, 84.3, and 81.8 mol%. Also included is the parent PVA sample, from which the three fractions were collected using preparative HPLC. The different elution times of the three fractions is easily observed and the wide hydrolysis distribution of the parent PVA is revealed by the broad chromatogram. Plots of retention time for fractions of known hydrolysis were used to construct calibration curves from which hydrolysis distributions were computed (7).

3 RECENT ADVANCES IN THE CHARACTERIZATION OF PVAC

Since 1995, the published material on SEC of PVAc has been somewhat limited. This section will briefly review some of the published works which have appeared in the literature dealing with PVAc.

PVAc is an amorphous, atactic polymer that is soluble in many organic solvents. THF is probably the most widely used solvent for SEC of PVAc (18). As an example, the SEC chromatogram and corresponding molecular weight distribution of a commercially available, PVAc broad standard (American Polymer Standards Corporation) is shown in Fig. 12.

There have been published several different values for the Mark–Houwink constants of PVAc over the years. These values fall in the range $K = 0.51 \times 10^{-4}$ to 3.50×10^{-4} and $a = 0.63$–0.79. It is interesting to note that Lawrey (18) points out the intrinsic viscosity behavior of PVAc is very close to that of polystyrene. Polystyrene and linear PVAc elute at nearly the same retention time for the same molecular weight in THF (18). The calculated molecular weight vs. polystyrene for the PVAc broad standard in Fig. 12 are very close to the

© 2004 by Marcel Dekker, Inc.

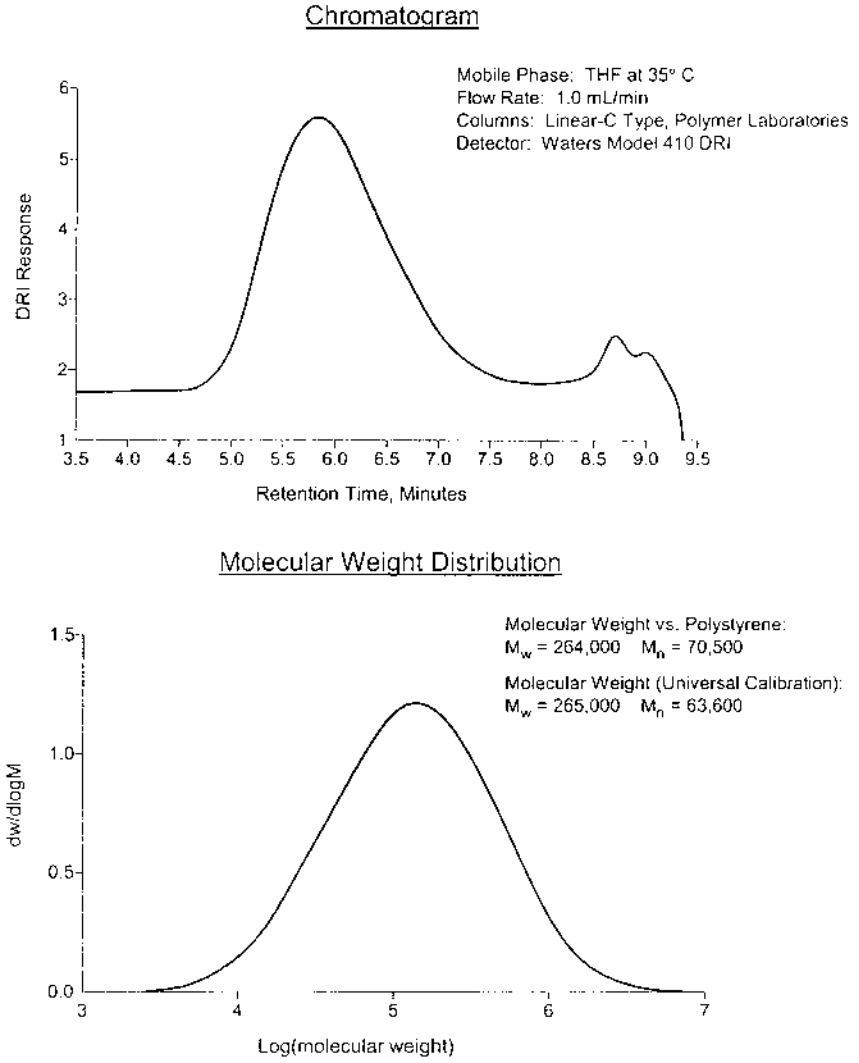

Figure 12 PVAc broad molecular weight standard, manufacturer's values: $M_w = 275{,}000$, $M_n = 65{,}700$.

manufacturer's values. The same is true for the molecular weights calculated using universal calibration, with $K = 3.50 \times 10^{-4}$ and $a = 0.630$ for PVAc and $K = 1.28 \times 10^{-4}$ and $a = 0.712$ for polystyrene (18).

A study on the use of a single capillary viscometer detector, utilizing a pulse-free pump on a Waters Alliance 2690 by Mendichi and Schieroni, was

© 2004 by Marcel Dekker, Inc.

conducted on a variety of commercial polymers including PVAc (19). Their calculated values for Mark–Houwink constants for PVAc ($K = 1.01 \times 10^{-4}$, $a = 0.760$) were in good agreement with the expected values reported for branched PVAc in THF at 35°C (20). The single capillary viscometer clearly revealed the presence of branched PVAc on a log–log plot of intrinsic viscosity vs. molecular weight.

PVAc is often used as a synthetic material to replace natural ingredients used in chewing gum. The masticatory properties of gum are highly dependent on the polymer molecular weight. For example, the greater the molecular weight, the stronger the film and hence the larger the bubble that the consumer can blow. However, increasing the molecular weight or size also tends to make gum more difficult to chew and a tradeoff is usually required. D'Amelia and Kumiega utilized TDS for the characterization of food grade PVAc used in chewing gum (21). They used an SEC system with a Model 250 refractometer/viscometer dual detector and a Model 600 right-angle laser light scattering detector, both from Viscotek Corporation. Later, they upgraded to a Viscotek Model T60A along with a Waters Corporation Model 410 Differential Refractometer.

A summary of the polymeric properties of several different PVAc resins used in various types of stick and bubble gums is given in Table 6 (21). The intrinsic viscosity, $[\eta]$, and radius of gyration, R_{gw}, are also summarized. As expected, the $[\eta]$ and R_{gw} values track the molecular weight. The TDS method can easily measure R_{gw} values less than 10 nm. The data in Table 6 are a good example of how TDS can be used to examine closely the microstructure of PVAc and how molecular weight impacts chewing gum properties.

The work described above uses right-angle light scattering as part of the TDS detection package. It should be noted that light scattering detection for PVAc in THF can be somewhat challenging, depending on the molecular weight. This applies whether using TDS or MALLS. The reason for this is that the specific refractive index increment for PVAc in THF is rather low. Values reported in the literature for a wavelength of 632 nm range between 0.047 to 0.054 mL/g (18).

Table 6 Molecular Weight Summary of Masticatory PVAc

Type	M_w	M_n	$[\eta]$, dL/g	R_{gw} (nm)
Stick	8,060	3,660	0.087	2.7
Stick	21,100	9,330	0.152	4.6
Bubble	54,500	14,300	0.297	7.6
Bubble	75,700	31,900	0.368	9.3

Source: Ref. 21.

© 2004 by Marcel Dekker, Inc.

4 SUMMARY

Advances in SEC characterization of PVA and PVAc for molecular weight and molecular weight distribution mirror the technological developments that have become mainstream in the field of SEC. Both polymers have been successfully characterized using TDS packages. MALLS detection has played a key role in the characterization of PVA under aqueous conditions. Molecular weight and polymer conformational information can be routinely measured using these techniques. The use of SEC for improved understanding of performance and product applications of these polymers is finding widespread use.

REFERENCES

1. DJ Nagy. Aqueous size exclusion chromatography of polyvinyl alcohol. In: Handbook of Size Exclusion Chromatography. New York: Marcel Dekker, 1996, pp 279–301.
2. DJ Nagy. Characterization of poly(vinyl alcohol) using SEC multiangle laser light scattering. Amer Labor 27:47J–47V, 1995.
3. DJ Nagy. Aqueous GPC triple detection of partially- and fully-hydrolyzed poly(vinyl alcohol). Proceedings of International GPC Symposium, Las Vegas, 2000, pp 1–22.
4. DJ Nagy. Applications and uses of columns for aqueous size exclusion chromatography of water-soluble polymers. In: Column Handbook for Size Exclusion Chromatography. San Diego: Academic Press, 1999, pp 559–581.
5. HJ Barth. Characterization of water-soluble polymers using size exclusion chromatography. In: Water-Soluble Polymers: Beauty with Performance, ACS Advances in Chemistry Series 213. Washington: American Chemical Society, 1986, pp 31–55.
6. M Weissmuller. Use of thermal field flow fractionation (TFFF) for characterization of polymeric materials. Proceedings of Werkstoffwoche ’98, Band VIII, 1999, pp 133–138.
7. JV Dawkins, TA Nicholson, AJ Handley, E Meehan, A Nevin, PL Shaw. Polymer 40:7331–7339, 1999.
8. TG Fox, PJ Flory. J Am Chem Soc 73:1904, 1951.
9. OB Ptitsyn, YE Eizner. Sov Phys Tech Phys 4:1020, 1960.
10. DJ Nagy. Aqueous SEC triple detection of poly(vinyl alcohol). Amer Labor 35, 2003.
11. DJ Nagy. J Liq Chrom 16:3041–3058, 1993.
12. AJ Beresniewicz. J Polym Sci 39:63, 1959.
13. H Staudinger, J Schneider. J Liebigs Ann 541:151, 1939.
14. A Nakajima, E Furutachi. Kobunshi Kagaku 6:460, 1949.
15. B Wang, S Mukataka, E Kokufuta, M Ogiso, M Kodama. J Polym Sci 38: 214–221, 2000.
16. KD Dunn. J Pharm Biomed Anal 25:539–543, 2001.

© 2004 by Marcel Dekker, Inc.

17. E Meehan, FP Warner, SP Reid, JV Dawkins. Characterisation of poly(vinyl alcohol) by liquid chromatography techniques. Proceedings of International GPC Symposium, Orlando, 1994, pp 145–160.
18. BD Lawrey. Size exclusion chromatography of polyvinyl acetate. In: Handbook of Size Exclusion Chromatography. New York: Marcel Dekker, New York, 1996, pp 303–310.
19. R Mendichi, AG Schieroni. Use of the single capillary viscometer detector, on-line to a size exclusion chromatography system with a new pulse free pump. In: Chromatography of Polymers, ACS Symposium Series. Washington: American Chemical Society, 1999, pp 66–83.
20. CY Kuo, T Provder, ME Koehler, AF Kah. Use of a viscometric detector for size exclusion chromatography. In: Detection and Data Analysis in Size Exclusion Chromatography, ACS Symposium Series 352. Washington: American Chemical Society, 1987, pp 130–154.
21. R D'Amelia, S Kumiega. Scientific Computing & Instrumentation 23–26, 1999.

© 2004 by Marcel Dekker, Inc.

11
Size Exclusion Chromatography of Vinyl Pyrrolidone Homopolymer and Copolymers

Chi-san Wu, James F. Curry, Edward G. Malawer, and Laurence Senak
International Specialty Products
Wayne, New Jersey, U.S.A.

1 INTRODUCTION

Polyvinyl pyrrolidone (PVP) is a polar and amorphous polymer that is completely soluble in water and some organic solvents, such as alcohols, chlorinated hydrocarbons, dimethylformamide, and *N*-methylpyrrolidone. It is an important polymer in the pharmaceutical, personal care, cosmetic, agriculture, beverage, and other industries.

PVP is a physiologically inert and biologically compatible polymer. PVP is known to reduce significantly the toxicity and irritant effects of many medications. PVP can form complexes with a variety of substances. For example, the PVP–iodine complex in the form of povidone or Betadine aqueous solution is the most widely used antiseptic in hospitals. It significantly reduces the toxicity and staining

© 2004 by Marcel Dekker, Inc.

effect of the tincture of iodine solution but retains the germicidal activity of the iodine.

Because of the excellent solubility of PVP in water, the dissolution rate of many drugs and compounds that are difficult to dissolve can be significantly improved if they are coprecipitated with PVP. PVP is amphiphilic in nature and is slightly surface active. It is frequently used in industries as a suspending aid and a protective colloid for polymers, emulsions, and lattices. PVP is also used as a dye stripper in the textile industry and in detergent formulation to prevent soil and dye redeposition. Because of its good adhesive and cohesive strengths and excellent water solubililty, PVP is one of the most widely used tablet binders for the pharmaceutical industry. It is also used as the major component in glue sticks and for bonding medical devices to a patient's skin.

The hydrophilic, hydrophobic, and ionic nature of PVP can be modified by copolymerization to enhance the properties of PVP for certain applications. Nonionic, anionic, and cationic VP copolymers have all been commercialized. A wide range of vinyl pyrrolidone and vinyl acetate copolymers, which are nonionic, have been made with optimized amphiphilicity and solubility in water or alcohol for the cosmetic and pharmaceutical industries. The surface activity of PVP can be further enhanced by copolymerization with acrylic acid. Vinyl pyrrolidone and acrylic acid copolymers, which are anionic in their major applications, with different molar ratios have been developed with well-balanced surface, associative, and film-forming properties for industrial applications.

Quaternized copolymers of vinyl pyrrolidone and dimethylaminoethyl-methacrylate, which is cationic, have been developed for the hair care and skin care industries because of their optimal substantivity, minimum buildup, and ability to form nontacky and continuous films. Other important comonomers include vinyl alcohol, styrene, maleic anhydride, acrylamide, acrylonitrile, crotonic acid, and methyl methacrylate.

2 MOLECULAR WEIGHT GRADES OF IMPORTANT VP-BASED POLYMERS

Many different molecular weight grades of VP-based polymers, characterized by viscosity, are available commercially. The determination of viscosity is historically satisfactory for quality assurance purposes; however, most physical properties of polymers are directly related to molecular weight (1). For example, the glass transition temperature and tensile strength of amorphous polymers are known to depend on molecular weight. The melt viscosity of polymers and the bulk viscosity of concentrated polymer solutions are also known to depend on molecular weight.

© 2004 by Marcel Dekker, Inc.

2.1 Molecular Weight Grades of PVP Based on *K* Value

The molecular weights of PVP have traditionally been characterized by the Fikentscher (2) *K* value, which is related to relative viscosity measured at 25°C by

$$\frac{\log \eta_{rel}}{C} = \frac{75K_0^2}{1 + 1.5K_0C} + K_0$$

where $K = 1000\,K_0$ and C is the solution concentration in g/dL. An increase in η_{rel} corresponds with an increase in *K* value. Table 1 shows the dependence of *K* value on η_{rel} for given values of relative viscosity, measured at 1 g/dL (or 1% wt/vol). As seen from Table 1, a PVP polymer with a relative viscosity of 2 would have a *K* value of 60 and the polymer would be referred to as a *K*-60. In industry, the *K* value is generally obtained from a table similar to Table 1, with concentrations specified by the U.S. Pharmacopoea (USP) for the different molecular weight grades of PVP. The USP specifies that *K*-30, *K*-60, or *K*-90 should be obtained from 1% solutions and *K*-15 and *K*-120 should be obtained from 5 and 0.1% solutions, respectively.

The molecular weight ranges of various commercial *K* value grades of PVP are shown in Table 2. The $\overline{M}_w$ of an unknown PVP sample can be calculated from intrinsic viscosity if the Mark–Houwink equation, which correlates intrinsic viscosity with $\overline{M}_w$ is known from the literature. The unknown PVP sample should be similar in branching and polydispersity to the PVP samples from which the Mark–Houwink equation is derived. Levy and Frank published the following Mark–Houwink equation in 1955 (3) for unfractionated PVP samples in water at 25°C: $[\eta] = 5.65 \times 10^{-2} \times \overline{M}_w^{0.55}$. Senak *et al.* published the following Mark–Houwink equation in 1987 (4) for unfractionated PVP samples in water–methanol (1:1 vol/vol) with 0.1 M $LiNO_3$ at 25°C: $[\eta] = 1.32 \times 10^{-4} \times \overline{M}_w^{0.65}$.

Table 1 *K* Value vs. Relative Viscosity at 1% Concentration (wt/vol)

K value	Relative viscosity	*K* value	Relative viscosity
20	1.120	60	2.031
25	1.175	65	2.258
30	1.243	70	2.527
35	1.325	75	2.846
40	1.423	80	3.225
45	1.539	85	3.678
50	1.677	90	4.219
55	1.839	95	4.870

© 2004 by Marcel Dekker, Inc.

Table 2 Molecular Weights of PVP

K value	$\overline{M}_w$	$\overline{M}_n$
K-15	7,000–12,000	− 2,500
K-30	40,000–65,000	− 10,000
K-60	350,000–450,000	− 100,000
K-90	900,000–1,500,000	− 360,000
K-120	2,000,000–3,000,000	—

If a *K* value vs. absolute weight-average molecular weight equation or table is available for PVP, then the *K* value can be easily determined from relative viscosity. Such a relationship, developed by Senak *et al.*, is shown in the equation $\log \overline{M}_w = 2.82 \log K + 0.594$ and in Table 3 for commercial grades of unfractionated PVP (L Senak, CS Wu, EG Malawer, unpublished results). It should be pointed out here that the *K* value is a function not only of molecular weight but also of molecular weight distribution and branching.

2.2 Molecular Weights of VP-Based Copolymers

Most VP-based copolymers are also characterized by *K* value. However, the literature on molecular weights of VP copolymers is very sparse. Wu and Senak reported in 1990 (5) the absolute molecular weights of cationic copolymers of quaternized vinyl pyrrolidone and dimethylaminoethyl methacrylate by size

Table 3 *K* Value vs. Weight-Average Molecular Weight for PVP[a]

K value	$\overline{M}_w$ (AMU)	*K* value	$\overline{M}_w$ (AMU)
10	2,594	70	626,869
15	8,139	75	761,505
20	18,319	80	913,511
25	34,371	85	1,083,831
30	57,475	90	1,273,397
35	88,771	95	1,483,135
40	129,363	100	1,713,957
45	180,326	105	1,966,770
50	242,714	110	2,242,474
55	317,558	115	2,541,955
60	405,870	120	2,866,099
65	508,646		

[a]The calculations are based on the regression formula $log\overline{M}_w = 2.82 \log K + 0.594$.

© 2004 by Marcel Dekker, Inc.

exclusion chromatography with low-angle laser light scattering (SEC/LALLS) and SEC with universal calibration (Table 8). The molecular weights (relative to polyethylene oxide standards) of nonionic copolymers of vinyl pyrrolidone and vinyl acetate, a nonionic terpolymer of vinyl pyrrolidone, dimethylaminoethyl methacrylate, and vinyl caprolactam, and anionic copolymers of vinyl pyrrolidone and acrylic acid were also reported in 1991 (6) by Wu *et al.* (Tables 6 and 7).

3 MOLECULAR WEIGHT DISTRIBUTION OF VP-BASED POLYMERS BY SIZE EXCLUSION CHROMATOGRAPHY

Many important properties of polymers depend not only on molecular weight but also on molecular weight distribution. For example, both viscosity and its dependence on the shear rate of polymer melt and concentrated polymer solution are dependent on molecular weight distribution. SEC is the most practical and the best method for determining the molecular weight distribution of a polymer without going through the tedious classic fractionation procedure using nonsolvent precipitation.

3.1 SEC of PVP: Historical Review

The SEC of PVP is not straightforward because of the polar nature of the polymer. Various interactions between PVP and columns, such as adsorption, partition, and electrostatic interactions, must be eliminated by prudent choice of column and mobile phase to obtain true separation by size with 100% recovery and compliance with universal calibration.

The SEC behavior of PVP has been of interest to many researchers. In the 10-year period from 1975 to 1984, seven papers, using seven different kinds of columns with various surface modifications and in both aqueous and nonaqueous mobile phases with and without modifiers and salts, were reported for the SEC of PVP with different degrees of success. Some of the columns used are commercially available; others are specially made.

Belenkii *et al.* reported in 1975 (7) the SEC of PVP with unspecified molecular weight using Pharmacia Sephadex G-75 and G-100 columns and a 0.3% sodium chloride solution as the mobile phase. Deviations from universal calibration behavior were noticed from PVP, dextran, polyethylene oxide (PEO), and polyvinyl alcohol. With the development of the important semirigid polymer gel, Toyo Soda TSK-PW columns for water-soluble polymers, Hashimoto *et al.* reported in 1978 (8) the SEC of PVP K-30 and K-90 using TSK-PW 3000 and two 5000 columns an 0.08 M Tris–HCl buffer (pH = 7.94) as mobile phase and PEO and dextran as calibration standards.

By using an E. Merck LiChrospher SI300 column, modified with an amide group chemically bonded to the surface, Englehardt and Mathes reported in 1979 (9) the SEC of PVP with molecular weights from 10,000 to 360,000 AMU. A 0.1 M

© 2004 by Marcel Dekker, Inc.

Tris–HCl buffer, pH 8.0, whose ionic strength was adjusted to 0.5 by Li_2SO_4, was used as the eluant. PVP was adsorbed by the column when water or buffer solution was used as eluant; upon the addition of 10% (vol/vol) ethylene glycol to the eluant, however, this interaction was eliminated.

Herman and Field synthesized monomeric diol onto E. Merck Lichrospher SI-500 and reported in 1981 (10) the SEC of PVP with molecular weight 10,000. Poor recovery (0–25%) of PVP was noticed using water as eluant. A 100% recovery was obtained using 40% acetonitrile in 0.01 M KH_2PO_4, pH 2.1. A 100% recovery of PVP was also reported using a TSK-PW-3000 column with 0.08 M Tris buffer. Mori reported in 1983 (11) the SEC of PVP with molecular weights from 11,000 to 1,310,000 AMU using two Shodex AD-80M/S columns with dimethylformamide (DMF) and 0.01 M LiBr as eluant at 60°C. Separation of PVP based on hydrodynamic volume in this SEC system was demonstrated by the applicability of universal calibration using PEO and polyethylene glycol as calibration standards. Domard and Rinaudo grafted quaternized ammonium groups onto silica gels with pore diameters 150, 300, 600, 1250, and 2000 Å and reported in 1984 (12) the SEC of PVP *K*-15, 25, 30, 60, and 90 using 0.2 M ammonium acetate as the eluant. Some adsorption of PVP *K*-15, 25, 30, 60 and 90 was noticed by deviation from the universal calibration curve.

In 1984, Malawer *et al.* (13) conducted a thorough study on the SEC of PVP *K*-15, 30, 60, and 90 using diol-derivatized silica gel column sets and aqueous mobile phase modified with various polar organic solvents. A log-linear calibration curve over three decades in molecular weights was obtained on a specially constructed Electronucleonics gylceryl-CPG column set consisting of two 75, 500, and 3000 Å columns and was found to provide better recovery and separation than the commercially available prepacked, 10 μm high-efficiency diol-derivatized silica gel columns. Methanol was found to be a better aqueous mobile-phase modifier to eliminate the adsorption effect than either dimethyl-formamide or acetonitrile. The best recovery (>90%) and separation were obtained with a mobile phase of 50:50 (vol/vol) methanol–water containing 0.1 M $LiNO_3$.

In summary, when commercially available SEC columns are used, successful SEC separation of PVP without polymer-column interactions has been reported in either an aqueous environment (8) or DMF (11). However, as indicated later, the aqueous environment has the advantage of providing better separation at the low-molecular-weight end of the SEC peak, especially for the lower molecular weight grades, PVP *K*-30 and *K*-15. Therefore, the remaining discussion of PVP concentrates on the aqueous environment.

3.2 SEC/LALLS and SEC with Universal Calibration for PVP

In a continuation of an earlier work (13), Senak *et al.* reported in 1987 (4) the most extensive SEC study on PVP to date with the determination of absolute molecular

© 2004 by Marcel Dekker, Inc.

weight and molecular weight distribution by SEC/LALLS and SEC with universal calibration of the four most widely used PVP grades, *K*-15, *K*-30, *K*-60, and *K*-90. The column set used consists of TSK-PW 6000, 5000, 3000, and 2000 columns and a mobile phase of 50:50 (vol/vol) water–methanol with 0.1 M $LiNO_3$; 100% recovery was reported. The highlights of this paper are reviewed in this section.

Because the principle of SEC with LALLS was discussed in Chapter 4, only the results of SEC with LALLS are presented here. The water–methanol mixed mobile phase used for SEC was also suitable for the determination of molecular weight by LALLS because no preferential solvation of PVP by water or methanol occurred in the mixed mobile phase. This was demonstrated by monitoring the equilibrium concentrations of water and methanol with crosslinked PVP. Furthermore, the differential refractive index increments of PVP in water and PVP in methanol are very close. Lack of preferential solvation in the mixed mobile phase was also demonstrated by the fact that the $\overline{M}_w$ of a PVP *K*-90 sample was found to be similar, as measured by static LALLS, in the mixed mobile phase (1.43×10^6 AMU) and in water with 0.1 M $LiNO_3$ (1.57×10^6 AMU).

Differential refractive index increments of PVP in the mixed mobile phase were found to be 0.174 mL/g and independent of molecular weight for PVP *K*-15, *K*-30, *K*-60, and *K*-90. Second virial coefficients of PVP, determined by static LALLS, were found to decrease with increasing $\overline{M}_w$ as expected. The $\overline{M}_w$ of PVP *K*-60 and *K*-90 determined by SEC/LALLS were found to be the same as those determined by static LALLS, respectively, indicating no shear degradation of PVP *K*-60 and *K*-90 by SEC in the mixed mobile phase.

Based on the SEC with LALLS results, Mark–Houwink constants of both fractionated and commercial unfractionated PVP samples were reported in the mixed mobile phase. The Mark–Houwink constants thus determined were later used in universal calibration to calculate absolute molecular weight and absolute molecular weight distribution. The absolute molecular weights of PVP based on the universal calibration curve calculated from the Mark–Houwink constants of fractionated PVP were found to be similar to those calculated from the Mark–Houwink constants of commercial unfractionated PVP. This indicates that for the purpose of calculating molecular weights by the universal calibration method, the Mark–Houwink constants may be obtained from broad distribution polymers without fractionation, as long as branching is similar for the polymer grades of interest. The molecular weights of PVP by SEC/LALLS and SEC with universal calibration are shown in Table 4. The results showed good agreement in $\overline{M}_w$ from SEC/LALLS and from SEC with universal calibration for PVP *K*-30, *K*-60, and *K*-90. This indicates PVP is separated by hydrodynamic volume in the mixed mobile phase with the TSK-PW column set and confirms the validity of universal calibration.

SEC/LALLS was found to overestimate $\overline{M}_n$ because of the lack of LALLS detector sensitivity in the low-molecular-weight portion of the SEC chromatogram.

© 2004 by Marcel Dekker, Inc.

Table 4 Molecular Weights of PVP Determined by SEC/LALLS and SEC with Universal Calibration

	$\overline{M}_w$		$\overline{M}_n$	
Grade	SEC/LALLS	Universal calibration	SEC/LALLS	Universal calibration
K-15	1.68×10^4	1.12×10^4	1.10×10^4	4.18×10^3
K-30	6.24×10^4	6.19×10^4	3.10×10^4	1.28×10^4
K-60	3.37×10^5	3.40×10^5	1.57×10^5	5.23×10^4
K-90	1.52×10^6	1.24×10^6	6.38×10^5	2.06×10^5

Source: From Ref. 4.

This overestimation is expected to be more significant for the broad molecular weight distribution polymers than for the narrow distribution polymers. The larger difference in $\overline{M}_w$ for PVP *K*-15 (vis-à-vis the higher *K*-value grades) could be caused by a combination of lower sensitivity of LALLS at low molecular weight and/or less accuracy of the universal calibration curve at the low-molecular-weight end. Absolute molecular weight distributions for PVP *K*-90, *K*-60, *K*-30, and *K*-15 grades based on universal calibration are shown in Fig. 1.

3.3 SEC of Commercial Grades of PVP with a Single Linear Column

One of the most important developments in the technology of semirigid polymeric gels for SEC of synthetic water-soluble polymers in recent years is the availability of the log-linear column with good separation range, from less than 1000 to several million in molecular weight. A linear calibration curve improves both the accuracy and precision of the determination of molecular weight and molecular weight distribution. The commonly used brand names for linear columns for aqueous SEC are Showa Denko Shodex OH pack, Toyo Soda TSK-PW, and Waters Ultrahydrogel. The column packing materials for these columns are all crosslinked, hydroxylated polymethyl methacrylate (PMMA) in nature. Using single linear columns also greatly reduces analysis time and solvent consumption, making SEC a practical method for quality assurance.

Linear PEO calibration curves generated in this laboratory for the Ultrahydrogel linear column in 20:80 methanol–water (vol/vol) with 0.1 M lithium nitrate and in 50:50 methanol–water (vol/vol) with 0.1 M lithium nitrate and for the Shodex KB-80M linear column in 20:80 methanol–water with 0.1 M lithium nitrate are shown in Figs 2, 3, and 4. The effect of methanol–water ratio of

© 2004 by Marcel Dekker, Inc.

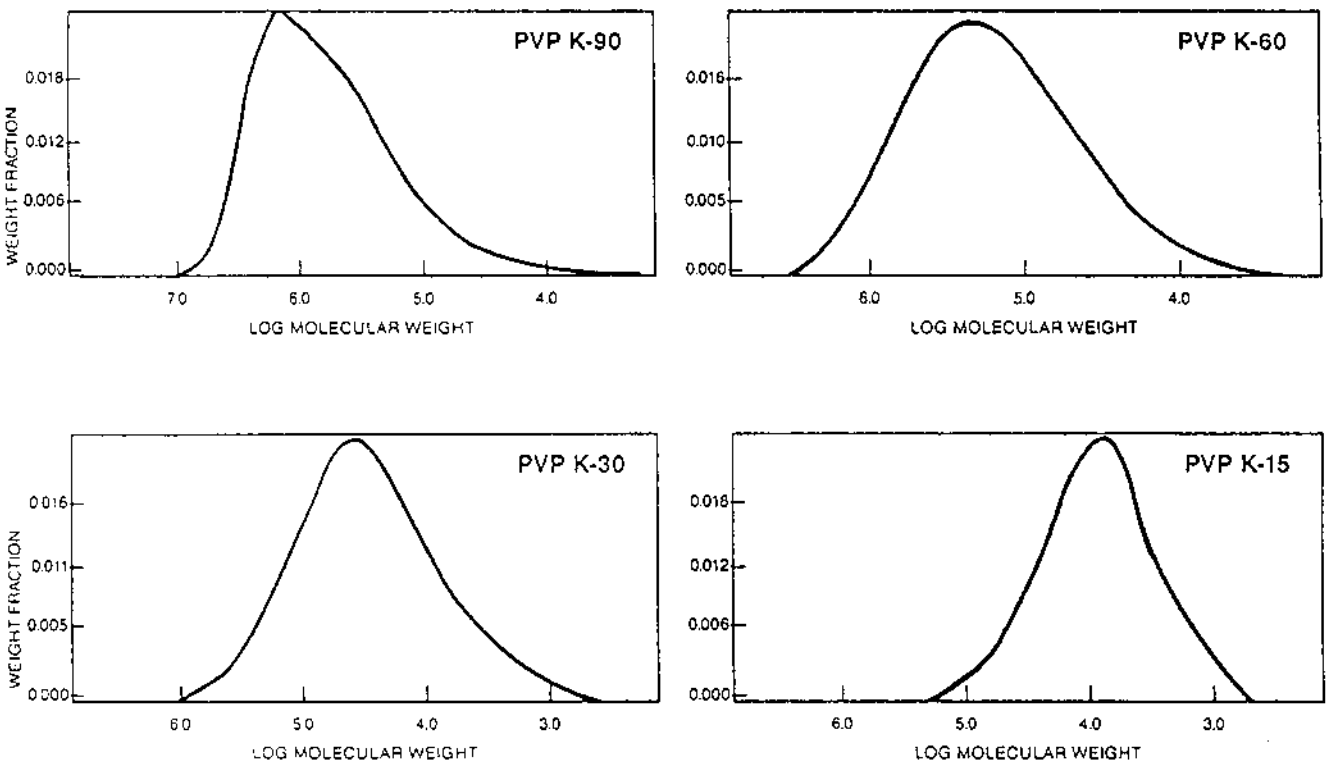

Figure 1 Molecular weight distributions of PVP polymers. (From Ref. 4.)

© 2004 by Marcel Dekker, Inc.

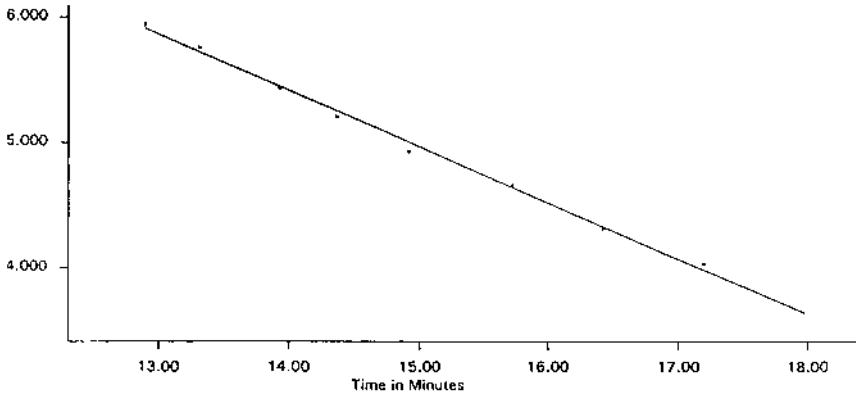

Figure 2 PEO calibration of Ultrahydrogel linear column in 50:50 (vol/vol) MeOH–water with 0.1 M $LiNO_3$.

the mobile phase on the elution time of PEO standards from a Ultrahydrogel linear column is shown in Table 5.

The PEO standards elute slightly earlier in the 50:50 methanol–water mixture than in the 20:80 methanol–water mixture. Because the viscosity of the 50:50 mixture (1.59 cP at 25°C) is higher than that of the 20:80 mixture (1.30 cP), the retention time in the 50:50 mixture theoretically should be longer than in the 20:80 mixture because of higher viscosity or backpressure on the column. This indicates the Ultrahydrogel linear column can swell slightly more in

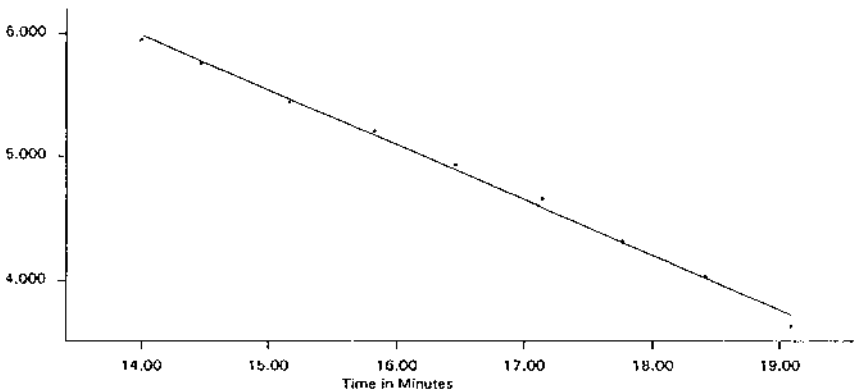

Figure 3 PEO calibration of Shodex KB-80M mixed column in 20:80 (vol/vol) methanol–water with 0.1 M $LiNO_3$.

© 2004 by Marcel Dekker, Inc.

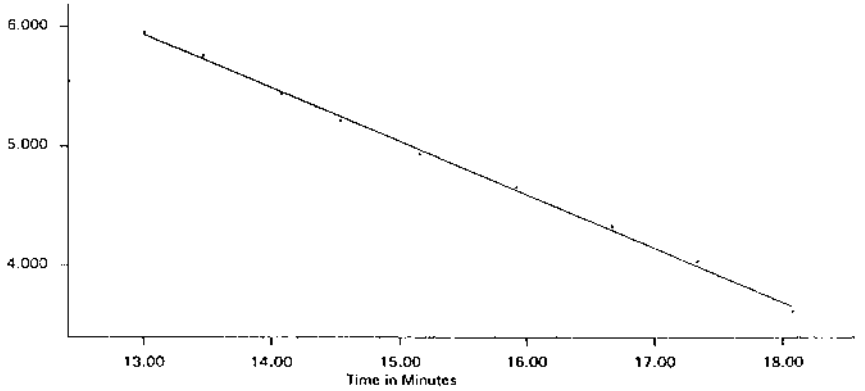

Figure 4 PEO calibration of Ultrahydrogel linear column in 20:80 (vol/vol) methanol–water with 0.1 M $LiNO_3$.

the 20:80 methanol–water mixture to generate larger pore sizes and volumes than in the 50:50 methanol–water mixture. As discussed later, the larger pore volume in the 20:80 mixture may provide better separation at the high-molecular-weight end.

Overlays of SEC chromatograms of five commercial grades of PVP using the Shodex KB-80M linear column with a mobile phase of 20:80 (vol/vol) MeOH/H_2O with 0.1 M $LiNO_3$ and the Ultrahydrogel linear column with a mobile phase of either 20:80 (vol/vol) MeOH/H_2O with 0.1 M $LiNO_3$ or 50:50 (vol/vol) MeOH/H_2O with 0.1 M $LiNO_3$ are shown in Figs 5, 6, and 7. Adequate separation of all commercial grades of PVP can be obtained from all three systems.

Table 5 Retention Times of PEO Using Ultrahydrogel Linear Column in Different 0.1 M Lithium Nitrate Mobile Phases

PEO (AMU)	20:80 Water/MeOH	50:50 Water/MeOH
885,000	13.00	12.88
570,000	13.47	13.33
270,000	14.08	13.92
160,000	14.53	14.33
85,000	15.15	14.93
45,000	15.92	15.73
21,000	16.67	16.40
10,750	17.33	17.17
4,250	18.08	17.97

© 2004 by Marcel Dekker, Inc.

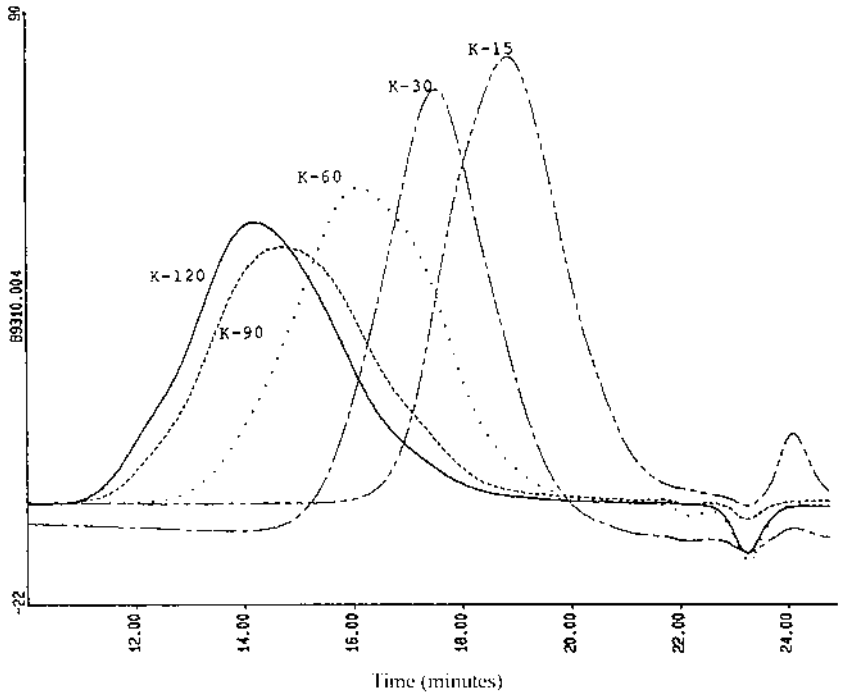

Figure 5 Overlay of gel permeation chromatogram (GPC) of commercial grades of PVP using Shodex KB-80M mixed column and 20 : 80 (vol–vol) methanol–water with 0.1 M $LiNO_3$.

The weight-average molecular weights (relative to PEO standards) of the five commercial-grade PVP samples obtained from these three systems with the respective mobile phases are shown in Table 6. Also shown is a Polymer Laboratories polyethylene oxide standard of reported $\overline{M}_w$ of 1,370,000 AMU. Good agreement in weight-average molecular weights were obtained for the low- and medium-molecular-weight grades PVP *K*-15, 30, and 60 samples among the three systems. However, the Shodex linear column yields higher molecular weight values for the high-molecular-weight grade PVP *K*-90 and 120 and the PEO standard than the Ultrahydrogel linear column. This indicates the Shodex linear column provides better separation at the high-molecular-weight end than the Ultrahydrogel linear column. The Ultrahydrogel column may also provide better separation at the high-molecular-weight end in the 20 : 80 methanol–water mobile phase than in the 50 : 50 methanol–water mobile phase; however, the difference is small.

© 2004 by Marcel Dekker, Inc.

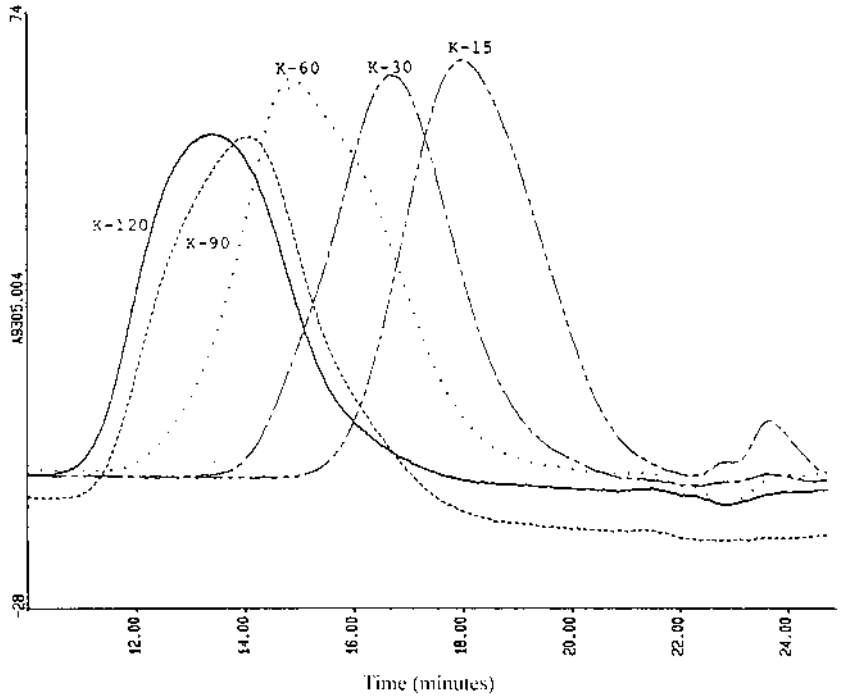

Figure 6 Overlay of GPC chromatograms of commercial grades of PVP using Ultrahydrogel linear column and 80:20 (vol/vol) water–MeOH with 0.1 M $LiNO_3$.

4 MOLECULAR WEIGHTS AND MOLECULAR WEIGHT DISTRIBUTIONS OF VP-BASED COPOLYMERS BY SEC

4.1 Nonionic Copolymers: Copolymers of Vinyl Pyrrolidone and Vinyl Acetate (VA) and Terpolymer of Vinyl Pyrrolidone, Dimethylaminoethyl Methacrylate (DMAEMA), and Vinyl Caprolactum (VC)

Wu *et al.* reported in 1991 (6) the SEC of PVP/VA copolymers and PVP/DMAEMA/VC terpolymer in both aqueous and nonaqueous systems. For the aqueous system the column set consisted of four Waters Ultrahydrogel columns of pore sizes 120, 500, 1000, and 2000 Å, and the mobile phase was 1:1 water–methanol (vol/vol) with 0.1 M $LiNO_3$. Aqueous mobile phases with no organic modifiers, such as methanol, cannot be used because of the poor solubility of some of the nonionic copolymers in pure water and the adsorption of the copolymers by the columns. For the nonaqueous system, the column sets were Shodex KD-80M

© 2004 by Marcel Dekker, Inc.

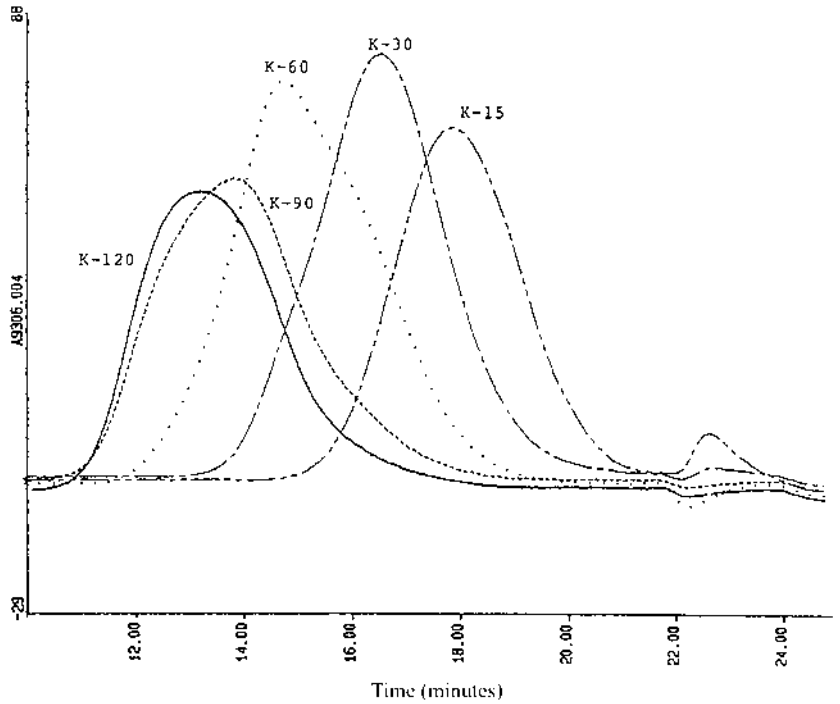

Figure 7 Overlay of GPC chromatograms of commercial grades of PVP using Ultrahydrogel linear column and 50:50 (vol/vol) water–MeOH with 0.1 M $LiNO_3$.

Table 6 Weight-Average Molecular Weights of Five Commercial Grades of PVP and a PEO Standard Obtained from the Shodex Linear Column and the Ultrahydrogel Linear Column

	Weight-average molecular weights (AMU)		
	Shodex	Ultrahydrogel	
Grade	20:80 Water–methanol	20:80 Water–methanol	50:50 Water–methanol
PEO	1,170,000	1,020,000	934,000
K-120	1,060,000	845,000	810,000
K-90	698,000	597,000	578,000
K-60	160,000	166,000	166,000
K-30	29,700	33,600	32,900
K-15	7,500	7,200	6,780

© 2004 by Marcel Dekker, Inc.

plus Ultrahydrogel 120 Å, Shodex KD-80M plus PLgel 100 Å, and PLgel 10^4 Å plus 500 Å, and the mobile phase was DMF with 0.1 M $LiNO_3$.

For the nonaqueous systems, the peak shapes are very similar for all three column sets; the Shodex KD-80M plus Ultrahydrogel 120 Å provides slightly better separation of the solvent peak and the low-molecular-weight end of the polymer peak. However, the aqueous system showed the best separation at the low-molecular-weight end, as shown in Figs 8 and 9. The weight-average molecular weights and intrinsic viscosities determined in aqueous and nonaqueous systems (Shodex KD-80M plus Ultrahydrogel 120 Å) are shown in Table 7. A 100% recovery was achieved in both aqueous and nonaqueous systems for PVP/VA in SEC.

4.2 Anionic Copolymers: Copolymers of Vinyl Pyrrolidone and Acrylic Acid (AA)

Even though this copolymer is soluble in the water–methanol (50:50, vol/vol) mobile phase with 0.1 M lithium nitrate, no recovery of the copolymer can be obtained in SEC with the Ultrahydrogel columns in this mobile phase. Wu *et al.* reported in 1991 (6) the SEC of PVP/AA using a 0.1 M pH 9 Tris buffer with 0.2 M $LiNO_3$ as the mobile phase and the Ultrahydrogel 120, 500, 1000, and 2000 Å column set. The PVP/AA samples were first dissolved in 0.25 N NaOH (1%,

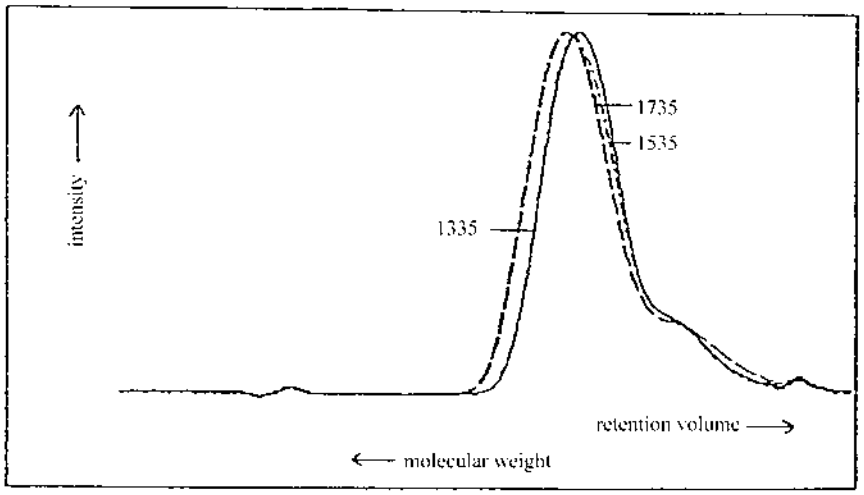

Figure 8 SEC traces of PVP/VA, I series, using the Shodex KD-80 M and Ultrahydrogel 120 Å columns with DMF solvent. (From Ref. 6.)

© 2004 by Marcel Dekker, Inc.

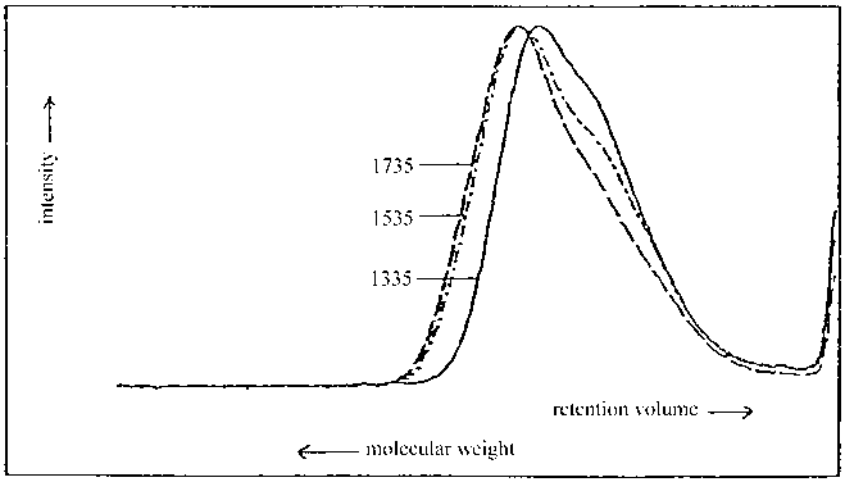

Figure 9 SEC traces of PVP/VA, I series, using the Ultrahydrogel columns of pore sizes 120, 500, 1000, 2000 Å with water–methanol solvent. (From Ref. 6.)

wt/vol) and then diluted with the pH 9 buffer to the proper concentration for analysis. The SEC chromatograms are shown in Fig. 10. The separation is reasonably good; however, a baseline separation between the solvent peak and the low-molecular-weight end of the copolymer peak could not be achieved. The

Table 7 Intrinsic Viscosities and Weight-Average Molecular Weights (Relative to PEO) of PVP/VA and PVP/DMAEMA/VC

Polymer	Composition (% VP)	Aqueous system		Nonaqueous system	
		$\overline{M}_w$	$[\eta]$ (dL/g)	$\overline{M}_w$	$[\eta]$ (dL/g)
PVP/VA					
E335	30	28,800	0.265	37,900	0.261
E535	50	36,700	0.363	38,700	0.241
E635	60	38,200	0.330	37,600	0.253
E735	70	56,700	0.429	52,200	0.310
I335	30	12,700	0.176	15,000	0.162
I535	50	19,500	0.222	20,300	0.174
I735	70	22,300	0.261	21,500	0.182
W735	70	27,300	0.265	25,000	0.238
S630	60	51,000	0.424	48,600	0.321
PVP/DMAEMA/VC	—	82,700	0.620	68,200	0.480

Source: From Ref. 6.

© 2004 by Marcel Dekker, Inc.

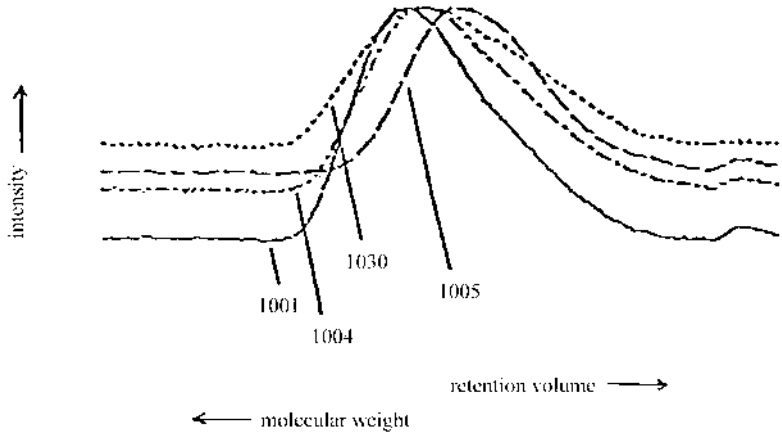

Figure 10 SEC traces of PVP/AA copolymers using the Ultrahydrogel columns of pore sizes 120, 500, 1000, 2000 Å with pH 9 solvent. (From Ref. 6.)

weight-average molecular weights (relative to PEO standards) and intrinsic viscosities of PVP/AA are shown in Table 8. A 100% recovery was achieved for PVP/AA in SEC.

4.3 Cationic Copolymer: Quaternized Copolymer of Vinyl Pyrrolidone and Dimethylaminoethyl Methacrylate

Wu and Senak reported in 1990 (5) the absolute molecular weights and molecular weight distributions of PVP/DMAEMA by SEC/LALLS and SEC with universal calibration using Waters Ultrahydrogel 120, 500, 1000, and 2000 Å columns and a 0.1 M Tris pH 7 buffer with 0.5 M $LiNO_3$ as mobile phase. The quaternized amino

Table 8 Weight-Average Molecular Weights and Intrinsic Viscosities of PVP/AA

PVP/AA	$\overline{M}_w$ (AMU)	$[\eta]$ (dL/g)
1001	318,800	1.33
1004	256,000	1.37
1005	135,000	1.04
1030	277,000	—[a]

[a]Not measurable because of poor solubility at high concentrations.
Source: From Ref. 6.

© 2004 by Marcel Dekker, Inc.

groups on PVP/DMAEMA are responsible for the cationic charge in a pH 7 buffer. Because of the cationic charges on the molecules, a much higher salt content is needed in the SEC mobile phase for the cationic PVP/DMAEMA copolymers (0.5 M $LiNO_3$) than the salt contents for nonionic and anionic copolymers (0.1 and 0.2 M $LiNO_3$) to improve separation and recovery of polymer. As indicated in the earlier discussions, these semirigid polymeric gels are hydroxylated PMMA in nature. They can be expected to have a small amount of free carboxyl groups on the gels as a result of hydrolysis, which can interact adversely with the cationic polymers. The much higher salt content (0.5 M) is required to neutralize the electrostatic interactions between the cationic polymer and the carboxylate groups on the column. A 100% recovery of the cationic PVP/DMAEMA was achieved in SEC in the pH 7 (0.5 M $LiNO_3$) mobile phase.

This cationic copolymer is also soluble in the 1:1 (vol/vol) water–methanol mobile phase with 0.1 M lithium nitrate, and SEC has been carried out in the past in this laboratory in this mobile phase with the Ultrahydrogel columns, with adequate results. The separation and recovery are generally better in the pH 7 buffer with 0.5 M lithium nitrate than in the water–methanol mixed mobile phase with 0.1 M lithium nitrate with the Ultrahydrogel columns and therefore is the preferred method for the PVP/DMAEMA polymer.

The Mark–Houwink constants K and α for cationic PVP/DMAEMA copolymers in pH 7 buffer were determined as 1.42×10^{-4} and 0.67, respectively. The intrinsic viscosities and absolute molecular weights of PVP/DMAEMA are shown in Table 9. The number-average molecular weights are overestimated by SEC/LALLS. The weight-average molecular weights determined by SEC/LALLS are the same as those determined by SEC with universal calibration, indicating the cationic PVP/DMAEMA copolymers are separated by hydrodynamic volumes in SEC. The overlays of molecular weight distributions of the cationic PVP/DMAEMA copolymers are shown in Fig. 11.

Table 9 Intrinsic Viscosities and Absolute Molecular Weights of Cationic PVP/DMAEMA Copolymers in pH 7 Buffer, 0.5 M $LiNO_3$

Polymer	Intrinsic viscosities	Absolute molecular weights (AMU)			
		SEC/LALLS		SEC-universal calibration	
		$\overline{M}_w$	$\overline{M}_n$	$\overline{M}_w$	$\overline{M}_n$
734	0.647	300,000	115,000	331,000	110,000
755	2.15	1,630,000	704,000	1,720,000	483,000
755N	2.22	2,020,000	889,000	2,020,000	523,000

Source: From Ref. 6.

© 2004 by Marcel Dekker, Inc.

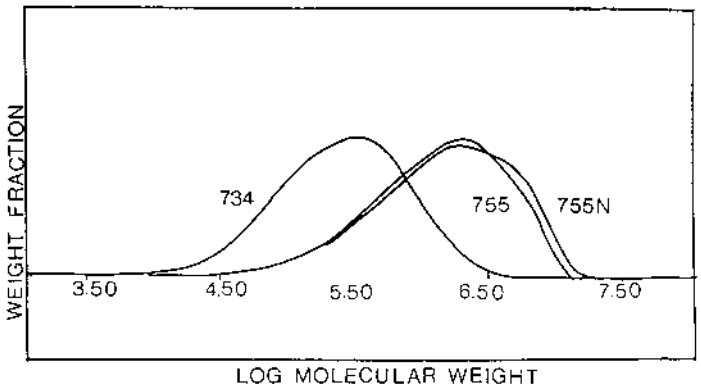

Figure 11 Molecular weight distributions of quaternized polyvinyl pyrrolidone–dimethylaminoethyl methacrylate copolymers. (From Ref. 5.)

5 SEC/MALLS OF PVP

SEC/MALLS has been found very useful in characterizing polymers including PVP in this laboratory in recent years. For example, excellent overlap of absolute M_w versus retention volume plot for all grades of PVP demonstrate similarity in branching among all commercial grades, despite different manufacturing processes (14).

6 CONCLUSIONS

Successful SEC of PVP- and VP-based copolymers in both aqueous and nonaqueous systems using commercially available columns has been reported in the literature. For PVP, separations based on hydrodynamic volume and universal calibration were also reported for both aqueous and nonaqueous SEC systems. In general, the aqueous SEC system (modified with methanol to eliminate polymer–column interactions) provides better separation than the nonaqueous SEC system, especially at the low-molecular-weight end. Therefore, aqueous SEC systems are preferred for PVP- and VP-based copolymers in general, as long as the aqueous system is applicable.

For PVP, the optimized SEC system is the Shodex linear column KB-80M with 20:80 water–methanol (vol/vol) and 0.1 M lithium nitrate. For low- to medium-molecular-weight nonionic copolymers, such as PVP/VA, the optimized SEC system is a Shodex linear column KB-80M plus a low-molecular-weight Shodex KB-802 column and a mobile phase of 50:50 water–methanol (vol/vol)

© 2004 by Marcel Dekker, Inc.

with 0.1 M lithium nitrate. For the anionic copolymers, such as PVP/AA, the optimized SEC system is the Shodex linear column KB-80M and a mobile phase of a pH 9 buffer with 0.2 M lithium nitrate. For the cationic copolymer, PVP/DMAEMA, the optimized SEC system is the Shodex linear column KB-80M and a pH 7 buffer mobile phase with 0.5 M lithium nitrate.

Depending on the molecular weight range of interest, the Shodex linear column KB-80M may have to be replaced with other Shodex OH-pack columns with different pore sizes to optimize separation. Ultrahydrogel columns or TSK-PW columns can also be used interchangeably with the Shodex OH-pack columns for PVP- and VP-based copolymers in the respective mobile phases. However, the Shodex OH-pack columns at the present time provide slightly better separation for high-molecular-weight PVP- and VP-based copolymers than the Ultrahydrogel columns or the TSK-PW columns.

REFERENCES

1. FW Billmeyer, Jr. Textbook of Polymer Science. 3rd ed. New York: Wiley & Sons, 1984, p. 341.
2. H Fikentscher. Cellulose-Chem 13:58, 1932.
3. B Levy, HP Frank. J Polym Sci 37:247–254, 1955.
4. L Senak, CS Wu, EG Malawer. J Liq Chromatogr 10(6):1127–1150, 1987.
5. CS Wu, L Senak. J Liq Chromatogr 13(5):851–861, 1990.
6. CS Wu, J Curry, L Senak. J Liq Chromatogr 14(18):3331–3341, 1991.
7. BG Belenkii, LZ Vilenchik, VV Nesterov, VJ Kolegov, SYA Frenkel. J Liq Chromatogr 109:223–238, 1975.
8. T Hashimoto, H Sasaki, M Aiura, Y Kato. J Polym Sci, Polym Phys Ed 16: 1789–1800, 1978.
9. H Engelhardt, D Mathes. J Chromatogr 185:305–319, 1979.
10. DP Herman, LR Field. J Chromatogr Sci 19:470–476, 1981.
11. S Mori. Anal Chem 55:2414–2416, 1983.
12. A Domard, M Rinaudo. Polym Commun 25:55–58, 1984.
13. EG Malawer, JK DeVasto, SP Frankoski. J Liq Chromatogr 7(3):441–461, 1984.
14. CS Wu, L Senak, J Curry, E Malawer. In: J Cazes, Encyclopedia of Chromatography. New York: Marcel Dekker, 2001, 869–872.

© 2004 by Marcel Dekker, Inc.

12
Size Exclusion Chromatography of Cellulose and Cellulose Derivatives

Elisabeth Sjöholm
Swedish Pulp and Paper Research Institute (STFI)
Stockholm, Sweden

1 INTRODUCTION

Cellulose is the most abundant renewable polymer on Earth, accounting for about 50% of the bound carbon. About 10^{11} tons are synthesized yearly (1,2), by plants, algae (for example, *Valonia*), some animals (tunicates), and enzymatically by some bacteria (for example, *Acetobacter xylinum*). Plants are quantitatively the most important source of cellulose. The chemical composition of plants depends on species but also varies between individual plants of the same species and between different anatomical parts of the same plant. Factors that may influence the chemical composition of a particular plant are, for example, age, place of growth, climate, and harvesting time of the year. The cellulose content of some natural fiber sources is shown in Table 1. Because there often is a lack of information regarding the sample, sampling, and analytical procedure, it is clearly impossible to review absolute figures of reported cellulose content. Thus, the figures shown in Table 1 should only be regarded as guidelines.

© 2004 by Marcel Dekker, Inc.

Table 1 Cellulose Content of Some Common Natural Sources

Source	Cellulose (%)
Softwood	33–42
Hardwood	38–51
Cotton	83–95
Flax (unretted)	63
Flax (retted)	71
Hemp	70–74
Jute	61–72
Ramie	69–76
Sisal	67–78

Source: Refs. 3–5.

Plant fibers are generally classified as seed-hair, bast, or leaf fibers. Seed-hair fibers, such as cotton, aid in the wind dispersal of the seed. Cotton lint fibers are used in the textile industry and the shorter fuzz fibers (linters) are mainly transformed into cellulose derivatives. The bast fibers (for example, ramie, hemp, flax, and jute), and leaf fibers (for example, sisal) have a supportive function. The bast fibers are strings of many individual cells and are used for manufacturing coarse textiles and textile-related products. Leaf fibers are coarser than bast fibers and are used as cordage and for rugs rather than for making clothes.

Today, wood is the main source of the cellulose used for industrial production of paper and board; highly refined wood pulps are the major raw material for regenerated fibers and films or manufacture of cellulose derivatives. Because cellulose is biodegradable, biocompatible, and derivatizable there is also a growing interest in extending the use of biofibers. Besides common derivatives like ethers and esters, efforts are made to find new applications through new derivatives, for example, graft copolymers and products with high net value such as composites (6–9). Size exclusion chromatography (SEC) is an invaluable tool to characterize cellulose, whether the interest is to study native cellulose fibers or to control and develop common or new cellulose-based products. In the present chapter, application and development of SEC for characterization of cellulose is reviewed. This will essentially include the main topics described in the corresponding chapter in the first edition of this handbook (10). The first edition covered the literature from 1970 to 1991, and the present review will give special attention to the literature published during the past decade.

© 2004 by Marcel Dekker, Inc.

2 CHEMICAL, MACROMOLECULAR AND MORPHOLOGICAL STRUCTURES

The molecular level of cellulose, that is, the chemical constitution, the steric conformation, the molecular mass, the three functional hydroxyl groups, and their molecular interactions through hydrogen bonding influence the supermolecular level of the cellulose polymer as well as the morphology of cellulose fibers. These factors are thus important to consider when cellulosic fibers, cellulose derivatives, or cellulose in itself are to be studied and/or characterized by SEC.

Cellulose is a linear polymer composed of β-D-(1$\rightarrow$4) glucopyranose units having a chair conformation with the hydroxyl groups in the equatorial conformation (Fig. 1). The elemental composition of cellulose, from which the empirical formula $C_6H_{10}O_5$ of cellulose could be established, was determined by Payen in 1838 (11), and the connecting β-(1$\rightarrow$4) glycosidic linkages and the linkages within the glucose molecule were established by Haworth. It was Staudinger, however, who proved the polymer nature of cellulose. Due to the β-link, the pyranose ring of every second glucose unit in the polymer chain is turned around about 180° along the longitudinal axis. Because of this, cellobiose can strictly be regarded as the smallest entity of cellulose. One of the terminal groups of the cellulose molecule is called the reducing end since the hydroxyl group at C1 of the cyclic hemiacetal is in equilibrium with the open-chain aldehyde form and thus has a reducing activity. The other end is called the nonreducing end due to its alcoholic hydroxyl group at C4.

The main functional entities that are available for derivatization are the three hydroxyls at C2, C3, and C6 in each glucose unit. These hydroxyl groups also form intra- and intermolecular hydrogen bonds with suitably positioned hydroxyls within the molecule and with adjacent cellulose molecules, respectively. The intermolecular hydrogen bonds are responsible for the stiffness of the cellulose molecule, which is reflected in its high viscosity in solution, its tendency to crystallize, and its ability to form fibrils. In its native state, the cellulose fibrils, sometimes called microfibrils, are assembled to fibril aggregates, which are the smallest morphological structure of the fiber. There is general agreement that

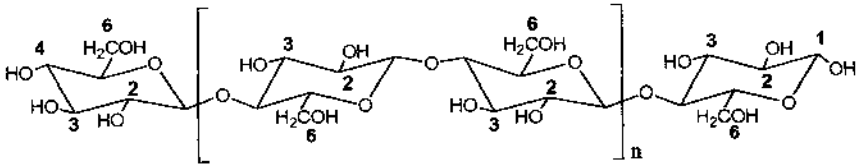

Figure 1 Chemical structure of cellulose. The bold figures denote the positions of the derivatizable hydroxyl groups, that is, carbon number 2, 3, and 6 within the cellulose chain, and carbon number 1 at the reducing end and carbon number 4 at the nonreducing end.

© 2004 by Marcel Dekker, Inc.

cellulose contains both ordered and less ordered regions although the exact arrangement in the microfibrils is still under debate.

According to x-ray diffraction analysis, the ordered cellulose may exist in four crystalline forms, that is, polymorphs: cellulose I, II, III, and IV (12). Cellulose I is a composite of two crystalline forms, I_α and I_β, giving rise to different chemical shifts and signal patterns in solid state (CP/MAS) ^{13}C-NMR spectroscopy. The ratio of I_α and I_β content varies depending on origin and treatment. The dominant polymorph in higher plants such as cotton and wood is cellulose I_β (13,14), whereas algal and bacterial cellulose are rich in cellulose I_α. It has been reported that cellulose I_α is more susceptible to enzymatic degradation and acetylation than cellulose I_β (15,16). Cellulose I can be transformed into cellulose II, during, for example, swelling in strong alkali (mercerization) but cellulose II can also be synthesized by certain bacteria (17) and algae (18). Cellulose III can be formed by treating cellulose I or II with liquid ammonia, and cellulose IV can be obtained by treating regenerated cellulose fibers in a hot bath under stretching (19).

The fiber walls of higher plants are built up by several layers differing from each other both in chemical composition and in the direction of the cellulose fibrils. The noncellulosic components of the plants are of importance to consider when choosing the most appropriate method for purification and isolation of cellulose. Molecules such as waxes, fats, pectins, and proteins present in, for example, cotton and ramie can be removed by dilute alkali or organic solvents. Other molecules, especially hemicelluloses and lignins that surround the cellulose fibrils in many plants like the wood tissue in trees, are more difficult to remove without concomitant degradation and loss of cellulose. The hemicelluloses are heteropolysaccharides and the lignins are amorphous polymers of phenylpropane units. To isolate cellulose from wood, harsh conditions are required and the isolated cellulose samples often remain more or less impure. The wood pulps used for papermaking are produced by chemical (alkaline and/or acidic) or mechanical treatment or by combining these types of treatments in order to liberate the fibers and partially or completely remove the lignin. The amount and state of the cellulose in the different processes differ widely; for more details the reader is referred to Sjöström (20). The kraft-pulping process, which is alkaline, produces about 76% of the wood pulp in the world (1). The condition is adjusted depending on the final use of the pulp and to avoid severe degradation of cellulose. The fibers to be used in the paper industry still contain fairly large amounts of both hemicelluloses and lignin (Table 2). The latter can be removed by acidic bleaching sequences. Thus, the pulp fibers are far from pure with respect to cellulose, which further complicates the dissolution and the chromatographic characterization.

The molecular mass is of interest when dissolving cellulose samples. Like most other natural polymers, cellulose is polydisperse, that is, it is a mixture of molecules of varying chain length. The chain length is often expressed as the number of glucose units, commonly known as the degree of polymerization (DP).

© 2004 by Marcel Dekker, Inc.

Table 2 The Relative Composition of the Main Polymers of Softwood and Hardwood Species, and of Kraft-Pulped Pine Wood and Birch Wood[a]

	Cellulose (%)	Hemicellulose (%)	Lignin (%)
Softwood	33–42	21–29	27–32
Hardwood	38–51	17–33	21–31
Pine kraft pulp[b]	35 (39)	9 (25)	3 (27)
Birch kraft pulp[b]	34 (40)	17 (33)	2 (20)

[a]The figures in parentheses refer to the original wood composition.
[b]Unbleached.
Source: Refs. 3. and 20.

The relation between DP and the molecular mass (M) of a cellulose molecule can thus be calculated by using the molecular mass of the glucan unit, that is, anhydroglucose, $M = 162 \times \mathrm{DP}$.

The M average of dissolved cellulose can be obtained by various techniques. The "zeta average" (M_z) from sedimentation equilibrium data is achieved by ultracentrifugation, the "weight average" (M_w) by light scattering, the "number average" (M_n) by osmometry, and "viscosity average" (M_v) from viscosity measurement. One clear advantage with SEC is the possibility to get all of the averages from the molecular distribution and in addition a measure of the polydispersity (M_w/M_n) of the cellulose sample.

As is true for the determination of the cellulose content, the reported M average of a cellulose sample depends on the source and origin, the isolation method, the solvent system, and conditions during dissolution. Because of this, reported DP averages of native cellulose differ widely. In Table 3 average $\mathrm{DP_v}$ is exemplified for some cellulose samples.

Table 3 $\mathrm{DP_v}$ of some Cellulose Fibers

Samples	$\mathrm{DP_v}$
Valonia	27,000
Acetobacter xylinum	4,000–6,000
Cotton fiber, open–unopened	8,000–15,000
Cotton linters, bleached	1,000–5,000
Bast fiber	8,000–9,600
Ramie fiber	6,500–11,000
Flax	8,800
Wood fiber	8,000–10,000

Source: Refs. 21–23.

© 2004 by Marcel Dekker, Inc.

3 CELLULOSE STRUCTURE AND SEC

To characterize cellulose by SEC, cellulose has to be purified or isolated from its native source and/or dissolved. The most common way to purify cellulose is to extract other molecules prior to dissolution of the cellulose. Holocellulose (cellulose + hemicellulose) can be obtained by removing lignin from wood or wood pulps by acid chlorite (24). Hemicelluloses in delignified fibers can be consecutively extracted with potassium hydroxide and barium hydroxide (25). Another way to reduce the hemicellulose content is by treating delignified fibers with hemicellulose-degrading enzymes (26,27), although a complete removal of hemicellulose is difficult, if not impossible, to achieve. Since the isolation procedure may degrade cellulose and the final sample may also contain impurities, it is important to report the applied isolation method when evaluating the molecular characteristics of the cellulose fraction.

To be defined as cellulose, the polymer must have a DP of at least several hundred (28). According to this definition, cellulose is not soluble in common solvents. The low solubility is partly due to the degree of crystallinity, the crystallite size, and crystallite size distribution (29). The strong interchain forces that bind the cellulose together restrict the accessibility and prevent complete penetration even of hydrophilic solvent systems. To facilitate direct dissolution or derivatization of cellulose, the hydrogen bonds in the ordered cellulose regions are partly broken by an activation step prior to dissolution. The activation is commonly achieved by solvent exchange using, for example, water or amines (30). To be able to chromatograph cellulose, solubility is generally achieved either by forming derivatives that are soluble in common solvents, or by using certain solvent mixtures capable of dissolving the cellulose directly. The main obstacle for a successful characterization of cellulose by SEC is the difficulty to achieve molecular dispersed solutions, both for cellulose and incompletely substituted derivatives (31–33).

3.1 Cellulose Derivatives

Cellulose can be derivatized by introducing functionalities at the primary and at the secondary hydroxyl groups of the glucose unit (Fig. 1). Five positions are available for derivatization; C2, C3, and C6 within the chain, C1 at the reducing end, and C4 at the nonreducing end of the chain, respectively. A variety of soluble cellulose derivatives suitable for SEC can thus be obtained such as esters, for example, cellulose nitrate, cellulose acetate, cellulose carbamate, and ethers such as methyl cellulose, carboxymethyl cellulose, trimethyl cellulose. The degree of substitution (DS) is defined as the average number of hydroxyl groups substituted in a glucose entity. Owing to the high molecular mass of cellulose, the substitution at C1 and C4 is disregarded and the maximum DS is

© 2004 by Marcel Dekker, Inc.

considered to be 3. After the DS has been determined, corrections are made to achieve the original molecular mass of the underivatized cellulose sample. The characterization is then assumed to reflect the molecular mass distribution (MMD) of the original cellulose.

The validity of the data depends, however, on whether a molecular dispersed solution is achieved, the cellulose has been degraded during the reaction, or the low molecular mass partly lost, rendering a nonrepresentative sample. Physical properties such as swelling and solubility are strongly affected by the DS. It is difficult to get a complete substitution or an even distribution of substituents in a cellulose molecule. This is partly due to the heterogeneous nature of cellulose, that is, within ordered and between ordered and less ordered regions. In heterogeneous derivatization systems the relative reactivity is commonly C2OH > C6OH > C3OH (34), but is strongly dependent on the derivatization conditions. Also, the reactivity between the different hydroxyl groups differs. When all hydroxyl groups are equally accessible the usual order of reactivity is C6OH $\gg$ C2OH > C3OH (35). Conventional derivatization procedures are heterogeneous, although it has become more common to perform derivatization in cellulose solvents. Examples of cellulose solvents used in conjunction with derivatizations are *N*-methylmorpholine-*N*-oxide/dimethylsulfoxide (MMNO/DMSO) (36), sulfur dioxide/diethylamine/dimethylsulfoxide (SO_2/DEA/DMSO) (37) but in particular lithium chloride/*N*,*N*-dimethylacetamide (LiCl/DMAc) (38–46). By performing the derivatization in a homogeneous system it is possible to achieve an even substitution throughout the cellulose molecule (47), controlled DS (48), and to use milder reaction conditions than for a corresponding heterogeneous derivatization. Another advantage in doing the derivatization in LiCl/DMAc is that SEC may be performed in the same solvents as used for derivatization.

3.2 Cellulose Solvents

Prior to performing SEC, the sample is dissolved in the same solvent as used as mobile phase. The requirements for a solvent to be used in SEC are that it must dissolve the sample completely, not degrade the sample, be stable, and be compatible with the stationary phase. In addition the solution obtained should not have too high viscosity. Although there are several solvents to dissolve cellulose, only a few are suitable for use in SEC.

Cellulose solvents are generally divided into four main categories (49); where (a) cellulose acts as a base, for example, concentrated acids or Lewis acids, (b) cellulose acts as an acid, for example, amines, sodium hydroxide solutions, (c) cellulose forms complexes, for example, with solvents such as cupriethylenediamine (Cuen), [cadmium tris(ethylenediamine)] dihydroxide (cadoxen), and (d) cellulose forms derivatives such as cellulose xanthate and methylol

© 2004 by Marcel Dekker, Inc.

cellulose. The latter category includes transient derivatives, which are dissolved simultaneously as derivative formation and the cellulose can easily be regenerated (50), in contrast to the stable cellulose derivatives discussed in the previous section. In the following, only relevant nonderivatizing solvents that form true cellulose solutions are considered.

In spite of the alkaline conditions, and thus the risk of degradation, alkaline metal complexes, such as Cuen, are commonly used for viscometric studies because of their capability to dissolve even high molecular mass cellulose. The qualities of the cellulose–metal solutions are still extensively studied (51,52) and compared to the solution characteristics of newer solvent systems. The solubility of low molecular mass cellulose in sodium hydroxide can be significantly improved with thiourea or acrylamide (53) or urea (54). Isogai and Atalla (55,56) have recently reported on complete dissolution of low molecular microcrystalline cellulose in aqueous sodium hydroxide solutions using a freezing procedure. Also, high molecular mass cellulose could be dissolved if regenerated in this solvent system from cellulose solutions of Cuen or SO_2/DEA/DMSO. Ammonia/ammonium thiocyanate (NH_3/NH_4SCN) has been reported to dissolve high molecular mass cellulose and form true cellulose solutions (57–59). Examples of investigated nonderivatizing, nonaqueous systems are MMNO/DMSO (60), lithium chloride/dimethylformamide (LiCl/DMF) (61) and lithium chloride/*N*,*N*-dimethylacetamide (LiCl/DMAc) (62–70). Comparative studies regarding LiCl/DMAc solutions and metal complex solutions of cellulose have been reported (71–73). Of the abovementioned solvents only cadoxen and LiCl/DMAc have been used in SEC of cellulose. Considering that an active solvent for cellulose can, within certain limits, be diluted with an inactive one without losing its dissolving ability, other solvents should also be possible to use.

4 SEC OF DERIVATIZED CELLULOSE

Apart from the interest in studying cellulose derivatives per se, the solubility of cellulose derivatives in common solvents offers many advantages compared to the complex solvent systems that are used for direct dissolution of cellulose. The compatibility with the stationary phase of modern high-performance columns and the possibility to use most kinds of detectors are the most obvious reasons.

4.1 Cellulose Trinitrate

As with other derivatives, the degree of substitution influences the solubility of cellulose nitrates in organic solvents. Cellulose trinitrate, which is easily dissolved in tetrahydrofuran (THF), was the derivative of choice at the time of introducing SEC for molecular mass characterizations (74,75). Cellulose trinitrate had then

© 2004 by Marcel Dekker, Inc.

been extensively studied by methods such as viscometry, osmometry, ultracentrifugation, and precipitation–fractionation and the SEC characterizations could thus be compared with known methods. The preparation procedure of the derivative was considered mild. Nitric acid together with either phosphoric acid and phosphoric pentoxide (76) or acetic acid and acetic anhydride (77) has been used for derivatization. The phosphoric acid or acid anhydride binds the water that is split off in the ester formation, and is thus of importance in the reaction to achieve a complete trisubstitution of cellulose, that is, a nitrogen content of 14.1%, corresponding to a repeating unit molecular mass of 297.

The SEC characterizations of cellulose trinitrate have preferentially been performed using series of columns packed with porous polystyrene particles of different exclusion limits (78–83). Besides THF, which was used in the given examples, ethyl acetate has also been used as mobile phase with polystyrene-packed columns (84). Silica particles, both underivatized and derivatized (85–87), have also been utilized as packing materials.

Today, cellulose trinitrates are rarely used to investigate the molecular mass of cellulose. During the past decade there have only been a few reports concerning cellulose trinitrate (88,89) or nitrocellulose (90,91). The decreased interest in using SEC of cellulose trinitrate as a means to characterize cellulose reflects the uncertainty of the method. The main doubt concerns possible acid hydrolysis of the cellulose chain during derivatization and instability of the derivative. Presence of microgels and the chromatographic behavior are also drawbacks to consider. For a more detailed review of cellulose nitrates, the reader is referred to the first edition of this handbook (10).

4.2 Cellulose Trimethylsilylates

Silylation is a well-known method for solubilizing and quantifying monosaccharides by gas chromatography. Silylation of cellulose has been investigated with a number of silylation agents and solvents. *N*,*O*-bis(trimethylsilyl)acetamide (92), chlorotrimethylsilane (93–95), hexamethyldisilazane (HMDS) (96–98) have been used for silylation of cellulose although HMDS requires addition of a catalyst. A drawback is the tedious purifications of the derivative, which are required to remove excess reagent, solvents, and salts. This is probably the main reason for the limited number of reports on SEC studies of cellulose trimethylsilylates. Trimethylsilylcellulose (TMSC) can be obtained with high DS (2.5–3); the reactivity depends on the solubility of the cellulose sample during derivatization. Pyridine (94), LiCl/DMAc (97,99), or formamide (96) are commonly used as solvent. The solubility of TMSC in THF, the preferred solvent for SEC of derivatives, depends on the DS and DP of the cellulose. Mormann and Demeter (100) studied cotton linter (DP 1100), microcrystalline cellulose (DP 220 and DP 290), and hydrocellulose (DP 40) and found that trimethylsilylates of

© 2004 by Marcel Dekker, Inc.

microcrystalline cellulose with a DS of 2.7 are completely soluble in THF whereas no sample having a DS of 3 was soluble in THF. Because soluble and insoluble fractions had similar DS it was concluded that the solubility depended not only on the DS of the derivative. The insolubility was suggested to be due to some kind of hydrophobic aggregation of high molecular mass cellulose samples. For SEC purposes, it is thus important to control the DS. During the past few years, systematic investigations of silylation conditions have been performed and some SEC applications reported (Table 4). The chromatograms have been evaluated using differential refractive index (DRI) detectors (98,100–102), dual detector systems consisting of either differential viscometry (DV) detector/DRI (97), or multi-angle laser light scattering (MALLS) detector/DRI (101), and also by using an evaporative light-scattering detector (95).

Complete (100) and controlled partial DS silylations, depending on reaction conditions and type of cellulose (98,103), have been reported. The derivatization was performed with HMDS, using liquid ammonia as solvent and saccharine as catalyst. The obvious advantage of the procedure, besides controlled substitution, is that no purification of the derivative is needed. According to SEC results no degradation takes place during derivatization. Another way to obtain cellulose samples with a controlled DS is to desilylate trimethylcellulose in THF/liquid ammonia (102). According to SEC characterizations, the molecular mass of microcellulose increases with increasing DS and no degradation could be observed.

Using partially substituted trimethylsilylates (DS 2.1 ± 0.2), Einfeldt and Klemm (97) studied bacterial cellulose by SEC using THF as mobile phase. The derivatives were synthesized in a homogeneous reaction in LiCl/DMAc with hexamethyldisilazane (HMDS). Continuous polymer fractionation (CPF) of cellulose has been investigated using silylated cotton linters (DP_{Cuoxam} 850) (101).

Table 4 SEC of Trimethylsilylcellulose using THF (1 mL/min) as Mobile Phase[a]

Packing material	Exclusion limits of each column (Å)[b]	DS of studied samples	References
Ultrastyragel	500, 10^4, and linear[c]	2.1 ± 0.2	97
Polystyrene	10^2, 10^3, 10^5, 10^6	2.5	98
PS/DVB[d]	10^3, 10^5, 10^6	3.00; 2.57	100
PS/DVB[d]	10^3, 10^5, 10^6	2.89	101
PS/DVB[d]	Linear[c]	1.53; 1.78; 2.37	102

[a]No information about temperature during analysis.
[b]Å $= 10^{-10}$ m, generally defined as the exclusion limit of polystyrene dissolved in THF.
[c]Exclusion limit not reported.
[d]Polystyrene/divinyl benzene.

© 2004 by Marcel Dekker, Inc.

The silylation was performed in LiCl/DMAc with a reagent mixture of hexamethyldisilazane (HMDS) and chlorosilane. The obtained DS was 2.89 and the cellulose derivative was reported to be completely soluble in THF. Both initial and fractionated TMSC were characterized using SEC.

4.3 Cellulose Acetate

Cellulose acetate is commercially one of the most important cellulose derivatives and is utilized, as, for example, fibers and filters. The application of the product is highly dependent on the DP as well as the DS of the derivative. The interest in characterization of cellulose acetate by SEC is thus primarily connected to commercial production rather than to the study of cellulose per se. Reported chromatographic conditions for various cellulose acetates are shown in Table 5.

Table 5 SEC Conditions for Characterization of Cellulose Acetate Samples

Cellulose sample	Packing material	Exclusion limits of each column (Å)[a]	Solvent	Temperature (°C)	Flow rate (mL/min)	Reference
Diacetate	—	3×10^3 8×10^3 10^5	THF	Ambient	1.0	110
Diacetate	Styragel	3×10^4 10^5 3×10^6 10^6	THF	Ambient	1.0	111
Triacetate	Styragel	7×10^5 5×10^6 5×10^3 $2–5 \times 10^3$	DCM	Ambient	1.0	112
Diacetate	TSK GMPW$_{XL}$ or CPG-10 or Toyopearl-75HW	—	Acetone	—	—	106
Diacetate	PL Gel+ Shodex A80M	10^3 10^4 10^5+ one mixed	DMAc[b] or NMP[b]	80 (DMAc) 60 (NMP)	1.5	104
DS 0.7–2.5	PL mixed B	$3 \times$ linear 10×10^6	0.5% LiCl/ DMAc	60	1.0	105

[a]Å $= 10^{-10}$ m, generally defined as the exclusion limit of polystyrene dissolved in THF.
[b]With and without addition of 10^{-2} M LiCl or LiBr.

© 2004 by Marcel Dekker, Inc.

Concentration-sensitive detectors (104,105) as well as low-angle laser light scattering (LALLS) detectors (106,107) have been used during the last decade.

Cellulose acetate is commonly produced by reaction with acid anhydride using a catalyst such as zinc chloride or sulfuric acid (35). In this solution process, the derivative formed is dissolved in glacial acetic acid or dichloromethane. For cellulose triacetate (CTA) (DS 2.8–3.0) the fibrous process is commonly applied. This process uses perchloric acid to catalyse the reaction and a nonsolvent of the derivative to maintain the fiber structure. Cellulose diacetate (CDA) can also be made by deacetylation of CTA.

The chemical and enzymatic reactivity is highly dependent on the DS of the cellulose acetate. The depolymerization of cellulose is catalyzed by sulfuric acid; that is, the latter does not only catalyze the acetylation reaction. By using GPC-LALLS, Shimamoto *et al.* (107) found that the depolymerization reaction is faster during the early stages of acetylation than for the fully substituted derivative, and also that the depolymerization of CTA proceeds randomly whereas the hydrolysis of cellulose does not. The degree of biodegradability is also closely connected to the DS, the lower DS the more biodegradable the cellulose acetate becomes (105).

Depending on application, the target DS is in the range 1.2–3. The solubility depends on the DS but also on the distribution of substituents between the three possible positions (108). CDA (DS 2.2–2.7) is soluble in acetone and THF whereas CTA requires chloroform or dichloromethane for dissolution. From light-scattering studies, various degrees of aggregation of dilute solutions of CTA in m-creosol, tetraethane, and mixtures of dichloromethane–methanol have been shown (109). SEC characterizations have been performed primarily on cellulose diacetates and triacetates using THF (110,111), chloromethane (112), or acetone (106) as solvent, but also polar solvents such as DMAc (104,105) or *N*-methylpyrrolidone (NMP) (104) with or without addition of salt have been used in the past (Table 5). Owing to the high viscosity of cellulose acetate solutions of DMAc or NMP, the chromatography is performed at elevated temperature.

A general problem encountered with SEC of cellulose acetate is the presence of extra humps and/or shoulders on the high molecular mass range of the main distribution and, in addition, a gel fraction (104,106,110–112). Whereas the gel fraction may be found in solutions of cellulose acetate samples from both cotton linter and wood pulps, the other anomalies are commonly only observed in cellulose acetates from wood pulps. The observed prehumps correlate with the hemicellulose content of the sample and can be reduced by optimizing the reaction conditions during acetylation or removed by fractional precipitation (110,111).

The extra peaks have also been attributed to ionic effects caused by sulfate groups in the CDA solutions of acetone (106,113). The prehumps could only be

© 2004 by Marcel Dekker, Inc.

observed using column materials having a slightly anionic charge ($GMPW_{XI}$ and CPG-10) and not when neutral column material (Toyopearl-75HW) was used (106), indicating an exclusion effect of the former column material. By addition of CaI_2 or NaI, the prehumps in the chromatograms were eliminated. Fleury *et al.* (104) thoroughly studied the humps of CDA from cotton linter and wood pulp samples seen in SEC by using polystyrene divinylbenzene (PS/DVB) columns and DMAc or NMP as mobile phase. The first eluting hump, the gel fraction, of the cellulose acetate samples was isolated by ultracentrifugation of acetone solutions of the samples prior to SEC. The amount of microgels in the wood pulp acetate was more than twice that of the corresponding cotton linter sample. After hydrolysis of the microgel fraction, it was found that the cotton linter sample consists almost exclusively of glucose while that of wood pulp also contains xylose, mannose, and galactose. By x-ray and electron diffraction analysis it was found that the microgel fraction from the cotton linter corresponds to CTA and the microgel fraction from the wood pulp sample is a mixture of CTA and xylan diacetate. The reason for the remaining prehumps was attributed to ionic associations of remaining sulfate groups on the CDA with residual calcium. The latter component proved to be directly correlated with size. By addition of 0.01 M LiBr or LiCl to DMAc or NMP, the ionic effects were eliminated and prehumps in the chromatogram were circumvented. Thus, the problems encountered with SEC characterizations of acetates can be regarded as solved utilizing Li-salt addition to the mobile phase, it being DMAc or NMP.

4.4 Cellulose Tricarbanilate

The first report concerning SEC application for characterization of cellulose triphenylcarbamate or tricarbanilate (CTC) was in 1968 (114). CTC is still the most utilized derivative for SEC studies on different kinds of cellulose samples, for example, microcrystalline cellulose, cotton linters, dissolving pulps, paper grade pulps, paper, ramie, and linen. The advantages in using CTC for cellulose characterizations are complete substitution, no depolymerization during the derivatization procedure, the stability of the formed derivative, and solubility and stability in THF. Fully substituted cellulose has a nitrogen content of 8.09%, corresponding to a repeating unit molecular mass of 519. Thus, the large molecular mass is important to consider in order to select columns with appropriate exclusion limits. The columns used are exclusively packed with porous crosslinked polystyrene particles. Owing to the aromatic group in the carbanilate, UV detection has frequently been used for SEC of CTC. Differential refractive index detectors (DRI) and on-line light-scattering detectors, such as low-angle laser light scattering (LALLS) and multi-angle laser light scattering (MALLS) detectors, have been used over the past few years. Commonly used SEC conditions for characterization of CTCs are exemplified in Table 6.

© 2004 by Marcel Dekker, Inc.

Table 6 SEC Conditions for Characterization of CTC Using THF as Mobile Phase Except for Where LiCl/DMAc Was Used

Packing material	Exclusion limits of each column (Å)[a]	Temperature (°C)	Detector(s) and wavelength (nm)	Flow rate (mL/min)	Reference
TSK-Gel HXL		—	UV (245)	—	128
G7000	4×10^8				
G6000	4×10^7				
G5000	4×10^6				
Shodex		—	UV (235)	1.0	119
KF-806	20×10^6				
KF-805	4×10^6				
KF-804	4×10^5				
Shodex		—	UV (235)	1.0	130,131
KF805	4×10^6				
KF803	7×10^4				
μStyragel	100				
Shodex		—	UV (236)	1.0	120
KF-806	20×10^6				
KF-805	4×10^6				
KF-804 or	4×10^5				
PL gel	10^6, 10^6, 10^3				
Ultrastyragel	10^6, linear, 10^5, 10^4	35	UV (278)	1.0	136
PL gel	10^6, 10^5	25	UV (225)	1.0	137
Phenogel		Ambient	DRI	1.0	125
PHOOH					
0447KO	10^6				
0446KO	10^5				
0445KO	10^4				
Waters		Ambient	DRI and UV (236)	—	129,138
Ultrastyragel	10^6, 10^5, 10^4, 10^3				
Shodex		—	—	—	139
KF807	2×10^8				
KF805	4×10^6				
KF803	7×10^4				
Waters					
μStyragel	100 Å				
LiChrogel		25	LALLS (633)/	0.5	121[b]
PS40000	—		DRI		
PS4					
Waters		20	UV (235)	1.0	132
Ultrastyragel	10^4, 10^3				
Shodex		Ambient	UV (254)/	0.6	117
KF-serie	10^6, 10^5, 10^5		MALLS (690)		

© 2004 by Marcel Dekker, Inc.

Table 6 (*Continued*)

Packing material	Exclusion limits of each column (Å)[a]	Temperature (°C)	Detector(s) and wavelength (nm)	Flow rate (mL/min)	Reference
Waters		—	RI/	0.735	122
HT6	2×10^5 to 10^6		MALLS (488)		
HT5	5×10^3 to 6×10^5				
HT4	5×10^2 to 3×10^4				
PL gel		80	UV (295)/DRI	1.0	134[c]
4 × mixed A	40×10^6				

[a]Å $= 10^{-10}$ m, generally defined as the exclusion limit of polystyrene dissolved in THF.
[b]CTCs having different DS of substituents on the phenyl group.
[c]Phenyl, ethyl, and propyl carbanilate, LiCl/DMAc as mobile phase.

Unbleached wood pulp samples need to be (chlorite) delignified prior to derivatization (115,116), but for cellulose fibers having a lignin content below approximately 2.5%, delignification is not necessary (117). The general procedure for derivatization of cellulose includes several steps: (a) activation, (b) reaction of cellulose with phenyl isocyanate ($OCNC_6H_5$), (c) addition of methanol to react with the excess reagent, (d) precipitation in a nonsolvent, (e) repeated washing of the precipitated derivative, (f) freeze-drying, and (g) dissolution in THF. The long preparation time and the risk of losing low molecular mass constituents of the sample in the precipitation step are some disadvantages of this procedure.

Activation to open up the structure of the sample prior to derivatization has been pointed out as necessary for some sample types such as regenerated cellulose samples and high molecular mass cellulose samples. The activation has been carried out in water (116,118), liquid ammonia:pyridine (119,120), ammonia (121), pyridine (122), ammonia:DMSO (119), DMSO (123), DMSO:pyridine (124), and LiCl/DMAc (125).

The heterogeneous carbanilation reaction is commonly performed in dimethylsulfoxide (DMSO) or pyridine. Since the reaction proceeds faster in DMSO (120), the reaction temperature is kept lower than when pyridine is used, typically 70°C for DMSO and 80°C for pyridine. It has however been reported that DMSO degrades high molecular mass samples when the reaction time is longer than 32 hours, although a CTC prepared from the same source, that is, bleached cotton linters, did not suffer appreciable loss of the molecular mass (M) after treatment in phenylisocyanate in DMSO at 70°C for 72 hours (120). Using an on-line MALLS detector during the chromatography, LaPierre and Bouchard (117,126) found that the DP of CTCs prepared from softwood kraft pulps was

© 2004 by Marcel Dekker, Inc.

higher when using pyridine than when using DMSO, whereas no difference was observed for microcrystalline cellulose or filter paper samples. The higher DP for the softwood kraft pulp samples was ascribed to incomplete derivatization in pyridine leading to aggregation of the cellulose part of the sample. Using LiCl/DMAc as solvent and only catalytic amounts of pyridine, the reaction proceeds homogeneously and the CTCs are formed within three hours for various samples (125). The chromatographic condition used was, however, not adequate for high M samples, giving a nonquantitative response and about half of the expected M_w as obtained from off-line LS measurements.

Precipitation and removal of byproducts (*N*,*N*-diphenylurea, methyl phenylcarbamate, and the phenylisocyanate trimer) are important for determination of the elemental composition, that is, determination of the DS. Precipitation has been carried out in neat EtOH (123,127,128) or neat MeOH (121,125,129). The conditions chosen for precipitation are a trade-off between complete removal of byproducts and complete recovery of the CTC (120). To circumvent the incomplete precipitation of the CTC in neat solvents, mixtures of water and MeOH (30:70 or 50:50) have been used with or without addition of salt (117,119,120). Coprecipitated trimer can be removed by extraction with toluene (120). Precipitation of CTC from the reaction medium has also been achieved using a mixture of MeOH, water, and acetic acid (122). In those cases where purification is not needed, a complete recovery of the derivative can be ensured by evaporation of the solvent (118,130–132).

Efforts to catalyze the carbanilation reaction have been made by adding different kinds of amines to the reaction mixtures consisting either of pyridine, DMSO, or DMF as solvents (124,133). 1,4-Diazobicyclo(2.2.2)octane (DABCO) and 4-*N*,*N*-dimethylaminopyridine accelerated the dissolution of cellulose during the reaction and DABCO in pyridine made it possible to carbanilate samples, which were otherwise unreactive in pyridine. However, several disadvantages were reported such as severe tailing of the elution curves due to incomplete carbanilation, loss of phenyl isocyanate by formation of phenyl isocyanate depolymerization, and retardation of the carbanilation reactions by some amines (133). Presence of pyridine or its derivatives in carbanilation reactions of Avicel or cotton linter samples in DMSO was found to cause severe depolymerization of the cellulose (124).

A method for carbanilation and direct SEC of lignin-containing hardwood kraft pulps and softwood kraft pulps using LiCl/DMAc has recently been reported (134). The samples were successfully carbanilated using phenyl, ethyl, or propyl isocyanate according to the procedure described by McCormick and Lichatowich (135), but without addition of catalyst. For studies of the pulp lignin and its interference with cellulose and hemicellulose the preferred reactants are ethyl isocyanate or propyl isocyanate, since the UV absorbance of the phenyl carbanilate interferes with the UV absorbance of lignin.

© 2004 by Marcel Dekker, Inc.

4.5 Other Cellulose Derivatives

Besides cellulose acetates, the previously described cellulose derivatives are made to study the cellulose itself. In this section, SEC of ether derivatives made for some given applications are mainly reviewed. These derivatives are heterogeneous; not only with respect to the types of substituents, but also because most of them are only partially substituted to attain the desired properties. SEC conditions used during the last decade for characterization of ionic and nonionic cellulose ethers are shown in Tables 7 and 8, respectively.

Examples of ionic cellulose ethers are carboxymethyl cellulose (CMC), mixed derivatives such as carboxymethyl hydroxyethyl cellulose (CMHEC), and amphoteric cellulose derivatives (140–142) such as carboxymethyl-2-diethylaminoethyl (CM-DEAE) cellulose. Examples of nonionic organic ethers that recently have been characterized by SEC are methyl cellulose (MC), hydroxyethyl cellulose (HEC), hydroxypropyl cellulose (HPC), ethyl(hydroxyethyl) cellulose (EHEC), hydroxypropyl(methyl) cellulose (HPMC), and benzylated pulps. In addition, different types of hydrophobically modified CMC (HMCMC), have been studied by SEC (143-147).

A common feature of partially derivatized cellulose is the tendency to form supermolecular structures in solution (148). This has been attributed to a nonrandom aggregation caused by an uneven derivatization along the cellulose chain, that is, blocks of less substituted chain segments. Commonly used mobile phases for SEC characterizations of cellulose ethers are aqueous saline or buffers. For polyelectrolytes, such as CMC, a high ionic strength of the mobile phase has the advantage of reducing the hydrodynamic volume, thereby reducing the effect of heterogeneity of the ionic groups along the polymer as well as reducing the viscosity of the sample (149). The relative viscosity of injected samples as compared to the mobile phase should be below 1.5 to obtain peak shapes and retention times that are independent of sample concentrations (150,151). On the other hand, too high salt concentrations promote hydrophobic interaction between the sample and the stationary phase. Addition of methanol to the mobile phase is commonly practiced to circumvent associations of nonionic derivatives of medium polarity (Table 8).

Sodium CMC is the most widely used cellulose ether. The most commonly used type of CMC has a DS of 0.65–1.0 (152), and is soluble in water. It has a wide range of utilization, for example, as an emulsion stabilizer, thickener, sizing agent, and binder. Water-insoluble CMC with a DS of less than 0.4 and crosslinked water-soluble CMC are used as superadsorbents and ion exchangers. Rinaudo and co-workers (153) concluded that the charge density of CMC does not change with M_w in the range 40,000–550,000 and that a DS between 1.0 and 2.9 neither influences the refractive index increment dn/dc nor the K and a parameters in the Mark–Houwink relationship. The latter means that the universal calibration

© 2004 by Marcel Dekker, Inc.

Table 7 SEC Conditions for Characterization of Ionic Cellulose Ethers

Celluose derivative	Packing material	Mobile phase	Detectors	Flow rate (mL/min)	Reference
CMC	Separon HEMA mono C60, G65 or	0.1 M or 0.1 mM NH_4NO_3	DRI/ Conducto-metry	—	153
	Shodex OH pak B804, B805	0.1 M NH_4NO_3	DRI/DV/ MALLS		
CMC DS 0.71–2.95	TSK 30, 40, 50, 60	0.1 M and 0.5 M $NaNO_3$ with 0.02% NaN_3	MALLS/DRI	—	155
CMC	Separon HEMA 1000	0.5 M NaOH or 0.4 M acetate buffer	UV/RI	0.5	154
CMC DS 0.75–1.25	TSK PW G6000, G5000, G3000	0.02 M or 0.1 M $NaNO_3$	MALLS/DRI	0.95	156
CMC	TSK PW_{XL} 30–60	0.1 M $NaNO_3$ with 0.02% NaN_3	MALLS/DRI	—	157
CMC	Analytical: TSK PW_{XL}[a] G5000, G4000, G3000	0.1 M $NaNO_3$	LS[b]/DV/RI	0.4	158–160
	Preparative: HiLoad 26/ 60 Superdex 75	0.1 M Ammonium acetate	RI	1.1	
CMC	TSK PW G6000, G3000	0.3 M NaCl/ 0.03 M Na_2HPO_4	DRI	0.5	161
CMC and CM-DEAE cellulose	Sepharose CL-2B	0.08 M–1.0 M[c] NaCl	—	0.4	140,142

[a]Guard column G2500.
[b]Two-angle LS.
[c]Concentration range used at pH 2.5, 6, or 12.

procedure can be used to determine the M_w of CMC. The neutral polymer dextran is commonly used for universal calibration of the SEC system. It has been proven valid for alkaline (0.5 M NaOH) and acid (0.4 M acetate buffer, pH 5) conditions (154). However, the authors recommended the alkaline eluent for MMD characterizations, due to the lower hydrodynamic volume of the CMC and to the lack of aggregation as compared to the acetate buffer system.

© 2004 by Marcel Dekker, Inc.

Table 8 SEC Conditions for Characterization of Nonionic Cellulose Ethers

Sample	Packing material and pore size designation	Mobile phase	Detector(s) and wavelength (nm)	Flow rate (mL/min)	Reference
MC, HEC, HPC, EHEC, HPMC	Diol modified LiChrospher 4000, 1000, 300	MeOH : 10 mM NaCl (aq) (50 : 50)	LALLS/DRI	—	162
HEC	TSK PW G5000, G4000	0.05 M NaCl with 0.02% NaN_3	LALLS/DRI or UV (208)/ DRI	0.8	163
HPMC	Methacrylate,[a] Hydroxylated polyetherbased[b]	Buffer[c] : MeOH (4 : 1)	DRI	1.0	164
HPMC	TSK PW G6000, G5000, G4000	Phosphate buffer, I = 0.1, pH 6.5	MALLS/RI	0.8	165
MC[d]	TSK PW G1000	0.05 M NaCl	RI	1.0	166
Benzylated pulps[e]	PL gel[f] 10000, 1000, 500	THF	UV	—	167
HEC, HMHEC[g], (CMC) HMCMC[g]	TSK PW G6000, G4000	0.1 M $NaNO_3$	MALLS/DRI	—	144
HMCMC[g]	TSK PW G6000, G4000 TSK SW_{XL}	0.1 M $NaNO_3$	MALLS/DRI	—	145
HPC-IND[h]	Ultrastyragel[f] 10^4, 10^3, 500, 2×100	THF	DRI/UV (265)	—	143
CEPAN[i]	[j]— 10^4, 10^3, 500	3% LiCl/ DMAc	—	1.0	146

[a]Exclusion limit 80,000 polyethylene glycols (PEG).
[b]Exclusion limit 1000 PEG.
[c]10 mM KCl, 13 μM sodium borate decahydrate, 1.5 mM dextrose, and 90 mM boric acid.
[d]Trade name: Methocel A15-LV.
[e]From sugar cane bagasse.
[f]Exclusion limit in Å ($= 10^{-10}$ m).
[g]HMHEC modified with C_{16} and HMCMC modified with hexadecylamine.
[h]Indometacin (IND) grafted onto hydroxypropyl cellulose (HPC).
[i]Cellulose–polyacrylonitrile copolymer.
[j]Packing material not reported.

© 2004 by Marcel Dekker, Inc.

5 SEC OF UNDERIVATIZED CELLULOSE

Historically, the two solvents used for SEC of underivatized cellulose are cadoxen and LiCl/DMAC. However, during the past decade hardly any reports of cadoxen in conjunction with SEC have appeared. During the same period, LiCl/DMAc has become the number one choice for various investigations of all kinds of cellulose samples.

5.1 Cadoxen

The cadmium–ethylene diamine complex possesses a number of desirable properties for studies of cellulose solutions. The solvent is colorless, easy to handle, and dissolves many kinds of cellulose samples. The main disadvantages are that it includes a toxic compound (Cd), it is time-consuming to prepare, and that the cellulose solutions have a high viscosity. It has also been reported that hardwood pulps have a limited solubility in cadoxen (168).

The preparation of cadoxen is usually a modification of the original procedure described by Jayme and Neuschaffer (169). Ethyleneamine is saturated with cadmium oxide in the presence of sodium hydroxide. The cadmium content ranges between 4.5 and 5.2%, ethyleneamine between 25 and 30%, and sodium hydroxide between 0.2 and 0.5 M; for a detailed description of the preparation of cadoxen see Ref. 170. The addition of sodium hydroxide increases the dissolving power but also increases the degradation of dissolved cellulose (171,172). The solvent as well as the cellulose solutions are fairly stable provided they are stored at 4°C in the dark. When the cellulose solution is used within a couple of days, degradation can be neglected (173). It has also been pointed out that water-miscible organic liquids should not, in general, be added to the cadoxen solution, since they induce turbidity and precipitation (173).

For dissolution of cellulose, cadoxen is brought to room temperature and added to the sample. The dissolution time for cellulose ranges from a few minutes up to two hours, depending on type and molecular mass of the cellulose, the degree of crystallinity, and the desired concentration of cellulose. Prewetting the sample with water facilitates the dissolution of high molecular mass samples. Commonly, the solution is diluted with an equal volume of water prior to chromatography. The diluted solution is not capable of dissolving additional cellulose, which makes it possible to use carbohydrate-based packing material in the subsequent chromatography.

SEC of cellulosic samples dissolved in cadoxen solutions was reported mainly during the late 1960s and 1980s (174–184). Various packing materials have been used such as polyacrylamide gel, agarose gel, vinyl polymer-based gels, and chemically modified silica gels (178) have also been tested. Since crosslinked

© 2004 by Marcel Dekker, Inc.

dextrans swell too much in cadoxen solutions, cellulose–cadoxen solutions have been characterized using 0.5 M NaOH as mobile phase.

5.2 Lithium Chloride/*N*,*N*-Dimethylacetamide

Among the investigated solvents for dissolution of cellulose, lithium chloride/*N*,*N*-dimethylacetamide (LiCl/DMAc) has proven to be the most successful to be used in SEC. The first report on LiCl/DMAc as solvent for cellulose appeared in 1981 (38,62). A number of models for the solvent–cellulose complex have been proposed and reviewed recently (66,68). The first report about the application of LiCl/DMAc for SEC of cellulose appeared in 1986 (185). Since then, a number of underivatized cellulosic samples have been characterized by SEC. Examples are cotton fibers (186–190), different kinds of cellulose samples from cotton (190–201), ramie (202), wood pulps from the sulfite process (191,201,203–207), and wood pulps from the kraft process (191,196,199,200,204,208–214). The stationary phase used is crosslinked PS/DVB particles. Reported chromatographic conditions are summarized in Table 9.

Cellulose–LiCl/DMAc solutions suitable for SEC are in principle simple to prepare. The sample, in the concentration range 0.8–1.25% (wt/vol) is dissolved using high concentrations of LiCl, typically 8–10% (wt/vol). The concentrated solution is then diluted about ten times. However, for successful dissolution of the cellulosic sample, activation prior to dissolution is necessary. There are two principal ways of activating the sample, in the following denoted procedures I and II, respectively. In both procedures, stirring during dissolution is recommended.

Swelling of cellulose in a polar medium followed by solvent exchange is the most common way of activation, here called procedure I. The sample is commonly soaked in water either at ambient temperature (190,197,198) or at 4°C (200,209,212). Swelling in steam or liquid ammonia has also been reported (62). Recently, the benefit of swelling sulfite pulp samples and cotton linter samples in a solution of 0.1 M LiCl in deionized water has been reported (206). In the same study, consecutive washing with chelating agents (DTPA and EDTA) and aqueous citric acid to remove metal ions was reported to facilitate the dissolution of the samples. Although the swelling requires a polar medium, it has to be carefully removed before dissolution in LiCl/DMAc. The solvent change is commonly made using acetone and/or methanol several times, and finally always by using neat DMAc. A solution of LiCl/DMAc is added to the sample, which is generally dissolved at 4°C. The time for complete dissolution is highly dependent on concentration, DP, crystallinity, and lignin content of the sample as well as on the LiCl concentration. Generally dissolution is obtained within one day, but high molecular mass samples, especially those containing hemicellulose and lignin, may need up to five days before dissolution is achieved.

© 2004 by Marcel Dekker, Inc.

Table 9 SEC Conditions for Characterization of Underivatized Cellulose Samples Using LiCl/DMAc as Solvent

Packing material	LiCl % (wt/vol)	Temperature (°C)	Flow rate (mL/min)	Detectors	References
Ultrastyragel 10^5, 10^4, 10^3	0.5	80	1.0	DRI	185
Styragel 10^6, 10^3	0.5	30–45	1.0	DRI	203
PL mixed A 1 × linear	0.5	80	1.0	DRI	191
Ultrastyragel 10^6, 10^5, 10^4, 10^3	0.5	80	1.0	DV/DRI	186,187,189
TSK GMHXL	5	Ambient	0.1	—	202
μStyragel 10^6, 10^5, 10^4	1	80	1	UV[a]/DRI	204,212,220,221
PL mixed B 3 × linear	0.5	80	1.0	DV/DRI or LS/DV/DRI	192–195
Ultrastyragel 10^6, 10^5, 10^4, 10^3	0.5	80	1.0	DRI	196
PL mixed B 1 × linear	0.5	80	1.0	DRI	205
PL mixed C 1 × linear	1	RT	0.7	DRI	190
PL mixed B 2 × linear	0.8	80	1.0	UV[a]/DRI	213
μStyragel 10^6, 10^5, 10^4, 10^3	0.5	60	0.72	DV/DRI	197
PS/DVB[b] or PL mixed B 2 × linear	0.5	40	1.0	MALLS/DRI	198,206
PL mixed A 4 × linear	0.5	80	1.0	UV[a] or UV[a]/DRI	200,208–211
Phenogel mixed[c] 4 × linear	0.5	55	0.3	DRI	201

[a]295 nm.
[b]Macroporous monodisperse polystyrene/divinylbenzene.
[c]Narrow bore columns.

The second common way of activating the sample is by treating the sample with hot DMAc (procedure II) at 145–150°C, commonly for one to two hours (62,186). The suspension is cooled to 100°C to avoid degradation (62) before LiCl is added to dissolve the sample. Different conditions with respect to temperature and time have been used to complete the dissolution of the cellulose. For instance, the sample can be dissolved at 100°C (213) or at 50°C (196), the latter followed by

© 2004 by Marcel Dekker, Inc.

stirring at room temperature for an extended time. Dissolution has also been achieved by maintaining the temperature at 100°C for a period of time before lowering the temperature to 50°C for an additional period of time (186,195). The total dissolution time is, as always for cellulosic samples, dependent on type, molecular mass, and degree of crystallinity of the cellulose.

Irrespective of the activation–dissolution procedure, the dissolved sample is diluted with DMAc prior to chromatography, and the final concentration of sample and LiCl is commonly 0.05–0.1% and 0.5–1.0%, respectively. Owing to the high viscosity of the final sample solutions, SEC is commonly performed at 80°C.

Since water has a deleterious effect on the dissolution, efforts to use dry salt and solvent are crucial. To completely avoid the presence of water is a difficult task, since LiCl as well as DMAc are highly hygroscopic. Thus, for practical applications, the solvent system should be regarded as a ternary solvent system, consisting of LiCl, DMAc, and water (215). Since the maximum solubility of LiCl in dry DMAc is 8.46%, reported concentrations above this value may be due to the presence of water. In order to obtain comparable SEC or light scattering results from cellulose–LiCl/DMAc solutions, Potthast and co-workers (215) recommend that the water content of the solvent system should be specified, and also describe a method by which this could be done. Another complication to consider is that heating/refluxing DMAc or LiCl/DMAc generates a number of chromophores in the solvent (216). One of these, *N*,*N*-dimethylacetoamide, is able to react with glucose and form a furan structure, which also was reported found in heated solutions of different pulps in DMAc or LiCl/DMAc. According to these findings, the dissolution procedure that includes heating, for example, procedure II, should be avoided. In a recent review on the characterization of cellulose by LiCl/DMAc-SEC, it was concluded that further improvements with respect to ionic strength and pH of the mobile phase are needed (217).

The formed solution is stable (218), although a slight decrease in the viscosity of solutions stored at 30°C for 30 days has been reported (64). Strlič *et al.* (190) found that oxidized cellulose samples are stable when the sample is dissolved at room temperature, that is, according to procedure I. Recently, Jerosch and co-workers (201) compared the stability of 8% LiCl/DMAc solutions of untreated and differently aged cellulose samples dissolved by procedure I. After 1–23 days storage at 35–40°C, the solutions were diluted and characterized by SEC. The solutions of untreated bleached sulfite softwood pulps and bleached cotton linters were found to be stable for 12 days and 6 days, respectively. The corresponding aged samples were more susceptible to degradation, the more initially degraded the faster was the solvent-initiated degradation. The authors recommend that the temperature as well as dissolution time should be lowered to avoid degradation.

Characterization of wood pulps is more complex since these types of samples also contain hemicellulose and lignin, the latter being absent only in

© 2004 by Marcel Dekker, Inc.

fully bleached pulps. Although isolated lignin samples are easily dissolved in LiCl/DMAc, unbleached samples containing high amounts of lignin cannot be completely dissolved. Hitherto, no systematic study concerning the limiting amount of lignin content has been reported, but unbleached hardwood kraft pulp samples can, in general, easily be dissolved. Irrespective of applied activation–dissolution procedure, I or II, softwood kraft pulps cannot be completely dissolved in LiCl/DMAc (67,200,219,220) and a gel-like residue can be isolated by ultracentrifugation (67). In addition, the chromatography of softwood kraft pulp samples has a poor reproducibility. Although the solution from this type of samples appears clear, the solution is difficult to filter and an increasing pressure during SEC is commonly observed also for ultracentrifuged sample solutions, indicating adsorption onto the stationary phase. At our laboratory we have found that the column material can be regenerated by increasing the LiCl concentration of the mobile phase to 8% LiCl, and continuing the washing at this high concentration over night. The limited solubility of kraft pulp samples in LiCl/DMAc, and the problems arising during chromatography have been attributed to glucomannan (67), a hemicellulose that is typical for softwood samples. The presence of glucomannan may also explain why not even fully bleached softwood kraft pulps can be completely dissolved. Since the chemical composition of the initial fibers and the residue differs, care must be taken when softwood kraft pulps dissolved and chromatographed in LiCl/DMAc are evaluated.

The shape of the MMD also differs between hardwood and softwood kraft pulp samples (209). This is true for the carbohydrate polymers of the pulps, as detected by differential refractive index (DRI) detector but also for the pulp lignin, as visualized by using an UV detector. Irrespective of detector used, hardwood kraft pulp samples always give a bimodal MMD (Fig. 2), representing cellulose and xylan, respectively, although the pulp lignin also contributes to the xylan distribution in the lower *M* range (209,212). Dissolved softwood kraft pulps have a more complex elution profile as compared to hardwood kraft pulps when using a DRI detector (209). From carbohydrate analysis of a fully bleached softwood kraft pulp sample (92% dissolved) it was found that the hemicellulose portion elutes over the entire *M* range (Fig. 3), although it is known that hemicelluloses (just as lignin) have a much lower *M* than cellulose. The MMD of lignin, as obtained by UV detection, differs between hardwood kraft pulps and softwood kraft pulps. The elution behavior of lignin has been proposed to be due to covalent linkage between lignin and cellulose (204,207) possibly through reaction between lignin and glucomannan during kraft cooking of softwood (221), even though no conclusive evidence has been found. In these studies about 80% of the untreated softwood kraft pulp was dissolved, whereas softwood pulps produced by bisulfite and acid sulfite are almost completely dissolved in LiCl/DMAc (204,207). The obtained MMD profiles of softwood pulps produced by these acid processes resemble those

© 2004 by Marcel Dekker, Inc.

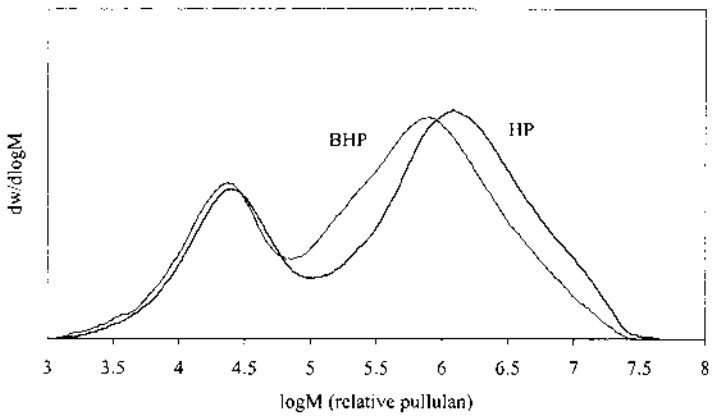

Figure 2 MMD of unbleached (HP) and bleached (BHP) hardwood kraft pulps. SEC was performed at 80°C on PL Mixed A columns using 0.5% LiCl/DMAc as mobile phase and a DRI detector. (From Ref. 209.)

of softwood kraft pulps, which the authors suggest to be due to bonds between residual lignin and cellulose.

Thus, dissolved wood pulps, and especially softwood kraft pulps, behave as copolymers during elution, rather than as separate polymers. By derivatization in LiCl/DMAc (Sec. 4.4), dissolution of softwood kraft pulps can be improved

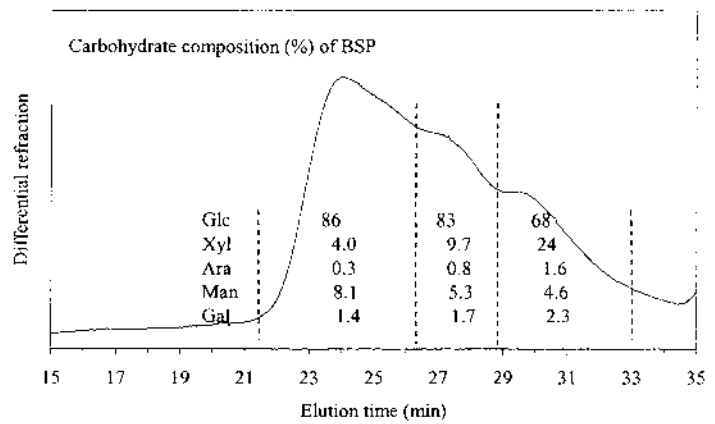

Figure 3 Chromatogram showing the relative carbohydrate composition (%) in different elution volumes (times) of bleached softwood kraft pulp (BSP). Glc = glucose, Xyl = xylose, Ara = arabinose, Man = mannose, Gal = galactose. Chromatographic conditions as in Fig. 2. (From Ref. 209.)

© 2004 by Marcel Dekker, Inc.

significantly (134). As a consequence of the derivatization, the profile of the MMD is changed to become more like those of hardwood kraft pulps, possibly due to decreased association between glucomannan and cellulose, that is, a better chromatographic separation between hemicellulose/lignin and cellulose.

The MMD corresponding to the cellulose portion of high molecular mass hardwood kraft pulps commonly has a shoulder on the high M end (196,199). This may be more or less pronounced depending on the M of the cellulose, and is commonly not seen for underivatized softwood pulp samples dissolved in LiCl/DMAc. A systematic study of the origin of this appearance revealed also that the MMD of a cotton linter (DP 8000) having about the same elution range as wood pulp cellulose also had a similar shoulder (199). The shoulder was attributed to aggregation/association of the cellulose. Using light scattering, stable aggregates have been demonstrated in concentrated LiCl/DMAc solutions of cellulose samples with lower M (DP $<$ 1500) (63,69,222). It was shown that even if aggregates were present in the stock solution, molecular dispersed, that is, nonaggregated, solutions for most of the samples could be obtained after dilution to 0.9% LiCl and 0.1% cellulose, that is, at concentrations used in SEC (69,222). Considering the additional dilution that occurs during chromatography, it was concluded that true molecular dispersed solutions exist under common SEC conditions.

Different approaches were investigated to avoid the formation of aggregates by using off-line LS and deconvoluting the MMD obtained by SEC (199). An optimized mechanical treatment by shaking the solutions was the only possible way to break the aggregates. The treatment only influenced the shoulder at the high molecular mass end of the cellulose MMD. The LiCl concentration during dissolution had a pronounced effect on the formation of aggregates, but at 6%, the lowest concentration possible for dissolution of the studied samples, the shoulder still remained. Different activation–dissolution procedures (I or II), urea addition, thermal treatment, decrease in sample concentration or dissolution time did not influence the shape of the MMDs. It should be pointed out that the used columns were packed with 20 μm PS/DVB particles. Using smaller particles, the sample solutions will experience a higher shear force during chromatography and aggregated cellulose may thus be disrupted.

Fundamental studies concerning the influence of different treatments of a fibrous sample on the MMD profiles of its polymers are of interest in order to interpret the effect of different types of degradation. In this context, hardwood pulps and pure cellulose samples have been studied. The relation between fiber strength and MMD obtained with LiCl/DMAc has been studied after degradation of unbleached hardwood kraft pulp with gamma irradiation, oxygen/alkali or alkali (210), and by ozone or acid hydrolysis (200), the latter study also included degradation of cotton linters. By comparing the profiles of hardwood kraft pulp with those of cotton linter, it was concluded that the MMD profiles depend on the type of degradation as well as type of fiber. A bimodal MMD profile (Fig. 4) of the

© 2004 by Marcel Dekker, Inc.

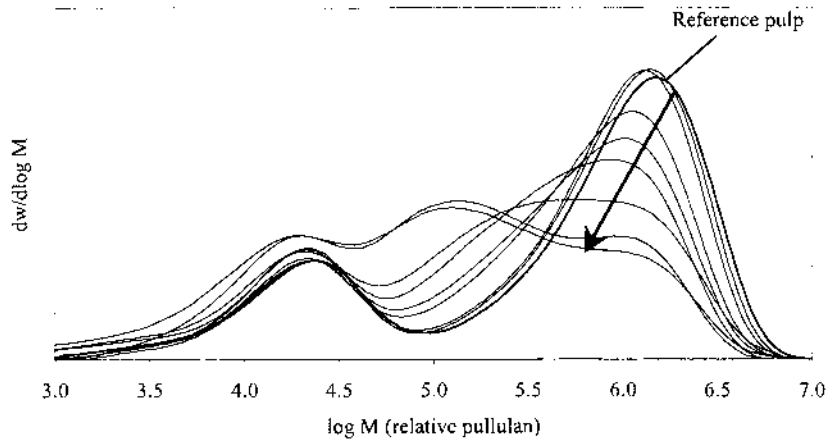

Figure 4 MMD of birch kraft pulp degraded by ozone. Reference = untreated pulp. The arrow indicates the gradual change of MMD obtained on increasing ozone dosage. Chromatographic conditions as in Fig. 2. (From Ref. 200.)

cellulose part of ozone-treated unbleached kraft pulp was obtained. Radicals formed in lignin–ozone reactions were suggested to cause heterogeneous degradation of the cellulose in the pulp fiber as visualized by the bimodal MMD of the cellulose fraction. In contrast, the cellulose part of the MMD of bleached hardwood kraft pulps, that is, lignin-free samples, showed a Gaussian shape (200). In another study concerning the aging of cotton linters, the MMD was shown to gradually change from a monomodal to a bimodal profile, but returned to the monomodal profile at a limiting DP value of 150–200 (197).

To summarize, when using LiCl/DMAc as solvent, the type and origin of the sample are of great importance to consider for applying adequate dissolution conditions. It seems that LiCl/DMAc is less suitable for direct dissolution of softwood kraft pulp samples. For this type of sample, derivatization and SEC in LiCl/DMAc provide a better way to study its MMD. Taken the new findings concerning the dissolution process into account, LiCl/DMAc offers a convenient way to characterize cellulosic samples by SEC in a reliable way.

6 DETECTORS AND CALIBRATION METHODS

The chromatogram obtained by SEC using differential refractive index (DRI) or UV absorbance detectors is merely a concentration profile of the polymeric sample with the larger molecules eluting first, that is, it does not provide direct information about *M*. Thus, to evaluate the MMD and the *M* averages of a sample, the elution

© 2004 by Marcel Dekker, Inc.

volume (or the elution time) scale of the chromatogram has to be transferred to a logarithmic M scale. For this purpose, three methods for evaluation have been used for dissolved cellulose or cellulose derivatives: (a) the direct standard calibration method, (b) the universal calibration method by using differential viscometry (DV) detector, or (c) by using a light scattering (LS) detector. These methods are described in detail elsewhere in this volume. The detectors used for SEC of different cellulose samples are exemplified in the previous sections. Multiple detectors (LS/DV/DRI) have been used for characterization of cellulose ethers, that is, by aqueous SEC (223).

The direct standard method requires the use of a set of monodisperse, (narrow) standards of known M, or polydisperse (broad) standards with known M_n, and either M_w or M_v. In either case the standards should preferably cover the entire elution range of the sample in hand. Unfortunately, there are no commercially available cellulose standards. During the last decade, monodisperse pullulan standards have frequently been used to obtain the MMD of cellulosic samples. Pullulan consists of polymaltotriose units linked together by α-(1→6) linkages. Because of its linearity and similar Mark–Houwink constants (192) it is commonly assumed to have about the same relation between molecular mass and hydrodynamic volume as cellulose. However, this is not true for all cellulose samples. The pullulan equivalent molar mass averages for cellulose ethers have been reported to overestimate the values determined by light scattering by a factor of 3.2 (224). Recently, an overestimation of the pullulan equivalent molar mass of cellulose in birch kraft pulp has been reported by using a multi-angle laser light scattering (MALLS) detector together with the DRI (225). Two ways of correlating the pullulan equivalent M to the absolute M as determined by MALLS were presented. One of the methods can be used to obtain reliable average molecular masses of the cellulose and the other method to obtain the MMD of the cellulose. A drawback with commercial pullulan standards is that the highest available standard has an M of around 1.6×10^6. For cellulosic samples having an M above this value, for example, the cellulose fraction of wood pulp samples, extrapolation of the calibration curve becomes necessary. Another obvious drawback in using pullulan for the evaluation of wood pulps is that these samples also contain other polymers than cellulose, such as hemicellulose and lignin. There are also reports of aggregation of pullulan dissolved in LiCl/DMAc (194). In spite of having a completely different structure, polystyrene standards have also been used to obtain an M value of cellulose samples (for example, 196). The advantage is that narrow polystyrene standards are available in a broader M range than the pullulan standards. Examples of other standards used for calibration are dextrans for evaluation of CMC (154), and polyethylene oxide/glycols for cellulose acetates (105). Thus, the reported molecular mass obtained from SEC in these cases is relative to the molecular mass of the used standards having the same hydrodynamic volume, that is, elution volume, as the sample, in the used solvent system. This is

© 2004 by Marcel Dekker, Inc.

adequate when evaluating the influence of different treatments on a cellulosic sample or to follow changes during a reaction, but should not be confused with the true M of the cellulose.

Calibration curves have also been constructed employing celluloses from different sources (79), celluloses obtained by acid hydrolysation of high M cellulose (83) or by fractional precipitation of cellulose derivative (111). The required characteristics of the homemade standards are then determined off-line by osmometry (M_n), viscometry (M_v), or light scattering (M_w) before use. Even if these latter methods give a better value of the M of cellulose than noncellulose standards they are rarely used today, primarily because they are much more time-consuming than using commercially available standards such as pullulan and polystyrene. Ultrasonic degradation has also been used to produce homologous series with respect to M of sulfoethyl celluloses (226). The degraded samples were evaluated with on-line MALLS/DRI.

To bypass the need for cellulose standards dual detectors have been used; one concentration detector, commonly DRI, and either a DV detector or a light-scattering detector. The use of a DV detector provides the intrinsic viscosity, which makes it conveniently possible to apply the universal calibration method (186,192). The universal calibration is based on the observation that the product of intrinsic viscosity and molecular mass ($[\eta]M$), that is, hydrodynamic volume is independent of polymer type (227). To determine the M of the cellulose sample at a given elution volume the column is calibrated with standards of known M, commonly polystyrene. Other molecular characteristics than M such as the Mark–Houwink coefficients for the cellulose under the chromatographic conditions employed can also be obtained. For the solvent LiCl/DMAc a number of different values of the constants for cellulose and polystyrene have been reported and reviewed recently (217). As mentioned before, the presence of water and variations of ionic strength in LiCl/DMAc also affect the conformation of the polymer in solution, and thereby the obtained constants. The root-mean-square radii of gravity (R_g) have also been studied as a parameter for universal calibration employing pullulan and dextran standards in aqueous SEC (228).

During the past decade there have been an increasing number of reports where LS detectors have been used for evaluation of the MMD of cellulose samples. The advantage in using LS detectors is that the absolute M can be obtained in the whole MMD range without using any standards. Low-angle laser light scattering (LALLS) and multi-angle laser light scattering (MALLS) detectors have been used both for aqueous and organic SEC. Besides giving the molecular mass of the eluting polymer, they also offer the possibility of detecting the occurrence of aggregates. When evaluating wood pulps, the presence of lignin has to be taken into account, especially when an argon laser (488 nm) is used, because the fluorescence of lignin adds to the scattered light (225,229,230). To avoid interference of any fluorescence, narrow band-pass filters should be used.

© 2004 by Marcel Dekker, Inc.

Table 10 Refractive Index Increment (dn/dc) of Cellulose Used for the Evaluation of SEC by On-Line Laser Light-Scattering Detectors[a]

Sample	Solvent	dn/dc (mL/g)	Wavelength (nm)	Temperature (°C)	References
CTC	THF	0.163	632.8	—	231
CTC	THF	0.155	633	25	121
CTC	THF	0.163	690	Ambient	117
TMSC	THF	0.059	646	25	101
CMC	0.02 M or 0.1 M $NaNO_3$	0.163	633	25	156
Cellulose ethers[b]	0.01 M NaCl	0.128–0.132	632.8	30	224
Cellulose ethers[b]	Phosphate buffer $I = 0.1$, pH 6.5	0.15	632.18	—	165
Cellulose	0.5% LiCl/DMAc	0.163	690	—	194
Cellulose	0.5% LiCl/DMAc	0.104	633	40	198
Cellulose	0.5% LiCl/DMAc	0.108	488	Ambient	225

[a]The literature reference contains dn/dc values of different types of carbanilates.
[b]Nonionic.

The accuracy of the obtained M_w value presupposes that the dn/dc has been properly determined under the conditions used for the SEC. Sample solutions should preferably be dialyzed against pure solvent prior to determination, but this is not possible for LiCl/DMAc solutions because the solvent will swell or dissolve the dialysis membranes. It is important to prepare the solvent in a reproducible way because an increase in the concentration of LiCl decreases the dn/dc value (222). In Table 10, reported dn/dc values of some types of celluloses used for evaluation of chromatograms by on-line light-scattering detectors are shown.

7 CONCLUSIONS

The great number of applications shows that SEC is the preferred technique to gain information about cellulose and its derivatives. During the past decade, SEC of cellulose has been focused on carbanilated cellulose samples or direct dissolution of cellulose samples in lithium chloride/*N*,*N*-dimethylacetamide (LiCl/DMAc). For derivatives, the trend is to perform derivatization of cellulose in homogeneous phase using LiCl/DMAc. Qualified evaluation of SEC results has become possible by using dual detection including differential viscometry (DV)/

© 2004 by Marcel Dekker, Inc.

differential refractive index (DRI) detectors, or light-scattering (LS)/DRI detectors.

As for all analytical techniques, the validity of the results obtained by SEC depends on all steps from sampling to evaluation. It is thus of importance to report carefully about the applied method, chromatographic conditions, and calibration method together with the SEC characterization of the actual cellulose sample. To facilitate comparison of different SEC methods, an interlaboratory evaluation of different cellulose samples should be valuable. This would provide guidelines for a suitable approach for future research and characterization of cellulose and cellulose derivatives by SEC.

REFERENCES

1. J Engelhardt. Sources, industrial derivatives and commercial application of cellulose. Carbohydr Eur 12:5–14, 1995.
2. DN-S Hon. Cellulose: a random walk along its historical path. Cellulose 1:1–25, 1994.
3. E Sjöström. Chemical composition of various wood species. In: Wood Chemistry. Fundamentals and Applications. San Diego, California: Academic Press, 1993, Appendix.
4. DN-S Hon. In: E Frollini, A Leao, LHC Mattoso, eds. Natural Polymers and Agrofibers based Composites. Sao Carlos, Brazil: Embrapa Instrumentacao Agropecuaria, 2000, p 3.
5. AK Mohanthy, M Misra, G Hinrichsen. Biofibers, biodegradable polymers and biocomposites: An overview. Macromol Mater Eng, 276/277:1–24, 2000.
6. RM Rowell. Opportunities for composites from agro-based sources. In: RM Rowell, RA Young, JK Rowell, eds. Paper and Composites from Agro-Based Resources. New York: CRC Press, 1997, pp 249–268.
7. RCR Nunes, LLY Visconte. Natural fibers reinforced elastomeric composites. In: E Frollini, A Leao, LHC Mattoso, eds. Natural Polymers and Agrofibers based Composites. Sao Carlos, Brazil: Embrapa Instrumentacao Agropecuaria, 2000, pp 135–158.
8. K Joseph, Mattoso, RD Toledo, S Thomas, LH De Carvalho, L Pothen, S Kala, B James. Natural fiber reinforced thermoplastic composites. In: E Frollini, A Leao, LHC Mattoso, eds. Natural Polymers and Agrofibers based Composites. Sao Carlos, Brazil: Embrapa Instrumentacao Agropecuaria, 2000, pp 159–202.
9. JMF Paiva, E Frollini. Natural fiber reinforced thermoset composites. In: E Frollini, A Leao, LHC Mattoso, eds. Natural Polymers and Agrofibers Based Composites. Sao Carlos, Brazil: Embrapa Instrumentacao Agropecuaria, 2000, pp 229–256.
10. AH Conner. Size exclusion chromatography of cellulose and cellulose derivatives. In: C-S Wu, ed. Handbook of Size Exclusion Chromatography. New York: Marcel Dekker, 1995, pp 331–352.

© 2004 by Marcel Dekker, Inc.

11. A Payen. “Troisième mémoire sur les developpements des végétaux.” Extrait des mémoires de l’Academie Royale des Sciences: Tomes III des Savants Étrangers, Paris: Impremerie Royale 1842.
12. RH Marchessault, A Sarko. X-ray structure of polysaccharides. Adv Carbohydr Chem 22:421–482, 1967.
13. RH Atalla, DL VanderHart. Native cellulose: a composition of two distinct crystalline forms. Science 223:283–285, 1984.
14. DL VanderHart, RH Atalla. Studies of microstructure in native celluloses using solid state ^{13}C NMR. Macromolecules 17:1465–1472, 1984.
15. N Hayashi, J Sugiyama, T Okano, M Ishihara. The enzymatic susceptibility of cellulose microfibrils of the algal–bacterial type and the cotton–ramie type. Carbohydr Res 305:261–269, 1998.
16. J-F Sassi, P Telely, H Chanzy. Relative susceptibility of the I_α and I_β phases of cellulose towards acetylation. Cellulose 7:119–132, 2000.
17. S Kuga, S Takagi, RM Brown, Jr. Native folded-chain cellulose II. Polymer 34(15):3293–3297, 1993.
18. WA Sisson. The existence of mercerized cellulose and its orientation in *Halicystis* as indicated by X-ray diffraction analysis. Science 87:350, 1938.
19. HA Krässig. The fiber structure. Supermolecular structure. In: Cellulose. Structure, accessibility and reactivity. Singapore: Gordon and Breach Science Publishers, 1993, pp 12–30.
20. E Sjöström. Wood pulping. In: Wood Chemistry. Fundamentals and Applications. San Diego, California: Academic Press, 1993, pp 114–165.
21. N Morohoshi. Chemical characterization of wood and its components. In: DN-S Hon, ed. Wood and Cellulosic Chemistry. New York: Marcel Dekker Inc, 1991, p. 338.
22. D Fengel, G Wegener. Cellulose. In: Wood: Chemistry, Structure, Reactions. Berlin: Walter de Gruyter, 1989, p. 75.
23. E Sjöström. Wood polysaccharides. In: Wood Chemistry. Fundamentals and Applications. San Diego, California: Academic Press, 1993, pp 51–70.
24. LE Wise, M Murphy, AA D’Addieco. Chlorite holocellulose, its fractionation and bearing on summative wood analysis and on studies on the hemicellulose. Paper Trade J 122(2):35–44, 1946.
25. TE Timell. Recent progress in the chemistry of wood hemicelluloses. Wood Sci Technol 1:45–70, 1967.
26. L Viikari, A Kantelinen, M Rättö, J Sundquist. Enzymes in pulp and paper processing. In: GF Leatham, ME Himmel, eds. Enzymes in Biomass Conversion. Washington DC: ACS Symp Ser 460, 1990, pp 12–21.
27. J Puls. Chemistry and biochemistry of hemicelluloses: Relationship between hemicellulose structure and enzymes required for hydrolysis. Macromol Symp 120:183–196, 1997.
28. RM Brown. The biosynthesis of cellulose. JMS—Pure Appl Chem A33(10):1345–1373, 1996.
29. HA Krässig. Effects of structure and morphology on accessibility and reactivity. In: Cellulose. Structure, Accessibility and Reactivity. Singapore: Gordon and Breach Science Publishers, 1993, pp 167–169.

© 2004 by Marcel Dekker, Inc.

30. HA Krässig. Effects of structure and morphology on accessibility and reactivity. Methods of activation. In: Cellulose. Structure, Accessibility and Reactivity. Singapore: Gordon and Breach Science Publishers, 1993, pp 215–276.
31. W Burchard. Macromolecular association phenomena. A neglected field of research? TRIP 1(7):192–198, 1993.
32. W Burchard. Polymer structure and dynamics, and polymer–polymer interactions. Adv Colloid Interface Sci 64:45–65, 1996.
33. B Morgenstern, H-W Kammer. On the particulate structure of cellulose solutions. Polymer 40:1299–1304, 1999.
34. HA Krässig. Methods of fiber structure characterization. Determination of the size of crystallites, fibrils and fibrillar aggregates. In: Cellulose. Structure, Accessibility and Reactivity. Singapore: Gordon and Breach Science Publishers, 1993, pp 66–149.
35. HA Krässig. Effects of structure and morphology on accessibility and reactivity. Morphology, structure and the course of substitution reactions. In: Cellulose. Structure, Accessibility and Reactivity. Singapore: Gordon and Breach Science Publishers, 1993, pp 277–315.
36. J-P Joseleau, G Chambat, B Chumpitazi-Hermoza. Solubilization of cellulose and other plant structural polysaccharides in 4-methylmorpholine *N*-oxide: an improved method for the study of cell wall constituents. Carbohydr Res 90:339–344, 1981.
37. A Isogai, A Ishizu, J Nakano. Preparation of tri-*O*-benzylcellulose by the use of nonaqueous cellulose solvents. J Appl Polym Sci 29:2097–2109, 1984.
38. CL McCormick. Novel cellulose solutions, U.S. Patent 4,278,790, 1981.
39. TR Dawsey, CL McCormick. The lithium chloride/dimethylamide solvent for cellulose: a review. JMS—Rev Macromol Chem Phys C30(384):405–440, 1990.
40. G Samaranyake, WG Glasser. Cellulose derivatives with low D.S. I. A novel acylation system. Carbohydr Polym 22(1):1–7, 1993.
41. SL Williamson, CL McCormick. Cellulose derivatives synthesized via isocyanate and activated ester pathways in homogeneous solutions of lithium chloride/N,N-dimethylacetamide. JMS—Pure Appl Chem A35(12):1915–1927, 1998.
42. AM Regiani, E Frollini, GA Marson, OA El Seoud. Investigation of Cellulose Dissolution and Acetylation in Lithium Chloride/*N*,*N*-Dimethylacetamide system. In: Proceedings of the Second International Symposium on Natural Polymer Composites, Sao Carlos, Brazil, 1998, pp 235–239.
43. T Heinze, K Rahn. New polymers from cellulose sulphonates. J Pulp Paper Sci 25(4):136–140, 1999.
44. N Kasuya, A Sawatari. A simple and facile method for triphenylmethylation of cellulose in a solution of lithium chloride in *N*,*N*-dimethylacetamide. Fiber 56(5):249–253, 2000.
45. B Tosh, CN Saikia, NN Dass. Homogeneous esterification of cellulose in the lithium chloride-*N*,*N*-dimethylacetamide solvent system: effect of temperature and catalyst. Carbohydr Res 327:345–352, 2000.
46. H-Q Liu, LN Zhang. Silylation of cellulose with trichlorosilane and triethoxysilane in homogeneous LiCl/*N*,*N*-dimethylacetamide solution. Chinese J Polym Sci 18(2):161–168, 2000.

© 2004 by Marcel Dekker, Inc.

47. S Takahasi, T Fujimoto, T Miyamoto, H Inagaki. Relationship between distribution of substituents and water solubility of *O*-methyl cellulose. J Polymer Sci, Part A, Polym Chem 25:987–994, 1987.
48. CL McCormick, PA Callais. Derivatization of cellulose in lithium chloride and *N*,*N*-dimethylacetamide solutions. Polymer 28:2317–2323, 1987.
49. AF Turbak, RB Hammer, RE Davies, HL Hergert. Cellulose solvents. Chemtech 10:51–57, 1980.
50. DC Johnson. Solvents for cellulose. In: TP Nevell, SH Zeronian, eds. Cellulose Chemistry and Its Applications. New York: Halsted Press, 1985, pp 181–201.
51. B Seger, W Burchard. Structure of cellulose in Cuoxam. Macromol Symp 83:291–310, 1994.
52. K Saalwächter, W Burchard, P Klüfers, G Kettenbach, P Mayer, D Klemm, S Dugarmaa. Cellulose solutions in water containing metal complexes. Macromolecules 33:4094–4107, 2000.
53. B Laszkiewicz, JA Cuculo. Solubility of cellulose III in sodium hydroxide solution. J Appl Polym Sci 50:27–34, 1993.
54. J Zhou, L Zhang. Solubility of cellulose in NaOH/urea aqueous solution. Polym J 32(10):866–870, 2000.
55. A Isogai, RH Atalla. Alkaline method for dissolving cellulose. U.S. Patent 5,410,034, 1995.
56. A Isogai, RH Atalla. Dissolution of cellulose in aqueous NaOH solutions. Cellulose 5:309–319, 1998.
57. SM Hudson, JA Cuculo. The solubility of cellulose in liquid ammonia/salt solutions. J Polym Sci, Polym Chem Ed 18:3469–3481, 1980.
58. JA Cuculo, CB Smith, U Sangwatanaroj, EO Stejskal, SS Sankar. A study on the mechanism of dissolution of the cellulose/NH_3/NH_4SCN system. I. J Polym Sci, Part A, Polymer Chem 32: 229–239, 1994.
59. JA Cuculo, CB Smith, U Sangwatanaroj, EO Stejskal, SS Sankar. A study on the mechanism of dissolution of the cellulose/NH_3/NH_4SCN system. II. J Polym Sci, Part A, Polymer Chem 32:241–247, 1994.
60. S Lee, H Park. A new sampling and SEC method for analysis of underivatized cellulose. J Korean Chem Soc 42(2):190–196, 1998.
61. B Morgenstern, W Berger. Investigations about dissolution of cellulose in the LiCl/*N*,*N*-dimethylformamide system. Acta Polym 44:100–102, 1993.
62. AF Turbak, A El-Kafrawy, FW Snyder, AB Auerbach. Solvent system for cellulose. U.S. Patent 4,302,252, 1981.
63. M Terbojevich, A Cosani, G Conio, A Ciferri, E Bianchi. Mesophase formation and chain rigidity in cellulose and derivatives. 3. Aggregation of cellulose in *N*,*N*-dimethylacetamide–lithium chloride. Macromol 18:640–646, 1985.
64. CL McCormick, PA Callais, BH Hutchinson, Jr. Solutions studies of cellulose in lithium chloride and N,N-dimethylacetamide. Macromol 18:2394–2401, 1985.
65. B Morgenstern, H-W Kammer, W Berger, P Skrabal. 7Li-NMR study on cellulose/LiCl/*N*,*N*-dimethylacetamide solutions. Acta Polym 43:356–357, 1992.
66. B Morgenstern H-W Kammer. Solvations in cellulose–LiCl–DMAc solutions. Trends Polym Sci 4(3):87–92, 1996.

© 2004 by Marcel Dekker, Inc.

67. E Sjöholm, K Gustafsson, A Colmsjö. Characterization of the cellulosic residues from lithium chloride/*N*,*N*-dimethylacetamide dissolution of softwood kraft pulp. Carbohydr Polym 32(1):57–63, 1997.
68. AM Striegel. Theory and application of DMAc/LiCl in the analysis of polysaccharides. Carbohydr Polym 34:267–274, 1997.
69. T Röder, B Morgenstern, O Glatter. Light scattering studies on solutions of cellulose in N,N-dimethylacetamide/lithium chloride. Lenzinger Ber 79:97–101, 2000.
70. T Röder, B Morgenstern, O Glatter. Polarized and depolarized light scattering on solutions of cellulose in *N*,*N*-dimethylacetamide/lithium chloride. Macromol Symp 162:87–93, 2000.
71. I Nehls, W Wagenknecht, B Philipp. ^{13}C-NMR spectroscopic studies of cellulose in various solvent systems. Cellulose Chem Technol 29:243–251, 1995.
72. H Pionteck, W Berger, B Morgenstern, D Fengel. Changes in cellulose structure during dissolution in LiCl:*N*,*N*-dimethylacetamide and in the alkaline tartrate system EWNN. I. Electron microscopic studies on changes in cellulose morphology. Cellulose 3:127–131, 1996.
73. L Ping, C Zili, T Yuan, L Zhaofeng. Study on the characteristics of macromolecular chains of cellulose in dilute solutions. J China Textile Univ 16(3):21–24, 1999.
74. G Meyerhoff. Molekulare Parameter und Gel-Permeation von Polymeren. Makromol Chem 89:282–284, 1965.
75. L Segal. Fractionation of cellulose trinitrates by gel permeation chromatography. J Polym Sci B 4:1011–1018, 1966.
76. WJ Alexander, RL Mitchell. Rapid measurement of cellulose viscosity by the nitration method. Anal Chem 21(12):1497–1500, 1949.
77. CF Bennett, TE Timell. Preparation of cellulose trinitrate. Svensk Papperstidn 58:281–286, 1955.
78. M Rinaudo, JP Merle. Polydispersity of celluloses and enzymic degraded celluloses by gel permeation chromatography. Europ Polym J 6:41–50, 1970.
79. M Chang, TC Pound, RSTJ Manley. Gel-permeation chromatographic studies of cellulose degradation. I. Treatment with hydrochloric acid. J Polym Sci, Polym Phys Ed 11:399–411, 1973.
80. RSTJ Manley. Gel-permeation chromatographic study of the degradation of regenerated cellulose by methanolysis. Text Res J 44:401–402, 1974.
81. RSTJ Manley. Gel-permeation chromatographic studies of cellulose degradation. III. Methanolysis of cellulose. J Polym Sci, Polym Phys Ed 12:1347–1354, 1974.
82. M Marx-Figini, O Soubelet. Size exclusion chromatography of cellulose nitrate. Molecular weight averages and molecular weight distributions. Polym Bull (Berlin) 11:281–286, 1984.
83. O Soubelet, MA Presta, M Marx-Figini. SEC on cellulose nitrate: DP–V_o relationship and evaluation of different methods to determine the calibration parameters. Angew Makromol Chem 175:117–128, 1990.
84. C Holt, W Mackie, DB Sellen. Gel permeation chromatography of high molecular weight cellulose trinitrate. Polymer 19:1421–1426, 1978.
85. M Marx-Figini, O Soubelet. Size exclusion chromatography (GPC) of cellulose nitrate using modified silicagel as stationary phase. Polym Bull (Berlin) 6:501–508, 1982.

© 2004 by Marcel Dekker, Inc.

86. TE Eremeeva, TO Bykova, VS Gromov. (In Russian.) Khim Drev 5:108–109, 1988.
87. TE Eremeeva, TO Bykova, VS Gromov. Problems in the size-exclusion chromatography of cellulose nitrates: non-exclusion effects and universal calibration. J Chromatogr 522:67–75, 1990.
88. M Marx-Figini, RV Figini. Studies on the mechanical degradation of cellulose. Angew Makromol Chem 224:179–189, 1995.
89. M Marx-Figini. Studies on the ultrasonic degradation of cellulose. Macromolecular properties. Angew Makromol Chem 250:85–92, 1997.
90. K Heppell-Masys, HW Bonin, VT Bui, M Bickerton, D Murphy. Effects of gamma and thermal neutron radiation on nitrocellulose. Proceedings of the Annual Conference—Canadian Nuclear Society, 1997, Vol. 2, Session 4C, Paper 4, p 5.
91. Z Jianchun, S Meiwu, L Gaoyong, Y Mu. Study of the super-molecular structure of lyocell fibers. Chem Fibers Int 49(4):314–315, 1999.
92. JF Klebe, HL Finkbeiner. Silyl celluloses: a new class of soluble cellulose derivatives. J Polymer Sci A1 7:1947–1958, 1969.
93. HA Schuyten, JW Weaver, JD Reid, JF Jurgens. Trimethylcellulose. J Am Chem Society 70:1919–1920, 1948.
94. G Keilisch, K Tihlarik, E Husemann. Über die Herstellung von Tries-O-Trimethylsilylpolysacchariden. Makromol Chimie 120:87–95, 1968.
95. N Aelenei, D Bontea, C Ioan. Synthesis and characterization of trimethylsilylcellulose in solution. JMS—Pure Appl Chem A35(10):1667–1680, 1998.
96. RE Harmon, KK De, SK Grupta. New procedure for preparing trimethylsilyl derivatives of polysaccharides. Carbohydr Res 31:407–409, 1973.
97. L Einfeldt, D Klemm. The control of cellulose biosynthesis by *Acetobacter xylinum* in view of molecular weight distribution. Part I: Change of molecular weight of bacterial cellulose by simple variation of culture conditions. J Carbohydr Chem 16(4&5):635–646, 1997.
98. W Mormann, T Wagner. Silylation of cellulose and low-molecular-weight carbohydrates with hexamethyldisilazane in liquid ammonia. Macromol Rapid Commun 18:515–522, 1997.
99. W Schempp, T Krause, U Seifried, A Koura. Herstellung hochsubstituierter Trimethylsilylcellulosen im System Dimethylacetamid/Lithiumchlorid. Papier 38:607–610, 1984.
100. W Mormann, J Demeter. Silylation of cellulose with hexamethyldisilazane in liquid ammonia—First examples of completely trimethylsilylated cellulose. Macromolecules 32:1706–1710, 1999.
101. T Stöhr, K Petzold, BA Wolf, DO Klemm. Continuous polymer fractionation of polysaccharides using highly substituted trimethylsilylcellulose. Macromol Chem Phys 199:1895–1900, 1998.
102. W Mormann, J Demeter. Controlled desilylation of cellulose with stoichiometric amounts of water in the presence of ammonia. Macromol Chem Phys 201:1963–1968, 2000.
103. W Mormann, T Wagner. Silylation of cellulose with hexamethyldisilazane in liquid ammonia. Macromol Carbohydr Polym 43(3):257–262, 2000.

© 2004 by Marcel Dekker, Inc.

104. B Fleury, J Dubois, C Léonard, JP Joseleau, H Chanzy. Microgels and ionic associations in solutions of cellulose diacetate. Cellulose 1:131–144, 1994.
105. E Samios, RK Dart, JV Dawkins. Preparation, characterization and biodegradation studies on cellulose acetates with varying degree of substitution. Polymer 38(12):3045–3054, 1997.
106. Y Funaki, K Ueda, S Saka, S Soejima. Characterization of cellulose acetate in acetone solution. Studies on prehump II in GPC pattern. J Appl Polym Sci 48:419–424, 1993.
107. S Shimamoto, T Kohomoto, T Shibata. Depolymerization of cellulose and cellulose triacetate in conventional acetylation system. In: TJ Heinze, WG Glasser, eds. Cellulose Derivatives. Modification, Characterization, and Nanostructures. Washington DC: ACS Symp Ser 688, 1998, pp 194–200.
108. K Kamide, K Okajima, K Kowsaka, T Matsui. Solubility of cellulose acetate prepared by different methods and its correlation with average acetyl group distribution. Polym J 19(12):1405–1412, 1987.
109. GC Berry, MA Leech. Properties of cellulose acetate in solution. Aggregation of cellulose triacetate in dilute solution. In: DA Brant, ed. Solution properties of polysaccharides. Washington DC: ACS Symp Ser 150, 1981, pp 61–80.
110. LJ Tanghe, WJ Rebel, RJ Brewer. Prehump in the gel-permeation chromatography fractionation of pulp cellulose acetate. J Polym Sci, Part A1 8:2935–2947, 1970.
111. WJ Alexander, TE Muller. Evaluation of pulps, Rayon fibers, and cellulose acetate by GPC and other fractionation methods. Separ Sci 6(1):47–71, 1971.
112. F Mahmod, E Chatterall. Fractionation and characterization of commercial cellulose triacetate by gel permeation chromatography. In: T Provder, ed. Size Exclusion Chromatography Methodology and Characterization of Polymers and Related Materials. Washington DC: ACS Symp Ser 245, 1984, pp 365–375.
113. K Kamide, M Saito. Cellulose and cellulose derivatives: recent advances in physical chemistry. Adv Polym Sci 83:1–56, 1987.
114. RJ Brewer, LJ Tanghe, S Bailey, JT Burr. Molecular weight distribution of cellulose esters by gel permeation chromatography and fractional precipitation. J Polym Sci, Part A1 6:1697–1704, 1968.
115. LR Schroeder, FC Haigh. Cellulose and wood pulp polysaccharides. Gel permeation chromatographic analysis. Tappi 62(10):103–105, 1979.
116. J Sundquist, T Rantanen. Characterisation of technical pulps by carbanilation of cellulose. Pap Puu 11:733–737, 1983.
117. L LaPierre, J Bouchard. Molecular weight determination of softwood kraft cellulose: Effects of carbanilation solvent, hemicelluloses and lignin. In: DS Argyropoulos, ed. Advances in Lignocellulosics Characterization. Atlanta: Tappi Press, 1999, pp 239–262.
118. BF Wood, AH Conner, CG Hill, Jr. The effect of precipitation on the molecular weight distribution of cellulose tricarbanilate. J Appl Polym Sci 32:3703–3712, 1986.
119. R Evans, AFA Wallis. Comparison of cellulose molecular weights determined by high performance size exclusion chromatography and viscometry. Proceedings of the Fourth International Symposium on Wood and Pulping Chemistry, Paris, 1987, Vol 1, pp 201–205.

© 2004 by Marcel Dekker, Inc.

120. R Evans, R Wearne, AFA Wallis. Molecular weight distribution of cellulose as its tricarbanilate by high performance size exclusion chromatography. J Appl Polym Sci 37:3291–3303, 1989.
121. N Aust, C Derleth, P Zugenmeier. Studies of lyotropic liquid crystalline mesophases of some novel regioselective substituted cellulose derivatives, 1 Synthesis and characterization. Macromol Chem Phys 198:1363–1374, 1997.
122. U Drechsler, S Radosta, W Vorwerg. Characterization of cellulose in solvent mixtures with *N*-methylmorpholine-*N*-oxide by static light scattering. Macromol Chem Phys 201:2023–2030, 2000.
123. J-M Lauriol, P Froment, F Pla, A Robert. Molecular weight distribution of cellulose by on-line size exclusion chromatography—low angle laser light scattering. Part I: Basic experiments and treatment of data. Holzforschung 41(2):109–113, 1987.
124. R Evans, RH Wearne, AFA Wallis. Pyridine-catalyzed depolymerization of cellulose during carbanilation with phenylisocyanate in dimethylsulfoxide. J Appl Polym Sci 42:821–827, 1991.
125. M Terbojevich, A Cosani, M Camilot, B Focher. Solution studies of cellulose tricarbanilates obtained in homogeneous phase. J Appl Polym Sci 55:1663–1671, 1995.
126. L LaPierre, J Bouchard. Molecular weight determination of softwood kraft cellulose. Proceedings of the Ninth International Symposium on Wood and Pulping Chemistry, Montreal, 1997, Vol 1, pp L6-1–L6-6.
127. AE El Ashmawy, J Danhelka, I Kossler. Determination of molecular weight distribution of cellulosic pulps by conversion into tricarbanilate, elution fractionation and GPC. Sven Papperstidn 77(16):603–806, 1974.
128. T Rantanen, P Färm, J Sundquist. The use of GPC in testing dissolving pulp and viscose fibre. Pap Puu 9:634–641, 1986.
129. TT Le, DJT Hill, M Darveniza. Aging of transformer insulation paper. JMS Pure Appl Chem A33(12):1885–1895, 1996.
130. BF Wood, AH Conner, CG Hill, Jr. The heterogeneous character of the dilute acid hydrolysis of crystalline cellulose. J Appl Polym Sci 37(5):1373–1394, 1989.
131. C-H Lin, AH Conner, CG Hill, Jr. The heterogeneous character of the dilute acid hydrolysis of crystalline cellulose II. Hydrolysis in sulfuric acid. J Appl Polym Sci 42:417–426, 1991.
132. B Saake, St Horner, J Puls. Progress in the enzymatic hydrolysis of cellulose derivatives. In: TJ Heinze, WG Glasser, eds. Cellulose Derivatives. Modification, Characterization, and Nanostructures. Washington DC: ACS Symp Ser 688, 1998, pp 201–216.
133. R Evans, RH Wearne, AFA Wallis. Effect of amines on the carbanilation of cellulose with phenylisocyanate. J Appl Polym Sci 42:813–820, 1991.
134. F Berthold, K Gustafsson, E Sjöholm, M Lindström. An improved method for the determination of softwood kraft pulp molecular mass distributions. Proceedings of the Eleventh International Symposium on Wood and Pulping Chemistry, Nice, 2001, Vol 1, pp 363–366.
135. CL McCormick, DK Lichatowich. Homogeneous solution reactions of cellulose, chitin and other polysaccharides to produce controlled-activity pesticide systems. J Polym Sci Polym Lett Ed 17:479–484, 1979.

© 2004 by Marcel Dekker, Inc.

136. D Miller, D Senior, R Sutcliffe. Determination of the molecular weight distribution of xylanase-treated pulps. J Wood Chem Technol 11(1):23–32, 1991.
137. PF Vidal, N Basora, RP Overend, E Chornet. A pseudouniversal calibration procedure for the molecular weight determination of cellulose. J Appl Polym Sci 42:1659–1664, 1991.
138. DJT Hill, TT Le, M Darveniza, T Saha. A study of the degradation of cellulosic insulation materials in a power transformer, Part 1. Molecular weight study of cellulose insulation paper. Polym Deg Stab 48:79–87, 1995.
139. KM Kleman-Leyer, M Siilka-Aho, TT Teeri, TK Kirk. The cellulases Endoglucanase I and Cellobiohydrolase II of *Trichoderma reesei* act synergistically to solubilize native cotton cellulose but not to decrease its molecular size. Appl Environ Microbiol 62(8):2883–2887, 1996.
140. G-z Zheng, G Meshitsuka, A Ishizu. Inter- and intra-molecular ionic interactions of polyampholyte: carboxymethyl-2-diethylaminoethylcellulose. Polym Int 34:241–248, 1994.
141. G-z Zheng, G Meshitsuka, A Ishizu. Properties of an amphoteric cellulose derivative containing anionic carboxymethyl and cationic 2-hydroxy-3-(trimethylammonio)-propyl substituents. J Polym Sci Part B, Polym Phys 33:867–877, 1995.
142. G-z Zheng, G Meshitsuka, A Ishizu. Interactions and chain mobilities of *O*-carboxymethyl-*O*-2-(diethylamino)ethylcellulose in aqueous solutions. Polymer 37(9):1629–1634, 1996.
143. GA Meyer, RT Lostritto, JF Johnson. Characterization of hydroxypropylcellulose-indomethacin grafts as a function of molecular weight. J Appl Polym Sci 42:2247–2253, 1991.
144. L Picton, L Merle, G Muller. Solution behavior of hydrophobically associating cellulosic derivatives. Int J Polym Analysis Character 2:103–113, 1996.
145. D Charpentier, G Mocanu, A Carpov, S Chapelle, L Merle, G Muller. New hydrophobically modified carboxymethylcellulose derivatives. Carbohydr Polym 33(2):177–186, 1997.
146. E Bianchi, E Marsano, L Ricco, S Russo. Free radical grafting onto cellulose in homogeneous conditions 1. Modified cellulose–acrylonitrile system. Carbohydr Polym 36(4):313–318, 1998.
147. J Zhang, L-M Zhang, Z-M Li. Synthesis and aqueous solution properties of hydrophobically modified graft copolymer of sodium carboxymethylcellulose with acrylamide and dimethyloctyl(2-methacryloxyethyl)ammonium bromide. J Appl Polym Sci 78:537–542, 2000.
148. L Schulz, W Burchard, R Dönges. Evidence of supramolecular structures of cellulose derivatives in solution. In: TJ Heinze, WG Glasser, eds. Cellulose derivatives. Modification, Characterization and Nanostructures. Washington DC: ACS Symp Ser 688, 1990, pp 218–238, 1998.
149. HG Barth, FE Regnier. High-performance gel-permeation chromatography of industrial gums: analysis of pectins and water-soluble cellulosics. In: JN BeMiller, RL Whistler, DH Shaw, eds. Methods in Carbohydrate Chemistry. New York: Academic Press, 1993, Vol 9 pp 105–114.

© 2004 by Marcel Dekker, Inc.

150. HG Barth. High-performance gel permeation chromatography of pectins. J Liq Chromatogr 3:1481–1496, 1980.
151. HG Barth, FE Regnier. High performance gel permeation chromatography of water soluble cellulosics. J Chromatogr 192:275–293, 1980.
152. A Ishizu. Chemical modification of cellulose. In: DN-S Hon, N Shiraishi, eds. Wood and Cellulosic Chemistry. New York: Marcel Dekker, 1991, pp 757–800.
153. M Rinaudo, J Danhelka, M Milas. A new approach to characterizing carboxymethylcelluloses by size exclusion chromatography. Carbohydr Polym 21:1–5, 1993.
154. TE Eremeeva, TO Bykova. SEC of mono-carboxymethyl cellulose (CMC) in a wide range of pH; Mark–Houwink constants. Carbohydr Polym 36(4):319–326, 1998.
155. W-M Kulicke, AH Kull, W Kull, H Thielking, J Engelhardt, J-B Pannek. Characterization of aqueous carboxymethylcellulose solutions in terms of their molecular structure and its influence on rheological behaviour. Polymer 37:2723–2731, 1996.
156. CW Hoogendam, A de Keizer, MA Cohen Stuart, BH Bijsterbosch, JAM Smith, JAPP van Dijk, PM van der Horst, JG Batelaan. Persistence length of carboxymethyl cellulose as evaluated from size exclusion chromatography and potentiometric titrations. Macromolecules 31:6297–6309, 1998.
157. J Kötz, I Bogen, U Heinze, T Heinze, D Klemm, S Lange, W-M Kulicke. Kolloideigenschaften statistisch, blockartig und regioselektiv substituierter carboxymethylcellulosen. Papier 12:704–712, 1998.
158. J Puls, HS Horner, Th Kruse, B Saake, T Heinze. Enzymunterstützte Charakterisierung von Carboxymethylcellulosen mit herkömmlicher und neuartiger Verteilung der funktionellen Gruppen. Papier 12:743–748, 1998.
159. S Horner, J Puls, B Saake, E-A Klohr, H Thielking. Enzyme-aided characterization of carboxymethylcellulose. Carbohydr Polym 40(1):1–7, 1999.
160. B Saake, S Horner, Th Kruse, J Puls, T Liebert, Th Heinze. Detailed investigation on the molecular structure of carboxymethyl cellulose with unusual substitution pattern by means of an enzyme-supported analysis. Macromol Chem Phys 201:1996–2002, 2000.
161. AR D'Almeida, ML Dias. Comparative study of shear degradation of carboxymethylcellulose and poly(ethylene oxide) in aqueous solution. Polym Degr Stab 56:331–337, 1997.
162. S Nilsson, L-O Sundelöf, B Porsch. On the characterization principles of some technically important soluble non-ionic cellulose derivatives. Carbohydr Polym 28(3):265–275, 1995.
163. A Huber, J Schurz, W Praznik, B Hinterstoisser. SEC/LALLS-Technik: Anwendung auf Polysaccharide. Papier 12:735–741, 1991.
164. G Delker, C Chen, RB Miller. Size exclusion chromatographic determination of hydroxypropyl methyl cellulose and polyethylene glycol 400 in an ophthalmic solution. Cromatographia 41(5/6):263–266, 1995.
165. K Jumel, SE Harding, JR Mitchell, K-M To, I Hayter, JB O'Mullane, S Ward-Smith. Molar mass and viscometric characterization of hydroxypropylmethyl cellulose Carbohydr Polym 29(2):105–109, 1996.

© 2004 by Marcel Dekker, Inc.

166. SS Cutié, CG Smith. Determination of Methocel A15-LV cellulose ether blends with microcrystalline cellulose. J Chromatogr A 693:371–375, 1995.
167. R Pereira, SP Campana Filho, AAS Curvelo. Benzylated pulps from sugar cane bagasse. Cellulose 4:21–31, 1997.
168. E Sjöström, B Enström. Spectrophotometric determination of the residual lignin in pulp after dissolution in cadoxen. Sven Papperstidn 69(15):469–476, 1966.
169. G Jayme, K Neuschaffer. Cadmiumaminkomplexbasen als Lösungsmittel für Cellulose. Makromol Chem 23:71–83, 1957.
170. L Segal, JD Timpa. Cellulose solubility in cadoxen and the effect of age of the solvent on viscometric data. Sven Papperstidn 72(20):656–661, 1969.
171. D Henley. A macromolecular study of cellulose in the solvent cadoxen. Ark Kemi 18(20):327–392, 1961.
172. WB Achwal, AB Gupta. Studies in a modified cadoxen solvent. Angew Makromol Chem 2(13):190–203, 1968.
173. MB Huglin, SJ O'Donohue. Cadoxen and solutions of cellulose in cadoxen. In: JF Kennedy, GO Phillips, PA Williams, eds. Wood and Cellulosics: Industrial Utilization, Biotechnology, Structure and Properties. Chichester: Ellis Horwood Limited, 1987, pp 119–126.
174. K-E Eriksson, F Johansson, BA Pettersson. Molecular weight fractionation of cellulose by gel filtration chromatography. Svensk Papperstidn 70(19):610–611, 1967.
175. K-E Eriksson, BA Pettersson, B Stenberg. Gel filtration chromatography of hemicelluloses and carboxymethylcellulose in cadoxen solution. Sven Papperstidn 71(19):695–698, 1968.
176. BA Pettersson. Gel filtration chromatography of regenerated cellulose. Sven Papperstidn 72(1):14–l5,1969.
177. K-E Amlin, K-B Eriksson, BO Pettersson. Determination of the molecular weight distribution of cellulose on calibrated columns. J Appl Polym Sci 16:2583–2593, 1972.
178. D Berek, G Katuščáková, I Novák. Some peculiarities of gel chromatography of non-modified cellulose on inorganic gels in cadoxen. Br Polym J 9:62–65, 1977.
179. YT Bao, A Bose, MR Ladisch, GT Tsao. New approach to aqueous gel permeation chromatography of nonderivatized cellulose. J Appl Polym Sci 25:263–275, 1980.
180. JD Cosgrove, BC Head, TJ Lewis, SG Graham, JO Warwicker. A GPC study of cellulose degradation. In: JF Kennedy, GO Phillips, DJ Wedlock, PA Williams, eds. Cellulose and its Derivatives: Chemistry, Biochemistry and Applications. Chichester: Ellis Horwood Limited, 1985, pp 143–152.
181. O Bobleter, W Schwald. Gelpermeationschromatographie zur Ermittlugn der Molekulargewichtesverteilung von Cadoxen gelösten, underivatisierten Cellulosen. Papier 39(9):437–441, 1985.
182. HD Burgess. Gel permeation chromatography use in estimating the effect of water washing on the long-term stability of cellulosic fibres. In: HL Needles, SH Zeronian, eds. Washington DC: ACS Adv Chem Ser 212, 1986, pp 363–376.
183. W Schwald, O Bobleter. Characterization of nonderivatized cellulose by gel permeation chromatography. J Appl Polym Sci 35:1937–1944, 1988.

© 2004 by Marcel Dekker, Inc.

184. M Teodorović, J Dănhelka, L Majdanac. Polydispersity of regenerated alkali celluloses during oxidative degradation. Acta Polymerica 42(9):458–461, 1991.
185. JL Ekmanis. Gel permeation chromatographic analysis of cellulose. Polymer Notes, Waters Chromatography Division, Millipore Corp 1(3), 1986.
186. JD Timpa. Application of universal calibration in gel permeation chromatography for molecular weight determinations of plant cell wall polymers: cotton fiber. J Agric Food Chem 39:270–275, 1991.
187. JD Timpa, BA Triplett. Analysis of cell-wall polymers during cotton fiber development. Planta 189:101–108, 1993.
188. JD Timpa, HH Ramey, Jr. Relationship between cotton fiber strength and cellulose molecular weight distribution: HVI calibration standards. Textil Res J 64(10):557–562, 1994.
189. JD Timpa. Characterization by size-exclusion chromatography with refractive index and viscometry. Cellulose, starch, and plant cell wall polymers. In: T Provder, MW Urban, HG Barth, eds. Chromatographic Separation of Polymers: Hyphenated and Multidimensional Techniques. Washington DC: ACS, Adv Chem Ser 247, 1995, pp 141–150.
190. M Strlič, J Kolar, M Žigon, B Pihlar. Evaluation of size-exclusion chromatography and viscometry for the determination of molecular masses of oxidized cellulose. J Chromatogr A 805:93–99, 1998.
191. JF Kennedy, ZS Rivera, CA White, LL Lloyd, FP Warner. Molecular weight characterization of underivatized cellulose by GPC using lithium chloride-dimethylacetamide solvent system. Cellulose Chem Technol 24:319–325, 1990.
192. A Striegel, J Timpa. Molecular characterization of polysaccharides dissolved in Me_2Nac–LiCl by gel-permeation chromatography. Carbohydr Res 267:271–290, 1995.
193. A Striegel, J Timpa. Gel permeation chromatography of polysaccharides using universal calibration. Int J Polym Analysis Character 2:213–220, 1996.
194. A Striegel, J Timpa. Size exclusion chromatography of polysaccharides in dimethylacetamide–lithium chloride. In: M Potschka, PL Dubin, eds. Strategies in size exclusion chromatography. Washington DC: ACS Symp Ser 635, 1996, pp 366–378.
195. M-A Rousselle, PS Howley. Molecular weight of cotton cellulose: effect of treatment with a total cellulase. Textile Res J 68(8):606–610, 1998.
196. AA Silva, ML Laver. Molecular weight characterization of wood pulp cellulose: dissolution and size exclusion chromatographic analysis. Tappi J 80(6):173–180, 1997.
197. AM Emsley, M Ali, RJ Heywood. A size chromatography study of cellulose degradation. Polymer 41:8513–8521, 2000.
198. T Schult, S Moe, BE Christensen, T Hjerde. Size exclusion chromatography of cellulose dissolved in LiCl/DMAc using macroporous monodispersed poly(styrene-*co*-divinylbenzene) particles. J Liq Chrom Rel Technol 23(15):2277–2288, 2000.
199. E Sjöholm, K Gustafsson, B Eriksson, W Brown, A Colmsjö. Aggregation of cellulose in lithium chloride/*N*,*N*-dimethylacetamide. Carbohydr Polym 41(2): 153–161, 2000.

© 2004 by Marcel Dekker, Inc.

200. R Berggren, F Berthold, E Sjöholm, M Lindström. Fibre strength in relation to molecular mass distribution of hardwood kraft pulp. Degradation by ozone and acid hydrolysis. Nordic Pulp Paper Res J 16(4):333–338, 2001.
201. N Jerosch, B Lavédrine, J-C Cherton. Study of cellulose–holocellulose solutions in *N*,*N*-dimethylacetamide–lithium chloride by size exclusion chromatography. J Chromatogr A 927:31–38, 2001.
202. M Hasegawa, A Isogai, F Onabe. Size-exclusion chromatography of cellulose and chitin using lithium chloride-*N*,*N*-dimethylacetamide as mobile phase. J Chromatogr A 635:334–337, 1993.
203. AL Kvernheim, E Lystad. Size-exclusion chromatography and methylation analysis of cellulose in N,N-dimethylacetamide/LiCl. Acta Chem Scand 43:209–211, 1989.
204. O Karlsson, U Westermark. Evidence for chemical bonds between lignin and cellulose in kraft pulps. J Pulp Paper Sci 22(10):397–401, 1996.
205. D Ciechanska, G Strobin, S Boryniec, N Struszczyk. Biotransformation of cellulose: GPC studies. Int J Polym Anal Charact 4:205–217, 1997.
206. T Schult, T Hjerde, OI Optun, PJ Kleppe, S Moe. Characterization of cellulose by SEC-MALLS. Cellulose, 9:149–158, 2002.
207. O Karlsson, B Pettersson, U Westermark. Linkages between residual lignin and carbohydrates in bisulphite (Magnefite) pulps. J Pulp Paper Sci 27(9):310–316, 2001.
208. E Sjöholm, K Gustafsson, J Kolar, B Pettersson. Characterization of chemical pulps by size exclusion chromatography. Proceedings of the Third European Workshop on Lignocellulosics and Pulp, Stockholm, 1994, pp 246–250.
209. E Sjöholm, K Gustafsson, F Berthold, A Colmsjö. Influence of carbohydrate composition on the molecular weight distribution of kraft pulps. Carbohydr Polym 41(1):1–7, 2000.
210. E Sjöholm, K Gustafsson, E Norman, T Reitberger, A Colmsjö. Fibre strength in relation to molecular weight distribution of hardwood kraft pulp. Degradation by gamma irradiation, oxygen/alkali or alkali. Nordic Pulp Paper Res J 15(4):326–332, 2000.
211. E Sjöholm, K Gustafsson, M Lindström. The influence of kraft cooking on the molecular mass distribution of pulp and dissolved polymers. Proceedings of the Sixth European Workshop on Lignocellulosics and Pulp, Bordeaux, 2000, pp 587–590.
212. U Westermark, K Gustafsson. Molecular size distribution of wood polymers in birch kraft pulps. Holzforschung 48:146–150, 1994.
213. M Tenkanen, T Tamminen, B Hortling. Investigation of lignin–carbohydrate complexes in kraft pulps by selective enzymatic treatments. Appl Microbiol Biotechnol 51:241–248, 1999.
214. O Karlsson, B Pettersson, U Westermark. The use of cellulases and hemicellulases to study lignin–cellulose as well as lignin–hemicellulose bonds in kraft pulps. J Pulp Paper Sci 27(6):196–201, 2001
215. A Potthast, T Rosenau, T Röder, R Buchner, G Ebner, H Sixta, P Kosma. The water content in the solvent system *N*,*N*-dimethylacetamide/lithium chloride and its effects on the dissolution of cellulose. Proceedings of the Eleventh International Symposium on Wood and Pulping Chemistry, Nice, 2001, Vol 3, pp 671–674.

© 2004 by Marcel Dekker, Inc.

216. T Rosenau, A Potthast, A Hofinger, H Sixta, P Kosma. Hydrolytic processes and condensation reactions in the cellulose solvent system *N*,*N*-dimethylacetamide/lithium chloride (DMAc/LiCl). Proceedings of the Eleventh International Symposium on Wood and Pulping Chemistry, Nice, 2001, Vol 3, pp 675–678.
217. T Bikova, A Treimanis. Problems of the MMD analysis of cellulose by SEC using DMA/LiCl: A review. Carbohydr Polym 48(1):23–28, 2002.
218. AF Turbak. Newer cellulose solvent systems. In: El Soltes, ed. Wood and Agricultural Residues. New York: Academic Press, 1983, pp. 87–99.
219. B Hortling, P Fäm, J Sundquist. Investigation of pulp components (polysaccharides, residual lignins) using an HP/SEC system with viscosimetric, RI and UV detectors. Proceedings of the Third European Workshop on Lignocellulosics and Pulp, Stockholm, 1994, pp 256–259.
220. O Karlsson, U Westermark. Condensation reactions between wood polymers during kraft pulping. Proceedings of Tappi Pulping Conference, San Diego, 1994, Vol 1, pp 1–4.
221. O Karlsson, U Westermark. The significance of glucomannan for the condensation of cellulose and lignin under kraft pulping conditions. Nordic Pulp Paper J 12:203–206, 1997.
222. T Röder, B Morgenstern, N Schelosky, O Glatter. Solutions of cellulose in *N*,*N*-dimethylacetamide/lithium chloride studied by light scattering methods. Polymer 42:6765–6773, 2001.
223. CM Keary. Characterization of METHOCEL cellulose ethers by aqueous SEC with multiple detectors. Carbohydr Polym 45(3):293–303, 2001.
224. DS Poché, AJ Ribes, DL Tipton. Characterization of Methocel™: Correlation of static light scattering data to GPC molar mass data based on pullulan standards. J Appl Polym Sci 70:2197–2210, 1998.
225. R Berggren, F Berthold, E Sjöholm, M Lindström. Improved methods for evaluating the molar mass distributions of cellulose in kraft pulp. J Appl Polym Sci 88:1170–1179, 2003.
226. N Schittenhelm, W-M Kulicke. Producing homologous series of molar masses for establishing structure–property relationships with the aid of ultrasonic degradation. Macromol Chem Phys 201(15):1976–1984, 2000.
227. Z Grubisic, P Rempp, H Benoit. A universal calibration for gel permeation chromatography. J Polym Sci B5:753–759, 1967.
228. ML Fishman, WC Damert, JG Phillips, RA Barford. Evaluation of root-mean-square radius of gyration as a parameter for universal calibration of polysaccharides. Carbohydr Res 160:215–225, 1987.
229. F Pla. Light scattering. In: SY Lin, CW Dence, eds. Methods in Lignin Chemistry. Berlin Heidelberg: Springer, 1992, pp 498–508.
230. GE Fredheim, SM Braaten, BE Christensen. Molecular weight determination of lignosulfonates by size-exclusion chromatography and multi-angle laser light scattering. J Chromatogr 942:191–199, 2002.
231. JJ Cael, DJ Cietek, FJ Kolpak. Application of GPC/LALLS to cellulose research. J Appl Polym Sci Appl Polym Symp 37:509–529, 1983.

© 2004 by Marcel Dekker, Inc.

13
Molar Mass and Size Distribution of Lignins

Bo Hortling, Eila Turunen, and Päivi Kokkonen
KCL
Espoo, Finland

1 INTRODUCTION

Lignin is a heterogenous material with respect both to chemical structure and molecular size (1–3). The structure of lignin varies with its origin, both according to species, site in the tree, and site in the cell wall. Also, the way of isolating lignin from the raw material affects its molar mass distribution (MMD).

Soft wood lignins are mostly built of guaiacyl units together with small amounts of p-hydroxyphenyl units, which are enriched in compression wood. The lignins from hardwoods contain about equal amounts of guaiacyl and syringyl units and a lower content of p-hydroxyphenyl units. Lignins from grasses contain guaiacyl, syringyl and p-hydroxyphenyl units. The main linkage between the different units in native lignins is the β—O—4 linkage.

The native lignins are mainly isolated by milling dry wood (grass) powder in a vibrational ball mill after which the isolation is performed by extraction using dioxane–water and purification. By performing enzymatic hydrolysis of cellulose and hemicelluloses in ball-milled wood (grass) powder enzymatic lignin (EHL) is obtained. Technical lignins are isolated from pulps or spent liquors obtained during cooking and bleaching processes and during other technical treatments of

© 2004 by Marcel Dekker, Inc.

lignocellulosic materials. The lignins from the spent liquors are mostly isolated by lowering the pH and collecting the precipitated lignin. The structures and molecular size of the lignins depend on the cooking and bleaching processes. The residual lignins left in the pulps after cooking and bleaching processes can be isolated either by dissolution in acidic dioxane/water or by enzymatic hydrolysis of the polysaccharides in pulps or other lignocellulosic materials or by a combination of the methods. Depending on which method is used, different fractions, and thus different MMDs, are obtained (4).

Although it should be advantageous to use one SEC method for all kinds of lignin, the different structures and properties of lignins imply that different methods have to be used depending on the origin of the lignins.

2 SIZE EXCLUSION CHROMATOGRAPHY (SEC) OF LIGNINS

2.1 General Background

In several recent investigations it has been emphasized that during SEC measurements of polymers in general (5) and especially of lignins there occur interactions between lignin molecules (association), lignin and solvent (solvatation), and lignin column packing material (adsorption), which should all be minimized in order to obtain absolute MMDs (6–9). However, it should be emphasized that in many practical applications the knowledge of relative molar masses gives important information about changes in the size of lignin molecules during different processes and reactions.

The molar masses (MM) calculated from the MMD are number-, weight-, and z-average values (M_n, M_w, and M_z) which are obtained according to what kind of detector is in use. Calculation and data collection programs are continuously developed but the results are essentially dependent on the performance of the SEC system during MMD determinations. The resolution of the columns, the eluent, the type of detectors, the standards used in the calibration of the columns and interactions between lignin, eluent, and column packing material determines the overall reliability of the results.

2.2 Determination of Molar Masses and Calibration of SEC Systems

2.2.1 Determination of Molar Masses

Theoretically, absolute molar mass values for lignin and polymers can be obtained from viscosity measurements, light-scattering measurements using multi-angle or low-angle laser light scattering (LALLS, MALLS), sedimentation equilibria

© 2004 by Marcel Dekker, Inc.

measurements, and vapor pressure osmometry (VPO). Recently, MALDI-TOF-MS (10) and electron spray/mass spectrometric (11) methods have been taken into use. These different absolute methods are used when calibrating different HP/SEC systems either by on-line detection using light-scattering techniques (MALLS, LALLS) and viscosity measurements for universal calibration or by isolating preparatively fractions with narrow MMDs for absolute molar mass determinations.

Absolute molar mass values are obtained by using LALLS detectors (7). By this method the size of the lignin molecules is obtained, which includes the possible occurrence of lignin aggregates, and the M_w and M_z can be calculated from the results together with the dimensions of the molecules. The possible occurrence of lignin aggregates emphasizes the importance of knowing the physicochemical properties of the lignin molecules in different eluents. During LS measurements no fluorescence should occur in the samples (12). It is possible to measure the absolute weight-average molar mass M_w, second virial coefficient, and the z-average root-mean-square radius of gyration. The theory and applications of light scattering for calculating sizes of lignin molecules have been described by Pla (7). The use of pulsed field gradient NMR has also been used in the determination of the size of the lignin molecules (13).

The theory of the sedimentation equilibrium has been described in detail earlier (6). If the lignin/THF system is considered as an ideal solution, then the following expression describing sedimentation–diffusion equilibrium in the centrifuge cell can be used.

$$M_{app} = \frac{2RT}{[(1 - v_2\rho)w_2]} \cdot \frac{d \ln c}{dr_2} \tag{1}$$

When solutes are polydisperse, as is the case for SEC of lignin, it is useful to recognize that M_{app} becomes M_{wr}, which is the weight-average molar mass at any given radial distance r from the center of rotation.

Absolute number-average molar mass (M_n) is obtained by vapor pressure osmometry, which, however, is restricted to lignins of low molar mass, approximately 500–10,000 g/mol. The best results are obtained if the lignins are soluble in organic solvents such as toluene or THF. This is often only partly the case, when acetylating and/or methylating the solublilities of lignin samples increase. The theory and application of this method are described by Pla (7).

Recently MALDI-TOF-MS (10) and electron-spray method mass spectrometry (11) have been applied. These methods are used for the determination of absolute molar masses for narrow fractions collected during MMD measurements. The heterogeneity of the kraft lignin makes it difficult to detect separate MALDI-MS peaks for the different components in the lignin. No structural information is therefore obtained for the lignin sample from the MALDI-TOF-MS spectrum. The electron-spray/mass spectrometry (ESI/MS)

© 2004 by Marcel Dekker, Inc.

detector is based on similar principles as the MALDI-TOF-MS detector. Preliminary results on lignin molar mass determinations using the ESI/MS technique (11) have been presented. The ESI/MS spectra showed the molar mass distribution of lignin as well as structural features of oligomers with molar masses between 500 and 2000 g/mol. The possibility of using ESI/MS analysis for monitoring lignin reactions in solution has also been demonstrated.

2.2.2 Calibration of SEC Systems

Conventional calibration of SEC systems results in absolute molar masses when the monodisperse calibration standards have the same chemical structure as the polymer under investigation. In the case of lignin this is not generally the case and the MMDs obtained for the lignins by conventional calibration are relative with respect to the calibration compounds and the type of eluent. However, if it should be possible to manufacture monodisperse lignin samples, with structures close to those of lignins, absolute molar masses could be determined.

Universal calibration is based on the Einstein viscosity law (6):

$$[\eta] = \text{const.} \times V_h \tag{2}$$

which relates the hydrodynamic volume V_h of a macromolecule to the intrinsic viscosity $[\eta]$ in cm^3/g.

The sphere equivalent to V_h for a flexible polymer has a radius R_e in which R_g is the radius of gyration:

$$R_e = \Psi \times R_g \tag{3}$$

By development of Eqs (1) and (2) the well-known Mark–Houwink equation is obtained:

$$[\eta] = K \times M^a \tag{4}$$

In SEC it is assumed that the penetration of the solutes into the pores of the column packing material determines the elution volumes of the solute. SEC separates molecules according to some function of size, of which V_h is the most commonly used. The radius of gyration (R_g) and the mean end-to-end distance ($h_{1/2}$) of a random coil polymer could also be used.

The universal calibration method is based on measuring simultaneously the response for the concentration with an RI detector and the viscosity of the sample on-line as a function of elution volume. By combining these two responses it is possible to calculate the intrinsic viscosity, which is proportional to V_h. Commercial programs are available by which it is possible to calculate different parameters related to the molecular size of polymers (6,9).

© 2004 by Marcel Dekker, Inc.

The calibration of SEC columns by conventional calibration, universal calibration, and sedimentation equilibrium studies have been compared for native lignins and acetylated organosolv lignins (5). Conventional SEC analysis calibrated with a polystyrene standard gave the lowest molar mass values. The use of universal calibration gave molar mass estimates higher by factors of 1.5–2.5 than conventional SEC. The sedimentation equilibrium studies gave values of $M_{w,app}$ that were roughly similar to those obtained by universal calibration. These results were not considered to be surprising because conventional HPSEC predicts the effective V_h of the lignin derivative, not its molar mass, and also because conventional calibration was performed relative to polystyrene standards. Universal calibration uses the relationship between $V_h([\eta]M)$ and elution volume for a specific column set throughout a wide range of polymer structures and sizes. The higher MM obtained by universal calibration than by conventional calibration is in line with the possibility that lignins are branched polymers. It is apparent that branched polymers of higher molar mass may occupy the same V_h as a linear polymer of lower molar mass.

Using THF as eluent and Styragel columns packed with crosslinked divinyl benzene–polystyrene, Jacobs and Dahlman (10) investigated matrix-assisted-laser-desorption-ionization time-of-flight mass spectrometry (MALDI-TOF-MS) for determination of absolute molar masses of lignins and hemicelluloses. During the SEC runs of lignins, fractions of different molecular size are collected and introduced in the the MALDI-TOF-mass spectrometer, and by this system it is possible to obtain absolute molar masses of the different fractions, which are then used for the calibration of the columns. The results were compared with apparent molar masses obtained using monodisperse polystyrenes for calibration. The main features of the MALDI technique are high sensitivity, wide mass range, relatively simple sample preparation, rapid generation of results, and almost no fragmentation of the molecules during the analyses. The heterogeneity of the kraft lignin makes it impossible to detect separate MALDI-TOF-MS peaks for the different components in the lignin polymer distribution, therefore no structural information besides the molar mass distribution can be obtained for the lignin sample from the MALDI-MS spectrum (Fig. 1).

It is possible to determine absolute molar masses of narrow lignin fractions directly by MALDI-TOF-MS.

3 DIFFERENT SEC METHODS FOR DIFFERENT LIGNIN SAMPLES

Currently, very few new experimental methods for SEC measurements of lignins have been developed, although several new applications have been reported. Programs for data collection and treatment of raw data obtained from different

© 2004 by Marcel Dekker, Inc.

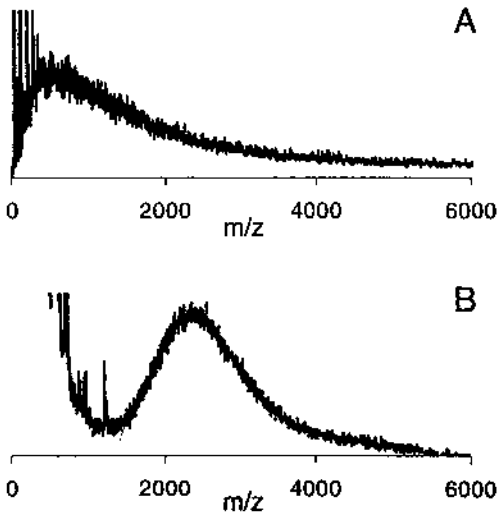

Figure 1 MALDI-MS positive ion spectra of (A) a whole Indulin AT sample, (B) a narrow MMD fraction of an Indulin AT sample isolated by SEC. (From Ref. 10.)

detectors are continuously developed. New column materials are also developed, falling into three different classes of column packing materials. The rigid crosslinked polystyrene-based materials may be derivatized in order to obtain hydrophilic properties. Semirigid synthetic hydrophilic packing materials can generally be used both with aqueous and weakly alkaline eluents and also with aprotic organic eluents. Soft packing materials are mainly based on different crosslinked polysaccharides and can be used in aqueous and alkaline eluents, but it should be pointed out that when using alkaline eluents the stability of the packing materials should be continuously monitored.

In several systems there are possibilties for connecting up to four different detectors that all detect the same sample as a function of V_h of the polymer molecule but measure different properties of the lignin molecule. The RI detector determines the concentration of the lignin molecules at a certain elution volume, the UV/VIS also measures the concentration of the lignin and is dependent on the extinction coefficient of the lignin, the light-scattering detectors (MALLS, LALLS) determine the size of the lignin molecules and also the interactions between lignin and the eluent. The viscosity detectors relate the hydrodynamic volume to the molar mass of lignin. The MALDI-TOF-MS and ESI/MS detectors give absolute molar masses by mass spectrometry of fractions obtained during SEC of lignins.

Some recent applications of known SEC systems using different types for mesurements of MMs and MMDs for lignins of different origin will be presented.

© 2004 by Marcel Dekker, Inc.

The division according to eluent type is applied because the solubilty of lignin samples of different origin varies as do the interactions between lignin, eluents, and column packing material. Some new approaches to the physicochemical behavior of lignins in aqueous solutions will also shortly be mentioned.

3.1 SEC Systems Using Organic Eluents (Mostly THF) as Eluent

THF is the most used eluent for HPSEC (high performance/size exclusion chromatography) systems using crosslinked polystyrene gels as column packing material. The solubilty of native lignins (milled wood lignin) and methylated or acetylated lignins and, in general, lignin fractions with low molar mass is good (9). Underivatized technical lignins and also enzymatically isolated native lignins are, however, only partly soluble in THF, as are hydrophilic technical lignins. The RI, UV, viscosity and light-scattering detectors and the new MALDI-TOF and electron-spray detectors have all been applied in HP/SEC systems using THF as eluent.

THF has been used as eluent (9) in the investigation of several commercial and semicommercial technical lignins, using the universal calibration with a differential viscosimeter including an RI detector. The solubility of partially soluble lignin samples was improved by acetylating and/or methylating of lignin samples. The measurements with the viscometric detector indicated that the lignin acetates are compact spherical molecules in THF. This seems to be a general property for lignin acetates in THF because according to light-scattering measurements (14) organosolv spruce lignin acetates are more compact in THF than in acetone. HPSEC measurements of lignin using THF as eluent have been described in an overview by Gellerstedt (15). In the interpretations of the results the lack of a full understanding of concentration, association, adsorption, and exclusion effects and their relationship to the hydrodynamic volume of lignin derivatives should be kept in mind. Himmel *et al.* (16) have demonstrated that commercially available molar mass standards, as well as low molar mass lignins, all follow the universal calibration curve. The universal calibration gives a more complete picture of molar masses and molecular size of lignins than conventional calibration using the elution volumes of monodisperse polystyrenes for calculation of the calibration line. However, conventional calibration has been used succesfully in several investigations for both native and technical lignins (7,9,17) when relative values for the molar masses are enough, which is often the case when following changes during specific processes. The difficulties in calibrating an HPSEC/THF system with linear polystyrenes on the one hand, and lignin fractions, lignin-like molecules, and lignin models on the other have been demonstrated. It was seen that for THF only a low amount of association between lignin molecules occurred but interactions between lignin, eluent, and packing materials did occur (18).

© 2004 by Marcel Dekker, Inc.

The determination of MMD by HPSEC using crosslinked polystyrene gels as column packing materials (19) and THF as eluent has been investigated in detail for acetylated and underivatized lignins. Also investigations with mixed solvent systems such as chloroform and dioxane were used. DMF and other polar eluents were also investigated and it was seen that for solvents such as DMF or a DMF/THF mixture, a strong association between lignin molecules occurred. However, the addition of LiCl breaks up the associates. A comparison of THF and DMF as solvents was performed for several purified kraft lignins from slash pine (20) using vapor pressure osmometry (VPO) and low-angle laser light scattering (LALLS). The molar mass distribution by high-temperature size exclusion chromatography (SEC) was investigated in THF, DMF, DMF with 0.1 M LiBr, and pyridine at conditions above the theta temperature. It was concluded that VPO may be used to determine M_n for kraft lignins if the purity of the lignins and the identity of the impurities are known. LALLS can be used to determine M_w for kraft lignins if measurements are made at or above the theta temperature of the lignin–solvent pair. SEC should be used at temperatures at, or above, the theta temperature of the lignin–solvent pair. The separation according to molecular size is highly dependent on the solvent used, and DMF is a much better solvent than THF for SEC at higher temperatures.

The molar masses of lignins from cork (21) and wine (22) have been determined. The cork lignin was significantly more crosslinked than wood-derived lignins. Also, lignins isolated from wheat straw (23) were investigated using this HPSEC system. The MMDs of lignin isolated from spruce wood at 50–110°C with mono-, di-, and trichloroacetic acid (24) were studied using THF and conventional calibration. Similar MMD measurements were performed for aspen and loblolly pine lignin samples (25) recovered from the spent liquor of several acetic acid-based pulping processes.

According to a new lignin isolation method (26), wood and pulp were subjected to ball milling, swelled in an organic solvent, and then treated with a cellulase. The MMDs of the lignins were determined using HP/SEC and THF as eluent. The thioacidolysis is used in the characterization of lignin structures and by determination of the MM for the reaction products indications of the degree of condensation of lignin and, hence, its reactivity toward pulping chemicals are obtained (27).

The molar masses of the residual lignin in softwood kraft pulp isolated by both enzymatic hydrolysis and acid hydrolysis extraction were characterized and their molar masses were determined using an HPSEC system including THF as eluent and a UV detector (28).

The MMD of chlorinated compounds of bleached kraft mill effluents (BKME) were studied by aqueous and nonaqueous SEC using THF as eluent and by ultrafiltration (29). In total 90% of the BKME halogenated organics, which originated from lignin, were soluble in THF, which was used as eluent when determining the MMD of these products.

© 2004 by Marcel Dekker, Inc.

A polymer produced by UV irradiation of a coniferyl alcohol solution was studied at the molecular levels using scanning tunneling microscopy (STM) (30). The molecular structure of the polymer was compared with the structure of a polymer obtained by the peroxidase-catalyzed polymerization of coniferyl alcohol. The results obtained by STM were in agreement with the MMD of the two polymers.

3.2 SEC Systems Using Mainly Aprotic Eluents, Alone and With Salts

The most common aprotic eluents for HPSEC are DMF and DMAC alone, or with the addition of salts such as LiCl and LiBr in order to decrease the association between lignin molecules. Both eluents are good solvents for lignins. DMF has also been used both with soft gels of the Sephadex type (31) and recently also with rigid crosslinked polystyrene packing materials.

SEC using DMF and DMAC alone and with salts as eluent and crosslinked polystyrene columns has been applied for acetylated, methylated, and underivatized kraft lignin fractions (32,33). Absolute molar mass determinations were performed using both universal calibration and analytical ultracentrifuge. The sets obtained from sedimentation equilibrium data for the pauscidisperse acetylated, methylated, and underivatized kraft lignin fractions isolated by preparative GPC could be curve fit to functions representing the sums of separate terms.

MMDs of soluble residual pine kraft lignin samples isolated during different stages of kraft flow-through cooking processes (34) have been measured in DMAC/LiCl, DMF/LiCl, and THF. It was seen that the relative MMs of the lignin samples changed in a similar way irrespective of the mobile phase used. The MM of the dissolved lignin increased during the cooking process. In contrast, the change in molar mass of the residual lignin samples did not show a clear trend with respect to cooking time. One explanation for this irregular change may be the low efficiency of the acid dioxane extraction of the pine kraft pulp obtained early in the cook. This is an example of the importance of knowing the origin of the samples when interpretating SEC results. For all samples, higher MMs of the MMD were seen when DMAC/LiCl was used as the mobile phase instead of THF (Fig. 2).

The explanation for this behavior is that the polystyrene standard elutes later from crosslinked polystyrene-based columns compared to the lignin samples when a mobile phase of higher polarity is used. The shapes of the distributions were different in LiCl/DMAc and THF, whereas LiCl/DMAc and LiCl/DMF gave similar distribution profiles. These results indicate the importance of using the same mobile phase and column packing material when comparing MMD and molecular size of different lignin samples. A similar investigation performed for

© 2004 by Marcel Dekker, Inc.

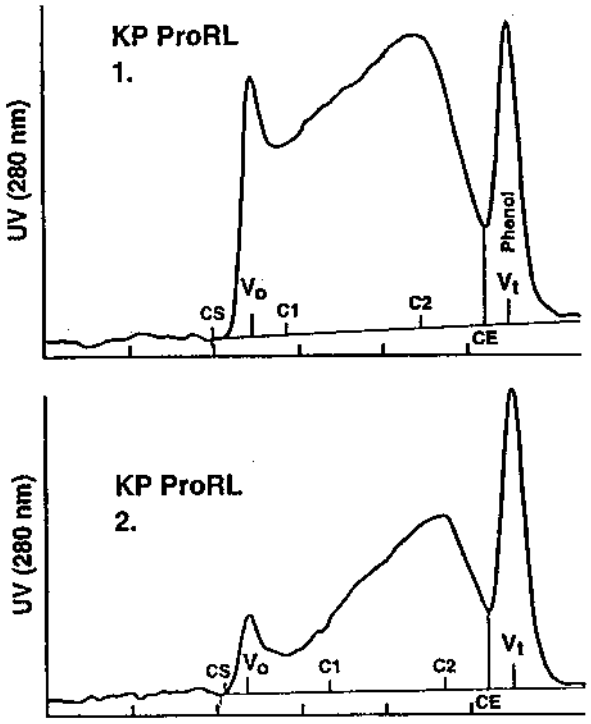

Figure 2 Elution curves of a residual lignin from an unbleached kraft pulp using 0.5 M NaOH as eluent and measured with the same column after 1 month (KP ProRL 1) and after 3 months (KP Pro RL2). (From Ref. 46.)

lignins obtained during flow-through kraft cooking of birch wood has also been studied (35). Underivatized and acetylated samples were investigated in DMAC/LiCl and compared to the MMDs of acetylated samples obtained when THF is used as eluent in a similar chromatographic system. The apparently larger molecular size obtained with the DMAc/LiCl system, as compared to the THF system, may be caused by interactions between the polystyrene standards and column matrix in combination with a more extensive conformation of the lignin polymer and or a higher degree of swelling of the polystyrene–divinylbenzene matrix.

The MMDs and structures of dehydrogenation polymer models of lignin (DHPs) (36) were analyzed using DMF as eluent. The selection of solvents for MMD measurements was considered to be important because some solvents, for example, DMF alone, are not able to destroy lignin aggregates. In this work the association effects were highly reproducible and influenced by the polymerization mode of the precursors. It was suggested that the mechanism of the association of lignin molecules should be investigated in detail.

© 2004 by Marcel Dekker, Inc.

Because DMAC/LiCl is also a good solvent for cellulose and pulps (see Chapter 12, This volume), it is possible to monitor molar mass distributions of the fiber lignin (residual lignin) left in the pulps after delignification. This kind of analysis should be possible for different kinds of cellulosics soluble in DMAC/LiCl. In investigations by Westermarck and Gustafsson (37) unbleached birch pulps were dissolved in DMAC/LiCl and the MMDs monitored using both RI and UV detectors so that both polysaccharides and lignin could be detected simultaneously. The molecular size profile of the unbleached pulp showed a cellulose peak with a low polydispersity and by the UV detector it was seen that the lignin in the pulp mainly eluted together with the low MM hemicellulose, indicating a possible chemical linkage. A similar system was applied to investigations of unbleached softwood pulp and the corresponding isolated residual lignins. Both universal and conventional calibrations were used (38). The results indicated that the isolated residual lignin had a lower molar mass than the same residual lignin *in situ* in the pulp, suggesting that there may also be linkages between lignin and cellulose in the pulp. The low intrinsic viscosity for the isolated residual lignins suggested a ball shape of the molecules, which is a generally approved result. Berthold *et al.* (39) have developed a system using ethylcarbanilation for the complete dissolution of softwood kraft pulps in DMAC/LiCl; this also made it possible to monitor the MMD of the total residual lignin in the pulp.

In investigations of properties of residual lignins isolated from kraft pulps of Eucalyptus globulus MMDs were determined using a HPSEC system with DMF/LiCl as eluent, a UV detector, and conventional calibration (40). Standards for HPSEC analysis of lignins in order to obtain better and precise results were prepared by preparative SEC from lignin fractions obtained during the acetosolv process of sugar cane bagasse (41).

A detailed study of the elution behavior of various preparations of lignins and lignocarbohydrate complexes by SEC have also been performed using pure dimethylformamide and dimethylsulfoxide as eluents and column packing materials such as porous silica and glycomethacrylate gels (42). The use of Spheron P-1000 and Sephadex G-50 columns have shown that lignins have polyelectrolytic properties and that their elution behavior is conditioned by the summed-up polyelectrolytic effects.

An HPSEC system based on the use of DMSO : water (90 : 10) as eluent and equipped with UV and RI detectors has been applied in the determination of MMDs, mainly for xylan, but also for lignin impurities (43).

3.3 SEC Systems Using Aqueous Eluents, Buffers, Salt, and Alkaline Solutions

3.3.1 MMD Determination for Native and Technical Lignins

SEC of lignins using aqueous eluents have been applied in several investigations together with structural characterization of lignins and lignin–carbohydrate

© 2004 by Marcel Dekker, Inc.

complexes. The relative molar mass information is often very useful as such. In the use of alkaline eluents, association of lignin molecules and their interactions with eluent and column packing materials should be considered (6). The benefits of using aqueous alkaline eluents are the good solubility of most lignins, and also the possibility of measuring MMDs directly from lignin containing spent liquors formed during pulping and bleaching processes and other treatments of lignocellulosics. UV detectors measuring at 280 nm are mainly used in aqueous SEC, but when a diode-array detector, covering a range from 200 to 700 nm is used, additional information is obtained. When quantitative conclusions are made one should be aware of possible differences in absorptivity of lignins of different origin. When RI detectors are added to the system, analyses of linkages and interactions between lignins and polysaccharides may be investigated in detail. Absolute molar masses can be determined with low-angle laser light scattering (LALLS) detectors coupled on-line with SEC measurements.

The characterization of both molecular size and structures of technical lignins is of great industrial interest. Aqueous SEC is mainly performed in alkaline solutions (0.1–0.5 M NaOH) using different soft and semirigid crosslinked agarose- and dextran-based packing materials. Semirigid synthetic resins are also prepared. Common soft packing materials include those under the Superdex, Sephacryl, and Sephadex trademarks. Semirigid hydrophilic synthetic gels such as Toyopearl HW-resins are also available. Recently, rigid hydrophilic synthetic packing materials such as Ultrahydrostyrgels have become available. For most materials the strength towards alkaline eluents is more or less restricted and should be considered when evaluating results.

A kraft lignin (6) isolated from an industrial black liquor was fractionated by preparative SEC using the Sephadex G-100 column and 0.1 M NaOH as eluent in nine paucidisperse fractions. Absolute molar masses for the kraft lignin fractions were determined from sedimentation equilibrium using an ultracentrifuge. These results were used for the calibration of the column and also in order to obtain information about the association behavior of the kraft lignins.

The MMDs of fractionated lignosulfonates (LS) were determined on Sephadex G-50, G-75, and Sephacryl S-300 gels using water as eluent. The molar masses were determined by light scattering and then used in the calibration of the columns (44). By comparing the retention volumes of proteins and lignosulfonate fractions with known molar masses, it was shown that several commercially available proteins can be used for calibration of the columns. The polyelectrolytic behavior of lignins (related to different numbers of free phenolic and carboxylic acid groups) affects strongly the elution behavior of lignins with the same molar mass but with different numbers of ionic groups. The shape of the elution curve is thus affected by ionic strength and alkalinity of the eluent. The effect of chemical stucture on fractionation according to molecular size was indicated by the Sephadex G-25 gel using 0.5 M NaOH as eluent for monomeric lignin model

© 2004 by Marcel Dekker, Inc.

compounds and was explained by adsorption effects of the packing material. It was suggested that with 0.5 M NaOH as eluent the most reliable results were obtained due to a good solubility of different lignins and a high ionic strength, which decreases association between lignin molecules.

The dependence on the strength of NaOH for the shape of the elution curves was described in detail in Ref. 6 and in references therein. One way of decreasing the association between residual lignins, which are isolated by enzymatic hydrolysis from the pulp is to determine the molar mass distributions directly from the hydrolysate using 0.5 M NaOH as eluent and a UV detector (4). In this way the formation of associates between lignin molecules during precipitation, which is needed for structural characterization, is avoided.

Aqueous eluents (45) have been applied in an SEC method for commmercial lignosulfonates, hard- and softwood kraft lignin, and birchwood dioxane lignin. In another investigation 0.5 M NaOH as eluent and Superdex gels of different pore size were used. Na-polystyrene sulfonates were used in the conventional calibration of the columns.

The relative molar mass distributions of enzymatically isolated residual lignins from pulps and spent liquor lignins were investigated. The possible changes in the performance of the gel filtration medium as a function of its age has to be considered, as seen in Fig. 2. This system was also used for the preparative fractionation of lignins for further characterization. The results were also compared with those obtained with an HPSEC system using DMAC/LiCl as eluent and pullulans as standards. Different shapes of the elution curves were obtained due to different void volumes of the column, interactions between lignin and eluent, and differences in column packing material. The orders of molar mass using the two systems were the same although the values differed.

Alkaline eluents were also used in SEC investigations of carbohydrate- and lignin-containing samples prepared from wood and pulp samples (47) (Fig. 3).

The elution of carbohydrates and lignin macromolecules was monitored by a pulsed amperometric detector resp. UV detector. In the investigation the importance of careful consideration of the stability of signals from samples stored in alkaline solutions was emphasized. Interactions between lignins and the column packing materials depend on the concentration of alkali in the eluent. The method can be used to follow the effect of chemical and enzymatic treatments on the MMs of lignins and polysaccharides, because no adsorptive interactions between carbohydrate and lignin macromolecules were seen. The SEC method has also been used to clarify the contribution of lignin–carbohydrate complexes to the mechanism occurring when xylanase enhances the bleaching of kraft pulp. In this work the MMD distribution of lignin and carbohydrate molecules were investigated using Toyopearl HW-50S and HW-55S resins (48) and 1 M NaOH as eluent. The elution curves were monitored using UV and differential refractometer detectors and dextrans were used as MM standards, which means

© 2004 by Marcel Dekker, Inc.

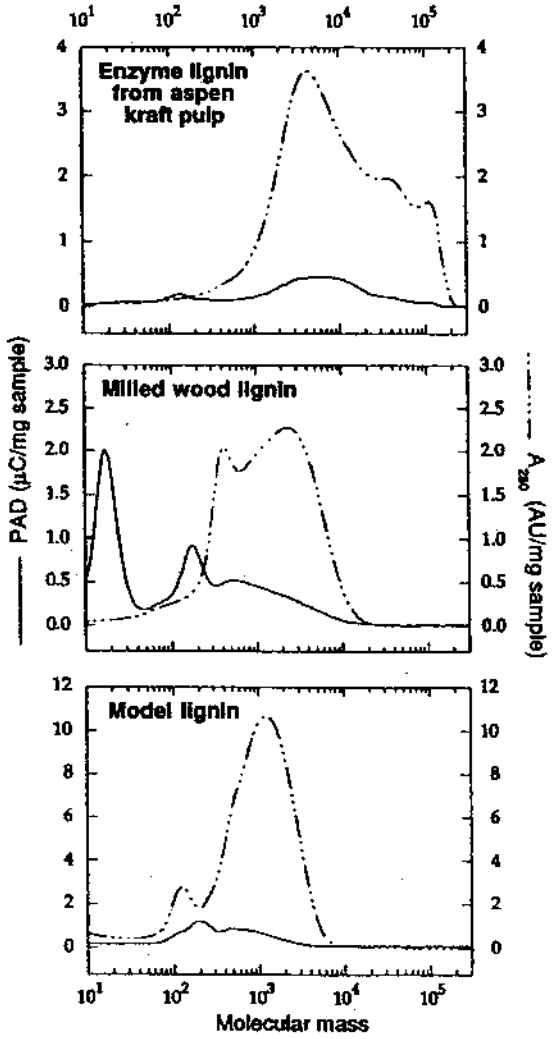

Figure 3 SEC of lignin preparations. Elution was carried out using 0.3 M NaoH with the UV lamp set low. The range of the ordinate for the PAD signals was chosen to provide a comparison with signals from carbohydrate samples. (From Ref. 47.)

that the MM values are relative with respect to dextrans. MMDs and structural analyses (49) for the acid-insoluble lignin fractions from *Caligonum monogoliacum* and *Tamarix* spp. have been investigated. The results revealed that alkaline peroxide post-treatment resulted in a substantial oxidation of the

© 2004 by Marcel Dekker, Inc.

isolated lignins because they are enriched in carbonyl and carboxyl groups. The fast pyrolysis of solid biomass into a liquid produces an insoluble residue (pyrolytic lignin) (50). The MMD and structure of the pyrolytic lignin has been determined and by combining results an average DP of 4 to 9 was obtained.

The use of HPSEC systems with alkaline eluents is restricted due to instability or interactions with the packing material. Recently several investigations have used Ultrahydrogel columns with eluents in the pH range of 6.5–12.0 and with salt solutions of 0.05 M LiCl, 0.1 M $NaNO_3$ as eluents (51,52). The ionic strength and pH value of the mobile phases have significant influences on the flow behaviors of the molar mass standards and lignins. It was shown that neutral aqueous eluents containing low concentration of electrolytes could separate degradation products of lignosulfonates. The best results were obtained by using 0.05 M LiCl at pH 6.5 as eluent. The above system was employed to measure relative MMD of lignin dispersants (53). Because of an increase in hydrophilicity, sulfonated lignins may be investigated in aqueous eluents.

The number- and weight-average MMs and MMDs of alkali lignins from eucalyptus and kraft lignin of birch have also been determined by aqueous HPSEC (54) taking into consideration the ionic strength and pH value of the eluent. The relative MM and MMD of lignosulfonates and sulfonated soda lignin samples (55) were determined by aqueous SEC. When 0.1 M $NaNO_3$ was used as mobile phase (eluent) an improved chromatographic resolution and decreased nonsize exclusion effect could be obtained. The MMs of alkali lignins were also determined by Ultrahydrogel columns calibrated with pullulans (56). Several mobile phases were tested and the ion strength and pH value of mobile phase affected greatly the adsorption of alkali lignin. It was shown, as expected, that the increase in ionic strength and pH caused a decrease in adsorption. When the pH was 12 adsorption disappeared. A review about SEC in determining the relative MM of lignin (57) has been presented. The molar masses of alkali lignins have also been determined using aqueous SEC, Ultrahydrogel column, and 0.01 M NaOH (pH 12) as eluent (58). The results were comparable to those obtained by a THF–SEC system. The MMD of kraft lignin from eucalyptus wood pulping was also investigated using aqueous eluents and Ultrahydrogel columns (59).

The structures and MMD of alkali lignins obtained by extraction with 5, 7.5, and 10% NaOH from fast growing poplar have also been investigated (60). A similar work was performed on soda-anthraquinone lignin, from oil palm empty fruit bunch (EFB), but the fractionation was obtained by successive extractions with dichloromethane, n-PrOH, and MeOH–dichloromethane (61). The relative molar masses of the fractions increased from 2630 to 4380.

A sulfomethylolated ALCELL lignin sample has been used as a water-reducing additive in cement paste. The importance of MM on the performance of the lignins was investigated by dividing it (62) into four fractions of different MM by means of membrane ultrafiltration. The MMD and average MM (M_n, M_w, M_z,

© 2004 by Marcel Dekker, Inc.

and M_{z+1}) and polydispersity of the original sample and its fractions were determined by high-performance aqueous SEC using Ultrahydrogel columns.

Preparative SEC using a Superdex column with 0.1 M NaOH as eluent has been used in investigations of MMDs of native lignins obtained by ball milling and enzymatic hydrolysis (63). The preparatively obtained fractions were precipitated and characterized. The results were compared to those obtained earlier for kraft pulps and it was suggested that at least a part of the high molar mass fraction in pulp residual lignin originates from native lignin galactan complexes.

The MMD and structures of lignins dissolved during organosolv delignification of eucalyptus batch and successive processes were investigated at various reaction times (64) and the possible occurrence of topochemical effects was considered.

The MMD of kraft lignin in alkaline solution (65) has also been investigated by calibrated ultrafiltration membranes. The membranes were first tested with probe macromolecules to obtain sieving curves at the same conditions as the lignin analyses. It was seen that the results were different from the nominal cut-off values when the MMD of a lignin sample was fractionated into five different fractions at pH 13.0. The SEC results confirmed the calibrated cut-off values for the MMD. The effect of pulping variables on the MM and MMD of dissolved kraft lignin prepared by cooking slash pine (*Pinus caribaea*) wood chips in a pilot-scale batch circulation digester was investigated (66). The effect of four pulping parameters on the MM of dissolved lignin was examined. Generally, the MM of dissolved lignin increased in both bulk and final phases as the delignification proceeded. Prolonged cooking at the end of the final phase delignification caused degradation of lignin in the liquor and decreased its MM. The MMD of lignin- and xylan-containing macromolecules that were isolated from kraft pulps derived from aspen and spruce have been determined using SEC under highly alkaline conditions (67). The changes in MMD as a result of treatment with xylanase and under acid conditions were evaluated in order to examine the role of lignin–carbohydrate complexes in enzyme prebleaching of kraft pulp. The MM and MMD of kenaf bast and core lignin during kraft pulping were determined together with the polydispersity and intrinsic viscosity, which increased with increasing cooking time (68). The MMD indicated the presence of only one component of high or low MM in the enzyme lignin of kenaf bast and core. Both the MM and polydispersity index of lignin in kenaf core were higher than those in kenaf bast under the same cooking condition, so the kenaf bast was easier to delignify than kenaf core.

In investigations of the delignification processes of *Eucalyptus grandis* wood the MMD of isolated native lignin, organosolv lignin, and kraft lignin were determined by an HP/SEC system (69). The weight-average MM (M_w) of the lignins decreased in the order MWL > organosolv lignin > kraft lignin. The weight-average MM decreased with increasing degree of delignification measured as the amount of extracted lignin.

© 2004 by Marcel Dekker, Inc.

The Separon HEMA and Separon HEMA BIO column packing materials, based on crosslinked polymethylmethacrylate, are suitable for SEC separations of lignins over a wide range of MMs (70). A minimum concentration of 0.005 M LiBr was enough to suppress the polyelectrolytic effects regardless of the sample concentration of the lignin samples that were analysed. The column packings and applied analytical conditions of SEC for lignin preparations allow fast analyses with good reproducibility; however, alkaline conditions may not be used in this system.

The organic material in effluent samples from a TCF (totally chlorine free) full-scale bleaching of kraft pulps has been characterized. The average MM of lignin and carbohydrates dissolved during the different stages of this bleaching sequence were characterized by SEC (29,71,72).

Six alkali soluble lignin fractions were extracted from the cell wall material of oil palm trunk and empty fruit bunch (EFB) fibers with 5% NaOH, 10% NaOH, and 24% KOH/2% H_3BO_3 (73). The lignin fractions contained low amounts of associated neutral sugars (0.8–1.2%) and uronic acids (1.1–2.0%). The lignin fractions isolated with 5% NaOH from the lignified palm trunk and EFB fibers gave a relatively higher DP shown by weight-average MMs ranging between 2620 and 2840, whereas the lignin fractions isolated with 10% NaOH and 24% KOH/2% H_3BO_3 from the partially delignified palm trunk and EFB fibers showed a relatively lower DP, as shown by weight-average MMs ranging between 1750 and 1980. In another investigation Abaca fiber was treated with 1, 2.5, and 5% sodium hydroxide at 25 and 50°C for 0.5–5 h (74). The dissolved alkali lignins were separated from the solubilized polysaccharides using a two-step precipitation method. All the lignin fractions were free of associated polysaccharides. Their weight-average MMs, ranging from 1960 to 2640, were determined by SEC using alkaline eluents. The use of size exclusion chromatography of lignin as ion-pair complexes has also been investigated (75).

3.3.2 MMD Determinations of Lignins During Enzymatic Treatments

Enzymatic treatments of pulps in order to improve bleachability and pulp properties is today widely investigated. One important parameter relates to the changes that occur in the MMDs of lignin during treatment. The use of alkaline eluents in the investigation of enzymatic treatments has several benefits due to the good solubility of the lignin samples.

The chemical and structural composition of native lignins from trunks of oil palm was isolated by ball milling and enzymatic hydrolysis and subsequent extraction (76). These lignins have been characterized and their MMDs have been determined.

© 2004 by Marcel Dekker, Inc.

Ball-milled straw lignin and enzymatically isolated lignin have been extracted from wheat straw and from straw residues, respectively (77). The alkali lignin was obtained by treatment of wheat straw with 0.5 M NaOH at 75°C. The effect of ball-milling time (BMT) on lignin yield and MM was examined. A comparative study of ball-milled lignin, enzyme lignin, and alkali lignin using structural determinations and SEC with an alkaline eluent was performed. The alkali lignin, which was relatively free of polysaccharides and appeared to have high MM, had the greatest potential for further investigation.

The effect of different hemicellulases on birch kraft pulp was evaluated by following the amount of lignin leached from kraft pulp after enzymatic treatment (78). An increase in the amount and MM, determined by SEC using an alkaline eluent, of the lignin extracted from the xylanase-treated pulps was observed when compared to the lignin extracted from the untreated pulp.

The effect of a commmercial xylanase preparation from *Trichoderma longibrachiatum* and *Trichoderma harzianum* E58 was tested on kraft pulp (79). By monitoring the MMD of untreated and treated pulps it was seen that the MM of lignin extracted from enzyme-treated brownstock was much larger than that from the control pulp.

The use of lignins fractionated according to molar mass in the investigations of effects of oxidative enzymes has been presented (80). In this system, alkaline eluents and preparative and analytical Superdex columns were used (Fig. 4).

Neutral-detergent fibers of cotton stalks was ball-milled for different times in a porcelain rotary ball mill and hydrolyzed by cellulase. The lignin was extracted by either dioxane:H_2O or 1 M NaOH (81). The effects of ball-milling duration and extraction procedure on yield, MMD, and carbohydrate content of lignin were investigated. The MMD patterns of the dioxane lignins were constant, irrespectively of the ball-milling time. It was also seen that the alkali system had probably extracted lignin molecules of larger size since the MM was two to three times higher than that in the dioxan lignin. The results of extractions of lignin from neutral-detergent fiber of wheat straw was performed by HP/SEC. The wheat was ball-milled for 7, 14, 21, and 28 days in a rotary ball mill and hydrolyzed by a cellulase for 4 days, and the residue was used for lignin extraction by either dioxane or 1 M NaOH (81). The effects of ball-milling time and extraction procedure on lignin yield and high-performance SEC features were examined. By increasing the ball-milling time, an increase in the proportion of high MM fraction was seen. MMD determinations were also used for evaluating how an enzymatic pretreatment modified the fiber surface. The MMD was studied using 0.5 M NaOH as eluent, a TSK HW-55S gel, and a UV detector. The MMD was determined for lignins extracted by alkali from the enzymatically treated pulps (83). The treatment of kraft pulp with hemicellulases removes some of the xylan and renders the fiber structure more permeable. The increased permeability allows the passage of lignin

© 2004 by Marcel Dekker, Inc.

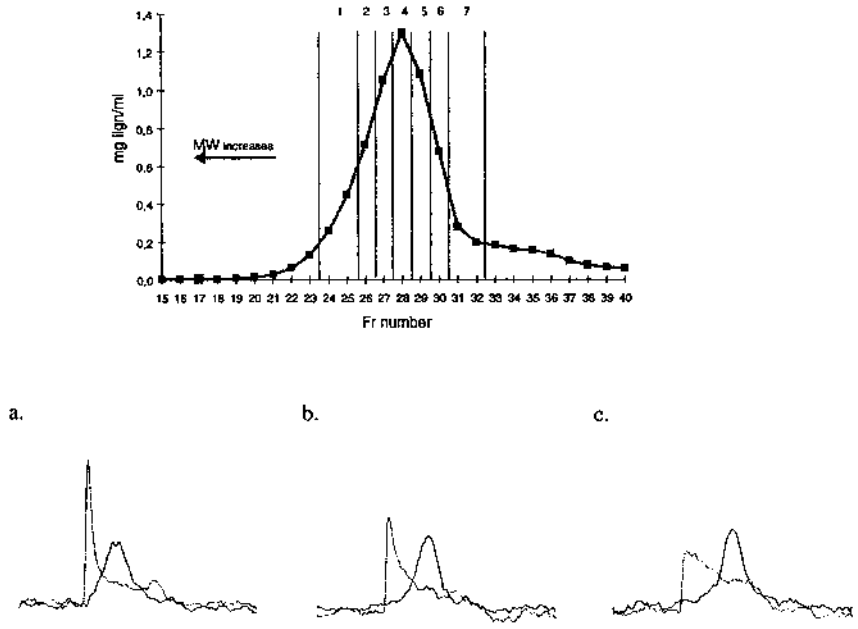

Figure 4 GPC elution curves of the kraft RL fractions before ———— and after – – – laccase treatment. Molar mass growing from right to left. Lignin concentration 0.13 mg/mL, laccase charge 170 nkat/mg. (a) Fr 1; (b) Fr 2; (c) Fr 3. High molar mass part after treatment with laccase. (From Ref. 80.)

or lignin–carbohydrate molecules in larger amounts and of higher MM in the subsequent chemical extraction performed as described above.

MMD value for brown-colored substances in biologically treated wastewaters from paper production plants (84) have also been investigated. When comparing the SEC chromatograms and the UV spectra of the eluted brown substances with those of humic acids and lignin sulfonic acids, the eluted substances could be identified as polymeric organic substances with acidic lignin-like character.

3.4 Physicochemical Investigations of Lignins

Important information about changes in the relative MMs of lignin occurring during different processes is obtained by performing SEC measurements using on-line detection. Using sophisticated detectors it is possible to obtain absolute MM

© 2004 by Marcel Dekker, Inc.

values for lignins that are soluble in suitable eluents. However, association phenomena between lignin molecules in organic solvents make any result difficult to evaluate if the association phenomena are not considered. The alkaline aqueous solvent in which most lignins are soluble is difficult to use with some packing materials and sophisticated detectors. In order to better understand the behavior of lignin molecules with different structures and the interaction between lignin molecules and between lignin molecules and solvent (eluent), a better knowledge about physicochemical phenomena should be obtained.

Detailed investigations of kraft lignins in alkali solutions have been investigated by Sarkanen and colleagues (6,85). The association–dissociation behavior of lignin molecules was investigated by precipitation of lignin at different pH values and also by isolating paucidisperse fractions 0.1 M NaOH elution profiles and determining the weight-average MM (M_w) of the fractions. At the same time physico-chemical properties of the lignin molecules in the system were investigated using light-scattering measurements. Pulse-field-gradient NMR has been used in order to obtain detailed information about the shape of lignin molecules (13). From intrinsic viscosity measurements the size and shape of lignin molecules can be estimated. The coefficients in the Kuhn–Mark–Houwink–Sakurada (KMHS) equations relate intrinsic viscosity data to the shape of molecules in different solvents and were determined based on the absolute molar mass determined with low-angle laser light scattering (86). The KMHS exponential factors of kraft lignin were found to be 0.11, 0.13, and 0.23 in DMF at 318.2 K in DMF at 350.7 K, and in 0.5 M NaOH at 302 K, respectively. It was seen that the lignin molecules in solution were approximately spherical particles and slightly solvated with solvent.

A new method to characterize underivatized lignins in aqueous solutions is capillary zone electrophoresis (CZE), by which separation is achieved due to differences in mobilities, which depend on differences in charge to molecular size ratios (87) (Fig. 5).

From flow-through kraft cooking of birch wood (88), a black liquor, an isolated spent liquor lignin, and residual lignin from pulps obtained at different cooking times were investigated by CZE. The average mobility (μ_{av}) of the lignin-containing samples was determined. It was seen that the lignin samples had a broad mobility distribution, which reflected the charge-to-size ratio of the molecules. At pH 12, when lignin is completely dissociated, μ_{av} of each type of sample increases during the cooking process, which is reflected as an increase in charge density of the lignin. The lower charge density of black liquor compared to dissolved lignin may be caused by association between lignin and carbohydrate fragments dissolved in the black liquor. The decrease in mobility when lowering the pH correlates with the degree of dissociation of the lignin phenol groups. At pH 10, approximately the pK_a of the phenolic groups in lignin, the μ_{av} of black

© 2004 by Marcel Dekker, Inc.

liquor is highest throughout the cooking process. The relative order of μ_{av} is then black liquor > dissolved lignin = residual lignin.

Kraft lignin fractions leached from a softwood pulp and fractionated by ultrafiltration (89) were characterized with respect to phenolic group content, MMDs, and self-diffusion coefficients. The self-diffusion coefficients obtained from the 1H-pulsed field gradient (PFG) NMR self-diffusion measurements and SEC analyses of the fractions were seen to correlate fairly well. From the self-diffusion measurements, the mass-weighted median hydrodynamic radii of the diffusants in the fractions were calculated assuming spherical fragments. Furthermore it was seen that the content of phenolic groups in the fractions decreased by increasing hydrodynamic radius and MM, but the calculated median surface charge densities of the macromolecules were in the range of oligomers of phenylpropane units up to at least 65 structural units (Fig. 6).

The dissociation of phenolic groups in a polydisperse, low MM kraft lignin (Indulin AT) was studied in alkaline aqueous solutions in the temperature interval 21–70°C, by a UV-spectrophotometric method (90). At a constant concentration of OH ions, the degree of dissociation decreased when the temperature was elevated. Dissociation curves and apparent pK_0 values were also calculated for the polydisperse sample at the same conditions, using the van't Hoff and the Poisson–Boltzmann equations. At dissociation degrees exceeding approximately 0.4, the outcome of the theoretical approach was shown to be in good agreement with the experimentally obtained results. Calculations were

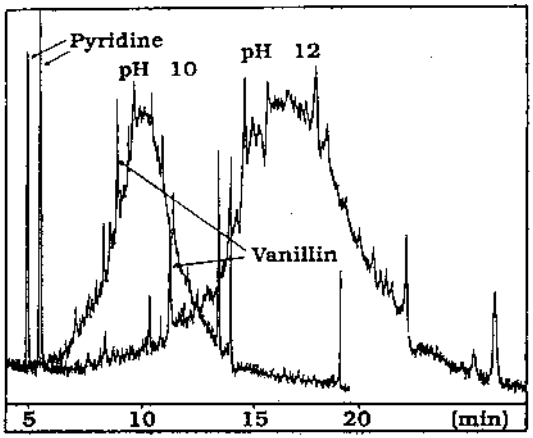

Figure 5 Electropherogram of underivatized dissolved lignin. The sample was separated at pH 10.0 and 12.0. The increased mobility at pH 12.0 is due to an increased number of ionized phenolic groups. (From Ref. 87.)

© 2004 by Marcel Dekker, Inc.

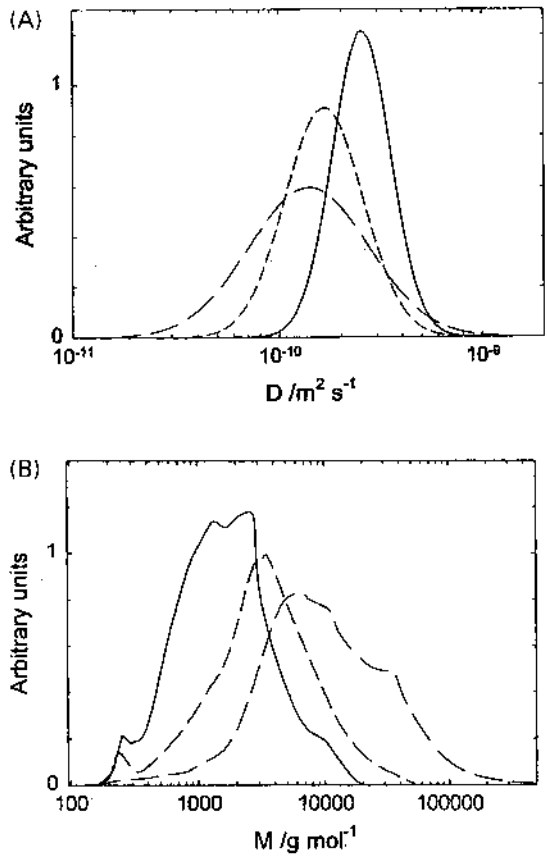

Figure 6 (A) Log-normal distribution curves of self-diffusion coefficients of the lignin fragments in some of the fractions, obtained by ^{1}H PFG NMR method. (B) Molar mass distribution curves for the fractions in Panel (A). (From Ref. 89.)

performed for kraft lignins with different MMs. The results indicated that the apparent pK_0 is shifted to higher values by increasing MM because of an increase in the electrostatic attraction of the H^+-ions, which arise from a less curved surface. Predictions of dissociation behavior at temperatures close to those in the kraft processes (approx. 160°C) were performed. Under these conditions, the higher MM kraft lignin molecules never seemed to reach the point of complete dissociation.

A non-solution technique, based on thermomechanical analysis of polymers (91), has also been presented and has been suggested to be used in studies of polymeric matrix structures of wood and some of its derivatives. Molecular and

© 2004 by Marcel Dekker, Inc.

topological anisotropy in the polymeric matrix of different kinds of wood were determined and analyzed. Molar mass characteristics of different types of viscose pulps and fir lignin were investigated. A way of obtaining information about sizes of lignin molecules has also been presented by Jurasek (92), who used modeling of lignin molecules by utilizing experimentally obtiained data for the lignin structures. Computational chemistry has also been used based on experimental data in order to mimic processes involved in lignin formation (93).

REFERENCES

1. D Hon, N Shiraishi. Wood and cellulosic chemistry. New York: Marcel Dekker, Inc., 1991.
2. W Glasser. Classification of lignin according to chemical and molecular structure. ACS Symp. Ser. (2000), 742(Lignin: Historical, Biological, and Materials Perspectives, 2000), pp 216–238.
3. D Argyropoulus, SB Menachem. Lignin. In: Th. Scheper, ed. Advances in Biochemical Engineering, Biotechnology, Vol. 57. Berlin: Springer-Verlag, pp. 127–158, 1997.
4. T Tamminen, B Hortling. Isolation and characterization of residual lignin. In: D Argyropoulus, ed. Progress in Lignocellulosics Characterization. Atlanta: TappiPress, 1999, pp 1–42.
5. W Yau, J Kirkland, D Bly. Modern Size-Exclusion Liquid chromatography. New York: John Wiley & Sons, 1979.
6. ME Himmel, J Mylnar, S Sarkanen. Size exclusion chromatography of lignin derivatives. In: Chi-san Wu, ed. Handbook of Size Exclusion Chromatography. Chromatographic Science Series 69, 1995, pp 353–379.
7. F Pla, Light scattering and vapor pressure osmometry. Determination of molecular weight, size and distribution. In S Lin, C Dence, eds. Methods in Lignin Chemistry. Berlin: Springer-Verlag, pp. 498–517, 1992.
8. E Sjöström, R Alen. Analytical Methods in Wood Chemistry, Pulping, and Papermaking, Springer Series in Wood Science. TE Timell, ed. Berlin: Springer Verlag, 1999.
9. WG Glasser, Vipul, CE Frazier. Molecular weight distribution of (semi-) commercial lignin derivatives. J Wood Chem Technol 13(4):545–559, 1993.
10. A Jacobs, O Dahlman. Absolute molar mass of lignins by size exclusion chromatography and Maldi-TOF mass spectroscopy. Nord Pulp Pap Res J 15:120–127, 2000.
11. DV Evtuguin, P Domingues, FL Amado, CP Neto, AJF Correia, Electrospray ionization mass spectrometry as a tool for lignins molecular weight and structural characterization (Short note), Holzforschung 53(5):525–528, 1999.
12. S Dutta, TM Garver, Jr, S Sarkanen. Modes of association between kraft lignin components. In: WG Glasser, S Sarkanen, eds. Lignin Properties and Materials, ACS Symposium Series 397, 195th National meeting of the American Chemical Society, Toronto, Ontario, Canada, June 5–11,1988.

© 2004 by Marcel Dekker, Inc.

13. TM Garver, PT Callaghan. Hydrodynamics of kraft lignins, Macromolecules 24(2):420–430, 1991.
14. G Merkle, S Auerbach, W Burchard, A Lindner, G Wegener. J Appl Polym Sci 45:407, 1992.
15. G Gellerstedt, Gel permeation chromatography. Determination of molecular weight, size and distribution. In S Lin, C Dence, eds. Methods in Lignin Chemistry. Berlin: Springer-Verlag, pp. 487–497, 1992.
16. ME Himmel, K Tatsumoto, KK Oh, K Grohmann, DK Johnson, HL Chum. Molecular weight distribution of aspen lignins estimated by universal calibration. In: S Sarkanen, W Glasser, eds. Lignin: Properties and Materials, Vol. 397. Washington, DC: American Chemical Society, 1989, pp 82–99.
17. C Lapierre, K Lundquist. Investigations of low molecular weight and high molecular weight lignin fractions. Nord Pulp Pap Res J 14(2):158–162,170, 1999.
18. O Faix, O Beinhoff. Improved calibration of high-performance size-exclusion chromatography of lignins using lignin-like model compounds. Holzforschung 46(4):355–356, 1992.
19. HL Chum, DK Johnson, MP Tucker, ME Himmel. Some aspects of lignin characterization by high performance size exclusion chromatography using styrene divinylbenzene copolymer gels. Holzforschung 41:97–108, 1987.
20. W Schmidl, D Dong, AL Fricke. Molecular weight and molecular-weight distribution of kraft lignins. Mater Res Soc Symp Proc 197(Mater Interact Relevant Pulp Pap, Wood Ind):21–30, 1990.
21. LG Akim, N Cordeiro, CP Neto, A Gandini. Cork lignin characterization with dry hydrogen iodide/1H NMR/GPC analysis: A comparative study. Book of Abstracts, 215th ACS National Meeting, Dallas, March 29–April 2 (1998), CELL-035. Washington, D.C.: American Chemical Society, 1998.
22. N Vivas, G Bourgeois, Y Glories, M Augustin, C Vitry. Tonnellerie Demptos, Universite Victor Segalen Bordeaux, Talence, 33405, Fr. GPC/MS detection of specific biomarkers of wine aging in barrels. Analusis 26(2):88–92, 1998.
23. R Sun, JM Lawther, WB Banks, B Xiao. Effect of extraction procedure on the molecular weight of wheat straw. Lignins Ind Crops Prod 6(2):97–106, 1997.
24. M Likon, J Zule, M Truden, A Moze, A Perdih, M Oblak-Rainer. Molecular weight distribution study of delignification of spruce wood meal with chloroacetic acids. J Wood Chem Technol 17(1&2):135–146, 1997.
25. JL Davis, RA Young. Production and characterization of lignins from acetic acid based pulping processes. Part 1. Lignin preparation and molecular weight distribution. Holzforschung 45(Suppl., Lignin and Pulping Chemistry):61–70, 1991.
26. JY Chen, Y Shimizu, M Takai, J Hayashi. A method for isolation of milled-wood lignin involving solvent swelling prior to enzyme treatment. Wood Sci Technol 29(4):295–306, 1995.
27. ID Suckling, MF Pasco, B Hortling, J Sundquist. Assessment of lignin condensation by GPC analysis of lignin thioacidolysis products. Holzforschung 48(6):501–503, 1994.
28. AP Duarte, D Robert, D Lachenal. Adv Lignocellul Chem Ecol Friendly Pulping Bleaching Technol, Eur Workshop Lignocellul Pulp, 5th, pp 523–526, 1998.

© 2004 by Marcel Dekker, Inc.

29. M Ristolainen, R Alen, J Knuutinen. Characterization of TCF effluents from kraft pulp bleaching. I. Fractionation of hardwood lignin-derived material by GPC and ultrafiltration. Holzforschung 50(1):91–96, 1996.
30. K Radotic, J Budinski-Simendic, M Jeremic. A comparative structural study of enzymic and photochemical lignin by scanning tunneling microscopy and molecular mass distribution, Center Multidisciplinary Studies, Belgrade, Yugoslavia Hem. Ind. 52(9):347–350, 1998.
31. WJ Connors. Gel chromatography of lignins, lignin model compounds and polystyrenes using Sephadex LH-60. Holzforschung 32(4):145–147, 1978.
32. EJ Siochi, MA Haney, W Mahn, TC Ward. Molecular weight determination of hydroxypropylated lignins. In WG Glasser, S Sarkanen eds. Lignin Properties and Materials. ACS Symposium Series 397, Washington DC, pp. 100–108, 1989.
33. ME Himmel, K Tatsumoto, K Grohmann, DK Johnson, HL Chum. Molecular weight distribution of aspen lignins from conventional gel permeation chromatography. Universal Calibration and Sedimentation Equilibrium. Crom. 21 947, Elsevier Science Publishers B. V., 1990.
34. E Sjoholm, K Gustafsson, A Colmsjo. Size-exclusion chromatography of lignins using lithium chloride/*N*,*N*-dimethylacetamide as mobile phase. II. Dissolved and residualpine kraft lignins. J Liq Chromatogr Relat Technol 22(18):2837–2854, 1999.
35. E Sjoholm, K Gustafsson, A Colmsjo. Size-exclusion chromatography of lignins using lithium chloride/*N*,*N*-dimethylacetamide as mobile phase. I. Dissolved and residual birch kraft lignin. J Liq Chromatogr Relat Technol 22(11):1663–1685, 1999.
36. B Cathala, B Saake, O Faix, B Monties. Evaluation of the reproducibility of the synthesis of dehydrogenation polymer models of lignin. Polym Degrad Stab 59(1–3):65–69, 1998.
37. U Westermark, K Gustafsson. Molecular size distribution of wood polymers in birch kraft pulps. Holzforschung 48(Suppl.):146–150, 1994.
38. B Hortling, T Tamminen, M Tenkanen, A Teleman, O Pekkala. Investigations of residual lignin and its interaction with polysaccharides in chemical pulps. Int Symp Wood Pulping Chem, 8th Volume 1, pp 231–238.
39. F Berthold, K Gustafsson, E Sjöholm, M Linström. An improved method for the determination of softwood kraft pulp molecular mass distributions, 11th International Symposium on Wood and Pulping Chemistry, Nice, France, Vol. I, pp. 363–366, 2001.
40. AP Duarte, D Robert, D Lachenal. Eucalyptus globules kraft pulp residual lignins. Part 1. Effects of extraction methods upon lignin structures. Holzforschung 54:365–372, 2000.
41. VR Botaro, AAS Curvelo, RAMC De Groote. Fractionation of acetosolv sugar cane bagasse lignin by preparative permeation chromatography. In: DP Veloso, R Ruggiero, eds. Proc Braz Symp Chem Lignins Other Wood Compon, 3rd, 1993, pp 195–199. Belo Horizonte, Brazil: Universidade Federal de Minas Gerais, Departamento de Quimica.
42. V Zakharov, MA Lazareva. Exclusion liquid chromatography of lignins and lignocarbohydrates complexes. Cellulose Chem Technol 26:567–589, 1992.

© 2004 by Marcel Dekker, Inc.

43. B Saake, Th Kruse, J Puls. Investigation on molar mass, solubility and enzymatic fragmentation of xylans by multi-detected SEC chromatography. Bioresource Technol 80(3):195–204, 2001.
44. K Forss, R Kokkonen, P-E Sågfors. Determination of the molar mass distribution of lignins by gel permeation chromatography. In: WG Glasses, S Sarkanen, eds. Lignin, Properties and Materials. ACS Symposium Series 397. Washington, DC: American Chemical Society, 1989, pp 124–133.
45. OM Sokolov, DG Chukhchin, LV Maier. High-performance liquid chromatography of lignins. Izv Vyssh Uchebn Zaved, Lesn Zh (2–3):132–136, in Russian, 1998.
46. B Hortling, E Turunen, P Kokkonen. Procedure for molar mass distributuion measurements of lignins of different origin. Proceedings of 10th International Symposium on Wood and Polymer Chemistry, Yokohama, Japan, 1999, Vol. 1. pp 54–57.
47. KKY Wong, E de Jong. Size-exclusion chromatography of lignin- and carbohydrate-containing samples using alkaline eluents. J Chromatogr A 737:193–203, 1996.
48. S Yokota, KKY Wong, JN Saddler, ID Reid. Molecular weight distribution of xylan/lignin mixtures from kraft pulps, Pulp & Paper Canada 96(4):39–41, 1995.
49. R Sun, Q Lu, XF Sun. Physico-chemical and thermal characterization of lignins from Caligonum. Polymer Degs Stab 72(2):229–238, 2001.
50. B Scholze, C Hanser, D Meier. Characterization of the water-insoluble fraction from fast pyrolysis liquids (pyrolytic lignin) Part II. GPC, carbonyl groups, and 13C-NMR. J Anal Appl Pyrolysis 58–59:387–400, 2001.
51. Fan-gen Chen. Determination of relative molecular mass distribution of electro-oxidative degradation products of lignosulfonate by gel permeation chromatography. Sepu 18(5):429–431, 2000 (Chinese).
52. Fangeng Chen, Jing Li. Aqueous gel permeation chromatographic methods for technical lignins. J Wood Chem Technol 20(3):265–276, 2000.
53. Shu-biao Zhang, Wei-hong Qiao, Zong-shi Li. Measurement for relative molecular mass distribution of lignin dispersants. Sepu 18(3):277–279, 2000.
54. Jing Li, Fangeng Chen. Determination of relative molecular weight distribution of alkali lignin and kraft lignin with aqueous gel permeation chromatography. Guangzhou Inst. Chem., Academia Sinica, Canton, 510650, Peop Rep China. Fenxi Huaxue 27(4):491, 1999.
55. Jing Li, Xiongjun Zuo. Determination of relative molecular weight distribution of lignosulfonate and sulfonated soda lignin by aqueous GPC. Fenxi Ceshi Xuebao 18(5):47–49, 1999.
56. Jing Li, Shiyu Fu, Hanying Zhang. Determination of molecular weight of alkali lignin with aqueous gel permeation chromatography. Sepu 16(3):235–237, 1998.
57. Fangeng Chen, Jing Li. Determination of molecular weight and molecular weight distribution of lignin by gel permeation chromatography. Xianweisu Kexue Yu Jishu 7(3):47–53, 1999.
58. Jing Li, Shiyu Fu. Determination of molecular weight and distribution of alkali lignin by aqueous GPC. Xianweisu Kexue Yu Jishu 6(1):63–66, 1998.
59. Fangeng Chen, Li Jing, Shuping Yu. Determination of molecular weight distribution of kraft lignin by aqueous gel permeation chromatography, Emerging Technol. Pulping Papermaking Fast-Grow Wood. In: Huanbin Liu, Huaiyuzhan, Yimin Xie,

© 2004 by Marcel Dekker, Inc.

eds. Proc Int Symp 1998. Canton, Peop. Rep. China: South China University of Technology Press, pp 116–121.
60. RunCang Sun, J Tomkinson, XF Sun, NJ Wang. Fractional isolation and physicochemical characterization of alkali-soluble lignins from fast-growing poplar wood. Polymer 41(23):8409–8417, 2000.
61. Runcang Sun, J Tomkinson, S Griffiths. Fractional and physico-chemical analysis of soda-AQ lignin by successive extraction with organic solvents from oil palm EFB fiber. Int J Polym Anal Charact 5(4–6):531–547, 2000.
62. J Zhor, TW Bremner. Influence of lignosulfonate molecular weight fractions on properties of fresh cement. Am Concr Inst SP SP-173 (Superplasticizers and Other Chemical Admixtures in Concrete):781–805, 1997.
63. B Hortling, T Tamminen, M Kleen, T Liitia, S Maunu. Morphological origin of residual lignin in spruce kraft pulp. Adv Lignocellul Chem Ecol Friendly Pulping Bleaching Technol, Eur Workshop Lignocellul Pulp, 5th, 1998, pp 535–538.
64. DT Balogh, AAS Curvelo. Successive and batch extraction of Eucalyptus grandis in dioxane–water–HCl solution. Pap Puu 80(5):374–378, 1998.
65. J Li, T O'Hagan, JM MacLeod. Using ultrafiltration to analyze the molar mass distribution of kraft lignin at pH 13. Can J Chem Eng 74(1):110–117, 1996.
66. Daojie Dong, AL Fricke. Effects of multiple pulping variables on the molecular weight and molecular weight distribution of kraft lignin. J Wood Chem Technol 15(3):369–393, 1995.
67. S Yokota, KKY Wong, JN Saddler, ID Reid. Molecular weight distribution of xylan/lignin mixtures from kraft pulps. Pulp Pap Can 96(4):39–41, 1995.
68. Molecular weight distribution of lignin during kraft pulping kenaf bast and core. Xianweisu Kexue Yu Jishu 2(2):21–27, 1994.
69. EA Nascimento, SAL Morais, AEH Machado, DP Veloso. Studies of Eucalyptus grandis lignin Part II: High-performance size-exclusion chromatography of milled wood lignin, kraft and organosolv lignins. J Braz Chem Soc 3(3):61–64, 1992.
70. F Kacik, R Solar, I Melcer. Gel permeation chromatography of lignins on the Separon HEMA columns. Drev Vysk 135:39–48, 1992.
71. M Ristolainen, R Alen. Characterization of effluents from TCF bleaching of hardwood kraft pulp. Int Pulp Bleaching Conf, 1996, Vol. 2, pp 523–525 Atlanta, Ga. TAPPI Press, 1996.
72. M Ristolainen, R Alen. Characterization of effluents from TCF bleaching of hardwood kraft pulp. J Pulp Pap Sci 24(4):129–133, 1998.
73. RunCang Sun, JM Fang, J Tomkinson, J Bolton. Physicochemical and structural characterization of alkali soluble lignins from oil palm trunk and empty fruit-bunch fibers. J Agric Food Chem 47(7):2930–2936, 1999.
74. RC Sun, JM Fang, A Goodwin, JM Lawther, AJ Bolton. Physico-chemical and structural characterization of alkali lignins from abaca fiber. J Wood Chem Technol 18(3):313–331, 1998.
75. A Majcherczyk, A Huttermann. Size-exclusion chromatography of lignin as ion-pair complex. J Chromatogr A 764:183, 1997.

© 2004 by Marcel Dekker, Inc.

76. Runcang Sun, L Mott, J Bolton. Isolation and fractional characterization of ball-milled and enzyme lignins from oil palm trunk. J Agric Food Chem 46(2):718–723, 1998.
77. JM Lawther, R-C Sun, WB Banks. Extraction and comparative characterization of ball-milled lignin (LM), enzyme lignin (LE) and alkali lignin (LA) from wheat straw. Cellul Chem Technol 30(5–6):395–410, 1996.
78. B Hortling, M Korhonen, J Buchert, J Sundquist, L Viikari. The leachability of lignin from kraft pulps after xylanase treatment. Holzforschung 48(5):441–446, 1994.
79. E de Jong, KKY Wong, LA Martin, SD Mansfield, FM Gama, JN Saddler. Molecular mass distribution of materials solubilized by xylanase treatment of Douglas-fir kraft pulp, ACS Symp Ser, 1996, 655(Enzymes for Pulp and Paper Processing):44–62, 1996.
80. ML Niku-Paavola, T Tamminen, B Hortling, L Viikari, K Poppius-Levlin. Reactivity of high and low molar mass lignin in the laccase catalysed oxidation, in Biotechnology in the Pulp and Paper Industry: 8th ICBPPI meeting, Eds. L Viikari, R Lantto. Amsterdam: Elsevier Science BV, 2002, pp. 121–130.
81. E Yosef, D Ben-Ghedalia. Effect of isolation procedure on molecular weight distribution and monosaccharide composition of cotton stalk lignins. Anim Feed Sci Technol 50(1–2):27–35, 1994.
82. D Ben-Ghedalia, E Yosef. Effect of isolation procedure on molecular weight distribution of wheat straw lignins. J Agric Food Chem 42(3):649–652, 1994.
83. A Kantelinen, B Hortling, J Sundquist, M Linko, L Viikari. Proposed mechanism of the enzymic bleaching of kraft pulp with xylanases. Holzforschung 47(4):318–324, 1993.
84. G Weinberger. Gel permeation chromatography for identification of brown-colored substances in biologically treated waste water. Papiertechnische Stiftung, Munchen, 80797, Germany SO PTS-Manuskr 1997, PTS-MS 66, PTS-Analytik-Tage: Aktuell Analyseverfahren, pp 6/1–6/18.
85. S Sarkanen, D Teller, C Stevens, J McCarthy. Lignin 20. Associative interactions between kraft lignin components. Macromolecules 17:2588–2597, 1984.
86. D Dong, AL Fricke. Intrinsic viscosity and the molecular weight of kraft lignin. Polymer 36:2075–2078, 1995.
87. E Sjöholm, N-O Nilvebrant, A Colmsjö. Characterization of dissolved kraft lignin by capillary zone electrophoresis. J Wood Chem Technol 13(4):529–544, 1993.
88. E Sjöholm, E Norman, A Colmsjö. Charge density of lignin samples from kraft cooking of birch wood. J Wood Chem Technol 20(4):337–356, 2000.
89. M Norgren, B Lindstrom. Physicochemical characterization of a fractionated kraft lignin. Holzforschung 54(5):528–534, 2000.
90. M Norgren, B Lindstrom. Dissociation of phenolic groups in kraft lignin at elevated temperatures. Holzforschung 54(5):519–527, 2000.
91. YA Olkhov, SS Chernikov, AI Mikhailov. Solutionless analysis of molecular mass distribution of wood polymer matrix, lignocellulosic and cellulose materials in real scale of time. 5th European Workshop on Lignocellulosics and Pulp, Aveiro, Portugal, August 1998, Proceeding, pp. 53–56.

© 2004 by Marcel Dekker, Inc.

92. L Jurasek. Towards a three dimensional model of lignin structure. J Pulp Paper Sci 21:J274, 1995.
93. WR Russell, AE Forrester, A Chesson. Predicting the macromolecular structure and properties of lignin and comparison with synthetically produced polymers. Holzforschung 54:505–510, 2000.

© 2004 by Marcel Dekker, Inc.

14
Contribution of Size Exclusion Chromatography to Starch Glucan Characterization

Anton Huber
Karl-Franzens-Universität Graz
Graz, Austria

Werner Praznik
Universität für Bodenkultur
Vienna, Austria

1 INTRODUCTION

Starch is a very common and ubiquitously available material, which is classified as "renewable raw material" for industrial production (Table 1) of food and nonfood goods (Table 2) with particular properties based on specific starch qualities (highly heterogeneous hydrophilic material, more or less insoluble in aqueous media, highly viscous when dispersed/dissolved, limited resistance against thermal, mechanical, and chemical stress, basically biodegradable). An on-line dictionary

© 2004 by Marcel Dekker, Inc.

Table 1 Selected Industries Connected with Processing and Manufacturing of Starch

Corn Refiners Association	http://www.corn.org/web/process.htm
National Starch	http://www.nationalstarch.com/
Eridania-Beghin-Say	http://www.eridania-beghin-say.com/
Archer Daniels Midland Company	http://food.admworld.com/corn/
Cargill Incorporated	http://www.cargill.com/
Corn Products International	http://www.cornproducts.com
Minnesota Corn Processors	http://www.mcp.net/
Penford Products Company	http://www.penford.com/
Roquette	http://www.roquette.fr
Agrana	http://www.agrana.com/
Novozyme	http://www.novo.dk/enzymes/ind_appl/star&sug.htm

of starch terms (http://www.foodstarch.com/dictionary/a.asp) and a collection of starch characteristics (http://www.orst.edu/food-resource/starch/index.html) provide information upon state of the art industrial and breeding attempts to obtain and develop parameters to control starch-based material properties (1,2).

Table 2 Industrial Application Spectrum of Starch

Food applications	Nonfood applications
Sauces	Paper and board
Soup	Textiles
Dressings	Plastics
Baked goods	Rubber
Diary products	Oil
Meat products	Pharmaceuticals
Drinks	Cosmetics
Ice cream	Adhesives
Refrigerated	Sewage and water treatment
Deep-frozen	Alcohol
Dry mix	Sizing coating
Thickening	Texturing
Gelling	Viscosity control
Stabilizing	Flocculation
Sweetening	Ion exchange matrix
Bulking	Adhesives
Texturing	Dusting
Fat replacement	Fuel

© 2004 by Marcel Dekker, Inc.

Table 3 Annually Assimilated Biomass with Details on Carbohydrate/Polysaccharide Fraction

Biomass	Dry matter annually, 10^9 tonnes (Gt)	
Lignin	~20–80	~20%
Lipids	~2–8	~2%
Proteins	~2–8	~2%
Others	~2–8	~1%
Carbohydrates/polysaccharides	~75–300	~75%
Nonbranched $\beta(1\rightarrow4)$ linked glucan cellulose	~50–200	~45% of 75%
Hemicellulose	~20–100	~20–25% of 75%
Others: mannan, xylan, glactan, fructan, etc.		
$\alpha(1\rightarrow4)$ linked + $\alpha(1\rightarrow6)$ branched glucan starch	~1–5	~2–5% of 75%
Industrial utilized starch glucan	~0.02	
Annual yield of petroleum	~2	
Synthetic polymers based on petroleum	~0.1–0.2	~5–10%

Starch or starch-equivalent glucans are produced by green plants, sea organisms, microbes, insects, and all kinds of mammals. The annually assimilated mass of biomaterials is in the range $100–400 \times 10^9$ tonnes (Gt) of dry matter (Table 3). Approximately three-quarters of this biomass is formed of polysaccharides, the major fraction of which consists of glucans, polymers made of glucose as basic building blocks. Cellulose and starch represent the most prominent glucan materials.

The mass of annually assimilated starch is in the same range as that of annually produced petroleum. However, the amount of industrially utilized/manufactured starch is approximately one-fifth of the share of petroleum used to produce synthetic polymers only.

2 BIOLOGICAL BACKGROUND: (BIO-)SYNTHESIS AND COMPOSITION OF STARCH

Most starch is produced by aboveground organs of green plants, in particular by their leaves, which transform CO_2, H_2O, and electromagnetic radiation (680 nm)

© 2004 by Marcel Dekker, Inc.

into C_3-metabolites, which then may be merged to form transient carbohydrates. The synthesis of starch from such metabolites involves interconversion of sugars, sugar-phosphates, and nucleotide-sugars (3–9).

The substrate for one of the key metabolites of starch synthesis, adenosine-diphosphate-glucose (ADP-glucose, Fig. 1a), glucose-1-phosphate is formed either by hydrolysis from UDP-glucose (E.2.7.7.9) or by isomerization from glucose-6-phosphate (E.5.4.2.2). ADP-glucose pyrophosphorylase (E.2.7.7.27) is the major controlling enzyme for the rate of starch synthesis and the amount of amylose-type glucans in starch granules (10).

Nonbranched (nb)/long-chain branched (lcb) starch glucans (amylose) and short-chain branched (scb) starch glucans (amylopectin) are synthesized in the amyloplast from ADP-glucose, primarily by the catalytic action of starch synthases [E.2.4.1.21; granular bound starch synthase (GBSSx) or soluble forms of starch synthase (SSx) and branching enzymes (BEx)]. Additionally, enzymes such as debranching enzymes and disproportionating enzymes are involved (Table 4).

Elongation of glucans by subsequential coupling of ADP-glucose to a Glc_n-chain, probably starting with a maltodextrosyl-protein as primer, via $\alpha(1 \rightarrow 4)$-glycosidic linkages, results in nonbranched (nb) glucans with high symmetry (helix) and complexing potential for hydrophobic and anionic materials within the helix. Catalytic action of branching enzymes (BE) introduces $\alpha(1 \rightarrow 6)$-glycosidic linkages and results in long-chain branched (lcb) and more or less short-chain branched (scb) starch glucans (Fig. 2b).

Branches act as symmetry breakers when compared to nonbranched compounds: hydrophilic and hydrophobic domains become less pronounced with increasing scb-characteristics. In general, branches increase molecular packing density (mass within occupied volume) and enforce intramolecular stabilization (11).

In the initial state a mix of nb-, lcb-, and scb-glucans form loose amorphous clusters, which are soluble in aqueous media. By subsequent action of disproportionating enzyme, these clusters are rearranged by increasing packing density and order (amorphous $\rightarrow$ crystallinity) and are precipitated in granules for temporary storage.

Simultaneously, debranching enzymes provide nb-glucans, which are elongated by granular bound starch synthase (GBSS), yielding amylose-type starch glucans. The amount of nb-starch glucans of course depends on the GBSS-concentration located in the amyloplast-matrix and local temperature (12–14). Although the formation of nb-glucans (amylose) by debranching of lcb- and scb-glucans is generally accepted, it should be noted that these nb-glucans are found in storage starch granules only and not in the transient cluster structures of leaves (15,16).

Many of the key enzymes of starch biosynthesis have been cloned (Table 5) from plant species, in particular from maize endosperm, rice endosperm, barley

© 2004 by Marcel Dekker, Inc.

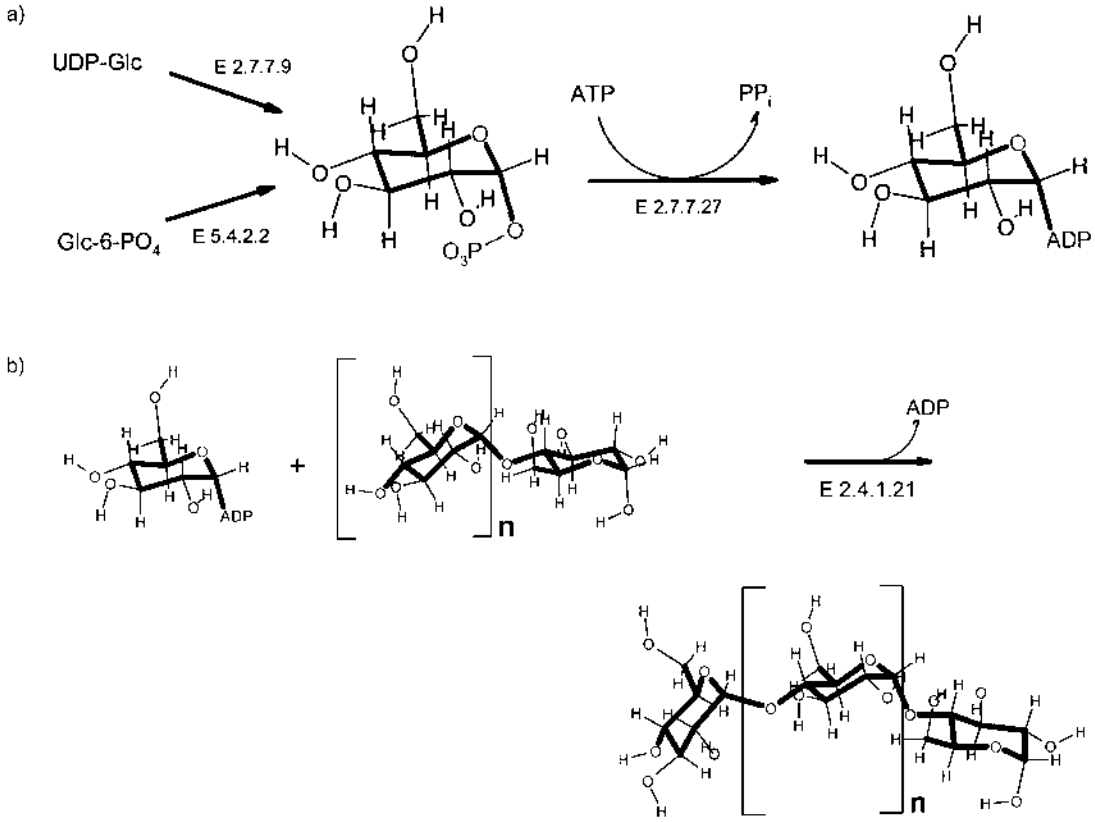

Figure 1 (a) Formation of the key metabolite of starch biosynthesis, ADP-glucose. (b) Formation of starch glucans.

© 2004 by Marcel Dekker, Inc.

Table 4 Key Enzymes in the Biosynthesis of Starch

Enzyme	Web-site → http://www.expasy.org/enzyme/
ADP-Glc-pyrophsophorylase	http://www.public.iastate.edu/~pkeeling/Enzpyro.htm
EC 2.7.7.27 Glc-1-PO_4-adenylyltransferase	http://www.expasy.org/cgi-bin/nicezyme.pl?2.4.1.27
Granule bound starch synthase (GBSS)	http://www.public.iastate.edu/~pkeeling/Enzgbss.htm
EC 2.4.1.21 starch (bacterial glycogen) synth.	http://www.expasy.org/cgi-bin/nicezyme.pl?2.4.1.21
Starch synthase (SS)	http://www.public.iastate.edu/~pkeeling/Enzss.htm
EC 2.4.1.11 glycogen (starch) synthase	http://www.expasy.org/cgi-bin/nicezyme.pl?2.4.1.11
EC 2.4.1.21 starch (bacterial glycogen) synth.	http://www.expasy.org/cgi-bin/nicezyme.pl?2.4.1.21
Branching enzyme (BE)	http://www.public.iastate.edu/~pkeeling/Enzbe.htm
EC 2.4.1.18 $(1 \rightarrow 4)\alpha$ glucan branching enzyme	http://www.expasy.org/cgi-bin/nicezyme.pl?2.4.1.18
EC 3.2.1.41 pullulanase	http://www.expasy.org/cgi-bin/nicezyme.pl?3.2.1.41
EC 3.2.1.68 isoamylase	http://www.expasy.org/cgi-bin/nicezyme.pl?3.2.1.68
Debranching enzyme	http://www.public.iastate.edu/~pkeeling/Enzdebe.htm
EC 3.2.1.41 pullulanase	http://www.expasy.org/cgi-bin/nicezyme.pl?3.2.1.41
EC 3.2.1.68 isoamylase	http://www.expasy.org/cgi-bin/nicezyme.pl?3.2.1.68
Disproportionating enzyme	http://www.public.iastate.edu/~pkeeling/Enzdispr.htm
EC 2.4.1.25 4-α-glucanotransferase	http://www.expasy.org/cgi-bin/nicezyme.pl?2.4.1.25

endosperm, potato tuber, and pea embryo to increase either the percentage of nb-/lcb-glucan fraction (amylose) or of scb-glucans (amylopectin).

No mutant has been found so far that lacks scb-glucans (amylopectin) completely; however, for several cases the ratio of lcb/scb-glucans could be significantly increased by breeding of hybrids such as amylomaize (17–19) or high amylose starch containing wrinkled pea varieties (20). Amylose-type nb/lcb-glucans are thus highly suspected to be some kind of remainders or byproducts of hydrolytic and transfer activities during starch biosynthesis.

A wide variety of mutants are, however, known that contain minor or negligible amounts of nb-glucans (21–26). The responsible maize waxy mutant was found decades ago and was optimized by breeding over a number of years to achieve starches with high yields of scb-glucans. Available waxy mutants include: maize, wheat (27), barley (28), rice (29) (monocots), pea (30), and amaranth (31) (dicots).

© 2004 by Marcel Dekker, Inc.

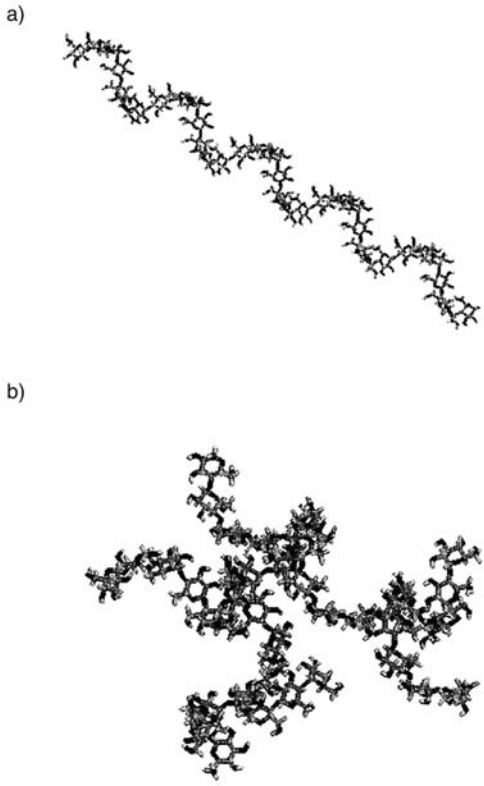

Figure 2 (a) Sequence (dp 30) of a nonbranched starch glucan formed by GBSS and SS helical structure with six anhydro-glucose units (AGU) per turn; hydrophobic cave; hydrophilic exterior; (b) Fragment (dp 43) of a branched starch glucan formed by GBSS and SS + BE; branches as symmetry-breaker compared to nonbranched starch glucan; increased packing density (molar mass within occupied volume).

General properties/qualities of mutants include:

- Single mutants (waxy, amylose, sugary) typically result in modified physico-chemical and technological (functional) properties.
- Double mutants (waxy/amylose, waxy/dull) provide new functionalities, but also poor yield, poor germination.
- Gene-dose of single mutants (aeae+ or ae++) yield no modified starch structure/functionality.
- Intermutants (wxwx+/++ae) provide novel functionality and high starch yield.

© 2004 by Marcel Dekker, Inc.

Table 5 Cloned Mutants of Starch Enzymes

Mutant	Abbreviation
Amylose extender locus	Ae → high amylose
Brittle 2 locus	Bt2
Dull locus	Dull
Shrunken 2 locus	Sh2
Sugary 1 locus	Su1
Sugary 2 locus	Su2
Waxy locus	Wx → low amylose

As an example for maize mutants detailed information may be found at the following sites:

- Waxy: http://www.agron.missouri.edu:80/cgi-bin/sybgw_mdb/mdb3/Variation/77802
- Sugary: http://www.agron.missouri.edu:80/cgi-bin/sybgw_mdb/mdb3/Variation/77153
- Shrunken: http://www.agron.missouri.edu:80/cgi-bin/sybgw_mdb/mdb3/Variation/76799

Plant-specific and environmental condition-induced activities of starch synthases and branching enzymes result in individual distributions of degree of polymerization and branching characteristics for any kind of starch glucans. For storage the crystallized insoluble form is preferred, and thus, formation of starch granules starts. Formation and growth of granules is a complex process and ends up with each granule as an individual object. Nevertheless, the major component of all types of starch granules are glucans with different percentages of proteins, lipids, water, and charges, primarily phosphates. In terms of order, granules are typically 20–40% crystalline (32,33), are of irregular, though plant- and variety-specific shape, with diameters in the range 1–120 μm and density of 1.5–1.6 g cm^{-3}, of white to creamy color, and internally organized in layers [dense layers (120–400 nm → formed by ~16 alternating crystalline, 5–6 nm, and semicrystalline, 2–5 nm, rings (34,35)) and less dense layers with higher content of water (36)].

In x-ray diffraction pattern classes of internal order may be discriminated as:

- A-type: left-handed parallel-stranded double helices crystallized in a monocline space group B2; compact packing of glucan-chains and low water-content [12 H_2O molecules with 12 anhydroglucose units (AGU); 6 AGU per helix turn, 1.04 nm height for each turn].

© 2004 by Marcel Dekker, Inc.

- B-type: double helices crystallized in the hexagonal space group P6; less compactly packed, higher water-content [36 H_2O molecules with 12 anhydroglucose units (AGU); 6 AGU per helix turn, 1.04 nm height for each turn].
- C-type: a mix of A- and B-type; however, listed as a distinct type.
- V-type: formed by 6 AGU in a helical structure with a height of 0.8 nm per helix turn.

By means of enzymatically supported fragmentation analysis, A-type starch glucans can be seen to also differ from B-type glucans in their branching pattern, in particular in their ratio of terminal (A-chains) and internal (B-chains) glucan segments (37–40).

Water definitely needs to be considered as a fundamental structural feature in the formation of starch granules and is not just another bulk material. All kinds of crystallinity represent more or less ordered structures on a more or less dominant amorphous background (41,42) (Fig. 3). ^{13}C CP/MAS spectra support the idea of amorphous single-chain and ordered double-helix glucans (43). Thermal stress on B-type glucans results in loss of water and transformation into A-type; swelling of A-type in aqueous media and destruction of crystalline structure yields B-type when recrystallizing.

Whereas scb-glucans (amylopectin) are assumed to form crystalline lamellae through parallel double helices with branching positions in amorphous regions, nb- and lcb-glucans (amylose) are preferably located in the amorphous layers (44) and are subject to complex formation with lipids. Additionally, limited cocrystallization of scb- and lcb-glucans forming small (~25 nm) and large (80–120 nm) blocks was observed by scanning electron microscopy (SEM) and atomic force microscopy (AFM) (45–48).

Based on differences in lcb/scb-glucan ratio, there are reasonable suggestions for preferred localizations of scb- (amylopectin) and lcb-glucans (amylose) within starch granules:

- Waxy maize starch granules represent an arrangement of more or less 100% scb-glucans (amylopectin) and 0% lcb-glucans (amylose). The scb-glucans are closely packed in concentric layers in dry waxy maize granules and expand on swelling in aqueous media. These concentric layers of scb-glucans represent the framework for the majority of starch granules.
- Potato starch granules are a mix of a major fraction of ~80% scb-glucans (amylopectin) and a minor fraction of ~20% lcb-glucans (amylose). The lcb-glucans are localized in distinct concentric layers alternating with scb-glucan layers. On hydration, these granules swell due to the expanding layers and simultaneously reduce the volume for

© 2004 by Marcel Dekker, Inc.

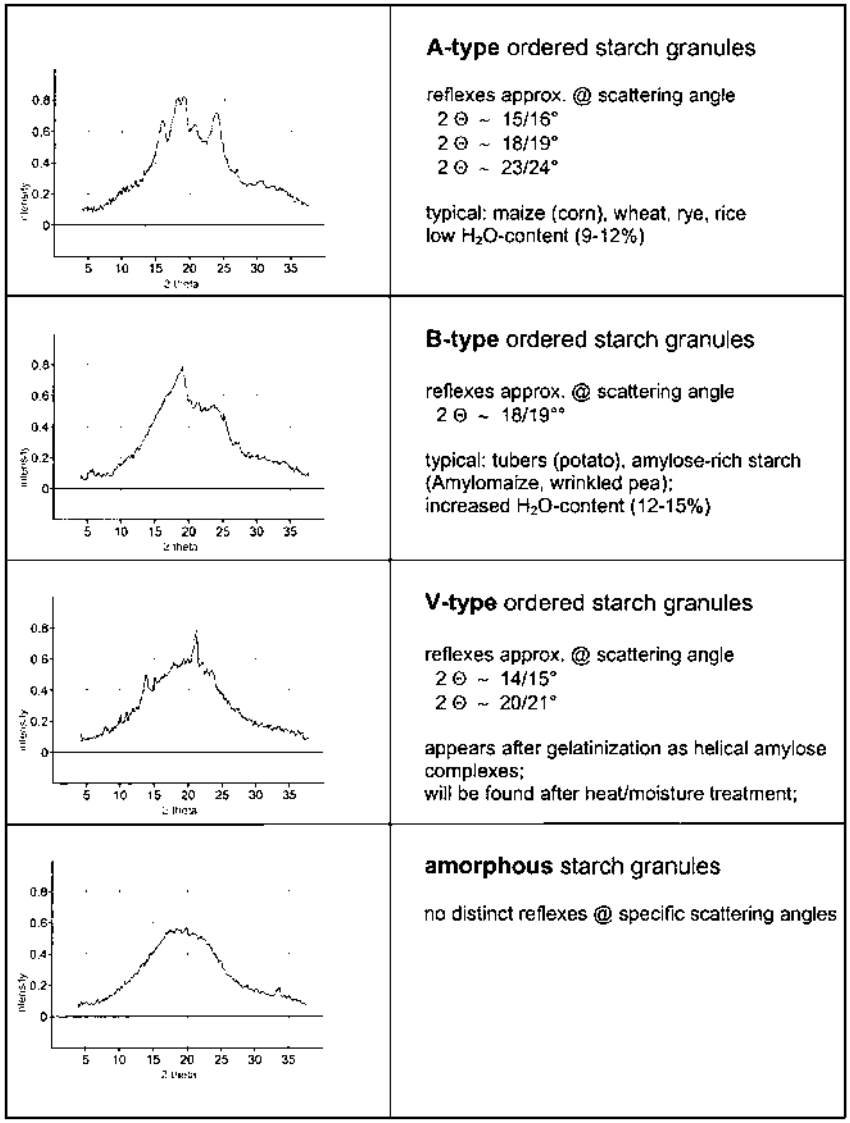

Figure 3 Modeled x-ray diffraction pattern of A-type (typically cereals), B-type (typically tubers), V-type (internal reorganized due to applied thermal/moisture treatments), and amorphous starch granules.

© 2004 by Marcel Dekker, Inc.

amorphous lcb-glucans by encapsulation. From such granules lcb-glucans (amylose) may even be extracted by leaching processes that similarly reduce the amorphous layer fraction.

- Amylomaize starch granules are composed of a minor fraction of ~30% of scb-glucans (amylopectin) and a major fraction of ~70% of lcb-glucans (amylose) with pronounced separation of scb- and lcb-glucans. On hydration lcb-glucans of such granules are diluted, but the granules do not swell. From such granules lcb-glucans may be extracted by leaching processes.

Starch granules (Fig. 4) are composed of a crystalline scb-glucan (amylopectin) framework and an amorphous lcb-glucan (amylose) fraction. Glucans of scb- and lcb-type are more or less incompatible: scb-glucans (amylopectin) form compact layers of high order lcb-glucans (amylose) form amorphous precipitates in less dense domains. Within the granules the tendency for separation increases with increasing percentage of lcb-glucans in a mixture of both types. No instance of an homogeneous scb/lcb-glucan blend in a starch granule is known.

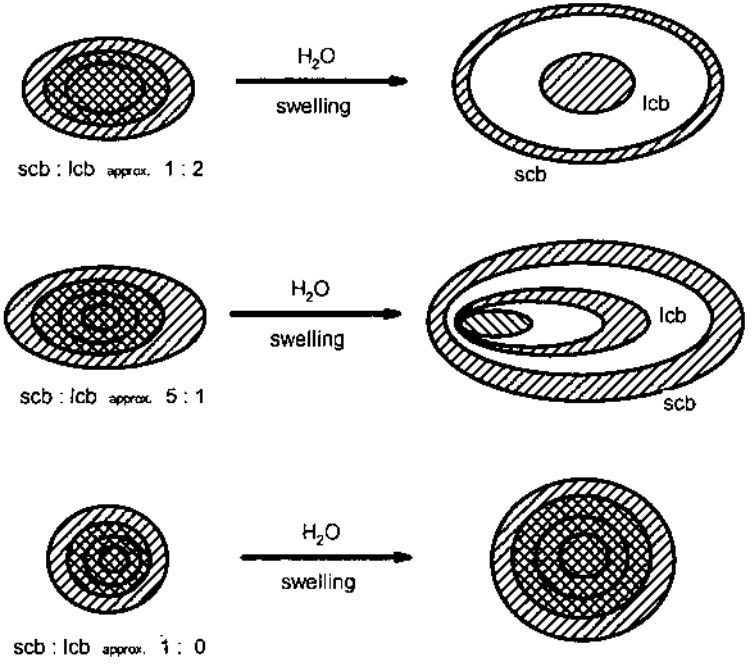

Figure 4 Schematic starch granule architecture with respect to different scb/lcb-glucan ratio and consequences on size and shape upon swelling in aqueous environment.

© 2004 by Marcel Dekker, Inc.

In the native environment (plant cell), starch granules are hydrated, and thus in a swollen status. In first order, these conditions match with industrially hydrated starch granules: in both cases the granules show up with increased order (birefringence) and reduced hilum opening. In such swollen granules lcb-glucans (amylose) diffuse out of amorphous regions, and, simultaneously, enable transfer ionic compounds into and out of the granules. Chemistry-supported extraction procedures (leaching) and drying result in the formation of compact granules with cracked hilum.

3 ISOLATION/PURIFICATION OF GLUCANS FROM STARCH RAW MATERIALS

Systematic analysis of technological qualities of starch materials includes different levels of information: environmental and biological conditions, granule properties, and molecular characteristics (Fig. 5).

Isolation of starch granules from native plant materials includes pulverization and milling of starch-containing parts and subsequent separation of granules from sliced cells with water. A sequence of repeated sieving and washing concludes this first step. In industrial isolation processes, due to technological limitations, an additional level of mechanical, thermal, and chemical stress on the granules cannot generally be avoided. However, the granule status after initial purification strongly controls "starch quality" for subsequent processes.

Isolation of cereal starch granules for analytical purposes includes elimination of adsorbed proteins (gluten), which may, for example, be achieved

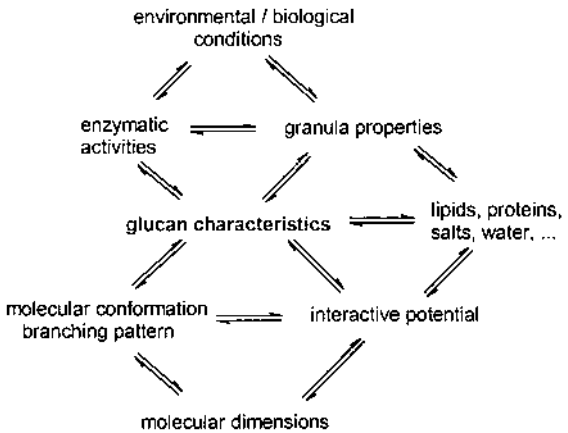

Figure 5 Interdependencies of controlling influences for starch glucan properties.

© 2004 by Marcel Dekker, Inc.

Table 6 Sequence of Techniques Applied to Isolated Potato Starch Granules to Obtain Reasonable Fractions/Pools

Isolation/ purification	Harvesting | cleaning | cutting | smashing | ... dispersing in H_2O → sieving | centrifugation | ...			
Pooling of starch granules: sedimentation in H_2O	• Small granules → fraction I (Fr.I) • Large granules → fraction II (Fr.II)			
Preparative SEC; Identification of fractions by staining: iodine: branching pattern	Iodine staining + vis-spectroscopy • E_{640} nb/lcb-quantification • E_{525} scb-quantification • $E_{640/525}$ lcb/scb-composition			
anthron: total carbohydrate	Anthron-Chromogen: • E_{540} total carbohydrates			
Precipitation of lcb- and scb-glucans from aqueous DMSO solutions	lcb-glucans: + n-butanol: → Fr.Ibut	scb-glucans: + methanol → Fr.Imet	lcb-glucans + n-butanol: → Fr.IIbut	scb-glucans: + methanol → Fr.IImet
Pooling: preparative SEC				
_a: initial V_{ret}-section	Fr.Ibut_a	Fr.Imet_a	Fr.IIbut_a	Fr.IImet_a
_b: midrange V_{ret}-section	Fr.Ibut_b	Fr.Imet_b	Fr.IIbut_b	Fr.IImet_b
_c: final V_{ret}-section	Fr.Ibut_c	Fr.Imet_c	Fr.IIbut_c	Fr.IImet_c
Glucan characterization bulk + fraction analysis	Molecule conformation/branching pattern; Molecular and supermolecular dimensions;			
enzymatically catalyzed debranching + fragment analysis	Coherent segments, dynamic interactions controlled enzymatically catalyzed step-by-step fragmentation			

© 2004 by Marcel Dekker, Inc.

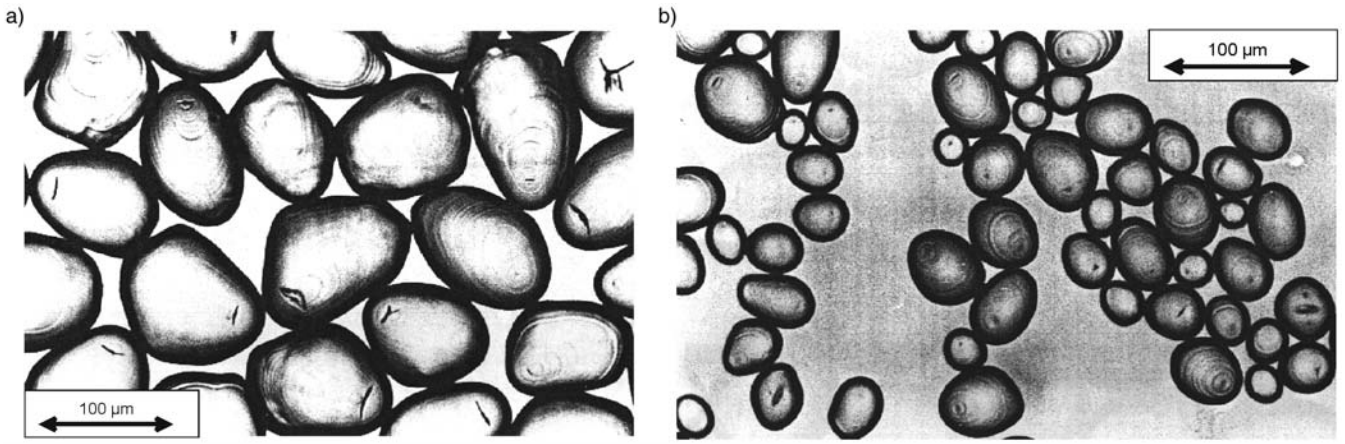

Figure 6 (a) Large starch granules of ripe potato tubers achieved after initial purification steps and final sedimentation of granules in pure water. (b) Small starch granules of ripe potato tubers achieved after initial purification steps and final sedimentation of granules in pure water.

© 2004 by Marcel Dekker, Inc.

by previous swelling in diluted aqueous SO_2 (diluted alkali or acetate buffer pH 6.5, 0.02 M). Swelling is followed by wet milling with a homogenizer and separation of starch and nonstarch materials by several sieving steps. Gluten, in particular, is separated by sedimentation on a sloped separation channel where gluten is washed out by water, and starch granules are accumulated at the bottom. Wheat starch granules are acquired by rinsing of dough made of wheat flour with a little water.

Starch granules from potato tubers are purified rather simply by washing, peeling, and smashing of the tubers, suspending the pulp in pure water and separating starch from fibers by sieving. After centrifugation, water-soluble components are removed with the supernatant. Either the resulting mix of different sizes of granules is taken to analysis or an additional separation procedure is applied: pooling of granules according their dimension by sedimentation in pure water (Fig. 6a, b)

To achieve molecular level analysis/characterization of starch glucans, isolation and dissolution, without generating artifacts, is required. Therefore, starch granules are typically dispersed in sodium or potassium hydroxide (0.5–2 M). Sonication and microwave heating have been suggested to improve "dissolution", however, these techniques support formation of artifacts and occurrence of uncontrolled destruction phenomena (49,50). For analytical purposes, dispersing in 90% aqueous dimethylsulfoxide (DMSO) is favorable. The glucan fraction dissolves in DMSO (0.5–1% wt/vol) when stirred for at least 15 hours (overnight) at 70°C. For distinct dissolution experiments dissolution temperature and periods of dissolution were varied between 50–95°C and 4–200 hours, respectively. After centrifugation (3000 rpm, 15 min) a clear starch glucan containing supernatant is achieved. In contrast with NaOH or KOH, proteins and lipids are insoluble in DMSO and for further processing no neutralization is required. DMSO-dissolved starch samples may be stored for several weeks without significant aging effects such as degradation, aggregation, or retrogradation.

4 STARCH GLUCAN CHARACTERISTICS AND THE SEC CONCEPT

Simplified starch glucans, similar to most polysaccharides, fill up volume [V_e; Eq. (1)] in a more or less regular way controlled by a fine-tuning mechanism on a molecular level which modifies coherent domains according to changing external and internal challenges. Major facets of macroscopic technological starch qualities therefore have to be correlated with molecular-level glucan features such as:

- Conformation [*mc*; Eq. (1)]: molecular symmetries in terms of helices, beta-sheets, branching pattern (short-chain, long-chain branches,

© 2004 by Marcel Dekker, Inc.

number of branching points); crosslinks; oxidation status; compatibility structures; packing density.
- Dimension [*md*; Eq. (1)]: molecular weight/degree of polymerization/ excluded volume; transition states between geometric molecular dimensions and coherence lengths of supermolecular structures.
- Interactive properties [*ip*; Eq. (1)]: water content; aggregation/ association; supermolecular dimensions (gel-formation); visco-elastic qualities; stress management.

$$V_e = ip \cdot md^{mc} \tag{1}$$

where V_e = excluded volume, ip = interactive potential, md = molecular dimension, and mc = molecular conformation. However, although variations of *md*, *mc*, and *ip* already provide countless options, diversity is increased even more by distributions of these features. In particular, starch glucans are a superimposed heterogeneous mix of regular and irregular modules:

- Highly symmetrical helices (multiple helices), primarily by lcb-glucans,
- Irregular "fractal" structures, primarily by scb-glucans,
- Compact and internally H-bond stabilized structures, predominantly by scb-glucans (crystallinity),
- Less compact "amorphous" domains with pronounced re-organization capability, predominantly by lcb-glucans,

which may easily be customized either with respect to mass [Eq. (2)] or molar [Eq. (3)] fractions of components for the major native purpose: to support optimum energy management.

$$m_V_eD = ipD \cdot m_mdD^{mcD} \tag{2}$$

where m_V_eD = mass fractions of excluded volumes distribution, ipD = distribution of interactive potentials, m_mdD = mass fraction of molecular dimensions distribution, and mcD = distribution of molecular conformation.

$$n_V_eD = ipD \cdot n_mdD^{mcD} \tag{3}$$

where n_V_eD = molar fractions of excluded volumes distribution, ipD = distribution of interactive potentials, n_mdD = molar fraction of molecular dimensions distribution, and mcD = distribution of molecular conformation.

In fact, the separation criterion in SEC is excluded volume (V_e: excluded volume). Thus, application of SEC on starch glucans should provide basic information about excluded volume heterogeneity (V_eD: excluded volume distribution). Combining SEC with several appropriate on-line detection

© 2004 by Marcel Dekker, Inc.

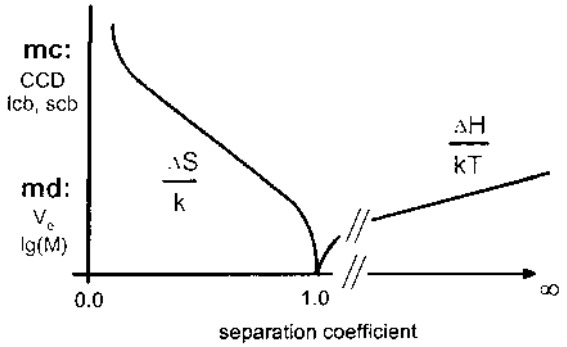

Figure 7 Separation criteria in liquid chromatography. Entropy controlled separation ($\Delta S/k$) according to differences in excluded volume (V_e): size exclusion chromatography (SEC); mc; molecular conformation; CCD, chemical composition distr; lcb, long chain branched; scb, short chain branched; md, molecular dimension. Enthalpy controlled HPLC-separation ($\Delta H/kT$) according to differences in interaction potential with the LC-matrix.

principles should provide even more detailed information about *ip*, *md*, and *mc* contributions to obtained V_e fractions (Fig. 7).

Because starch glucans at any time fill up volume in a very characteristic way, it is of utmost importance to understand the controlling factors of how this is done and why it is done that way. By gaining such knowledge, diversity of biological raw materials may be understood much better, and efficiency of processing of such raw materials could be improved. The key characteristics that need to be determined are:

- branching characteristics,
- molecular weight distribution,
- supermolecular dimensions and coherent segment dimensions.

Several approaches, which include SEC, provide information with respect to these key characteristics. In particular, molecular weight of starch glucans may be determined in several ways:

- Calibrated: applying reference glucan materials (e.g., dextrans) via peak position calibration or broad standard calibration;

or absolutely by:

- Light scattering (LS) combined with universal mass detection (SEC-mass/LS); or
- Viscosity combined with universal mass detection (SEC-mass/visc).

© 2004 by Marcel Dekker, Inc.

Both absolute approaches are extraordinarily sensitive towards high molecular components, in particular towards glucan aggregates. Thus, the molecular weight of superstructures and not of the constituting molecules will primarily be determined using these techniques. An alternative approach to obtain information about molecular weight of constituting glucans is a combined chemical/analytical one:

- Quantitative derivatization of each glucan molecule combining specific molar detection (e.g., UV/VIS or fluorescence of a unique chromophor in each molecule) and universal mass detection (SEC-mass/molar).

SEC elution profiles are also affected by variations in the branching pattern and the more or less pronounced presence of supermolecular structures. However, these phenomena are superimposed, somewhat secondary influences, which need complementary analyses to evaluate them from SEC experiments.

5 STARCH GLUCAN ANALYSIS: EXPERIMENTAL APPROACH

Benefits and limitations of SEC in starch glucan characterization will be discussed and illustrated for wheat starch glucan in the following sections. Wheat starch is an important industrial source of starch, and is a mix of lcb/scb-glucans and, thus, shows a mix of characteristics from both "extreme" components. In particular, results from different detector combinations with SEC providing fraction information will be compared to data from bulk techniques which provide integral characteristics (Table 7).

5.1 Preparative SEC: Purification and Pooling

Mass detection of separated glucan fractions in preparative SEC is typically obtained off-line as total carbohydrates (Fig. 8). Therefore an equivalent of 1 mL of each fraction is mixed with 2 mL anthron reagent (200 mg crystalline anthron pA dissolved in 100 mL H_2SO_4 96% pA) and heated for 10 min in a boiling water bath. After cooling and degassing by ultrasound, extinction at 540 nm is determined. Carbohydrate concentration is obtained from extinction values via calibration with D-glucose (51,52).

5.2 Semipreparative SEC: Branching Analysis

Whereas the granular consistency of starch glucans typically is considered to be rather relevant for starch material quality, importance of molecular level characteristics such as branching pattern, potential to form supermolecular

© 2004 by Marcel Dekker, Inc.

Table 7 Analytical Approach for Starch-Glucan Characterization and Parameters that may be Obtained

Approach	Experimental	Parameter	Information
Preparative SEC; purification + pooling	Total hydrolysis + anthron coupling → E_{540} (total carbohydrates); iodine staining: E_{525}, E_{640}	E_{540} → mass (V_{ret}) E_{640}/E_{525} (V_{ret})	Mass fractions distribution; lcb/scb ratio
Fragmentation	Step by step fragmentation; → pure chemical; → enzymatically catalysed; fragment analysis	Type of fragments; mol of fragments; mass of fragments;	Constituting glucan distribution; mean glucan conformation; branching characteristics: → chain lengths of branches → br% (percentage of br.) → # of branching positions
Semipreparative SEC; in-line elution profile; off-line complexing	In-line DRI-detection offline iodine-complexing + E_{640}, E_{525} detection	Mol (V_{ret}) mass (V_{ret}) E_{640}/E_{525} (V_{ret})	Mass fractions distribution; molar fractions distribution; lcb/scb ratio
Analytical SEC: mass detection + molecular weight calibration	In-line DRI detection → mass_ev	Mass (V_{ret}) concentration dn/dc	Mass fractions distribution; molar fractions distribution; recovery info on preferential dissolution
Analytical SEC: mass/ LALLS-detection	Elution profiles: DRI → mass_ev LALLS → LS_5_EV	Mass (V_{ret}) R_Θ (V_{ret}) M (V_{ret})	Apparent absolute molecular weight calibration (log(M) vs. V_{ret}) → M_n, dp_n/M_w, dp_w → m_MWD_d, m_dpD_d → n_MWD_d, n_dpD_d
Analytical SEC: mass/ viscosity detection	Elution profiles: DRI → mass_ev visc → eta_spec	Mass (V_{ret}) $[\eta]$ (V_{ret}) V_e (V_{ret})	Excluded volume V_n distribution → m_VeD_d, n_VeD_d

© 2004 by Marcel Dekker, Inc.

Table 7 (*Continued*)

Approach	Experimental	Parameter	Information
Analytical SEC: mass/molar detection	Elution profles: DRI → mass_ev UV/VIS/ fluorescence → mol_ev	Mass (V_{ret}) mol (V_{ret}) M (V_{ret})	Absolute molecular weight distribution → M_n, dp_n/M_w, dp_w → m_MWD_d, m_dpD_d
Analytical SEC: mass/LS/ visc detection	Elution profiles: DRI → mass_ev LS → LS_θ_EV visc → eta_spec	Mass (V_{ret}) R_Θ (V_{ret}) M (V_{ret}) $[\eta]$ (V_{ret}) V_e (V_{ret})	Universal SEC calibration → V_eD_d
Bulk viscosity η below overlapping concentration c^*	Viscosity of concentration series	$\eta(c \to 0) \equiv [\eta]_{av}$ $c^*_{av} = 1/[\eta]_{av}$	Mean value of excluded volume $[\eta]_{av}$; overlapping concentration c^*_{av}
Bulk viscosity η at varying mechanical stress (shear deformation D)	Complex viscosity at varying shear deformation; for dissolution periods	$\eta^*_{(o)}$ $\eta^*_{(D)}$ (t)	Visco-elastic properties of starch glucan solutions: → Newtonian/ non-Newtonian
Bulk viscosity η above overlapping conc c^* at varying thermal stress (T)	Viscosity at increasing temperature	T_{dis} ΔT_{dis}	Conformational stability; gelatinization temperature; disintegration temperature
Bulk viscosity η above overlapping conc c^* at varying thermal stress (T) and const. mechanical stress	Brabender viscosity: constant shear deformation period of incr. T period of holding elev. T period of decr. T	Viscosity as function of temperature, deformation and application time: $\eta(T, D, t)$	Stability/resistance towards applied energy (T, D, t): → disintegration characteristics → re-organization capability
Photon correlation spectroscopy (PCS)	Translational diffusion coefficient D_T	$D_T \to R_H \to l_{coh}$ Distribution of mass fractions → m_D_TD Distribution of LS-intensity fractions → intensity_D_TD	Population analysis: translational diffusion coef. D_T; sphere equivalent radii of diffusing molecular objects R_H; coherence length of molecular and supermolecular segments

© 2004 by Marcel Dekker, Inc.

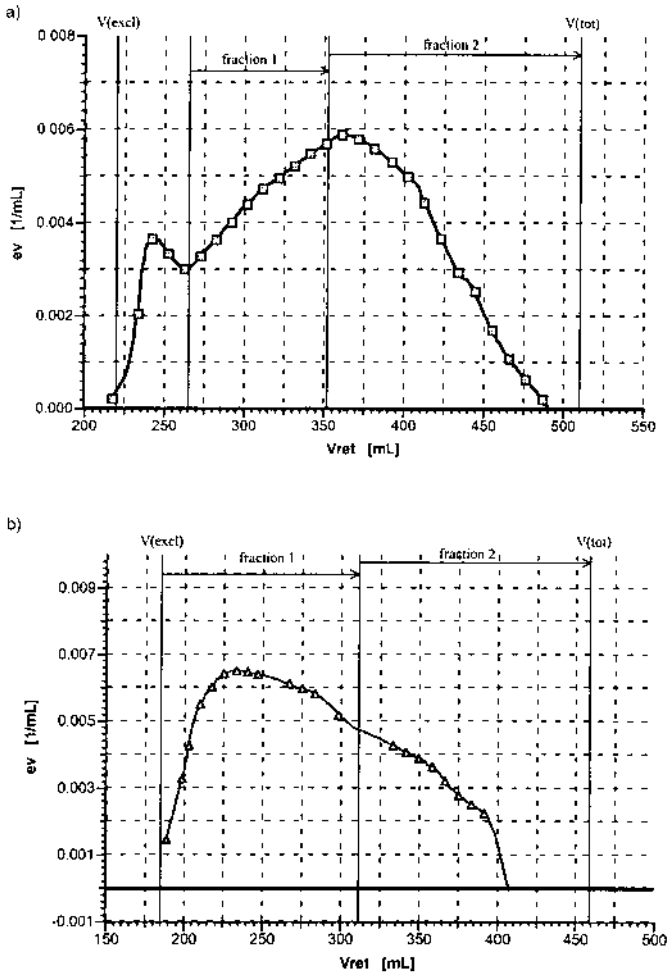

Figure 8 (a) Preparative SEC of lcb-glucans. Glucans from small ($d < 35$ μm) granules of potato species Ostara; separated on Sephacryl S-200/S-400/S-500/S-1000 ($12 + 55 + 66 + 135 \times 1.6$ cm); eluent, 0.005 M NaOH; injected volume, 2 mL (20 mg/mL); normalized chromatogram (area = 1.0) was constructed from off-line determined carbohydrate content of succeeding 5 mL fractions; flow rate, 0.67 mL/min; $V_{excl} = 220$ mL; $V_{tot} = 510$ mL; exclusion limit cut-off; impurities; fraction 1, large-V_e fraction; fraction 2, small-V_e fraction. (b) Preparative SEC of scb-glucans; glucans from small ($d < 35$ μm) granules of potato species Ostara; separated on Sephacryl S-1000 (88×2.6 cm); eluent, 0.005 M NaOH; injected volume, 2 mL (20 mg/mL); normalized chromatogram (area = 1.0) was constructed from off-line determined carbohydrate content of succeeding 5 mL fractions; flow rate, 0.67 mL/min; $V_{excl} = 185$ mL, $V_{tot} = 460$ mL; fraction 1, large-V_e fraction; fraction 2, small-V_e fraction.

© 2004 by Marcel Dekker, Inc.

structures, excluded volumes, and the way to fill excluded volumes, is often underestimated (53). Key characteristics for this molecular level are branching characteristics. It is well known that the ratio of lcb/scb-glucans (amylose-type/amylopectin-type) in particular controls macroscopic starch qualities (54,55). Bad solubility in aqueous media, high tendency for retrogradation and gelatinization of amylose-type nb/lcb-glucans is as well known as the potential of such starches to form gels and films. Amylopectin-type scb-glucans on the other hand are soluble in aqueous media as long they are not organized in supermolecular H-bond stabilized clusters. Additionally, scb-glucans are capable of fixing a high percentage of water and are less sensitive towards varying environmental conditions (56–63).

Investigation of branching characteristics includes determination of a complex package of parameters:

- Type of branching pattern; composition of branching pattern for starch glucan fractions sampled with respect to identical excluded volume; identical molecular weight (degree of polymerization); identical internal stabilization; identical potential for formation of supermolecular characteristics;
- Number and/or percentage of branching position within individual glucan molecules and type of distribution of number of branching positions in supermolecular domains;
- Heterogeneity/homogeneity of branching positions within individual glucan molecules and distinct supermolecular domains;
- Degree of local symmetry (crystallinity) due to certain types of branching characteristics; influence of increased branching to symmetry and interactive properties.

However, the experimental approaches to branching characteristics are rather laborious and often result in rough estimations only:

- Destructive techniques: pure chemical directed and/or enzymatically catalyzed step-by-step fragmentation followed by fragment analysis and recalculation of mean molecules as a puzzle from fragment characteristics;
- Complexing/staining of starch glucans (native glucans, glucan fractions, glucan fragments) with polyiodide anions in hydrophobic caves of terminal helical starch glucan branches, and spectroscopy in terms of extinction-ratio E_{640}/E_{525} provides relative information about lcb/scb-characteristics of investigated samples (Fig. 9); application to fractions from semipreparative SEC (Fig. 10a, b) yields a profile of lcb/scb-ratio with respect to glucan fractions with decreasing excluded volume.

© 2004 by Marcel Dekker, Inc.

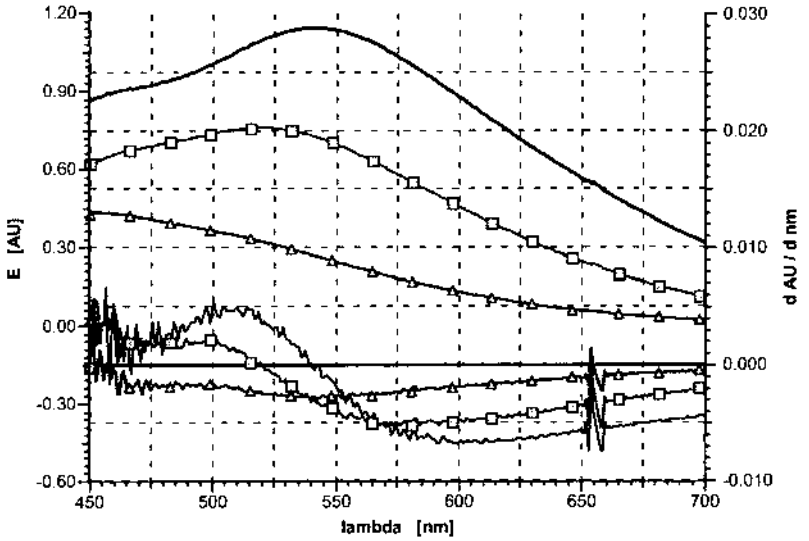

Figure 9 VIS spectrum of potato maltodextrin (——) with starting-type of branching characteristics. Introduction of additional branching positions by branching enzyme to the initial potato maltodextrin at 20°C (—□—); introduction of more branching positions by branching enzyme to the initial potato maltodextrin at 4°C (—△—); first derivative of spectra illustrates a shift of absorption maximum (zero-intercept) and a broadening of absorbance in the wavelength range below 550 nm for increasing scb characteristics of polyiodide–glucan complexes. Absorbance maxima: potato maltodextrin, 540 nm; branching-enzyme modified maltodextrin at 20°C, 520 nm, branching-enzyme modified maltodextrin at 4°C, approx. 460 nm.

Branching characteristics for glucan mixtures or individual fractions in a first approach may be estimated by determining complexation potential of helical glucans with polyiodide anions. Experimentally, 125 mg of freshly sublimated iodine is dissolved in the presence of 400 mg kJ in 1000 mL demineralized water and diluted 1 : 1 with 0.1 M acid to ensure a final pH 4.5–5.0 when mixed with the alkaline eluate from SEC. Polyiodide anions complexed in the helical starch glucan segments shift the extinction maximum from E_{max} 525 nm of free aqueous iodine to higher wavelengths (64,65). In fact, the shift is also controlled by the length of helical segments and by the number of available helical segments; however, correlation of E_{640} values is an appropriate indication for lcb-glucans. Correlation of scb-glucans with E_{525} values is supported by corresponding maxima in ORD/CD-spectra for $\alpha(1 \rightarrow 4)$-glucans with dp < 40 (66,67). The (E_{640}/E_{525}) ratio also indicates branching characteristics of complexed glucans, glucan fractions, or glucan fragments as lcb/scb-glucan ratio.

© 2004 by Marcel Dekker, Inc.

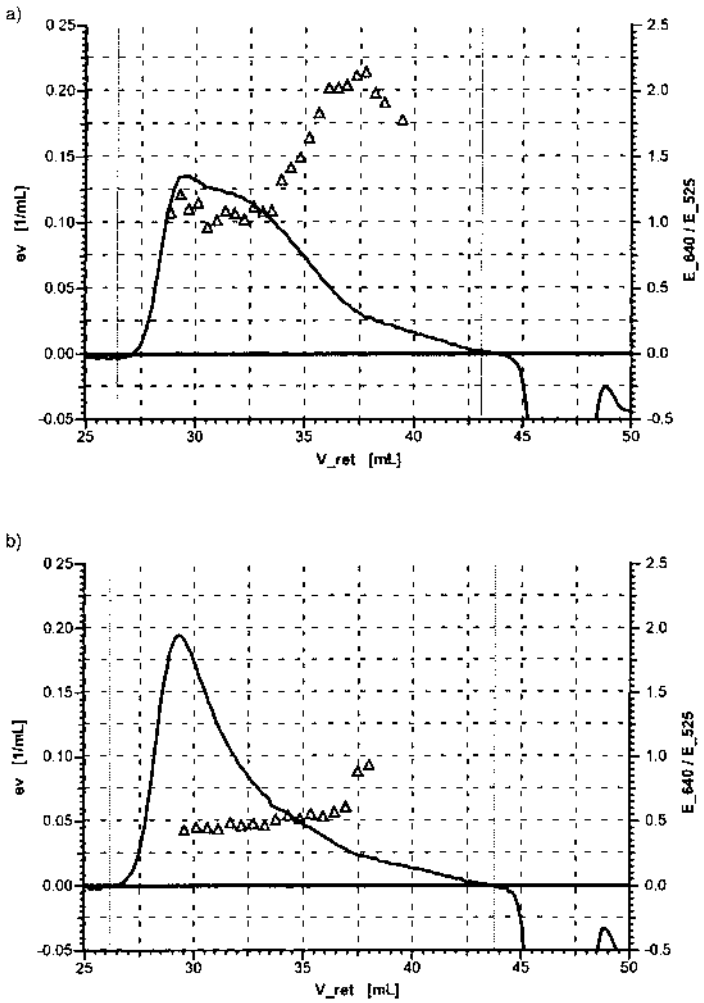

Figure 10 (a) SEC elution profile of wheat starch glucans with indicated lcb/scb ratio as indicator for kind and homogeneity of branching characteristics. SEC system: TosoHaas guard PWH + GMPWM + GMPW6000 + 5000 + 4000 + 3000 (150 × 7.5 mm); eluent, 0.005 M NaOH; sample volume, 0.4 mL (5 mg/mL); flow rate, 0.80 mL/min; E_{640}/E_{525}-values in the range 1–2 indicating a mix of lcb rather than scb glucans. (b) SEC elution profile of waxy maize starch glucans with indicated lcb/scb ratio as indicator for kind and homogeneity of branching characteristics. SEC system: TosoHaas guard PWH + GMPWM + GMPW6000 + 5000 + 4000 + 3000 (150 × 7.5 mm); eluent, 0.005 M NaOH; sample volume, 0.4 mL (5 mg/mL); flow rate, 0.80 mL/min; E_{640}/E_{525}-values dominantly in the range close to 0.5, indicating scb glucans with "lcb impurities."

© 2004 by Marcel Dekker, Inc.

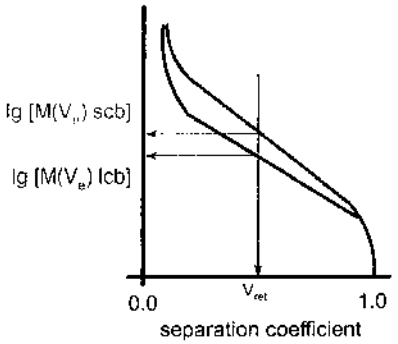

Figure 11 SEC separation of starch glucans with differences in branching pattern. At identical retention volume V_{ret} (identical excluded volume V_e) lcb-glucans typically contain less molar mass than scb-glucans.

In the analysis of the elution profile from SEC with respect to absolute molecular weight and excluded volume of individual glucan fractions, for identical characteristics of two glucans except differences in branching pattern different elution positions are expected: the more scb-characteristics, the later the position on the elution grid (the higher the V_{ret} value) (Fig. 11).

Although such an ideal constellation will never be found for native starch glucans, the principle however, might be useful for glucan fractions and/or glucan fragments.

5.3 Analytical SEC

5.3.1 Mass Detection and Calibrated Molecular Weight Distribution

Elution profile of mass fractions for DMSO-dissolved starch glucans from analytical SEC is obtained by in-line (differential) refractive index detection. However, total molecular dissolution of starch glucans in the concentration range around 5 mg/mL can hardly be achieved, neither in aqueous media nor in DMSO. Nevertheless, the percentage of truly dissolved glucans can be increased by a continuous dissolution process in DMSO at elevated temperature (80–90°C), reflux-cooling, and permanent stirring. Monitoring of reductive potential, an indicator for the number of molecules, proved that only a negligible degradation occurs at such conditions.

From the elution profile area of an interferometric refractometer (area_DRI) the actual glucan concentration within a selective separation range may be obtained according to Eq. (4) with known applied sample volume (loop_vol), selected DRI sensitivity factor (DRI_sens), previously determined DRI calibration

© 2004 by Marcel Dekker, Inc.

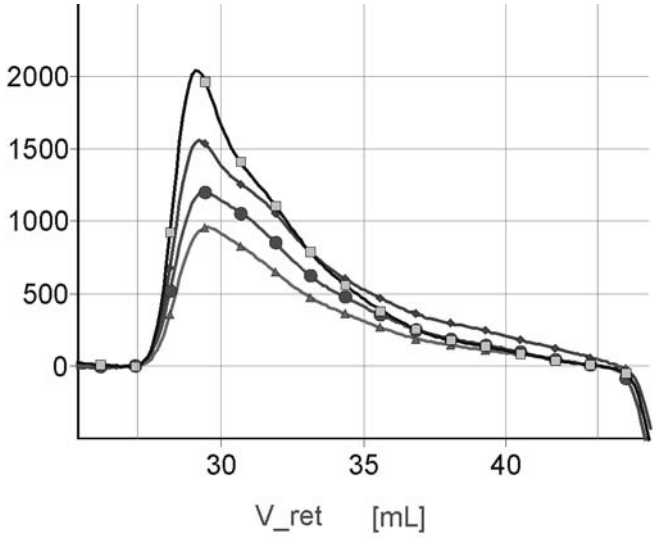

Period of dissolution process (h)	4	48	96	170
Mass within selective separation range (%)	30	38	50	52
Symbol	—▲—	—●—	—◆—	—□—

Figure 12 Wheat glucans: DRI elution profiles → raw_mass; Wyatt Optilab R 903: interferometric refractometer at $\lambda = 630$ nm. SEC system: TosoHaas guard PWH + GMPWM + GMPW6000 + 5000 + 4000 + 3000 (150 × 7.5 mm); eluent, 0.1 M NaCl(aq) + 0.005 M Na_2CO_3(aq) + NaN_3; flow rate, 0.80 mL/min.

constant (DRI_cal_const) and specific refractive index increment [$(\text{srii})_\lambda$ or $(dn/dc)_\lambda$].

$$\text{conc} = \text{DRI_cal_const} \cdot \text{DRI_sens} \cdot \frac{\text{area_DRI}}{(dn/dc)_\lambda \cdot \text{loop_vol}} \tag{4}$$

where conc = glucan sample concentration → [mg/mL], dn/dc = specific refractive index increment → [mL/g], loop_vol = applied volume of glucan solution → [μL], DRI_cal_const = slope of "conc vs. detector signal" → [nL/area], DRI_sens = attenuation/amplification factor, and area_DRI = integral of DRI chromatogram within selective separation range.

As illustrated in Fig. 12 for wheat starch glucans, the percentage of molecular dissolved glucans increases, but, typically remains far away from total recovery. The missing percentage of 40–70%, however, remains not fixed to the matrix but forms supermolecular aggregates that elute below the DRI detection limit superimposed to the molecular dissolved glucans in the selective SEC separation range and continue to elute for several void volumes. An indication of

© 2004 by Marcel Dekker, Inc.

this fact is provided by the elution profiles of low-angle scattering (Fig. 18), which do not approach baseline for several void volumes.

For aqueous dissolved glucans $(dn/dc)_{630}$ is in the range 0.150 ± 0.03 mL/g and no major error is introduced working with this value for starch glucans. Any possible small error is partially compensated by computation of absolute molecular weights from mass and laser light-scattering experiments if concentration (DRI-profile) and optical constant (LS-profile) are also processed with this value.

If sample concentration (conc) is known and recovery from the SEC system can be assumed to be 100%, specific refractive index increment may be determined from area of the SEC elution profiles according to Eq. (5):

$$\left(\frac{dn}{dc}\right)_{\lambda} = \text{DRI_cal_const} \cdot \text{DRI_sens} \cdot \frac{\text{area_DRI}}{\text{conc} \cdot \text{loop_vol}} \tag{5}$$

For DMSO-dissolved native starch glucans a typical recovery of 30–60% will be obtained with aqueous SEC eluents. Recovery increases with increasing dissolution process; however, no preferential dissolution of individual glucans is observed: normalized DRI-eluograms (mass_ev), which are computed from raw data DRI elution profiles (raw_mass) according to Eqs (6) and (7) for several dissolution periods for more than 7 days match within experimental error (Fig. 13).

$$\text{mass_ev} = \frac{\text{raw_mass}}{\int_{\text{int_start}}^{\text{int_stop}} \text{raw_mass}} \tag{6}$$

$$\int_{\text{int_start}}^{\text{int_stop}} \text{mass_ev} = 1.0 \tag{7}$$

where mass_ev = normalized elution profile of mass fractions, raw_mass = elution profile of mass fractions (raw data), and int_start, int_stop = integration range = limits of selective separation range.

Molecular weights for starch glucans may be obtained from SEC separation combined with mass detection by means of molecular weight calibration obtained either from peak position calibration or broad standard calibration, for instance with dextrans (Fig. 14). Results, however, are relative results in terms of calibration material (e.g., dextran) equivalent molecular weights. Typically, molecular weight distributions are visualized as normalized (area = 1.0) differential distribution of mass fractions (m_MWD_d) according to Eq. (8) and molar (number) fractions (n_MWD_d) according Eq. (9) (Fig. 15).

$$m(M)_i = \frac{dm(M)}{dM} \quad \text{with} \quad \int_0^{\infty} m(M)\,dM = \text{m_MWD_d} = 1.0 \tag{8}$$

$$n(M)_i = \frac{m(M)_i/M}{\int_0^{\infty} [m(M)_i/M]\,dM} \quad \text{with} \quad \int_0^{\infty} n(M)\,dM = \text{n_MWD_d} = 1.0 \tag{9}$$

© 2004 by Marcel Dekker, Inc.

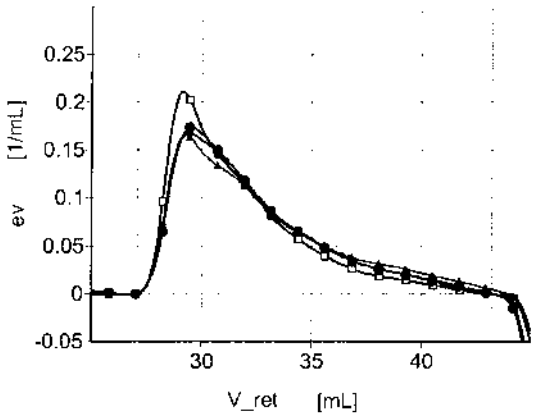

Figure 13 Wheat glucans. Normalized DRI elution profiles from DRI mass-detection of Fig. 12, raw_mass → mass_ev [Eqs (6) and (7)]. SEC system: TosoHaas guard PWH + GMPWM + GMPW6000 + 5000 + 4000 + 3000 (150 × 7.5 mm); eluent, 0.1 M NaCl(aq) + 0.005 M Na_2CO_3(aq) + NaN_3; flow rate, 0.80 mL/min.

where MWD = molecular weight distribution, $i = i$th fraction, m_ = mass fractions, n_ = molar (number) fraction, and _d = differential fraction.

Construction of universal SEC calibration (Fig. 16) with dextran calibration and Staudinger–Mark–Houwink constants K and a from $[\eta] = KM^a$ enables computation of molecule dimensions in terms of excluded volume for individual

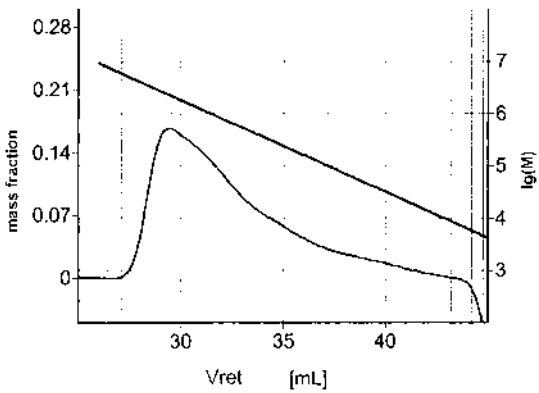

Figure 14 Wheat glucan. Molecular weight calibration with standard glucans (dextran). Normalized DRI elution profiles → mass_ev [Eqs (6) and (7)]. Molecular weight calibration → fit_MWV established by standard glucans (dextrans): either peak position calibration or broad standard calibration.

© 2004 by Marcel Dekker, Inc.

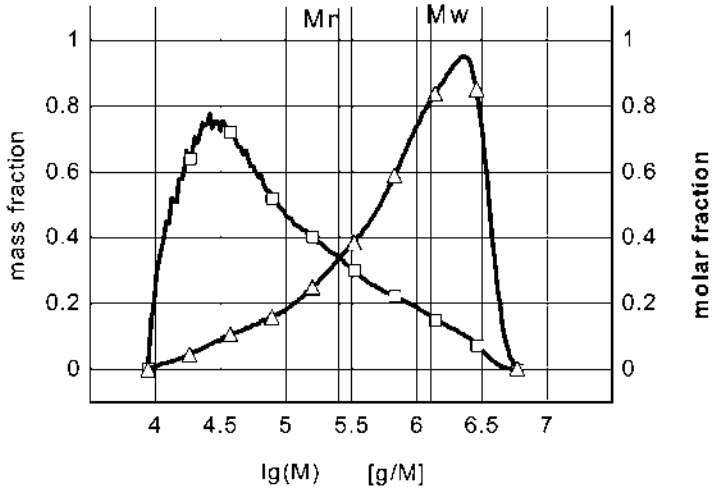

Figure 15 Wheat glucan. Dextran equivalent normalized molecular weight distribution. Differential mass fractions: m_MWD_d (—△—) [Eq. (8)], differential molar fractions: n_MWD_d (—□—) [Eq. (9)]. Dextran equivalent molecular weight averages: M_n: number average, 256,600 g/M; M_w: weight-average, 1,295,000 g/M polydispersity: M_w/M_n: 5.06.

SEC separated fractions $V_{e,i}$ and distribution either as distribution of mass fractions (m_$V_e D$_d) or molar fractions (n_$V_e D$_d) according Eq. (10).

$$V_{e,i} = \frac{KM_i^{a+1}}{2.5N_A} \rightarrow \text{m_}V_eD\text{_d} \wedge \text{n_}V_eD\text{_d} \tag{10}$$

Sphere equivalent radii of excluded volume and correlated mass and molar distributions of molecule radii are computed according Eq. (11) (Fig. 17).

$$R_{e,i} = \left[\frac{3V_{e,i}}{4\pi}\right]^{1/3} \rightarrow \text{m_}R_eD\text{_d} \wedge \text{n_}R_eD\text{_d} \tag{11}$$

5.3.2 Mass/LS: Absolute Molecular Weight

Absolute weight-average of molecular weight (M_w) of polymers can be obtained from static light-scattering experiments if sample concentration (c), specific refractive index increment $(dn/dc)_\lambda$, wavelength of laser light (λ), experimental scattering angle (θ), and ratio of intensities of applied and scattered intensity of laser light (Rayleigh-factor R_θ) at scattering-angle θ are known. Starting from a triplet elution profile (mass → raw_mass, applied laser intensity → raw_LS_0, scattered laser intensity → raw_LS_θ) via several intermediates [Eqs (12)–(14)]

© 2004 by Marcel Dekker, Inc.

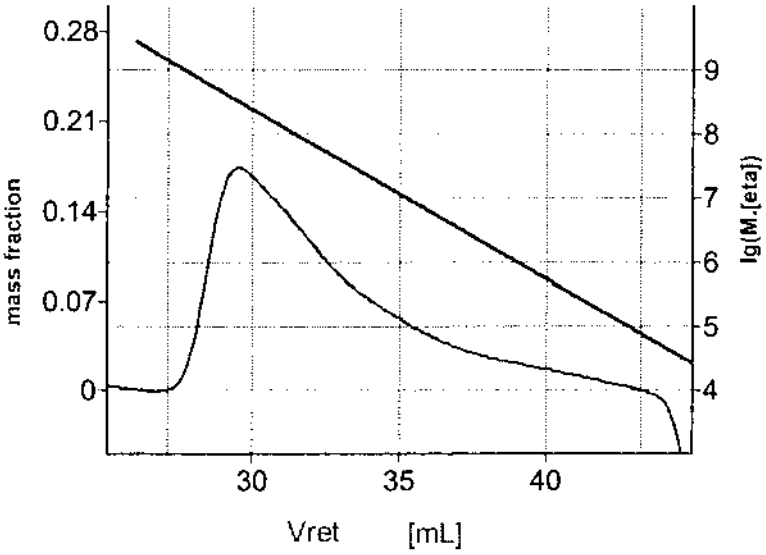

Figure 16 Wheat glucan. Normalized DRI elution profiles → mass_ev [Eqs. (6) and (7)]. Universal SEC calibration constructed from: dextran SEC calibration + SMH_K = 0.0978 mL/g, SMH_a = 0.500.

absolute molecular weight distribution (m_MWD_d, n_MWD_d) and degree of polymerization distribution (m_dpD_d, n_dpD_d) may be computed.

Although such molecular weights are assigned as absolute, due to superimposed glucan aggregates that dominate the scattering signal, these molecular weights for starch glucans are apparent absolute molecular weights.

With the elution profile of Excess–Rayleigh factors [Eq. (12)] and information about glucan concentration for each SEC separated fraction, a normalized scattering profile for scattering angle θ (e.g., $\theta = 5^\circ \rightarrow$ LS_5_EV) may be established [Eq. (13)] with area equivalent to weight-average molecular weight (M_w) according to Eq. (14) (Fig. 19a).

$$R_\theta = \frac{P_\theta}{P_{(0)}} \text{ att const} \rightarrow \text{R_5} = \frac{\text{raw_LS_5}}{\text{raw_LS_0}} \tag{12}$$

$$\text{LS_5_EV} = \frac{\text{R_5 mass_ev}}{k_{\text{opt}}\,\text{conc}} \tag{13}$$

$$M_w\text{_raw} = \int_{\text{int_start}}^{\text{int_stop}} \text{LS_5_EV} \tag{14}$$

The raw data scattering profile (Fig. 18) as well as the normalized scattering profile (Fig. 19a) illustrate the presence of aggregates below the detection limit

© 2004 by Marcel Dekker, Inc.

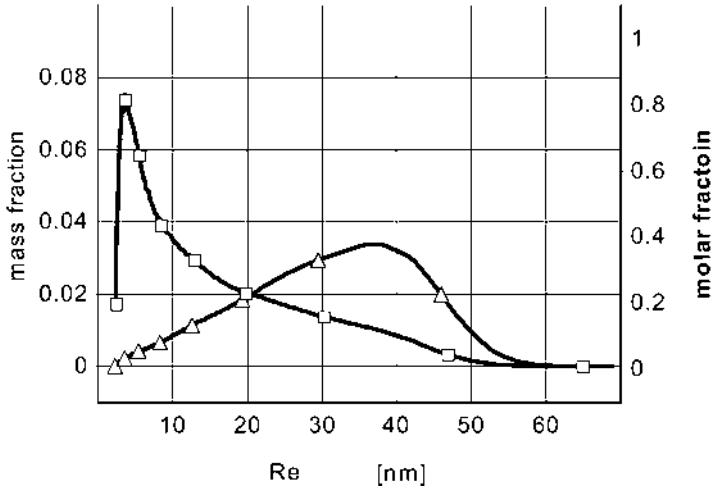

Figure 17 Wheat glucan. Sphere equivalent radii distribution (R_eD) of SEC-separated wheat glucans. Differential mass fractions: m_R_eD_d (—△—) [Eq. (11)]. Differential molar fractions: n_R_eD_d (—□—) [Eq. (11)].

of the mass detector but with huge molar masses. Scattering in general, and low-angle scattering in particular, is enormously sensitive to aggregates (the signal is proportional to the coherent segment length with the power of 6) and thus LS-signals are dominated by minimum amounts of huge molecules or aggregates. However, absolute molecular weight calibration (raw_MWV) for the mass and scattering profiles is obtained using Eqs (15) and (16), and if applied to each fraction, absolute molecular weight calibration is achieved.

$$\left(\frac{K\,c}{R_\Theta}\right)_{\substack{c\to 0\\ \Theta\to 0}} = \frac{1}{M_w} + 2A_2c \tag{15}$$

$$M_w = \left[\left(\frac{K\,c}{R_\Theta}\right)_{\substack{c\to 0\\ \Theta\to 0}} - 2A_2c\right]^{-1} \rightarrow \log(M) \text{ vs. } V_{ret} \tag{16}$$

which can be done by simply computing the ratio of normalized scattering and mass profiles and taking the logarithm of the result [Eq. (17)].

$$\text{raw_MWV} = \log\left(\frac{\text{LS_5_EV}}{\text{mass_ev}}\right) \tag{17}$$

© 2004 by Marcel Dekker, Inc.

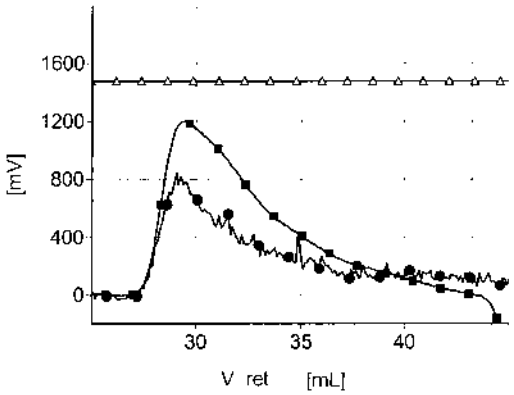

Figure 18 Wheat glucan. Elution profile triplet: mass by DRI → raw_mass_ev; (—■—) [Eqs (6) and (7)]. Applied laser intensity → raw_LS_0; (—△—). Scattered laser intensity → raw_LS_5 (—•—) SEC system: TosoHaas guard PWH + GMPWM + GMPW6000 + 5000 + 4000 + 3000 (150 × 7.5 mm); eluent, 0.1 M NaCl(aq) + 0.005 M Na_2CO_3(aq) + NaN_3; flow rate, 0.80 mL/min; sample (inject) volume, 0.4 mL (5 mg/mL).

Depending on the applied dissolution process and the characteristics of superimposed glucan aggregates, molecular weights in the range of several 10^7 g/mol will typically be achieved from light-scattering data (Figs 19c and 20). Even for extremely long periods of dissolution only minor changes in molecular weight will be observed; supermolecular structures are still present and dominate the light-scattering signal. Thus, although absolute, light scattering primarily provides information about molecular weight of glucan aggregates and not of constituting glucan molecules.

5.3.3 Mass/Viscosity: Excluded Volume Profile

If SEC separation of starch glucans is connected with mass and viscosity detection, excluded volume profile and overlapping concentration profile may be obtained (Fig. 21).

The specific viscosity profile (eta_spec) is computed according to Eq. (18) from monitored typically constant inlet pressure profile (raw_ip) and differential pressure profile (raw_dp).

$$\text{eta_spec} = \frac{4\ \text{raw_dp}}{\text{raw_ip} - 2\ \text{raw_dp}} \tag{18}$$

Combining specific viscosity profile of starch glucans with mass information (mass_ev, actual fraction mass: inj_mass) for each SEC separated

© 2004 by Marcel Dekker, Inc.

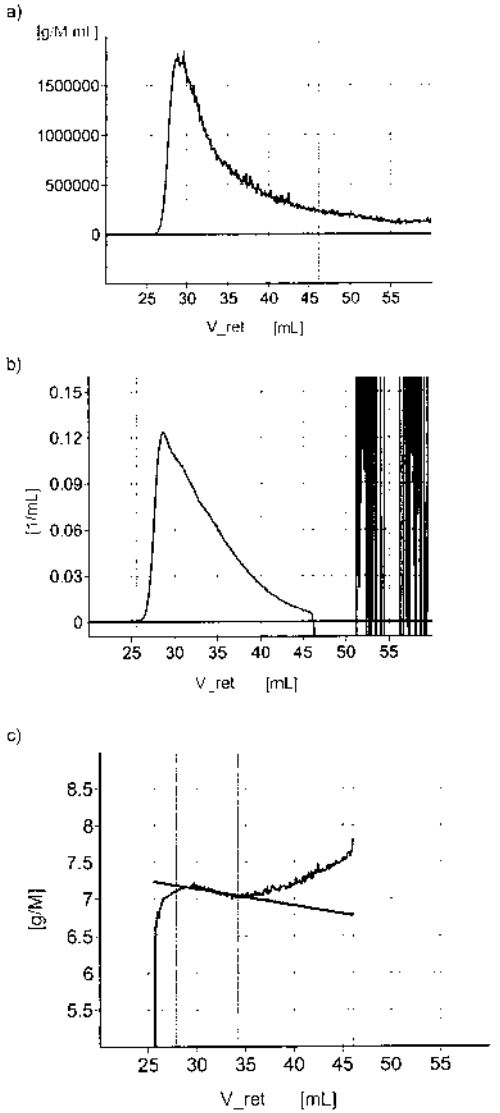

Figure 19 Wheat glucan. (a) Normalized elution profile of scattering intensity at scattering angle $\theta = 5^{\circ}$. raw_LS_5, raw_LS_0 → R_5 [Eq. (11)] → LS_5_EV [Eq. (13)] Normalization: area within selective separation range (int_start–int_stop) equivalent to weight-average molecular weight: Mw_raw = 27,100,000 g/M [Eq. (14)]. (b) Normalized elution profile of mass detection. raw_mass → mass_ev [Eqs (6) and (7)]. (c) Absolute SEC-calibration function; established from → mass_ev [Eqs (6) and (7)] → LS_5_EV [Eq. (13)] → raw_MWV/fit_MWV [Eq. (17)].

© 2004 by Marcel Dekker, Inc.

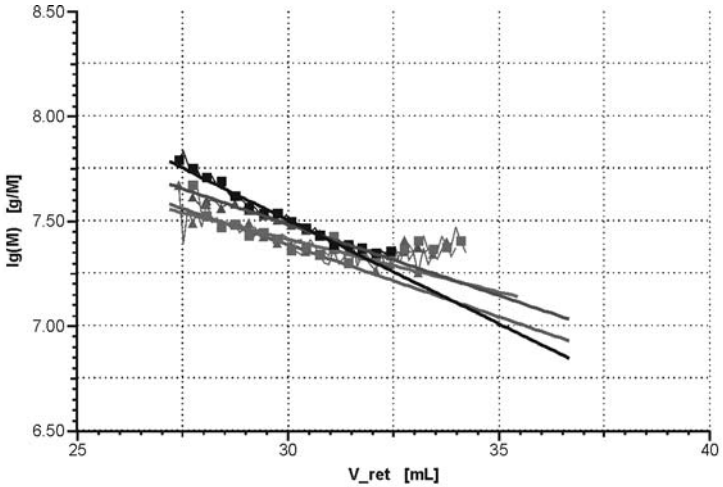

Period of dissolution process (h)	4	48	96	170
Weight average molecular weight M_w (g/M)	$21 \cdot 10^6$	$19 \cdot 10^6$	$23 \cdot 10^6$	$26 \cdot 10^6$
Symbol	—■—	—▲—	—▲—	—■—

Figure 20 Wheat glucans. Absolute molecular weight calibration achieved from scattering and mass detection at increasing periods of dissolution process; → raw_MWV [Eq. (17)].

fraction, intrinsic viscosity profile (eta_int) may be obtained according to Eq. (19):

$$\text{eta_int} = \frac{\text{eta_spec}}{\text{mass_ev} \cdot \text{inj_mass}} \tag{19}$$

Mean intrinsic víscosity (68) may be obtained according to Eq. (20):

$$[\eta]_{\text{av}} = \int_{\text{int_start}}^{\text{int_stop}} \text{eta_int}\, dV_{\text{ret}} \tag{20}$$

Similar to light scattering, even viscosity preferentially senses high molecular and supermolecular components. However, if these components are present in below ppm-amounts—as is the case for starch glucan aggregates—their contribution to overall viscosity is negligible. Thus, viscosity detection of SEC separated starch glucans dominantly is structural viscosity of molecular dissolved glucans. The reciprocal of intrinsic viscosity is a crude measure of overlapping concentration for these glucan molecules (Fig. 22).

© 2004 by Marcel Dekker, Inc.

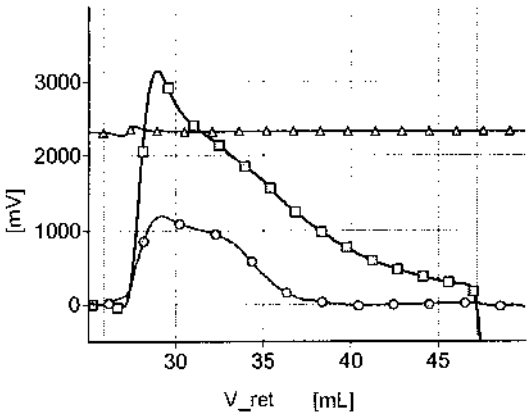

Figure 21 Wheat glucan. Elution profile triplet: mass by DRI → raw_mass_ev (—□—) [Eqs (6) and (7)]. Viscosity: inlet pressure → raw_ip (—△—). Viscosity: differential pressure → raw_dp (—○—). SEC system: TosoHaas guard PWH + GMPWM + GMPW6000 + 5000 + 4000 + 3000 (150 × 7.5 mm); eluent, 0.1 M NaCl(aq) + 0.005 M Na_2CO_3(aq) + NaN_3; flow rate, 0.80 mL/min, sample (injected) volume, 0.4 mL (5 mg/mL).

5.3.4 Mass/Molar: Absolute Molecular Weight Distribution

To obtain the true molecular weight of constituting glucans for a starch sample without perturbing influences of aggregates, the number of molecules, as well as their mass, is required. Molar concentration (number of molecules) for starch glucans may be achieved by quantitative pyridylamination (PA) of the terminal reducing OH-group and vis-spectroscopy of formed PA-glucans (69–71) (Fig. 23).

SEC combined with universal mass detection by an interferometric DRI detector (DRI → mass_ev) and detection of the chromophor with a fluorescence detector ($\lambda_{ex} = 315$ nm; $\lambda_{em} = 400$ nm) (fluorescence → mol_ev) (Fig. 24) enables computation of absolute molecular weights [Eqs (21) and (22)] without the influence of aggregates as there is good basis for the assumption that individual as well as associated glucans are derivatized.

$$M_i = \frac{c_i[g/L]}{n_i[mol/L]} = \left(\frac{g}{mol}\right)_i \tag{21}$$

$$\text{raw_MWV} = \lg\left(\frac{\text{mass_ev}}{\text{mol_ev}}\right) \tag{22}$$

Figure 25a illustrates the results indicating that molecular weight of constituting wheat starch glucans is in the range of several 10^5 g/mol (Figs 25b, c), which is at

© 2004 by Marcel Dekker, Inc.

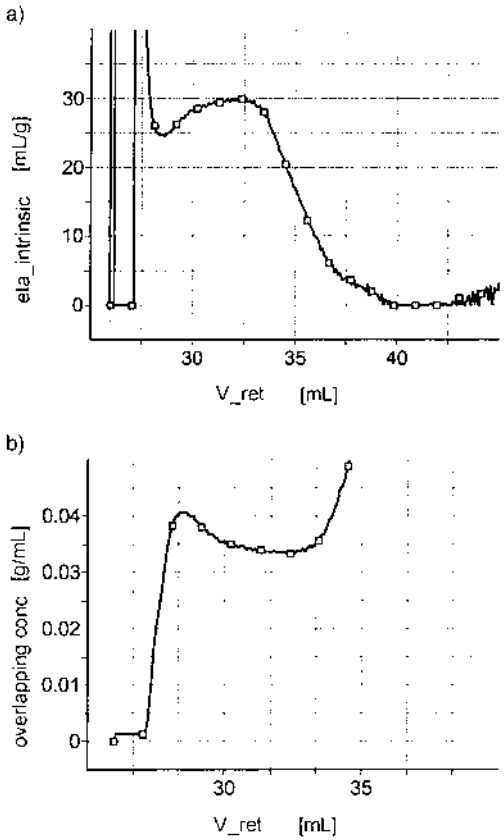

Figure 22 Wheat glucan. (a) Intrinsic viscosity profile obtained from mass detection: raw_mass → mass_ev [Eqs (6) and (7)]. Viscosity detection: raw_ip/raw_dp → eta_spec [Eq. (18)] → eta_int [Eq. (19)]. $[\eta]_{av}|V_{ret}27-37$ mL| = 26 mL/g [Eq. (20)]. (b) Overlapping concentration profile: → $c^* = 1/\text{eta_int}$ vs. V_{ret}; $c^*_{av}=1/[\eta]_{av} = 38$ mg/mL.

least some two magnitudes less than that proposed by data from light scattering. Data from viscosity detection, on the other hand, match quite well with results from molar and mass detection.

For verification of the presence of glucan aggregates, and for evidence for actual glucan molecular weights (10^7 g/mol from mass and light scattering or 10^5 g/mol from mass and molar detection) bulk solutions of starch glucans were investigated, in particular:

- Rheology below overlapping concentration to investigate development of excluded volume for the starch glucan/glucan aggregate systems;

© 2004 by Marcel Dekker, Inc.

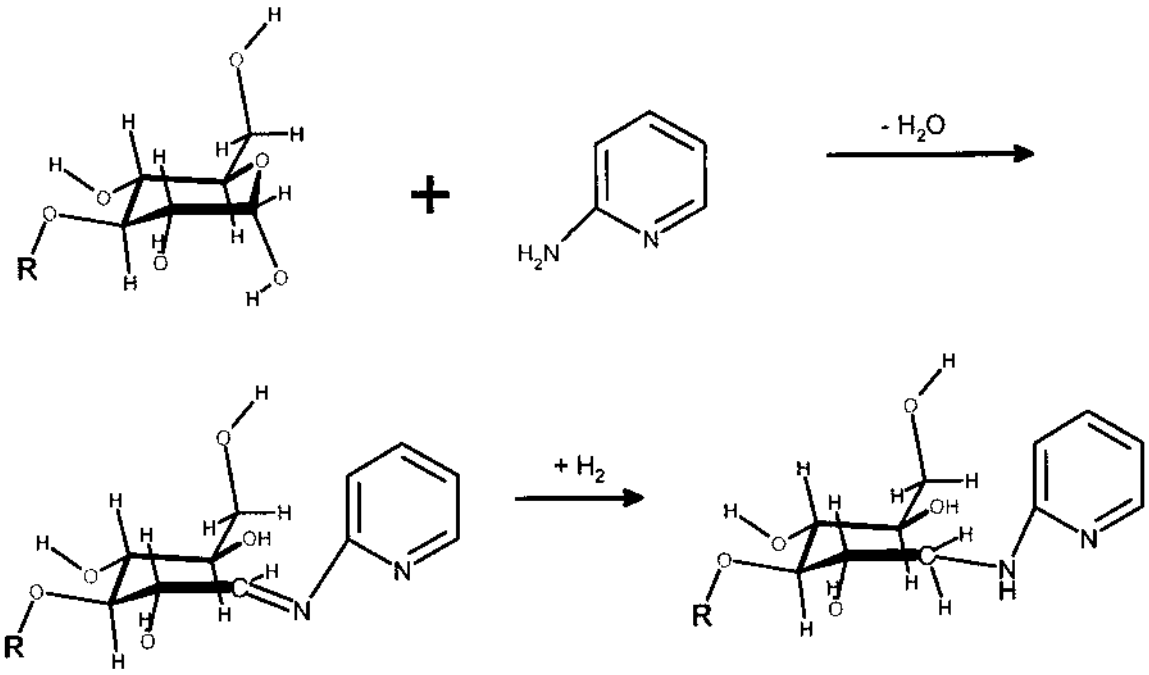

Figure 23 Reductive pyridylamination of glucans at the terminal reducing OH group: glucose (R = H)/glucan (R = Glc_n), and 2-aminopyridin form an intermediate Schiff base by opening the hexose ring; reduction yields the secondary pyridylamino glucose (R = H)/glucan (R = Glc_n).

© 2004 by Marcel Dekker, Inc.

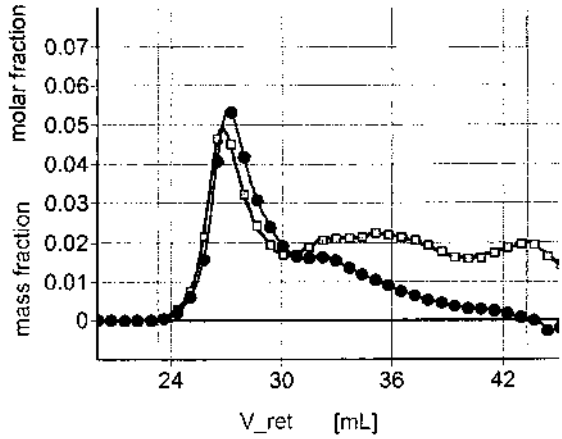

Figure 24 Wheat PA-glucan. Elution profiles: mass by DRI → mass_ev (—●—) molar PA-glucan fractions → mol_ev (—□—). SEC system: TosoHaas guard PWH + GMPWM + GMPW6000 + 5000 + 4000 + 3000 (150 × 7.5 mm); eluent, 0.1 M NaCl(aq) + 0.005 M Na_2CO_3(aq) + NaN_3; flow rate, 0.80 mL/min; sample (injected) volume, 0.4 mL (5 mg/mL).

- Rheology at increasing shear rates to determine stability of glucan/glucan aggregate systems under applied mechanical stress;
- Rheology at increasing temperature to determine stability of glucan/glucan aggregate systems under applied thermal stress;
- Rheology at constant shear rate and temperature program to determine disintegration behavior and reorganization capability of glucan/glucan aggregate systems; and
- Photon correlation spectroscopy to obtain diffusion mobilities of glucan and glucan aggregates, that is, of coherent glucan segments, without significant destructive energy input.

5.4 Bulk Properties of Starch Glucans: Rheology

For investigations with respect to presence and influence of glucan aggregates, wheat starch glucans were dissolved in DMSO by stirring at elevated temperature (90°C) and reflux cooling for more than 200 hours. At increasing times of this dissolution process, aliquots were taken and investigated with respect to component characteristics by means of SEC (Fig. 12) as well as with respect to bulk characteristics, primarily by rheology. First experiments were performed with

© 2004 by Marcel Dekker, Inc.

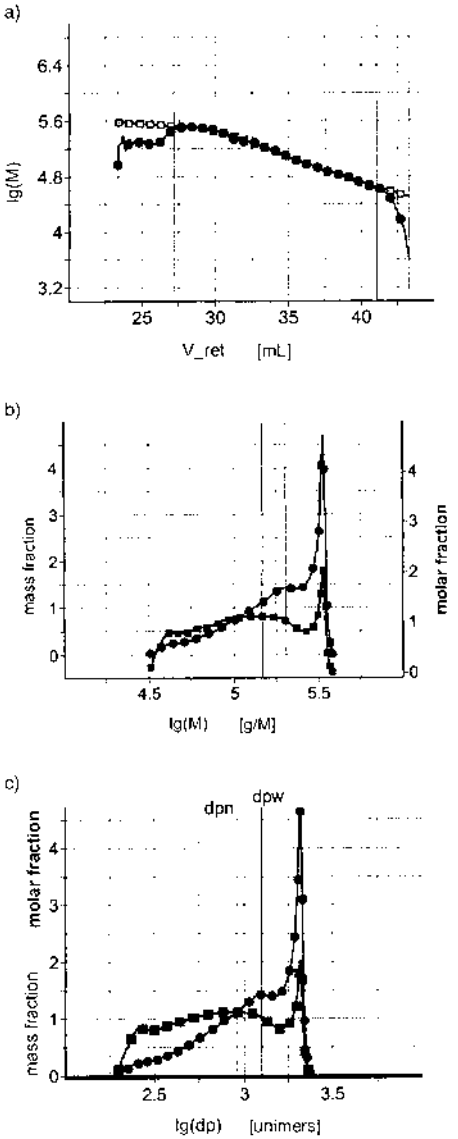

Figure 25 Wheat PA glucan. (a) Absolute molecular weight calibration without influence of aggregates: → mass_ev (DRI) [Eqs (6) and (7)] → mol_ev (fluorescence) → raw_MWV [Eq. (22)] → fit_MWV (fit to [Eq. (22)]). (b) Differential mass fractions: m_MWD_d [Eq. (8)]; differential molar fractions, n_MWD_d [Eq. (9)]. Molecular weight averages: M_n, number-average, 147,000 g/M; M_w, weight-average, 204,000 g/M polydispersity; M_w/M_n, 1.39. (c) Differential mass fractions, m_dpD_d; differential molar fractions, n_dpD_d. Degree of polymerization averages: dpn, number-average: 907 Glc; dpw, weight-average: 1260 Glc; polydispersity, dpw/dpn, 1.39.

© 2004 by Marcel Dekker, Inc.

an Ubbelohde-viscometer for concentration series at increasing times of the dissolution process. Extrapolation of reduced viscosity values for each concentration series [Eq. (23)] to $c \rightarrow 0$ yields intrinsic viscosity [Eq. (24)] for investigated states of dissolution (Fig. 26).

$$\eta_{\text{red}} = \frac{t_{\text{solution}} - t_{\text{solvent}}}{t_{\text{solvent}}\, c} \tag{23}$$

$$[\eta] = \eta_{\text{red}}(c \rightarrow 0) \tag{24}$$

Obviously, intrinsic viscosity ($[\eta]$) and, thus, excluded volume (V_e), decreases and overlapping concentration (c^*) increases with increasing time: an indication that matches with degradation of huge glucan molecules as well as with the presence of supermolecular glucan aggregates that disintegrate by the continuous dissolution process. However, a significant difference between data from bulk investigations (Fig. 26) and data from component analysis (Fig. 22a) is observed from the initial state: in bulk solutions supermolecular glucan aggregates shift results for intrinsic viscosity and overlapping conentration more than sixfold (approx.).

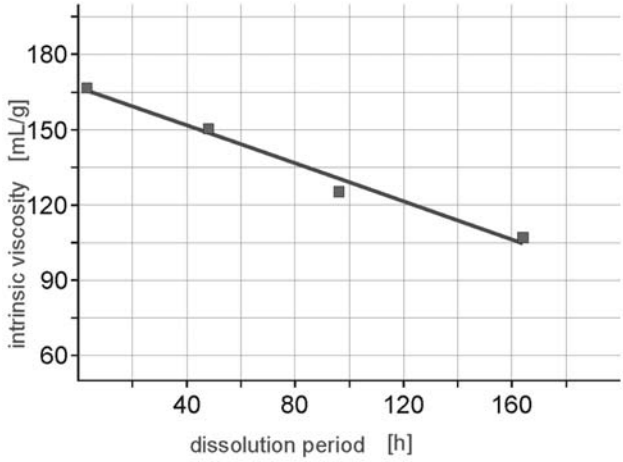

Period of dissolution process (h)	4	48	96	170
Excluded volume $[\eta] \rightarrow V_e$ (mL/g)	167	150	125	**107**
Overlapping concentration $1/[\eta] \rightarrow c^*$ (mg/mL)	6.0	6.7	8.0	**9.3**

Figure 26 Wheat glucans. Intrinsic viscosity $[\eta]$ of the bulk solution for increasing periods of dissolution process.

© 2004 by Marcel Dekker, Inc.

Stability of wheat starch glucan/DMSO solutions against mechanical stress for increasing times of dissolution process was investigated by means of a dynamic capillary viscosimeter by varying shear deformation (D). From these experiments complex viscosity (η^*) results as a contribution of viscous (η': in-phase) and elastic (η'': out-of-phase) contributions [Eq. (25)].

$$\eta^* = \eta' + i\eta'' \tag{25}$$

For the investigated wheat starch glucan non-negligible elastic contributions were observed, at least in the initial states of dissolution. In general, according to Ubbelohde viscosimeter investigations, viscosity decreases with increasing periods of dissolution; additionally, elastic contributions, showing up as *D*-dependence of complex viscosity, vanish for longer periods of dissolution (Fig. 27). Typically, such types of *D*-dependence of viscosity will be found for dynamically stabilized "soft gels," a finding that perfectly matches the situation of molecular dissolved glucans in the presence of minor amounts of supermolecular glucan aggregates.

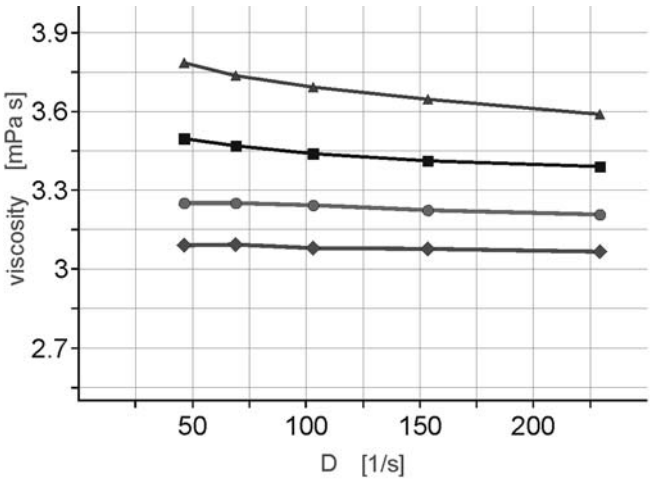

Period of dissolution process (h)	4	48	96	170
Complex viscosity η^* (mPa s)	3.2	3.45	3.27	3.08
Elastic (η') contribution	++	+	–	–

Figure 27 Wheat glucans. Visco-elastic properties of bulk solution for increasing periods of dissolution process.

© 2004 by Marcel Dekker, Inc.

Rheological investigations of stability of starch glucans against applied thermal stress yields information in terms of so-called gelatinization temperature: a critical temperature where disintegration of supermolecular glucan structures starts and a significant temperature range for the disintegration process. Obviously the critical temperature and disintegration temperature range strongly depend on branching pattern characteristics: scb-type starch glucans such as waxy maize are typically better stabilized and thus stand applied thermal stress better than starch glucans with dominant lcb-contributions such as wheat (Fig. 28). Increasing thermal energy disintegrates wheat starch glucans at significantly lower temperatures and over a smaller temperature range (56–62°C; $T_{max} = 58°C$) than waxy maize glucans (65–85°C; $T_{max} = 78°C$). A much more pronounced increase in viscosity upon disintegration of scb-type waxy maize starch glucans compared to lcb-type wheat starch indicates a comparably pronounced glucan/glucan stabilization of scb-type starches compared to lcb-type glucans, which need much more energy for destruction.

For simultaneously applied thermal and mechanical stress [Brabender viscosity for an applied temperature program with three states (heating, holding, cooling) and constant shear deformation] another significant difference between scb- and lcb-type starch glucans becomes apparent (Fig. 29). Although much more energy is required comparably to disintegrate scb-glucans in the heating period (20–40 min), once liberated from supermolecular formations, scb-glucans do not

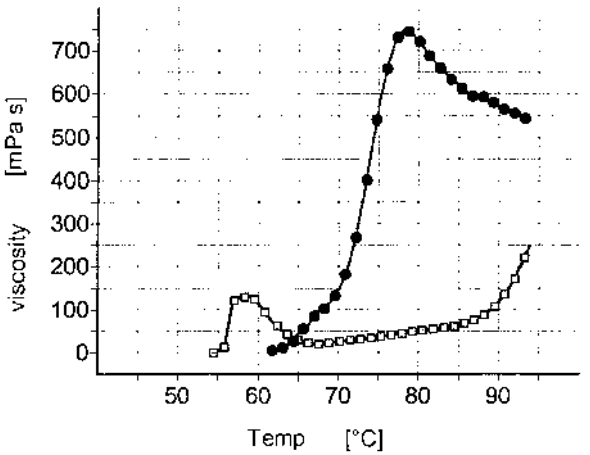

Figure 28 Stability of starch glucans on applied thermal stress. Viscosity at increasing temperature: Wheat (—□—): minor initial stability; disintegration peak, 56–62°C. Waxy maize (—○—): high initial stability; disintegration peak, starting at 65°C.

© 2004 by Marcel Dekker, Inc.

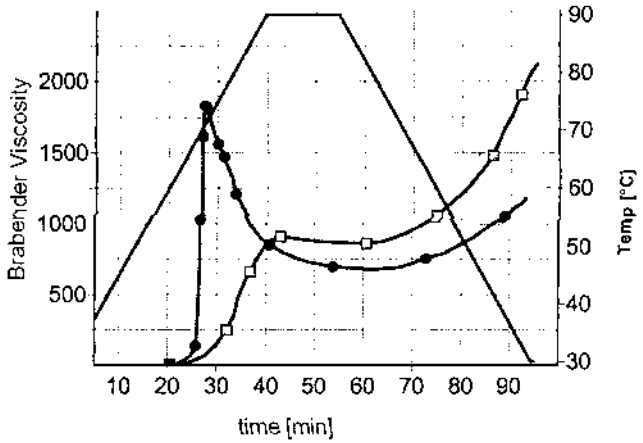

Figure 29 Brabender viscosity for (a) wheat glucans (—□—): Broad disintegration → parallel reorganization of supermolecular structures; pronounced reorganization on cooling; (b) waxy maize glucans (—•—): more sharp disintegration → minor reorganization of supermolecular structures; constant shear deformation; applied temperature program: heating, 30 → 90°C within 40 min; holding, 90° for 15 min; cooling, 90 → 30°C within 40 min.

tend to re-establish supermolecular structures, neither in the high temperature holding nor in the subsequent cooling period. Quite different behavior is observed for lcb-dominated starch glucans: their disintegration is achieved much more easily than that for scb-glucans; however, the tendency of liberated lcb-glucans to re-establish supermolecular structures is much more pronounced. The level of glucan/glucan interaction after disintegration remains constant at the initially elevated level as long thermal stress is kept constant (holding period) and even increases in the cooling period, significantly exceeding the level of initial disintegration status. Thus, however less perfectly stabilized compared to scb-glucans, lcb-glucans tend to form new supermolecular structures and show a significant re-organization capability.

5.5 Supermolecular Structures of Starch Glucans: Dynamic Light Scattering

Dynamic light scattering (DLS)/photon correlation spectroscopy (PCS) experiments for starch glucan solutions provide data about diffusive mobility of glucan molecules and supermolecular structures formed by glucan molecules. In particular, translational diffusion of glucans and glucan aggregates causes Doppler

© 2004 by Marcel Dekker, Inc.

shifts to applied laser light, which may be monitored via the autocorrelation function $G_2(\tau)$ [Eq. (26)].

$$G_2(\tau) = \frac{1}{T}\int_0^{\tau} I(t)\, I(t+\tau)\, dt \tag{26}$$

where T = temperature [K], t = time, I = intensity of scattered laser light, and τ = correlation period.

Indirect Laplace transformation of $G_2(\tau)$ yields $G_2(t)$, which contains the translational diffusion coefficient (D_T) (72) [Eq. (27)].

$$G_2(t) = A\left[1 + C_i\left(\int_{\tau_{\min}}^{\tau_{\max}} \frac{D_T(\tau)}{\tau^2} e^{(-t/\tau)}\, d\tau\right)^2\right] \qquad \text{with} \qquad \tau = \frac{1}{D_T h^2} \tag{27}$$

where D_T = translational diffusion coefficient, h = scattering vector, and A, C = coefficients.

According to Stokes/Einstein [Eq. (28)] D_T of observed glucans and glucan aggregates may be correlated with radius R_H or diameter (d) of a moving equivalent sphere. In the case of glucan aggregates, diameter d rather is the length of coherent segments and, thus, d for glucans is used as coherence length l_{coh} of molecular and/or supermolecular glucan segments.

$$D_T = \frac{k_B T}{6\pi\eta R_H} \rightarrow l_{coh} \tag{28}$$

where k_B = Boltzman constant, T = temperature [K], and η = viscosity of solution.

Results from mobility investigations within glucan solutions by means of photon correlation spectroscopy reflect a situation having two main populations:

- A major mass fraction (Fig. 30a) with dimensions (l_{coh}) in the range 10–30 nm, which represents the molecular dissolved starch glucans;
- A minor, but not negligible, fraction (Fig. 30b) with dimensions (l_{coh}) in the range 100–800 nm representing glucan aggregates.

Additionally, translational diffusion coefficient analysis of starch glucan solutions shows the source of many problems in the analysis of these materials. Depending on the applied principle of observation, (mass-sensitive refractive index variations or volume-square of coherent objects by scattering intensities) either individual glucan molecules (Fig. 30a) or glucan aggregates (Fig. 30b) dominate the experimental data. If this fact is not considered, SEC-DRI/LS experiments of starch glucans in particular provide information about supermolecular aggregates and not about constituent glucan molecular weights.

© 2004 by Marcel Dekker, Inc.

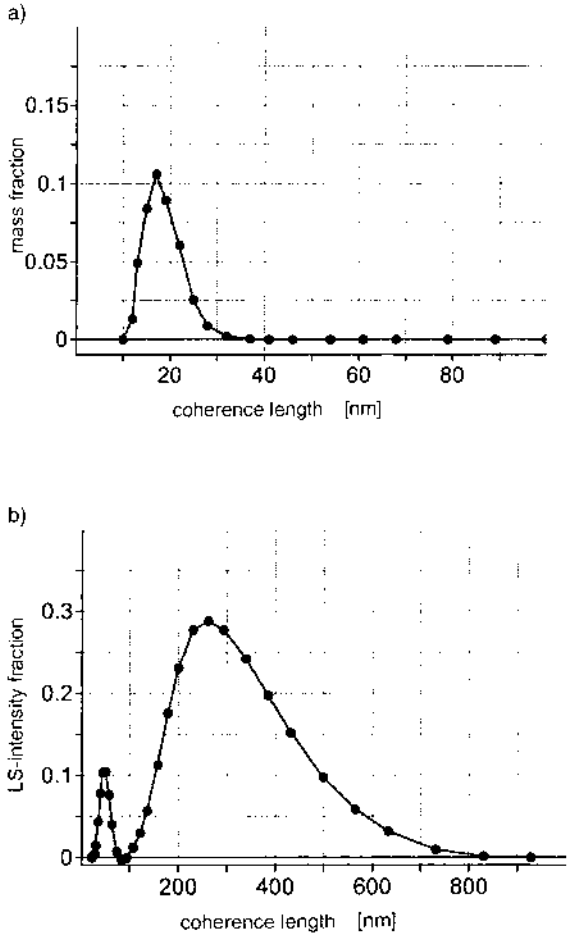

Figure 30 Wheat glucans. (a) Photon correlation spectroscopy analysis after 4 hours of dissolution process; mass fractions of observed sphere equivalent objects with radii (R_H); "seen" through the eyes of a DRI-detector. (b) Photon correlation spectroscopy analysis after 4 hours of dissolution process; intensity fractions of observed sphere equivalent objects with coherence lengths (l_{coh}); "seen" through the eyes of a light-scattering detector.

6 SUMMARY OF STARCH GLUCAN CHARACTERISTICS

From the point of view of system theory, starch glucans, just like many other polysaccharides, may be seen as transformed energy packages: electromagnetic radiation from sunlight captured in chemical linkages of basic compounds CO_2

© 2004 by Marcel Dekker, Inc.

Table 8 Characteristic Parameters for Starch Glucans

	Source/specification	
	Wheat glucans	Waxy maize glucans
	Chamtor/France; moisture: 9.8% 98.3% glucan content	Agrana/Austria; lot #2100740; moisture: 11.4% 97.4% glucan content
Applied modifications (gene technology/breeding)	No information	No information
Growth period/point of harvesting/ storage period	No information	No information
Granule size/conformation	No information	No information
Type of x-ray diffraction pattern	A	A
Branching characteristics: general classification	scb & lcb	scb
Branching characteristics: E_{640}/E_{525} high V_e-range	1.0–1.2	0.4–0.55
Branching characteristics: E_{640}/E_{525} small V_e-range	1.8–2.1	0.6–1.0
Branching characteristics: scb-fraction (mass %)	78	100
Branching characteristics: lcb-fraction (mass %)	22	—
lcb-fraction fragmentation analysis:		
Primary C-chains (dp/%)	112/46	—/—
Secondary B-chains (dp/%)	40/14	—/—
Terminal A-chains (dp/%)	13/40	—/—
scb-fraction fragmentation analysis:		
Primary C-chains (dp/%)	50/5	50/5
Secondary B-chains (dp/%)	40/25	50/23
Terminal A-chains (dp/%)	13/70	15/72
Molecular dissolved after 4 hours (mass %)	30	
Preferential dissolution of individual glucans	No	No
Excluded sphere equivalent radii $V_e \rightarrow R_e$ in SEC separation		
Range (nm)	2–55	2–55
Maximum of molar fractions distribution (nm)	5	5
Maximum of mass fractions distribution (nm)	38	38

© 2004 by Marcel Dekker, Inc.

Table 8 (*Continued*)

	Source/specification	
	Wheat glucans	Waxy maize glucans
	Chamtor/France; moisture: 9.8% 98.3% glucan content	Agrana/Austria; lot #2100740; moisture: 11.4% 97.4% glucan content
Excluded volume from component analysis: SEC-mass/viscosity		
Range: $[\eta]$ (mL/g)	10–30	
Mean value: $[\eta]_{av}$ (mL/g)	26	
Overlapping concentration from component analysis		
Range: c^* (mL/mg)	20–40	
Mean value: c^*_{av} (mL/mg)	38	
Excluded volume from bulk investigations (Ubbelohde)		
Intrinsic viscosity: $[\eta](4\text{ h}) \rightarrow [\eta]$ (mL/g)	167 → 107	
Overlapping concentration from bulk investigtions (Ubbelohde)		
c^*: $1/[\eta](4\text{ h}) \rightarrow 1/[\eta]$ (mg/mL)	5.9 → 9.3	
Molecular weight: SEC-mass + dextran calibration		
Range (g/mol)	10,000–6,000,000	10,000–8,500,000
Weight-average molecular weight, M_w (g/mol)	1,295,000	1,543,000
Number-average molecular weight, M_n (g/mol)	256,000	271,000
Molecular weight: apparent absolute from SEC-mass/LS		
Range (g/mol)	$10–120 \times 10^7$	$5–100 \times 10^7$
Molecular weight: absolute from derivatization + SEC-mass/molar		
Range (g/mol)	32,000–380,000	
Weight-average molecular weight, M_w (g/mol)	204,000	
Number-average molecular weight, M_n (g/mol)	147,000	
Visco-elasticity at increasing times of dissolution process		
After 4 h	Present	
After 48 h	Decreased	
After 100 h	Vanished	

© 2004 by Marcel Dekker, Inc.

Table 8 (*Continued*)

	Source/specification	
	Wheat glucans	Waxy maize glucans
	Chamtor/France; moisture: 9.8% 98.3% glucan content	Agrana/Austria; lot #2100740; moisture: 11.4% 97.4% glucan content
Disintegration upon thermal stress	56–62°C	65–80°C
Reorganization capacity after disintegration	+++	+
Populations in terms of coherent mobility		
Molecular dissolved glucans, l_{coh} (nm)	10–30/Max = 18	10–45/Max = 25
Glucan aggregates, l_{coh} (nm)	10–800/Max = 250	10–800/Max = 370
Disintegration of 5% paste at 95°C: η (mPas)	107	340
Shear stress stability	High	Medium
Acid resistance	None	None
Status of starch suspensions after first freeze/thaw cycle	Soft gel	Pasty, High-viscous
Freeze/thaw stability	None	Medium

and H_2O. A particular property of starch glucans is their capability to "fill volume" in an adaptive and easy-to-modify way. Constituting modules are glucan molecules with pronounced variety-, species-, and history-specific interactive qualities for forming supermolecular structures. Therefore, a comprehensive characterization of starch glucans includes determination of molecular characteristics of the basic modules (individual glucan molecules) as well as specification of supermolecular characteristics. A feasible list of parameters from the molecular and supermolecular level as well as from the technological level is given in Table 8.

7 ACKNOWLEDGEMENT

This work was supported by the Austrian FWF "Fonds zur Foerderung wissenschaftlicher Forschung" project P-12498-CHE.

© 2004 by Marcel Dekker, Inc.

8 APPENDIX

8.1 Starch and Starch-Related Topics on the Web

Biosynthesis and phosphorylation of starch: http://www.plbio.kvl.dk/plbio/starch.htm

Starch and sucrose metabolism: http://www.genome.ad.jp/htbin/show_pathway?MAP00500 + 2.4.1.29

Pathway of starch biosynthesis: http://www.public.iastate.edu/~pkeeling/Pathway.htm

Enzymes of starch biosynthesis: http://www.public.iastate.edu/~pkeeling/Enzymes.htm

Enzyme nomenclature database: http://www.expasy.org/enzyme/

The maize page: http://maize.agron.iastate.edu/

Starch/Die Stärke: http://www.wiley-vch.de/publish/en/journals/alphabeticIndex/2041/

The Food Resource Homepage: http://food.orst.edu/

Starch—Information about different starches and their technological properties:http://www.orst.edu/food-resource/starch/index.html

Processing of starch: http://www.corn.org/web/process.htm

REFERENCES

1. DM Stark, KP Timmerman, GF Barry, J Preiss, GM Kishore. Science, 258:287–292, 1992.
2. B Muller-Rober, J Kosman. Plant Cell Environ, 17:601–613, 1994.
3. DJ Manners. Recent development in our understanding of amylopectin structure. Carbohydr Polym 11:87–112, 1989.
4. AM Myers, MK Morell, MG James, SG Ball. Recent progress toward understanding biosynthesis of the amylopectin crystal. Plant Physiol 122:989–997, 2000.
5. J Preiss. Specific functions of starch biosynthetic enzymes. Carbohydr Eur 15:11–14, 1996.
6. SR Erlander. Starch biosynthesis. 1. The size distributions of amylose and amylopectin and their relationships to the biosynthesis of starch. Starch/Stärke 50:227–240, 1998.
7. SR Erlander. Starch biosynthesis. 2: The statistical model for amylopectin and its precurser plant glycogen. Starch/Stärke 50:275–285, 1998.
8. SR Erlander. Starch biosynthesis. 3: The glycogen precursor mechanism using phosphorylase in the production of the precursor glycogen. Starch/Stärke 50:319–330, 1998.
9. AM Smith, K Denyer, C Martin. The synthesis of the starch granule. Annu Rev Plant Physiol, Plant Mol Biol 48:67–87, 1997.

© 2004 by Marcel Dekker, Inc.

10. SG Ball, MHBJ van de Wal, RGF Visser. Progress in understanding the biosynthesis of amylose. Trends Plant Sci 3:462–467, 1998.
11. W Praznik, G Rammesmayer, T Spies, A Huber. Characterisation of the (1→4)-α-D-glucan-branching 6-glycosyltransferase by *in vitro* synthesis of branched starch polysaccharides. Carbohydr Res 227:171–182, 1992.
12. AM Myers, MK Morell, MG James, SG Ball. Recent progress toward understanding biosynthesis of the amylopectin crystal. Plant Physiol 122:989–997, 2000.
13. J Preiss. Specific functions of starch biosynthetic enzymes. Carbohydr Eur 15:11–14, 1996.
14. AM Smith, K Denyer, C Martin. The synthesis of the starch granule. Annu Rev Plant Physiol, Plant Mol Biol 48:67–87, 1997.
15. SG Ball, H-P Guan, M James, A Myers, P Keeling, G Mouille, A Buleon, P Collona, J Preiss. From glycogen to amylopectin: a model for the biogenesis of the plant starch granule. Cell 86:349–352, 1996.
16. NK Matheson. The chemical structure of amylose and amylopectin fractions of starch from tobacco leaves during development and diurnally-nocturnally. Carbohydr Res 282:247–262, 1996.
17. A Huber, W Praznik. Molecular characteristics of glucans: High amylose corn starch; In: M Potschka, PL Dubin, eds. ACS Symposium Series No. 635, Strategies in size-exclusion chromatography. Ch. 19, 1996, pp 351–365.
18. V Fergason. High amylose and waxy corns. In: A Hallauer, ed. Specialty Corns. Boca Raton, FL: CRC Press Inc., 1994, pp 55–77.
19. W Praznik, A Huber, S Watzinger, HF Beck. Molecular characteristics of high amyloses starches. Starch/Stärke 46:88–94, 1994.
20. P Colonna, C Mercier. Macromolecular structure of wrinkled and smooth-pea starch components. Carbohydr Res 126:233–247, 1984.
21. P Weatherwax. A rare carbohydrate in waxy maize. Genetics 7:568–572, 1922.
22. OE Nelson, HW Rines. The enzymatic deficiency in the waxy mutant of maize. Biochem Biophys Res Commun 9:297–300, 1962.
23. CD Boyer, LC Hannah. Kernel mutants of corn. In: A Hallauer, ed. Speciality corns. CRC Press Inc., 1994, pp 2–28.
24. M Obanni, JN BeMiller. Identification of starch from various maize endosperm mutants via ghost structures. Cereal Chem 72:436–442, 1995.
25. RGF Visser. Some physicochemical properties of amylose-free potato starch. Starch/Stärke 49:443–448, 1997.
26. RA Graybosch. Waxy wheats: Origin, properties, and prospects. Trends Food Sci Technol 9:135–142, 1998.
27. T Nakamura, M Yamamori, H Hirano, S Hidaka, T Nagamine. Production of waxy (amylose-free) wheats. Mol Gen Genet 248:253–259, 1995.
28. T Ono, H Suzuki. Endosperm characters in hybrids between barley varieties with starchy and waxy endosperm. Seihen Ziho 8:11–19, 1957.
29. T Murata, T Sugiyama, T Akazawa. Enzymic mechanism of starch synthesis in glutinous rice grains. Biochem Biophys Res Commun 18:371–376, 1965.
30. K Denyer. The isolation and charcterisation of novel low-amylose mutants of *Pisum sativum* L. Plant Cell Environ 18:1019–1026, 1996.

© 2004 by Marcel Dekker, Inc.

31. Y Konishi. Characterisation of starch granules from waxy, nonwaxy and hybrid seeds of *Amaranthus hypochondriacus* L. Agric Biol Chem 49:1965–1971, 1985.
32. HF Zobel. Molecules to granules: A comprehensive review. Starch/Stärke 40:1–7, 1988.
33. S Hizukuri. Starch: analytical aspects. In: AC Elliasson, ed. Carbohydrates in food. New York: Dekker, 1996, pp 347–429.
34. RE Cameron, AM Donald. A small-angle X-ray scattering study of the annealing and gelatinization of starch. Polymer 33:2628–2635, 1992.
35. PJ Jenkins, RE Cameron, AM Donald. A universal feature in the structure of starch granules from different botanical sources. Starch/Stärke 45:417–420, 1993.
36. D French. Organisation of starch granules. In: RL Whistler, JN BeMiller, EF Paschal. Starch Chemistry and Technology. 2nd ed. London: Academic Press, Inc., 1984.
37. S Hizukuri, T Kaneko, Y Takeda. Measurement of the chain length of amylopectin and its relevance to the origin of crystalline polymorphism of starch granules. Biochim Biophys Acta 760:188–191, 1983.
38. S Hizukuri. Polymodal distribution of the chain length of amylopectin and its significance. Carbohydr Res 147:342–347, 1986.
39. H Fredriksson, J Siverio, R Andersson, A-C Eliasson, P Aman. The influence of amylose and amylopectin characteristics on gelatinization and retrogradation properties of different starches. Carbohydr Polym 35:119–134, 1998.
40. MJ Gidley, PV Bulpin. Crystallisation of malto-oligosaccharides as models of the crystalline forms of starch: minimum chain-length requirement for the formation of double helices, Carbohydr Res 161:291–300, 1987.
41. A Imberty, A Buleon, V Trans, S Perez. Recent advances in knowledge of starch structure. Starch/Stärke 43:375–384, 1991.
42. S Perez, A Imberty. Structural features of starch. CiE 15:17–21, 1996.
43. MJ Gidley, SM Bociek. Molecular organization in starches: a ^{13}C CP/MAS NMR study. J Am Chem Soc 107(7):7040–7044, 1985.
44. PJ Jenkins, RE Cameron, AM Donald, W Bras, GE Derbyshire, GR Mant, AJ Ryan. In situ simultaneous small and wide-angle X-ray scattering: a new technique to study starch gelatinization. J Polym Sci, Polym Phys Ed 32:1579–1583, 1994.
45. PJ Jenkins, AM Donald. The influence of amylose on starch granule structure. Int J Biol Macromol 17:315–321, 1995.
46. DJ Gallant, B Bouchet, PM Baldwin. Microscopy of starch: evidence of a new level of granule organization. Carbohydr Polym 32:177–191, 1997.
47. DJ Gallant, B Bouchet, A Buleon, S Perez. Physical characteristics of starch granules and susceptibility to enzymatic degradation. Eur J Clin Nutr 46:S3–S16, 1992.
48. PM Baldwin, RA Frazier, J Adler, TO Glasbey, MP Keane, CJ Roberts, SJB Tendler, MC Davies, CD Melia. Surface imaging of thermally-sensitive particulate and fibrous materials with the atomic force microscope: a novel sample preparation method. J Microscopy 184:75–80, 1996.
49. LA Bello-Perez, P Colonna, P Roger, O Parades-Lopez. Starch/Stärke 50:137, 1998.
50. DS Jackson. Starch/Stärke 43:422, 1991.
51. GR Noggele. The identification and the quantitative determination of carbohydrates. In: W Pigman, ed. The Carbohydrates. New York: Academic Press Inc., 1957, pp 602–640.

© 2004 by Marcel Dekker, Inc.

52. W Praznik, R Beck. J Chromatogr 387:467–472, 1987.
53. A Huber, W Praznik, Molecular characteristics of glucans: High amylose corn starch. In: M Potschka, PL Dubin, eds. ACS Symposium Series No. 635, Strategies in Size-Exclusion Chromatography. Ch. 19, 1996, pp 351–365.
54. W Praznik, A Huber, S Watzinger, RHF Beck. Molecular characteristics of high amylose starches. Starch/Stärke 2(94):82–93, 1994.
55. W Praznik, A Huber. Modification of branching pattern of potato maltodextrin with Q-enzyme zywnosc. Technologia Jakosc (Food Technol Quality) 4(17):202–216, 1998.
56. B Pfannemüller, Stärke. In: W Burchard, ed. Polysaccharide. Berlin, Heidelberg, New York, Tokyo: Springer Verlag, 1985, pp 25–42.
57. VM Leloup, P Colonna, SG Ring, K Roberts, B Wells. Microstructure of amylose gels. Carbohydr Polym 18:189–197, 1992.
58. S-H Yun, K Matheson. Structural-changes during development in the amylose and amylopectin fractions (separated by precipitation with concanavalin-A) of starches from maize genotypes. Carbohydr Res 270:85–101, 1992.
59. M Schmidt, W Burchard. Moleküleigenschaften in verdünnten Lösungen. In: W Burchard, ed. Polysaccharide. Berlin, Heidelberg, New York, Tokyo: Springer Verlag, 1985, pp 25–42.
60. J Springer, MD Lechner, H Dautzenberg, W-M Kulicke. Overview. Macromol Chem, Macromol Symp 61:1–23, 1992.
61. W Praznik, G Rammesmayer, T Spies, A Huber. Characterization of the (1→4), α-D-glucan-branching 6-glycosyltransferase by *in vitro* synthesis of branched starch polysaccharides. Carbohydr Res 227:171–182, 1992.
62. TJ Schoch. The fractionation of starch. In: WW Pigman, ML Wolfrom, eds. Adv Carbohydr Chem 1:247–277, 1945.
63. A Huber, W Praznik. Dimensions and structural features of aqueous dissolved polymers. In: W. Praznik, A Huber, eds. Carbohydrates as organic raw materials IV. Wien: WUV-Universitätsverlag, Ch. 19, 1998, pp 230–246.
64. W Banks, CT Greenwood, KM Khan. Carbohydr Res 17:25–33, 1971.
65. T Handa, H Yajima, T Ishii, T Nishimura. Deep blueing mechanism of triiodide ions in amylose being associated with its conformation. In: DA Brant, ed. Solution Properties of Polysaccharides. ACS Symposium Series 150, 1981, pp 455–475.
66. B Pfannemüller, G Ziegast. Properties of aqueous amylose and amylose–iodine solutions. In: DA Brant, ed. Solution Properties of Polysaccharides. ACS Symposium Series 150, 1981, pp 529–548.
67. SV Bhide, MS Karve, NR Kale. The interaction of sodium dodecyl sulfate, a competing ligand, with iodine complexes of amylose and amylopectin. In: DA Brant, ed. Solution Properties of Polysaccharides. ACS Symposium Series 150, 1981, pp 491–511.
68. ST Balke, RT Thitiratskul, R Lew, P Cheung, TH Mourey. A Strategy for Interpreting Multidetector Size-Exclusion Chromatography Data II. ACS Symposium Series 521, T Provder, ed. 13, 1993, pp 199–219.
69. S Hase. Precolumn derivatization for chromatographic and electrophoretic analysis of carbohydrate. J Chromatogr A 720:173–182, 1996.

© 2004 by Marcel Dekker, Inc.

70. J Suzuki, A Kondo, I Kato, S Hase, T Ikenaka. Analysis by high-performance anion exchange chromatography of component sugars as their fluorescent pyridylamino derivatives. J Biol Chem 55:283–284, 1991.
71. D Marx. Molekulare Charakterisierung von Stärkeglucanen mittels selektiver Fluoreszenzmakierung. PhD thesis, Universität für Bodenkultur, Vienna, 2001.
72. M Hofer. Basic concepts in static and dynamic light scattering: Application to colloids and polymers. In: P Lindner, Th Zemb, ed. Neutron, X-Ray and Light Scattering. Amsterdam, Oxford, New York, Tokyo: North-Holland, 1991.

© 2004 by Marcel Dekker, Inc.

15
Size Exclusion Chromatography of Proteins

John O. Baker, William S. Adney and Michael E. Himmel
National Renewable Energy Laboratory
Golden, Colorado, U.S.A.

Michelle Chen
Wyatt Technology Corporation
Santa Barbara, California, U.S.A.

1 INTRODUCTION

Researchers in the biophysical sciences have been concerned with the rapid and gentle isolation of macromolecules of all sizes and types. Although the exact dates of early thoughts on the subject are difficult to place, records from *Discussions of the Faraday Society* in 1949 (1) reflect on both speculation and evidence that porous media may be useful in separating biomolecules by size. The chronology of the subsequent discovery of the particle-sieving effects of starch and crosslinked dextran gels in the 1950s at the Institute of Biochemistry, University of Uppsala, Sweden, is well reviewed in a recent article by Hagel and Janson (2). The separation and collection of many water-soluble biopolymers has since been possible using the principle first called gel filtration. Sephadex® (Pharmacia, Uppsala, Sweden) was the first commercial separation media made from water

© 2004 by Marcel Dekker, Inc.

insoluble crosslinked polydextran gel and was originally described by Porath and Flodin in 1959 (3). Soon after this initial breakthrough, Granath and Flodin clearly demonstrated the relationship between the elution of fractionated dextrans and proteins and some function of the molecular size of the solute (4). In fact, the early work showed a tendency for elution in reverse order of molecular weight. This observation then stimulated interest in finding a simple relationship between the absolute molecular weights of macromolecules and their elution volumes in the hope that such a relationship might be useful as a predictive analytical tool for unknown systems. The early uses of Sephadex® were broadly reviewed by Porath (5) in 1967; however, the popularity of these packing materials diminished with the availability of stronger, more efficient preparations.

The success of size exclusion chromatography (SEC) for protein separation is undeniable and has been well chronicled. Milestone reviews of protein SEC present treatments of applications and theory and, in chronological order, include the works of Bly (6), Yau *et al.* (7), Barth (8), Giddings (9), Regnier (10), Dubin and Principi (11), Gooding and Regnier (12), and Barth *et al.* (13). Column and/or packing material selection guidelines have also been well described by Montelaro (14), Unger and Kinkel (15), Makino and Hatano (16), and Gooding and Freiser (17). Protein SEC in detergents has been recently reviewed (14,18). In the present review, we shall explore fundamental partition parameters appropriate to protein SEC and SEC theory, and then focus on several important aspects of protein SEC that are not well and widely treated. These topics are column/elution calibrations, non-SEC partitioning, and industrial-scale protein SEC.

2 COLUMN COMPARTMENTALIZATION

The volume elements found in the chromatography column filled with porous media are usually defined in a manner that follows the first suggestions by Porath (19) and later modified by Andrews (20). Here, the total geometrical volume of the SEC column, V_g, is defined as the sum of the total mobile phase volume, V_t, and the volume of the packing material or stationary phase, V_s. The mobile phase volume is further defined as the sum of the volume external to the pores in the packing material or void volume, V_0, and the volume occupied by the "stagnant" mobile phase found in the internal pore structural elements, V_i. V_0 has been shown to be near $0.2595 \times V_g$ for columns of rigid SEC packing materials (21) by approximating the gel bed as an assembly of hexagonal closest-packed spheres. It is thought that the differential solute distribution between the volumes internal and external to the pores results in the separation of the solutes. The volume of elution of these solutes is known as V_e.

© 2004 by Marcel Dekker, Inc.

3 PROTEIN PARTITIONING IN SEC

3.1 General Retention Mechanisms

Retention mechanisms for SEC are generally given on both hydrodynamic (actually hydraulic) or thermodynamic grounds. The validity of interpreting SEC behavior in terms of thermodynamic generalities has been well expressed and defended by Yau *et al.* (22–24), and will not be stressed here. The hydrodynamic description of the SEC process, especially when describing well-behaved protein systems, has been reasonably rewarding in its ability to converge theory and predictive elution. Fundamentally, V_e is the sum of the void volume occupied by all solutes and a portion of the internal pore volume defined by the size exclusion differential equilibrium constant, K_{SEC}, and a portion of the surface of the column packing defined by the distribution coefficient describing interactions between the column and solute, K_{LC}. This condition leads to the general equation

$$V_e = V_0 + K_{SEC}V_i + K_{LC}V_S \tag{1}$$

In the execution of SEC procedures it is usual and desirable, however, to reduce adsorptive effects as much as possible using appropriate packing materials, buffers, or detergents so that the last term in Eq. (1) is reduced to insignificance.

While solute partitioning in other forms of liquid chromatography involve primarily the solute/stationary phase interactions, solute partitioning in SEC can be described loosely as an entrapping effect, where solute molecules lose configurational freedom upon entering the gel pores, a process that results in entropic changes with the occupation of different column volumes (25). This explanation, then, represents the basis for thermodynamic characterization of K_{SEC}. K_{SEC} may also be explained in terms of column compartmentalization and geometry, however.

3.2 Protein Elution Calibration

We now understand that two parameters must be understood before such a tool could be usable: the correct description of the solute (protein) exposed to the SEC process, and the physical description of the internal pore spaces seen by the eluting species, usually as some function of V_e. The correct physical or hydrodynamic description of the protein solute and the column packing material exists as a challenge today.

3.2.1 Column Partitioning Effects: Pore Geometries

The early work of Andrews (20) is typical of the approach used to first study the elution of proteins from SEC columns. Here the volume, V, passing through the

© 2004 by Marcel Dekker, Inc.

column before the protein emerges in maximum concentration was plotted as a function of the logarithm of protein molecular weight. The agreement was considered, at the time, to be surprisingly good. Also in the early 1960s, Whitaker (26) reported good correlations between the ratio of the elution volume to the void volume, V/V_0, and the logarithm of the molecular weight. A new elution volume parameter, K_{av}, based on comparisons with the void and total column volumes, was soon derived (7,27,28).

$$K_{av} = \frac{V_e - V_0}{V_t - V_0} \tag{2}$$

The relationship described as K_{av} was recommended by Pharmacia (Uppsala, Sweden) as the method of choice for column calibration from the earliest days of Sephadex® use. These results, and others like them, set the stage for a unique analytical tool at the time, one capable of predicting the molecular weights of unknown proteins. The elution of 37 purified proteins and two small solutes was plotted by this method and is shown in Fig. 1.

Modern theoretical models used to describe SEC elution behavior must allow for possible variations in both the solute and bead pore size and shape, while remaining consistent with current concepts regarding SEC as an equilibrium-controlled process. The shape of the "pore" in SEC is important in the prediction of elution behavior. Gel pores were originally described in terms of the penetrability of "hard-sphere" solutes, and extensions of this model are still employed today. Early theories of hard sphere solute models, in chronological order of appearance in the literature, are the random-spheres pore model of Ogston (29), the randomly occurring cones, cylinders, and crevices pore model of Squire (30), and the random-rod pore model of Laurent and Killander (31). The model proposed by Squire for the description of pores in Sephadex® for a solute eluting at V_e was given as

$$V_e = V_0 + kV_0\left(1 - \frac{r}{R}\right)^3(\text{cones}) + k'V_0\left(1 - \frac{r}{R}\right)^2(\text{cylinders}) + k''V_0\left(1 - \frac{r}{R}\right)(\text{crevices}) \tag{3}$$

where r is the protein radius. The cones and cylinders are of radius R, and the crevices of width $2R$. An arbitrary assignment of the distribution of these pores, $k'' = 9g$, $k' = 9g^2$, and $k = 3g^3$, leads to the simplified equation describing the contribution of all pore types to elution volume:

$$\frac{V_e}{V_0} = \left[1 + g\left(1 - \frac{r}{R}\right)\right]^3 \tag{4}$$

© 2004 by Marcel Dekker, Inc.

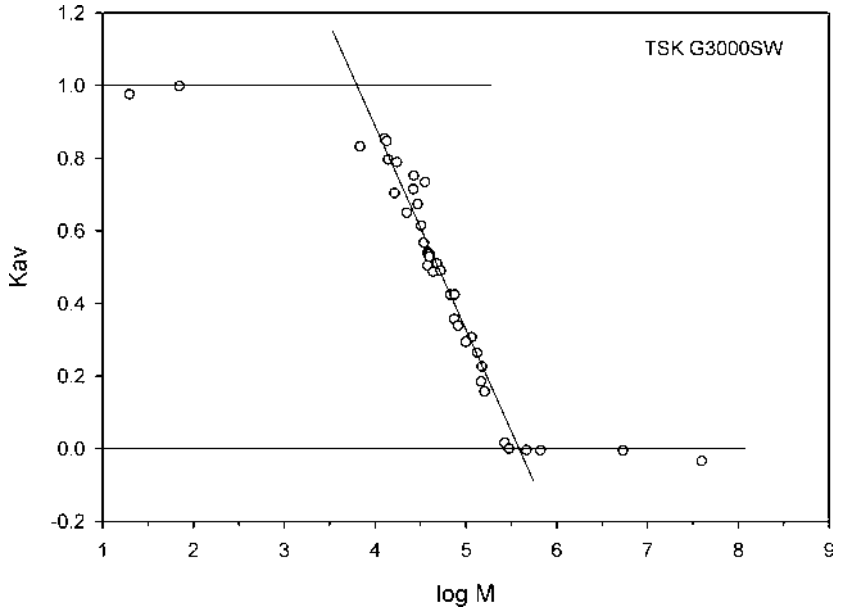

Figure 1 Plot of K_{av} vs. log M for 37 purified proteins and two V_t markers. Solutes, from low to high M, are: D_2O, NaN_3, trypsin inhibitor, cytochrome C, elastase (subunit), ribonuclease A, myoglobin, chymotrypsinogen A, carboxypeptidase, hemoglobin (subunit), elastase, carbonic anhydrase, myokinase, deoxyribonuclease, malate dehydrogenase, superoxide dismutase, peroxidase, alcohol dehydrogenase (subunit), α-galactosidase II, ovalbumin, α-amylase, 3-phosphoglycerate kinase, lactate dehydrogenase (subunit), bovine serum albumin, malate dehydrogenase, aldolase (subunit), catalase (subunit), glucose 6-phosphate dehydrogenase (subunit), bovine serum albumin (dimer), glucose oxidase, lactate dehydrogenase, β-glucouronidase (subunit), aldolase, fructosidase, β-glucouronidase, apoferritin, thyroglobulin, turnip yellow mosaic virus, and tobacco mosaic virus. The chromatography was performed at 1.0 mL/min with two 7.8 mm × 30 cm TSK G3000 SW columns. The mobile phase was 10 mM phosphate pH 7 buffer in 100 mM NaCl. Each injection included D_2O as an internal standard for V_t. The correlation coefficient for the linear portion of the data is 0.989.

It is generally agreed today that the random-sphere models (resulting in uniform pore geometry systems), based on the close packing of spherical gel beads, are best suited to describing SEC using porous silica microspheres or controlled pore glass beads. The random pore models given above and the models based on statistical distributions of shapes, which followed, may indeed be more accurate for the majority of the rigid SEC packings used today.

The first of such statistical pore models was proposed by Giddings *et al.* (32) in 1968. In this landmark study, general expressions were formulated that

© 2004 by Marcel Dekker, Inc.

described the partitioning of hard-sphere solutes in a random pore system described as a "porous network." Also unique to this study was an attempt to express SEC partitioning as a function of both complex pore and solute contributions. Furthermore, the authors treated the distribution of solutes of various shapes (spherical, thin rod, dumb-bell, and capsular shaped) in pores described as cylinders, slabs, spheres, and rectangular pockets. Giddings concluded that SEC partitioning may best be defined as

$$K = e^{(-s\bar{L}/2)} \tag{5}$$

where K is the SEC equilibrium constant for a random plane pore model and $s\bar{L}$ is the product of the mean external molecular length, $\bar{L}$, and the effective pore radius, s. The equilibrium partitioning of rigid solutes in a random-fiber pore model was also proposed by Giddings (32). Here the SEC equilibrium constant was defined as

$$K = e^{-\bar{A}h} \tag{6}$$

where $\bar{A}$ is the projection of the molecular dimension, A_x, averaged over all directions in space and h is the fiber length per unit volume. The fiber diameter is assumed similar to the size of the solute molecule.

Further contributions to SEC theory were made by Glandt (33) for the description of the spatial density distribution for "crowded pores." This work contrasts earlier with studies based solely on dilute solutions of solutes where solute-wall effects are primarily considered.

3.2.2 Proteins as SEC Solutes

It is noteworthy that the field of SEC elution theory turned largely to the description of partitioning of random-coil polymers during the late 1960s and throughout the following decade. Contributions from Cassassa and Tagami (34), based on Flory theory (35), served to further the understanding of high polymer SEC. This work focused on new descriptions of flexible solutes. When considering the elution of proteins as SEC solutes, the treatment of solution conformation becomes somewhat simplified when viewed from the perspective of the statistical mechanical arguments needed to describe high polymers. The hard shell or rigid sphere solute models described above are probably adequate for proteins. This approach was used by Squire (30) to extend Eq. (4) to

$$\frac{V_e}{V_0} = \left[1 + g\left(1 - \frac{M^{1/3}}{C^{1/3}}\right)\right]^3 \tag{7}$$

© 2004 by Marcel Dekker, Inc.

by considering the protein solutes to be spherical. The term r is proportional to the cube root of the molecular weight. Equation (7) may then be rearranged in the manner described by Himmel and Squire (36), yielding two forms, one relating elution to the void volume of the column and the other to the total volume accessible to the mobile phase:

$$F'_{\mathrm{v}} = \frac{V_{\mathrm{e}}^{1/3} - V_0^{1/3}}{V_{\mathrm{t}}^{1/3} - V_0^{1/3}} = \frac{C^{1/3} - M^{1/3}}{C^{1/3} - A^{1/3}} \tag{8}$$

$$F_{\mathrm{v}} = \frac{V_{\mathrm{e}}^{1/3} - V_0^{1/3}}{V_{\mathrm{t}}^{1/3} - V_0^{1/3}} = \frac{C^{1/3} - M^{1/3}}{C^{1/3} - A^{1/3}} \tag{9}$$

where C and A correspond to the molecular weights of solutes just large enough to be rejected from the column pores, and solutes small enough to be included in all volumes of the column, respectively. Note that the right-hand quantity in Eqs (8) and (9) predicts a linear relationship between F_{v} and $M^{1/3}$. The set of 37 proteins shown in Fig. 1 are replotted according to the equation for F'_{v} and are shown in Fig. 2.

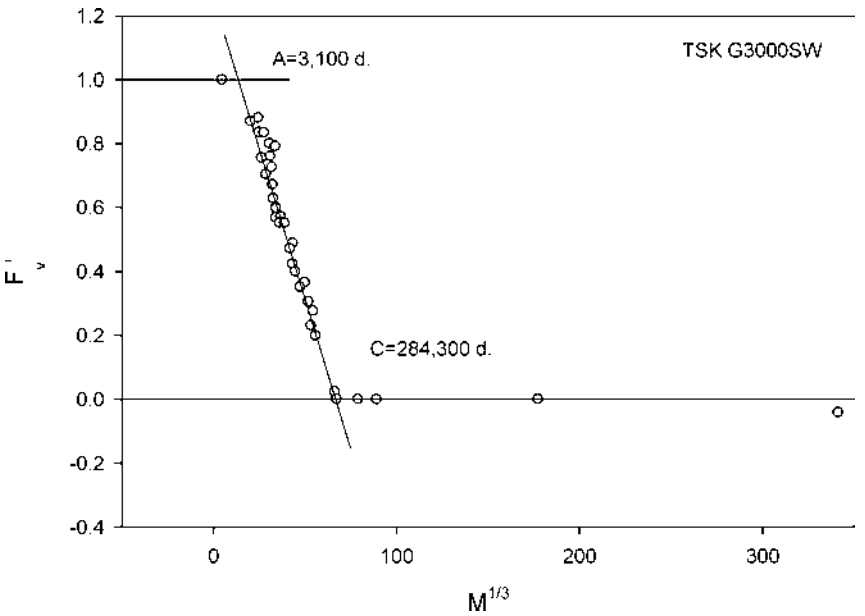

Figure 2 Plot of F'_{v} vs. $M^{1/3}$ for the data given in Fig. 1. The correlation coefficient for the linear portion of the data is 0.992.

© 2004 by Marcel Dekker, Inc.

To use Eqs (8) and (9) effectively, one must decide if, in the context of a given experiment, V_0 or V_t may be determined less ambiguously. Himmel and Squire assumed that in most cases V_t may be less accurately determined than the void volume because of adsorptive effects experienced with most small solutes and hence recommended the use of F'_v. However, Noll *et al.* have recently shown (37) that the elution of deuterium oxide can be used as a reliable marker for V_t and re-evaluation of the use of Eq. (9) may be in order. A further benefit of Eqs (8) and (9) is that the values C and A can be accurately calculated from the limiting chromatographic conditions, that is, at $F'_v = 1, M^{1/3} = A^{1/3}$, and at $F'_v = 0, M^{1/3} = C^{1/3}$. The calculation of the column parameters C and A for a series of similar columns, in different laboratories, is shown in Table 1.

The method of Himmel and Squire (38) has been applied to a wide range of native protein SEC conditions, including TSK columns (39), Waters I125 columns (40), as well as denatured protein SEC using Sephadex® (41). An important extension to the method based on Eq. (8) was proposed by Bindels and Hoenders (42), where F_v was plotted against $(M\bar{\nu})^{1/3}$. These workers found that this approach gave better results than plots of $M^{1/3}$ or $\log M$.

Assuming that the left-hand side of Eqs (8) and (9) provides an adequate description of the column pores in SEC, then the predictive power of this method may be improved by enhancing the picture of the solute during SEC beyond MW. Although proteins are indeed roughly spherical, they can usually be more accurately described as ellipsoids of revolution, either prolate or oblate, with axial ratios normally ranging from 1.0 to 6 (35). And, as found by Bindels and Hoenders, the correct SEC molecular radius must consider other factors. A thorough treatment of proteins and nonflexible chain polymers as SEC solutes has been contributed by Potschka (43). In this study, the parameters considered included the equivalent (or effective) hydrodynamic radius, R_e, the Stokes radius, R_s, the root-mean-square radius of gyration, R_g, and the root-mean-square end-to-end distance, r_{rms}. In an important recent contribution by Dubin and Principi (44),

Table 1 Calibration Constants for Toyo Soda TSK SW Series SEC Columns

TSK column support type	A (daltons)	C (daltons)
G2000 SW	940	91,000
G3000 SW	2460	340,000
G3000 SW	3900	330,000
G3000 SW[a]	3100	284,000
G4000 SW	550	3.4×10^6

[a]From this study.
Source: Adapted From Ref. 38.

© 2004 by Marcel Dekker, Inc.

globular proteins and selected flexible chain polymers were found to elute predictably when the "viscosity radius", R_η, (equal to $[\eta]M$) was used as the solute parameter. These authors found that rodlike molecules did not obey this elution rule, however, and concluded that the universal "SEC radius" had not been found. This may indeed be true for the broad-based SEC of biomacromolecules; however, the R_{SEC} (Dubin's term) must be similar, if not equal, to the effective hydrodynamic radius proposed by Cassassa and Tagami (34), and must occupy the effective hydrodynamic volume, V_h. For many proteins, R_e may be equivalent to R_η. Yet, R_e may also be calculated from known parameters, such as the molecular weight (from sedimentation equilibrium or gene sequence), molecular dimensions (from x-ray crystallography), surface hydration (from titration or modeling), and partial specific volume (from composition or actual measurement). Following Oncley's approach (45), based on an extension of the Stokes relationship for a perfectly spherical protein, $f_0 = 6\pi\eta R_0$, globular proteins may be described more accurately than as simple spherical, hydrated structures (34). This frictional coefficient, f, is defined as:

$$f = 6\pi\eta \frac{f}{f_0}\left[\frac{3M(\bar{\nu}_2 + \delta_1 \nu_1^0)}{4\pi N}\right]^{1/3} \tag{10}$$

where f/f_0 is the frictional ratio, $\bar{\nu}_2$ is the protein partial specific volume, ν_1^0 is the pure solvent specific volume, δ_1 is the protein hydration, and N is Avogadro's number. The product of the bracketed quantity in Equation (10) and the shape factor, f_e/f_o, is the highly protein-specific radius, R_e. If needed, the frictional ratios may be found from experimental data (s, M, and $\bar{\nu}_2$; where s is the sedimentation coefficient) or from protein dimensional information, assuming best fit for x-ray structural data to either prolate or oblate spheroids of revolution. This estimation may be accomplished using the relationships developed long ago by Perrin (46) and modified by Herzog *et al.* (47). For prolate ellipsoids (semi-axes a, b, b)

$$\frac{f}{f_0} = \frac{(1 - \mathrm{b}^2/\mathrm{a}^2)^{1/2}}{(\mathrm{b/a})^{2/3}\ln[1 + (1 - \mathrm{b}^2/\mathrm{a}^2)^{1/2}]/(\mathrm{b/a})} \tag{11}$$

and for oblate ellipsoids (semi-axes a, a, b):

$$\frac{f}{f_0} = \frac{(\mathrm{a}^2/\mathrm{b}^2 - 1)^{1/2}}{(\mathrm{a/b})^{2/3}\tan^{-1}(\mathrm{a}^2/\mathrm{b}^2 - 1)^{1/2}} \tag{12}$$

where R_0 is the radius of a sphere of equal volume to the ellipsoid, that is, $\frac{4}{3}\pi R_0^3 = \frac{4}{3}\mathrm{ab}^2$ (prolate ellipsoid) or $\frac{4}{3}\pi\mathrm{a}^2\mathrm{b}$ (oblate ellipsoid).

Unfortunately, these parameters are known accurately for only a relatively small group of globular proteins: the 21 globular proteins reported by Squire and Himmel in 1979 (48). The test of fit for globular protein elution from SEC based

© 2004 by Marcel Dekker, Inc.

on the estimation of R_e from such a database is promising but has not yet been examined.

4 NON-SEC PARTITIONING

In connection with the SEC of proteins, the term "nonsize effects" refers, inclusively, to all phenomena affecting the retention of proteins on size-exclusion columns, other than the classical partitioning of solutes between pore volume and interstitial volume based on the ratio of solute dimensions to pore dimensions. These nonsize effects may include attractive interactions such as ion-exchange and hydrophobic (44) binding, which will tend to increase the elution volumes of solutes, thus causing them to appear smaller than they actually are, and forces of electrostatic repulsion (ion-exclusion), which will have the effect of denying otherwise accessible volumes to the solutes and thereby causing them to appear larger than they are.

In some applications, such as development of purification protocols, these additional effects may not be regarded as problems, but may instead be exploited in the "fine-tuning" of procedures for separating proteins that would co-elute if separated purely on the basis of size (49). It is when investigators attempt to use SEC data to draw quantitative conclusions concerning absolute or relative sizes of proteins that these nonsize effects pose a major problem. The most obvious example is, of course, the use of SEC to estimate the molecular weight of proteins, but distortions resulting from nonSEC effects can potentially be even more severe when SEC is used to measure changes in the shape of a given protein (i.e., experiments measuring conformational changes and/or subunit dissociation/recombination phenomena, which may expose new and different protein surfaces for potential contact with packing materials) (50,51).

A variety of modifications of stationary and mobile phases have been made in order to eliminate, or at least reduce, nonsize effects. The results of these measures are complicated, however, because of the fact that there are at least three general categories of phenomena that can be affected (often differently) by these measures: packing material/solute interactions, geometrical changes in the column itself, and changes in the physico-chemical state of the proteins being studied.

4.1 Packing-Material/Solute Interactions

4.1.1 Electrostatic Interactions

The surfaces of most packing materials used for aqueous SEC tend to have slight negative charges under the conditions most often used for chromatography of proteins. Silica-based packings are negatively charged because of weakly acidic

© 2004 by Marcel Dekker, Inc.

silanol groups (52–54); even capped silica materials tend to exhibit some of this property inasmuch as the "capping" process usually leaves some unmodified silanols (51,52), and more silanols may be produced by erosion of capping groups during use of the column (52). Some polymeric packing materials tend to be negatively charged because of the presence of small numbers of carboxyl groups (54). Proteins with net positive charges will therefore tend to be adsorbed on the matrix, be retained longer on the column, and be assigned erroneously small molecular sizes. Negatively charged proteins will (to a first approximation; see below) tend to be repelled from the surface of the packing material, which repulsion will result in their being denied access to some of the pore volume and eluted earlier than would be expected on the basis of size alone.

For a given packing material, the most generally useful means of suppressing electrostatic interactions with proteins is to vary the ionic strength of the mobile phase until a region of ionic strength is encountered in which elution volume is essentially independent of ionic strength (56–59). It should be kept in mind that high ionic strengths tend to promote hydrophobic interactions; if a simple minimum in elution volume is observed in the dependence of elution volume on ionic strength, instead of a flat plateau of significant width, the results may not mean that ideal SEC is taking place at the ionic strength producing the minimum elution volume. Both electrostatic and hydrophobic binding to the packing may be influencing the elution significantly, with the minimum elution volume simply marking the ionic strength at which the sum of the two interactions is at its minimum (60,61).

Another approach to suppressing electrostatic interactions is to adjust the charges on the protein, the packing material, or both, by adjusting the pH of the mobile phase (49,55–57). In (oversimplified) theory, if the positive and negative charges on the protein can be equalized, so that the net result is an electrically neutral molecule, there should be no electrostatic attraction or repulsion between protein and packing material. In practice, however, one rather extensive evaluation of this strategy found that the most nearly ideal SEC occurred when the mobile phase pH was slightly above the isoelectric point of the protein (48).

Strategies based on protein pI values appear to work well in a number of instances (55,56), although pH adjustment will not be an appropriate response to non-SEC effects in the not-unlikely event that a given pH value is an integral part of the experiment being conducted and not a variable that can be varied for purely analytical reasons, or, as will be discussed below, in the event that protein stability becomes a problem at the pH that would be chosen for chromatographic reasons. Deviations from predictions based solely on net charges of proteins and packing materials may also arise from chromatographic implications of the macromolecular nature of proteins. In most cases, charged proteins cannot be represented adequately as point charges equal to their net charges; the charged groups on the exterior of proteins have definite distributions about quite appreciable diameters,

© 2004 by Marcel Dekker, Inc.

and these distributions are by no means always symmetrical. Chromatographic behavior may reflect attraction between charged packing materials and local patches of opposite charges on the protein, even when the net charge on the protein as a whole has the same sign as the charge on the packing material (62). Small-molecule examples of such local interactions are to be found in the binding of polyelectrolytes to proteins even at pH values such that the net charges on the polyelectrolytes and proteins are of the same sign (63).

4.1.2 Hydrophobic Interactions

Significant hydrophobic interactions between proteins and packing material may be inferred from increases in elution volume as ionic strength is increased to fairly high values (generally 0.5 or higher, for ionic strength supported by NaCl). A strong "salting out" salt, such as ammonium sulfate, is especially useful in assessing the potential for such interactions in the case of a particular protein/matrix pair (51). Hydrophobic adsorption of proteins may be reduced by decreasing the ionic strength of the mobile phase (which may concurrently increase electrostatic interactions, however) or by adding organic solvents (64).

4.2 Geometrical Changes in the Packing Material

Gels such as Sephadex® and the BioGel®-P series (BioRad, Hercules, California, U.S.A.) depend upon swelling of the gel material in solvent for the formation of pores; the pores collapse completely upon removal of the solvent (65). This critical dependence of the gel structure on solvation of the polymeric material raises the possibility of changes in effective pore size when the chemical nature of the mobile phase is changed significantly in an attempt to suppress adsorptive effects, as in the addition of detergents or organic solvents (64) for the chromatography of hydrophobic proteins. Such considerations may also apply to hybrid gels (65) in which a hydration-dependent material has been bonded inside the large pores of a macroreticular supporting framework. A second type of pore-size change may affect rigid, permanent-pore packing materials as well as the solvent-swollen materials, in that detergents added to the mobile phase in order to solubilize or denature proteins, or to suppress hydrophobic interactions between proteins and packings, may bind to the surfaces inside the pores to such an extent that the effective pore size is significantly decreased (66). The straightforward, though laborious, countermeasure to both of these effects is the calibration of the SEC column under each and every set of conditions employed experimentally.

4.3 Changes in the Physico-Chemical State of the Proteins

When changing the pH of the mobile phase to eliminate electrostatic interactions between protein and packing material, one should keep in mind the tendency of

© 2004 by Marcel Dekker, Inc.

most proteins to be maximally stable at a certain pH value or range of values, and to display diminishing stability as the pH is varied in either direction from this optimal value (or range). As has been pointed out previously (67,68), considerable evidence exists that some proteins (those that can be described as deformable, or "soft", in that they have relatively low structural stability) are bound to surfaces in a two-step process (69). First, the native protein forms a fairly weak interaction with the surface (this interaction may be either hydrophobic or electrostatic, depending on the nature of the surface and of the exterior of the protein). A subsequent conformational change in the loosely bound protein allows a substantial increase in the extent of contact between the protein and the surface, and therefore in the number of binding interactions (68–71). If the second step (the conformational change in the bound protein molecule) proceeds to a sufficient extent, this may result in an overall tight binding of such a soft protein to the packing material, even under conditions such that the equilibrium in the first step (the original association of the protein with the packing material) is in favor of the protein remaining in the mobile phase. In contrast to this behavior, a more structurally stable, relatively "hard", or nondeformable protein, even though it has the same surface chemistry as the soft protein, will exhibit only the first, weak step of binding, and will remain principally in the mobile phase.

The relevance of the foregoing to the question of adsorptive interactions in SEC is that as the pH of the mobile phase is moved away from the pH of maximum protein stability, the protein will be progressively softened, becoming much less resistant to structural changes induced upon contact with the packing material. It is important to note that this softening of the structure can proceed to a significant extent, long before the pH change reaches the point of causing denaturation of the protein in solution.

The result of all of these concurrent and often opposing effects is that an experimenter who wishes to use protein SEC data to support specific, quantitative conclusions concerning protein sizes and shapes will be required to test multidimensional arrays of sets of conditions, rather than a one-dimensional array in which only the variable of specific interest is changed.

5 USE OF MALS DETECTION FOR ABSOLUTE MOLAR MASS DETERMINATION IN SEC

As discussed in the previous section, the molecular weight of protein measured by column calibration in SEC may be erroneous due to the nonsize effect and the assumption that the conformation of the protein sample is the same as that of the standard proteins used for column calibration. Because of its ability to measure absolute molecular weight of protein eluted from the SEC column and easy interface with any SEC system, on-line multi-angle light scattering (MALS)

© 2004 by Marcel Dekker, Inc.

detection has gained increasing popularity among protein chromatographers during the past decade (72–76).

A MALS detector together with a concentration detector, typically UV or differential refractive index (DRI) detector, measures the molar mass of protein independent of the shape of the protein or the elution volume in SEC as demonstrated by Figs 3 and 4. In Fig. 4, the elution of protein X is much later than expected from its actual molecular weight, therefore prediction of the molecular weight of protein X from SEC elution volume alone would provide an erroneously low molecular weight. The theory and applications of MALS detection for polymer characterization are summarized elsewhere in this book.

More recently, therapeutic proteins are often modified with polymers, such as polysaccharides and polyethylene glycol, to reduce immunogenicity and the clearance rate from the body as well as to improve drug efficacy (77). The

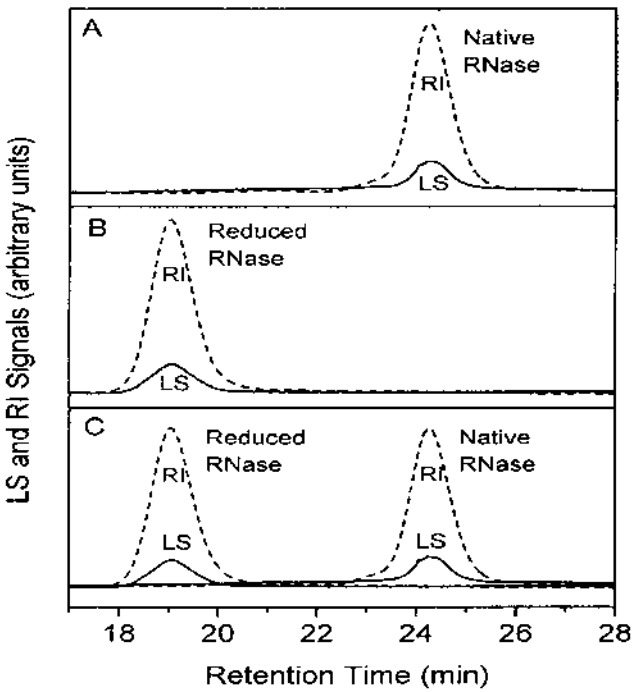

Figure 3 Chromatograms from native and reduced carboxymethylated RNase. Reduced RNA is unfolded with a more extended structure and thus eluted much earlier. Column calibration estimated a molecular weight of 41 kD. The combination of light-scattering and refractive index detectors determines the molecular weight of both reduced and native RNAse to be 13.7 kD, as theory suggests. (From Ref. 2.)

© 2004 by Marcel Dekker, Inc.

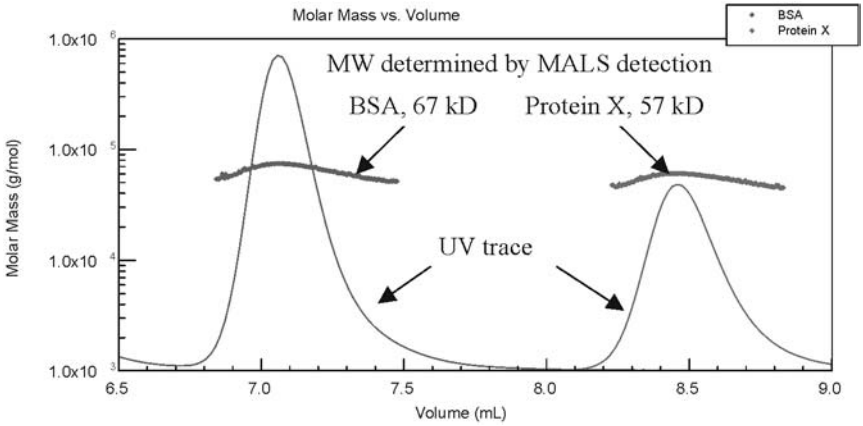

Figure 4 Chromatograms of BSA and Protein X obtained under identical SEC conditions. Owing to interaction with the stationary phase, Protein X eluted much later than the BSA monomer. MALS detection determined a molecular weight of 57 kD for Protein X, as expected from its sequence.

conformation of glycosylated or pegylated proteins are much more extended than the unmodified proteins but more dense than the free polysaccharides and polyethylene glycol. Therefore, molecular weight of the modified proteins measured by traditional column calibration with either protein or polymer standards will lead to significant errors (78). Wen and co-workers demonstrate the use of combining MALS, UV, and RI detectors to measure both the molecular weight of each component in the complex and the degree of modification (73).

6 PREPARATIVE PROTEIN SEC

The inherent effectiveness of SEC for large-scale protein purification is based on the equilibrium nature of the method, which results in high yields because little solute is denatured, and in predictability of elution once column parameters are known.

6.1 Applications

The first industrial application of SEC for protein solutions was for desalting dairy products (79). Large columns (2500 L) were used to separate proteins in whey or skim milk from low molecular weight sugars and salts. SEC is also used in the "de-ethanolization" of human serum albumin (HSA) (80) produced by the Cohn cold ethanol procedure. The purification of insulin was the first successful

© 2004 by Marcel Dekker, Inc.

industrial application of SEC for protein fractionation (81), followed by the fractionation of HSA proteins (82).

The term preparative SEC encompasses all forms and scales of SEC depending on requirements for the product. Preparative protein SEC has been categorized by the scale of the separation (83), which include the following.

1. Preparative–analytical: analytical columns (diameter <1 cm), single injection, microgram to milligram quantities prepared.
2. Semi-preparative: analytical columns (diameter 0.7–2 cm), multiple injections, milligram quantities prepared.
3. Standard–preparative: preparative columns (diameter 2–20 cm), single or multiple injections, milligram to gram quantities prepared.
4. Large-scale preparative: large preparative column (diameter ≥ 20 cm), automated injections, gram to kilogram quantities prepared.

The complexities of large-scale applications arise from the absolute requirements for optimal productivity (gram product/cm^2/hour), cost effectiveness, and product purity. There are many technical factors that affect these issues. Evaluating these factors for a given application is paramount to successfully utilizing SEC at the industrial scale.

Column diameter and length are primary factors affecting the scale of preparative SEC. For preparative separations, it is most cost-effective to operate at the highest sample loading and flow rate possible without loss of adequate resolution. In general, both the sample size and the flow rate can be increased proportionally to the column's cross-sectional area (Pharmacia). However, with soft gels, bed compression is a major factor for large-diameter columns, even at moderate flow rates (>50 cm/h). This compression imposes an additional physical limitation, beyond that of resolution, on the throughput that can be attained in scaling up from analytical columns using soft resins. Column length is also a major factor affecting productivity. The chromatographic resolution (R_{sc}) is weakly affected by the length ($R_{sc} \propto \sqrt{L}$), so doubling the bed length will only increase the R_{sc} by 40%. However, doubling the bed length will double the overall backpressure at a given flow rate. Moreover, R_{sc} is a weak inverse function of linear velocity, and in some preparative applications it may even be advantageous to the overall productivity to actually shorten the bed length and run at higher flow rates (84). This approach may be taken to a point of diminishing returns or to the physical flow limitations described above. In general, this optimum must be determined empirically for each resin and protein sample.

Sample loading is also important to the overall productivity of SEC. Different loadings are recommended for desalting ($\cong 30\%$ bed volume), and protein fractionation ($\leq 5\%$ bed volume). These loadings are low compared to other forms of chromatography, and tend to limit the use of SEC to the final (more

© 2004 by Marcel Dekker, Inc.

concentrated) steps of protein purification schemes. In fact, recent advances in ultrafiltration membrane technology have further limited the large-scale use of SEC for protein desalting. In many cases, SEC has been replaced by ultrafiltration as the more cost-effective method for buffer exchange in all but the most shear-sensitive proteins.

Resin particle size has a pronounced effect on chromatographic resolution and column backpressure. However, large-scale applications usually dictate that the only cost-effective choice of resin particles is for those with a diameter of $\geq 30\,\mu m$. It is important to realize this limitation before scaling up based on information gained from analytical resins ($d_p \leq 20\,\mu m$).

One issue of SEC unique to processes involving the production of parenteral drugs, and of many proteins, is that of validated resin regeneration. This is especially important for large-scale, cost-challenged processes, where resins must be reused hundreds of times. Resins used to purify proteins from bacterial sources must be depyrogenated (to remove cell wall fractions) while resins used to purify proteins from other sources must be disinfected (destruction of viruses, and so on). This can be carried out effectively by exposure to sodium hydroxide (85). Sodium hydroxide solutions have many advantages over organic solutions, including low cost, ease of disposal, and minimal risk of product contamination.

6.2 Selection of Resins

In all chromatographic work, the most critical choice before scale up is that of resin selection. The separation can never be better than the selectivity of a given packing material allows. Therefore, time spent on identifying the required selectivity for the separation and subsequent choice of the appropriate resin is invaluable. Once several resins have been identified as possibilities, empirical data, technical parameters, and cost must be considered in the final selection. Selected performance parameters are presented for modern SEC resins in Tables 2 to 5.

All of the resins described in Tables 2 to 5 have been utilized extensively for analytical protein purifications and those in Tables 2 to 4 have been successfully applied to preparative scale separation. Superdex® (Pharmacia) prep resins are an agarose/dextran composite (86) and became commercially available in late 1991. Superdex® resins are reported to have higher productivities than earlier gels because of the increased physical stability of agarose coupled with the steep selectivity of dextran. Note that the resins normally used for analytical-scale protein purifications display maximum linear flow rates much lower than the preparative resins. The new generation of preparative resins are smaller in size and more rigid than earlier materials, making rapid high-efficiency separations possible.

© 2004 by Marcel Dekker, Inc.

Table 2 Characteristics of Agarose and Agarose/Acrylamide Mixed Resins for Protein SEC

Support name and manufacturer	V_{max}[a]	Selectivity[b]	pH Stability	Particle size (μ)	Exclusion limit (kDt)
Sepharose®[c]					
6B	30	10–4000	4–9	45–165	
4B	26	60–20,000	4–9	45–165	
2B	15	70–40,000	4–9	60–200	
Sepharose®[c] CL					
6B	30	10–4000	3–14	45–165	
4B	26	60–20,000	3–14	45–165	
2B	15	70–40,000	3–14	60–200	
Superose[c] 12 Prep Grade	30	1–300	1–14	20–40	
Superose[c] 6 Prep Grade	30	5–5000	1–14	20–40	
Ultrogel[d]					
AcA202		1–15	3–10	60–140	22
AcA54		5–70	3–10	60–140	90
AcA44		10–130	3–10	60–140	200
AcA34		20–350	3–10	60–140	750
Bio-Gel[e]					
A-0.5 m	20	1–500	4–13	40–80	
A-1.5 m	20	1–1500	4–13	80–150	
A-5 m	20	10–500	4–13	150–300	
A-15 m	20	40–15,000	4–13		
A-50 m	15	100–50,000	4–13		

[a]Maximal linear velocity (cm/hr) for columns in the 1–6 cm diameter range.
[b]Selectivity is defined as the fractionation range for globular protein in Daltons.
[c]Amersham Biosciences Corp., 800 Centennial Ave., P.O. Box 1327, Piscataway, New Jersey 08855-1327.
[d]Ciphergen Biosystems, Inc., 6611 Dumbarton Circle, Fremont, California 94555.
[e]Bio-Rad Laboratories, 2000 Alfred Nobel Dr., Herules, California 94547.

6.3 Selection of Hardware

Once the most productive resin has been identified, an appropriately configured column must be selected. Information about the required throughput, sample volume, chemical resistance, and cycle time must be included in choice of column(s). Conventional preparative and process SEC columns (packed or empty) are available from Amicon/Wright (Danvers, MA), Pharmacia Biotechnology (Lund, Sweden), TosoHaas (Philadelphia, PA), and Millipore/Waters (Milford, MA). The Pharmacia Process Stack™ Column PS 370 is the most noteworthy

© 2004 by Marcel Dekker, Inc.

Table 3 Characteristics of Dextran-Based Resins for Protein SEC

Support name and manufacturer	V_{max}[a]	Selectivity[b]	pH stability	Particle size (μ)
Sephadex[c]				
G-10		< 0.7	2–13	40–120
G-25F	5	1–5	2–13	20–80
G-50F	5	1.5–30	2–13	20–80
G-75		3–80	2–13	20–100
G-100		4–100	2–13	100–300
G-150		5–300	2–13	
G-200		5–600	2–13	
PDX[d]				
G.F. 50–150		1–5		50–150
G.F. 50–150		1.5–30		50–150
G.F. 100–300		1.5–30		100–300
G.F. 100–300		1–5		100–300

[a]Maximal linear velocity (cm/hr) for columns in the 1–6 cm diameter range.
[b]Selectivity is defined as the fractionation range for globular protein in kDaltons.
[c]Amersham Biosciences Corp., 800 Centennial Ave., P.O. Box 1327, Piscataway, New Jersey 08855-1327.
[d]Polydex Biologicals.

because of the configuration and versatility of the stack (87). The stack may contain up to six individual columns (37 cm × 15 cm) connected in series. This translates into a 90-cm bed height or a 96-L total bed column. The separation of the total bed into a series of discrete 16-L beds allows high throughput and resolution by supporting the gel and alleviating the bed compression associated with large bed volumes, while introducing minimal band spreading.

Table 4 Characteristics of Acrylamide and Porous Polystyrene Based Resins for Protein SEC

Support name and manufacturer	Selectivity[a]	pH stability	Particle size (μ)	Exclusion limit (kDt)
Trisacryl[b]				
GF05, M	0.2–2.5	1–11	40–80	3
GF05, LS	0.2–2.5	1–11	80–160	3
GF2000, M	10–15	1–11	40–80	20
GF2000, LS	10–15	1–11	80–160	20

[a]Selectivity is defined as the fractionation range for globular protein in kDaltons.
[b]Ciphergen Biosystems, Inc., 6611 Dumbarton Circle, Fremont, California 94555.

© 2004 by Marcel Dekker, Inc.

Table 5 Characteristics of Silica-Based Resins for Protein SEC

Support name and manufacturer	Selectivity[a]	pH stability	Particle size (μ)	Exclusion limit (kDt)
TSK-GEL[b]				
G2000SW	0.5–600	2.5–7.5	10	
G3000SW	1–300	2.5–7.5	10	
G4000SW	5–1000	2.5–7.5	13	
Synchropak[c] GPC 100A	3–630		5	
BioSep[c]				
S2000	1–300	2.5–7.5	5	
S3000	5–700	2.5–7.5	5	
S4000	15–2000	2.5–7.5	5	
Protein-Pak[d]				
60	1–20	2–8	10	
125	2–80	2–8	10	
200SW	0.5–60	2–8	10	
300SW	10–300	2–8	10	
Lichrosorb Diol[e]	0.8–450	2–8	10	
Shodex[f]				
KW-802.5	0.1–50	3–7.5	5	150
KW-803	0.1–150	3–7.5	5	700
KW-804	0.5–600	3–7.5	7	1000
Zobax[g]				
GF-250	4–400	3–8.5	4	
GF-450	10–900	3–8.5	6	

[a]Selectivity is defined as the fractionation range for globular protein in kDaltons.
[b]TOSOH Biosep LLC, 156 Keystone Drive, Montgomeryville, Pennsylvania 18936.
[c]Phenomenex U.S.A., 2320 W. 205th St., Torrance, California 90501-1456.
[d]Waters Corporation, 34 Maple St., Milford, Massachusetts 01757.
[e]Varian Inc., 2700 Mitchell Dr., Walnut Creek, California 94598.
[f]Showa Denko K.K., Tokyo, Japan.
[g]Agilent Headquarters, 395 Page Mill Rd., P.O. Box #10395, Palo Alto, California 94303.

Finally, process automation is also essential for efficient, reproducible, preparative SEC of proteins. Several companies produce automated chromatography systems equipped for preparative sanitary protein SEC. The Dorr-Oliver Protein LC™, Pharmacia BioProcess™ and BioPilot™, TosoHaas Protein Prep LC™, Separations Technologies (Wakefield, RI) Pilot/Production Preparative HPLC, Millipore Kiloprep™ LC, and Waters KiloPrep™ systems are all fully automated liquid chromatography systems designed to support "turn-key"

© 2004 by Marcel Dekker, Inc.

preparative SEC. The capabilities of these systems range from low-throughput, high-resolution preparative HPLC systems to low-pressure, high-throughput, skid-mounted systems. These systems can be custom designed to a limited extent, however.

7 MICROBORE SEC

Although microbore SEC has been used routinely for GPC (primarily in organic solvents) and products are available from MZ-Analysentechnik GmbH, only Pharmacia offers microbore prepacked columns for SEC of proteins. For the SMART^{TM} Chromatography System, Pharmacia offers Superdex 75 and 200 and Superose 6 and 12 in Precision Columns (PC) 3.2 × 30 cm columns. Using the SMART System, Superdex 75 is excellent for separating monomeric and dimeric forms of lower molecular weight recombinant proteins and peptides. Superdex 200 is designed to separate larger protein molecules, including antibodies, and nucleic acids up to 200 base pairs. These MPSEC media are prepacked with 13 μm media.

Most narrow-bore columns have an inner diameter (ID) of 4.6 mm, directly between the standard-analytical columns with 8 mm inner diameter and the microbore columns are usually 3 mm, 2 mm, or 1.6 mm in ID. While the microbore columns can only be used in specially equipped chromatography hardware, the narrow-bore columns may directly be run (with modest optimization) in standard equipment. The use of reduced-bore columns instead saves up to 70% of eluent and narrow-bore columns are less sensitive to variations in flow and require less sample. They also show a more flat MW calibration curve than analytical columns. There is ample evidence that narrow and microbore columns give excellent SEC separations.

8 ACKNOWLEDGEMENTS

The authors again wish to dedicate this work to the memory of Phil G. Squire. His passion for gel filtration began with a visit to Uppsala in 1960, before widespread interest in the field of column chromatography ignited. This work was funded by the U.S. Department of Energy Office of the Biomass Program.

REFERENCES

1. Discuss Faraday Soc 7:114, 1949.
2. L Hagel, J-C Janson. In: E Heftmann, ed. Chromatography, Part A: Fundamentals and Techniques. Vol. 51A, Amsterdam: Elservier, 1992, pp A267–A307.
3. J Porath, P Flodin. Nature 183:1647, 1959.

© 2004 by Marcel Dekker, Inc.

4. KA Granath, P Flodin. Macromol Chem 48:160, 1961.
5. J Porath. Lab Pract 16:838, 1967.
6. DD Bly. In: B Carroll, ed. Gel Permeation Chromatography in Polymer Chemistry, Physical Methods in Macromolecular Chemistry. Vol. 2. New York, NY: Dekker, 1972.
7. WW Yau, JJ Kirkland, DD Bly. Modern Size Exclusion Chromatography. New York, NY: Wiley, 1979.
8. HG Barth. J Chromatogr Sci 18:409, 1980.
9. JC Giddings. In: JC Giddings, E Grushka, J Cazes, PR Brown, eds. Advances in Chromatography, Vol. 20, New York, NY: Marcel Dekker, 1982, p 217.
10. FE Regnier. Adv Enzymol 91:137, 1983.
11. PL Dubin, JM Principi. Macromolecules 22:1891, 1989.
12. KM Gooding, FE Regnier. HPLC of Biological Macromolecules. New York, NY: Marcel Dekker, 1990.
13. HG Barth, BE Boyes, C Jackson. Anal Chem 70:251R, 1998.
14. RC Montelaro. In: PL Dubin, ed. Aqueous Size Exclusion Chromatography. Amsterdam, The Netherlands: Elsevier, 1988, p 269.
15. KK Unger, JN Kinkel. In: PL Dubin, ed. Aqueous Size Exclusion Chromatography. Amsterdam, The Netherlands: Elsevier, 1988, p 193.
16. K Makino, H Hatano. In: PL Dubin, ed. Aqueous Size Exclusion Chromatography. Amsterdam, The Netherlands: Elsevier, 1988, p 235.
17. KM Gooding, HH Freiser. In: CT Mant, RS Hodges, eds. High Performance Liquid Chromatography of Peptides and Proteins. Boca Raton, FL: CRC Press, 1991, p. 135.
18. GW Welling, S Welling-Wester. In: CT Mant, RS Hodges, eds. High Performance Liquid Chromatography of Peptides and Proteins. Boca Raton, FL: CRC Press, 1991, p. 155.
19. J Porath. Biochem Biophys Acta 39:193, 1960.
20. P Andrews. Nature 196:36, 1962.
21. PG Squire, A Magnus, ME Himmel. J Chromatogr 242:255, 1982.
22. WW Yau, CP Malone, SW Fleming. J Polym Sci 6:803,1968.
23. WW Yau, HL Suchan, CP Malone. J Polym Sci 6:1349, 1968.
24. WW Yau, CP Malone, HL Suchan. Sep Sci 5:259, 1970.
25. JV Dawkins. J Polymer Sci 14:569, 1976.
26. JR Whitaker. Anal Chem 35:1950, 1963.
27. Sephadex Filtration in Theory and Practice. Pharmacia Fine Chemicals, Uppsala, Sweden, 1979.
28. P Andrews. Biochem J 96:595, 1965.
29. AG Ogston. Trans Faraday Soc 54:1754, 1958.
30. PG Squire. Arch Biochem Biophys 107:471, 1964.
31. TC Laurent, J Killander. J Chromatogr 14:317, 1964.
32. JC Giddings, E Kucra, CP Russell, MN Meyers. J Phys Chem 72:4397, 1968.
33. ED Glandt. J Colloid Interface Sci 77:512, 1980.
34. EF Cassassa, Y Tagami. Macromolecules. 2:14, 1969.
35. C Tanford. Physical Chemistry of Macromolecules. New York, NY: Wiley, 1961.
36. ME Himmel, PG Squire. Int J Peptide Protein Res 17:365, 1981.

© 2004 by Marcel Dekker, Inc.

37. GR Noll, N Nagle, JO Baker, DJ Mitchell, K Grohmann, ME Himmel. J Liq Chromatogr 13:703, 1990.
38. ME Himmel, PG Squire. In: PL Dubin, ed. Aqueous Size Exclusion Chromatography. Amsterdam, The Netherlands: Elsevier, 1988, p 3.
39. TS Burcham, DT Osuga, H Chino, RE Feeney. Anal Biochem 139:197, 1984.
40. M Dennis, C Lazure, NG Seidah, M Chretien. J Chromatogr 266:163, 1983.
41. C Lazure, M Dennis, J Rochemont, NG Seidah, M Chretien. Anal Biochem 125:406, 1982.
42. JG Bindels, HJ Hoenders. J Chromatogr 261:381, 1983.
43. M Potschka. Anal Biochem 162:47, 1987.
44. PL Dubin, JM Principi. Macromolecules 22:1891, 1989.
45. JL Oncley. In: EJ Cohn, JT Edsall, eds. Proteins, Amino Acids, and Peptides. New York, NY: Reinhold, 1943, Ch. 22.
46. F Perrin. J Phys Radium 7:1, 1936.
47. RO Herzog, R Illig, H Kudar. Z Phys Chem A167:329, 1934.
48. PG Squire, ME Himmel. Arch Biochem Biophys 196:165, 1979.
49. W Kopaciewicz, FW Regnier. In: MTW Hearn, FE Regnier, CT Wehr, eds. High-Performance Liquid Chromatography of Proteins and Peptides: Proceedings of the First International Symposium, Washington, DC, 1981. New York: Academic Press, 1983, p. 151.
50. JE Dyr, J Suttnar. J Chromatogr 408:303, 1987.
51. R Majuri. J Chromatogr 387:281, 1987.
52. W Flapper, AGM Theeuwes, JTG Kierkels, J Steenbergen, HJ Hoenders. J Chromatogr 533:47, 1990.
53. LG Daignault, DC Jackman, DP Rillema. J Chromatogr 462:71, 1989.
54. Y-B Yang, FE Regnier. J Chromatogr 544:233, 1991.
55. B-L Johansson, J Gustavsson. J Chromatogr 457:205, 1988.
56. I Drevin, L Larsson, I Eriksson, and B-L Johansson. J. Chromatogr. 514:137, 1990.
57. KM Gooding, HH Freiser. In: CT Mant, RS Hodges, eds. High-Performance Chromatography of Peptides and Proteins: Separation, Analysis, and Conformation. Boca Raton, FL: CRC Press, 1991, p. 135.
58. M Potschka. J Chromatogr 441:239, 1988.
59. RD Ricker, LA Sandoval. J Chromatogr A 743:43, 1996.
60. PL Dubin. In: PL Dubin, ed. Aqueous Size-Exclusion Chromatography. New York: Elsevier, 1988, p 55.
61. VA Romano, T Ebeyer, PL Dubin. In: M Potshka, PL Dubin, eds. Strategies in Size-Exclusion Chromatography. ACS Symp Ser, 635, 1996, p 88.
62. W Kopaciewicz, MA Rounds, J Fausnaugh, FE Regnier. J Chromatogr 266:3, 1983.
63. JM Park, BB Muhoberac, PL Dubin, J Xia. Macromolecules 25:290, 1992.
64. K Inouye. Agric Biol Chem 55:2129, 1991.
65. L Kagedal, B Engstrom, H Ellegren, A-K Lieber, H Lundstrom, A Skold, M Schenning. J Chromatogr 537:17, 1991.
66. RM Chicz, FE Regnier. Methods Enzymol 182:392, 1990.
67. MA Cohen Stuart, GJ Fleer, J Lyklema, W Norde, JMHM Schleutjens. Adv Colloid Interface Sci 34:477, 1991.

© 2004 by Marcel Dekker, Inc.

68. A Sadana, RR Raju. Bioseparation 1:119, 1990.
69. K Benedek, S Dong, BL Karger. J Chromatogr 317:227, 1984.
70. JL McNay, EJ Fernandez. Biotechnol Bioeng 76:225, 2001.
71. K Benedek. J Chromatogr 646:91, 1993.
72. H Zhu, DW Ownby, CK Riggs, NJ Nolasco, JK Stoops, AF Riggs. J Bio Chem 271:30007–30021, 1996.
73. J Wen, T Arakawa, JS Philo. Anal. Biochem. 240:155–166, 1996.
74. PJ Wyatt. LC-GC, 15:160–168, 1997.
75. E Folta-Stogniew, KR Williams. J Biomol Techniques 10(2):51–63, 1999.
76. RL Woodbury, SJS Hardy, LL Randall. Protein Sci 11:875–882, 2002.
77. MJ Knauff, DP Bell, P Hirtzer, ZP Luo, JD Young, NV Katre. J Biol Chem 263:15064–15070, 1988.
78. IL Koumenis, Z Shahrokh, S Leong, V Hsei, L Deforge, G Zapata. Int J Pharmaceutics 198:83–95, 2000.
79. LO Lindquist, KW Williams. Dairy Ind Int 38:459, 1973.
80. H Friedli, P Kistler. Chimia 26:25, 1972.
81. J-C Janson. Agric Food Chem 19:581, 1971.
82. JM Curling. In: JM Curling, ed. Methods of Plasma Protein Fractionation. London, UK: Academic Press, 1980, p. 77.
83. GL Hagnauer. In: BA Bidlingermeyer, ed. Preparative Liquid Chromatography. New York, NY: Elsevier, 1987, p. 289.
84. Gel Filtration: Theory and Practice, Pharmacia Fine Chemicals, Rahms i Lund, Sweden, 1984, p. 45.
85. GK Sofer, L-E Nystrom, eds. Process Chromatography: A Practical Guide. New York, NY: Academic Press, 1989, p. 93.
86. Downstream. Piscataway, NJ: Pharmacia LKB Biotechnologies, No. 7, 1990.
87. Process Stack Column. Piscataway, NJ: Pharmacia LKB Biotechnology, Data file No. 5040, 1990.

© 2004 by Marcel Dekker, Inc.

16
Size Exclusion Chromatography of Nucleic Acids

Yoshio Kato
TOSOH Corporation
Yamaguchi, Japan

Shigeru Nakatani
TOSOH Bioscience LLC
Montgomeryville, Pennsylvania, U.S.A.

1 INTRODUCTION

Conventional size exclusion chromatography (SEC) has been employed for a long time for the separation and purification of nucleic acids, but it has not been very successful. High-performance SEC, however, was applied to the separation of nucleic acids in 1979 (1), and the performance in SEC of nucleic acids was greatly improved. As a result, SEC became one of the effective methods to separate various types of nucleic acids according to molecular size. Since then, successful separations of RNAs (1–9), DNA fragments (8–18), plasmids (18–24), and oligonucleotides (25) have been reported. In this chapter, separations of these types of nucleic acids by high-performance SEC and guidelines to optimize chromatographic conditions are described.

2 RNA

SEC has been applied to various types of RNA, such as transfer RNA (tRNA), ribosomal RNA (rRNA), messenger RNA (mRNA), and retroviral genomic RNA.

© 2004 by Marcel Dekker, Inc.

Although there are a variety of species in tRNA, their molecular weights are in a narrow range, approximately 25,000–30,000. Therefore, it is rather difficult to separate different species of tRNA by SEC. Single peaks are usually observed in SEC of tRNA samples even if they contain many species. Only one example of the separation of tRNA species has been reported. Two species, tyrosine-specific and *N*-formylmethionyl-specific tRNAs, were separated on a MicroPak TSK 3000SW column (30 cm × 7.5 mm inner diameter, ID), although only partially (1). However, it is easy to separate tRNA from other types of RNA such as rRNA, as exemplified in Fig. 1. tRNA was separated from rRNA on a TSKgel G3000SW two-column system (each column 60 cm × 7.5 mm ID).

Separation of different species of rRNA is also easy. Figure 2 shows an example of the separation of 5S, 16S, and 23S rRNAs, whose molecular weights are approximately 39,000, 560,000, and 1,100,000; they were separated well on a TSKgel G4000SW two-column system (each column 60 cm × 7.5 mm ID) in

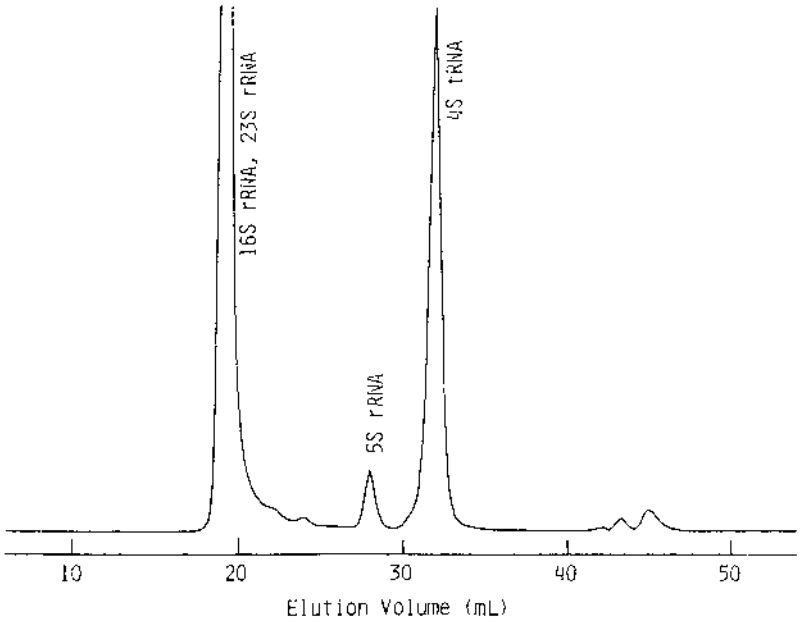

Figure 1 Separation of total *E. coli* RNAs containing 4s tRNA and 5S, 16S, and 23S rRNAs obtained on a TSKgel G3000SW two-column system (each column 60 cm × 7.5 mm ID) in 0.1 M phosphate buffer (pH 7.0) containing 0.1 M sodium chloride and 1 mM EDTA at a flow rate of 1 mL/min. (From Ref. 9.)

© 2004 by Marcel Dekker, Inc.

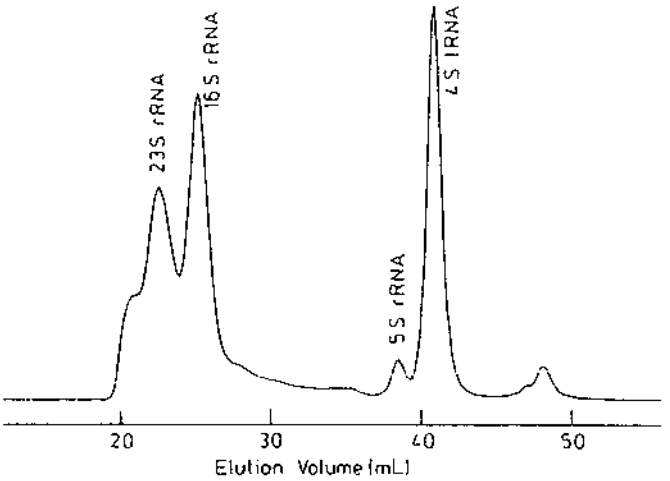

Figure 2 Separation of total *E. coli* RNAs containing 4S tRNA and 5S, 16S, and 23S rRNAs obtained on a TSKgel G4000SW two-column system (each column 60 cm × 7.5 mm ID) in 0.1 M phosphate buffer (pH 7.0) containing 0.1 M sodium chloride and 1 mM EDTA at a flow rate of 1 mL/min. (From Ref. 8.)

about 40 minutes. Although the separation between 16S and 23S rRNAs seems insufficient, this is a result of other components eluting at the same position as the rRNAs. A pure mixture of 16S and 23S rRNAs was separated almost completely. The 5S and 5.8S rRNAs with approximate chain lengths of 120 and 158 were also separated well on a TSKgel G3000SW column (60 cm × 7.5 mm ID) in about 20 minutes (2).

Samples of mRNA usually contain many components whose molecular weights differ continuously in a rather wide range. Consequently, single broad peaks are usually obtained in the SEC of mRNA mixtures. However, it has been confirmed by an *in vitro* translation test of the fractionated mRNA samples that the separation of mRNA is roughly based on molecular size (3,6). mRNA easily aggregates in nondenaturing buffers, which results in inferior resolution. Therefore, it is recommended to separate mRNA under denaturing conditions in the presence of 6 M urea. Under denaturing conditions, aggregation formation is avoided and the resolution is considerably improved (3,6). SEC under denaturing conditions has a resolution equivalent to or even better than that of sucrose gradient centrifugation, which has been the most common method to separate mRNA.

Satisfactory separation has also been obtained for small nuclear RNAs on UltroPac TSK SW type columns (4).

© 2004 by Marcel Dekker, Inc.

A retroviral genomic RNA of approximately 16,600 bases has successfully been purified from viral lysate on Spherogel TSK 6000PW (7). In spite of its long chain length, the retroviral RNA was not excluded in the void volume of the column, probably due to the tridimensional structure, and it was separated from other components. The preparation of the genomic RNA was 20 times more efficient than the sucrose gradient ultracentrifugation in terms of yield.

According to the test for loading capacity in SEC on columns of 7.5 mm ID, RNA samples could be applied without a decrease in resolution up to a few milligrams (5).

3 DNA FRAGMENTS

DNA fragments of up to approximately 7,000 base pairs have successfully been separated by SEC. Figure 3 shows chromatograms of HaeIII-cleaved plasmid pBR322 obtained on column systems consisting of two TSKgel G3000SW columns or two G4000SW columns (each column 60 cm × 7.5 mm ID). The numerals above the peaks represent the base pairs of DNA fragments contained in the peaks. On G3000SW, DNA fragments of less then 124 base pairs were well separated, whereas larger DNA fragments were eluted together in the void volume of the column system (approximately 20 mL). On G4000SW, DNA fragments up to 267 base pairs were separated. According to these results, it can be said that relatively small DNA fragments can be separated by SEC if they differ by more than 10% in chain length. The chain length of DNA fragments is plotted against elution volume in Fig. 4. The average chain lengths were used for peaks containing more than one DNA fragment. The results demonstrate that DNA fragments were separated according to their chain length. Therefore, it is possible not only to purify fragments but also to estimate the chain length of unknown DNA fragments. Figure 5 shows the separation of larger DNA fragments. A mixture of EcoRI-cleaved plasmid pBR322 and BstNI-cleaved plasmid pBR322 was separated on a TSKgel DNA-PW four-column system (each column 30 cm × 7.8 mm ID). The sample contains seven fragments of 13, 121, 383, 928, 1,060, 1,857, and 4,362 base pairs. Peaks a–f contained fragments of 4,362 (a), 1,857 (b), 1,060 and 928 (c), 383 (d), 121 (e), and 13 (f) according to polyacrylamide gel electrophoresis of collected eluates corresponding to the peaks. Although two fragments of 928 and 1,060 base pairs were eluted together as one peak, all the other fragments were well separated from each other. The separations of 1,060 and 1,857 base pair fragments and of 1,857 and 4,362 base pair fragments were also almost complete. This means that even fragments of greater than 1000 base pairs can be separated with little cross-contamination, provided that the chain length of one is more than twice that of the other. The void volume of the column system was determined with λ-DNA. The exclusion limit of

© 2004 by Marcel Dekker, Inc.

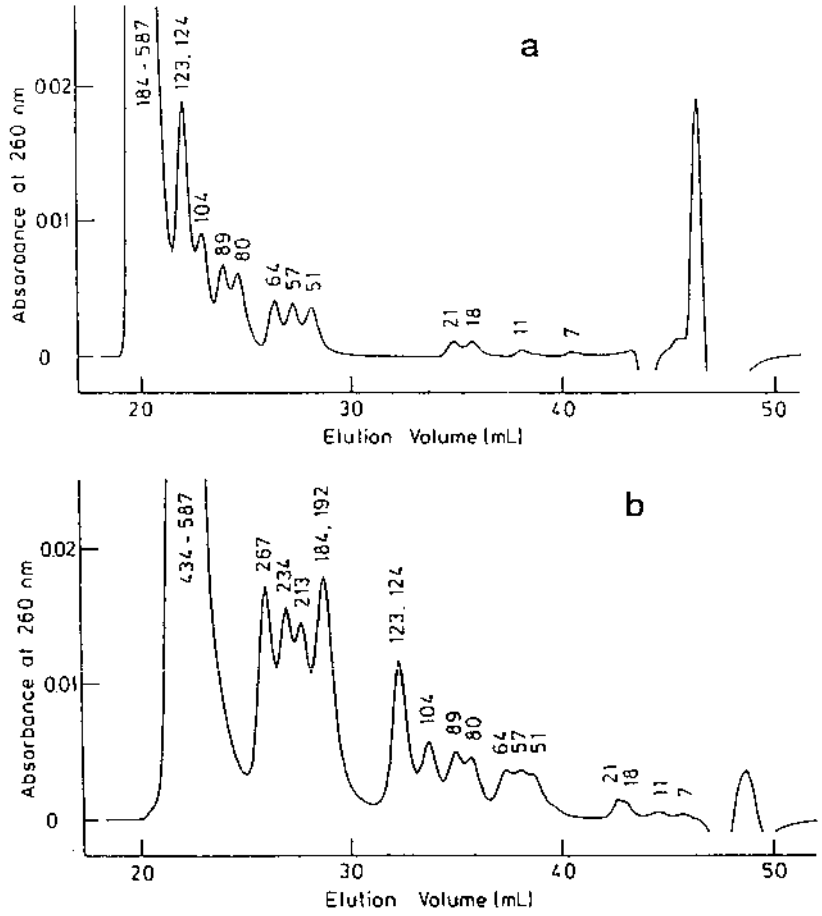

Figure 3 Separation of HaeIII-cleaved pBR322 obtained on a TSKgel G3000SW two-column system at a flow rate of 1 mL/min (a) or on a TSKgel G4000SW two-column system at a flow rate of 0.33 mL/min (b) (each column 60 cm × 7.5 mm ID) in 0.05 M Tris–HCl buffer (pH 7.5) containing 0.2 M sodium chloride and 1 mM EDTA. (From Ref. 11.)

TSKgel DNA-PW estimated by utilizing the value of void volume was approximately 7,000 base pairs. Therefore, SEC should be very useful in the field of genetic engineering, in which the separation of large DNA fragments in the range of 1,000–5,000 is important. However, it seems that DNA fragments larger than 7,000 base pairs cannot be separated at present because no commercially available aqueous SEC columns have higher exclusion limits than TSKgel DNA-PW.

© 2004 by Marcel Dekker, Inc.

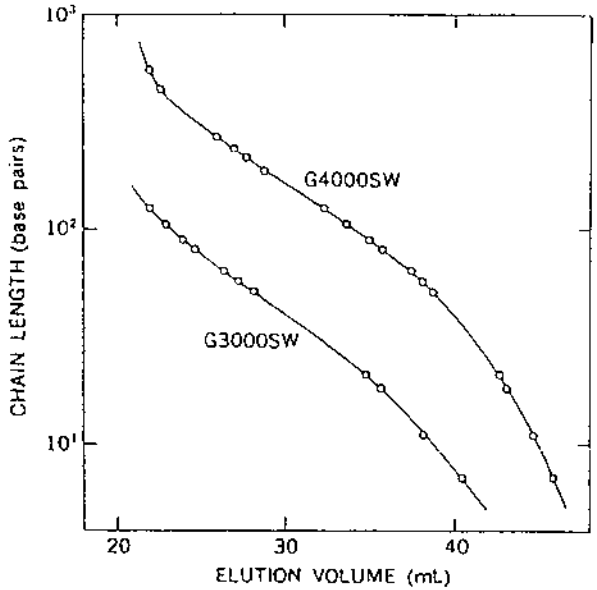

Figure 4 Plots of chain length against elution volume for double-stranded DNA fragments obtained in SEC on TSKgel G3000SW and TSKgel G4000SW in Fig. 3. (From Ref. 11.)

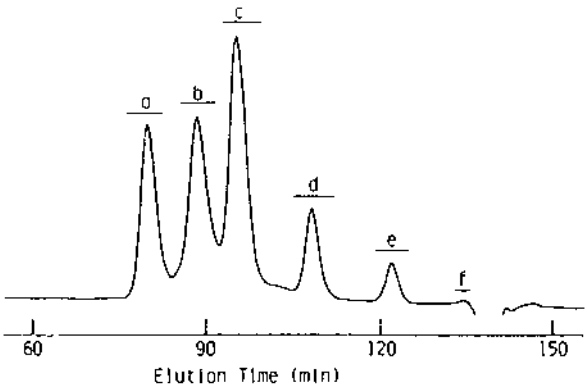

Figure 5 Separation of a mixture of EcoRI-cleaved plasmid pBR322 and BstNI-cleaved plasmid pBR322 obtained on a TSKgel DNA-PW four-column system (each column 30 cm × 7.8 mm ID) in 0.1 M Tris–HCl buffer (pH 7.5) containing 0.3 M sodium chloride and 1 mM EDTA at a flow rate of 0.3 mL/min. (From Ref. 12.)

© 2004 by Marcel Dekker, Inc.

The recovery of DNA fragments has been reported to be almost quantitative (10,11).

4 PLASMIDS

Recently, there has been an increasing interest in the purification of plasmids for use as vectors in gene therapy. Plasmid-mediated gene delivery systems, in which plasmids are injected directly, should be a good alternative to viral-mediated gene delivery systems, due to the potential safety and simple delivery of the gene. The use of plasmids in clinical trials requires the reproducible and scalable production process of highly purified plasmids to meet regulatory criteria for manufacturing of biopharmaceuticals. The purification of plasmids has been traditionally performed by extraction with toxic reagents and CsCl gradient centrifugation. The purification process using SEC, however, would eliminate these undesirable reagents for the clinical use of plasmids.

SEC has been applied to the purification of various forms of plasmids. It is possible to obtain plasmid free of proteins, RNA, and chromosomal DNA from cleared lysate of *Escherichia coli* cells. Figure 6 shows an example of the purification of plasmid. Cleared lysate of *E. coli* cells containing amplified

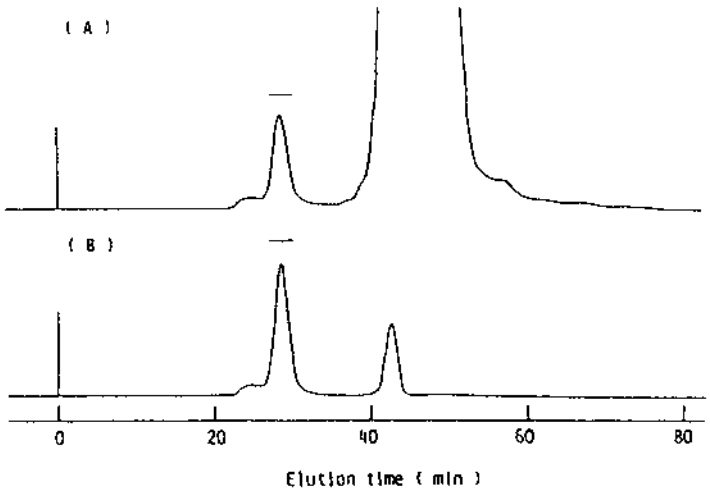

Figure 6 Separation of cleared lysate of *E. coli* cells (A) and its phenol extract (B) obtained on a TSKgel G6000PW two-column system (each column 60 cm × 7.5 mm ID) in 0.1 M Tri–HCl buffer (pH 7.5) containing 0.3 M sodium chloride and 1 mM EDTA at a flow rate of 1 mL/min. (From Ref. 21.)

© 2004 by Marcel Dekker, Inc.

plasmid pBR322 and its phenol extract were separated on a TSKgel G6000PW two-column system (each column 60 cm × 7.5 mm ID). Plasmid pBR322 was eluted between 27 and 31 minutes and was perfectly separated from RNA and proteins, which were eluted after 36 minutes. Chromosomal DNA was also removed fairly well, but not completely, because it was eluted continuously after 22 minutes. The purities of plasmid fractions collected from cleared lysate and phenol extract were almost equivalent. The phenol extract sample was treated with ATP-dependent deoxyribonuclease to digest linear double-stranded DNA-like chromosomal DNA and was subjected to SEC on a TSKgel G6000PW column (30 cm × 7.5 mm ID). The result is shown in Fig. 7. The chromatogram suggests that chromosomal DNA was almost completely eliminated from the plasmid fraction. According to a purity test by agarose gel electrophoresis, the collected plasmid fraction was free of RNA, proteins, and chromosomal DNA. The separation between plasmid and other components was sufficient even when a 0.5 mL solution of the enzyme-treated phenol extract was applied to a column of 30 cm × 7.5 mm ID and the separation was completed in about 15 minutes.

The major contaminants in the plasmid fraction obtained by SEC are generally high molecular weight species such as *E. coli* chromosomal DNA and rRNAs. The careful preparation of cell lysate would reduce the level of these contaminants and, as a result, make it easy to separate these contaminants from plasmids by SEC. The yields of plasmids would also be affected by the preparation step of cell lysate (22).

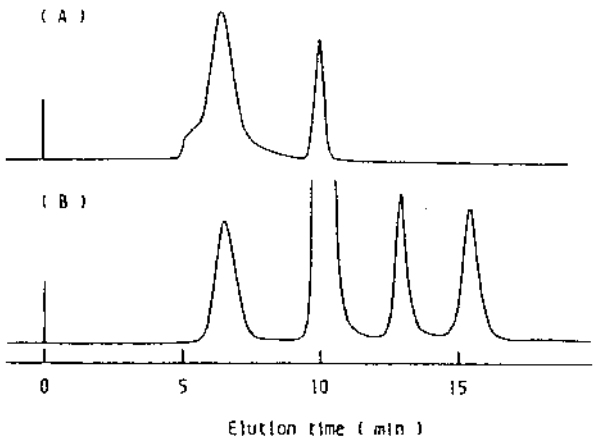

Figure 7 Separation of phenol extract of cleared lysate of *E. coli* cells before (A) and after (B) treatment with ATP-dependent deoxyribonuclease on a TSKgel G6000PW column (30 cm × 7.5 mm ID) in 0.1 M Tris–HCl buffer (pH 7.5) containing 0.3 M sodium chloride and 1 mM EDTA at a flow rate of 1 mL/min. (From Ref. 21.)

© 2004 by Marcel Dekker, Inc.

Endotoxin should also be removed from the plasmid fraction, especially in clinical use. SEC could effectively remove endotoxin from the plasmid fraction for use in a clinical trial (24).

From the partially purified plasmid, the separation of the supercoiled form and the nicked or the relaxed form was achieved by SEC (20), although the importance of the supercoiled form for clinical use is still under investigation.

5 OLIGONUCLEOTIDES

SEC has also been applied to oligonucleotides. However, there have not been many applications of SEC to oligonucleotide separation because SEC generally has a considerably lower resolution than other modes of high-performance liquid chromatography such as reversed-phase and ion-exchange chromatography. One example of the separation of oligonucleotide is shown in Fig. 8. A mixture of oligodeoxyadenylic acids was separated on a TSKgel G2000SW two-column system (each column 60 cm × 7.5 mm ID). It is also possible to separate other types of homogeneous oligonucleotides, such as oligodeoxythymidylic acid, and heterogeneous oligonucleotides by SEC.

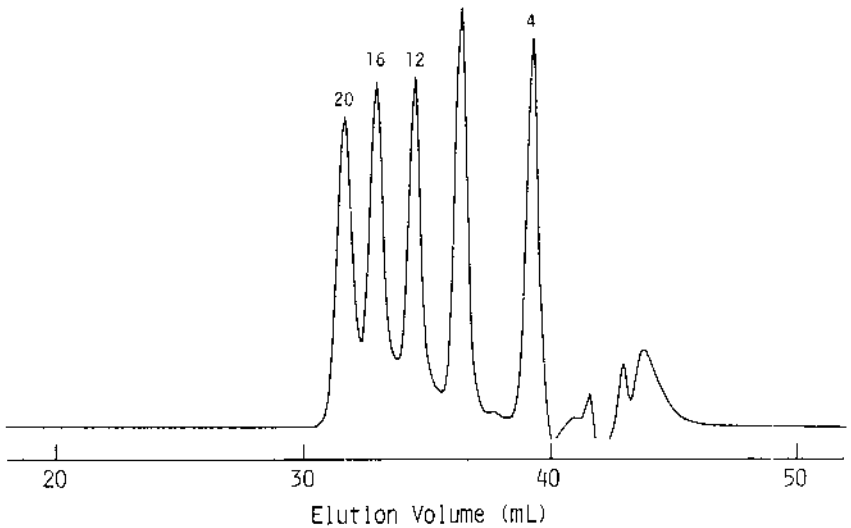

Figure 8 Separation of a mixture of oligodeoxyadenylic acids with chain lengths of 4, 8, 12, 16, and 20 nucleotides on a TSKgel G2000SW two-column system (each column 60 cm × 7.5 mm ID) in 0.1 M phosphate buffer (pH 7.0) containing 0.1 M sodium chloride and 1 mM EDTA at a flow rate of 1 mL/min. (Y Kato, unpublished data.)

© 2004 by Marcel Dekker, Inc.

Table 1 Exclusion Limits of TSKgel SW and PW Columns for RNA and Double-Stranded DNA Fragments[a]

	Exclusion limit (molecular weight)	
Column	RNA	Double-stranded DNA fragment
G2000SW	70,000	50,000 (70)[b]
G3000SW	150,000	100,000 (150)
G4000SW	1,500,000	300,000 (500)
G5000PW	>5,000,000	1,000,000 (1,500)
G6000PW	—[c]	5,000,000 (7,000)
DNA-PW	—[c]	5,000,000 (7,000)

[a]In 0.1 M phosphate buffer (pH7.0) containing 0.1 M sodium chloride and 1 mM EDTA.
[b]Values in parentheses are the exclusion limits in base pairs.
[c]Not determined.
Source: Refs. 8 and 12.

6 COLUMNS

Two types of columns have been employed in the SEC of nucleic acids: chemically bonded porous silica columns and hydrophilic resin columns. Among them, TSKgel SW and PW columns have been well accepted. They are available in different pore sizes, and each has a different separation range. The exclusion limits for RNA and double-stranded DNA fragment are listed in Table 1. A sample of a certain molecular weight can be in general separated on different columns. However, the resolution depends on the column employed. For example, in the separation of HaeIII-cleaved plasmid pBR322, the best separation is obtained for base pairs of 7–21, 51–104, 123–267, and 434–587 on G2000SW, G3000SW, G4000SW, and G5000PW, respectively. Therefore, it is very important to select the best column depending on the molecular weights

Table 2 Best Columns for the Separation of RNA

Molecular weight range	Best column
<60,000	G2000SW or G3000SW
60,000–120,000	G3000SW
120,000–1,200,000	G4000SW
1,200,000–10,000,000	G5000PW

Source: Ref. 8.

© 2004 by Marcel Dekker, Inc.

Table 3 Best Columns for the Separation of Double-Stranded DNA Fragments

Molecular weight range	Best column
$<$40,000 ($<$60)[a]	G2000SW or G3000SW
40,000–80,000 (60–120)	G3000SW
80,000–250,000 (120–400)	G4000SW
250,000–800,000 (400–1,200)	G5000PW
800,000–5,000,000 (1,200–7,000)	G6000PW or DNA-PW

[a]Values in parentheses are ranges in base pairs.
Source: Ref. 8.

of the samples to be separated. Tables 2 and 3 summarize the best columns in relation to molecular weight range.

7 ELUANT

Eluant ionic strength affects the elution volume and resolution in the SEC of nucleic acids, and therefore it must be properly adjusted to obtain good results. Figure 9 shows the effect of eluant ionic strength on the elution volumes obtained on TSKgel G3000SW, G4000SW, and G5000PW columns. Elution of both RNA and DNA fragments is delayed by increasing the eluant ionic strength. Elution volumes vary greatly in the low ionic strength region, but at high ionic strength the elution volumes seem to become constant. Furthermore, the elution volumes of small molecules are more markedly affected than those of large molecules. The peak widths broaden with increasing eluant ionic strength, although slightly. Accordingly, in general, an eluant ionic strength of 0.3–0.5 may be optimum. When an eluant of low ionic strength is used, the exclusion limits of the columns are considerably lowered. The main source of variation in elution volume with eluant ionic strength is probably the repulsive ionic interaction between samples and column packing materials, because both nucleic acids and TSKgel SW and PW are negatively charged. TSKgel SW is based on silica and contains some residual silanol groups on its surface, whereas TSKgel PW is based on hydrophilic synthetic resin and contains some carboxyl groups. Most other commercially available columns for aqueous SEC are also negatively charged, and the phenomenon of increasing elution volume with increasing eluant ionic strength has been observed on them, too. Other sources may also be responsible in some cases. For example, elution volumes increase regularly with eluant ionic strength, even in the high ionic strength region, where ionic interactions should diminish, in the case of 16S and 23S rRNAs (see 16S rRNA in Fig. 9b). The retardation of

© 2004 by Marcel Dekker, Inc.

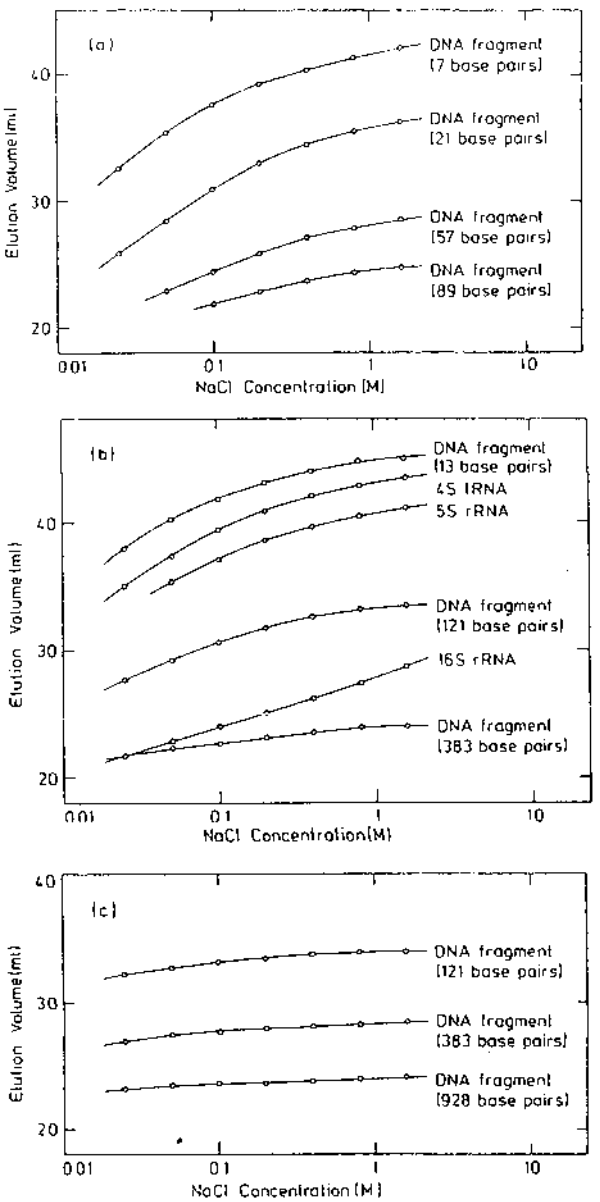

Figure 9 Dependence of elution volume on eluant ionic strength obtained on TSKgel G3000SW (a), G4000SW (b), and G5000PW (c) two-column systems (each column 60 cm × 7.5 mm ID) in 0.01 M Tris–HCl buffer (pH 7.5) containing 0.025–1.6 M sodium chloride and 1 mM EDTA at a flow rate of 1 mL/min. (From Ref. 8.)

© 2004 by Marcel Dekker, Inc.

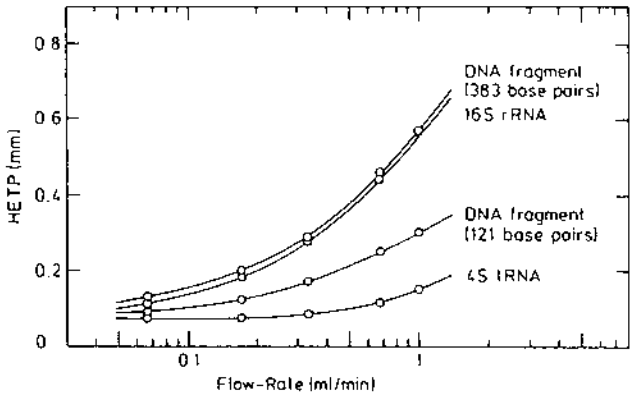

Figure 10 Dependence of HETP on flow rate for RNAs on a TSKgel G4000SW two-column system and for DNA fragments on a TSKgel G5000PW two-column system (each column 60 cm × 7.5 mm ID). (From Ref. 8.)

elution in the high ionic strength region may be attributed to the adsorption of samples on column packing materials by hydrophobic interaction.

8 FLOW RATE

Figure 10 shows the dependence of height equivalent to a theoretical plate (HETP) on flow rate observed in the SEC of RNA and DNA fragment on 7.5 mm ID columns. The HETP decreased with decreasing flow rate. Especially with high-molecular-weight samples, such as 16S rRNA and a DNA fragment of 383 base pairs, the HETP was significantly dependent on flow rate and reached a minimum at flow rates lower than 0.1 mL/min. Flow rates of 0.3–0.5 mL/min seem to be a good compromise when separation time and resolution are taken into consideration.

9 CONCLUSIONS

A wide range of nucleic acids including RNAs, DNA fragments, plasmids, and oligonucleotides can be separated effectively by SEC on the basis of molecular size. Accordingly, it is possible to adopt SEC as an alternative to gel electrophoresis for analytical purposes. Furthermore, because the separated components in samples can be recovered easily and yet almost quantitatively by collection of column effluent, SEC should be superior to gel electrophoresis for preparative

© 2004 by Marcel Dekker, Inc.

purposes. Moreover, the purification process of nucleic acids using SEC would eliminate the use of toxic reagents, which are not desirable for clinical purposes. Consequently, SEC seems to be a useful technique for the separation and purification of nucleic acids.

10 APPENDIX

Polymer	Columns	Mobile phase	Comments	Ref.
RNA	MicroPak TSK 2000SW and 3000SW (Varian)	67 mM potassium phosphate buffer (pH 6.8) containing 0.1 M potassium chloride and 0.6 mM sodium azide		1
RNA	TSKgel G3000SW (Tosoh)	0.2 M sodium phosphate buffer (pH 7.0) containing 0.1% sodium dodecyl sulfate (SDS)		2
RNA	UltroPac TSK G4000SW (LKB)	A. 50 mM Tris–HCl buffer (pH 7.5) containing 25 mM potassium chloride and 5 mM magnesium chloride B. 75 mM Tris–HCl buffer (pH 7.5) containing 6 M urea, 0.1% SDS, and 1 mM EDTA		3
RNA	UltroPac TSK G2000SW, G3000SW, and G4000SW (LKB)	A. 0.1 M acetate buffer (pH 7.0) containing 0.75 M sodium chloride, 0.1% velcorin, and 1% methanol B. 10 mM acetate buffer (pH 5.5) containing 0.2 M sodium chloride, 5 mM magnesium chloride, and 0.2% SDS C. 75 mM Tris–HCl buffer (pH 7.5) containing 6 M urea, 1 mM EDTA, and 0.1% SDS		4
RNA	TSKgel G4000SW (Tosoh)	50 mM Tris–HCl buffer (pH 7.5) containing 0.2 M sodium chloride and 1 mM EDTA		5

© 2004 by Marcel Dekker, Inc.

Appendix (*Continued*)

Polymer	Columns	Mobile phase	Comments	Ref.
RNA	TSKgel G4000SW and G5000PW (Tosoh)	A. 0.25 M acetate buffer (pH 5.4) containing 1 mM EDTA B. 10 mM phosphate buffer (pH 7.0) containing 0.1 M potassium chloride		6
RNA	TSKgel G6000PW (Tosoh)	50 mM Tris–HCl buffer (pH 8.0) containing 0.1 M sodium chloride and 1 mM EDTA		7
RNA and DNA fragment	TSKgel G2000SW, G3000SW, G4000SW, and G5000PW (Tosoh)	A. 0.1 M phosphate buffer (pH 7.0) containing 0.1 M sodium chloride and 1 mM EDTA B. 10 mM Tris–HCl buffer (pH 7.5) containing 0.025–1.6 M sodium chloride and 1 mM EDTA		8
RNA and DNA fragment	TSKgel G2000SW, G3000SW, and G4000SW (Tosoh)	0.1 M phosphate buffer (pH 7.0) containing 0.1 M sodium chloride and 1 mM EDTA		9
DNA fragment	UltroPac TSK G3000SW and G4000SW (LKB)	50 mM triethylammonium acetate (pH 7.0)		10
DNA fragment	TSKgel G3000SW and G4000SW (Tosoh)	50 mM Tris–HCl buffer (pH 7.5) containing 0.2 M sodium chloride and 1 mM EDTA (and 7 M urea)		11
DNA fragment	TSKgel DNA-PW (Tosoh)	0.1 M Tris–HCl buffer (pH 7.5) containing 0.3 M sodium chloride and 1 mM EDTA		12
DNA fragment	Spherogel TSK 6000PW (Beckman)	50 mM Tris–HCl buffer (pH 7.6) containing 0.3 M sodium chloride and 1 mM EDTA		13

© 2004 by Marcel Dekker, Inc.

Appendix (*Continued*)

Polymer	Columns	Mobile phase	Comments	Ref.
DNA fragment	TSKgel G4000PW, G5000PW, and G6000PW (Tosoh)	0.1 M sodium nitrate		14
DNA fragment	UltroPac TSK G4000SW, G5000PW, and G6000PW (LKB)	0.25 M ammonium acetate (pH 6.0) containing 0.1 mM EDTA		15
DNA fragment	Bioseries GF-250 (DuPont)	Tris–acetic acid buffer (pH 7.5) containing 0.5 mM EDTA		16
DNA fragment	Superose 6 (Pharmacia LKB)	20 mM Tris–HCl buffer (pH 7.6) containing 0.15 M sodium chloride		17
Plasmid and DNA fragment	TSKgel G5000PW (Tosoh)	50 mM Tris–HCl buffer (pH 7.4) (containing 15 mM EDTA)		18
Plasmid	Bioseries GF-250 (DuPont)	0.2 M phosphate buffer (pH 9.0)		19
Plasmid	Fractogel TSK HW75S (Merck)	10 mM Tris–HCl buffer (pH 8.0) containing 0.2 M sodium chloride and 1 mM EDTA		20
Plasmid	TSKgel G6000PW (Tosoh)	0.1 M Tris–HCl buffer (pH 7.5) containing 0.3 M sodium chloride and 1 mM EDTA		21
Plasmid	Sephacryl S-1000 (Pharmacia)	50 mM Tris–HCl buffer (pH 8.0) containing 0.1 M sodium chloride and 5 mM EDTA		22
Plasmid	Superose 6 (Pharmacia)	6 mM Tris–HCl buffer (pH 8.0) containing 6 mM sodium chloride and 0.2 mM EDTA		23
Plasmid	Sephacryl S-1000 (Pharmacia)	10 mM Tris–HCl buffer (pH 8.0) containing 0.15 M sodium chloride and 1 mM EDTA		24
Oligonucleotide	I-125 Protein Column (Waters)	0.1 M triethylammonium acetate (pH 6.4–7.0)		25

© 2004 by Marcel Dekker, Inc.

REFERENCES

1. CT Wehr, SR Abbott. J Chromatogr 185:453, 1979.
2. S Uchiyama, T Imamura, S Nagai, K Konishi. J Biochem (Tokyo) 90:643, 1981.
3. L Graeve, W Goemann, P Fdldi, J Kruppa. Biochem Biophys Res Commun 107:1559, 1982.
4. L Graeve, J Kruppa, P Foldi. J Chromatogr 268:506, 1983.
5. Y Kato, T Hashimoto, T Murotsu, S Fukushige, K Matsubara. HRC & CC 1:626, 1983.
6. T Ogishima, Y Okada, T Omura. Anal Biochem 138:309, 1984.
7. J Pager. Anal Biochem 215:231, 1993.
8. Y Kato, M Sasaki, T Hashimoto, T Murotsu, S Fukushige, K Matsubara. J Chromatogr 266:341, 1983.
9. Y Kato, H Parvez, S Parvez. In: H Parvez, Y Kato, S Parvez, eds. Gel Permeation and Ion-Exchange Chromatography of Proteins and Peptides. Utrecht: VNU Science Press, 1985, p 1.
10. J Kruppa, L Graeve, A Bauche, P Fdldi. LC Magazine 2:848, 1984.
11. Y Kato, M Sasaki, T Hashimoto, T Murotsu, S Fukushige, K Matsubara. J Biochem (Tokyo) 95:83, 1984.
12. Y Kato, Y Yamasaki, T Hashimoto, T Murotsu, S Fukushige, K Matsubara. J Chromatogr 320:440, 1985.
13. J-M Schmitter, Y Mechulam, G Fayat. J Chromatogr 378:462, 1986.
14. T Nicolai, LV Dijk, JAPPV Dijk, JAM Smit. J Chromatogr 389:286, 1987.
15. R Dornburg. LC/GC 6:254, 1988.
16. BE Boyes, DG Walker, PL McGeer. Anal Biochem 170:127, 1988.
17. H Ellegren, T Lais. J Chromatogr 467:217, 1989.
18. ME Himmel, PJ Perna, MW McDonnell. J Chromatogr 240:155, 1982.
19. PAD Edwardson, T Atkinson, CR Lowe, DAP Small. Anal Biochem 152:215, 1986.
20. N Moreau, X Tabary, FL Goffic. Anal Biochem 166:188, 1987.
21. Y Yamasaki, Y Kato, T Murotsu, S Fukushige, K Matsubara. HRC & CC 10:45, 1987.
22. GJ Raymond, PK Bryant III, A Nelson, JD Johnson. Anal Biochem 173:125, 1988.
23. JK McClung, RA Gonzales. Anal Biochem 177:378, 1989.
24. NA Horn, JA Meek, G Budahazi, M Marquet. Human Gene Ther 6:565, 1995.
25. D Molko, R Derbyshire, A Guy, A Roget, R Teoule, A Boucherle. J Chromatogr 206:493, 1981.

© 2004 by Marcel Dekker, Inc.

17
Size Exclusion Chromatography of Low Molecular Weight Materials

Shyhchang S. Huang
Noveon, Inc.
Brecksville, Ohio, U.S.A.

1 INTRODUCTION

Low molecular weight (MW) polymers, or oligomers, have been used as plasticizers, detergents, lubricants, food additives, and prepolymers for copolymerizations. The MW distribution of these materials is an important parameter for their performance.

Common MW determination methods, such as light-scattering photometery, membrane osmometry, and ultra-centrifuge, do poorly with low MW oligomers because of their low sensitivities. Low MW oligomers are normally analyzed by colligative property measurements, such as vapor phase osmometry, boiling-point elevation (ebulliometry), freezing-point depression (cryoscopy), end group analyses by titration, and by various spectroscopic techniques. All these methods only generate one number-average MW (M_n) and are normally time consuming (1). The recently developed technique of

© 2004 by Marcel Dekker, Inc.

MALDI-MS has been applied to determine the absolute MW of many relatively low MW materials. However, it is limited to samples with narrow MW distribution and with certain polarity (2).

Traditionally, the chromatographic analysis of low MW material has been done by enthalpic interaction chromatography, where the retention mechanism is based more upon chemical structure than MW. These methods include gas chromatography, supercritical fluid chromatography, and normal-phase and reversed phase liquid chromatography (commonly referred to as HPLC, high-performance liquid chromatography). However, for MW determination for even low MW material, size exclusion chromatography is by far the most frequently used method just as for high MW material, because of its high speed, automation capability, and rich information (MW distribution and its averages of various modes).

The small-pore-size gels for size exclusion chromatography (SEC) are more difficult to prepare and use than large-pore gels for at least two reasons. (1) Small-pore gels are more fragile than larger-pore gels. In order to achieve a good resolution, the total pore volume of SEC gels needs to be as large as possible. The volume of interstitial voids of an SEC column, regardless of particle size, is approximately 40% of the total column volume. Therefore, the smaller the pore size the thinner the solid wall, and the more fragile. (2) The applications for low MW separation normally demand high resolution, which may he achieved by reducing particle size or using several columns in series. Either method results in a high backpressure, which is detrimental to the fragile nature of a small-pore gel. SEC column technology has recently been improved significantly. The commercially available small-pore columns have become more and more popular.

This chapter will also discuss other difficult issues for SEC of small molecules, such as MW dependence of detection sensitivities, calibration methods, and solvent mismatch interference.

2 RESOLUTION

2.1 Columns

The SEC study of small molecules often demands a high resolution, especially when the resolution of an individual molecule is needed. The peak resolution, R_S, of any chromatographic separation, including SEC, can be calculated using (3):

$$R_S = \tfrac{1}{4}(\alpha - 1)N^{1/2}\left(\frac{k'}{1+k'}\right) \quad (1)$$

© 2004 by Marcel Dekker, Inc.

where α is the separation factor, N is the number of theoretical plates, and k' is the capacity factor. In SEC, k' equals 1. Therefore, the calculation of resolution can be simplified to:

$$R_S = \frac{1}{8}(\alpha - 1)N^{1/2} \tag{2}$$

In order to improve resolution in SEC, α and N should be maximized. As in HPLC, N can be increased by increasing the column length or by reducing the particle size of the gels. To increase the total column length, one can simply run several low MW columns in series. Regarding particle size, 5 μm SEC gels for low MW are currently very popular. Several SEC column manufacturers also provide columns with 3 μm gels. However, either method will induce higher backpressure. Unfortunately, the small-pore gels are more fragile than the SEC gels with larger pore sizes as mentioned previously. The pressure fluctuation during sample injection, when the zero-pressure sample loop is connected to the high-pressure flow line, will reduce the lifetime of the small-pore gels. Placing a small guard column, which serves as a pulse damper, before the analytical low MW columns will greatly reduce the pressure fluctuation on the analytical column. Because of the low viscosity nature, the concentration effect in SEC of high MW polymer samples is usually not taken into account in the case of low MW material (4). Therefore, in order to reduce the pressure fluctuation and to extend the lifetime of a column, injection of a small sample volume with a high concentration is also preferred.

The α in SEC depends mainly on the slope of the calibration curve: the flatter the slope the better resolution, as shown in Fig. 1. There are at least two ways to reduce the slope of the calibration curve and to maximize α: first, increasing Δt_r by increasing the total pore volume of the gels, and secondly, minimizing the MW separation range ($\Delta \log MW$) by selecting columns with minimum but adequate MW range.

In order to increase the total pore volume, one may simply connect more columns of the same pore size in an SEC (column set B in Fig. 1). In this case, the number of theoretical plates will also be approximately doubled. The other way to increase the pore volume is to increase the pore-to-solid-body ratio, because the interstitial volume of an SEC column is inherently fixed at approximately 40% of the total column volume. The OligoPore column, recently introduced by Polymer Laboratories, is designed based on this principle (5). The calibration curve for the OligoPore column compared to that of a regular low MW column is shown in Fig. 2. However, larger total pore volume with the same pore size means a thinner solid wall, and thus more fragile particles. This type of column should be used with care. Yet another means to increase the total pore volume is to use a larger internal diameter column. This also has the advantage of reducing backpressure.

© 2004 by Marcel Dekker, Inc.

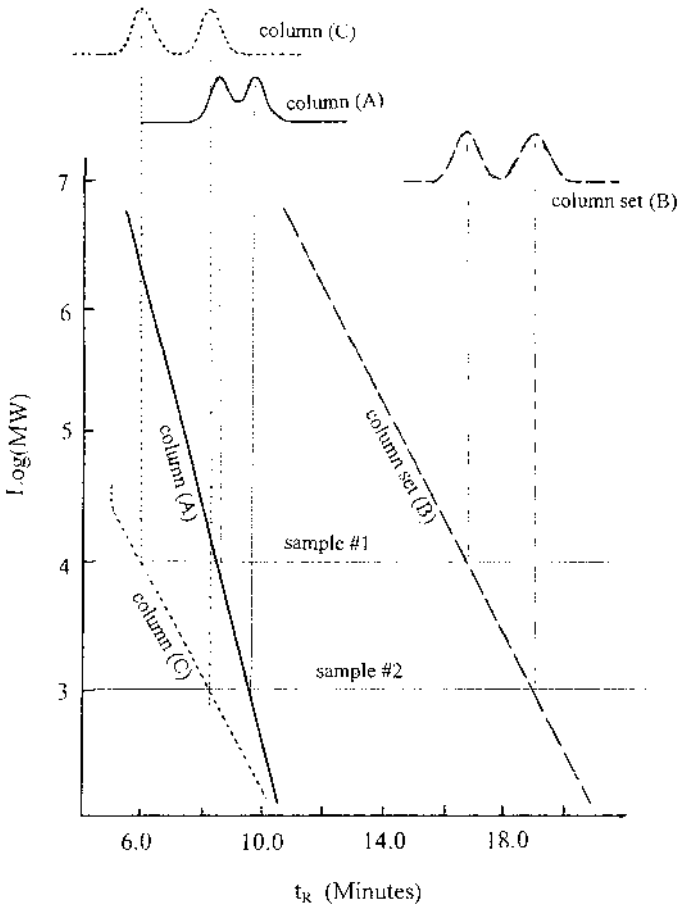

Figure 1 Calibration curves of SEC columns. Column (A): one typical column; column set (B): two typical columns; Column (C): one column with a narrow MW range.

A narrow but adequate MW range is another very effective way to increase the resolution in SEC, which is demonstrated by column C in Fig. 1. Figure 3 is an example of separating low MW epoxy resins using different pore-size columns (6). The lowest MW sample, Epikote 828, is well separated by either the Shodex A801 column (equivalent to a 50 Å column) or the A802 column (100 Å). However, the analysis using the A801 column takes less time. The Epikote 1001 sample is clearly partially excluded by the A801 column. The A802 column gave good separation at the low MW region; however, the A803 column (10^3 Å) separates better in the higher oligomer area. The A803 column is a clear choice for the other

© 2004 by Marcel Dekker, Inc.

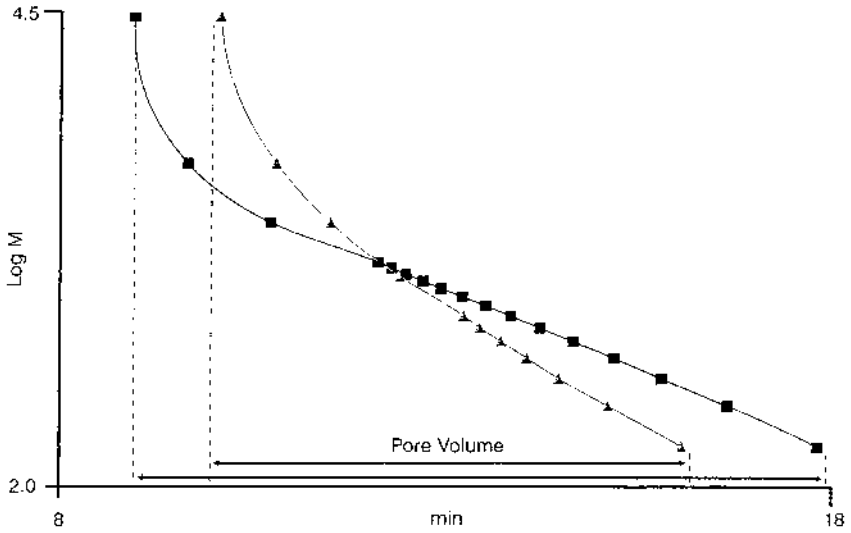

Figure 2 Calibration curve of PLgel OligoPore (■) compared to a conventional, low pore size GPC column (▲).

two samples. The two-column set consisting of A802 and A803 columns, or a mixed-bed column with a linear MW calibration covering the same MW range, may be used for the analysis of all these samples.

In summary, in order to maximize resolution in low MW analyses, one should select a column set with minimum but adequate MW range, large internal diameter, small particle size, and large pore volume gels (Table 1). If analysis time is allowed, as many columns in series should be run as possible. Using a guard column before the analytical columns will help to extend the lifetime of analytical columns.

2.2 Other Chromatographic Conditions

In SEC of high MW polymers, a low sample concentration with a large injection volume is normally preferred to prevent any viscosity effect. However, a small injection volume and high sample concentration is preferred in low MW SEC for better resolution.

The other parameter that may increase the resolution is higher temperature. At higher temperatures, the motion of both polymer chains and solvent molecules is increased, while the viscosity of the solvent is lower. All these factors increase N, and thus improve the resolution. Table 2 shows the value of N for BHT,

© 2004 by Marcel Dekker, Inc.

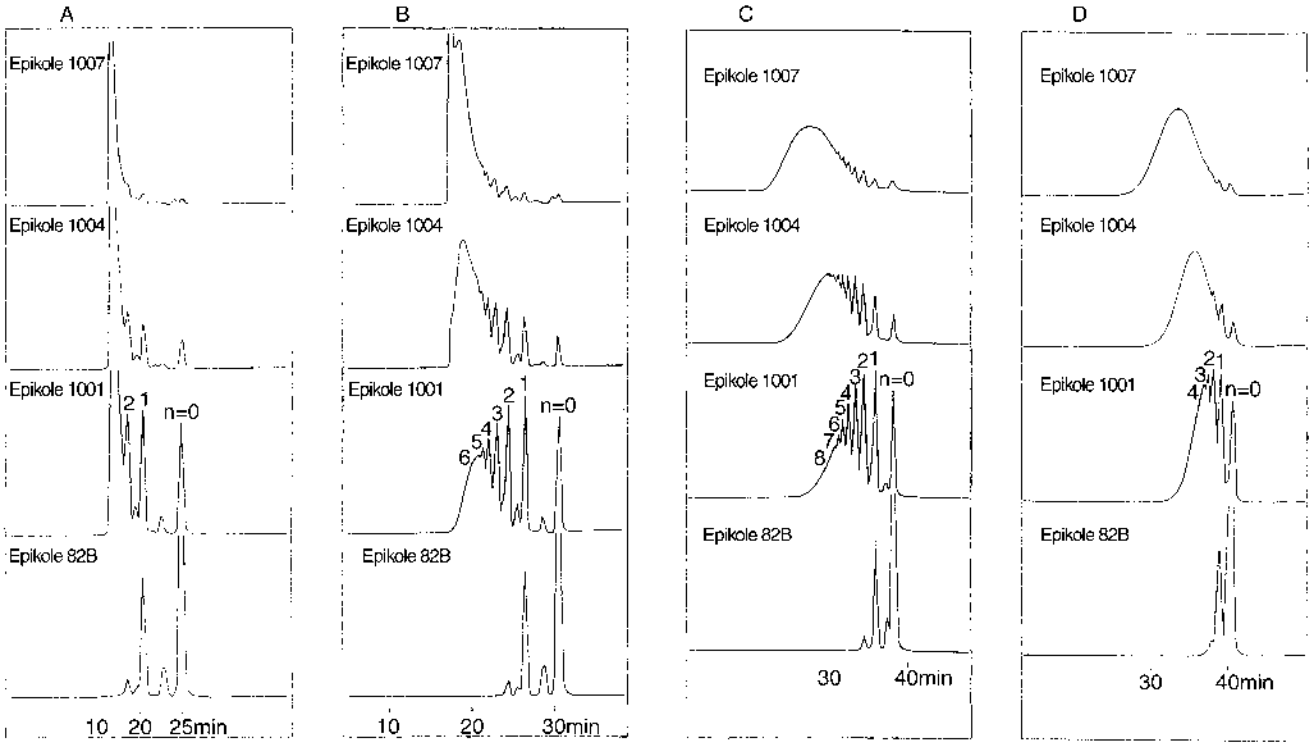

Figure 3 Chromatograms of epoxy resins. Columns: (A) Shodex A801 × 2; (B) Shodex A802 × 2; (C) Shodex A-803 × 2; and (D) Shodex A-804 × 2; mobile phase: THF; flow rate: 1.0 mL/min; detector: UV (254 nm); column temperature: room temperature. (From Ref. 6.)

© 2004 by Marcel Dekker, Inc.

Table 1 Factors for GPC Resolution

Factors	N/α	To increase R	Remarks
Column length	N, α	Longer or multicolumn	Increased backpressure
Particle size	N	Smaller	Increased backpressure
Internal width of column	α	Wider	Reduced backpressure
MW range of separation	α	Narrow but adequate	
Pore volume/solid body	α	Larger ratio	More fragile
Injection volume	N	Small	Less pressure fluctuation
Column temperature	N	Higher	Reduced backpressure Bubbles may form after column

Table 2 Number of Theoretical Plates at Different Temperatures

Temperature	Peak[a]		
	1,320[b]	BHT	162[c]
Room temperature	1,230	19,200	18,300
35°C	1,480	19,400	19,300
50°C	1,520	21,800	21,000

[a]Samples were run using one PLGel 100 Å column in THF, at 1.0 mL/min.
[b]This sample is polystyrene with MW 1,320, from Polymer Laboratories. This is not a real monodispersed material; the number of theoretical plates is an apparent number.
[c]This is 1-phenylhexane, the unimer of oligostyrene.

1-phenylhexane (the unimer), and a low MW oligostyrene at three different temperatures. All increased roughly by 15% from room temperature to 50°C.

3 DETECTOR SENSITIVITIES

Unlike high MW polymers, the SEC detector sensitivity of oligomeric material varies with respect to MW. In the case of the most oftenly used SEC detector, the refractive index (RI) detector, the signal is the excess refractive index (Δn) due to solute, which can be expressed as:

$$\Delta n = (n - n_0) = k\frac{dn}{dc}c \tag{3}$$

© 2004 by Marcel Dekker, Inc.

where n and n_0 are the RIs of the sample and solvent, respectively, k is a constant, dn/dc is the specific refractive index (the increment of refractive index to the concentration of a solute), and c is the concentration of the solution. The dn/dc approximately equals the difference of refractive indexes of solute and solvent (7):

$$\frac{dn}{dc} \approx n_{\text{solute}} - n_{\text{solvent}} \tag{4}$$

The refractive index of an oligomeric material has a linear relation to the reciprocal of its MW, as demonstrated with hydrocarbons in Fig. 4. Therefore, dn/dc is proportional to the reciprocal of solute MW (8):

$$\frac{dn}{dc} = \left(\frac{dn}{dc}\right)_{\infty} + \frac{k'}{M_{\text{n}}} \tag{5}$$

where k' is a constant. As shown in Fig. 4, k' is often a negative number. However, it can be positive if the chain ends with a high refractive index functional group, such as phenyl, chloride, and bromide. For a polymer with high M_{n}, the k'/M_{n} term is insignificant, and dn/dc reaches a constant value, $(dn/dc)_{\infty}$. For the low MW material, dn/dc varies according to k'/M_{n}. When dn/dc is relatively large, the variation due to MW may be not obvious. However, when dn/dc is small, the variation will become significant. Figure 5 shows that the signal of hydrocarbons in THF gradually diminishes and changes to negative as the MW is reduced. Solvent selection may exaggerate or minimize the dn/dc effects on MW. Therefore, it is important to choose a mobile phase that has a refractive index as far from the samples as possible for SEC of low MW samples.

Figure 6A shows that the SEC curve of a silicone copolymer sample in THF starts with a negative signal (around 4.8 min), becomes positive around 5.6 min, and becomes negative again around 6.6 min. The variation of polymer refractive index, and thus dn/dc and detector sensitivity, may be due to a combination of changes in MW and chemical structure. The peaks after 8.8 min are solvent mismatches. The solvent mismatches show the concentration differences of small molecules, such as H_2O, N_2, O_2, and other additives in the mobile phase, introduced during the sample preparation procedure. Owing to the low sensitivity of this sample, the solvent mismatches appear to be exaggerated. When it is analyzed in toluene, the entire chromatogram is negative and the mismatches became negligible, as shown in Fig. 6B, in which case the MW distribution can be calculated easily.

It is convenient to create a chart like Fig. 7, which lists the refractive index of commonly used solvents on one side and commonly analyzed polymers on the other. Using this chart, the selection of a good polymer/solvent pair for SEC analyses becomes much easier.

© 2004 by Marcel Dekker, Inc.

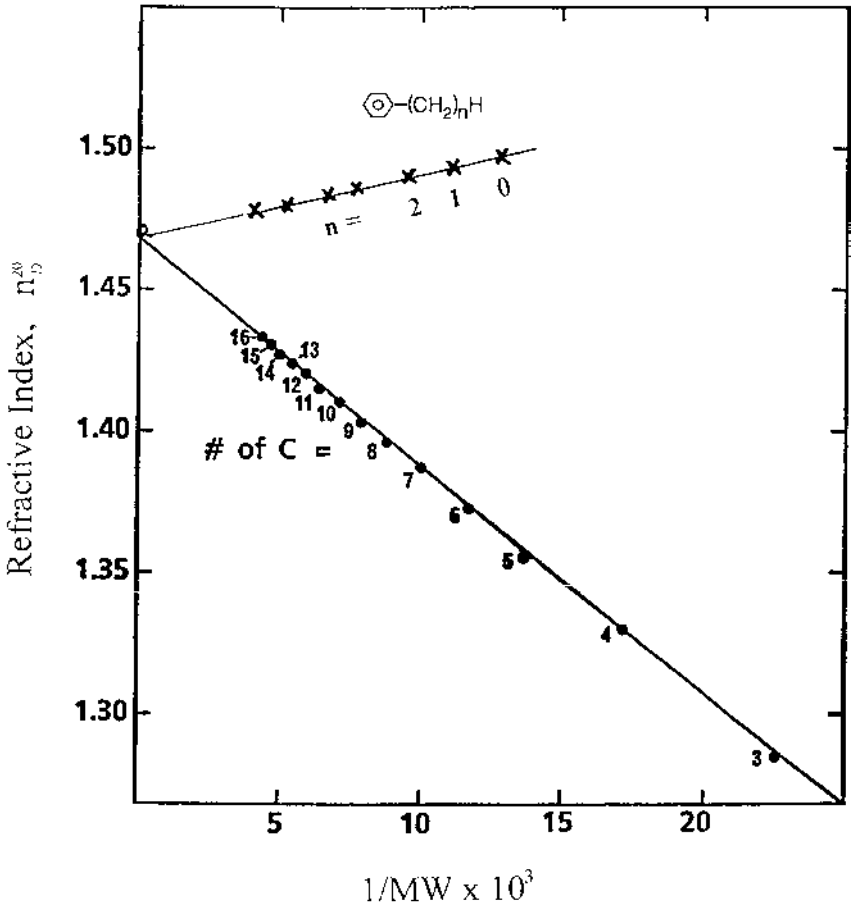

Figure 4 Refractive index of *n*-alkanes vs. 1/MW.

The second most common SEC detector is a UV detector, which is very useful for polymers with UV-absorbing chromophores on their backbone. The SEC signal using this detector may also have a chain end effect if the end group absorbs in the UV more strongly than the functional group on the backbone. The chain end effect will be more pronounced in the SEC of low MW oligomers than for high MW polymers as shown in Fig. 8, in which the UV intensity is relatively higher at the lower MW area than the RI. The UV detector also shows several peaks of polymer additives, but not the RI detector.

© 2004 by Marcel Dekker, Inc.

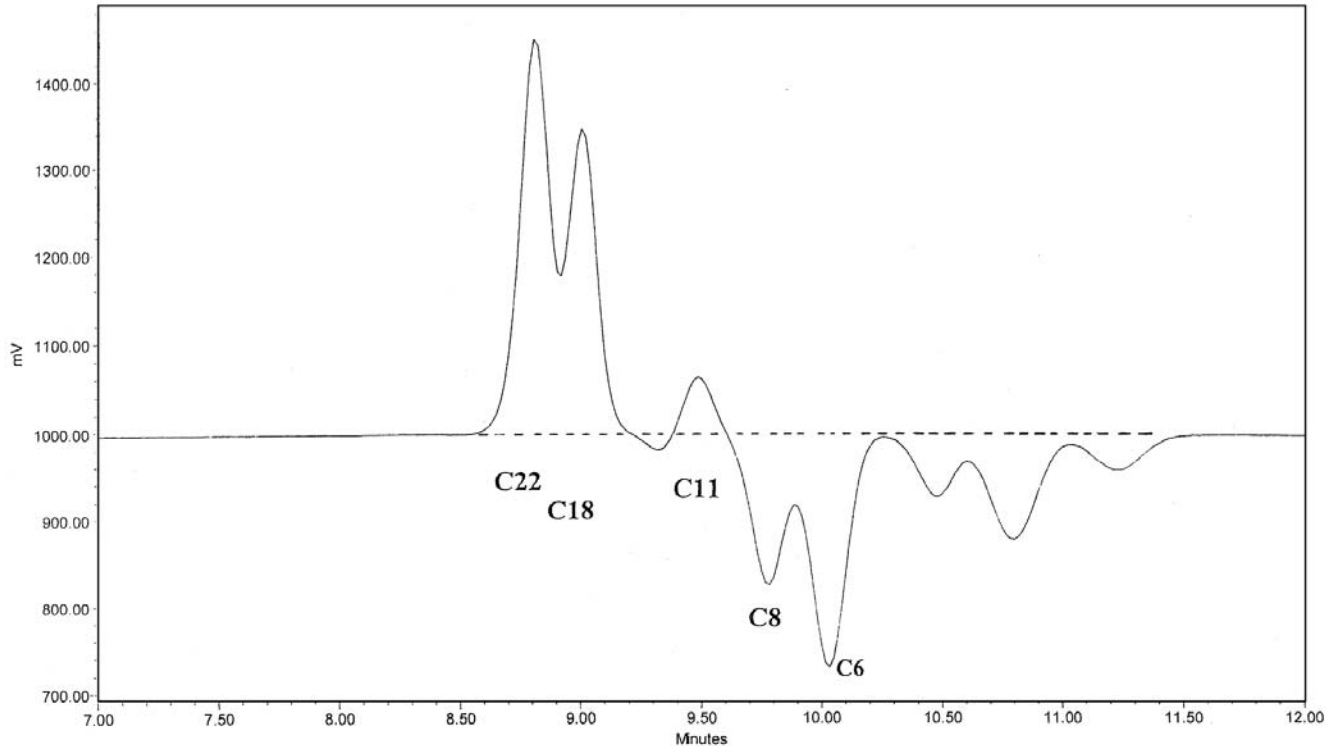

Figure 5 SEC chromatogram of *n*-alkanes. Column: PLgel, MiniMix-E Guard + MIXED-E; mobile phase: THF with 250 ppm BHT; flow rate: 1.0 mL/min; detector Waters 410 DRI; column temperature: 50°C.

© 2004 by Marcel Dekker, Inc.

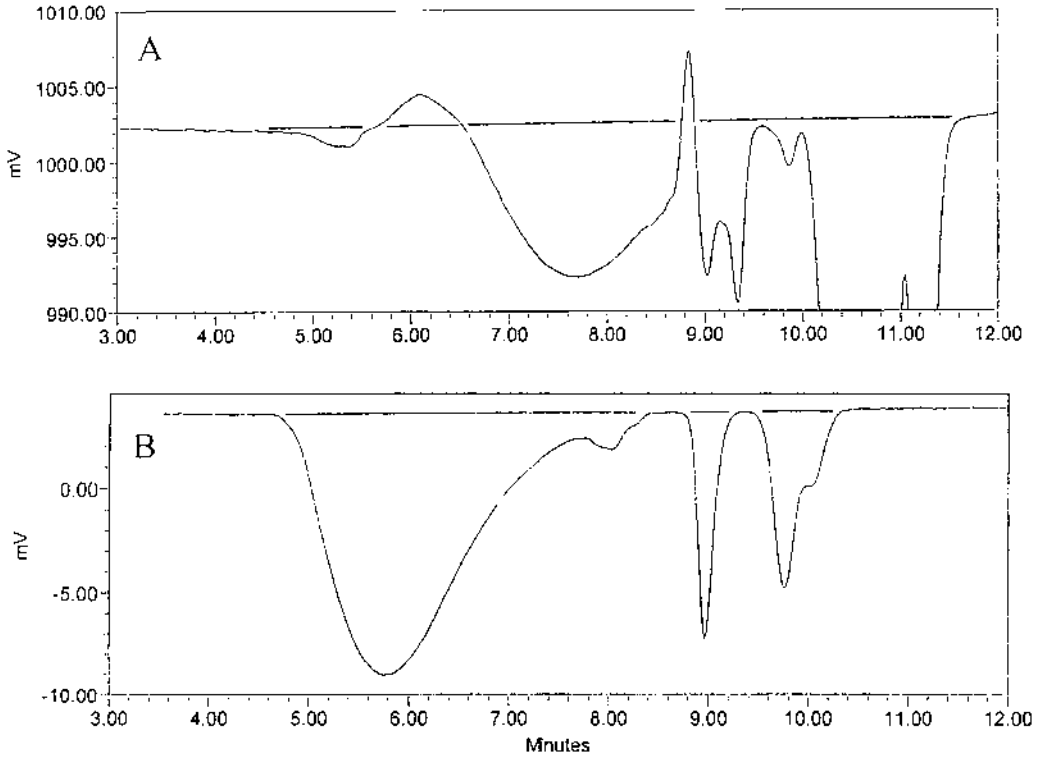

Figure 6 SEC chromatograms of a silicone copolymer sample. (A) Same SEC conditions as in Fig. 5. (B) PLgel, MIXED-E; mobile phase: toluene with 250 ppm BHT; flow rate: 1.0 mL/min; detector: RI in PL220 GPC; column temperature: 75°C.

© 2004 by Marcel Dekker, Inc.

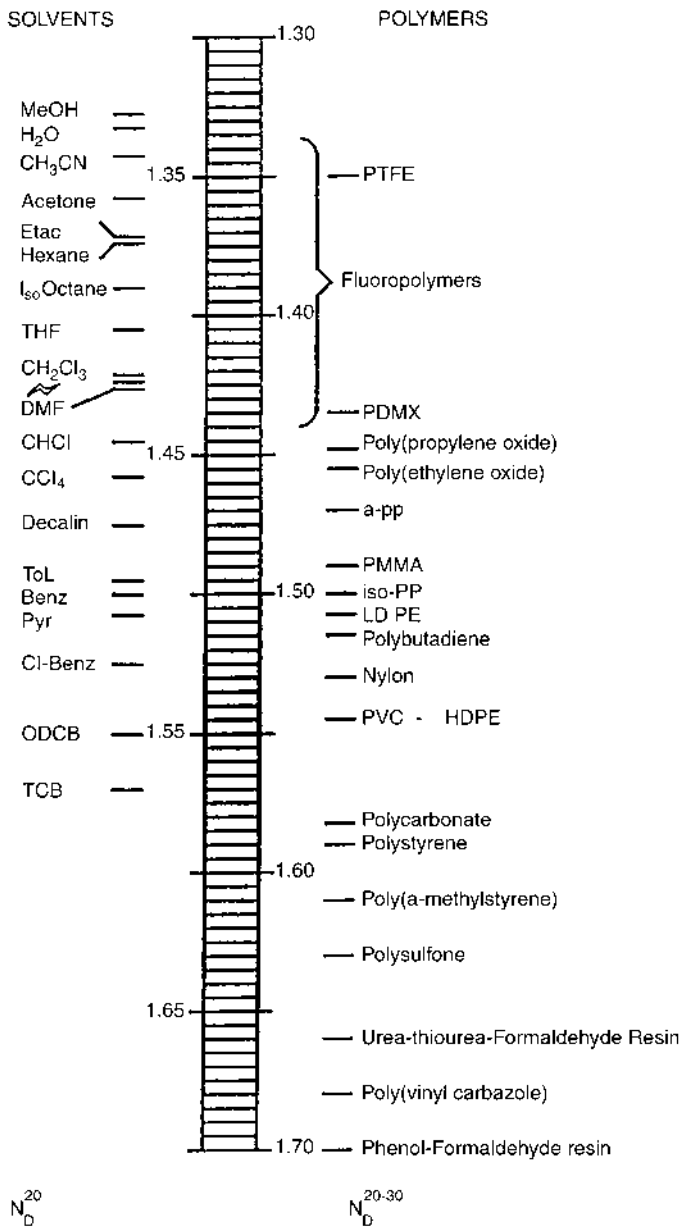

Figure 7 Refractive indexes of common liquid chromatography solvents and common polymers.

© 2004 by Marcel Dekker, Inc.

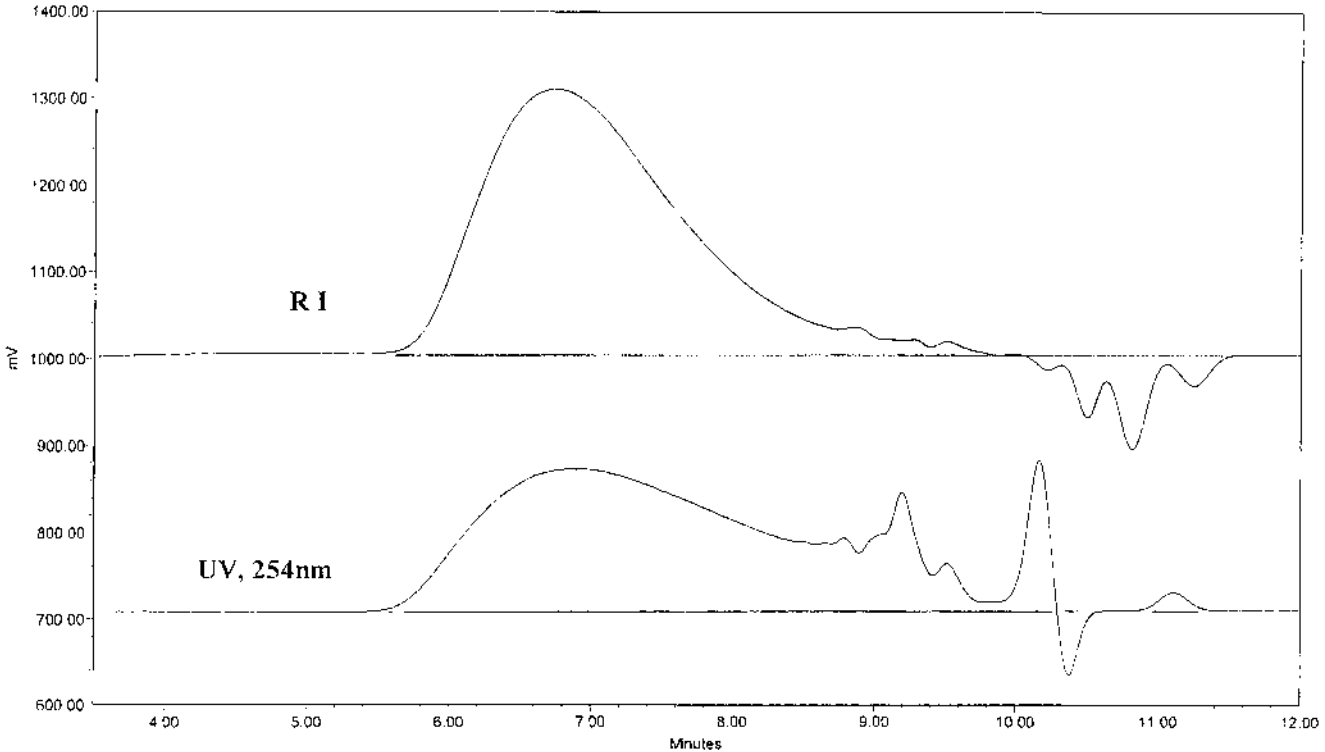

Figure 8 SEC chromatograms of a styrene/acrylate copolymer sample (same SEC conditions as in Fig. 5, except an additional UV detector: LDC SpectroMonitor III).

© 2004 by Marcel Dekker, Inc.

Another detector recently applied in SEC is the evaporative light-scattering detector (ELSD). This detector is not used for oligomers as often as the RI and UV detectors are, because some very low MW oligomers may be evaporated. However, if it is used without the evaporation effect, the nonlinear sensitivity effect should he considered. Figure 9 shows that the sensitivity of this detector is lower at lower concentration ranges (9), which happen to be around the range for a typical LC or SEC analysis. Because the concentrations at both ends of a peak are underestimated, the calculated polydispersity (M_w/M_n) will he smaller than the actual number.

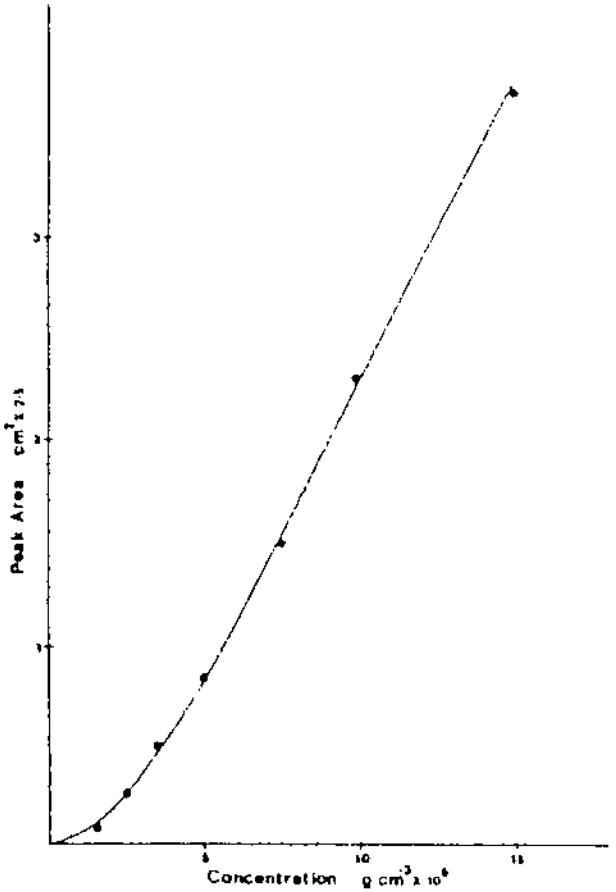

Figure 9 Plot of the detector response for *p,p′*-diaminodiphenylmethane solutions in the concentration range 1.5×10^{-5} to $1.5 \times 10^{-4}\,g/cm^3$. From Ref. 9, copyright 1978 American Chemical Society.

© 2004 by Marcel Dekker, Inc.

4 CALIBRATION AND CALCULATION

The most commonly used polymer MW standard is probably the polystyrene (PS) standard, because of availability of narrow distribution standards over a wide MW range, from close to 10×10^6 to unimer, and because of its solubility in various common organic solvents for SEC studies. In many applications, when the absolute MW is not necessary, the MW results calculated using PS standards are acceptable for relative comparison. It is highly recommended to add the unimer, hexylbenzene, MW = 162, in calibration, especially when stabilized THF is used as the mobile phase. The BHT stabilizer peak often shows up between the trimer, 370 MW, and the unimer peaks. It is important to note that the refractive index of trichlorobenzene (TCB) happens to be very close to the trimer. Therefore, the trimer becomes invisible, while the dimer and the unimer become negative peaks (Fig. 10).

Poly(ethylene glycol) (PEG) is another useful MW standard for SEC in THF and more polar solvents. The higher MW standards (> 1,000) are difficult to dissolve in THF at room temperature. They can he dissolved at elevated temperature and will stay in solution when the solution is cooled. It is also important to note that the retention times of very low MW oligomers of PEG (< 200) are not linear relative to higher MW PEG standards for an unknown reason (10).

It is difficult to use an on-line MW detector, such as light-scattering photometer or viscometer, for absolute MW analysis of low MW oligomers by SEC because of lack of sensitivity. However, an absolute MW calibration curve may be created if the low oligomer peaks can be resolved and the MWs can be assigned. Figure 11 is an example for polyols, where the low MW oligomer peaks

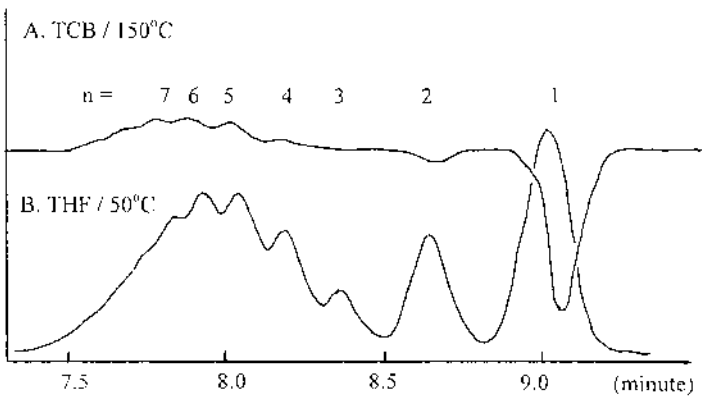

Figure 10 FSEC chromatograms of styrene oligomers in THF and in TCB. (A) Column: PLgel MIXED-E; mobile phase: TCB with 250 ppm BHT, 1.0 mL/min. (B) Same conditions as in Fig. 5.

© 2004 by Marcel Dekker, Inc.

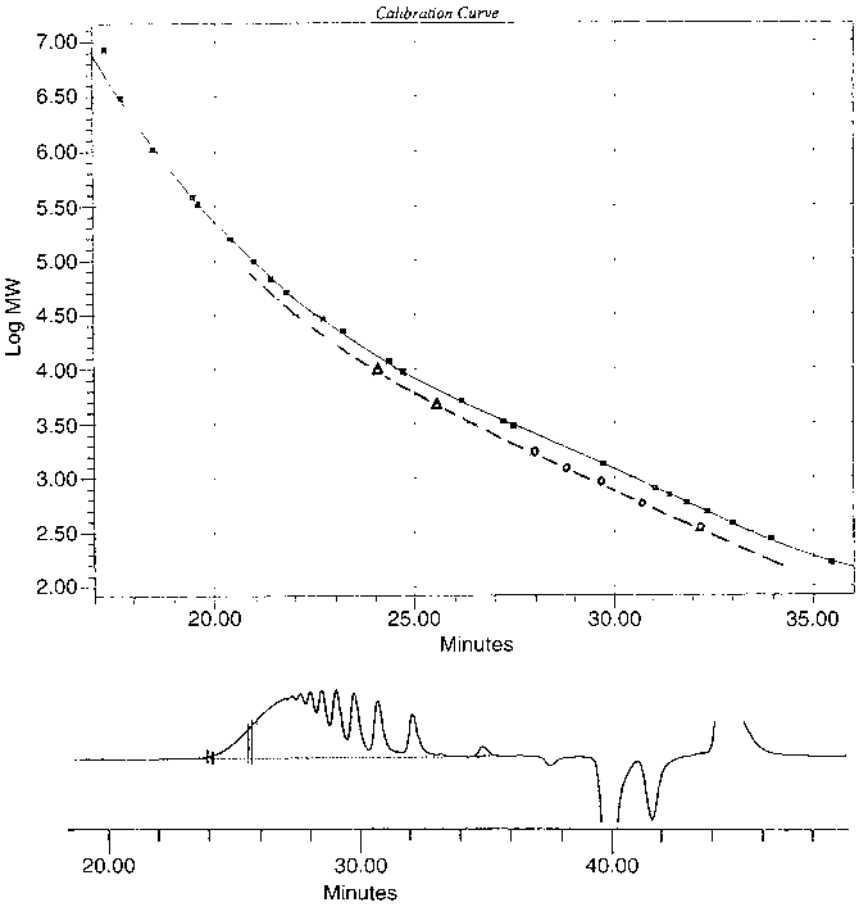

Figure 11 Absolute MW calibration polyols. Column set: PLgel, 2 × MIXED-D + 500 Å + 100 Å; mobile phase: THF with 250 ppm BHT; flow rate: 1.0 mL/min; detector: Waters 410 DRI; column temperature: 40°C. Solid line: (■) polystyrene; dashed line: (○) polyol oligomers, (△) fractions identified by MALDI/MS.

were resolved well enough up to, at least, the pentamer. Two fractions of high MW SEC effluent were collected for MW determination with mass-assisted laser desorption ionization/mass spectroscopy (MALDI/MS). An absolute MW calibration curve was then created using these data points. The calibration curve can be extended to higher MW using a PS calibration by assuming that the ratio of $MW_{polyol} : MW_{PS}$ remains the same at all retention volumes, which indicates

© 2004 by Marcel Dekker, Inc.

Table 3 Comparison of M_n Results by Various Methods

Sample	By titration[a]	By NMR (500 MHz)	By GPC[b1] (PS)	By GPC[b2] (Polyol)
Polyol-1A	974	966	1808	1079
Polyol-1B	1032	1088	1933	1121
Polyol-2	2370	2590	3283	2311
Polyol-4	3993	4520	4599	3573

[a]Determined using ASTM Standard Test Method D1957-86.
[b]GPC conditions: see Fig. 11. M_n results in column b1 were calculated using a PS calibration. Those in column b2 were calculated using the polyol absolute MW calibration.

that a, the exponential constant in the Mark–Houwink–Sakurada equation of two polymers, is the same. Fortunately, the M_n is normally more important than M_w for low MW material. A slight deviation of the calibration curve on the higher MW side can normally be tolerated. The MWs of polyol samples calculated using this calibration curve agree well with other primary methods, such as NMR and titration (Table 3).

It is important to note, during the above procedure, that the peak maximum MW (M_p) of MALDI/MS is different from that of SEC for two reasons: (1) the peak height in MALDI/MS is approximately proportional to the number of polymer molecules, instead of the concentration, weight by volume, as in SEC; (2) the x-axis in MALDI/MS is linear in MW, instead of roughly log(MW) as in SEC. The M_p needs to be converted before creating the calibration curve. The dead volume between the RI detection cell and the outlet for collection, which is normally significantly large, should be adjusted for a correct calibration.

It is not uncommon that the MW distribution of a low MW material covers the solvent mismatch peaks. As mentioned earlier, the concentration effect is normally not significant for low MW samples. The solvent mismatch problem can be reduced by increasing sample load, which means higher sample concentration and larger sample volume.

5 SPECIAL SUBJECT: ANALYSIS OF POLYMER ADDITIVES USING SEC

Owing to improved resolution in low MW SEC, many polymer additives, if they are soluble in a common solvent with the polymer, can be directly analysed using SEC without tedious extraction steps. Acrawax C (*N*,*N*′-ethylene-*bis*-stearamide) as an additive in polyurethane is a good example, because of the difficulty in finding a good solvent for HPLC analysis. Both Acrawax C and polyurethane are

© 2004 by Marcel Dekker, Inc.

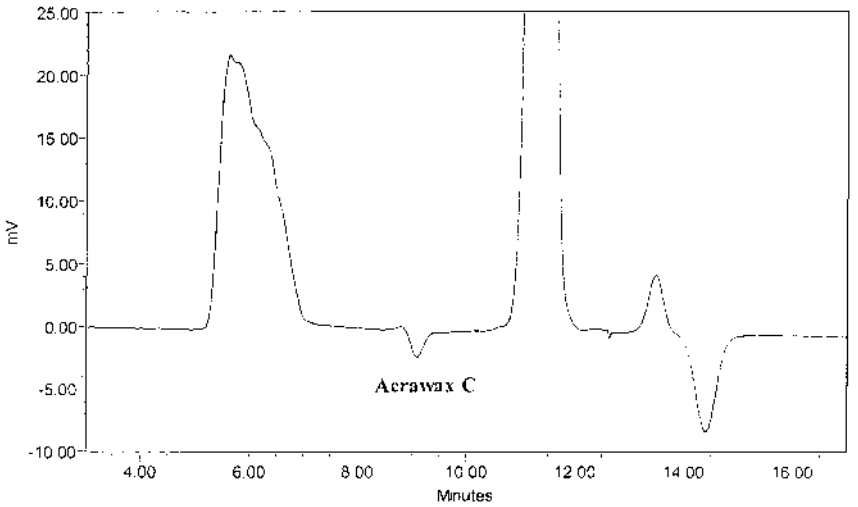

Figure 12 Chromatogram of Acrawax C in polyurethane. Column: Jordi DVB 100 Å, 250 × 10 mm; mobile phase: benzyl alcohol, 250 ppm BHT; flow rate: 1.0 mL/min; temperature: 150°C; injection volume: 200 μL.

soluble in benzyl alcohol at 150°C. The concentration of Acrawax C can be analyzed using a high-temperature SEC with a small-pore (100 Å) column. Acrawax C, which appears as a negative peak at 9.1 min (Fig. 12), is well separated from the polyurethane and other additives. In this type of method, the viscosity of the polymer should not be too high.

ACKNOWLEDGEMENTS

The author expresses his appreciation to Noveon, Inc., for its permission to publish this article and for its support on all research work, to Dr CS Wu for his encouragment and discussion, and to D Hanshumaker for his help in preparation of this article.

REFERENCES

1. JM Mays, N Hadjichristidis. In: HG Barth and JM Mays, eds. Modern Methods of Polymer Characterization. New York: Wiley-Interscience, 1991, Chs. 6, 7.
2. G Montaudo, MS Montaudo, F Samperi. In: G Montaudo and RP Lattimer, eds. Mass Spectroscopy. Boca Raton: CRC Press, 2002, ch. 10.

© 2004 by Marcel Dekker, Inc.

3. LR Snyder, JJ Kirkland. In: Introduction to Modern Liquid Chromatography, 2nd ed. New York: Wiley-Interscience, 1979, p 36.
4. S Mori, HG Barth. Size Exclusion Chromatography. Springer, 1999, p 58.
5. Polymer Laboratories Chromatography Products, Issue 2, 2001/2002, p 18.
6. Shodex Application Data, 1994, Showa Denko, 1994.
7. SS Huang. Estimation of the refractive index increment of polymer solutions. 1st International Symposium on Polymer Analysis and Characterization, Toronto, Canada, June 2, 1988.
8. JW Lorimer, DFG Jones. Polymer 13:52, 1972.
9. JM Charlesworth. Anal Chem 50:1414, 1978.
10. S Mori. J Liq Chromatogr 3:329, 1980.

© 2004 by Marcel Dekker, Inc.

18
Two-Dimensional Liquid Chromatography of Synthetic Macromolecules

Dušan Berek
Polymer Institute of the Slovak Academy of Sciences
Bratislava, Slovakia

1 INTRODUCTION AND BASIC TERMS

Properties of macromolecular systems depend on molecular characteristics of polymers and on relative concentrations of constituents in polymer mixtures, as well as on the mutual arrangement of macromolecules and on the presence of low molecular admixtures. The determination of molecular characteristics of both natural and synthetic polymers is of prime importance for science and technology of macromolecular systems, from understanding of life secrets to production of tailored advanced materials.

Many natural polymers, for example numerous proteins, can be considered uniform chemical substances. On the other hand, all synthetic polymers known thus far are arrays of macromolecules with different molar masses. Many synthetic polymeric materials also contain macromolecules differing in their physical architecture and chemical structure. We can define three basic or primary

© 2004 by Marcel Dekker, Inc.

molecular characteristics of macromolecules, namely their molar mass (MM), physical (molecular) architecture (MA), and chemical structure (CS). As is known, molar masses of macromolecular substances range from a few hundreds, through a few thousands (oligomers), to a few millions [(high) polymers] and, eventually up to tens of millions (ultra-high molar mass polymers). The term physical (molecular) architecture of polymers represents differences between linear and short- — or long- — chain branched macromolecules, as well as between species of various stereoregularities, head-to-head and head-to-tail structures, and so on. Chemical structure of polymers includes mainly their chemical composition (CC) corresponding to relative concentration of building units in copolymers and constituents of polymer blends, as well as functional groups, both type (FT) and concentration (FC), in functional polymers.

The nonuniformity of molecular characteristics is expressed by differences of various mean (average) values of molecular characteristics, that is, MMM, MMA, and MCS, as well as with the distribution of molecular characteristics, that is, MMD, MAD, and CSD (CCD, FTD, FCD).

Besides primary molecular characteristics, we can also define secondary molecular characteristics of macromolecules. For example long-chain branches in branched macromolecules including also comblike, grafted, or starlike structures may simultaneously exhibit differences in their molar mass, architecture, or chemical structure.

Polymeric substances that exhibit more than one distribution of their molecular characteristics are called complex polymer systems.

Mean values of molecular characteristics can be determined by various bulk methods while for assessment of distributions, macromolecules are usually separated. Both bulk and separation procedures utilize differences in particular physical and chemical properties of macromolecules. Information on distribution of molecular characteristics is generally more conclusive than the mean values and therefore separation methods are often preferred over bulk methods. Presently, separations of macromolecules are dominated by chromatographic and mass spectrometric procedures. Chromatographic separation is based on different extents of retention for different macromolecules within chromatographic columns. Separated macromolecules are transported along the chromatographic column by the mobile phase (eluent), which is a liquid or supercritical fluid. Correspondingly, we speak about liquid chromatography (LC) and about supercritical fluid chromatography (SFC). In this chapter, we shall deal mainly with the former. Chromatographic columns contain an array of porous or nonporous particles, which form a packing or a rodlike monolith. Monoliths possess larger flow-through channels with usual sizes in the range of 1 or 2 μm and smaller "separation pores." Particles of typical column packings have narrow size distribution with a maximum in the range 3–20 μm, depending on the separation task. The smaller the packing particles, the more efficient is separation (narrower peaks), but also the

© 2004 by Marcel Dekker, Inc.

larger is pressure drop and resulting experimental problems. Particles in the upper size range are used mainly for preparative work and for separation of ultra-high molar mass macromolecules in order to reduce mechanical degradation of analytes by shearing.

Pore sizes in column packings and sizes of separation pores in monoliths should match the sizes of macromolecules. This is especially important for exclusion-based separations (Sec. 4.1.1).

In most cases, separation efficiencies of modern liquid chromatographic columns are high enough so that a general term high-performance liquid chromatography (HPLC) can be applied. Monolithic column fillings typically exhibit much lower flow resistance than packed columns and, they are therefore more suitable for high-speed separations. The sizes and volumes of separation pores so far available in monoliths are, however, less favorable for polymer HPLC than those in packed columns.

Separation pores that are suitable for macromolecules range from a few nanometers up to several hundreds of nanometers in size (Sec. 4.1) depending on preferred retention mechanisms (Sec. 3). Pore volume should be as large as possible. Unfortunately, increased pore volume is connected with a lowering in mechanical stability of the porous gel matrix, which must withstand high pressures of up to several tens of megapascals (hundreds of bars) and frequent pressure strokes. Therefore, a compromise must be sought and pore volumes of modern HPLC column packings assume barely more than 60 to 70% of total particle volume.

The chemical nature of HPLC column packings strongly affects analyte retention. This feature will be discussed in more detail in Secs. 3 and 4.

At present, the most popular method for molecular characterization of synthetic polymers is size exclusion chromatography (SEC), which is also termed gel permeation chromatography (GPC) in the case of lipophilic macromolecules and gel filtration chromatography (GFC) in the case of hydrophilic macromolecules. Modern SEC belongs to the family of high-performance liquid chromatographic methods and, consequently, it is improper to speak about HPLC *and* SEC. SEC separates macromolecules according to their size in solution. This means that macromolecules with particular size will be eluted from a column within a specific volume of mobile phase that is within a specific retention volume, V_R. As a result, molar masses of macromolecules leaving the SEC column can be easily evaluated on the base of their retention volumes using appropriate calibration. Alternatively, the molar mass of macromolecules in the column effluent can be continuously monitored applying on-line light-scattering measurement or viscometry. Concentration of macromolecules leaving the SEC column is measured by appropriate flow-through HPLC detectors, for example, by differential refractometers, photometers, evaporative light-scattering detectors, and so on (Sec. 10). Knowing both concentration and molar mass of

© 2004 by Marcel Dekker, Inc.

macromolecules in the column effluent, one can directly calculate mean molar mass values (mass, number, z, $z + 1, \ldots$ averages) of the analysed polymer sample and also determine its molar mass distribution function. SEC measurements are easy to automate and SEC results are usually highly repeatable. Moreover, high-speed, high-throughput SEC systems allow at least semiquantitative on-line characterization of samples in polymer production plants and in combinatorial polymer laboratories. These features make SEC extremely popular in both polymer science and technology. As a result, SEC has almost fully substituted or at least suppressed the use of various bulk methods such as membrane and vapor pressure osmometry, light-scattering measurements, and even viscometry.

Unfortunately, SEC cannot be applied directly to molar mass determination of many complex polymers which, as mentioned, exhibit more than one single distribution of their molecular characteristics. This situation is schematically represented in Fig. 1, which shows a typical SEC chromatogram that is a dependence of polymer concentration in the effluent on retention volume.

In the case of complex polymers, size of macromolecules usually depends on all molecular characteristics, that is, not only on molar mass but also on chemical structure (for example, the composition of copolymers) and on physical architecture (for example, the long-chain branching) of macromolecules. To convert V_R values into particular local molar mass (M) values, functional dependence between size or molar mass and composition or architecture of macromolecules must be known. This last condition is only rarely fulfilled. Therefore various interpolation approaches are used in which, for example,

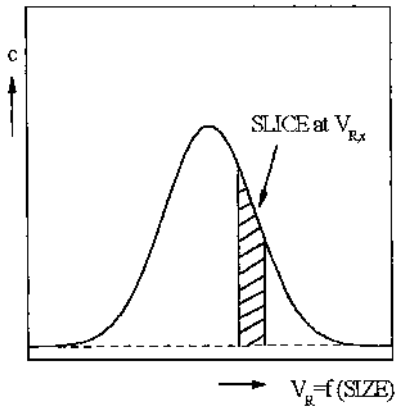

Figure 1 SEC chromatogram of a statistical binary copolymer. Each slice contains macromolecules of similar sizes; however, polymer species in each slice have different molar masses, chemical compositions, and sequence lengths.

© 2004 by Marcel Dekker, Inc.

relations between molar masses and sizes of macromolecules for complex polymers are calculated from corresponding relations for homopolymers. The success of these approaches may be rather selective; in many cases they fail completely (1).

Similarly, the "absolute" detectors, such as viscometers or light-scattering detectors, respond not only to molar mass but also to chemical structure and often also to architecture of macromolecules (Sec. 10). As a result, it is rarely possible to determine exactly two independent distributions from one single SEC measurement, even if using hyphenated detection (multidetector systems), except for mass spectrometry. Also, for the same reasons, data on molar mass distribution of complex polymers determined by simple SEC measurement will often be disturbed by the presence of further distribution(s). The situation seems to be easier in polymer blends in comparison with many other complex polymers. If two or several different detectors enable us to independently monitor concentrations of each blend constituent, calculation of molar mass/distribution data appears rather simple. However, the chemically different macromolecules can mutually affect their retention volumes ("concentration effects") so that the calculated MMD values may be inaccurate. Consequently, full separation polymer blend components is advised for exact determination of molar mass/distribution values (Secs 7 and 12.2).

SEC is often applied to direct determination of mean molar mass values and molar mass distribution of copolymers. For the above reasons, the data obtained can be regarded for most cases as only semiquantitative. The resulting information can be utilized in the investigation of various important tendencies in copolymerization processes but hardly for an exact evaluation of copolymerization kinetics. For binary statistical copolymers, the situation is schematically represented in Fig. 2a, which originates from considerations of Balke and Patel (2).

Statistical copolymers, composed from two different monomer units, for example, A and B, usually exhibit distribution in their molar mass, chemical structure [various compositions between homopolymers poly(A) and poly(B)] and architecture (from an alternating copolymer ABABAB to a block-copolymer AAAA–BBBB). Each molecular characteristic affects the size of polymer species in solution in a different way. The resulting dependences of polymer size on molecular characteristics can be represented by the contour plot shown in the center of the triangle in Fig. 2a. Evidently, the shape of the contour plot can be rather nonsymmetrical. If the sequence length distribution in a binary statistical copolymer is neglected, we arrive at a simplified scheme, which is shown in Fig. 2b. MMD and CCD are bimodal, though still continuous in this case. A scheme of a contour plot for a copolymer with discontinuous multimodal molar mass and chemical composition distributions is shown in Fig. 2c. Although simplified, the schemes in Figs 2a–c objectively illustrate the necessity of determination of all molecular characteristics for complex polymer systems by two or several independent but complementary procedures. In this

© 2004 by Marcel Dekker, Inc.

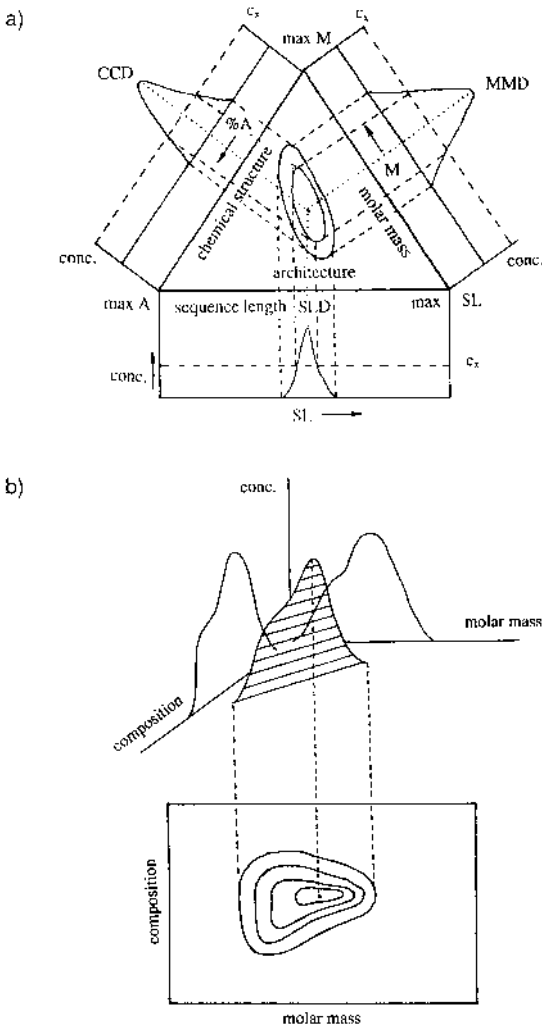

Figure 2 Schematic representation of multiple distributions of molecular characteristics in binary statistical copolymers. Three-dimensional diagrams and contour plots are shown. (a) Molecular size of statistical binary copolymers dependent on molar mass (MM), chemical composition (CC), and sequence length (blockiness-SL) and on distributions of the above characteristics. (b) Three-dimensional diagram and contour plot of a copolymer with bimodal, continuous molar mass distribution and chemical composition distribution. Sequence length distribution is neglected. (c) Contour plot of a copolymer mixture exhibiting multimodal, discontinuous molar mass, and chemical composition distribution.

© 2004 by Marcel Dekker, Inc.

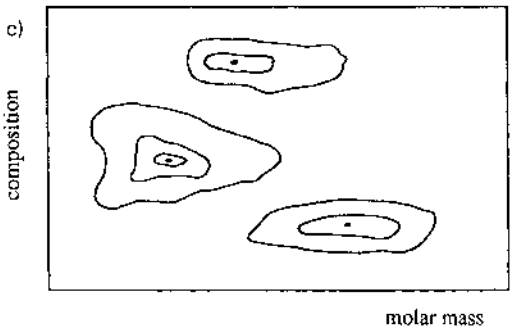

Figure 2 (*Continued*)

chapter, one of the emerging approaches for solving the above problems will be introduced, namely multidimensional liquid chromatography. Difficulties connected with complex polymer systems characterization grow exponentially with the number of characteristics to be independently determined. So far, systems possessing two distributions have been treated, and presence of further distribution(s) has been neglected. For that reason and also for the sake of clarity, we shall concentrate on two-dimensional liquid chromatography (2D-HPLC or 2D-LC) of complex polymer systems. The scope of this chapter does not allow us to provide a detailed survey of the literature. Therefore, we shall refer mainly to reviews and to monographs. At this time the excellent monograph by Glöckner (3) should be mentioned first. More recent broader publications describing several applications of 2D-HPLC for complex polymers are those by Pasch and Trathnigg (4) and Kilz and Pasch (5). Further, we include some basic papers, and other important experimental works which, for various reasons, have not been mentioned in the books of Refs 4 and 5, and will also select some very recent publications. We shall not treat in detail the hyphenated methods that combine chromatographic separations with the nonchromatographic separations such as mass spectrometry, TREF and CRYSTAF, field flow fractionation, and so on. Some other hyphenations of HPLC with nonchromatographic methods of measurement will be briefly mentioned as important detection approaches (Sec. 10). We shall also deal with hyphenation of HPLC methods with the HPLC-like procedures, which enable reconcentration, storage, and transfer of samples, as well as eluent exchange in 2D-HPLC instruments (Sec. 7). We anticipate that the so far less-known HPLC-like procedures, together with hyphenated detection will in future constitute expedient and often even indispensable components of many 2D-HPLC methods. As is typical for a handbook, we shall give simplified, general method descriptions, basic explanations, and practical hints. Selected 2D-HPLC

© 2004 by Marcel Dekker, Inc.

applications will be mentioned only for illustration and as a guide for the choice and evaluation of appropriate methods to solve a particular analytical problem.

2 STRATEGIES FOR TWO-DIMENSIONAL LIQUID CHROMATOGRAPHY OF COMPLEX POLYMERS

Two-dimensional HPLC instruments comprise at least two different and independent separation systems C#1 and C#2 (Fig. 3). The latter are represented either by different column fillings or different mobile phases, or both. Temperature variations are so far less common in 2D-HPLC of polymers. In some specific systems pressure changes may be utilized [for example, in supercritical fluid chromatography of complex polymer (6)].

Two-dimensional chromatographic separations were pioneered in gas chromatography and in thin layer chromatography. Their development was motivated by an effort to increase resolution of analytical separations, that is, to raise the number of substances that could be resolved by the enhanced peak capacity of chromatographic systems. Grushka (7) has shown that the number of peaks n that can be separated in a one-dimensional isocratic chromatographic system, that is, its peak capacity, can be calculated from the following equation:

$$n = 1 + \frac{N^{0.5}}{4} \ln\left(\frac{V_{R,n}}{V_m}\right) \tag{1}$$

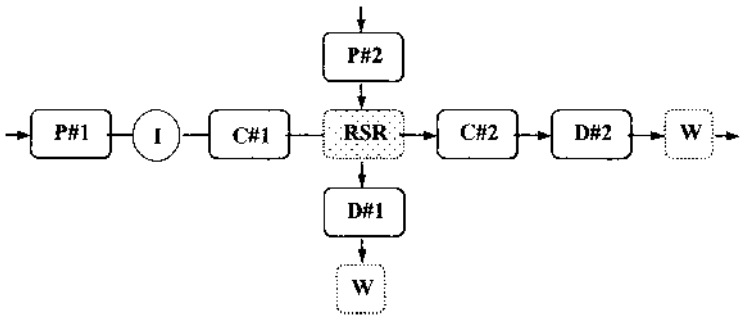

Figure 3 Schematic representation of a two-dimensional HPLC system for complex polymer separation. P stands for pumping systems, C for column systems, and D for detectors. Pumping system P#2 is needed if two different mobile phases or different flow rates of eluents are applied. I is the sample injector and RSR is the sample reconcentration, storing, and reinjection, as well as eluent switching system. W denotes waste vent (for explanation see also Sec. 9).

© 2004 by Marcel Dekker, Inc.

where N is the column efficiency expressed as theoretical plate number, $V_{R,n}$ is retention volume of the nth component, and V_m is the total volume of the liquid in the column (void volume).

The peak capacity for a two-dimensional chromatographic system n_{2D} is

$$n_{2D} = n_1 n_2 \sin \theta \tag{2}$$

where n_1 and n_2 are peak capacities of one-dimensional chromatographic systems, which are included into the two-dimensional system, and θ is called the separation angle between particular dimensions. $\theta = 90^\circ$ holds for two procedures that separate analytes exclusively according to one, different, property. It is evident that the peak capacity of two-dimensional chromatographic separations largely exceeds selectivity of one-dimensional procedures.

The above considerations can be extended also to polymeric analytes which, of course, can be separated into chemical individuals only in the range of oligomers with rather low molar masses.

Fractions leaving the first separation system C#1 are off-line or on-line transferred into the second separation system C#2 (Fig. 3). The off-line arrangements are generally more flexible but also time, sample, and labor intensive. Therefore, we shall deal in this chapter mainly with the on-line 2D-HPLC systems.

The two HPLC systems are to be selective to particular molecular characteristics of polymer sample (θ between 60 and 90°), that is, each system must separate macromolecules preferably or exclusively according to one molecular characteristic. The option $\theta = 90^\circ$ strongly simplifies data processing. If the first separation system C#1 discriminates macromolecules exclusively according to one single characteristic, the second HPLC system C#2 often does not at all need to be selective only to the second characteristic. For example, if C#1 separates molecules of copolymers exclusively according to their chemical composition and molar mass does not affect retention volumes, the second separation system may be a normal SEC column, because each fraction from the first separation system contains only species within a narrow composition range (sequence length distribution is neglected). On the contrary, if both separation systems discriminate macromolecules according to both characteristics with similar selectivities, the quantitative data evaluation is practically impossible. Therefore, the sequence of particular separation systems is very important. One of the first attempts for two-dimensional separation of statistical copolymers was published by Balke and Patel (2). These authors combined two liquid chromatographic systems, both of which separated macromolecules mainly according to their size. The first dimension separation system was an SEC column. Fractions from the SEC column, each containing species of different molar masses and compositions, were forwarded into the second dimension separation column, which combined entropic

© 2004 by Marcel Dekker, Inc.

(exclusion) and enthalpic (interaction) retention mechanisms. The nonselective SEC retention of complex polymers concerning their three different molecular characteristics was described in the preceding section. Therefore, the second column, even if selective enough to separate polymer species mainly or exclusively according to their composition, could not provide a set of information needed for full copolymer characterization because each fraction from the second column still contained macromolecules with different molar masses.

Concerning separation selectivity, we can define an important condition for a successful 2D-HPLC of complex polymers; namely different selectivities of separation systems, and especially of the first dimension separation system C#1, toward one of the molecular characteristics to be determined. This can be achieved by:

1. Full or at least substantial suppression of sample separation according to one molecular characteristic while selectivity of separation according to the second characteristic remains essentially unchanged.
2. Considerable enhancement of separation selectivity according to one molecular characteristic so that it fairly exceeds selectivity of separation according to the second characteristic.
3. Suppression of separation according to one characteristic and enhancement of separation according to another characteristic.

Evidently, the latter, ideal case is difficult to reach. Most liquid chromatographic approaches directed to these goals are based on the controlled combinations, coupling, of various HPLC retention mechanisms within the same column (Sec. 5).

Further features of combinations of various chromatographic methods include sample dilution and detectability. The latter aspects of two-dimensional separations together with efficiencies of both 2D partner procedures were theoretically analysed by Schure (8). In this broad discussion, he included gas chromatography, field flow fractionation, eluent gradient HPLC, SEC, and capillary electrophoresis. The binary combinations of the latter three methods should give the best results.

Sample dilution represents an important practical problem in 2D-HPLC. Fractions leaving the first dimension separation system C#1 (Fig. 3) may be too diluted to allow their quantitative detection. In this case, the reconcentration step must be introduced into the 2D-HPLC chromatograph. The corresponding system is denoted RSR in Fig. 3, where the first R stands for "reconcentration." If necessary, the RSR system should allow also for storage of fractions from system C#1 and/or sample solvent and mobile phase exchange in the second dimension system C#2. RSR enables direct forwarding of effluent from the column C#1 into the (set of) detector(s) for independent monitoring of sample concentration/

© 2004 by Marcel Dekker, Inc.

composition/architecture/molar mass in the column C#1 effluent. Thus S in the RSR abbreviation denotes "switching" and "storage" because column C#1 effluent can wait in the RSR system for reinjection into column C#2. A very important role of the RSR system is the defined reintroduction (second R) of (reconcentrated) fractions from column C#1 into column C#2 so that retention volumes of macromolecules leaving the second dimension separation column can be exactly identified.

The pecularities of sample purification, as well as their reconcentration, storage, and reinjection, and also of eluent exchange by means of RSR systems will be discussed in Secs 7, 8, and 9.

Various experimental arrangements of 2D-HPLC of polymers are possible and the complexity of the particular instrument applied depends on the separation problem to be solved. The most simple 2D-HPLC apparatus utilizes two different columns with just one pump P#1 and one (set of) detector(s) D#2 while the RSR system is simplified or fully abandoned. The complicated 2D-HPLC systems comprise two (systems of) columns C#1 and C#2, an isocratic pump plus a complete gradient making device P#1 and P#2, further a multicolumn/multivalve RSR system, and two series of detectors D#1 and D#2 (Sec. 11).

3 RETENTION MECHANISMS IN LIQUID CHROMATOGRAPHY OF MACROMOLECULES

In any HPLC separation, the retention volume V_R of an analyte is determined by the distribution constant K of sample molecules between a certain part of the eluent and column filling. K is expressed as a ratio of sample concentration in the (quasi) stationary phase C_S and the free mobile phase C_M. The free mobile phase is situated in the interstitial volume of the column packed with particulate material or in the flow-through channels of the monolithic column. The volume of the SEC stationary phase corresponds to the mobile phase within the separation pores, as well as to that situated near the outer surface of the column packing particles or near the surface of the transport channels of a monolith. In other words, we deal with the mobile phase volume from which macromolecules are partially or fully excluded. The stationary phase in the interactive (enthalpic) HPLC mainly includes the outer and inner (situated within the separation pores) column filling surface on which or near which adsorption, or ionic effects of analyte molecules occur. Enthalpic partition of analyte molecules takes place between the (quasi) stationary liquid phase and the mobile phase provided these two phases have different natures or compositions. Phase separation of macromolecules usually takes place in the mobile phase. The stationary phase can be either chemically bonded to an appropriate particulate or monolithic carrier, or formed by the stagnant molecules of eluent adsorbed on the column filling surface.

© 2004 by Marcel Dekker, Inc.

If the role of the stationary phase volume is neglected, an approximative relation can be written:

$$V_R \sim K = \frac{C_S}{C_M} \sim \exp\left(\frac{-\Delta G}{RT}\right) = \left(\frac{\Delta S}{R} - \frac{\Delta H}{RT}\right) \tag{3}$$

where ΔG is the Gibbs function, ΔS and ΔH are the respective changes in entropy and enthalpy of sample molecules largely connected with their transfer from mobile into (quasi) stationary phase or vice versa, R is the gas constant, and T is temperature. This simplified thermodynamic consideration allows classification of the retention mechanism in HPLC of macromolecules into two basic groups: entropic (exclusion) and enthalpic (interaction) retention mechanisms.

Before explaining HPLC retention mechanisms of macromolecules, some basic terms will be elucidated. In any HPLC system, three essential constituents must be considered; namely column filling, mobile phase, and separated sample molecules. Enthalpic contributions to the distribution constant K and to the sample retention volume result from interactions among the above three constituents. These ternary interactions can be in the first approximation described by a set of binary interactions; namely packing–mobile phase, mobile phase–sample, and sample–packing. In HPLC of small molecules, mobile phases are, as a rule, formed by two and more (usually liquid) constituents. Interactions between mobile phase constituents may also affect sample retention. This effect is often overlooked in HPLC of both small and large molecules. Single mobile phases are preferred in entropic HPLC (SEC) of polymers; however, they may contain substantial amounts of unwanted admixtures.

Mobile phases (components) that exhibit large affinity toward column packing are termed *strong*, in contrast to *weak* mobile phases (components). Thus the term *strength* of the mobile phase (components) expresses the extent of its (their) interactions with column packing. Mutual interactions between mobile phase components in mixed eluents may affect their interaction with column packing. This means that the strength of eluent component 1 toward column packing may change in the presence of eluent component 2, not only due to dilution of 1 by molecules of 2.

Enthalpic interactions between separated macromolecules and mobile phase (components) are described by the term *thermodynamic quality* of solvent (eluent). We speak about (thermodynamically) *good* and *poor* solvents and about *nonsolvents*. It is well known in polymer science that coils of macromolecules with the same molar mass assume a larger volume in good solvents than in poor solvents. This means that expansion coefficients of polymer species are larger than 1 in good solvents while only reaching a value of 1 in thermodynamically poor, theta solvents (9). In mixed solvents, macromolecules are, as a rule, preferentially solvated by one of the solvent components, usually but not exclusively with a better

© 2004 by Marcel Dekker, Inc.

solvent. Here again, solvent–solvent interactions play an important role. It should also be noted that a mixture of two nonsolvents for a polymer may together form a good solvent for it (*co-solvency phenomenon*). The opposite situation may also sometimes appear, when a mixture of two good solvents will not dissolve a given polymer (*co-nonsolvency phenomenon*). With rising temperature, solubility of a polymer in a liquid may either improve (*upper critical solubility temperature*) or (sometimes) also deteriorate (*lower critical solubility temperature*).

From the viewpoint of HPLC, interactions between macromolecules and column packing have a practical sense only in the presence of a mobile phase. Enthalpic interactions between column packing and polymer analytes are sometimes expressed by means segmental interaction energy parameter ε. The value of ε strongly depends on the eluent strength (Sec. 3.2).

3.1 Entropic Retention Mechanism

Changes of entropy within an HPLC column separating polymers result not only from mixing phenomena but also from large conformation and possibly also from orientation changes of macromolecules that get confined in the pores or excluded from the pores and/or from the outer column packing surface. The conformational contribution to the ΔS term in Eq. (3) is very large for polymer analytes and therefore important entropic effects accompany all HPLC separations of macromolecules. Evidently, the term "nonexclusion HPLC of polymers" is not appropriate, although the nonexclusion, enthalpic retention mechanisms dominate in some HPLC separation procedures. On the contrary, enthalpic interactions between macromolecules and column packing can be successfully suppressed ($\varepsilon \sim 0$). This is the case of "ideal" size exclusion chromatography.

Retention of macromolecules in liquid chromatographic systems is often analysed from the point of view of rules that are valid for low molar mass substances. However, already, a brief comparison of macromolecular and low molecular bulk static systems reveals important differences in their behavior. Neglecting these differences makes it difficult to understand retention behavior of macromolecules.

The entropic retention mechanism that is the entropic partition of macromolecules in porous systems forms a base for size exclusion chromatography and *hydrodynamic chromatography* (HDC). Differences in entropy changes for macromolecules of different sizes, which take place in stationary phase regions (mainly in the pores of different sizes and shapes) are responsible for different retention volumes of eluted polymer species. This results in separation of macromolecular analytes according to their size.

To date SEC is performed mainly with columns packed by porous particles. It is anticipated that improved technology of monolithic columns (improved control of sizes and volumes of separation pores) will allow their application also in SEC. HDC is carried out either with capillaries or with columns packed with

© 2004 by Marcel Dekker, Inc.

nonporous particles. The quasi stationary phase volume in HDC is much smaller than in SEC and, correspondingly, selectivity of separation is lower in the former case. SEC column packings will be further discussed in Sec. 4.1.1.

In entropy-driven separations such as SEC and HDC, retention volumes increase with decreasing sizes of macromolecules, that is, with decreasing molar masses of linear homopolymer samples. A typical dependence of SEC retention volumes on polymer molar mass is schematically depicted in Fig. 4, curves 1–5.

Dependences of this type are used for determination of local molar masses of polymeric analytes from retention volumes. They are obtained by elution of a series of polymer samples with known molar masses and are called *SEC calibration dependences*. We shall explain some general features of polymer retention in HPLC columns by means of this kind of diagram applying the term "calibration dependences," though these plots are often constructed for other than calibration reasons.

3.2 Enthalpic Retention Mechanisms

Total change of enthalpy connected with the transfer of macromolecules from mobile into (quasi) stationary phase [ΔH in Eq. (3)] is composed of enthalpic interactions of polymer segments with the column filling. Therefore ΔH is large in polymer HPLC provided attractive interactions of macromolecules with column filling exceed attractive interactions between eluent molecules and column filling,

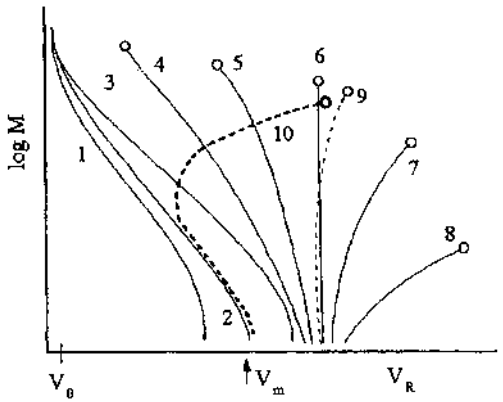

Figure 4 Schematics of calibration dependences in polymer HPLC for a constant exclusion contribution and different enthalpic interaction contributions expressed with segmental interaction energies, ε. 1: $\varepsilon < 0$; 2: $\varepsilon \sim 0$; 3,4: $\varepsilon > 0$; 5: $\varepsilon \gg 0$; 6: $\varepsilon = \varepsilon_{cr}$ (full entropy − enthalpy compensation); 7: $\varepsilon > \varepsilon_{cr}$; 8: $\varepsilon \gg \varepsilon_{cr}$; 9: $\varepsilon \sim \varepsilon_{cr}$ (nearly complete entropy − enthalpy compensation, ε slightly depends on polymer molar mass); 10: ε strongly depends on polymer molar mass. For further explanation see Sec. 3.2.1.

© 2004 by Marcel Dekker, Inc.

or repulsive interactions between macromolecules and eluent exceed repulsive interactions between stationary phase and macromolecules. The ΔH contribution to K rises with molar mass of separated macromolecules, and so do their retention volumes. However, the overall value of ΔH cannot be expressed by a single sum of segmental interaction energies because for steric and conformational reasons all parts of a macromolecule cannot simultaneously interact with the column filling. The overall situation is depicted in the scheme in Fig. 4. Curve 1 shows the course of calibration dependence for negative values of segmental interaction energy, $\varepsilon < 0$ while curve 2 holds for $\varepsilon = 0$, that is for "ideal" SEC. Curves 3 and 4 reflect low positive values of ε. The course #3 is explained with an increase of column filling surface or volume of stationary phase available for weak interactions of smaller macromolecules. This course is especially typical for oligomers containing end groups (generally, functional groups) which are attracted by column packing ($\varepsilon > 0$), while the main chain is less interactive ($\varepsilon \sim 0$). The role of end groups is largest for low molar masses and diminishes with rising size of analyte molecules. In any case, curve 3 indicates an increase of SEC separation selectivity due to the presence of enthalpic interactions between the column filling and analyte. The effect is usually small for high polymers but may be remarkable in the case of oligomers (10,11). The calibration curve of type 3 can also appear as a result of enthalpic partition of oligomer molecules, that is, when solubility of oligomers decreases in the eluent and/or increases in the stationary phase with decreasing sample molar mass (12). The prevailing role of total polymer segment number (molar mass of sample) over effect of accessible filling surface or stationary phase volume is evidenced for higher values of segmental interaction energy, $\varepsilon \gg 0$ (curve 5). As a result, V_R only increases rather little with increasing polymer molar mass. It should however, be stressed that the leading mechanism in case 5 is still size exclusion.

Curve 6 corresponds to a special situation when segmental interaction energy assumes a "critical" value ε_{cr} at which point entropic and enthalpic contributions to K mutually compensate. In this case, V_R assumes a value which is at least roughly independent of polymer molar mass and which is situated in the area of total volume of liquid in the column (column void volume V_m).

A further increase of ε values denotes the HPLC area where enthalpic interactions prevail over entropic effects and retention volumes (rapidly) grow with polymer molar mass (calibration dependences 7 and 8). For $\varepsilon \gg \varepsilon_{cr}$ (curve 8), this tendency is so pronounced that retention volumes became impractically high even for molar masses of a few $kg\,mol^{-1}$ and the applicability of corresponding HPLC systems is limited to oligomers. For large positive ε values, full retention of macromolecules in HPLC columns is often observed, which corresponds with "infinitive" retention volumes of samples (depicted with $\circ$ in Fig. 4). This situation may be rather pronounced with narrow pore column packings in HPLC systems working under a strong adsorption regime

© 2004 by Marcel Dekker, Inc.

and especially in the area of excluded molar masses (Sec. 3.2.1). Full retention is preceded with decreased sample recovery. Evidently, the highest molar masses are fully retained while smaller macromolecules are still eluted. If overlooked, this phenomenon may cause large errors in determined polymer characteristics. This is one of the important limitations of many enthalpy-affected HPLC polymer separations, especially of liquid chromatography at the critical adsorption point (Sec. 5.1). Curve 9 in Fig. 4 corresponds to the system where entropic and enthalpic contributions to V_R fully compensate only in a limited area of molar masses. The back-turn shaped calibration dependence 10 will be discussed in Sec. 3.2.1.

Four principal retention mechanisms in HPLC of macromolecules are *adsorption*, *enthalpic partition*, *phase separation*, and *ion interactions*. Ion interactions comprise ion exchange, ion inclusion, ion exclusion, and polyelectrolyte expansion. The latter phenomena plays an important role in HPLC of macromolecules bearing charges on their main chains, or branches (polyelectrolytes), or on their functional groups, especially when working with charged column fillings. Ion interactions may, however, appear also if low molecular ions (eluent additives and/or sample impurities) are adsorbed on macromolecules (pseudo-polyelectrolytes) and/or on the column filling surface. Most analysts involved in characterization of synthetic macromolecules try to systematically suppress possible ion interactions in HPLC systems rather than to utilize them in separation. Therefore, we shall deal only with the remaining three enthalpic retention mechanisms, namely adsorption, enthalpic partition, and phase separation. While the former two retention mechanisms play a decisive role in many HPLC separations of small molecules, the phase separation retention mechanism is an almost exclusive domain for macromolecules. Surprisingly, the differences between the three principal retention mechanisms in HPLC of macromolecules are not recognized in most papers and even in monographs (4,5) dealing with polymer separation. This results in confusing statements such as "polymer adsorption was promoted by adding a nonsolvent to eluent." The following sections should help orientation of readers, in particular those just entering the field of polymer HPLC.

3.2.1 Adsorption

Adsorption of macromolecular substances on solid surfaces and on liquid interfaces plays an important role in many systems containing biopolymers and synthetic polymers and also in numerous areas of technology. Therefore, the science of polymer adsorption keeps developing rather intensively, as it has over 100 years (see, for example, Refs 13 and 14). The adsorption retention mechanism of low molecular substances has already been studied in the initial stages of development of various chromatographic techniques. However, adsorption of

© 2004 by Marcel Dekker, Inc.

macromolecules may strongly differ from that of small molecules. Therefore, some conclusions on the role of adsorption of low molecular analytes cannot be directly applied in HPLC of macromolecules.

The schematics of polymer adsorption on the solid surface are shown in Fig. 5. A similar picture is valid also for adsorption of macromolecules on liquid (mobile phase)–(quasi) stationary phase interfaces. The extent of polymer adsorption depends both on the affinity of macromolecules to the surface and the eluent strength (see also Secs 1 and 4.2). Weakly adsorbed macromolecules are attached to solid surfaces and to interfaces with relatively short parts of their chains (*trains* are short, *free ends* are long, and *loops* are large). As ε increases, trains become longer while the loops and free ends become less frequent and their sizes decrease. To adsorb, macromolecules usually change their conformation (*de-coiling*). Consequently, adsorption of macromolecules is accompanied by large changes in their conformational entropy. This is one of the reasons why extent of polymer adsorption may increase with rising temperature of the system. De-coiling of macromolecules also allows us to understand adsorption of large macromolecules in narrow pores. At a certain, large ε value, de-coiled macromolecules are able to reptate into pores from which they would be excluded in the weak interaction regime ($0 \sim \varepsilon \ll \varepsilon_{cr}$) (Fig. 6) (15).

It is anticipated that in some systems the summing effect of otherwise not very large segmental interactions may start playing a role at certain molar masses. As a result, the calibration dependence would exhibit an unusual back-turn curvature (Fig. 4, curve 10). We have also revealed that macromolecules can penetrate along rather bulky groups bonded on a solid surface to adsorb on active surface groups (for example, silanols in case of silica gel C_{18} bonded phase) (16). In this case, polymer adsorption may be limited to rather short trains or even to single active groups situated on macromolecules. To attain a measurable change in retention volume, macromolecules must bend and attach on the surface simultaneously with several moieties. This is possible only if polymer molar mass is high enough and therefore the back-turn kink on calibration dependences affected by adsorption is observed only at a certain "limiting" size of macromolecules. We speak about "U-turn adsorption" (Fig. 7) (15–17). Evidently, conformation of this hypothesis will need

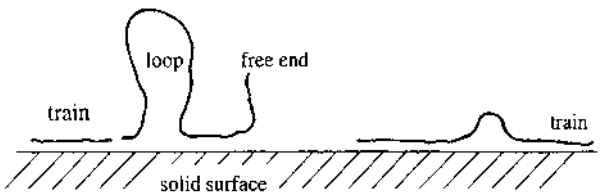

Figure 5 Schematic representation of macromolecules adsorbed on a solid surface.

© 2004 by Marcel Dekker, Inc.

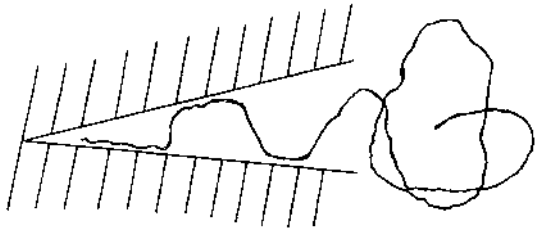

Figure 6 Schematic representation of a (large) macromolecule adsorbed in a narrow adsorbent pore at high ε value.

further experimental material and also calculation of steric and conformational feasibility of the U-turn arrangement macromolecules (kinked conformation).

The usual source of adsorption for electroneutral species are dipole–dipole and dipole-induced dipole interactions between analyte and column fillings. Therefore, important adsorption phenomena are observed mainly for polar macromolecules. The most common HPLC adsorbents are silica gels with active silanol groups. Adsorption on siloxane groups is expected to be much weaker. Unexpectedly large polar adsorptive activity was, however, also observed in poly(styrene-co-divinyl benzene) column packings (18,19) (see also Secs 4.1.1 and 4.1.2). HPLC column fillings will be discussed in Sec. 4.1.

As mentioned, analyte adsorption is strongly affected by the nature of the eluent (Secs 1 and 4.2). A strong solvent, which fully suppresses adsorption of a polymer on a given column packing at given temperature (and pressure) ($\varepsilon \sim 0$) is termed a *desorli* while a weak solvent, which promotes full adsorption of a polymer on a given column packing at given temperature (and pressure) is called an *adsorli* ($\varepsilon \gg \varepsilon_{cr}$). Evidently, the adsorli for a polymer on a sorbent may turn out to be a desorli for another polymer on the same or another sorbent, or at another

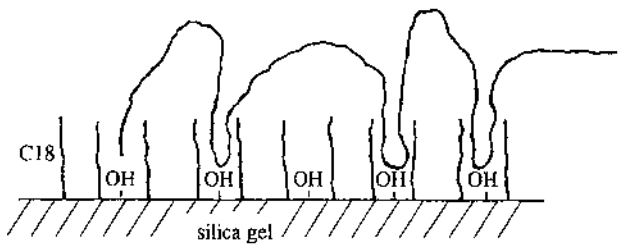

Figure 7 Schematic representation of adsorption of a large macromolecule (containing polar moieties) on silica gel C_{18} bonded phase containing free silanols.

© 2004 by Marcel Dekker, Inc.

temperature. The efficacy of an adsorli depends on the length of adsorbed macromolecular trains it allows. For an onset of full polymer retention already relatively short trains may be sufficient. Similarly, efficacy of a desorli depends on its ability to block active sites on both packing surface and macromolecules. In HPLC systems, an important role may also be played by kinetic parameters of both train formation and destruction. So far, little is known about these features of polymer adsorption. Our measurements have, however, revealed that attachment of macromolecules onto nonoccupied adsorbent surface, which causes their full retention, is a fast process. Similarly, detachment of polymer chains from a nonporous adsorbent surface, which results from a desorli action, is quick provided the system is well mixed (20,21). It seems that an instantaneous contact between strongly interacting polymer and adsorbent pair or a twinling desorli action are sufficient for the full adsorption or desorption of macromolecules, respectively. On the other hand, conformational changes of adsorbing macromolecules and the diffusion-controlled mutual displacements of polymer species from the nearly saturated adsorbent surface may be much more dilatory. As a result, the equilibrium adsorption of polymers is considered a slow process, which needs hours or even days to fully develop (13). In any case, kinetic effects must be considered when evaluating adsorptive retention of macromolecules within porous HPLC column fillings.

A single liquid or a mixture of adsorli and desorli that is strong enough to allow elution of at least a fraction of polymer sample from a column packing at a temperature is denoted a *displacer* ($0 \sim \varepsilon < \varepsilon_{cr}$). Some basic parameters of HPLC eluents will be discussed in Sec. 4.2.

In conclusion, adsorption within an HPLC column causes a change in analyte retention in addition to retention due to the ever present entropic exclusion. In the weak adsorption regime (low ε values) the exclusion mechanism prevails and retention volumes of macromolecules increase with decreasing molar mass. On the contrary, retention volumes increase or even strongly rise with analyte molar mass in the strong adsorption regime (high ε values). Strong adsorption of analyte molecules can lead to their full retention (Fig. 4 and Sec. 7). Moreover, adsorption of analytes can bring about chromatographic band broadening and splitting. These two phenomena frequently appear with narrow pore HPLC column packings and, in particular for high molar mass (excluded) analytes. Often, it is difficult to remove large macromolecules adsorbed within narrow pores of the column packing. Very effective desorli must be applied and the desorbing process may be rather slow (15).

A phenomenon that is termed "column history" can complicate experimental work with the adsorbing solutes. (Macro)molecules that were fully retained within packing and were not entirely removed by a careful column flushing procedure may promote adsorption of subsequent analytes. As a result, retention volumes may change in the course of a series of experiments. Column

© 2004 by Marcel Dekker, Inc.

history may also play an important role in conventional SEC measurements. It can substantially reduce the precision and accuracy of results. The successive deposition of sample constituent(s) within packing is often responsible for limited life-time of HPLC columns, which is evidenced by irrepeatability of retention volumes and by large band broadening effects.

Adsorption of analytes depends also on temperature and pressure within HPLC columns. Temperature can be used as an important parameter to affect retention of macromolecular analytes (22). Correspondingly, temperature must be carefully controlled in enthalpy-driven HPLC of polymers. This may be difficult due to heat evolved in a column by the friction of the flowing mobile phase. As a result, both axial and radial temperature gradients may be created in HPLC columns (23). Direct pressure effects are anticipated only at very high pressures of hundreds of MPa (thousands of bars). On the other hand, important V_R variations may already appear at much lower pressure changes when working with mixed mobile phases. Preferential sorption of the mixed eluent components within the column packing (Sec. 4.1) is often strongly affected by pressure variations as low as a few MPa and, consequently, analyte retention can be altered (24,25). This may happen, for example, due to flow rate adjustment or due to partial blocking of the exit column filter.

3.2.2 Enthalpic Partition

Enthalpic partition of analyte molecules between (at least) two chemically different liquid phases gives rise to the second important retention mechanism in polymer HPLC. The stationary liquid phase can be created, for example, by adsorption or absorption of a liquid immiscible with eluent on the inner and outer surface or within the pore volume of a particulate or monolithic column filling. Alternatively, a dynamic (quasi) stationary phase can be formed as a result of preferential adsorption of a mixed eluent component on the filling surface. The HPLC approaches, which are based on the above phenomena are accompanied with important experimental problems connected with stationary phase relating to both "bleeding" and composition changes. Therefore, chemically bonded stationary phases are preferred in modern HPLC. In spite of numerous attempts to modify surfaces of various carriers based on inorganic oxides with polymers (for review see Ref. 26) the HPLC field is presently dominated by materials prepared by bonding short aliphatic groups C_4, C_8, C_{14}, C_{22}, C_{30}, and mainly C_{18} onto porous and nonporous SiO_2 particles (Sec. 4.1). Recently, monolithic silica C_{18} also became available (27). Other important HPLC column fillings represent heterogeneously crosslinked porous, nonporous, and monolithic systems based on natural or synthetic polymers (Sec. 4.1).

At present, silica C_{18} materials are almost exclusively used in enthalpic partition HPLC of polymers. Consequently, the enthalpic partition retention mechanism seems to be limited to weak London nonpolar interactions. In fact,

© 2004 by Marcel Dekker, Inc.

however, aliphatic bonded groups may exhibit a rather "polar" character if solvated with eluent molecules that contain both nonpolar and polar moieties. The advantage of working with weaker enthalpic interactions is the "softness" of the corresponding HPLC systems. In contrast to the adsorption-based retention mechanism, fine control of retention volumes is easier in enthalpic partition HPLC of macromolecules. On the other hand, silica-based C_{18} column packings contain many remnant free silanols which, for steric reasons, cannot be bonded with C_{18} groups. In spite of numerous attempts to block these free silanols with low molar mass silanes ("end capping"), even the best "deactivated" silica gel C_{18} materials still contain some 50% of initial silanols. The latter are, surprisingly, accessible for macromolecular analytes and under certain conditions may be responsible for their extensive adsorption (16,17). As result, enthalpic partition of macromolecular analytes in silica C_{18} phases is often accompanied with their adsorption. This may hold even for less polar polymers such as poly(methyl methacrylate), and so on, in nonpolar mobile phases. For the sake of clarity, the adsorption effects will be neglected in the following discussion.

The enthalpic partition of macromolecules in favor of the bonded (e.g., C_{18}) phase takes place if solvated bonded groups represent a thermodynamically better solvent than the mobile phase for analyte macromolecules. This often happens if mobile phase is a poor to very poor solvent for polymer sample (Secs 1 and 4.2). When eluent quality for a polymer sample decreases, the phase separation threshold may be attained. As a rule, phase separation starts with the largest macromolecules. We arrive at a hybrid separation mechanism, enthalpic partition plus phase separation. In some systems, even all three enthalpic retention mechanisms, that is, enthalpic partition, adsorption, and phase separation, can be present simultaneously and act antagonistically. Evidently, it may be difficult to understand and to control elution of analytes under hybrid retention mechanism conditions. The strength of interaction between the mobile phase and the bonded phase has somewhat different meaning between adsorption and enthalpic partition HPLC mechanisms. At least one strong eluent component that is able to solvate the bonded phase must be present to prevent the stationary phase (C_{18} groups) from a collapse and to allow efficient enthalpic partition of analytes. At the same time, the mobile phase (usually one of the eluent components) must efficiently repel macromolecules and push them into the stationary phase.

The enthalpic partition of a macromolecule between the C_{18} phase and eluent is schematically depicted in Fig. 8. It is evident that the enthalpic partition process is also accompanied with de-coiling of macromolecules and with large entropic effects.

Similar to adsorption, enthalpic partition phenomena directly affect retention volumes of analytes. Owing to a relatively low strength of interactions between the C_{18} phase and macromolecules, the enthalpic partition effects are generally less pronounced when compared with adsorption. Therefore,

© 2004 by Marcel Dekker, Inc.

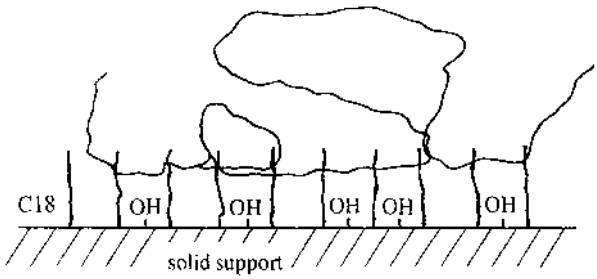

Figure 8 Schematic representation of a macromolecule partitioned between bonded C_{18} groups and mobile phase.

adjustments of enthalpic partition usually require relatively larger changes in eluent composition or in temperature. Full retention of macromolecules within the column may be more difficult than in the case of adsorption (28) unless a very poor solvent is used as mobile phase.

It is anticipated that enthalpic partition of macromolecules, especially in the narrow pore column packings and when approaching polymer phase separation limits, may lead to band broadening and splitting phenomena. Retention volumes of polymers subject to enthalpic partition depend on temperature and possibly also on pressure.

The schematics of a situation depicting the hybrid enthalpic partition/adsorption retention mechanism of macromolecules is shown in Fig. 9.

3.2.3 Phase Separation: Solubility

As shown in Sec. 3.2.2, the thermodynamic quality of the mobile phase toward eluted polymers strongly affects enthalpic partition of macromolecules. Moreover, quality of eluent also somewhat influences exclusion behavior of macromolecules

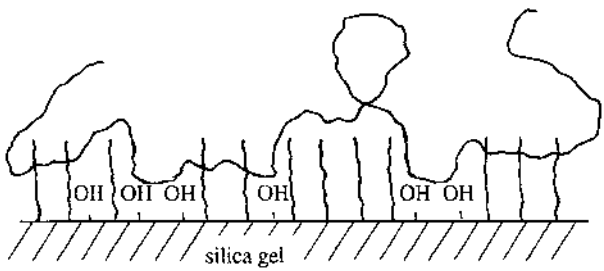

Figure 9 Schematic representation of macromolecules simultaneously adsorbed on free silanols of silica gel and partitioned between bonded C_{18} groups and mobile phase.

© 2004 by Marcel Dekker, Inc.

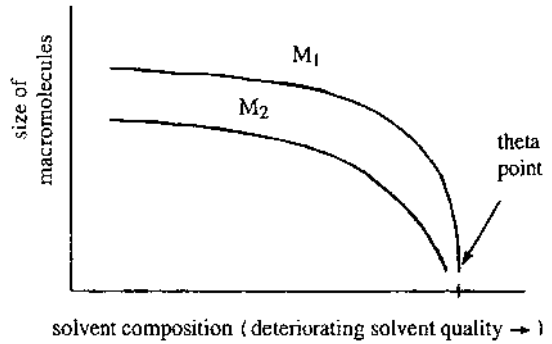

Figure 10 Schematic representation of polymer coil dimensions as function of thermodynamic quality of solvent, $M_1 > M_2$.

through changing their sizes. Figure 10 shows a typical course of polymer size changes with changing thermodynamic quality of the solvent (Fig. 10).

Swollen coils of macromolecules usually extensively shrink in the vicinity of theta conditions where mutual interactions between polymer segments are equal to interactions between solvent molecules and polymer segments (9). Important changes in polymer–column filling interactions, both adsorption and enthalpic partition, are expected in the vicinity of the theta point (29,30). If the thermodynamic quality of solvent further deteriorates, macromolecules may collapse and assume less than 50% of their theta dimensions. The instable, collapsed state of a macromolecule may last for several minutes (31), which is comparable with the duration of normal HPLC experiments. The deteriorated solvent quality, however, inevitably leads to a phase separation (32). The macro-phase separation in polymer systems is often preceded by a micro- or nano-phase separation that is by complexation of macromolecules (association or aggregation). The latter processes, whether solute concentration dependent (association) or not (aggregation), further complicate HPLC elution of polymer analytes because of their slow kinetics. Although SEC was used for polymer association studies (see, for example, Refs. 33–35), it seems that attaining repeatability of retention volumes and peak shape values for complexing macromolecules is rather difficult. Block-, graft-, and star-copolymers dissolved in selective solvents (liquids that dissolve one kind of polymer chain but precipitate another kind) create micellar systems. The core of micelles is formed by aggregated insoluble chains while the soluble chains create a protective cloud that prevents macrophase separation. Sizes of micelles depend on thermodynamic quality of solvent and may change with time.

During phase separation of polymer solutions, at least two phases are formed. One of them is concentrated ("gel phase") and contains larger macromolecules. The other, diluted ("sol") phase contains smaller polymer species. In

© 2004 by Marcel Dekker, Inc.

many cases, the diluted phase contains only pure solvent (32). Alternatively, solid particles of a precipitate appear when the quality of solvent rapidly deteriorates and also if macromolecules tend to crystallize. Solubility of macromolecules in a solvent is affected by all molecular characteristics of polymers. It depends rather strongly also on temperature and pressure. Before SEC was introduced, phase separation phenomena were extensively used for polymer fractionation (3). In the case of copolymers, solvent–nonsolvent systems were sought in which effect of either molar mass or composition was suppressed (36). In the case of crystalline polymers, such as polyolefins, the solubility-based phenomena form a base for the important methods, TREF (37) and CRYSTAF (38). Phase separation phenomena are directly used in high-performance precipitation/redissolution liquid chromatography of macromolecules (3) termed also gradient polymer elution chromatography (GPEC^{R}) (39). Phase separation processes of macromolecules, precipitation, and (re)dissolution of polymer species, are usually slow compared to adsorption and enthalpic partition. Slow redissolution processes are rather frequent with very high molar mass polymers, and with species that may undergo crystallization (40). Thus, the kinetics of phase separation may contribute to chromatographic band broadening and splitting. Moreover, if both separated phases contain macromolecules, band broadening and splitting may be very important. Complex polymers may even form multiphase systems. In many cases, phase separation is accompanied by adsorption and/or partition phenomena. The resulting hybrid separation mechanism may be difficult to control.

For the above reasons, the phase separation retention mechanism is mainly used in HPLC of nonpolar polymers and oligomers and under conditions that prevent sample crystallization.

4 MATERIALS FOR TWO-DIMENSIONAL HPLC OF MACROMOLECULES

4.1 Column Filling Materials

Some general features of HPLC column fillings were briefly outlined in Sec. 1.

4.1.1 Column Packings for Size Exclusion Chromatography

Particulate column packings dominate SEC because sizes of separation pores in monoliths are difficult to control. Silica gels exhibit high mechanical stability and advantageous pore structure with fast mass transfer kinetics. Their limited stability in basic mobile phases is not important in most HPLC applications to synthetic polymers. However, silica gels are rather active, largely due to the presence of surface silanols, and it is difficult to reach $\varepsilon \sim 0$ for polar polymers with bare silica column fillings. Therefore heterogeneously crosslinked poly(styrene-co-divinylbenzene) (PS/DVB) resins represent the most common

© 2004 by Marcel Dekker, Inc.

packing materials for SEC of synthetic lipophilic polymers. Different mean pore diameters are applied in SEC. They range from about 4 to over 400 nm. PS/DVB SEC column packings are considered noninteractive, yet important enthalpic interaction and, consequently, retention volume increase, has been observed for polymers of medium and high polarity with some PS/DVB packings (16,18,19). The extent of polar interactivity of PS/DVB column packings varies from producer to producer (18,19). It is anticipated that polar interactivity of PS/DVB HPLC column packings is caused by various polar groups present on the packing surface (Secs 3.2.1 and 4.1.2). Highly polar substances such as formic acid, trifluoroacetic acid, dimethylformamide, and so on, are sometimes added to eluents in order to prevent adsorption of analytes within SEC column packings. Alternatively, polar eluents may be applied. If, however, the eluent appears to be a poor solvent for the polymeric analyte (for example dimethyl formamide for polystyrene samples), enthalpic partition phenomena may appear and V_R again increase (41). The general condition for the ideal SEC ($\varepsilon \sim 0$) is a certain degree of symmetricity in the system. In other words, interactions between all three essential constituents of the HPLC systems should be similarly positive with the slightly prevailing role of eluent. This means that eluent must be strong toward column packing and rather good for the polymer sample while polymer and column packing should not exhibit strong attractive or repulsive interactions. It is evident that new, tailored SEC column packings should be synthesized to cover the broad range of polarities of the polymer analytes.

4.1.2 Column Fillings for Enthalpic Interaction HPLC

Numerous particulate column packings and several monolithic HPLC materials have been synthesized in various research laboratories. Practically all of them were designed for HPLC of low molar mass substances. Consequently, the choice of interactive column fillings for polymer HPLC is limited to a few materials widely applied in HPLC of low molar mass substances. Tailored column fillings that would allow the fine tuning of retention of macromolecular analytes are practically nonavailable. The HPLC column packing market is dominated with porous and nonporous particulate, as well as monolithic SiO_2 materials both bare and bonded with various groups. Other inorganic bonded phase carriers such as zirconia, titania, and alumina so far have not found wide application. Of the many different bonded groups prepared on a laboratory scale, only a few are suitable for polymer separation and are commercially available. Unfortunately, composite stationary phases comprising a mechanically stable (inorganic) carrier, pores of which are filled with a homogeneously crosslinked network of organic macromolecules (26), are missing from the market.

Alternative column filling materials are those based on heterogeneously crosslinked synthetic and natural polymers. Styrene–divinyl benzene resins are

© 2004 by Marcel Dekker, Inc.

largely used, being complemented by only a few other, mainly hydrophilic materials. The chemical structure of the organic column fillings is often non-disclosed by column producers. Quite popular are fillings based on hydroxyethyl methacrylate and (hydrolysed) glycidyl methacrylate resins.

Rapid progress in SiO_2 binding chemistries (42) and in synthetic polymer column filling materials including monoliths (43,44) raises the hope that the situation regarding column fillings for polymer HPLC will soon improve. Also, further developments in polymer HPLC and 2D-HPLC may eventually attract the attention of column producers.

Silica gel is a very complex material with complicated physical and chemical structures (45,46). Many parameters of silica gels have been studied in detail, and technology for the production of HPLC silica-based column fillings has substantially improved in recent years. This is manifested, for example, in better batch-to-batch reproducibility of silica gel HPLC column packings from most producers. Still, numerous questions concerning this material remain so far unanswered and further progress in controlling silica gel properties is needed. As mentioned, the structure of silica gel pores is advantageous for fast mass transfer of samples, which results in increased column efficiency. Silica gels with various pore diameters D (up to several hundreds and even thousands of nm) and pore volumes (up to $2\,mL\,g^{-1}$) have been synthesized; however, the market of HPLC columns for separation of low molar mass substances dictates parameters of most commercial silica gels. Mean values of D for most silica gels in the range 6–12 nm (60–120 Å). Their relatively low pore volumes in the range of $1\,mL\,g^{-1}$ allow high pressure resistance. Silica gel based bonded phases with diameters of 30 nm and sometimes 50 nm are applied to HPLC of proteins. Silica gels with pore sizes up to 400 nm that were on the market a few years ago are hardly available any more. As a result, most HPLC separations of polymers are carried out with mesoporous column packings. Macromolecules with molar masses above $50–100\,kg\,mol^{-1}$ are excluded from pores of such packings under weak interaction regimes. Evidently, the outer surface of 5 or 10 μm particles, which lies in the range of hundreds of $cm^2\,g^{-1}$, is too small to allow selective retention of macromolecules. This supports the hypothesis on the barrier mechanism of polymer retention in many isocratic and gradient procedures of polymer HPLC (Sec. 5.2). It is widely accepted that polar interactivity of silica gel is caused mainly by the presence of surface silanol groups. Siloxane moieties are less interactive. The adsorption activity of silanols depends on their topology and concentration. As was shown for low molar mass analytes, the most active are isolated silanols, followed by geminal and vicinal silanols. The adsorptive activity of latter types of silanols is reduced by their mutual hydrogen bonding. Therefore the activity of silica gel in terms of polymer adsorption seems to reach its maximum at the intermediate silanol concentration at which the highest population of isolated silanols is anticipated (47).

© 2004 by Marcel Dekker, Inc.

Quantitative relations between silanol concentration and column filling interactivity toward polymer species are, however, difficult to establish because the affinity of macromolecules toward column packing depends also on pore size and shape, as well as on polymer nature. One must rely on trial-and-error tests and optimizations.

The activity of silanols is also strongly influenced by the presence of metal impurities in the silica matrix. Modern technology of ultra-pure silica production (silica of B type) allows the more efficient control of silica gel interactivity compared to the A type of silica, which contains metal impurities.

Differences in bonding chemistries, as well as in endcapping and polymer coating procedures, represent another source of limited producer-to-producer silica-based filling reproducibility. Further problems are brought about by chemical attack of eluents and sometimes also of samples on both the silica gel matrix and the bonded groups. Generally, pH below 2 and above 8 as well as elevated temperatures above 80°C should be avoided to keep high repeatability of retention. The former conditions are usually unproblematic for lipophilic synthetic polymers; however, traces of moisture in hygroscopic eluents may affect the column lifetime.

Macroporous, heterogeneously crosslinked organic resins do not only interact with polymer analytes by their (smooth) surfaces. It is anticipated that the free ends and loops of macromolecular chains protrude over filling surfaces and create a sort of "bonded phase," which may take part in enthalpic partition processes.

As mentioned, most commercial nonpolar poly(styrene-co-divinylbenzene) column packings were found to exhibit surprisingly high polar interactivities, which cause increased retention of medium and polar polymer species (Secs 3.2.1 and 4.1.1). This phenomenon may be caused by polar substances such as initiators, chain transfer agents, porogenes, and protective colloids, which are added to polymerization systems to control porosity, size, and (spherical) shape of packing particles. Another source of polar interactivity of commercial styrene–divinylbenzene HPLC column packings may be the additional crosslinking of some organic resin-based materials (48).

4.2 Mobile Phases

Properties of HPLC mobile phases are discussed in many HPLC textbooks (49,50). As has been repeatedly stressed in Secs 1 and 3, adsorption of macromolecules within a column filling largely depends on eluent strength. Snyder, in his classic monograph (49) proposed solvent strength parameter, ε^0, for characterization of potential eluents and eluent components. Originally, ε^0 values were determined for alumina adsorbents, which possess a more homogeneous and less interactive surface than silica gels. Still, the same tabulated ε^0 values are

© 2004 by Marcel Dekker, Inc.

widely used also for the semiquantitative characterization of eluent strength toward silica gel and other polar column packings. Snyder proposed to express the solvent strength for binary eluents AB, ε^0_{AB} as

$$\varepsilon^0_{AB} = \varepsilon^0_A + \frac{\log N_B}{\alpha n_B} \tag{4}$$

where ε^0_A is solvent strength of the weaker eluent component, A, N_B is mole fraction of the stronger component B, and n_B is the effective molecular area of an adsorbed molecule B. The adsorbent surface activity function, α, is defined as

$$\log K^0 = \log V_a + \alpha f(X, S) \tag{5}$$

where K^0 is sample adsorption distribution coefficient (milliliters per gram), V_a is the volume of an adsorbed solvent monolayer per unit weight of adsorbent, and $f(X, S)$ is a function describing properties of sample X and solvent S. The simplified Eq. (4) holds for A plus B mixed eluents with not very low concentration of the stronger component B. The role of molecular interactions between A and B solvents is not considered.

Solubility of analytes plays an important role not only in phase separation but also in partition-based HPLC of macromolecules. Thermodynamic quality of the eluent allows controlling of both phase separation and enthalpic partition polymer retention mechanisms and to some extent it may also influence polymer adorption. The thermodynamic quality of a solvent for a polymer is expressed by the Flory–Huggins interaction parameter χ (6) or by the exponent in the Staudinger–Mark–Houwink–Sakurada viscosity law

$$[\eta] = K_v M^a \tag{6}$$

where $[\eta]$ is the limiting viscosity number of linear macromolecules with molar mass M (in practice, molar mass of the species that is most abundant in the sample), and a and K_v are constants for a given polymer–solvent system. $[\eta]$ reflects the volume of polymer coils in the infinitively diluted solution. In thermodynamically good solvents, $[\eta]$ values little depend on temperature (Fig. 10) while they rapidly change at the vicinity of the theta point. The product of $[\eta]$ and M is the hydrodynamic volume of polymer coils and represents a base for the famous Benoit's SEC "universal calibration dependence" (51), which is a plot of $\log[\eta]M$ vs. V_R for appropriate polymer standards (largely polystyrenes). In the absence of enthalpic interactions ($\varepsilon \sim 0$) universal calibration plots for a particular SEC column coincide for different coiled polymer species in different eluents.

For many linear macromolecules, exponent a in Eq. (6) assumes values from 0.5 (for theta solvents) up to 0.7–0.8 (for thermodynamically good solvents).

Both χ and a values for numerous polymer–solvent systems are collected, for example, in *Polymer Handbook* (52).

© 2004 by Marcel Dekker, Inc.

Both strength and thermodynamic quality of eluents can be adjusted by temperature variation and, especially, by mixing two or several substances. Unfortunately, mixed eluents possess several complicating features. In order to efficiently control the resulting strength and quality of a mixed eluent, its components must exhibit rather different polarities, that is, different strengths toward the column packing or different quality toward macromolecular analyte. This results in preferential sorption of eluent components in the domain of column packing and/or in preferential solvation of analyte macromolecules. Preferential sorption causes an increase of a particular eluent component concentration near the packing surface or within the bonded stationary phase. The term preferential solvation stands for increased concentration of one eluent component in the domain of sample macromolecules. The extent of both preferential sorption and preferential solvation depends on temperature and pressure. Variations in preferential sorption resulting, for example, from temperature or pressure (19) changes may complicate retention control. Preferential sorption is co-responsible for the appearance of system peaks on HPLC chromatograms due to displacement effects (53). System peaks appearing on chromatograms obtained with mixed eluents are also due to preferential solvation of the sample (54). Both phenomena, preferential sorption and preferential solvation, complicate sample detection and appropriate corrections are necessary (4,55).

Adsorption of analytes within polar HPLC column fillings is efficiently controlled by adding polar, strong modifiers into a nonpolar, weak mobile phase. Historically, this approach is called HPLC with normal (straight) mobile phase (NPLC or NP HPLC) in liquid chromatography of low molar mass substances. Extent of retention due to enthalpic partition in favor of nonpolar (bonded) phases is controlled by adding less polar modifiers into a more polar major eluent constituent (usually water). This approach is widely known as reversed mobile phase (high-performance) liquid chromatography (RPLC or RP HPLC) of small molecules. The terms NP HPLC and RP HPLC are sometimes also used in polymer liquid chromatography.

Numerous other parameters are important for the eluent component choice (50). They include, for example, transparency in the ultraviolet and sometimes in the infrared wavelength range, high boiling point, as well as viscosity, corrosive properties, toxicity, and price. In 2D-HPLC systems, further important eluent parameters must be considered such as mutual miscibility of mobile phases in both separation systems and overall compatibility of the column #1 eluent with the column #2 packing. Also for this reason, it is useful to apply SEC eluent (column #2) as one of the column #1 eluent components.

4.3 Polymer Reference Materials (Standards) for HPLC

Dependences of polymer retention volumes on molar mass (Fig. 4) are constructed by eluting a series of homopolymer probes with different molar

© 2004 by Marcel Dekker, Inc.

masses and narrow molar mass distributions. Such polymer standards are used also in optimization of HPLC column/eluent/detector systems and for evaluation of band broadening/splitting phenomena. Several—but not too many—series of homopolymers with different MMM and narrow MMD are available from a handful of producers. SEC calibration dependences can be constructed also by applying well-characterized broad molar mass polymers. The latter are especially suitable for periodic checking of SEC instrument performance. Unfortunately, only few well-defined complex model polymers are commercially available, such as block-, graft-, and statistical-copolymers, further star-, cyclic-, branched-, stereoregular-, and so on, species. These models are very much needed for HPLC method development, otherwise many separations will be evaluated using poorly defined polymer species. Many polymer synthesists are reluctant to make their samples available to chromatographers, probably in order to prevent bad disclosures, or because they try (or hope to be able to in the future) to characterize their samples themselves. In any case, the lack of well-defined polymer models hampers progress in HPLC of complex polymers including 2D-HPLC method development.

5 FIRST-DIMENSION SEPARATION SYSTEMS (COUPLED HPLC PROCEDURES)

As mentioned in Sec. 2, an important part of each polymer 2D-HPLC strategy is either to suppress or to strongly increase separation selectivity according to one molecular characteristic in the first separation column while separation according to the second molecular characteristic may remain essentially unchanged. Selectivity of SEC separation is limited by column packing pore volume. Augmentation of entropy-dominated separation selectivity according to polymer molar mass can be achieved by adding an enthalpic retention mechanism ($\varepsilon > 0$). The resulting benefit is, however, rather limited except in the case of some oligomers (Sec. 3.2 and Fig. 4).

Much more promising seems to be the suppression of HPLC separation selectivity according to one molecular characteristic, especially according to polymer molar mass. One can speak about one-parameter HPLC separation of macromolecules. An inspection of Eq. (3) and Fig. 4 reveals one such possibility. If ΔS and ΔH contributions to ΔG are equal, K in Eq. (3) is 1 and V_R is a constant, independent of molar mass of polymer analyte. The linear part of SEC calibration dependence can be expressed with the following equation:

$$V_R = C - D \log M \tag{7}$$

© 2004 by Marcel Dekker, Inc.

where C and D are constants for a particular polymer–eluent system in a given column, or

$$V_R = E - F \log[\eta] M \tag{8}$$

(universal calibration dependence) (51), where E and F are constants for a given column provided enthalpic interactions are negligible ($\varepsilon \sim 0$) and macromolecules form isolated, flexible coils.

According to Eqs (7) and (8), retention volumes decrease with increasing polymer molar mass. For V_R of macromolecules retained in the strong interaction regime ($\varepsilon > \varepsilon_{cr}$) we have

$$V_R = G + H \exp M \tag{9}$$

where G and H are constants for a given polymer species in a given HPLC column/eluent system and at a given temperature. It is attractive to intentionally combine, to couple entropic and enthalpic retention mechanisms so that they mutually compensate and the molar mass dependence of retention is suppressed or even absent.

Several approaches to such coupling of retention mechanisms were recently described in a review (56). Therefore, we shall abridge the present discussion on this matter.

The result of isocratic coupling of exclusion and enthalpic interaction retention mechanisms, which leads to molar mass independent retention of polymer analytes is evident from Fig. 4, curve 6, for $\varepsilon = \varepsilon_{cr}$.

5.1 Liquid Chromatography of Macromolecules Under Critical Conditions (LC CC)

Depending on the retention mechanism applied, the method can also be termed liquid chromatography at critical adsorption point or liquid chromatography at critical partition point. LC CC should not be confused with supercritical liquid chromatography of polymers. Recently, critical chromatography in supercritical fluids was also attempted (6,57). At this point, tribute should be paid to three groups of Russian authors. One group discovered the "critical approach" in the 1970s and applied it to high polymers (for a review see, for example, Ref. 58), another independently applied critical chromatography for the successful separation of various oligomers (59), and the third elaborated theory of LC CC and proposed its application to various complex polymer systems (60). After a longer period, LC CC was applied to numerous complex polymers and oligomers including binary polymer blends, and block-copolymers (3–5). LC CC was also

© 2004 by Marcel Dekker, Inc.

rendered useful in the separation of polymers according to their stereoregularity (61,62) and for discrimination of linear and cyclic macromolecules with similar molar masses (63–65). Numerous critical systems are listed in Refs. 4, 5, and 66. LC CC was also included in two-dimensional HPLC (4,5,62,67). During application of LC CC, its numerous important experimental limitations were revealed (68,69). Most of them are mentioned at the end of this section. Unfortunately, the drawbacks of LC CC were ignored in some recent books (4,5). Cifra and Bleha (70) also showed by Monte Carlo modelling that the molar mass region in which perfect entropy–enthalpy compensation takes place may be limited (Fig. 4, curve 9). Still, LC CC remains attractive for characterization of many complex polymers both in direct (one separation system) and two-dimensional arrangements. LC CC proved especially successful in molecular characterization of oligomers (4) where, for example, the problems connected with strong interaction of large polymer species with walls of narrow pores (Sec. 3.2.1) are less important and also relatively high concentration of analytes are experimentally feasible. The latter feature of oligomer HPLC, including LC CC, allows application of a less sensitive flow-through densitometer as an additional detection system (4).

A situation similar to entropy/enthalpy compensation may also appear in systems where two enthalpic retention mechanisms, for example, adsorption and enthalpic partition, affect retention volumes in an opposite way (71).

The following practical hints may be useful for LC CC users:

1. Whenever possible, the enthalpic partition retention mechanism is preferential. It is difficult to maintain the HPLC system at the critical adsorption point. Minute variation in eluent composition due to preferential evaporation and moisture absorption may strongly affect adsorption of polymer analytes. Consequently, the LC CC system must be frequently controlled and critical conditions adjusted for example by temperature variations. If, however, the adsorption mechanism has to be applied, try to identify both adsorli and desorli, which are as good solvents for the analysed polymer as are possible. Critical composition of the eluent, which is situated in the vicinity of the theta point or even near the precipitation threshold, may further increase instability of the critical adsorption point and increasingly deteriorate repeatability of measurements.
2. Avoid using very narrow pore column packings. The danger of backward curvature of critical calibration curves, as well as problems connected with peak broadening and decreased sample recovery decrease with rising pore diameter (47). Unfortunately, the selectivity of SEC separation for lower molar mass polymer species is at least partially sacrificed when narrow pore column packing is removed.

© 2004 by Marcel Dekker, Inc.

This is important when LC CC is applied to characterization of polymer blends and block-, graft-, or star-copolymers where one kind of polymer chains elutes under critical conditions, irrespective of its molar mass (chromatographic invisibility). Another kind of polymer chain is eluted under SEC conditions and its MMM/MMD is to be determined in the conventional way. Reduced separation selectivity of the latter chains affects the accuracy of the results obtained.

3. Single-component critical eluents are rather rare (30). Therefore, one is forced to use mixed mobile phases in LC CC. If possible, binary eluents are preferred over multicomponent eluents. Usually, experimental problems increase with the increasing number of eluent components. Temperature and pressure dependence of preferential sorption and preferential solvation (Sec. 4.2) as well as preferential evaporation from the mobile phase increasingly complicate not only critical point stability but also sample detection. Evaporative light scattering detectors (ELSD) may be used to suppress detection problems, although the response of ELSD is often rather nonlinear and depends on polymer composition, molar mass, as well as on eluent composition (72) (Sec. 10).

5.2 Barrier Coupled Procedures

When compared with HLPC of low molar mass substances, polymer HPLC exhibits several specific features. For example, in the case of porous particulate or monolithic column fillings, we are confronted with generally large differences between mobilities of macromolecular analytes and eluent molecules. With the exception of LC CC, macromolecules that are partially or fully excluded from the filling pores tend to move along the HPLC column much faster than molecules of eluent that penetrate most filling pores. This allows the creation of "barriers" of small molecules, which are impermeable for macromolecules possessing certain enthalpic interactivity. Such barriers force macromolecules to decelerate their progression along the column and to elute at the barrier edge. In other words, macromolecules accumulate on the corresponding barrier of small molecules and may elute irrespectively of their molar mass. This is a specific approach to the mutual compensation of entropic and enthalpic effects within HPLC columns. Adsorption-promoting barriers, that is, zones of liquids with low solvent strength, are utilized for adsorbing macromolecules. Enthalpic partition and phase separation barriers are created from thermodynamically poor solvents or nonsolvents for polymer analytes. Barriers can be

- *Continuous*, created by the mobile phase, or
- *Local*, formed by pulses of appropriate liquids. The local barriers can be *single* or *multiple.*

© 2004 by Marcel Dekker, Inc.

Mobile phase barriers can be of

- *Isocratic* or
- *Stepwise/continuous gradient* type.

Schematic representations of particular barrier approaches are shown in Figs. 11–13. Figure 11 shows the action of an isocratic barrier of mobile phase. Eluent with constant composition promotes full retention of polymer analytes B and C due to their adsorption or enthalpic partition or phase separation (precipitation) within the column, while analyte A is not retained by the eluent barrier. Sample containing polymers A, B, and C is dissolved and injected in a liquid that prevents their adsorption, partition, or precipitation (desorli/displacer or good solvent). Macromolecules tend to travel faster than the zone of their initial solvent. However, polymer B cannot leave the zone of its original solvent and elute corresponding to the exclusion retention mechanism because the eluent barrier hinders its fast progression. Nonretained polymer A will freely leave the initial solvent zone and elute in the SEC mode separately from retained species B and C. Molar mass and molar mass distribution of polymer A can be determined in the conventional way. Retention properties of eluent and displacement properties of sample solvent can be optimized so that polymer species of identical or similar chemical structure or architecture (polymer B) will travel with the same velocity near the front of the initial sample solvent zone and elute from the HPLC column independently of their molar mass (5,6,73). A sample which exhibits still higher affinity toward the column filling

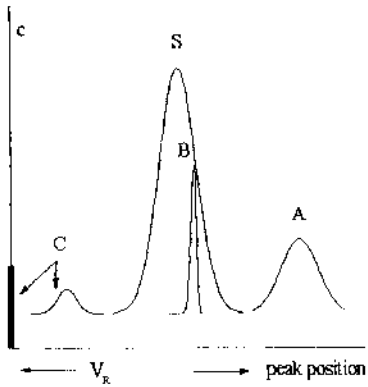

Figure 11 Schematic representation of liquid chromatography under limiting conditions of adsorption. A, B, and C are polymers injected, S is the elution (desorption) promoting sample solvent. Eluent promotes adsorption of polymers B and C. For detailed explanation see the text.

© 2004 by Marcel Dekker, Inc.

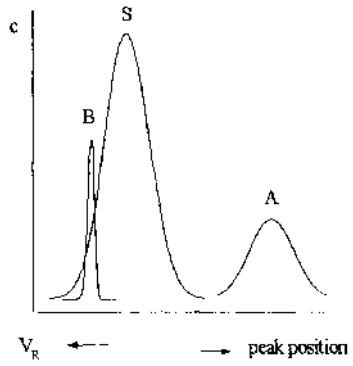

Figure 12 Schematic representation of liquid chromatography under limiting conditions of desorption. A and B are polymers injected, S is the sample solvent (adsorbing barrier for polymer B). Eluent promotes desorption of both polymers. For detailed explanation see the text.

and/or which is completely insoluble in eluent (polymer C) will be strongly retained within the column immediately after its injection or when the sample solvent zone becomes diluted and cannot prevent sample immobilization. Polymer C can be eluted with a subsequent zone of liquid, that is, with a more efficient displacer or a better solvent. A series of liquid pulses with increasing

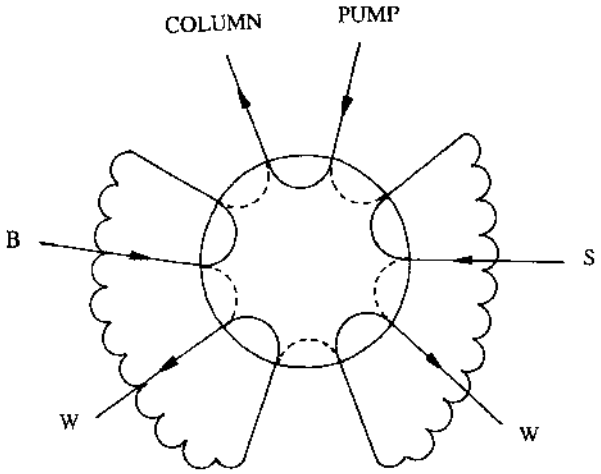

Figure 13 Scheme of a ten-port two-way valve equipped with two loops. S is sample solution and B is the barrier liquid (nonsolvent, adsorli, and so on); W is the waste vent.

© 2004 by Marcel Dekker, Inc.

displacing effectivities could allow fractionation of multicomponent polymers according to their chemical structure or architecture irrespectively of their molar masses.

The corresponding methods are termed liquid chromatography under limiting conditions (LC LC) of adsorption, enthalpic partition, or solubility, respectively. The sample solvent and displacing zones can be formed, for example, by mixtures of eluent components with increasing displacing efficacies.

Figure 12 depicts a reversed situation when mobile phase is a displacer but sample solvent promotes polymer retention (74). Alternatively, a zone of liquid that forms a barrier can be injected into the column just before sample introduction, applying, for example, a ten-port two-way valve provided with two loops (Fig. 13) or an autosampler. Macromolecules of A type that exhibit low retentivity can surmount the solvent barrier and are eluted, for example, in the SEC mode. Polymer B, however, is decelerated by the barrier and elutes irrespective of its molar mass just behind the barrier. Again, a series of barriers with increasing efficacies can be created to selectively block fast progression of macromolecules with different retentivities due to differencies in their chemical structure or architecture. Adsorption, enthalpic partition, or phase separation retention mechanisms can be applied. In dependence on the prevailing retention mechanism taking part in the barrier action, the corresponding methods are termed liquid chromatography at limiting conditions of desorption, repartition, or insolubility. The six possible LC LC procedures for separation of complex polymer systems are at present only in the first stage of their development.

The principle of polymer fractionation applying the continuous eluent gradient barrier is shown in Fig. 14. The action of a stepwise barrier is in principle similar, although the latter may exhibit some advantages and also drawbacks.

In the gradient elution approach, the polymer is injected into a mobile phase, which brings about its effective full retention within the column due to adsorption, enthalpic partition, or phase separation. It is preferable also if the sample solvent strongly promotes adsorption or enthalpic partition in favor of the stationary phase. Eluent must be either an adsorli, a poor solvent promoting enthalpic partition, or a nonsolvent. Next, the displacing efficacy of the eluent starts to increase continuously or stepwise. Macromolecules of similar retentivities are successively displaced; they move along the column with different velocities and undergo fractionation. A very important feature of the described eluent gradient HPLC (EG HPLC) is the possibility of identifying experimental conditions under which macromolecules of different retentivities elute independently of their molar masses. This situation is typical for many high polymer systems (usually with molar masses above $50\,\mathrm{kg\,mol^{-1}}$) using narrow pore columns so that macromolecules can be fully excluded from the pores in the weak interaction regime. The simplified explanation of molar mass independent retention in EG HPLC considers the barrier effect of eluent gradient, similar, for example, to

© 2004 by Marcel Dekker, Inc.

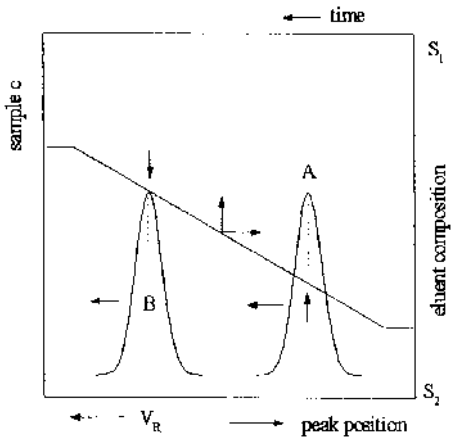

Figure 14 Schematic representation of eluent gradient HPLC of two polymers A and B with different chemical structures or physical architectures. The linear eluent gradient is used with isocratic periods in the starting and final stage. Arrows denote the eluent composition, which acts as a barrier for progression of macromolecules with a particular composition. Solvent S_1 promotes sample elution, S_2 promotes sample retention. Sample B exhibits larger enthalpic interaction with the column filling than sample A.

limiting conditions of desorption (74). Macromolecules that are retained near the column inlet start eluting at different eluent compositions in dependence on their molar mass, chemical structure, and architecture. During their passage along the column, polymer species are, however, stacked on the eluent barrier only according to their chemical structure and/or architecture while the molar mass effect may be suppressed, similarly as in, for example, liquid chromatography under limiting conditions of desorption (Fig. 12) (73). In adsorption and partition EG HPLC, the eluent composition that just decelerates macromolecules nearly corresponds with critical conditions (75,76).

This hypothesis explains several features of polymer EG HPLC. The column is used mainly for sorting of macromolecules by selective hampering of their fast progression. Macromolecules with different molar masses but similar composition and/or architecture are stacked within the same loci of eluent composition. Therefore, EG HPLC columns have much higher loadability than, for example, SEC columns. Further, EG HPLC columns can be short, just to allow larger macromolecules that are stronger interacting species, which started moving later, to catch smaller species with similar chemical structure and architecture. Zones of species with similar chemical structure or architecture are narrow due to focusing effects (77,78), which is similar to HPLC of macromolecules under limiting conditions (Figs 11 and 12). With well chosen column packing and nature of

© 2004 by Marcel Dekker, Inc.

eluent components, as well as with optimized eluent gradient shape, EG HPLC can give very high separation selectivities. Polymers of different compositions (79–83) and architectures (84) have been successfully discriminated applying adsorption and enthalpic partition retention mechanisms. The application of a phase separation retention mechanism (3–5,39,40) (eluent gradient phase separation liquid chromatography, high-performance polymer precipitation chromatography, precipitation–redissolution liquid chromatography) seems to be more complicated. Solubility of polymers often too strongly depends on their molar masses and their redissolution may be slow. The ultimately dissolved highest molar mass species may be too much delayed to catch lower molar mass fractions before these leave the column. This is especially important with crystalline polymers where dissolution kinetics are often rather slow (40). Creation of two phases during the precipitation/redissolution processes may lead to zone splitting, especially if both phases contain macromolecules that inevitably differ in their molar masses (Sec. 3.2.3). On the other hand, the phase separation based EG HPLC exhibits very high separation selectivities and may give valuable information about many practically important complex systems, in particular if quantitative interpretation of chromatograms is possible, for example, if HPLC is hyphenated with mass spectrometry.

Eluent gradient HPLC of polymers is at present the most important group of separation methods for a variety of complex polymer systems. Abovementioned chance to attain molar mass independ retention at high selectivity with compressed chromatographic zones and at high column loadability predestine EG HPLC to be applied as the first dimension separation system. The second dimension separation SEC column can be often directly attached.

Barrier-coupled liquid chromatographic procedures have undergone long periods of development, with a distinct acceleration during the 1990s. Precipitation–redissolution liquid chromatographic separations have been proposed by the father of size exclusion chromatography, Porath (85), and its high-performance arrangement was pioneered by Glöckner (3). Adsorption/partition-based eluent gradient procedures were initiated by Belenkii *et al.* (86) and Inagaki *et al.* (87) in the TLC arrangement, and column EG HPLC separation of complex polymers was proposed by Teramachi *et al.* (88). Local gradient approaches have been suggested in this laboratory. Additional literature sources on barrier methods of polymer HPLC can be found in a number of reviews (3–5,56,78).

Some practical hints for HPLC barrier methods users include the following:

1. Apply the possibly mildest conditions for retention of separated macromolecules. Using narrow pore column fillings (narrow pore particulate column packings and monoliths with narrow separation pores) is advantageous for suppression of molar mass retention volume dependence and for enhancement of peak compression (focusing).

© 2004 by Marcel Dekker, Inc.

However, strong adsorption of macromolecules in very narrow filling pores (15,17) may deteriorate results due to band broadening and splitting, as well as due to decreased sample recovery. Presence of macromolecules trapped in the narrow pores can often be revealed by a blank experiment performed after the actual separation experiment and under identical experimental conditions but without polymer sample. Trapped macromolecules are successively eluted in the course of blank experiments with retention volumes (practically) identical to the originally eluted sample (17). Similar to LC CC, enthalpic partition is usually easier to fine tune than adsorption. Interfacial adsorption on polar bonded groups (amino-, nitril-, nitro-, glyceryl-, propyl-, and so on) is preferred over that on a bare silica gel surface. Strong desorli eluent components should be applied if column filling material contains surface silanols accessible to macromolecules (this includes many C_{18} silica bonded phases, see Sec. 4.1.2) and analytes are highly polar.

2. Application of a phase separation mechanism should be carefully reconsidered and tested. The danger of band broadening and splitting increases with both polymer molar mass and crystallization tendency. However, EG HPLC in the phase separation mode is very useful for separation of many nonpolar polymers and oligomers (3).
3. Avoid hybrid separation mechanisms and, in particular, the combinations of phase separation with adsorption or with enthalpic partition. Use thermodynamically good solvents for analyzed samples as mobile phase components, and beware of the co-nonsolvency phenomenon.

6 SECOND DIMENSION HPLC SEPARATION SYSTEMS

Once a complex polymer has been separated primarily or exclusively according to one single characteristic, the second dimension separation of fractions is substantially simplified. Fractions leaving the first dimension HPLC system are usually forwarded into a "regular" SEC system. If the molar mass effect is suppressed/deleted in the first dimension HPLC system the SEC data for each fraction leaving the first separation column and possessing narrow distribution in chemical structure or architecture directly reflect its molar mass distribution. Still, determination of true molar masses from retention volumes may be complicated. For example, sequence length distribution will be present in statistical copolymers. Even if this third property distribution is neglected, we encounter problems connected with selective detection (Sec. 10) and with the complicated relation between retention volume and molar mass of fractions. To apply Benoit's universal calibration dependence (51), functional dependence of viscosity law constants

© 2004 by Marcel Dekker, Inc.

[Eq. (6)] on copolymer composition is needed. Various procedures have been proposed which interpolate these constants from those for homopolymers (89). Montaudo *et al.* (1) have demonstrated their limited validity using a MALDI mass spectrometry. Viscometric detectors and hyphenations of polymer HPLC with mass spectrometry help in mitigating these problems while application of light-scattering detectors for copolymers is somewhat limited.

In a few practical cases, the usual order of separation systems in 2D-HPLC that was described in Sec. 2 can be changed. A typical example represents stereoregular polymers. For example, limiting viscosity numbers of poly(methyl methacrylate) in good eluents does not depend on their tacticity (M Bohdanecky, personal communication). As a result, universal calibration dependences for polymers of the same nature but differing in their stereoregularities should coincide and SEC can be used as the first dimension separation system to discriminate macromolecular analytes almost exclusively according to their molar mass. SEC fractions can be forwarded into the second dimension column, for example into an LC CC system for separation of polymer species according to stereoregularity (61,62). However, this approach cannot be used for 1,2- and 3,4-polyisoprenes because their calibration dependences are mutually shifted (89).

Size exclusion chromatographic methodology is treated in detail in several chapters of this book and does not need to be elucidated here. It is, however, necessary to again mention the danger of enthalpic interactivity of many SEC columns. The latter may be augmented by some mobile phases used in the first dimension column. Therefore, eluent and consequently also sample matrix must sometimes be changed between the first and second dimension columns (Sec. 9). The problems connected with sample storage and reconcentration between both column systems will also be discussed in Sec. 9.

If the first dimension separation system only partially suppresses and does not fully eliminate the effect of one characteristic, the calculation of corresponding distributions is complicated (Sec. 1). However, the contour representation of results allows estimation at least of the distribution limits (4,5).

A specific problem of 2D-HPLC of complex polymer systems consists in determination of the entire polymer concentration and/or relative concentration of complex polymer constituents in the column effluent (Sec. 10).

7 HPLC-LIKE PROCEDURES

Separations of numerous complex polymer systems can be achieved using HPLC-like procedures, which apply the same instrumentation and retention mechanisms as the true HPLC methods. The multitude of retention–elution steps are responsible for chromatographic separations. However, if retention–elution processes are selective enough, one single (full) retention and subsequent (full)

© 2004 by Marcel Dekker, Inc.

elution step may be sufficient for sample separation. The one-step approaches are called also "on-and-off procedures" or full retention–elution methods (FRE). The best known FRE method utilizes an adsorption retention mechanism and is also called the full adsorption–desorption (FAD) method. The present state of development of the FAD method is described in the recent review (90) and therefore only basic ideas will be repeated here and some new information about this powerful approach will be added.

FRE procedures are similar to solid phase extraction, which is well known in HPLC of low molar mass substances. However, a unique ability of macromolecules is utilized in FRE, namely to be quantitatively and irreversibly immobilized within a column filling under particular experimental conditions. The immobilization is so strong that polymer is not eluted by any volume of mobile phase ("infinitive retention volume"). On the other hand, a sudden change of experimental conditions quantitatively releases either the whole polymer sample or its particular fraction from the FRE column. Sample immobilization and its controlled release seem to be easiest when the adsorption retention mechanism is applied. The high affinity adsorption isotherm (Fig. 15) is applicable to many polymers of medium and high polarity. FAD procedures work below saturation onset, that is, at the situation when virtually all macromolecules are attached to the adsorbent surface.

It was shown that the adsorptive attachment of polymer species is a very fast process (20). The sample residence time within a FAD column is as short as a few seconds and is fully sufficient for trapping virtually all macromolecules within adsorbent under mobile phase flow (and therefore under intensive mixing) conditions. Similarly, detachment of macromolecules is fast and quantitative

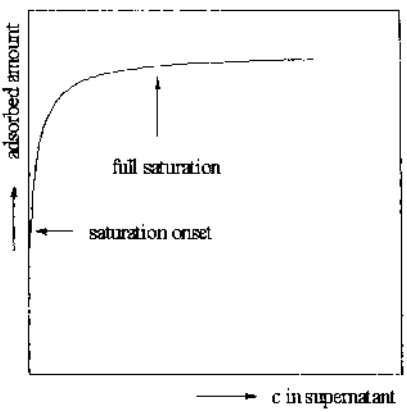

Figure 15 Typical course of a high affinity adsorption isotherm for macromolecules.

© 2004 by Marcel Dekker, Inc.

provided the FAD column is packed with nonporous particles (see Sec. 4.1.2 and the role of polymer adsorption with narrow pores).

The full entrapment of nonpolar macromolecules within the silica C_{18} phase from a polar eluent (reversed phase) utilizing partition mechanism in FRE is more problematic. In this case, the extent of retention within the column packing may depend on the degree of silica coverage with C_{18} groups and on polymer molar mass. For example, full retention of narrow molar mass polystyrenes from dimethylformamide on silica nonporous C_{18} was attained only above a molar mass of $90\,\mathrm{kmol\,g^{-1}}$ (28). FRE procedures based on phase separations may be even more difficult because they are affected by (slow) dynamics of phase separation processes (Secs 3.2.3 and 5.2).

FAD allows extensive compression of chromatographic bands, that is, the reconcentration of diluted polymer solutions. For example, a reconcentration factor of 600 was easily achieved for poly(methyl methacrylate) using bare, nonporous silica-based FAD column packing (91). FRE procedures can also be used for sample storing and sample matrix exchange (Sec. 9). FRE column(s) can be directly connected with an SEC system. In this way we arrive at the FRE/SEC quasi two-dimensional HPLC system. An optimized FAD/SEC method was used for separation and molecular characterization of multicomponent polymer blends (up to six components) (92) and also for determination and characterization of minor macromolecular admixtures ($\sim$1%) in polymer blends (93). Using FAD, Lazzari *et al.* (94) also successfully separated four-arm highly syndiotactic star poly(methyl methacrylate)s from their linear PMMA pendant.

Many different arrangements are possible for pursuing full retention–elution separations. A typical FAD/SEC system is shown in Fig. 16. The system can be altered to meet particular needs. For example, instead of a mixing device (an HPLC gradient maker) a series of displacing liquids with precisely adjusted compositions can be stored in separate containers. Several FAD columns can be arranged in parallel or in series. Fillings used in these columns may be identical or have different interaction activities. Further, sample injection valve (V_2 in Fig. 16) can be substituted by an independent HPLC system and in this way we arrive at the real 2D-HPLC system enforced with a FAD system (Sec. 9). In the latter case, the FAD column may act also as an additional separation unit to form a quasi three-dimensional HPLC system. Further, an efficient retention promoting liquid, for example, an adsorli, can be continuously added to the sample (that is to the HPLC column effluent) to assure retention of analytes leaving (95). A full retention approach can also be used for sample purification (Sec. 8).

FRE procedures may also assist sample detection in the second dimension column effluent, for example, by additional reconcentration of fractions leaving column #2, or by eluent exchange for NMR and infrared spectroscopic measurements.

© 2004 by Marcel Dekker, Inc.

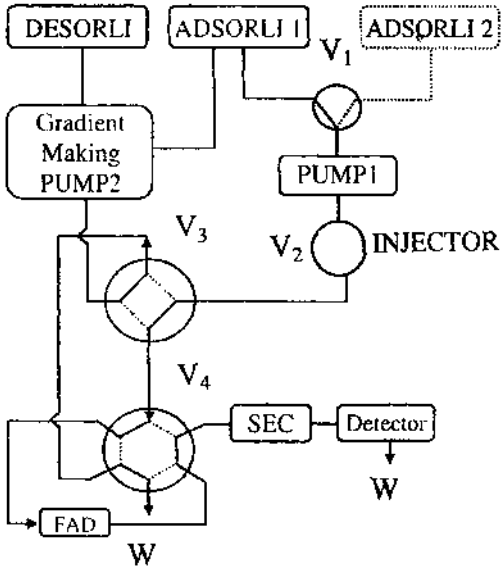

Figure 16 Block scheme of a full adsorption–desorption/SEC system. V_2 is sample injector, FAD and SEC are full adsorption–desorption and SEC columns, respectively. P#1 and P#2 are pumping systems. For further explanation see the text.

8 REMOVAL OF POLYMERIC INTERFERENCES FROM SAMPLES

Polymeric admixtures often complicate accurate characterization of macromolecular analytes of interest. A typical example represents characterization of products of block-, graft-, star-, and so on copolymer syntheses and also analyses of polymers that were chemically transformed by analogous reactions, including functionalization and oxidization processes. Complex polymer systems of these kinds are frequently characterized by conventional SEC, although it is evident that interfering admixtures can be discriminated in this way only if their molecular sizes differ substantially from the sizes of analyte molecules. Presence of admixtures is often masked by the chromatographic band broadening phenomena. Macromolecular admixtures in broad molar mass polymers easily remain undiscovered even if the size of analyte and admixture differs by a factor of two. Evidently, conclusions about purity of products (for example, about absence of homopolymers in statistical-, block-, graft-, and miktoarm-copolymers or diblocks in triblock species and vice versa can hardly be drawn from an SEC chromatogram if a thorough evaluation of SEC band broadening is omitted. Unfortunately, many papers entitled "Synthesis and characterization of . . ." are based on this

© 2004 by Marcel Dekker, Inc.

oversimplified approach. It seems that too many scientists consider the SEC method in its present stage of development a "concluded story" which enables sufficiently exact molecular characterization of synthetic polymers and does not need any further improvements. As result, the sections on bulk and HPLC methods for polymer characterization practically disappeared from the program of many broad-scope international symposia on polymers (see for example, Brisbane IUPAC Macro Symposium 1998). Besides the limited intrinsic accuracy of SEC even in the case of homopolymers, as demonstrated by a series of IUPAC round robin tests (96), the possible influence of interfering macromolecular admixtures on the SEC data for complex polymer systems represents another reason to develop more advanced methods for molecular characterization of complex polymers.

The most straightforward way to avoid negative effects of interfering polymer admixtures is their removal from the analyzed mixture. In many cases this can be done by utilizing differences in enthalpic interactivities of analyte and admixture in the HPLC system. As a result we arrive at a special case of a quasi two-dimensional HPLC arrangement in which the only role of the first separation system is purification of the analyte from unwanted macromolecular admixtures. If, however, the resulting purified analyte is a complex polymer system one will need also to engage a true 2D-HPLC method for its characterization and we again arrive at a quasi three-dimensional HPLC.

The elegant method for sample purification renders the full retention approach, a mainly full adsorption procedure. The interfering admixture is trapped either within the interactive SEC column (97) or within an extra full retention guard column in the apparatus similar to a full retention–elution instrument (Sec. 7, Fig. 16). The full adsorption approach is very efficient in the case of admixtures that are more polar than the macromolecules of analyte. Nonpolar admixtures can be better removed under application of enthalpic partition and phase separation retention mechanisms. After its saturation the guard column is regenerated by appropriate displacing liquid.

It is, however, possible also to apply a reversed approach. Analyte is trapped within the full retention precolumn while admixtures are eluted. In the next step, analyte is displaced into the analytical HPLC or 2D-HPLC system(s).

The HPLC-like procedures of sample purifications are used in many industrial analytical laboratories. Unfortunately, their results remain largely unpublished.

9 SAMPLE TRANSFER BETWEEN FIRST AND SECOND DIMENSION SEPARATION SYSTEMS

Defined reintroduction of eluent from the first dimension separation column into the second dimension column is an important condition for unambiguous

© 2004 by Marcel Dekker, Inc.

processing of 2D-HPLC data. Knowledge of the exact elution start is especially important for the molar mass calculation based on SEC retention volumes.

The least complicated way for sample transfer is collection of effluent from column #1 by means of a fraction collector and their successive reinjection into column #2. Fractions from column #1 can easily be further manipulated, for example, concentrated, or combined (either adjacent fractions from one single run or corresponding fractions from several independent runs of column #1). Fractions from column #1 can also be reinjected into column #2 only partially ("heart cut approach"). Usually the effluent part with maximum concentration is further analyzed. The entire off-line procedure is, however, too sample, time, and work intensive to compete with modern on-line approaches as far as the latter can be automated by using electrically or pneumatically operated valves that are controlled by appropriate software.

Some experimental setups for on-line reintroduction of eluent from the first dimension separation column into the second dimension separation column are shown in Figs 17–20. The simple arrangement in Fig. 17 utilizes one six-port two-way valve provided with a sample loop. The procedure necessitates a stop-and-go operation of the first dimension column, if the entire effluent from column #1 is to be transported into column #2. The loop size must be appropriately adjusted and a partial loop filling procedure can also be applied.

Two further setups (Figs 18 and 19) allow continuous operation of the first dimension separation column C#1. However, the flow rate in C#1 must be adjusted so that filling time of the injection loops is matched with the duration of elution in the second dimension separation column. The highest detected retention volume of column #2 limits throughput of the whole 2D analysis. For SEC column #2, the late eluting peaks are system peaks or peaks of eluent from the first dimension separation column, which was introduced into the second dimension separation column together with the sample fraction. Large volumes of eluent from column #1

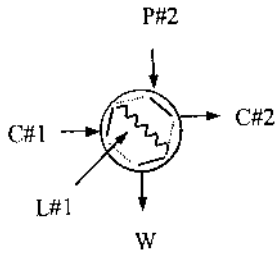

Figure 17 Schematic representation of the 2D-HPLC sample transfer system with one six-port two-way valve. C#1 and C#2 are column systems, P#2 is the second pump, W is waste. Column #1 works in the stop-and-go mode. L is the loop. For further explanation see the text.

© 2004 by Marcel Dekker, Inc.

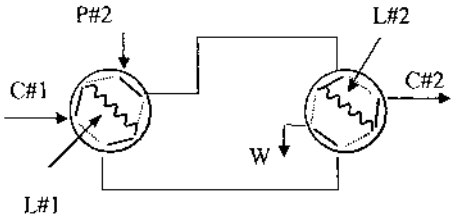

Figure 18 Schematic representation of the 2D-HPLC sample transfer system with two six-port two-way valves. Column #1 works in continuous mode. Loops #1 and #2 are filled alternatively. Both valves are operated simultaneously. Other symbols as in Fig. 7. For further explanation see the text.

introduced into C#2 may also affect sample retention within column #2, stability of column #2, as well as detection of effluent from column #2. Therefore eluent exchange between C#1 and C#2 may bring several advantages.

An important query of any 2D-HPLC procedure relates to sample dilution (98), which complicates detection of polymer in the column #2 effluent. Reinjection of a large number of diluted fractions from column #1 into column #2 also prolongs total time of analysis. The reinjection of only the most concentrated parts of the column #1 fractions (heart cut approach) may bring about unintentional disregard of important information about the sample.

It seems that several of the above problems can be solved by means of the FRE procedures (Fig. 20). The full retention–elution method allows storage of fractions from column #1 and thus practically independent operation of column #2. If only fraction storage is needed, "FRE columns" can be packed with nonactive nonporous particles to reduce diffusion-induced mixing within each fraction (99). Alternatively, FRE columns can be substituted by a set of capillary loops. FRE columns can also serve for the reconcentration/focusing of fractions from the first dimension column and thus for at least partial exchange of sample solvent injected into column #2. Separation in column #1 can be repeated and corresponding

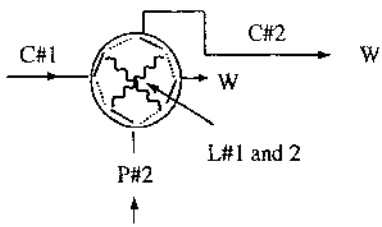

Figure 19 Eight-port two-way valve system for the 2D-HPLC sample transfer. Two loops L#1 and L#2 are filled alternatively. Other symbols as in Fig. 17. For further explanation see the text.

© 2004 by Marcel Dekker, Inc.

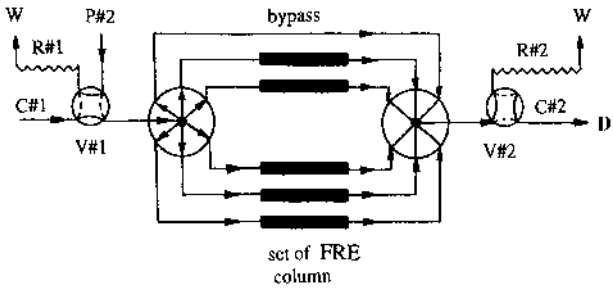

Figure 20 Set of full retention–elution (FRE) columns, a real RSR system (sample storing and reconcentration device that also allows eluent switching). Combination of the corresponding fractions is feasible. Column C#1 works continuously. V#1 and V#2 are $n + 1$ port n-way switching valves, which are operated simultaneously. R#1 and R#2 are hydrodynamic resistors. D is a detector. C#1 and C#2 do not operate simultaneously in this simpler arrangement. For further explanations see the text.

fractions combined within corresponding FRE column(s). The entire arrangement can easily be automated for unattended operation.

The conditions for the FRE retention mechanism choice were discussed in Sec. 7.

10 DETECTION AND DATA REPRESENTATION IN 2D-HPLC OF COMPLEX POLYMER SYSTEMS

Detectors and detection procedures are discussed in several chapters of this book. It is shown that detection in polymer HPLC made much progress in the 1990s. However, detectors remain one of the weak points of coupled and two-dimensional HPLC procedures of complex polymers.

Concentration/mass detectors should selectively detect each constituent of the complex polymer, for example, each type of monomer in the copolymers. There are, however, only a few complex polymer constituents that can be detected both universally and selectively by conventional detectors. For example, the total concentration of copolymers of styrene and methyl methacrylate can be monitored by means of UV photometers at about 235 nm and polystyrene concentration can be measured selectively at a wavelength of 254–260 nm (100). In any case, the photometric detectors, including UV-VIS diode array detectors, as well as infrared and fluorescence detectors, find important applications in 2D-HPLC of many complex polymer systems. Serious drawbacks of infrared spectroscopic detection lie in its relatively low sensitivity, as well as in the poor IR transparency of most mobile phases. Important progress was achieved by introduction of interfaces that

© 2004 by Marcel Dekker, Inc.

allow removal of mobile phases and creation of a continuous film of polymer eluted from the column (LC transform instruments). The inhomogeneities of the polymer film that is deposited onto a germanium disc are partially compensated for by measurements at two appropriate wavelengths. Further progress in IR polymer detection depends on improvement in both sample film deposition technology and sensitivity of IR measurement itself.

In spite of their relatively low sensitivity, differential refractometers are very popular in SEC. Their response is affected by the chemical composition of the polymer sample. Evidently, refractive index (RI) detectors can hardly be applied in gradient procedures. In the case of mixed mobile phases the RI detector response is affected also by preferential solvation of the sample. Pasch and Trathnigg (4) proposed corrections for this later effect by applying hyphenation of refractometric and densitometric detectors. Unfortunately, densitometric detectors are even less sensitive than RI detectors and, therefore, they afford sample reconcentration. This is feasible practically only with oligomers. Refractometers also detect system peaks that are caused by preferential evaporation, displacement, and preferential solvation effects typical for mixed mobile phases (Sec. 4.2).

Dependences between detector response and sample concentration are usually rather nonlinear for evaporative light-scattering detectors (ELSD) and their slopes depend on the polymer chemical structure and to some extent also on sample molar mass. The response of present ELSD instruments depends also on the eluent nature/composition (72). This latter feature represents an important limitation of ELSD for all types of barrier procedures and, especially, for eluent gradient methods.

Absolute detectors such as (solution) light-scattering photometers and viscometers continuously monitor molar mass of macromolecules in the column effluent. They are discussed in several chapters of this book. Molar mass detectors render important services in SEC of homopolymers and also polymers with complex architectures, such as branched species. Unfortunately both types of detectors suffer from serious drawbacks for most complex polymer systems with changing chemical structure. They are practically incompatible with procedures that utilize mobile phases with varying composition. On the other hand, if SEC is used as the second dimension separation system, both above detectors can produce valuable information on macromolecules in the effluent.

A very important group of detectors for HPLC of complex polymers and a good hope for future developments includes nuclear magnetic resonance and mass spectrometry devices. These are discussed in detail in other chapters of this book. In spite of both their high acquisition price and operational cost, these instruments will certainly find application in many 2D-HPLC procedures.

Without solving important detection problems, many 2D-HPLC separations of complex polymers produce only semiquantitative data on their molecular characteristics. This holds especially for high polymer systems because oligomer detection is often less problematic. However, even semiquantitative data on binary

© 2004 by Marcel Dekker, Inc.

distributions of complex polymers are very important for both science and technology, provided they are evaluated critically. These data may allow a better understanding of many polyreactions, optimization of polymer production processes, and tracing sources of problems in manufacturing of complex polymers.

The data from 2D-HPLC of complex macromolecules are usually represented by contour plots (see Fig. 2) or contour maps in which detector response, sample composition, or relative concentration are represented against retention volume or fraction molar mass (4,5). The contour plots allow fast orientation and identification of unwanted sample components.

11 TYPICAL EXPERIMENTAL ARRANGEMENTS FOR 2D-HPLC OF COMPLEX POLYMER SYSTEMS

The general scheme for two-dimensional high-performance liquid chromatographic instruments is depicted in Fig. 1. The strategy and conditions for separation column (systems) selection was outlined in Secs. 2, 5, and 6. Sample transfer options were discussed in Sec. 9 and some detection problems were mentioned in Sec. 10. It is evident from the above sections that no universal 2D-HPLC arrangement does exist. The actual setup must be tailored for each characterization task or even for each group of samples. Therefore, it is necessary to evaluate carefully relations between available investment and expected benefits. The investments include mainly the cost of both method development and current measurements such as work, time, instrumentation, and material. Benefits, evidently, lie in more profound information about molecular characteristics of samples.

The most simple 2D-HPLC includes an off-line approach. RSR system in Fig. 3 is deleted and effluent from column #1 flows directly into the detector(s) and a fraction collector. Each fraction or its selected part is manually reinjected (possibly after reconcentration) into a completely independent column (system) #2, which is equipped with another set of appropriate detectors. As mentioned, this approach is labor- and time-intensive. It can help in the course of scouting experiments.

Column #1 can be operated in the stop-and-go mode. In this case, the RSR system in Fig. 3 can be substituted by a simple four-port two-way switching valve or with a six-port two-way valve equipped with the sample loop (Fig. 17). After necessary adjustment of experimental conditions for the first dimension separation system (column #1 filling, mobile phase, and temperature) which are evaluated by detector(s) #1, effluent segments from column #1 are directed into column #2.

RSR setups with the reinjection valves depicted in Figs 18 and 19 allow continuous operation of column #1; however, elution rates in column systems #1 and #2 must be well matched.

© 2004 by Marcel Dekker, Inc.

RSR arrangement with one or several full retention–elution column(s) allows sample storing and reconcentration/focusing, as well as partial exchange of sample solvent in column #2 (Fig. 20).

12 APPLICATIONS OF 2D-HPLC TO COMPLEX POLYMER SYSTEMS

In this section, we shall briefly discuss application strategies of two-dimensional polymer HPLC to the most important groups of complex polymer systems. Several practical applications of 2D-HPLC to particular complex polymers are reviewed, for example, in recent monographs (3–5). To avoid unnecessary disappointment, the readers are advised to evaluate and optimize each procedure published and carefully check its applicability to the system of interest. 2D-HPLC of complex polymer systems possesses many pitfalls, for example due to:

- differences in exclusion and interaction retention properties of commercial columns from different producers,
- often rather limited reproducibilities of HPLC columns from the same producer,
- large effects of minute variations in mixed eluents composition on the sample retention, and problems with repeatability of mixed eluents preparation,
- important influence of small amounts of admixtures/impurities present in many solvents. Content of solvent admixtures may change from batch to batch and also with time, for example, due to preferential evaporation, moisture absorption, and oxidization reactions, and
- possible pressure dependence of retention volumes, in particular with mixed mobile phases. Pressure may vary in the course of the experiment due to partial column exit blockage.

All above effects may negatively affect retention volumes in regard to both repeatability and reproducibility.

An important negative aspect of 2D-HPLC method design is also "optimism" of some authors who tend to overlook even well-known general shortcomings of procedures they apply (4,5).

As mentioned, researchers dealing with synthesis of complex polymers very often characterize their products using conventional SEC. Average values of molar masses and molar mass distributions of synthesis products are calculated directly from polystyrene calibrations. The resulting data should be designated as "polystyrene equivalent values." They can give valuable preliminary, semiquantitative information on synthesized polymers, but in some cases they may also be quite misleading, for example, when a product is *de facto* a polymer mixture in which

© 2004 by Marcel Dekker, Inc.

constituents were not discriminated by SEC. On the other hand, some authors who have characterized complex polymers with coupled or two-dimensional HPLC procedures failed to compare their results with the data from simple, conventional SEC and with data calculated from polymerization kinetics. Further, molar mass values obtained from coupled or 2D-HPLC are often calculated again from the peak retention volumes using polystyrene calibration while peak widths/broadening are neglected. This all casts some doubt on the advantages and even on the necessity of complicated HPLC measurements. We believe that it is very important, if a coupled or two-dimensional HPLC at least reveals the presence of macromolecular admixtures in the polymer characterized. In no way can 2D-HPLC and coupled HPLC procedures be substituted by simple SEC measurements if a complex polymer system contains two or ore constituents differing in their composition and/or architecture but possessing similar molecular sizes.

In 2D-HPLC it is very important to choose an appropriate first dimension separation procedure and retention mechanism. Enthalpic partition with nonpolar column fillings and phase separation are preferred retention mechanisms for noncrystalline nonpolar polymers, while the adsorption retention mechanism is more attractive for medium-to-highly polar polymeric analytes (Sec. 3.2). A hybrid retention mechanism such as adsorption and partition of macromolecules within silica C_{18} column packings seems presently to be the most universal approach for many complex polymer systems.

12.1 Oligomers

Coupled HPLC procedures for separation of oligomers have been studied rather intensively for more than two decades. Very important results were obtained with HPLC under critical conditions (Sec. 5.1) by Entelis *et al.* (59), Pasch and Trathnigg (4), and Kruger *et al.* (101,102). LC CC enables the separation of oligomers according to the type and number of functional groups. The danger of reduced sample recovery is much less pronounced with oligomers than with high polymers. In the second dimension separation system (SEC, eluent gradient or isocratic interaction liquid chromatography, or supercritical chromatography) the oligomer species in fractions from column #1 are separated according to molar mass of the main chain. If an oligomer sample contains two different kinds of chains, for example, two blocks, LC CC can be used for separation exclusively according to the length of one block in the first dimension and the fractions are further separated according to the length of the second block in the second dimension separation system. The full retention–elution approach can also be applied for some oligomers, especially if efficient retention promoting liquid is continuously added to the column #1 effluent (95).

Detection problems are mitigated by the fact that the initial sample concentration may be rather high. On the other hand, responses of all common

© 2004 by Marcel Dekker, Inc.

detectors depend on the oligomer molar mass and chemical composition (end group effect) and the data must be corrected (4). An evaporative light-scattering detector may produce erroneous results due to evaporation of very low molar mass sample constituents (72). Mass spectrometry of fractions obtained by coupled or 2D-HPLC separations of oligomers produces, as a rule, a very valuable, unequivocal set of information.

12.2 Polymer Mixtures

As mentioned, all synthetic polymers are multicomponent in their nature and contain macromolecules exhibiting different sizes (molar masses), and possibly also different architectures, and compositions. Thus, in a general sense, all synthetic polymers represent mixtures of different macromolecules. By convention, however, the terms polymer mixtures and polymer blends denote only those multicomponent macromolecular systems in which the distributions in molar mass, architecture, and chemical composition exhibit pronounced discontinuities. In many papers, the term "polymer mixtures" is used as a general one while the term "polymer blends" is reserved for multicomponent systems in which two and more macromolecular substances are combined intentionally. Polymer blends are frequently encountered in both technology and everyday life. A macromolecular additive may improve various processing and utility properties of the major polymer component and/or decrease the price of the resulting material. Polymer mixtures may, however, come into existence where they are not wanted. For example, parent homopolymers are often formed in the course of copolymer syntheses and also many chemical transformations of polymers including oxidization lead to polymer mixtures. A rather particular group polymer mixtures represent some technological scraps and (municipal) waste.

Analysis of polymer mixtures and molecular characterization of their constituents belong to the most important applications of coupled and two-dimensional (or quasi two-dimensional) high performance chromatographic methods. This is also due to the fact that conventional SEC often cannot produce even semiquantitative data on polymer mixtures because particular constituents of similar sizes cannot be discriminated by an exclusion retention mechanism.

Binary polymer mixtures can be separated applying "critical" or "barrier" HPLC procedures (Secs 5.1 and 5.2). One component is eluted according to an exclusion mechanism while another remains unseparated and elutes near V_M. The latter component can be further characterized, for example, by the second dimension SEC column.

Various multicomponent polymer mixtures can be discriminated using full retention–elution procedures (Sec. 7) and their constituents may be successively characterized by SEC or, if needed, by appropriate coupled or two-dimensional HPLC methods. FRE methods allow reconcentration of diluted polymer solutions

© 2004 by Marcel Dekker, Inc.

(Sec. 7) and therefore they can be applied also to molecular characterization of minor (~1% or less) macromolecular admixtures that were added to major component(s) or which were created during processing (93).

The highest separation selectivity of multicomponent polymer mixtures generally exhibits eluent gradient HPLC (Sec. 5.2).

12.3 Statistical Copolymers

Statistical copolymers were among the first and most popular complex polymer targets for chromatographic characterization (2,3). Initially, statistical copolymers were subject to tedious solubility-based cross-fractionations and only relatively recently have HPLC procedures have taken over the field. Skvortsov and Gorbunov (103) stated that critical conditions apply only to sequenced complex polymers and that the critical behavior is limited to the macromolecular chains that possess free ends. On the contrary, Brun (75,76) showed that entropy–enthalpy compensation can appear also with chains of statistical copolymers. However, LC CC is so far only rarely used as a first dimension separation system for the latter species. Very good selectivities of statistical copolymer separations were obtained with eluent gradient HPLC procedures (3–5,81,82) where molar mass independent retention was frequently observed, especially when an adsorption and partition retention mechanism was applied (Secs 3.2.1, 3.2.2, and 5.2). Second dimension separation system can be SEC.

12.4 Segmented Copolymers

Di-, tri-, and multiblock copolymers, graft copolymers and star (miktoarm) copolymers are the most typical representatives of this group of complex polymers. Most common are diblock copolymers and so are the attempts for their characterization by means of HPLC. Skvortsov and Gorbunov (104) proposed application of LC CC for diblock of copolymers and first experimental measurements were published by Zimina *et al.* (105,106). Interestingly, Zimina *et al.* (105) stated in their paper from 1991 that "... we did not evaluate experimental data quantitatively because of large band broadening ..." Later, Pasch published a series of papers describing successful LC CC of di- and triblock copolymers without mentioning the band broadening problems (4,5). Several further experimentally observed and anticipated problems connected with LC CC in general and with its application to block copolymers in particular were reviewed in Refs. (56,68,69 and 78) (see also Sec. 5.1). Mutual influence of chemically different blocks on their retention at critical conditions was recently confirmed by Lee *et al.* (107). Retention volumes of "critically retained" or "chromatographically invisible" homopolymers differ from V_R of identical chains in the block copolymers.

© 2004 by Marcel Dekker, Inc.

Unfortunately, applications of eluent gradient HPLC to block copolymers so far has not led to clearly positive conclusions. On the other hand, graft copolymers were successfully separated by EG HPLC (108).

LC CC is the most important first dimension separation system for block copolymers in the present state of 2D-HPLC method development (5). However, numerous pitfalls of this method should be considered. The situation with graft copolymers and miktoarm copolymers is even more complicated. For example, LC CC results were reasonable for graft copolymers poly(styrene-graft-ethylene oxide) with short grafts but less satisfactory for the same copolymers with long grafts (109).

12.5 Macromolecules with Complex Architectures

The most frequent and practically important polymers with distributions in their architecture are long-chain branched species. They belong to the few examples for which a single exclusion mechanism can produce decisive molecular information. SEC of branched polymers is discussed in several chapters of this book.

LC CC, LC LC, and eluent gradient HPLC can discriminate macromolecules according to their fine structural features, such as *cis–trans* isomerism (84) or stereoregularity (62,110). In the 2D-HPLC of stereoregular poly(ethyl methacrylate)s, macromolecules were first separated by conventional SEC according to their molar mass/size and LC CC was used as the second dimension separation system (61). An NMR detector confirmed good overall separation selectivity (62). LC CC also discriminates linear and cyclic macromolecules with similar molar masses (63–65).

12.6 Unknown Samples

In the preceding sections, we tried to assist polymer analysts in orientation among presently available HPLC procedures for molecular characterization of complex polymer systems The aim was to help in identifying appropriate steps in method development for solving a particular analytical problem, that is, when the basic information on the polymer type were available or it could be reasonably assessed. Unfortunately, owing to the existence of a large variety of complex polymers, so far no universal protocol for 2D-HPLC can be prepared. The situation is even more complicated when a completely unknown polymeric material appears, a "sample." The following proposed actions and their sequence should be considered as tentative only:

1. Determine the chemical composition of the unknown sample by applying all conventional solid-state bulk methods available, including (reflectance) infrared spectroscopy or pyrolysis gas chromatography.

© 2004 by Marcel Dekker, Inc.

2. Identify sample solvents. First apply single and, if necessary also mixed liquids of various polarities. Good advice on polymer solubility can be found in the *Polymer Handbook* (52). Once the sample is dissolved, several bulk methods of polymer analysis and characterization in solution can be applied from conventional spectrometry and NMR up to SEC. The latter method may also reveal the presence of species with large differences in their molar masses (molecular sizes) in the sample. If so, preparative SEC separation can produce fractions for further identification procedures. In any case, SEC also gives valuable first estimate(s) on molar mass(es) of the sample (components).
3. Full retention–elution (FRE) (Sec. 7) with nonporous bare silica and later with nonporous silica C_{18} packing can help to separate the sample into chemically different components, which are further characterized with on-line SEC (Fig. 16). Apply bare silica FRE column packing for the sample (constituents) carrying polar groups. Adsorption will be the leading retention mechanism (Sec. 3.2.1). Nonpolar sample constituents will be more easily mutually separated with silica C_{18} FRE column packing, in which macromolecules will be retained mainly by enthalpic partition (Sec. 3.2.2). For nonpolar sample constituents, a phase separation retention mechanism can also be applied (Sec. 3.2.3), preferably with bare silica FRE column packing. For full adsorption–desorption (FAD) columns packed with bare silica use the least polar solvent available for sample adsorption and polar solvent(s) for sample desorption. The experimental approach wih silica C_{18} FRE column is reversed. Evidently, the initial eluent must be an efficient nonsolvent for the sample if the FRE retention mechanism is based on the phase separation retention mechanism.
4. Fractions from repeated or preparative FRE separations can be further analyzed by spectrometry including NMR and MS. The FRE fractions of the sample can also be injected into an eluent gradient HPLC system for further, more selective discrimination. An EG HPLC system is to be chosen on the base of sample behavior in the FAD column. This means that polar sample constituents are separated by applying a polar column packing (for example, bonded amino-phase) and eluent gradient with increasing concentration of polar solvent.
5. If necessary, fractions from the EG HPLC system can be forwarded into the SEC column for the final molecular characterization (quasi three-dimensional HPLC).

Good luck!

© 2004 by Marcel Dekker, Inc.

ACKNOWLEDGEMENTS

This work was supported by the Slovak Grant Agency VEGA, project No. 2-7037-20. The author thanks Mrs J. Tarbajovska for her technical assistance.

APPENDIX

List of Selected Abbreviations

CSD	Chemical structure distribution
2D-HPLC, 2D-LC	Two-dimensional (high-performance) liquid chromatography
EG HPLC	Eluent gradient HPLC
ELSD	Evaporative light-scattering detector
FCD	Distribution of functional group concentration
FT	Functional group type
FTD	Distribution of functional group type
GFC	Gel filtration chromatography
GPC	Gel permation chromatography
HDC	Hydrodynamic chromatography
HPLC	High-performance liquid chromatography
K	Chromatographic distribution constant
$K_{V,\alpha}$	Constants in viscosity law [Eq. (6)]
LC CC	Liquid chromatography under critical conditions
LC LC	Liquid chromatography under limiting conditions
M	Local molar mass of polymer, usually the most abundant molar mass within sample or within its fraction
MAD	Molecular architecture distribution
(M)CC	(Mean) chemical composition
MCS	Mean (average) chemical structure
(M)FC	(Mean) functional group concentration
MMA	Mean (average) molecular architecture
MMD	Molar mass distribution
MMM	Mean (average) molar mass
PS/DVB	Polystyrene/divinylbenzene copolymers, important column packings for HPLC of polymers
RSR	Reconcentrating, eluent switching, sample storing, and reintroducing system
SEC	Size exclusion chromatography
V_m	Total volume of liquid within column, void volume of column
V_R	Retention volume

© 2004 by Marcel Dekker, Inc.

ε	Segmental interaction energy parameter describing interaction of a polymer segment (e.g., monomeric unit) with column packing
ε_{cr}	Critical value of ε
ε^0	Solvent strength parameter
ε^0_{AB}	Solvent strength of a binary mixture A plus B
χ	Flory–Huggins polymer–solvent interaction parameter
$[\eta]$	Limiting viscosity number of polymer

REFERENCES

1. MS Montaudo, C Puglisi, F Samperi, G Montaudo. Macromolecules 31:3839, 1998.
2. ST Balke, RD Patel. J Polym Sci, Polym Lett Ed 18:453, 1980; Adv Chem Ser 203:281, 1983.
3. G Glöckner. Gradient HPLC of Copolymers and Chromatographic Cross-fractionation. Berlin: Springer, 1991.
4. H Pasch, B Trathnigg. HPLC of Polymers. Berlin: Springer, 1998.
5. P Kilz, H Pasch. Coupled liquid chromatographic techniques in molecular characterization. In: RA Meyers, ed. Encyclopedia of Analytical Chemistry. Chichester: Wiley, 2000, p. 7495.
6. I Souvignet, SV Olesik. Anal Chem 69:66, 1997.
7. E Grushka. Anal Chem 42:1142, 1970.
8. MR Schure. Anal Chem 71:1645, 1999.
9. PJ Flory. Principles of Polymer Chemistry. Ithaca: Cornell Press, 1953.
10. D Berek, D Bakoš. J Chromatogr 91:237, 1974.
11. B Trathnigg, A Gorbunov. J Chromatogr A 910:207, 2001.
12. D Berek. Chromatography of Polymers and Polymers in Chromatography (in Slovak). DSc Thesis, Polymer Institute of the Slovak Academy of Sciences, Bratislava, 1989.
13. YuS Lipatov, LM Sergeeva. Adsorption of Polymers. New York: Wiley, 1974.
14. GJ Fleer, MA Cohen Stuart, JMHM Scheintjens, T Cosgrove, B Vincent. Polymers at Interfaces. London: Chapman and Hall, 1993.
15. M Šnauko, D Berek. Chromatographia 57:5–55, 2003.
16. D Berek. J Chromatogr. A950:75, 2002 and Chromatographia 57:5–45, 2003.
17. D Berek, J Tarbajouská. J Chromatogr A976:27, 2002.
18. D Berek. Interactive Properties of polystyrene/divinylbenzene and divinylbenzene-based commercial size exclusion chromatography column. In: C-S Wu, ed. Column Handbook for Size Exclusion Chromatography. New York: Academic Press, 1999, p 445.
19. D Berek, J Tarbajovská. Polar Interactivity of Poly(styrene-co-divinylbenzene) and Poly(divinylbenzene). Commercial Gel Permeation of Chromatographic Columns. Int GPC Symposium, Las Vegas, Oct. 2000 (to be published).

© 2004 by Marcel Dekker, Inc.

20. SH Nguyen, D Berek. Colloids Surf A 162:75, 2000.
21. SH Nguyen, D Berek. Colloid Polym Sci 277:1179, 1999.
22. T Chang, HC Lee, W Park, C Ko. Macromol Chem Phys 40:2188, 1999.
23. H Poppe, JC Kraak. J Chromatogr 282:399, 1983.
24. D Berek, T Macko. Pure Appl Chem 61:2041, 1989.
25. T Macko, M Chalányová, D Berek. J Liq Chromatogr 9:1123, 1986.
26. M Petro, D Berek. Chromatographia 37:549, 1993.
27. F Rabel, K Cabrera, D Lubda. Int Lab 31(1):23, 2001.
28. SH Nguyen, D Berek, O Chiantore. Polymer 39:5127, 1998.
29. K Baran, S Laughier, H Cramail. Int J Polym, Anal Charact 60:123, 2000.
30. T Macko, D Hunekeler, D Berek. Macromolecules 35:1797, 2002.
31. O Karal-Yilmaz, EE Gurel, N Kayaman-Apohan, BM Baysal, FE Karasz. Polymer 42:9433, 2001.
32. R Koningsveld, WH Stockmayer, E Nies. Polymer Phase Diagrams. Oxford, UK: Oxford University Press, 2001.
33. EE Brumbaugh, GK Ackers. Anal Biochem 41:543, 1971.
34. GA Gilbert, GL Kellet. J Biol Chem 246:6079, 1971.
35. PA Baghurts, LW Nichol, AG Ogston, DJ Winzor. J Biochem 147:575, 1975.
36. V Juranićová, S Florián, D Berek. Eur Polym J 6:57, 1970.
37. L Wild. Adv Polym Sci 98:1, 1991.
38. B Monrabal. Macromol Symp 110:81, 1996.
39. HJA Philipsen, HA Claessens, H Lind, B Klumperman, AL German. J Chromatogr A 790:101, 1997.
40. HJA Philipsen, M Oestreich, B Klumperman, AL German. J Chromatogr A 775:157, 1997.
41. JV Dawkins, M Hemming. Makromol Chem 176:1795, 1975.
42. B Buszewski, M Jezierska, M Welniak, D Berek. J High Res Chromatogr 21:267, 1998.
43. F Sinner, MR Buchmeiser. Macromolecules 33:5777, 2000.
44. F Švec, EC Peters, D Sykora, MJ Fréchet. J Chromatogr A 887:3, 2000.
45. RK Iler. The Chemistry of Silica. New York: Wiley, 1979.
46. KK Unger. Porous Silica. Amsterdam: Elsevier, 1979.
47. D Berek, M Jančo, G Meira. J Polym Sci A, Polym Chem 36:1363, 1998.
48. B Gawdzik, J Osypiuk. Chromatographia 54:323, 2000.
49. LR Snyder. Principles of Adsorption Chromatography. London: Arnold, 1967.
50. LR Snyder, JL Glajch, JJ Kirkland. Practical HPLC Method Development. New York: Wiley, 1988.
51. H Benoit, Z Grubisic, P Rempp, D Decker, J Zilliox. J Chim Phys 63:1507, 1966.
52. J Brandrup, EH Immergut, EA Grulke, A Abe, DR Bloch, eds. Polymer Handbook. Ch. 7. New York: Wiley, 1999.
53. DJ Solms, TW Smuts, V Pretorius. J Chromatogr Sci 9:600, 1971.
54. D Berek, T Bleha, Z Pevná. J Chromatogr Sci 14:560, 1976.
55. B Trathnigg, M Kollroser. Int J Polym, Anal Charact 1:301, 1995.
56. D Berek. Progr Polym Sci 25:873, 2000.
57. H Yun, SV Olesik, HH Marti. Anal Chem 70:3298, 1998.

© 2004 by Marcel Dekker, Inc.

58. BG Belenkii. Pure Appl Chem 51:1519, 1979.
59. SG Entelis, VV Evreinov, AV Gorshkov. Adv Polym Sci 76:129, 1987.
60. AA Gorbunov, AM Skvortsov. Adv Colloid Interface Sci 62:31, 1995.
61. M Janco, T Hirano, T Kitayama, K Hatada, D Berek. Macromolecules 33:1710, 2000.
62. T Kitayama, M Janco, K Ute, R Niimi, K Hatada, D Berek. Anal Chem 72:1518, 2000.
63. IV Blagodatskich, AV Gorshkov. Polymer Sci A 39:1135, 1999.
64. HC Lee, H Lee, T Chang, J Roovers. Macromolecules 33:8119, 2000.
65. B Lepoittevin, MA Dourges, M Masure, P Hemery, K Baran, H Cramail. Macromolecules 33:8218, 2000.
66. D Hunkeler, M Janco, D Berek. ACS Symp Ser 635:259, 1996.
67. D Berek. Macromol Symp 174:413, 2001.
68. HAJ Philipsen, B Klumperman, AM van Herk, AL German. J Chromatogr A 727:13, 1996.
69. D Berek. Macromol Symp 110:33, 1996.
70. P Cifra, T Bleha. Polymer 41:1003, 2000.
71. P Jandera, M Holcapek, L Kolarova. Int J Polym, Anal Charact 6:261, 2001.
72. B Trathnigg, M Kollroser, D Berek, SH Nguyen, D Hunkeler. ACS Symp Ser 731:95, 1999.
73. D Berek. Macromolecules 32:3671, 1999.
74. D Berek. Macromolecules 31:8517, 1998.
75. Y Brun. J Liq Chrom Relat Technol 22:3027, 1999.
76. Y Brun. J Liq Chrom Relat Technol 22:3067, 1999.
77. C Degoulet, R Perrinaud, A Ajdari, J Prost, H Benoit, M Bourrel. Macromolecules 34:2667, 2001.
78. D Berek. Mat Res Innovat 4:365, 2001.
79. S Mori. Adv Chem Ser 247:211, 1995.
80. S Mori. Macromol Symp 110:87, 1996.
81. TH Mourey. J Chromatogr 357:101, 1986.
82. HG Barth. ACS Symp Ser 352:29, 1987.
83. TC Shunk. J Chromatogr A 656:591, 1993.
84. H Sato, M Sasaki, K Ogino. Polym J 21:965, 1989.
85. J Porath. Nature (London) 196, 1962, p. 47.
86. BG Belenkii, ES Gankina, GE Kasalainer, MB Tennikov. ACS Symp Ser 635:274, 1996.
87. H Inagaki, H Matsuda, F Kamiyama. Macromolecules 1:520, 1968.
88. S Teramachi, A Hasegawa, Y Shima, M Akatsuka, M Nakajima. Macromolecules 12:992, 1976.
89. JM Sebastian, RA Register. J Appl Polym Sci 82:2056, 2001.
90. SH Nguyen, D Berek. Int J Polym, Anal Charact (in press).
91. SH Nguyen, D Berek. J Polym Sci A, Polym Chem 37:267, 1999.
92. SH Nguyen, D Berek. Colloid Polym Sci 277:318, 1999.
93. SH Nguyen, D Berek. Int J Polym, Anal Charact 6:223, 2001.
94. M Lazzari, T Kitayama, M Janco, K Hatada. Macromolecules 34:5734, 2001.

© 2004 by Marcel Dekker, Inc.

95. B Trathnigg, SH Nguyen, in preparation.
96. D Berek, R Bruessau, D Lilge, I Mingozzi, S Podzimek, E Robert. Reproducibility of Molar Mass Values of Commercial Polymers Determined with Size Exclusion Chromatography, HPLC 2001, Maastricht, p. 307 (to be published).
97. M Jančo, T Prudskova, D Berek. J Appl Polym Sci 55, 1995, p. 393.
98. RE Murphy, MR Schure, JP Foley. Anal Chem 70:1585, 1998.
99. D Berek. J Chromatogr 132:128, 1977.
100. S Mori. J Chromatogr 541:375, 1991.
101. R-P Krüger, H Much, G Schulz. J Liq Chromatogr 17:3069, 1994.
102. R-P Krüger, H Much, G Schulz, O Wachsen. Macromol Symp 110:155, 1996.
103. AM Skvortsov, AA Gorbunov. J Chromatogr 507:487, 1990.
104. AM Skvortsov, AA Gorbunov. Vysokomol Soedin A21:339, 1979.
105. TM Zimina, EE Kever, EYu Melenevskaya, VN Zgonnik, BG Belenkii. Vysokomol Sojedin A33:1349, 1991.
106. TM Zimina, A Fell, JZ Castledine. Polymer 33:4129, 1992.
107. W Lee, D Cho, T Chang, KJ Hanley, TP Lodge. Macromolecules 34:2353, 2001.
108. S Teramachi. Macromol Symp 110:217, 1997.
109. R Murgašová, I Capek, E Lathová, D Berek, S Florián. Eur Polym J 34:659, 1998.
110. D Berek, M Jančo, K Hatada, T Kitayama, N Fujimoto. Polym J 29:1029, 1997.

© 2004 by Marcel Dekker, Inc.

19
Methods and Columns for High-Speed Size Exclusion Chromatography Separations

Peter Kilz
PSS Polymer Standards Service GmbH
Mainz, Germany

1 INTRODUCTION

Size exclusion chromatography (SEC) is the established method for determining macromolecular properties in solution. It is the only technique that allows the efficient measurement of property distributions for a wide range of application. Recently, a major goal in industry and research alike has been focused on increasing the throughput of analytical instrumentation. This has been forced by increasing productivity demands in QC/QA and by the use of high-throughput screening techniques in materials science for faster development of new products. Increased analytical throughput can save time and resources (e.g., instrumentation) in production-related fields. In combinatorial research, high-throughput analytical techniques are a bare necessity, because of the huge numbers of samples being synthesized (1,2; and references therein). In either situation, the slowest step in the

© 2004 by Marcel Dekker, Inc.

process will determine the turn-around time. The importance of high-speed analytical techniques gets obvious when it is considered that research companies synthesize over 500 targets per day, but only about 100 samples can be analyzed. The potential of new synthetic methods and in-line production control cannot be fully utilized until the typical SEC run times of 30 minutes are substantially reduced.

2 APPROACHES FOR FAST SEC SEPARATIONS

This section reviews very briefly different methods that have been used to increase the number of SEC analyses per unit time. The key benefits and requirements of each method are discussed and summarized in Table 1.

2.1 Parallelization

Early answers to such challenges have been parallelization and automation of analytical processes. More samples can be analyzed by using fully automated instruments, which work day, night, and over the weekend. The number of processed samples can be increased proportionally by setting up identical systems in parallel. The time and analytical requirements for each sample are not changed but the number of samples per hour can be increased. Since no change in analytical methods is necessary, implementation of parallel systems is not very complex and is not straightforward.

This approach, however, is clearly limited by a number of important prerequisites like space, operator instruments, and computers. All of this will cost a lot of money for initial investment, maintenance, and operation. Practical experience with this concept has shown that this approach will hold if the number of samples increase much less than one order of magnitude.

2.2 Shorter Columns

Column length reduction is the traditional method to reduce analysis time. This was done in SEC applications in the 1960s and 1970s when more efficient column packings allowed smaller column dimensions. Today, the efficiency of SEC columns is at a stage where a further column length decrease cannot be compensated without a loss of resolution. Cutting down on column length is also very limited. Therefore some column manufacturers (most notably PL and TSK, in Freiburg, Germany) cut column length in half to increase throughput (3). However, this reduces run times proportionally and only low time and solvent savings are possible (Fig. 1).

Please note that shorter columns cannot easily meet the polymer resolution requirements of ISO 13885 or DIN 55672 SEC standards (9).

The advantages and disadvantages of this approach are summarized in Table 1.

© 2004 by Marcel Dekker, Inc.

Table 1 Summary of Methods for Increased SEC Throughput

Approach	Advantages	Disadvantages	Beneficial for...
Parallization	No method change Easy to implement No additional training	High investment cost High maintenance Higher operating cost More people More space Limited throughput gain	Sample increase of up to 3×
HighSpeed	No method change Uses existing equipment 1 : 1 Application transfer No additional training Minimizes investment (column only) SEC separations in 1 min Time gain ca. 10× No additional shear High efficiency Runs with conventional software	No eluent savings	QC/QA Increased throughput (10×) Use with existing methods
FIA	Uses existing equipment Saves eluent	No separation Limited time gain Not applicable for copolymers/blends Requires expensive equipment (LS and/or viscometer) Only primary information (conc., M_w, IV) Needs method change Needs special software	Samples difficult to separate Utilizes existing instruments
Short or thin columns	Uses existing equipment Minimizes investment Saves eluent Runs with current software	Limited time saving Needs method adaption Optimization of injection volumes Optimization of detection systems Shear degradation Low efficiency Needs training Limited throughput increase	Low resolution applications Low time-saving requirements Single detector applications

© 2004 by Marcel Dekker, Inc.

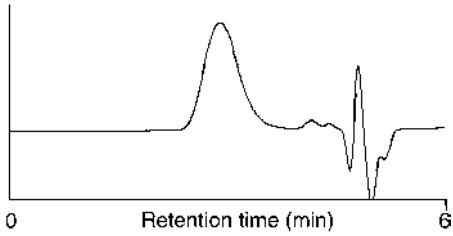

Figure 1 SEC chromatogram of column with 15 cm column length run in THF at a flow rate of 1.0 mL/min and temperature of 40°C. (From Ref. 3.)

2.3 Flow Injection Analysis (FIA)

Another method to cut down on analysis time is to avoid separation altogether and inject samples directly into detector cells. Unfortunately, this cannot be done in dilute solutions, because the signals from the solvents must be separated out from the sample response (Fig. 2).

This method has to be used with expensive molar mass sensitive detectors (like light scattering and/or viscometry) to obtain a single result from each detector (M_w and/or IV, respectively). A concentration detector is also needed in most applications to obtain the concentration of the sample. If only a concentration detector is used, the only measured parameter is polymer content in a sample, which can also be determined with various other well-established methods. The FIA approach requires expensive and well-maintained equipment and will

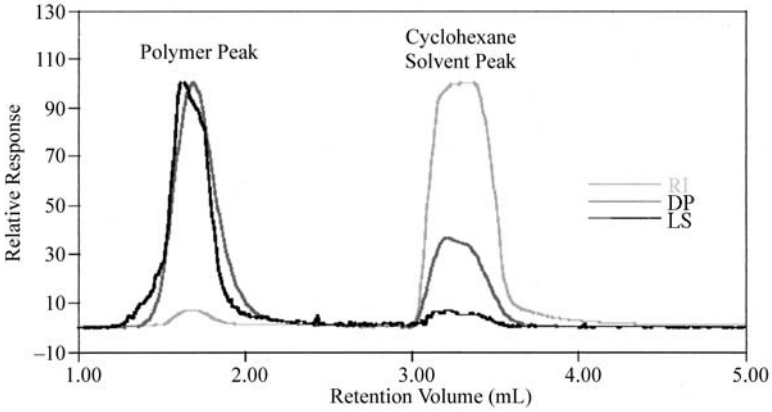

Figure 2 Flow injection analysis with short column to separate solvent and sample run in THF at a flow rate of 1.0 mL/min and temperature of 60°C. (From Ref. 4.)

© 2004 by Marcel Dekker, Inc.

not save a lot of time and solvent, despite the fact that no distribution information is available. All major producers of molar mass sensitive detectors have published initial results on this technique (4,5). A summary of pros and cons is listed in Table 1.

2.4 High-Speed SEC Columns

PSS investigated the limitations of different approaches to reduce time requirements and decided to start a research project on fast SEC separations evaluating and quantifying the effects of different column dimensions and packings (6). The results of this work are presented in Sec. 3. The data presented there will allow the reader to understand and apply the different principles for fast SEC separations in their own environment. A summary of advantages and limitations are given in Table 1.

3 COLUMN DESIGN CONCEPTS FOR HIGH-SPEED SEC

Time requirements for chromatographic separations can be reduced most simply by changing the column dimensions. This is the easiest adaptation for column manufacturers, because they will not need to change the chemical and or physical nature of the packings. However, chromatographic theory predicts a number of important limitations, which have to be taken into account (7,8).

Alternatively, the packing of columns can be optimized for shorter run times. PSS investigated the efficiency of packings with different particle size and their potential to increase throughput. Table 2 discusses effects of column parameter modifications and summarizes their advantages and limitations.

3.1 Quantitative Investigation of Ideal Column Dimensions

Identical experimental conditions have been used to compare the results of columns with different dimensions in the investigation carried out by PSS. They used a styrene–divinyl benzene-based column packing with 5 μm particle size and a wide pore size range (PSS SDV 5 μm linear column). A single column was used in all cases. All experiments were run on the same instrument (to avoid any influence by the instrument hardware), evaluated with the same software (PSS WinGPC), and by a single operator. All experiments were performed with a polystyrene standard cocktail containing seven narrow standards (from 2.5 million down to 1900 g/mol) in THF as the eluent. Only flow rates and injection volumes were adjusted accordingly.

© 2004 by Marcel Dekker, Inc.

Table 2 Effects of Column Dimensions on Chromatographic Performance

Column change	Result	Advantage	Disadvantage
Reduce length	Run time reduction	Shorter runs with less solvent	Lower resolution Lower pore volume Time gain very limited
Reduce diameter	Sensitivity increase	Less injected mass and eluent needed	Needs microbore instrumentation Lower resolution Lower pore volume Higher shear rates Polymer degradation Very limited time gain
Reduce column aspect ratio	Constant separation volume	Shorter run times with identical pore volume and similar resolution	No solvent savings
Reduce particle size	Band broadening reduction Efficiency increase	Increases resolution (most notable in oligomer region)	High backpressure High shear rates Polymer degradation Limited time gain
Increase flow rate	Run time reduction	Shorter runs	High backpressure Shorter column lifetime Lower resolution High shear rates Polymer degradation

3.1.1 Results of a Conventional Column

Figure 3 shows a typical chromatogram for a conventional SEC experiment using a standard column of 30 cm length and 8 mm internal diameter (ID) at the usual flow rate of 1.0 mL/mm. All results from columns with different dimensions were compared to the performance of this experiment. The overall run time of this experiment was about 13 minutes. As expected, the seven polymer standards show

© 2004 by Marcel Dekker, Inc.

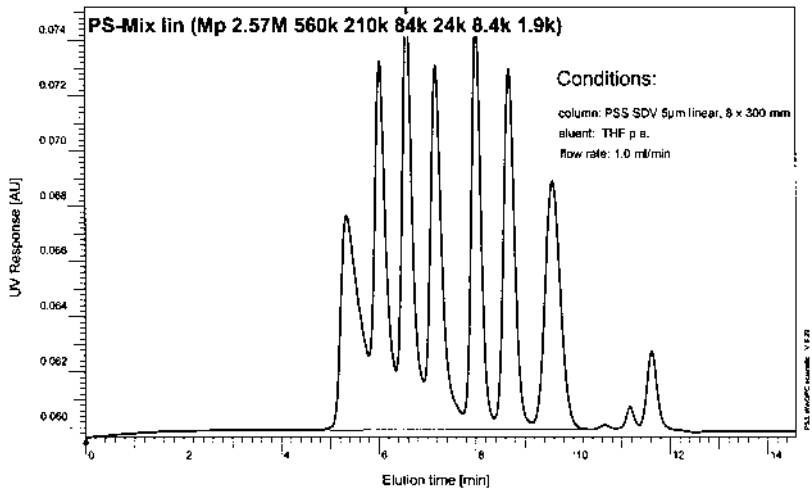

Figure 3 Conventional SEC chromatogram of seven polymer standards showing state-of-the-art performance run in THF at a flow rate of 1.0 mL/min and at ambient temperature.

very good resolution across the total molar mass range. The peaks are very well separated from the solvent peaks. The shape of all the peaks is symmetrical, indicating a homogeneously packed column bed. There is no indication of sample degradation in the high molar mass regime. The number of theoretical plates for BHT was calculated as 92,500 plates/m and the specific resolution was 5.2 [determined according to ISO 13885 standard (9)]. These are very good values for a mixed-bed column indicating a perfect system for efficient and reliable separations and molar mass calculations.

3.1.2 Increasing Eluent Flow Rate

Because SEC is based on the diffusion of molecules between a mobile phase and a stagnant mobile phase in the pore structure of the packing, the eluent flow rate will influence the efficiency of the separation. This is a very well-known and well-understood phenomenon, which can be described by the van Deemter relation (Fig. 4). The efficiency of the separation is expected to drop continuously with increased linear flow velocity (the speed of the solvent front that travels along the column).

In order to understand visually the importance of the linear flow rate on separation efficiency, the experiment with the conventional column was repeated at a flow rate of 4.0 mL/min instead of 1.0 mL/min (above). Figure 5 shows the

© 2004 by Marcel Dekker, Inc.

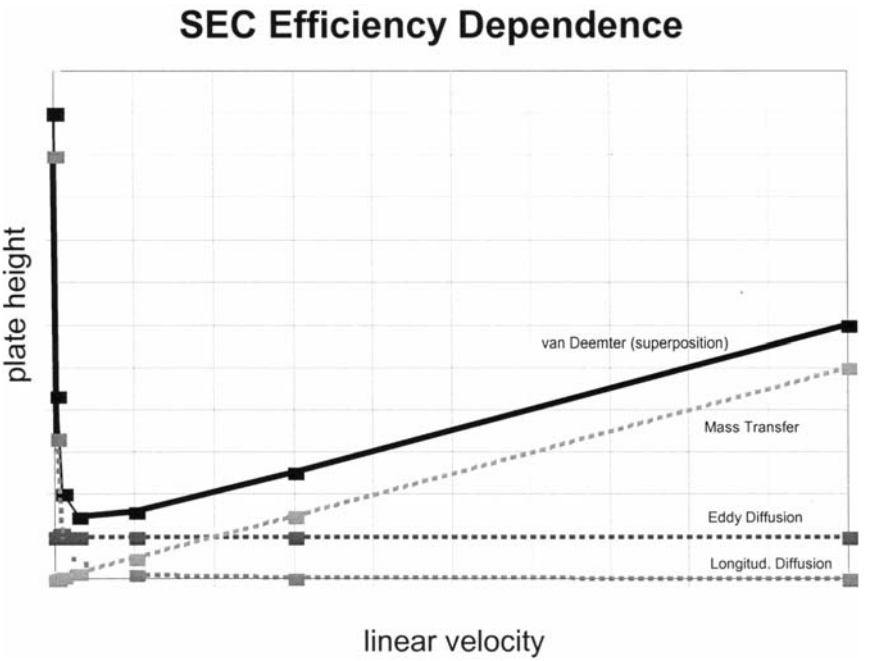

Figure 4 Schematic representation of contributions of column packing properties to overall column performance (van Deemter relation).

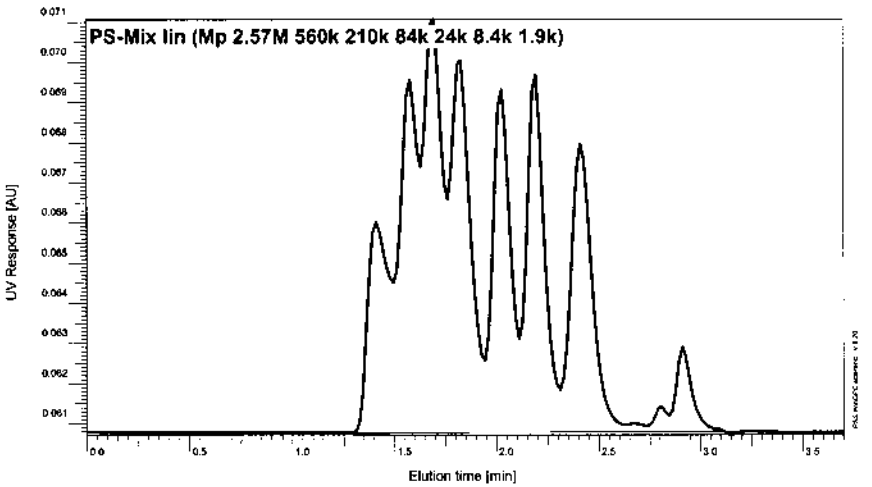

Figure 5 Reduction of column performance caused by too high flow rates (sample and conditions similar to Fig. 3).

© 2004 by Marcel Dekker, Inc.

chromatogram at 4 mL/min, which is finished after about 3.5 min instead of 13 min. The price to pay for this time gain is clearly visible in the chromatogram:

- Peak separation is dramatically reduced compared to Fig. 3,
- High molar mass peaks show tailing (degradation).

The number of theoretical plates is reduced by more than a factor of 2 (43,000 instead of 92,500) and the asymmetry factor of 0.7 shows peak skewing. The specific resolution and other performance criteria are affected in the same way. Running columns far beyond their flow rate rating will also reduce the effective lifetime of the column and lead to higher costs.

3.1.3 Reducing Column Length

Column length and chromatographic run times are directly proportionally related, while column efficiency changes with the square root of column length only. This means a column cut in half will generate results twice as fast, while the resolution will be reduced by a factor of 1.4 only. The bad news is that cutting run times by larger factors is very limited. In order to reduce the run time by a factor of 10 the column length has to be reduced from 30 cm to 3 cm. Obviously, this is not possible without sacrificing too much performance. Additionally, the pore volume will also be reduced proportionally with column length. Therefore it is very important to check experimentally how much the resolution of such columns will be affected by their reduction in length.

An identical experiment using a column of only 5 cm length (while maintaining the internal diameter of 8 mm) was performed in order to relate these results to conventional separation. Figure 6 shows the chromatogram of the short column (length cut by a factor of 6). As expected the run time in this experiment is significantly reduced (to about 2.5 min). However, the resolution of peaks is much lower again and peaks show significant tailing. The fine structure of the solvent peaks is no longer visible and all components are merged into a single peak at the end of the chromatogram.

Short columns like this one cannot be used, if tests have to carried out according to ISO 13885 or DIN 55672 SEC standards. They require that peak positions (as a direct measure of resolution) have to be at least 6 cm apart in the column (9).

3.1.4 Reducing Column Diameter

So far, limitations from chromatographic theory have been found to be effective in real-life scenarios for polymers too. Reducing internal column diameters has long been used in GC and HPLC to speed up separations and overcome sensitivity issues. PSS checked out this approach for macromolecules in their investigation.

© 2004 by Marcel Dekker, Inc.

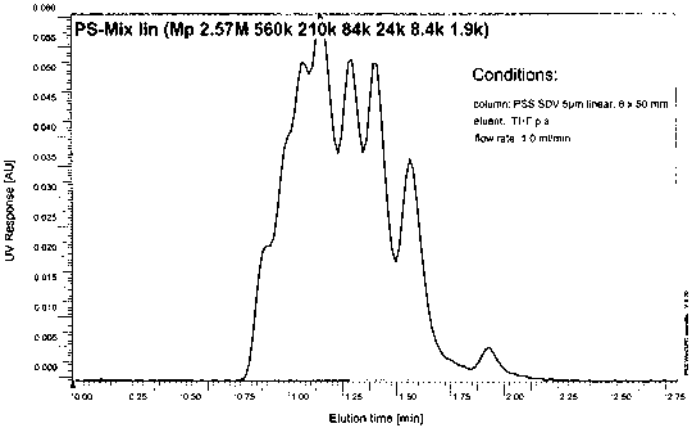

Figure 6 Substantial performance loss caused by reducing column length from 30 cm to 5 cm compared to a conventional SEC column (sample and conditions similar to Fig. 3).

They used a 4 mm ID column (half the diameter of their conventional column) to investigate the effects of reduced column size on polymer separation efficiency and run time. A 4 mm ID column was chosen because it is compatible with existing instruments. It does not require µ-bore ready equipment, which is not available for RI detection (e.g., low cell volumes). Figure 7 shows the raw chromatogram obtained under otherwise identical experimental conditions. As expected, the run time in this experiment is significantly reduced (to about 3 min).

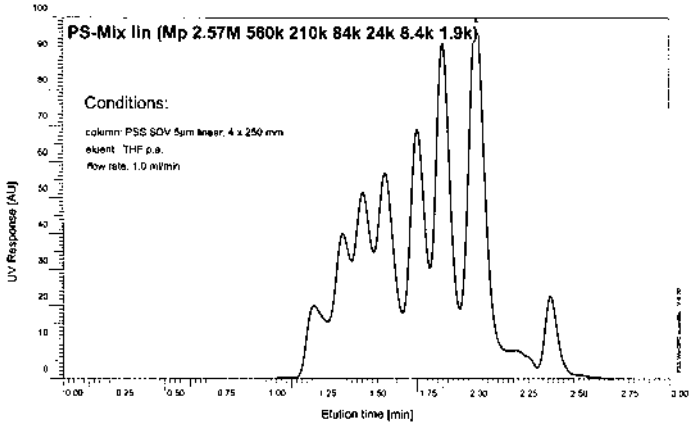

Figure 7 Efficiency loss and poor peak shapes caused by a column with 4 mm internal diameter (sample and conditions similar to Fig. 3).

© 2004 by Marcel Dekker, Inc.

Since the reduction of the internal diameter drastically reduces the pore volume of the column (squared relationship), a substantial influence on performance has to be expected. This is clearly visible in the raw chromatogram. Resolution is much poorer as compared to the reference chromatogram of the conventional column in Fig. 3. Moreover, the peak shapes are badly affected as can be seen in the relative change of the peak heights of the standards. The higher the molar mass of a standard the broader the peak gets (and the lower the corresponding peak height will be). This is caused by the high linear flow rate inside the column, which is necessary to drive the eluent through it; please note that the pump flow rate was kept constant at 1.0 mL/min. Samples with high molar mass will be affected by shear degradation under such conditions. The limited efficiency in this setup is also seen in the poor separation of sample peaks from the solvent peaks at the end of the chromatogram.

3.1.5 Changing Column Aspect Ratio

The simultaneous adaption of column length and diameter allows the internal volume of the separation system to be kept constant. This is important for SEC, because the column volume and the pore volume of the packed bed are directly related. As pointed out above, the pore volume is one of the major factors influencing peak resolution. Cutting down the column length and *increasing* the internal dimension of the column at the same time can, in theory, reduce the chromatographic run time while maintaining the efficiency of the separation. Obviously such columns have to be operated at higher flow rates to reduce the run times. Solvent cannot be saved significantly without interfering with resolution.

Moreover, other effects can influence the separation. In such a scenario, the accessibility of the pores in the packing will be most important. If the architecture of the pores in the column will restrict diffusional migration of the solutes, the column will not and cannot perform as expected. Wall effects might also influence the separation and have to be watched closely as column length is reduced. PSS studied such short wide-bore columns extensively for their use in fast separations.

Figure 8 shows the separation on a test column of 50 mm length and 20 mm ID run at a flow rate of 6 mL/min. The same packing material as in all other columns was used in this experiment. All other experimental parameters were kept constant. The first impression of the separation is favorable:

- All peaks are present in their correct height (concentration) ratios,
- A good peak symmetry is kept throughout the whole chromatogram,
- No indication of sample degradation at high molar masses,
- Separation is carried out in less than 2 min, and
- Sufficient separation of solvent peaks from sample.

© 2004 by Marcel Dekker, Inc.

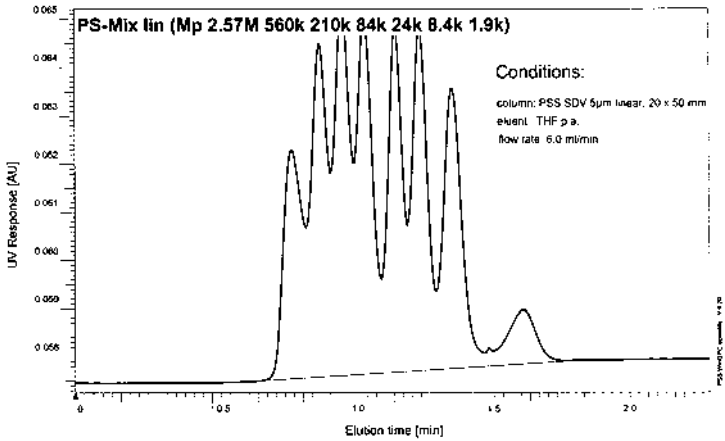

Figure 8 Column performance of short wide-bore SEC column with 20 mm internal diameter and 50 mm length (sample and conditions similar to Fig. 3).

The separation efficiency is not as good as in the case with a conventional column. It could be shown (6) that this is related to the nonoptimized flow profile inside the column and is not related to wall effects. Influence of the wall will, however, be a parameter affecting the efficiency of the separation when columns are further reduced in length.

A quantitative investigation of column performance showed that the specific resolution of 4.3 is about 20% lower than on a conventional column. The plate count is influenced even more: using BHT as a probe molecule only 58,500 plates/m could be measured (using the ISO 13385 test) as compared to 92,500 for the conventional column.

3.2 Evaluation of Different High-Speed Column Design Approaches

The performance of different column designs with regard to key criteria in macromolecular separations such as resolution, pore volume, and peak symmetry are summarized in Table 3.

The available pore volume in an SEC column directly determines peak resolution and separation efficiency, while the flow rate setting will influence shear degradation of the sample, the effective mass transfer, and consequently resolution.

Figure 9 compares the raw chromatograms of different column designs under identical experimental conditions using the same volume flow rate. The deterioration of column efficiency at identical volume flow is directly related to columns with low pore volume (see chromatograms [2] and [3] in Fig. 9), that is,

© 2004 by Marcel Dekker, Inc.

Table 3 Summary of Column Performance Criteria with SEC Columns of Different Dimensions

Column design	Parameter				
	Resolution	Plate count	Symmetry	MMD range	Solvent peak separation
Analytical	☺	☺	☺	☺	☺
High flow analytical	☹	😐	☹	☺	😐
Short	☹	😐	☹	☺	😐
Narrow-bore	☹	☹	☹	☺	😐
Short wide-bore	😐	☺	☺	☺	😐

Performance criteria are met well (☺), adequately (😐), or poorly (☹).

short and narrow-bore columns. These are, unfortunately, the same columns that separate the fastest. Those columns with high pore volume (see chromatograms [1] and [4] in Fig. 9) shows much better resolution. This figure underlines the importance of pore volume for optimum SEC separations.

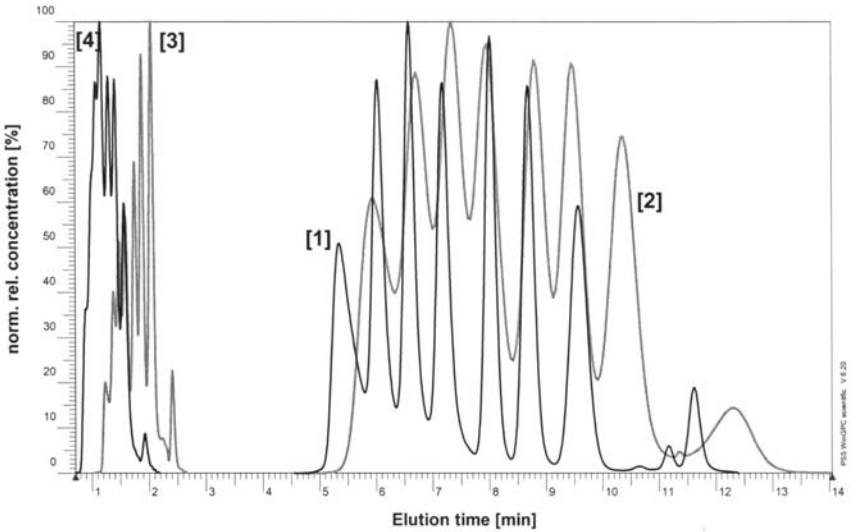

Figure 9 Comparison of chromatograms of SEC columns with different dimensions tested with identical polystyrene standards in THF shows the required run time, pore volume, and efficiency (all run at equal volume flow rate of 1.0 mL/min). [1] Traditional analytical SEC column (8 × 300 mm), [2] short SEC column (8 × 50 mm), [3] narrow-bore SEC column (4 × 250 mm), and [4] short wide-bore SEC column (20 × 50 mm).

© 2004 by Marcel Dekker, Inc.

Narrow columns require lower flow rates for optimal operation. Figure 10 shows the same columns as above, but this time under identical *linear* flow velocity. This means that the standards travel with identical speed through each of the different columns and all columns perform close to the optimum in the van Deemter plot.

This view allows the comparison of the efficiency of the separation and its time requirement. Because narrow-bore columns need lower volume flow rates for best performance, almost no time can be gained. The resolution difference between the conventional analytical column and the narrow-bore column in Fig. 10 can, in part, be attributed to the fact that the same instrument was used that was not optimized for narrow-bore use. The shorter run time for the narrow-bore column must only be attributed to its shorter column length (25 cm instead of 30 cm for the analytical column).

The fastest column is the short wide-bore column, which is about six times faster than the other columns in the comparison and nevertheless shows satisfactory resolution.

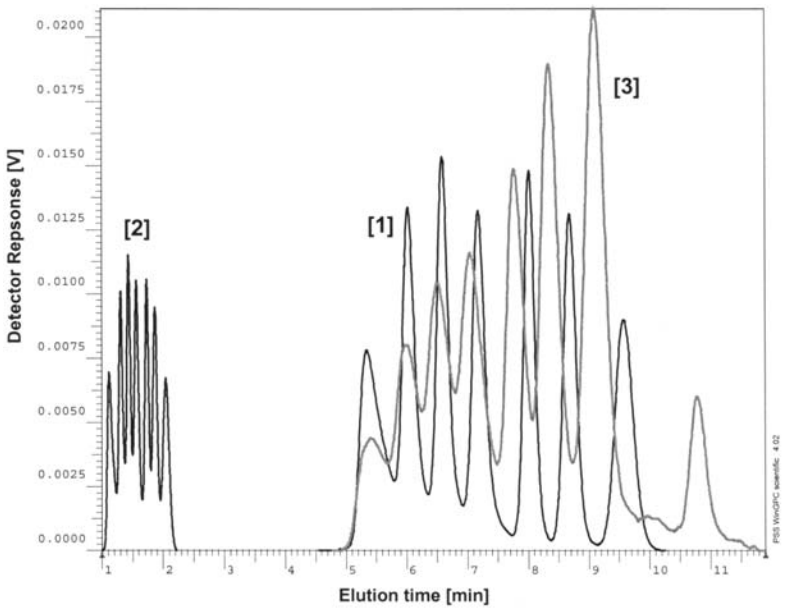

Figure 10 Overlay of SEC chromatograms of columns with different dimensions tested with identical polystyrene standards in THF at identical linear flow rates reveals time requirements and related column efficiency. [1] Traditional analytical SEC column (8 × 300 mm), [2] short SEC column (8 × 50 mm), [3] narrow-bore SEC column (4 × 250 mm).

© 2004 by Marcel Dekker, Inc.

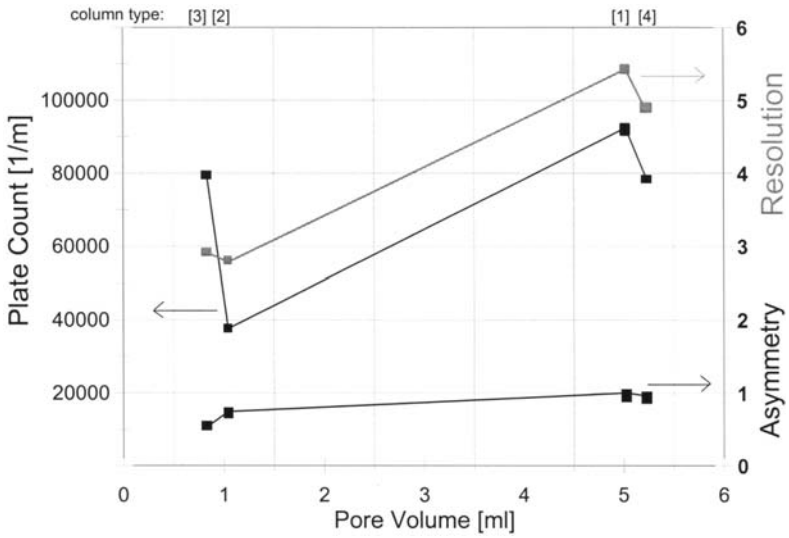

Figure 11 Dependence of column performance parameters on SEC column dimensions and pore volume. [1] Traditional analytical SEC column (8 × 300 mm), [2] short SEC column (8 × 50 mm), [3] narrow-bore SEC column (4 × 250 mm), and [4] short wide-bore SEC column (20 × 50 mm).

The column with the best overall performance is certainly the conventional column. This is no surprise since this product has been optimized for highest performance/price and has been in use in many laboratories for years. The conventional column performs extremely well in all areas studied. The next best design for polymeric applications is the short wide-bore column. It is quite obvious that the resolution must be enhanced by using a specially designed packing with optimized pore architecture. This can also be seen in Fig. 11.

As a general rule the following conclusions can be drawn:

- For least time requirement a short wide-bore column should be used, and
- For lowest eluent consumption a short and thin column is best.

4 HOW CAN HIGH-SPEED SEC COLUMNS BE MADE?

The previous chapter has shown the potential and shortcomings of various methods to overcome the time restraints in conventional SEC experiments. In order to utilize the short wide-bore columns best, new packing materials have to be designed that overcome the pore access limitations of conventional packings. Conventional analytical columns have been optimized for their typical flow rates

© 2004 by Marcel Dekker, Inc.

(between 0.5 and 1.5 mL/min). Higher or lower flow rates will lead to inferior performance. This can be explained by the van Deemter equation, which relates plate height, h, with the linear flow rate, u:

$$h = A + \frac{B}{u} + Cu$$

where A represents the eddy diffusion term (Fig. 4), which mainly depends on the particle size, B is related to longitudinal diffusion effects, which are not very prominent in densely packed SEC columns, and C is the so-called mass transfer term, which describes (in a simple analogy) the movement of the solute between the mobile and stationary phase. The higher the linear flow velocity the more difficult it will get for the solutes to penetrate the pores of the packing and the lower the resolution will be.

4.1 Properties of PSS HighSpeed™ SEC Columns

Because parallelization of SEC analyses did not meet the requirements PSS set for optimal implementation and easy use of fast SEC analyses, PSS decided to design SEC packing materials that allow the true high-speed separations. The design of new SEC packing materials requires a lot of experience from synthetic chemists on copolymerization and network formation as well as from analytical chemists who have to test that the design criteria are met (10).

Every change in column packing materials is critical for the manufacturer (market acceptance) and for the users (method compatibility). Therefore the key requirement for PSS HighSpeed SEC packings has been the trouble-free method transfer from an existing conventional application to a PSS HighSpeed application. The only thing a PSS HighSpeed user should have to do is replace a conventional column with a similar HighSpeed column. This is only possible if a number of other design criteria are met:

- SEC separations must be possible in 1 min,
- There must be no change in sample separation ranges, resolution, and efficiency,
- The column must run on already existing instrumentation (no need for special equipment),
- There must be simple transfer of existing methods (one-to-one column exchange),
- All packings must be available in conventional and HighSpeed types,
- The same samples must be able to be run as before (no shearing, high efficiency, and so on),
- Existing SEC instruments must be utilized more efficiently (no need to buy new equipment with increasing sample numbers), and

© 2004 by Marcel Dekker, Inc.

- Two-dimensional chromatography run times must be reduced to about 1 hour.

If all these requirements are met, new application areas will become really attractive for SEC as an analytical tool for:

- Monitoring *and* controlling production processes in-line,
- Using SEC methods routinely in high-volume QC labs,
- Allowing high-throughput screening for new materials design,
- Playing a role in combinatorial chemistry, and
- Being useful in monitoring time-critical processes.

4.2 Optimized HighSpeed Column Packings for Fast Separations

HighSpeed columns require polymer packings that are crosslinked in a way that allows easy access of macromolecules to the inner parts of their network structure. The optimum flow characteristics of conventional analytical SEC columns are schematically shown in Fig. 4. Best column performance is achieved with volume flow rates of about 0.5–1.5 mL/min. Above that value the plate height increases (performance decreases), because of the higher mass transfer contribution. A similar investigation with PSS HighSpeed column packing shows a flat (shallow) dependence of plate height on flow rate (Fig. 12).

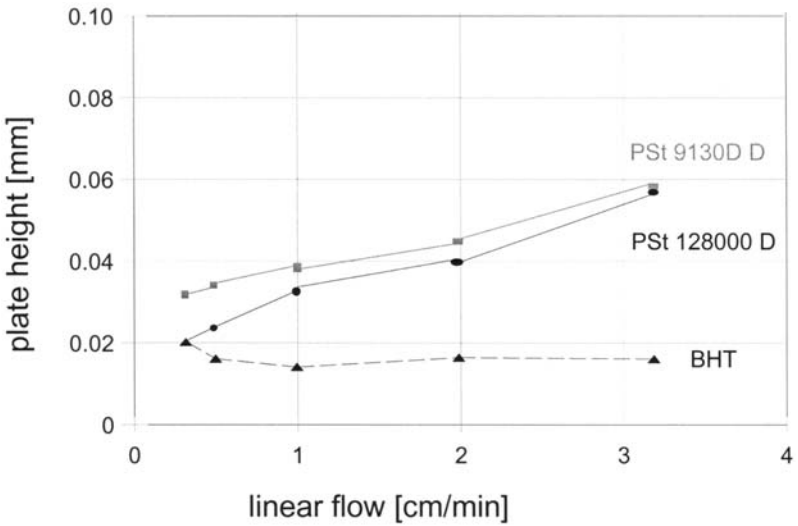

Figure 12 Flow rate dependence of column efficiency for HighSpeed column (PSS SDV 5 μm HighSpeed linear) determined by polystyrene standards in THF.

© 2004 by Marcel Dekker, Inc.

The van Deemter equation was measured for different molar masses (using polystyrene standards in THF) over a wide molar mass range. The lower the molar mass, the more flat the dependence becomes. Even for samples beyond 100,000 g/mol, very shallow flow dependence was determined. This means that these columns can be operated at higher flow rates *without* losing too much of their efficiency.

4.2.1 Precision of HighSpeed Separations

Time requirement and resolution are not the only criteria for a good HighSpeed column. It should also be able to generate results with the same precision and accuracy as conventional analytical columns. It should also last as long as conventional columns and should not be more expensive.

Reproducibility of SEC measurements can be checked more easily by HighSpeed columns because the time requirements are much lower. This allows for better result accuracy and higher statistical security. Figure 13 shows the overlay of 10 commercial polycarbonate chromatograms in THF; every sixth run out of 60 runs in total is represented in the overlay. They overlap almost perfectly. Each run took about 2.5 min, the total run time for 60 repeats was about 2 hours.

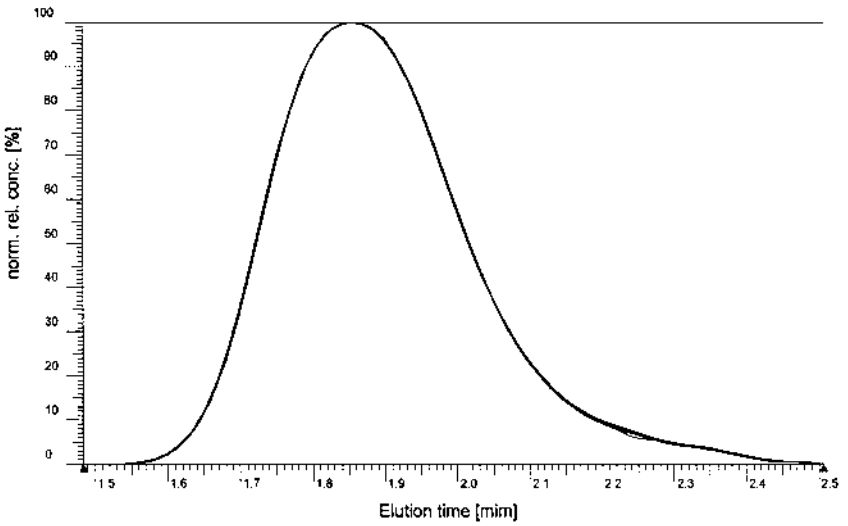

Figure 13 Overlay of 10 (out of 60) repeats of a commercial polycarbonate run in THF on PSS SDV 5 μm HighSpeed, 10^3, 10^5 Å column; measured $M_w = (29{,}610 \pm 150)$ g/mol (nominal sample molar mass by producer, 30,000 g/mol).

© 2004 by Marcel Dekker, Inc.

The standard deviations for the molar mass results are in the order of 0.5% RSD for this HighSpeed separation. They are similar to analyses using conventional columns on good instrumentation. It has been shown that not the column but the instrument determines result precision (11). In particular, in HighSpeed separations, the pumps must be able to deliver constant flow at higher flow rates and with high precision.

4.2.2 Accuracy of HighSpeed Columns

Correct molar mass results are very important and they should not be compromised even in HighSpeed applications. PSS checked the absolute accuracy of molar masses using various narrow and broad standards in various solvents and compared measured molar mass averages with the accepted values of the polymer standards.

Table 4 compares results of 10 repeats of a broad polystyrene standard with the measured molar mass averages and their standard deviation. The accuracy of the HighSpeed results is excellent, while the standard deviation is similar to normal SEC separations. RSD values will depend directly on the maintenance status of the instrumentation. Different instruments have shown different RSD levels while the molar mass averages have been very close to those reported for the reference standard.

Similar results have been reported by Alden (15) and Nielson (private communication), who investigated the accuracy and precision of polystyrene runs using short columns (6 × 150 mm) on an optimized SEC system (Fig. 14).

4.2.3 Saving Time with HighSpeed SEC Columns

HighSpeed SEC is certainly nice to have, but how much can be gained with respect to time and money? Analysing the analytical process shows that calibration, validation runs, and sample runs are areas where the PSS HighSpeed SEC column concept must show its validity.

Typical conventional calibrations require a minimum of 10 calibration points. Also typical are SEC run times of 40 to 60 min (3 to 4 columns per instrument) for high-quality analyses. Please note that these conditions are very close to the requirements of the international (ISO 13885, Ref. 9) and national

Table 4 Accuracy of HighSpeed Separation for Polystyrene Reference Standard

	M_n	%SD	M_w	%SD	M_p	%SD
Reference polymer	47,500	n/a	93,300	n/a	85,300	n/a
HighSpeed results	47,200	5.2	93,100	3.0	85,200	1.1

n/a, not applicable.

© 2004 by Marcel Dekker, Inc.

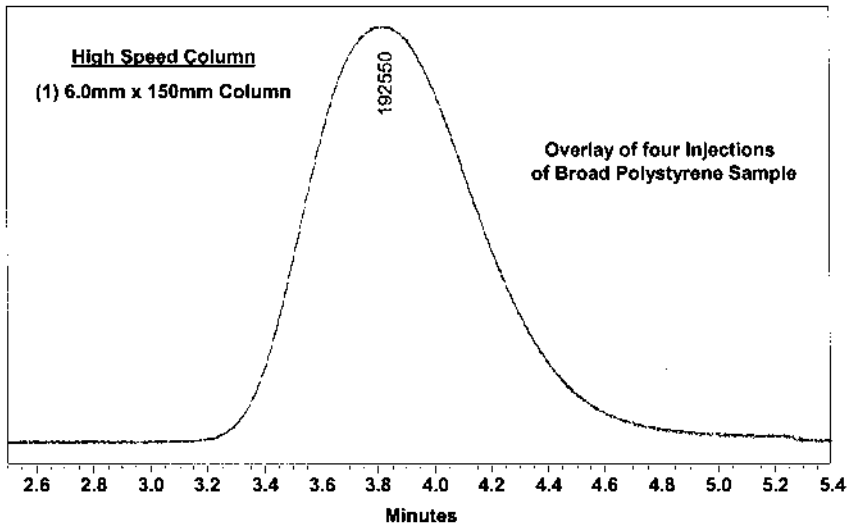

Figure 14 Reproducibility of broad polystyrene (four repeats) analyzed on a short SEC column using an optimized instrument with an analysis time of 7.5 min (Rick Nielson, private communication).

SEC standards (DIN 55672 in Germany). Equilibration time for an instrument prior to calibration is about 10 hours (overnight).

The total calibration time using conventional columns is about: 600 min (prep time) + 10 × 60 min (standards run time) = 1200 min = 20 hours (that is, about 2.5 workdays).

Running a HighSpeed SEC system 10 times faster than a conventional one will reduce total calibration time accordingly: 60 min (prep time) + 10 × 6 min (standards run time) = 120 min = 2 hours (that is, about a quarter of a workday).

Analysis time for checkout samples and unknowns is the same. Assuming that 10 samples are run in a sequence on a conventional system, the total analysis time is 10 × 60 min = 600 min (more than an average workday). Whereas on a HighSpeed system only 60 min will be required (less than 15% of a typical workday).

This means that in our scenario equilibration, calibration, validation, and unknown sample analysis can be done on the *same* day in the HighSpeed case; there is even room for more samples or other work on that day. However, a conventional system will require about two days and a night (for equilibration), tying up substantial manpower and instrument time.

Figure 15 shows a practical calibration example from work done by the author using only a single conventional column (run time 15 min per sample)

© 2004 by Marcel Dekker, Inc.

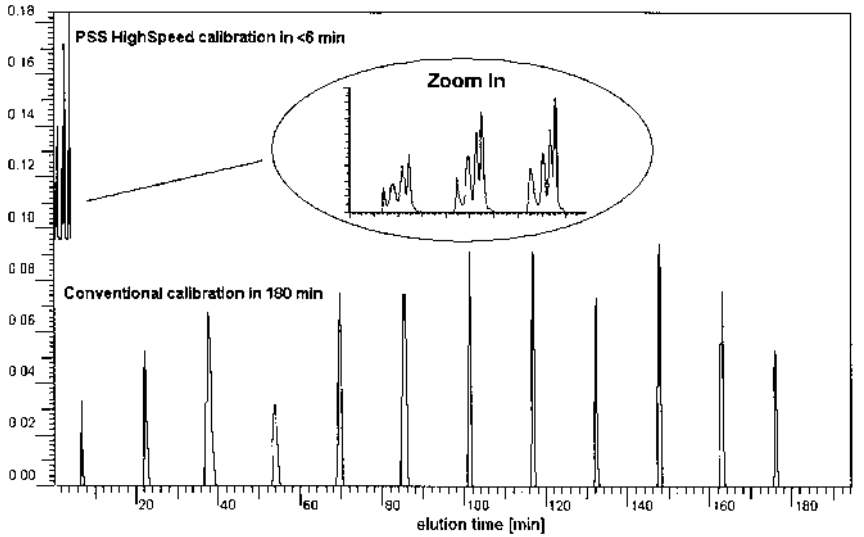

Figure 15 Comparison of time requirements for a traditional 12-point polystyrene calibration on a single analytical SEC column (bottom) vs. a single HighSpeed column using PSS ReadyCal premixed standards (top); HighSpeed separation magnified to show resolution (insert).

running 12 polystyrene standards in THF on a PSS SDV 5 μm linear column (bottom trace). Total run time for this 12-point calibration was 180 min (3 hours). Each standard was injected only once and separately.

In order to find the best and fastest SEC calibration three mixtures of four polystyrene standards were used to create the calibration on a single PSS HighSpeed SDV 5 μm linear column (Fig. 15, top traces). Total run time in this case is only 6 min, a 30-fold increase in time savings! Please note that a similar resolution is obtained in both cases. The HighSpeed method did not hamper chromatographic performance.

4.2.4 Cost-Saving Aspects of HighSpeed GPC Analyses

Saving time is obviously the foundation for saving money. Because the throughput of existing equipment can be increased, operating cost and capital investment are reduced. Laboratories can calculate efficiency increase and cost savings easily taking their own parameters into account.

Hofe and Reinhold (14) published an example of how much money can be saved by converting from conventional to HighSpeed applications (Table 5).

© 2004 by Marcel Dekker, Inc.

Table 5 Model Calculations for Reducing Instrument Cost by HighSpeed SEC

Number of samples		Time required		Number of instruments required	
Per year	Per day	Traditional	HighSpeed	Traditional	HighSpeed
20,000	100	≈15,000 h ≈2000 days	≈1500 h ≈200 days	≈11 ($390,000)	≈1 ($39,000)
200	10	≈1500 h ≈200 days	≈150 h ≈20 days	≈1 ($39,000)	≪ 1

Calculations based on: 45 min/run, 7 h/day, 200 days/yr up-time.
Source: Ref. 14.

4.3 Applications of PSS HighSpeed™ SEC Columns

Published applications are still rare because the broad use of HighSpeed SEC is very recent. However, Gray and Long (12) and Kilz and Montag (13) have published the first results on HighSpeed analyses for polyolefins in high-temperature applications (Fig. 16). Initial data show that it is possible, but information on accuracy, repeatability, and stability have not yet been published.

The comparison of conventional and HighSpeed SEC results for poly(siloxanes) in toluene with RI detection showed good agreement of results, while cutting analysis time down to about 2 min.

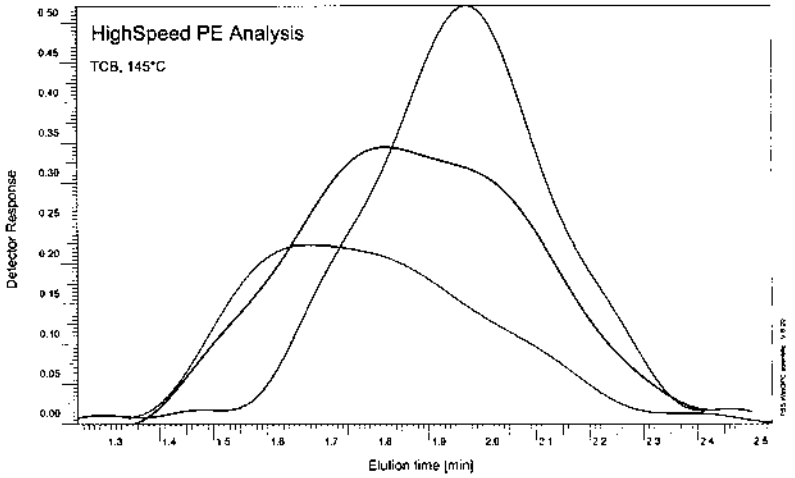

Figure 16 HighSpeed SEC separation of different polyethylene samples run in TCB at 145°C using two PSS Polefin HighSpeed columns. (From Ref. 13.)

© 2004 by Marcel Dekker, Inc.

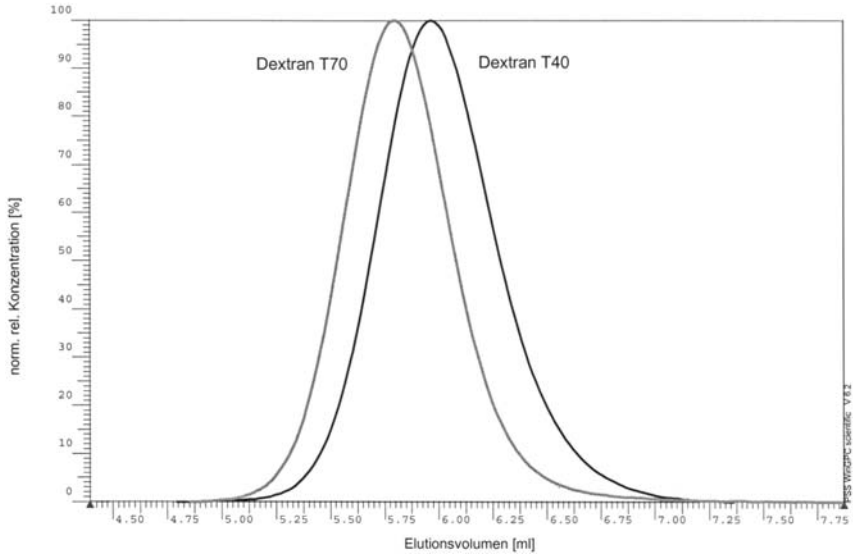

Figure 17 Accuracy and precision of fast SEC analysis in water tested with reference dextran samples (PSS Suprema HighSpeed 100 + 1000 columns).

Aqueous samples can also be analyzed by HighSpeed SEC methods. Polyacrylic acids, pullulans, and dextrans have been investigated. The accuracy and reproducibility of dextran results tested with various dextran samples (T-series by Pharmacia) have been evaluated (Fig. 17). Result precision has been similar to conventional analyses, while good accuracy has been reported for M_w and M_p (14). M_n results have been low, because of nonideal flow profiles in water at ambient temperature. Owing to the high viscosity of water, the use of elevated temperatures is recommended for increased resolution.

Kilz and Pasch used HighSpeed columns to speed up analysis time of two-dimensional chromatography experiments (17). They were able to cut down 2D run times from 10 hours to about 1 hour, while maintaining the efficiency of the 2D separation as shown for a separation of polystyrene and polybutadiene standards of different molar mass (Fig. 18). About 60 transfer injections have been made in this experiment.

4.4 Can HighSpeed Columns also be used for FIA Applications?

FIA (or FIPA as it is called by Viscotek) does not rely on any separation of the sample, but can be considered as a sample preparation and introduction method in

© 2004 by Marcel Dekker, Inc.

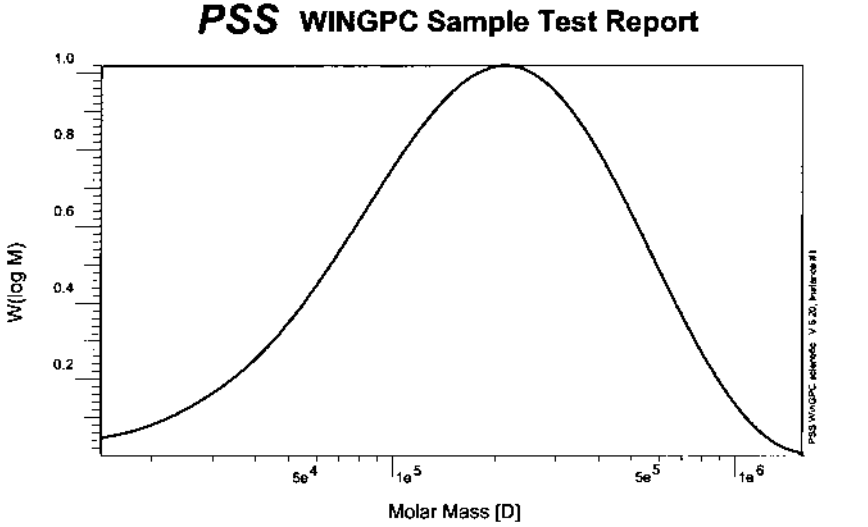

Figure 18 Molar mass distribution report on HighSpeed SEC separation with viscosity detection.

© 2004 by Marcel Dekker, Inc.

polymer analysis. Samples are "run" on HPLC instrumentation for practical reasons only. FIA methods can only determine results that are derived directly from the overall detector response:

- In the case of concentration detectors this would be the concentration (in most cases not very useful for polymer samples);
- In the case of light-scattering detectors, this would be the weight-average molar mass, M_w, determined by a single concentration only; in multi-angle instruments radius of gyration, R_g, of certain samples can also be measured;
- Similarly, in the case of viscometer detectors, the only result is the intrinsic viscosity, $[\eta]$, determined from a single concentration only.

Detector combinations of RI, LS, and viscometry allow M_w and $[\eta]$ to be obtained as before. Mathematical treatment of primary information allows the *calculation* of molecular size from viscosity measurements (16), which the author does not consider primary (reliable and sample independent) information.

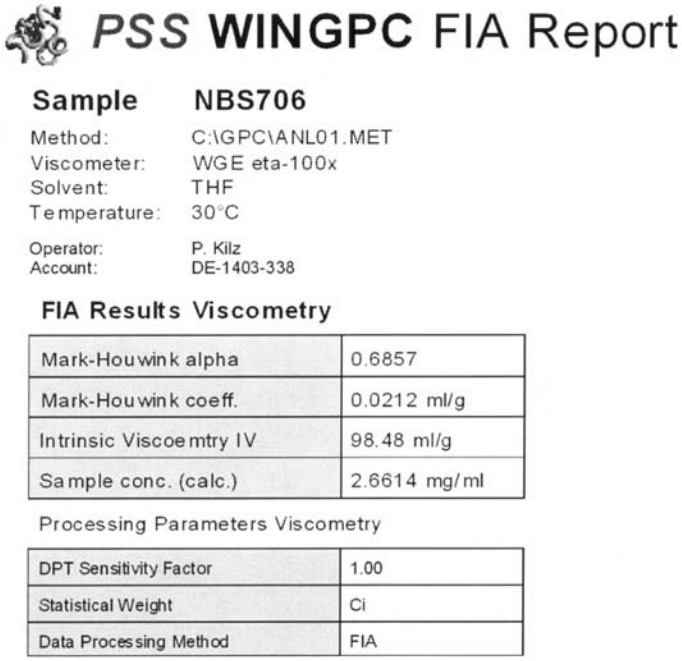

PSS WINGPC FIA Report

Sample NBS706

Method: C:\GPC\ANL01.MET
Viscometer: WGE eta-100x
Solvent: THF
Temperature: 30°C

Operator: P. Kilz
Account: DE-1403-338

FIA Results Viscometry

Mark-Houwink alpha	0.6857
Mark-Houwink coeff.	0.0212 ml/g
Intrinsic Viscoemtry IV	98.48 ml/g
Sample conc. (calc.)	2.6614 mg/ml

Processing Parameters Viscometry

DPT Sensitivity Factor	1.00
Statistical Weight	Ci
Data Processing Method	FIA

Figure 19 Viscosity result report by FIA method using identical raw dataset as in Fig. 18, but ignoring distribution information from HighSpeed column.

© 2004 by Marcel Dekker, Inc.

The main benefit of these FIA methods is that they can be automated without buying additional equipment (for example, automated solution viscometers) and training additional users. However, the information is just the same as that for dedicated static (non-FIA) systems; the accuracy and precision should be compared with static methods.

PSS HighSpeed columns allow similar or shorter run times as compared to the few published FIA experiments (4,5). The major improvement, however, is that the samples are separated in the system and distribution information is also available from the same analysis. This means that an instrument running a HighSpeed application can be used to report detailed distribution results and/or only the averages depending on the need of the client. No instrument changes are necessary to switch from an FIA to an SEC report. The only change is the report template. The FIA report will neglect the slice information (separation) and calculations are based on the integrated detector responses.

The SEC results from a HighSpeed separation of NBS 706 are shown in Fig. 19 using a prototype HighSpeed viscosity detector (WGE, Berlin, Germany). The corresponding FIA report in Fig. 20 is generated from the same raw dataset,

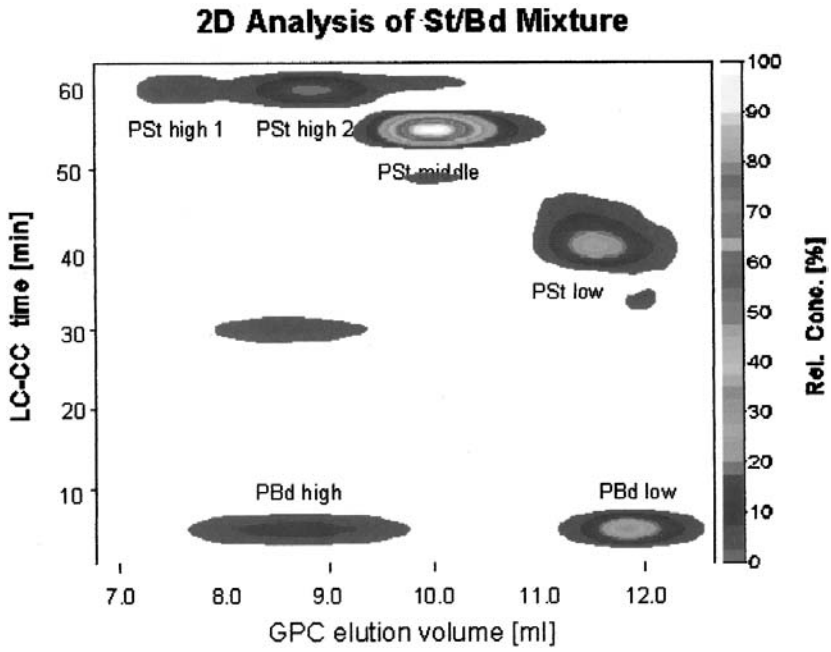

Figure 20 Contour map of four polystyrene and two polybutadiene standards separated in a two-dimensional HPLC-SEC experiment during 1 hour using a HighSpeed SEC column.

© 2004 by Marcel Dekker, Inc.

just ignoring the fractionation of the sample in the PSS HighSpeed column. The HighSpeed SEC separation took about 3 min. The viscosity results of the SEC and the FIA method agree within 2%. This example shows very nicely how much flexibility can be gained by using HighSpeed columns, which really separate the sample (in contrast to the delay columns in FIA methods that separate off the solvent peaks only). If analyses are carried out in this way, the clients can decide post-run which results they need without having to repeat the actual analysis.

5 CONCLUSIONS

SEC separations can now be carried out 10 times faster than before (in about 1 min) using specially designed HighSpeed SEC columns. They offer similar resolution and can be run on existing equipment just by replacing a conventional column with a HighSpeed column one by one. This allows the opening up of SEC applications to new fields where results have to be in fast (as in in-line production control) or many samples have to be run (as in high-throughput systems) and space, money, and staff are limited. Because HighSpeed SEC columns separate the samples they can be used for distribution reports (e.g., molar mass) and/or for the determination of property averages only (e.g., intrinsic viscosity or M_w), similar to FIA experiments.

Because HighSpeed SEC columns are available in different packings they can be used in different solvents for different applications (including high-temperature applications). If sample separation is never required, then the FIA method can be used to obtain molar mass or viscosity averages determined on a similar time scale.

ACKNOWLEDGEMENTS

The author would like to thank his colleagues Dr. G. Reinhold and Dr. C. Dauwe from PSS who did the design, the optimization and testing of PSS HighSpeed columns. He would also like to thank PSS for allowing this work to be published.

REFERENCES

1. RB Nielson, AL Safir, M Petro, TS Lee, P Huefner. Polym Mat Sci Eng 80:92, 1999.
2. S Brocchini, K James, V Tangpasuthadol, J Kohn. J Am Chem Soc 119:4553, 1997.
3. E Meehan, S O'Donohue, JA McConville. Proc Intern GPC Symp 2000. Waters, Milford, 2001.
4. WS Wong, M Haney, S Welsh. Proc Intern GPC Symp 2000. Waters, Milford, 2001.
5. PJ Wyatt, T Scherer, S Podzimek. Proc Intern GPC Symp 2000. Waters, Milford, 2001.

© 2004 by Marcel Dekker, Inc.

6. P Kilz, G Reinhold, C Dauwe. Proc Intern GPC Symp 2000. Waters, Milford, 2001.
7. JC Giddings, E Kucera, CP Russell, NM Myers. J Phys Chem 72:4397, 1968.
8. G Glöckner. Liquid Chromatography of Polymers. Hüthig, 1982.
9. International Organization for Standardization. ISO 13885-1:1998, Gel permeation chromatography (GPC)—Part 1: Tetrahydrofuran (THF) as eluent. Geneva: ISO, 1998.
10. P Kilz. Design, properties and testing of PSS SEC columns and optimization of SEC separations. In: Chi-san Wu, ed. Column Handbook for Size Exclusion Chromatography. New York: Academic Press, 1999, Ch. 9, pp 267–304.
11. P Kilz, G Reinhold, C Dauwe. PSS Project Report HighSpeed GPC Columns. PSS, 1999.
12. M Gray, B Long. Proc Intern GPC Symp 2000. Waters, Milford, 2001.
13. P Kilz, P Montag. Proc IUPAC Polym Conf, published on PolymerEd 2001 CD Rom. Stellenbosch: University of Stellenbosch, 2001, RSA.
14. G Reinhold, T Hofe. GIT Fachz Lab 44:556, 2000.
15. P Alden. Proc Intern GPC Symp 2000. Waters, Milford, 2001.
16. OB Ptitsyn, YE Eizner. Zh Fiz Khim 32:2464, 1958.
17. P Kilz, H Pasch. Coupled LC techniques in molecular characterization. In: RA Meyers, ed. Encyclopedia of Analytical Chemistry. Chichester, UK: Wiley, 2000, Volume 9, pp 7495–7543.

© 2004 by Marcel Dekker, Inc.

20
Automatic Continuous Mixing Techniques for On-line Monitoring of Polymer Reactions and for the Determination of Equilibrium Properties

Wayne F. Reed
Tulane University
New Orleans, Louisiana, U.S.A.

1 INTRODUCTION AND BACKGROUND

This chapter deals with the use of automatic continuous mixing techniques in a wide variety of contexts: on-line monitoring of polymerization reactions, polymer degradation, aggregation, and dissolution, and equilibrium characterization of complex systems. The technique is composed of a "front end," that is, a system of pumps and mixers to ensure automatic mixing, and a "detector end," which includes any number of detectors that function with flowing samples. Detectors can include multi-angle light scattering, UV/visible absorbance, differential refractometry, viscosity, evaporative light scattering, near IR, electron spin resonance (ESR), and others.

© 2004 by Marcel Dekker, Inc.

The idea of making time-resolved measurements *per se*, for example, with time-dependent static light scattering (TDSLS), has been explored by a number of groups. Aggregation (1,2), gelation (3), degradation (4–6), dissolution of dry polymers (7), and phase separation have been followed with TDSLS.

The notion of following polymerization reaction kinetics has been around at least since Flory's original, manual measurements (8), and is now an active field including the use of near infrared (9–13), rheology (14–16), electron spin resonance (17,18), ultraviolet absorbance (19–21), and pulsed laser techniques (22,23).

Automatic continuous online monitoring of polymerization reactions (ACOMP) was first introduced by the present author and his colleagues in 1998 (24). ACOMP allows simultaneous monitoring of weight-average molecular mass M_w, certain measures of polydispersity (25), monomer conversion, and intrinsic viscosity, and will be discussed in detail below.

1.1 Automatic Continuous Mixing (ACM)

Automatic continuous mixing (ACM) differs from SEC and flow injection analysis in that it provides a continuous, diluted stream of sample to the detectors. Hence, there are no detector signal peaks, but rather a continuous record of the sample behavior. There is, however, a lag-time between the extraction/dilution and the detection. This is strictly dependent on flow rates and "plumbing," and can range from tens to hundreds of seconds. Likewise, there is a finite response time for ACM. It is normally the integrated product of a Gaussian spreading of an extracted/mixed volume on its way to the detector, and an exponential "mixing chamber" response time, related to any mixing chambers associated with ACM.

Several configurations have been used for ACM. For ACM in equilibrium characterization, the simplest is the use of a simple syringe pump, or even a gravity feed, to dilute continuously a sample reservoir. The sample issuing from the detector lines can optionally recirculate to the sample, usually to conserve sample, or flow to waste. More refined methods can use a commercial tertiary or quaternary mixing pump, such as from ISCO (Lincoln, Nebraska, U.S.A.) or Waters (Milford, Massachusetts, U.S.A.). These were designed to provide gradients of different solvents for use in HPLC, but can also provide mixing of any desired, low-viscosity solutions for ACM (e.g., dilute polymer solutions, electrolytes, surfactants, colloids, and so on). Some mixing pumps allow the time profile of the gradient to be chosen, which can be very useful when samples respond in a logarithmic fashion to a component, for example, the reaction of polyelectrolyte conformations, interactions, and hydrodynamics to ionic strength.

For situations where polymer reactions are to be monitored, the use of a programmable mixing pump is viable, as long as the solution viscosity in the reactor is not too high, that is, where solution viscosities do not exceed a few hundred centipoise (cP). Degradation and aggregation reactions are often carried

© 2004 by Marcel Dekker, Inc.

out at low enough concentration that the viscosity poses no problem to a commercial mixing pump.

For monitoring polymerization reactions, however, viscosities in the reactor can reach millions of cP (e.g., nylons), and even far more modest viscosities (in the many hundreds or thousands of cP) seriously compromise the performance of HPLC-grade piston pumps. Low-pressure mixing pumps (for example, an ISCO programmable mixer with an isocratic pump withdrawing from it) have proportioning valves that rely on timing for withdrawing the nominal percentage mix from two or more reservoirs. If one of the reservoirs is a reactor, and the viscosity of the reactor solution is increasing, then the preset percentage withdrawn from the reactor will decrease in time as viscosity increases. As long as at least two separate detector signals are available, so that the two unknowns, polymer concentration in the detector stream and percentage actually withdrawn from the reactor, can be solved for, accurate values for the polymer characterization will still be obtained. The lag and response times, however, increase as the percentage withdrawn from the reactor decreases, and can become unacceptably high in some cases.

Another alternative is provided by high-pressure mixing. In this case two separate isocratic pumps can be used, one of which draws from the reactor, the other from the solvent reservoir. The two pumps then feed a micro-mixing chamber on the outlet side, so that high-pressure mixing occurs. In this case, the isocratic pump guarantees the selected withdrawal and flow rate at the expense of increasing pressure on the outlet side. Isocratic pumps are usually built to withstand at least 100–200 bar, so that such pressures are not normally a problem, and the pump can be set to shut down if a certain pre-set limit is reached. The problem with this arrangement is that piston pumps cause cavitation of high-viscosity liquids, so a point arises at which the pump will deprime, usually at moderate viscosities. Another problem that occurs with this scheme is bubbling. Many reactor liquids are bubbly, due to the exothermicity of the reactions, and bubbles entering the isocratic pump will cause it to lose prime. Hence, a variety of debubblers have been used.

In these approaches it is important to be careful that no plugging of the pumps occurs, so a rapid return to pure solvent to flush polymer from pumps and detectors is required between experiments.

Ultimately, high-performance ACM devices are required. These will not be based on piston or other suction-type pumps. Development based on hybrid schemes with gear and screw pumps is currently under way.

1.2 Detectors

As mentioned, any number and variety of detectors can be used. A common configuration is a series containing a multi-angle light-scattering detector, a

© 2004 by Marcel Dekker, Inc.

differential refractometer, a viscometer, and a UV/visible spectrophotometer. Interdetector dead volumes are critical in SEC applications (26) because fractionated material elutes in peaks that pass fairly quickly through the detectors. Most time-dependent reactions that have been the subject of ACM techniques, however, occur on a scale of minutes or hours, so interdetector dead volume is not a critical issue.

A specific configuration involving a home-built multi-angle light-scattering instrument, Shimadzu SPD-10AV UV/visible detector, Waters 410 RI, and a home-built viscometer has been treated in several references.

Light scattering data is normally analyzed according to the well-known Zimm approximation (27)

$$\frac{Kc}{I(q,\,c)} = \frac{1}{M\,P(q)} + 2A_2c + [3A_3Q(q) - 4A_2^2M\,P(q)(1 - P(q))]c^2 + O(c^3) \quad (1)$$

where c is the polymer concentration (g/cm^3), $P(q)$ the particle form factor, q is the amplitude of the scattering wave-vector $q = (4\pi n/\lambda)\,\sin(\theta/2)$, where θ is the scattering angle, and K is an optical constant, given for vertically polarized incident light by

$$K = \frac{4\pi^2 n^2 (\partial n/\partial c)^2}{N_A \lambda^4} \quad (2)$$

where n is the solvent index of refraction, λ is the vacuum wavelength of the incident light, and $\partial n/\partial c$ is the differential refractive index for the polymer in the solvent. $Q(q)$ involves a sum of complicated Fourier transforms of the segment interactions that define A_2. In the limit of $q = 0$, $P(0) = Q(0) = 1$, so that for a polydisperse polymer population, this becomes

$$\frac{Kc}{I(0,\,c)} = \frac{1}{M_w} + 2A_2c + 3A_3c^2 + O(c^3) \quad (3)$$

For low enough concentrations that the c^2 term in Eq. (1) is negligible, and for $q^2\langle S^2\rangle_z < 1$, another, frequently used form of the Zimm equation becomes

$$\frac{Kc}{I(q,\,c)} = \frac{1}{M_w}\left(1 + \frac{q^2\langle S^2\rangle_z}{3}\right) + 2A_2c \quad (4)$$

where $\langle S^2\rangle_z$ is the z-average mean square radius of gyration. As pointed out in other polyelectrolyte studies (28,29), in this limit $\langle S^2\rangle_z$ can be determined at low concentrations if M_w is known, without a full extrapolation to $c = 0$.

The voltage $V(t)$ of the single capillary viscometer is directly proportional to the total viscosity of the solution flowing through the capillary. This allows the

© 2004 by Marcel Dekker, Inc.

reduced viscosity, η_r, to be computed at each instant, without any calibration factor, according to

$$\eta_r(t) = \frac{V(t) - V(0)}{V(0)c(t)} \tag{5}$$

The intrinsic viscosity $[\eta]$ is related to η_r according to

$$\eta_r = [\eta] + \kappa_H[\eta]^2 c + \kappa_{H,2}c^2 + O(c^3) \tag{6}$$

where κ_H is ~ 0.4 for neutral polymers, and $\kappa_{H,2}$ has no generally accepted theoretical form for coil polymers, although empirical expressions exist (30). $[\eta]$ measures the hydrodynamic volume V_H, per unit mass according to

$$[\eta] = \frac{5V_H}{2M} \tag{7}$$

Shear rates in the capillary viscometer were of the order $500\,s^{-1}$.

1.3 Heterogeneous Time-Dependent Static Light Scattering (HTDSLS)

Recently, HTDSLS was introduced as a detection and analysis technique, in order to permit the simultaneous characterization of solutions containing co-existing populations of polymers and colloids (31). Such solutions occur in many contexts: (1) bacteria that produce or degrade natural products, such as proteins and polysaccharides, (2) microgels and microcrystals that form inside polymer reaction solutions, aggregates of proteins, and other polymers in otherwise homogeneous solutions, (3) solutions containing "dust" and other optical contaminants that would normally have rendered the solution uncharacterizable by classical light-scattering techniques. Other scenarios also exist.

The main notion of HTDSLS is to make a very small scattering volume V_s (of the order of nanoliters, as opposed to the total sample volume, which is typically tens of microliters) and to use a flowing sample, so that each time a colloid particle passes through the scattering volume a large scattering spike is produced. It has been shown (31) that the "clear window time," CWT, that is, the fraction of time no large scatterers are in the illuminated scattering volume, has the limiting form

$$\text{CWT} \cong \exp(-nV_s) \tag{8}$$

where n is the number density of large particles. In the meantime, the average scattering level within the scattering volume is a result of the polymeric population. Built-in algorithms then allow for discriminating and counting the spikes due to colloids, while simultaneously measuring the baseline scattering due to the polymer. Thus, absolute molecular mass and size characterization, and its

© 2004 by Marcel Dekker, Inc.

evolution, can be carried out on the polymer, while evolution in colloid particle density is measured.

HTDSLS has been demonstrated in contexts where large amounts of colloidal contaminant were added to a polymer solution, and a full Zimm-style analysis of the polymer was recovered, and in a case where the evolution of *Escherichia coli* bacteria in a population of water-soluble polymer (polyvinyl pyrrolidone, or PVP) was monitored, while the PVP itself was characterized. Figure 1 shows data taken at a scattering angle of 90° from co-existing *E. coli* and PVP populations, adapted from Ref. 31. Each spike corresponds to a single *E. coli* bacterium passing through the scattering volume, and the increasing spike density shows the increase in time of the *E. coli* population density. The *E. coli* density is shown in the top inset graph. The baseline due to PVP is recoverable at each instant, and yields the characterization in terms of Kc/I shown in the lower inset graph.

HTDSLS can be incorporated as an integral part of light-scattering detection in the many cases where colloids co-exist with polymers.

2 ON-LINE MONITORING OF POLYMER PROCESSES

2.1 Automatic Continuous On-line Monitoring of Polymerization Reactions (ACOMP)

The ability to monitor conversion and the evolution of mass and composition distributions during polymerization reactions is important in three broad areas. First, polymer scientists working on new material development can obtain detailed, quantitative information on kinetics and mechanisms that can accelerate the process of discovery and understanding. Secondly, chemists and engineers seeking to optimize reaction conditions can immediately assess the effects of changing initiators, catalysts, temperature, concentration, solvents, and so on. Finally, it is expected that ACOMP will provide a process analytical approach to on-line control of polymerization reactors. This should lead to considerable increases in efficiency and product quality, and lead to important savings in terms of nonrenewable resources, energy, personnel, and reactor time.

Some of the attractive features of ACOMP include the fact that it provides an absolute characterization of the polymerization process and products in real time, and that it does not rely on chromatographic columns or flow injection devices. It requires that a very small stream of sample be continuously withdrawn from the reactor and diluted with a much larger quantity of solvent. This is because a highly dilute polymer solution is required in order to suppress strong intermolecular effects and arrive at the intrinsic properties of the polymer molecules themselves.

© 2004 by Marcel Dekker, Inc.

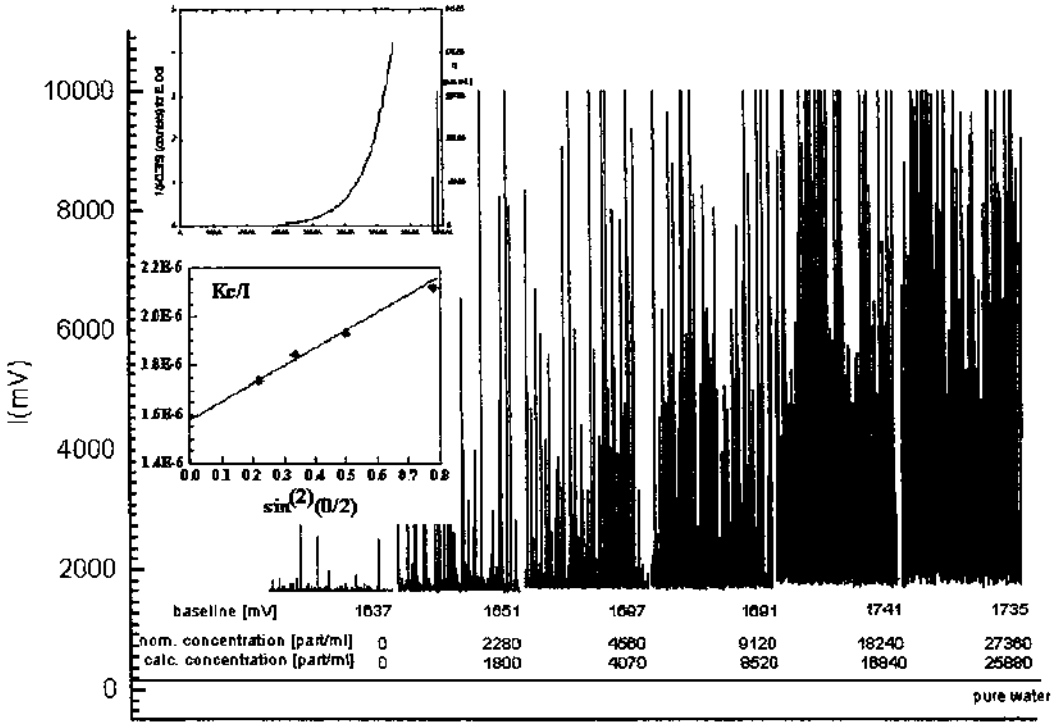

Figure 1 Raw intensity data at 90° scattering angle for a mixed population of *E. coli* bacteria and neutral polymer, PVP. The increasing spike density shows the increase in the bacterial number density, which is shown in the top inset graph. The recovered baseline is a result of the PVP whose Kc/I representation allows recovery of M_w and $\langle S^2 \rangle_z$, and is shown in the lower inset graph. (From Ref. 31.)

© 2004 by Marcel Dekker, Inc.

2.1.1 Free Radical Polymerization in a Batch Reactor

Ideal free radical polymerization involves initiation, propagation, and termination. The production of the free radicals with rate constant k_d is expressed by

$$I_2 \xrightarrow{k_d} 2I^*$$

where I_2 is the initiator and I^* the primary radical formed by initiator decomposition.

The second initiation step is the production of the first monomer radical R_1 by combination of I^* with monomer m, with rate constant k_i

$$I^* + m \xrightarrow{k_i} R_1$$

Propagation ensues with rate constant k_p (assumed equal for all chain lengths).

$$R_1 + m \xrightarrow{k_p} R_2$$

Termination can occur by disproportionation

$$R_m + R_n \xrightarrow{k_t} P_m + P_n$$

and/or by recombination

$$R_m + R_n \xrightarrow{k_t} P_{m+n}$$

An often used approximation is the so-called quasi-steady-state approximation (32), in which the concentration of radical $[R]$, varies slowly with respect to the time scale for propagation and termination reactions. This yields

$$[R] = \sqrt{\frac{2Fk_d[I_2]}{k_t}} \tag{9}$$

If $[I_2]$ decreases negligibly during conversion, the monomer disappears in a first-order process

$$[m] = [m]_0 e^{-\kappa t} \tag{10}$$

where the rate constant κ is given by $\kappa = k_p[R]$.

Figure 2 shows typical raw data for free radical polymerization of acrylamide (AAm) initiated by sodium persulfate at $t = 60^\circ$C (33). Pure water is pumped through the detector train during the first 500 s, in order to obtain baselines for each instrument. After this the reactor withdrawal pump begins to pull the initial aqueous monomer solution (0.034 g/mL of AAm) from the reactor to achieve 4% of the flow to the detectors. The other 96% of the flow comes from the pure water reservoir, so that the total amount of monomer initially in the detector train was 0.00136 g/mL. The flow rate was 2 mL/min, so that 4.8 mL per hour of reactor fluid was withdrawn during the reaction. The increase in the UV absorbance monitored at 225 nm during the monomer pumping period is due to the double bonds in the AAm, which are lost,

© 2004 by Marcel Dekker, Inc.

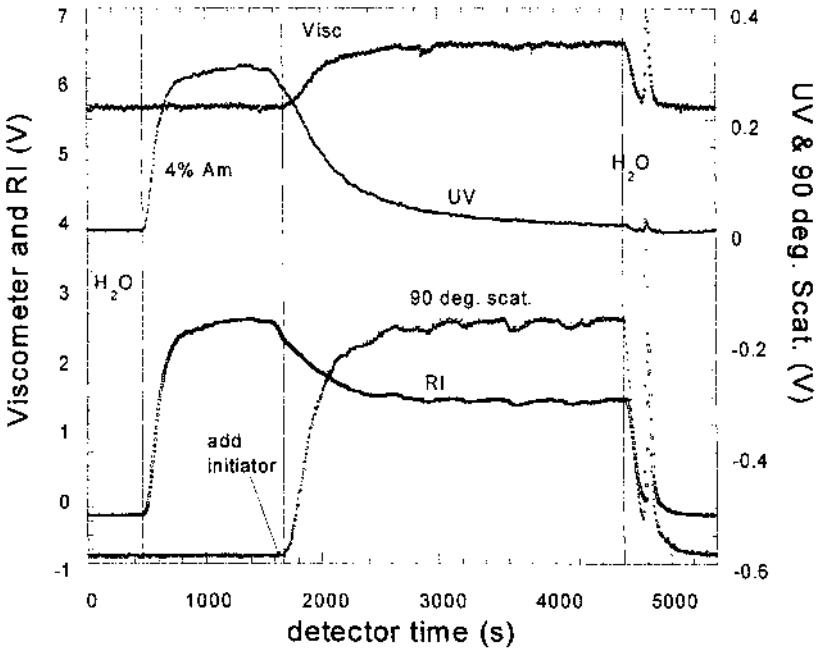

Figure 2 Raw ACOMP signals from multiple detectors during the free radical polymerization of AAm. (From Ref. 33.)

along with the UV absorbance, when AAm is incorporated into a polymer chain. The increase in the RI during this period is due to a dn/dc of 0.153 for AAm. Neither the viscometer nor TDSLS respond to the presence of the dilute monomer.

At 1700 s the persulfate initiator was added, and the onset of the polymerization reaction is quickly seen; the decrease in the UV monitors AAm conversion, and the increase in TDSLS and viscosity indicate the presence of an increasing amount of polymer. The decrease in RI is due merely to the fact that the ISCO mixing pump used in the low-pressure mixing scheme for this experiment could not maintain the initial 4% withdrawal rate as the reactor liquid viscosity increased. This poses no problem for exact determination of M_w, conversion, and so on, since the RI signal, together with the UV, allow the exact concentration of monomer (and hence polymer from mass balance) and the true withdrawal rate to be computed. A high-pressure mixing technique developed subsequent to Ref. 33, using two isocratic pumps, maintains a fixed withdrawal rate, and hence avoids "wasting" a detector signal solving an equation for withdrawal pump rate. This feature becomes crucial in copolymerization, where the RI signal can be used to determine the concentration of a comonomer.

© 2004 by Marcel Dekker, Inc.

Figure 3 shows AAm conversion vs. time for the reaction in Fig. 2, as well as several others, where the ratio of AAm to initiator was varied. In all cases the conversion is fit fairly well by a first order (exponential) fit. As the amount of initiator decreases and conversion slows, however, the fit is less good, and it was demonstrated in Ref. 33 that the deviations from the ideal free radical polymerization paradigm were due to impurity and cage effects.

Figure 4 shows M_w vs. conversion for several AAm polymerization experiments. The QSSA above predicts that M_w at any value of monomer conversion f, should obey

$$M_w(f) = M_w(0)\left(1 - \frac{f}{2}\right) \tag{11}$$

Both the linearity and ratio of $M_w(0)/M_w(1) = 2/1$ are seen in Fig. 4. Deviations at early values of conversion (up to 5–15%) before the straight line, ideal regime is reached, are also due to impurity and cage effects. The solid circles in Fig. 4

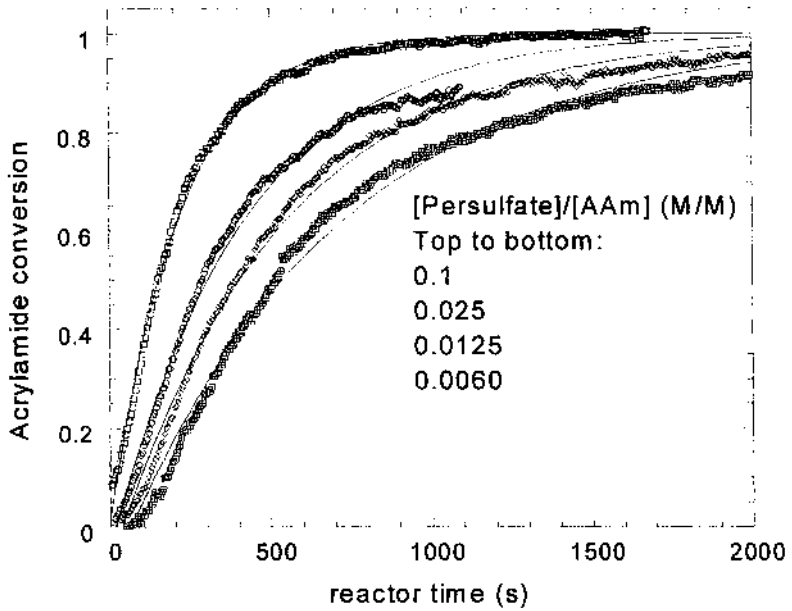

Figure 3 Monomer conversion during the free radical polymerization, from data in Fig. 2 and other, similar reactions, where the ratio of AAm to persulfate initiator varied. At high initiator concentrations the conversion is almost perfectly first order (exponential), with deviations from first order becoming more apparent as initiator concentration decreases. (From Ref. 33.)

© 2004 by Marcel Dekker, Inc.

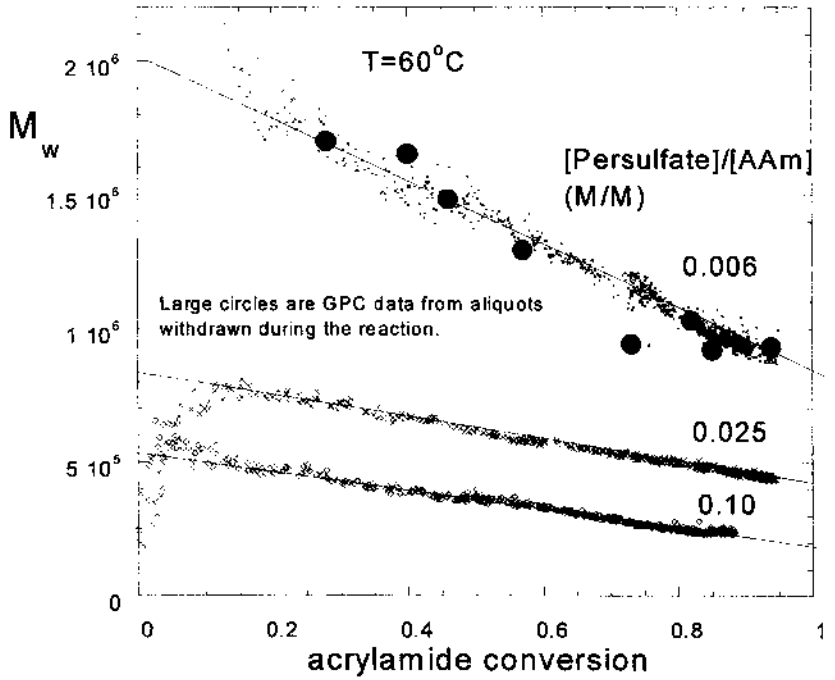

Figure 4 M_w vs. monomer conversion, f. Data from Fig. 2 and similar experiments. The linear decrease in M_w, beginning at early values of conversion, is expected from ideal free radical polymerization kinetics [Eq. (11)]. The solid circles are M_w determinations for the top experiment, obtained by manually withdrawing aliquots from the reactor during the reaction. (From Ref. 33.)

represent the value of M_w obtained by GPC measurements on aliquots manually withdrawn during the reaction. The agreement both confirms that ACOMP measures the same M_w as traditional GPC, and that no additional reaction takes place once a sample volume is automatically withdrawn from the reactor and quickly diluted 25-fold and cooled to $T = 25°C$.

2.1.2 Monitoring Polydispersity During Polymerization, Without SEC Columns

Several methods were recently proposed for following the evolution of polydispersity using ACOMP (25). One method involves the use of the slope of $Kc/I(q, c)$ vs. q^2 as a direct measure of the quantity $\langle S^2 \rangle_z / M_w$, which is itself closely related to the polydispersity index M_z/M_w. A second method compares the viscosity-averaged mass, M_η, with M_w. M_η for most polymers lies between M_n and

© 2004 by Marcel Dekker, Inc.

M_w, so that M_η/M_w is a valuable measure of polydispersity. A third method, which applies when dead chains are produced on a time scale that is fast compared to total conversion (for example, free radical polymerization, but not anionic or controlled radical polymerization), involves finding the instantaneous weight-average mass $M_{w,inst}$, which is related to the measured, cumulative M_w via

$$M_{w,inst}(f) = M_w(f) + f\frac{dM_w}{df} \tag{12}$$

Figure 5 shows M_w and $M_{w,inst}$ for a PVP reaction in which an additional amount of hydrogen peroxide initiator ("booster") was added after about 20% conversion. When a fixed amount of hydrogen peroxide was added at the outset of the PVP reactions, M_w would remain constant throughout conversion, as found in Ref. 24. Hence, a booster of hydrogen peroxide was expected abruptly to cause subsequent conversion to proceed at a fixed, lower M_w. The curve of M_w in Fig. 5

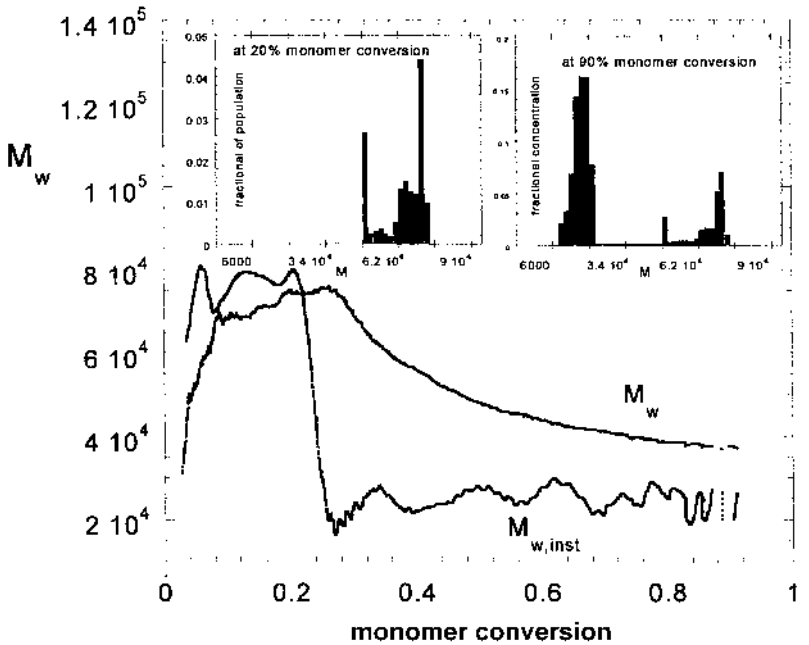

Figure 5 M_w is the cumulative value of M_w measured directly by light scattering, whereas $M_{w,inst}$ represents the instantaneous value of M_w, obtained from the M_w data via Eq. (12). An initiator "boost" at 20% conversion led to the production of smaller chains for the remainder of the reaction. The on-line histograms are derived from the $M_{w,inst}$ data at two different conversion points (20 and 90%), and show how the initial, unimodal population becomes bimodal after the initiator boost. (From Ref. 25.)

© 2004 by Marcel Dekker, Inc.

decreases smoothly and monotonically after the booster, and there is no obvious indication that a bimodal population is actually present. When Eq. (12) is applied to M_w, however, the curve of $M_{w,inst}$ gives dramatic evidence that M_w falls abruptly to the predicted lower value, and remains constant. Histograms of the evolving mass distribution can be built up at each point in conversion, which resemble GPC chromatogram-based mass distributions. Two of these are shown in the insets to Fig. 5. The first shows the unimodal, large M_w distribution prevailing just before the booster initiator was added. The second inset, to the right, shows the bimodal character of the population at 90% conversion, weighted heavily towards the small masses that began to be produced after the initiator boost.

2.1.3 Free Radical Polymerization in a Continuous Reactor

It is advantageous in many industrial situations to produce polymers in a continuous process. This allows a steady state of production to be reached, with a continuous input of reactants and output of product. We recently adapted ACOMP to a common type of continuous reactor, a homogeneous, continuously stirred tank reactor (34). In this arrangement a solution of monomer/initiator was continuously fed at a flow rate r (mL/s) to a reactor thermostatted to a desired temperature, from which reactor liquid was continuously withdrawn at the same rate.

If a given monomer/initiator mix is fed into a reactor of volume V at flow rate r, and fluid is pumped from the reactor at the same rate, then the steady-state value of conversion reached is

$$f_{\text{steady state}} = \frac{k_p[R]}{p + k_p[R]} \tag{13}$$

and the number-average, steady-state degree of polymerization is

$$N_{n,\text{steady state}} = \frac{pk_p[m]_s}{k_t[R](p + k_p[R])} \tag{14}$$

where p is the reciprocal of the average residence time, given by

$$p = r/V \tag{15}$$

and $[m]_s$ is the molar concentration of monomer in the reservoir that feeds the reactor at rate p, $[R]$ is the concentration of propagating free radical, and k_p and k_t are the propagation and termination rate constants, respectively. The concentration of monomer in the reactor reaches its steady-state value according to

$$[m](t) = \left\{[m]_r - \frac{p[m]_s}{p + k_p[R]}\right\} \exp\{-(p + k_p[R])t\} + \frac{p}{p + k_p[R]}[m]_s \tag{16}$$

where $[m]_r$ is the concentration of monomer initially in the reactor.

© 2004 by Marcel Dekker, Inc.

Figure 6 shows the results of a continuous reactor experiment in which the concentration of initiator in the monomer feed was varied, as shown, while the monomer feed concentration and r were kept constant. As the initiator concentration increases, the amount of conversion increases according to Eq. (13). Similarly, Eq. (14) predicts that M_w will decrease as initiator concentration increases, which is also seen in Fig. 6. The exponential approaches to the steady state are seen between the increments in initiator concentration.

The inset to Fig. 6 shows the extrapolation of M_w to $f = 0$. In the QSSA $M_w(f = 0)$ should be proportional to the inverse square root of the initial initiator concentration, a prediction born out in the inset. Combining the M_w and f data allows for the determination of k_p^2/k_t from a single experiment, such as in Fig. 6. The value is $11.7\,\mathrm{L/M} \times \mathrm{s}$.

Figure 7 shows the effect of fluctuating conditions on f and M_w. In the first part an uninterrupted steady state is obtained. Then, deliberate temperature

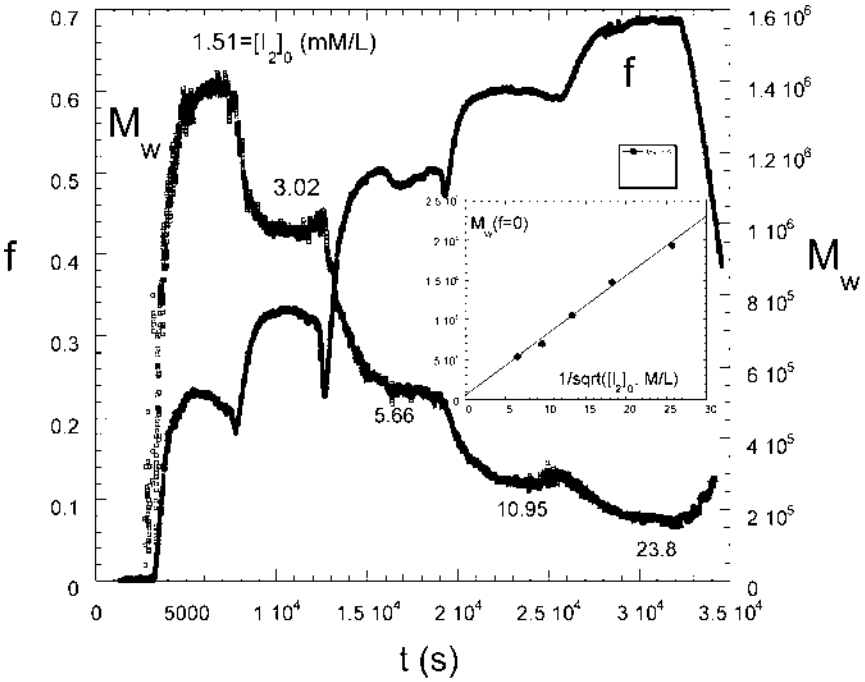

Figure 6 M_w and f from ACOMP of a continuous reactor, where the feed reservoir ratio of initiator to monomer increased after the steady state for each condition was reached. The inset shows the expected inverse square root dependence on initiator of M_w ($f = 0$). (From Ref. 34.)

© 2004 by Marcel Dekker, Inc.

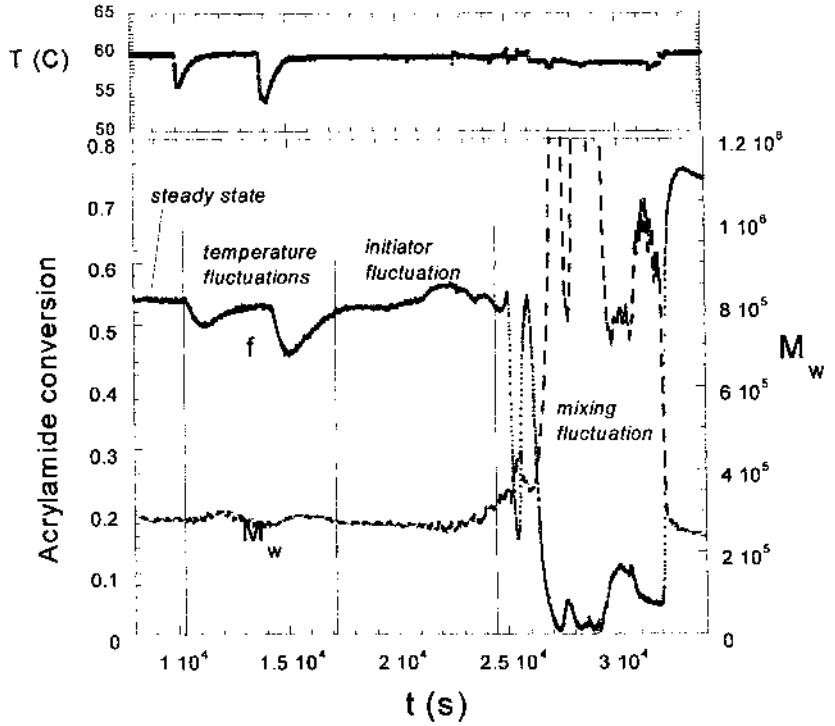

Figure 7 Effects of fluctuating reactor conditions on the steady state of M_w and f. (From Ref. 34.)

fluctuations in the reactor cause immediate fluctuations in both f and M_w; as T decreases conversion decreases and M_w increases. After this, the concentration of initiator was made to fluctuate, leading to corresponding fluctuations in f and M_w, in the sense expected. Finally, mixing fluctuations were produced by changing agitation speed, and ceasing to stir altogether. The latter had a drastic effect on both f and M_w.

2.1.4 Controlled Radical Polymerization (CRP)

CRP combines the control performance of living polymerization with the robust, economical aspects of free radical polymerization. Several types of CRP exist, most of which are based on a reversible combination between the growing radicals $P^{\bullet}$, and a molecular species X*, shown in Scheme 1. The majority of initiated chains are normally "dormant" in the P–X form, since, typically the equilibrium constant $K_{eq} = k_{act}/k_{deact}$ is much smaller than one, and those chains that are active add monomer M with a rate constant k_p, or terminate with a much smaller probability via rate constant k_t, until they again associate with X* and fall dormant.

© 2004 by Marcel Dekker, Inc.

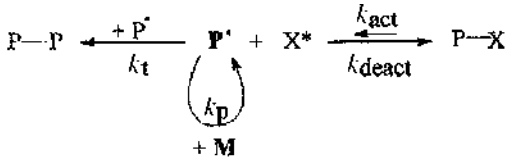

Scheme 1

Usually, a nitroxide acts as the counter-radical X*. TEMPO (2,2,6,6-tetramethylpiperidine nitroxide) and SG1 (*N*-tertiobutyl-1-diethylphosphono-2, 2-dimethylpropyl nitroxide) are among the agents commonly used in CRP. An extensive literature exists on the theoretical (35) and applied aspects of CRP (36–39).

ACOMP was adapted to CRP monitoring for the SG1 controlled, bulk polymerization of butyl acrylate (40). A high-pressure mixing scheme was used to deal with the high reactor viscosities. The monomer conversion kinetics closely resembled a first-order process, and M_w increased linearly with f, although the initial M_w is finite, not zero, as often reported. GPC sampling during the reactions showed that, as in anionic polymerization, the polydispersity decreases during the CRP.

2.1.5 Copolymerization

There are many ways of producing copolymers, including free and controlled radical copolymerization (41). Average sequence lengths of a comonomer can run from one, for a strictly alternating copolymer, to very large numbers for block copolymers. Additionally, copolymers can have widely varying architectures, such as combs, stars, dendrimers, and others.

As an initial entry into the field of copolymerization, ACOMP was recently applied to free radical copolymerization (42). The classical system of polystyrene/methyl methacrylate was chosen. Exploiting the differences in refractive index increment and UV absorption between each comonomer and the polymers, it was possible to obtain a continuous, on-line record of the conversion of each comonomer. This means that at every instant the remaining concentration of each comonomer is known, and, from the derivative of these concentrations, the instantaneous rate of comonomer incorporation into polymer is known. This immediately provides a record of the average copolymer composition at every instant, so that the entire average compositional distribution of the copolymer is obtained during the reaction. Furthermore, by running two or more experiments at different initial relative comonomer concentrations it is possible to obtain the reactivity ratios of the comonomers without the need for the many approximations that have often been made in order to use single point techniques (43,44). Knowledge of the reactivity ratios, together with the instantaneous comonomer concentrations allows the average sequence length of the copolymer population also to be followed.

© 2004 by Marcel Dekker, Inc.

Finally, the use of a light-scattering detector allows simultaneous monitoring of the evolution of molecular weight during the reaction. It is important to realize that Eqs (1), (3), and (4) cannot be used directly for determining M_w in the case of copolymers, because the different values of $\partial n/\partial c$ of each comonomer, together with compositional heterogeneity, lead to apparent values of M_w from which the true value of M_w could traditionally only be determined by running light-scattering experiments in three different solvents (45,46). Reference 42, however, gives a means of computing M_w on-line, by exploiting the continuous knowledge of composition. The use of a viscometer furnishes an additional crosscheck on molecular weight evolution, and can potentially also be used to study differences in branching and copolymer viscosity characteristics.

Hence, use of ACOMP, with no model-dependent assumptions, can provide average composition, and molecular mass distributions. These are typically found after copolymer production by laborious crossfractionation techniques (47,48). If models for mass, composition, and sequence length are evoked, then the average distributions from ACOMP can be folded with the appropriate instantaneous distribution forms to arrive at full distribution representations, including the composition/mass bivariate distribution (49).

2.1.6 Current and Future Directions for ACOMP

Research and development are currently under way both to improve the instrumentational base for ACOMP and to extend the method to more complex polymerization reactions. Instrumentational developments include improved front- end modules that can withdraw and mix from high-viscosity reactor liquids (over one million centipoise), and sample conditioning modules for "flashing monomer," rapidly dissolving and treating slurries and grains, and removing polymer from emulsions. Ultimately, a fully ruggedized extraction/dilution/conditioning system should be available that will be suitable for use in full-scale industrial reactors. Extension to other detectors including electron spin resonance (ESR), near infrared, and evaporative light-scattering are also expected.

New types of reaction scenarios include the use of CRP to produce more complex polymer architecture, atom transfer radical polymerization (50), hydrophobically modified copolymers (51,52), photopolymerization, polymerization in microemulsions (53), high-pressure polymerization, and fluidized bed reactions. Additional strategies for on-line characterization of branching and crosslinking are also being developed.

2.2 Degradation Reactions

When a polymer is degraded by agents such as radiation, acids, bases, enzymes, heat, ultrasound, and so on, its mass decreases, and hence also the intensity of scattered light at small angles. It is possible to find quantitative relationships

© 2004 by Marcel Dekker, Inc.

between the time dependence of the scattered light, and features of the degradation process, including degradation rates and degree of branching, and to make deductions about the mechanism of degradation, and the structure of the polymer being degraded.

In the case of a polydisperse initial population of polymers, with initial concentration distribution $C_0(M)$, the Zimm approximation can be adapted to incorporate the way scattering changes as a function of average cuts r per initial polymer. In this method the effect of the cuts is embodied in $P(q, r)$, such that (54)

$$Kc_0/I(q, r) = \frac{c_0}{\int_0^\infty MC_0(M)P[q, r(M)]\,dM} + 2A_2c_0 \tag{17}$$

where $P(q, r)$ is given for a polymer composed of N monomers by

$$P(q, r) = (2/N^2)\sum_{i=2}^{N}\sum_{j=1}^{i-1} W(r, i, j)\langle\langle \exp(-i\vec{q}\cdot\vec{r}_{ij})\rangle\rangle \tag{18}$$

Here, $\vec{q}$ is the scattering wave vector, and $\vec{r}_{ij}$ is the vector connecting monomers i and j. This procedure weights the double sum over all polymers by the probability $W(r, i, j)$ that monomers i and j are still connected after r cuts. If they are no longer connected, the resulting fragments are presumed to diffuse away from each other, leaving no phase correlation between monomers on separate fragments. $W(i, j, r)$ can include virtually any model, such as random, midpoint, or endwise scission, and the corresponding $I(q, r)$ found r itself is a function of time $r(t)$, and depends on the rate and fashion in which the cuts occur. For example, random scission of a random coil molecule of s strands and initial concentration c_0 yields

$$Kc_0/I(0, t) = \tfrac{1}{2}M_{n,0} + m^{s-1}\dot{\beta}^s t^s/2 + 2A_2c_0 \tag{19}$$

where $M_{n,0}$ is the initial number average mass of the undegraded polymer and $\dot{\beta}$ is the number of random cuts per second per dalton of initial polymer (which is constant as long as there are many uncleaved sites with respect to the number already cleaved). The striking feature is that the reciprocal of the scattering intensity is proportional to the s power of time; that is, it will be linear for random scission of a single strand coil, quadratic for a double strand, and so on.

Figure 8 shows examples of random degradation of single and triple strand linear polymers, due to the action of laminarinase (DP Norwood and WF Reed, unpublished results). The single strand is sodium hyaluronate, whose reciprocal intensity signature in time is linear ($s = 1$), and the triple strand polymer is schizophyllan ($s = 3$), yielding a cubic time dependence.

Another interesting case involves polymers with branches off a central backbone. Figure 9 shows TDSLS for degradation of a galactomannan (GM), whose backbone consists of mannose, a fraction of which bear galactose side

© 2004 by Marcel Dekker, Inc.

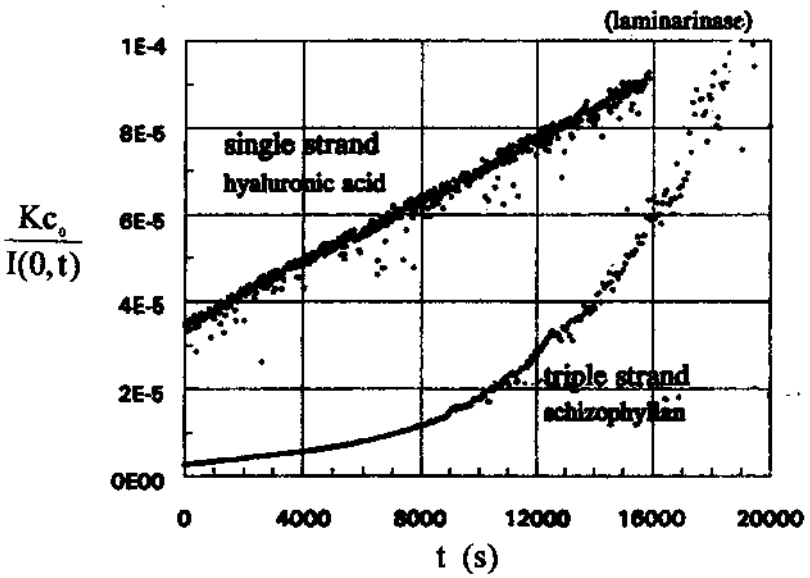

Figure 8 Linear and cubic increases due to single and triple stranded degradation. (DP Norwood and WF Reed, unpublished results.)

chains (55). The upper left inset in Fig. 9 shows the action of galactosidase on the GM, which is to strip off the galactose side chains. The signature for this type of reaction was predicted to be (56)

$$\frac{Kc_0}{I(q,\,t)} = \frac{1 + u(t)/3}{M_{t,0}[f_p + (1 - f_p)\exp(-\alpha t)]^2} + 2A_2(t)c_0 \tag{20}$$

where $M_{t,0}$ is the total initial polymer mass ($= M_p + M_{s,0}$, where $M_{s,0}$ is the initial side chain mass), f_p, is the initial fraction of mass in the backbone, and

$$u(t) = q^2\langle S^2\rangle_z(t) \tag{21}$$

where $\langle S^2\rangle_z(t)$ is the mean square z-average radius of gyration. It is assumed that the stripped side chains themselves scatter insignificantly compared to the remaining backbone. The above form will hold for stripping side chains from *any* polymer conformation, as long as $u < 1$. For the case of stripping from an ideal random coil (which GM resembles), the numerator $1 + u/3$ can be replaced by $u/2$ for the case where $u > 3$.

The upper right inset to Fig. 9 shows the reciprocal scattering signature when the GM is exposed to mannanase, which can cleave the mannose backbone that has no "protection" by galactose side chains. The signature corresponds to the

© 2004 by Marcel Dekker, Inc.

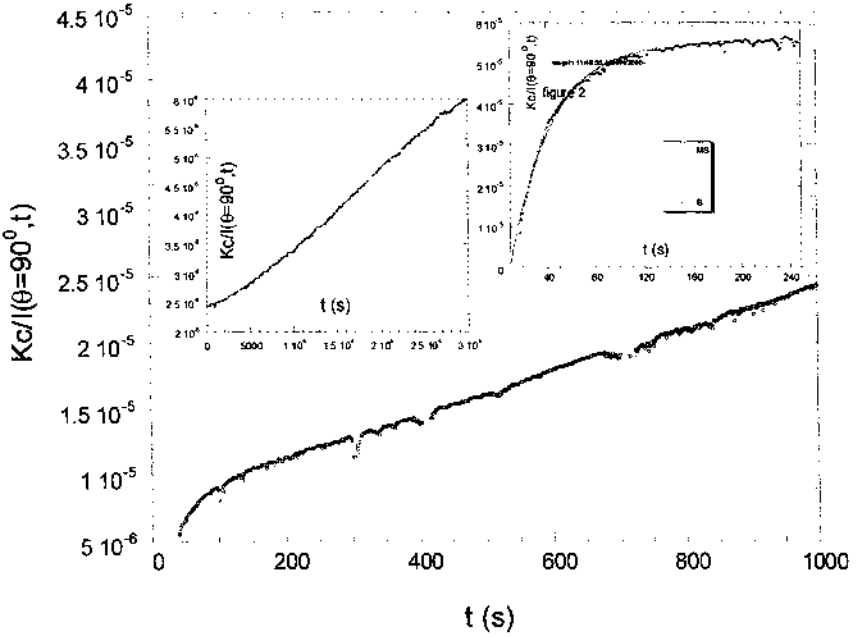

Figure 9 Upper left inset shows random stripping of the galactose side chains of a galactomannan by galactosidase, according to Eq. (20). The right upper inset is the action of mannase, which cleaves only mannose backbone sites unprotected by galactose. The main figure shows simultaneous stripping of the side chains and backbone degradation, caused by mixing the enzymes, according to Eqs. (22) and (23). (From Ref. 55.)

case when the number of bonds cleaved is of the order of the number of cleavable bonds. The experiments revealed that an average of about three sequential mannoses with no galactose side chains was necessary for mannanase to act. The plateau reached in this figure corresponds to the residual scattering from the GM fragments, which cannot be further digested because of galactose side chain protection.

The main portion of Fig. 9 shows the effect of treating GM with both mannanase and galactosidase simultaneously. Instead of reaching a plateau, the degradation continues as galactosidase continues to strip side chains from the GM fragments, allowing the mannanase to digest the GM backbone beyond what it could when no galactose was stripped. The light scattering signature describing this reaction is

$$\frac{Kc_0}{I(q,\,t)} = \frac{1}{[f_{\mathrm{p}} + (1 - f_{\mathrm{p}})\exp(-\alpha t)]^2}\left[\frac{1}{2M_{n,0}} + \frac{\gamma q^2}{2} + \frac{R(t)}{2} + 2A_{2,0}c_0\right] \qquad (22)$$

© 2004 by Marcel Dekker, Inc.

where $r(t)$ is now given by

$$r(t) = N + kn_0 \left[\frac{\left(1 - \frac{N}{n_0}\right)e^{-\alpha t} + \left(\frac{\alpha N}{kn_0} - 1\right)e^{-kt}}{k - \alpha} \right] \tag{23}$$

where $r(t) = R(t)M$. Since f_p and α are known from the analysis of the side chain stripping data, and k and n_0 are known from the random mannose backbone degradation data, the only unknown parameters in the expression involving the two enzymes are N/M, the total number of cleavable sites per g/moles of initial polymer mass, and α.

It is hoped that TDSLS methods will become frequently used for both degradation and structural studies. Whereas TDSLS can aid in determining biodegradability, stability against UV radiation, enzymatic resistance, rheological processability, and so on, it should prove useful in its own right for "deconstructing" branched and crosslinked polymers to understand their architecture.

2.3 Aggregation

Oftentimes, polymer solutions are unstable, in that they can undergo a host of reversible and irreversible associative processes; aggregation, microcrystallization, coacervation, liquid–liquid phase separation, microgel formation, and so on. Sometimes these associations are desirable (for example, water purification, bioimmunoassays, and others), whereas in other cases they can render a product useless or harmful (for example, aggregation in a pharmaceutical formulation). Because TDSLS is exquisitely sensitive to even small changes in molecular mass, it provides a powerful tool for monitoring such instabilities.

There are many scenarios for such associative processes, and a review is beyond the scope of this chapter. Many references exist (57,58). Each associative model yields predictions about TDSLS. Figure 10 shows raw light scattering intensity data for the aggregation of gold nanospheres that were coated with a protein and the corresponding antibody (T Nguyen and WF Reed, unpublished results). The aggregation process is immediately detectable, whereas with standard techniques, such as turbidity, there is a long latent period before any change in signal is measurable.

2.4 Dissolution

The rate at which dry polymer, in the form of pellets, powders, granules, and so on, dissolves in solution is often of paramount importance for a particular application. In many instances the most rapid dissolution possible is desired, whereas in others

© 2004 by Marcel Dekker, Inc.

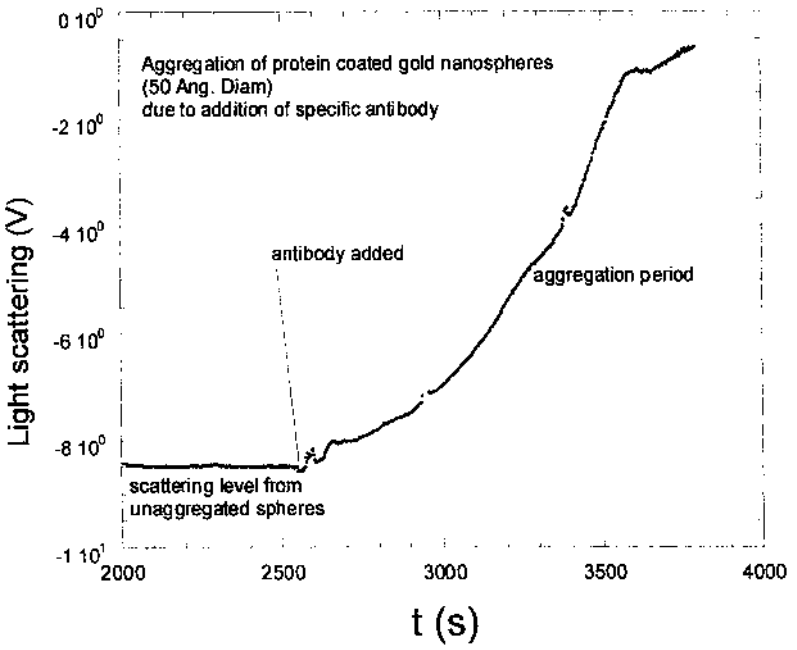

Figure 10 Aggregation of a solution of protein-coated gold nanospheres after an antibody specific to the protein was introduced into the solution. (WF Reed and T Nguyen, unpublished results.)

(for example, time release encapsulation) a very slow dissolution is needed. There have been a number of experimental and theoretical studies of dissolution (59–62).

The basic detector train used in the foregoing systems is readily used for dissolution monitoring. Normally, the sample to be dissolved is placed in a vessel in a temperature-controlled bath, and a peristaltic pump is used to recirculate solution in the dissolution vessel through the detectors and back to the vessel. Usually, in-line filters of a chosen pore size are used to ensure that no macroscopic particles are pumped through the detectors.

In some cases, in-line filters can affect the dissolution behavior if micro-aggregates or microgels are present during dissolution. An example of this latter case is given in Fig. 11, which shows the dissolution behavior of a polyelectrolyte, sodium polystyrene sulfonate (PSS) in pure water and also in water with a 100 mM concentration of NaCl, with several different in-line filter pore sizes (adapted from Ref. 7). The inset shows the refractometer response, which measures the concentration of polymer dissolved in the solvent at each instant. There is very little difference between the way the PSS dissolves in pure water and in salt water,

© 2004 by Marcel Dekker, Inc.

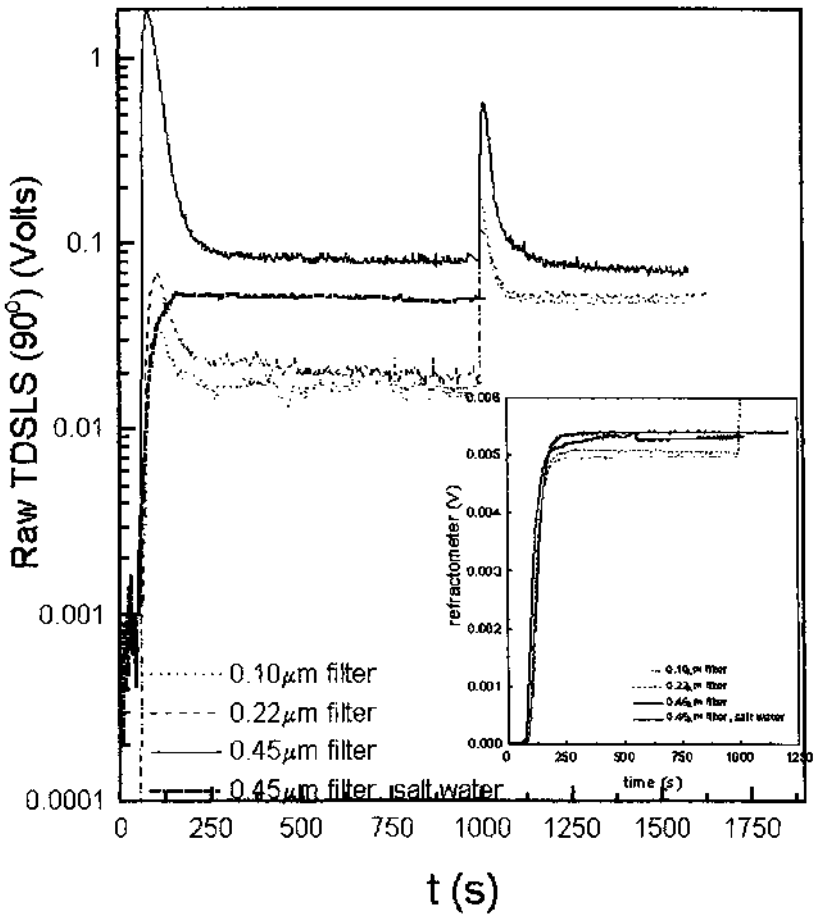

Figure 11 Light scattering from solutions of dissolving polyelectrolytes under different conditions; in pure water with different on-line membrane filter pore sizes, and in salt water (0.1 M NaCl) with a 0.45 μ filter. The initial sharp peaks in scattering are due to "bursts" of micro-aggregates that appear upon dissolution in pure water, whose heights depend critically on filter pore size. The inset shows the actual concentration of polymer in solution, obtained from simultaneous RI measurements, which are insensitive to aggregates. The different conditions have little effect on the dissolution kinetics themselves. (From Ref. 7.)

and the type of in-line filter size also has no appreciable effect. In dramatic contrast, however, is the TDSLS signal, which is proportional to the quantity cM_w at the very low concentrations used in these experiments. Large scattering spikes are seen at the outset of the dissolution in pure water, being largest for the coarsest

© 2004 by Marcel Dekker, Inc.

filter size, so large in fact that a logarithmic scale is used to show the peaks. In salt water there is no peak at all, and the TDSLS and RI curves are virtually identical.

The data were interpreted in terms of a very small population of aggregates that are present upon initial dissolution in pure water, and which very slowly dissolve. Although the initial burst of aggregates dissolved mostly in minutes, the residual amount of aggregates, seen by the higher level plateaus for the largest filter, took several weeks to dissolve totally. This was the first kinetic demonstration of the existence of aggregates and their tendency to dissolve, and lends considerable strength to demonstrations made earlier that the puzzling "slow modes" of diffusion in polyelectrolyte solutions at low ionic strength are due to incompletely dissolved aggregates (63,64). Hence, the slow modes do not represent an equilibrium property of such solutions. Others had interpreted the slow modes in terms of ordering or other equilibrium phenomena, and had even given the name "extraordinary regime" to solutions manifesting these modes (65).

3 EQUILIBRIUM CHARACTERIZATION OF MULTICOMPONENT SOLUTIONS

While equilibrium characterization is not the main focus of this chapter, the time-dependent approach to monitoring allows significant strides in characterizing equilibrium systems by providing a continuous, automatic record of behavior as solution conditions are changed. This not only provides much more detailed data than normally found, but also eliminates tedious manual solution preparations and data gathering.

One of the pre-eminent approaches to equilibrium characterization is SEC, the main topic of this book. Light-scattering and viscosity detectors have now been in use for many years in conjunction with SEC (26,66), so that their use in that context can now be termed "traditional," even if many SEC users still lag in obtaining and using the detectors.

We are interested, hence, in finding new applications of the basic ACM and detector train. A strong feature of this approach is that gradients of multiple components can be produced in time, allowing the equilibrium behavior along any path in the composition space of components to be monitored. This is illustrated by three separate examples: (1) a single component polymer system, (2) the effect of simple electrolytes on polyelectrolytes, and (3) the complex association properties of polymers and micelles.

Although the following experiments were performed using an ISCO 2360 programmable mixer, even simpler means of obtaining ACM can be used, because an RI is used to obtain the polymer concentration at every point; that is, gravity feed a stirred vessel containing polymer solution with pure solvent to dilute it slowly, or use a syringe pump to dilute it.

© 2004 by Marcel Dekker, Inc.

3.1 A Simple System: Equilibrium Characterization of PVP

This simplest application of ACM in the equilibrium context is to ramp the concentration of the polymer in a given solvent, thus obtaining an automated Zimm plot, plus intrinsic viscosity characterization. This can be useful in contexts where one wants to determine $[\eta]$ and the virial coefficients, A_2 and A_3, where it suffices to have M_w instead of the full population distribution, or where appropriate SEC columns either do not exist or may be damaged by the sample.

Figure 12 shows typical analysis results when RI, TDSLS, and viscosity signals were monitored during an experiment where polymer (PVP) concentration was ramped continuously from 0 to 0.008 g/mL (67). The RI signal allows conversion of the data from the time domain to the concentration domain of the component being ramped. The automated Zimm plot yielded M_w (g/mole) = 646,300 $\pm$ 5%, $A_2(\text{cm}^3\ \text{mole/g}^2) = 3.50 \times 10^{-4} \pm 7\%$, $A_3(\text{cm}^6\ \text{mole/g}^2) = 0.0186 \pm 8\%$, $\langle S^2 \rangle_z^{1/2}(\text{Å}) = 390 \pm 6\%$, and the viscosity curve gave $[\eta](\text{cm}^3/\text{g}) = 154 \pm 8\%$, with a coefficient $k_H = 0.34 \pm 3\%$ in Eq. (6).

3.2 Effect of Salts on Polyelectrolytes

The conformations, interactions, and hydrodynamics of polyelectrolytes are very sensitive to the concentration of simple electrolyte in the solution; that is, the ionic strength. When ionic strength decreases polyelectrolytes interact more strongly, and if they are flexible their static and hydrodynamic dimensions increase. Numerous experimental and theoretical studies have been carried out on these issues (68). ACM has recently been used to make detailed studies of electrostatically enhanced second and third virial coefficients, static and hydrodynamic dimensions, and strong interparticle correlations (69,70). The detail and resolution of these latter studies surpasses anything the author is aware of in traditional manual gathering of individual data points.

3.3 Interaction of Neutral Polymers and Surfactants

A more complex multicomponent system is represented by solutions containing polymer, ionized surfactants, and simple electrolytes (salts); that is, there are now three independent component axes in component space. It is well known that surfactant micelles can form complexes with neutral polymers (71,72), but it is a daunting task to choose and perform manual experiments at a collection of individual points chosen from component space. ACM allows behavior along arbitrary paths in component space to be followed.

An illustrative system is the interaction of PVP and sodium dodecyl sulfate (SDS) (73). SDS forms micelles at its critical micelle concentration (CMC), which depends on the concentration of salt. One ACM strategy for exploring the

© 2004 by Marcel Dekker, Inc.

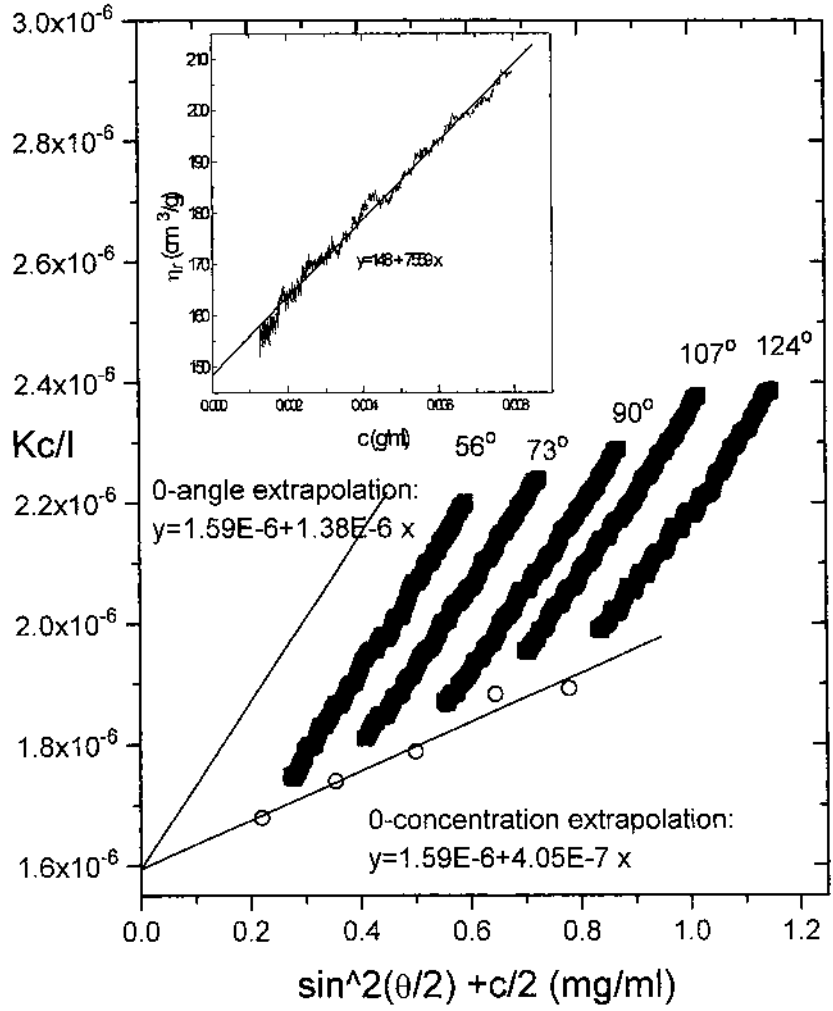

Figure 12 Zimm plot data obtained from the ACM technique for PVP in water. The inset shows the viscosity data vs. c_{PVP} obtained simultaneously. (From Ref. 67.)

interactions between SDS and PVP is to run separate experimental paths parallel to each coordinate axis.

Figure 13a shows how light scattering intensity and viscosity change as a solution of 0.002 g/mL PVP ($M_w = 2 \times 10^6$ g/mole) in pure water is mixed with SDS. The immediate decrease in scattering intensity with increasing SDS implies that the charged SDS monomers are associating with the PVP below and beyond

© 2004 by Marcel Dekker, Inc.

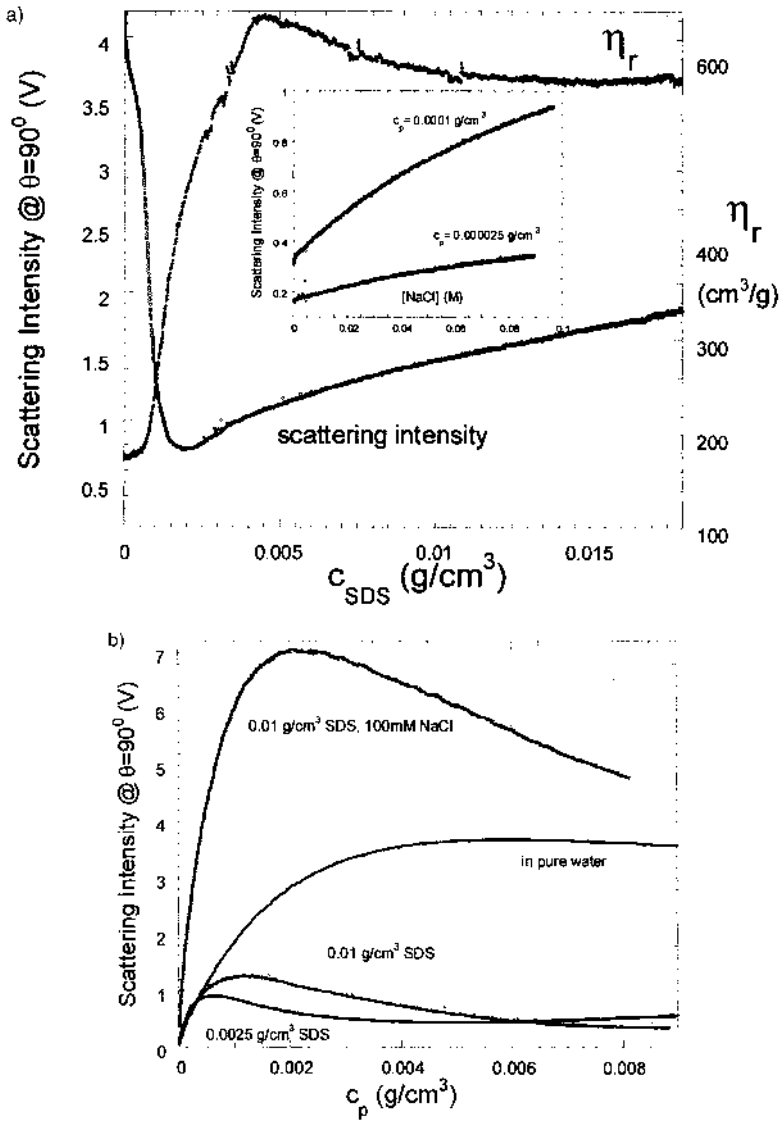

Figure 13 (a) ACM applied to the characterization of a complex system; a neutral polymer (SDS), surfactant (SDS), and a simple salt (NaCl). Shown is the behavior of raw scattering and of η_r as the concentration of SDS increases, at a fixed concentration of PVP in pure water. The inset shows scattering behavior vs. [NaCl] for different values of c_{PVP}. Strong association and polyelectrolyte effects are seen in both figures. (b) ACM for the system of Fig. 13a, except now the concentration of PVP is ramped while holding c_{SDS} and [NaCl] fixed at different values. (From Ref. 70.)

© 2004 by Marcel Dekker, Inc.

the normal CMC (about 0.002 g/mL), and charging the PVP, turning it into a polyelectrolyte whose A_2 increases as linear charge density increases, leading to the decrease in scattered intensity, according to Eq. (3). Similarly, the charging of the PVP leads to an electrostatically based expansion of the polymer coil, increasing the hydrodynamic volume (and hence viscosity). The inset to Fig. 13a shows how the scattering intensity increases for fixed concentration PVP saturated by SDS (1% SDS) as [NaCl] increases. The increase in the scattered intensity is due to the ionic shielding between the charged PVP chains, leading to a decrease in A_2. The viscosity (not shown) likewise decreases as [NaCl] increases. In the absence of SDS, the scattering and viscosity behavior of PVP are independent of [NaCl].

Figure 13b shows the complex way scattering intensity varies as the concentration of PVP saturated with a fixed concentration of SDS increases. The maxima reached are due to the effect of A_3, which can be computed from the value of c_p at which the maximum occurs at $q = 0$, $c_{p,\max,q=0}$, according to

$$A_3 = \frac{1}{3M_w c_{p,\max,q=0}^2} \tag{24}$$

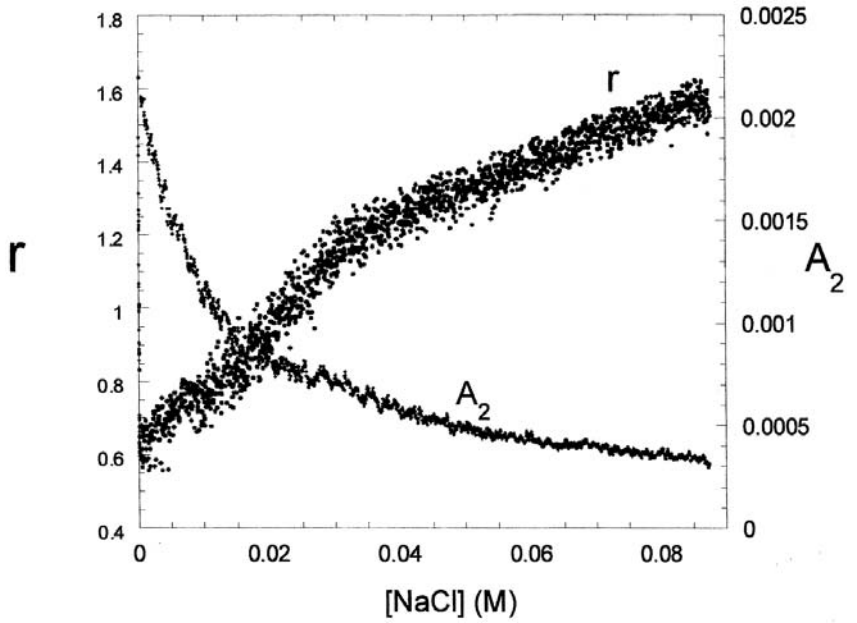

Figure 14 The value of the association constant r (mass of SDS bound per mass of PVP) vs. [NaCl], at saturating levels of SDS. Also shown is A_2 which decreases strongly with [NaCl] due to ionic shielding. (From Ref. 70.)

© 2004 by Marcel Dekker, Inc.

Also of note in Fig. 13b is how highly the scattering is suppressed when SDS is present with the PVP in a salt-free solution. This is again a manifestation of the electrostatically enhanced A_2 due to the electrical charging of PVP by SDS. In contrast, when such a solution is exposed to salt (e.g., 0.1 M NaCl in Fig. 13b) the scattering is actually higher than when no SDS is present, reflecting the fact that A_2 has been greatly lowered by the NaCl, and that the mass of the complex formed by SDS and PVP is significantly greater than the mass of the PVP alone.

Figure 14 shows how these two latter factors are affected by salt. A procedure for determining the mass ratio of SDS to PVP in the aggregates r, was presented in Ref. 7. Figure 14 shows that r increases from 0.6 to 1.6 as [NaCl] increases, for PVP under saturating SDS conditions, due to the decrease in repulsion among the charged SDS groups. A significant decrease in A_2 from 0.0022 to 0.0003 is also seen as [NaCl] increases.

4 SUMMARY

Use of automatic continuous mixing, together with multiple detectors provides state-of-the-art characterization for polymers in a variety of equilibrium and nonequilibrium contexts. ACOMP is one of the ACM family of techniques that promises the greatest long-term economic impact, both in terms of fundamental research and on-line reactor control. ACOMP is rapidly being adapted to a wide variety of polymerization reaction contexts, including batch and continuous reactors, homogeneous and inhomogeneous media, and those that produce slurries, pellets, and phase-separated products. Significant improvement in the front end, involving the ACM portion, is expected to augment greatly the versatility of ACOMP.

ACM should steadily find new monitoring applications for degradation, aggregation, microcrystallization, and other phase-separation processes. ACM in the equilibrium characterization milieu should prove to be immensely labor saving, especially for the study of complex systems, such as those involving polyelectrolytes, salts, and surfactant agents.

Also on the horizon is a new application for light scattering; simultaneous multiple sample light scattering, or SMSLS (74). This takes advantage of the greatly lowered expense of light-scattering sample cells (75), laser light, and sensitive photodetection to gang many independent cells together to form an instrument unified under the control of a single computer. Applications are expected in combinatorial and high-throughput methods applied to new polymer synthesis (76–78), shelf-life and stability measurements, aggregation, dissolution, and multiple reactor sampling.

© 2004 by Marcel Dekker, Inc.

ACKNOWLEDGEMENTS

I would like to acknowledge support from the U.S. National Science Foundation CTS 0124006, Atofina Elf, International Specialty Products, Brookhaven Instruments, Firmenich, SKW, and many people who have contributed throughout the recent years: Alan Parker, Jean Luc Brousseau, David Norwood, Roland Strelitzki, Fabio Florenzano, Stephan Moyses, Bruno Grassl, Gina Sorci, Huceste and Ahmet Giz, Alina Alb, Erica Bayly, Florence Chauvin, Joana Ganter, Ricardo Michel, Ruth Schimanowski, and others.

REFERENCES

1. H Holthoff, SU Egelhaaf, M Borkovec, P Schurtenberger, H Sticher. Coagulation rate measurements of colloidal particles by simultaneous static and dynamic light scattering. Langmuir 12:5541–5549, 1996.
2. A Chowdhury, P Russo. Static light scattering instrument for rapid and time-resolved particle sizing in polymer and colloidal solutions. Rev Sci Instrum 67:3645–3648, 1996.
3. T Norisuye, M Shibayama, S Nomura. Time-resolved light scattering study on the gelation process of poly(*N*-isopropyl acrylamide). Polymer 39:2769–2775, 1998.
4. CA Thomas. The enzymatic degradation of desoxyribose nucleic acid. J Am Chem Soc 78:1861–1866, 1956.
5. CE Reed, WF Reed. Light scattering power of randomly cut random coils with application to the determination of depolymerization rates. J Chem Phys 91:7193–7199, 1989.
6. CE Reed, WF Reed. Effect of polydispersity and second virial coefficient on light scattering by randomly cut random coils. J Chem Phys 93:9069–9076, 1990.
7. RC Michel, WF Reed. New evidence of the non-equilibrium nature of the "slow modes" of diffusion in polyelectrolyte solutions. Biopolymers 53:19–39, 2000.
8. PJ Flory. Kinetics of polyesterification: a study of the effects of molecular weight and viscosity on reaction rate. J Am Chem Soc 61:3334–3340, 1939.
9. RL Grob, DJ Shahan, K Dix, K Nielsen. Remote on-line monitoring of polyol production using near-infrared spectrophotometry. Process Control & Qual 2:225–235, 1992.
10. A Penlidis, JF MacGregor, AE Hamielec. Continuous emulsion polymerization reactor control. Proc of Amer Control Conf 2:878–880, 1985.
11. P Dallin. Near IR analysis in polymer reactions. Process Control of Qual 9:167–172, 1997.
12. RF Storey, AB Donnalley, TL Maggio. Real-time monitoring of carbocationic polymerization of isobutylene using in situ FTIR-ATR spectroscopy with conduit and diamond-composite sensor technology. Macromolecules 31:1523–1526, 1998.
13. R Reshadat, ST Balke. Correlating inline near IR and off-line MIR spectra using partial least squares: further assessment. App Spectroscopy 53(10):1309–1311, 1999.
14. MG Hansen, S Vedula. In-line measurement of copolymer composition and melt index. Polym Process Eng 97:89–102, 1997.

© 2004 by Marcel Dekker, Inc.

15. JM Starita, CL Rohn. Rheological measurements for quality control of thermoplastics. Plast Compound 10:46–51, 1987.
16. O Brand, JM English, SA Bidstrup, MG Allen. Micromachined viscosity sensor for real-time polymerization monitoring. Sensors and Actuators 1:121–124, 1997.
17. SE Bresler, EN Kazbekov, VN Shadrin. Study of radical polymerization by means of ESR. Makromole Chem 175:1875–2880, 1974.
18. J Shen, Y Tian. ESR study of the propagating rate constant and radical concentration of bulk polymerization of methyl methacrylate. Makromole Chem Rapid Comm 8:615–620, 1987.
19. RS Saltzman. On line UV-visible analysis increases process efficiency. I&CS 67:49–51, 1994.
20. YS Kim, C Sook, P Sung. UV and fluorescence characterization of styrene and methyl methacrylate polymerization. J Appl Polym Sci 57:363–370, 1995.
21. HJ Paik, NH Sung. Fiberoptic intrinsic fluorescence for in-situ cure monitoring of amine cured epoxy and composites. Polymer Eng Sci 34:1025–1032, 1994.
22. IN Kotchetov, DC Neckers. Fluorescence probe studies of UV laser-induced polymerization of polyolacrylates. J Imaging Sci & Technol 37:156–163, 1993.
23. WF Reed, L Guterman, P Tundo, JH Fendler. Polymerized surfactant vesicles: kinetics and mechanisms of photopolymerization. J Am Chem Soc 106:1897–1907, 1984.
24. FH Florenzano, R Strelitzki, WF Reed. Absolute, online monitoring of molar mass during polymerization reactions. Macromolecules 31:7226–7238, 1998.
25. WF Reed. A method for online monitoring of polydispersity during polymerization reactions. Macromolecules 33:7165–7172, 2000.
26. WF Reed. Data evaluation for unified multi-detector size exclusion chromatography–molar mass, viscosity and radius gyration distributions. Macromol Chem Phys 196:1539–1575, 1995.
27. BH Zimm. The scattering of light and the radial distribution function of high polymer solutions. J Chem Phys 16(12):1093–1098, 1948.
28. WF Reed. Light scattering results on polyelectrolyte conformation, diffusion, and interparticle interactions and correlations. In: KS Schmitz, ed. Macroion Characterization. Washington, DC: ACS, 1994.
29. S Ghosh, X Li, CE Reed, WF Reed. Apparent persistence lengths and diffusion behavior of high molecular weight hyaluronate. Biopolymers 30:1101–1112, 1990.
30. M Bohdanecky, J Kovar. Viscosity of Polymer Solutions. In: AD Jenkins, ed. Polymer Science Library 2. New York: Elsevier, 1982.
31. R Schimanowski, R Strelitzki, DA Mullin, WF Reed. Heterogeneous time dependent static light scattering. Macromolecules 32:7055–7063, 1999.
32. NA Dotson, R Galvan, RL Laurence, M Tirrel. Polymerization process modeling. New York: VCH Publishers, 1996, Ch. 3.
33. A Giz, HC Giz, A Alb, JL Brousseau, WF Reed. Kinetics and mechanisms of acrylamide polymerization from absolute online monitoring of polymerization reactions. Macromolecules 34:1180–1191, 2001.
34. B Grassl, WF Reed. Online polymerization monitoring in a continuous tank reactor. Macromol Chem & Phys 203:586–597, 2002.

© 2004 by Marcel Dekker, Inc.

35. M Souaille, H Fischer. Kinetic conditions for living and controlled free radical polymerizations mediated by reversible combination of transient propagating and persistent radicals: the ideal mechanism. Macromolecules 33:7378–7394, 2000.
36. NA Listigovers, MK Georges, PG Odell, B Keoshkerian. Narrow-polydispersity diblock and triblock copolymers of alkyl acrylates by a "living" stable free radical polymerization. Macromolecules 29:8992–8993, 1996.
37. S Grimaldi, JP Finet, F Le Moigne, A Zehdaoui, P Tordo, B Benoit, M Fontanille, Y Gnanou. Acyclic-phosphonylated nitroxides: a new series of counter-radicals for "living"/controlled free radical polymerization. Macromolecules 33:1141–1147, 2000.
38. DH Salomon, E Rizzardo, P Cacioli. Polymerization process and polymers produced thereby U.S. Patent 4,581,429, 1985.
39. A Goto, T Fukuda. Kinetic study on nitroxide-mediated free radical polymerization of tert-butyl acrylate. Macromolecules 32(3):618–623, 1999.
40. F Chauvin, AM Alb, D Bertin, P Tordo, WF Reed. Kinetics and molecular weight evolution during controlled radical polymerization. Macromol Chem Phys 203:2029–2041, 2002.
41. G Odian. Principles of polymerization. 3rd ed. New York: John Wiley & Sons, 1991.
42. H Çatalgil-Giz, A Giz, AM Alb, A Öncül Koç, WF Reed. Online monitoring of composition, sequence length, and molecular weight distributions during free radical copolymerization, and subsequent determination of reactivity ratios. Macromolecules 35:6557–6571, 2002.
43. FR Mayo, FM Levis. Copolymerization I. A basis for comparing the behavior of monomer in copolymerization; the copolymerization of styrene and methyl methacrylate. J Am Chem Soc 66:1594–1601, 1944.
44. S Duc, A Petit. Copolymerization of phenylacetylene and 1-hexyne using Ziegler–Natta and methathesis catalyst systems: copolymer compositions and reactivity ratios by ^{1}H NMR spectroscopy. Polymer 40:589–597, 1999.
45. W Buschuk, H Benoit. Light scattering studies of copolymers. 1. Effect of heterogeneity of chain composition on the molecular weight. Canadian J Chem 36:1616–1626, 1958.
46. WH Stockmayer, LD Moore, M Fixman, BN Epstein. Copolymers in solution. 1. Preliminary results for styrene-methyl methacrylate. J Polym Sci 16:517–530, 1955.
47. A Faldi, JBP Soares. Characterization of the combined molecular weight and composition distribution of industrial ethylene/α-olefin copolymers. Polymer 42:3057–3066, 2001.
48. Y Feng, JN Hay. The measurement of compositional heterogeneity in a propylene–ethylene block copolymer. Polymer 39:6723–6731, 1998.
49. WH Stockmayer. Distribution of chain lengths and compositions in copolymers. J Chemical Phys 13:199–207, 1945.
50. TE Patten, K Matyjaszewski. Copper(I) catalyzed atom transfer radical polymerization. Acc Chem Res 32:895–903, 1999.
51. F Candau, J Selb. Hydrophobically modified polyacrylamides prepared by micellar polymerization. Adv Colloid & Interface Sci 79:149–172, 1999.

© 2004 by Marcel Dekker, Inc.

52. M Hulden. Hydrophobically modified urethane–ethoxylate associative thickeners: rheology of aqueous solutions and interactions with surfactants. Colloids and Surfaces A82:263–277, 1994.
53. E Larson. Method for producing polymers using micellar polymerization. U.S. Patent 6,127,494, 2000.
54. WF Reed. Time dependent light scattering from singly and multiply stranded linear polymers undergoing random and endwise scission. J Chem Phys 103(17): 7576–7584, 1995.
55. JL Ganter, WF Reed. Real time monitoring of enzymatic hydrolysis of galactomannans. Biopolymers 59:226–242, 2001.
56. S Ghosh, WF Reed. New light scattering signatures from polymers undergoing depolymerization with application to proteoglycan monomer degradation. Biopolymers 5:435–450, 1995.
57. Kinetics of aggregation and gelation. In: FF Family, DP Landau, eds. Amsterdam: Elsevier Science Publishers, 1984.
58. JW Cahn, JE Hilliard. Free energy of a non-uniform system. J Chem Phys 28:258–267, 1958.
59. F Brochard, PG De Gennes. Kinematics of polymer dissolution. Physicochem Hydrodynam 4:313–321, 1983.
60. MF Herman, SF Edwards. A reptation model for polymer dissolution. Macromolecules 23:3662–3667, 1990.
61. A Parker, F Vigouroux, WF Reed. The dissolution kinetics of polymer powders. Am Inst Chem Eng Journal 46:1290–1299, 2000.
62. NA Peppas, JC Wu, ED von Meerwall. Mathematical modeling and experimental characterization of polymer dissolution. Macromolecules 27:5626–5634, 1994.
63. S Ghosh, RM Peitzsch, WF Reed. Polyelectrolyte aggregates and other particles as the origin of the “extraordinary” diffusional phase. Biopolymers 32:1105–1122, 1992.
64. RG Smits, ME Kuil, M Mandel. Quasi-elastic light scattering study on solutions of linear flexible polyelectrolytes at low ionic strengths. Macromolecules 27: 5599–5608, 1994.
65. KS Schmitz. On the “filterable aggregates and other particles” interpretation of the extraordinary regime of polyelectrolytes. Biopolymers 33:953–959, 1993.
66. JP Wyatt. Light scattering and the absolute characterization of macromolecules. Analytica Chimica Acta 272:1–40, 1993.
67. R Strelitzki, WF Reed. Automated batch characterization of polymer solutions by static light scattering and viscometry. J Appl Polym Sci 73:2359–2368, 1999.
68. S Förster, M Schmidt. Polyelectrolytes in solution. Adv Polym Sci 120:53–133, 1995.
69. E Bayly, JL Brousseau, WF Reed. Continuous monitoring of the effect of changing solvent conditions on polyelectrolyte conformations and interactions. Int J Polymer Characterization and Analysis, in press.
70. GA Sorci, WF Reed. Electrostatically enhanced second and third virial coefficients, viscosity and interparticle correlations for linear polyelectrolytes. Submitted for publication.

© 2004 by Marcel Dekker, Inc.

71. P Dubin, P Tong, eds. Colloid–polymer interactions. ACS Symposium Series 532, 1993.
72. DP Norwood, E Minatti, WF Reed. Surfactant/polymer assemblies: 1. Surfactant binding properties. Macromolecules 31:2957–2965, 1998.
73. GA Sorci, WF Reed. Electrostatic and association phenomena in aggregates of polymers and micelles. Langmuir: in press.
74. WF Reed. U.S. Patent 09/690,099, 2003.
75. WF Reed. A miniature, submersible, light scattering probe for absolute macromolecular and colloidal characterization. U.S. patent 6,052,184, 2000.
76. JC Meredith, A Karim, EJ Amis. High throughput measurement of polymer blend phase behavior. Macromolecules 33:5760–5762, 2000.
77. LA Thompson. Recent applications of polymer supported reagents and scavengers in combinatorial, parallel, or multistep synthesis. Current Opinions in Chemical Biology 4:324–337, 2000.
78. EW McFarland, WH Weinberg. Combinatorial approaches to materials discovery. Trends in Biotechnology 17:107–115, 1999.

© 2004 by Marcel Dekker, Inc.

21
Light Scattering and the Solution Properties of Macromolecules

Philip J. Wyatt
Wyatt Technology Corporation
Santa Barbara, California, U.S.A.

1 INTRODUCTION

It has now been many years since Burchard and Cowie (1) stressed the importance of light scattering in "... providing information in depth on ... polymers ..." Although light scattering was not the only method in use at that time (early 1971), the authors expressed their hope that it would become obvious "... to the unconverted that to neglect light scattering [MALS] would be to proceed under a distinct disadvantage ..." Since that time, there has been a great increase in the number of laboratories throughout the world that now use such techniques. A major impetus to this increased use of light scattering measurements, especially in combination with chromatographic separations, has been the advent of exceptional instrumentation and software.

Of the three "absolute" techniques for the measurement of molar mass in solution (sedimentation equilibrium, membrane osmometry, and light scattering), only light scattering covers a great breadth of application (from a few 100 to 10^9 g/mol). It also represents the fastest and most versatile of the methods. Traditionally, measurements of light scattered by molecules in solution have been made over a

© 2004 by Marcel Dekker, Inc.

broad range of scattering angles. Such measurements have permitted the deduction of molar mass, molecular mean square radius, and the second virial coefficient. Because measurement of scattered light at many angles seemed a difficult and time-consuming task, instrumentation was introduced to make measurements at fewer angles than theoretically desirable. With them came the need to retain the absolute concept of the terminology "light scattering" while at the same time differentiating their measurements from those capable of making the determinations over a full "range of angles." The term "multi-angle light scattering," or simply MALS, is often used to describe this full light scattering concept. To comply with this more recent designation, the term MALS will be used throughout this chapter to refer to general light scattering measurements.

The term "absolute" is frequently seen in reference not only to results derived from MALS measurements, but also, inappropriately, to methods requiring calibration against standards of known molar mass. Just what is meant by the term "absolute"? A measurement of molar mass is said to be absolute if, and only if:

- The measurement requires no reference to any mass standards.
- All parameters of the measurement are determined directly. These include
  - refractive indices of all cells and fluids;
  - geometries of the sample cells and detectors (distances, shape, composition, and solid angles subtended at the sample by the scattered light detectors);
  - wavelength of the light source;
  - concentrations of the solutes;
  - response of the detectors (for example, for a DRI detector, the relation between the output voltage change and the corresponding change of fluid refractive index);
  - temperature and its effects on the physical parameters of the experiment.
- There is no *a priori* assumption of molecular conformation and/or structure.

Some types of instruments use light scattering for their determinations, but require calibration, as the solvent refractive index is changed, with mass standards for each such solvent. They are not absolute as they become totally dependent on the stability and reproducibility of the standards employed.

This chapter focuses on many of the elements of the MALS measurement technique that can affect the final results. It lists some of the causes of erroneous results and (hopefully) provides helpful guidance to various features of the instrumentation that are often overlooked. A major objective of the chapter,

© 2004 by Marcel Dekker, Inc.

therefore, is to remove any lingering doubts about the power of the method. A summary of some of the key historical events of the light scattering method are mentioned in the next section. This is followed by a brief description of the theory and its implementation via modern instrumentation. Next follows an explicit explanation of the significance of absolute measurements and the importance of the multi-angle, traditional measurement itself.

Discussions follow of the many problem areas relating to chromatographic separations in general and their effects on light scattering. Included here are discussions of band broadening and mobile phase preparation.

2 SOME BRIEF HISTORICAL NOTES

Although light scattering techniques were well known and understood in many respects in the 19th and 20th centuries, it was not until the seminal works of Einstein (2), Raman (3), Debye (4), and Zimm (5,6) were all brought together by the mid 1940s that the true power of the technique became recognized. By the 1930s, the possibility that proteins were distinct macromolecules was resolved by the early 90° light scattering experiments of Putzeys and Brosteaux (7). Their measurements appeared to confirm this hypothesis since the scattered light intensity, from light scattering theory, was known to be directly proportional to the weight-average molar mass times the molecular concentration.

The first commercial light scattering photometer incorporating a laser was introduced by Wyatt and Phillips (8) in 1970. The early applications of these instruments were directed almost entirely to measurements of colloids and microorganisms. In about 1972, Beckman Instruments introduced instrumentation, with the primary focus of measuring macromolecules, incorporating a laser to make measurements at very small scattering angles (9,10). The instrumentation (referred to as low-angle laser light scattering, or LALLS) was developed further and fully commercialized by the Chromatix. As discussed further in the next section, such low-angle measurements permitted the deduction of the molar mass of light-scattering molecules directly.

Although size exclusion chromatography (SEC) was developed by Moore (11) in 1964, it was not until the early 1970s that Ouano and Kaye (12) showed how the combination of SEC separation and LALLS could produce a quantitative distribution of molar mass. Whereas until that time, the classical light scattering methods of Zimm could yield at best a weight-averaged molar mass, here at last was a remarkable result that showed finer details of the samples so examined.

3 SOME ELEMENTS OF THE THEORY

In Zimm's earlier papers, he showed the relationship between the light scattering quantities measured and the physical elements of the measurement itself. In

© 2004 by Marcel Dekker, Inc.

addition, he developed graphical means by which such measurements could be related directly to the weight-averaged molar mass, the mean-square radius, and the second virial coefficient. For the light scattering measurements made at vanishingly small solute concentrations c, the familiar result of Zimm relating the measurements of solute concentration c and the excess Rayleigh ratio $R(\theta, c)$ to the derived macromolecular properties is given by

$$\frac{K^* c}{R(\theta, c)} = \frac{1}{M_w P(\theta)} + 2A_2 c \tag{1}$$

where M_w is the weight-average molar mass, $P(\theta)$ is the scattering form factor, A_2 is the second virial coefficient, and $K^* = 4\pi^2 (dn/dc)^2 n_0^2/(N_a \lambda_0^4)$. Following separation by SEC, at each slice (collection interval), both the MALS measurement and a concentration measurement [corrected for its corresponding interdetector volume (13) displacement] are made. The excess Rayleigh ratio $R(\theta, c)$ is the ratio of the scattered intensity per unit solid angle about the direction θ with respect to the direction of the incident beam to the incident light intensity per unit area.

From Zimm's graphical methodology, the extrapolated values of the left hand side (l.h.s.) of Eq. (1) as $c \to 0$ and $\theta \to 0$ yielded molar mass directly, since in this limit, $P(\theta) = 1$ and the term proportional to A_2 vanishes. We may expand Eq. (1) for the case of small scattering angle and vanishingly small concentrations to yield

$$\begin{aligned} \frac{K^* c}{R(\theta, c)} &= \frac{1}{M_w P(\theta)} + 2A_2 c \\ &\approx \frac{1}{M_w}\left[1 + \left(\frac{16\pi^2 n_0^2}{3\lambda_0^2}\right)\langle r_g^2 \rangle \sin^2 \frac{\theta}{2} - O\left\{\sin^4 \frac{\theta}{2}\right\} + \cdots\right] \end{aligned} \tag{2}$$

From Eq. (2) it is easily seen that at these limits, the variation of the l.h.s. of Eq. (2) with respect to $\sin^2 \theta/2$ is $16\pi^2 n_0^2 \langle r_g^2 \rangle/(3M_w \lambda_0^2)$, where $K^* = 4\pi^2 (dn/dc)^2 n_0^2/(N_a \lambda_0^4)$, λ_0 is the vacuum wavelength of the incident light, N_a is Avogadro's number, and dn is the solution refractive index increment with respect to a concentration change dc of the solute molecules. The mean square radius of a molecule of mass M is defined by

$$\langle r_g^2 \rangle = \left(\frac{1}{M}\right) \int r^2 \, dM \tag{3}$$

where the integration is over all mass elements of the molecule with respect to its center of mass. For the case of a distribution of molecules, this result is often referred to as the z-average mean-square radius. The misnomer *radius of gyration*

© 2004 by Marcel Dekker, Inc.

is often found in the literature when referring to the square root of the mean square radius (r.m.s. radius).

From the theoretical summaries above, we see that light scattering measurements and their interpretation depend simply on two fundamental principles: 1) the intensity of light scattered by a sample is directly proportional to the *product* of the molar mass and concentration (that is, measure the concentration and then read off the molar mass!), and 2) the variation of the scattered light intensity with angle is proportional to the molecules' average size. These are somewhat simplified versions of the following more exact statements.

1) The scattered light flux per unit solid angle about a direction θ, in excess of that scattered by the solvent, divided by the incident light intensity is directly proportional to the product of the weight-average molar mass and the molecular concentration. This means that $R(\theta, c) \propto M_w c$ in the limit as c and $\theta \to 0$. 2) The variation of scattered light flux with respect to $\sin^2 \theta/2$ is directly proportional to the average molecular mean-square radius in the limit as c and $\theta \to 0$. Equivalently, $dR(\theta, c)/d(\sin^2 \theta/2) \propto \langle r_g^2 \rangle$ in the limit as c and $\theta \to 0$.

A more detailed review of the theory and its interpretation may be found in Ref. 14.

4 INSTRUMENTATION

Figure 1 is a schematic of the MALS measurement showing a light source (generally a laser) producing a fine beam incident on the sample. The sample may be contained in a cuvette of a flow cell. The scattered light from the sample is collected over a range of angles with respect to the forward direction. Most MALS measurements are made with light polarized perpendicular to the plane of measurement. In recent years, solid-state lasers have replaced the formerly used

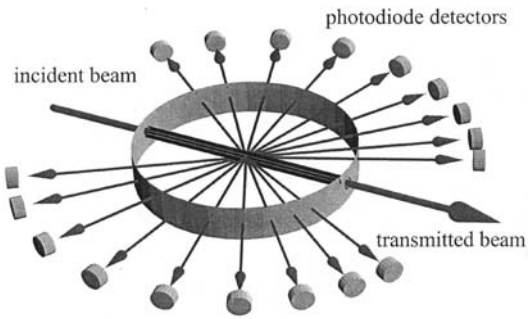

Figure 1 Schematic of an MALS measurement.

© 2004 by Marcel Dekker, Inc.

gas lasers as the solid state lasers are more efficient, produce higher power levels, and are far more compact. They do have one serious problem and that is stability. Despite their normalization capability by means of an internal beam monitor, they generally suffer from so-called "mode hopping" and this can result in large output power fluctuations, irrespective of the efficiency of power normalization or feedback control. Such mode hopping depends critically upon laser temperature and age. Because these fluctuations can be very rapid, they are often unsusceptible to monitoring correction. Solid-state laser sources are now available over a range of wavelengths from blue through infrared. Most commonly, a wavelength around 680 nm is used. In recent years, elimination of mode hopping has been achieved by some vendors without relying on temperature stabilization attempts.

The detectors shown are generally selected as high-gain transimpedance photodiodes or even small CCD arrays. The former span a far greater dynamic range. An important characteristic of all detectors is their collimation and angular resolution. Very large macromolecules produce scattering patterns exhibiting considerable curvature. With detectors subtending large solid angles, the derived results can be compromised by this unnecessary smoothing of the angular variation of the scattered light. In addition, if detectors accept too great a range of angles, it becomes difficult to separate noise contributions within the collected data.

Detectors should be capable of being fitted with narrow band pass interference filters for the measurement of fluorescent materials, such as lignins and asphaltines. The depolarizing effects of some molecules are best studied with the fitting of polarization analysers, an application of increasing importance in the field of nanoparticle characterization.

Other elements useful for light scattering detectors include temperature and (as needed) humidity control of the optics. Indeed, a great amount of SEC work relates to the high temperature environment (100–220°C). Not only must the optical train be able to withstand such temperatures without distortion, but the detectors must often be shielded from long-wavelength radiation as they are often very sensitive well into the infrared region. Without such filtering, the noise contributions arising from black body radiation may overwhelm the sample signatures themselves.

Figure 2 shows a typical configuration for collecting MALS data from the sample following separation in the columns shown. Note several key elements: the mobile phase is both degassed and filtered, the latter generally through 0.1 μm filters. Either UV or DRI detectors may be used to determine concentration [needed to solve Eq. (1)], an essential element of the measurement. The UV detector is generally placed before the MALS detector, the DRI after it. For most SEC separations, a DRI detector is preferred. This is particularly true for proteins whose refractive index increment is about 0.175 within 5% for most proteins. With UV detection, the protein extinction coefficients must be known before the

© 2004 by Marcel Dekker, Inc.

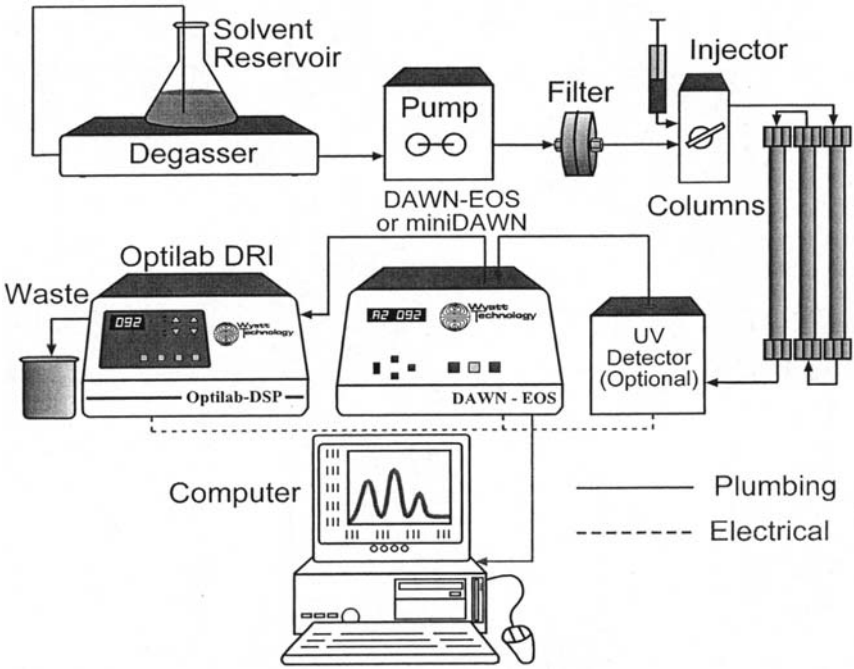

Figure 2 Configuration of an SEC separation with MALS.

detector may be used to determine concentration. For various types of copolymers, especially conjugated proteins, both UV and DRI detectors are often used in combination (see Sec. 6, below).

Preparation of the mobile phase for light scattering is a task too often neglected. Not only can the presence of dust affect the quality of recorded signals and the precision of the masses and sizes extracted from such measurements, but very small signals from minor components of the sample are often lost if the noise levels are too great. There are three major sources of noise (apart from the usually very small contributions from the photometer's electronics): the columns, the mobile phase, and the sample itself.

Because of their high sensitivity to dust and aggregates, MALS detectors provide an excellent measure of column quality. Deteriorating columns are often first noticed by means of the detection of particulate materials shed by the columns. Nevertheless, by the judicious use of appropriate collection software, the life times of such deteriorating columns may often be extended by means of suitable statistical analyses (see section on software, below). The larger the shed particles, the more pronounced is their forward scattering.

© 2004 by Marcel Dekker, Inc.

The use of freshly distilled organic solvents is always recommended. For aqueous mobile phases, the use of Nanopure™ (Barnstead International, Dubuque, Iowa, U.S.A.) or equivalently purified and filtered water must be used. Particular care must be exercised in preparing the buffered solutions so often required for various types of biopolymers. Despite the high purity listed on containers of these fine chemicals, rarely is there mention made of the dust content of the ingredients. Thus such mobile phases must be filtered with great care throughout their preparation.

Finally, the sample itself may contain large quantities of extemporaneous debris introduced during sample preparation. For this reason, a guard column is often used to protect the columns from the clogging that such debris may cause. For certain types of separation mechanisms, such as asymmetric flow field flow fractionation (AsFFF), the debris is often removed directly by the separation process itself (15).

The columns shown in Fig. 2 generally refer to SEC columns, although the MALS measurement is independent of the separation (or *non*separation) method. Reversed phase HPLC columns are often used instead of the SEC columns, especially for the measurement of proteins. For these measurements, the DRI detector is generally replaced by a UV detector because most DRI detectors do not have the dynamic range needed to cope with the refractive index range of the mobile phase. As mentioned earlier, a guard column is often included for many such separations.

In recent years, the development of more robust instrumentation for the field flow fractionation method of separation has permitted the incorporation of such instrumentation without the steep learning curve associated historically with its implementation. The AsFFF device alluded to earlier and introduced by Wyatt Technology Europe as the *Eclipse*™ (Woldert, Germany) is a particular case in point. For many polymers, particularly water-soluble polymers, the separations achieved rival SEC. Mastery of the device can be achieved within a few hours. This should be compared with weeks or months formerly required to learn the subtleties of such separation devices. In addition to so-called "cross-flow" FFF (exemplified by the AsFFF devices), there are several other FFF separation techniques (16) based on thermal, centrifugal, electrical, or other properties of the molecules undergoing separation. A current reference list of all articles published in the field of FFF may be found at the website developed by Dr. Mark Shure of Rohm and Haas (http://www.rohmhaas.com/fff/).

The FFF separation techniques are particularly useful for the separation of nanoparticles and giant molecules such as DNA. SEC separations, while generally inapplicable to particles, have been used for many years to separate (or attempt to separate) large molecules, often beyond the exclusion limit. Unfortunately, such molecules tend to shear during separation, which results in a distribution of molecules separated that includes often substantial amounts of such fragmented contributions.

© 2004 by Marcel Dekker, Inc.

5 THE IMPORTANCE OF SOFTWARE

Like any other analytical procedure, MALS requires special interpretive software to insure the precision of results derived from such measurements. Foremost among the objectives of the software is the determination at each elution slice of the molar mass and root-mean-square radius of the sample within that slice. Following separation in SEC columns (or by other fractionation processes such as field flow fractionation or reversed phase chromatography), the concentration of the fractionated polymer at each such elution slice is assumed to be so low that the second term on the right-hand-side of Eq. (1) may be neglected. [In other words, at such low concentrations, the second virial coefficient may not be determined directly. However, the value of A_2 determined off-line, following Zimm's method (5,13), may be supplied directly as an input parameter for the software.]

Figure 3 shows in graphical form the calculational basis for the determination of the weight-average molar mass M_j and average mean-square radius $\langle r_g^2 \rangle_j$ based on the Zimm plot procedure when there is no 2nd virial coefficient dependence of the derived Rayleigh ratios, $R_j(\theta_i, c_j)$. At each slice j and corresponding concentration c_j, the ratios $K^* c_j / R_j(\theta_i, c_j)$ for each measured scattering angle θ_i are plotted as a function of $\sin^2 \theta_i/2$. Associated with each measured $R_j(\theta_i, c_j)$ is a corresponding standard deviation based upon the plethora of multiple measurements characteristic of the MALS method, as well as errors in measurement of the corresponding concentration. The data fit shown in Fig. 3 is obtained by a least-squares fitting of a linear function in $\sin^2 \theta_i/2$ to the correspondingly weighted deviations of the data to the function. The associated weights are taken proportional to the square of the reciprocal standard deviations. Once the least-square fit has been determined, the intercept with the ordinate axis is readily calculated to yield the weight average molar mass value M_j for that slice. The initial slope of the least squares fit with respect to $\sin^2 \theta_i/2$ yields

$$\frac{1}{M_j}\left(\frac{16\pi^2 n_0^2}{3\lambda_0^2}\right)\langle r_g^2 \rangle \tag{4}$$

This may be written also as

$$[\text{ordinate intercept}]\left(\frac{16\pi^2 n_0^2}{3\lambda_0^2}\right)\langle r_g^2 \rangle \tag{5}$$

Using the concept of error propagation, the standard deviation of the derived value M_j may be calculated directly from

$$\Delta M_j = \sqrt{\sum_i \left(\frac{\partial M_j}{\partial R_j(\theta_i, c_j)}\right)^2 [\Delta R_j(\theta_i, c_j)]^2 + \left(\frac{\partial M_j}{\partial c_j}\right)^2 (\Delta c_j)^2} \tag{6}$$

© 2004 by Marcel Dekker, Inc.

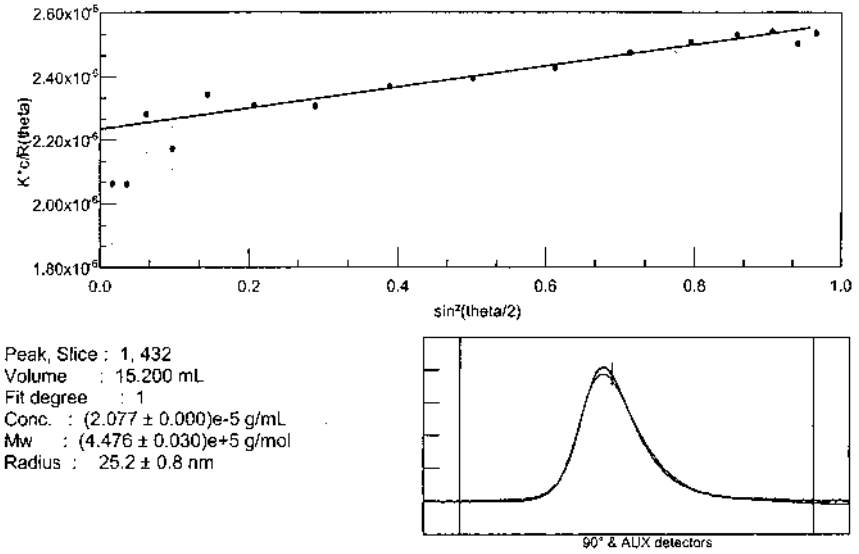

Figure 3 Data for a single slice plotted with error bars.

where $\Delta R_j(\theta_i, c_j)$ is the calculated standard deviation of the measured excess Rayleigh ratio at θ_i and Δc_j is the standard deviation of the concentration c_j. Similar calculations are performed to establish the errors associated with the mean square radius values.

The calculations discussed briefly above are both complex and essential for any MALS determinations of molecular and particle properties. With today's armamentarium of high-speed and low-cost computing, all the benefits of MALS should be realized by all laboratories. Most important among such benefits is the ability to judge the precision of the results reported.

A variety of other quantities essential for the characterization of molecular and particle samples must also be reported with a measure of their precision. Once again, only by performing detailed analyses based upon the well-proven application of error propagation can MALS measurements, or for that matter any measurements, be considered a valid and reproducible technique.

Other quantities determined from MALS directly whose precision is essential include the various moments of the mass and size distributions so calculated. Typical among them are the weight, number, and z-average molar mass (see Sec. 9). In the case of fractionated proteins, for example, the monomeric masses must be presented as precisely as possible to provide the user continuing "cold comfort" for the MALS measurement. Protein masses are generally known *a priori* in any event from calculations based on DNA sequencing. References to so-called standards used for empirical studies are always valuable. With precision insured by reporting of

© 2004 by Marcel Dekker, Inc.

standard deviations of the measured quantities, systematic errors are more easily identified. Such might include selecting the wrong wavelength for the light source used, entering the wrong value of the refractive index increment, erroneous calibration of the refractive index or other concentration sensitive detectors, errors in calibrating the MALS photometer, and so on.

The importance of the Zimm plot procedure to yield the second virial coefficient, weight-average molar mass, and average mean-square radius for unfractionated samples requires that MALS software be capable of performing such determination, as well. This is easily implemented by preparing a set of aliquots spanning a broad range of unfractionated sample concentrations. Using a syringe pump or large injection loop plus chromatographic pump, individual aliquots are injected sequentially during a "collection" event. The resulting chromatograph at each scattering angle appears as a series of plateaus such as shown in Fig. 4 for the scattering at 90° from aliquots of starch sample in 90% DMSO. A peak region is selected from each plateau as indicated by the vertical lines. The software then combines the corresponding data from all scattering angles averaged over each peak region with the user-entered concentration of each prepared aliquot to yield a Zimm plot such as that shown in Fig. 5. From this plot, the software calculates the molar mass $(7.46 \pm 0.09) \times 10^6$, the r.m.s. radius 85.7 ± 1.7 nm, and the second virial coefficient $(1.46 \pm 0.19) \times 10^{-5}$ mol mL/g^2. All software should be able to calculate and plot the important distributions of mass and r.m.s. radius (for MALS, the latter has a lower limit of about 8–10 nm).

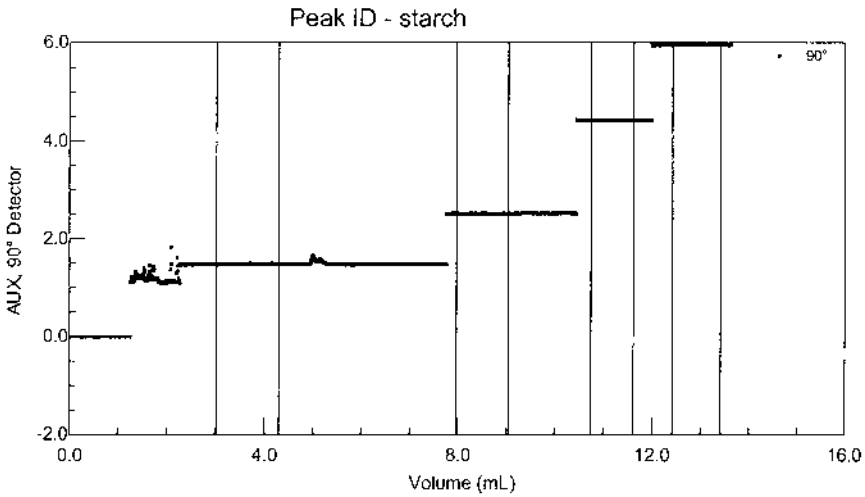

Figure 4 Series of plateaus at 90°, each corresponding to a different starch concentration injected into a flow cell using a syringe pump.

© 2004 by Marcel Dekker, Inc.

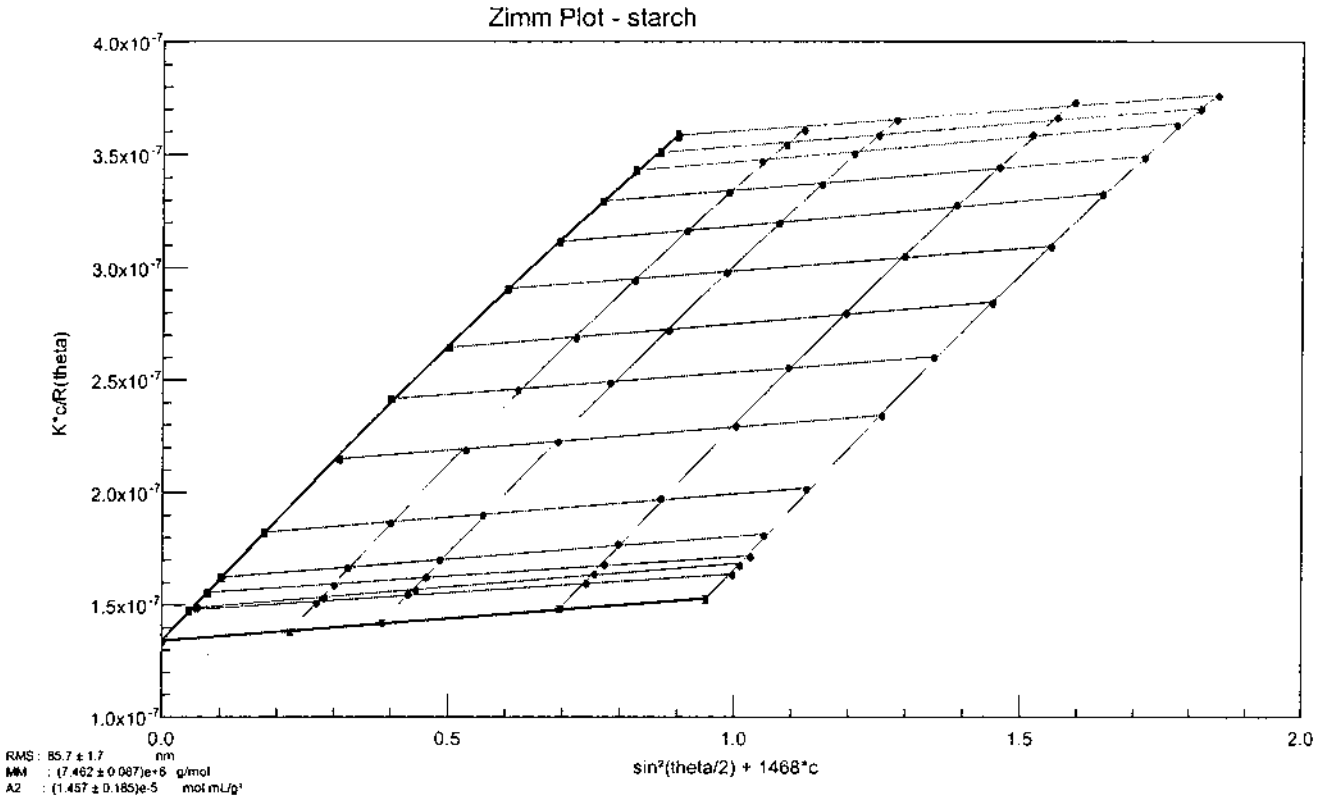

Figure 5 Software generated Zimm plot for the data of Fig. 4.

© 2004 by Marcel Dekker, Inc.

These include the differential weight fraction distributions of both mass and size, the corresponding cumulative distributions, the conformation plot ($\log M_w$ vs. $\log r_g$), as well as the "calibration" curve ($\log M_w$ vs. elution volume) and related plots. Details of these quantities are described in Shortt's article (17).

Because the MALS software calculates both M_w and r_g (for large enough molecules) throughout the separated distributions present in the samples, for a variety of molecular species one may calculate the eluting sample's intrinsic viscosity, $[\eta]$, at each slice using the Flory–Fox equation (18):

$$M_w[\eta] = \Phi(\sqrt{6}r_g)^3 \tag{7}$$

where $\Phi(\equiv\Phi_0 = 2.87 \times 10^{23})$ is the so-called Flory viscosity constant. In general, the excluded volume effect is taken into account via the Ptitsyn–Eizner equation (19) $\Phi = \Phi_0(1 - 2.63\varepsilon + 2.86\varepsilon^2)$ and ε ranges from 0 at the theta point to 0.2 for a good solvent. The software can then calculate and plot the so-called Mark–Houwink–Sakurada plot. An example for the NIST broad polystyrene standard NBS706 is shown in Fig. 6.

Band broadening plays a major role in distorting the calibration curve ($\log M_w$ vs. elution volume V) of eluting species of extremely narrow size distribution. This is particularly noticeable for proteins whose masses (following separation of aggregates) should be monodisperse. Over the years, numerous papers and books have been written on the subject of correcting for such

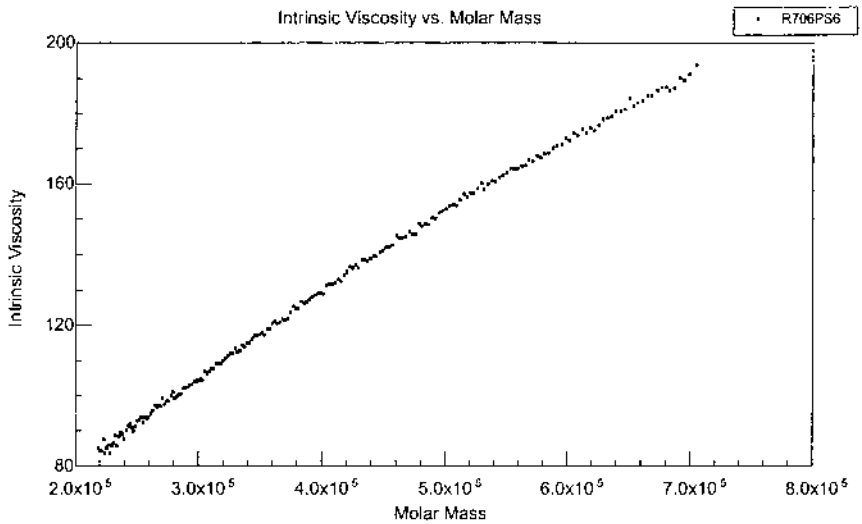

Figure 6 MHS plot of NBS706.

© 2004 by Marcel Dekker, Inc.

broadening, yet for the most part, it has been difficult to implement such methods. The problems associated with band broadening are clearly shown in Fig. 7 where MALS data of a BSA (bovine serum albumin) sample containing various aggregate states have been processed. Most of the band broadening arises from the large dead volume of the DRI unit relative to the MALS detector. The MALS peak has been broadened by the DRI (after concentration and MALS data are combined to calculate molar mass of the separated sample) resulting in a "grimace-like" appearance to the mass presentation instead of a flat, constant mass vs. elution volume. Figure 8 shows these same data corrected by the software using a proprietary correction method developed by Steven Trainoff. The monomer (largest peak) and dimer aggregate are clearly shown to be monodisperse, whereas the peaks corresponding to higher aggregates clearly show (after correction for band broadening) their unresolved polydisperse composition.

Another important object of MALS software relates to its handling of noise. Such noise, especially at very low angles, literally can overwhelm the associated signals (see Sec. 6 for additional comments.). Although careless sample preparation is often associated with the presence of dust or related debris affecting most the smaller scattering angles, aging columns that have begun to shed both column packing materials as well as remnants of prior samples can produce overwhelming scattering at smaller scattering angles. These contributions to noise can be especially troublesome in the presence of elutions of relatively small molar mass. If any significant filtering of such noise contributions is to be achieved by the

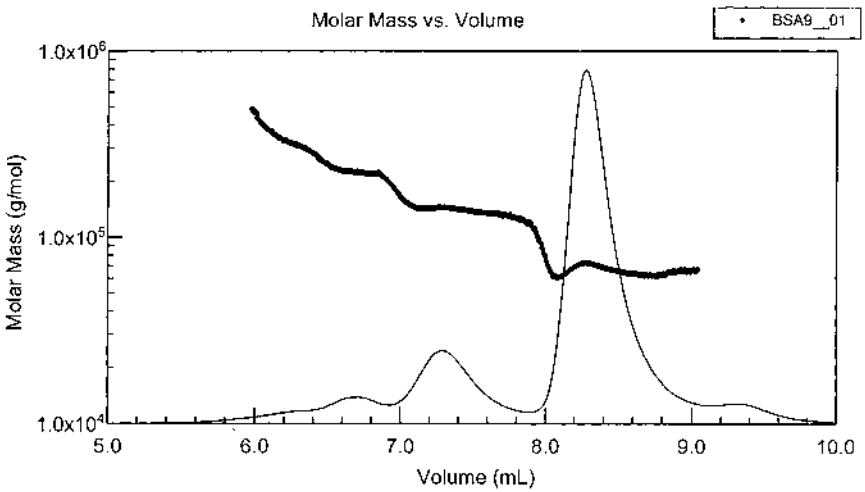

Figure 7 Calculated molar mass vs. elution volume for a BSA sample clearly showing the effects of band broadening.

© 2004 by Marcel Dekker, Inc.

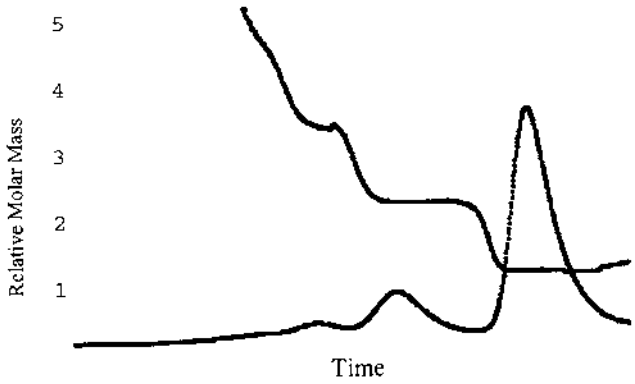

Figure 8 Data of Fig. 7 corrected for band broadening.

software, control of such functions must remain with the software user and cannot be performed automatically. Consider the data shown in Fig. 9 corresponding to the light scattering signals reported by software associated with a low-angle light scattering (LALS) device at about 7°. This same sample was then allowed to flow through a MALS detector whose light scattering signals at a larger angle of 14° are shown in Fig. 10. Note that despite the smaller collection angle associated with the LALS measurement, the noise appears even *smaller* than that corresponding to the

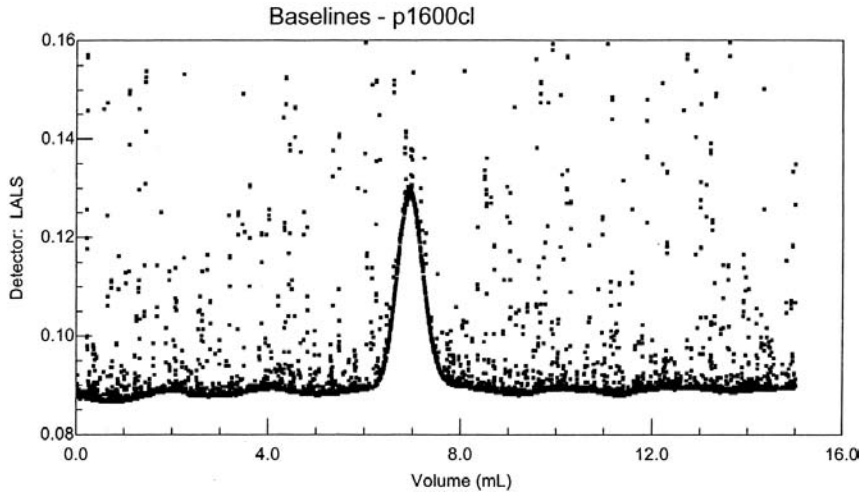

Figure 9 Light scattering data presented by software associated with a low-angle light scattering instrument from a measurement at about 7°.

© 2004 by Marcel Dekker, Inc.

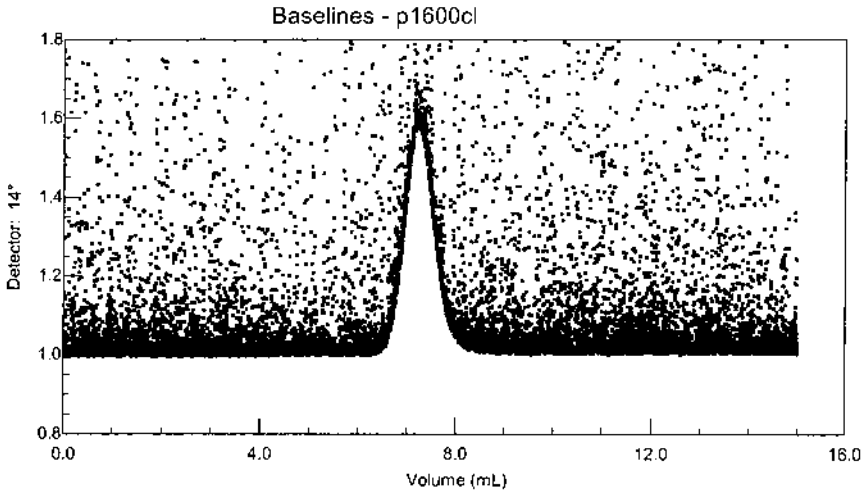

Figure 10 Light scattering data presented by ASTRA software from a measurement of the same sample shown in Fig. 9 but at a scattering angle of about 14°.

larger scattering angle signals collected by the MALS detector. Applying moderate data spike removal algorithms to the data of Fig. 10, the data are modified to appear as shown in Fig. 11. Without knowledge that the data of Fig. 9 had been preprocessed by the software (as well as passing through an on-line prefilter), the sample associated with Fig. 10 would appear to be quite different. In addition, were the source of the noise of Fig. 10 caused by a failing column, the user would have been warned by reference to the poor data quality. However, software that attempts to "beautify" the data without warning the user of such attempts at cosmetic repair must be avoided. Interestingly, such hidden data beautification also affects the "cleaned" data quality by changing the shape of the eluted peak with increased filtering.

Software that doctors collected data without knowledge of the user will often present the user with a feeling of comfort of his/her preparative work to the detriment of the quality of the final report. In recent years, the Federal Food and Drug Administration (FDA) has introduced new rules for the pharmaceutical industry to ensure that data are not modified by the software without providing a clear, traceable record. Indeed, all drug development and production dependent upon software-processed data collected by compliant instrumentation must be compliant with the FDA's associated Code of Federal Regulations (Title 21), Section (or "Rule") 11 (21 CFR 11, for short) (www.fda.gov/ora/compliance_ref/part11). It is the responsibility of the pharmaceutical user to confirm (generally by independent audit) that MALS software is compliant with 21CFR11.

© 2004 by Marcel Dekker, Inc.

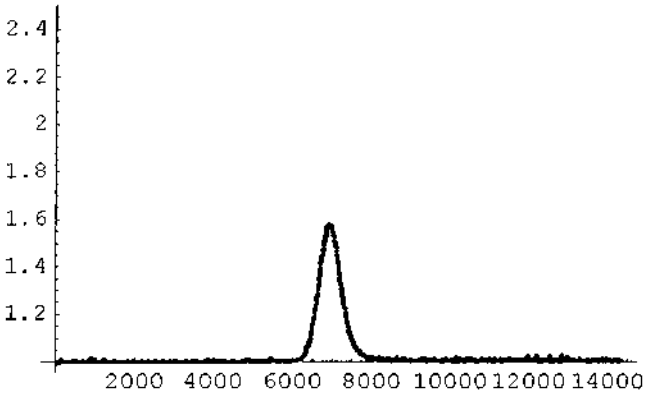

Figure 11 Data of Fig. 10 with spike removal software activated.

6 WHY MULTI-ANGLES?

It should be evident from Fig. 3 that noisy data presented without a measure of its statistically expected fluctuations can result in the reported measurements being both erroneous and misleading. In addition, if the data are processed properly, there should be no need to discard them because of the presence of such noise; only the reported *precision* of the results presented will be affected. To within the limits proscribed by such precision limits, the data will have an associated validity. It is those limits of precision by which the experimentalist will decide to keep, discard, or repeat the experimental determinations. Unfortunately, without those quantitative measures of experimental precision, as has been the case historically with many light-scattering instruments, there is virtually no objective basis for excluding data known to be flawed.

The use of a plurality of measurements over a broad range of scattering angles has three benefits. First, of course, is the increased *precision* of the measurement. This is most easily understood if we consider as an example measurement of a sample of relatively small size. For such molecules, the scattering should be the same at all angles. Thus low molar mass samples are processed as if the measurements at each angle were independent of those made at other angles. So for the case of N angles, we have made the determination N times with an expectation of a $\sqrt{N}$-fold increase in precision. The same holds true when fitting the measured excess Rayleigh ratios as a function of $\sin^2 \theta/2$ (the Zimm plot). Each measurement included in the fitting procedure improves the precision of the final result. Here, however, each measurement is weighted statistically, so that points with high uncertainties have an associated low weight.

© 2004 by Marcel Dekker, Inc.

The second most important element of multi-angle measurements is their built-in redundancy. In the event that any detector became unusable and whose results, therefore, had to be discarded (a failed photodiode because of electrical problems, solution-borne obstructions that may block the scattered light from certain detectors, and so on), the deletion of one or more such detector signals from the final analysis would have a far smaller effect on the resultant calculations because there would be so many additional detectors to compensate for any losses.

Finally, with measurements spanning a broad range of scattering angles, the ability to measure larger particles whose scattering characteristics show much steeper, and/or nonlinear behavior with scattering angle is enhanced by the presence of more detector angles.

Let us consider a simple comparison of so-called "clean" chromatography with "poor" chromatography: the distinction related qualitatively to the contributions of noise to the signals. (See also the discussion of Sec. 5.) The sources of noise could be the shedding of the separation columns, the careless preparation of the samples, faulty mobile phase filtering, degassing problems, and so on. Figure 12 shows the excess Rayleigh ratios measured from a sample of acid-degraded amylopectin, which resulted in very clean signals at all detectors. The trace labeled AUX corresponds to the DRI detector (corrected for the delay volume between it and the MALS unit. Figure 13 shows the resultant fits at a single

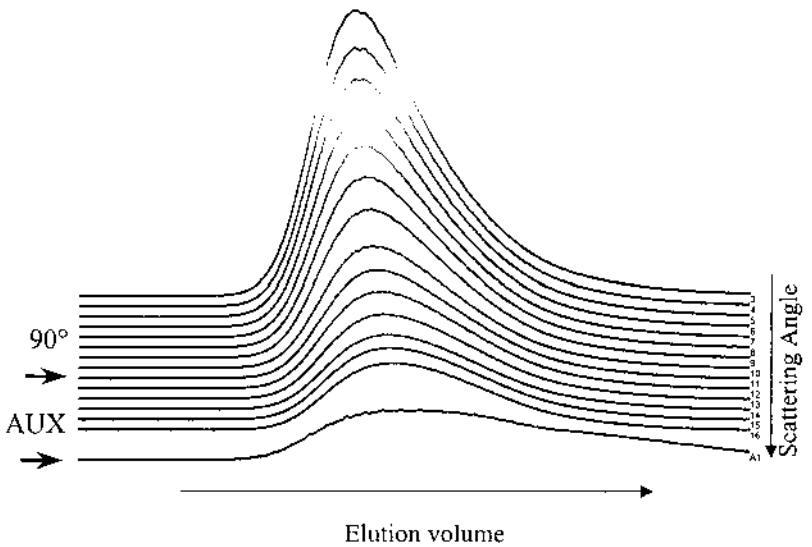

Figure 12 Three-dimensional plot of excess Rayleigh ratios as a function of elution volume for "good" chromatography: one trace for each scattering angle.

© 2004 by Marcel Dekker, Inc.

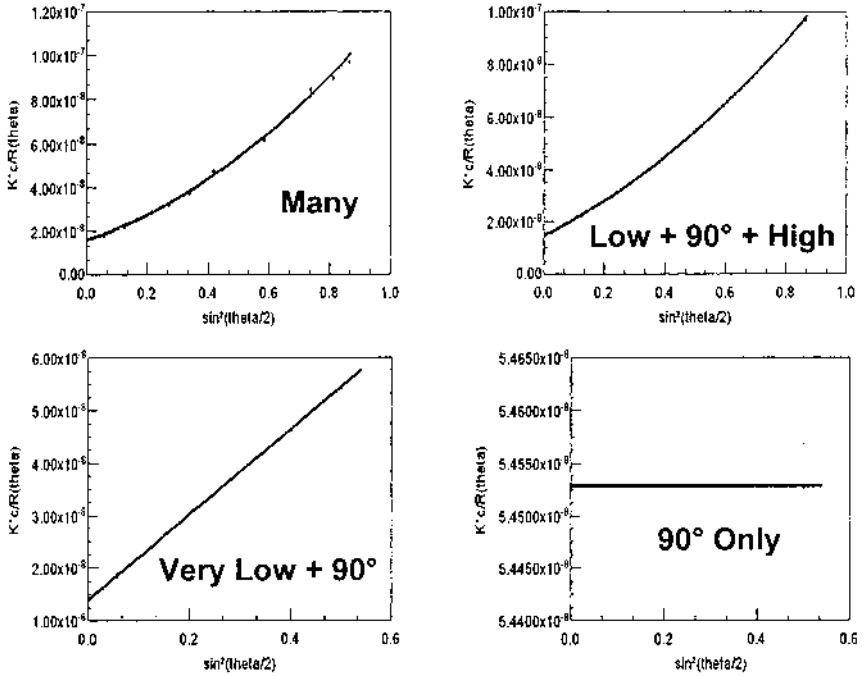

Figure 13 Fits to data collected at a slice near the peak of Fig. 12 for MALS, three-angle detector, dual angle detector, and single 90° detector.

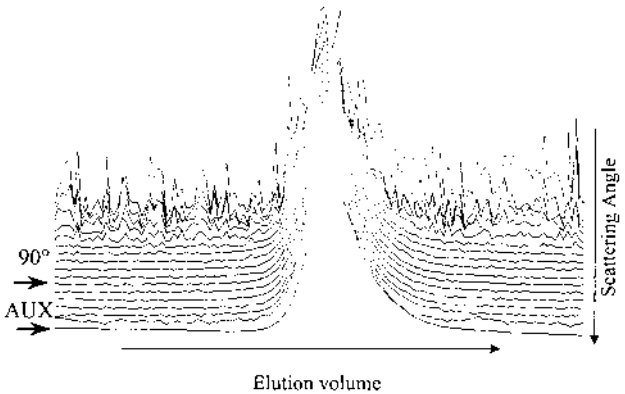

Figure 14 Three-dimensional plot of excess Rayleigh ratios as a function of elution volume for "poor" chromatography: one trace for each scattering angle.

© 2004 by Marcel Dekker, Inc.

slice (near the top of the peak region of Fig. 12) for the many detectors (MALS), a triple detector, a dual angle detector, and a single (90°) detector. Note the extremely small error bars associated with the data points fit.

For a poor chromatography example, consider Fig. 14, which shows the excess Rayleigh ratios measured from a sample of 400k pullulan which resulted in very noisy signals at the low-angle detectors. Figure 15 shows the resultant fits at a single slice (near the top of the peak region of Fig. 14) for the many detectors (MALS), a triple detector, a dual angle detector, and a single (90°) detector. Note the extremely large error bars associated with the smaller angle data points. (We have seen similar fits in Fig. 3.) For this case of poor chromatography, the errors associated with the points add tremendous uncertainty to the two-angle results. Naturally with a light scattering detector situated at 90° only, for all but the smallest molecules, the results will be far from correct.

Table 1 summarizes the errors associated with the use of two, three, and many detectors in the calculation of molar mass and r.m.s. radius under conditions

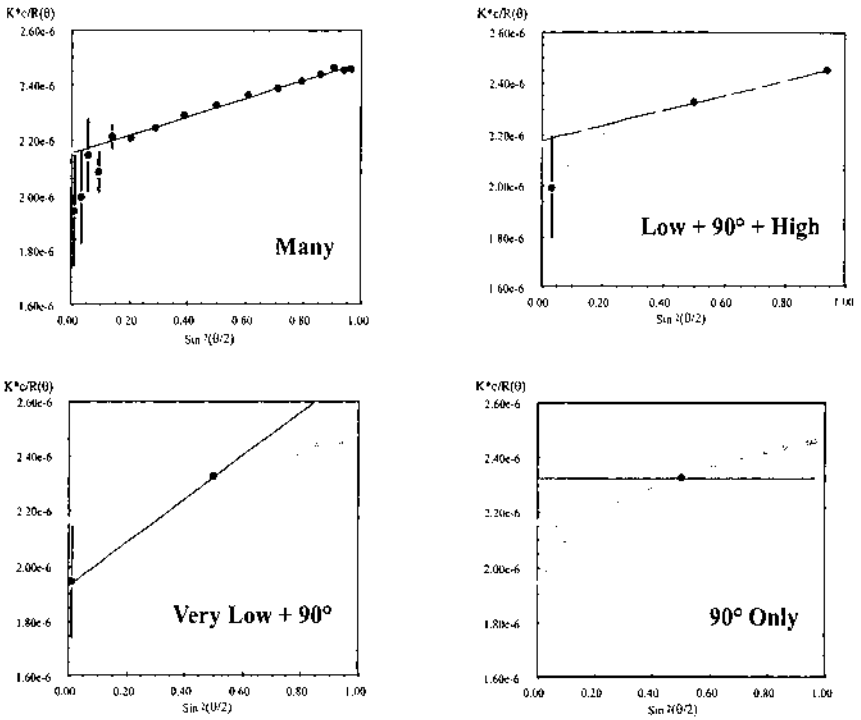

Figure 15 Fits to data collected at a slice near the peak of Fig. 14 for MALS, three-angle detector, dual angle detector, and single 90° detector.

© 2004 by Marcel Dekker, Inc.

Table 1 Errors (in %) Characteristics of Good and Poor Chromatography

Angles	Molar mass	Radius
Good chromatography		
Many	0.07	0.6
Low + 90° + High	0.2	2
Very low + 90°	0.6	10
Poor chromatography		
Many	0.5	3.0
Low + 90° + High	1	5
Very low + 90°	14	80

of good and poor chromatography. Naturally, single 90° detectors cannot be expected to yield any reliable results for molecules whose size may be measured from MALS.

7 COPOLYMERS

Copolymers may be formed of monomers A and B in a random manner, that is, of a structure such as AABABBABABAABBABA, or with monomer blocks such as AAA and BBB to form a block copolymer such as AAABBBBBBAA-ABBBAAAAAA, and so on. These copolymers, in turn, may be homogeneous (that is, with relative contribution of each homopolymer independent of molar mass) or heterogeneous (that is, with varying relative compositions that vary with molar mass). Since each homopolymer has its corresponding dn/dc, it becomes very difficult to characterize the scattered light from chromatically separated species of such copolymers in terms of a specific molar mass at each elution. However, if the copolymer is homogeneous, we may then take a *weighted* average of the two dn/dc values dn_A/dc and dn_B/dc. Heterogeneous copolymers present a challenge for MALS because there are many combinations that could produce copolymers having identical hydrodynamic sizes, that is, that therefore would co-elute if separated by SEC columns, for example. For such separations, each slice would be expected to contain a variety of molecular structures and molar masses.

The reader should be aware that the light scattering characteristics of polymers (and copolymers) are assumed to be described by the Rayleigh–Gans–Debye (RGD) approximation discussed, for example, in Refs 5 and 14. In this approximation, each constituent of a molecule scatters light independently

© 2004 by Marcel Dekker, Inc.

of any other constituent. One might be tempted, therefore, to assume that a copolymer composed of various combinations of two monomers could be treated as if the different monomeric components scattered light in the absence of the other monomeric constituents. Thus, were it possible to know the relative composition of each homopolymer at each slice, then one might obtain a weight-average value of each constituent eluting in that slice and, therefrom, a weight-average of the copolymer in that slice. Unfortunately, the polarizability of a copolymer molecule, and therefore its effective dn/dc value, depends critically upon the composition of the molecule. The problem is far more complicated here for an unfractionated sample than for the case discussed earlier of a homogeneous copolymer whose composition is independent of molar mass. The difficulties and complex means by which the weight-average molar mass of such an unfractionated sample be determined was described by Benoit and Froelich (20). It should be emphasized that even after separation by SEC, a particular slice still contains a distribution of molar masses since the different molar masses present can have a large variation despite the fact that they share an equivalent hydrodynamic size.

Because MALS has proven to be so successful a means for the determination of molar mass for homogenous copolymers, attempts always persist to find a means by which molar mass may be deduced even for such complex systems of heterogeneous copolymers. Since the thermal conductivity of a copolymer molecule depends on its composition, the possibility of using thermal FFF as a separation technique (16) remains a possibility to be explored. Unfortunately, the actual result of such separation in terms of molar mass or size remains unknown. Other attacks on the problem have been suggested in the past including finding a solvent that is isorefractive for one component, thereby permitting the measurement of the "visible" component. From the measured concentration of this component, one could change solvents to obtain a measure of the sum of the contributions and from those, attempt to determine the sample's weight-average molar mass. However, note all the additional complications such an approach would entail. As each solvent is introduced, the dn/dc values for each homopolymer constituent would change, as would the separation mechanism itself. Alternatively, one might try to find a solvent whereby the differential refractive index of each homopolymeric constituent would be of the same magnitude but of different sign. Thus the $(dn/dc)^2$ factor of K^* in Eq. (1) would be the same for each component. Yet, the concept of separating the molecules by molar mass remains elusive and unpredictable for such heterogeneous copolymers. The objective of determining the molar mass distribution often remains elusive.

Generally, attempts to separate compositional distributions from molar mass distributions for such heterogeneous copolymers have been all but abandoned by the decision to treat all such copolymers as having the properties of a

© 2004 by Marcel Dekker, Inc.

homogeneous copolymer, that is, taking some kind of average dn/dc value measured experimentally from a set of unfractionated sample aliquots. The "accuracy" of such an assumption may then be checked by integrating the concentration detector response and comparing this recovered mass with the known injected mass. The greater the departure from homogeneity, the greater should be the discrepancy of these two results. Unfortunately, the total mass recovered may not be complete because of column retention of some components: a further complication. Although some form of molar mass distribution may be generated on this basis, its accurately reflecting the true nature of the real molecular structure must remain uncertain.

There are certain classes of copolymers for which mass, size, and compositional distributions (stoichiometry) may be obtained following separation by using MALS in combination with both UV and DRI detectors. These copolymers have a homopolymeric component that produces no UV signal, that is, it has no absorption at the UV wavelength commonly used. Among them are so-called conjugated proteins comprised of a protein to which has been attached (either by natural or synthetic means) a polymer (conjugate) that has no chromophoric components. Most common among these are polysaccharides (producing "glycosylated proteins") and poly(ethylene) glycol (producing "pegylated proteins"). The stoichiometry of protein–protein complexes where each protein constituent may be conjugated has been studied by many groups. Wen *et al.* (21) and Kendrick *et al.* (22) illustrate the techniques most frequently applied using UV, DRI, and MALS detectors, although there are some questions remaining as to how the weighted dn/dc values are calculated. The Wen *et al.* paper provides an interesting discussion of an iterative approach whereby the relative proportions of the (possible) two conjugated proteins are derived iteratively. The special case whereby the UV detector may be used adds some simplification to the Benoit and Froelich (20) method that introduced the concept of an apparent molar mass that varied with the solvent used. The UV detector adds additional information of help in establishing the stoichiometry of the molar mass distribution expected to be present even within an SEC-separated elution slice.

A particularly simple example associated with such conjugated structures occurs when the "core" is a single protein monomer. Separation of the conjugate by SEC should be by hydrodynamic size and this in turn depends only on the amount of *conjugate* attached. Each component has its distinct value of dn/dc and the MALS measurements are combined with both UV and DRI measurements of the eluting sample. The UV signal at each elution volume yields the concentration of the polypeptide (protein) in that elution. If ε_p is the protein extinction coefficient whose corresponding differential refractive index increment (for the solvent used) is $(dn/dc)_p$, the protein concentration c_{pi} at elution slice i is simply UV/ε_p where UV is the calibrated UV detector response. If $(dn/dc)_B$ is the differential refractive index increment of the conjugate, the weighted differential refractive index

© 2004 by Marcel Dekker, Inc.

increment for the copolymer at slice i is just

$$\left(\frac{dn}{dc}\right)_{\mathrm{pB}i} = \frac{c_{\mathrm{p}i}}{c_{\mathrm{p}i} + c_{\mathrm{B}i}}(dn/dc)_{\mathrm{p}} + \frac{c_{\mathrm{B}i}}{c_{\mathrm{p}i} + c_{\mathrm{B}i}}(dn/dc)_{\mathrm{B}} \tag{8}$$

Returning to Eq. (1) and extrapolating to $\theta = 0$, we have for slice i

$$\frac{K^* c_i}{R_i(0^\circ)} = \frac{4\pi^2 n_0^2}{N_A \lambda_0^2 R_i(0^\circ)} \left[\frac{c_{\mathrm{p}i}}{c_{\mathrm{p}i} + c_{\mathrm{B}i}}(dn/dc)_{\mathrm{p}} + \frac{c_{\mathrm{B}i}}{c_{\mathrm{p}i} + c_{\mathrm{B}i}}(dn/dc)_{\mathrm{B}}\right]^2$$

$$= \frac{1}{M_{\mathrm{p}} + M_{\mathrm{B}i}} \tag{9}$$

Since $c_i = c_{\mathrm{p}i} + c_{\mathrm{B}i}$ is measured by the DRI as

$$c_i = c_{\mathrm{p}i} + c_{\mathrm{B}i} = \frac{RI}{[c_{\mathrm{p}i}/(c_{\mathrm{p}i} + c_{\mathrm{B}i})](dn/dc)_{\mathrm{p}} + [c_{\mathrm{B}i}/(c_{\mathrm{p}i} + c_{\mathrm{B}i})](dn/dc)_{\mathrm{B}}} \tag{10}$$

where RI is the calibrated RI detector response, Eq. (10) is easily solved for $c_{\mathrm{B}i}$ ($c_{\mathrm{p}i}$ having been determined from the UV detector). Since M_{p} is the known protein monomer, the measurement of $R_i(\theta)$ extrapolated to $\theta = 0^\circ$ combined with the determinations of $c_{\mathrm{p}i}$ and $c_{\mathrm{B}i}$ yields the conjugate mass $M_{\mathrm{b}i}$ from Eq. (9). Calculating the distributions of the amount of conjugate in the sample becomes a straightforward exercise. It should be noted, however, that the polarizabilities of the molecules have been assumed to be additive in Eq. (8). Stockmayer *et al.* (23) have shown that for the case of block copolymers, this assumption should be particularly true, but for random copolymers the hypothesis is more difficult to justify. As conjugated proteins are very similar to block copolymers, this assumption has been used.

A far more difficult analysis is required if the protein exists in several aggregated states. Each of these states may be conjugated and a distribution of copolymers may be present in each slice. A given slice may contain a range of such protein aggregates whose varying conjugate coats have produced the same hydrodynamic size and, therefore, co-elution. The presence of such aggregates can be a major impediment to quantifying the stoichiometry. These slice-by-slice determinations become even more difficult because of band broadening which, if not suitably corrected, can seriously distort the results (22). In such cases, peak areas are used to obtain rather crude results relative to what one might have obtained with software correcting such band broadening. Fortunately, new software corrects for these band broadening distortions.

Finally, a few comments about protein–protein interactions and their quantitation. The association of various nonchromophoric conjugates with proteins may be determined by similar techniques as long as each slice contains a single protein–protein associate. Wen *et al.* (21) have shown how an iterative

© 2004 by Marcel Dekker, Inc.

process may be used to identify the correct association of the protein component. However, if a distribution of associates is present, the method described above well may yield misleading and quantitatively wrong results.

8 BRANCHING

The characterization of branching by MALS has long been an objective beginning with the seminal paper on the subject by Zimm and Stockmayer (24). At that time SEC had not been invented. Indeed, the only means of fractionating a sample was by precipitation fractionation, which yielded broad fractions and rendered attempts to measure distributions present futile. Nevertheless, by making a plot of $\log(M)$ vs. $\log\langle r_g^2\rangle$, even of such crude fractions should reveal some quantitative elements of the presence of branching. Indeed, this approach was used later by Podzimek *et al.* (25) who plotted $\log(r_g)$ vs. $\log(M)$ instead. Further details of Podzimek's approach are discussed in Sec. 10 and in Ref. 25.

The quantitation of branching generally begins from calculation of the so-called branching ratio

$$g = \frac{1/M \int r_b^2 \, dm}{1/M \int r_l^2 \, dm} = \frac{\langle r_{gb}^2 \rangle}{\langle r_{gl}^2 \rangle} \tag{11}$$

where the mean-square radii are calculated for the branched (b) and linear (l) molecules at the *same* molar mass. For the same molar mass, the branched molecules will be more compact than their linear counterparts and, therefore, the branching ratio will be less than unity. The ASTRA® software (Wyatt Technology Corporation, Santa Barbara, California, U.S.A.) provides means to calculate the average number of branch units per molecule, B, for both trifunctional (three units joined at one point) and tetrafunctional (four units) branching based on the corresponding relations (24)

$$g_3(B) = \left[\sqrt{\left(1 + \frac{B}{7}\right)} + \frac{4B}{9\pi}\right]^{-\frac{1}{2}} \tag{12}$$

and

$$g_4(B) = \left[\sqrt{\left(1 + \frac{B}{6}\right)} + \frac{4B}{3\pi}\right]^{-\frac{1}{2}} \tag{13}$$

From these results one may calculate long-chain branching defined as the number of branches per 100 repeat units. Further details and examples, especially for the

© 2004 by Marcel Dekker, Inc.

case of a highly branched high-temperature metallocene, are found in the article by Trainoff and Wyatt (26).

The improvement in branching analyses, especially since the work of Zimm and Stockmayer and with the advent of SEC, has been significant. Unfortunately, there still remain some problems. Foremost among them is the requirement that a linear analog of the branched sample be available for the calculation of the branching ratio of Eq. (11). This is often difficult to find. Then there is the equally serious problem that an elution slice actually corresponds to a single mass. Because of branching, there will be many different masses that are branched to varying degrees yet have the same hydrodynamic size and thus co-elute. Each slice, therefore, may contain a relatively large mass distribution and not be monodisperse. Analyses based upon the assumption of monodispersity must be weighed carefully, especially if anomalous results are derived. This problem is very similar to MALS measurements of copolymers whereby for heterogeneous copolymers, a given elution slice may contain a broad range of molar masses.

Interestingly, the Zimm–Stockmayer paper contained two paragraphs about viscometry and discussed how measurement of the ratio of *intrinsic viscosities* for branched and linear molecules might provide a parameter similar to the *g*-factor of Eq. (11), that is, a measure of the degree of branching in a sample. This hope has been used extensively as the basis of the belief that viscometric measurements could be used to quantitate branching. However, the last sentence of the viscometry discussion (24) concludes with the statement "... clearly it is still hazardous to draw inferences about branching from empirical viscosity–molecular weight relationships, and the method based on evaluations of $\langle r_g^2 \rangle$ from light scattering is much to be preferred."

9 MASS AND SIZE DISTRIBUTIONS

An important result derivable from MALS measurements following chromatographic separation is the ability to determine both differential and cumulative distributions in both mass and r.m.s. size for each sample successfully separated. Shortt (17) has described these and related quantities in depth in his 1993 article. There are few measurements able to characterize a sample more precisely than the differential weight fraction distribution. Indeed, because of the associated error analyses, such quantitation has been used extensively in quality control applications. Until Shortt's article, the definitions were confusing and some were erroneous (28) because of confusion with the meaning of the logarithm to base 10.

In addition to the differential and cumulative distributions, an important measure of a molecular species are the number-, weight-, and z-averages of the

© 2004 by Marcel Dekker, Inc.

fractionated sample. They represent three moments of the distributions present. In terms of the numbers of molecules present in each slice separated by, for example, SEC, these quantities are given simply by

$$M_{\mathrm{n}} = \frac{\sum_i n_i M_i}{\sum_i n_i} \tag{14}$$

$$M_{\mathrm{w}} = \frac{\sum_i n_i M_i^2}{\sum_i n_i M_i} \tag{15}$$

$$M_{\mathrm{z}} = \frac{\sum_i n_i M_i^3}{\sum_i n_i M_i^2} \tag{16}$$

where n_i is the number of molecules in slice i whose weight-average molar mass is M_i. Since MALS measurements measure the *concentration* at each slice by the concentration detector (DRI or UV) rather than the number density, Eqs (14), (15), and (16) must be re-expressed in terms of the concentrations c_i. Since M is expressed in g/mol and c in terms of g/mL, $c_i = n_i M_i / N_A$ with N_A Avogadro's number. Thus we re-write these in terms of the measured concentrations to obtain

$$M_{\mathrm{n}} = \frac{\sum_i c_i}{\sum_i (c_i / M_i)} \tag{17}$$

$$M_{\mathrm{w}} = \frac{\sum_i c_i M_i}{\sum_i c_i} \tag{18}$$

and

$$M_{\mathrm{z}} = \frac{\sum_i c_i M_i^2}{\sum_i c_i M_i} \tag{19}$$

The *polydispersity* of a sample is then defined (17) as the ratio of $M_{\mathrm{w}}/M_{\mathrm{n}}$, or simply

$$P = \frac{M_{\mathrm{w}}}{M_{\mathrm{n}}} = \sum_i c_i M_i \sum_i \frac{c_i}{M_i} \tag{20}$$

Although an important quantity often referred to as an essential characterization parameter, MALS software must present each result with its measured precision. Once again, this complex calculation is based on the errors associated with both mass and concentration at each slice measured.

Equation (20) is often misunderstood and exaggerated in its use as a characterization tool. For example, it is a simple matter to calculate the

© 2004 by Marcel Dekker, Inc.

polydispersity of a sample comprised as 50% by weight of two monodisperse polymers, one of molar mass M and the other of molar mass $2M$. The result is simply $P = 1.125$, which is generally believed to be a "small" polydispersity despite the 100% range of molecules present. Results of polydispersity calculations performed by MALS have been criticized repeatedly in the literature as being too *small* as the sensitivity of MALS measurements decreases with decreasing molar mass. Certainly M_w is best measured by MALS and M_n by membrane osmometry, yet this idea has been debunked recently by Podzimek (29) who made meticulous MALS measurements as well as membrane osmometry determinations for several polymers. His conclusion was that MALS yields the most plausible values of polydispersity despite its decreasing sensitivity with decreasing molar mass. A powerful example of a truly (confirmed by MALS) monodisperse sample was analysed by Shortt (27). His study showed that certain polystyrene standards are actually far narrower than their manufacturers believe.

10 THE PERFECT COMPANION FOR SEPARATION SCIENCES: MALS

There are virtually no liquid chromatography techniques for which the addition of sequential classical light scattering measurements through MALS cannot benefit inordinately. Not only are all results previously based on calibration methods and related empirical methods rendered absolute, but information regarding the separation processes themselves is often revealed. An extensive bibliography of well over 1,500 peer-reviewed papers describing the ever-increasing range of results and applications may be found at www.wyatt.com.

Poor chromatography (that is, a possible wrong choice of columns or mobile phase, or both) is often seen immediately by examining the MALS output. Thus Fig. 16, for example, shows the MALS r.m.s. radius vs. SEC elution volume for a high molar mass polysaccharide. Note that the elution is not characteristic of SEC where we expect radius to decrease with elution volume. The separation indicates that the method was flawed because of poor chromatography.

The presence of long-chain branching is detected quite easily through MALS when a so-called conformation plot (14) is made following sample elution. Figure 17 shows such a plot (25) of the log(r.m.s. radius) vs. log(mass) for linear and randomly branched polystyrene. The linear molecules exhibit a slope consistent with a random coil (0.5–0.6) whereas the branched molecules produce a conformation whose compactness increases with molar mass (slope decreasing from that of the linear polymer).

Many powerful examples of MALS may be seen in reversed phase chromatography where the elution depends on the molecular/column affinity

© 2004 by Marcel Dekker, Inc.

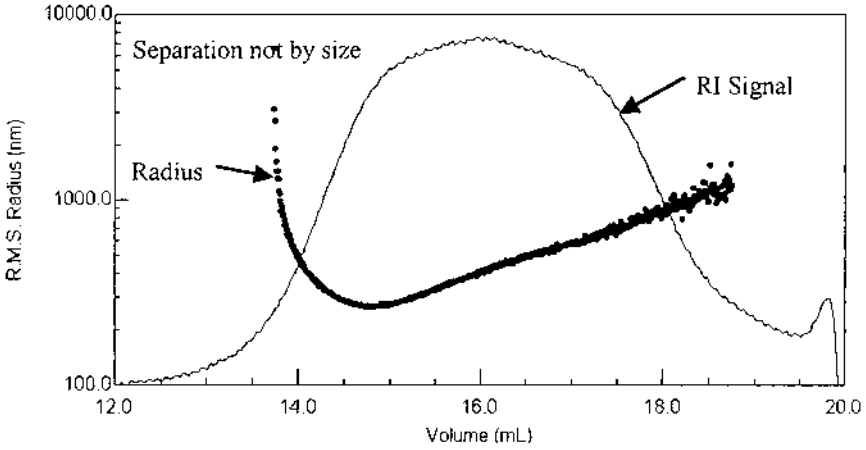

Figure 16 An example of poor SEC chromatography.

with respect to the variable mobile phase. Figure 18 shows (30) the UV detector signal and the 90° MALS signal for the elution profile of some fibroblast growth factor multimers. Two dimer forms with identical mass are seen to elute at different times. Calibration techniques are generally useless for reversed phase separations.

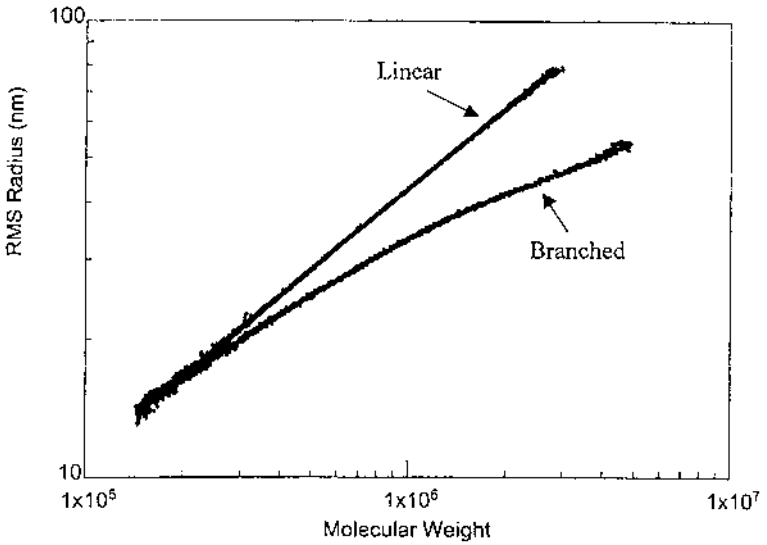

Figure 17 Conformation plots of linear and randomly branched polystyrene.

© 2004 by Marcel Dekker, Inc.

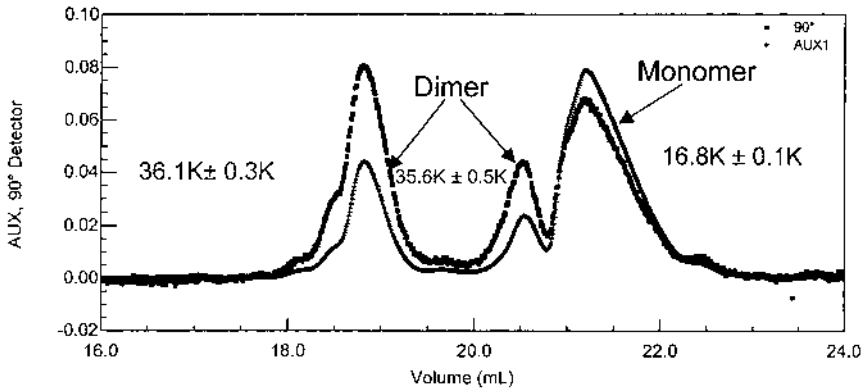

Figure 18 Elution profile of some fibroblast growth factor multimers. Two dimer forms with identical mass elute at different times.

Numerous studies have been presented in the literature confirming the absolute measurement capability of MALS. Proteins in particular have been useful examples of such validation since many protein masses are known *a priori* from sequence and amino acid and carbohydrate composition. Jiu *et al.* have shown (31) good agreement for MALS-derived results of protein complexes with both sedimentation equilibrium and molar masses calculated from amino acid and carbohydrate composition. Li *et al.* have compared (32) MALS results with small angle x-ray scattering and calculated masses for some chimeric proteins. Another powerful comparison (33) was carried out by Singer *et al.*, wherein the authors report a comparison of MALS with analyses of similar molecules by SDS-PAGE, SE, and MALDI-TOF mass spectroscopy.

Although at this time, the only commercial MALS systems that may be coupled to chromatographs are the DAWN® detectors of Wyatt Technology Corporation, there can be little doubt that in the years ahead there will be others. A seven-angle detector has been introduced by Brookhaven Instruments Corporation (Holtsville, New York), though no published chromatography results have been seen at the time of this writing. Two-angle light-scattering detection systems are manufactured by both Precision Detectors, Inc. (Bollingham, Massachusetts) and Viscotek, Inc. (Houston, Texas). Both are available in single 90° angle modes with application to small molar mass samples, although the former actually collects scattered light over a broad range of scattering angles about 90° (detector acceptance solid angle reported by the manufacturer (34) as 0.8 steradians!). Both require calibration to known molar mass standards for each mobile phase used (see Sec. 6).

In recent years, photon correlation spectroscopy (also known as quasi-elastic light scattering QELS, inelastic light scattering, dynamic light scattering, and so

© 2004 by Marcel Dekker, Inc.

on) methods, whereby the average diffusion coefficient associated with a light-scattering sample is determined, have been combined with SEC chromatography to yield a characterizing diffusion coefficient at each eluting slice. If the assumption is made that the molecules being measured are spheres, the so-called hydrodynamic radius (r_h) may be determined as a function of elution volume. For very small molecules whose r.m.s. radius (r_g) cannot be measured (that is, below about 10 nm), QELS can make such measurements down to below 1 nm and permit conformation studies to be completed. For larger molecules, when both r_h and r_g may be measured, molecular conformation may be determined directly following the methods of Burchard *et al.* (35). The combination of MALS and QELS is expected to have very important applications for the years ahead. The DAWN instruments (Wyatt Technology Corporation) permit full MALS measurement coupled with a QELS measurement at a range of selected angles for an eluting sample. Instruments (capable of being combined with a chromatographic separation) that incorporate a single 90° QELS measurement and single 90° light-scattering measurement are manufactured by Wyatt Technology Corporation, Precision Detectors, Inc., and Protein Solutions, Inc. (Charlottesville, Virginia).

There is a huge range of applications for MALS measurements, not the least of which are those listed at www.wyatt.com. This chapter has touched briefly on but a few of these applications and the significance of an integrated MALS system complete with software and error analysis. There can be no doubt that Burchard and Cowie were Cassandras when they stated that those not using MALS were at a distinct disadvantage. Unfortunately, it took almost a quarter of a century before their words began to be treated seriously.

ACKNOWLEDGEMENTS

Kudos to Dr. Steve Trainoff for his brilliant solution of the band-broadening problem that, in a practical sense, had remained unsolved to this day. Many thanks also to Drs. Michelle Chen and Miles Weida for their continuing contributions.

REFERENCES

1. W Burchard, JMG Cowie. Selected topics in polymer systems. In: MB Huglin, ed. Light Scattering from Polymer Solutions. Ch. 17:725–787, London: Academic Press, 1972.
2. A Einstein. The theory of opalescence of homogeneous fluids and liquid mixtures near the critical state (Theorie der Opaleszenz von homogenen Flüssigkeitsgemischen in der Nädes kritischen Zustandes). Ann Phys 33:1275–1298, 1910.
3. CV Raman. Relation of Tyndall effect to osmotic pressure on colloidal solutions. Indian J Phys 2:1–6, 1927.

© 2004 by Marcel Dekker, Inc.

4. PJ Debye. Light scattering in solutions. J Appl Phys 15:338–342, 1944.
5. BH Zimm. The scattering of light and the radial distribution function of high polymer solutions. J Chem Phys 16:1093–1099, 1948.
6. BH Zimm. Apparatus and methods for measurement and interpretation of the angular variation of light scattering; Preliminary results on polystyrene solutions. J Chem Phys 16:1099–1116, 1948.
7. P Putzeys, J Brosteaux. The scattering of light in protein solutions. Trans Faraday Soc 31:1314–1325, 1935.
8. DT Phillips. Evolution of a light scattering photometer. Bioscience 21:865–867, 1971.
9. W Kaye, AJ Havlik. Low angle laser light scattering—absolute calibration. Appl Optics 12:541–550, 1973.
10. W Kaye, JB McDaniel. Low angle laser light scattering—Rayleigh factors and depolarization ratios. Appl Optics 13:1934–1937, 1974.
11. JC Moore. Gel permeation chromatography. I. A new method for molecular weight distribution of high polymers. J Polym Sci A 2:835–843, 1964.
12. AC Ouano, W Kaye. Gel-permeation chromatography: X. Molecular weight detection by low-angle laser light scattering. J Poly Sci A 12:1151–1162, 1974.
13. PJ Wyatt, LA Papazian. The interdetector volume in modern light scattering and high performance size exclusion chromatography. LC-GC 11:862–872, 1993.
14. PJ Wyatt. Light scattering and the absolute characterization of macromolecules. Analytica Chimica Acta 272:1–40, 1993.
15. K-G Wahlund, A Litzen. Application of an asymmetric flow field-flow fractionation channel to the separation and characterization of proteins, plasmids, plasmid fragments, polysaccharides, and unicellular algae. J Chromatogr 461:73–87, 1989.
16. JC Giddings. Field-flow fractionation: separation and characterization of macromolecular, colloidal, and particulate materials. Science 260:1456–1465, 1993.
17. DW Shortt. Differential molecular weight distributions in high performance size exclusion chromatography. J Liquid Chromatogr 16:3371–3391, 1993.
18. PJ Flory, TG Fox. Treatment of intrinsic viscosities. J Am Chem Soc 73:1904–1908, 1951.
19. OB Ptitsyn, YuE Eizner. J Phys Chem USSR 32:2464, 1958; J Tech Phys USSR 29:1117, 1959.
20. H Benoit, D Froelich. Applications of light scattering to copolymers. In: MG Huglin, ed. Light Scattering from Polymer Solutions. London: Academic Press, 1972, Ch. 11, pp. 467–501.
21. J Wen, T Arakawa, J Talvenheimo, AA Welcher, T Horan, Y Kita, J Tseng, M Nicolson, JS Philo. A light scattering/size exclusion chromatography method for studying the stoichiometry of a protein–protein complex. Techniques in Protein Chem VII:23–31, 1996.
22. BS Kendrick, BA Kerwin, BS Chang, JS Philo. Online size-exclusion high-performance liquid chromatography light scattering and differential refractometry methods to determine degree of polymer conjugation to proteins and protein–protein or protein–ligand association states. Anal Biochem 299:136–146, 2001.

© 2004 by Marcel Dekker, Inc.

23. WH Stockmayer, LD Moore Jr, M Fixman, BN Epstein. Copolymers in dilute solution. I. Preliminary results for styrene-methyl methacrylate. J Polym Sci 16:517–530, 1955.
24. BH Zimm, WH Stockmayer. The dimensions of chain molecules containing branches and rings. J Chem Phys 17:1301–1314, 1949.
25. S Podzimek, T Vlcek, C Johann. Characterization of branched polymers by size exclusion chromatography coupled with multiangle light scattering detector. 1. Size exclusion chromatography elution behavior of branched polymers. J Appl Polym Sci 81:1588–1594, 2001.
26. SP Trainoff, PJ Wyatt. High temperature GPC defined by MALS. 1998 International GPC Symposium Proceedings, 1999, pp 108–134.
27. DW Shortt. Measurement of narrow-distribution polydispersity using multi-angle light scattering. J Chromatogr A 686:11–20, 1994.
28. WW Yau, JJ Kirkland, DD Bly. Modern Size-exclusion Liquid Chromatography. New York: John Wiley & Sons, 1979.
29. S Podzimek, in press.
30. V Astafieva, GA Eberlein, YJ Wang. Absolute on-line molecular mass analysis of basic fibroblast growth factor and its multimers by reversed-phase liquid chromatography with multi-angle laser light scattering detection. J. Chromatogr A 740:215–229, 1996.
31. L Jiu, J Ruppel, SE Shire. Interaction of human IgE with soluble forms of IgE high affinity receptors. Pharmaceutical Res 14:1388–1393, 1997.
32. H Li, MJ Cocco, TA Seitz, DM Engelman. Conversion of phospholamban into a soluble pentameric helical bundle. Biochem 40:6636–6645, 2001.
33. E Singer, R Landgraf, T Horan, D Slamon, D Eisenberg. Identification of a heregulin binding site in HER3 extracellular domain. J Biol Chem 276:44226–44274, 2001.
34. [0.8 steradians at 90°, 0.06 steradians at 15°] Precision Detectors, Inc. PD2000W-1-D Users' Manual, pp 2:2–2:3, 1992.
35. W Burchard, M Schmidt, WH Stockmayer. Information on polydispersity and branching from combined quasi-elastic and integrated scattering. Macromolecules 13:1265–1272, 1980.

© 2004 by Marcel Dekker, Inc.

22
High Osmotic Pressure Chromatography

Iwao Teraoka and Dean Lee
Polytechnic University
Brooklyn, New York, U.S.A.

1 INTRODUCTION

High osmotic pressure chromatography (HOPC) was developed in 1995 as a tool for preparative separation of polydisperse polymers by molecular weight (MW) using analytical-size columns (1). Since then, HOPC has been applied to separation of various polymers, demonstrating a high resolution and a large processing capacity (2–10).

In HOPC, a concentrated, viscous solution of polymer is injected into a column packed with porous materials. The concentration is much higher than the overlap concentration; the solution is in a semidilute range. The pore diameter must be sufficiently small to exclude most of the polymer at low concentration but not too small to exclude low-MW components at high concentrations. The injection continues typically until the whole column is filled with the solution. Upon detecting the first polymer in the eluent, solvent is injected to wash the column, and the eluent is collected by a fraction collector. The collection continues until the eluent concentration drops to a low level.

Any soluble polymer can be separated by HOPC. Advantages of HOPC over conventional preparative-scale chromatography include a high processing capacity and a high resolution. The latter requires fine-tuning of the separation

© 2004 by Marcel Dekker, Inc.

condition, as is explained in this chapter. The injected solution is concentrated, as is the eluent. Therefore, it is easy to recover solid polymer in each of the fractions. With minimal consumption of often hazardous organic solvents, HOPC is an environmentally friendly separation method for a wide variety of polymers.

The first half of this chapter explains the separation principle of HOPC in a good solvent condition. A couple of examples of separation are given. The second half focuses on recent extension of HOPC into theta solvent condition. The latter solvent allows a superior resolution and a greater processing capacity compared with the good solvent. In particular, use of weakly adsorbing porous packing makes it possible to produce narrow-distribution fractions from early to late eluent, yet rejuvenating the column at the end of each batch.

2 SEPARATION PRINCIPLE: HOPC IN A GOOD SOLVENT

The separation in HOPC is based on partitioning of a concentrated solution of polymer between a pore space (stationary phase) and a surrounding unconfined space (mobile phase). When the polymer is monodisperse and the solution is dilute (much lower than the overlap concentration c^*), the partition coefficient K is a sharply decreasing function of MW of the polymer (dashed line in Fig. 1). This principle is widely used in size exclusion chromatography (SEC). As in

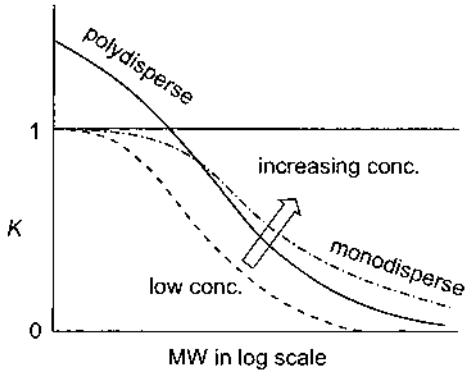

Figure 1 Partition coefficient K is schematically drawn as a function of MW in a logarithmic scale. Dashed lines, low concentrations; dash-dotted lines, higher concentrations; monodisperse polymer, solid lines; higher concentrations, polydisperse polymer.

© 2004 by Marcel Dekker, Inc.

SEC, the pore surface in HOPC is assumed not to interact with the polymer except for steric interactions. It is well known (11) that SEC requires that the concentration of the injected solution be sufficiently low. Overloading deforms chromatograms, because K increases rapidly with concentration when it is not sufficiently low compared with c^*. In solutions of a monodisperse polymer, K at c^* can be several times as large as its value in the dilute solution limit. The strong increase in K is caused by the high osmotic pressure of the solution. The osmotic pressure forces more chains into the pore, resulting in an increase of K toward $K = 1$. The increase occurs for polymers of different lengths, and thus the sharp MW dependence of K is lost (dash-dotted line in Fig. 1) (12). Pores that exclude a given polymer at low concentrations can admit it at high concentrations. Note that K never exceeds one in solution of a monodisperse polymer at any concentration.

The partitioning can be different when the polymer is polydisperse. At low concentrations, each polymer chain is partitioned independently, and therefore its K is exactly the same as the dashed line. At higher concentrations, repulsive interactions between polymer chains, especially those between long chains, change the landscape. The osmotic pressure drives polymer chains into the pore at higher proportions than it does at low concentrations. In the forced migration, low-MW components are preferentially partitioned to the pore space. As shown by the solid line in Fig. 1, K of a low-MW component in the polydisperse polymer is much higher compared with solutions of that component alone at the same concentration (dash-dotted line), whereas K of a high-MW component in the solution of polydisperse polymer is lower than the counterpart in the solution of that component alone at the same concentration (13,14). The concentration of the low-MW components can be higher in the pore than it is in the unconfined space. As a result, the span of K may exceed one (2). This phenomenon is exclusive to concentrated solutions of a polydisperse polymer. The plot of K in semidilute solutions of the polydisperse polymer reminds us of normal-phase and reversed-phase chromatography, which makes use of a large span of K through enthalpic interaction between the analyte and the stationary phase to induce high-resolution separation (11). SEC, by contrast, can attain reasonable resolution only with a long column or a bank of columns, because K is bound to the range $0-1$.

Computer simulation using Monte Carlo methods on a cubic lattice verified how the partition coefficient depends on the concentration, the chain length, and the pore size (15,16). A slit space constituting the pore was adjacent to the surroundings, allowing exchange of polymer chains. A chain that consists of 100 beads, each bead representing a monomer, was used as a long chain; a chain of 20 beads was for a short chain. Results for monodisperse solutions of the long chains only and of the short chains only (dotted lines) and an equal mass mixture of the long and short chains (solid lines) are compared in Fig. 2 (16). The

© 2004 by Marcel Dekker, Inc.

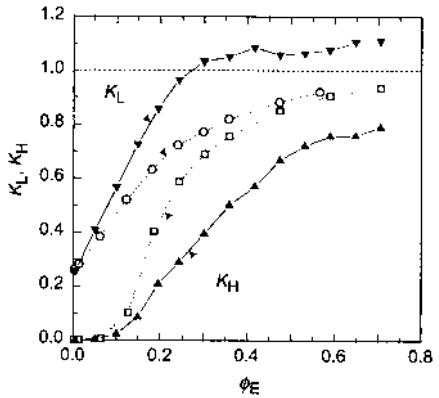

Figure 2 Partition coefficients K_L and K_H (solid lines) of short and long chains (20 and 100 beads) in an equal-mass mixture in a good solvent with a slit of width 6 (unit length = lattice unit), plotted as a function of the total volume fraction ϕ_E of the chains in the surrounding unconfined space. The partition coefficients for solutions of monodisperse polymer, namely a solution of the short chains only and a solution of the long chains only, are drawn as dotted lines. (From Ref. 16.)

partition coefficients of long and short chains, K_H and K_L, are plotted as a function of the total volume fraction ϕ_E of the chains in the surrounding solution. Overlapping of chains occurs at around $\phi_E = 0.40$, 0.12, and 0.19 in solutions of short chains only, long chains only, and their mixture, respectively. At low concentrations, each component of the polymer is partitioned independently. Therefore, a pair of dashed and solid lines share the intercept. With a slight increase in ϕ_E, K_L rises rapidly, whereas K_H remains near zero until ϕ_E reaches the overlap concentration. The increase in K_L occurs at concentrations well below the overlap concentration. Enhancement of K_L and suppression of K_H compared with the monodisperse counterparts are evident: the solid line of K_L for the short chains runs above the curve for the monodisperse system of short chains; the solid line of K_H for the long chains runs below the curve for a monodisperse system of long chains. K_L exceeds one, and the disparity between K_L and K_H is greater compared with independent partitioning of each component. If the long chains are longer and the short chains are shorter, the disparity between K_L and K_H in Fig. 2 will be greater.

As in HPLC, a greater $K_L - K_H$ leads to a greater difference between retention times of the two components. The separation resolution is better when the injected solution is concentrated, rather than dilute. SEC, however, does not make use of this principle, because universality, as represented by the SEC calibration curve, fails at high concentrations. When the purpose of separation is

© 2004 by Marcel Dekker, Inc.

fractionation rather than analysis of the MW distribution, injection of a concentrated solution has an edge. HOPC uses this principle.

3 HOPC SYSTEMS

At this moment, commercial HOPC systems are not available. Fortunately, off-the-shelf HPLC components can be assembled to construct an HOPC system, except for the columns (1–10). A typical system consists of an HPLC pump, a column, and a fraction collector. Two parts of Fig. 3 illustrate different injection methods. Figure 3a shows the injection of a concentrated solution by using an injection valve equipped with a sample loop of a large volume (2–4 mL for a column of 3.9×300 mm), swept by an HPLC pump of any type. The sample loop needs to have a large interior diameter to minimize the backpressure. In Fig. 3b, a simple HPLC pump directly injects the viscous solution through a pump head into the column. In the latter, a tubing of minimal length should connect the outlet check valve of the pump and the inlet end fitting of the column, bypassing a pulse damper, a pressure transducer, and other auxiliary components. A single-head pump will be preferred.

A detector may be connected to the column outlet. Upon detection of the first polymer, the eluent should be diverted to the fraction collector to avoid damage to the flow cell in the detector and to minimize band broadening in the fluid path between the column and the fraction collector. Any SEC detector can be used, but dropping the eluent into a solvent that does not dissolve the polymer and mixes with the eluent and visually inspecting the drops may be sufficient; precipitation signals the first polymer. If such a solvent is not readily available, dropping the eluent into the mobile phase solvent may be a good alternative. Because the polymer concentration in the eluent shoots up as the polymer enters, the human eye will detect spatial fluctuations of the refractive index to signal the first polymer.

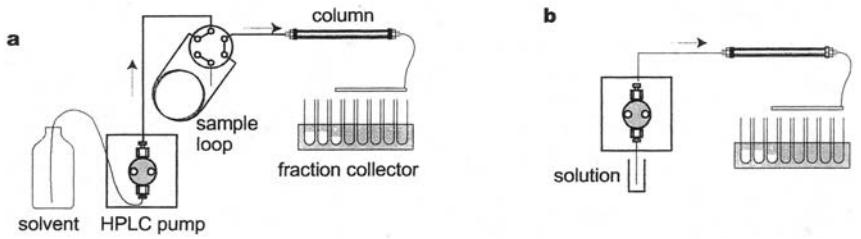

Figure 3 HOPC systems: (a) a polymer solution is injected into the sample loop, and then into the column, (b) the solution passes through the pump head.

© 2004 by Marcel Dekker, Inc.

4 COLUMNS FOR HOPC

Details are given in Chapter 23 of Ref. 6. However, in short, porous silica particles with a narrow pore size distribution are preferred to the polymeric gel beads commonly used in SEC. Specifically, controlled pore glasses (CPG) (17) available from CPG, Inc. (http://www.cpg-biotech.com/) and Prime Synthesis (http://www.primesynthesis.com/) offer excellent separation. CPG is available in average pore diameters that range from ~80 Å to ~3000 Å. The surface of CPG needs to be modified to prevent adsorption of polymer. Adsorption may lead to clogging of the column. Various silanization agents are available from Gelest (http://www.gelest.com/) and Fluka of Aldrich (http://www.sigmaaldrich.com/). Surface modification methods are described in the literature (1–10).

The mean pore diameter should be sufficiently small to exclude most of the injected polymer at low concentrations but admit its low-MW components at high concentrations. Specifically, the ratio of the mean pore diameter to the radius of gyration R_g of the polymer at its average MW should be between 1 and 2 (2,3,6). This size criterion is equivalent to ~1/4 of the pore size in the columns used in SEC to analyze the same polymer. If the polymer can be analyzed by nonaqueous SEC, its chromatogram will give an estimate of R_g of the polymer. The following approximate formula (18) is convenient:

$$R_g\,(\text{nm}) = 0.0125 \times [M(\text{g/mol})]^{0.595}$$

where M is the polystyrene-equivalent average MW (weight-average or peak MW).

Analytical-size columns can be used in HOPC for preparative purposes. Past studies indicate that columns of dimension 3.9 × 300 mm and 7.8 × 300 mm give a better resolution than thinner columns (6). Using a longer column or cascading a few columns, a practise that improves resolution in SEC, does not necessarily improve the resolution in HOPC.

5 OPERATION OF HOPC

Once a column (or a bank of columns) is selected according to the criteria described above, there are still several parameters a user can choose or must decide upon. They include the solvent, the concentration, the injection volume, the flow rate, and the column temperature.

The solvent must dissolve the polymer at high concentrations. A good solvent, a theta solvent, and any solvent between them can be used.

The concentration should be as high as possible unless the solution is too viscous for injection. Typically, the viscosity of honey at room temperature is adequate.

© 2004 by Marcel Dekker, Inc.

The injection volume should be comparable to the mobile phase volume of the column. Most conveniently, injection can be switched from solution to solvent upon detection of polymer at the column outlet. This practice guarantees that transport of the polymer solution through the column is uniform at least for the front end of the transported solution. When the solvent is injected into the column filled with viscous polymer solution, displacement of the viscous solution by the nonviscous solvent may not be uniform. Rather, solvent channels may be formed to facilitate penetration of the nonviscous fluid through the packed bed imbibed with the viscous fluid. Then, mass transfer between the stationary phase and the mobile phase will not be efficient. This phenomenon is known as *viscous fingering*, and is widely observed at the interface between two fluids vastly different in viscosity (19). The viscous fingering will affect mostly middle to late fractions in HOPC.

There is a severe restriction on the flow rate available in HOPC. On the one hand, extremely slow flow will cause a problem at the fraction collector, especially when the solvent is volatile. Evaporation of solvent at the tip of the tubing will clog the tubing or form a column of partially dried polymer hanging from the tip. On the other hand, a high flow rate not only increases the already high backpressure but also increases the chance of nonuniform transport of the solution through the column. Furthermore, the mass transfer problem will become more serious. Typically, a flow rate of 0.1 or 0.2 mL/min should be used for a column of 3.9 mm interior diameter.

It must be borne in mind that a large-volume injection of the viscous solution poses a serious problem of high backpressure, often exceeding several thousand psi, which is the limit of most HPLC pumps and hardware. Injection of a solution of a high-MW polymer through the pump head (Fig. 3b) may be especially troublesome, because the concentrated solution can be viscoelastic, causing malfunction of the check valves when the pump head employs a reciprocating plunger.

HOPC is a batch separation process. A typical procedure is summarized as follows. Prior to injection, the column is washed with the same solvent as the one used to dissolve the polymer to separate. A solution of the polymer is injected into the column at a constant flow rate. When the first polymer is detected in the eluent, the injection of the solution is stopped, and instead pure solvent is injected into the column to collect the polymer by the fraction collector and wash the column. Polymer can be recovered from solution by evaporation or by adding a nonsolvent.

6 EXAMPLES OF SEPARATION IN A GOOD SOLVENT

HOPC studies have been carried out nearly exclusively in good solvent conditions (1–10). This is partly to avoid deposition of injected polymer onto the pore surface

© 2004 by Marcel Dekker, Inc.

and concomitant clogging of columns. More importantly, however, it was believed that the high osmotic pressure of a concentrated solution in good solvent, the driving force of segregation by MW, was critical in HOPC (1). Figure 4 shows examples of separation in the good solvent condition. Figure 4a was obtained in HOPC of poly(methyl methacrylate) ($M_w = 7.9 \times 10^4$ g/mol, $M_w = 4.0 \times 10^4$ g/mol, with reference to polystyrene) in tetrahydrofuran (3). In total, 2.1 g of 25 wt% solution was injected at 0.1 mL/min into a column of 3.9×300 mm packed with CPG particles [mean pore diameter 128 Å, particle size 200/400 mesh; the surface was modified with trimethylsilanol (TMS) to avoid possible adsorption of the polymer]. The figure shows chromatograms obtained by off-line SEC (Phenogel, 10^3, 10^4, and 10^5 Å; Phenomenex, Torrance, California, U.S.A.). Each chromatogram is normalized by the peak area above the baseline. Early fractions collected the high end of the MW distribution of the original polymer. With an increasing fraction number, the peak MW shifts lower, and the peak broadens. Late fractions are not much different from the polymer injected.

Another typical separation in a good solvent condition is shown in Fig. 4b (5). This example is for poly(vinyl pyrrolidone) K30 (Fluka, Buchs, Switzerland) [$M_w = 1.7 \times 10^4$ g/mol, $M_w = 4.4 \times 10^3$ g/mol, with reference to poly(ethylene glycol)] in water. Then, 2.2 g of 30 wt% solution was injected at 0.1 mL/min into a column of 3.9×300 mm packed with CPG particles (mean pore diameter 130 Å, particle size 200/400 mesh; CPG was washed with acid) at room temperature. The figure shows chromatograms obtained by off-line aqueous

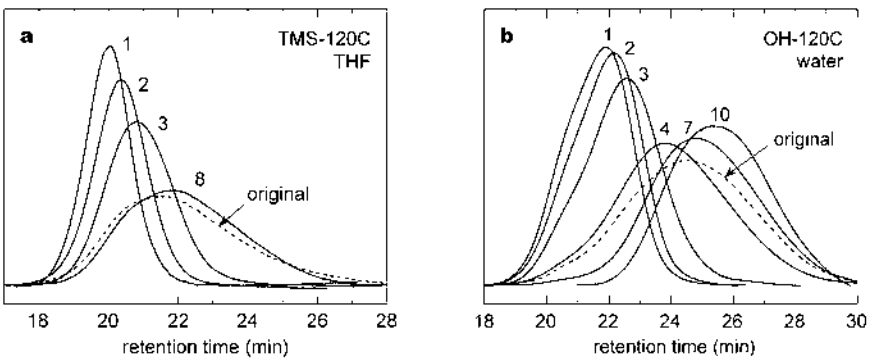

Figure 4 Examples of HOPC separation in a good solvent. Chromatograms obtained in off-line SEC are shown for some of the fractions. Each chromatogram is normalized by the peak area above the baseline. The chromatogram for the original polymer is shown as a dashed line. Fraction numbers are indicated adjacent to each curve. (a) Separation of poly(methyl methacrylate) in tetrahydrofuran. (b) Separation of poly(vinyl pyrrolidone) K30 in water. (From Refs 3 and 5.)

© 2004 by Marcel Dekker, Inc.

SEC with Shodex columns (OH Pak SB803, 804, 805). The overall transition of MW distribution in early to late fractions is similar to the one in Fig. 4a. There is a difference, however. The early fractions (1–3) have a greater leading edge than trailing edge. Late fractions collected low-MW components, and therefore their MW distribution is narrower than that of the original polymer. The difference between the two separations is ascribed to a weak adsorption of poly(vinyl pyrrolidone) onto the silica surface. We will see the effect of adsorption more clearly when we examine HOPC separation in the theta condition.

A need to inject a concentrated solution was demonstrated, substantiating the separation mechanism (1). It was also shown that use of porous packing with a narrow pore size distribution is essential (3). Performance of separation was compared for columns packed with CPG and silica gels that have similar mean pore diameters. CPG is known to have a narrower pore size distribution. The resolution was far better when separated by CPG.

Good separation applies to a few early fractions only. The mass of polymer with a narrowed MW distribution is at best 20% of the mass of polymer injected. Often, the number is less than a few percent. Nevertheless, those early fractions can provide a sufficient amount of polymer for further purification by HOPC (5) and further spectroscopic analysis (8) and thermal analysis. In fact, HOPC was applied repeatedly to early fractions to prepare standard-grade polymer samples (5). Using the preparative capability of HOPC, it was verified that multimeric impurity components in presumably monomethoxy-, monohydroxy-terminated poly(ethylene glycol) are diol-terminated (8).

7 SEPARATION PRINCIPLE: HOPC IN A THETA SOLVENT

In a solution of polymer in a good solvent, the second virial coefficient A_2 is positive. Positive A_2 makes the osmotic pressure deviate upward from that of an ideal solution, as illustrated in Fig. 5. A solution in the theta condition has $A_2 = 0$. Then, the osmotic pressure remains that of the ideal solution until a contribution by the third virial coefficient becomes sufficiently large, which occurs at a concentration much higher than the overlap concentration c^*. In most polymer solutions, lowering the temperature decreases A_2 to zero (upper critical solution temperature), although it may not be possible in an accessible temperature range. Exceptions are solutions in which polymer is solubilized by hydrogen bonding. Examples include poly(ethylene glycol) in water and poly(isopropyl acrylamide) in water. In these solutions, raising the temperature causes the polymer to precipitate (lower critical solution temperature). For details on the theta solvent condition, see Ref. 12.

In the theta solvent, the absent second virial coefficient drastically alters the partitioning at high concentrations. Again, lattice Monte Carlo simulation was used

© 2004 by Marcel Dekker, Inc.

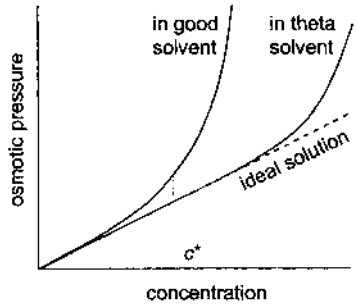

Figure 5 Concentration dependence of the osmotic pressure of polymer solution in good solvent and in theta solvent. The dashed line represents the osmotic pressure in the ideal solution of the same concentration.

to study the effect of the solvent quality on the partitioning of a mixture of short (20 beads) and long (100 beads) chains (16). Figure 6 compares the partition coefficients K_L and K_H of short and long chains with a slit of width 6. For reference, the partition coefficients for a monodisperse polymer in the theta condition are plotted as dotted lines. Unlike in the good solvent, K_L and K_H of dotted lines remain flat until the concentration becomes very high, when the positive third virial coefficient starts to force the chains into the slit. The same rule applies to the

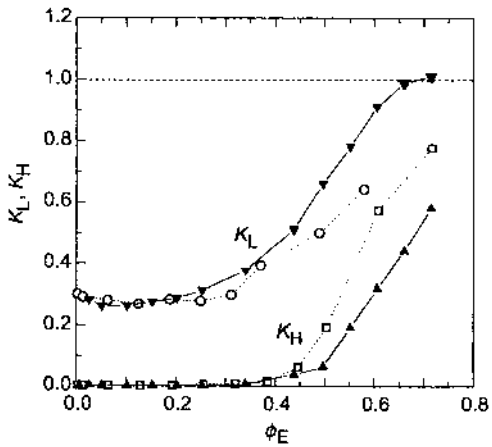

Figure 6 Partition coefficients K_L and K_H (solid lines) of short and long chains (20 and 100 beads) in an equal-mass mixture in theta condition with a slit of width 6, plotted as a function of the total volume fraction of the chains in the surrounding space. The partition coefficients for solutions of monodisperse polymer are drawn as dotted lines. (From Ref. 16.)

© 2004 by Marcel Dekker, Inc.

partition coefficients in the bimodal mixture. Only at high concentrations does the enhancement of K_L and the suppression of K_H compared with the monodisperse counterparts occur. When a concentrated solution of a polydisperse polymer in theta solvent is partitioned between the pore and the surrounding space, the high osmotic pressure will drive low-MW components into the pore more than it does in a solution of a monodisperse polymer of the low-MW components. This part is the same as in a good solvent, except that the concentration needs to be much higher. More importantly, though, the flatness of the plots of the partition coefficients, especially K_H, can help improve the resolution of HOPC. The low K_H over a broad range of concentrations indicates that the purity of low-MW components in the pore remains high, unchanged from that at low concentrations, until K_H starts to increase at quite a high concentration. This means that, in HOPC, only low-MW components will be able to enter the pores in nearly all steps of partitioning in all theoretical plates in the column during the separation. This property may help narrow the MW distribution in late fractions. In the good solvent condition, in contrast, some of high-MW components can enter the pores at a lower concentration, degrading the purity of the polymer partitioned to the pore and eluting later. Thus, the theta solvent may offer superior separation in HOPC, especially for late fractions, as long as strong adsorption by the pore surface in the unfavorable solvent condition is avoided.

8 COMPARISON OF SEPARATIONS IN A GOOD SOLVENT AND A THETA SOLVENT

The difference in the separation performances in the two solvent conditions was demonstrated for poly(ε-caprolactone) (PCL), a biodegradable polymer (9). Dioxane is a good solvent for PCL. Toluene gives a near-theta solvent condition at 30°C. PCL–toluene has an upper-critical solution temperature of around 15°C (9). The column used (3.9 × 300 mm) was packed with octyldimethylsilanol (C8)-modified CPG (pore diameter 130 Å, 120/200 mesh). In each separation, the solution of PCL10K ($M_w = 1.02 \times 10^4$ g/mol, $M_n = 0.61 \times 10^4$ g/mol, $M_w/M_n = 1.66$) was injected into the column at 30°C until the whole column was filled with solution. The concentration of the solution was 0.228 g/mL (21.9 wt% for dioxane; 25.0 wt% for toluene). The injection amount was 1.95 mL and 2.53 mL, respectively. Table 1 shows the number of drops, the volume of the solution, and the mass of the polymer in each fraction for the separation in toluene. A similar collection schedule was employed in the separation in dioxane.

Figure 7 shows the concentration of the eluent as a function of the cumulative volume of the eluent since the polymer solution was injected in the two separations. If one drop were collected in each fraction, then the curve would be smooth. We call this curve an HOPC retention curve. In dioxane, the eluent

© 2004 by Marcel Dekker, Inc.

Table 1 Solution Volume, Polymer Mass, and Average Molecular Weights in Each of Fractions Collected in Separation of PCL10K by a C8-120B Column in Toluene

Fraction	Drops	Volume of solution (mL)	Mass of polymer (g)	$M_w/10^4$ (g/mol)	$M_n/10^4$ (g/mol)	M_w/M_n
1	20	0.233	0.0010	2.64	2.38	1.11
2	20	0.223	0.0052	2.17	1.90	1.14
3	20	0.229	0.0153	1.62	1.34	1.21
4	20	0.236	0.0337	1.37	1.08	1.27
5	20	0.243	0.0475			
6	20	0.246	0.0532	1.15	0.80	1.43
7	20	0.246	0.0550			
8	20	0.245	0.0556	1.05	0.69	1.53
9	20	0.245	0.0558			
10	20	0.243	0.0528	0.91	0.57	1.59
11	40	0.476	0.0784			
12	40	0.464	0.0458	0.81	0.49	1.63
13	100	1.123	0.0452			
14	100	1.127	0.0144	0.60	0.35	1.70
15	300	3.395	0.0091	0.53	0.25	2.08
16	300	3.398	0.0028	0.50	0.17	2.88
Total	1080	12.373	0.5708			

increases its concentration gradually to reach a plateau in fraction 9. The plateau level is nearly equal to the concentration of the injected solution. In toluene, the increase is more rapid, and the plateau is broader. A decrease in concentration occurs in the same way for the two solvents except it is delayed in toluene because of a greater injection volume. Both separations recovered more than 99% of the

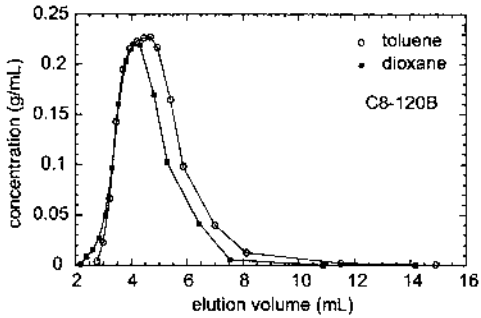

Figure 7 HOPC retention curve in separation of PCL10K by a C8-120B column in dioxane (closed squares) and toluene (open circles).

© 2004 by Marcel Dekker, Inc.

polymer injected in the first 19 fractions. Apparently, adsorption was absent in these two separations. A greater injection volume in toluene indicates easier partitioning of polymer to the pore, especially at low concentrations. The latter is reasonable when we consider the smaller chain dimension in the theta solvent compared with fully swollen chains in the good solvent.

A difference in the separation performance of dioxane and toluene is evident in SEC chromatograms of the separated fractions (Fig. 8). The values of M_w, M_n, and M_w/M_n in the separation in toluene are listed in Table 1 for fractions analyzed. The molecular weights of PCL, M_{PCL}, were converted from M_{PS}, polystyrene-equivalent MW, using the formula, $M_{PCL} = M_{PS} \times 0.462$. The latter was obtained in SEC with a multi-angle laser light-scattering detector (Wyatt; Dawn DSP, Santa Barbara, California) by comparing the plots of M_w as a function of the retention volume for broad-distribution polystyrene and PCL.

The chromatograms for the separation in dioxane are typical of HOPC in the good solvent condition. The transition in early to late fractions is similar to the one

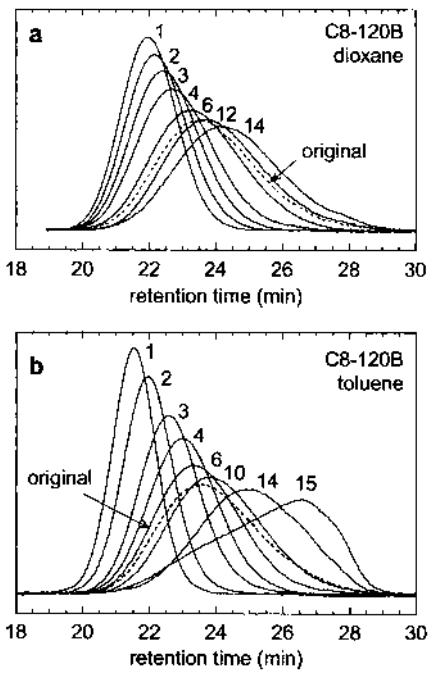

Figure 8 SEC chromatograms for some of the fractions obtained in separation of PCL10K by a C8-120B column in (a) dioxane and (b) toluene. The chromatogram for the original PCL10K is shown as a dashed line.

© 2004 by Marcel Dekker, Inc.

in Fig. 4a. The middle fractions (8–12) are indistinguishable from the original PCL10K. Later fractions have a lower MW, but fractions 15 and 16 return to a distribution not much different from that of the original PCL (recoiling). In the theta solvent, early fractions have quite a high MW. Middle fractions maintain a narrower distribution than that of the original PCL10K. Late fractions have enriched low-MW components. Recoiling was absent.

The advantage of HOPC in the theta solvent is obvious. The resolution is better from early to late fractions, in agreement with the result of the computer simulation study. Furthermore, the theta solvent had a higher loading capacity. Nevertheless, the amount of fractions with a narrow MW distribution, say $M_w/M_n < 1.2$, is less than 1% of the polymer injected, which is still greater than the counterpart in the dioxane separation. The amount was drastically increased by separating with a weakly adsorbing medium as shown below.

9 HOPC IN A THETA SOLVENT WITH WEAKLY ADSORBING MEDIA

Using porous media that weakly adsorb the polymer may improve the separation performance in HOPC. In the past, SEC in the theta condition was attempted, but adsorption impaired the separation (20). All the polymer injected failed to come out. In HOPC, in contrast, adsorption of some of the polymer injected does not prevent most of the polymer from eluting from the column, separated by the pore, unless the adsorption is too strong.

The theta solvent offers an excellent environment for fine-tuning the degree of adsorption. In the theta solvent, polymer chains are on the verge of associating each other. A slight decrease in A_2 will lead to precipitation or phase separation. Therefore, in the solution placed near a surface, weak attractive interactions between the polymer and the surface will be sufficient to adsorb the polymer.

We compare the separation performance for the same PCL10K. When the pore surface weakly adsorbs the polymer, the performance of HOPC is better. TMS-120B (CPG120B modified with TMS), TMS-75B [CPG75B (mean pore diameter 81 Å) modified with TMS], and C8-75B (CPG75B modified with C8) weakly adsorb PCL10K in toluene. None of these media adsorbs the same polymer in dioxane. HOPC was conducted using a column packed with one of the three media at 30°C. A 25 wt% solution of PCL10K in toluene was injected into a toluene-filled column. Injection volumes were 3.45, 3.41, and 2.16 mL, respectively, much greater than the injection volumes in separation with the nonadsorbing medium (C8-120B). Figure 9 compares HOPC retention curves for the three separations. When the surface was TMS, the polymer did not elute until nearly twice as much volume as the typical injection volume in a good solvent was loaded into the column. The tailing of the retention curve is obvious. In the smaller

© 2004 by Marcel Dekker, Inc.

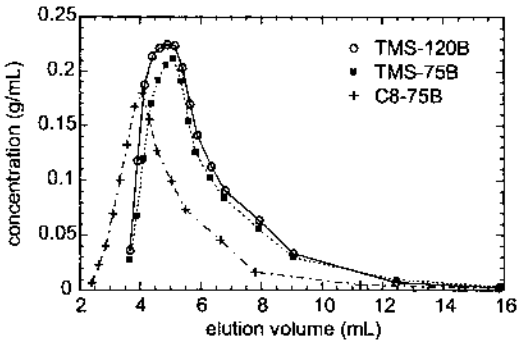

Figure 9 HOPC retention curve in separation of PCL10K by a TMS-120B column (open circles), a TMS-75B column (closed squares), and a C8-75B column (crosses).

pore size with TMS surface, the peak concentration did not reach the level of the injected solution. With the C8-75B, the injection was less, probably because of an even smaller pore size due to surface modification and some repulsion from the octyl moieties. The peak concentration was considerably lower. Recovery was below 100% (85, 86, and 85%, respectively, in the three separations), but washing the column in dioxane at 80°C released all the polymer adsorbed.

The three parts of Fig. 10 show SEC chromatograms. Fractions 1 to 16 were eluted in toluene at 30°C. Later fractions were collected at a higher temperature either in toluene or dioxane. These last fractions reveal which components of PCL10K were adsorbed onto the pore surface. The overall tendency is similar among the three columns, but distinctly different from the one obtained with nonadsorbing environment (C8-120B). The increase in the peak retention time with an increasing fraction number is more gradual compared with Fig. 8, especially in Fig. 10c. Middle fractions maintain a narrower distribution compared with that of the original PCL10K. Late fractions are enriched with low-MW components, especially in the separation by TMS surfaces. The multimodal nature of the MW distribution is revealed. Unlike the column C8-120B, the C8-75B column adsorbed PCL10K. It was considered that a lower degree of substitution of surface silanols with octyl moieties in C8-75B than in C8-120B resulted in adsorption (9). Separation of the same polymer by octadecyl (C18)-modified CPG75B was attempted, but there was little adsorption, and the fractions had a broader MW distribution compared with the weakly adsorbing surfaces.

Table 2 lists the mass of polymer and its average MW for some of the fractions obtained in the separation with the C8-75B column. Now the mass of polymer with $M_w/M_n < 1.2$ is 88.6 mg as opposed to a mere 6.2 mg in the separation with the C8-120B column in toluene.

© 2004 by Marcel Dekker, Inc.

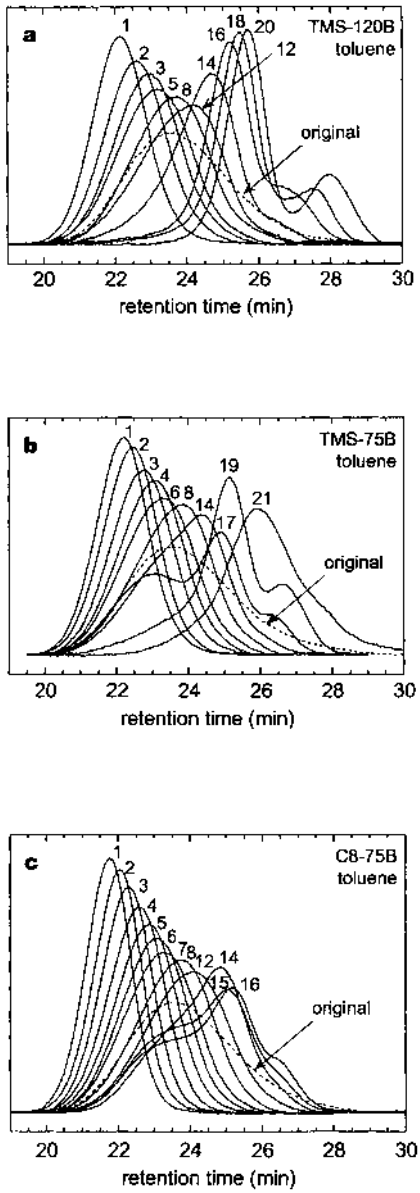

Figure 10 SEC chromatograms for some of the fractions obtained in separation of PCL10K by (a) a TMS-120B column, (b) a TMS-75B column, and (c) a C8-75B column. The chromatogram for the original PCL10K is shown as a dashed line. (Part c, from Ref. 9.)

© 2004 by Marcel Dekker, Inc.

Table 2 Solution Volume, Polymer Mass, and Average Molecular Weights in Each of Fractions Collected in Separation of PCL10K by a C8-75B Column in Toluene

Fraction	Drops	Volume of solution (ml)	Mass of polymer (g)	$M_w/10^4$ (g/mol)	$M_n/10^4$ (g/mol)	M_w/M_n
1	20	0.231	0.0016	2.39	2.18	1.10
2	20	0.230	0.0053	2.13	1.92	1.11
3	20	0.231	0.0093	1.91	1.71	1.12
4	20	0.235	0.0164	1.71	1.50	1.14
5	20	0.238	0.0239	1.53	1.31	1.17
6	20	0.242	0.0321	1.38	1.16	1.19
7	20	0.244	0.0409	1.29	1.06	1.22
8	20	0.246	0.0443	1.10	0.88	1.25
9	20	0.244	0.0379			
10	20	0.242	0.0307			
11	40	0.476	0.0474			
12	40	0.469	0.0346	0.95	0.72	1.32
13	100	1.147	0.0521			
14	100	1.150	0.0189	0.78	0.57	1.36
15	300	3.460	0.0172	0.81	0.54	1.51
16	300	3.460	0.0084	0.76	0.48	1.59
Total	1080	12.545	0.4210			

A closer look at the chromatograms in Fig. 10, in particular Fig. 10c, reveals that the middle fractions have a smaller trailing edge compared with the leading edge, although the original PCL has them the other way around. In separation in a good solvent or in a nonadsorbing medium, in contrast, SEC chromatograms of separated fractions have always a greater trailing edge, as shown in Fig. 4a and Figs 7a and b. Cutting the tail increases M_n, and thus decreases M_w/M_n.

Curtailing the low-MW components was explained by the following mechanism (9). As the polymer is introduced to the column, it starts to coat the pore surface, thus decreasing the pore size. The coating will remove the polymer from the transported solution. This is why an excess solution needs to be injected before the first polymer comes out of the column. If the pore is sufficiently small (as in CPB75B), the coated layer will consist mostly of low-MW components. The coating will occur beyond the monolayer coverage to further narrow the pore. The increasing layer thickness will force later-eluting polymer to partition with a narrower pore size. The adjustable pore size results in a narrowed MW distribution even for late fractions; in the absence of adsorption, late fractions are almost indistinguishable from the original polymer injected, because the pore size

© 2004 by Marcel Dekker, Inc.

appropriate for the early fractions is too large to narrow the distribution in late fractions.

It is important not to have a strong adsorption. When polymer is injected into a column filled with strongly adsorbing media, polymer of any MW will be adsorbed. Selective partitioning of low-MW components into the stationary phase will not occur. Strong adsorption can be prohibited by using small pores, since high-MW components will find it difficult to enter the pore to be adsorbed.

Using a thicker column or cascading the columns increases the processing capacity. The results obtained (21) are promising. By carefully choosing the right combination of columns in the right order, an even higher resolution with an increased capacity was demonstrated (21).

Good separation with a weakly adsorbing medium in the theta condition raises a hope that a weakly adsorbing medium may also offer a better separation than nonadsorbing medium in a good solvent. It now appears that good resolution enjoyed in the separation of PVP in water (5) (good solvent) is ascribed to the weak adsorption. The smaller trailing edge compared with the leading edge in early fractions in Fig. 4b indicates adsorption. Enriching low-MW components in late fractions, which is uncommon in HOPC in good solvent, was helped by the adsorption and concomitant narrowing of the pores. Another evidence of the adsorption is gradual degradation in separation performance as separation is repeated on the same column (5). In fact, the first-time use of the column resulted in a higher resolution from early to late fractions than those shown in Fig. 4b. In that study, the total mass of the polymer recovered was not measured, however. We expect it will be difficult to find a solvent that removes all of the adsorbed polymer when the adsorption occurs in a solvent that solvates the polymer well.

To utilize adsorption, a theta solvent in HOPC has an advantage that a good solvent does not have: when washed in a good solvent after separation in the theta solvent, the adsorbed polymer will be released, and the column will return to the state before the run and be ready for the next batch of separation. Another batch of separation conducted under the same condition produced identical results (9). Adsorption occurs as a result of a precarious balance of polymer–polymer interactions and polymer–pore surface interactions. A slight change in the surface such as octyl modification is sufficient to suppress the adsorption. The surface modification is not limited to TMS, C8, and C18. Another surface may give an even better separation.

10 SUMMARY

The advantage of HOPC in a theta solvent was demonstrated, especially with a column that weakly adsorbs the polymer. The same method was applied to a higher-MW sample of PCL. Again, the resolution was better when separated in

© 2004 by Marcel Dekker, Inc.

toluene and the surface was weakly adsorbing than otherwise. Unlike SEC, selection of the optimal surface and solvent requires time-consuming trial-and-error separations in order for each polymer to separate, but it is rewarding.

REFERENCES

1. M Luo, I Teraoka. Macromolecules 29:4226, 1996.
2. I Teraoka, M Luo. Trends Polym Sci 5:258, 1997.
3. M Luo, I Teraoka. Polymer 39:891, 1998.
4. A Dube, I Teraoka. Isolation and Purification 3:51, 1999.
5. Y Xu, I Teraoka, L Senak, C-S Wu. Polymer 40:7359, 1999.
6. I Teraoka. In: C-S Wu, ed. Column Handbook for Size Exclusion Chromatography. New York: Academic Press, 1999.
7. S Matsuyama, H Nakahara, K Takeuchi, R Nagahata, S Kinugasa, I Teraoka. Polym J 32:249, 2000.
8. D Lee, I Teraoka. Polymer 43:2691, 2002.
9. D Lee, Y Gong, I Teraoka. Macromolecules 35:7093, 2002.
10. D Lee, I Teraoka. Biomaterials 24:329, 2003.
11. UD Neue. HPLC Columns: Theory, Technology, and Practice. Wiley-VCH, 1997.
12. I Teraoka. Polymer Solutions: An Introduction to Physical Properties. New York: John Wiley, 2002.
13. I Teraoka, Z Zhou, KH Langley, FE Karasz. Macromolecules 26:3223, 1993.
14. I Teraoka, Z Zhou, KH Langley, FE Karasz. Macromolecules 26:6081, 1993.
15. Y Wang, I Teraoka, P Cifra. Macromolecules 34:127, 2001.
16. P Cifra, Y Wang, I Teraoka. Macromolecules 35:1146, 2002.
17. W Haller. Nature 206:693, 1965.
18. K Huber, S Bantle, P Lutz, W Burchard. Macromolecules 18:1461, 1985.
19. J Bear. Dynamics of Fluids in Porous Media. New York: Elsevier, 1972 (New York: Dover, 1988).
20. C-S Wu. PhD thesis, The University of Akron, 1978.
21. D Lee, I Teraoka. J Chrom A 996:71, 2003.

© 2004 by Marcel Dekker, Inc.

23
Size Exclusion/ Hydrodynamic Chromatography

Shyhchang S. Huang
Noveon, Inc.
Brecksville, Ohio, U.S.A.

1 INTRODUCTION

Size exclusion chromatography (SEC) is currently the most widely used method for determining the molecular weight (MW) and molecular weight distributions (MWD) of polymers. What is less known is that during a SEC run another chromatographic separation mechanism, hydrodynamic chromatography (HdC), is also taking place. Figure 1 shows polystyrene standards that were separated by these two mechanisms in a single injection (1) using small-pore columns. The calibration curve for the chromatogram in Fig. 1 is plotted in Fig. 2. It shows that standards larger than MW 5×10^5 are separated by HdC. Those smaller than 5×10^4 are separated by SEC. In a larger pore-size column, the MW ranges separated by these two mechanisms overlap and it becomes difficult to distinguish from the calibration curve. HdC is currently used more for particle size distribution studies. It has also been investigated for MW studies (2,3). This chapter discusses the combination of these two mechanisms, whereby an analysis benefits from the separation abilities of both.

© 2004 by Marcel Dekker, Inc.

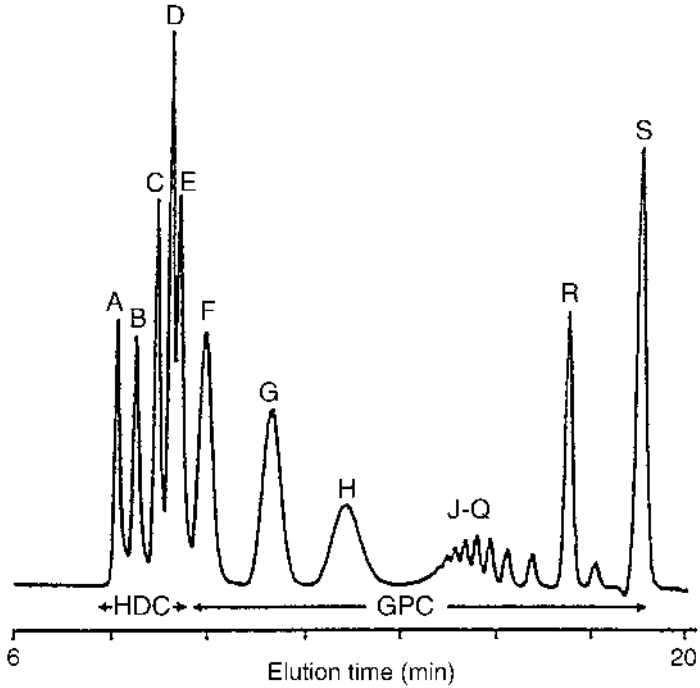

Figure 1 Chromatogram showing SE/HdC separation of narrow polydispersity polystyrene standards. Column: two 300 × 7.5 mm PLgel Mixed-E columns in series; flow rate, 1.0 mL/min. A = 4,000,000; B = 1,550,000; C = 550,800; D = 156,000; E = 66,000; F = 30,300; G = 9200; H = 3250; J–Q = oligomers; R = 162; S = toluene. (From Ref. 1.)

2 HYDRODYNAMIC CHROMATOGRAPHY

The basic principles of HdC are easily explained by considering the transport of spherical macromolecules in laminar flow through an open microcapillary tube (Fig. 3). The solvent velocity profile in an open tubular tube is a parabolic Poiseuille flow. Macromolecules are considered as rigid spheres and are neutrally buoyant. As a result of Brownian motion, macromolecules will disperse throughout the capillary cross-section. Because of their finite sizes, the centers of the polymer molecules cannot approach the column wall any closer than their own radii. Owing to the fluid velocity profile, a larger solute molecule travels through the capillary at a greater average velocity than a smaller solute. In other words, the separation of HdC is not due to size exclusion itself, but to the faster average

© 2004 by Marcel Dekker, Inc.

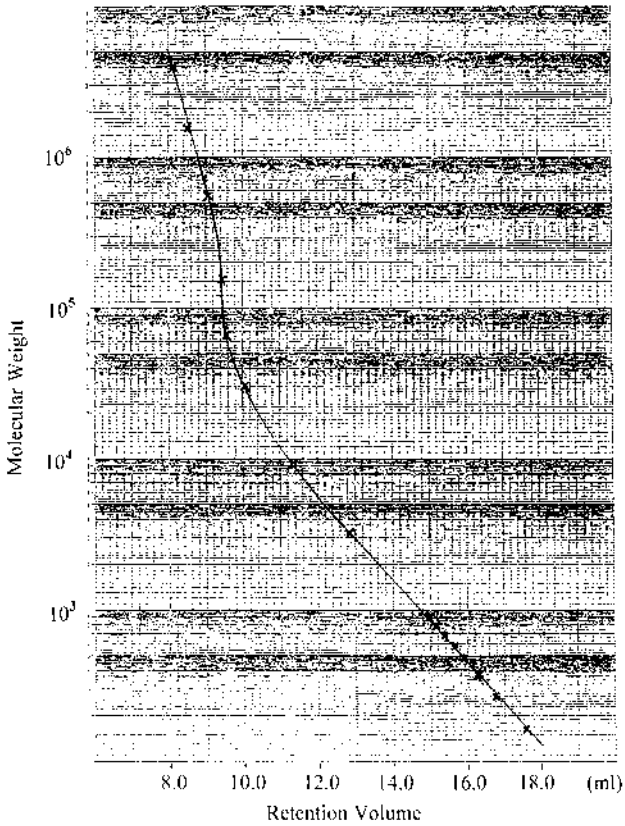

Figure 2 Calibration curve for the chromatogram in Fig. 1.

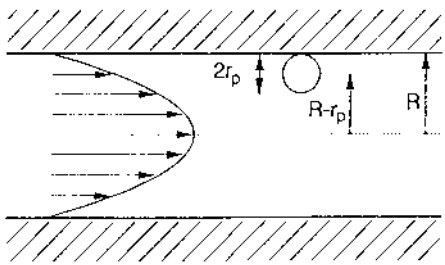

Figure 3 Transport of a spherical particle undergoing Poiseuille flow through a cylindrical capillary. (From Ref. 5, Copyright 1993, Elsevier.)

© 2004 by Marcel Dekker, Inc.

solvent speed in the area where the macromolecules (or particles) are restricted due to their size.

HdC separation also occurs in the interstices of a packed column, although the configuration of channels is not as simple as in a microcapillary tube. Owing to the three-dimensional void structure of a packed column, the exact form of the velocity profile is not clearly defined as it is in the microtubular columns. The mechanism is much more complicated than for an open tubular HdC. However, we may consider these voids as a set of equivalent capillaries. Bird *et al.* (4) found that the radius of equivalent capillaries is roughly 0.2 times the mean diameter of the packing beads.

Most current liquid chromatographic columns, including SEC and HPLC, are packed with porous gels. With porous packings, SEC separation is more noticeable than HdC separation. A pure HdC separation can be demonstrated using a column packed with nonporous solid gels. Figure 4 shows an example of an HdC chromatographic separation using 1.50 μm solid beads (5). The calibration curves of polystyrene standards separated in THF mobile phase with

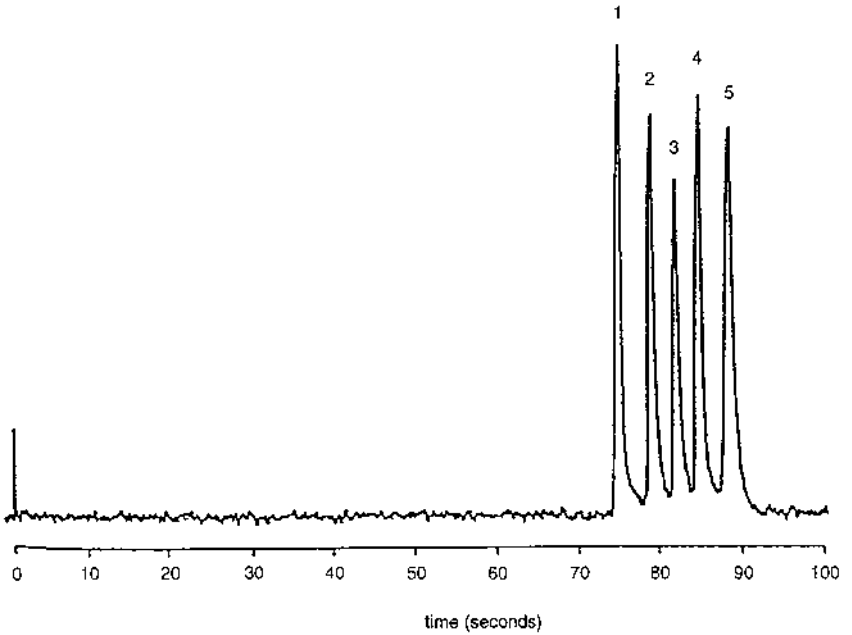

Figure 4 High-speed packed column HdC separation of polystyrenes dissolved in THF. Column, 150 × 4.6 mm; packing, 1.50 μm nonporous silica particles; pressure drop, 200 bar; detection, UV. (1) PS 775,000, (2) PS 336,000, (3) PS 127,000, (4) PS 43,900, and (5) toluene, 0.2 mg/mL each. (From Ref. 5, Copyright 1993, Elsevier.)

© 2004 by Marcel Dekker, Inc.

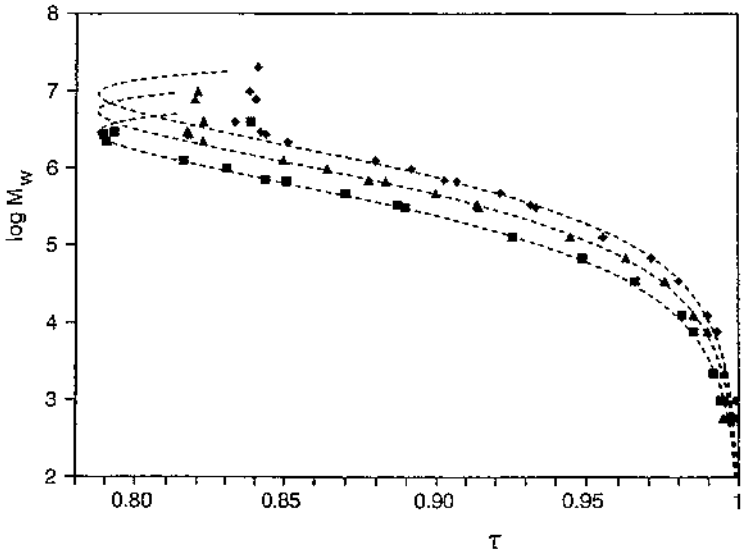

Figure 5 Elution behavior of polystyrene standards in THF in packed-column HdC with different packing diameters: ■ = 1.40 μm, ▲ = 1.91 μm, and ◆ = 0.87 μm. Theoretical curves (dashed lines). (From Ref. 6, Copyright 1990, Elsevier.)

1.40, 1.91, and 2.69 μm solid beads are shown in Fig. 5 (6). The dashed lines in Fig. 5 are theoretical curves.

3 COMPARISON OF HdC AND SEC

The separation range of an SEC column, in terms of MW, is determined by the pore size of the packed gels. The calibration curves of columns with single pore-size gels are shown in Fig. 6 (7). A broader MW range of separation can be obtained by mixing various pore size gels. The slope of the calibration curve, or resolution of separation, then depends on the pore volume. The greater the pore volume, the less steep will be the calibration curve, and the better the resolution; and vice versa. A linear calibration curve with broad separation range in MW can be achieved by packing specially-mixed different pore-size gels of the same particle size in a column. Linear calibration curves with various MW ranges of commercialized mixed-bed columns are shown in Fig. 7 (8). In the HdC case, optimal chromatographic separation requires a close packing, uniform particle size, and as spherical gels as possible. Given these conditions the calibration curve depends only on the particle size. The MW separation range of an HdC column, as

© 2004 by Marcel Dekker, Inc.

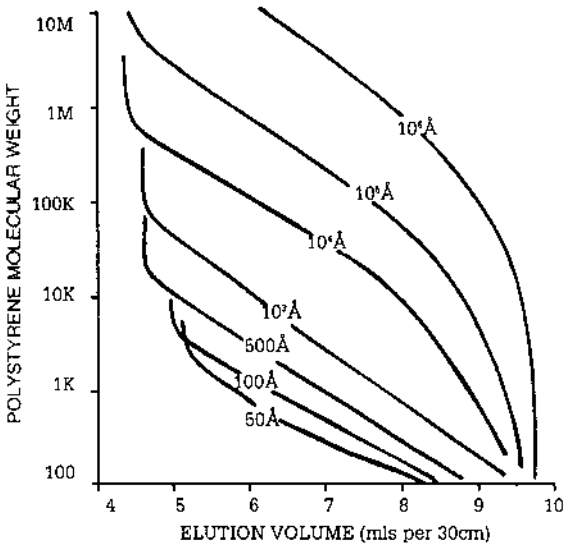

Figure 6 Calibration curves of PLgel columns with single pore-size gels. Calibrants, Polystyrene; eluent, THF; flow rate, 1.0 mL/min. (From Ref. 7, courtesy of Polymer Laboratories.)

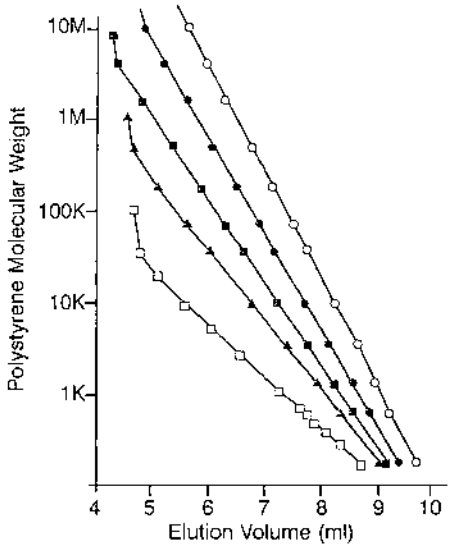

Figure 7 Calibration curves of mixed-bed PLgel columns. ○ = MIXED-A, ● = MIXED-B, ■ = MIXED-C, ▲ = MIXED-D, □ = MIXED-E. (From Ref. 8, courtesy of Polymer Laboratories.)

© 2004 by Marcel Dekker, Inc.

Table 1 Comparison Between SEC and HdC Separations

	SEC	HdC
Location where separation occurs	Pores inside gels	Interstitial area between gels
Factors affecting separation	Pore size & pore volume	Particle size
For low MW material	MW range & slope of calibration curve can be easily designed	Separation diminishes below 10^4 MW
For high MW material	Poorer separation due to slow process, and possible degradation	More favorable

shown in Fig. 5, is slightly narrower than that of a single-pore-size SEC column. More importantly, it becomes more and more difficult to use a column packed with particles smaller than 1.0 μm due to the increase in backpressure. The separation of low MW species by HdC quickly diminishes below 10^4 MW.

The SEC separation mechanism of high MW polymers, which involves an in-and-out-of-pore process, becomes more difficult for high MW polymers. The higher the MW, the slower the movement, and the more difficult the separation. The high MW polymer chains are also more susceptible to degradation during this in-and-out-of-pore process. Therefore, the peak shape of high MW standards, $> 10^6$, separated by large-pore columns tends to be broader and exhibits tailing. On the other hand, the separation mechanism of HdC does not involve this in-and-out-of-pore process. This is the reason that the high MW peaks in Fig. 1, separated by small pore columns, tends to be sharp.

These two separation mechanisms co-exist in a chromatographic run and complement each other, as shown in Table 1. It would be ideal to design a column that uses the advantages of each mechanism and provides a linear calibration curve.

4 COMBINATION OF SEC AND HdC

Currently, HdC studies for MW separations emphasize the same MW ranges as regular SEC studies (2). The particle size of HdC packings is normally less than 3 μm. In order to separate polymers in the higher MW range for the SEC/HdC combination, the particle size should be larger. Three columns are custom-packed with 3, 5, and 10 μm solid beads by Jordi's Associate (Bellingham, MA, USA). The calibration curves of polystyrene standards in THF are shown in Fig. 8. All three columns appear to have an inflection point around $\sim 5 \times 10^5$. The curves are steeper below this point, and are less steep above it. The slopes at the upper MW

© 2004 by Marcel Dekker, Inc.

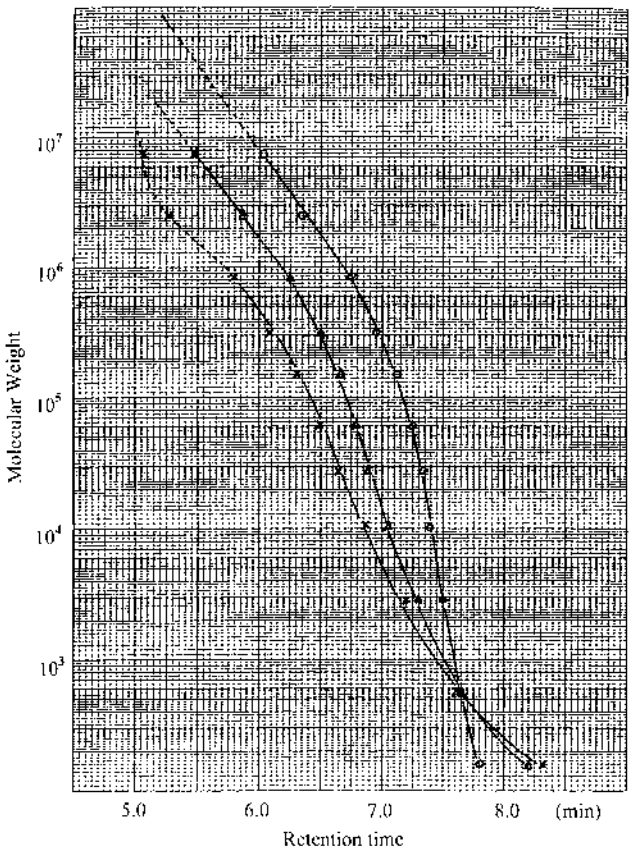

Figure 8 Calibration curves of solid-bead HdC columns. Columns, $\times = 3\,\mu m$, $\triangle = 5\,\mu m$, $\bigcirc = 10\,\mu m$; mobile phase, THF with 250 ppm BHT, at 1.0 mL/min; column temperature, 50°C.

range of the three columns are approximately the same. The curve of the 3 μm column turns upward above $\sim 3 \times 10^6$ MW, while both 5 μm and 10 μm columns do not reach their upper MW limits with the available PS standards, up to 7.5×10^6. It seems that the 10 μm column would separate the highest MW range among three columns. For an ideal SEC/HdC column, it is possible to adjust the SEC separation so that the portion of the calibration curve for 5×10^5 and below is colinear with the HdC high MW portion of the curve. This adjustment can be accomplished by controlling the total pore volume of the packing gel.

As discussed previously, the slope of an SEC calibration curve depends on the pore volume. Figure 2 shows the calibration curve of an SEC separation in a

© 2004 by Marcel Dekker, Inc.

regular SEC column in which the pore volume is roughly 30 to 40% of the entire column volume. In the curve, the linear portion above 3×10^5 is due to the HdC mechanism separating large molecules while the portion below 5×10^4 is due to the SEC mechanism separating lower MW species. It can be seen that the portion of the curve due to the SEC mechanism has a flatter slope than that region due to the HdC mechanism. In order to obtain a linear calibration curve over the entire MW range, the total pore volume must be reduced so that the slope of the lower MW portion of the curve matches that of the upper region. From experience, the ratio of the total pore volume to total column for such an ideal SEC/HdC column should be roughly one-third that of a regular SEC column.

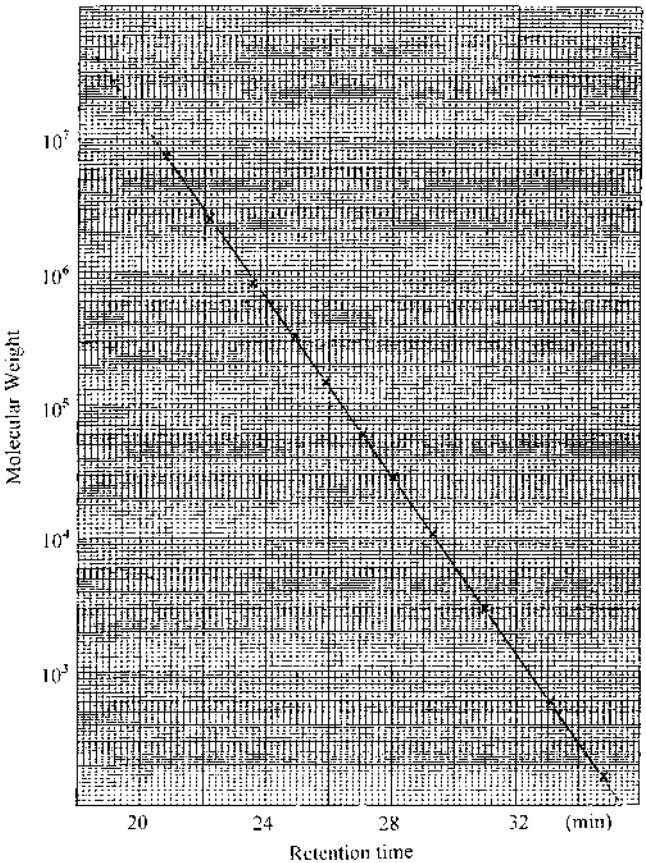

Figure 9 Calibration curve of SE/HdC. Column, 10 μm solid-bead column (250 × 10 mm) + 5 μm PLgel MIXED-D column (300 × 7.5 mm); mobile phase, THF with 250 ppm BHT, at 0.5 mL/min; column temperature, 50°C.

© 2004 by Marcel Dekker, Inc.

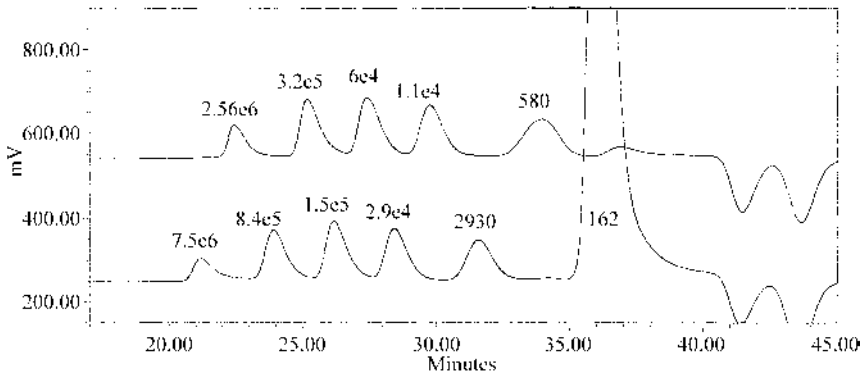

Figure 10 SE/HdC chromatograms of two polystyrene standard mixtures. Chromatographic conditions as in Fig. 9.

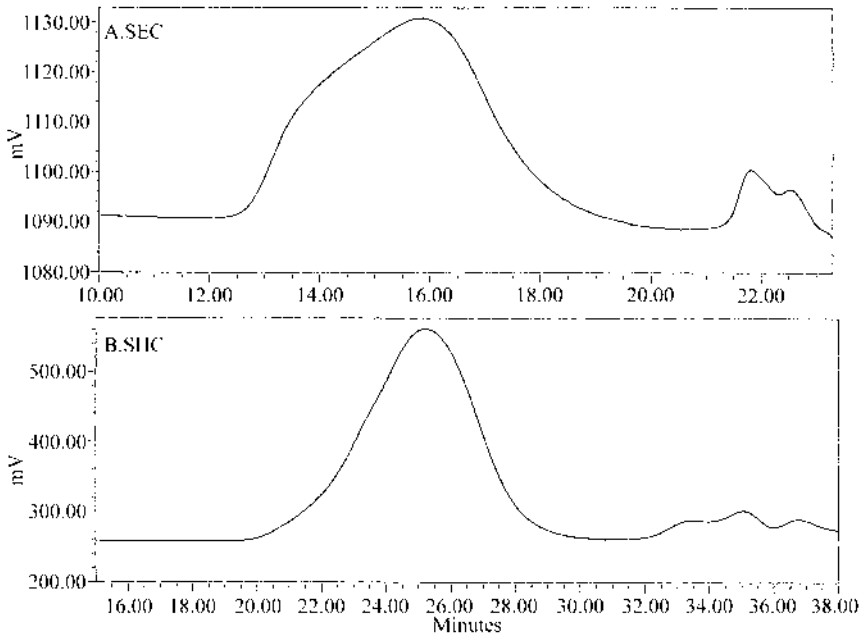

Figure 11 Comparison of SEC and SE/HdC chromatograms of a high MW sample. Chromatographic conditions of both runs are the same as Fig. 9, except the column set of run A, which consists of PhenoGel columns: 5 μm, Guard (50 × 7.8 mm) + 2 × Linear(2) (300 × 7.8).

© 2004 by Marcel Dekker, Inc.

Such an ideal separation can be obtained by connecting a 10 μm solid-bead column and a PLgel Mixed-bed D column in series. The calibration curve of PS standards is shown in Fig. 9. It is surprisingly almost perfectly linear, even up to the highest MW standard, 7.5×10^6. According to Fig. 8, the curve may be linear to a much higher MW region. The chromatograms of two PS standard mixtures are shown in Fig. 10. The shapes of the 7.5×10^6 and 2.56×10^6 peaks are sharp and considerably less tailing than in a regular SEC chromatogram.

A broad MW distribution sample was studied using both SEC alone and SEC/HdC. These chromatograms are compared in Fig. 11. This sample is largely excluded from a typical mixed-bed SEC column, such as PLgel Mixed-B columns. There is better separation with the SEC/HdC column; the entire sample is within the separation range.

The above example demonstrates the feasibility of combining SEC and HdC in one chromatographic run with a linear calibration curve. It would be more convenient to use a mixed-bed packing that combines the separation mechanisms of these two columns in one column. The recipe for such a packing can be calculated according to the above study: (1) 10 μm particle size, (2) with pores of size distribution similar to PLgel's Mixed-D column, and (3) a total pore volume of about 40% of a regular SEC packing material. This configuration can also be obtained by mixing 60% of 10 μm solid bead with 40% mixed-D gels. Efforts are under way to make such an ideal SEC/HdC packing.

ACKNOWLEDGEMENTS

The author expresses his appreciation to Noveon, Inc., for permission to publish this article and for support on all research work, to Dr. C. S. Wu for his encouragement and discussion, and to D. Hanshumaker for his help in preparation of this article.

REFERENCES

1. E Meehan, S Oakley. LC-GC 5(11):32, 1992.
2. SS Huang. Column Handbook for Size Exclusion Chromatography. San Diego: Academic Press, 1999.
3. J Bos, R Tijssen. J Chromatogr Lib Ser 56(4):95, 1995.
4. R Bird, WE Stewart, EN Lightfoot. Transport Phenomena. New York: Wiley, 1960.
5. G Stegeman, JC Kraak, H Poppe, R Tijssen. J Chromatogr A 657:253, 1993.
6. G Stegeman, R Oostervink, JC Kraak, H Poppe, KK Unger. J Chromatogr 506:547, 1990.
7. Polymer Laboratories, Chromatography Products, Issue 2 2001/2002, p 14.
8. Polymer Laboratories, Chromatography Products, Issue 2 2001/2002, p 5.

© 2004 by Marcel Dekker, Inc.